practice guide

NIST recommended

Fractography of Ceramics and Glasses

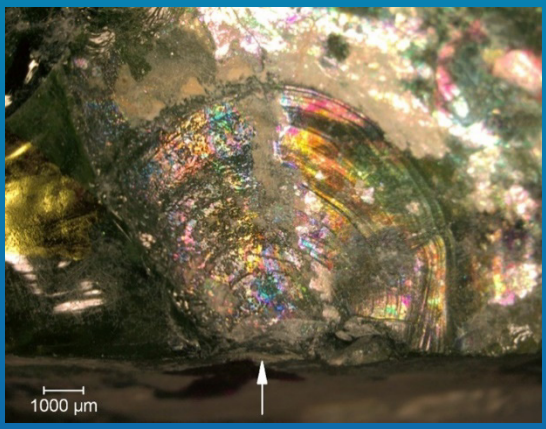

George D. Quinn

This publication is available free of charge from:

https://doi.org/10.6028/NIST.SP.960-16e4

NATIONAL INSTITUTE OF STANDARDS AND TECHNOLOGY
U.S. DEPARTMENT OF COMMERCE

Special Publication 960-16e4

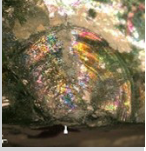

NIST Recommended Practice Guide

Special Publication 960-16e4

Fractography of Ceramics and Glasses

George D. Quinn
Materials Measurement Laboratory
National Institute of Standards and Technology

This publication is available free of charge from:
https://doi.org/10.6028/NIST.SP.960-16e4

April 2026

U.S. Department of Commerce
Howard Lutnick, Secretary

National Institute of Standards and Technology
Craig Burkhardt, Acting Under Secretary of Commerce for Standards and Technology and Acting NIST Director

The cover illustration shows an impact fracture in a piece of glass cullet that was excavated in the mid-1960s from an ancient Roman Empire glass factory (»350 AD) in Jalame, Israel. Although the glass surface is heavily weathered and has a colorful patina, the concentric tertiary Wallner lines that are characteristic of an ancient impact are still recognizable.

Certain equipment, instruments, software, or materials, commercial or non-commercial, are identified in this paper in order to specify the experimental procedure adequately. Such identification does not imply recommendation or endorsement of any product or service by NIST, nor does it imply that the materials or equipment identified are necessarily the best available for the purpose.

National Institute of Standards and Technology
Special Publication 960-16e4
Natl. Inst. Stand. Technol.
Spec. Publ. 960-16e4
683 pages (April 2026)
CODEN: NSPUE2
This publication is free of charge from:
https://doi.org/10.6028/NIST.SP.960-16e4

Preface to the Fourth Edition

Fractography is a powerful but underutilized tool for the analysis of fractured glasses and ceramics. It may be applied to fractures in the laboratory or for component failures in service. Fractography can identify the cause of failure and can even provide quantitative information about the loading conditions. The goal of this Guide is to make fractographic analysis of brittle materials less an art and more an engineering practice for scientists and engineers. This Guide is a free public service of NIST for the benefit of American industry, and the worldwide ceramic and glass communities. I am gratified that this Guidebook has been very popular over the years since it was first published in 2007 in both printed and digital forms. This encouraged me to keep it up to date and add new knowledge.

This guide emphasizes practical approaches for problem solving and failure analyses, but it also distills the state of the art in our "important minor branch of physical science." I respect the know-how developed over more than a century by conscientious researchers, materials scientists, and engineers. I salute them and have done my best to credit their contributions by the liberal use of citations and the bibliographies.

I have been able to update the Guide about every 4 to 5 years. My goal always has been to provide as much information as possible to help the user solve problems. I have struggled to "get my arms completely around" the subject matter. Fractography has been a continual learning experience even for me. The book has grown appreciably in size and there are more than 450 more figures than in the first edition and almost double the number of references. Judicious changes to the text font size and layouts have kept the overall size manageable. The risk is that these expansions will make the Guide unwieldy, but so far there have been no complaints! I also have been able to add new techniques, new science, and yes, new flaws. [a,b]

Two new trends are worth noting here: innovative ceramics are being created by additive-manufactured processes. This field has enormous potential, but these new processes are introducing many new and exotic flaws. These will keep fractographers busy for many years! As for glasses, new trends of making them stronger and thinner are challenging fractographers. It will be

---

[a] A separate document file that lists chapter-by-chapter all the changes by edition is available upon request. I also maintain "errata sheets" for each edition.

[b] The book has almost doubled in content. There now are well over 1000 references and 1200 figures. Appendices A Bibliography, B Case Studies, and E Terminal; Crack Velocities are only in the digital on-line version of this book.

difficult or impossible to detect classic markings such as Wallner lines or fracture mirrors. There is a new specimen size effect section 5.10 in this edition that explains why.

The follow-on editions have enabled me to correct of few major mistakes in earlier editions. In the 1st edition there was a typographical mistake in the Newman-Raju stress intensity formulas for semielliptical surface cracks in bending (chapter 7) and the definition of "vicinal illumination" (chapter 3) was incorrect. I also have corrected some faulty notions by other scientists and engineers. Preston's original crack branching angle analysis of 1935 was in part incorrect. It was corrected in the 3rd edition of this Guide in 2020. I also reanalyzed the literature about crack terminal velocities for ceramics and glasses. There are many faulty notions about this topic carried over from the metals dynamic fracture mechanics community. For example, notions of microcavities nucleating ahead of fast-moving cracks in ceramics and glasses are wrong. How fracture mirrors form is reviewed in much greater depth than in the 1st edition. In this 4th edition I also call attention to the wild confusion and contradictions in the literature about scratch/dig specifications for optical materials.

The fundamentals of fractographic analysis of ceramics and glasses have not changed since the 1st edition in 2007. These include the classic breakage patterns, the fracture surface markings, fracture mechanics principles, and the examination techniques. Nonetheless, I have added major new definitions of: "Griffith flaw," (chapter 6), "fracture toughness, K_{Ic}" (chapter 7), and even "fractography" (chapter 1). There are many new examples and illustrations, expanded failure mode discussions (thermal shock, compression, multiaxial loading), new examination equipment and microscopes, and the marriage of the computer to the microscope. Obsolete equipment has been deleted (e.g., Polaroid instant film). New ceramics and glasses and processing techniques are emerging along with inevitable new types of flaws. Chapter 6 on flaw origins has almost doubled in length from the 1st edition.

Overall, there is a lot more on new applications including additively-manufactured ceramics, terminal crack velocities, dynamic compression fractures, thermal shock, glue chip fractures, human bone fractures, and fractures in museum glasses. Artificial intelligence systems are discussed in the Conclusion chapter 11. From the beginning, special effort has been put into carefully structuring this book with a detailed Table of Contents and a thorough Index at the end. Only a few will read this Guide from cover to cover, and it is more likely that the user will be seeking some specific information on a particular problem.

There are many cross references in this book. A single broken part may be shown in multiple chapters. Inevitably in a work of this size and magnitude a few cross-referencing or reference number mistakes crop up. I apologize if this leads to reader confusion or frustration.

Acknowledgements

The author derived much inspiration from the late Professor Van Derck Fréchette of Alfred University who wrote the 1990 seminal book: *Failure Analysis of Brittle Materials*. The author has had a fruitful collaboration with Professor James Varner in teaching the short summer course on Fractography at Alfred University from 1996 to 2021. The author thanks Dr. Jeffrey Swab, of the U.S. Army Research Laboratory; Aberdeen Proving Ground, Maryland and Mr. Michael J. Slavin (formerly of ARL) for their help in crafting the U.S. Army Military Handbook (MIL HDBK) 790 in 1990, a precursor to ASTM practice C 1332 adopted in 1996. The latter was the first formal standard for fractographic analysis of ceramics and brittle materials in the world. Dr. Swab and I learned much about how fractographers work from our 1994 Versailles Advanced Materials and Standards round robin on ceramic fractography.

Special thanks are to Mr. Roy Rice and Dr. Jack Mecholsky. Dr. Roger Morrell of the National Physical Laboratory has been an inspiration with his practical applications of fractography and his own Guide to Fractography.

I also acknowledge the insightful work of Dr. Janet B. Quinn formerly of the American Dental Association, who made her own contributions to the science of brittle materials fractography before she prematurely passed away in 2008. She and her friend Dr. Susanne Scherrer pioneered the application of fractography to ceramic, glass-ceramic, and composite dental crowns and bridges. Some of their illustrations are in this Guide.

TABLE OF CONTENTS

Preface

1.	**Introduction**	1-1
2.	**Resources**	2-1
3.	**Tools and Equipment**	3-1
3.1	Low Power Optical Examination	3-2
3.2	Photographing the Overall Component: Cameras, Cellphones, and Simple Digital Microscopes	3-7
3.3	Stereo Optical Microscope	3-11
3.4	Stereo Optical Microscope Camera Port and Digital Cameras for Microscopes	3-14
3.5	Digital Image Processing and Focus Stacking	3-16
3.6	Discussion Stereomicroscope	3-19
3.7	Digital Microscopes	3-19
3.8	Illumination Sources and Techniques	3-21
3.9	Coatings on Fracture Surfaces	3-28
3.10	Size Measurements	3-31
3.11	Compound Optical Microscope	3-33
3.12	Replication Equipment	3-36
3.13	Scanning Electron Microscope (SEM)	3-43
3.14	Stereo SEM Imaging	3-55
3.15	Field Emission SEM	3-57
3.16	Environmental SEM	3-57
3.17	Transmission Electron Microscope (TEM)	3-58
3.18	Atomic Force Microscope (AFM)	3-58
3.19	Optical Profilometer	3-59
3.20	Confocal Scanning Light Microscope	3-60
3.21	Stress Wave and Ultrasonic Fractography	3-61
3.22	High Speed Photography	3-62
3.23	X-ray Topography	3-62
3.24	Dye Penetration and Staining	3-63
3.25	Polariscope	3-67
3.26	Other Equipment	3-68
3.27	Other Resources	3-69
3.28	The Future	3-69
4.	**General Examination, Fracture Modes, and Patterns**	4-1
4.1	Specimen Reconstruction	4-2
4.2	Crack Branching Patterns	4-5
4.3	Crack Branching Angles	4-8

4.4	Crack Branching Distances	4-13
4.5	Fragmentation Patterns	4-13
4.6	Laboratory Test Fracture Patterns	4-14
4.6.1	Tension strength	4-15
4.6.2	Flexural strength	4-16
4.6.3	Biaxial flexural strength	4-22
4.6.4	Laboratory tests: additional tips	4-27
4.7	Component Fracture Patterns – General	4-27
4.8	T Intersections and Crossing Cracks	4-31
4.9	Invisible cracks	4-33
4.10	Plates and Windows	4-33
4.11	Tempered Windows and Objects	4-35
4.12	Thermally-Induced Plate and Window Fractures	4-37
4.13	Bottles and Pressure Vessels	4-41
4.14	Torsional Fractures	4-46
4.15	Edge Chipping	4-48
4.16	Complementary Laboratory Test Fractures to Aid Component Fracture Analysis	4-54
4.17	Controlled Component Fractures, Replicates, Exemplars	4-55
4.18	Finite Element Analysis	4-58
4.19	Characteristics of Some Common Fracture Modes	4-59
4.19.1	Mechanical overload fracture	4-59
4.19.2	Thermal fracture and thermal shock, crackle glass	4-59
4.19.3	Coating fractures, crazing, and craquelure	4-63
4.19.4	Corrosion, oxidation, crizzling	4-69
4.19.5	Impact or contact fractures	4-70
4.19.6	Residual stresses	4-71
4.19.7	Time-dependent fracture and slow crack growth	4-73
4.19.8	Compression fracture	4-73
5.	**Fracture Surface Examination**	5-1
5.1	Introduction	5-1
5.2	Fracture Mirrors, A Fractographer's Best Friend	5-4
5.2.1	Fracture mirrors in glass	5-4
5.2.2	Terminal crack velocities	5-7
5.2.3	How fracture mirrors form	5-11
5.2.4	Fracture mirrors in ceramics	5-23
5.2.5	Fracture mirrors, special cases	5-26
5.2.6	Fracture mirrors in other materials	5-35
5.3	Hackle	5-36
5.3.1	Coarse microstructural hackle	5-36
5.3.2	Wake hackle	5-38

5.3.3	Twist hackle	5-42
5.3.4	Shear hackle	5-47
5.3.5	Corner hackle	5-48
5.3.6	Step hackle	5-49
5.4	Wallner Lines	5-50
5.4.1	Introduction	5-50
5.4.2	Primary Wallner lines	5-52
5.4.3	Secondary Wallner lines	5-55
5.4.4	Tertiary Wallner lines	5-58
5.4.5	Wallner Lambda lines	5-63
5.5	Arrest Lines (Interruption marks)	5-63
5.6	Scarps	5-66
5.7	Transgranular and Intergranular Fracture	5-69
5.8	Stable Crack Growth	5-71
5.8.1	Slow crack growth (SCG) at ambient temperature	5-71
5.8.2	Stable extension from local residual stress or R-curve effects	5-75
5.8.3	High temperature slow crack growth in ceramics	5-76
5.8.4	High temperature creep fracture	5-79
5.8.5	Mechanical fatigue from cyclic loading	5-83
5.9	Organizing all the Information - Fractographic Montages	5-86
5.10	Specimen Size Effects in Fractographic Analysis	5-88
6.	**Origins of Fracture**	6-1
6.1	Origins, Flaws, and Defects	6-1
6.2	The Spatial Distribution of Flaws	6-2
6.3	Are Flaws Intrinsic or Extrinsic?	6-4
6.4	Matching Fracture Halves	6-6
6.5	External Surfaces	6-6
6.6	Volume-Distributed Flaws	6-8
6.6.1	Pores and Bubbles	6-8
6.6.2	Porous regions	6-15
6.6.3	Porous seams	6-16
6.6.4	Agglomerates	6-18
6.6.5	Inclusions	6-20
6.6.6	Compositional inhomogeneities	6-26
6.6.7	Large grains	6-27
6.6.8	Grain boundaries	6-30
6.7	Surface-Distributed Flaws	6-32
6.7.1	Surface voids or pits from processing	6-32
6.7.2	Pits from environmental exposure	6-33
6.7.3	Handling scratches and polishing scratches	6-34
6.7.4	Sharp object impact or contact	6-42

6.7.5	Blunt object impact or contact	6-45
6.7.6	Grinding and machining cracks	6-51
6.7.7	Chips	6-64
6.7.8	Glue Chips	6-65
6.8	Other Flaws	6-70
6.8.1	Processing and firing cracks in ceramics	6-70
6.8.2	Blisters in ceramics	6-76
6.8.3	Knoop and Vickers controlled flaws, glasses and ceramics	6-77
6.8.4	Other glass origins	6-79
6.9	Fracture Oddities and other flaws	6-88
6.10	Contaminants	6-92
6.11	Combined or Hybrid Flaws	6-94
6.12	Baseline Microstructure Origins	6-95
6.13	Geometric Sharp points or Cusps	6-98
6.14	Partially-Exposed Flaws	6-99
6.15	Glaze and Coating Flaws	6-100
6.16	Microfault Pockets	6-102
6.17	Polished Microstructural Sections	6-104
6.18	Flaw Size	6-105
6.19	What to Report	6-105
7.	**Quantitative Analysis**	7-1
7.1	Introduction	7-1
7.2	Stresses from the Extent of Fragmentation	7-2
7.2.1	Annealed parts	7-2
7.2.2	Fragmentation of tempered parts	7-5
7.3	Stresses from the Branching Distances	7-7
7.3.1	Annealed plates and bars	7-7
7.3.2	Tempered plates	7-8
7.4	Stresses from the Fracture Mirror Size	7-10
7.4.1	Fracture Mirror analysis and constants	7-10
7.4.2	How to measure fracture mirror sizes	7-17
7.5	Fracture Mechanics Analysis of the Flaw Size	7-19
7.5.1	Introduction to fracture mechanics	7-19
7.5.2	Fracture mechanics solutions for internal penny-shaped cracks	7-29
7.5.3	Fracture mechanics solutions for surface cracks	7-32
7.5.3.1	The Newman-Raju Y factors for semielliptical surface flaws in bending	7-33
7.5.3.2	Newman-Raju formulas for deep (a/c > 1) semielliptical surface cracks	7-38
7.5.3.3	Accuracy of the Newman-Raju formulas and alternatives	7-38

7.5.3.4	Bansal's approximation for semielliptical surface flaws	7-39
7.5.3.5	Murakami's equation for irregular surface cracks	7-39
7.5.4	Three-dimensional, blunt, and inclined flaws	7-40
7.6	Relationship of K_{Ic} and A	7-41
7.7	Fracture Mirror to Flaw Size Ratios	7-42
7.8	Comparing Measured to Calculated Flaw Sizes	7-43
7.9	Crack Velocities from Wallner Line Analysis	7-46
7.10	Slow Crack Growth	7-51
7.11	R- curve Behavior	7-54
7.12	Indentation Mechanics	7-59
7.13	Fractal Analysis	7-63
7.13.1	General	7-63
7.13.2	Fractal analysis of fragmentation	7-65
7.13.3	Fractal analysis of the fracture surface	7-66
7.14	Estimation of Residual Stresses	7-68
7.14.1	Introduction	7-68
7.14.2	Estimates of residual stresses from fragmentation	7-69
7.14.3	Estimates of residual stresses from fracture mechanics analysis of flaws	7-69
7.14.4	Estimates of residual stresses from fracture mirror size analysis	7-70
7.14.5	Estimates of residual stresses from indention crack sizes	7-71
7.14.6	Estimates of residual stresses by other means	7-71
7.15	Weibull Analysis	7-71
8.	**Single Crystals**	8-1
8.1	General	8-1
8.2	Preferred Cleavage Planes	8-4
8.3	Fractographic Techniques	8-6
8.4	Fracture Surface Markings	8-10
8.5	Origins	8-23
8.6	Other Sources	8-32
9.	**Ceramic and Glass Composites**	9-1
9.1	Particulate, Whisker, or Self-Reinforced Ceramic Composites	9-1
9.2	Fiber-Reinforced Composites	9-2
9.3	Dental composites	9-5
10.	**Case Studies**	10-1
Case 1	Ruptured Rotor (Ceramic gas turbine rotor)	10-1
Case 2	Busted Barrel (SiC machine gun liner)	10-4
Case 3	Conflicting Carbide Data (SiC flaws, slow crack growth)	10-7

Case 4 Vulnerable Vials (Broken medicinal vials) 10-10
Case 5 Damaged Dome (Coarse-grained AlON IR dome) 10-11
Case 6 Suffering Setter Plate (SiC furnace plate) 10-13
Case 7 Ruptured Radomes (Fused silica missile nosecones) 10-15
Case 8 Maligned machinists (Bend bars from machine shops) 10-17
Case 9 Modeler's Match (Fracture origins in MEMS scale SiC micro tensile specimens) 10-20
Case 10 Fractious Fractographers (A fractography round robin) 10-22
Case 11 Perilous Prostheses (Three ceramic dental crowns) 10-25
Case 12 Mangled Margins (Twenty alumina dental crowns) 10-33
Case 13 Ruined Refractors (Sapphire lenses) 10-35

11. Conclusions 11-1

Appendix A Bibliography

Appendix B Fractographic Case Studies

Appendix C Fracture Mirror and Branching Constants

Appendix D Guidelines for Measuring Fracture Mirrors

Appendix E Terminal Crack Velocities

Index

1. Introduction

Why did it break? What was the origin of failure? Did it break as expected or from an unexpected cause? Was there a problem with the material or was the part simply overloaded or misused? Why did this part break and others not? What was the stress at fracture? Was the laboratory strength test successful or was there a misalignment? These are common practical questions and the fractographer can often give straightforward definitive answers.

The curse of brittle materials is that they are prone to catastrophic fracture. Brittle fracture is fracture that takes place with little or no plastic deformation. Nature has partially compensated for this shortcoming by furnishing clear fracture patterns and fracture surface markings that provide a wealth of interpretable information. Indeed, in many respects, fractographic analysis of ceramics and glasses is easier and can produce more quantitative information than the fractographic analysis of metals or polymers.

Figure 1.1 shows broken glass and ceramic rods. Using the techniques described in this Guide, fractographers are able to determine that the rods were broken in bending, from surface flaws, and even determine the fracture stress.

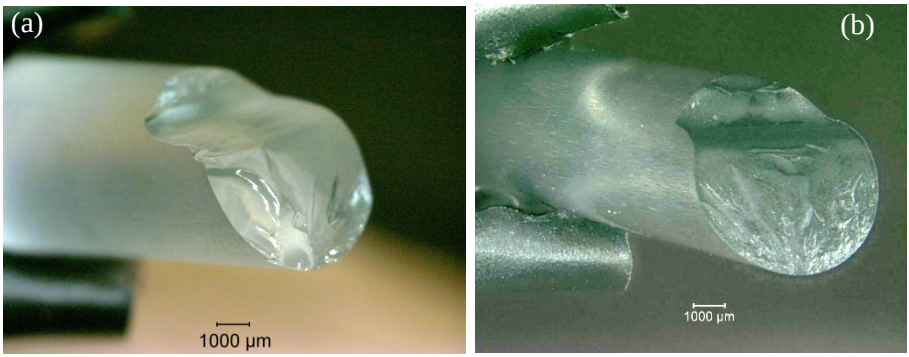

Figure 1.1 *Fractured glass (a) and ceramic (b) rods.*

This Guide takes a broader view of fractography than merely the examination of the fracture surface. The author wrote a broad definition of fractography that was adopted in ASTM standard C1322[1] in 1996:

> **fractography,** n – means and methods for characterizing fractured specimens or components

Alternative definitions that say: "fractography is the study of fracture surfaces of materials," are far too narrow in my opinion. Much can be gleaned by first looking at the sizes, shapes, and breakage patterns of the fragments. In some cases, the breakage pattern is all that is necessary and examination of fracture surfaces is unnecessary. For example, even novices can recognize an impact site on an auto windshield without examining the fracture surfaces. In other cases, a simple visual examination can tell the observer whether a fracture was thermally or mechanically driven, whether the stress was large or small, and whether the stresses were uniaxial or multiaxial.

The reader might wonder about the words "fractography" and "fractology.[a]" The suffix "-graphy" has Greek roots and in English usually means the "written or photographic description" of something, e.g., photography, tomography, xerography, cartography. Its meaning has evolved over the years, however. It now commonly means "field of study." The suffix "-ology" in most modern English references is defined as "field of study" or "branch of science," or "branch of knowledge," e.g., anthropology, biology, mineralogy. In summary, fractography and fractology are now used interchangeably. The preponderance of usage in the technical literature in the late 20th and early 21st century is "fractography." This leads us to an alternative definition:

> **fractography,** n – the field of study of fractures in materials, components and structures.

Getting back to the matter of how and where to look at a fractured piece, it is surprising how many instances where undue attention was spent on small fracture surface regions that were probably not even in the area of fracture initiation. It behooves one to look at the overall breakage pattern first, before one jumps to a microscopic examination of the fracture surfaces.

Most people recognize that fractography is a valuable tool for failure analysis, but fewer appreciate its value in routine mechanical testing or support of materials processing. Although thousands of ceramic or glass items and test specimens are broken daily, only a tiny fraction is examined fractographically. A wealth of information is lost about the causes of fracture and the nature of the material. The flaw type may be just as important as the fracture stress in a strength test.

Some of the reluctance to apply fractographic analysis is that it is unfamiliar to most engineers and scientists. Fractography is rarely taught in schools and is

---

[a] I am indebted to Drs. P. Oikonomopoulou and T. Bristogianni of the Technical University of Delft in the Netherlands who brought the distinctions to my attention in mid-2019.

often learned gradually and autodidactically by experience over many years. Some erroneously regard fractographic analysis as mysterious and a subjective practice that is too interpretive. It is in fact very objective and quantitative.[b] Brittle materials often have unequivocal markings on fracture surfaces that are the direct consequence of crack perturbations during propagation.

An important element of fractographic analysis is **pattern recognition**. Fracture leaves telltale fracture patterns on the fracture surfaces, or have telltale breakage patterns or fragment shapes. For example, hackle lines radiating from a fracture mirror are features that lead an observer back to the origin. Other markings may be more subtle and can be overlooked by the casual or inexperienced observer. Pattern recognition skills can be reinforced by studying multiple examples in a set of specimens. The novice may be tentative at first, but fractography is a cumulative learning experience. The more fractography one does, the easier and faster it becomes.

A good starting place to gain experience is by examining simple objects such as bend bars broken under laboratory conditions. Component failure analysis is often much more difficult, especially if only a single example is available, or the fracture occurred under unknown loading conditions.

Fractographers ideally should have knowledge of materials science, microscopy, mechanics (stresses and strains), and an aptitude for problem solving and troubleshooting. Puzzle-solving skills can be helpful. The ability to sketch or draw is important. Fractographers should be comfortable with microscopy, since many of the features to be studied are smaller than the unaided eye can discern. Some knowledge of materials science is necessary since strength-limiting flaws and crack propagation behavior are controlled by processing and the microstructure.

Cracks propagate in response to stresses and strains, and thus fractography often comes quite naturally to mechanical engineers. Other scientists, physicists and geologists will have to learn the fundamentals of stress analysis. At a minimum, a fractographer should be comfortable with concepts of uniaxial *tensile* stresses (stresses primarily in one direction, such as in a direct tensile strength test specimen), uniaxial *bending* stresses (such as in a beam or plate loaded in bending), and *biaxial* tensile stresses (whereby there are tensile stresses in two different directions such as in a pressurized flat plate or a

---

[b] This is reminiscent of Arthur C. Clarke's Third law, which is: "Any sufficiently advanced technology is indistinguishable from magic." *Profiles of the Future: An Inquiry into the Limits of the Possible*, A. C. Clarke, Bantam, 1973.

pressurized bottle). Some important stress configurations are illustrated in Figure 1.2.

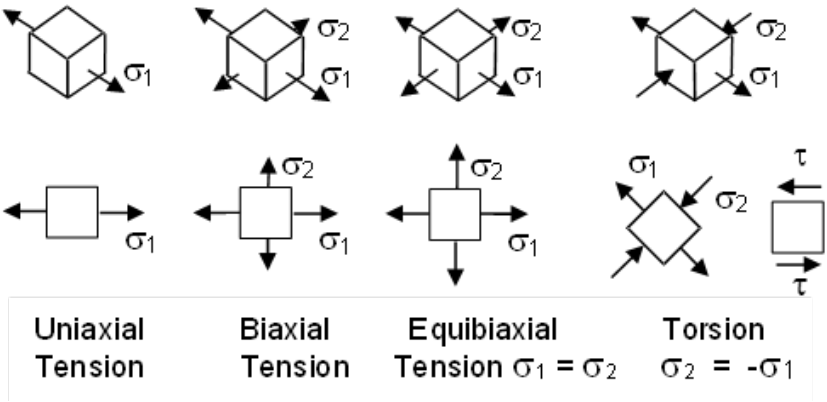

Figure 1.2 *Uniaxial or biaxial stress states may be represented by stresses (arrows) acting on the surfaces of tiny differential volume elements. They are shown here as 3-dimensional (top row) or 2-dimensional (bottom row) views. The lengths of the arrows are in proportion to the stress magnitudes.* s_1 *and* s_2 *are normal stresses and* t *are shear stresses. In some cases, the stress state is triaxial, and a third stress direction,* s_3*, may be added to the diagrams above.*

Most fracture problems the reader will encounter will be uniaxial or biaxial stress cases, but there are very important cases (e.g., projectile-impacted ceramic or glass armor plates, or Hertzian or sharp contact problems) where the stress state is *triaxial;* that is, there are stresses in all three directions, s_1, s_2, and s_3. Some of these are tension stresses that by convention are denoted with a positive sign (e.g., +100 MPa), and some may be compressive stresses, denoted by a minus sign (e.g., - 300 MPa). Mechanical engineers are very comfortable with multiaxial stress problems, and can convert the stresses in any arbitrary orientation at a given point to the specific orientation that has the *principal stresses.* (The X-Y-Z axes at any point can be rotated and are reoriented so that the small differential volume element has three normal stresses s_1, s_2, and s_3 and no shear stresses acting on its faces.) Mechanical engineers commonly use a Mohr's circle analysis or finite element analysis to find this orientation and the maximum principal stresses. <u>Maximum principal tensile stresses usually control fracture in ceramics and glasses.</u> Shear stresses usually do not. Only in specialized cases do compression or shear stresses cause fracture. This is an important difference in how ceramics and glasses break as compared to metals and polymers. Many mechanical engineers (and

finite element modelers) focus too much attention on shear stresses particularly with multiaxial loading conditions when they should instead be focusing on the maximum principal tensile stresses. Exceptions are for laminated structures and multiaxial compression problems, where shear is important.

It should also be borne in mind that most parts and laboratory specimens have stress *gradients* and may even have internal *residual stresses*. It is rare that a component has a uniform stress throughout. Simple loading configurations are typically covered in the first chapters of an elementary strength of materials engineering textbook, which may be consulted to gain a basic familiarity with stresses and strains. It is beyond the scope of this Guide to delve too far into multiaxial stress fracture criteria, but the reader should be aware that what causes fracture in a tensile-loaded ceramic part may be completely different than for a compressively-loaded ceramic part, or for a part with mixed tension and compression stresses. Engineers often use stress diagrams with fracture envelopes to illustrate fracture versus no-fracture boundaries in multiaxial stress problems. Mechanical engineers not versed in ceramic or glass behavior do not appreciate the nuances of multiaxial failure criteria for ceramics and glasses. For example, many finite element modelers who are new to the ceramic field erroneously use the Von Mises (or maximum distortion energy) criterion in their models. While this criterion works quite well for metals, it is inappropriate for ceramics and glasses. Another thing that surprises many mechanical engineers is how different the Poisson's ratios are for glasses and ceramics (e.g., 0.15 to 0.25) as compared to those for metals.

There are two special stress conditions that warrant explanation. Mechanical engineers may say that parts are loaded in *plane stress* or *plane strain* conditions. Plane stress refers to a case where there are only two principal stresses, s_1 and s_2. The third stress $s_3 = 0$. In other words, all the stresses lie in a flat plane. This is commonly the case with thin parts, such as a thin-walled cylinders or pressurized bottles. The principal stresses are parallel to the surface. In contrast, with thick parts, there can be a s_3 internal stress. If the part is very thick, lateral contraction strains may be inhibited and the strain through the thickness, $e_3 = 0$. There are only two principal strains e_1 and e_2 and they are parallel to the part's surface. This is called the *plane strain* condition and it is especially important for metallic fracture toughness test specimens. The matter usually is not important for ceramics and glasses, since the plastic yield zones in ceramics are tiny if they exist at all.

It is customary in stress analyses to treat the ceramic or glass as a continuum. "Continuum mechanics" is used to analyze the stresses and strains throughout the body. There is a growing awareness, however, that there can be significant

microstructural-level stresses within- and between-grains in ceramics, due to elastic property and thermal expansion anisotropies in the ceramic crystals. This is true even in cubic ceramic crystals, but can be very dramatic in hexagonal, rhombohedral or tetragonal structures. The internal microstructural stresses can be very large even if no external stresses are applied. If the grain size is small, then these will average out and continuum mechanics may be safely used. On the other hand, with coarse-grained ceramics, these microstructural level stresses can be pronounced and can affect fracture, particularly if the critical flaw size itself is comparable to the grain size.

Part of the skill of a fractographer is knowing where to look and how to look. A specimen that breaks into only two pieces may not be too difficult to interpret. Medium to high strength specimens with multiple fractures can initially be confusing, but with a little experience one can find the primary fracture. Component or service failures may be difficult since the loading conditions may be unknown. Key pieces may be missing or the evidence incomplete or contradictory. Multiple crack systems from different causes and events may intersect and confound an interpretation.

One reason that fractography is sometimes held with suspicion or is deemed subjective is that some incautious fractographers have jumped to conclusions and reached questionable interpretations. It is unwise to make conclusions based on limited or incomplete evidence. Novices often force fit a fracture scenario to their limited experience base. Some fracture patterns may be difficult to detect or be very subtle and may not be recognized. Good fractographers recognize their strengths and the limitations of their experience base and do not overreach or extrapolate. They should be alert to unusual or new fractographic markings or to failure modes with which they are not familiar and should be ready to search the literature, consult colleagues, or try to create comparable markings in the laboratory. Step-by-step accumulation of experience is necessary. One may consult textbooks, reference articles, and this Guide to help acquire knowledge, but there is no substitute for hands-on direct eyeball and microscopy experience.

There is a wealth of information in the technical literature about fractography of glasses and ceramics, but until the first edition of this book was written in 2007, it was scattered in book chapters, journals, and conference proceedings. Fréchette's 1990 seminal book, *Failure Analysis of Brittle Materials*,[1] was a good starting point for the practical fractography of glasses. This NIST Guide dramatically expands what he did and includes an extensive bibliography. There now are formal standard practices in ASTM Int.[1,2,3] and the European Committee for Standardization.[4]

Fractography is a tool for the broader topic of **failure analysis**. Figure 1.3 suggests a simple but apt analogy. The fractographer is called upon to solve a fracture mystery. The detective uses his or her powers of observation to study the scene of the fracture and meticulously collects and preserves the available evidence. The clues are contemplated and weighed against the available background information furnished by witnesses. Comparable cases are

Figure 1.3 *The fractographer as detective.*

considered to determine whether there are similarities and whether there is a *pattern*. Scientific analysis of the material may be done to verify its quality, composition, and authenticity. Pondering all the information, and keeping an open mind for all possible scenarios, the fractographer detective formulates a hypothesis and checks it against the known facts. In summary, fractographic analysis is not merely looking at fracture surfaces, but is the integration of knowledge from a variety of sources to solve the puzzle of how fracture occurred (Figure 1.4).

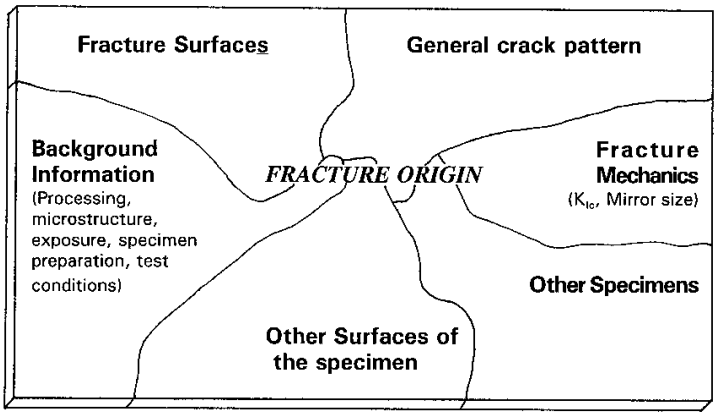

Figure 1.4*. Fractographic analysis is more than examining fracture surfaces.*[5] *The fractographer integrates a variety of information.*

Failure analysis is: "A process that is performed in order to determine the causes or factors that have led to an undesired loss of function."[6] Failure may be due to fracture, corrosion, excessive deformation, or wear. Readers interested in the broader topic of failure analysis in general should refer to the ASM handbook on Failure Analysis and Prevention[6] that has pragmatic recommendations such as: "don't jump to conclusions," "keep an open mind," and "avoid 5-minute best guess analyses."

It is beyond the scope of this book to delve into issues of litigation, fault, or blame. Readers who are interested in these matters are referred to: an article by B. Adams in the 2nd Alfred conference on fractography,[7] an article by C. O. Smith in Volume 11 of the ASM handbook,[8] or a review by Bradt in the 3rd Conference on Fractography of Advanced Ceramics in Slovakia:[9] "The Expert Witness," or Chapter 11 in Van Fréchette's book.[10]

A few words about nomenclature are appropriate here. Readers may be surprised that terms for ceramics and glasses are somewhat different than for other materials. For example, "hackle lines" and "lances" refer to steps or lines on the fracture surface running parallel to the direction of crack propagation. "Striae" or "striations" means completely different things to metallurgical fractographers, ceramic and glass fractographers, and glass manufacturers. Fréchette proposed a fractography nomenclature scheme for glasses and ceramics in a paper at a 1982 conference on fractography[11] and later incorporated it in his 1990 book.[10] His logical scheme was adopted in this Guide. His terms usually described what the feature was, rather than how it looked.[c] For example, he defined the term "twist hackle" and used it rather than "river delta." This Guide has added only six new terms for the basic fracture surface markings beyond Fréchette's. This author resisted the temptation to devise new and colorful terms, since a proliferation of terms will only lead to confusion. Anne Roulin-Moloney, in the preface of her outstanding book on the fractography of polymers and composites,[12] wrote about the "myriad of weird and wonderful terms to describe the features observed. Some examples are "laceration, shish-kebab, cusps, welts, mist, and shards." There are a myriad of terms in use in the glass container industry including: "blisters, bird cages, bird swings, monkey swings, bruises, letter checks, cat scratch cords, bump checks, and percussion cones." The Euronorm EN 843-6 [4] includes "blind cracks." In the rock fracture community, one finds the terms: "en echelon fractures, fringe cracks, plumose patterns, and conchoidal ribs, and fringe lines." These are analogous to terms in this Guide: hackle, twist hackle, arrest lines and so forth. Fracture origins in rocks may be

[c] One notable exception was his "Sierra scarps." These were scarps with shapes that remined him of the Sierra-Nevada mountains.

a variety of irregularities in siltstones such as: groove casts, flute casts, gutter casts, or discrete faults such as inclusions, pores, fossils or even worm hole burrows! The latter is a network of pore tunnels formed by ancient worms as sedimentary rock was being formed. I made a few exceptions in chapter 8 on single crystals when I copied the terms coined by Rice:[13] "cathedral mirrors," "gull wing mirrors," "skewed cathedral mirrors," and "whisker lances."

There are only six primary types of markings described in chapter 5: fracture mirror, mist, hackle, arrest lines, Wallner lines, and scarps. Subsets of these help differentiate the fundamental cause of the feature, not how they look. So, for example, there are ten variations of hackle: mist hackle, velocity hackle, fine- or coarse-microstructural hackle, twist hackle, wake hackle, shear hackle, corner hackle, step hackle, and cleavage step hackle. Following Fréchette's scheme, there are three types of Wallner lines: primary, secondary, and tertiary. In addition, fracture surfaces in polycrystalline ceramics can be either transgranular, or intergranular, or a mixture. Thus, there are a total of twenty-one basic fracture surface markings defined in this Guide. A few other unique fractographic terms are scattered through this book. Excessive differentiation of minor variations of fracture markings (such as has been done by the rock fracture community) can be confusing and counter-productive. Prof. Frechette's approach of keeping it simple seems wise.

The history of fractography of brittle materials is a fascinating story of advances in microscopy, material science, fracture mechanics, and people. Fig. 1.5, adapted from my review articles,[14,15] chronicles how the field evolved with contributions from famous scientists and engineers. The pioneering fractographer Frank Preston in 1942[16] made a profound statement about whether pieces from different fractured parts would match and he also summarized the art of fractographic analysis:

> "From the beginning of time to its end, no two cracked surfaces will fit each other, unless originally they were part of the same piece. Cracks are as distinctive as fingerprints. … Now the important thing about cracks is that they must be propagated. They do not originate all over the final fracture surface, but at one tiny spot, and from thence are propagated out to the rest of the area. This fact and the fact that the telltale marks or "fingerprints" of the process are left on the surface, provide the groundwork for the subject of Fracture Diagnosis, which in the last decade has become an important minor branch of physical science."

At this point it is appropriate to point out a critical aspect of fracture analysis problems. Final fracture often occurs after a chain of events. One event may

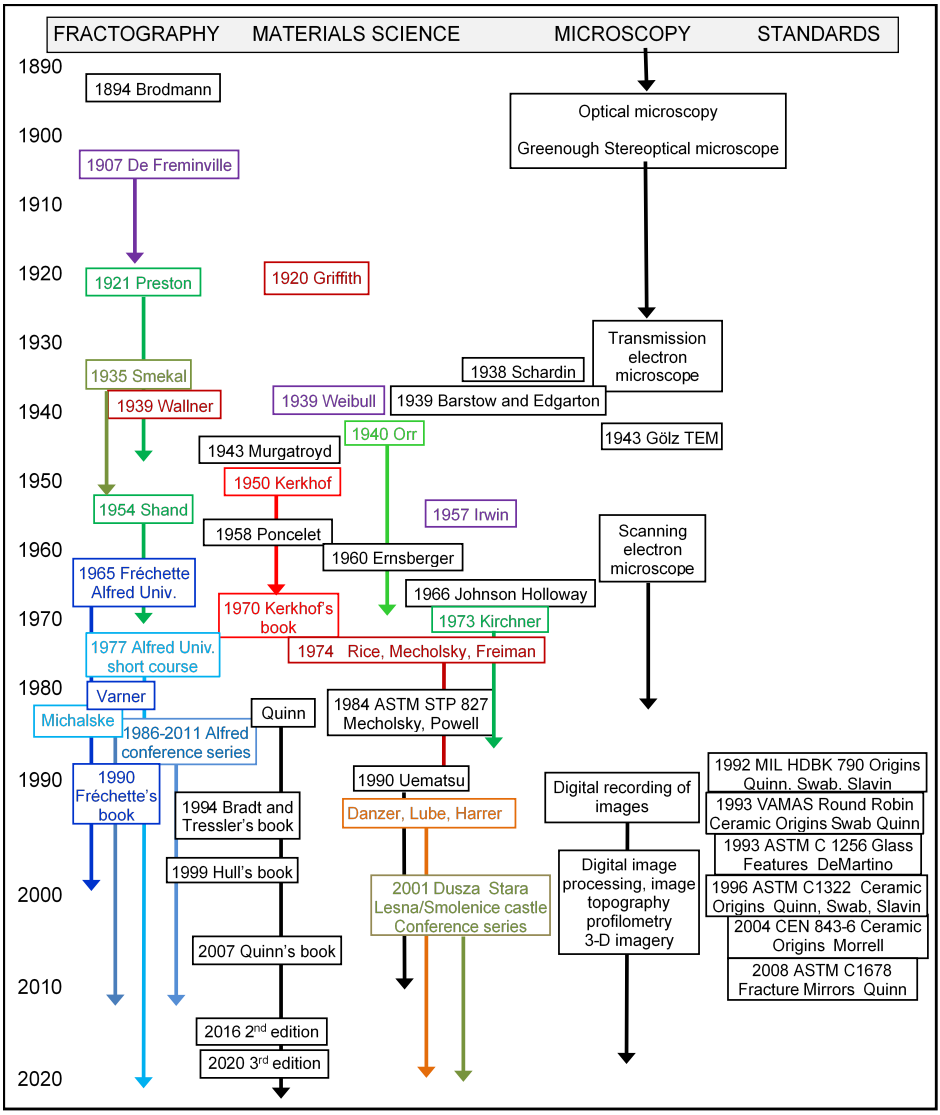

***Figure 1.5**. The history of fractography of brittle materials.*

create a flaw, but then a second or even third event may be necessary to cause fracture. For example, drinking glasses commonly sustain internal impact damage from knives, forks and spoons that are carelessly dropped into the glass. Subsequent thermal stresses generated in the dishwasher may cause these cracks to grow gradually around the base. If the large crack is not noticed, an unwary user who picks up a liquid-filled glass may have an

unpleasant surprise when the bottom falls off spilling the liquid. What was the cause of failure in this case: the user pouring a liquid into the glass and lifting it to quench a thirst, the initial impact damage, or the thermal stresses that cause the crack to grow? The answer is all of the above.

The fractographer is warned that there can be exceptions. For example, Chapter 4 has the "law of normal crack propagation" which, in brief, states that cracks run perpendicular to the maximum tensile stress. This is usually the case, but there are exceptions. Similarly, curved lines on a fracture surface usually are Wallner lines, unless they are "cleavage step hackle lines" on a single crystal and have the exact opposite curvature sense as discussed in chapter 8. Similarly, many hackle lines radiating outward from a single point almost always indicate a fracture origin, unless it is a "hackle terminus node" of converging hackle lines on a single crystal as described in Chapter 8. Although fracture usually commences from a single fracture origin, this is not always true. Things sometimes are not as simple as they seem! Do not force fit an interpretation to every case. A good fractographer is always on the lookout for exceptions.

Finally, the matter of whether machine or artificial intelligence can reliably do fractographic analysis is discussed in Chapter 11, Conclusions.

Chapter 1 References

1. ASTM C1322-20, "Standard Practice for Fractography and Characterization of Fracture Origins in Advanced Ceramics," Annual Book of Standards, Vol. 15.01, ASTM Int., West Conshohocken, PA, 2020. (originally 1996, ASTM standards are typically renewed at five-year intervals.)
2. ASTM C1678-21 "Standard Practice for Fractographic Analysis of Fracture Mirror Sizes in Ceramics and Glasses," Annual Book of Standards, Vol. 15.01, ASTM Int., 2021 (originally 2007).
3. ASTM C1256-25, "Standard Practice for Interpreting Glass Fracture Surface Features," Annual Book of Standards, Vol. 15.02, ASTM Int., 2025 (originally 1993).
4. CEN EN 843-6, "Advanced Technical Ceramics - Monolithic Ceramics – Mechanical Properties of Monolithic Ceramics at Room Temperature – Part 6: Guidance for Fractographic Investigation," European Committee for Standardization, Brussels, 2009.
5. J. J. Swab and G. D. Quinn, "The VAMAS Fractography Round Robin: A Piece of the Fractography Puzzle," pp. 55 - 70 in *Fractography of Glasses and Ceramics III*, Ceramic Transactions, Vol. 64, eds., J. R. Varner, V. D. Fréchette, and G. D. Quinn, ACS, Westerville, OH, 1996.
6. *Failure Analysis and Prevention*, ASM Handbook, Vol. 11, American Society for Materials, Materials Park, OH, 2002.
7. P. B. Adams, "Fractography in the Courtroom," pp. 219 – 226 in *Fractography of Glasses and Ceramics, II*, Ceramic Transactions, Vol. 17, eds V. D. Fréchette and J. R. Varner, American Ceramic Society, 1991.
8. C. O. Smith, "Products Liability and Design," pp. 71 - 78 in Ref. 6.

9. R. C. Bradt, “Fractography, Some Legal Aspects and Challenges,” pp. 28 – 42 in *Fractography of Advanced Ceramics, III,* eds., J. Dusza, et al., Transtech Publ., Zurich, 2009.
10. V. D. Fréchette, “Failure Analysis of Brittle Materials,” *Advances in Ceramics,* Vol. 28, American Ceramic Society, Westerville, OH, 1990.
11. V. D. Fréchette, “Markings on Crack Surfaces of Brittle Materials: A Suggested Unified Nomenclature,” pp. 104 - 109 in *Fractography of Ceramic and Metal Failures,* ASTM STP 827, J.J. Mecholsky, Jr. and S.R. Powell, Jr. eds., ASTM Int., 1984.
12. A. C. Roulin-Moloney, *Fractography and Failure Mechanisms of Polymers and Composites*, Elsevier, Essex, England, 1989.
13. R. W. Rice, “Ceramic Fracture Features, Observations, Mechanisms and Uses,” pp. 5 –102 in *Fractography of Ceramic and Metal Failures,* ASTM STP 827, eds. J. Mecholsky and Powell, ASTM Int., 1984.
14. G. D. Quinn, “A History of the Fractography of Brittle Materials,” in *Fractography of Advanced Ceramics, III*, ed. J. Dusza, R. Danzer, R. Morrell, G. Quinn, TransTech Publ., Zurich, 2009. *Key Engin. Materials*, **409** (2009) 1 - 16.
15. G. D. Quinn, “A History of the Fractography of Glasses and Ceramics,” pp. 1 – 56, in *Fractography of Glasses and Ceramics,* Vol. 6, Ceramic Transactions, Vol. 230, eds, J. R. Varner, M. Wightman, American Ceramic Society, 2011.
16. F. W. Preston, “The Mechanical Properties of Glass,” *J. Appl. Phys*., **13** (1942) 623 – 634.

2. Resources

This Guide is designed to be a stand-alone resource. Each chapter contains a list of references for the chapter. A wealth of additional information is scattered in books and technical articles that delve into specific topics in more detail. Some important books are listed below.

The 1990 book *Failure Analysis of Brittle Materials* by Professor Fréchette is a seminal work.[1] His book covered all aspects of the fractography of glasses including fundamental markings on crack surfaces (Wallner lines, hackle, and so forth), crack branching, failure origins, and estimates of stress at fracture, and fractographic techniques. It was superbly illustrated with many service failures and amazing case histories. This NIST Guide follows his nomenclature scheme.

Professors Bradt and Tressler's 1994 book: *Fractography of Glass* has eight superb technical articles written by experts in the field.

Professor Hull's 1990 book *Fractography* is a masterpiece of fractography of metals, ceramics, and polymers.[2] It is printed on high-quality paper and is superbly illustrated and laid out. It is strong on the science and physics underlying fracture markings, but limited on practical applications.

ASM International publishes two famous handbooks: *Fractography, Vol. 12*,[3] and *Failure Analysis and Prevention, Vol. 11*[4]. The former is the seminal work for metals fractography and includes a large atlas of metal failures, but only a brief chapter on ceramics or glasses. Ceramics and glasses almost seem to be an afterthought. Nevertheless, it includes excellent chapters on the history of fractography, metal models of fracture, photographic equipment and techniques, optical and electron microscopy that are directly relevant to ceramics and glasses. Note that some cleaning and preparation techniques such detergent cleaning prescribed for metals are *not recommended* for ceramic fracture surfaces. Vol. 11 includes sections on fractography, and fractographic equipment and techniques, but deals more with the broader issues of failure analysis philosophies and approaches. Why does a component fail to perform its intended function? Fracture is but one of many failure modes. The fracture mechanics chapter is tailored towards metals fracture and not ceramic or glass fracture. Gokahle's quantitative fractography chapter is excellent and has information about quantitative microscopy and fractals and their limitations.

Roulin-Moloney's 1989 book *Fractography and Failure Mechanisms of Polymers and Composites*[5] is by far the best book on fractography of polymeric

materials and composites. It has chapters on microscopy, analytical techniques, materials including unfilled and filled composites, and failure mechanisms. Some brittle composites and polymers have similar fracture markings to those on glasses and ceramics, but there are important differences.

Morrell's masterful *Fractography of Brittle Materials*,[6] is an 86-page long measurement guide, one of a series of practice Guides published by the National Physical Laboratory in the United Kingdom. It is a superb treatment of the subject. It begins by saying:

> "Fractography can tell us why something broke. It can help us understand material or processing limitations, what features of materials need to be removed in order to improve their mechanical properties, and sometimes, who is to blame for something gone wrong."

The NPL Guide starts with 27 pages covering the fundamentals and is followed by an extended 59-page annex that includes 15 strength specimen examples followed by 4 component case studies. This NPL Guide is harmonious with ASTM Standard C1322 and this NIST Guidebook.

Kerkhof's 1970 German language book *Bruchvorgange in Gläsern* (*Fracture Processes in Glass)*[7] is not normally thought of as a fractography book, but it is a brilliant treatment of crack propagation in brittle materials, especially in glass. It is richly-illustrated and strong on fracture mechanics.

A new book on fractography of human bones was published in 2022 by Christensen *et al*..[8] I cooperated with her team. Many concepts from ceramics and glasses are applicable to skulls, femurs, and other bones.

Appendix A of this Guide is a bibliography featuring many good publications of special interest to the glass and ceramic communities. Appendix A includes books from two conference series devoted exclusively to the fractography of glasses and ceramics. One was organized by Profs. Fréchette and Varner at Alfred University and me and was held six times at four- or five-year intervals in the United States from 1986 to 2011. There is a conference proceeding book for all six. Dr. Dusza of the Institute of Materials Research of the Slovak Academy of Sciences, Košice, Slovakia began a conference series in 2001 that repeated in 2004, 2008, 2013, 2016 and 2019. Conference proceedings for the first three were published as bound books. Selected papers from the later conferences were published in topical issues of the Journal of the European Ceramic Society.

Appendix B is a list of publications dealing with specific case studies. Some of the cases deal with the mundane and some with the exotic. It is included for the benefit of readers who wish to investigate specific problems. Key papers on rock fractography are listed as well.

Appendix C is the most complete tabulation of fracture mirror constants ever compiled for ceramics and glasses. It is an expansion of a similar listing in ASTM C1322.

Appendix E is a comprehensive compilation of terminal crack velocities.

There are three formal documentary standards from ASTM[9,10,11] and one from CEN on fractography of glasses and ceramics.[12] The ASTM standards are periodically renewed or updated at five-year intervals.

References

1. V. D. Fréchette, *Failure Analysis of Brittle Materials, Advances in Ceramics*, Vol.28, American Ceramic Society, Westerville, OH, 1990.
2. D. Hull, *Fractography*, Cambridge University Press, 1999.
3. *Fractography*, Vol. 12 ASM Handbook, ASM Int., Materials Park, OH, 1987.
4. *Failure Analysis and Prevention*, Vol. 11, ASM Handbook, ASM Int., Materials Park, OH, 1987
5. A. Roulin-Moloney, *Fractography and Failure Mechanisms of Polymers and Composites*, ed., Elsevier, 1989.
6. R. Morrell, *Fractography of Brittle Materials*, Measurement Good Practice Guide #15, National Physical Laboratory, Teddington, UK, 1999.
7. F. Kerkhof, *Bruchvorgange in Gläsern*, German Technical Glass Society, Frankfurt, Germany, 1970.
8. A. Christensen, M. I. Isa, M. A. Smith, J. T. Hefner, H. Berryman, J. B. Webb, and I. S. Saginor, *A Guide to Forensic Fractography of Bone*, Federal Bureau of Investigation Laboratory, Quantico, VA, Feb. 2022.
9. ASTM C1256-13, "Standard Practice for Interpreting Glass Fracture Surface Features," ASTM Int., West Conshohocken, PA, originally from 1993.
10. ASTM C1322-15, "Standard Practice for Fractography and Characterization of Fracture Origins in Advanced Ceramics," ASTM, International, West Conshohocken, PA, originally from 1996.
11. ASTM C1678-15, "Standard Practice for Fractographic Analysis of Fracture Mirror Sizes in Ceramics and Glasses," ASTM, International, West Conshohocken, PA, originally from 2007.
12. EN 843-6, "Advanced Technical Ceramics, Monolithic Ceramics, Part 6: Guidelines for Fractographic Examination," European Committee for Standardization, Brussels, originally from 2004.

3. Tools and Equipment

The most important tools of the fractographers craft are a digital camera, a zoom stereomicroscope, and a scanning electron microscope. The stereo microscope affords to the eyes a magnified, naturally-appearing, three-dimensional view of the fracture surface that retains all color and reflectivity information. Fracture origins and flaws in ceramics and glasses can often be detected with the stereo optical microscope, but higher magnifications are often needed to see the flaw more clearly. The scanning electron microscope serves this need and has good depth of field, high magnification capability, and chemical analysis features.

The “marriage” of the microscope with digital cameras and computers has revolutionized the field. The new technologies rendered film photography obsolete by the 1990s and opened up marvelous new capabilities not heretofore available. The shortcomings of conventional compound microscopes (e.g., limited depth of field) or of scanning electron microscopes (e.g., flat-appearing images) can be overcome. Virtual three-dimensional images can be constructed with automatically-rastering optical microscopes or by analysis of multiple scanning electron microscope images taken with slightly different specimen tilts. The pseudo three-dimensional images can be displayed, tilted, and rotated to afford different perspectives. Various quantitative numerical analyses of surface topography (e.g., surface roughness or even fractal dimension analysis) can be performed at almost no extra effort since the surface topography has been recorded digitally.

Simple low-cost software programs are now available that can simply and conveniently overcome the depth of field limitations of virtually any microscope. A series of photos at the same magnification are taken while slightly readjusting the focus. The software interprets the regions that are in focus in each photo and stitches these together to create a single image with an infinite depth of field. This is called: “focus stacking.”

In this chapter, traditional and new tools of the trade and are reviewed with an emphasis on their applicability to fractography. Digital cameras are discussed in four sections of this chapter: first in section 3.2 as simple tools for overall photographs, then in sections 3.4 and 3.5 as recording devices attached to conventional microscopes, and finally in section 3.7 as components of new digital microscopes which do not even have eyepieces for the viewer to look through.

3.1 Low Power Optical Examination

The examination of fractured pieces begins with a visual examination using the unaided eye. Some fractographer prefer to use lint-free gloves when handling fragments, but gloves usually are not necessary. Ceramics and glasses are hard, durable materials and may be cleaned fairly easily.

It may be tempting to rush to a microscopic examination of the fracture surfaces, but study of the general fracture and the overall condition of the component is time well spent. This examination and reconstruction of the specimen may be aided by a simple (1.2X to 1.4X) magnifying glass, whether hand-held or mounted on a stand as shown in Figure 3.1. A stand-mounted lens frees the fractographer's hands for manipulation of the specimen. Larger versions with built-in ring lamps are ideal. A clean, tidy table or bench top is desirable, lest the fractographer inadvertently knock critical fragments onto the floor or against each other, or contaminate or damage the fracture surfaces.

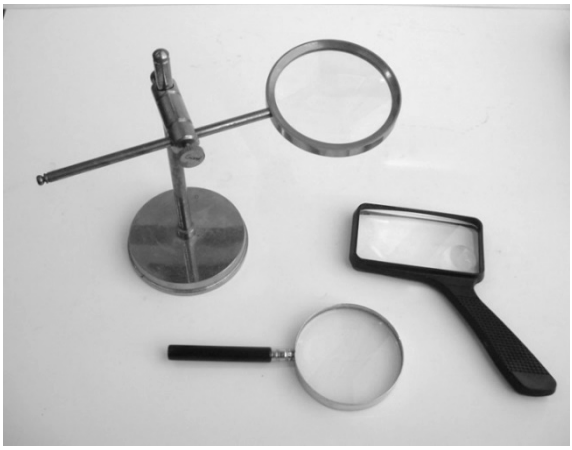

Figure 3.1 *Simple magnifiers.*

Small jeweler's loupes as shown in Figures 3.2 and 3.3 also are handy, particularly in the field. Their working distances range from 50 mm for the low power (5X) loupe, to about 25 mm for a 10X loupe. Some practitioners may be adept at holding a watchmaker's loupe in one eye without using a hand, thereby freeing up both hands. Most fractographers will use one hand to hold the loupe and the other to hold the examined fragment. Machinist loupes and pocket optical comparators with magnifications up to 20X (two are shown on the right of Figure 3.2) have built-in measuring scales with graduations as fine

as 0.1 mm (0.005 in). Rapid measurements of mirror sizes or even fracture origin sizes may be made with these inexpensive tools. Remember, the more powerful the magnification, the smaller the field of view and the shallower the depth of field, so a good general duty loupe or comparator with a 7X or 10X magnification may be perfectly suitable and more versatile than one with a 20X magnification. At these low magnifications, illumination is usually not a problem and ambient light is adequate.

Figure 3.2 *Hand loupes and optical comparators. From the left, 5X and 7X watchmaker loupes; a 20X loupe, a 7X comparator with an internal 20 mm scale marked in 0.1 mm increments attached to the bottom, and an 8X to 16X zoom comparator with a 16 mm scale marked in 0.1 mm increments.*

Figure 3.3 *Loupes (5X to 20X) may either be held by the eye or by hand. The part is a single-crystal silicon rod. Note the convenient working distance.*

Simple holders or clamps may be useful as shown in Figures 3.5 and 3.6, particularly if the fractographer is examining repetitive examples of a particular specimen or component. It can be exasperating to hold a part in one hand at just the right angle, while holding a magnifier with the second, but then need an extra hand to apply some alcohol with a cotton swab to clean the part. Similarly, the fractographer may wish to jot down some important information as part of a written record.

Figure 3.4 *A jeweler's or hobbyist's head mounted magnifier (2X to 3.5X).*

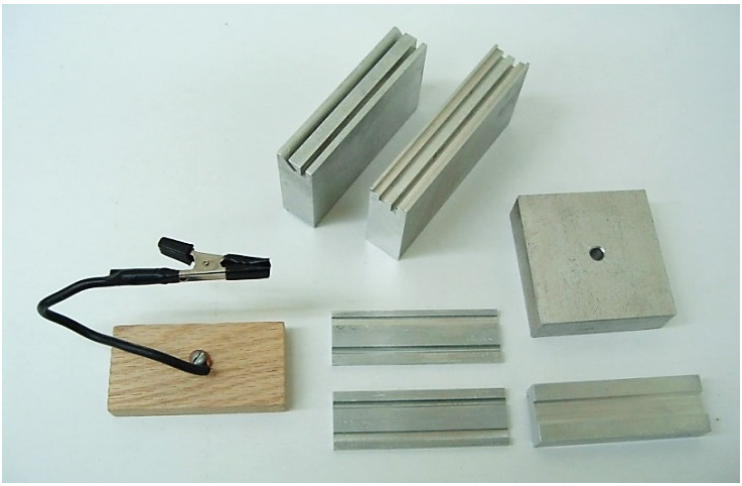

Figure 3.5 *Specimen holders. Clockwise from the lower left are: a bend bar holder made with an alligator clip on a bendable (10 gage electrical) wire with black electrical tape wrapped around the teeth to cushion the specimen; two aluminum jigs with slots and grooves for flexure or tension strength specimens; an aluminum block with hole; and three aluminum holders with groves to hold bend bars on their flats or on their edges for chamfer examination.*

Conventional clays should not be used for mounting specimens unless there is no alternative. Clay is a pernicious material that can easily contaminate the fracture surfaces and blend into the fracture features. Natural clays have colors and compositions similar to ceramic products. They are next to impossible to clean off. Their electrostatic surface charge and extremely fine plate-like structure cause them to cling to the fracture surface. Clays often have an oil to keep them plastic and this makes things even worse, since the oils can smear over the fracture surfaces even on glasses. Clay often gets on one's hands and then tends to get on everything. Clay contamination is shown in section 6.10.

A completely satisfactory alternative is polymer clay that is available from arts and crafts stores. Figure 3.6 shows the type the author uses. [a] Some polymer clays can be easily dissolved and cleaned with paint thinner, acetone, and even ethanol. The color in these polymer clays can easily be distinguished on the fracture surfaces. The best colors are deep blues or greens. White or gray should not be used since they cannot be distinguished from many ceramics. Garish colors like yellow or red should not be used, since they are a distraction in photographs.

(a) (b)

Figure 3.6 *Component or specimen holders. (a) Clockwise from the lower left: a homemade plastic platform mounted on a swivel base; a pivoting wooden holder; a cork ring; a clamp on a stand; an alligator clip on a stand (with electrical tape on the teeth to cushion the specimen); an inverted miniature wood flowerpot with a hole; and two wooden candleholders with dolls heads and polymer mounting clay. The doll's head balls can be rotated to obtain optimum illumination angles onto the specimen's surface. (b) shows a polymeric clay that is safe to use and is easily removable.*

---

[a] Sculpey III Polymer, "Oven bake clay" made by Polyform products, Elk Grove, Ill. It is easily dissolved by paint thinner or acetone.

Simple cleaning tools and markers such as shown in Figure 3.7 should be conveniently located at the examination work station. Acetone, ethanol, or methanol with tissues and cotton swab applicators ("Q-tips") are handy for cleaning. Compressed air from air lines should be used with caution since there may be traces of oil mixed with the air. Water-soluble ink pens (with fine tips) are handy for marking the specimen. Ceramic fracture surfaces should never be cleaned with metallic tools or probes. It may be tempting to try to scrape or poke off a contaminant, but metallic tools are easily abraded by the harder ceramic causing metallic traces to be smeared on the fracture surface. Fractured dental restorations often have plaque on them. The plaque can even be on a fracture surface if it has been exposed to the oral environment for any period of time. An example of what plaque looks like is shown in section 6.10 of this guide, where contaminants are discussed. Plaque can be removed by using an ultrasonic bath with a 16% solution of NaOCl ("bleach") for 8 minutes, then rinsing well with water (courtesy S. Scherrer). Cotton swab applicators should be used with discretion on very rough, porous ceramics or on rock and lithic specimens. The cotton fibers may come off the applicator and cling tenaciously to the fracture surfaces.

In many instances, specimens *should be examined before cleaning.* Firstly, staining or discoloration of a flaw may provide important information about the flaw itself. A good example on a broken dental crown is shown in chapter 10 as Figure 10.24e. Secondly, fine debris of the material itself on the fracture surface may be a clue that cyclic fatigue has occurred such as shown in Figure 5.72 on a silicon nitride. Examination before cleaning is discussed further in section 5.1 in Chapter 5, Fracture Surface Examination.

Figure 3.7 *Convenient tools and cleaning agents*

3.2 Photographing the Overall Component: Cameras, Cellphones, and Simple Digital Microscopes

It is often prudent to photograph the entire specimen or component. An overall photo provides an essential context for subsequent close up photos. A variety of scales or rulers should be available, which may be set alongside the component in order to show the size or scale. It is wise to get size markers on the recorded image as soon as possible, otherwise much time can be wasted afterwards deducing or guessing what magnification was used. It is very easy to make mistakes with the size markers added after the fact. Fractographers would do well to follow the example of the archeological community, wherein rulers and meter sticks are ubiquitous features of any formal record of a dig site. In lieu of scales, simple props such as coins or other common objects may be set alongside the component, but perhaps on the side or bottom where they subsequently can be cropped or replaced with marker bars.

A variety of camera types may be used to photograph an entire component. Cell phones or digital cameras (Figure 3.8b) are the tools of choice. Modern digital cameras and even simple consumer digital cameras with a macro option can be used at very close distances (»100 mm or less) from the object. Digital cameras, either professional high-resolution models or simple consumer versions such as shown in Figure 3.8b, have auto focus and exposure controls and can capture good images in ambient lighting without a flash. Images taken with digital cameras seem to be less sensitive to the illumination source color than obsolete color films that used to be used. A digital camera chip with 2 million to 5 million pixels is adequate for most applications. The camera should have a close up or macrophotography option for close-ups at distances as short as 100 mm. File storage format should include a

Figure 3.8 *Photographing the whole component. (a) shows an old photo stand with an obsolete Polaroid camera with bellows. (b) shows a simple consumer digital camera with macro capability, auto exposure, and auto focus.*

Joint Photographic Experts Group (JPEG) or Tagged Image File Format (TIFF) option. Sometimes Bitmap (BMP) format files are used with Microsoft Windows operating system computers. Some professionals prefer the raw image format (RAW), which is image data with very little processing or compression.

JPEG images have an option that they may be saved with variable amounts of compression, but users should record images with little or no compression. A copy of the image can be made at a later time with some compression to reduce the file size so that electronic documents or presentations with many images do not become unwieldy. For example, most of the JPEG images in this Guide ranged in size from 300 kB to 2 MB in size. There are over 1,100 JPEG and TIF figures, so compression was used to prepare the master pdf that is available from the NIST web site. JPEG files are as much as $1/5^{th}$ to $1/10^{th}$ the size of an uncompressed TIFF file, with very little or no loss of detail. JPEG is available only for true color or grayscale images. JPEG reduces the number of bits in the image by eliminating repetitive image data or image data that is hard to see. The software may allow various compression levels and the higher the level of compression, the lower the quality of the image. JPEG may compress more than other methods and the results may not be fully reversible. At higher compression ratios (> 20:1 or a 50% setting), JPEG can degrade the quality of the image. A JPEG file is automatically uncompressed when it is opened.

TIFF is either an uncompressed format or a LZW (Lempel-Ziv-Welch) compressed format. LZW compression translates common patterns in an image into short codes and is best at preserving all the image data and achieving good compression. It doesn't achieve the high compression ratios that JPEG does. LZW is available for monochrome, grayscale, palette, and true color images. Most of the graphs in this Guide were saved as TIFF files with LZW compression. Most of the line drawings and sketches were done by hand with pen and ink and then scanned and saved as TIFF files also with LZW compression.

The RAW format is used by manufacturers to contain the raw (minimally processed) data from the image sensor in a digital camera. RAW file formats are proprietary and can differ greatly from one manufacturer to another and sometimes between cameras made by one manufacturer. RAW files are normally only used when additional computer processing is intended. The author has never used RAW files.

More elaborate single lens reflex (SLR) digital cameras have more options, more versatile lenses, and higher resolutions. Some may have extremely high

resolutions, but the stored image file sizes may be very large. SLR cameras should be ordered with close up macro lenses as an option.

Cell phone cameras take very good overall images and have surprisingly high resolutions as shown in Figure 3.9. Most models can be used in a magnifier

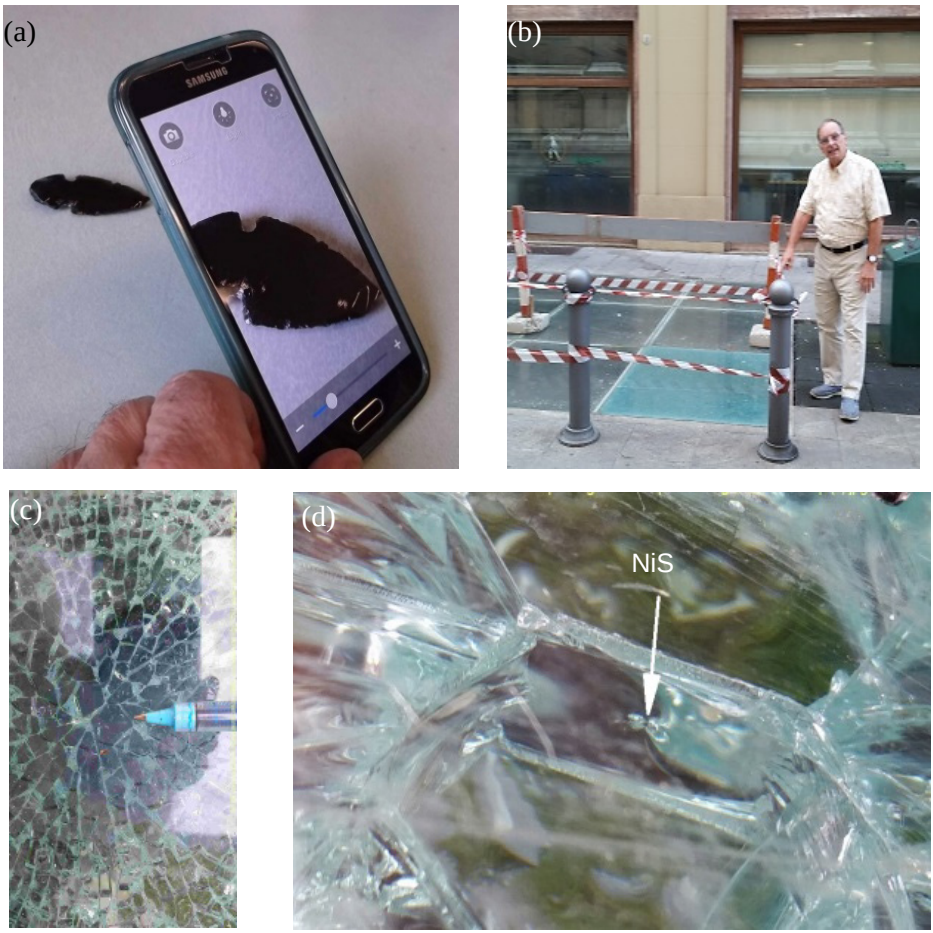

Figure 3.9 *Cell phones can be used for fractographic analysis (a) shows an obsidian arrowhead as viewed at 2X magnification in a cell phone; (b) is a street photo showing the author near Santo Stefano Basilica in Bologna, Italy in 2014; (c) is a close-up of the laminated, tempered glass fracture pattern that I was pointing at. The tip of a blue ink pen is shown for a size comparison. (d) is the close-up at 5X of the small (< 1 mm) internal NiS inclusion fracture about 60 mm below the surface while aiming through the glass at an angle.*

mode. The camera automatically determines which of several built-in lenses gives best focus at a given working distance. Autofocus can be done over a broad range of magnifications. Some cell phone manufacturers have clip-on close-up lenses and simple holder-stand accessories that can reach even greater magnifications. Users can construct their own little stands to hold the camera steady when taking close-up images (e.g., some are shown on the Internet). The author has also been surprised in some of his courses on fractography when students used cell phones to take images through one eyepiece of a stereo microscope.

Digital camera photography has eliminated many of the color problems associated (e.g., sensitivity to incandescent bulb temperature) with older film technology. In some cases, the best results can be obtained by photographing the component outdoors with ambient lighting on a neutral-colored background, such as a white or gray poster board. The author often photographs specimens on the window sill of his office on a white poster board base as shown in Figure 3.10. An additional white cardboard is placed vertically as a reflector on the inside of the room (behind the camera) to reflect some external natural light to back-fill the lighting on the specimen.

Figure 3.10 *Natural lighting is often effective. This is the window sill of the author's office at NIST. White poster or cardboards provide back-fill. On the left is a small whiteware bowl held together with blue tape. On the right is a single-crystal sapphire missile dome (#SN37), that fractured during wind tunnel testing at a high Mach number at high temperature. This dome is also shown in Figure 4.21.*

3.3 Stereo Optical Microscope

More powerful magnification will be needed in most cases to observe small fracture origins or markings on the fracture surfaces. The fractographer's single most valuable tool is the stereo optical microscope or stereo microscope as shown in Figure 3.11. Basic stereo microscopes have zoom magnification ranges to the eyes of only 8X to 32X or 10X to 40X. Greater magnifications are needed to see small flaws clearly. Upper magnifications of 100X or as high as 300X are available and are better for fractographic analysis. On the other hand, having a small magnification at the lowest limit (e.g., 5X) facilitates taking an overall picture of a small component. Hence, a stereo microscope with a broad zoom range (e.g., range of 10, 16, or even 20 power) is desirable. *A 50/50 beam splitter is strongly recommended* if the microscope has a camera. Half the light reflected from the specimen is sent to the eyes and half is sent to a camera. It allows one to look through the eyepieces at the same time an image is sent to the camera. The alternative, an either/or lever which diverts light *either* to the eyes *or* to the camera, is cumbersome and is exasperating to use.

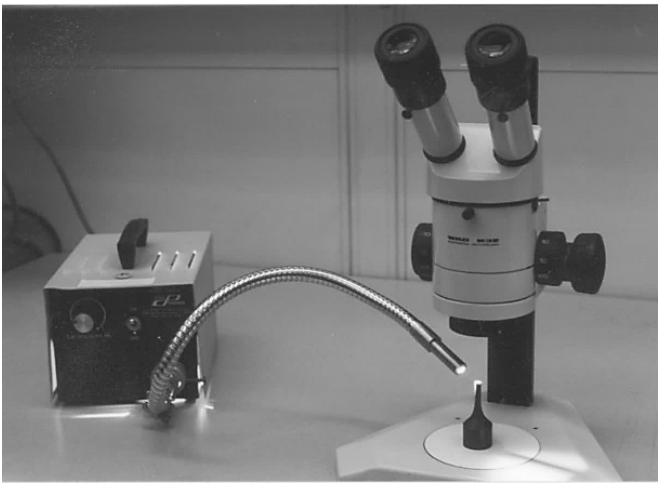

Figure 3.11 *Stereo binocular microscope with a fiber optic light source for low-angle, grazing illumination. This particular microscope has interchangeable 0.63X, 1.0X, and 2.0X objective lenses, a body zoom range of .65X to 4X, and 25X eyepieces for an overall magnification range of 10X to 200X. The moderately tall (300 mm) mounting post enables specimens up to 150 mm tall to be placed under the microscope. The "gooseneck" light bundle often gets loose in the clamp and it can be a big nuisance to precisely align the bundle to highlight a critical feature. A better light source is shown in Figure 3.17 later in this chapter.*

The stereo microscope is designed such that each eyepiece views the object from a slightly different angle, thereby creating two different images. The brain interprets these as a three-dimensional view. The stereo microscope is in reality two separate microscopes. Older rudimentary Greenough design stereo microscopes had two completely different optical paths (including two separate objective lenses), one for each eye. They had very limited capabilities. Most contemporary stereo microscopes use a common objective lens and then two separate internal optical light paths in the body up to the eyepieces. Parfocality, whereby the object remains in focus while the magnification is changed, is a very advantageous feature of the microscope. Follow the manufacturer's guidelines to set the eyepieces for parfocality.

Stereo microscopes present an image that is *right side up and is laterally correct.* Images are therefore easy to correlate to a specimen held in the hands or on the stage. The long working distance from the objective lens and the good depth of field make it possible to clearly see surface features despite the inherent roughness or curvatures of fracture surfaces. Some microscopes also have diaphragm apertures that can be stopped down to enhance the depth of field. Many stereo microscopes are modular and easily modified or expanded.

The total magnification *to the eyes* is the product of the magnifications of the objective lens, the body, and the eyepieces. There often are different <u>objective lenses</u> (0.5X to 2.0X) that screw into the bottom of the microscope. Low power 0.5X or 0.63X lenses are useful for examining or photographing an entire test specimen or viewing large areas of the fracture surface. Higher power lenses (1.6X or 2.0X) may be screwed in for close-up examination. It may come as a surprise that the objective lenses have such low magnifying power, but a large diameter lens is needed to allow the two optical views at slightly different viewing angles. The low power also means that the working distance from the objective lens to the object is very large, on the order of 20 mm to 200 mm. This is a very important and desirable feature for the examination of irregular components. One advantage of the long working distance is that illumination sources such as fiber optic gooseneck light guides can be brought into close proximity to the work piece and the angle can be adjusted with plenty of room as shown in Figure 3.11. A good fractographic examination set up should have both a low power objective lens (0.5X or 0.63X) and a high-power lens (1.6X or 2.0X). An intermediate power lens (1.0X) may also be handy. Objective lenses can cost anywhere from $ 400 to $ 4,000 each. The more expensive lenses have better sharpness at greater magnifications and have less chromatic aberration. The latter is a color distortion or slight blurriness that occurs when a lens refracts the light wavelengths (colors) differently.

Basic student-model stereo microscopes have a limited magnification range. They have little or no capability for expansion (e.g., addition of different objective lenses or camera ports) and have short posts and very limited working distances. Their limitations can make them very frustrating to use and they are not a wise investment for the serious fractographer. Nevertheless, when such a microscope is the only one available, it is possible to use a cell phone to take an image through one eyepiece.

Much of the magnification occurs in the body of the stereo microscope. Most bodies have multiple magnifications either through the use of discrete lenses that can be rotated into the optical path, or better, through stepless-zoom magnification. Modern stereo microscopes have been vastly improved over older models that may have only had a 2X or 4X zoom range. Modern bodies can zoom over a 10X, 16X, or even 20X range while keeping the object in focus. *A very desirable feature is discrete click stops on the zoom knob corresponding to specific magnifications.* This feature is critical for size measurement purposes, either by the use of a graduated reticule in the eyepiece, or by a camera mounted on the microscope.

Final magnification to the eyes is provided by the wide-field eyepieces that are usually 10X, 16X, or 25X. 10X eyepieces are the most common. Stereo microscopes may be used either with or without eyeglasses. The distance between the eyepiece tubes usually can be adjusted for the interpupilary distance. Eyepieces may have rubber boots that attach to the eyepieces for screening out stray light coming into the eyes. These can be removed or slid out of the way for eyeglass wearers. Typical overall magnifications can range from as low as 5X to as high as 200X. Some modern microscopes can achieve as much as 300X to 400X magnification with 16X or 20X body magnifications and 1.6X objectives.

The stereo microscope should be mounted on a tall mounting post so that large objects can be placed on the stage. Often it is necessary to mount long specimens end on that the fracture surface is viewed directly. Figure 3.11 showed a model with a » 300 mm post that allows specimens as large as 100 mm to 150 mm tall to be placed on the stage.

One or both eyepieces should be adjustable, so that the operator can focus each eyepiece independently. One reticule should have a cross hair, which is valuable if the microscope will be used for size measurements in conjunction with a traversing stage as will be described below. If no independent measurement system is incorporated, then a built-in graduated reticule should be mounted in one of the eyepieces. The reticule readings will have to be

calibrated at various magnifications. A valuable but expensive optional feature is a *tilting eyepiece head* that may be adjusted up or down so that the viewer does not have to extend or bend his or her neck to see through the eyepieces, or to have to move a chair or stool up or down. Figure 3.14b later in this chapter shows an example on a discussion stereo optical microscope. A tilt head can cost between $ 3,000 and $ 4,000.

3.4 Stereo Optical Microscope Camera Port and Digital Cameras for Microscopes

Stereo microscopes may be equipped with a camera port for a video or digital camera. The port will be in line with *either* the left or right optical paths. The camera cannot record or display both images that the eyes see and the brain interprets as a three-dimensional image. The camera commonly will be mounted on the camera port through a C-mount or an F-mount that must be chosen with care. It must fit the camera port's diameter, but also have with an appropriate internal lens to match the image size to the camera chip size. Some microscope bodies have a lever switch that directs the light to *either* the eyepiece *or* to the camera. This is extremely inconvenient and very frustrating to use. A much better scheme is a beam splitter that directs 50 % of the light to the eyepiece and 50 % to the camera so that the image can be viewed at the same time it is projected onto a computer monitor.

Digital cameras designed to be attached to microscopes can show "live" images at up to 10 to 20 fames/sec with nominally reduced resolutions on the computer monitor. Once the object is framed and focused, a higher quality image can be acquired or "snapped." A small piece of white paper is often handy, since it can be momentarily placed in the field of view and the camera color-balanced by pressing a camera software button. A fast "live" image mode makes focusing on a computer monitor very efficient. Cameras with slow refresh rates should be avoided since focusing is exasperating as one makes a slight focus adjustment, and then has to wait a few seconds to see the effect on a monitor. A digital camera chip with 2 million to 5 million pixels is adequate for most applications. The most common image formats in 2020 are JPEG, TIFF and sometimes BMP or RAW as discussed in section 3.2. Image compression should be minimized or not used at all when capturing and saving images. Sometimes excessive emphasis is placed on having large pixel counts in digital cameras. There is no harm in having digital cameras with larger pixel counts, but storing and handling very large files might become cumbersome, especially if the images are embedded in documents. Refresh rates on "live" images may also be slowed down. Nearly all the microscope images in this Guide were captured with a CCD (charge-coupled device) digital camera

having a 11.8 mm x 8.9 mm RGB color mosaic chip having 2 megapixels (1600 x 1200) and saved as 24 bit color jpg files. The price of these cameras is cost effective and resolutions of 3 megapixels or more are common at prices less than $ 4,000 as this Guide was written originally in 2007. CMOS (complementary metal oxide semiconductor) chip cameras are also becoming more popular. A microscope digital camera specialist or salesman can be consulted for the advantages and disadvantages of each.

The camera input can be fed to software provided with the digital camera as part of a complete package, or to a separate image processing software package. Contemporary digital cameras and software packages now are much more user friendly than in the past. If there is any doubt, it probably is best to have digital cameras and their software installed by a digital camera or microscope company representative who has experience trouble shooting installation and compatibility problems. *The simpler the software the better!* The author has used digital software packages that are excessively complicated, in large part since they had lots of options and clever additions. They were slow and cumbersome, and were a nuisance to use. Users should beware of salespersons who are eager to sell expensive software packages that the user does not really need. A lot of time may be lost later every time one has to train students and new users.

A very important attribute of a digital camera is <u>the ease which a magnification marker bar can be added</u> to an image. Some digital cameras come with free software that allows not only the usual image adjustments (brightness, contrast, sharpness, cropping, etc.) and file-saving options, but annotations and arrows as well. This is important, and the fractographer can mark a feature on an image immediately and not have to use a secondary software package back in his or her office. It is crucial to be able to put a magnification – size marker bar onto an image and *the fractographer should get into the habit of doing this immediately*. It can be confusing afterwards to know just what magnification a photo was taken with, and an erroneous marker bar might be put on. One recommended additional option is to save a file with an image name that includes the magnification, e.g., “specimen 6 side view at 32X.jpg”.

If a microscope with a digital camera has a variety of lenses and body magnifications, then calibration factors for each combination will have to be established in the software. Usually this is not too difficult. Once the calibration factors are set, they can be retrieved automatically by the software afterwards. The author uses a scheme whereby the camera software has a list of files with all possible lens magnification combinations, with file names that are easy to understand, e.g., “1.6X obj 4X body 102X” which is short for: “1.6

X objective lens, 4X body magnification, 102X total magnification to the eyes" that is the case for his Wild M10 stereooptical microscope with 16X eyepieces." Alternatively, it may be as simple as "M10-102X." I routinely need only 5 to 10 seconds to put an accurate magnification marker bar on my digital images. The author has gone to fractography laboratories around the world and has been pleasantly surprised that others have used simple schemes like this, and it is possible to start using their microscope with little or no confusion.

3.5 Digital Image Processing and Focus Stacking

Digital image technology has revolutionized techniques for processing images. Brightness, contrast, sharpness, and gamma adjustments can easily be made to captured images. Complex discussions about the *gamma adjustment* and luminance of pixels can be found on the internet or in software packages, but can be confusing to newcomers. Simply put, gamma settings adjust the brightness of the pixels that are between the limits of the very bright and very dark regions in an image. In other words, a gamma adjustment does not alter the bright or dark regions, but everything in between.

Inexpensive commercial software now overcomes the *depth of field limitations* of common microscopes. A series of ten to twenty JPEG or TIFF digital images of an object are taken in sequence by an ordinary digital camera with the focus adjusted slightly between each photo. There is no need to use exact vertical refocusing steps. Only a portion of the object is in focus in each image. Later, the software evaluates each image, assesses which portions are in focus, and then constructs a composite final image with all elements in focus in just a few seconds. This is called "focus stacking" or "Z-axis stacking." It does not matter whether the images are from a camera mounted on a tripod, an optical microscope, or a scanning electron microscope. The software for focus stacking need not be expensive. The author uses a software package from a company in the Ukraine that cost a little over $100 in 2007.[b] Figures 3.12 and 3.13 show examples. Even if the images shift slightly sideways after refocusing in a stereo optical microscope, the software compensates for the shifts. The practical ramifications of this technology are that infinite depths of field are achievable with all microscopes, dramatically enhancing the versatility of all microscopes. More sophisticated versions of such software are available with digital microscopes (described in section 3.7 below) or in a scanning

[b] The author first learned about this Helicon Focus software from reading a model train magazine. The technique was used to get in focus photographs of an entire model train as it recedes into the distance along the train tracks on a long hobby table.

electron microscope. Focusing is automatically done in precise vertical steps. A virtual 3-D rendition of the fracture surface can be constructed.

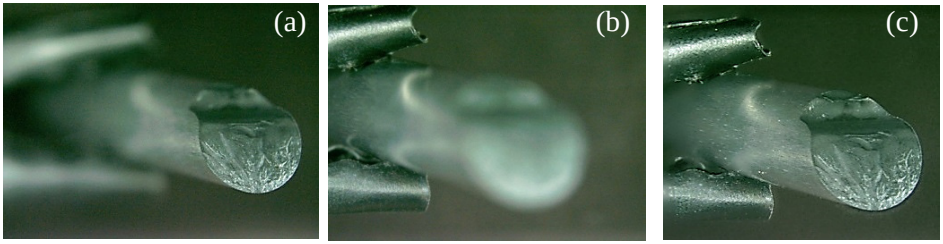

Figure 3.12 *A silicon nitride 6 mm diameter rod broken in flexure (801 MPa). (a) and (b) show stereo microscope digital images. The compression curl and holder are out of focus in (a). (b) shows the holder in the back in focus. (c) shows the digitally reconstructed composite image from 15 separate images.*

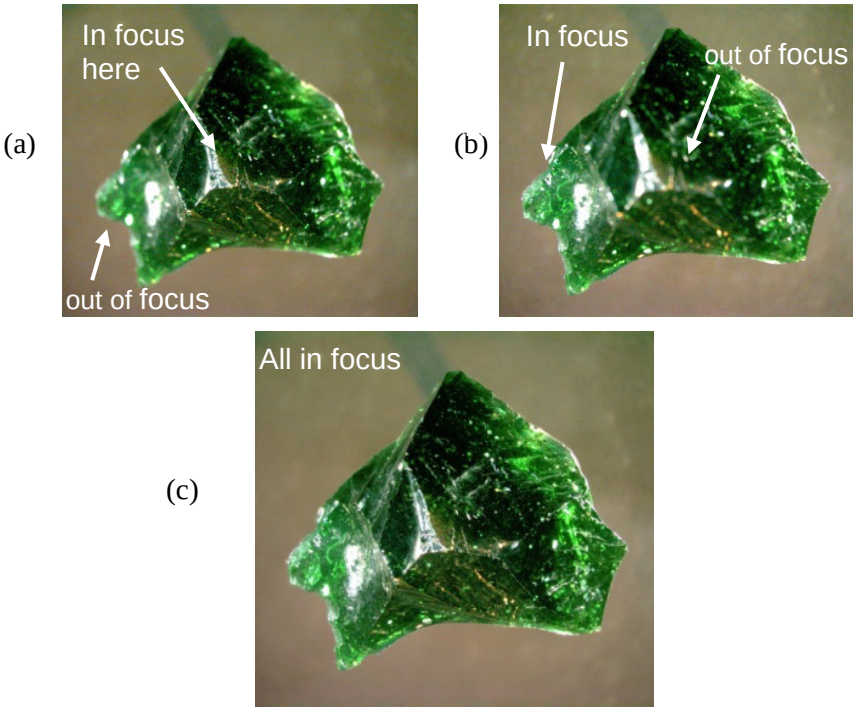

Figure 3.13 *A 25 mm glass fragment. (a, b) show typical images made by a stereo microscope at low magnification. Although it has excellent depth of field, portions of the fragment are out of focus in each view. (c) shows the digitally reconstructed image made from 16 separate images focused from the top to bottom. The digital reconstruction took less than 1 minute.*

(a)

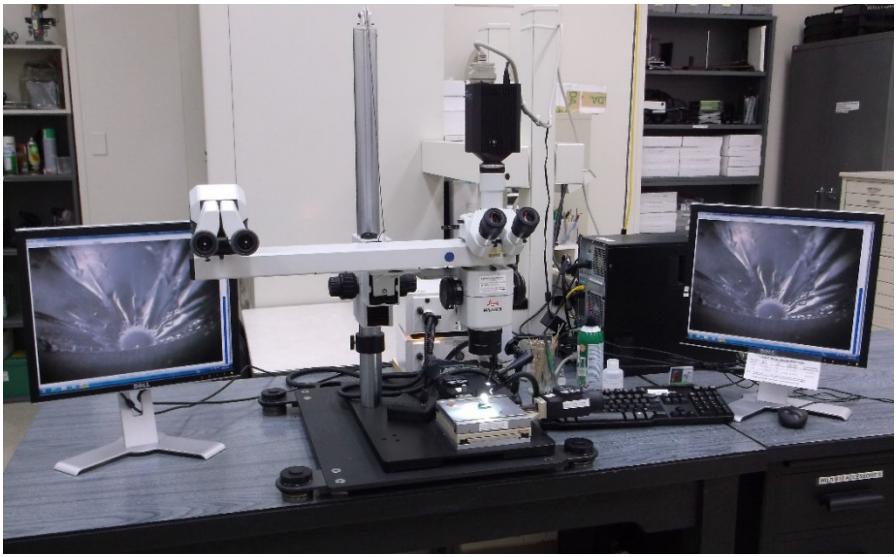

(b)

Figure 3.14 *A discussion stereo optical microscope (a) allows two observers to simultaneously view an object. (b) shows the same microscope in 2006 with an older monitor and camera. The author is demonstrating fractographic analysis to the then director of NIST, Dr. Ray Kammer. Notice how his eyepieces are on a tiltable head. Beam splitters in the optical path enable simultaneous viewing by both viewers through their eyepieces at the same time the camera views the object. Also note the very tall post (800 mm) on which the microscope body is mounted. The entire assembly can be moved up or down as required to accommodate very large or very small specimens. The microscope is mounted on a low-profile vibration isolation table.*

3.6 Discussion Stereo microscope

Figure 3.14 shows a "discussion stereo optical microscope" that enables two observers to simultaneously see the image. These are also known as "dual head discussion stereo microscopes" or "dual head discussion training microscopes." A beam splitter diverts half of the light to the auxiliary viewing station. The configuration shown is a side-by-side model which is preferred for most fractographic analysis. Discussion microscopes often have a built in moveable pointer that can be seen by both observers. Discussion microscopes are extremely valuable for training new fractographers or for showing features to clients or colleagues. The auxiliary viewing station should also have adjustable eyepieces so that the secondary observer can adjust the focus to match the focus of the primary observer. A camera port can be included with another beam splitter so that the image can be projected onto a monitor at the same time it is viewed through the eyepieces.

3.7 Digital Microscopes

Simple digital microscopes, also known as USB microscopes, connect directly to an ordinary computer. They do not have eyepieces to look through. Everything is projected onto a computer monitor. They can range from inexpensive low-power, hand-held models such as shown in Figure 3.15a to elaborate, high-power, expensive models mounted on a rigid platform with full Z-axis control and digital image stitching capabilities as shown in Figure 3.15b.

The mid-priced model (~$ 1,000 plus $130 for the stand in 2016) shown in Figure 3.15a has variable magnifications from 20X to 250X and corresponding working distances of 48 mm to 2 mm. It may be difficult to obtain sharp, focused images with the simpler models that are handheld, so a stand is advisable. Simple digital microscopes may <u>not be parfocal</u>. As the magnification is changed, the working distance is changed significantly, and the image must be completely refocused. This is a <u>major nuisance</u> and dramatically slows down the examination process. The greatest limitation of such simple digital microscopes is that they <u>do not provide a three-dimensional</u> view of the surface, as a stereo optical microscope does. Another limitation is illumination, which is usually provided by built-in light-emitting diodes surrounding the lens. This limits their ability to highlight or even discern critical fracture surface features. For example, shadowing, or low-angle grazing illumination, which is essential for ceramic examination and fracture mirror examination, cannot be done. A separate light source is recommended for use with a digital microscope.

(a)

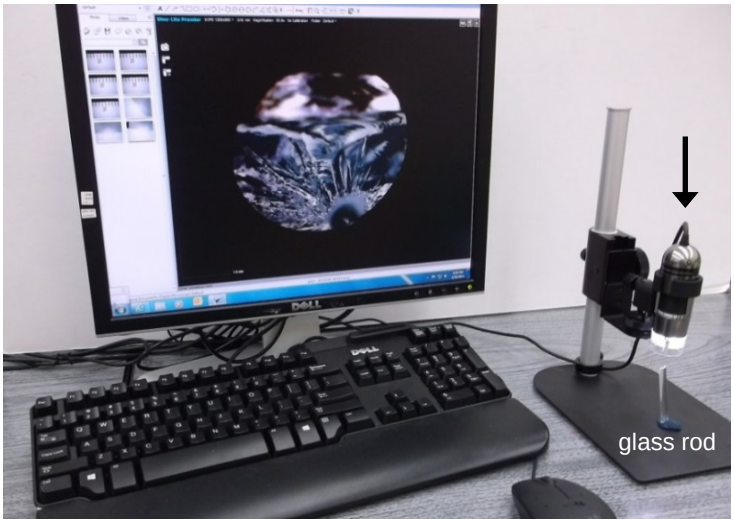

(b)

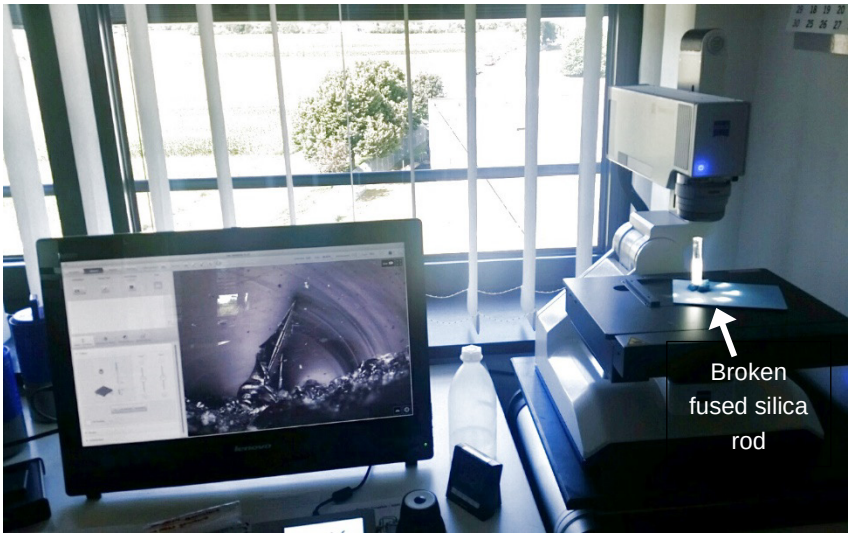

Figure 3.15 *Digital microscopes. (a) shows a simple model (arrow) that is mounted on a stand on the right. It is focused on the fracture surface of a broken 6 mm diameter glass rod that is mounted on polymer clay. The monitor and computer (not shown) are separate components. (b) shows a sophisticated model with full Z-axis control and digital image stitching capabilities, interchangeable objective lenses, and tiltable head. Some models have a zoom range of 10x and a total magnifications capability from 10x to 2000X. A broken silica glass rod is on the stage and is illuminated by built-in LED lights. The monitor shows the surface damage fracture origin. Neither of these microscopes have eyepieces and the 2-D image appears on a flat screen. (b is courtesy of C. Schenk, Heraeus, Germany)*

At the other end of the spectrum are high-end digital microscopes mounted on very rigid fames and bases and which may have built-in vibration dampers. Interchangeable objective lenses with magnifications up to 10X can be used. Figure 3.15b shows such a model. They may have motorized positioning stages and automated Z-axis focusing and even have tilting heads. Camera and stage controls are via joysticks, electronic knobs, or even touch-screen monitor manipulation. These systems can automatically conduct Z-axis focus stacking analysis and, combined with the stage control, can generate quantitative three-dimensional profiles of the fracture surface. The virtual three-dimensional image can be displayed on the monitor and rotated and viewed from different perspectives. Despite this extraordinary versatility, the illumination systems with such microscopes (usually a ring of LEDs) are very limited. Many of the techniques described in this Guide require fully-independent illumination control. It is recommended that independent illumination sources such as shown in the next section be acquired for use even with such high-end digital microscopes. The working distances between the lens and the piece should be large enough that independent light can be directed onto the specimen at variable angles.

3.8 Illumination Sources and Techniques

Illumination is critical. Figures 3.16 and 3.17 show some options. Bright light sources are advisable to facilitate the examination of dark ceramics and the use of high magnifications. Ring lights that clamp to the objective lens or built-in uniform lighting sources are <u>not</u> preferred since they provide uniform lighting that is ineffective in highlighting ridges or valleys. Directional illumination is essential and can be achieved with fiber optic gooseneck light guides that direct an intense light beam onto the fracture surface at an angle. Dual gooseneck guides from a single light source as shown in Figure 3.17 are highly recommended. This particular model has a single locking knob at the elbow that locks or loosens all the arm positions. One guide may be used for illuminating the key features while the second guide can be used as filler or for adjusting the overall illumination.

A good fractographer uses lighting to not only discern the key fractographic features, but also to <u>highlight them</u> so that <u>convincing photographs</u> can be taken to show others. Some artistic skill and common-sense techniques apply. For example, most good photos of a fracture origin have the origin centralized in the photo with radiating hackle lines. The photo should have the lighting adjusted to emphasize both the origin and the hackle lines. This can be time consuming but rewarding.

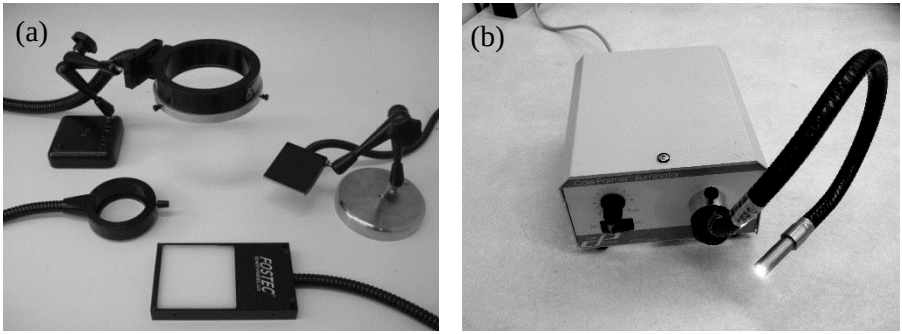

Figure 3.16 *Illumination sources for use with a stereo microscope. (a) shows clockwise from the middle left: a ring light intended to be clamped to the objective lens, a ring dark light illuminator on an adjustable stand, a line light source on a stand, and a transmitted light platform. These are interchangeable in the source light box. (b) shows a simple single gooseneck light guide. See also Figure 3.11.*

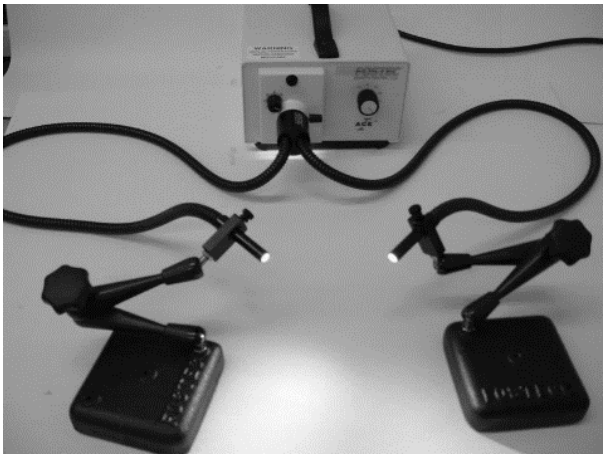

Figure 3.17 *Dual gooseneck fiber optic light guides allow flexibility in directional illumination. The single knob locks-unlocks all the joints.*

Low-angle grazing illumination is very effective for accentuating peaks and valleys on fracture surfaces as shown in Figure 3.18.[c] The ability to adjust the angle of the illumination source by just a few degrees is critical. Easily-adjustable holders (e.g., Fig 3.17) are a great time saver. Low angle grazing illumination is sometimes called "raking angle illumination." Notice in Figure 3.18 how white and black cards may be used to adjust the lighting.

---

[c] Low-angle grazing illumination was erroneously termed "vicinal illumination" in the 1st edition of this Guide in 2007. It was corrected in the 2nd edition in 2016.

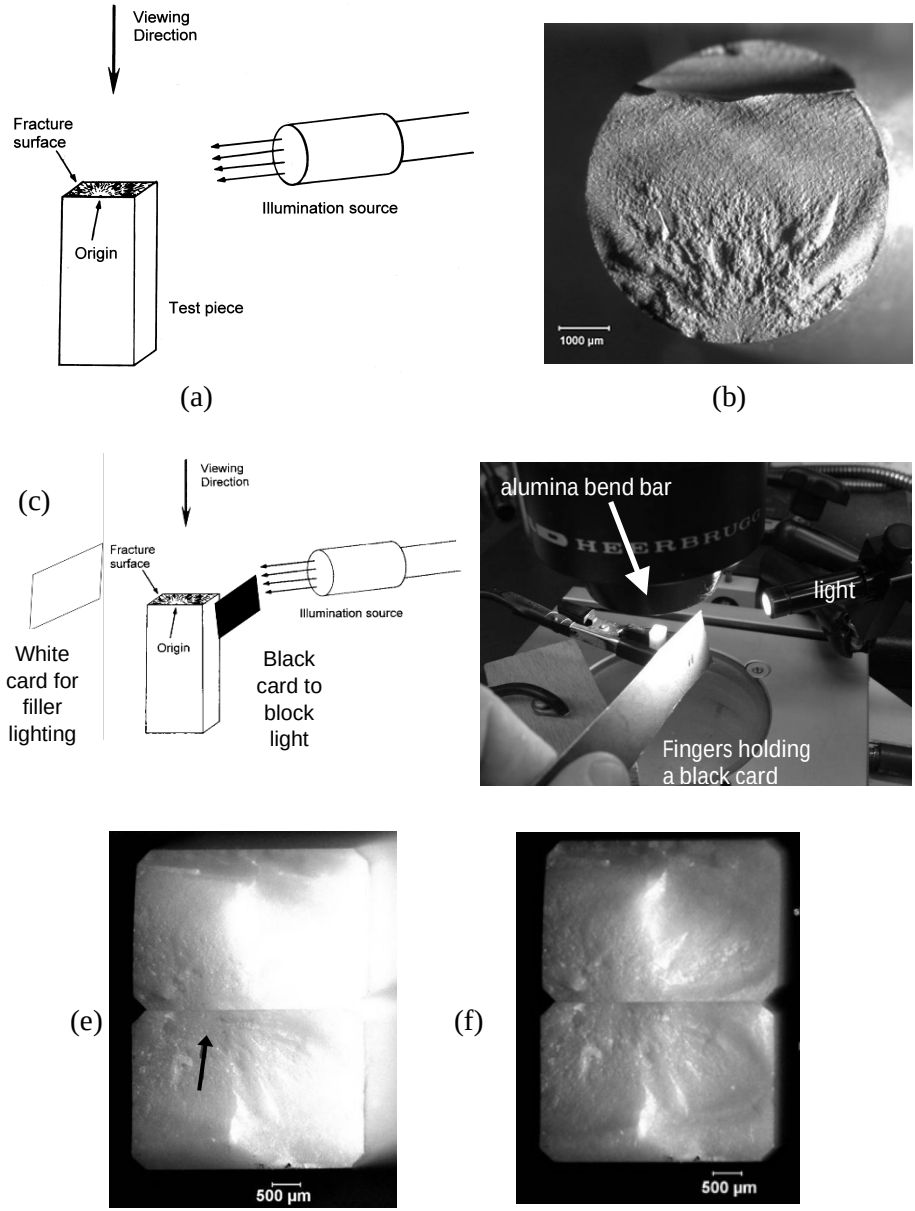

Figure 3.18 *Low-angle grazing illumination (a) is effective in highlighting fracture surface topography as shown in (b), which is the fracture surface of a ceramic rod broken in flexure. (c) and (d) show how a piece of black card interposed between the light source and the specimen helps with translucent specimens. Alternatively, a white card on the backside of the specimen can provide some filler illumination. (e) and (f) show a translucent alumina without and with a black card blocking light from the right side.*

"Vicinal illumination," illustrated in Figures 3.19 and 3.20 helpful in detecting cracks that may be difficult to see by other means in a translucent material. A bright light illuminates an area *near to* ("in the vicinity"), but not directly on the area to be studied. Light is scattered sideways in the translucent material. If the light encounters a crack, much of the light is reflected. Only some is transmitted across the crack. This creates a sharp delineation between light and dark areas that highlights the crack.

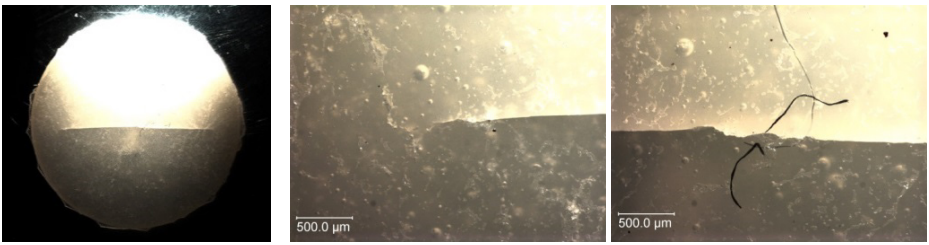

(a) (b) (c)

Figure 3.19 *Vicinal illumination of a Polyethylene glycol (PEG) dental resin with amorphous calcium phosphate filler. The 15 mm diameter disk specimen (a) broke in a biaxial strength test at only 35.5 MPa. There was insufficient elastic energy to completely break the specimen into two pieces. (b) is a close-up of one crack tip, and (c) is a close-up of the* <u>*tensile*</u> *surface at the fracture origin. The flaw is a trapped hair or fiber confirmed by examination of the fracture surfaces once the specimen was snapped in half.*

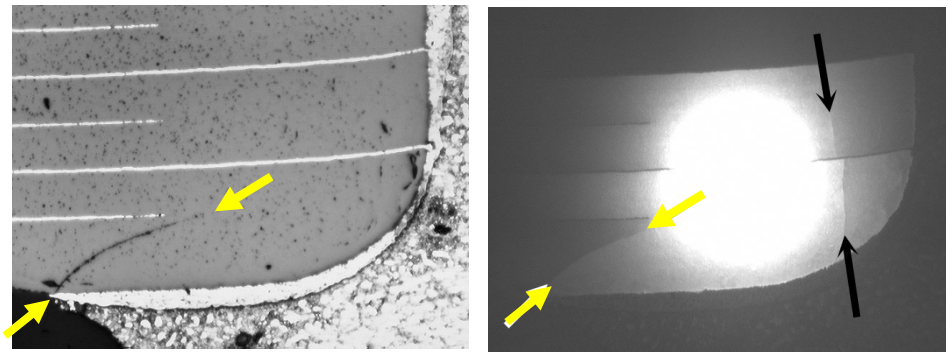

(a) (b)

Figure 3.20 *Bright field reflected light (a) and vicinal illumination (b) of a multilayer ceramic capacitor. Both images are at the same magnification. Only one crack is apparent in (a) as marked by the yellow arrows. Vicinal illumination revealed the second crack on the right marked by black arrows in (b). These images are from a compound optical microscope. (Unreported image size. Courtesy of S. Hull, NASA, Goddard Research Center.)*

An inexpensive hand-held laser pointer may be used with translucent or transparent ceramics to highlight internal cracks.[d]

Dark field illuminators such as shown in Figure 3.21 may also be handy. The dark field illuminator is similar to a normal ring light, but the light is directed sideways from the ring towards an object in the middle. It is in essence low-angle grazing illumination from all directions. This sideways illumination accentuates subtle surface features and scratches.

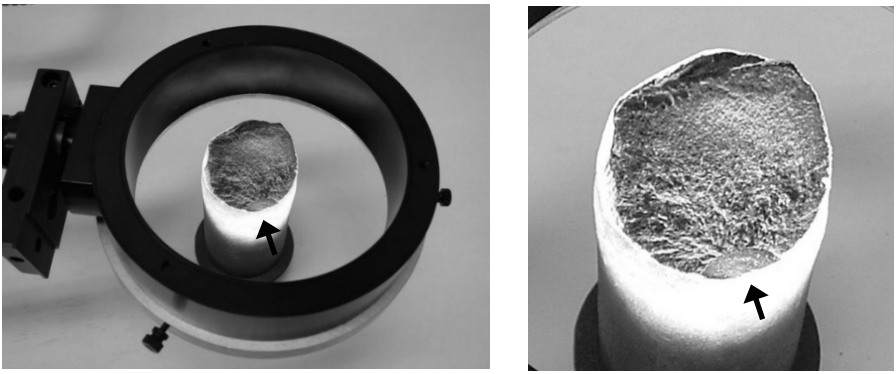

Figure 3.21 *Dark field illumination of the fracture surface of a fractured 40 mm diameter steel railroad coupler pin. The arrows point to a fatigue crack.*

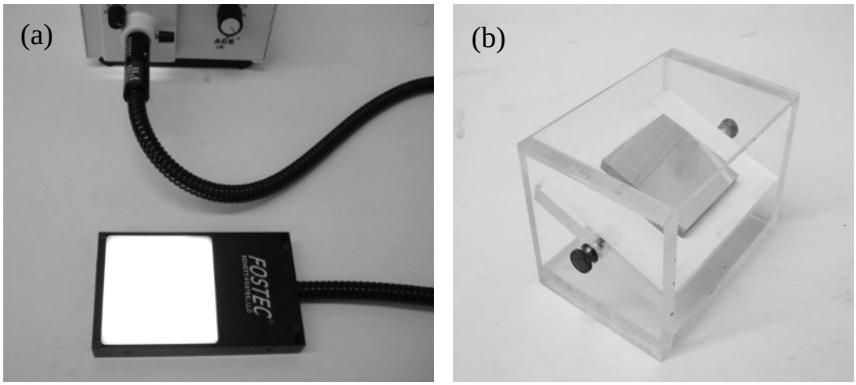

Figure 3.22 *Transmitted light can be from an illuminator plate as shown in (a) or in (b), an improvised stage made of Plexiglas and white paper or a mirror. A fiber optic light source can be directed onto the tiltable inclined plane so that light is reflected up through a specimen mounted on the top. (b is based on a suggestion by Dr. Daniel Shechtman.)*

---

[d] This tip is new to the 4th edition. It was suggested to me in 2022 by Henning Leidecker and Scott Hull of the NASA Goddard Space Center, Greenbelt, MD. Use care with such lasers.

Sometimes it is better to illuminate glasses and transparent or translucent ceramics with transmitted light from the bottom and up through the specimen. Some stereo microscopes have a light source in the base for transmitted illumination. Illuminated bases as shown in Figure 3.22 may also be used.

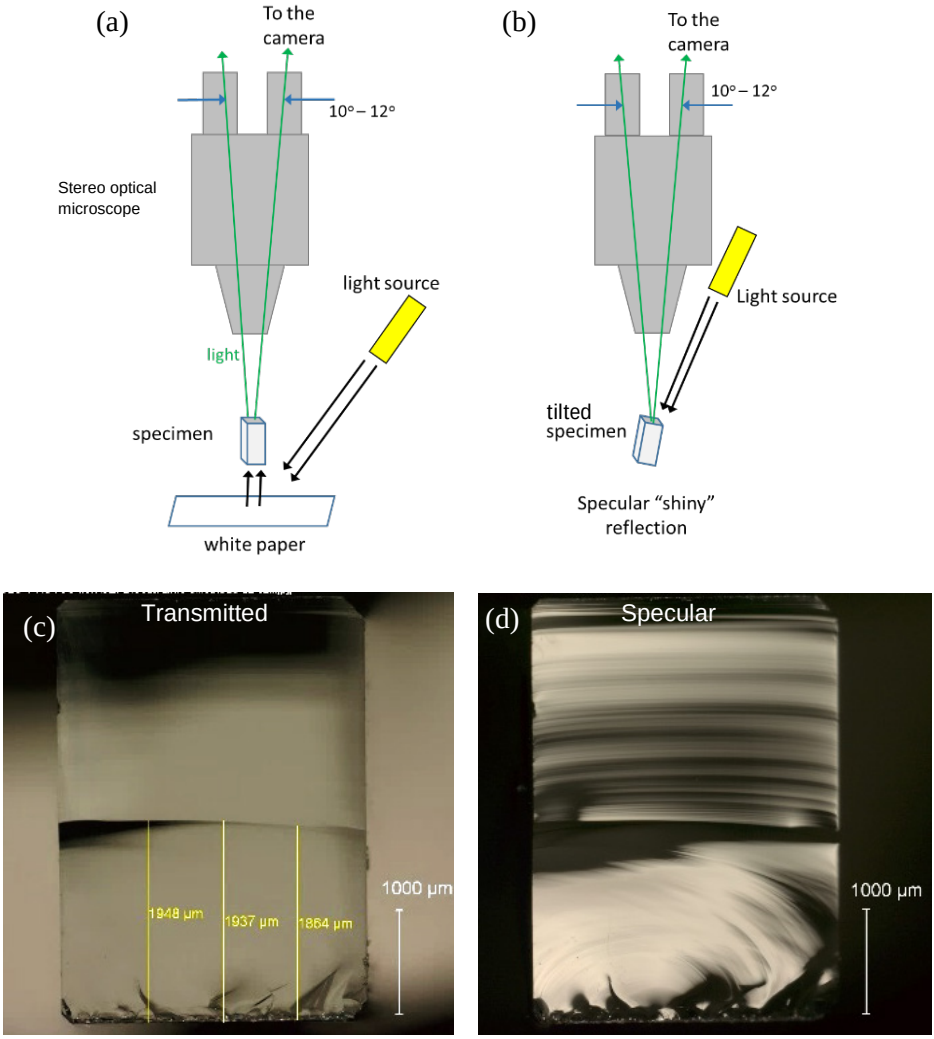

Figure 3.23 *Transmitted (a and c) and specular reflected (b and d) light illumination of the fracture surface of a glass single-edged precracked beam (SEPB) fracture toughness specimen with a 1.95 mm deep precrack. The specular view in (d) shows a lot of crack front and crack propagation detail.*

Another approach with ceramics is “transillumination” whereby light is shone through the side of the specimen. Figure 4.2 in the next chapter shows examples. The fiber optic light source is directed through the material from one side. Usually the side surface nearest the light guide will be washed out, but internal features and subtle fracture surface features may stand out elsewhere on the fracture surface.

Figure 3.23 shows matching images of a glass fracture toughness test specimen with either transmitted illumination or specular reflected illumination. For transmitted light illumination, the light source is simply directed at a piece of white paper beneath the specimen. The test piece is straight up and down. For the specular reflected light illumination, the light source is brought in at a very high incident angle and the specimen is tilted so that the fracture surface acts like a mirror to shine light up into the microscope and camera. Different levels of brightness are observed in the two stereo optical microscope eyepieces due to the different light path angles. Very careful and minute adjustments of the light source angle and specimen tilt lead to dramatic differences in fracture surface reflections. Specular illumination works best with stereo optical microscopes with low magnification objective lenses since the working distances are greater and one has more flexibility in bringing the incident light from a highly inclined direction. Even though it is tilted, nearly all of the fracture surface will be in focus, since the depth of field is greater with the lower power objective. Very subtle and important fracture features can be detected by specular illumination, that are not evident in the transmitted mode.

Polarizers (Figure 3.24) may be valuable for examining transparent materials. They may reveal residual strains in glasses or twins in single crystals. One

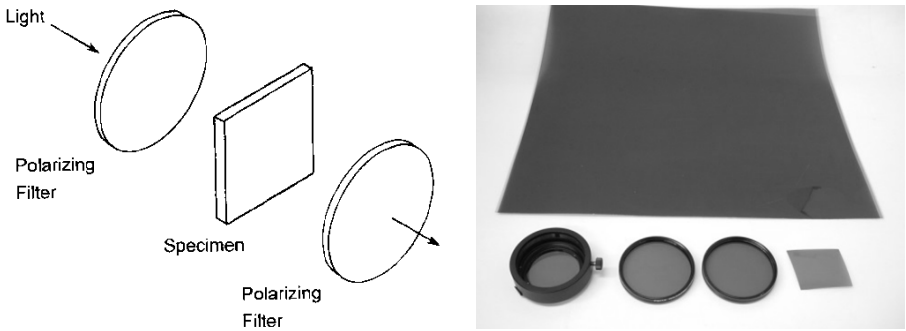

Figure 3.24 *Crossed polarizing filters or plastic sheets. Polarizers can either be dedicated accessories for the stereo microscope, or can be improvised from ordinary single lens camera lens attachments or plastic polarizing sheets.*

polarizing filter may be placed between the transmission light source and the specimen and an analyzer (another polarizing filter) attached to the objective lens. The analyzer can be rotated as required to achieve the desired color or brightness differences. Polariscopes are discussed in section 3.25 below.

3.9 Coatings on Fracture Surfaces

Coatings may be applied to specimens that have poor reflectivity or which are translucent and scatter light from beneath the surface, thereby washing out the surface detail. A thin layer of gold or platinum may be sputtered onto the surface in a small vacuum chamber. Such equipment is commonly used to prepare a specimen for scanning electron microscope examination, but the coating enhances optical examinations as well. Figure 3.25 shows an example. Notice how the gold coating blocks the internal light scattering. Gold and platinum coatings may be removed later without harm to most ceramic specimens by soaking the pieces for about 1 minute in "aqua regia." This is a combination of 1 part by volume of nitric acid and 3 to 4 parts hydrochloric

(a)

(b)

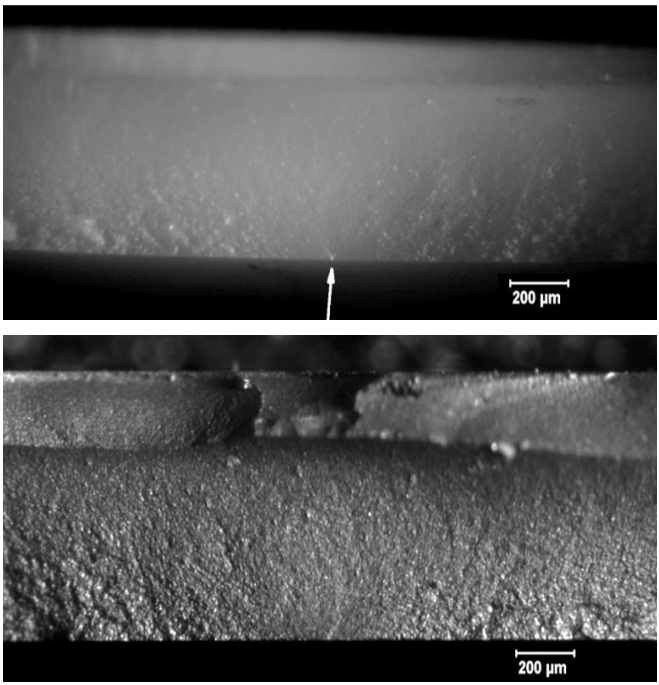

Figure 3.25 *Two views of a fractured yttria-stabilized tetragonal zirconia disk with reflected light illumination. (a) shows the uncoated fracture surface and (b), the same region after a thin gold coating was applied. The fracture surface and fracture mirror are much easier to interpret in (b).*

acid. This is a hazardous combination and appropriate precautions must be taken (e.g., gloves and eye protection). Only mix the amount to be used in a cleaning session. *Never store it, since it releases gasses that build up pressure in a sealed container*. The specimens should be rinsed in water afterwards. When disposing of used aqua regia, water should not be added to the acid mix. Instead, the acid mix should be carefully poured into a large container of water or a sink with ample flowing water. Aqua regia can cause harm to a specimen if the specimen contains anything metallic, such as a metallic-inclusion fracture origin. The author once had a highly-filled resin matrix dental composite bend bar that had some trapped contamination covering the origin during the initial SEM examination. The original gold coating had to be removed, the specimen recleaned, and recoated for a second SEM examination. The fracture origin was a calcium rich inclusion. The aqua regia not only removed the gold coating, but it also reacted with the fracture origin forming calcium chloride. The EDX analysis during the second SEM session showed chlorine at the origin, which was puzzling until the author remembered the aqua regia cleaning step and realized that the HCl had reacted with the flaw.

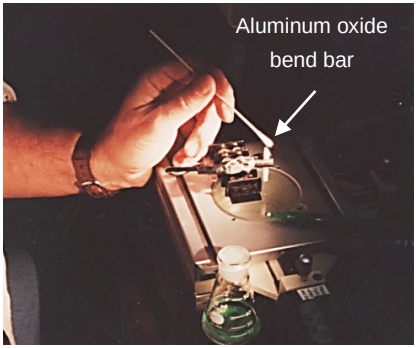

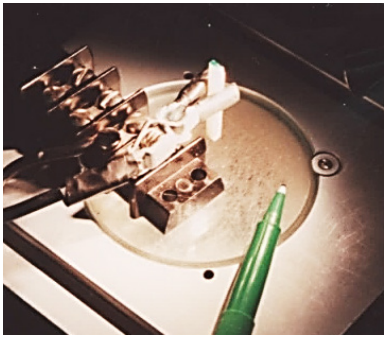

Figure 3.26 *A simple but effective coating technique on white ceramics is to stain the surface with a green felt tip pen. The staining can be watched in real time through the microscope. The green stain can be easily removed with ethanol alcohol on a cotton swab applicator and the process repeated.*

A simple expedient that works very well for many white or gray ceramics is a common *green felt tip pen* as shown in Figures 3.26 and 3.27. Green felt tip pens work the best, partly because the eye is most sensitive to green wavelengths, but probably also due to the character of the green dye.[e] The dyes can easily be removed with ethanol within a few seconds or minutes and the process repeated in a matter of seconds. Most dye will come off, but some may penetrate into crack branches and may be more persistent. If the green dye is allowed to sit for longer periods of time, it can be removed by soaking the part for 1 to 2 minutes in a 30% solution of H_2O_2 (hydrogen peroxide). Note this is a much greater concentration than is use for topical cleaning of wounds. Gloves and eye protection should be used. Additional dye and staining techniques are discussed in section 3.24 later in this chapter.

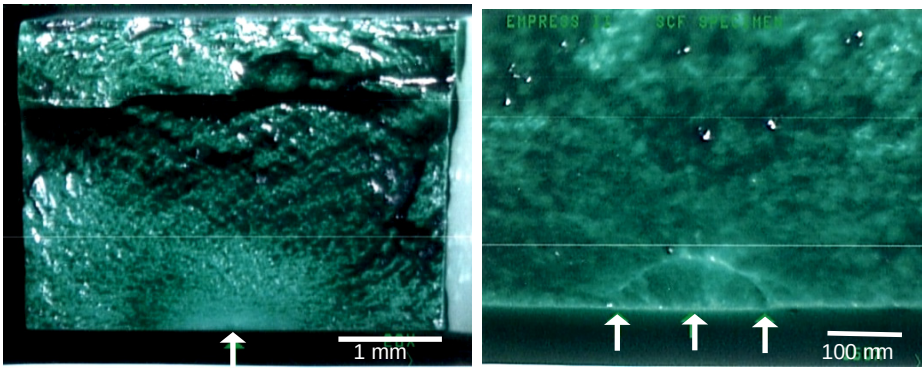

(a) (b)

Figure 3.27 *An example of green dye staining on a lithium disilicate dental glass ceramic bend bar. (a) shows the entire fracture surface illustrating how the stain drains into valleys and accentuates hackle lines and ridges and how easily the fracture mirror region stands out (arrow). (b) shows the fracture origin: a surface crack (arrows) made by Knoop indentation for a fracture toughness measurement. The pictures were older generation video prints and the thin horizontal white lines are an artifact from a defect in the print head.*

People have been creative with coatings for other materials. For example, Dr. A. Christensen at the FBI Forensics laboratory in Quantico, Virginia has found that *black fingerprint powder*[1] can be effective with fracture surfaces of broken human bones. Figure 5.25 later in this guide shows an example.

---

[e] Papermate Flair, 1.1 mm, Sanford Corporation, Division of Newell, Rubbermaid.

Prof. T. Engeleder of the Department of Geosciences, Pennsylvania State University has used *chalk* effectively on geologic fracture surfaces as shown in Figure 3.28.[2]

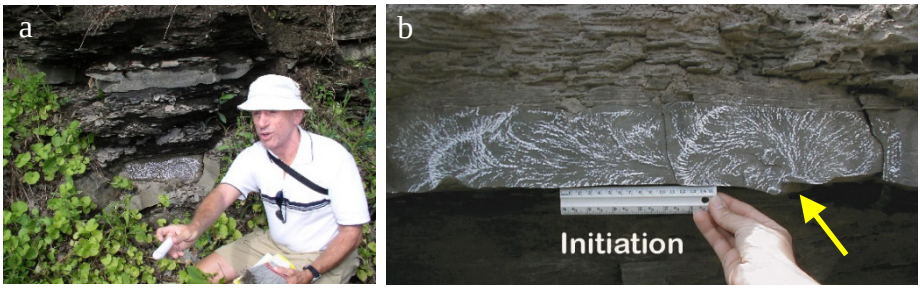

Figure 3.28 *Prof. Terry Engelder demonstrates the use of chalk to highlight hackle and arrest lines ("plume" or "plumose" pattern) in siltstone fracture surfaces exposed in the Ithaca Formation along route 414 near Watkins Glen, NY in 2006. (b) shows a nearby siltstone example, along route 14 between Montour Falls and Watkins Glen. The fracture origin is at an asymmetrical site ("flute cast") marked by the yellow arrow. Crack growth occurred in multiple stable extension stages. See also Figure 4 of Ref. 2.*

3.10 Size Measurements

Sizes may be measured by means of a graduated reticule in a microscope eyepiece. The graduations must be calibrated by means of a stage micrometer

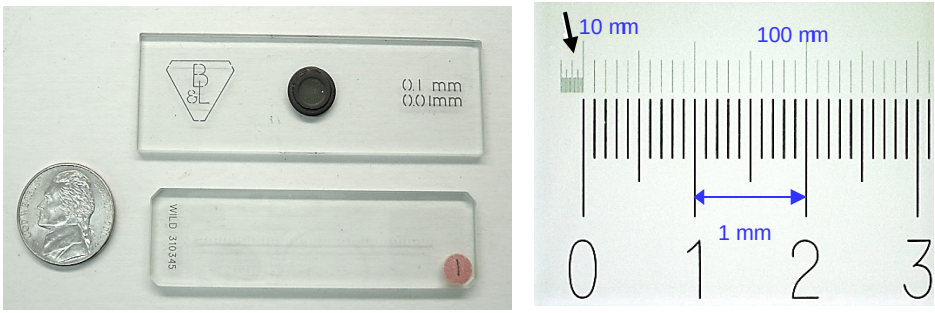

Figure 3.29 *Two stage micrometers (a). A close-up of the bottom one is in (b). The numbers show 1 mm spacings. The thin lines on the top right are 100 μm apart. The thin lines on the top left (arrow) are 10 μm apart. This model was accurate to an amazing 0.01 %.*

such as shown in Figure 3.29. Users should be cautious about the accuracy of stage micrometers. Some are rudimentary and only meant to furnish an approximate magnification for photography and can be as much as several percent in error. Others may be very accurate. If a stereo microscope has a zoom capability, it is best that the body have discrete click steps or detents so that precise magnifications can be calibrated and recorded at the discrete steps.

A powerful accessory to a microscope is a traversing X-Y stage with micrometer positioning heads such as shown in Figure 3.30. This accessory is especially valuable for precisely aligning a specimen in the field of view, particularly when photographing an image. (A lot of time can be lost when nudging a specimen around with one's hands.) The micrometer heads in conjunction with a crosshair in one eyepiece also facilitate accurate size measurements of features. One advantage of such a system is that if the fracture surface is viewed directly from above through both eyepieces, and the fracture plane is horizontal, then the micrometer-measured sizes need not be corrected for foreshortening, as long as the surface being examined is parallel to the X-Y stage.

If size measurements are made on recorded images, care must be taken to ensure that the camera axis is near to perpendicular to the fracture surface plane. Cameras mounted on a stereo microscope view the fracture surface at a small angle (» 7°) to the fracture surface, so its view may be foreshortened. The specimen may have to be tilted a few degrees to obtain a true view of the

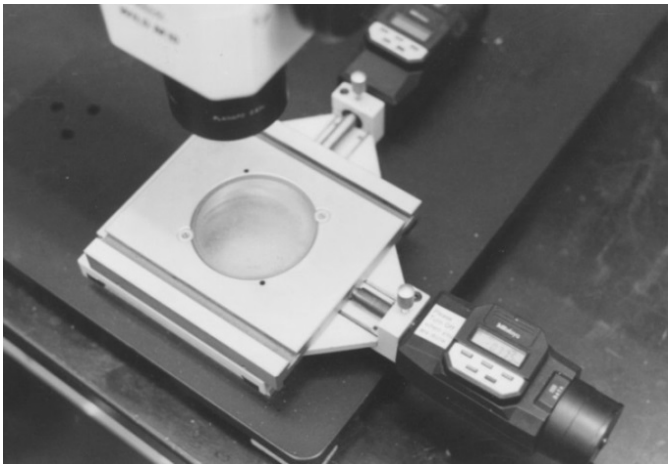

Figure 3.30 *A X-Y traversing stage with digital micrometer heads is very convenient for positioning a piece and making accurate size readings.*

size of the fracture surface. For example, one can tilt a bend bar sideways a little bit until the camera does not “see” the sides of the bend bar.

An additional advantage for the X-Y stage measurement is that the size readings are independent of the magnification used to view the specimen. In contrast, images captured by the camera must be calibrated for the exact magnification. One drawback to the traversing stage is that it takes up vertical space and hence the microscope body must be moved up higher and possibly may limit the working range under the objective if the microscope is mounted on a short post. As noted above, stereo microscopes should be mounted on tall posts for maximum versatility.

3.11 Compound Optical Microscope

Compound optical microscopes such as shown in Figures 3.31 and 3.32 may be used for fractographic analysis but are less versatile than stereo microscopes. Compound microscopes are best suited for small specimens with relatively flat surfaces. They magnify much more (up to 1600X) than a stereo microscope, but three-dimensional topographical effects are lost. Virtually all work is now done with air lenses. Oil immersion lenses are no longer needed.

Objective lenses from 5X to 100X may be used in the lens turret, but in practice the limited depth of field makes it difficult to see a fracture surface in focus at larger magnifications. Only portions of a fracture surface may be in focus even at lower magnifications. Working distances are also very small, and care must be taken not to contact and damage the objective lens with a specimen. Long focal length objectives are ideal. These have greater working distances, but at the cost of some loss of light collecting power and resolution. The author uses a compound microscope with long focal length lenses. The 100X objective has a 1.3 mm clearance and 0.8 numerical aperture. Some 100X lenses are available with working distances as long at 13 mm, but these have lower numerical apertures (0.5 to 0.6) and less resolving capability. The clearance between a stage and the objective lenses may preclude examination of large fractured pieces. Low-angle grazing illumination is difficult to achieve with compound microscopes, especially at greater magnifications.

Dark field illumination may be very effective for examining cleavage planes in <u>single crystals</u>. Direct reflected light illumination may be too bright or wash out details due to the mirror-like reflection from a cleaved crystal surface. Dark field illumination blocks the central portion of the illumination light coming through an objective, allowing only oblique rays in a ring to strike the specimen. Only light that is scattered by features on the fracture surface is

reflected back up into the objective for the viewer to see. Fracture surfaces appear as small bright lines and spots against a dark background. Dark field can highlight subtle cleavage steps and make the symmetry of a fracture mirror more evident. Figure 8.6a in the chapter on single crystals shows a classic example of this.

Figure 3.31 *Compound reflected light microscope. The two eyepieces view the same image collected by the objective lens. Overall magnifications can be as much as 1600X, but the working distances and the depths of field are very small. Only relatively flat specimens may be examined.*

Compound microscopes are useful for measuring very small features, such as tiny fracture mirrors in optical fibers or other strong test specimens. Compound microscopes can also be used in transmitted illumination mode. These microscopes are also optimal for measuring fracture mirror sizes in glasses as discussed in Chapter 7 and Appendix D.

Compound microscopes may be very useful for examining fine detail in replicas such as shown in Figures 3.33 to 3.35 in the next section. Thin polymer replicas of curved surfaces may be flattened by taping the ends of a

replica on a glass microscope slide, or the replica may be placed between two glass slides so that the curved surface can be flattened and examined at high magnification in either transmitted or reflected light.

Compound microscopes are essential for examining polished specimens for microstructural analysis, a useful adjunct to the fractographic analysis.

(a)

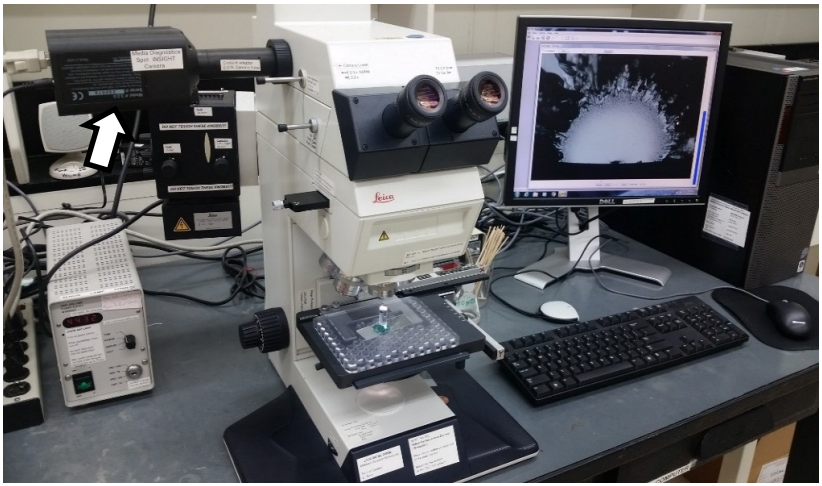

(b)

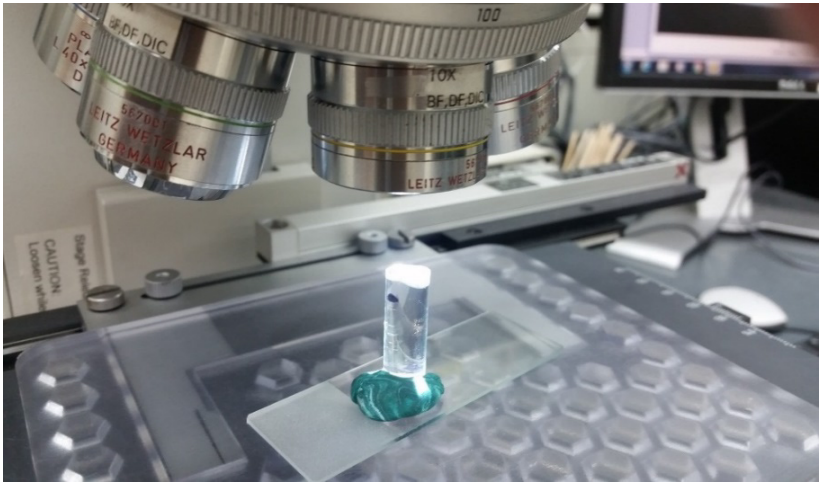

Figure 3.32 *A research compound microscope with a digital camera (white arrow). Linear encoders with a 1 micrometer resolution are attached to the traversing X-Y stage and facilitate rapid size measurements. The monitor on the upper image shows the fracture mirror of a fractured glass rod that is mounted on green polymeric clay as shown in (b). The fracture mirror can be viewed through the eyepieces at the same time it is projected on the monitor.*

3.12 Replication Equipment

Replicas of fracture surfaces may be valuable in some instances. Figure 3.33 shows the concept of making replicas. Some fractured parts may be so large or unwieldy that it may be difficult to position them under an optical microscope. A small replica may be taken of the area of interest. In other instances, the fractured part may be a critical piece of evidence that cannot be taken to the fractography laboratory. Replicas can also be an important backup source of critical fracture surface information if the component is lost or damaged. Replicas are sometimes easier to interpret than the original piece. They can be valuable teaching aids in a course on fractography since every student gets to examine the same object with the same features!

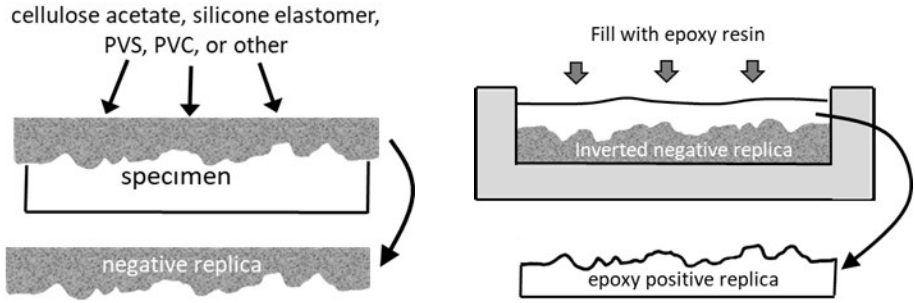

(a) (b)

Figure 3.33 *Replicas copy the information on a fracture surface. (a) shows a negative replica. (b) shows a positive replica which requires an extra step.*

There are two types of replicas: "positive replicas" and "negative (or reversed) replicas" as shown in Figure 3.33. Some replica materials are laid over a fracture surface then removed after they dry sufficiently to retain the critical surface features. The material preserves a mirror image of the fracture markings: what was left is now right, and so forth. This is a "reversed replica" or a "negative replica." Other replicas may be made in multiple steps to create a "positive replica." For example, a silicone impression or mold may be made around an object, and then pulled off the fracture surface. An epoxy resin is then cast into the mold and allowed to dry. The mold is removed, and now the epoxy represents a positive replica (i.e., a clone) of the original part. The dental materials community has a good line of products suitable for making mold impressions of teeth and these materials are suitable for general fractographic applications as well, as discussed by Scherrer *et al.* [3] Fréchette also describes replication techniques in his book.[4] Two excellent summary papers with practical tips are by Varner.[5,6]

Disadvantages of replicas include they may have artifacts form the preparation procedure. They also lose color and reflectivity differences that would be observed on the original fracture surface. They also have no information about the chemistry of the material or a fracture origin. They may create confusion with respect to orientation or location of a feature if they are negative replicas.

In some cases, fracture surface features may actually be easier to observe on the replica than on the original surface. In transparent or translucent ceramics such as porcelains or coarse grain ceramics light scattering from below the surface can obscure the fracture surface details. For example, subtle wake hackle lines behind pores may be easier to see on replicas. Curved surfaces can be made more amenable to high magnification examination, since a replica can be flattened. Since some replicas are a negative of the fracture surface, depressed features such as pores or cracks are converted to raised features on the replica that sometimes are more easily imaged in the scanning electron microscope.

Figure 3.34 *Thin cellulose acetate replica tape, acetone, applicator, and bend bar specimens. These are used to make reversed (negative) replicas.*

There are a variety of materials that may be used to make a replica as shown in Figures 3.34 to 3.38. The replica must be made without the introduction of artifacts. The replica material must also not damage the original material nor chemically react with it! Cellulose acetate tapes or films are convenient replica materials that may be made at room temperature as shown in Figure 3.34. The specimen surface should be clean.

(a)

(b)

(c)

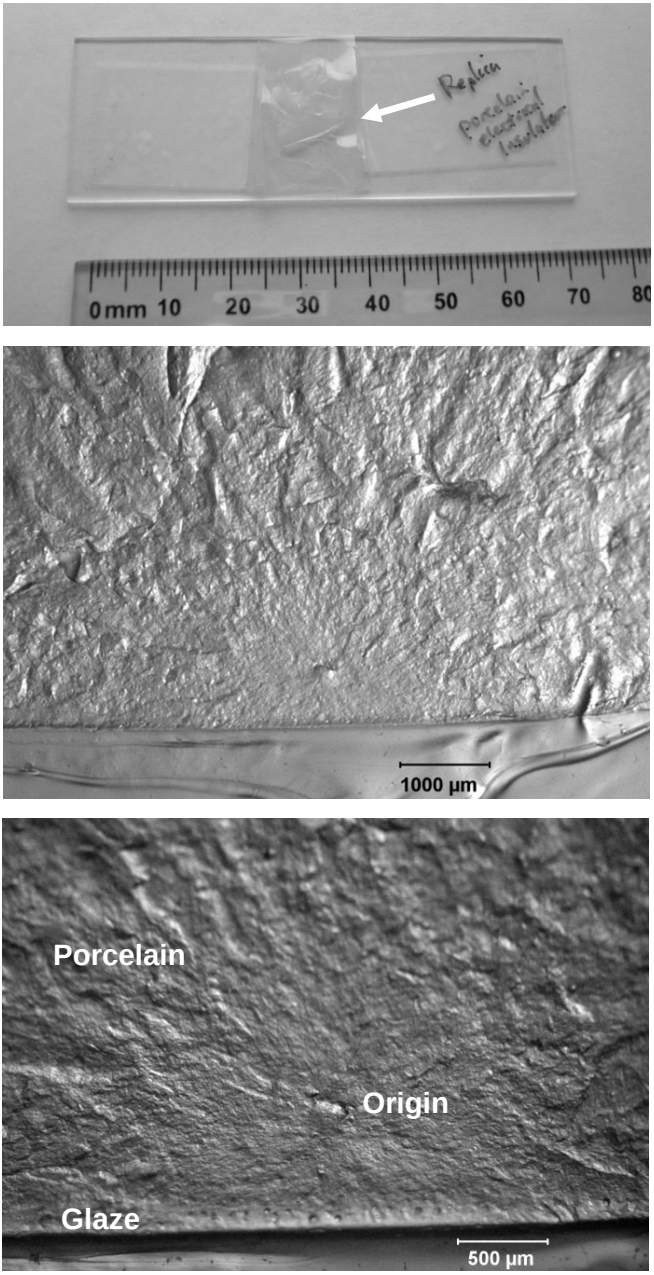

Figure 3.35 *Cellulose acetate replica of a fracture surface of a porcelain electrical insulator. (a) shows the replica taped to a glass microscope slide for convenience in handling. (b) and (c) show close-ups of the replica which reveals the fracture mirror and an inclusion flaw.*

A short strip of 0.13 mm to 0.25 mm thick tape is cut from the sheet or roll and then moistened on one side with acetone. Thick tapes or films may be immersed in acetone for 10 s to 15 s, whereas thin tape may be wetted by a few drops from an eye drop applicator. The specimen surface may also be wetted by acetone, although that step is not always necessary. The tacky film or tape is applied to one side of the fracture surface and then is gradually brought into contact with the remainder. The replica material should be applied so as not to entrap any air. Pressure is applied to the replica for 15 s up to two or three minutes as required, taking care to not slide or shift the replica material. A small pad (or if the specimen is small enough, a finger or thumb) may be used to apply the pressure. If a finger is used, a folded tissue or small pad between the finger and the tape should be used so that one's fingerprints do not get superimposed on the back side of the replica tape! The pressure is carefully removed without disturbing the replica which remains in contact with the fracture surface for 10 min to 15 min more drying time. The replica is peeled from the fracture surface (or it may pop off) and may be trimmed with scissors or mounted on a glass microscope slide such as shown in Figure 3.35.

Cellulose acetate replicas may be viewed with reflected or transmitted illumination in an optical microscope. An interesting advantage of a replica over an original surface is that even if the original surface is curved, the replica can be flattened out and examined in a compound optical microscope at greater magnifications (in either reflected or transmitted light mode) than if the replica were only examined with a stereo microscope. Gold or carbon coatings can be sputtered onto negative replicas to enhance viewing in reflected light or to prepare the replica for SEM examination.

Since "reversed" replicas like the cellulose acetate tapes are flipped versions of the fracture surface, it is prudent to label them clearly as to their location on the component, lest the fractographer confuse top-bottom, or left-right orientations. Special care should be taken to avoid artifacts in the replicas such as trapped air pockets, tears, or handling artifacts. Replicas should be kept clean and carefully stored in containers.

If it is possible to warm a specimen, then negative replicas made with the thermoplastic compound polyvinyl chloride (PVC) (180 ^{o}C) or, alternatively, silicon elastomers may also be used (100 ^{o}C).[4] If PVC is used, the specimen is heated and the PVC applied with a Teflon rod.

Positive replicas may be made with filled silicone rubbers, unfilled (transparent silicone rubber, and polyvinylsiloxane (PVS).[1,2,3] The latter material is commonly used in dentistry to make impressions in patient's mouths as shown

(a)

(b)

Figure 3.36 *Dental replica equipment. (a) shows a typical PVS applicator gun which has interchangeable tips and compounds. (b) shows Dr. S. Scherrer demonstrating the technique in a dental materials fractography class.*

in Figures 3.36 and 3.37. Extraction of a damaged dental crown from the mouth typically requires its destruction. Therefore, it is prudent to make a replica before the crown is extracted as discussed by Scherrer *et al* [3] and shown in Figure 3.37. Sometimes just one PVS compound is adequate, but in other cases it is optimal to use two PVS compounds. The first is a very fluid PVS that can retain very fine detail (e.g., Ultra-Light Body) when applied to the fractured part. Once it sets, a second PVS that is a fast setter is applied over the first layer. It is used to build up a larger, more handleable mold.

Once the mold has set, an epoxy resin may be poured into it to make the positive replica. One interesting advantage of this procedure is that the mold

(a) Top view of the fractured all-ceramic alumina crown (first upper left molar) in the patient's mouth. The broken crown is cleaned with alcohol on a cotton swab.

(b) The crown is water spray rinsed and air dried.

(c) A light body precision impression material is injected around the fracture surface.

(d) The whole crown is covered with more impression material.

(e) The mold is removed.

(f) A positive replica is cast with epoxy resin. It is then gold coated for SEM examination.

Figure 3.37 *Steps in the preparation of a dental replica that is a positive duplicate of a fractured alumina crown. Photos a-d were taken in the patient's mouth. (Photos and technique courtesy of S. Scherrer, Univ. Geneva)*

can be reused to make multiple epoxy replicas. They are useful as teaching aids since every student examines the same object with the same features. Gold or carbon coatings can be sputtered onto positive replicas to enhance viewing in reflected light or to prepare the replica for SEM examination.

Figure 3.38 shows a broken whiteware plate. Both cellulose acetate and PVS replicas were made for comparison as shown in (a). Closeups of the positive epoxy replicas of the origin area that were made by the PVS mold are shown in (b – d). The image in (d) could have even been sharper and clearer if the colorless epoxy had been gold coated.

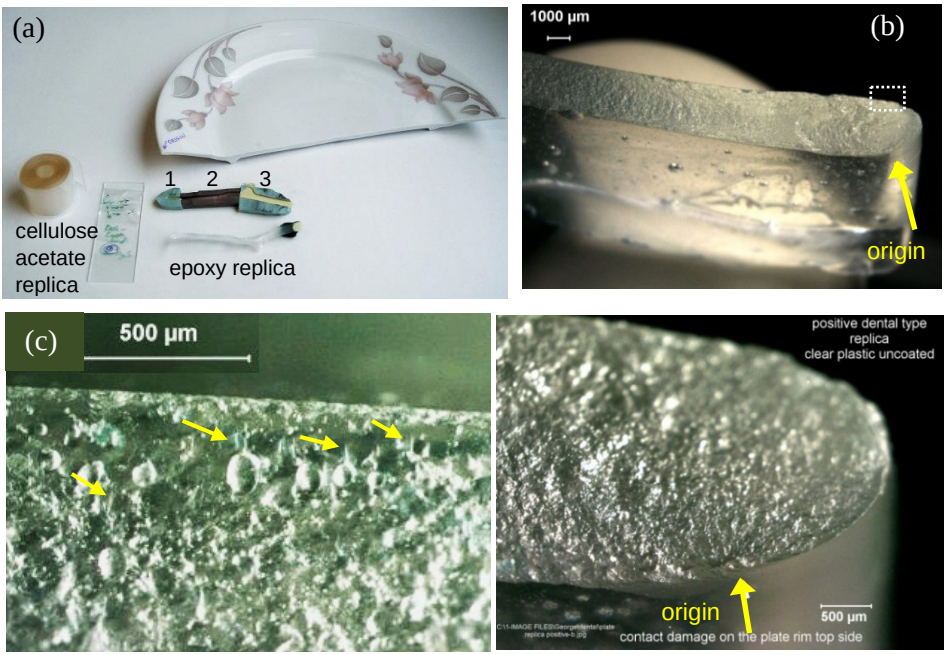

Figure 3.38 *Replicas of a broken whiteware plate. (a) shows both a cellulose acetate tape negative replica on the left, and a dental PVS mold and epoxy positive replica on the right. The PVS mold was cut into 3 pieces (labeled 1,2,3). The middle one was gold coated for easier examination. (b) shows the cast epoxy resin positive made from mold piece #1 from the plate rim area. (c) is a close-up of the boxed region shown in (b). Tiny wake hackle lines (yellow arrows) in (c) in the glaze are little "weathervanes" that are more easily seen in the glaze than in the whiteware body. They help direct one's attention back to an origin area that is <u>on the opposite surface</u> shown in (d). Coarse hackle lines (chapter 5) in (d) also lead back to the origin which is a contact damage crack on the rim marked by the arrow.*

Sections on replication techniques are in both the Visual Examination and Light Microscopy and the Transmission Electron Microscopy (TEM) chapters in the ASM Handbook on Fractography.[7]

In general, some practice is needed to create successful replicas with good detail and without artifacts. Before a critical component is replicated, it is prudent to practice with the materials to optimize one's techniques.

Figure 3.39 *A conventional 1980s – 1990s model scanning electron microscope. Figure 3.40 shows the same instrument.*

3.13 Scanning Electron Microscope (SEM)

Despite the versatility of optical microscopy, there inevitably will be cases where the fracture initiating flaw is too small to be clearly discerned and the scanning electron microscope (SEM) is required (Figure 3.39). The SEM is a *complementary tool* to the optical microscope. They "see things" differently. The optical microscope has a resolving power that is limited to about half the wavelength of visible light, that is, about 0.2 um under ideal conditions.[4] Even so, it is best to examine specimens with the optical microscope first, since much valuable information such as color, reflectivity, subsurface flaws in translucent or transparent materials, Wallner lines and scarps *cannot be*

detected by the SEM. Nevertheless, the SEM is a versatile tool that can view large portions of a specimen at low magnifications and yet instantly zoom in for high-resolution close-ups of regions of interest. It can also provide compositional information. The usual range of magnifications for fractographic analysis are of the order of 10X to 20,000X, but sometimes greater magnifications are necessary.

A basic scanning electron microscope and how it functions is described first. Special versions of electron microscopes including modern table top models are described later in this chapter. Modern SEMs are not difficult to use and materials scientists and engineers can perform their own routine examinations without the need of an expert operator. The advent of commercial SEMs and transmission electron microscopes in the 1960s led to a quantum jump in the quality of fractography of ceramics and glasses. Researchers and engineers could finally see and characterize the strength-limiting flaws that previously were too small to be clearly discerned with optical microscopy. It is fair to say that the SEM opened up a whole new world of possibilities for fractographers, processors, and mechanical testers and led to many major advances in materials science and engineering.[f]

The SEM uses electrons as a signal source and, since the probe size can be made smaller than the wavelength of light, smaller features can be resolved and much greater magnifications achieved. A vacuum is necessary to remove gas that would interfere with the electron beam. The SEM has superb depth of field over a broad magnification range. For a working distance of 20 mm, the depth of field may be 0.4 mm at 100X or 40 μm at 1000X and 4 μm at 10,000X.[8] Sometimes the SEM is preferred for this reason at even low magnifications (100X to 500X) that are well within the range of optical microscopes. On the other hand, SEM images often look flat and tend to deemphasize large surface topography changes. The SEM image can also be deceptive and it may be confusing to interpret whether a feature projects above the surface or is a depression below the surface. Stereo SEM viewing, described below, can help solve this dilemma. A great advantage of the SEM is that compositional analysis can also be done using accessories that detect X-rays emitted from the fracture surface.

Specimens must fit into the vacuum chamber and are usually cut and mounted on a small aluminum stub that will be placed into the SEM as shown in Figure 3.40. The SEM should have a large opening to accommodate broken fragments and test specimens without having to cut or trim them to small sizes.

---

[f] The coincidental advent of modern fracture mechanics in the late 1950s, described in chapter 7, also led to major breakthroughs in the study of ceramics and glasses.

The stage has external controls that permit the specimen to be positioned in X, Y, and Z directions, rotated, and tilted. The size of the chamber and the mount station, plus the clearance to the electron optics all put limits on the size of specimens than can be examined. A good SEM for fractography has a large chamber, a large entry port, and can pump down with a minimum of difficulty.

Specimens on an aluminum stub are shown in Figure 3.40b and 3.41. It is convenient to cut the specimens so that they will sit square and facing upward. Irregular specimens can be propped up by small metallic pieces. If multiple specimens are to be examined in one session, it is best to cut them to similar lengths to minimize refocusing time in the SEM. A small laboratory cut off wheel with a thin diamond wafering saw is also handy for cutting long specimens into manageable lengths for the SEM. The specimens should be cut so that the fracture surface is approximately perpendicular to the incident beam in order to avoid distortions from foreshortening. Once in the SEM, the specimen can be tilted to enhance the emissions and signal responses if necessary.

Figure 3.42 shows some common accessories and tools for SEM examination. The specimens must be cleaned carefully of greases, dust, or debris. It can be exasperating to find a tiny piece of dust right on top of the origin site when the specimen is in the chamber. Soaking the specimen in a small beaker of acetone in an ultrasonic bath for a minute or so is often effective. After removal, a

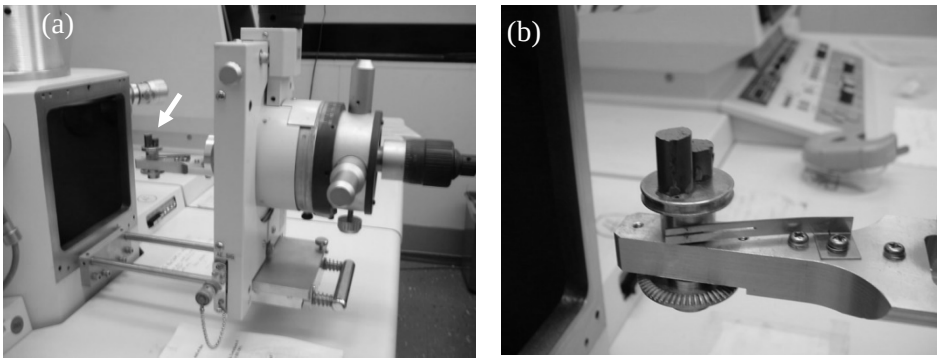

Figure 3.40 *(a) shows an open SEM vacuum chamber showing the specimen station on the left (arrow) and the positioning controls on the right, outside of the chamber. (b) shows a close up of the two fracture specimens on their stub on the examination mount. Both fragments had to be cut from longer pieces to fit in the chamber. This model has a large opening and the stage can accommodate specimens as tall as 25 mm. With some modifications it was possible to insert an entire 150 mm diameter grinding wheel into the chamber and image the diamond abrasive particles.*

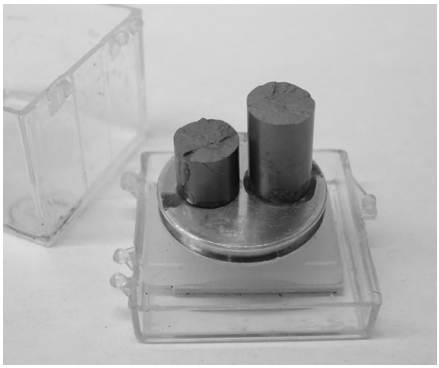

Figure 3.41 *Two matching fracture halves of a broken round tension specimen on a stub in a protective plastic box. Silver paint was used to attach the specimens to the stub. Ideally, the halves should have been cut to similar lengths to save time refocusing in the SEM.*

Figure 3.42 *SEM specimen preparation tools. Clockwise from the top left are two SEM length calibration standards, two silver paint bottles, a double-sided conductive adhesive tape roll, two sheets of double-sided conductive adhesive disks, and an assortment of aluminum stubs.*

gentle blast of compressed air can eliminate any acetone residue. Sometimes it may be sufficient to swipe the fracture surface with a cotton swab soaked in acetone. Small trays or plastic boxes are convenient for holding the specimens and protecting them from contamination prior to examination. Special containers are available for mounting stubs. The best procedure is to keep the

specimens as clean as possible from the moment the fragments are recovered. There may be times when gloves should be used, but author rarely uses them.

There must be a good electrical contact between the specimen and the stub. The specimen can be affixed to the stub by silver paint or by conductive carbon double-sided sticky tape. Sometimes it may be convenient to use a special holder, e.g., a slotted stub to hold multiple bend bar fragments. Sometimes a specimen can be propped up on the stub with a metallic bolt or nut that is also taped to the stub. These steps are prudent if the stage will be tilted in the SEM. If multiple specimens are placed on a stub, it *is a good idea to make a hand drawn sketch or map to show which specimen is where on the stub,* lest the viewer become confused when viewing the array in the SEM. Furthermore, *all the specimens should be oriented in a similar way*. For example, if a series of bend bar fracture surfaces are being examined, they all should have their tensile surfaces facing the same way. Otherwise, much time can be lost getting oriented or searching the wrong areas during the SEM session. A set of optical photos of the fracture surfaces can be handy when the specimens are examined in the SEM.

The next step for most SEM examinations is to apply a thin 5 nm to 40 nm conductive gold, gold-palladium, or carbon coating by means of a sputter coater shown in Figure 3.43 or a thermal evaporator. The former is preferred for rough surfaces. The coatings are needed for ceramics and glasses in order to eliminate surface charge build up from the electron bombardment. For most applications, the coating does not interfere with the image. A coating is not needed for conductive ceramics or for examinations with low accelerating voltages (1 keV to 5 keV). Low accelerating voltage examinations may have a

Figure 3.43 *A gold sputter coater used to apply a conductive coating. Coatings are helpful for both optical and scanning electron microscopy.*

diminished resolution, however. Carbon coatings are used if X-ray information of lighter atomic weight elements is desired. Coating with gold or carbon is a simple procedure that only takes a few minutes. Sometimes a gold coating may be applied to facilitate some *optical microscopy*. The coating reflects light that would otherwise pass through a fracture surface in translucent or transparent specimens (see Section 3.9 on coatings).

The sputter coater will preferentially coat from one direction, and sometimes it is advantageous to position the specimen and the stub at an angle so that shadow coating will occur on the surface. Slight charging on some edges of the fracture surface may enhance the image by promoting contrast. Coating along the specimen sides may be incomplete, so sometimes it is wise to add a thin silver paint line along the specimen sides from the fracture surface to the stub. Of course, the silver paint should be kept well away from the fracture origin or any features of interest on the fracture surface. The conductive coating step may be omitted for some modern SEMs that operate at low accelerating voltages and low vacuums as described in a later section on environmental SEMs. Additional details and tips on coatings for SEM examination may be found in the paper by Healy and Mecholsky.[9]

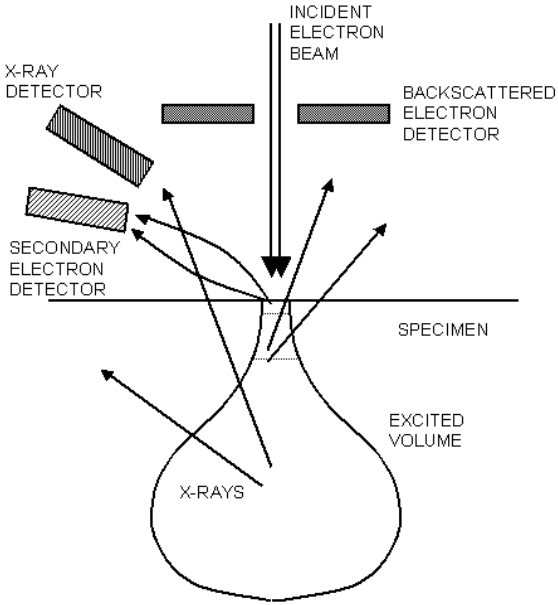

Figure 3.44 *The electron beam interacts with the specimen surface and volume creating emissions that may be analyzed. Signals are generated in all directions, but they come from different depths of the material. The beam is rastered over the surface and an image is sequentially formed.*

The SEM can be operated in several modes. A focused beam of high-energy electrons (typically 1 keV to 30 keV) is rastered over a rectangular portion of the specimen. Some electrons interact with the specimen surface and some penetrate into the volume. Figure 3.44 shows that the interaction volume is larger than the size of the incident beam, which may be as small as 10 nm diameter.[10] The three most important signals are secondary electrons, backscattered electrons, and X-rays. Secondary electrons reveal the surface topography. Backscattered electrons give a combination of the topography and atomic number and crystallographic information. X-rays reveal compositional information.

The initial working distance can be adjusted to enhance the field of view and the depth of field. Long working distances allow a lower minimum magnification which is sometimes helpful in initial orientation or in photographing the whole part or as much as possible. A longer working distance also allows the specimen to be tilted more. On the other hand, longer working distances reduce resolution and may reduce X-ray signal acquisition. Image clarity is also affected by specimen tilt. As noted above, having the surface perpendicular to the incident beam minimizes foreshortening, but secondary electron and X-ray collection can be maximized by tilting the specimen towards the detectors.

The secondary electron mode of operation provides the best spatial resolution and produces a surface topographical image. Secondary electrons are low energy electrons (10 eV to 50 eV) primarily produced from the material close to the surface. Since they are low energy, a positively charged detector off to one side can capture the emitted electrons for the image. These electrons may even follow a curved trajectory from the surface to the detector. Edge charging can be a problem with very rough surfaces or those with sharp corners and cracks, in which case gamma adjustments to the image may help. Gamma adjustments can suppress bright areas and enhance dark areas. For some edge charging cases, backscattered imaging may be preferred.

Backscattered electrons are higher energy electrons (5 keV to 40 keV), up to the energy of the incident beam and are emitted from a larger volume than the secondary electrons. The backscattered electrons travel in straight lines and are registered by a different detector that may have to be slid into proximity with the fracture surface. They often have a central hole for the incident electron beam. Backscattered electrons include both topographical and compositional responses. Detectors can be split ring or four quadrant (or more) versions and, by turning different elements on or off in the detector, it is possible to emphasize topographical or compositional information. Backscattered electron

imaging is effective in detecting phase distributions in heterogeneous or composite microstructures and also aberrant features such as inclusions or second phase concentrations. Such information is often completely missed by secondary electron imaging.

Figures 3.45 through 3.48 show matching secondary electron and backscattered electron images of fracture origins. Figure 3.45 shows how the backscatter mode can even help highlight a controlled flaw made by a Knoop indenter.

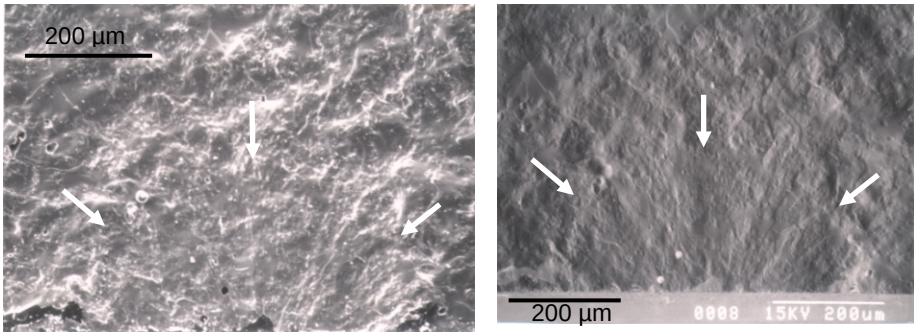

(a) (b)

Figure 3.45 *Comparative secondary electron (a) and backscattered electron (b) images of the fracture surface of a Knoop semi-elliptical precrack in a silicon nitride fracture toughness test specimen. The edge charging in (a) emphasizes certain features, but (b) shows that the flattening effect of the backscattering mode tends to better reveal the overall crack (arrows).*

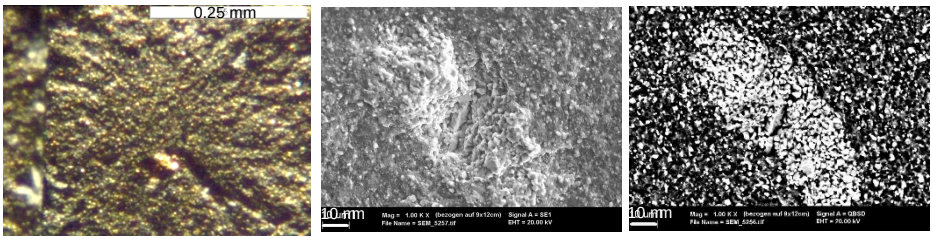

(a) (b) (c)

Figure 3.46 *Backscattered mode electron scanning electron microscopy is effective in showing compositional difference of fracture origins flaws relative to the background. (a) is an optical image of a silicon nitride with 30 mass % TiN bend bar illustrating the origin has a gold color (722 MPa). (b) is an SEM secondary electron image of the origin. (c) is a backscattered electron image of the flaw. This origin may be termed either a TiN agglomerate or a compositional inhomogeneity. (Courtesy J. Kübler, EMPA).*

X-ray emissions provide valuable information about the elemental composition. This energy-dispersive spectroscopy by X-ray analysis (EDS or EDX) is especially useful for detecting and characterizing inclusions, second phase variations, or compositional inhomogeneities, which all may act as strength-limiting flaws. The analysis is over a region of the order of size of a few micrometers, but penetrates into the interior 1 mm to 2 mm. With most SEMs and with coated surfaces, elements from sodium (Z = 11) or heavier can be detected simultaneously. A better resolution of the lighter elements is obtained with very thin gold or carbon coatings, or even uncoated specimens with low accelerating voltage. Newer detectors and vacuum-tight polymer windows allow lighter elements including boron, carbon, nitrogen and fluorine to be detected.[11] Modern SEM machines can rapidly EDX scan the surface and make chemical element maps of a fracture surface. Modern machines also do not require liquid nitrogen cooling of the EDX detectors.

(a)

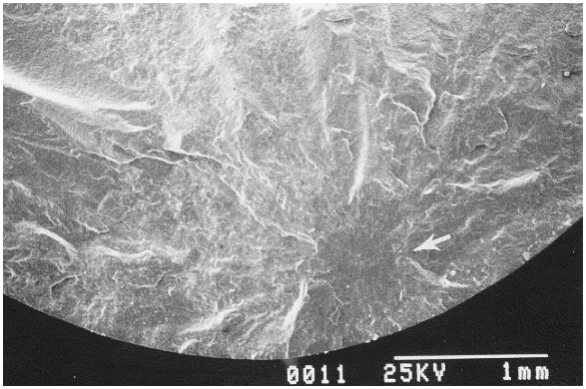

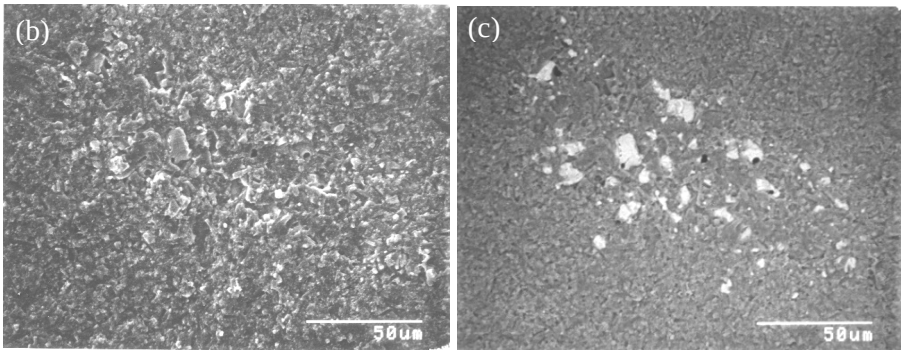

Figure 3.47 *A cluster of iron particles acting as an origin in a silicon nitride rod broken in flexure. The origin is below the surface. The stress at the origin was 682 MPa. (a) and (b) show secondary electron images and (c) is the backscattered image at the same magnification as (b).*

An X-ray scan may require several minutes as the electron beam illuminates the surface and the detector accumulates a sufficient signal of a range of emitted X-rays. A typical scan appears as shown in Figure 3.48c where signal intensity is plotted versus X-ray energy or wavelength. The specimen response is compared to known characteristic wavelengths of the various elements to identify which elements are present. A common procedure is to scan the critical feature, then rescan a different area away from the feature and compare the patterns. The accelerating voltages should be high enough to activate emissions from the elements. This should be 1.5 times the threshold energy of the element. For example, to detect copper which has Ka X-rays of 8.0 keV, it is best to use an accelerating voltage of 12 keV or greater. Otherwise, if the voltage is too low, then the X-rays will not be emitted or detected, even if copper is present.[12] Similarly, for zirconium, which has Ka X-rays of 15.7 keV, it is best to use an accelerating voltage of 25 keV or greater.

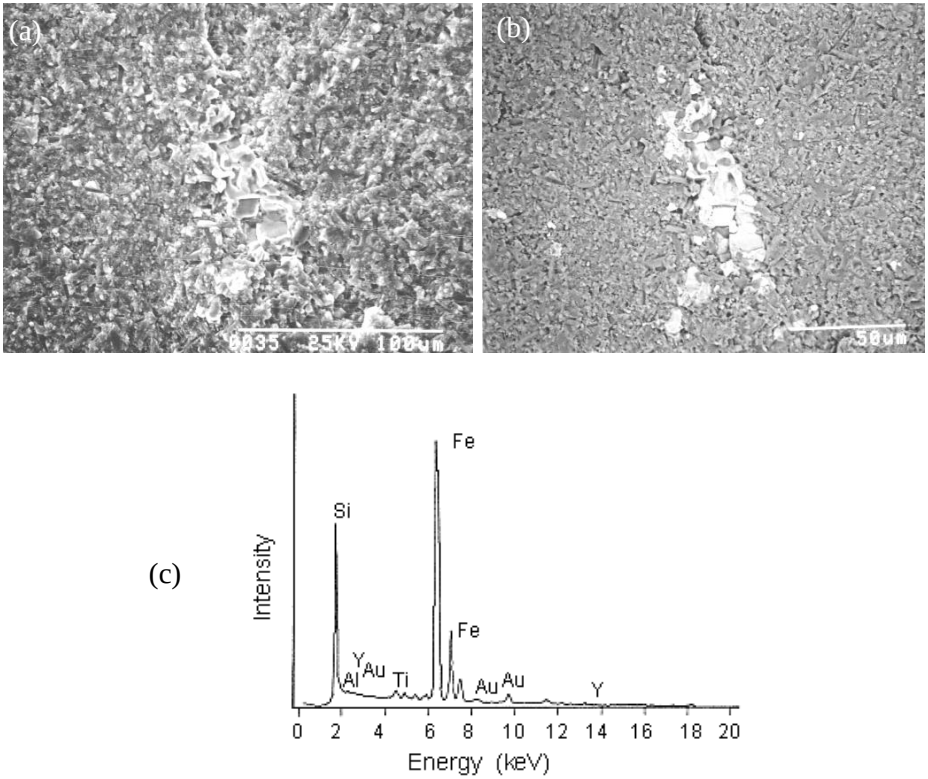

Figure 3.48 *An iron inclusion in a silicon nitride rod broken in tension (684 MPa). Matching secondary electron (a) and backscattered electron images (b). (c) is the EDX pattern of the inclusion revealing it is iron.*

Figures 3.48a,b shows matching secondary electron and backscattered electron images of an inclusion in a silicon nitride tension specimen. Figure 3.48(c) shows the EDX analysis from a close-up view of the inclusion. In this case the iron peak stands out prominently. At other times, the inclusion peaks may appear only as a small fraction of the intensity of the primary constituent (Si in this case) due to the averaging effect of the area being imaged. Several peaks at different energies and intensities characterize each element. Sometimes these will overlap with peaks from other elements confusing the interpretation. Gold or palladium peaks from the coating may also be present. EDX analysis is usually semi quantitative, and even under the most ideal conditions, the mass fraction concentration is only precise and accurate to ± 1%.[13] The minimum concentrations that can be detected are 0.5 to 1.0 mass fraction % under ideal conditions, but more typically is several mass fraction % or more.

X-ray compositional maps, tailored to a particular element, may be made of the region being examined. The areas that contain the element in question emit X-rays and create bright spots on the map, whereas regions without the element appear dark. Digital image maps may be constructed with false colors representing areas of similar composition.

Colorization of SEM fracture surface images can be done with commercial software. Currently it must be done manually by adjusting grey scale settings,

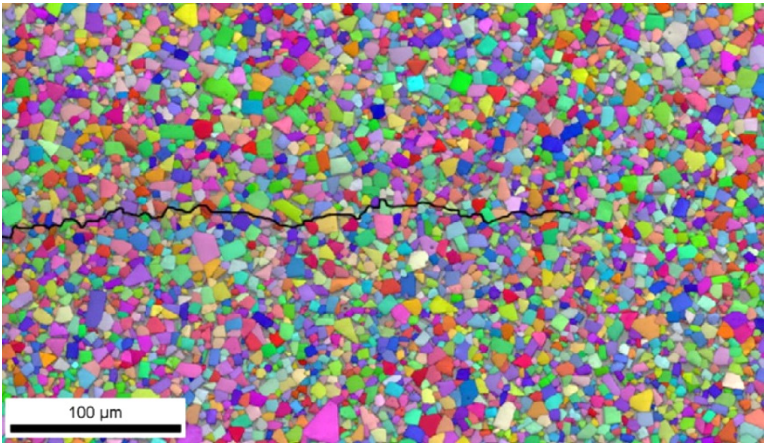

Figure 3.49 *Electron backscatter diffraction map of the flat exterior surface of a WC/11 mass % Co fracture toughness test specimen. Individual grains with different crystallographic orientations are shown in color. A black crack propagated through the microstructure under static loading and was mixed inter- and transgranular, with the latter crossing through the grains on* $[10\bar{1}0]$ *slip planes. (Courtesy R. Morrell and K. Mingard, NPL, ref. 15.)*

or alternatively by manually highlighting areas for color adjustments, aided by automatic grain or feature recognition. A useful article by Caja and Diego[14] compares colorized images made by Adobe Photoshop, Mountain, and ImageJ software packages. Their article discusses the pros and cons and ease of usage of software packages.

Electron backscatter diffraction (EBSD) is a valuable tool for studying microstructures and can discern the variation of crystallographic orientation of individual grains, but it requires a flat specimen surface. Figure 3.49 is an example of the exterior surface of a fracture toughness test specimen. [15] A focused electron beam is scanned across a crystalline material and at each point an electron diffraction pattern is created and analyzed. At the present time EBSD is not amenable to analysis of rough fracture surfaces.

Magnifications displayed on the SEM monitor (e.g., 1,000X) may not be accurate. Brooks and McGill state that accuracies of 5 % are typical.[13] The superimposed micrometer bars on the photos or images are usually better than a nominal magnification, but are not necessarily exact either. If quantitative measurements are made with the SEM, then care should be taken to ensure the fracture surface is not foreshortened. An SEM length calibration standard such as shown in Figure 3.50 should be used to check the magnifications. Some older SEMs have magnifications that vary across the field of view and which are not the same vertically and horizontally.

A paper by Healey and Mecholsky on SEM techniques and their application to brittle materials is very instructive.[9] An excellent, detailed article on the use of the SEM for fractography is by Brooks and McGill.[13]

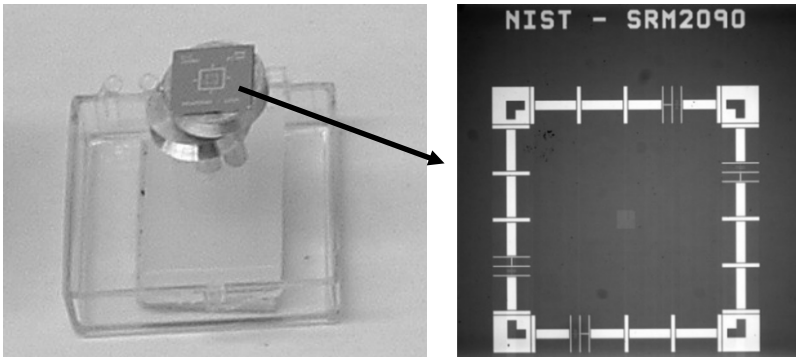

Figure 3.50 *A NIST Standard Reference Material 2090 SEM length calibration standard. Finely spaced reference lines are located at intervals along the sides of the box on the right close-up view.*

Table-top scanning electron microscopes recently have become available that are suitable for fractographic analysis. Some have large working chambers with good specimen height flexibility. The one shown in Figure 3.51 has a motorized specimen positioning stage and an internal optical camera that facilitates locating the specimen to be examined. It is capable of 80X to 100,000X magnifications. It has secondary electron and backscattered electron detectors and an EDX detector that does not need liquid nitrogen cooling.

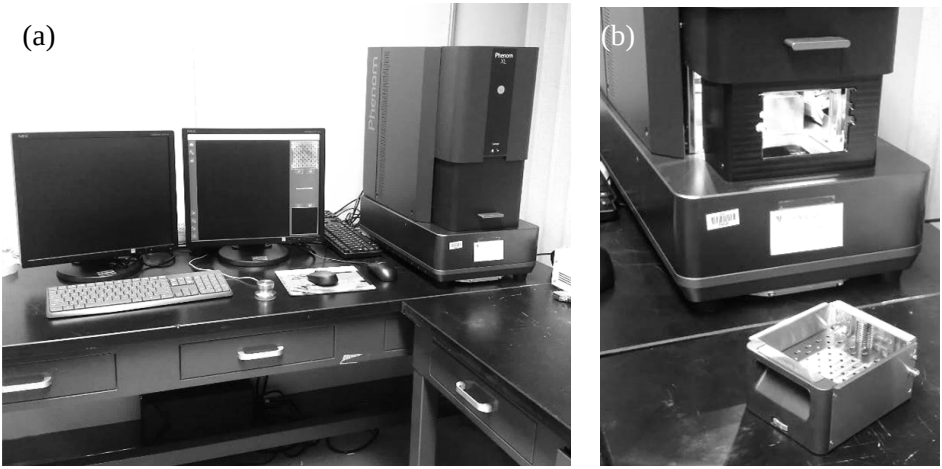

Figure 3.51 Tabletop scanning electron microscope. (a) shows one sitting on a common laboratory table. (b) shows it with the chamber open and the specimen holder assembly removed.

3.14 Stereo SEM Imaging

The SEM takes pictures that make the surface look flat and do not show the topography clearly. A much better sense of the full topography can be revealed by the simple process of taking matching stereo photographs. Two photos of the same area are taken, but with the specimen tilted 5º to 15º in the SEM chamber between shots. A minor adjustment to the brightness and contrast may be necessary for the second photo, but is not essential. Some people are able to hold the two images in front of their eyes and focus the left eye on the left photo and the right eye on the right photo. The distance between the photos is adjusted and the eyes are “relaxed.” The brain merges the images and interprets them as a single three-dimensional view. Most people find it easier to put the images under a **stereoscope,** which is a stereo viewing optical device shown in Figure 3.52. The fractographer looks into two eyepieces and the

photos are spaced apart and adjusted slightly back and forth until the three-dimensional effect is achieved. It may take a little practice to get the two images to register, but the usual trick is to focus each eye on an identical spot in the two photos. Initially the two eyes will discern the spot as two separate spots, but by carefully sliding one or the other photos around, the spots can be made to merge. At that instant the three-dimensional effect should be detected since each eye will be viewing the same surface, but from different angular perspectives. This may take a little practice, but the viewer helps make it easy for most people. One curious effect is that the perception of what features

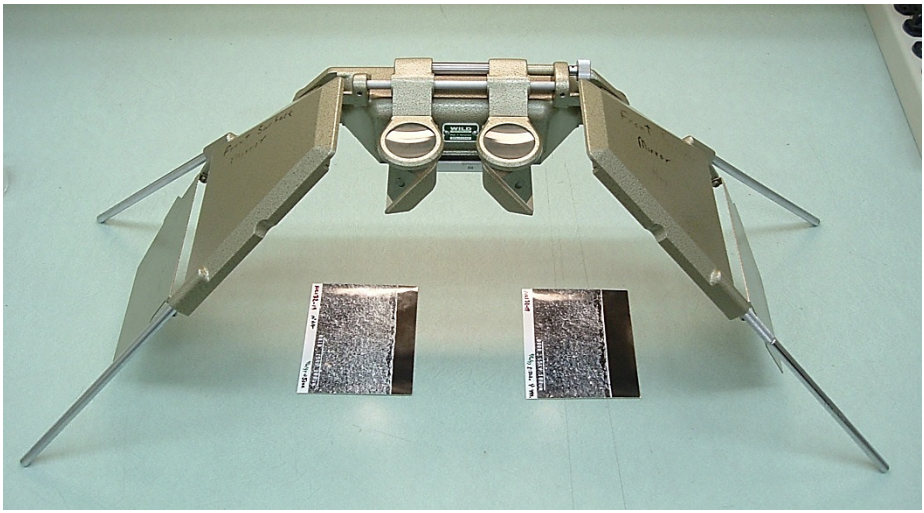

Figure 3.52 *Stereoscope. The two photos are placed under the viewer and the viewer looks into the two eyepieces. The photos are moved around slightly until they appear as one image in three dimensions.*

are up or down may change depending upon which photo is on the left and which is on the right. It may be necessary to swap the photos to get the correct rendition. The orientation of the photos may have to be turned 90º as well in order to match the tilt angle used in the SEM. Photos taken with optical microscopes may also be put in a stereoscope to get a 3-D perspective.

Some modern SEMs can digitally capture the pair or of tilted images, or even three images at different tilts. Image analysis software can then interpret the multiple images and constructs a pseudo three-dimensional rendition that is displayed on a monitor. The computer image can be rotated or displayed from different vantage points and height profiles through various sections can be displayed. Quantitative analysis may be done by a procedure known as stereophotogrammetry. A few applications to ceramics so far were hampered

by contrast limitations[16] or lack of computing power,[17] but the latter problem probably is less of a concern now.

3.15 Field Emission SEM (FESEM)

The FESEM offers dramatic increases in magnifications (600,000X) compared to the SEM and improved resolutions down to 1 nm (Figure 3.53). They rival the resolution and contrast of many transmission electron microscopes. The field emission cathode replaces conventional tungsten cathodes on the common SEM. A smaller probe beam is used. Accelerating voltages are lower and conductive coatings are not needed in many cases. Energy dispersive X-ray spectroscopy (EDX) can be applied to smaller regions than in a conventional

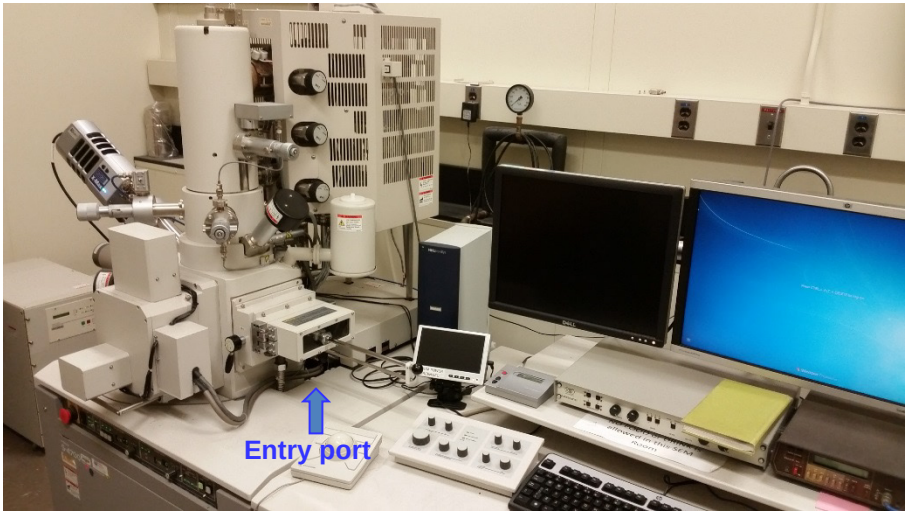

Figure 3.53 *A field emission scanning electron microscope.*

SEM. The FESEM is used much the same way that a conventional SEM is used for fractographic analyses. One problem with such microscopes is that the working distances and the pre-evacuation chambers are very small and it may not be possible to get large pieces into the microscope. The author used such a FESEM to take Figures 6.93 and 8.24 which show origin flaws in single-crystal silicon as small as 50 nm to 200 nm, possibly the smallest fracture origin flaws ever detected.[18]

3.16 Environmental Scanning Electron Microscope (ESEM)

The ESEM is designed to operate either in a high or low vacuum unlike conventional scanning electron microscopes, which require a high vacuum.

Low accelerating voltages can be used however this may hamper or even preclude EDX analysis. Insufficient energy may be imparted to the material to stimulate x-ray emissions from some elements as discussed on page 3-52. The environmental SEM can operate with environments having water vapor or other gases. A specimen coating is not needed, as static charges do not develop on the specimen since the gasses ionize and can neutralize excess electron charge build up on the specimen. Magnifications up to 100,000 are possible, but resolutions are less than that from a conventional SEM. One advantage of the ESEM is that dynamic processes such as corrosion or chemical reactions can be studied by time-lapse imaging. The ESEM is primarily used for biological materials or with materials when it is undesirable to apply a coating.

3.17 Transmission Electron Microscope (TEM)

The TEM is capable of extraordinarily high magnifications and high resolutions (< 0.1 nm). It is limited to specimens about 0.5 mm or less in thickness, however. The TEM can reveal critical microstructural details. Prior to the advent of modern scanning electron microscopy, TEM was applied to replicas of fracture surfaces in order to study the fracture morphology. Today, the TEM is not used for routine fractographic analysis, but is a critical tool for research projects studying the effect of microstructure on properties. It can reveal crucial information about defect densities in grains, grain boundary sliding, cavitation, twin formation, damage accumulation, phase changes, fracture mode (intergranular or transgranular), and grain boundary phases and their thickness. TEM specimens are cut from the bulk and then electro-chemically or ion milled to very thin foils that are transparent to electrons. Alternatively, carbon replicas may be made for examination. Since the TEM examines only tiny portions of the material, it is almost never used to find and characterize fracture origins or classical fracture surface markings.

3.18 Atomic Force Microscope (AFM)

The AFM is a powerful microscope that uses a tiny tip (radius about 2 nm to 20 nm) at the end of a cantilever to probe the surface. The tip is brought into close proximity to the sample surface and either gently contacts the surface or taps it while the tip is oscillated close to the cantilever's resonant frequency. The probe is held at a fixed location in the X-Y plane and the surface to be examined is rastered in the X-Y plane. The Z-deflection of the cantilever is magnified by a laser beam that reflects off the cantilever into a position sensitive photo detector or interferometer. A computer records the X, Y, and Z displacements and a three-dimensional image of the surface can be constructed. The AFM is capable of extremely fine resolution (10 pm) and does not require

any special specimen preparation or testing environment, but the specimen must be very nearly flat and has to be mounted flat on a holder. The AFM is most frequently used in microelectronic and biological studies. It has been applied to the study of fatigue crack markings in metals and fracture mirror roughness measurements in glasses. There are limitations to the AFM. The scanned area is usually quite small. Depending upon the resolution it can be as small as 1 mm square to as large as 150 mm square. The vertical surface features can only be a few micrometers in size. Acquisition times may be long. Color and reflectivity information are lost. Therefore, the AFM is almost never used to search for fracture origins or other telltale fracture markings, but instead is used for very close up, high-resolution examination of surface roughness detail or coating evaluations. Hull used it to study mist and hackle lines in brittle epoxies.[8]

3.19 Optical Profilometer

Optical profilometers are designed to make non-contact three-dimensional surface roughness measurements from 0.1 nm to several millimeters. The sub nanometer resolution for an optical system with white light illumination source (halogen bulb) may seem surprising, but interferometry allows the small height variations to be resolved. Optical profilometers either translate the specimen vertically or, if the specimen is tilted slightly, laterally in front of an interferometer. Reflected light from the specimen and a reference surface are combined to form fringes that are projected onto a digital camera. Height variations are denoted by color and contrast differences in a computer-

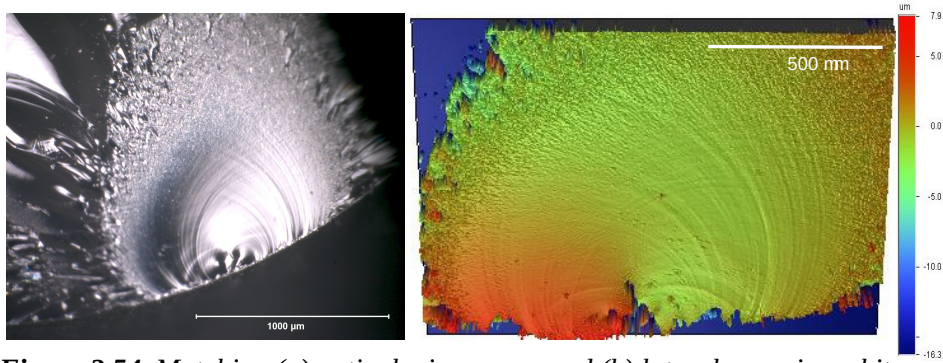

Figure 3.54 *Matching (a) optical microscope and (b) lateral scanning white light interferometer (optical profilometer) images of a fracture mirror in a ground glass rod. (b) is an area 1.0 mm tall x 1.3 mm wide. The colors correspond to the scale range shown on the right (+7.9 mm to -16.3 mm). Wallner lines and mirror mist are readily detected and displayed. The origin is a surface crack from a scratch at the bottom middle. (b courtesy of R. Gates)*

generated image as shown in Figure 3.54. One advantage of the optical profilometer is that precise height and roughness variations are quantitatively recorded and can be interpreted by the program software.

3.20 Confocal Scanning Light Microscope

This is a variant of an optical microscope. Rather than broadly illuminate a fracture surface, a point source of light (often from a laser) is scanned over the surface and reflected into the microscope through a pinhole aperture. A lens with a large numerical aperture is used and on uneven surfaces only a small portion of the surface will be in focus. A photo-multiplier tube records the strong return signal from the in-focus regions. Optical slices of in-focus surface are registered and recorded by a computer as the focus is finely adjusted. The final product is a computer generated three-dimensional topographic map of the specimen surface, often in false color corresponding to the surface heights. Figure 3.55 shows an example for a glass fracture mirror.

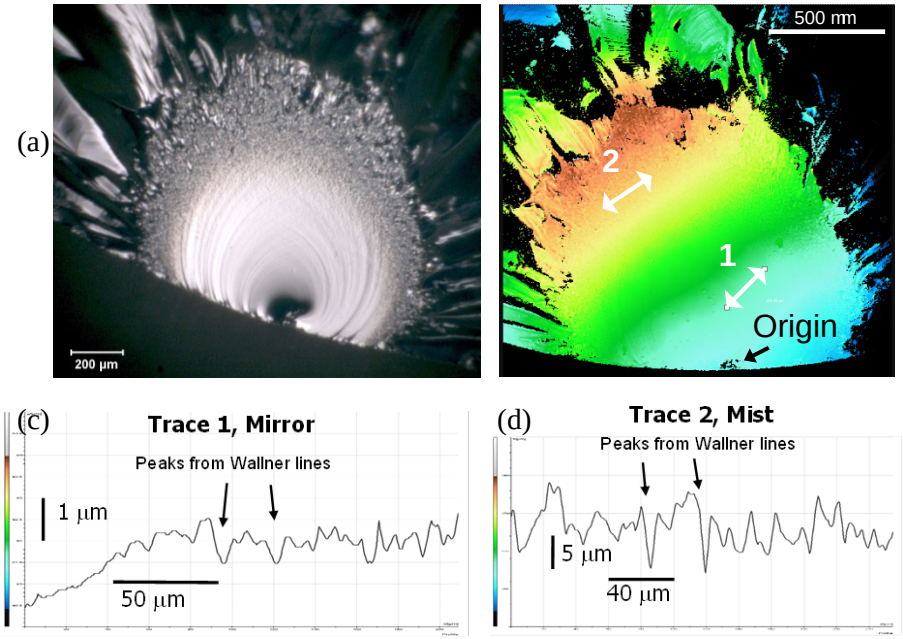

Figure 3.55 *Matching stereo optical (a) and confocal microscope (b) images of a glass rod fracture mirror. Height profiles for tracks 1 and 2 are shown in (c) and (d). The major peaks are from Wallner lines. The minor peaks show the inherent roughness in the mirror and mist regions. (b) and traces are courtesy of J. López-Cepero Borrego and A. Ramirez de Arellano Lopez, Univ. Seville.)*

Resolutions are of the order of 0.25 mm or greater. The primary virtue of the confocal microscope is that in-focus images can be collected that would not otherwise be possible due to the limited depth of field of the light microscope. Quantitative information about height differentials can also be recorded. Confocal microscopes usually have longer image acquisition times than common optical microscopes with cameras, although some contemporary models can acquire and display images in as fast as 1/30th s which is suitable for video rate imaging. A full topographical characterization can require 10 s or more. Some fracture surfaces are difficult to view with a confocal microscope. Carbon and graphite surfaces reflect very little light back up to the lens. Single crystals can act as specular mirrors and reflect light away from the lens. Diffuse reflection may be enhanced by application of a coating in such cases.

3.21 Stress Wave and Ultrasonic Fractography

Ultrasonic or stress wave fractography is an effective fractographic tool in the laboratory that was pioneered by Kerkhof.[19,20] A transducer attached to the specimen creates continuous elastic waves at a specific frequency. The elastic waves create ripples (tertiary Wallner lines) on the fracture surface as shown in Figure 3.56. Local crack velocity can be simply calculated on the basis of the spacing between the lines and the pulse frequency. Richter and Kerhof [20] used 5 MHz lead zirconium titanate (PZT) transducers to measure cracks running at terminal velocities in glass. Their review article has a wealth of additional details about this method and many fascinating examples of its use. Additional examples of their work are in section 5.4.4 on tertiary Wallner lines. Tsirk improvised[21] with a simple hand-held woodworking palm sander that vibrated in a circular motion at 11,000 rpm (183 Hz) and was able to create makings on the fracture surfaces of obsidian pieces that he was knapping. Figures 5.56 b-d in chapter 5 show his images. Michalske and Fréchette showed how refinements to the procedures can sharpen up the Wallner lines and extend the range of measured crack velocities in a single experiment.[22]

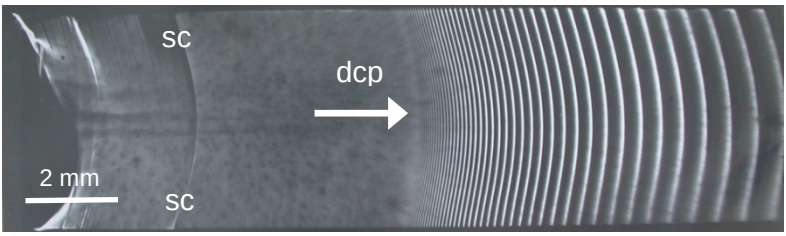

Figure 3.56 *Fracture in a glass plate. Fracture originated at the starter crack "sc" on the left and accelerated to the right as attested to by the increased spacing between the timing ripples. (Courtesy H. Richter)*

3.22 High Speed Photography

Studies of impact fractures have benefited from high speed photographic techniques. Field's review is good starting point.[23] The first extensive use of high-speed photography to study fracture in glasses was by Schardin and colleagues.[24] In 1937, Schardin and Struth used a multiple spark camera to observe that the terminal velocity of cracks in soda lime glass was about 1500 m/s. Barstow and Edgerton in 1939[25] did pioneering work on high-speed photography with spark photography as well. Ballistic impact studies are ongoing and Strassburger and colleagues at the Fraunhofer Institute in Kandern, Germany have been producing spectacular results.[26]

3.23 X-Ray Topography

X-ray topography is a specialized technique for single crystals.[27,28] An X-ray beam illuminates the test specimen and images formed using the diffracted beams are recorded. The image from an ideal crystal is completely homogeneous, but imperfections that distort or "strain" the crystal lattice produce image contrast. Often the defects themselves are not visible. It is the

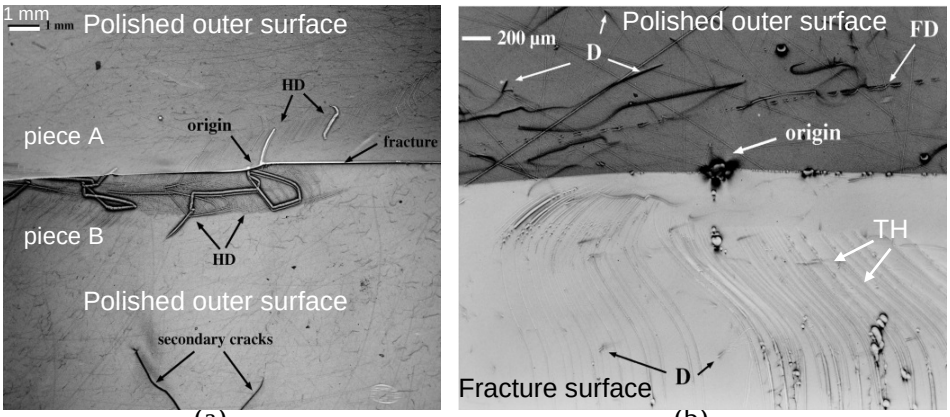

(a) (b)

Figure 3.57 *X-ray topographs of a fractured sapphire hemispherical dome (#1087). (a) shows the outer polished surfaces of the matching fracture halves. The broken halves were carefully realigned for this image. It reveals handling damage (HD) cracks not readily visible to the optical or scanning electron microscopes. (b) shows a close up of one piece tilted to show both the fracture surface and outer polished surface. Twist hackle – cleavage step lines (TH), dislocations (D), and fabrication damage (FD) are apparent. An overall photo of this dome and the fracture origin are shown in Figure 8.7 in the chapter on single crystals. (topographs courtesy D. Black).*

disturbances to the lattices that are revealed, and these are often magnified in size relative to the defect size. X-ray topographs will reveal dislocations, stacking faults, inclusions, and surface damage. Since diffracted X-rays form the image, interpretation is not always straightforward. Figure 3.57 shows handling damage on and below the polished surfaces of a sapphire hemi-spherical domes**.** The damage was not visible with the optical or scanning electron microscopes.

3.24 Dye Penetration and Staining

Dye penetration is a staple of nondestructive testing, but it also has value for fractographic analysis. It is commonly used to search for hidden cracks in a ceramic part prior to usage or after exposure to some loading or environmental conditions. Simple colored staining dyes or felt tip pens may be used with white ceramics. Level 4 ultrahigh sensitivity fluorescent dyes are used with dark ceramics.

Simple staining with common dyes such as the felt tip pens shown in section 3.9 can aid post-fracture interpretation in porous or coarse-grained materials that are otherwise very difficult to interpret. The dye can be applied to the fractured parts. For example, Figure 3.58 shows a portion of a fractured porcelain toilet tank. Simple staining revealed tiny incomplete crack branches that gave a clear indication of the direction of crack propagation. Figure 4.42 in the next chapter shows thermal shock cracks highlighted by red dye.

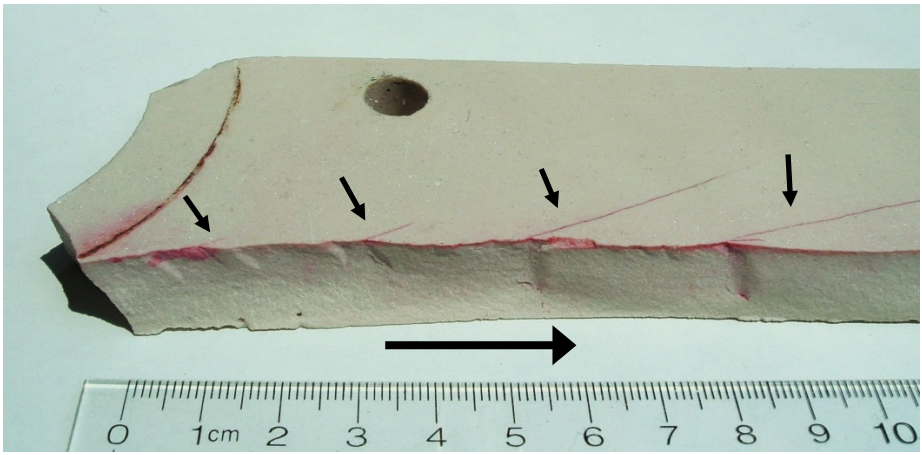

Figure 3.58 *Fractured porcelain part with dye penetration by a common felt-tip red pen. The dye reveals crack branching patterns (small arrows) and thus the direction of crack propagation (large arrow).*

Ultrahigh penetrating fluorescent dyes are needed to get into the tiny cracks. Special precleaning and soaking steps sometimes are necessary to facilitate dye penetration. Sometimes it may even be necessary to heat or vacuum treat a part to eliminate adsorbed gasses on the crack faces prior to dye penetration. After penetration, ultraviolet or "black light" illumination (Figure 3.59) is used to excite the dye such that it fluoresces and can be seen by the eye. Parts may be examined under a stereo microscope, but the images are dim since the amount of light emitted is very slight. It is difficult or impossible to photograph features under these conditions. Compound optical microscopes, on the other

Figure 3.59 *Fluorescent dye penetration equipment. Two double torsion fracture toughness specimens are shown.*

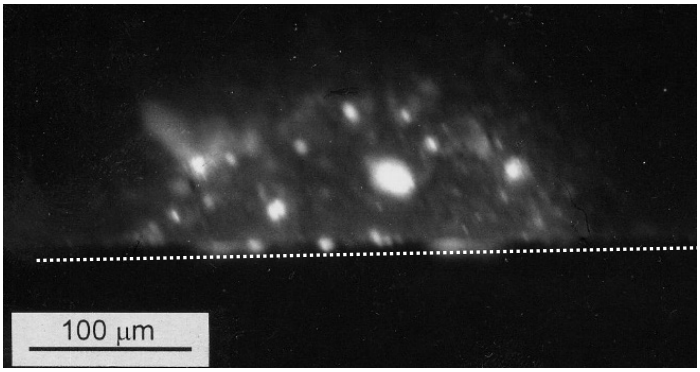

Figure 3.60 *Fracture surface of a silicon nitride specimen with a Knoop semielliptical surface crack that was penetrated by a fluorescent dye prior to fracture. The dashed line is the specimen bottom surface. This photo was made with a compound microscope with xenon bulb illumination and a fluorescence filter at a nominal 200 X magnification. The dim blurred image is typical for the weakly-emitting dye penetrant.*

hand, may be used with intense xenon bulb light sources and fluorescent filters so that images may be captured as shown in Figure 3.60. The photo shows an image made on an older generation instant developing film that was exposed for several minutes. Digital cameras would have made a better recorded image. Figure 3.61 shows a C contact damage crack in a large notched silicon nitride ball prior to and after a controlled fracture.[29] Fischer et al.[30] have used fluorescent dyes to detect flaws in dental ceramics.

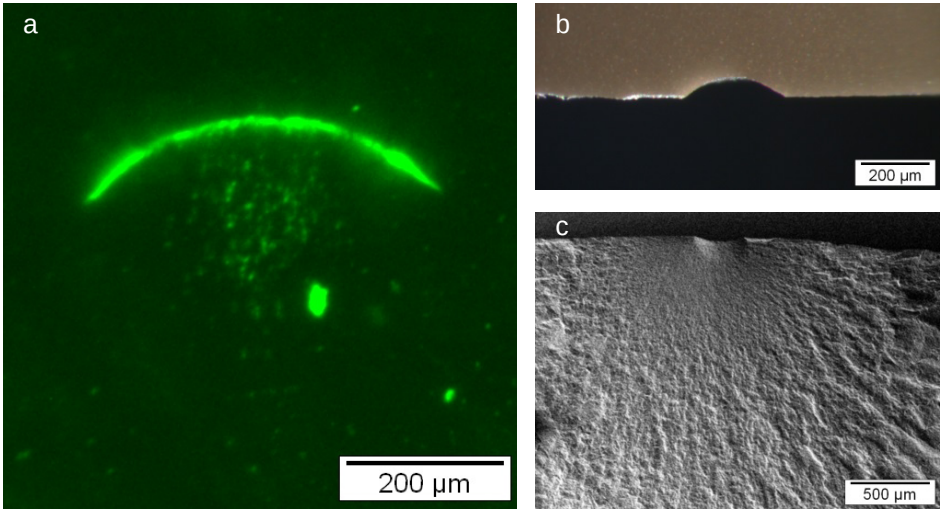

Figure 3.61 *C contact damage crack (also known as a crescent crack) in a silicon nitride ball bearing. (a) shows the outer surface and the crack highlighted by fluorescent dye penetrant. (b) shows one half of the notched ball with normal illumination after it was broken. (c) shows the fracture surface. (Courtesy T. Lube and R. Danzer, Mountain University Leoben).*

Dye penetration is sometimes used with ceramics to try to penetrate grinding induced cracks, but these are often very small and tight, making penetration problematic. Examinations of the fracture surfaces are done after fracture to ascertain whether the dye has penetrated beneath the ground surface. Dye "bleeding" can be a problem if the dye migrates into the fracture surface either during the fracture event or afterwards. Part of the problem is that there usually is a thin zone (of the order of only a few micrometers) on the surface that is in residual compression. It clamps the cracks tight at the surface. Mizuno et al.[31] devised a clever procedure to use a metallic solution with $Pd(NO_3)_2$ impregnation in a vacuum. The solution normally would not penetrate the as-ground surfaces, but this was overcome by two methods. One was to polish off the surface compression layer. The alternative method was to apply a small

amount of bending to open up the cracks for penetration on the tensile surface. The palladium-penetrated cracks were evident on the fracture surfaces when viewed by SEM, presumably in the backscattered mode. Kanematsu used this methodology but with an electron micro probe to study machining cracks by using cold-isostatic pressing to infiltrate the dye. [32,33,34] He further used plasma etching to highlight the surface and subsurface damage around grinding damage and indentations.[33,35] Figure 3.62 shows matching SEM images and palladium maps for three different specimens ground with a 100 grit, 75% concentration, resin-bonded diamond wheel.

The Nagaoka University of Technology in Japan has done fine work with novel dye penetration methods to investigate three-dimensional structures and flaws

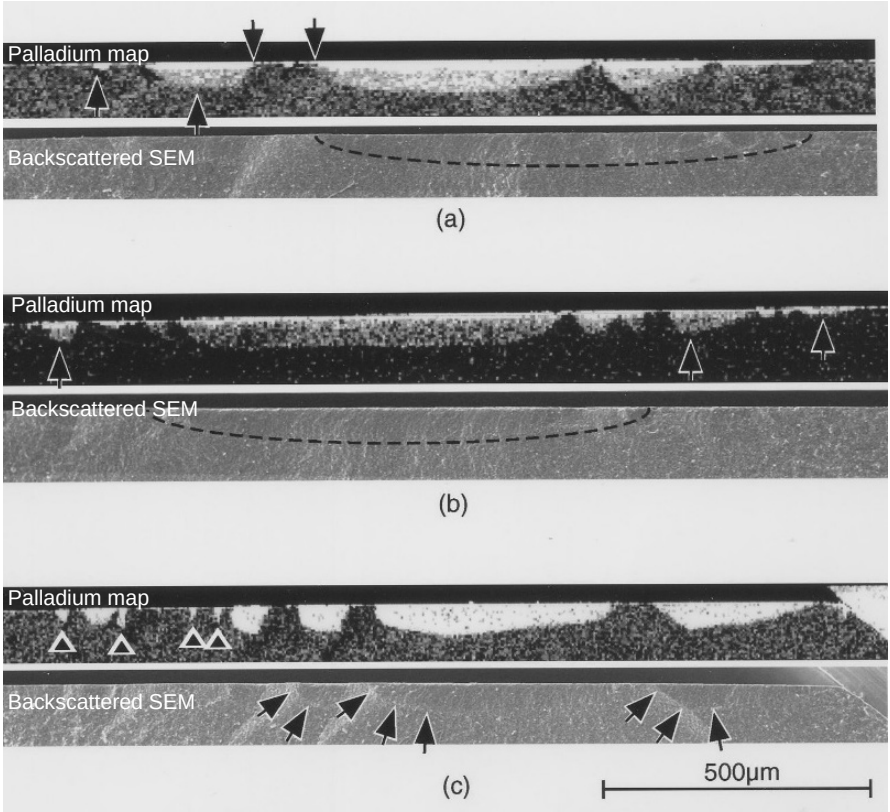

Figure 3.62 *Grinding cracks in silicon nitride revealed by palladium nitrate solution impregnation. These are three paired views of fracture surfaces for different specimens. The first image in each pair is a palladium map. The second image is a conventional backscattered SEM image at the same magnification. (Courtesy of W. Kanematsu, ref. 33).*

in powdered compacts and fired ceramic structures. For example, Professors Uematsu and Tanaka and students used potassium iodide and iodine in diluted water mixed with saturated boric acid to study the uniformity and lack of uniformity in pressed compacts.[36,37]

3.25 Polariscope

As discussed in section 3.8 on illumination and lighting, transparent objects may be viewed through crossed polarizers. A dedicated polariscope such as shown in Figure 3.63 may be used to examine large objects such as bottles or plates held between the rear polarizer and illumination source and the front polarizer (or eyepieces). In photoelastic materials the existence of residual stresses may be revealed by light and dark patterns or color bands. Glasses and plastics are photoelastic. The method is based on the property of birefringence, whereby a light ray passing through the material may have two refractive indices. Many crystals are naturally birefringent. Plastics and glasses become birefringent when stressed. The strains in the body cause the horizontally- and vertically-polarized light waves to travel at different velocities through the stressed material in the directions of the maximum principal stresses. Photoelastic analysis is usually applied to two-dimensional X-Y problems, such as plates or bottles and vials. The stresses that are revealed are those that are in the X-Y plane of the structure and not those that may exist through the thickness. If the stress

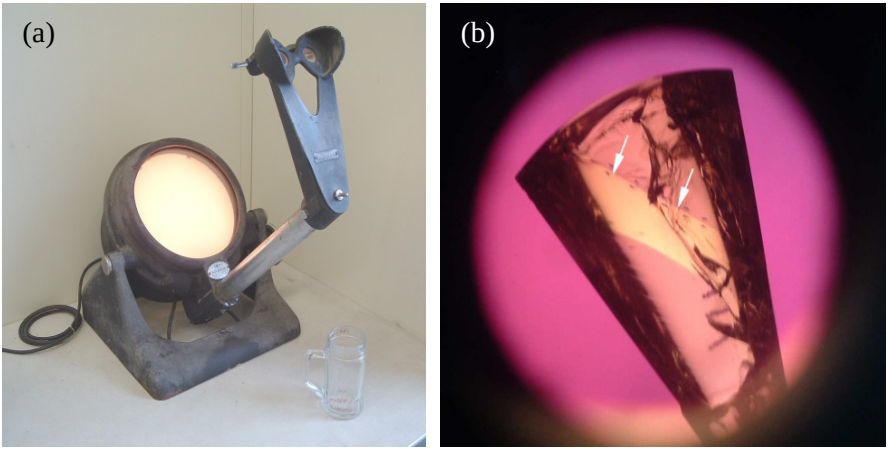

Figure 3.63 *(a) shows an old but still very useful polariscope. (b) shows a twin band (arrows) in a complex single-crystal sapphire part described in detail as case 13, "The Ruined Refractors," in Chapter 10. The photo was taken by a simple digital consumer camera held up to the eyepiece.*

optical coefficient for the material is known, then quantitative stress estimates may be made. Highly stressed parts will have a sequence of alternating light and dark bands, or "fringes," that can be counted and used with the stress-optic law to estimate the stresses. One thing a fractographer should keep in mind is that once a part breaks, the internal strains can be relieved to some extent, and the stress distribution will be different than that in the unbroken part.

Polariscopes are also valuable with single crystals. Twins may be revealed as shown in Figure 3.63b. Additional examples are in Chapter 8. Polariscopes are also used to detect and even estimate the magnitude of residual stresses in transparent birefringent materials.

3.26 Other Equipment

Figure 3.64 shows a simple ultrasonic cleaner that is helpful for cleaning small specimens prior to SEM examination. The specimens may be placed into small beakers with a solvent such as acetone and then placed into the sonic cleaner bath which is partially filled with water. Methyl alcohol is effective in removing fingerprints. A few minutes vibration is usually sufficient to remove

Figure 3.64 *An ultrasonic cleaning bath.*

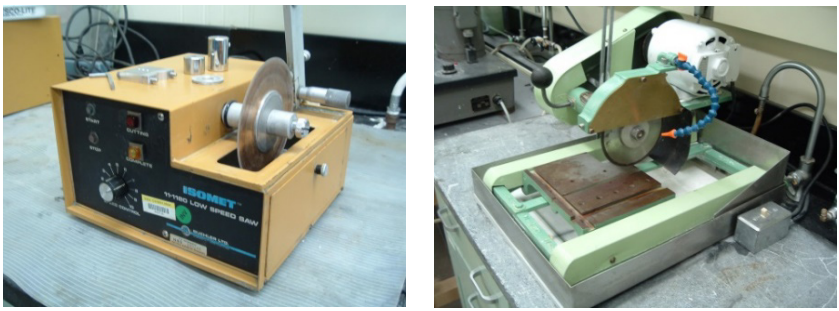

Figure 3.65 *Wafering and cut off wheel machines.*

common contaminants and cutting debris. Simple cutoff or wafering machines (Figure 3.65) are handy for cutting large specimens to sizes that can be mounted in optical or scanning electron microscopes. Cutting should be done wet to flush debris away and to minimize heating of the specimen.

3.27 Other Resources

The ASM Handbooks Volume 11 on Failure Analysis and Prevention and Volume 12 on Fractography have articles on fractographic equipment.[7,38] Appendix A of this Guide (on-line) lists additional sources of information.

3.28 The Future

The merger of the microscope with digital cameras and computers will continue and virtual imaging with computer-generated topographical images will become commonplace. Despite all the advantages of the new tools and advanced technologies, the author believes they will never replace direct optical imaging. The stereo microscope will always be a primary tool since it is easy to use and retains color and reflectivity information and can capture internal reflections. Most of the new digital technologies emphasize topographic detail to the exclusion of all else and thus miss key information. Very often a key feature will be fleetingly observed through the microscope eyepieces during the rotation of a specimen or the angle of lighting.

New computer software and digital camera technologies will enhance the capabilities of the conventional compound optical microscope so that it partially replaces the scanning electron microscope. The latter is most commonly used at 200X to 1,000X for fractographic work, since this is all the magnification that is ordinarily needed to find and record 5 mm to 100 mm size flaws. These magnifications are well within the reach of enhanced compound optical microscopes with digital cameras and Z-axis image stacking. On the other hand, the chemical (energy dispersive x-ray analysis) and structural analysis (electron diffraction) capabilities of the SEM will ensure it is a staple of the fractographers tool box for many years to come.

Microanalytical techniques in the SEM will continue to improve. Spatial variations in microstructure can have a strong influence on crack propagation. We tend to envision a microstructure as uniform with all the grains being randomly oriented, but materials scientists know otherwise. Variations in composition, grain orientations, second phase distributions and preferred orientations can have a profound influence on local properties and local crack propagation. Colorization of SEM images may now be done manually by post

processing of the SEM black and white images, but will be commonly integrated with the SEM software. Electron backscatter diffraction is limited at the present to very flat surfaces, but imagine how our eyes will be opened if it or some other technology can be applied to rougher fracture surfaces.

Perhaps one of the greatest current limitations of the art of image storage and display is that it is all two-dimensional. Fracture surfaces are by their very nature three-dimensional, so something is lost when an image of a fracture surface is captured and stored in a computer's memory. This is partially solved by new image analysis computer programs used in conjunction with multiple SEM images (taken with different tilts) or optical microscopes with Z-axis rastering such that a computer-generated model or depiction of the surface can be displayed. Such virtual images can be color enhanced and can be tilted, rotated, or viewed from different angles. They are all displayed on two-dimensional computer monitors.

One can imagine the future fractographer donning special eyepieces or a visor that enable him or her to traverse over or "fly over" a virtual fracture surface. These will certainly have considerable novelty value, but one wonders whether they will lead to better diagnoses than those made by an experienced observer looking through a simple stereo microscope. It is very common for the fractographer, while wiggling and tilting a fracture surface under a stereo microscope, to detect a fleeting reflection or stray subtle fracture line, which upon further examination unlocks the secret of a particular problem. Will future computer software and image analysis programs ever match this skill?

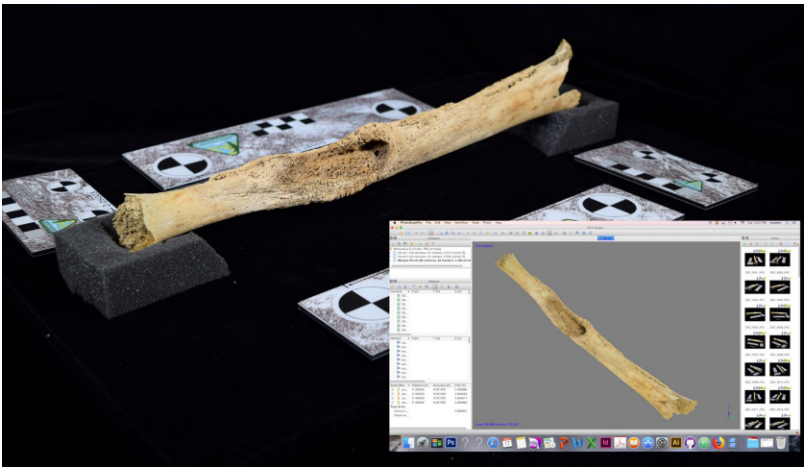

Figure 3.66 *Photogrammetry model of a broken bone.*[39,40] *(Courtesy A. Christensen)*

As this 4th edition was being written, the author became aware of the field of photogrammetry as applied to bone fractography.[39,40] Lasers or structured light scanners can be used for three-dimensional documentation of broken structures and fracture surfaces. Photogrammetry uses a series of two-dimensional photographs from different viewpoints. These are analyzed and a "point cloud" is created that represents the surface of the object and a virtual three-dimensional model is created such as shown in Figures 3.66 and 3.67. Surface scanners that use lasers to scan an object are becoming more convenient to use and can also construct virtual three-dimensional models as shown in Figure 3.67. These new techniques may be valuable for making renditions of a broken part, but it is not clear whether they have sufficient resolution to capture fine fracture surface details (e.g., Wallner lines).

Figure 3.67 *A handheld metrological three-dimensional scanner using blue-light technology applied to a broken bone. (Courtesy A. Christensen)*

Perhaps the great breakthrough will occur when technology is invented that can capture genuine images with fine detail and retain full color, reflectivity, and internal reflection information *and display* them with full fidelity in three dimensions. The author can personally attest to the hours of desperate struggle to acquire the best two-dimensional image to capture a critical detail, only to feel despair when showing the image later and realizing that it "just doesn't show what the eyes saw."

Chapter 3 References

1. A. M. Christensen, M. A. Smith, J. T. Hefner, J. Blakely Webb, M. C. Bottrell, and T. W. Fenton, "Forensic Fractography of Bone: A New Approach to Skeletal Trauma Analysis," *Forensic Anthropology*, **1** [1] (2018) 32 - 51.

2. T. Engelder, "Propagation Velocity of Joints: A Debate Over Stable vs. Unstable Growth of Cracks in the Earth," pp. 457 - 482 in *Fractography of Glasses and Ceramics V*, eds. G. D. Quinn, M. Wightman, and J. R. Varner, *Ceram. Trans*., Vol. 199, American Ceramic Society, Westerville, OH, 2007.
3. S. S. Scherrer, J. B. Quinn, G. D. Quinn, and H. W. Anselm Wiskott, "Fractographic Ceramic Failure Analysis Using the Replica Technique," *Dental Materials*, **23** [11] (2007) 1397 -1404.
4. V. D. Fréchette, *Failure Analysis of Brittle Materials*, Advances in Ceramics, Vol. 28, American Ceramic Society, Westerville, OH, 1990.
5. J. R. Varner, "Using Replicas in Fractography of Glasses and Ceramics – Advantages and Pitfalls," pp. 299 - 307 in *Fractography of Glasses and Ceramics, VI*, eds. J.R. Varner and M. Wightman, Ceramic Transactions, Vol. 230, Wiley, Hoboken, NJ, 2012.
6. J. R. Varner, "Replicas as a Technique for Examining Fracture Surfaces of Ceramics," pp. 107 - 112 in *Fractography of Advanced Ceramics, III*, eds. J. Dusza *et al*., Transtech Publ. Zurich, 2009.
7. *Fractography*, Vol. 12, ASM Handbook, ASM Int., Materials Park, OH, 1987.
8. D. Hull, *Fractography, Observing, Measuring and Interpreting Fracture Surface Topography*, Cambridge University Press, Cambridge, 1999.
9. J. T. Healy and J. J. Mecholsky, Jr., "Scanning Electron Microscopy Techniques and Their Application to Failure Analysis of Brittle Materials," pp. 157 – 181 in *Fractography of Ceramic and Metal Failures, ASTM STP 827*, ASTM, West Conshohocken, PA,1984.
10. B. L. Gabriel, "Scanning Electron Microscopy," pp. 166 – 178 in *Fractography*, Vol. 12, ASM Handbook, ASM Int., Materials Park, OH, 1987.
11. S. Burgess, X. Li, and J. Holland, "High Resolution Energy Dispersive X-ray Spectrometry in the SEM and the Detection of Light Elements Including Lithium," *Microscopy and Analysis*, May 2013, pp. S8 - S13.
12. L. S. Chumbley and L. D. Hanke, "Scanning Electron Microscopy," pp. 516 – 526 in *Failure Analysis and Prevention*, Vol. 11, ASM Handbook, ASM Int., Materials Park, OH, 2002.
13. C. R. Brooks and B. L. McGill, "The Application of Scanning Electron Microscopy to Fractography," *Mater. Charact.*, **33** (1994) 195 - 243.
14. M. A. Caja and L. G. Diego, "SEM Colorized Images from Oil and Gas Reservoirs: Petrology in Technicolor," *Microscopy and Analysis*, Sept./Oct. 2017, pp. 14 - 18.
15. K. P. Mingard, H. G. Jones, M. G. Gee, B. Roebuck, and J. W. Nunn, "In situ Observation of Crack Growth in a WC-Co Hardmetal and Characterization of Crack Growth Morphologies by EBSD," *Int. J. Refr. Met. Hard Mater*., **36** (2013) 136 - 142.
16. H. U. Marschall, R. Danzer, and R. Pippan, "Three-Dimensional Analysis of Decorated Ceramic Fracture Surfaces by Automatic Stereophotogrammetry," *J. Am. Ceram. Soc*., **83** [1] (2000) 223 – 225.
17. T. D. Fletcher, J. J. Petrovic, and J. E. Hack, "Quantitative Fractography of SiC Whisker-Si_3N_4 Matrix Composites," *J. Mat. Sci.*, **26** (1991) 4491 – 4498.
18. G. D. Quinn, "Fractographic Analysis of Miniature Theta Specimens," *Ceram. Eng. Sci. Proc.*, **29** [3] (2008) 189 – 199.
19. F. Kerkhof, "Bestimmung der Maximalen Bruchgeschwindigkeit Verschiedener Gläser Nach Der Ultraschalmethode," *Glasstechn. Bericht*, **35** (1955) 267 - 272.
20. H. G. Richter and F. Kerkhof, "Stress Wave Fractography," pp. 75 – 109 in *Fractography of Glass*, eds., R. C. Bradt and R. E. Tressler, Plenum, NY, 1994.
21. A. Tsirk, *Fractures in Knapping*, Archaeopress, Oxford, UK, 2014.
22. T. A. Michalske and V. D. Fréchette, "Modified Sonic Technique for Crack Velocity Measurement," *Int J. Fract*., **17** [3] (1981) 251 – 256.

23. J. E. Field, "High-Speed Photography," *Contemp. Phys*., **24** [5] (1983) 439 – 459.
24. H. Schardin and W. Struth, "Neuere Ergibnisse der Funken-kinemographie," *Zeitschrift Tech. Phys.*, **18** (1937) 474 - 477.
25. F. E. Barstow and H. E. Edgerton, "Glass Fracture Velocity," *J. Am. Ceram. Soc.*, **22** [9] (1939) 302 – 307.
26. J. W. McCauley, E. Strassburger, P. Patel, B. Paliwal, and K. T. Ramesh, "Experimental Observations on Dynamic Response of Selected Transparent Armor Materials," *Exp. Mech.*, **53** (2013) 3 – 29.
27. D. R. Black and G. G. Long, *X-Ray Topography*, NIST Recommended Practice Guide, NIST Special Publication 960-10, April 2004.
28. D. Black and G. D. Quinn, "X-ray Topography for Fractography of Ceramic Single Crystals," *J. Fail. Anal. Prev.*, **6** [3] (2006) 69 - 76.
29. T. Lube, S. Witschnig, P. Supancic, R. Danzer, and O. Schöppl, "The Notched Ball Test – Characterization of Surface Defects and Their Influence on Strength," pp. 225 – 234 in *Fractography of Glasses and Ceramics, VI*, eds. J.R. Varner and M. Wightman, Ceramic Transactions, Vol. 230, Wiley, Hoboken, NJ, 2012.
30. H. Fischer, F. Karaca, and R. Marx, "Detection of Microscopic Cracks in Dental Ceramic Materials by Fluorescent Penetrant Method," *J. Biomed. Mater. Res.*, **61** [1] (2002) 153-158.
31. S. Mizuno, N. Kobayashi, and K. Miyata, "Analysis of Sintered Silicon Nitride Grinding Damage," SAE Technical Paper 930163, March 1-5, 1993, SAE Int., Warrendale, PA, 1993.
32. W. Kanematsu, M. Sando, L. K. Ives, R. Marinenko, and G. D. Quinn, "Determination of Machining Crack Geometry by Dye Penetration Technique," *J. Am. Ceram. Soc.*, **84** [4] (2001) 795 - 800.
33. W. Kanematsu, "Visualization of Subsurface Damage in Silicon Nitride from Grinding by a Plasma Etching and Dye Impregnation Method," *J. Am. Ceram. Soc.*, **89** [8] (2006) 2564 - 2570.
34. W. Kanematsu and L. K. Ives, "Propagation Behavior of Machining Cracks in Delayed Fracture," *J. Am. Ceram. Soc*., **87** [3] (2004) 500 - 503.
35. W. Kanematsu, T. Miyajima, and M. Sando, "Visualization of Knoop Indentation Damage of Silicon Nitride by Plasma Etching," *J. Am. Ceram. Soc*., **84** [10] (2001) 2427 - 2429.
36. Z. Kato, S. Tanaka, N. Uchida, and K. Uematsu, "A Novel Method to Investigate the Non-uniformity of the Internal Structure of Granule Compacts," in *Key Engineering Materials, Vols. 206-213, Proc. 7th Eur. Cer. Soc.*, (2002) pp. 341 – 344, Trans Tech Publ., Zurich, Switzerland.
37. Y. Saito, S. Tanaka, N. Uchida, and K. Uematsu, "Direct Observation of Three-Dimensional Structure in Powder Compact," in *Key Engineering Materials, Vols. 206-213, Proceedings of the 7th Eur. Cer. Soc.*, (2002) pp. 657 – 660, Trans Tech Publ., Zurich, Switzerland.
38. *Failure Analysis and Prevention*, Vol. 11, ASM Handbook, ASM Int., Materials Park, OH, 2002.
39. A. Christensen, M. I. Isa, M. A. Smith, J. T. Hefner, H. Berryman, J. B. Webb, and I. S. Saginor, *A Guide to Forensic Fractography of Bone*, Federal Bureau of Investigation Laboratory, Quantico, VA, Feb. 2022.
40. Z. Obertova, A. Leipner, C. Messina, A. Vanzulli, B. Fless, C. Cattaneo, L. Sconfienza, "Postmortem Imaging of Perimortem Skeletal Trauma, *Forensic Sci. Intl*., 2019 **302** (2019):109921.

4. General Examination, Fracture Modes, and Patterns

Analysis begins with a simple visual examination of the broken pieces. The general patterns of crack extension and branching point the way back to a fracture origin and provide information about the cause of fracture, the energy of fracture, and the stress state. The majority of brittle fractures start at one origin and radiate outward. There are exceptions.[a] Severe thermal stresses or impact loadings can create multiple origin sites. Sometimes once one primary fracture occurs, large fragments remain that are still under load, and they can have secondary fractures.

Fréchette defined the fracture origin as: "that flaw (discontinuity) from which cracking begins."[1] A slightly broader definition considers that the fracture origin is both a location and a flaw:

***fracture origin**: the source from which brittle fracture begins.*

Even if the primary objective is to find the fracture origin, the overall breakage pattern should be examined first. Most of this chapter is concerned with breakage patterns in general. Examination of the fracture surfaces is covered in Chapter 5. An experienced fractographer may simultaneously examine the general breakage pattern and the fracture surfaces. Chapter 6 covers the types of fracture origins that one might find.

Breakage may be sudden, unstable, and catastrophic as in a laboratory strength test or a dropped glass. Alternatively, it may be in stages as in a fractured dental crown restoration, or a crack growing in an automobile windshield.

Most but not all origins in glass are from surface- or edge-located origins. Ceramics fracture from volume, surface, or edge sources. The fracture origin is the site that had the worst combination of tensile stress and flaw severity. The latter is determined by the flaw size, shape, and thermoelastic or chemical interactions with the matrix. A large flaw may not necessarily trigger fracture, especially if it is located in a portion of a part that has low stress or it is very blunt such as a spherical pore. The severity of a flaw and whether local stresses are sufficient to trigger fracture are covered by principles of fracture mechanics presented in Chapter 7. This Chapter 4 begins with some generic breakage patterns and shows some common examples, both for laboratory tested specimens and component fractures. The end of the chapter has some general

[a] Figure 5.14 in Section 5.2.5 shows a bend bar fracture surface with two fracture mirrors centered on two flaws of identical size. Section 4.13 on impacted bottles shows examples of multiple origin sites. Compression fractures in section 4.19.8 also involve many flaws.

observations about fractures caused by mechanical overload, impact or contact, thermal, corrosion or oxidation, and some observations on how residual stresses may affect fracture patterns.

4.1 Specimen Reconstruction

The general examination often begins with specimen reassembly. Ideally all fragments are available. Even if the pieces with the origin are lost, valuable information can be gleaned from the fragments. With some experience and with a familiar breakage pattern, irrelevant shards or secondary fracture fragments may be ignored. At this point the fractographer should take care not to introduce contamination to the fragments and especially the fracture surfaces. Sometimes an experienced fractographer is able to look at fragments of a familiar component or test specimen type and be able to immediately find the piece with the fracture origin. For example, experienced fractographers are able to sift through a bucket of tempered glass fragments and find the origin pieces on the basis of their telltale morphology. A common concern is whether it is safe to put the pieces together. This step is discouraged for analysis of polymer or metal fractures. In contrast, ceramic and glasses are hard and durable materials. The pieces usually fit perfectly together. It is acceptable to fit pieces together gently, taking care to avoid abrasion or chipping. Single crystals and glasses are more sensitive to chipping than polycrystalline ceramics and must be handled more carefully.

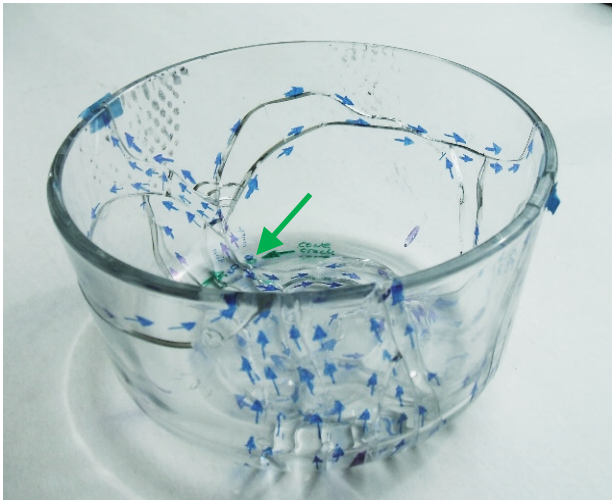

Figure 4.1 *A reconstructed Pyrex bowl that was broken intentionally by thermal shock. Directions of crack propagation are marked with blue arrows from a felt tip marker pen. The fracture origin is marked by the green arrow.*

Figure 4.1 shows a reconstructed Pyrex (in this case, a heat-strengthened soda lime silica) bowl that was intentionally broken by thermal shock.[b] The bowl was removed from an oven, inverted, and then a slightly-damp towel was placed over it, and it broke. The towel prevented the pieces from flying about. The pieces were individually examined, and directions of crack propagation marked with blue arrows from a felt tip marker. These directions of crack propagation were ascertained by studying the crack branching patterns (described later in this chapter) plus observations of features on the fracture surfaces such as Wallner lines as described in chapter 5. The single fracture origin on the base is marked by the green arrow. Reference 2 has a similar example of a reconstructed kitchenware glass ceramic vessel (Corningware 9608 glass ceramic) with a comprehensive fractographic analysis. (Additional information about that case is in Appendix B of this Guide.)

Simple adhesive tapes may be used to temporarily hold pieces together. Apply the tape sparingly and only on external surfaces and not between fracture surfaces. Small strips of masking tape may be used judiciously, but it should be borne in mind there is a risk of contamination. Whatever tape is used, it should be a type that is easily removable. Blue painter's tape is useful. Keep in mind that a reassembled body held together by tape strips may be unwieldy.

In complex cases with multiple fragments, it may even be necessary to glue fragments together. Glues should be used sparingly and preferably in a tack-bonding mode away from candidate fracture origin regions. Avoid getting glue on the fracture surfaces. The overall assembly will fit better if there is no build up or misfits from glue joints between fracture planes. Simple cheap nitrocellulose air-drying cements[c] are suitable and set fast. They can easily be removed by peeling off with a fingernail or razor knife or by dissolving with common solvents. In special cases it may be necessary to use a strong cement to glue the pieces together on their fracture surfaces. Cyanoacrylate ester ("super") glues may be used since they can set with very thin bonds such that cumulative misfits are held to a minimum. Such glues can be removed by soaking in acetone or nail polish remover. *In any case, glues should be used sparingly and every precaution taken to prevent them from coming into contact with fracture origin areas*.

---

[b] This fracture was done intentionally by the author to study the characteristics of thermal shock fractures of the modern heat-strengthened (or tempered) soda lime silica version of Pyrex kitchenware. Early generations of Pyrex cookware were made of low-expansion borosilicate glass that was less susceptible to thermal shock fracture.

[c] Duco cement or Scotch "All purpose adhesive, Super strength."

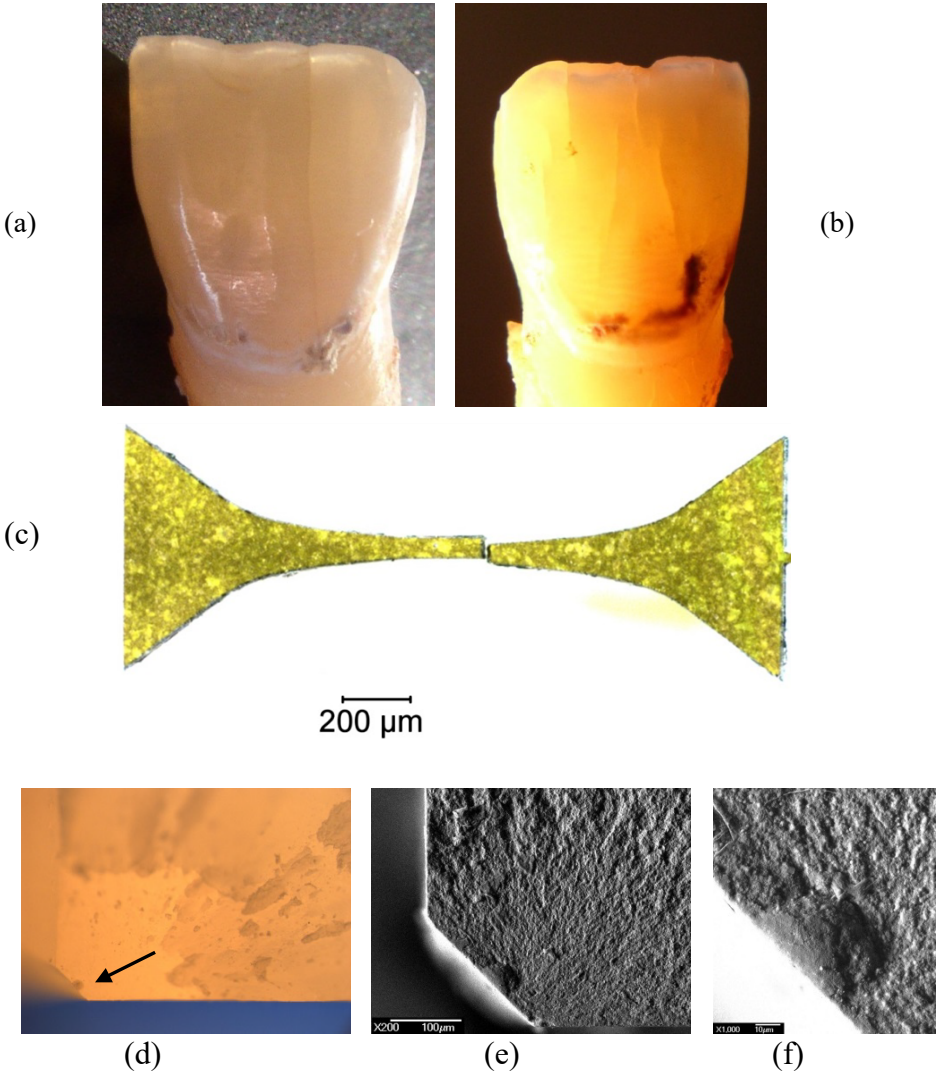

Figure 4.2 *Transillumination examples. (a) and (b) are an extracted human tooth from an approximately 80-year-old patient. Transillumination from the side shows internal enamel cracks. (courtesy S. Scherrer) (c) shows transmitted illumination of a chemical vapor deposited SiC micro tensile specimen. Very coarse grains acted as light pipes through the body. Relatively pure SiCs are green. (d) – (f) show an aluminum-rich inclusion origin, in a highly-filled resin-matrix dental composite bend bar. (d) is a trans-illumination view with light from below. Although the fracture surface features are blurred by the material's translucency, the origin flaw stands out at the chamfered corner. The SEM images (e) and (f) show the inclusion.*

During reconstruction it may be helpful to mark the pieces with a number or letter scheme in order to expedite the examination and to minimize specimen–to-specimen refitting exercises. Use a pencil or fine tip felt tip marker pens, but care should be taken to avoid contaminating the fracture surfaces or the fracture origin. Felt tip pen markings can usually be removed with alcohol or acetone.

During the initial examination it may be advantageous to try *transillumination* on white and translucent ceramics. Figure 4.2 shows three examples. Transillumination, whereby the part is illuminated from behind or from the side, may reveal internal cracks, flaws, and microstructural irregularities not detected by examination of the outer surface.

4.2 Crack Branching Patterns

Crack branching and radiating patterns may be interpreted before the fracture surfaces are examined. Much of the fractographer's craft is in the observation and interpretation of these patterns. Crack branch patterns can lead back to an origin and also tell much about the stress state and stress magnitude. A simple example is a glass biaxial strength test specimen shown in Figure 4.3. The radiating pattern is intuitive and leads the observer back the origin which is in the disk middle.

Sometimes multiple fractures can be simultaneously triggered. Examples are severe thermal shock fractures, or mid-body fractures on each side of an impacted bottle. Secondary origins are often present in components that initially break from one origin, but then the fragments themselves fracture. The first general rule is the:

Law of Normal Crack Propagation*: a crack propagates normal to the direction of the maximum local principal tension stress.*

The word "normal" means "perpendicular." There are exceptions. As the crack propagates, minor perturbations in the direction of local principal tension can modify the plane of cracking. These minor perturbations can create telltale markings such as Wallner lines or hackle on the fracture surface as described in Chapter 5. Internal stresses or inhomogeneities can also cause crack local deviations. In single crystals and laminated structures, cracks may not necessarily run perpendicular to the maximum principal stress.

Once fracture has commenced, the propagating crack can fork or branch into multiple propagating cracks. These may be at non-normal angles to the far-field stress direction. Nevertheless, the initial fracture starts out as a single

radiating crack that separates the part into two pieces. Often the search for the fracture origin entails studying the branching patterns and tracing them back to the region of first fracture where the two pieces with the origin join across a flat surface as shown in the center of Figure 4.3b.

Branching may not occur at all if the failure stresses are low, or if they drop off in the direction of crack propagation, or if the opening up of the crack makes a specimen more compliant such that the stresses are relieved (e.g., Fig. 3-19). Figures 4.4 and 4.5 on the next page show other examples.

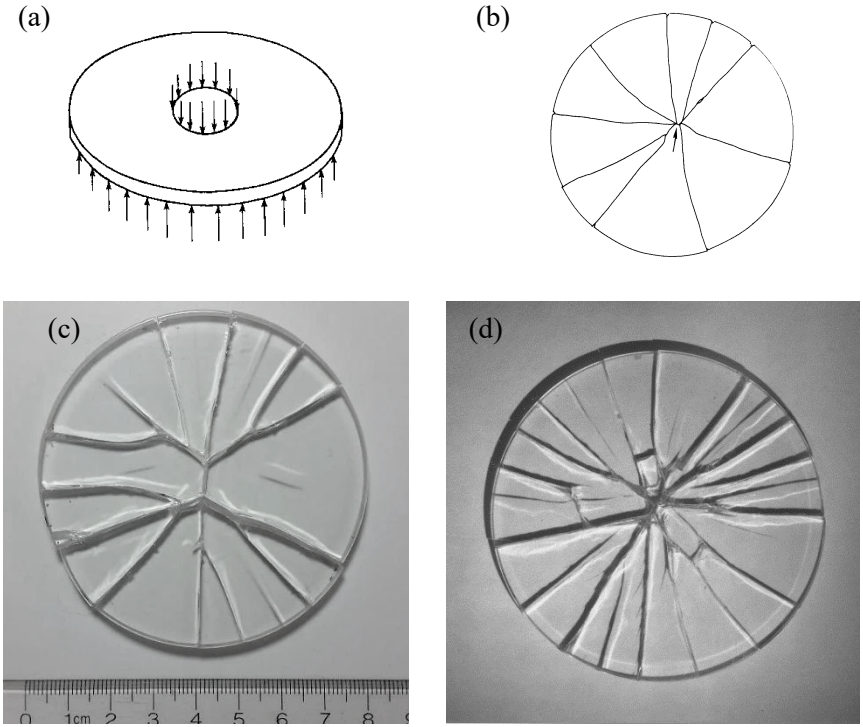

Figure 4.3 *Fracture patterns in glass disks tested in ring-on-ring biaxial strength tests. (a) shows the test arrangement, (b) shows a schematic of a fracture pattern of a moderately strong piece. The arrow marks the origin. (c) and (d) show BK-7 borosilicate crown glass disks that broke at a peak stress of 52 MPa and 73 MPa, respectively. It is difficult to photograph these since the crack faces in the interior cast shadows or reflect the light off slightly-inclined crack faces. A black background might have been better.*

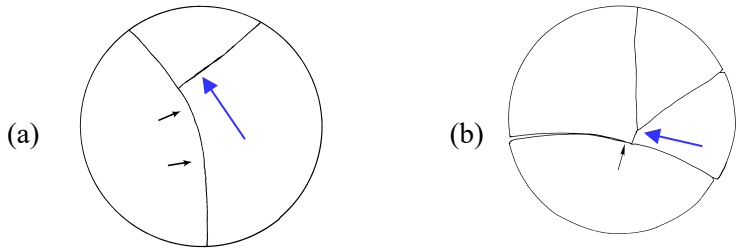

Figure 4.4 *Low-strength plates that break in bending (e.g., ring-on-ring test coupons) may have an initial fracture that splits the piece into two halves. Continued loading causes secondary breaks marked by the blue arrows.*

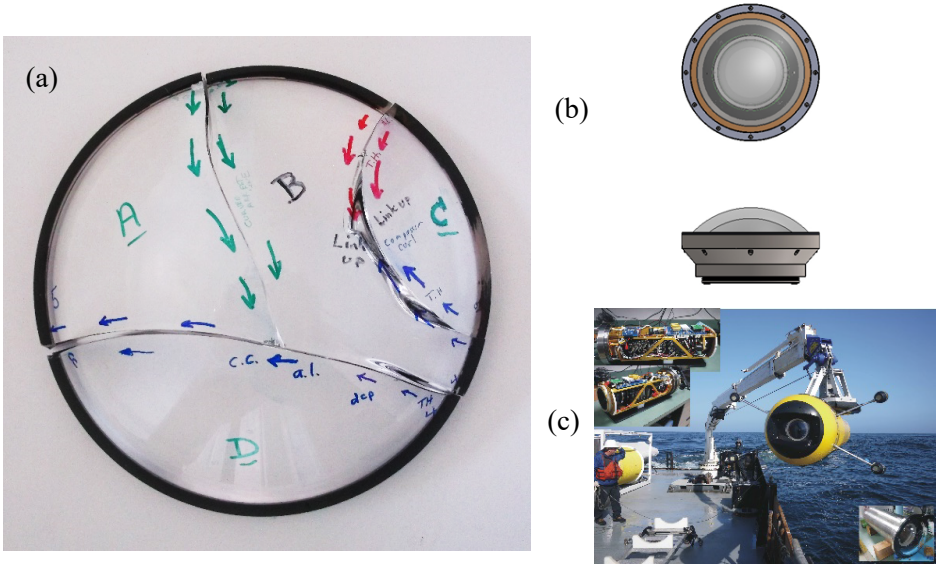

Figure 4.5 *A very large, dome-shaped borosilicate-crown glass window (250 mm outside diameter, 162 mm spherical radius, and 22 mm thick) for an ocean submersible is shown in (a). (b) shows top and side drawings of the dome and its mounting structure. (c) shows the submersible The dome fractured from external pressure on the convex outer surface during proof testing, not when in service. In figure (a) the initial break that formed large fragment "D" occurred from right to left as shown by blue arrows made by a felt tip pen. Continued loading caused the green-colored crack that split the top half into pieces "A" and "B". Cracks from two separate origins (red and blue) on the rim curved inwards then linked up and formed piece "C." (Ref. 3, b and c courtesy of F. Cazenave.)*

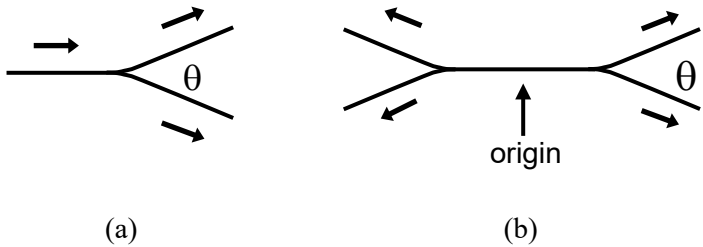

Figure 4.6 *Crack branching indicates the direction of crack propagation.*

4.3 Crack Branching Angles

Cracks which have reached their terminal velocity may split into two cracks with an acute angle between them as shown in Figure 4.6a. Fréchette[1] terms this *velocity branching, velocity forking, or velocity bifurcation.* Branching patterns are a valuable aid in diagnosing the direction of crack propagation. For example, a pair of branches in opposite directions typically brackets the origin as shown in Figure 4.6b. Sometimes cracks trifurcate, and a middle crack continues from the original crack. A closeup of the branching point as shown in Figure 4.7 shows the angle starts small and then stabilizes as the cracks propagate. The branching angle should be measured once the branch angle stabilizes as shown in the figure.

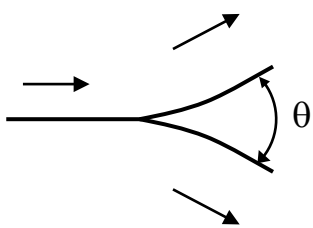

Figure 4.7 *Close up of the branching point.*

Another very useful observation is that the angle of forking varies with the stress state as shown in Figure 4.8. This figure is for the <u>first crack branch</u> and has been revised from the one in the 1st and 2nd editions of this Guide. A new solid trend line is shown. The earlier version of this figure emphasized Preston's original trend line of 1935 which is shown here as a dashed line.[4] Although Preston specifically said that branch angles should be measured near the point of branching, it appears that he actually showed fully-included angles after multiple branches.

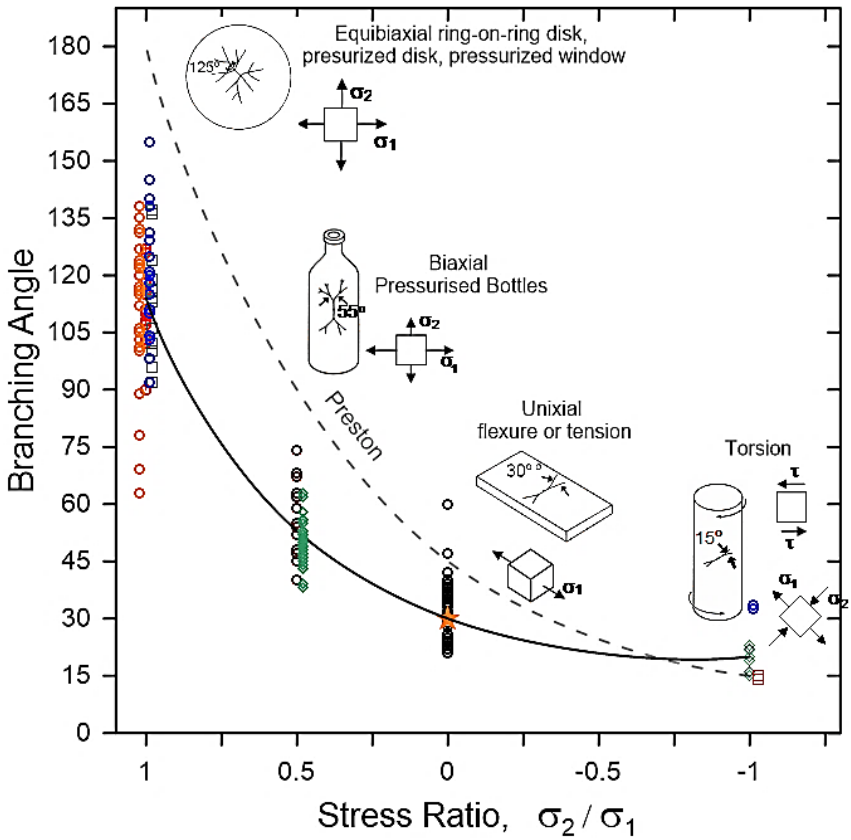

Figure 4.8 *First branching angle versus stress state. The branching angle is the angle between the first branches. The colored circles and squares show first branching angles for ceramics and glasses from many studies including new data by the author as explained in ref. 5. The red star for the uniaxial stress condition,* $\sigma_2/\sigma_1 = 0$, *is from Kalthof's study.*[7,8]

Table 4.1 *Average branch angles as a function of stress ratio. Uncertainties are one standard deviation.* n *is the number of branch angles measured and includes values from photos in the literature and new results in reference 5.*

Stress Ratio			
Equibiaxial $\sigma_2/\sigma_1 = 1$	Biaxial $\sigma_2/\sigma_1 = 0.5$	Uniaxial $\sigma_2/\sigma_1 = 0$	Biaxial Torsion $\sigma_2/\sigma_1 = -1$
113.8° ±16.3° n = 76	52.4° ± 7.2° n = 66	32.4° ± 7.2° n = 55	20.8° ± 6.3° n = 13

Figure 4.8 has a solid main trend line and actual data that is discussed in detail in the author's 2020 review paper.[5] Table 4.1 shows the results from that study that involved measurements on both glasses and ceramics. These are discussed further on the following pages. The evidence so far suggests the branch angles are independent of material property or component shape. This would be a good topic for additional investigation. If cracks trifurcate, the included branch angle of the outer branches are as much as 13° larger.

One must be careful interpreting stress-ratios versus branching angles since the branch angle can vary quite a bit depending upon the exact stress ratio and locations of the branch within a stressed part. Stress states often vary with location. J. Quinn used magnification to study branch angles in biaxially-stressed glass disks and also observed angles that started small, but then stabilized at a larger angle.[6] She observed that the final included angle depended upon the stress magnitude: highly-stressed disks had angles that approached the 180° degree limit, whereas lower-stressed disks had smaller final included angles. For example, in a ring-on-ring loaded disk the stresses are equal in the middle circle, but the radial stresses decrease faster than the hoop stresses with distance as fractures propagate out to the rim. Furthermore, as cracks progressively branch, they may begin to interact with each other. Hence, it is common for an initial branch angle to be large in the middle near an origin in a biaxially stressed disk, but the subsequent branch angles diminish out towards the rim.

(a) 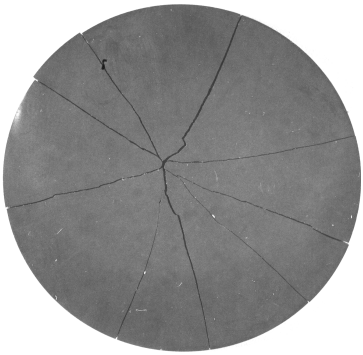 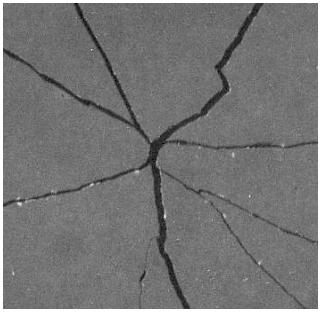 (b)

Figure 4.9 *Fracture pattern in a 44.5 mm silicon nitride ring-on-ring (10 mm x 40 mm) equibiaxial strength test disk. The stress at fracture in the inner ring was 447 MPa. The branching is curved near the origin. Successive secondary branching occurs over short distances. (b) is a close up of the origin area showing that the initial branch angles are 140° and 145°. Additional branching is minimized as the crack propagated into lower stress areas away from the disk center.*

Uniaxially-stressed parts, such as direct tension strength or bend bar specimens, have $\sigma_2/\sigma_1 = 0$. Many researchers have shown that ≈30° is the average first branching angle although there often is a large scatter. Kalthoff[7,8] studied the matter in detail in the early 1970s and used fracture mechanics analysis (using a static stress distribution) to show that cracks at greater or lesser angles than 30° had some Mode II stress intensity that tended to steer the cracks back to 30°, a direction where the maximum principal tension stress controls fracture. Cracks with angles less than 30° tended to "repel" each other, whereas cracks with larger angles tended to "attract" each other. He supported his finding with experimental evidence on glass and Araldite B polymer plates. Figure 4.8 shows a red star at $\sigma_2/\sigma_1 = 0$ and an angle of 30° that anchors the trend line.

Pressurized bottles, which have axial stresses (σ_2) that are one-half of the circumferential hoop stresses (σ_1) so that $\sigma_2/\sigma_1 = 0.5$, initially fork at about 50° to 55°. This is from measurements that the author made of photos of forty-nine branch angles from burst small vials, plus angles found in papers on pressurized-bottle fractures.[1,4,9,10,11]

In equibiaxially-stressed parts $\sigma_2/\sigma_1 = 1$, the initial branching angles are typically 110° to 125° although there is considerable scatter. Table 4.1 shows the average for seventy-six values from plates, bottles, and tempered glass was 113.8° with a standard deviation of 16.3°. The full range was 63° to 155°. Fourteen tempered glass fragments had average first branch angles of 111.4° ± 9.8°. Caution should be exercised in interpreting branch angles if fractures initiate from origins that are <u>not</u> in the middle of pressurized plates, or within the inner circle of ring-on ring disks specimens, since the stress ratios are $\sigma_2/\sigma_1 < 1$. Branch angles should be measured within the equibiaxially-stressed regions of such specimens. Disks loaded in ball-on-ring loading are problematic since the stress ratio varies dramatically with origin location. Only at the exact center is the stress ratio $\sigma_2/\sigma_1 = 1$ and if the crack propagates any significant distance away from the middle, the ratio will be less.

In the other direction on the graph, torsion fractures have a stress ratio of $\sigma_2/\sigma_1 = -1$, since one principle stress is tensile, the other is compressive. The branching angles are very small, typically 15° to 20°.

In general, initial branching angles can vary with location within a broken part. This is often due to spatial variations of the stresses. Thus, a fracture in a ring-on-ring specimen that initiated off center, near the inner loading ring, may have one branch angle for the crack that runs inward toward to the disk middle, but a smaller branch angle for the crack that runs outward to the rim due to the stress gradient.

The focus of the discussion so far has been on the first branching, whereby there is no influence of other nearby cracks. Once fracture and branching start, the stress distributions are altered. For example, Kolsky showed[12] how stresses are altered through the cross section of a bend bar as a crack propagates through it during fracture. The stress changes plus reverberations lead to the formation of the famous compression curl pattern. Rice suggested that branching patterns tend to split a component into regions of approximately similar area.[13] This implies that the cracks partition the component into pieces with comparable areas and strain energies, a reasonable supposition. It is common for an initial branch angle to be large in the middle near an origin in a biaxially-stressed disk, but subsequent branch angles diminish out towards the rim as additional branches occur. Bullock and Kaae[14] also noted that the branching angles diminished with progressive branching. Other crack systems often become operative and the physics dramatically changes. For example, biaxial glass disks tested in ring-on-ring flexure initially partition the disk into pie-shaped sections as cracks run radially out to the rim. These pie-shaped fragments are then subjected to bending and interactions with the inner loading ring and reverberations. The pie-shaped pieces then fracture in bending causing circumferential fractures in the pie-shaped fragments such as shown in Figure 4.16 later in this chapter. Secondary circumferential cracking is common around the inner loading ring. Secondary fragmentation from stress wave reverberations is common even in simple loading cases such as flexure of beams[12] or tension of rods.[15] The subject of fragmentation is covered in sections 4.5 later in this chapter, section 7.2, and section 7.13 on fractal analysis.[16] The computer-generated fracture patterns in reference 16 closely simulated real crack patterns for moderately-stressed disks. Modelers are warned that as fragmentation occurs, the stress states evolve, cracks interact, and new fracture modes occur. The author has seen many instances where irregularities on a first fracture plane can act as fracture origins on subsequent secondary fractures.

It is worth noting that in very high-energy fractures, such as high-strength glass plates broken in bending or ballistic impact fractures, that a swarm of radial cracks can form so fast that the stable branching angle shown in Figure 4.7 is not achieved. Branching and rebranching occurs quickly and the radial cracks affect each other causing them to repel each other. This gives rise to the swarm of closely-spaced “fan cracks” that resemble a folding fan.

In summary, branching angles provide at least a *qualitative* indication of the stress state. There may be material property or component shape effects. This may be a good topic for a graduate thesis.

4.4 Crack Branching Distances

The distance a propagating crack travels before branching is directly related to the stresses and stored energy in the component. The greater the stored energy, the shorter the distance to branching. If the crack travels through a region of constant stress, the empirical relationship is:

$$\sigma\sqrt{R_b} = A_b \tag{4.1}$$

where σ is the stress, R_b is the branching distance (radius), and A_b is a material constant called the fracture branching constant. A table of branching constants is in Appendix C. Additional details about equation 4.1 and A_b, including the latter's similarity to fracture toughness, are discussed in chapter 7 on Quantitative Analysis. There is some evidence that A_b may not be a material constant[17,18] and may depend upon geometry and stress state.

4.5 Fragmentation Patterns

A qualitative assessment of the stresses in a part can be made from the number of fragments. Quantitative analysis is discussed in Chapter 7. Low stress, low energy fractures create minimal branching and hence few fragments. High energy fractures cause extensive fragmentation. The extent of fragmentation depends upon the stress state throughout the body and the total energy available for fracture. A small pebble or BB gun shot creates only localized damage in a window, but a hurled brick will cause window bending in addition to localized impact damage. Sometimes a general observation about fragmentation patterns is sufficient for a quick diagnosis. For example, if a fracture occurs at an unexpectedly low stress the fractographer might suspect and search for a gross material, handling, or impact flaw that has weakened a part. Many thermal breaks are low energy fractures. High local or transient stresses may precipitate initial crack propagation, but the stress levels may be low in most other portions of a part. Low energy fractures often have few or no telltale markings on the fracture surfaces, as discussed in the next chapter.

Processing cracks that occur on firing also generate minimal fragmentation. That is because the cracks are so large that they significantly weaken the part. Differential shrinkage or out-gassing often create local stresses that can initiate a crack in the green state or during final firing, but the stresses may relax as the crack opens. Such cracks are often rough, twisted, and winding. Their internal fracture surfaces may have telltale thermal rounding or discoloration from being exposed during processing. Section 6.8.1 in the chapter on Origins has examples of large processing and firing cracks.

Moderate-stress failures create more fragments that can be reassembled so that branching patterns can be interpreted. There will be more fracture surface markings.

High-energy fracture may create so many fragments that reconstruction may be impractical. Critical pieces may be lost. That is not to say fractographic analysis is hopeless. Sometimes telltale pieces that contain the origin can be culled out of a mass of fragments and the critical information gleaned while the majority of pieces are ignored. Analysis of the fracture surfaces can reveal whether fracture was caused by tension or bending, as will be discussed in the next chapter.

Uneven stress states may be manifested in many ways. For example, Fréchette[1] showed an example of a tempered, high-powered lamp that cracked spontaneously as a result of heating in-service. The fragments were large in the fracture origin area, attesting to a low to moderate stress level. Elsewhere in the lamp, extensive fragmentation and dicing typical of tempered glass was observed. Fréchette concluded that the intense heating in service caused the middle of the lamp to lose its temper and weaken such that it was more susceptible to fracture from thermal stresses.

Although similar techniques are applied to analyze laboratory-generated fractures and component service fractures, it is convenient to treat them separately in the following paragraphs. Even if one is primarily interested in component analysis, the experience gained with laboratory fractures can help.

4.6 Laboratory Test Fracture Patterns

In the laboratory the cause of fracture is known. Fractographic analysis may be done to identify strength-limiting flaws or to study crack microstructure interactions. It also may be done to verify that the test was done correctly and that the fixtures and specimen were aligned properly. It also may be done to gain valuable experience in examining fracture patterns in a particular material that can help with component failure analysis.

A simple precaution should be taken before the testing commences: *Shielding or buffering material should be placed around the specimens to catch all the fragments and to minimize secondary fractures and impact damage.* Cotton or tissue buffering and paper shields can be placed around the test specimens. In some instances, the specimens may be partially taped before the test so that the pieces remain attached to the tape after fracture. This must be done judiciously and in no instance should tape interfere with the load application.

Tape should not be used on the tensile surfaces. Ring-on-ring loaded disks may be taped on the compression side of the specimen with a tape circle inside the loading ring and a tape annulus outside the inner loading ring. The portion of the surface in direct contact with the loading ring should not be taped.

Specimens should be premarked with orientation or location marks. This preliminary step can dramatically aid post fracture analysis. For example, the orientation of round specimens tested in tension should be marked to ascertain whether fracture occurs preferentially from one side or another. Similarly, flexural strength specimens should always have the loading points marked on the side once the specimen has been inserted and preloaded in the bend fixtures. The marks will help ascertain whether breakages occur at the load pins. Sometimes a grid may be marked on a specimen to help with reconstruction. This may help with biaxial disks loaded in flexure, but again, any such markings should be on the compression side of the specimen.

4.6.1 Tension strength

This category includes machined specimens with grip holes or shoulders, glass optical fibers pulled in tension, or long tubes or rods that are pulled apart.

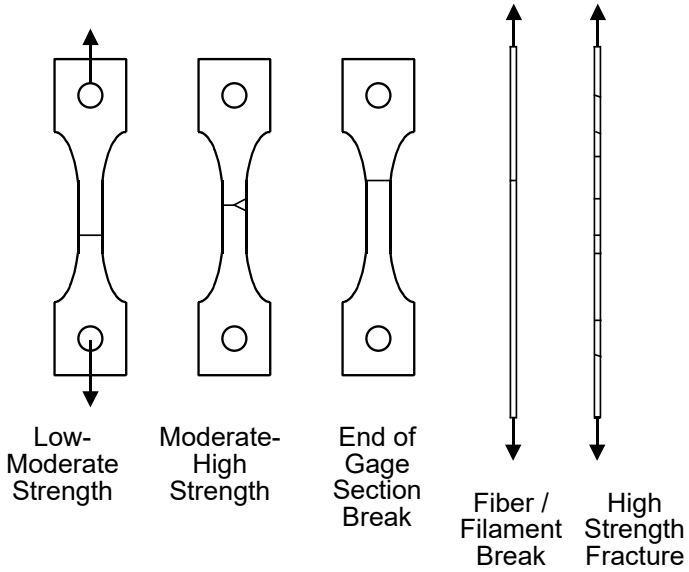

Figure 4.10 *Tension specimen and fiber fractures.*

Direct tension is conceptually one of the simplest loading configurations, but in practice it can be tricky to achieve. Slight loading misalignments or test specimen irregularities can create superimposed bending stresses. Breakage patterns in properly aligned specimens are usually quite simple as shown in Figure 4.10. Fractures initiate and run perpendicularly to the loading axis until and if they branch. Moderate-to-high strength specimens may branch with the telltale 30° to 45° angle as discussed in section 4.3. Fractures at a nonperpendicular angle to the loading direction (or with compression curls as discussed in the next section) should be cause for concern and suggest misalignments in the load train. It is especially important to ascertain whether fracture origins are located on the specimen surface, in the interior, or at an edge as will be discussed in the next chapter. Breakages in a group of test specimens should be randomly distributed within the gage section. An occasional break near the end of the gage section is probably not too serious, but if all specimens break from the end, then the tester should review the test specimen design. The stress concentration at the end of the gage section, the fixture and grip alignments, and the machining of the blend junction at the end of the gage section should be checked.

High strength fibers have the added complication that secondary fractures are common. After initial fracture, the intense stored elastic energy in the fiber releases, sending stress waves through each broken portion. Reverberations and fiber whipping cause additional breakages. Fragmentation may be so thorough that it may be impractical to find a primary fracture. Testing in oil or coating the fibers with grease may minimize the whipping and secondary breakage, at the risk of contaminating the primary fracture and altering the environmental sensitivity of fiber strengths.

4.6.2 Flexural strength

Flexural strength testing with rod or bar specimens is often done in lieu of direct tension testing. Flexure is much easier to do. Specimens and testing equipment cost considerably less. A drawback is that much less volume and area are exposed to the full tensile stresses. Hence, flexural strengths are typically greater than direct tension test strengths. Reference 19 is a review of flexural strength testing of ceramics. For our purpose here, it is convenient to briefly review the stress state in linearly-elastic materials as shown in Figure 4.11. The bending loading creates a stress distribution such that the maximum tensile stress is on the bottom as shown in (b) and (c). This is often described as the “maximum outer fiber stress.”

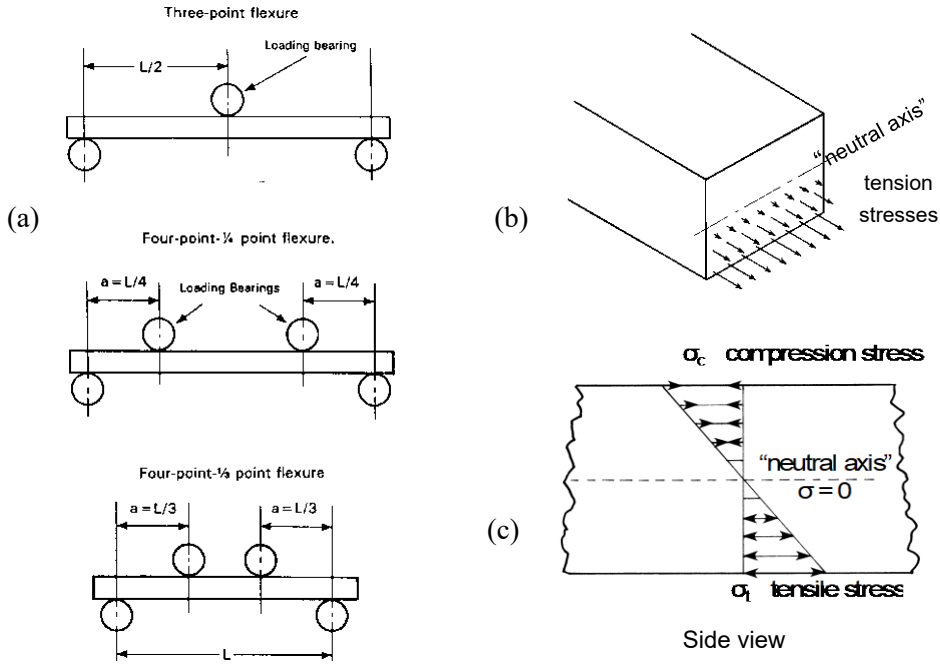

Figure 4.11 *Three- and four-point flexure test configurations are shown in (a). The stress distribution on a cross section is illustrated in (b) and (c).*

The tensile stresses diminish into the interior until they are zero in the middle, at the "neutral axis." The tensile stresses are balanced by compression stresses on the opposite side. The maximum stress exists only directly opposite the middle loading point in three-point loading and diminishes linearly with distance from the middle loading point to the outer support points. In four-point flexure, the maximum stress occurs over a larger region between the two inner loading points. Additional information on the stress distribution is given on pages D-24 and D-25 in Appendix D. (There are significant shear stresses in these beams, but they usually do not cause fracture unless the beam is a laminated composite.)

It is worth noting at this point that the "flexural strength of a test piece" is the maximum stress in the piece at the instant of fracture, *irrespective of the actual fracture origin location.* The maximum stress is used to compute the "strength" of one bar or rod. It is a nominal, reference stress level in the beam when it broke. Weibull analysis of flexural strength data requires one to use this maximum-reference stress level. In other words, use the maximum stress for most normal uses of flexural strength data. There are two exceptions: a fracture mechanics analysis of the size of the fracture origin flaw, or a fracture mirror size analysis. In these latter two cases, use the actual tensile stress <u>at the</u>

origin site. This is explained further and illustrated on pages D-24 and D-25 of Appendix D.

A very telltale feature of bend fractures is the *compression curl*, also known as the *cantilever curl*, shown in Figures 4.12 and 4.13 and later in Figure 5.1. Once the crack has propagated from the tensile half of the specimen into the compression side, it slows down and changes direction. In stronger specimens the crack can branch, creating a double curl. The existence of a compression curl is an important sign that the specimen either was loaded primarily in

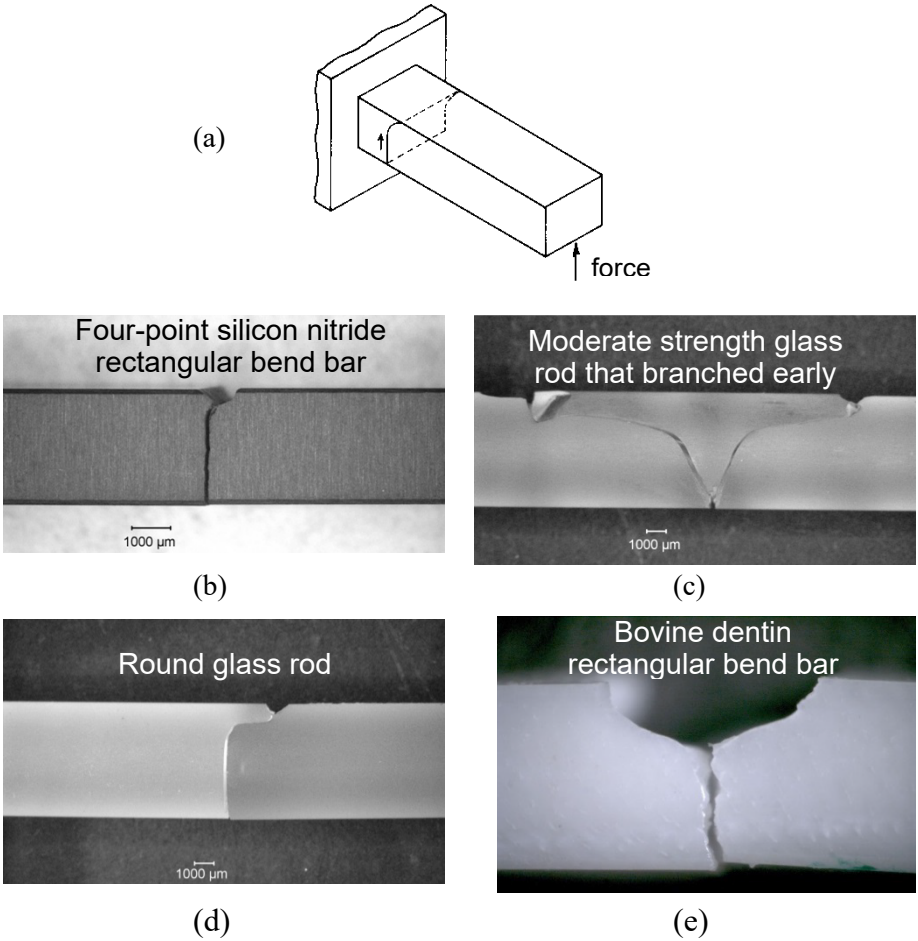

Figure 4.12 *Compression or cantilever curls are a telltale feature of flexural fractures. (b) – (e) show side views of four-point flexure specimens. In each case shown, the tension surface is on the bottom and compression is on top.*

bending or had a strong bending component. Compression curls are not normally present in direct tension specimens, unless they were badly misaligned such that some bending was superimposed on the gage section. The origin of fracture on a fracture surface is directly opposite the compression curl. The presence or absence of compression curls may be important for interpreting not only test specimens, but component fractures as well. Thermal fractures usually do not have compression curls. Tsirk argued in his book[20] that in simply supported beams as shown here in Figure 4.12a, the curl tends to run back towards the support. He argued this is due to shear stresses and that the maximum principle stresses steers the crack in that direction. To verify this, I tested fourteen glass rods supported in a vise with cushioned grips, by tapping with a small mallet hammer on the rod ends as shown in Figure 4.12a. The rods had a small score mark on the tensile surface near the support to weaken them. If the score mark was within the contact area of the grips, the curl came out toward the applied force. If the score was right at the end of the cushioned support, the curl went back into the grips. If the score was just outside the gripped area, the curl went back to the grips, but sometimes came outward towards the force as shown in Figure 4.12a. The angle of the force was a critical parameter, and if the force were angled slightly away from the vise, the curl came outward toward the force. I concluded that the direction of the curl varied with the location of the origin and the precise angle of the force.

Kolsky,[12] used very high-speed photography in glass and showed the compression curl in beams in bending is formed late in a fracture, often due to elastic wave reverberations interacting with the slowly moving crack in its final stages of breakthrough. This may seem counter-intuitive since the fracture surface shows that fracture very quickly reaches terminal velocity (if a fracture mirror and hackle form as discussed in the next chapter), but cracks may in fact slow down very rapidly once they get to the compressively-loaded half of the beam. Furthermore, Kolsky showed that the local stress state around the crack is dramatically altered during the fracture event. It is very much a dynamic situation. Most of this is of secondary importance, however. The key point here is quite simple: a compression curl indicates a part was loaded in bending.

Figure 4.13 shows a variety of fracture patterns in bend bars. Low strength fractures are often the easiest to interpret since the specimen breaks into only two or three pieces. Often a small “T” shaped piece will be opposite the origin, but this fragment can be ignored since it never has the origin on it. The origin is below the “T” fragment on the two matching pieces nearer to the tensile stressed surface. Sometimes it is handy to keep the “T” fragments to confirm the other fragments do fit together.

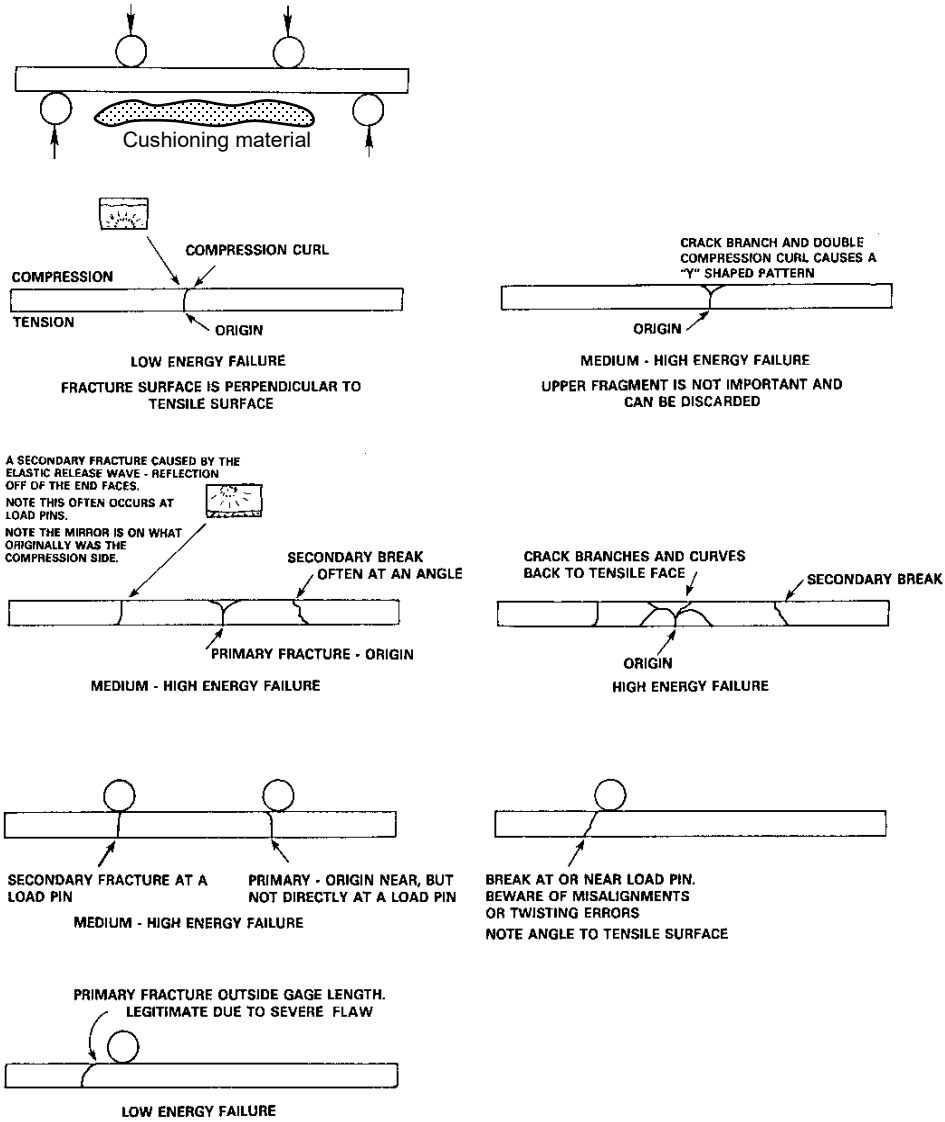

Figure 4.13 *Fracture patterns in four-point flexure specimens. Cushioning material under the specimens minimizes damage to the fracture surface edge.*

Higher strength bars have two or more fractures, and it must be deduced which was primary. Secondary fractures are caused by reverberations and stress reflections after the first fracture has occurred.[12,21] Secondary breaks frequently occur at the loading points. If there are two fractures and one is located at an inner loading point and the other is in the inner gage section, the latter is probably the primary fracture with the first origin. If the two breaks are

close to the two inner loading points, then the exact locations on the tensile surface should be examined closely. Often one fracture will be right under a loading point, whereas the other may be close, but not right at the loading point. The latter is usually the primary fracture. If both are exactly under the two inner points, it may be difficult to deduce which was first. There is also the possibility the specimen might have been loaded unevenly causing stress concentrations at both sites. If this occurs for more than a few specimens in a set, then the fixture should be checked as well as the specimen's parallelism.

Properly aligned specimens and fixtures almost always cause a perpendicular primary fracture in the middle gage section. Secondary fractures are often but not always at a slight non-perpendicular angle to the specimen axis. Misaligned specimens or fixtures can cause twisted crack planes as shown in Figure 4.14 and described in Ref. 22.

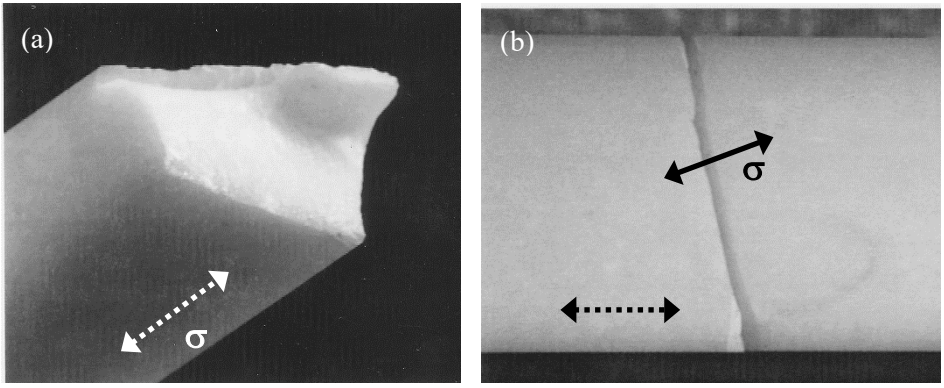

Figure 4.14 *A twisted fracture surface in a misaligned alumina bend bar in a fixture that did not articulate properly. (a) shows the fracture surface, and (b) the tensile surface of both halves. The principal stress direction (solid black arrow) was 14 degrees off the expected direction (dotted arrows).*

An unusually large flaw <u>outside</u> the gage section can trigger a fracture with crack plane tilted towards an inner loading pin. Specimens with such low strength fractures usually do not have secondary breaks. *A fracture outside the inner gage section in properly aligned specimens and fixtures is usually completely valid and a warning that an unusually large flaw is present.* An example is shown in Figure 4.15. It should not be dismissed as an invalid test.

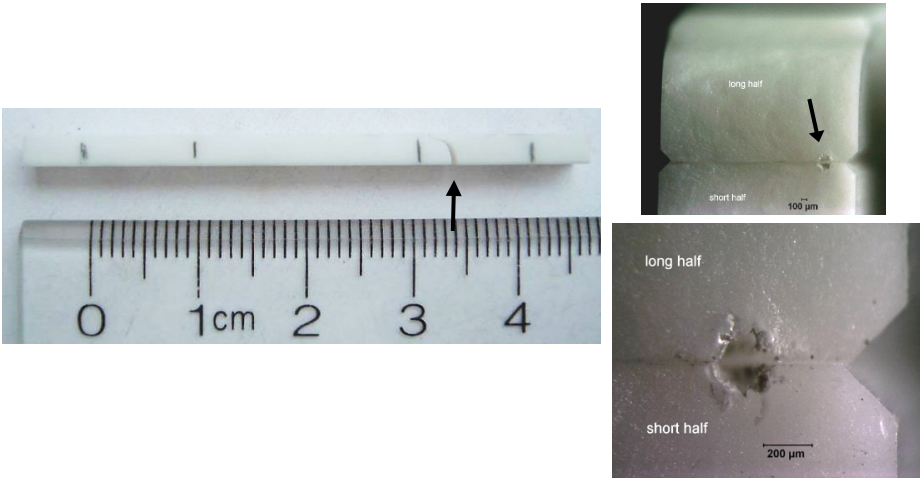

Figure 4.15 *An 4 5 mm long alumina bend bar (313 MPa) with the 4-point contact points marked by a pencil. The fracture origin (arrow) was a very large material flaw outside the gage section (arrow). It was a valid test.*

Figure 4.16 shows an interesting example of a human leg bone broken in bending from a new FBI Guide to Forensic Fractography of Bone.[23] Here the "T" shaped piece so large it is called a "wedge fragment" and the overall pattern is called a "wedge fracture." The origin is opposite the wedge piece.

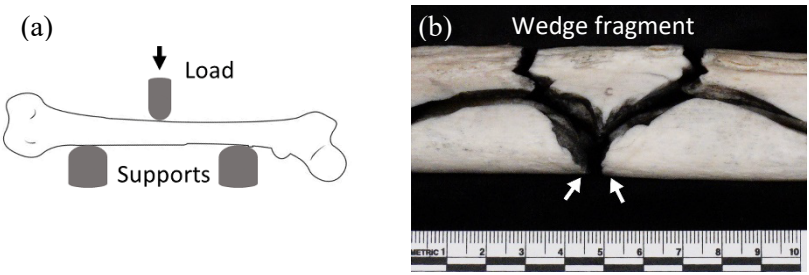

Figure 4.16 *A human leg bone broken in bending. In (b) the middle top piece is deemed a "wedge fragment" in Ref. 23. The white arrows mark the origin. (a courtesy A. Christensen, b courtesy M. Isa)*

4.6.3 Biaxial flexural strength

Plates or disks may be tested in biaxial tension by a variety of methods including: pressure on-ring, ring-on-ring, piston-on-ring, ball-on-ring, and ball-on-three balls. Pressure-on-ring loading (whereby a specimen is supported on a

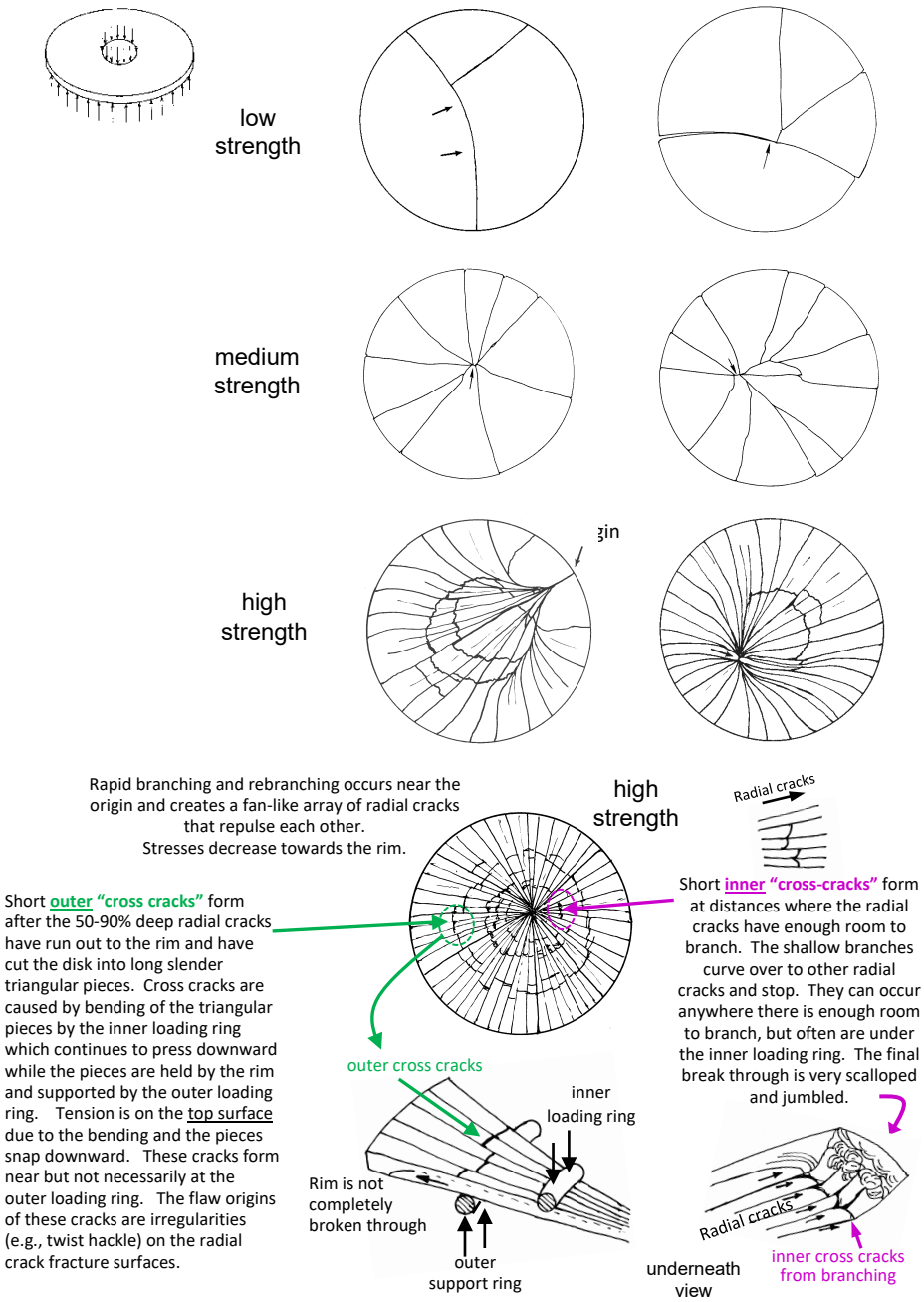

Figure 4.17 *Fragmentation patterns in ring-on-ring loaded specimens. In low strength parts, after the first break has occurred, the larger remnant may still bear load from the inner loading ring, and it in turn will break in bending. In high strength disks, secondary circumferential "cross cracks" occur.*

ring and is loaded by a uniform pressure on the opposite surface) has the virtue that a large area is stressed biaxially. There are no loading point or stress concentration problems with the inner loaded area. Ring-on-ring loading is more commonly done since it is simpler to do. It creates an equibiaxially-stressed region within the inner circle. Pressure-on-ring and ring-on-ring are best used with specimens that have flat and parallel surfaces for even contact with the loading and support fixture rings. Figure 4.17 shows fracture patterns in ring-on-ring specimens.

The single ball loading schemes have the drawback that only a tiny spot directly under the loading point experiences the maximum stress. The concentrated forces of the ball distort the stress field in the vicinity. Fracture almost always starts directly below the loading ball. The ball-on-three balls or piston-on-three balls schemes are better suited for uneven specimens, but the stress state is not very symmetric. Cracks often align themselves to run between the supporting balls. *Excessively thick test specimens should not be used, since breaking forces are so high that Herztian cone cracks can be initiated by the middle loading ball*. These disturb the stress state. In the worst case, the cone cracks will propagate through the specimen thickness and reach the tensile side and cause unintended fracture. This is an invalid test.

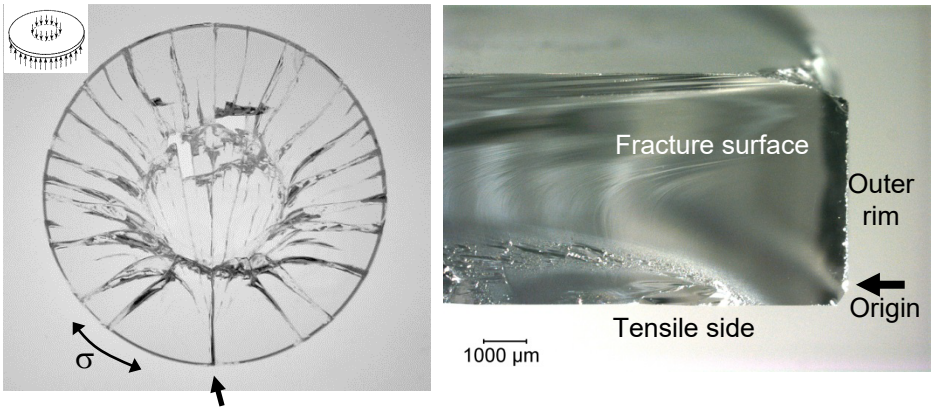

Figure 4.18 *A fractured BK-7 glass ring-on-ring tested disk. (a) shows the overall breakage pattern. Fracture started on the rim (large arrow) in response to the uniaxial hoop stress σ (small arrows), propagated towards the middle, and branched in response due to the greater biaxial stresses in the middle. (b) shows the fracture surface. The origin is a grinding crack on the outer rim (large arrow). Notice the partial fracture mirror.*

A common misperception about ring-on-ring testing is that the edge condition is unimportant, since the maximum stresses are within the inner loading circle. This notion is only partly correct. Figure 4.18 shows one of several fractured BK-7 borosilicate crown glass specimens that were part of a large set of specimens intended to generate a comprehensive design and reliability database. The overall fracture pattern showed the origin was on the rim. Fracture surface examination confirmed that outer rim grinding cracks caused fracture. Stress analyses for ring-on-ring specimens (e.g., Fessler and Fricker[24] or Salem and Powers[25]) show that the maximum hoop and radial stresses are in the inner circle. The radial stresses gradually diminish to zero out at the rim. *Hoop stresses also diminish, but are finite at the rim and depend upon the specimen dimensions, the fixture sizes, and Poisson's ratio.* In the case of the disk shown in the Figure, the hoop stresses were as large as 48 % of the maximum stresses in the middle. It was not surprising that with a highly-polished tensile surface, the disk fractured from grinding flaws on the rim. In this testing episode, the problem was detected early after only six disks had been tested. The remaining disks were reground and HF acid etched to diminish the severity of the grinding cracks. Subsequent fracture testing was successful and almost always initiated fracture from the central disk region. If this precaution had not been taken and the remaining disks tested to fracture, the database would have been nearly worthless. The point here is that fractography is a valuable aid to mechanical property testing.

One way to mitigate edge fractures is to use a large overhang. This is often done with square plates that are as cut and have no edge treatment. Large overhangs alter the stress state, and the maximum stress in the inner circle must take the overhang into account. A large overhang can have an unexpected consequence as explained below.

Additional common plate and disk crack branching patterns are shown in Figure 7.39 in Chapter 7, in section 7.13 on fractal analysis.

Sometimes spiral cracks can form in biaxially strength-tested plates if there is a large overhang.[26] Figure 4.19 shows examples. The plate shown in Figures a,b had an overhang that was so large that it stiffened the rim of the plate and led to the formation of tensile stresses on the top (nominally the compression) side of the plate in the overhang region and over the outer loading ring. These are illustrated by Figure 4.19c. By chance, a very large flaw was located in the overhang on the top surface and it initiated a fracture whereby cracks ran to the top and bottom and spiraled almost all the way around the plate. These cracks actually led on the top surface (which one normally thinks of as being in compression) in response to the radial tensile stress in the overhang.

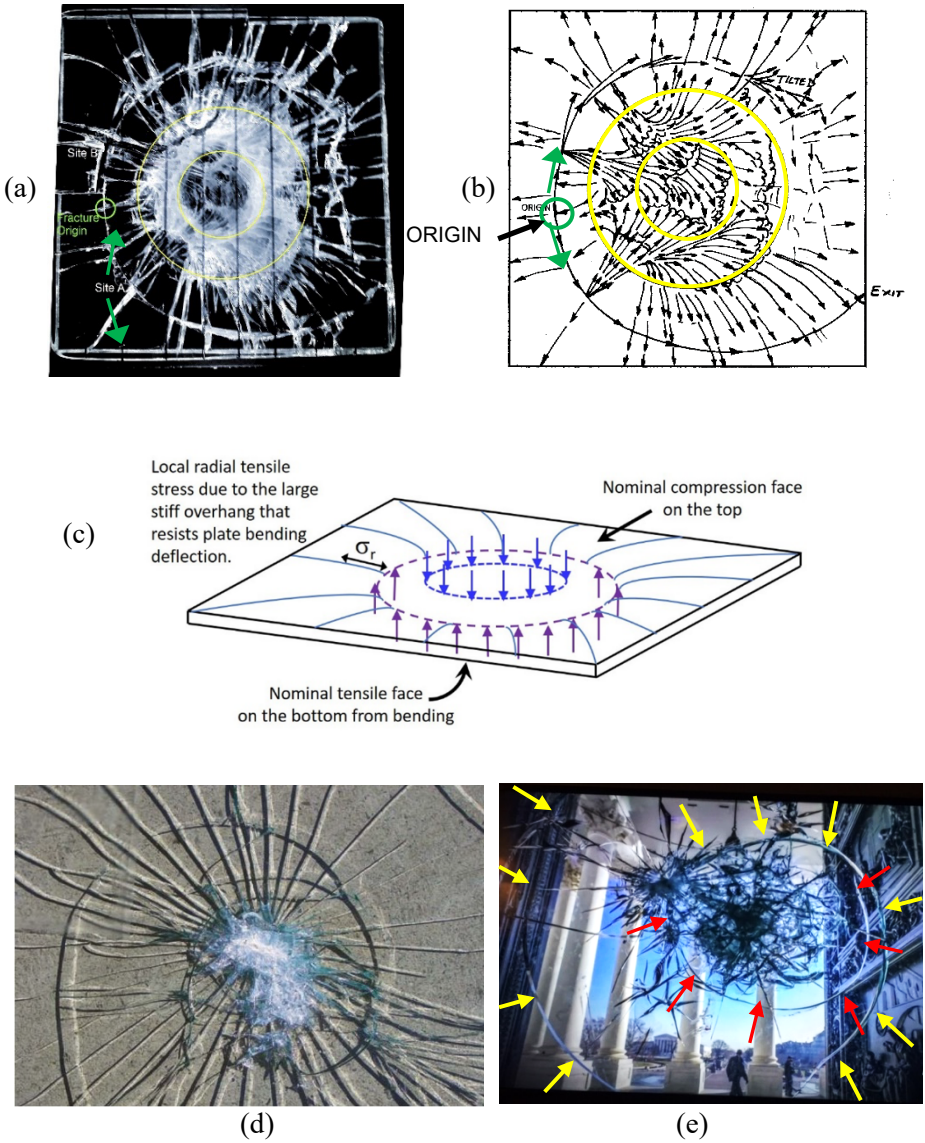

Figure 4.19 *Spiral cracks (a) and (b) in a 152 mm square glass plate broken in a ring-on-ring strength test. The inner loading and the outer support rings are shown by the yellow circles. The origin is marked by the green circles on the top surface of the plate. (c) shows how radial tensile stress can develop as shown. (d) shows a spiral crack in a heat-strengthened plate (courtesy J. Wurm[27]). (e) shows an example of dual spiral cracks (yellow and red arrows) in a window pane that broke in the U. S. Capitol Building on January 6, 2021. The multilayered safety glass was repeatedly impacted by rioters.*

Similar spiral cracks can form in flexed or impacted glass window panes or ballistic armor glass whereby the frame or mounting resists the backward flexing of the plate. Figure 4-19e shows an example. In summary, spiral cracks can form and propagate on the front side of a flexed plate that is rigidly supported at its rim or is supported from underneath and has a large overhang that resists flexing.

4.6.4 Laboratory test specimen analysis: additional tips

It is often helpful to look at contact marks or scuff marks where the specimen was loaded, whether it was in tension, uniaxial or biaxial bending. Such surface marks are one type of *witness marks:*

Witness marks: *marks on a specimen surface that attest to contact with a foreign body.*

Witness marks help one to ascertain whether loading was in fact uniform or not. Contact marks in a bend specimen may also help with the interpretation of whether a break occurred directly opposite a loading pin.

Test specimens are often broken in batches of ten, thirty, or more. Which specimens should be examined first? The pragmatic answer is that the weakest ones should be examined first, since they are the easiest to interpret. The experience gained from these easy specimens facilitates examination of the more complex fractured specimens, since the fractographer will be better prepared to recognize primary fractures and distinguish them from secondary breaks.

4.7 Component Fracture Patterns – General

Component fractures have the complication that the state of stress or the cause of failure may be unknown. The general fragmentation pattern can provide powerful clues. The fractographer first should obtain whatever ancillary information is possible about the component. What exactly was the material? What were the circumstances of the fracture? Was it an isolated case or part of a series? Had some change been made to the material or the loading conditions? Was there a noise (e.g., shattering sounds or water hammer)? Were there other parts or evidence found with the fractured material (impact debris)? Was there a witness? Is the witness honest? Does the witness have a good memory? Background information such as this may be crucial for the broader failure analysis. Nevertheless, the fractographer must keep an open mind, and let the pieces tell their story.

A wise precaution is to retrieve as many pieces as possible. In some instances where there is an obvious pattern, the fractographer can cull out important fragments. On the other hand, if other people have the fragments, you *cannot expect them to know* which are the important pieces. They should retrieve all pieces. If remnants are in a mount or assembly, then they should not be retrieved or extracted until after the fractographer has had an opportunity to examine them in situ. Of course, this may not always be practical, but the fractographer should try to see the fracture scene and fragments in as close to in situ state as possible. At the minimum, photographs of the overall fracture

Figure 4.20 *Dr. J. Quinn with a window fracture problem at NIST. Evidence collected at the scene included foreign material (animal fur!) attached to the impact site as shown in (c). The crack patterns indicated impact from the exterior. That, plus the height of the impact above the ground, the tuft of fur, the time of the year (November, the rutting season) and similar occurrences elsewhere suggested the cause of failure shown in (d). The deer saw its reflection in the window and attacked it!*

pattern and close-ups as necessary should be taken. Figures 4.20 illustrate some of these recommendations for a practical failure problem. This window fracture also illustrates how witness marks or traces of the impactor material aided the interpretation.

The impulse is to jump directly to an examination of the fracture surfaces to find an origin. While there may be no harm in this (and it is human nature for most fractographers to take this step), there is one extra step that is prudent to take immediately, especially if a moderate or great amount of time will be spent in specimen reconstruction or the part will be involved in serious failure analysis or litigation:

The entire component or part should be photographed or sketched.

There are several reasons why it is wise to capture an image of a whole structure or sketch it at an early stage. There are obvious instances, for technical or legal purposes, why a permanent record is required. It is best to make the record as soon as possible, lest pieces be lost, misplaced, or mangled in handling. An early record is essential if pieces need be cut up for microscopic examination. If the pattern of fracture is complex and an origin location not obvious, the fractographer may have to examine many pieces in order to track the cracking pattern back to the origin. A sketch or photo that can be marked up aids this process. Figure 4.21 shows an example of a broken component and an accompanying sketch with work notes.

An overall sketch or photo will help the analyst show other fractographers, engineers, managers, or clients the overall context of the fracture origin or fracture pattern. Is the fracture from the same location as other parts, is the pattern of breakage the same, or has a new failure mode been triggered? Much time and accuracy may be lost in orally explaining or drawing sketches from memory the fracture patterns days or weeks later. A handy overall photo of the part can save time and reassure others that the correct fracture origin photos indeed have been taken. A ruler, magnification marker, or a common object such as a coin should be placed next to the component when a photo is taken. Many close-up images of fracture features that I have seen in the technical literature are unconvincing or may in fact have nothing to do with a bona fide fracture origin.

If many examples of a particular part are to be studied, then a sketch or photo of an *unbroken* part may be useful as a <u>blank</u> onto which fracture patterns may be sketched or drawn.

There is another very important and overlooked reason why a fractographer ought to make sketches. In the very process of drawing a line, the fractographer must think: "where exactly is that line, exactly what does it mean, and which way does it go?" Why did it start here and not there? The

(a)

(b)

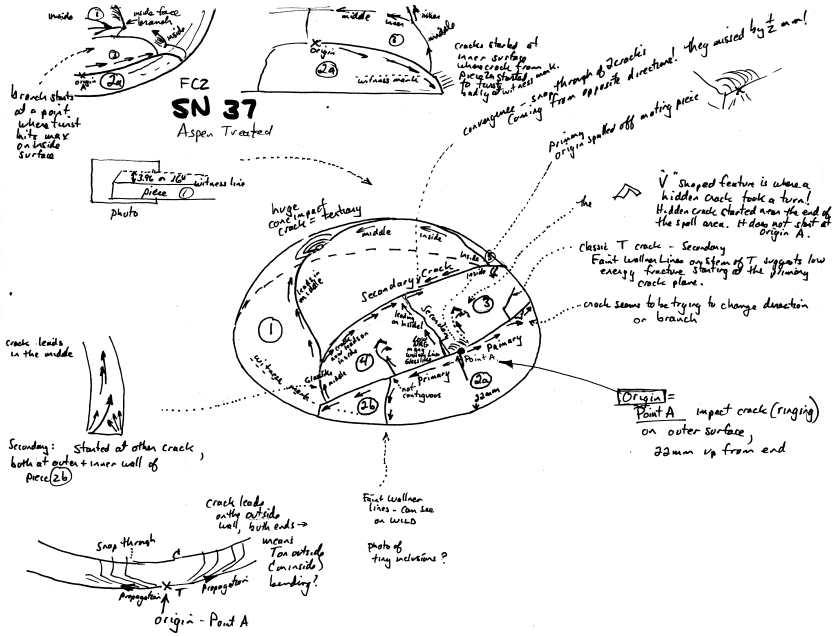

Figure 4.21 *A fractured single-crystal sapphire hemispherical 90 mm dome #SN37 that broke in a high temperature, high Mach wind tunnel. It was shown previously as Figure 3.10. The crack progression along individual pieces was used to back track to the origin (arrow). The sketch (b) helped integrate and keep track of the information from examination of the individual pieces. The origin is marked by the arrow in (a) and is labeled "origin" in (b). Figure 8.22 in Chapter 8 shows the actual origin flaw which was a tiny particle impact site. Thermal stresses then caused the dome fracture. Figure 5.55 in chapter 5 shows an example of a scarp that was detected on a fragment of this dome.*

fractographer must contemplate and interpret what has happened as the sketch is being made. This is an important step in an interpretation and diagnosis of fracture. Professor Varner at Alfred University put the matter rather succinctly: "One can take a photo without thinking, but one cannot make a drawing without thinking." One study noted that students who took a museum tour had more difficulty remembering the objects if they only photographed them, rather than if they looked at the objects without taking a photo. The popular author David Maccauley, who has written a series of well-illustrated books such as Cathedral,[28] and City,[29] has said that when he creates his drawings, he must contemplate how the structures were designed, what materials were used, and how they were assembled. Leonardo da Vinci's drawings underscore the depth of his knowledge about objects both natural and manmade and how they worked.

Some common fracture patterns are shown in the following examples. The reader is referred to the bibliography for more information. Fractographers who are dealing with specific component failures are strongly advised to search the literature for prior examples and documentation of similar fracture patterns. Appendix B of this guide is a compilation of fractographic case studies.

4.8 T Intersections and Crossing Cracks

Intersecting cracks may pose interpretation problems in component fracture analysis. A fractographer may initially be confused by the multitude of intersecting cracks. Which came first? Which way was the crack going? With a little experience and applying the process of deduction, it usually is not too difficult to answer these questions. Figure 4.22 offers some guidance.

Crack branching creates patterns shown in (a). The branch angle depends upon the stress state as shown previously in section 4.3. Even with biaxial loading and branch angles near 180°, a close examination of the branching point will show which way the crack was moving as it split. Hence the determination of the crack propagation direction is easy. Intersecting cracks as shown in (b) are also easy to interpret. The first crack is continuous and passes through the plate undisturbed. The second crack approaches and is stopped at the intersection since it is unable to traverse the previously cleaved material. Intersections are commonly at 90° since the second crack moves at right angles to tensile stresses and tensile stresses cannot be carried across the previously cleaved crack. Examination of the fracture surfaces (to be discussed in the next chapter) will also corroborate the interpretation, since the fracture surface of the first crack is planar and undisturbed though the intersection. Wallner lines and hackle lines

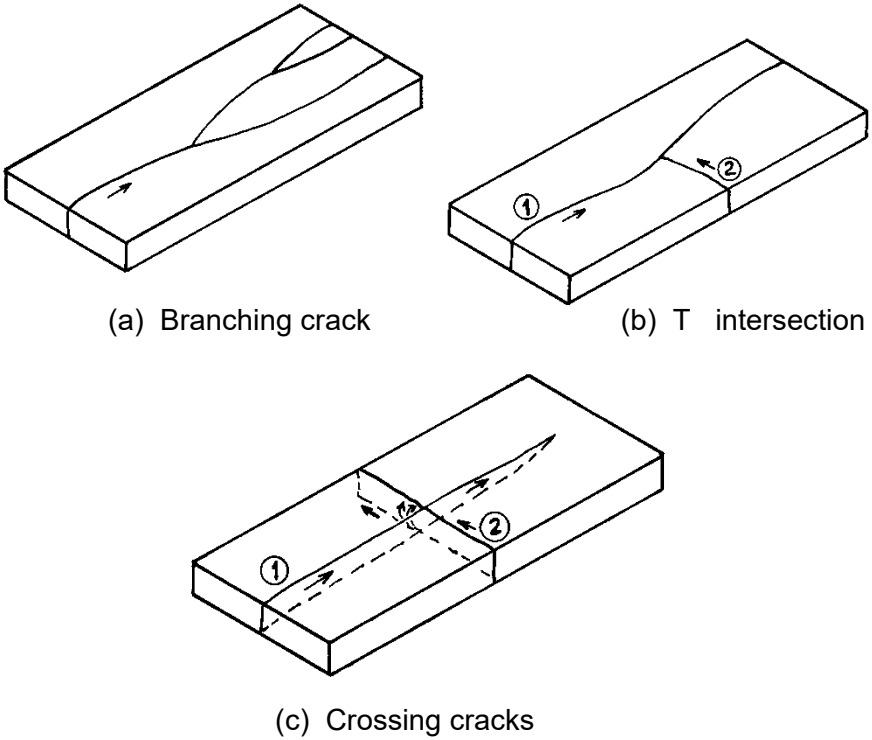

Figure 4.22 *Intersecting cracks. (a) shows common crack branching, which can be distinguished by the gradual forking. (b) shows a T intersection. The numerals indicate the first and second cracks. (c) shows a crossing crack, which may occur if the first crack does not completely cleave the part.*

for the first crack plane are continuous and connected on each side of the intersection.

The scenario shown in Figure 4.22c occurs in cases where an initial crack does not completely cleave the plate. This can easily occur with bending fractures wherein the crack leads on one side that is in tension, but does not necessarily go all the way through on the compression side. The window in Figure 4.20 has examples. In such cases, the remnant ligament of unbroken material provides a path for a crossing crack to traverse the first crack. The key features to look for are disturbances in the fracture surface. The fracture surface markings (Wallner lines and hackle) on the first plane are continuous on either side of the intersection. On the other hand, the second crack has a pronounced change in the markings on its crack plane, often a jog, or a hook around and up to complete the fracture just on the other side of the first crack. Sometimes two cracks seem to cross exactly over each other at exactly 90°, but a very close

inspection of the exact intersection will show that the second crack has a slight offset or step where it intersects the other.

4.9 Invisible Cracks

Incomplete fractures sometimes create cracks that are difficult or impossible to see. The interfacial separations may be less than the wavelengths of light and the cracks are not visible even under a microscope. The cracks may even be partially healed. Interfacial adhesion may be due to hydrogen bonding from water molecules adsorbed onto the fresh surfaces following the initial crack opening.[30,31,32,33] The healing can occur even in inert environments and vacuum, and indeed, the literature shows that dangling-ruptured silicate bonds do link back up. When a crack is created but closes quickly, as in the case of a window impact, pockets of air may be trapped between the crack faces. These pockets may be visible if light is reflected off the glass-air interface. Sometimes the light is refracted creating elusive but colorful reflections that are visible only at certain angles. This is one reason why it is wise to rotate and shift a piece while inspecting it, or to move around it if the piece is stationary. "Chill check" cracks, described in section 6.8.4 and shown in Figure 6.76, are tiny cracks formed by transient, very-localized thermal shock. They can be very difficult to see. Sometimes crack segments will *appear* to be isolated and not connected to other cracks or to an origin, but they are in fact connected by invisible segments. Fréchette[1] described a case wherein an invisible long crack in an intravenous bottle went unnoticed in a hospital, leading to a fatality. Internal cracks may be invisible in bottles that are filled with liquid.[34] Schaut et al. [35] described a number of instances when visual and automated inspections of pharmaceutical containers did not detect cracks since they were too tight.

Ernsberger[36] stated that the surface of plate and sheet glass is populated by invisible microcracks. The crack faces are in very tight contact and will be activated when the glass is placed in tension. These microcracks can be formed by contact, friction and abrasion during forming and handling. Shallow surface cracks can also form in glasses during cooldown from processing temperatures. Such cracks are sometimes called "checks."

4.10 Plates and Windows

Plates and windows can exhibit a wide variety of fracture patterns. Some common modes are shown in Figure 4.23. Shinkai's excellent article[37] shows subtle variations in the fracture patterns depending upon whether the plate edges are freely supported or are built in. Variations also occur with plate

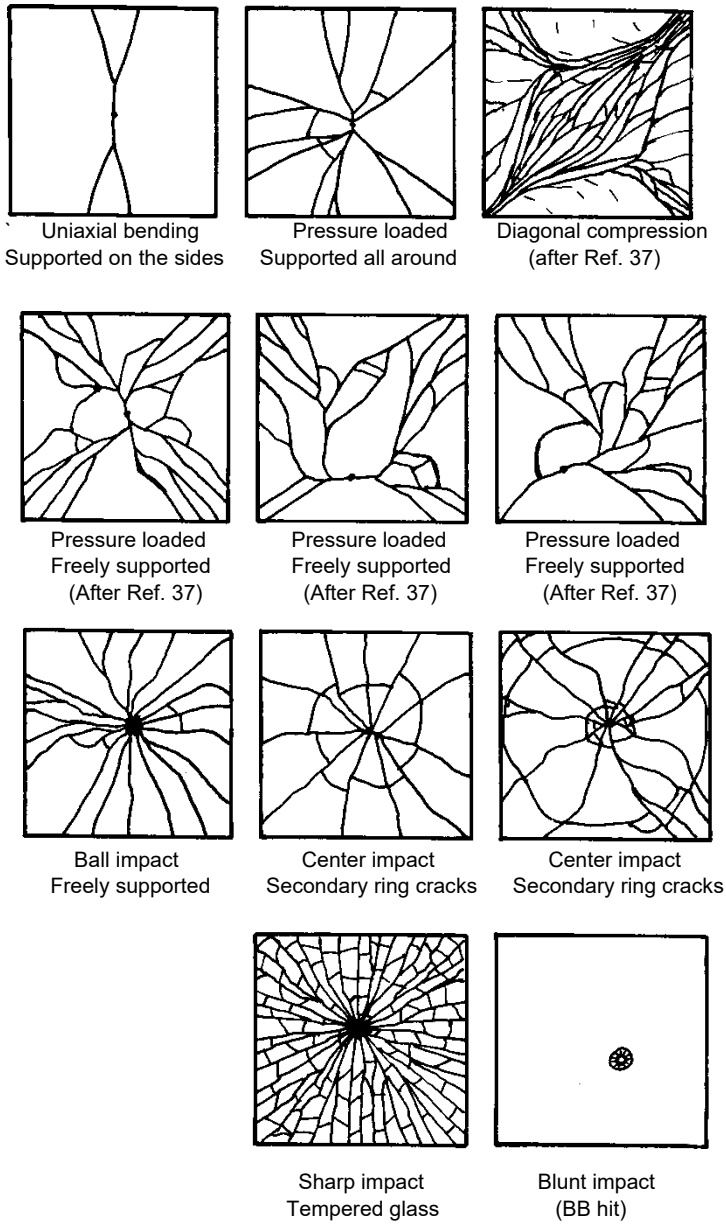

Figure 4.23 *Plate and window fracture patterns. Figures 4.19e and 4.20b show examples of a center impact plate with secondary ring cracks.*

thickness. The extent of residual stress in tempered glass plates may also be estimated from the size of the diced fragments as discussed in 7.2.2. Heat strengthened glasses also have compressive residual stresses such that the glass

is twice as strong as an annealed plate, but the pieces do not dice into small fragments. They break into triangular shards similar to annealed plate breaks.

Blunt objects may create a Hertzian cone crack that penetrates partially or completely through the plate. Such a flaw may or may not necessarily constitute a failure, since the plate is essentially intact. At higher velocities, radial cracks may be generated from the impact site. Radial cracks also may be triggered by impact of sharp objects.

In other cases, the bending forces from the impact may cause the crack (once it is away from the immediate impact site) to run on the opposite side of the plate from the direction of impact. At even higher velocities, many radial cracks fan outward from the impact site. The continued loading of the plate causes the radially-fractured segments to bend inward, causing them to break in bending leading to circumferential secondary cracking. In these secondary fractures, the maximum tension is on the impacted side of the plate. These rings around the impact often have offsets at the radial cracks, confirming that the radial cracks occurred first. Figures 4.17, 4.20b and 4.23 show examples. Sometimes a secondary ring crack may step across a radial crack if the latter has not completely severed the plate. Very blunt objects may not necessarily create cracking at the impact side. Bending forces can create tension opposite the impact side and can trigger crack growth from flaws on the opposite side. In some instances, the very blunt object can generate bending forces in the plate that triggers a crack from a flaw at the plate edge. A crack runs to the impact site, and then radiates and branches repeatedly outward as in Figs. 4.17 and 4.18. In analyzing such fracture sequences, it is often very useful to combine the overall crack pattern analysis with an examination of the fracture surfaces, as described in the next chapter. The fracture surface examination reveals whether the crack was running uniformly through the thickness or was leading on the inside or outside plate surfaces. The latter information can establish whether the plate was in bending, and if so, which side was in tension.

4.11 Tempered Windows and Objects

Tempered glasses fracture into many small fragments. It is said that the glass "diced up." Occasionally such fractures are triggered by internal flaws such as nickel sulfide inclusions (Chapter 6). More commonly, the fracture is triggered by impact or sharp contact loading on the surface. If the loading is sufficient, it drives a surface crack through the surface compression temper zone and into the interior tensile stresses. The cracks hit terminal velocity very quickly and branch repeatedly into small fragments since the internal stresses are more than sufficient to cause propagation and repeated branching. If there is no continued

external loading, the window might remain in place. Evidently the internal cracks have not broken all the way out to the external surface. Sometimes there is a noticeable time delay and slow crack growth or an elastic wave reverberation, may eventually cause one crack to break through throwing the forces out of balance. Then the window or object will erupt into pieces. Figure 3.9 in chapter 3 showed an example of a street skylight that fractured but was held in place by a bonded second glass layer. Figures 6.20 and 6.37 in chapter 6 show two examples. The origins can often be deduced from the branch crack patterns as shown in Figures 3.9 and 4.24. Close examination of the origin area often reveals that in moderate impact or loading cases, the crack branching creates matching symmetrical hexagonal (or pentagonal or heptagonal) shaped pieces at the origin as shown in Figures 3.9 and 4.24c. This symmetric pattern is often described as a "butterfly pattern." As will be discussed in Chapter 7 (section 7.3.2) and Figure 7.6, the first branch distances may be used to estimate the temper stress. An excellent article on the fracture of tempered flat glass is by Shinkai, reference 37. He states that some higher energy impacts may not have the two telltale fragments at the origins, and may instead have cone cracks that penetrate from the surface. Gardon's review article[38] also showed variations in fragmentation patterns near the origin depending

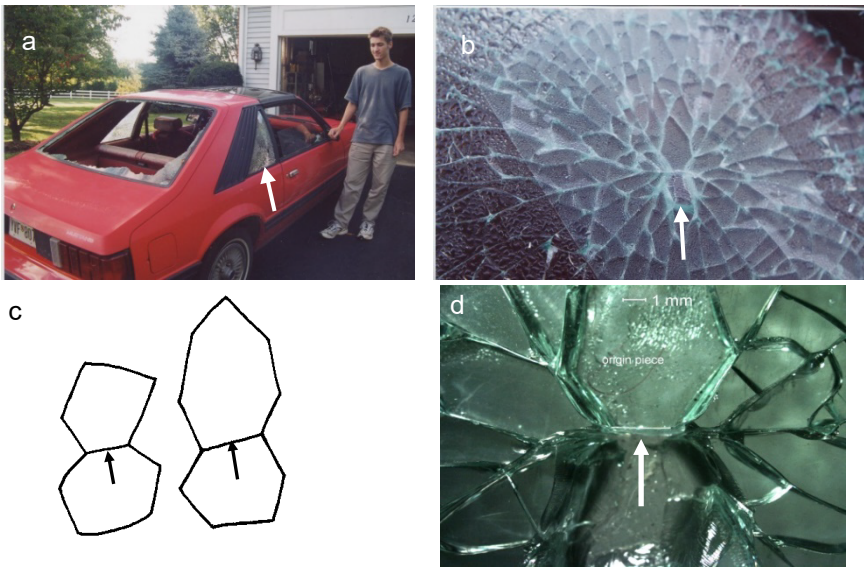

Figure 4.24 *Tempered glass fractures in the author's son's car. Flying debris from a tornado in College Park, Maryland in September, 2001 caused the impact fractures (a, b, d). The arrows show the actual origin in one window and (c) shows some variations of shape of typical matching origin pieces. The fracture surface of the origin piece is shown in Figure 5.24b in Chapter 5.*

upon whether impact was by a sharp or blunt object.

The hexagonal fragments are distinctive and can be found by simply sifting through rubble. With persistence and a little luck, the patient fractographer may be rewarded. In some instances, tempered plates do not break up into uniform fragments. Atypical fragments are a sign that the temper was non-uniform either by design (e.g., Shinkai,[37] p. 288 and Gardon[38]) or not (e.g., Fréchette,[1] case 10.18), or relieved by high temperature exposure (e.g., Fréchette,[1] case 10.22). See Figure 5.24 for more on tempered glass fracture.

4.12 Thermally-Induced Plate and Window Fractures

A center-heated plate is one which is heated in the middle while the rim is cooler. Differential strains put the middle of the plate into compression and the rim into tension. The plates fracture as shown in Figures 4.25 and 4.26. The

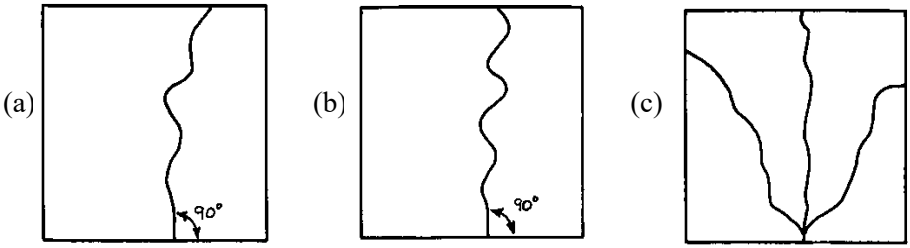

Figure 4.25 *Fractures in center-heated plates. (a) and (b) are low stress fractures (less than 10 MPa {≈ 1,500 psi} in glass), and (c) is a higher stress fracture such that branching occurred.*

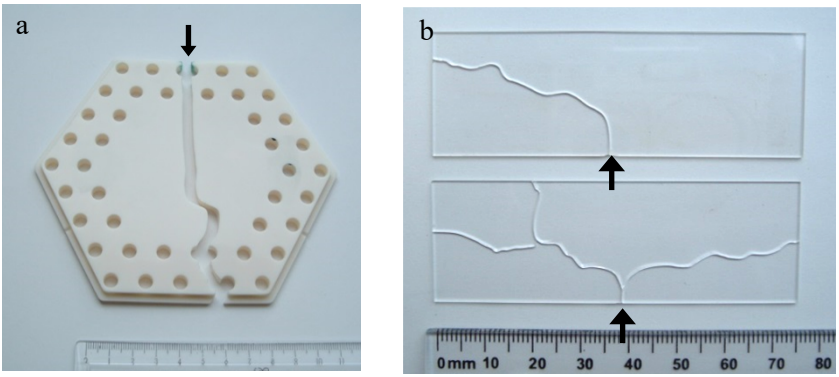

Figure 4.26 *Thermal fractures with origins marked by arrows. (a) shows an alumina furnace baffle plate. Fracture started from grinding cracks associated with a hole. (b) shows glass slides broken by heating them on a hot plate.*

crack starts from an edge origin in tension and initially propagates at 90° to the edge, but then changes to a meandering wavy pattern as it approaches the initially biaxial compression stressed middle portions of the plate. The waves are often periodic as shown in (b). Figure 4.26 shows thermal failures in an alumina plate and glass microscope slides. The alumina plate is a classic center-heated plate case. Case 6 in Chapter 10 shows another center-heated plate example in a SiC furnace plate. Fréchette[1] noted that meandering cracks are not proof of thermal stresses, and they can also form in impact cases in the final stages of breakup.

The waviness is an example of Hopf bifurcation problem that can occur in nonlinear systems.[39,40] It is possible to create such wavy cracks in controlled experiments. Thermal gradients create a biaxial stress field in center heated plates. Time is an important variable as the problem involves both heat transfer

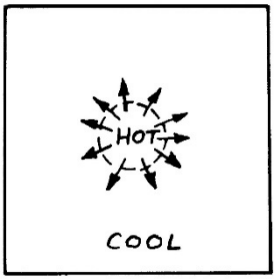

The center-heated zone tries to expand, but it is constrained by the cooler outer portions.

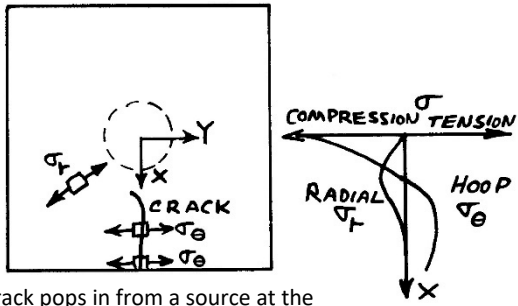

A crack pops in from a source at the outer edge. It starts at 90° to the edge and runs straight. The crack experiences diminishing hoop tensile stresses and approaches the initial compressive stressed region. It curves to one side.

The crack and the stress field interact.
The crack alters the stress distribution

The tensile stresses are relocated to near the crack tip.
The crack turns and propagates further.
The process repeats itself and a wavy pattern is formed.

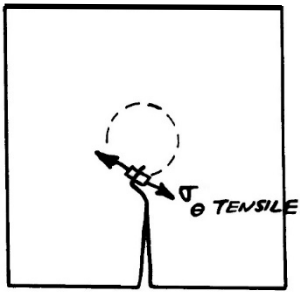

Changes to the temperature distribution as the plate cools can also cause the crack to meander.

Figure 4.27 *Center-heated plate thermal stress fracture.*

and stress distributions that change with time. The problem is non-linear since the stresses create and propagate the crack, but in turn, the crack alters the stresses in the plate. The crack may even alter the temperature distribution, but that is not necessary for the wavy pattern to appear. Although some engineering and dynamic fracture mechanics literature suggests that wave-like cracks form under fast, dynamic conditions, the thermal stress induced wavy cracks are slow and are created in quasi static conditions. Figure 4.27 illustrates how they form. It shows that the center heated portion tries to expand, but is constrained by the cooler rim. The rim is put into tension by the expanding core of the plate. There are radial stresses, σ_r, and hoop circumferential stresses, σ_θ, that vary with location in the plate. (Reference 41 illustrates the stress distribution in a similar case.) The initial stress condition is illustrated in the Figure. The hoop stresses vary from tensile at the rim to compressive in the plate middle. The radial stresses are zero at the plate rim and the exact plate middle, but are compressive everywhere in between. They are of a lower magnitude than the hoop stresses. The hoop stress σ_θ causes the crack to pop in from the rim and run towards the middle. The crack encounters diminishing tensile stresses and, eventually, compression stresses that deflect it to one side or the other. Yet as this has occurred, the stresses in the plate are changing. The plate is now a center heated plate with a gap in the plate that cannot transmit stresses across the crack face. Circumferential stresses are redistributed and now become tensile near the crack tip. The crack is redirected back toward the plate center. The crack propagates to the other side, the stresses redistribute, and a wavy crack pattern is formed.

Thermal stress fractures in general often have localized tensile stresses that start fracture, but diminish away from the origin site. Branching may be minimal and the fracture surfaces may be relatively featureless and flat in regions away from the origin. Wallner lines or hackle lines (discussed in the next chapter) are rare. There may be multiple arrest lines attesting to stepwise propagation of the crack. Scarps may be present on the initial parts of the fracture surface if the part was thermally shocked by a cooler fluid.

In the center heated plate case, the relatively featureless fracture surfaces mean that the crack is moving slowly when the wavy pattern forms. The crack alters the stress distribution and it in turn alters the crack path. This nonlinear interaction causes the crack to curve back and forth.

Thermal stress cracks can take other surprising forms. Figures 4.28a,b show odd circular and spiral cracks in a thick glass plate bonded to a metal plate. Fractures occurred when the combination was cold-tested in an autoclave then brought back to room temperature. Biaxial tensile stresses formed due to

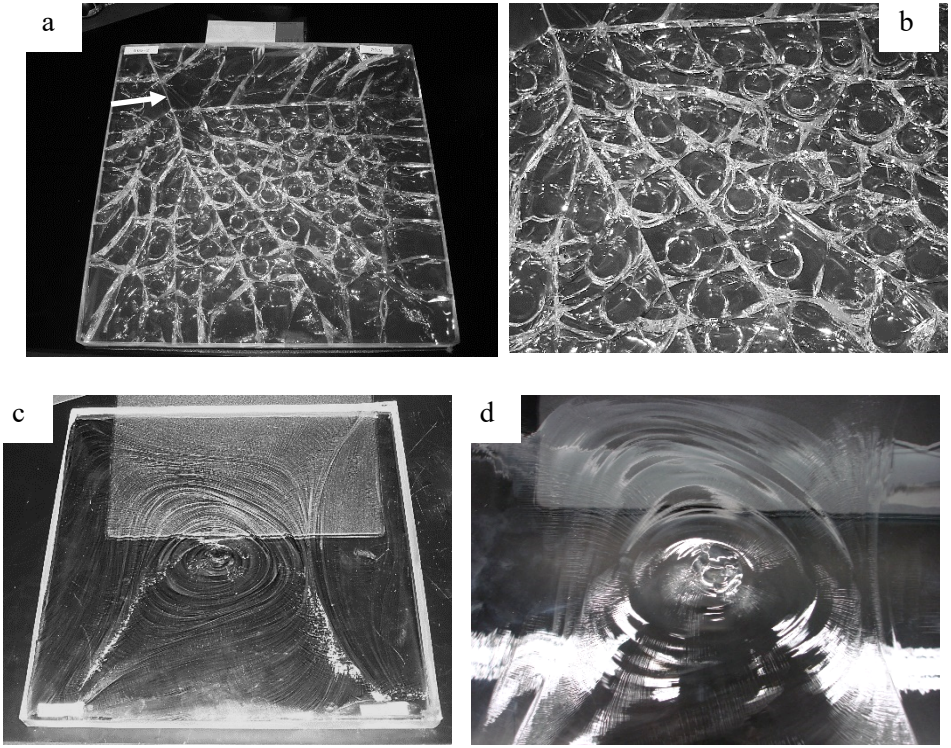

Figure 4.28 *Wavy circular and spiral cracks in thick glass plates. (a) and the closeup (b) show one plate that was bonded to a metal plate. The first fracture started at the top left of the plate (arrow). The main crack branched repeatedly forming polygonal- and square-shaped pieces. Circular cracks then formed in these pieces. (c) and (d) show another plate with a single large circular pattern. (Courtesy J. Swab and P. Patel)*

differential plate expansions. A single fracture crack branched repeatedly portioning the glass into fragments. Wavy circular cracks then formed in the fragments. Bahat[42] has shown similar wavy concentric circular and spiral cracks in a glass that was melted in an alumina crucible and air cooled. The 1 mm thick glass first broke into distorted square-shaped pieces, then wavy circular and spiral cracks formed in the squares. A common element in both Bahat's fractures and the plates shown in Fig. 4.28 is the waviness of the cracks and lots of twist hackle.

Other thermal shock and thermal stress fractures are covered in sections 4.19.2 and 4.19.3 later in this chapter. Glaze and coating fractures are discussed in section 6.15 in Chapter 6.

4.13 Bottles and Pressure Vessels

Bottles and pressure vessels are susceptible to a variety of failure scenarios. Figure 4.29 shows some common modes, but this illustration is by no means

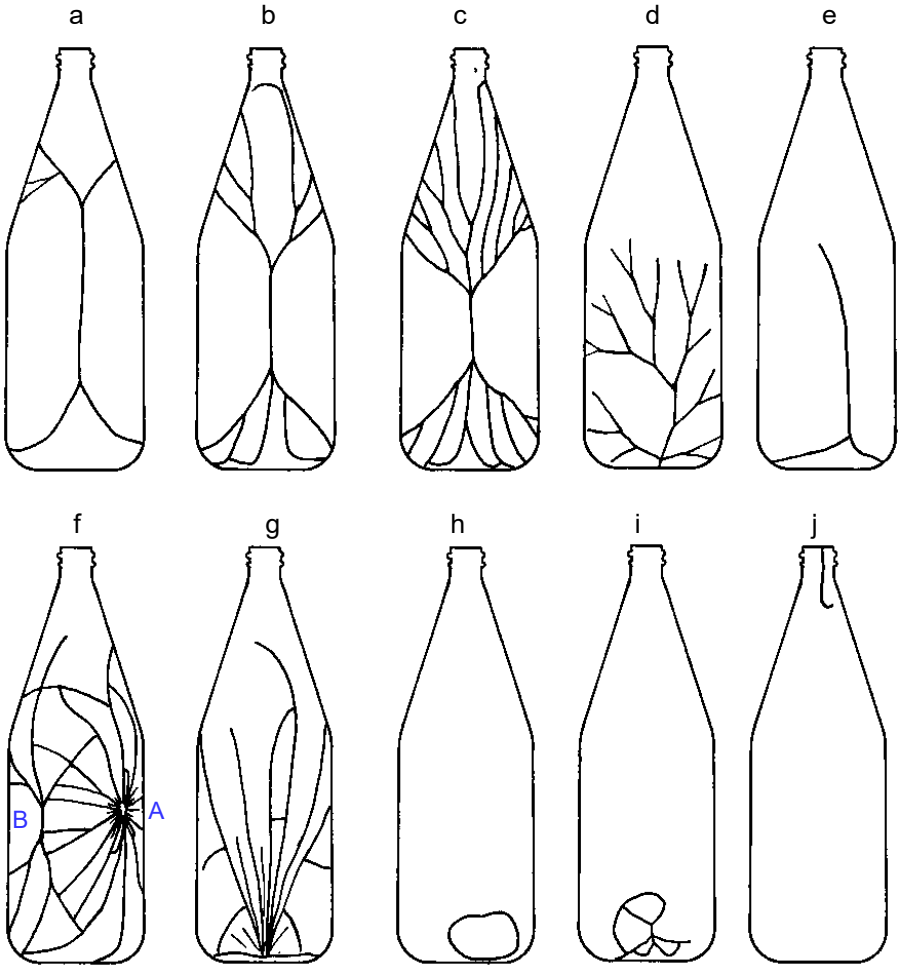

Figure 4.29 *Bottle fracture patterns. (a-c) sidewall fractures due to internal pressure at progressively greater pressures. (d) internal pressure fracture starting from the base. (e) is a thermal fracture from sudden cooling of the base. (f) is an impact fracture on the right side (labeled A) with a hinge fracture on the side (labeled B). Sometimes a "leader" crack will run from B (not shown here) over to site A and trigger the A site fractures (see Fig. 4.50)! (g-i) show water hammer fractures and (j) shows a fracture from diametral rim clamping.*

complete. The reader is referred to the excellent review article by Kepple and Wasylyk[43] for a more detailed presentation with more illustrations. Preston's article[44] in 1939 was an outstanding early contribution. Kepple and Wasylyk cite F. W. Preston's earlier work from the 1930s and 1940s in their review. Fréchette[1] also illustrated a number of interesting glass bottle fractures. Spangenberg[34] wrote about the many causes of pressurized bottle fractures from both a legal and technical perspective. He even discussed cases of beer bottle fractures due to continued fermentation in the sealed bottles. In one instance, burst fractures were caused by decaying mouse carcasses inside beer bottles! More recent reviews of bottle, vial, and pharmaceutical fractures may be found in book by Aldinger and De Haan,[45] a book by the Bucker Emhart Glass Company,[46] and a review article by Schaut et al.[35]

Fracture origin types that one may find in bottles and vials are covered in Chapter 6, Origins.

Fractures from internally-pressurized bottles (e.g., carbonated beverages, Fig. 4.29 a-c, have vertical initial cracks since hoop tensile stresses are double the axial stresses (as discussed in detail below). Fractures usually initiate on the outside wall and branch in a symmetrical pattern about the vertical axis. The number of branches is proportional to the stress in the glass. Fractures start on the outside wall since larger flaws are more apt to be present there, but as the crack propagates it will extend to the interior and then lead slightly on the internal surface, since the stress is slightly higher there. Secondary breaks from bending have crack fronts that strongly lead on the *inside* surface. Pressure fractures from the base will also have extensive forking as shown in Figure 4.29d. Thermal fractures have very little, or no branching as shown in Figure 4.29e. Sudden temperature differentials can occur in a variety of different ways. Tensile stresses are generated when a portion of the body is suddenly cooled and attempts to shrink. The warm portions resist the contraction and put the cooler portions into tension. The temperature gradients can be either through the thickness or from one part of the body to another. Exposure of a hot vessel to a cold liquid often leads to thermal shock fracture. Figure 4.1 showed an example in a Pyrex bowl. Fracture often starts and runs around the base and may extend up into the sidewall. Fréchette[1] and Kepple and Wasylyk[43] cover more thermal stress fractures of glass containers. Additional information about thermal fractures is in section 4.19.2 later in this chapter.

Sometimes impact damage sites may be found around the base, either on the inside or the outside. Impact damage sites on the <u>inside</u> of drinking glasses or beer mugs are often due to careless dropping of eating utensils like knives or forks into the glasses.

External impact fractures on the side walls often have a starburst pattern at the impact site as shown in Figure 4.29f and 4.30. A network of cracks from the impact site can start on either the inside or outside of the impact site, depending upon the sharpness of the impactor. Fracture may not necessarily start at the impact site, however. Depending upon the circumstances, fracture can initiate from three possible sites: at the impact site, or one or both sides of the bottle.[47,48] Thus, there may be between one and three fracture origins. The force of impact can cause the sidewall of the vessel to flex outwards creating a tension bending stress in the sides of the vessel. This can trigger so-called "hinge fractures" 45° to 90° to the sides of the impact site. These can even precede fracture at the impact site. Wallner lines indicate that fracture starts on the outside surface of the hinge fracture origin sites. The hinge site fractures then send a *leader crack* over to the impact site that triggers new cracking or exacerbates the cracking already occurring at the original impact site. Figure 4.30 below shows an example of this in a glass tube that was not impacted, but statically loaded on its sides by the author. Cracks from the one origin site can halt later radiating cracks from another site. See Frechette,[1] Dimmick,[47] and Mould[48] for additional details.

Filled glass containers dropped on their side trigger fracture from origins on the inside surface.

Water hammer is a phenomenon that can cause vessel fractures as shown in Figures 4.29g-i. The sudden arrest of a liquid in motion or a surge of liquid that collapses a void in a partially-filled vessel can create transient intense internal localized pressures. Figure 4.29g shows a base fracture initiated by water hammer when a filled bottle was dropped. There may be a high concentration of cracks at the origin, but little branching afterwards since the stresses were focused at the base. Collapse of a void can occur in vacuum-sealed or incompletely-filled vessels. Base fractures shown in Figures 4.29h,i can result.

Vessel necks are vulnerable to many forms of damage from chipping due to capping-clamping stresses. Figure 4.29j shows a crack triggered by diametral clamping around the rim.

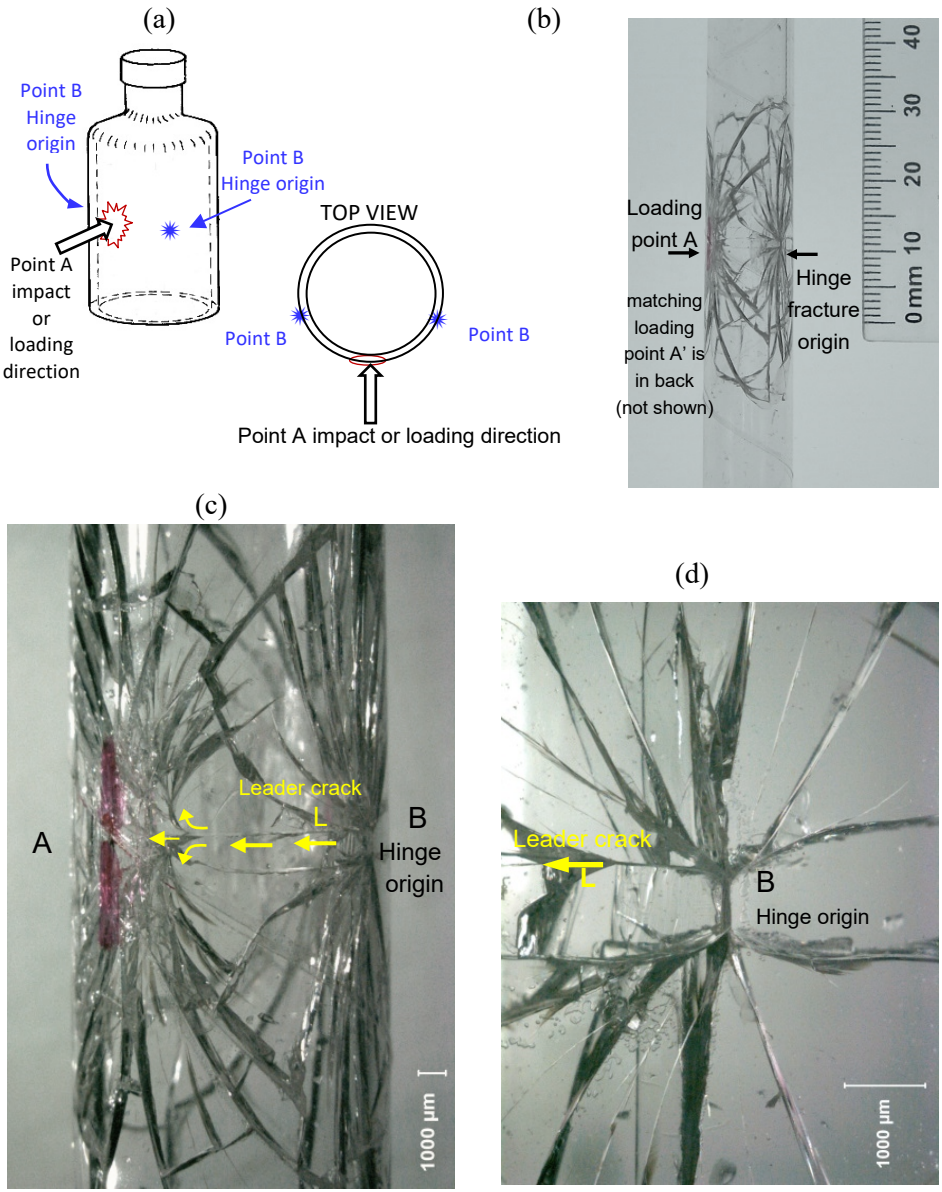

Figure 4.30 *Side impacts or loading can activate hinge fracture origins from side wall bulging. (b) show a small glass tube statically-loaded sideways at opposing points A (only the front is shown). Fracture started at the side hinge points B (about 90° to the side) which generated an array of radiating cracks. One of these is the "leader crack" L running in the direction of the arrows in photos (c) and (d) which went to the loading site A where it branched repeatedly and fanned out yet again.*

As noted above, fractures from internally pressurized bottles (e.g., carbonated beverages, Fig. 4.29 a-c, or medicinal vials Fig. 4.31) usually have vertical initial cracks since hoop tensile stresses are double the axial stresses, irrespective of the pressure. This is a good opportunity to show a stress analysis of a simple structure. Imagine making a vertical cut through the

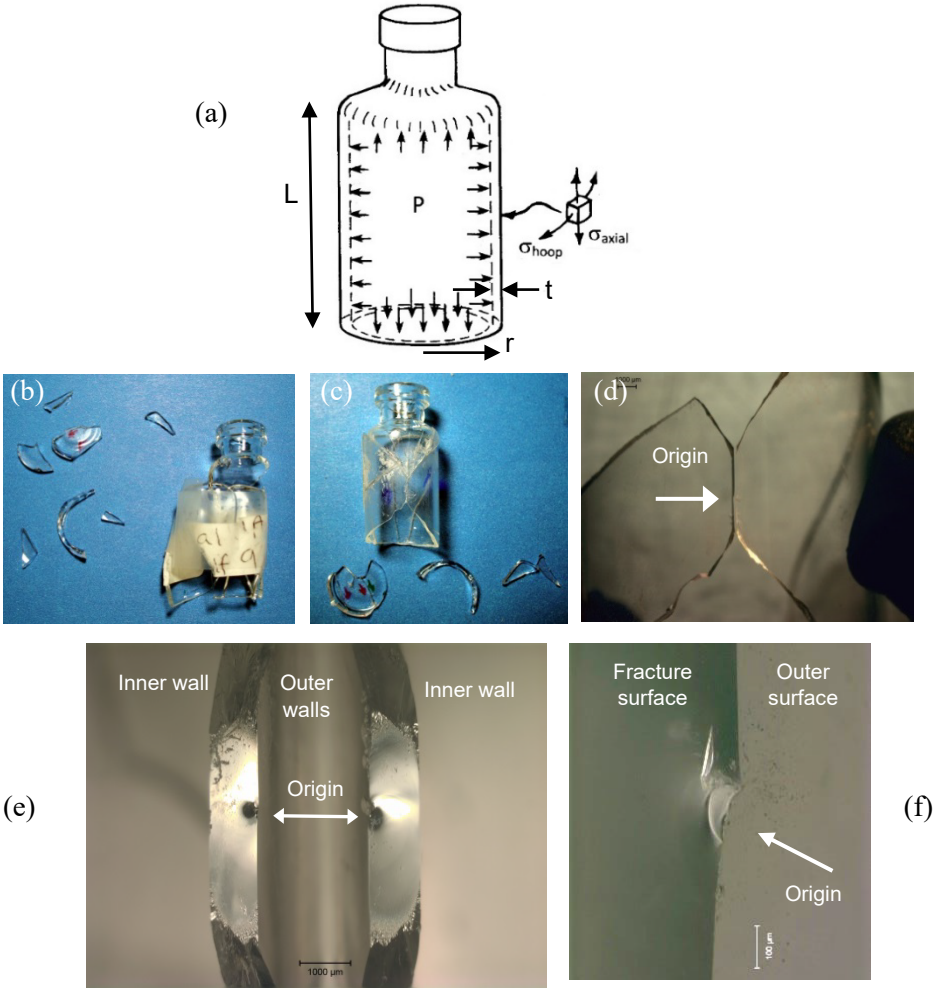

Figure 4.31 *Pressurized thin-walled vessels. (a) shows that the side walls are stressed in biaxial tension. Hoop stress is double the axial stress and therefore the first fracture is usually vertical as shown in the medicinal vial shown in (b)–(f). (e) shows the matching fracture surfaces at the origin. There is a distinct fracture mirror centered on the origin. (f) shows the origin was an arc shaped crack in the outer wall, a clear indication of blunt contact damage. It is termed "bump check" in the glass container and pharmaceutical fields.*

middle of the bottle with height L, radius r, and wall thickness t, under pressure P. This is a common practice for mechanical engineers to do when they construct "free body diagrams" to analyze stress problems. A part is cut in an imaginary sense. The external forces and moments acting on one half of the component are balanced with internal stresses in the walls. For the vertically-split bottle, the forces from the sideways expanding pressures that act on the arc of the inside surface are balanced against the constraining forces in the side walls. These are the sum of the hoop stresses in the two side walls that have a total cross-sectional area of $2Lt$:

$$\int_{-\pi/2}^{\pi/2} P\cos\theta r d\theta L = 2rLP = 2Lt\sigma_{hoop} \tag{4.2}$$

$$\sigma_{hoop} = \frac{Pr}{t} \tag{4.3}$$

For the axial stress (vertical direction), imagine splitting the vessel in a horizontal plane midway along its height. The force created by the sum of the pressures on the bottom circular surface of area πr^2 is balanced by the sum of the vertical axial stresses in the vessel side walls which have a total cross-sectional area of $2\pi rt$:

$$P\pi r^2 = 2\pi rt\sigma_{axial} \tag{4.4}$$

$$\sigma_{axial} = \frac{Pr}{2t} \tag{4.5}$$

Hence:

$$\sigma_{hoop} = 2\sigma_{axial} \tag{4.6}$$

This solution is for thin-walled vessels where it may be assumed there is negligible stress gradient through the wall thickness. Engineering textbooks should be consulted for thick–walled vessels or finite element analysis done since there will be a stress gradient through the wall thickness.

4.14 Torsional Fractures

Torsional loadings such as shown in Figure 4.32 produce twisted fracture surfaces at an angle to the part length. Torsional stresses usually do not induce a special failure mode in ceramics or glasses. Fracture starts at a flaw and the crack propagates normal to the plane of maximum tensile stress, which is aligned at 45° to the shear stress direction. In other words, the shear stress (τ) state is equivalent to one in which a material element is pulled in tension (σ_1) in one direction and compressed laterally (σ_2) as shown in Figure 4.32a. Fracture primarily occurs due to σ_1 tensile stress and fracture propagates perpendicular to σ_1. If branching occurs, the included angle is quite small and is usually

between 15° and 21°. One branch may become dominant and the other may arrest as shown in Figure 4.32.

Many parts that fail in torsional loading also have some bending as well. Fracture surfaces often have ample twist hackle markings as discussed later in section 5.3.3. Previous figure 4.14 showed fracture in a bend bar that had superimposed bending and torsional stresses. Figure 5.37 showed the fracture surface of a glass rod with mixed tension and torsional loading.

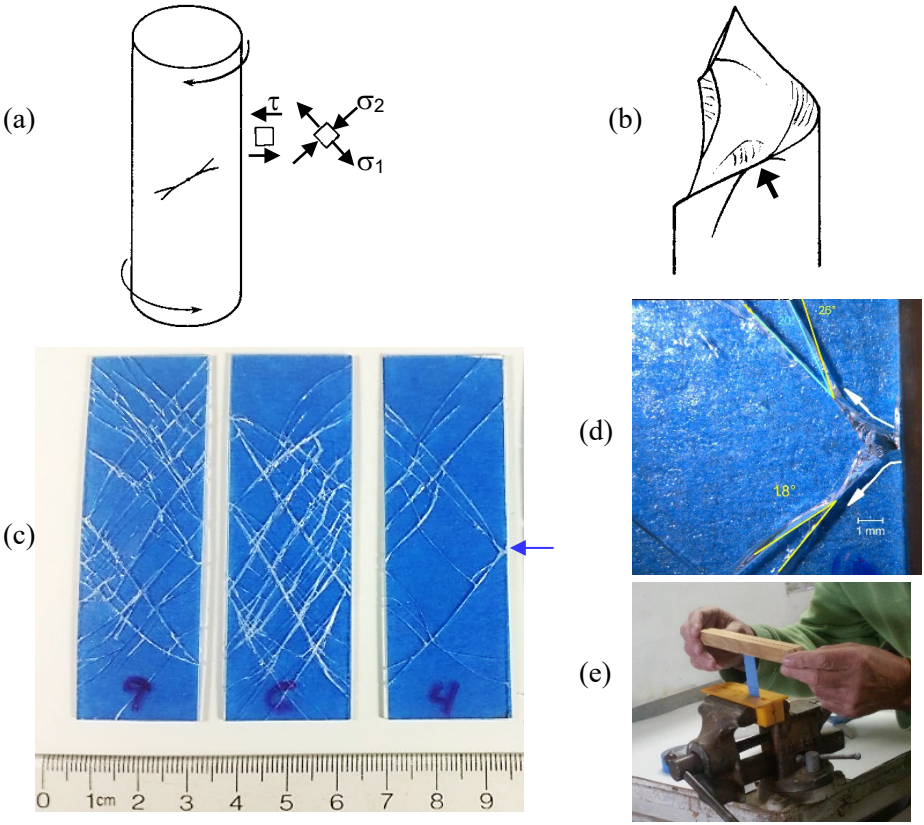

Figure 4.32 *Torsional loading causes fractures at an angle to the longitudinal axis of a part. The shear stresses are τ. These generate equivalent principal stresses σ_1 in tension and σ_2 in compression as shown in (a). Fracture occurs perpendicular to σ_1. (b) shows a schematic of a glass rod fractured in torsion. (after Michalske[10]) The origin is at the arrow. Note how branching occurs to either side of the origin, but that only one branch in each case continues, giving rise to the curved fracture surface. (c) shows glass microscope slides broken in torsion. Blue painter's tape on one side holds the pieces together. (d) is a closeup of (c). (e) shows how the slides were loaded.*

Torsion failures of plates start from edge flaws and have a distinctive pattern of crisscrossing cracks as shown in Figure 4.32c. It is caused in part by cracks that start on one side of a plate do not go all the way through the plate thickness. Then, other cracks from other origins and directions cross over them. These glass microscope slides were tested by the author as described in Reference 5. In brief, glass slides were tested straight out of the box, but with a single layer of blue painter's tape on one side to hold the pieces together. Care was taken to gently clamp the bottom end in a simple vise with polymer inserts. At the top end, a simple clamp was made with two strips of wood separated by washers that were just a bit thicker than the microscope slide. This holder was slid over the top end of the slide as shown in Figure 4.32e. Care was taken to torque the slides evenly and with no bending. The crisscrossing patterns of fracture were remarkably similar to what Grabau showed in a 1920 book on geology.[49] The fractures started from the edges with the first crack strongly inclined ($\approx 45^{o}$) to the edge. Many of the secondary cracks that ran perpendicular to the initial cracks were initiated from twist hackle and lips on the fracture surface of the first crack. In other words, the first cracks had so many irregularities on them that they triggered additional perpendicular cracks thereby creating the crisscross pattern.

4.15 Edge Chipping

Concentrated loads near an edge can chip off a portion of the body. Figure 4.33 shows some examples. Chipping can either be a primary mode of fracture, or it can be a secondary nuisance. For example, it is one of the leading causes of failure of all-ceramic dental restorations such as crowns or bridges, and hardmetal (e.g., tungsten carbide) or ceramic cutting tools. On the other hand, it may be a nuisance if there is so much post fracture chipping that it interferes with interpretation of a fracture from some other cause. Thus, it is important to be careful when fitting pieces together during an initial examination.

The force to cause fracture depends upon the shape of the object that applies the contacting force, the distance from the edge, the angle of the applied force P, the angle of the edge, and the material's fracture toughness. The greater the distance away from an edge, the greater the force that is necessary to create a chip. Modern use of this test for engineering materials was started in 1986 at the National Physical Laboratory in United Kingdom by Almond and McCormick.[50] A remarkable finding was that the shape of the chip was invariant with material. Quite interestingly, Charles de Freminville's seminal 1907 treatise on fracture of brittle materials included excellent illustrations (his Fig. 5) of edge chips in glass.[51] There was a full session on edge chipping

at the 2000 Alfred Conference on Fractography of Ceramics and Glasses.[52] Edge chipping also has been a topic in the lithic fracture literature and flint knappers have a good practical knowledge on the topic.[20,50]

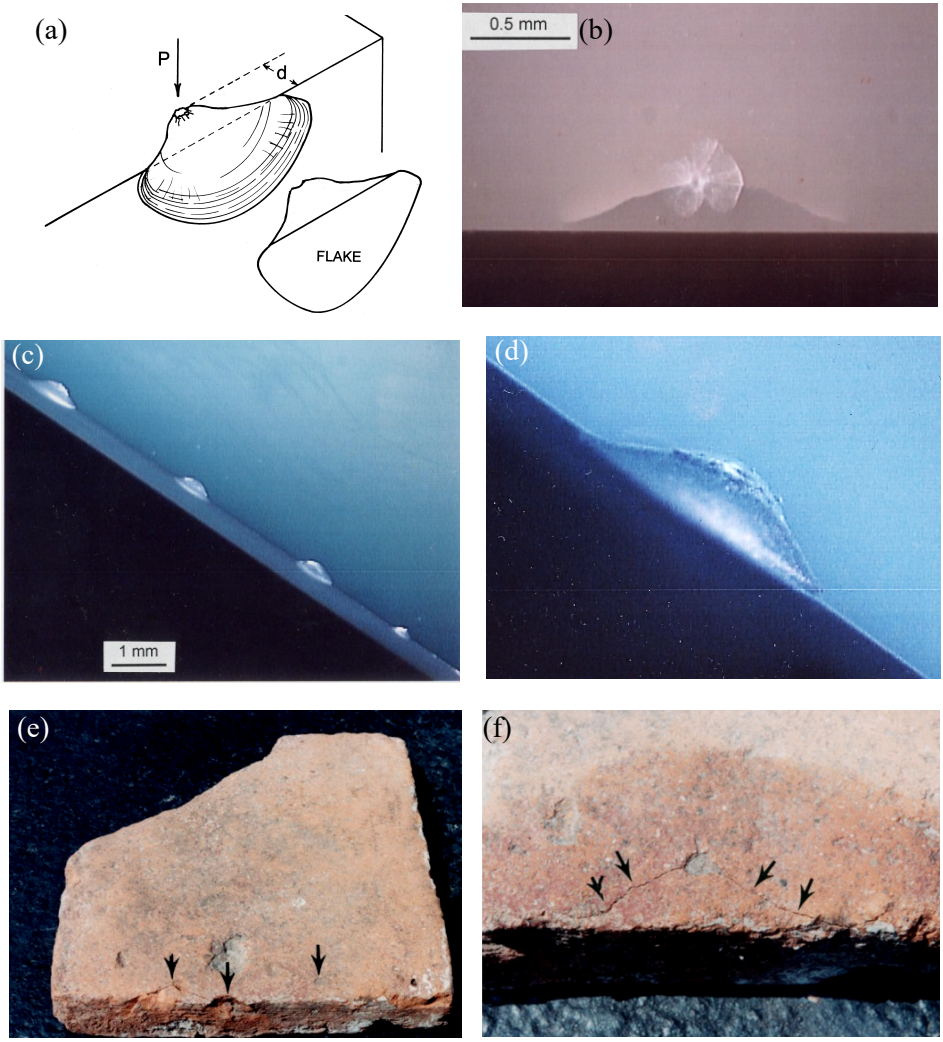

Figure 4.33 *Examples of chip fractures. (a) is a schematic that shows how a chip is formed and the telltale shape. (b) shows a top view of a chip that is just about to pop off a lithium disilicate foundation dental glass-ceramic. The loading point is obvious. (c) shows a row of edge chips created in a dental porcelain under controlled conditions in the laboratory. (d) is a close-up. (e) and (f) show edge chips in an ancient Roman (circa 300 AD) 22 cm square by 3.4 cm thick hypocaust brick from Trier, Germany. (b,c,d, courtesy J. Quinn)*

The exact force-distance trend depends upon the type of indenter (sharp or blunt). In a laboratory setting, sharp diamond indenters (Rockwell, Vickers, Knoop) or sharp conical tools are used, but in practice any contact type loading can create a chip at an edge. Lab-scale indenters initiate cracks around the contact site which then grow to form a chip. On the other hand, some loadings with blunt contactors near an edge cause a pre-existing crack to propagate parallel to the specimen side and to form a long flake. The top of the flake, where the force is applied, is called the "platform" in the lithics literature. The fracture mechanics of chip formation and how long slender flakes may be formed by stable crack extension are fascinating.[53,54] The long slender flakes can be used as cutting tools. Cotterell discussed how the ability to form such long slender stone tools was a critical step in the evolution of mankind.[53]

(a)

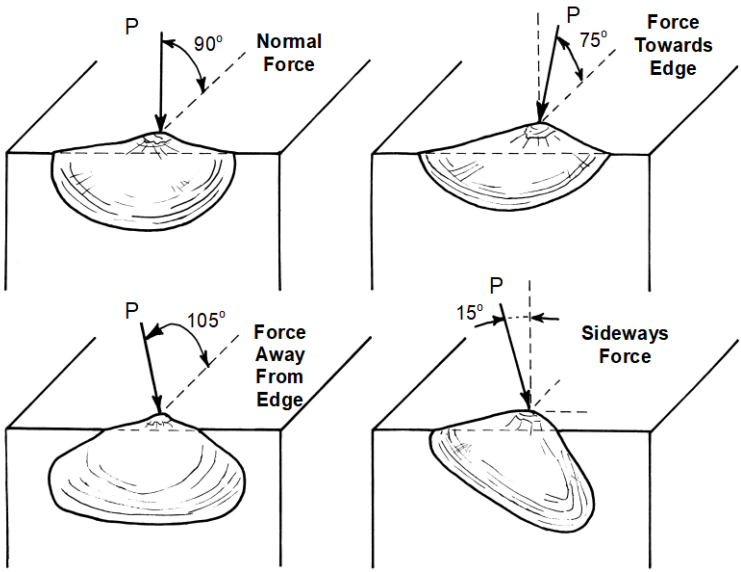

(b)

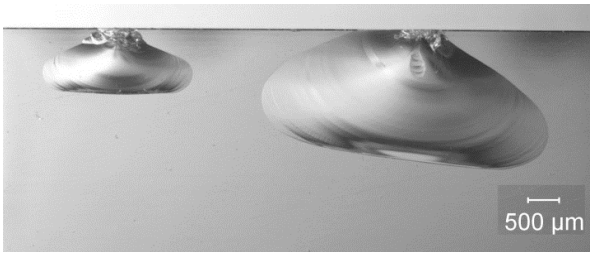

Figure 4.34 *The angle of the applied force, P, load affects the shape of edge chips. (a) is a schematic that shows the patterns. (b) shows front views of chips in glass (at different loads and distances from the edge) made by a conical indenter tool angled away from the edge at 105°. (J. Quinn, R. Mohan, Ref. 55).*

Fracture surfaces of edge chips have twist hackle and concentric wavy tertiary Wallner lines as described in the next chapter. The latter are caused by elastic wave reverberations as the chip fractures off. (See the cover of this Guide.)

The shape of chips varies with the angle of the applied load as shown in Figure 4.34.[55] This has practical significance, since the shape of the chip can tell a fractographer the direction of the force that caused the chip. Since the first edition of this book was written, I have followed up on the edge chipping work of my departed spouse Dr. J. Quinn. We published a number of papers on edge chipping of dental ceramic and composite restorative materials and structural engineering ceramics and with a new quantitative model.[56,57,58] Early work emphasized a linear relationship between force and distance the force is applied away from the edge, but new results indicate nonlinear trends can result from the partitioning of indenter energy into competing deformation and fracture modes in the material. Figures 4.35 and 4.36 show some new chips.

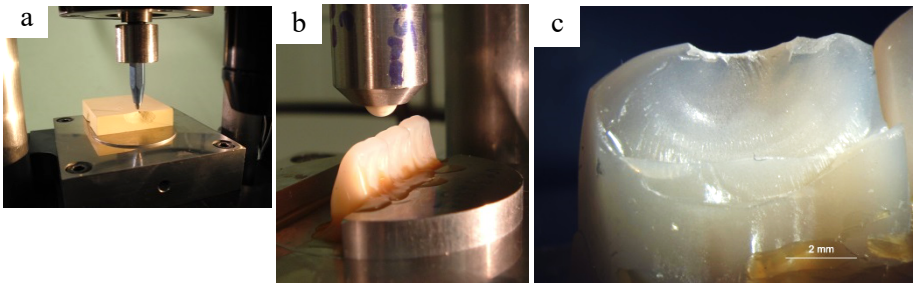

Figure 4.35 *Edge chipping. (a) shows the test machine with a 120º sharp diamond scriber making a chip in a dental stone material. (b, c) show a ceramic ball indenter that chipped brittle denture material tooth specimens.*

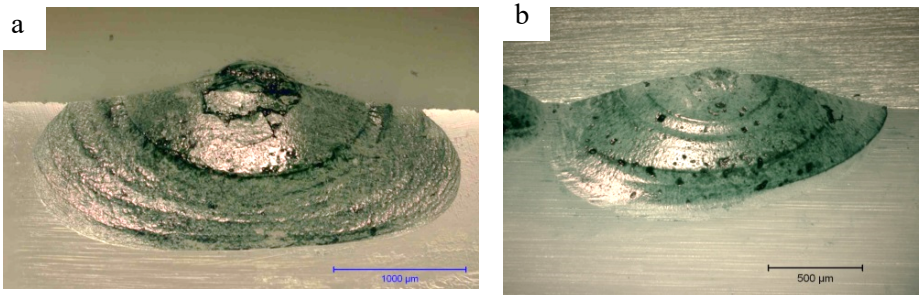

Figure 4.36 *Edge chips formed in (a) dental lithium disilicate glass ceramic; (b) dental 3Y-TZP zirconia; (c) dense alumina; and (d) laminated alumina/alumina-zirconia ceramic. The chips were stained with a green felt tip pen to make the fracture surfaces easier to see in these translucent materials.*

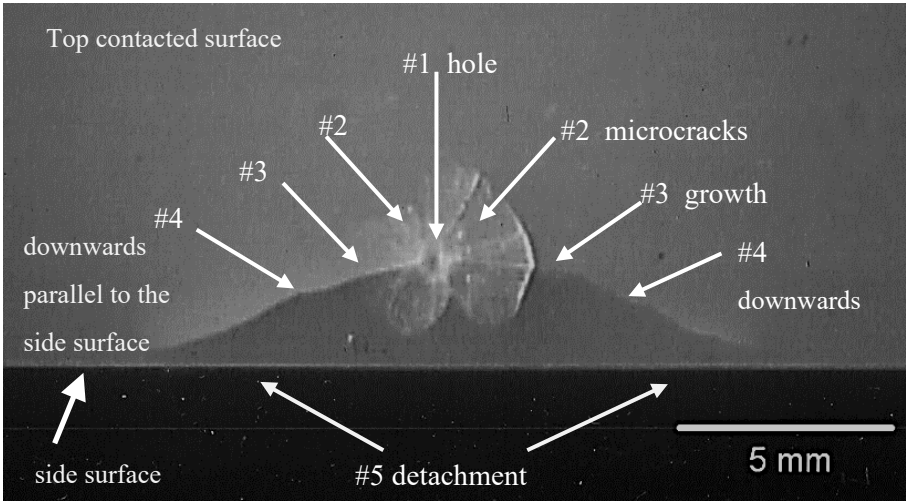

Figure 4.37 *Top view of a lithium disilicate glass ceramic block showing the 5 steps of the formation of an edge chip from a 120º sharp conical indenter. Detachment Step 5 is on the verge of occurring.*

Edge chipping is a multistep process as illustrated in Figure 4.37 which is a magnified view of Figure 4.33b. Step #1 is contact. The contact may be from a sharp indenter (such as a Vickers, Knoop, Rockwell, or sharp conical indenter as in laboratory type experiments), or from a blunt object. With a sharp contactor, a hole may form. Step #2 is nucleation of radiating micro cracks from the contact site. If the contactor is a faceted indenter such as a Vickers or Knoop indenter, there will be just a few microcracks approximately aligned with the indenter axes. Sharp indenters initiate such microcracks much sooner and at lower forces than blunt objects. With a blunt object contact on a rigid ceramic or glass, there may not be a hole, but a partial ring crack. Step #3 is growth of some of the microcracks outwards from the contact site. Many microcracks become dormant. The ones which grow are usually those that are parallel to the side surface. Step #4 is growth of these cracks down into the object and parallel to its side surface. Step #5 is breakthrough of the chip to the side surface. In many cases the chip or flake will detach, i.e., "pop off." All of these steps can happen in one instant if a strong contact-impact occurs. Lower force or transient contact may start the chipping process to make some damage, but not cause the final breakthrough. So sometimes edge damage can occur without a flake popping off, but the damage has been done. Subsequent handling or additional contact can pop the flake off. The author had an unpleasant experience when drinking from a glass of beer. A very sharp small fragment landed on my tongue. I was able to extract it. Lo and behold, it was a

sharp edge chip from prior damage at the glass rim. It finally detached as I took a sip. It was fortunate indeed that I did not swallow it.

With brittle ceramics and glasses, most of the damage is in the form of cracking with only a small "plastic" damage zone or hole. Less rigid or softer materials (with low elastic modulus or which plastically deform) can expend a lot of the energy of contact into hole formation[59] as shown in Figure 4.38. An energy balance model of edge chipping was presented in references 56 and 58.

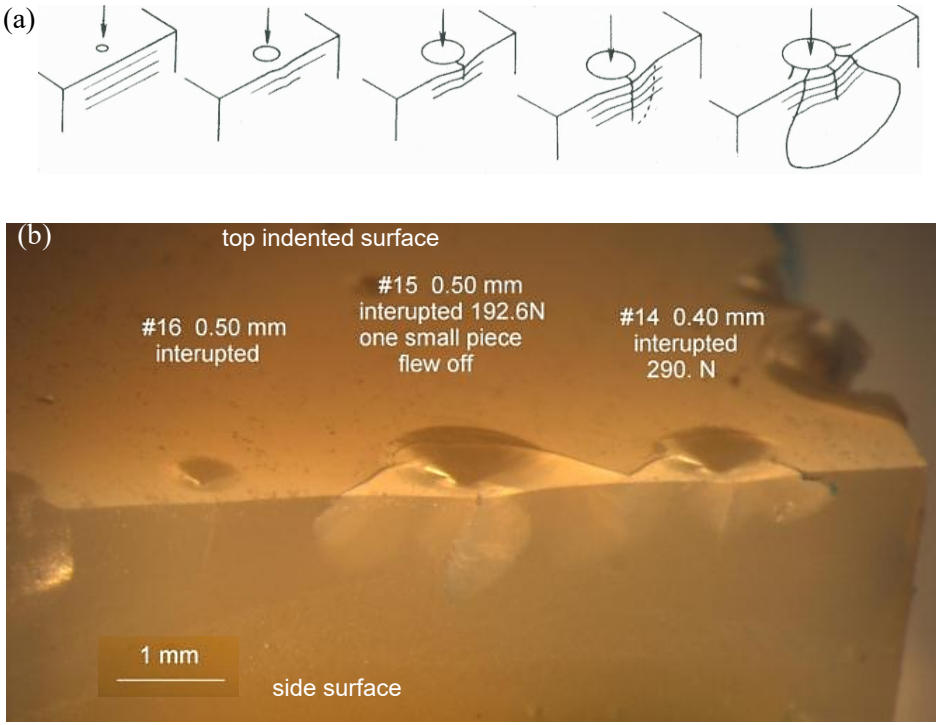

Figure 4.38 *Softer brittle materials may form large holes at the contact site. This photo shows a block of a glass particle filled resin-matrix composite with three chip contact sites made by a sharp 120º conical indenter. The low elastic modulus and deformability of the material made it more complaint to the degree that chips did not "pop off." Much of the indenter contact energy went into hole formation. The chips are in the process of being pried off.*

Edge chips are very common as *secondary fractures* on broken ceramic or glass fragments. They may have had nothing to do with the original cause of fracture. They easily occur if fragments bump into each other or impact other objects during breakage or subsequent handling. If there is any doubt as to whether an edge chip is a secondary or a primary fracture, compare the matching fracture halves. If the chip is only on one half, then it is a secondary fracture. It is quite common, especially with glasses, to have one fracture half rub against the edge of the matching fracture half, causing chips in the latter. Undesirable secondary fracture chips can occur in bend bar strength specimens and other test coupons if the pieces fly around and impact the fixtures after the first break. Often the tensile edge of a bend bar will hit first, and the genuine fracture origin may be chipped off! Soft cushioning material should be placed in the fixtures under the bars as discussed in section 4.6. Some additional means to prevent the fragments from flying about should also be used (e.g., cotton or rolled paper or tape pieces).

4.16 Complementary Laboratory Test Fractures to Aid Component Fracture Analysis

Examination of laboratory test coupon fracture surfaces can often aid interpretation of component failures. It is not unusual to be confronted with only one or two component fractures. The fracture surface markings may be unfamiliar and common fracture markings such as hackle lines or cantilever curls may be hard to recognize. A few broken bend bars, tension specimens, or fracture toughness specimens of the same material may be invaluable in such cases. The fractographer can study the crack propagation behavior and markings for these familiar configurations.

The author used this approach to aid the interpreting of broken large (≈1 m) sintered porous fused-silica missile radomes in the mid-1980s. This is Case 7 discussed in Chapter 10. Only a few broken components were available and an initial examination of the weak material with its rough fracture surfaces was unsuccessful. Examination of bend bar and double torsion fracture toughness specimens gave the author more experience in interpreting crack propagation directions. Optimum examination conditions for detecting hackle and Wallner lines were discovered. This know-how was then applied to the full-size components, with the result that fracture surfaces which initially confounded the author became tractable on the reexamination.

In an ideal case, exemplars or models of the components may be tested as described in the next section.

4.17 Controlled Component Fractures, Replicates, Exemplars

Sometimes the cause of an in-service component fracture is not known with certainty but there may be a working hypothesis. The hypothesis can be checked by conducting controlled fractures on other components or replicates to try to match the service fractures. If one can duplicate the component fracture patterns, then one has good evidence as to the cause of fracture. Figure 4.1 in this chapter is an example of an intentional thermal shock fracture of a glass kitchenware bowl. Several other examples are shown below.

Morrell and colleagues[60] and Richter[61] documented two superb examples of exemplar testing for ceramic hip joint balls. Figure 4.39 shows how the testing was done by Morrell in accordance with ISO standards and how cracks propagated. They complemented their component testing with biaxial disk and bend bar fracture testing as suggested in the previous section.

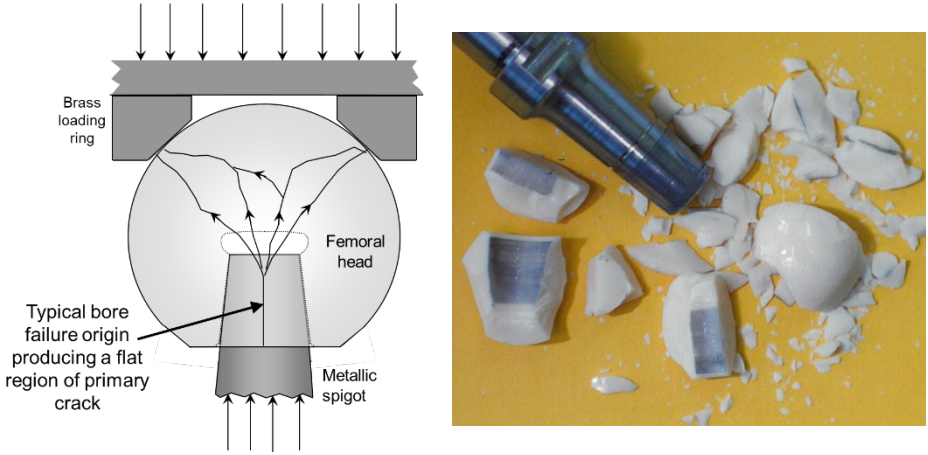

Figure 4.39 *Controlled laboratory fracture of alumina femoral heads (courtesy R. Morrell).*

An excellent analysis of 27 *in vivo* (in the patient's mouth) all-ceramic dental crown fractures was described by Øilo et al.[62] Crowns are shell-like ceramic restorations which are cemented onto a tooth that is too damaged for repair by amalgam or composite fillings. The crowns were a dense alumina, primarily from one source. Most of the clinical fractures split the crowns vertically into two or more pieces such as shown in Figure 4.40. Laboratory testing (*in vitro)* of 30 model crowns of the same material system was done using three different loading schemes. Two loading schemes produced fractures that did not match

the patient *in vivo* fractures. The third loading scheme matched quite well and generated nearly identical fracture patterns as in *in vivo* fractures. It was with occlusal (top surface) loading of the crown with a large 30 mm diameter ball pressing on a 3 mm thick rubber disk. The rubber disk distributed the load and prevented localized contact damage. Fractographic analysis of both the model and clinical fractures confirmed that the occlusal loading generated internal expansion of the shell-like crown, creating high hoop stresses along the margins (the open end of the crown that is in contact with the gum line). Subsequent work verified that the clinically fractured pieces had excessive faults (chips, cracks, irregularities) at much too sharp (~0.1 mm) margins. Figure 6.92 is one example, and several more are shown in Case 12 in Chapter 10. The combination of the faults with the hoop stresses led to premature splitting fractures. Clearly the crown design had to be revised.

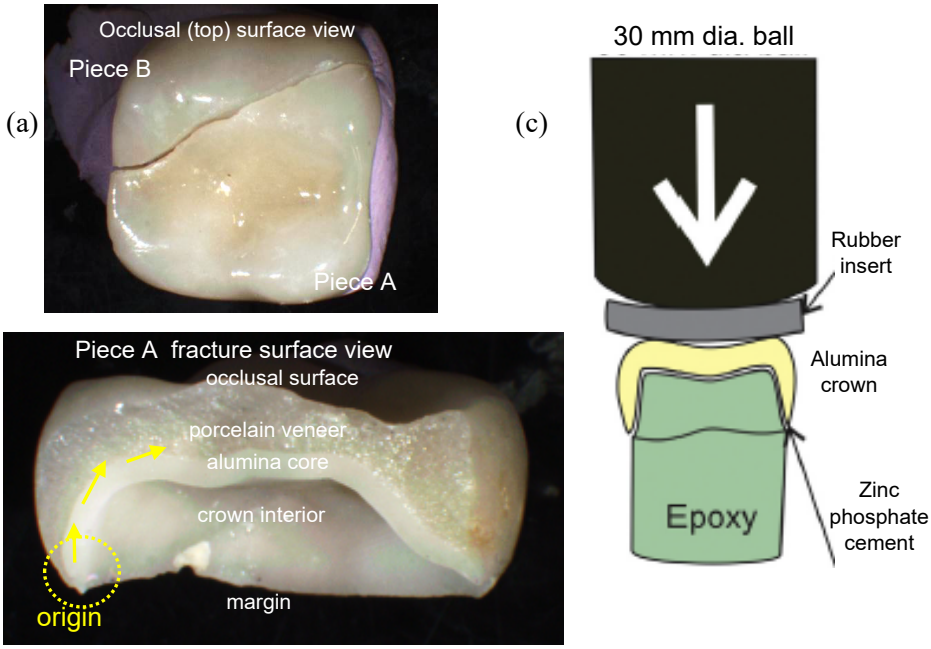

Figure 4.40 *Alumina molar crown (clinical 33) which fractured after 6 years in the patient's mouth. (a) shows an occlusal surface (top) view. (b) shows a side view and the fracture surface of piece A. Careful examination showed the origin was on the margin on the left, and the fracture ran up through the crown and to the other side, splitting it in half. (c) shows the laboratory test set up which produced nearly identical fracture patterns. The epoxy base simulated the dentin of the reduced human tooth. (courtesy M. Øilo)*

Another dental example on an actual human tooth, was by Dr. J. Quinn et al.[63] She mimicked a fracture of an upper right canine tooth that broke at the root several days after the patient had heart surgery. This led to litigation against the anesthesiologist. It was speculated that blunt force damage during intubation by the anesthesiologist caused damage that led to the fracture. Fractographic analysis showed that fracture started from the lingual (tongue) side and caused a curved fracture plane from cantilever loading. Dr. J. Quinn obtained a comparable tooth from an extraction (from another patient) and loaded it in cantilever loading in a laboratory setting. It broke in an almost identical manner. This, plus tooth decay in the heart surgery patient's tooth, evidence of step wise crack growth, and evidence of bruxism, showed the tooth was damaged before the surgery. The anesthesiologist was not at fault. Nevertheless, it was recommended that mouth guards (commonly used by bruxers when sleeping) ought to be used during intubation for surgery in the future.

Fractures or partial cracking in pharmaceutical containers is a serious problem that can lead to major product recalls and even fatalities. Schaut et al.,[64] surveyed such episodes for borosilicate containers and listed examples. They identified "bump checks," "lens cracks," and "neck cracks" as common container damage. Sections 6.8.4 in chapter 6 and section 4.13 in this chapter have more information about glass container flaws. Schaut et al.[64] described how they were able to duplicate such damage in the laboratory. They compared results for a common borosilicate glass to results for a modern chemically-strengthened glass.

A recent failure analysis was applied by Costello et al. [65] to glass "post horns" as shown in Figure 4.41. These were made in the Netherlands in the 17th and 18th centuries. More than one dozen of them exhibited cracking around the mouthpieces even though they had been careful preserved in museums. Was this yet another example of "crizzling" or "glass disease" as described in the following section 4.19.4 of this Guide? Was this due to an environmental attack of an unstable composition glass? What should the conservators do to protect the pieces from further degradation? These questions were answered by fractographic analysis. The cracking extended as much as 2 cm to 3 cm down the tube from the mouthpieces. The cracking pattern did not resemble crizzling fractures (section 4.19.4) but instead looked more like a biaxal thermal shock cracking and was only on the outer surfaces. It was hypothesized that the mouthpieces may have been intentionally quenched during early stages of glass blowing of the horns to preserve the mouthpiece shape. This was verified when modern glassblowers duplicated the cracking by quenching the mouthpieces in water when they prepared replicas by a trial-and-error process. Annealing

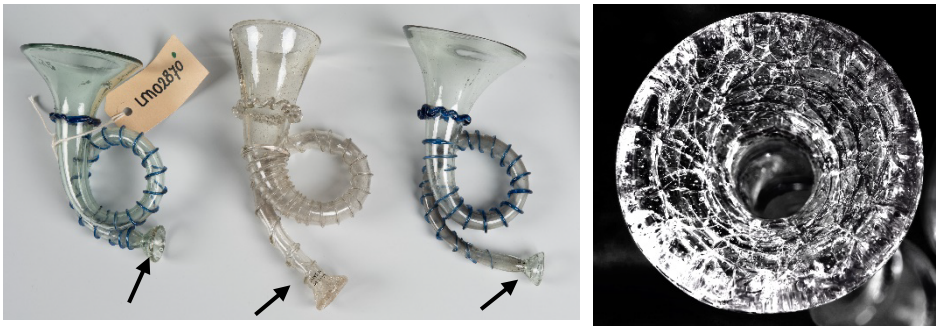

(a) (b)

Figure 4.41 *Glass "post horns." The arrows point to cracking extending from the rim down to as far as 2 or 3 cm below the mouthpieces. (b) is an end view of one mouthpiece. The cracking pattern is typical of thermal shocking. (courtesy T. Costello)*

made the horns strong enough to be handled and even blown in the mouthpiece. Polariscope examination showed no internal strains.

4.18 Finite Element Analysis

Stress solutions may be straightforward for simple shapes and loadings, but many components have complex shapes and asymmetrical loadings. Closed-form solutions for the stress state may not be available. Finite element analysis (FEA) is a valuable tool for such problems. FEA models partition a body into small elements and uses computer analysis to obtain the stresses and strains in each using the theory of elasticity. In principle, the entire stress distribution in a body can be analyzed, provided that the loading conditions are accurately simulated. Software for FEA is becoming increasingly easy to use, but some skill is needed in setting up the problem, applying a good mesh, and identifying the correct boundary conditions. Richter utilized FEA results to help interpret the ceramic hip ball fractures.[61]

FEA analysis can be a case of "garbage in and garbage out." Modelers may be so enamored of the models with their assumed loading conditions and anticipated fracture modes that they are unreceptive to obvious evidence that a component is not fracturing "the way it is supposed to break." A good modeler should be flexible and not afraid to modify or adapt the simulation based on the fractographic findings. In reference 66 "Design and Reliability of Ceramics, Do Modelers, Designers and Fractographers See the Same World?" I reviewed several case studies and compared model predictions to actual fracture modes.

4.19 Characteristics of Some Common Fracture Modes

4.19.1 Mechanical overload fracture

This chapter has illustrated only a sampling of mechanical fractures. The general breakage patterns can sometimes lead one directly back to an origin site, but often it is necessary to examine the fracture surfaces of the fragments to interpret the directions of crack propagation as shown in Chapter 5. Once a fracture pattern is recognized and an origin site identified, the next step is to assess whether the flaw is intrinsic to the manufacture of the part (as in a pore or inclusion), or from surface finishing, or from handling, contact or impact damage, or environmental attack (e.g., corrosion, oxidation, or erosion). Origins are covered in chapter 6.

4.19.2 Thermal fracture and thermal shock, crackle glass

Thermal stresses are created by differential strains created when portions of the body try to stretch or contract, but are constrained by other portions of the body at different temperatures. The key word here is "constraint." Some examples of thermal-stress induced fractures were shown earlier in this chapter. If the body can expand or contract freely, then thermal stresses do not arise. The constraint may be within the ceramic or glass body itself as portions of it inhibit the expansion or contraction of other portions, or the constraint may be from an external source such as a support or frame that holds the ceramic. Linear temperature gradients in a body do not create thermal stresses if the body is unconstrained.[67,68]

Thermal stresses may either be steady state (invariant with time) or time dependent. Thermal shock is the case where the temperature of a body is suddenly changed. The simplest one-dimensional thermal stress case entails a rod or prism that is heated and tries to expand lengthwise but is constrained by rigid walls on the ends. The thermal strain, $\varepsilon = \Delta l/l = \alpha\Delta T$, where α is the coefficient of linear thermal expansion and ΔT is the temperature change. The rigid walls prevent the expansion by exerting stresses on the ends of the rod or prism. The thermal stress is compressive:

$$\sigma = \varepsilon E = \alpha E \Delta T \tag{4.7}$$

where E is the elastic modulus. This combination of parameters, $\alpha E \Delta T$, appears in many thermal stress problems. A $(1-\nu)$ term is often included (where ν is Poisson's ratio) in plate or surface problems where the stresses are biaxial, and

$$\sigma = \frac{\alpha E \Delta T}{(1-v)} \qquad 4.8$$

This relationship can be rearranged to give the "R factor," with the material properties on one side.

$$R = \frac{\sigma_f (1-v)}{\alpha E} \qquad 4.9$$

where σ_f is the material's strength. R is a common index of a brittle material's thermal shock resistance and has units of temperature. It can be correlated to the instantaneous (or very sudden) ΔT temperature shock to the surface of a ceramic or glass that will cause fracture. Complex heat transfer problems have additional terms such as the material properties: thermal conductivity, thermal diffusivity, and Biot's modulus and external factors such as the surface heat transfer coefficient, *h*, and various geometry terms (e.g., diameter, radius, or thickness). The *R* factor and other factors such as *R', R'', R'''*, etc.,[67,69] are used to rank a material's resistance to various thermal stress or thermal shock conditions. The *R* factors often do not exactly match the ΔT to cause a fracture, since component shape and geometry factors are involved. They allow material ranking, but sometimes they can match measured ΔT values.

Five common types of thermal stress cases that cause fracture are (a) a component is constrained or stretched by an external structure, such as a window in a frame, or the ceramic is bonded to a metal; (b) a ceramic or glass has a coating, glaze or enamel that expands differently than the bulk; (c) a component has strains within itself from overall temperature gradients between different portions of the body; (d), a component has through-the-thickness strains from temperature gradients through-the-thickness; and (e) the component is a polycrystalline ceramic with anisotropic crystals or a mix of phases and stresses arise from differences in expansion between crystals or phases. In the latter instance, cracking may be is very localized around and between the grains.

The center-heated plate problem discussed in section 4.12 and shown in Figures 4.25 – 4.27 are classic cases of scenario (c). The differential expansion of the middle regions of the structure relative to the rim creates uniaxial hoop type tensile stresses at the rim that trigger fracture from an edge origin. The crack initially propagates perpendicularly to the edge, but then slows down and meanders in the interior biaxial compression stress field. The interior stresses are of insufficient magnitude to cause crack branching. The fracture surface markings (discussed in the next chapter) may be sharp and clear near the origin but then fade away to a very smooth featureless appearance as the crack slows down in the interior. Case 6 in Chapter 10 is an example of a center heated plate fracture in a silicon carbide furnace part. Center-cooled plates have the

opposite stress state: tension in the interior and compression at the rim. Fracture is less likely to occur since the edge, which is likely to have the more serious flaws, is in compression.

Thermal shock occurs during transient (sudden) cool down or heat up events. Figure 4.1 at the beginning of this chapter showed an example of a Pyrex soda lime silica kitchenware that broke in thermal shock. The fracture origin was a surface crack that propagated despite the piece having been heat strengthened. Thermal shock can cause strains between portions of a body (scenario b above) or through-the-thickness (scenario d above). Ceramics and glasses are most susceptible to sudden cool down thermal stresses, since tensile stresses are created at the surface. The surface layer of the part cools quickly and tries to contract, but the hotter interior portion prevents the contraction thereby creating tensile strains and stresses in the outer layer. Compressive stresses are generated in the interior. Suddenly cooling the surface with a fluid such as water can generate substantial tensile stresses and fracture since the fluid promotes rapid heat transfer from the surface.

Depending upon the circumstances (heat transfer rates, material properties, size and shape of ceramic or glass, the quenching medium) temperature cooldowns of as little as 100° C may be enough to cause fractures in common glasses. Some glasses with low thermal expansion coefficients such as fused silica, almost never fracture from thermal shock. Ceramics may fracture with a few hundred degrees shock. There are exceptions. In an exotic case described by Suratwala,[70] a weak and very brittle (K_{Ic} = 0.10 $MN/m^{1.5}$) single-crystal of potassium dihydrogen phosphate (KDP) fractured during fabrication. Despite an extremely slow cooling at 3° C per day from the processing temperature of 62° C, the crystal boule fractured. An astonishing conclusion was that flowing dry air (that was used to remove the liquid salt solution in which the boule was fabricated) caused the thermal shock fracture. It was estimated that the temperature change ΔTc was less than 5.7° C. In other words, simple evaporative cooling of just a few degrees Celsius was sufficient to cause thermal shock. This was an extreme case! Suratwala also showed an example where a layered structure with special light-absorbing glass plates mounted on aluminum backing plates failed when exposed to sunlight.[70]

Some procedures, such as laboratory quenching of hot bend bars into water, create sharp stress gradients with a biaxial stress state at the surface. This leads to the formation of a two-dimensional network of surface cracks that may not necessarily penetrate completely into the interior. Examples are shown in Figure 4.42. Shao et al. [71] showed some images showing how cracking patterns in alumina plates changed with increasing temperature shock. At low shock, a

few looping cracks formed. With greater shock, a dense cellular structure formed. With the maximum shock, a cellular structure with enveloping larger cracks appeared.

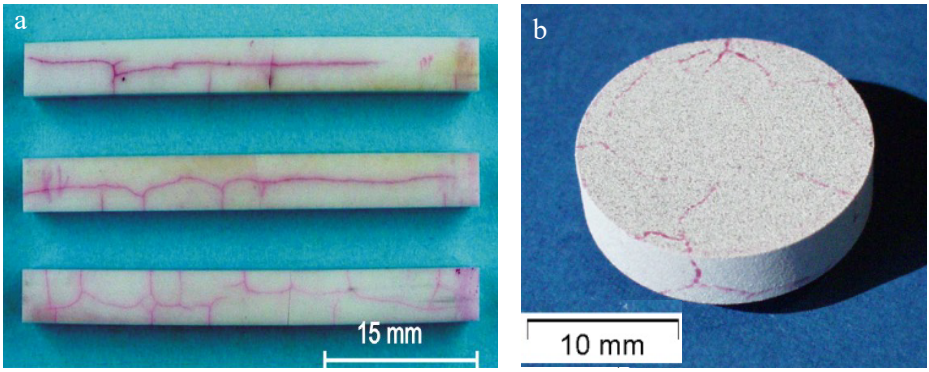

Figure 4.42 *Thermal shock cooldown cracks in alumina bend bars (a), and a disk (b). The cracks are highlighted by red dye penetrant. (courtesy of R. Danzer and T. Lube, Mountain Univ. Leoben)*

Very-localized thermal fractures from contact of a warm or hot component surface with a cooler contacting object (such as a metal tool) can create "chill checks" that are small cracks described in section 6.8.4 and shown in Figure 6.76. They do not penetrate far or very deep since thermal strains are very localized. The cracks are susceptible to later extension leading to fracture by subsequent events or loadings.

Other cases of thermal shock or thermal stress fracture in this Guide include Figure 4.1 for the Pyrex glass kitchenware bowl, Figure 4.21 for a sapphire missile dome, Figures 4.25 and 4.26 for a center-heated ceramic furnace plates, Figure 4.28 for bonded glass plates, Figure 4.29e for a glass bottle, Figures 8.27 - 8.29 for sapphire furnace tubes, Figure 10.13 for a center-heated SiC furnace plate, and Figure 10.31 for a large sapphire space lens.

An interesting anecdote about avoidance of glass thermal shock fractures related to the fire in the Notre Dame cathedral in Paris on 15 April 2019.[72] The firefighters who rushed to the scene had been expertly-trained in protocols for fire management of Paris' historical monuments. They knew to keep water away from the medieval stained-glass windows to prevent thermal shock that would have destroyed them.

"Crackle glass" is a novelty or artistic cracked glass with intentional thermal shock cracking as shown in Figure 4.43. It is sometimes called "ice glass" or even "craquelle." Crackle glass is made by blowing a gather of molten glass and then dipping it into cold water. This step may be repeated. The glass outer surface is cracked but the cracks do not penetrate all the way through the glass thickness since the inside glass may still be warm/hot and be either ductile or under compression from the contracting outer surface. The glass can be reheated or flash heated to seal the outer surface, or another layer of glass may be added. Crackle glass can also be created in glass rods heated by a gas torch then plunged into water.

Figure 4.43 *A 120 mm diameter crackle glass globe from a common yard ornament. It is erected on a small post stuck in the ground. A photocell and battery illuminate an internal small light bulb at night.*

4.19.3 Coating fractures, crazing, and craquelure

Coating fractures are an example where large-scale localized fracturing occurs and one's attention is not on finding a single fracture origin. They often have a cellular pattern as shown in Figures 4.44 and 4.45. Coating fractures are a broad class of problems ranging from glazes on pottery, enamels on metals such as bathtubs, to crazing on paintings, to layered ceramics, to thermal barrier or environmental barrier coatings on advanced high-temperature engine parts.

Crazing is surface cracking in coated or glazed brittle materials. The patterns can be variable or quite symmetric such as for dried-out mudflats. Hodges[73] wrote: "Crazing has long been the bane or delight of potters depending upon the aesthetic effects for which they are aiming." Crazing commonly arises

from the glazes or coatings that have higher coefficients of thermal expansion than the body to which they are applied. During cooling they try to contract more than the body but are prevented from doing so by the body. Tensile stresses develop in the coating causing cracking. Crazing is usually undesirable, but some artwork is intentionally crazed. Many crack patterns are possible, but the pattern can provide some insights as to the cause of crazing.[71,74,75,76] The patterns even provide guidance on artwork authentication!

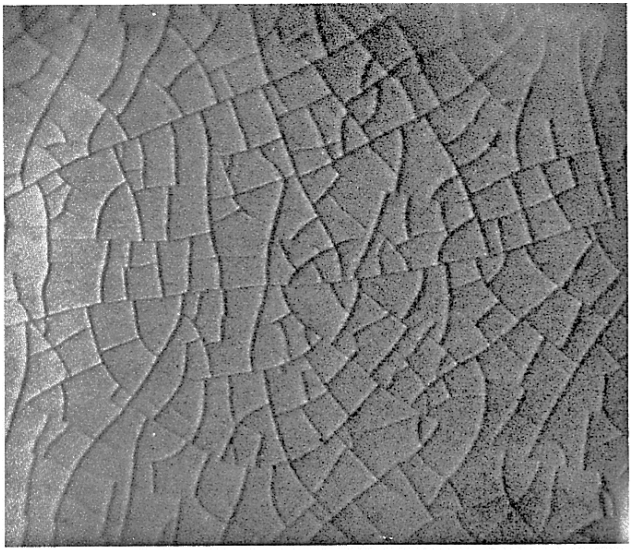

Figure 4.44 *Coating cracking, in the form of crazing in a glazed ceramic whiteware as the result of moisture expansion of the underlying body. (size not reported, from Fréchette, ref. 1)*

At first glance, the patterns may seem random, but crazing does not occur instantaneously. It can occur in steps. Many cracks can initiate and grow and intersect. Since cracks run perpendicular to the principal tension stresses at the crack tip and the cracking pattern shows the stress distribution at the time of cracking. Once one set of cracks forms, tensile stresses are redistributed. New cracks form as the glaze contracts, often running at angles or perpendicular to the first cracks. This divides and subdivides the surface into little squares, rectangles or other shapes. T-crack intersections can help determine which cracks came first. Figure 4.44 shows such an example. Figure 4.45a is a matching schematic of the same pattern. Several approximately horizontal cracks formed first, followed by cross cracking between them. Eggert's 2006 example[75] for a glaze on a figurine is redrawn here as Figure 4.45b and had as many as nine separate cracking and subcracking stages.

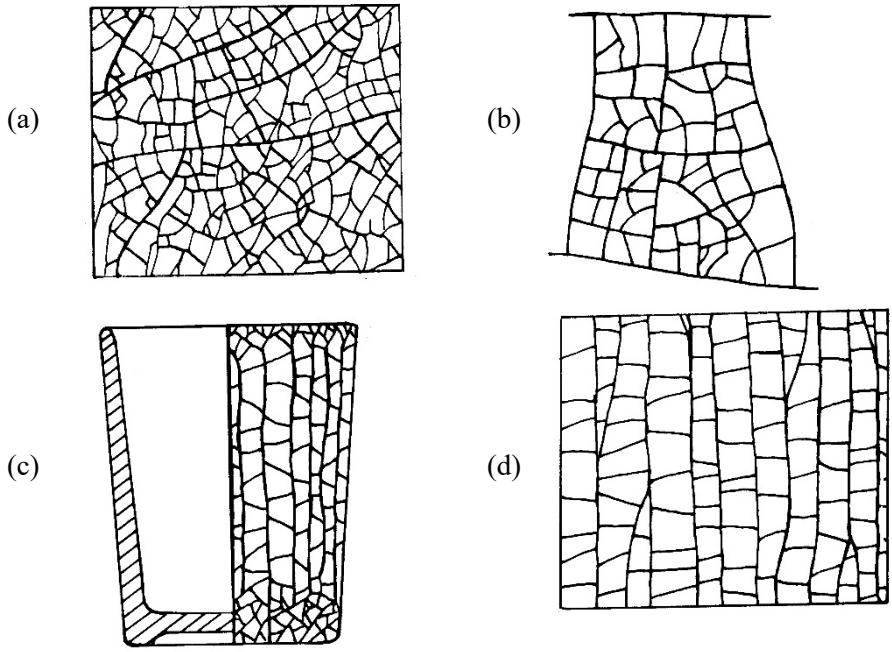

Figure 4.45 *Examples of crazing patterns retraced from several original sources. (a) is after Fréchette.*[1] *(b) is after Eggert*[76] *(c) and (d) are after Hodges.*[73] *See text for descriptions.*

Figures 4.45c,d are from Hodges' article.[73] The first shows a cylindrical vessel with theoretical zones of crazing formed during rapid cooling of a glazed ware in a kiln. The rim and base have randomly arranged cracks, but the body has vertical cracks that formed first from hoop tensile stresses followed by cross cracking. His article has a good discussion of various causes of crazing including the differential thermal expansion, glaze composition issues, unreacted quartz in the glaze, thermal cooldown rate effects (too fast or too slow) in kilns, and thermal gradients in furnaces or within the body, devitrification or quartz inversion effects. Crazing can also occur after firing. Crazing can occur in many applications including glazes on ceramics, glazes on metals, coatings, layered ceramics or glasses, paintings in museums, veneers on ceramic dental restorations, thermally shocked glasses or ceramics (see the previous section 4.19.2 and Figure 4.41 with the Dutch post horns), and even fire-damaged glass.

Eggert showed fascinating examples of fire-damaged glass fragments from an ancient Roman Empire era burial site. He was able to replicate the effect with modern glass plates.[75,76] He did the same for an ancient Roman glass bottle,

also from a cremation. These were excellent examples of laboratory replication of fracture patterns as a means to verify a hypothesis as to the cause of fracture as discussed in the section 4.17 in this chapter. Similar words "*craquelé*" and "*craquelure*" are used to describe a pattern of undesirable fine cracks on artworks such as paintings or pottery. Sometimes these words are used in the art community for desirable cracking, as in wares made intentionally to have such patterns. Note these are not the same as "*crizzling*," which is an attack on glass by the environment that is discussed in the next section, 4.19.4.

Fréchette's book has a subsection on failure of coatings.[1] He noted that cracking across a coating and substrate depends on whether the interfaces are constrained and whether coatings are applied equally on both sides of a part. Part geometry plays a large role. Coatings on tubular shaped parts may behave differently. Coating and substrate materials may interact forming interphases or they may interfuse) affecting the stresses.

It is common practice to use coatings (e.g., glazes) that are fused to a body at elevated temperatures. The coatings have a lower thermal expansion coefficient than the substrate. As the object is cooled, the substrate tries to contract more, putting the outer coating into residual compression. One would expect this improve resistance to cracking, yet it is not necessarily that simple. Fréchette pointed out[1] that excessive residual compression stresses in a coating can cause "*shivering*" that causes material to spall at corners and edges.

One example of dental coating cracking was from the 2000s, when premature *in vivo* veneer fractures occurred in veneered zirconia ceramic tooth restorations.[77] High-strength yttria-stabilized zirconia crowns and bridges had recently been introduced to the dental restoration market. The contemporary zirconias were too white and had a "chicklet" appearance. A cosmetic porcelain veneer was applied to the core zirconia ceramic and bonded at high temperature. The color and translucency of the porcelain veneer could be matched to colors in the individual patient's mouth. The thermal expansion of the veneer was less than that of the zirconia in order that the veneer would be in residual compression, but service chipping failures of the veneer occurred at an unexpected rate. Failure analysis showed that thermal conductivities of the materials were a key factor since thermal gradients were created during fast cooldown. During cooldown the restorations had gone too quickly through the porcelain's glass transition temperature T_g of about 600° C in the furnace. It may seem surprising, but in the interest of fast production, conventional practice (such as had been done for decades with porcelain to metal crowns) was to fuse a veneer to the core substrate at temperatures such as 840° C or greater, hold for ten minutes, and then open the chamber and shut the small

furnace off. A combination of tempering and thermal expansion mismatch stresses in the veneer caused high tensile residual stress to form on the inside of the veneer. These made it more vulnerable to chipping once a crack penetrated from the exterior surface. The remedy was to cool more slowly through T_g, so as to minimize the residual stresses and only then open the furnace chamber door.[77] The point here is that coating stresses are due not only due to thermal expansion mismatches, but a variety of other thermal factors and firing schedules and part geometries. Hodges' article is instructive.[73]

The stresses that develop in planar interfaces were mathematically analyzed and experimentally verified by Oel and Fréchette in a clever study in 1967.[78] They bonded glasses of different properties in both constrained and unconstrained configurations. The constrained configuration involved two identical glass layers bonded to an inner different glass layer. The unconstrained configuration involved one glass bonded to another glass such

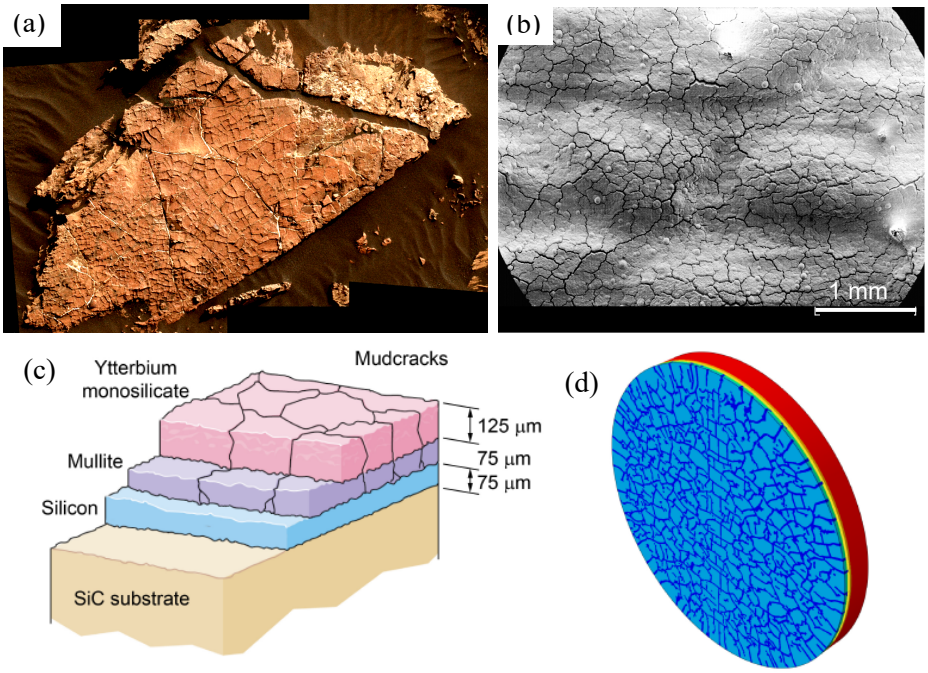

Figure 4.46 *Example of "mud cracks" from Nemeth et al.[79] (a) is a composite photo of fossilized desiccation mudcracks solidified on the Martian surface 3.5 billion years ago. (b) is an environmental barrier coating (EBC). (c) is an example of a 3-layer EBC coating with mudcracks and channel cracks. (d) shows simulated cracking in a 3-layer EBC coating.*

that the structure could bow. The study used optical glasses with known thermal expansions, refractive indices, and stress optical coefficients so that the stresses through each glass layer could be spatially measured and compared to mechanics theory. Although only glasses were used, the authors noted that the results were applicable to glass to metal structures such as sheet steel enameled on both sides. These results were quite interesting and showed that the actual stress profiles could vary from the predicted distributions, especially at the exact interface. Uncertainties in the exact point the respective glasses stiffened up (e.g., went through T_g, or the strain point) depended upon the cooling rates. Interdiffusion of the glasses also blurred the interface, and in one example there was a spectacular divergence of measured from calculated stresses such that the stress sign reversed.

Interesting examples of environmental barrier coating (EBC) cracks are in a 2020 NASA Technical publication by Nemeth *et al.*[79] Some of the coatings are multilayered. The report has an interesting review of nomenclature including the terms: "desiccation cracks," "mudcracks," "channel cracks," and "shrinkage cracks." The report has a emphasis on modelling but includes fascinating illustrations and a good review of the literature especially in its Appendix. Figure 4.46 shows mudcracks.

Additional examples of cracked glazes and veneers are in this Guide section 6.15 in Chapter 6 on Glaze and Coating Flaws. Glaze flaws that acted as fracture origins are shown.

Cracking from the <u>edges of coatings</u> can occur, even if the coatings are designed to be in residual compression. Fréchette[1] observed that in such cases a crack can occur first at the coating edge and run into the compression-stressed partner (the coating) at 45°, and then curve to run parallel to the interface. (This is related to but opposite the edge chipping case discussed and illustrated in section 6.7.8 in the Origins chapter of this Guide.) Fréchette then said additional cracks might form in the tension partner perpendicular to the interface, but they might run into the coating and then branch to run parallel to the interface.

Fréchette[1] also noted that in unconstrained cases (coating applied to one side of a thin substrate), the specimen may bow towards the tension side. This may relax the stresses, possibly to the extent that they reverse in sign. A coating in originally in compression may go into tension leading to spontaneous fracture!

The reader is referred to the Glue Chipping problem discussed in section 6.7.8 in the Origins chapter. Additional examples of dental coating (veneer) fractures are in section 6.15 in the Origins chapter.

4.19.4 Corrosion, oxidation, crizzling

Oxidation and corrosion can weaken a part and leave it susceptible to fracture. In ceramics, telltale surface reactions are often apparent on the surface in the form of numerous pits, discoloration, and surface scale. Sometimes the damage is confined to small localized pits, bubbles, or blisters that can act as fracture origins as shown in Figure 6.28 in chapter 6. In some difficult to interpret cases, the reactions are localized along grain boundaries and can only be discerned with the SEM. Chemical analysis can show cation migration to or from a reaction site. It can also indicate contamination or reaction with the environment or furnace linings or insulation. Richerson[80] shows several examples of corrosion-oxidation fracture origins in silicon nitrides.

Crizzling is a corrosion process that can severely damage glasses and even lead to fractures as shown in Figure 4.47. It is sometime described as "glass disease" and can cause severe deterioration and even fracture of some glasses in normal air environments. Koob explains the process in his book on

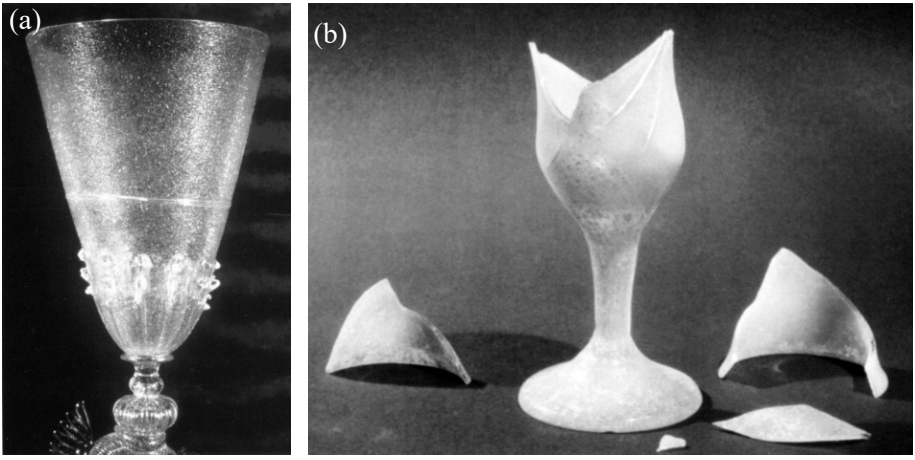

Figure 4.47 *Crizzling can result from of water attack on glasses. It can even occur on pieces stored in a museum. It can progress to form microcracks as shown in the vessel in (a) or even outright fracture as shown by the example in (b). The composition of the glass and the humidity of the environment are key factors. (photos courtesy S. Koob, Corning Museum of Glass.)*

conservation and restoration of glass.[81] Water is attracted to the surface of glasses. The alkali in glass is hygroscopic and can attract moisture directly from the air. As the alkali is hydrated, it leaches out to the surface of the glass. This eventually can result in an attack on the silica network. This can free up more alkali and the process can become progressively worse. Koob characterized this process by five stages, beginning with a light clouding up of the glass surface, then continuing with the formation of microcracks on the surface (Figure 4.47a). As the process progresses the cracking becomes quite distinct. Pieces may even flake off. The vessel may completely fracture into pieces all by itself, or with simple handling or cleaning (Figure 4.47b).

Certain glasses are more susceptible to this mechanism of damage, most notably those with too little silica content, inadequate lime (or magnesia) stabilizer content, or too much alkali in general, particularly from potash. Indeed, ancient Roman era glass makers made glass with good proportions of soda (natron), lime, and silica that made the glass very durable over time. European glass makers in medieval times made glasses that used plant ash (rich in potassium) rather than natron and these glasses were far less durable and sometimes deteriorated sitting on shelves in museums. Venetian glass makers also made glasses that were susceptible in their efforts to make glass with clarity of rock crystal. Problems with the susceptibility of glasses to crizzling continued well into the 19th century, and continues even today with studio glasses made by artists who are not careful.

Additional information on crizzling and fracture may be found in the books by Tennent[82] and Davidson.[83] For many years, it was thought there was little hope to restore such heavily damaged pieces, by new work by Koob[84] offers a practical remedy and some hope for conservationists.

Surface cracking from environmental effects can be a problem for high tech materials as well, as described by Suratwala in his book on optical materials fabrication.[70] Examples were shown for phosphate glasses and potassium-dihydrogen-phosphate (KD_2PO_4) single crystals.

4.19.5 Impact or contact fractures

Impacts may create <u>localized damage sites</u> that can become the origin of fracture if the impactor is small or sharp. Impact may also cause fracture by <u>flexing the structure</u> such that fracture initiates on the <u>side opposite the impact</u> site or elsewhere in the body. Section 4.13 on bottle and plate fractures earlier in this chapter shows both scenarios. Sharp and blunt impacting objects create different types of localized damage origins as shown in sections 6.7.4 and 6.7.5

in chapter 6. When an impact or contact fracture is suspected, the surface should be carefully examined for "witness marks" as discussed in section 7. Figure 4.48 shows a human bone broken in three-point loading with some superimposed axial compression. An impact could be expected to create a similar breakage pattern. The fracture origin is on the bottom to one side of the loading axis. A new FBI Guide[22] refers to this as a "*Remote origin*" since the origin of fracture was not exactly opposite the loading axis, but remote to it.

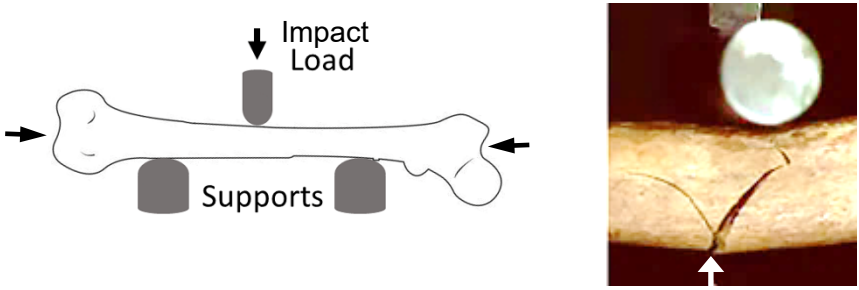

Figure 4.48 *Human bone in bending with some axial compression. Side view of an impact fracture. The origin location is marked by the white arrow. (Ref. 22, courtesy A. Christensen)*

4.19.6 Residual stresses

Residual stresses can arise from many sources. They may be either beneficial or harmful. They can be intentional as in tempered or heat-strengthened glass or unintentional as in ceramics sintered in furnaces with thermal gradients. They can be highly variable within a structure. Residual stresses can exist at different scales within a structure. It is convenient to differentiate them as: *bulk, through the thickness, localized, or microstructural residual stresses.*

Bulk residual stresses in a part are such that one portion or side is straining against other portions due to differential contractions during cooling. They can even cause spontaneous fractures in the absence of external stresses. For example, there are reported cases of improperly-sintered porcelain toilets that fractured spontaneously leading to catastrophic house flooding. Residual stresses may also exist through the thickness of a part, as in heat-strengthened or tempered glass plates. Residual stresses may be very localized, such as around a sharp impact or contact damage site (e.g., a sharp particle impact site or Vickers indentation). Shallow residual stresses are also common on machined and ground surfaces. They typically are compressive within a few

micrometers of the outer surface and change to tensile further beneath the surface. As such they can affect origins located on the surface. Finally, residual stresses may exist at a microstructural level, such as at the grain boundaries between grains or between two phases in polycrystalline materials, or between an inclusion and the matrix. The inclusion may have very different thermal contraction or elastic properties than the matrix. Even in pure ceramics localized microstructural stresses can occur within or between anisotropic grains. Alumina is a good example. Such stresses are more likely to exist in noncubic ceramics, but they can exist even in cubic materials.

Thus, it is simplistic to say: "the piece had residual stresses." One must be more specific and recognize that there may be multiple types of residual stress in a part. Residual stress may not necessarily be harmful. Some are compressive and some are tensile. Where an origin is located and the type of residual stress it is exposed to are important factors to consider. Crack propagation and branching may be dramatically affected as a crack moves from one type of stress field into another (e.g., compressive to tensile). Residual stresses may be highly variable within a part. Reference 85 is an interesting new paper on the variability of residual stresses in air-jet tempered glass plates. Reference 86 has other examples of nonuniformly-tempered glass including one illustration of a large automobile windshield. Uneven fragmentation and crack patterns are telltale signs of nonuniform tempering.

The fractographer may be tipped off to the existence of residual stresses by the overall fracture patterns. They may also be signaled by Wallner line markings on the fracture surfaces as shown in the next chapter. Distortions in the size and shape of a fracture mirror can be evidence of residual stresses. Analysis of flaw sizes can be used to estimate residual stresses as shown in section 7.14.

A sudden change in crack propagation direction may be another sign. They can also be indicated by abrupt, seemingly spontaneous fractures when a component is being cut or machined. A machinist once told me this had happened with large SiC tubes he was slicing. Fréchette described a case of boron carbide blanks fracturing during machining.[87] Fractographic analysis showed that the fracture started at the root of the machine cut and then spread rapidly along the middle of the slabs and then outward to the free surfaces. This indicated the interior was in tension and the outer portions were in compression. The firing schedule was reviewed, and it was learned that the part was allowed to free cool between 1950 ºC to 1800 ºC followed by very gradual cooling thereafter. The free cooling occurred in a range where creep was possible which could have set up a final stress state not unlike tempered glass. Afterwards, no matter how carefully the slicing was done, once it

reached the interior the part fractured. The problem was simply remedied by changing the cool down rate through the creep regime to minimize differential strains during the cool down, thereby eliminating the residual stresses.

4.19.7 Time-dependent fracture and slow crack growth

Delayed fracture can occur due to slow crack growth (SCG) from preexistent flaws. The loading conditions and stresses may initially be insufficient to cause breakage, but a flaw may slowly grow when it is under tensile stress until it reaches a critical condition and then triggers breakage. The rate of crack growth is very sensitive to the stresses and stress intensities acting on a flaw, and growth can be very slow or rather fast. Section 7.10 in chapter 7 covers quantitative aspects of SCG and shows how it may appear on a glass fracture surface. For constant stress, cracks accelerate with time in accordance with fracture mechanics analyses shown in section 7.10. There may be little or no warning of the imminent failure since the extent the crack grows to become critical may be very small. The mechanisms of slow crack growth and additional illustrations showing some telltale signs of SCG are in section 5.8 in chapter 5.

4.19.8 Compression fracture

Genuine compression fractures with ceramics and glasses are rare. They are more common in concretes and rocks. Compression failure is a factor in ballistic impact or geological fractures. The uniaxial compression strength of ceramics and glasses is ten times or more greater than the tensile strength. Fracture does not start from a single flaw but instead involves damage accumulation that leads to fracture with a lot of fragmentation. Fractographic analysis is often focused on verifying that a proper compression fracture has occurred in laboratory tests. Important changes in fracture mode can occur in multiaxial compression cases and the fractographer should be on the lookout for them as described below. Confining pressures dramatically increase strengths and alter the failure modes. We begin here with a discussion of uniaxial compression fracture.

Unless special precautions are taken in uniaxial compression strength testing many specimens actually break from tensile stresses and not from genuine compression. Tensile stresses can arise from even slight misalignments or elastic property mismatches, and the tensile stresses will cause fracture.[88,89,90,91] Specimen design is critical. End splitting can occur if the compliance of the loading anvils creates lateral stresses at the ends of the specimen. Cylindrical specimens are prone to these problems, and often fractures occur due to end

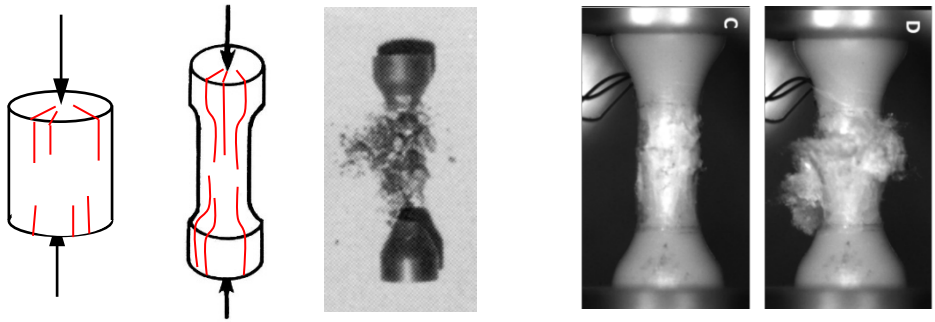

(a) (b) (c) (d) (e)

Figure 4.49 *Compression strength specimens. Cylindrical specimens (a), are very susceptible to end splitting shown by the red cracks. Dumbbell specimens (b) are also susceptible to end splitting if the loading anvils are not carefully chosen or are misaligned. (c) shows a valid B_4C compression quasistatic fracture from Tracy[88] in 1987 whereby the gage section is pulverized but the end caps are intact. (d) and (e) show a 2017 high-speed photo of a dynamic Kolsky bar fracture of alumina 995 taken at the instant of failure from Swab and Quinn.[93] (d, e, courtesy C. Meredith)*

splitting as shown in Figure 4.49a. Such results are invalid. Dumbbell tapered specimens are preferred, as shown in Figure 4.49b.[88,89,92,93,94] Properly tested specimen fractures are shown in Figures 4.49c-e. The extraordinary fragmentation of the gage section is notable. There is no point in looking for a single fracture origin. The goal of a fractographic analysis is more to verify that a test was done correctly, and to identify the mechanism of compression fracture as described in the next paragraphs. Figures 4.49d,e show a gage length fracture in a high-speed Kolsky bar experiment.[93,94]

Unlike tension fracture, compression fracture activates <u>many flaws</u> in a body. These may either be preexisting flaws or those newly-generated by the high compressive stresses. Preexisting flaws such as open inclined elliptical pores may be such as shown in Figure 4.50.[95,96] Although the overall stress state is compression, the flow lines of stress cannot pass through such an open flaw. They bend around it and create localized, sideways tensile stresses at the pore ends. Microcracks initiate, then grow stably and alter the flow lines of stress such that the local tensile stresses gradually rotate to a horizontal orientation. The microcracks propagate and align themselves parallel to the compression loading axis and eventually stop as shown in Figure 4.50a. These cracks are often called “wing cracks.” To the best of the author’s knowledge, Adams and Sines were the first to use the word “wing” in 1978 (Ref. 95, page 109).

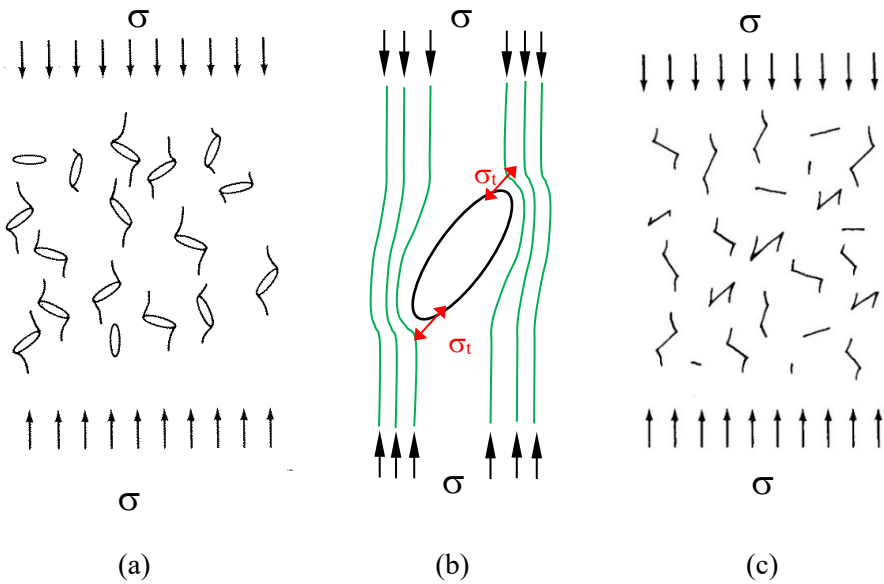

Figure 4.50 *Mechanisms of wing crack formation that leads to compression fracture. (a) shows microcracks ("wing cracks") that form from preexisting flaws such as inclined ellipsoidal pores. (b) is a close-up of the flow lines of stress around the pore. Localized tensile stress occurs at the flaw ends. (c) shows that wing cracks can also form from closed planar flaws.*

New microcracks initiate at other pores with different orientations and sizes. Wing cracks can also form at closed flaws as shown in Figure 4.50c due to shear across the crack faces. Friction across the microcrack surface and geometric interlocking can affect behavior. As uniaxial compression loading on the open or closed flaws continues, the structure becomes saturated with a high density of microcracks. The extreme stresses can even activate dislocations or twins within grains leading to localized plasticity that is not experienced in tensile loadings. Final fracture occurs with a sudden dramatic structural collapse and "explosion" of the specimen. This could entail buckling collapse of vertical columns in the damaged structure or shear bands of damaged material. Enormous stored elastic energies are released in the form of pulverization, kinetic energy of the fragments, sound waves and reverberations, and even triboluminescent light emission.[d] The key point here is that compression strength is not controlled by a single large flaw. It is controlled by the flaw density and size distribution. An interesting 1978 paper about the

[d] Once this collapse begins, stored elastic energy in a testing machine may be pumped back into the specimen further contributing to pulverization. The machine compliance may be a factor.

latter (that builds on their earlier work correlating the Weibull distribution to tensile strengths, flaw densities, fracture mechanics, and statistical theory) is by Jayatilaka and Trustrum.[97] Open ellipsoidal pores are used in the explanation above, but other flaws (e.g., inclusions) can induce the same response if the elastic properties of the flaw do not match the matrix or there are localized residual stresses around the flaws. One problem with compression strength or ballistic impact loading models is that they often assume one type of idealized flaw, whereas as this Guide shows, there can be a variety of flaw types in a material. They will behave differently.

Figure 4.51 shows several alternative modes of fracture that do not necessarily require initial flaws. During compression loading microcracks can be generated in a microstructure by several mechanisms.[98,99,100] Grain boundary microcracks can be initiated due to elastic property mismatches between the

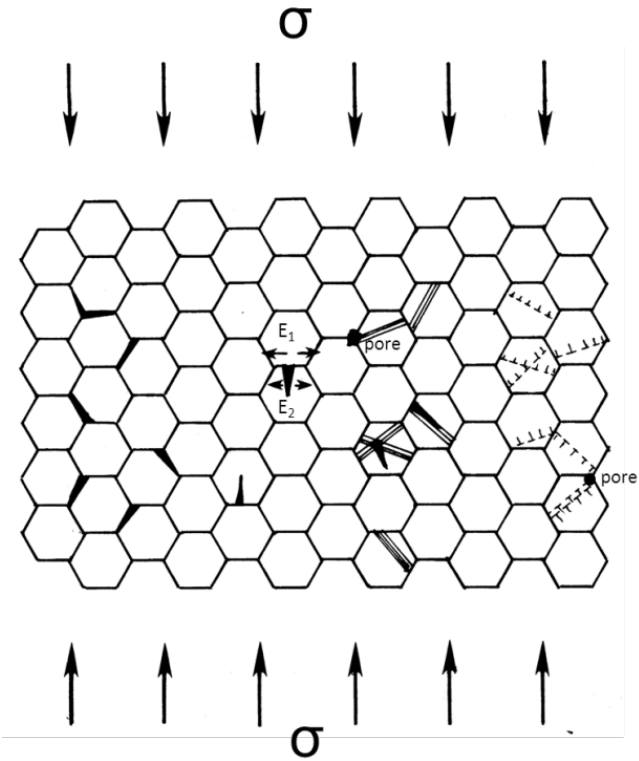

Figure 4.51 *Compression loading may create microcracks in the microstructure of a ceramic. This simulated microstructure with hexagonal grains shows how microcracks can be generated at grain boundaries (left), or from elastic property mismatch at grain boundaries (middle), or from twinning or dislocation activity within grains (middle and right side).*

adjoining grains that have different orientations. The elastic moduli and crystal constants can be dramatically different on different orientations, especially in non-cubic materials. Furthermore, strong residual stresses can exist along grain boundaries due to differential shrinkage between adjoining grains with different orientations. The middle of Figure 4.51 shows two grains with different orientations and moduli and, as vertical force is applied, the lateral strains can be very different, causing the nucleation of wedging cracks in one or the other grain. On the right of Figure 4.51 twins or dislocations within grains are shown initiating microcracks. Usually there are not enough independent slip systems active at low temperatures to lead to generalized plasticity, but the very large compression stresses can create sufficient dislocation activity and buildups to form microcracks within grains or at grain boundaries.

A very different failure mode occurs for cases of "confined compression." By this it is meant that the material is in a triaxial compression stress state. Triaxial compression suppresses the formation of even localized tensile stresses at inclined flaw tips. The case of equal principal stresses ($\sigma_1 = \sigma_2 = \sigma_3$) is called "hydrostatic compression" and fracture is inhibited. Nonetheless, high pressure compression cell and diamond anvil research has shown that failure can occur under hydrostatic conditions due to densification in glasses, phase

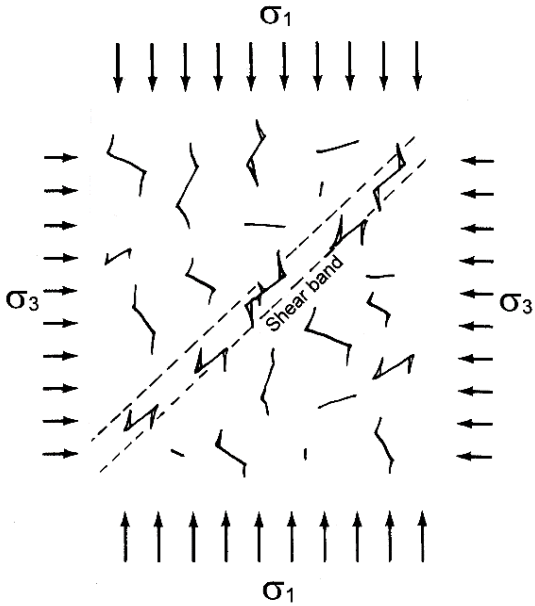

Figure 4.52 *Shear bands can form in triaxial compression if the stresses are unbalanced as shown in (a) where $\sigma_1 > \sigma_2, \sigma_3$. The principal stress σ_2 out of the plane of paper is not shown.*

changes in ceramics, or collapse of porosity. This could lead to local faulting at grain boundaries or at flaws, and even within grains particularly if they are noncubic.

Alternatively, unbalanced triaxial compression ($\sigma_1 = \sigma_2 > \sigma_3$), ($\sigma_1 > \sigma_2 = \sigma_3$) or ($\sigma_1 > \sigma_2 > \sigma_3$) leads to shear failures, often in bands as shown in Figure 4.52. This shear localization leads to apparent "plasticity with work hardening" and eventually fracture.[101] The array of interacting wing cracks is sometimes described as "en echelon cracks." Since flaws are often more pronounced on a free surface, shear bands often initiate at a free surface. In some famous

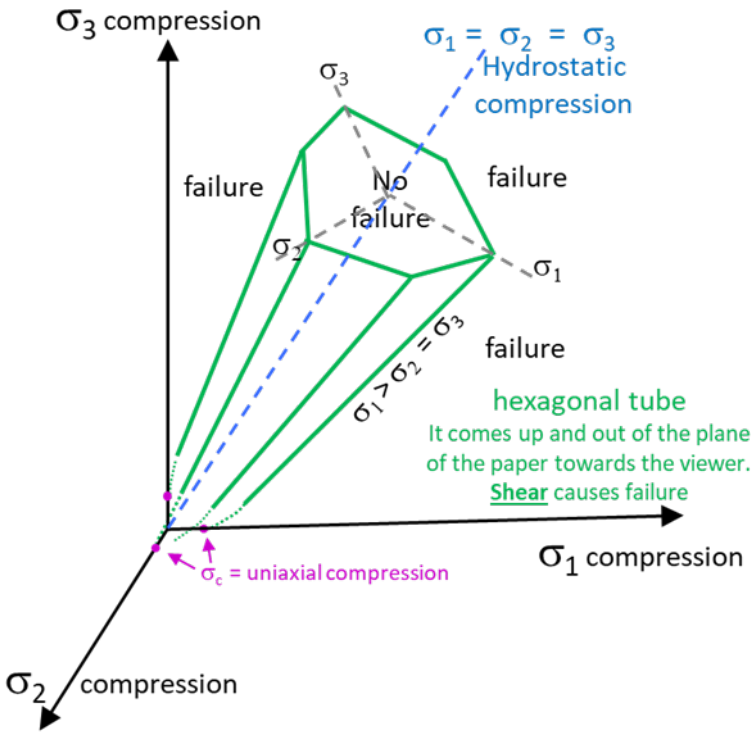

Figure 4.53 *The failure envelope based on the Mohr-Coulomb criterion. Failure does not occur for combinations within the tube. This triaxial loading condition is sometimes described as "confined compression." Unbalanced compression principal stresses create shear stresses. Failure occurs for stress combinations outside the expanding hexagonal tube. Failure may eventually occur in hydrostatic compression if densification or phase changes occur so the failure envelope may be "closed off" on the upper right.*

experiments, Heard and Cline[102] showed that confining pressure suppressed brittle fracture from flaws and led to a brittle-ductile transition whereby dislocations and twins became active within grains leading to pronounced plasticity. The greater resistance to fracture with increasing compression stresses was shown by Bridgeman's pioneering confined compression work in the 1930s to 1950s.[103,e] There is an extensive literature on confined compression fracture in the rock fracture literature. Concrete fractures often involve shear banding.

The Mohr-Coulomb failure criterion is often applied to analyze fracture in triaxial compression loading problems. This is shown by the expanding hexagonal tube failure envelope shown in Figure 4.53. Up to this point, this fractography Guide has not covered the topic of multiaxial stress failure envelopes. Engineers are trained in the more common ones such as the maximum normal stress theory, the maximum shear stress theory (Tresca), or the distortion energy theory (Von Mises). They are covered in any mechanical engineering textbook, but the books usually focus on tensile or combined tensile-compression loadings. Multiaxial compression failure envelopes are not commonly taught and are less familiar to engineers and scientists so a few words about it are added here. The Mohr-Coulomb criterion takes into account the shear stresses created by the imbalance of the compression stresses. Failure occurs when the difference between the maximum (σ_1) and minimum (σ_3) principal stresses create shear stresses that exceed a limiting criterion. (The intermediate compression stress σ_2 usually plays a small role.) In other words, fracture will not occur for any principal stress combination within the hexagonal tube in Figure 4.53. It does occur for stress combinations outside the tube. An interesting complication is that the shear limit depends upon the overall magnitude of the compression stresses. The greater the overall compression stresses, the greater the resistance to fracture, hence the tube expands as shown. The tube may not necessarily continue upwards indefinitely, however. A limit for the hydrostatic condition may occur if densification or phase changes occur. At low stresses, the tube pinches inward for uniaxial and biaxial compression, since a completely different flaw density failure criterion applies. The tube does not extend into the tension quadrants.

A curious new phenomenon identified as a failure mechanism in confined compression of rock entails the formation of "anticracks" shown in Figure 4.54.

---

[e] It is curious that Bridgman's 1938 paper showed "tensile fractures" in the complete absence of any applied tensile stresses. His tensile fracture planes were perpendicular to the minimum principal compression stress. This paradoxical and controversial finding came as a surprise. He argued that tensile strain ought to be the criterion for fracture, not stress. He did observe shear failures in some of his experiments (his "compression set") in his 1947 paper.

Sometimes these are accompanied by cracks. The combination can lead to volume-conserving bulk deformation and shear faults.[104] An "anticrack" is a confined crack like elastic irregularity that has concentrated compression stresses acting on its tips. Figure 4.54 shows they can either be "open" or "closed" anticracks. The open anticrack is an elastic irregularity like a microcrack or void that is compressed by remote compression stresses causing the zone to collapse. The tips of the collapsed zones are under extreme compression and have a negative stress intensity K_I field. Hence the name "anticrack." Alternatively, there can be "filled anticracks" that are zones of material that that undergo a phase transformation that contracts the zones. This pulls the tips into compression.[105,106] Microcracks and assorted faults, sometimes with zig-zag patterns, may emerge from the tips or sides of the anticrack. Patterns of parallel en echelon crack patterns can appear. Whichever way the anticracks form, they can evolve into arrays of anticracks, cracks, and fault lines that lead to deformation bands in confined rocks. Although this is an area of active attention in the geological community, it is unknown whether anticracks play a role in ceramics or glasses subjected to confined compression loadings.

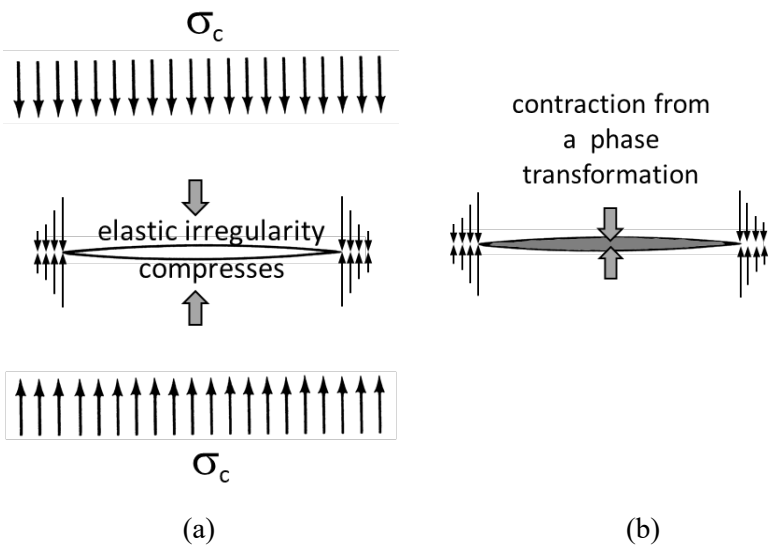

Figure 4.54 *Anticracks. (a) shows an "open anticrack." An open zone or open crack is exposed to remote compression stresses that cause the zone to collapse. Material at the tip is "scrunched" creating a negative K_I stress intensity field. (b) shows a "filled anticrack" whereby a phase transformation causes contraction of a lens-shaped zone. Local compression stresses are created at the zone tips.*

The explanations of compression-induced cracking in this section are a first order explanation of how accumulated damage can lead to structural collapse. The rock fracture literature has many papers and models on compression fractures in geological materials. A recent publication[107] showed that wing cracks as shown earlier in Figure 4.50 are just one category of localized damage. "Wrapped wing cracks" and even "anti-wing cracks" can also arise depending upon the triaxial stress states and proximity of flaws to each other. Wrapped wing cracks extend from the inclined flaw as shown above, but partially wrap around the inclined flaw. Anti-wing cracks are similar to the wing cracks shown above, but the curvature at the end of the inclined flaw is mirror-reversed. Although the rock literature has many useful lessons for structural ceramics and glasses, the fact remains that rocks can behave differently since they are anisotropic and inhomogeneous, and generally have coarser microstructures. A recent review[108] of "brittleness" of rocks points this out and has a fascinating discussion of just what the word "brittleness" means. No less than eighty different rock brittleness parameters are reviewed, one of which is this author's own.[109] Hundreds of papers have been written on brittleness and attempts to quantify it, and we should not digress too far on this topic here. Nonetheless, this author likes Van Frechette's definition of brittle fracture,[1] which I paraphrase here: "the broken pieces fit back together perfectly matched."

Chapter 4 References

1. V. D. Fréchette, *Failure Analysis of Brittle Materials*, Advances in Ceramics, Vol. 28, American Ceramic Society, Westerville, OH, 1990.
2. P. B. Adams and S. E. DeMartino, "Glass-Ceramic Cookware Failure Analysis," pp. 669 – 673 in *Ceramics and Glasses, Engineered Materials Handbook*, Vol. 4, ed. S. Schneider, ASM, Metals Park, OH, 1991.
3. F. Cazenave, E. H. Baker, N. D. Card, G. D. Quinn, P. Remijan, J. Salem, and A. Varshneya, "Design and Testing of a Large Sub-hemispherical Glass Port for a Deep-Sea Camera Housing," presented at the GOMD Division meeting of the American Ceramic Society, San Antonio, TX, May 2018.
4. F. W. Preston, "The Angle of Forking of Glass Cracks as an Indicator of the Stress System," *J. Am. Ceram. Soc.,* **18** [6] (1935) 175 - 176.
5. G. D. Quinn, "On Crack Branching Angles in Glasses and Ceramics," *J. Eur. Ceram. Soc*., **40** (2020) 4711 – 4721.
6. J. B. Quinn, "Extrapolation of Fracture Mirror and Crack-Branch Sizes to Large Dimensions in Biaxial Strength Tests of Glass," *J. Am. Ceram. Soc*., **82** [8](1999)2126–32.
7. J. F. Kalthoff, "On the Propagation Direction of Bifurcated Cracks," pp. 449 – 458 in *Dynamic Crack Propagation*, ed. G. C. Sih, Noordhoff, Leyden, NL, 1973.
8. J. F. Kalthoff, "On the Characteristic Angle for Crack Branching in Brittle Materials," *Int. J. Fract. Mech*., **7** (1971) 478 – 480.
9. V. D. Fréchette and T. A. Michalske, "Fragmentation in Bursting Glass Containers," *Bull. Amer. Ceram. Soc*., **57** [4] (1978) 427 – 429.

10. T. A. Michalske, "Quantitative Fracture Surface Analysis," pp. 652 – 662 in *Ceramics and Glasses, Engineered Materials Handbook, Vol. 4*, ASM Int., Materials Park, OH, 1991.
11. J. B. Kepple, and J. S. Wasylyk, "Fracture of Glass Containers," pp. 207 –252 in *Fractography of Glass*, eds. R. C. Bradt and R. E. Tressler, Plenum, NY, 1994.
12. H. Kolsky, "The Waves Generated by Brittle Fracture in Glass," *Trans. Soc. Rheology*, **20** [3] (1976) 441 – 454.
13. R. W. Rice, ""Ceramic Fracture Features, Observations, Mechanisms and Uses," in *Fractography of Ceramic and Metal Failures,* STP 827, ASTM, 1984, pp. 5 – 103.
14. R. E. Bullock and J L. Kaae, "Size Effect on the Strength of Glassy Carbon," *J. Mat. Sci.,* 14 (1979) 920 – 930.
15. J. Miklowitz, "Elastic Waves Created During Tensile Fracture," *J. Appl. Mech*., 20 [1] (1953) 122 – 130.
16. G. W. Quinn, J. B. Quinn, J. J. Mecholsky, Jr. and G. D. Quinn, "Computer Modeling of Crack Propagation Using Fractal Geometry," *Ceram. Eng.Sci. Proc.,***26** [2](2005) 77 - 84.
17. D. Shetty, A Rosenfield, and W. Duckworth, "Crack Branching in Ceramic Disks Subjected to Biaxial Flexure," *Comm. Amer. Ceram. Soc.,* Jan. 1983, C10 - C12.
18. D. Hull, "Influence of Stress Intensity and Crack Speed on the Fracture Surface Topography: Mirror to Mist to Macroscopic Bifurcation," *J. Mat. Sci.*, **31** (1996) 4483 – 4492.
19. G. D. Quinn and R. Morrell, "Design Data for Engineering Ceramics: A Review of the Flexure Test," *J. Am. Ceram. Soc*., **74** [9] (1991) 2037 - 2066.
20. A. Tsirk, *Fractures in Knapping*, Archeopress, Oxford, U.K., 2014, page 171, Figure 11.3.
21. J. Miklowitz, "Elastic Waves Created During Tensile Fracture, The Phenomenon of a Second Fracture," *J. Appl. Mech.,* Mar. 1953, 122 – 130.
22. G. D. Quinn, "Twisting and Friction Errors in Flexure Testing," *Ceram. Eng. Sci. Proc*., **13** [7-8] (1992) 319 - 330.
23. A. Christensen, M. I. Isa, M. A. Smith, J. T. Hefner, H. Berryman, , J. B. Webb, and I. S. Saginor, *A Guide to Forensic Fractography of Bone*, Federal Bureau of Investigation Laboratory, Quantico, VA, Feb. 2022.
24. H. Fessler and D. C. Fricker, "A Theoretical Analysis of the Ring-on-Ring Loading Disk Test," *J. Am. Ceram. Soc.,* **67** [9] (1984) 582 – 588.
25. J. A. Salem and L. Powers, "Guidelines for the Testing of Plates," *Ceram. Eng. Sci. Proc.,* **24** [4] (2003) 357 - 364.
26. G. D. Quinn, J. J. Swab, and P. Patel, "On Radial, Circumferential, and Spiral Cracks in Fractured Glass Plates," *Int. J. Appl Glass Sci.,* **12** [23] (2021) 189 - 197.
27. J. Wurm, *Glass Structures: Design and Construction of Self-Supporting Skins*, Birkhauser Verlag, Berlin, 2007.
28. D. Maccauley, *Cathedral: The Story of Its Construction*, Houghton Mifflin, NY, 1981.
29. D. Maccauley, *City: A Story of Roman Planning and Construction,* Houghton Mifflin, New York, 1974.
30. D. G. Holloway, "The Fracture Behavior of Glass," *Glass Techn.,* **27** [4] (1986) 120 - 133.
31. T. A. Michalske and E. R. Fuller, Jr., "Closure and Repropagation of Healed Cracks in Silicate Glasses," *J. Am. Ceram. Soc*., **68** [11] (1985) 586 - 590.
32. S. M. Wiederhorn and P. R. Townsend, "Crack Healing in Glass," *J. Am. Ceram. Soc*., **53** [9] (1970) 486 – 490.
33. B. Stavrinidis and D. G. Holloway, "Crack Healing in Glass," *Phys. Chem. Glasses,* **24** [1] (1983) 19 - 25.
34. C. Spangenberg, "Exploding Bottles," *Ohio State Law Journal*, **24** [3] (1963) 516 – 533.
35. R. A. Schaut, K. C. Hoff, S. E. Demartino, W. K. Denson and R. L. Verkleeren, "Enhancing Patient Safety Through the Use of a Pharmaceutical Glass Designed to Prevent Cracked Containers," *PDA J. Pharm. Sci. and Tech*., **17** (2017) 511 - 518.

36. F. M. Ernsberger, "Current Status of the Griffith Crack Theory of Glass Strength," pp. 58 – 76 in *Progress in Ceramic Science*, *Vol. 3*, Ed. J. E. Burke, Pergamon Press, NY, 1963.
37. N. Shinkai, "The Fracture and Fractography of Flat Glass," pp. 253 – 297 in *Fractography of Glass*, eds. R. C. Bradt and R. E. Tressler, Plenum, NY, 1994.
38. R. Gardon, "Thermal Tempering of Glass," pp. 145 – 216 in *Glass: Science and Technology, Vol. 5, Elasticity and Strength in Glasses,* eds. D. R. Uhlmann and N. J. Kreidel, Academic Press, NY, 1980.
39. A. Yuse and M. Sano, "Instabilities of Quasi-static Crack Patterns in Quenched Glass Plates," *Physica D,* **108** (1997) 365 - 378.
40. A. Yuse and M. Sano, "Transition Between Crack Patterns in Quenched Glass Plates," *Nature,* **362**, 25 March 1993, 329 - 331.
41. K. C. Deshmukh, Y. I. Quazi, S. D. Warbhe, and V. S. Kulkarni, "Thermal Stresses Induced by a Point Heat Source in a Circular Plate by Quasi-Static Approach," *Theo. Appl. Mech. Lttrs*., 1 (2011) 031007
42. D. Bahat, "Thermally Induced Wavy Hertzian Fracture," *J. Am. Ceram. Soc.,* **60** [1-2] (1977) 118 – 120.
43. J. B. Kepple and J. S. Wasylyk, "Fracture of Glass Containers," pp. 207 – 252 in *Fractography of Glass,* ed. R. C. Bradt and R. E. Tressler, Plenum, NY, 1994.
44. F. W. Preston, "Bottle Breakage – Causes and Types of Fractures," *Bull. Am. Ceram. Soc*., **18** [2] (1939) 35 -60.
45. B. S. Aldinger and P. de Haan, *Color Atlas of Glass Container Defects,* AGR, Butler, PA, 2022.
46. *Glass Container Defects, Causes and Remedies*, Bucher Emhart Glass Company, Steinhausen, Switzerland, 2017.
47. H. M. Dimmick, "Observed Direction of Leader Cracks from Hinge Failures of Glass Bottles," *J. Am. Ceram Soc*, **35** [9] (1952) 235 - 236.
48. R. E. Mould, "The Behavior of Glass Bottles Under Impact," *J. Am. Ceram. Soc,* **35** [9] (1952) 235 - 236.
49. A. W. Grabau, *A Textbook of Geology,* Pat 1, D. C. Heath &Co,, N. Y., 1920, pp. 640 - 641.
50. E. A. Almond and N. J. McCormick, "Constant-Geometry Edge-Flaking of Brittle Materials," *Nature*, **321** [6065] (1986) 53 - 55.
51. Ch. De Freminville, "Caractères Des Vibrations Accompagnant Le Choc Dé L'Examen Des Cassures," *Review de Metalugie*, **4** (1907) 833 - 884.
52. *Fractography of Glasses and Ceramics IV*, eds. J. R. Varner and G. D. Quinn, *Ceramic Transactions*, Vol. 122, Amer. Ceram. Soc., Westerville, OH, 2001.
53. B. Cotterall, *Fracture and Life,* Imperial College Press, London, 2010.
54. M. D. Thouless, A. G. Evans, M. F. Ashby, and J. W. Hutchinson, "The Edge Cracking and Spalling of Brittle Plates," *Acta Metall*., **35** [6] (1987) 1333 - 1341.
55. J. B. Quinn and R. Mohan, "Geometry of Edge Chips Formed at Different Angles," *Ceram. Eng. Sci. Proc.,* **26** [2] (2005) 85 – 92.
56. G. D. Quinn and J. B. Quinn, "A New Analysis of the Edge Chipping Resistance of Brittle Materials," *Ceram. Eng. Sci. Proc.*, **35** [1] (2015) 209 - 224.
57. G. D. Quinn, A. A. Giuseppetti, and K. H. Hoffman, "Chipping Fracture Resistance of Dental CAD/CAM Restorative Materials: Part 1, Procedures and Results," *Dent. Mater.*, **30** (2014) e99 – e111.
58. G. D. Quinn, A. A. Giuseppetti, and K. H. Hoffman, "Chipping Fracture Resistance of Dental CAD/CAM Restorative Materials: Part 2, Phenomenological Model and the Effect of Indenter Type," *Dent. Mater.*, **30** (2014) e112 - e123.

59. G. D. Quinn, A. A. Giuseppetti, and K. H. Hoffman, "Chipping Fracture Resistance of Denture Tooth Materials," *Dental Materials*, **30** (2014) 545 – 553.
60. R. Morrell, L. Byrne, and M. Murray, "Fractography of Ceramic Femoral Heads," pp. 253 – 266 in *Fractography of Glasses and Ceramics IV,* eds. J. Varner and G. D. Quinn, Cer. Trans., Vol. 122, Amer. Ceram. Society, Westerville, OH, 2001.
61. H. Richter, "Fractography of Bioceramics," pp. 157 - 180 in *Fractography of Advanced Ceramics*, ed. J. Dusza, Key Engineering Materials, **223** (2003), Trans Tech Publ., Switz.
62. M. Øilo, A. K. Kvam, J. E. Tibballs, and N. Gjerdet, "Clinically Relevant Fracture Testing of All-Ceramic Crowns," *Dent. Mater.*, **29** (2013) 815 - 823.
63. J. B. Quinn, L. W. Schultheis, and G. E. Schumacher, "Failure Analysis of a Broken Tooth," *J. Fail. Anal. Prev.*, **4** [1] (2004) 41 – 46.
64. R. A. Schaut, K. C. Hoff, S. E. Demartino, W. K. Denson and R. L. Verkleeren, "Enhancing Patient Safety Through the Use of a Pharmaceutical Glass Designed to Prevent Cracked Containers," *PDA J. Pharm. Sci. and Tech*., **17** (2017) 511 - 518.
65. T. Costello, L. Megens, G. Verhaar, G. D. Quinn, M. Barreda, and M. Slager, "Interdisciplinary Analyses for Diagnosing a Cracking Phenomenon on 17th- to 18th--century Dutch Glass Horns," pp. 163 – 171 in *Recent Advances in Glass and Ceramics Conservation 2022*, proc. 6th Interim Meeting of the ICOM-CC Glass and Ceramics Working Group, 9 – 11 Nov. 2022, Lisbon, Portugal.
66. G. D. Quinn, "Design and Reliability of Ceramics, Do Modelers, Designers and Fractographers See the Same World?" *Ceram. Eng. Sci. Proc*., **26** [2] (2005) 239 – 252.
67. W. D. Kingery, "Factors Affecting Thermal Stress Resistance of Ceramic Materials," *J. Am. Ceram. Soc.,* **38** [1] (1955) 3 - 15.
68. S. P. Timoshenko and J. N. Goodier, "*Theory of Elasticity,"* 3rd ed., McGraw Hill, NY, 1970.
69. D. P. H. Hasselman, "Thermal Stress Resistance Parameters For Brittle Refractory Ceramics: A Compendium," *Bull. Am. Ceram. Soc*., **49** [12] (1970) 1033 - 1037.
70. T. I. Suratwala, *Materials Science and Technology of Optical Fabrication*, Wiley, Hoboken, NJ, 2018. Section 6.4.1.2.
71. Y. Shao, X. Xu, S. Meng, G. Bai, C. Jiang, and F. Song, "Crack Patterns in Ceramic Plates after Quenching," *J. Am. Ceram. Soc*., **93** [10] (2010) 3006 – 3008.
72. C. Lesté-Lasserre, "Saving Notre Dame," *Minerva, Archeology & Ancient Art,* **31** [5], Sept/Oct. (2020) 48 - 54.
73. H. W. M. Hodges, "The Formation of Crazing in Some Early Chinese Glazed Wares," in *The Conservation of Far Eastern Art : Contributions to the IIC Kyoto Congress, Sept. 1988,* eds. J.S. Mils et al., International Institute Conserv., London (1988) pp. 155 - 157.
74. S. Bucklow, "The Description of Craquelure Patterns," *Studies in Conservation,* **42** (1997) 129 – 140.
75. G. Eggert, "Hot Glass, Cold Water: Experiments in the History of Glass Fracture," pp. 8-14 in *proc. Glass and Ceramics Conservation 2007, interim meeting of the ICOM-CC Working Group, Nova Gorica, Slovenia,* ed. L. Pilosi.
76. G. Eggert, "To Whom the Cracks Tell," A Closer Look at Craquelure in Glass and Glaze," *Studies in Conservation,* **51** (2006) 69 – 75.
77. M. J. Tholey, M. V. Swain, and N. Thiel, "Thermal Gradients and residual Stresses in Veneered Y-TZP Frameworks," *Dent. Mater*., **27** (2011) 1102 - 1110.
78. H. J. Oel and V. D. Fréchette, "Stress Distributions in Multiphase Systems: Composites with Planar Interfaces," *J. Am. Ceram. Soc,* **60** [10] (1967) 542 – 549.
79. N. Nemeth, S. Mital, Evan Pinea, P. Murthy, D. Zhu, H. Wadley, and S. Arnold, "Stochastic Simulation of Mudcrack Damage Formation in an Environmental Barrier Coating," NASA Technical Publication-2020-220185, Dec. 2019.

80. D. W. Richerson, Chapter 16 in *Modern Ceramic Engineering, 2nd ed,* Decker, NY, 1992.
81. S. P. Koob, *Conservation and Care of Glass Objects*, Archetype Publ., London, 2006.
82. N. H. Tennent, *Conservation of Glass and Ceramics*, James and James, London, 1999.
83. S. Davidson, *Conservation and Restoration of Glass, 2nd ed*. Butterworth and Heineman, Oxford, 2003.
84. S. P. Koob, "Crizzling Glasses: Problems and Solutions," *Glass Technology: Eur. J. Glass Sci and Tech. A,* **53** [5] (2012) 225 - 227
85. J. Anton, A. Errapart, M. Paemurru, D. Lochegnies, S. Hödemann, and H. Aben, "On the Inhomogeneity of Residual Stresses in Tempered Glass Panels," *Estonian J. Engineering*, **18** [1] (2012) 3 - 11.
86. K. Blank, "Some Practical Aspects of Thermally Strengthened Glass," pp. 485 – 499 in *Strength of Inorganic Glass*, ed. C. Kurkjian, Plenum, NY, 1985.
87. V. D. Fréchette, "Fractography and Quality Assurance of Glass and Ceramics," pp. 227 - 236 in *Quality Assurance in Ceramic Industries*, eds. V. D. Fréchette, L. D. Pye, and D. E. Rase, Plenum, NY, 1978.
88. C. A. Tracy, "A Compression Test for High Strength Ceramics," *J. Test. and Eval.,* **15** [1] (1987) 14 - 19.
89. A. Rudnick, C. W. Marschall, W. H. Duckworth, and B. R. Enrick, "The Evaluation and Interpretation of Mechanical Properties of Brittle Materials," U.S. Air Force Materials Laboratory Technical Report, AFML TR 67-316, April 1968.
90. W. Dunlay, C. Tracy, P. Perrone, "A Proposed Uniaxial Compression Test for High Strength Ceramics," MTL TR 89-89, US Army Mat. Tech. Lab., Watertown, Mass., 1989.
91. G. Sines and M. Adams, "Compression Testing of Ceramics," pp. 403 - 434 in *Fracture Mechanics of Ceramics, Vol. 3,* eds. R.C. Bradt et al., Plenum, NY, 1978.
92. J. J. Swab, C. S. Meredith, D. T. Cassem, and W. R. Gamble, "Static and Dynamic Compression Strength of Hot-pressed Boron Carbide Using a Dumbbell-Shaped Specimen," *J. Mat. Sci.,* **52** [17] (2017) 10073 – 10084.
93. J. J. Swab and G. D. Quinn, "Dynamic Compression Strength of Ceramics: Results from an Interlaboratory Round-Robin Exercise," U.S. Army, ARL Technical report 8860, Nov. 2019.
94. J. J. Swab, W. Chen, J. Hogan, H. Liao, C. Lo, S. Mates, C. Meredith, J. Pittari, R. Rhorer, and G. D. Quinn, "Dynamic Compression Strength of Ceramics: What was Learned from an Interlaboratory Round Robin Exercise?" *J. Dyn. Beh. Mater*., 7 [1] (2021) 34 – 47.
95. M. Adams and G. Sines, "Crack Extension from Flaws in a Brittle Material Subjected to Compression," *Tectonophysics,* **49** (1978) 97 - 118.
96. F.M. Ernsberger, "Tensile and Compressive Strength of Pristine Glasses by an Oblate Bubble Technique," *Physics and Chemistry of Glasses,* **10** (6) 1969 pp. 240 - 245.
97. A. DeS. Jayatilaka and K. Trustrum, "Fracture of Brittle Materials in Uniaxial Compression," *J. Mat. Sci., Lttrs.,* **13** (1978) 455 - 457.
98. J. Lankford, "Compressive Strength and Microplasticity in Polycrystalline Alumina," *J. Mat. Sci*., **12** (1977) 791 – 796.
99. J. Lankford, W. W. Predebon, J. M. Staehler, G. Subhash, B. Pletka, and C. A. Anderson, "The Role of Plasticity as a Limiting Factor in the Compressive Failure of High Strength Ceramics," *Mech. Mater*., **29** (1998) 205 - 218.
100. R. W. Rice, "The Compressive Strength of Ceramics," pp. 195 – 229 in *Ceramics in Severe Environments*, eds. W. W. Kriegel and H. Palmour III, Plenum Press, NY, 1971.
101. "Fracture in Compression of Brittle Materials," National Materials Advisory Board report, NMAB-404, National Academy of Sciences, Washington, DC, August 1983.
102. H. C. Heard and C. F. Cline, "Mechanical Behavior of Polycrystalline BeO, Al_2O_3 and AlN at High Pressure," *J. Mat. Sci.,* **15** (1980) 1889 – 1897.

103 P. W. Bridgman, "The Effect of Hydrostatic Pressure on the Fracture of Brittle Substances," *J. Appl. Phys.,* **18** [246] (1947) 246 – 258.
104. R. C. Fletcher and D. D. Pollard, "Anticrack Model for Pressure Solution Surfaces," *Geology,* **9** (Sept. 1981) 419 – 424.
105. H. W. Green II, T. E. Young, D. Walker, and C. H. Scholz, "Anticrack-Associated Faulting at Very High Pressure in Natural Olivine," *Nature,* **348** (Dec. 1990) 720 -722.
106. H. W. Green and P. C. Burnley, "A New Self-Organizing Mechanism for Deep-Focus Earthquakes," *Nature,* **341** (October 1989) 733 - 737.
107. Y. Sun, F. Fei, L. Wong, and J. Choo, "Intermediate Principal Stress Effects on the 3-D Cracking Behavior of Flawed Rocks Under True Triaxial Compression," *Rock Mech. and Rock Eng.,* **57** (2024) 4607 - 4634.
108. F. Meng, L. Wong, and H. Zhou, "Rock Brittleness Indices and their Applications to Different Fields of Rock Engineering: A Review," *J. Rock Mech. Geotech. Eng.,* **13** (2021) 231 - 247.
109. J. B. Quinn and G. D. Quinn, "Indentation Brittleness of Ceramics: A Fresh Approach," *J. Mat. Sci*., **32** (1997) 4331 - 4346.

5. Fracture Surface Examination

5.1 Introduction

Fracture surfaces have a wealth of information that may help determine the cause of fracture. Oftentimes (but not always) the fractographer looks for a single fracture origin. The fracture surfaces should have an initial examination to look for any signs of contamination, and they should be cleaned as discussed in section 3.1 if necessary. There are two important cases where it may be wise to *examine fracture surfaces before cleaning*. First, surface contaminants may provide clues about the fracture event and may not be merely contamination picked up afterwards from handling. Figure 10.24e in Chapter 10 is a good

(a)

(b)

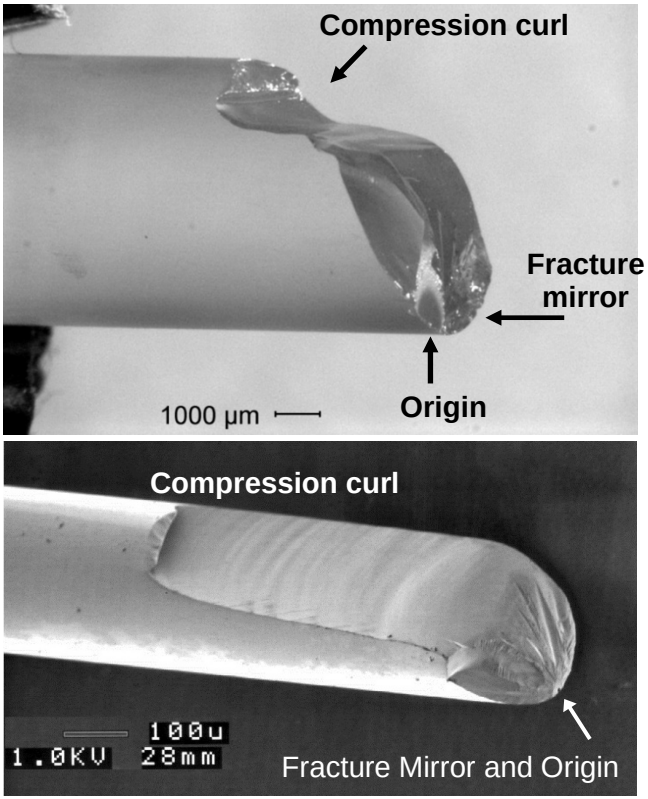

Figure 5.1 *Classic fracture patterns. (a) shows a low-power stereo optical microscope image of a 6 mm fused silica rod fractured in bending at 88.5 MPa (12.8 ksi) (b) is an SEM image of a 240 µm telluride chalcogenide fiber ($Ge_{30}As_{10}Se_{30}Te_{30}$) fractured in bending at 368 MPa (53.4 ksi). (b is courtesy of J. Quinn)*

example where discoloration at the origin was an important clue to understanding the initial flaw in a broken dental crown. Second, fine debris on a fracture surface may be a clue that cyclic fatigue may have occurred, if the debris is crushed material that was dislodged from the microstructure. This is covered in section 5.8.5 and shown in Figure 5.72.

The origin may range from a type and location anticipated by the fractographer (as in a broken bend bar) to an unexpected type from an unexpected location or cause (as in a broken component). In some cases, there may be multiple fracture origins. With familiar laboratory strength test specimens, the fractographer may proceed directly to the primary fracture surface and quickly locate the origin area. The fractographer usually seeks a fracture mirror, a key feature centered on the origin. Figure 5.1 shows two examples. The origins are often very small and magnification by a microscope is necessary. Stereo optical microscopes are ideal for initial fracture surface examinations. Sometimes this examination may be all that is needed for a full characterization of the origin. In other instances, the flaw at the origin is so small that scanning electron microscopy is needed.

Unexpected failure modes or component fractures require more time to study. The crack propagation markings on fracture surfaces allow one to evaluate the state of stress, the crack velocities, and interpret crack propagation paths back to an origin. In instances where an origin is not obvious, it may be necessary to study many fragments and carefully determine the local direction of crack propagation. Stereo optical microscopes are ideal for this initial fracture surface examination. Wallner lines and hackle markings are helpful indicators of the direction of crack propagation (dcp) in each piece. It is helpful to mark which way the crack was running in a fragment. This can be repeated for other fragments and then the pieces reassembled so that the lines of crack propagation can be tracked back to an origin site. Even very complex fractures may be interpreted if the fractographer is patient and systematic.

The greater the stress in the part at fracture, the more the stored energy, and the richer the fracture markings. Weak parts with low stored energy are often difficult to interpret. The part breaks into two pieces with relatively featureless fracture surfaces. Very porous or coarse-grained materials also can mask fracture surface fractographic markings. On the other hand, very strong components such as some glass optical fibers may have so much stored elastic energy at fracture that excessive fragmentation occurs and the origin cannot be found.

The nomenclature of fracture markings is varied. For example, “twist hackle” as defined in this Guide is also known as “river delta” lines. A common term in the older literature is “rib marks” that are arc-shaped lines that are almost always curved in the direction from which the crack was coming.[1] They may actually be “Wallner lines,” “arrest lines” or even “scarps.” This Guide avoids the term “rib marks” since the feature can be caused by so many different mechanisms. This Guide adopts and expands the nomenclature system devised by Fréchette.[1] His system is practical, logical, and designed to be easily remembered. Some of the definitions in the next sections are from Fréchette and many are new.

As noted in the Introduction to this book, Chapter 1, this Guide restricts itself to only five fundamental types of markings on the fracture surfaces:

fracture mirror, hackle, arrest (interruption) marks, Wallner lines, scarps

Subsets to these help differentiate the fundamental cause of the feature. There are ten types of hackle: mist hackle, velocity hackle, fine or coarse micro-structural hackle, twist hackle, wake hackle, shear hackle, corner hackle, step hackle, and cleavage step hackle. There are three types of Wallner lines: primary, secondary, and tertiary. Fracture surfaces in polycrystalline ceramics can be either transgranular, or intergranular, or a mix. Thus, there are only twenty primary fracture surface markings defined in this Guide.

A few other unique fractographic terms are scattered through this book. These include “gull wings”, a specific type of primary Wallner line. “Cathedral” and “Batman” mirrors are very distinctive fracture mirrors in single crystals shown in Chapter 8.

“Conchoidal fracture” and “cleavage fracture” are terms commonly used in the geological community. Cleavage fractures are smooth and planar fractures such as those on preferred breakage planes in single crystals. Conchoidal fractures do not follow natural planes of separation and often are curved, in a manner reminiscent of curved seashells. Conchoidal is derived from the Greek word for a mussel shell. Glass and many ceramic fractures are conchoidal. “Joint” is a common term in the geological community and means a fracture surface. Joints are defined as a fracture or crack in a rock mass along which no appreciable movement has occurred. “Parting” is another geological term describing flat fractures in a mineral, but is not necessarily along preferred cleavage planes. Parting is sometimes associated with twinning. Fréchette[1] discussed how parting can occur in ceramics along planes of weakness introduced during processing.

5.2 Fracture Mirrors, A Fractographer's Best Friend

5.2.1 Fracture mirrors in glass

Fracture mirror: *Relatively smooth region surrounding and centered on the fracture origin.* (ASTM C 1322, C 1678, and C 1145)

Once a fractographer finds a fracture mirror, he is reasonably sure that the fracture origin has been found. Figures 5.1 to 5.3 show mirrors in glass. They are telltale features that can be recognized by even novice fractographers. In strong specimens, they are approximately circular or semicircular in shape, but significant deviations may occur as discussed later. Usually there is only one mirror corresponding to a single fracture origin, but there are exceptions that are discussed later in this chapter. Fracture mirrors are typically 10 to 13 times larger than the origin flaw, but there can be considerable variability. This matter is discussed in detail in section 7.7 later in this book. There won't always be a fracture mirror and, if the fractographer cannot find one, he or she should not worry. More about this will be covered later in this chapter, but for now let us take a closer look at the fractographer's best friend.

The fracture mirror is the region where a crack radiates outwards from a flaw at the fracture origin. The crack accelerates from near zero velocity to terminal velocity within the fracture mirror region. Using ultrasonic stress wave fractography on soda lime silica specimens, Richter and Kerkhof[2,3] showed that mist formed at approximately 800 m/s which is 53% of the terminal crack velocity of 1,500 m/s. The crack continued to accelerate and formed hackle at the terminal velocity. Field et al.[4,5] showed similar ultrasonic stress wave fractography results and said that initial roughening (presumably hackle) occurred at the terminal velocity. The remarkable acceleration of a crack over a very short distance occurs in microseconds. Smekal[6] arrived at the same conclusion from his analysis of the Wallner lines (described later in this chapter) that had formed inside the fracture mirrors.

The term fracture mirror came in to being as a result of early optical microscopy of glasses wherein the mirror region was so smooth that it reflected light like a mirror. From my research into the history of fractography of brittle materials, it appears that Brodmann[7] first used the word *"mirror"* in 1894. Figure 5.2c shows a bright mirror region. (The illumination in this figure also accentuates the faint curved Wallner lines within the mirror, about which more shall be said later in this chapter.) In polycrystalline ceramics or composites, the qualifier "relatively," as in "relatively smooth," must be used, since there is

an inherent microstructural roughness even in the area immediately around the origin flaw.

Since fracture mirror boundaries are formed by cracks running close to or at the terminal crack velocity, this topic is discussed in detail in the next section, 5.2. Then, in the following section 5.3, the smooth fracture mirror, the mist region, and the hackle region are described and defined.

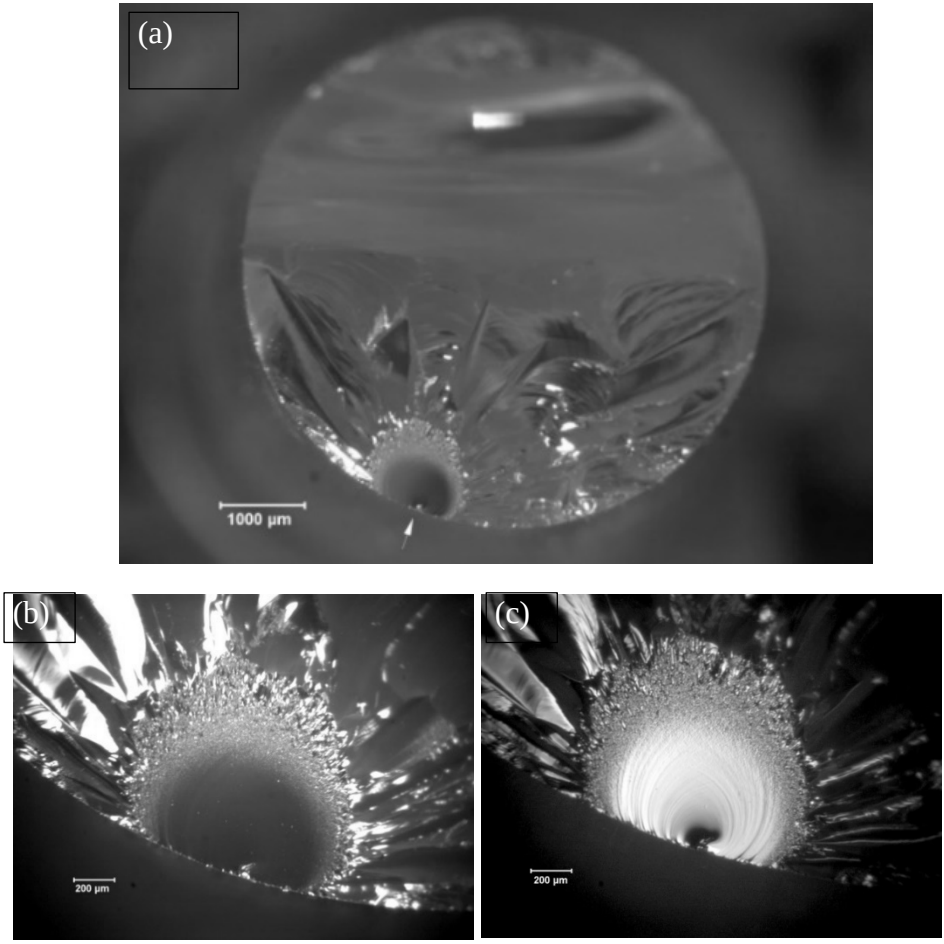

Figure 5.2 *Three views of a fracture mirror in fused silica glass rod broken in bending at a high stress level (96.2 MPa, 13.9 ksi). (a) shows the entire fracture surface. (b) is a close-up of the mirror, and (c) is the same view but with the illumination adjusted. Maximum tension was at bottom center in view (a). The mirror is asymmetric due to the bending stress field.*

(a)

(b)

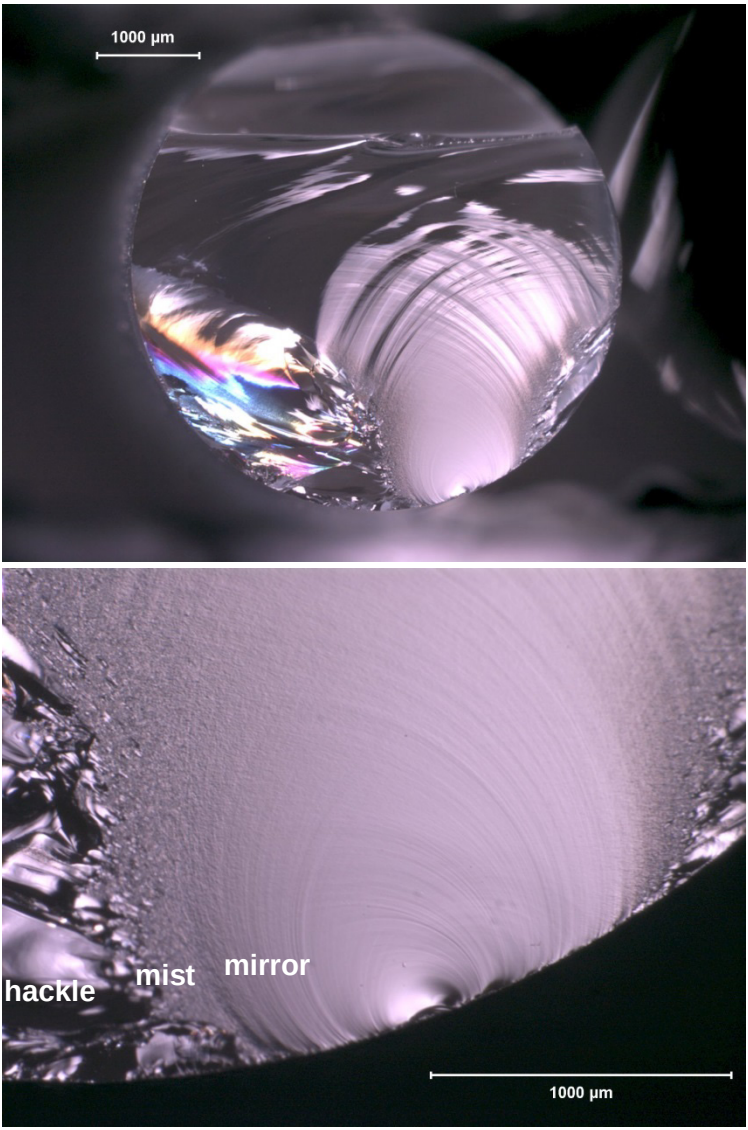

Figure 5.3 *Two views of a fracture mirror in a moderate strength (76.2 MPa, 11.0 ksi) fused silica glass rod broken in bending. The mirror is incomplete since it was large relative to the cross-section size. The advancing crack propagated into a decreasing stress field in the interior and did not have sufficient energy to form the mist and hackle in a complete circle. If this rod had been loaded in direct tension instead of bending, the mirror would have been fully formed and semicircular. The incomplete mirror in the direction of the interior is a telltale sign of bending.*

5.2.2 Terminal Crack Velocities

The terminal velocity, v_{ct}, in glasses typically ranges from 700 m/s to 2200 m/s depending upon composition, density, and elastic properties. Some values are shown in Table 5.1. The velocities in Table 5.1 are very high and fracture can occur "in the blink of an eye." The fastest glass velocities are in fused silicas (or fused quartz). Values between 2100 m/s and 2200 m/s are often shown in textbooks or reviews for fused silica, although some have reported velocities from ballistic impact experiments as high as 2500 m/s. Ceramics have greater terminal velocities. Brittle polymers have much slower terminal velocities.

Terminal velocities in glasses and ceramics are limited by two factors:

1. The elastic wave propagation speeds in the material
2. Anything that causes cracks to deviate from the main plane of fracture.

There are conflicting theories about terminal crack velocities in brittle materials, but all agree that the elastic wave velocities put an upper limit on how fast a crack may run.[a] The material in the highly-strained region around

Material	Terminal Crack Velocity v_{ct} (m/s)
Soda lime glass	1500 - 1600
Various flint glasses	700 - 1627
Borosilicate crown glass (BK-7)	1677 - 1800
Zinc borosilicate crown glass (ZK-7)	1760
Borosilicate glasses	1920 - 2034
Aluminosilicate glass (Corning 1723)	1740
Fused silica (quartz glass)	2100 – 2200
Glass ceramics	2000 - 2157
Reaction bonded Si_3N_4 (AME)	2950
Hot pressed Si_3N_4 (HS 130)	3500
KCl, single crystal	700, 1039
LiF, single crystal {100}	1700- 2000
MgO, single crystal, cleavage {100}	5100
MgO, polycrystalline (85% dense, 15 mm)	1800
Diamond, cleavage {111}	7200
Al_2O_3, sapphire, cleavage on m $\{10\bar{1}0\}$ or r $\{10\bar{1}2\}$ planes	4500 - 5438
AlON, polycrystalline	4377
Tungsten	2200
Steels	1370 - 2012
Resins, Plastics, Polymers	100 - 770

Table 5.1 *Representative terminal crack velocities. Appendix E has a detailed tabulation with the original references.*

[a] Some exceptions are mentioned in Appendix E. Shock loading conditions apply energy so fast to a crack front that it can run faster than the normal terminal velocity. Cracks running on cleavage planes in single crystals can also travel faster than the predictions here.

the moving crack has a mass and inertia. It takes time for the elastic energy to be transmitted from atom to atom. Elastic waves transmit the energy. There are three types of elastic waves: longitudinal (dilational), shear (transverse), and Rayleigh surface waves. The longitudinal wave is the fastest, followed by the shear wave, and then the slower Rayleigh surface waves. These velocities are shown normalized by the one-dimensional, rod longitudinal wave velocity in Figure 5.4. The 1-D longitudinal wave velocity in a homogeneous isotropic body is:

$$V_{L\,rod} = \left(\frac{E}{\rho}\right)^{1/2} \tag{5.1}$$

where E is the elastic modulus and r is the density. The stiffness of the atomic bonds between atoms directly relates to the speed of wave propagation. The other relationships for wave velocities have this basic $(E/r)^{1/2}$ term, but have additional terms with Poisson's ratio as shown in Appendix E. The 3-D bulk longitudinal wave velocity is somewhat faster than the 1-D rod longitudinal velocity. The transverse and Rayleigh waves speeds are slower as shown in Figure 5.4.

There is significant confusion in the literature about which wave velocity controls the terminal crack velocity. This author believes that the longitudinal

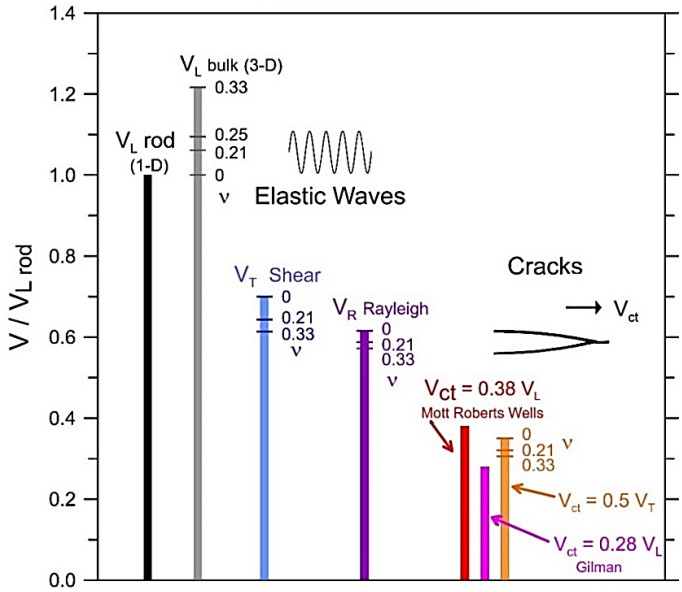

Figure 5.4 *Relative wave and crack terminal velocities. All velocities are normalized by the one-dimensional (1-D) rod longitudinal wave velocity. The velocities depend upon Poisson's ratio, n.*

Wave velocity is the determining factor. In my 2019 review of this topic,[8] I concluded that a simple elastic energy model by Mott[9,] and expanded by Roberts and Wells[10] (with help from G. Irwin) is fundamentally sound. It correlates the terminal crack velocity v_{ct} to the longitudinal wave velocity in a homogeneous and isotropic brittle material:

$$v_{\mathrm{ct}} = 0.38\ V_{\mathrm{L}} \tag{5.2}$$

where V_L is the longitudinal elastic wave velocity in a rod (the 1-D case). A simple modification to this equation is presented later as equation 5.3 after some discussion about whether materials are really homogenous and isotropic and whether fast cracks are flat and planar. Gilman arrived at a similar relationship.[11]

The Mott-Roberts-Wells model is a simple modification of the classic Griffith energy model. It is a <u>two-dimensional (2-D) model.</u> This is a major simplify-cation as will be shown below. When a crack propagates <u>rapidly</u>, the strain energy release is balanced by the energy to create the fractured surfaces <u>plus</u> the kinetic energy associated with the rapid displacement of material on each side of the crack. Data from studies of cracks propagating in glasses that have relatively open structures (that do not cause much crack deviations at the nanoscale) support the Mott-Roberts-Wells model. Their model may be very simple, but it has considerable merit and the predicted crack velocities very closely match measured velocities in some important glasses.[b] I believe that arguments that the terminal crack velocity is related to the Rayleigh wave velocities are incorrect. This entire matter is discussed below and in detail in Appendix E and Reference 8.

Sometimes there is a direct correlation between the elastic wave velocities and terminal crack velocities in accordance with equation 5.2 but often there is not. For example, two materials (e.g., glasses) may have identical density and elastic properties, but the terminal velocities differ by as much as a factor of two. There are other factors at play beyond just the density and elastic properties. These are described in the next two paragraphs.

The second factor that limits terminal crack velocities are any out-of-plane deviations of the crack. Local deviations of the crack front can occur up and down out of the main propagation plane. They are what form the mist and hackle in glasses and ceramics as shown in the next section. These deviations consume some energy and limit the maximum crack velocity. There are two

[b] The beauty of a global energy fracture mechanics approach like the Mott-Roberts-Wells model is that it avoids getting lost with details at the precise crack tip.

sources of local crack front deviations for fast-moving cracks in glasses and ceramics. First, even in a perfect continuum, the direction of maximum principal tensile stress ahead of the fast crack shifts out of plane. Second, microstructural and even nanoscale material variations and irregularities cause a crack to locally move out of plane. It is not fully appreciated that nanoscale compositional, bonding, and structural variations in glasses can cause local crack front perturbations that affect the terminal crack velocity. Glasses are often considered to be homogenous and isotropic, but at the nanoscale they most certainly are not.

The mist and hackle lines associated with the formation of fracture mirror markings retard crack velocities. It will be shown in the next section that mist and microhackle in glasses are caused by local deviations of the crack front out of plane. With ceramics, local crack front deviations are also caused by interactions with the microstructure or flaws. For example, several silicon carbides may have very different v_{ct} even if they have similar elastic moduli and densities, since they have different microstructures. In ceramics, porosity can affect terminal velocities by not only triggering crack front perturbations, but also by reducing the density and elastic modulus.

In view of the above discussion, equation 5.2 for the terminal velocity of a crack V_{ct} in a brittle material may be modified as follows:

$$V_{ct} = 0.38\, q\, V_L \tag{5.3}$$

where q is a dimensionless structure factor that takes into account nano or microstructural factors that can cause local perturbations of the crack tip out of the main plane of crack propagation. For an ideal homogenous and isotropic medium, $q = 1$ but it can be < 1 for a real material with structural variations.

Wave and crack velocities will be referred to again in Chapter 7, Quantitative Analysis, but for now we return to the topic of fracture mirrors. Fracture mirrors have an important practical significance. The fact that a fracture mirror with defined boundaries exists in a part is evidence that the fracture was a high energy event. The part had high stress acting on it. Conversely, if there are no clear fracture mirror boundaries, the fracture was a low energy event and occurred at low stress. The part must have been weak. What exactly happens at a crack tip in brittle materials is discussed in the next section.

5.2.3 How Fracture Mirrors Form

The underlying principal that accounts for the micro and macro branching that form a fracture mirror has been variously attributed to the crack reaching a critical velocity,[12] a critical energy level,[13] a critical stress intensity,[14,15,16,17] or a critical strain intensity.[18] A velocity criterion for crack branching was discounted by data shown by Congleton and Petch.[15] Richter and Kerkhof[2,3] and Field[4] used ultrasonic fractography to show that mist formed in glass as the accelerating cracks were running at about 1,000 m/sec or faster as the cracks approached the terminal velocity of 1500 m/s. Döll[19] showed similar results at the point of hackle and branch formation. There was no pronounced change in velocity when the mirror boundaries formed. Figure 5.5 shows Richter and Kerkhof's[2,3] results in glass. Field[4] showed almost identical figures and results. He said that "the first serious roughening" formed at about 1400 m/s. (There was a slight change in the crack speed, but it was within the scatter of the data.) Kirchner et al.[16,17] showed convincing evidence that a stress intensity criterion accounts for the mirror sizes and shapes. Congleton and Petch[15] demonstrated that a stress intensity criterion controlled the branching. They also showed that the Johnson and Holloway energy criterion[13] was related to the stress intensity

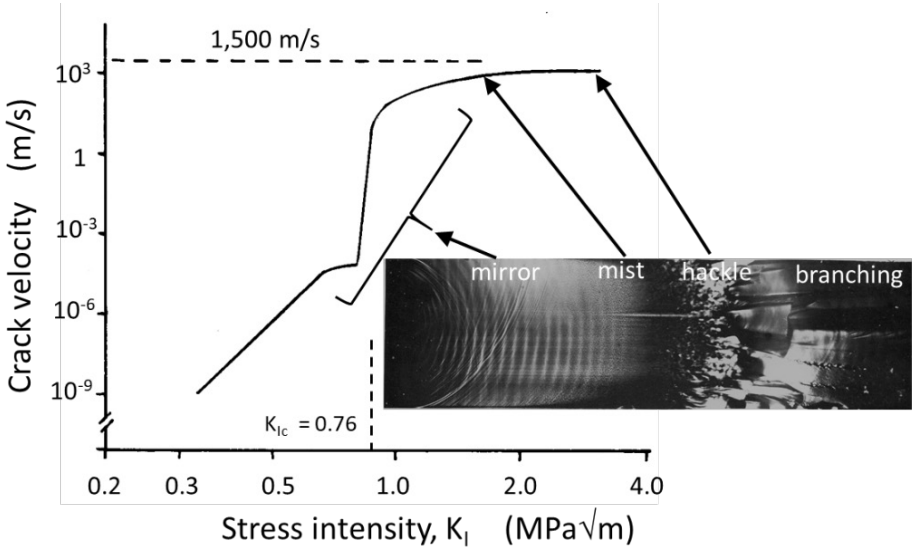

Figure 5.5 *Ultrasonic fractography, using externally applied sound pulses, was used by Richter and Kerkhof [2,3] to correlate crack velocities with fracture mirror markings in soda lime silica. The spacing between the wave ripples is used to calculate the local velocity. The crack is running very close to terminal velocity when the mist forms. This figure is adapted from their figure in ref 3. The fracture surface image is courtesy of H. Richter.*

criterion. Tsai and Mecholsky[20] noted that for isotropic materials it is difficult to distinguish between the energy, stress intensity, or strain intensity criteria since they are all related. This topic will be discussed again in Chapter 7 on Quantitative Analysis and in Appendix D on Guidelines for How to Measure Fracture Mirrors.

Careful electron microscopy, atomic force microscopy, and optical microscopy have shown that the formation of the mirror is a gradual progression of very localized crack path deviations from the main plane. Figures 5.6 a-e show superb transmission electron microscope images of various regions in a glass fracture mirror collected by Beauchamp in 1971.[21,22] Gölz[23] may have been the earliest with extraordinary electron microscope photos published in 1943 that showed features identical to those in Beauchamp's work. Poncelet[24] in 1958 and Peter[25] in 1968 also showed superb images that support Beauchamp's interpretations. Johnson and Holloway showed superb optical micrographs of the same features in 1968.[26] Beauchamp's figures, shown here as Figures 5.6 a-e, show that rounded ridges that are elongated in the direction of crack propagation gradually coarsen in amplitude. At some point, they develop slight hackle steps where over-running and under-running fingerlike crack segments link. This point, where nano to micro scale hackle lines begin to form, could be an important transition point. Close examination of Figure 5.6b shows they are not present inside the mirror, but they are just visible in Figure 5.6c near the mirror-mist boundary.

There is no evidence in glasses of microcracking occurring ahead of a rapidly moving crack. Hull concluded the same in his book on Fractography: [c,27]

> "Most of the explanations of micro-branching, and associated roughening, have been based on the idea that Griffith cracks are nucleated in the high stress regions ahead of the crack. . . . For brittle glasses, there are many difficulties with this explanation. First, there is no convincing experimental evidence for the initiation of cracks ahead of the growing crack in these materials. . . . . Third, the stresses needed to activate very small flaws close to the crack tip would have to approach the theoretical strength of the materials. It is difficult to envision why a growing crack should expand by micro-crack initiation rather than by bond breakage at the tip."

---

[c] The dynamic fracture mechanics community has been misled by behavior in brittle polymeric materials which have relatively slow terminal crack velocities and in which it is possible for plastic damage and flaw initiation to occur <u>ahead of the crack</u>. This leads to hyperbolic or parabolic markings on a fracture surface. It sometimes occurs in metals. There is <u>no evidence</u> that this occurs with fast cracks in glasses and ceramics. This is discussed further in the following paragraphs.

(a)

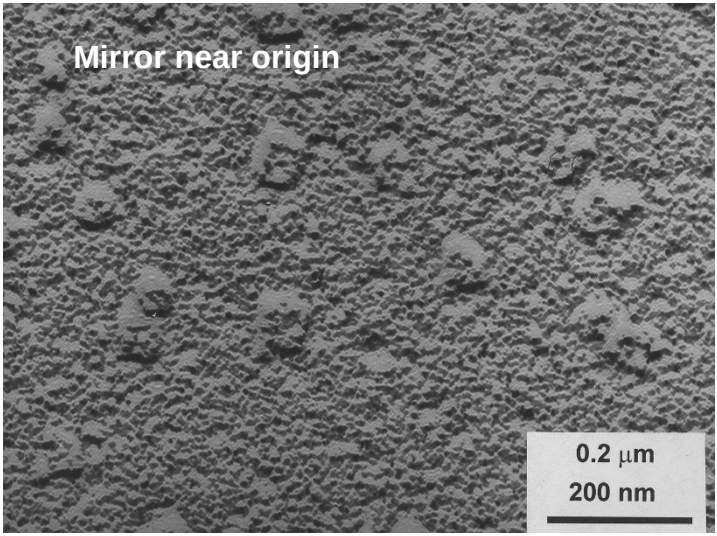

(b)

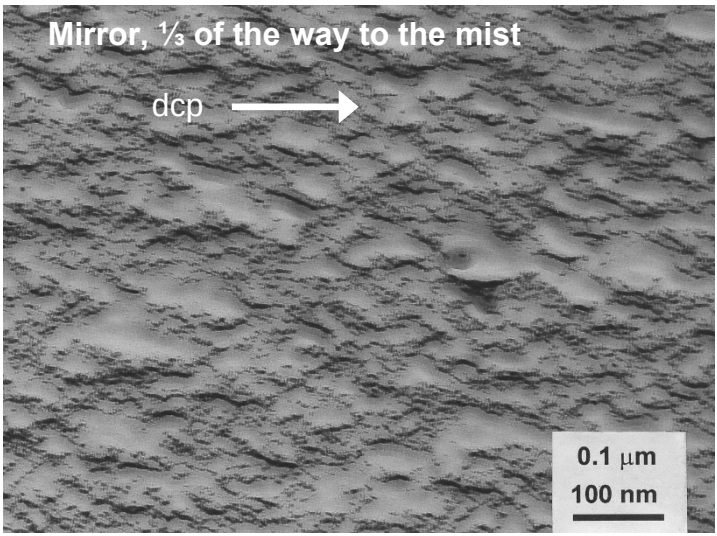

Figure 5.6 *Transmission electron microscope pictures from parts of the fracture mirror in a lightly-tempered soda lime glass sheet. (courtesy E. Beauchamp, refs. 21,22) (a) is in the smooth mirror area near the critical flaw. The tiny black dots are an artifact of the specimen preparation, but the larger (50 nm) round bumps are genuine. (b) is in the mirror region about 1/3rd of the way to the mirror/mist boundary. The arrow shows the direction of crack propagation (dcp). The ridges and valleys are elongated in the direction of crack propagation, but they are too small to be detected optically.*

(c)

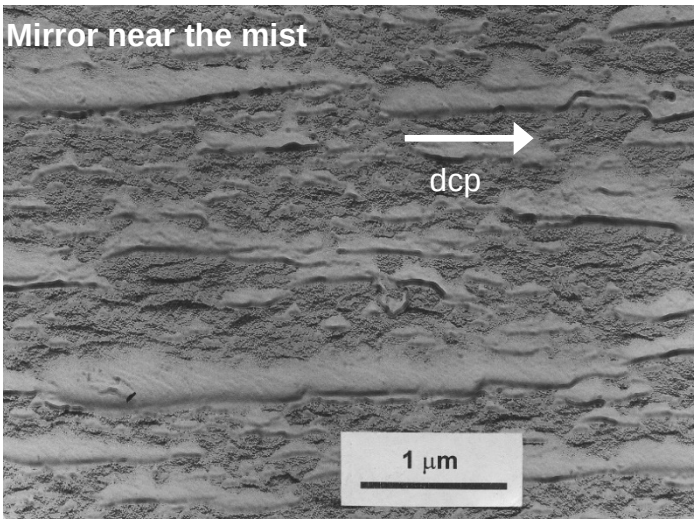

(d)

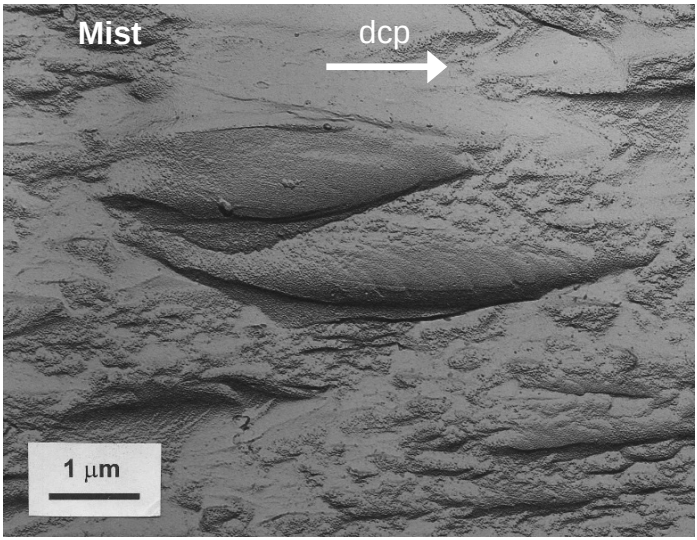

Figure 5.6 continued *(c) is a region still inside the mirror before the mist is detected but close to the mist boundary. The ridges are longer and wider. Nanoscale hackle steps have formed running parallel to the direction of crack propagation. (d) is in the mist, just beyond the mirror/mist boundary. The features are similar to the prior figure, except that they are now large enough to be detected optically. Close examination of (c) and (d) reveals faint but distinct twist hackle lines in some of the large features, attesting to some localized lateral crack growth.*

(e)

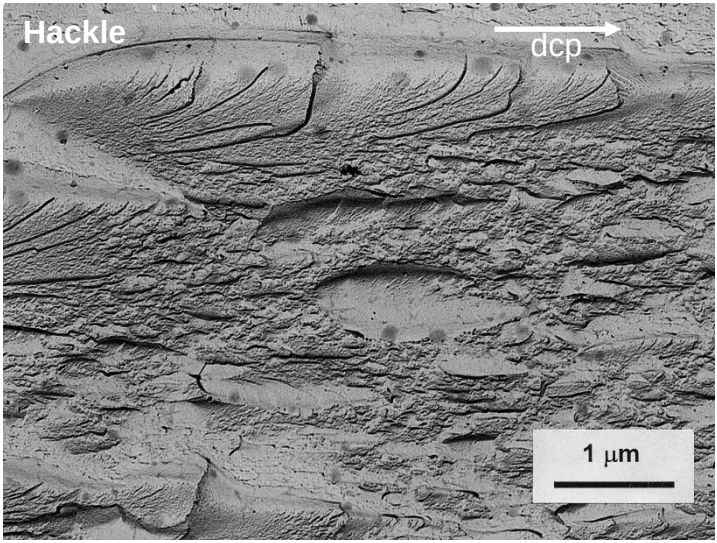

Figure 5.6 continued *(e) shows features in the hackle zone. The features are now larger than 10 μm, but are similar in character to those in the mist and mirror zones.*

Attempts to correlate the mirror boundaries with surface roughness parameters have had only limited success, as discussed in more detail in Appendix D. Hull pointed out that different surface roughness characterization devices such as atomic force microscopes (AFMs), mechanical profilometers, and laser optical profilometers all have different advantages, disadvantages, sensitivities, and scanning zone sizes. AFMs can measure tiny regions with very high sensitivities, but may miss large hackle steps in a mist or hackle zone. These latter features can dramatically alter the average or root mean square roughness. Mist and hackle regions may have different roughness at different scales. Hull discusses these various scales of roughness in detail in his book.[27]

Figure 5.7 schematically shows the three-dimensional nature of the process. The explanation below closely follows Fréchette's[1] general discussion as well as Beauchamp's[21,22] convincing analysis. As the crack accelerates away from the origin, micro portions of the crack front begin to twist slightly or tilt up and down out of the main fracture plane. Yoffe[12] and Freund[28] have shown that when a crack moves with a velocity greater than about 0.5 to 0.6 times the shear wave velocity in a material, the maximum stress in front of the crack shifts from directly ahead of the crack on the same plane to directions about 60° above and below the crack plane. This causes small local crack deviations above and below crack plane as shown schematically in Figure 5.7. The

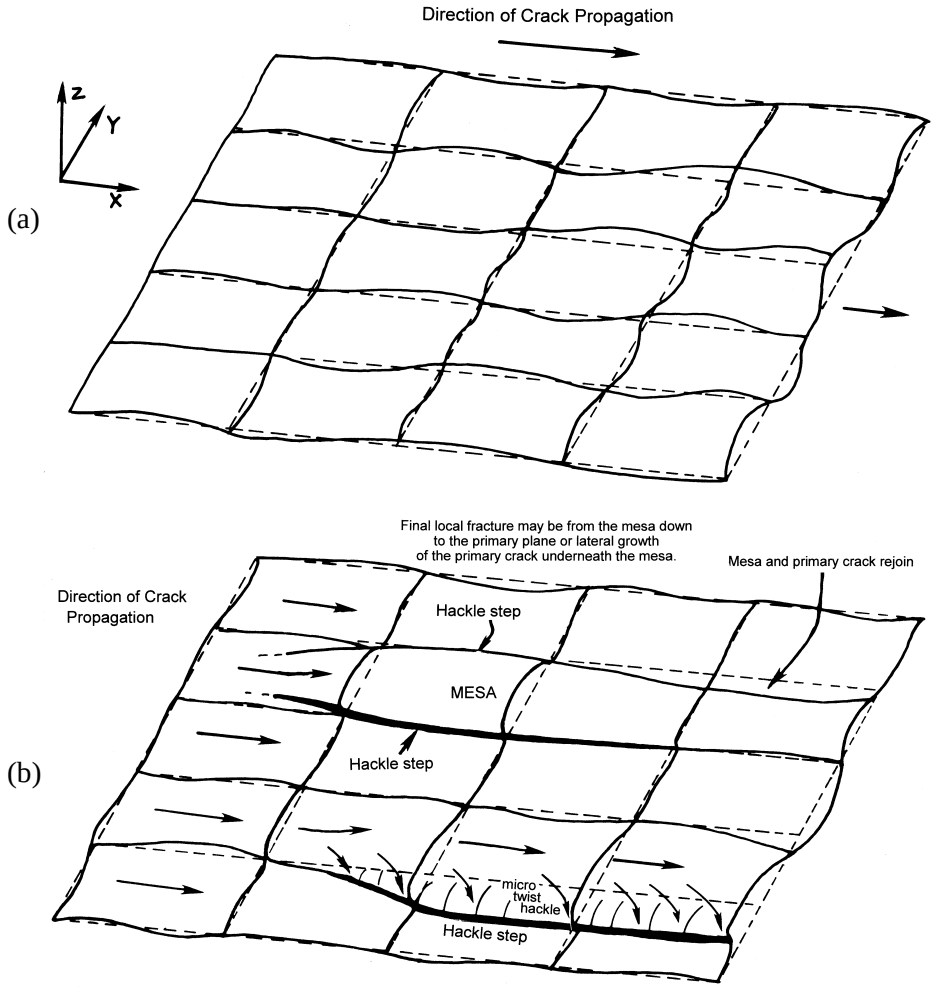

Figure 5.7 *Fast cracks deviate from the main fracture surface plane as the peak stress shifts out of plane as shown in (a). Different portions of a crack front may go up or down out of plane. The crack becomes three dimensional. The waviness increases in magnitude and eventually forms tiny hackle steps running parallel to the direction of crack propagation as shown in (b). The deviations may be one-sided as shown in the bottom half of (b), or double-sided as shown in the upper half of (b) where a "mesa" plateau structure forms.*[21,22] *Segments of the crack front are retarded where they are inclined. Such crack plane deviations and microhackle limit the terminal crack velocity.*

momentary tilting or twisting does not persist for very long since crack plane deviations are restricted by the energetic cost of creating additional crack surface. The slight tilt or twist variations in crack plane quickly rejoin the main propagating crack plane. These tiny local crack perturbations exist well within the mirror region, but are too small to be optically discernable. The small perturbations may also be influenced by nanoscale structural variations in the glass. As the crack advances, the local crack perturbations eventually become large enough to be just discernable with the optical microscope as the "mist" zone surrounding the origin (Figure 5.6d). Little hackle steps appear. The mist has a slight frosty appearance such as when water condenses on a reflecting mirror. As the crack continues to advance, the local perturbations increase and begin to oscillate and form larger tongue-like segments that may deviate from the average fracture plane to the degree that micro steps are generated running parallel to the direction of crack propagation. Beauchamp described these tongue like miniature plateaus as "mesas." (Others have described the out-of-plane perturbations as "fingers.") The perturbations gradually coarsen such that the tongue-like elements can overcut other portions of the crack front thereby generating large "velocity hackle" lines that run parallel to the direction of crack propagation. Beauchamp[21,22] pointed out that many of these features are similar in character from within the mirror out to the hackle zone. They differ only in scale. The transitions between the regions are gradual. They are not abrupt. One intriguing observation by Beauchamp was that tilted or twisted hackle segments that relink with the main crack plane may generate elastic pulses and Wallner lines that could trigger additional hackle along the crack front. This could be the impetus to form a band of hackle along the crack front and hence the mist-hackle boundary. Reflected elastic waves off specimen surfaces also might trigger mist and hackle.

So far in this discussion, the material has been considered to be a continuous medium and continuum mechanics has been applied. Modern research using advanced equipment such as atomic force microscopes with sub-nanometer resolutions has revealed that in glasses, localized sub-nanometer scale compositional and structural variations cause a crack to move up or down out of plane.[29,30,31,32] Even in the shiniest, smoothest regions at the beginning of a fracture mirror, or in regions where slow crack growth occurs, there are such perturbations. They occur even in fused silica due to localized structural variations in the silicate tetrahedral structure. The work by Poggemann, Frischat, and colleagues at T.U. Clausthal[30] is particularly noteworthy, since the fracture surface variations were correlated with individual silicon and oxygen atoms. (Their work even supported the Zachariasen model of the network structure of glass!) Glasses with more complex compositions have rougher

fracture surfaces, because compositional and structural variations are greater. With ceramics, the microstructure can cause crack deviations out of plane.

At this point a word of caution is injected here about some studies that use polymers as model "brittle materials." Their use as model brittle materials can be very misleading. The elastic modulus of most polymers is quite low and terminal crack velocities are much less than for glasses and ceramics. Polymers have much more ductility, may not be linearly-elastic, are much more loading rate sensitive, and may have deformation modes (e.g., crazing) not seen in glasses and ceramics. For example, defects ahead of a moving crack front can be nucleated and a circular crack radiates outward from the flaw. This localized crack can run back towards the advancing main crack front. The intersections of the main crack front and the localized microcrack create parabolic or hyperbolic markings on the fracture surface. These are also known as Kies markings.[1,33] Although common in polymeric materials, they do not exist in ceramics and glasses. Markings that resemble Kies marks have very rarely been seen, but they actually are double wake hackle lines described in 5.3.2 later in this chapter and are a different marking.[8,34,35] Figure 5.32 later in this chapter shows rare examples. They are usually only seen in poor quality glass or natural obsidian with inclusions. Kies markings do not form in glasses and ceramics since cracks run very fast and flaws ahead of the crack front are usually not activated. In the fracture mechanics engineering literature, which often uses polymers as model brittle materials, it has been suggested that mist and hackle form in glasses and ceramics because of microfractures ahead of the main crack tip. This is wrong. The mist and hackle markings are generated at the crack tip.

In summary, although the process of roughening through the fracture mirror boundaries has often been described as gradual, there are two potential transition points. The mirror to mist boundary may be a transition where nano-micro steps form between ridges that are tens of nanometers tall. The mist to hackle transition boundary may be where a band of microhackle forms that is triggered by self-generated or external elastic pulses (Wallner lines).

When crack branching occurs, the daughter branches slow down momentarily. This is not surprising since the specimen strain energy now forms two cracks. They initially have smooth fracture surfaces, but as they run onward, mist and hackle rapidly form again.

There are three zones around a fracture mirror: the smooth mirror zone, the mist zone, and the hackle zone. Fracture mirror (sometimes shortened to just "mirror") was defined previously on page 5-4 as:

Fracture mirror: *Relatively smooth region surrounding and centered on the fracture origin.*

Mist: *A zone of markings on the fracture surface of an accelerating crack close to its effective terminal velocity, observable first as a misty appearance and with increasing velocity revealing a fibrous texture, elongated in the direction of crack propagation. The fibrous texture is due to the formation of tongues of local out-of-plane crack front deviations and submicroscopic hackle lines.*

This definition of mist is new to this 4th edition of the Guide.[d] It seems reasonable to distinguish the mist region inside the fracture mirror from the hackle region for practical reasons that will become evident when ceramic mirrors are discussed in the next paragraphs. Mist is fairly obvious in glasses but is difficult or impossible to discern in ceramics due to the microstructure. The definition includes the clause "of an accelerating crack" since this is the traditional way they have been explained for over 100 years. In truth, fast cracks that *decelerate* can form mist as they slow down to velocities less than the terminal crack velocity.

Hackle: *A line on the surface running in the local direction of cracking, separating parallel, but noncoplanar portions of the crack surface. (Fréchette, ref. 1)*

This hackle line definition originally from Fréchette[1] is broad. It is not merely for fracture mirrors. It may be a few lines on a fracture surface, or profusion such as around a fracture mirror. Hackle lines can be formed by a variety of processes as shown later in this chapter. Nonetheless, many small hackle lines fan radially outward around a fracture mirror, and it is customary to refer to these as the hackle zone. Hackle lines are physical steps on the fracture surface, as opposed to undulations or minor ripples. They can form with fast or slow cracks. There may be instances when it may be convenient to refer to the tiny hackle lines around a fracture mirror as: "Mist-hackle."

Velocity hackle*: Hackle markings formed on the fracture surface of the crack close to its terminal velocity, observable as discrete elongated steps aligned in the direction of cracking.*

---

[d] The earlier Guide editions copied Fréchette's definition[1] that combined the words "mist" and "hackle" as "mist-hackle." He did not define mist separately. Fréchette's combination of the two words created confusion. Fréchette regarded *mist* as a very fine version of *hackle.* He was correct that there are nano- and sub-micrometer hackle lines in the mist, but they are not discernable at low magnifications with an optical microscope.

Additional types of hackle lines are described below in section 5.3 below.

Fracture mirrors are very important since they not only draw attention to the fracture origin, but their size may be used to estimate the stress in the part at the moment of fracture. For a long time, it was common practice to interpret the mirror as having distinct boundaries between the mirror and mist and between the mist and hackle. Extensive empirical work showed that the relationship between the mirror size and the stress at the instant of fracture is:

$$s\sqrt{R} = A \tag{5.4}$$

where s is the tensile stress at the origin at the instant of fracture, R is the mirror radius, and A is a constant, known as the "mirror constant" and is considered by many to be a material property constant. It has units of stressÖlength, which are the same units as stress intensity which is discussed in detail in section 7.5.1. The mirror radius may either be the mirror-mist boundary or the mist-hackle boundary for glasses. There are different A's for each boundary. For polycrystalline ceramics there usually is simply a single mirror-hackle boundary. Equation 5.4 is discussed in great detail in Chapter 7, Quantitative Analysis and in Appendix D (how to make mirror measurements), but for the moment we need only consider some general ramifications.

This simple relationship has tremendous practical value. It can be used to estimate the fracture stress. It is not necessary to have a-priori information about the how the part was loaded. The smaller the mirror, the larger is the stress at the origin site. A small mirror is proof that the part was strong and had a small strength-limiting flaw. Conversely, large mirrors mean the failure stress was lower and implies a large flaw. In some instances, a part may be so weak that the mirror size is larger than the part cross-section and hence the mirror markings are not visible. That, in and of itself, is valuable information. The existence of a mirror boundary implies that the part was stressed to a moderate or high level. Alternately, very strong parts (e.g., pristine optical fibers) may have such high strengths that mirrors are so small as to be not practically measurable with optical microscopes or the mirror may not even be found due to excessive fragmentation.

Mist and hackle are sometimes triggered earlier than they would otherwise form by material flaws or microstructural features. Figures 5.8a-c show examples. Strong Wallner lines, described later in this chapter, may also trigger mist formation in fracture mirrors such as shown in Figures 5.9. Figures 5.2 and 5.3 shown earlier also hint at this possibility. Beauchamp has described

cases like these where perturbations of the crack front can trigger early mist and hackle[36] and long, persistent "hackle streaks."

Surface irregularities often cause a fracture mirror to depart from a semicircular shape and turn inward towards a surface origin as previously shown in Figs. 5.2 and 5.3.

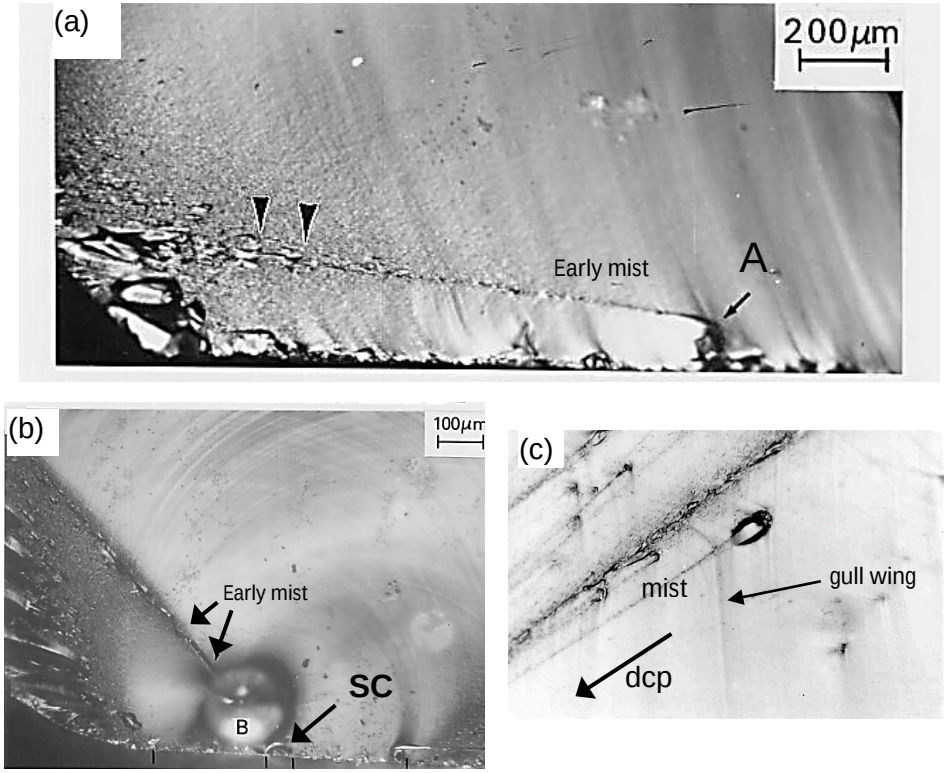

Figure 5.8 *Early mist and hackle streaks associated with flaws. (a) shows mist and hackle triggered by a surface crack at site "A" in a soda lime glass specimen at 65 MPa. The origin was well to the right, beyond the photo edge. (b) shows early mist and hackle triggered by a large bubble "B" in a 70 MPa strength specimen. The origin is not the bubble, but is a surface crack "SC" near the bubble (c) shows mist behind inclusions in obsidian. Gull wings (described later in this chapter) are also evident. (a, b courtesy R. Rice, c is courtesy A. Tsirk.)*

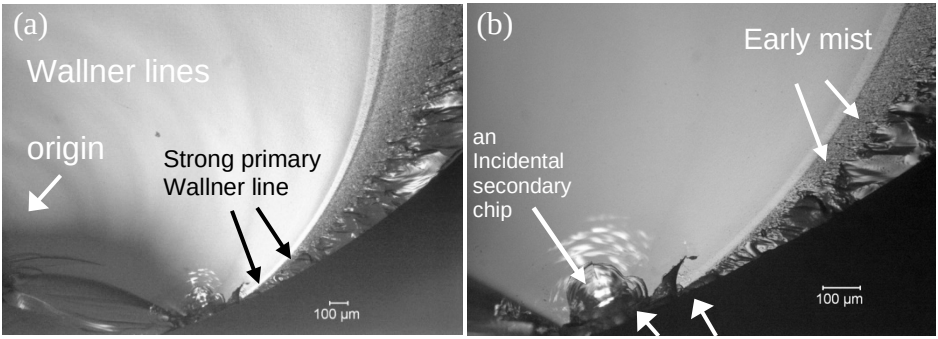

Figure 5.9 *Early mist and hackle. (a) and the enlargement (b) show an example of early formation of mist in a Pyrex borosilcate glass rod broken in flexure. The Wallner lines in (a) suggest the origin is off to the left in the image. The crack radiating outwards from the origin encounters other surface flaws shown by the arrows on the bottom in (b). A strong primary Wallner line is generated. It triggers mist earlier than normal during mirror formation.*

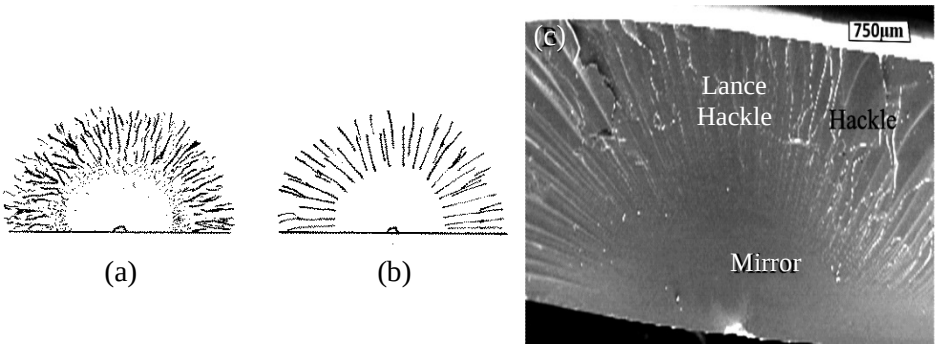

Figure 5.10 *Mixed-mode loading creates fracture mirrors without mist but with a systematic array of "lance hackle." (a) shows a normal mirror from pure opening mode I loading in glass. (b) and (c) show mirrors from mixed opening/shear modes I/II, (c is courtesy J. Mecholsky).*

Gopalakrishnan and Mecholsky[37,38] showed that mist does not form around glass fracture mirrors if the loading has some in-plane shear (Mode II loading) acting on the crack at the same time it is under Mode I opening loading (see chapter 7). Hackle markings are very distinct in such cases as shown in Figure 5.10. The boundary is comprised of "lances" or "lance hackle" that are very similar to twist hackle. These steps on the fracture surface probably all step up (or step down) systematically as one goes around the crack front periphery, unlike the case of Mode I loading, where hackle steps are random or alternating up and down out of the fracture surface. The size of the mirror is not altered by

the mixed-mode loading. The mirror/mist boundary for pure Mode I loading and the onset of lances in mixed Mode I/II loadings are comparable in size. The practical significance of this difference in appearance is that if a glass fracture mirror is comprised of lances with no mist, then the loading was not pure tension, Mode I, but mixed mode with some shear. Sommer[39] showed similar fracture surfaces with lance hackle and no mist in glass rods loaded in combined tension and torsion (i.e., mixed Mode I and Mode III loading).

5.2.4 Fracture mirrors in ceramics

The microstructure and polycrystalline nature of most ceramics obscures most of the fine details of fracture mirrors. Figures 5.11 - 5.13 show some variants of mirrors in ceramics. Mist is usually not recognizable. Sometimes coarse microstructural elements or flaws in a mirror may trigger early hackle lines within the mirror, prior to the onset of the generalized velocity hackle that forms the mirror boundary. The mode of crack propagation, whether it is trans- or intergranular, also affects the mirror markings. Transgranular fracture is a

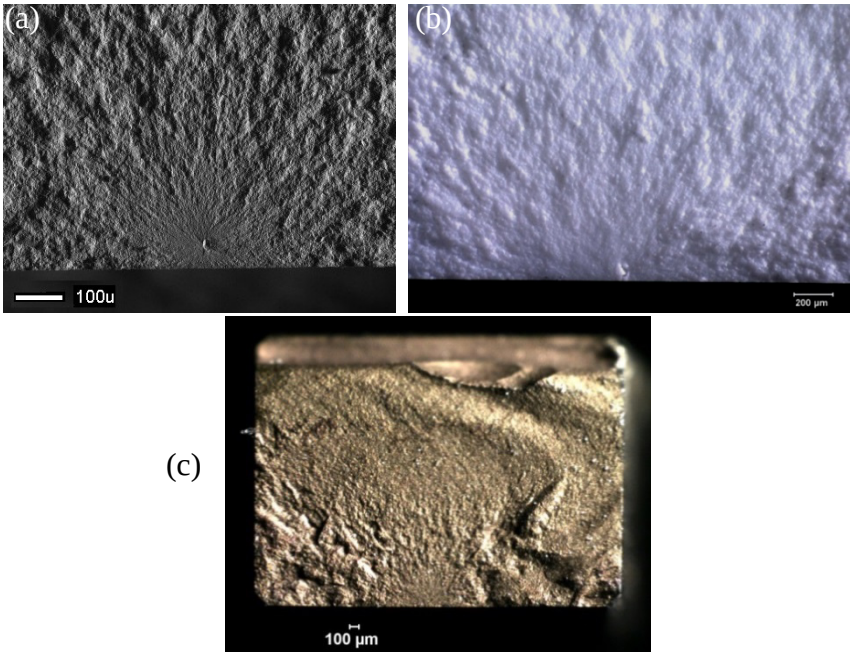

Figure 5.11 *Fracture mirrors in ceramics. (a) is a SEM image of a strong bend bar (1024 MPa) of Y-tetragonal zirconia polycrystal (Y-TZP) for dental crowns. (courtesy J. Quinn) (b) is a stereo optical microscope image of another Y-TZP bend bar (486 MPa) for an engine application. (c) is a stereo optical microscope image of a silicon nitride bend bar (487 MPa).*

mode whereby the crack propagates directly through grains on cleavage planes, whereas intergranular fracture is a mode whereby the crack takes paths along grain boundaries between grains. These modes will be discussed later in section 5.7. Mirrors may be easier to see in materials that start out with transgranular fracture, but then develop increasing fractions of intergranular fracture. On the other hand, it may be more difficult to define mirrors when the fracture mode is intergranular from the origin right through the entire mirror. For these reasons it is appropriate to add the qualifier "relatively" as in relatively smooth when describing the mirror region since there is an inherent roughness from the microstructure even in the area immediately surrounding the origin. Rice observed that mirrors are more detectable in strong specimens and are less clear in weak specimens.[40] Mirrors may not be detectable in coarse grained materials or those with more than 10 % porosity. Mist can only be detected in fine-grained ceramics or those that fracture transgranularly.[41]

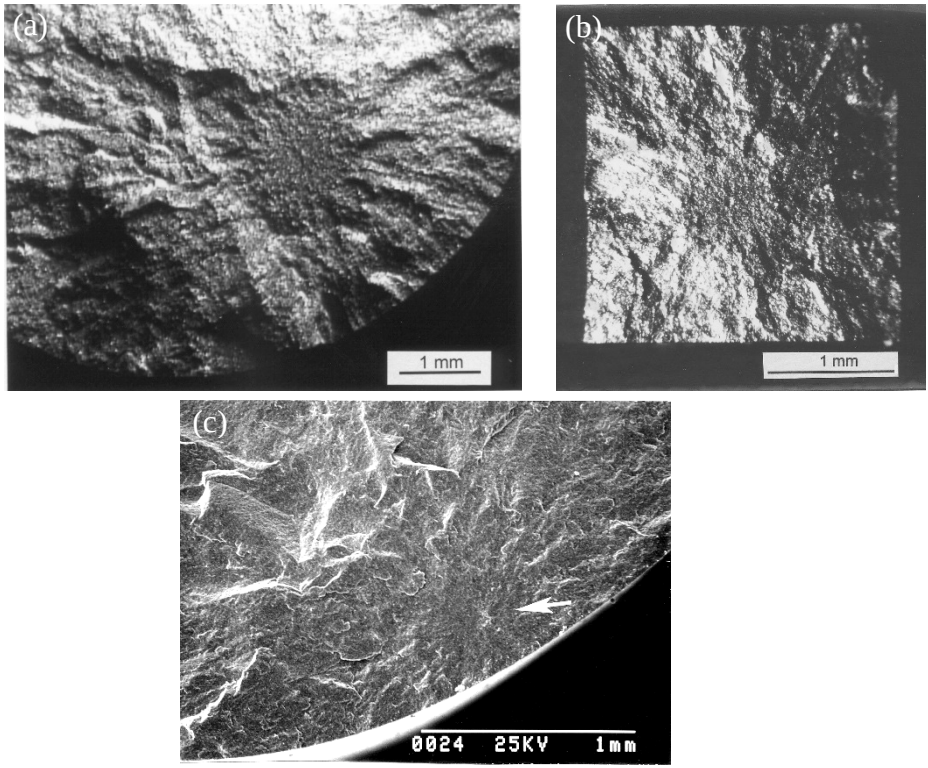

Figure 5.12 *Fracture mirrors in ceramics. (a) is an optical image of hot-pressed silicon carbide tensile specimen (371 MPa). (b) is an optical image of a silicon carbide tension specimen and (c) is a SEM image of a silicon nitride rod broken in flexure. Many beams and rods broken in flexure have internal flaw origins if the specimens are ground carefully.*

(a)

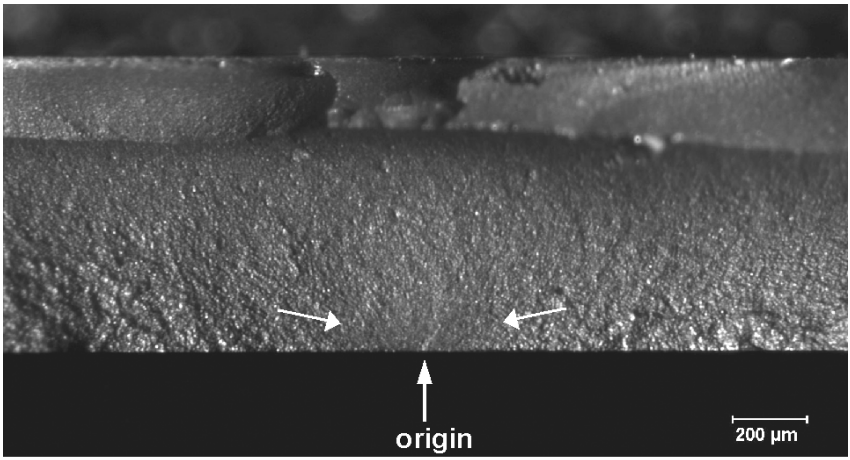

(b)

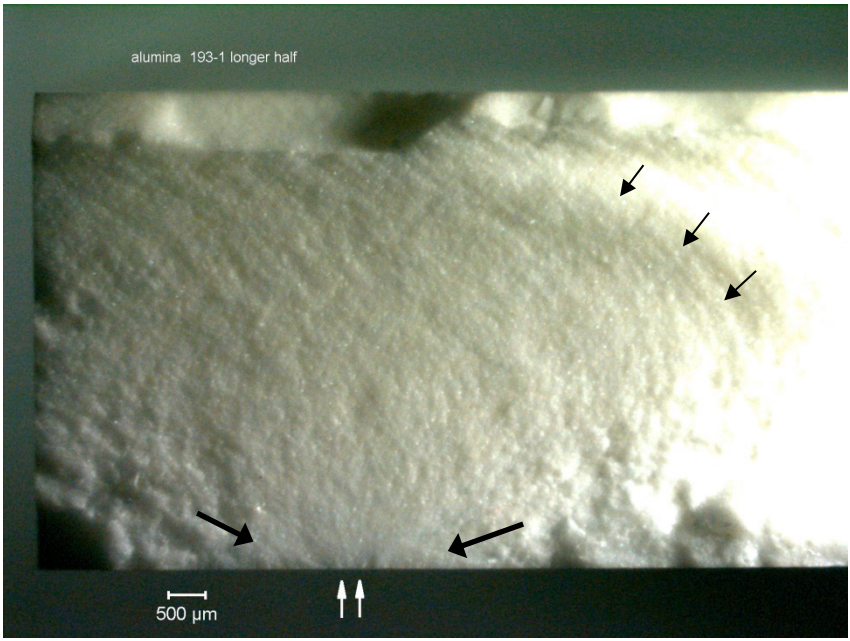

Figure 5.13 *Examples of incomplete ceramic mirrors due to bending stress fields. (a) shows an optical image of a gold-coated biaxial Y-TZP zirconia disk. The arrows mark the origin and the mirror. (b) is an alumina bend bar with low-angle grazing illumination to reveal the mirror in this stereo optical microscope image of this translucent material. The small white arrows mark a grinding crack origin, and the large black arrows mark the mirror. The small black arrows mark one of many coarse, arced Wallner lines.*

5.2.5 Fracture mirrors, special cases

In most of the above discussion, it is assumed the stress in the body is constant over the cross section, or at least approximately constant. Once the crack becomes unstable and radiates outward it forms circular or semicircular mirrors. In many structures this is not the case. Sometimes the crack accelerates and forms mist and hackle, but then slows down when it reaches an area of decreasing stress. The markings revert back to mist and then a smooth mirror. Other conditions that lead to altered mirror shapes are described below. Sometimes the crack itself alters the stress distribution. A large crack may make the specimen unload itself and the stresses decrease so that the crack slows down and even stops. An example was shown as Figure 3.19 ion page 3-24 where a compliant, low elastic modulus resin biaxial disk unloaded itself once a large crack formed.

Multiple fracture mirrors
In many cases, only one origin is activated, and there is only one fracture mirror. The crack propagates and reaches terminal velocity after only a short extension and in a period of microseconds. In rare instances, two virtually identical flaws may be triggered simultaneously in a laboratory strength test such as shown in Figure 5.14.

Sometimes there will be multiple simultaneously-activated origins in a component or test specimen due to severe loadings such as laser heating or thermal shock by water quenching.[42] Another example is a side-impacted

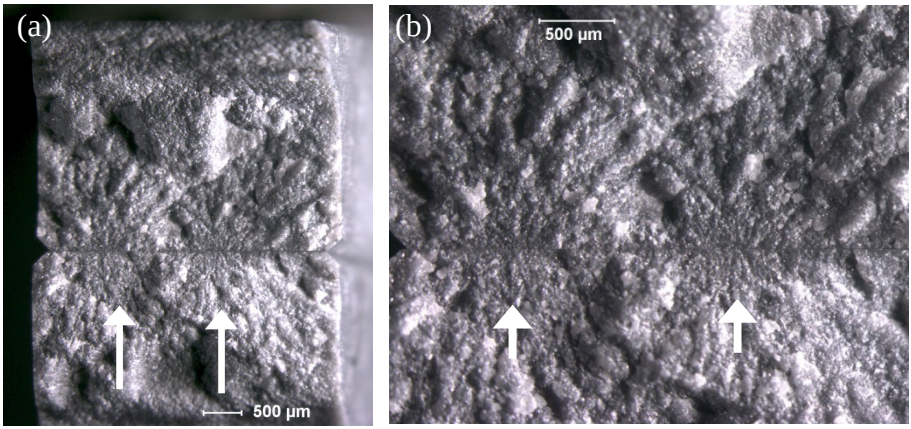

Figure 5.14 *Multiple mirrors from grinding damage in a silicon nitride bend bar. (b) is a close-up of (a). Grinding damage caused fracture in these examples and the origins in each mirror were nearly identical. (Ref. 43)*

bottle as shown in Figure 4.29f in the previous chapter where the impact causes the sidewalls of the vessels to flex outwards. The bending stresses activate "hinge fractures" to either side of the impact site. When there are multiple origins, each generates a crack system and the fractographer must deduce the sequence of events that causes them. Sometimes, once one origin starts a crack system, the component stresses are redistributed, and then a second origin is activated. The burst gas turbine rotor Case 1 in chapter 10 is an example.

Secondary fractures can occur due to a variety of causes. Elastic wave reverberations after an initial fracture can cause secondary fractures. These complicate the interpretation of high strength four-point bend specimens and it can be difficult to determine which one was the primary fracture as shown in Figure 4.13. An observation that a fracture mirror is on what once was the *compressively*-loaded surface in a bend bar is proof the break was secondary. If there are two fracture planes with mirrors on the tensile side in the inner gage section, the larger mirror may be the primary break and the smaller mirror may be secondary due to stress reverberations that momentarily created a greater local stress.

Concentric mirrors have been reported by Ramulu et al.[44] and correspond to a crack front that is alternately decelerating and accelerating. Such markings also occur in high-strength tensile specimens when a crack branches repeatedly. At each branch, the crack slows down somewhat, then accelerates back to near terminal velocity and branches again.

Steps or jogs in a mirror

In some cases, a pronounced step or jog may start at the origin. This usually occurs when the origin flaw is irregular, three-dimensional, or inclined at an angle to the principal stress. Crack extension from the irregular flaw may occur on slightly-offset, parallel planes and thereby create a step or jog which may persist up into the mirror or even further. These steps are one type of "hackle" as described later in section 5.3. They usually point back to the origin and are an additional aid to locating the origin flaw.

Curved or bent mirrors

Cracks propagate perpendicular to the maximum principal tension stress, but some parts may have maximum stresses that are invariant with orientation. Equibiaxial stressed ring-on-ring test coupons (Figure 4.3) are an example. Curved or wavy fracture mirrors may occur in equibiaxial-loading cases. Figure 5.15 shows an example of a bent mirror.

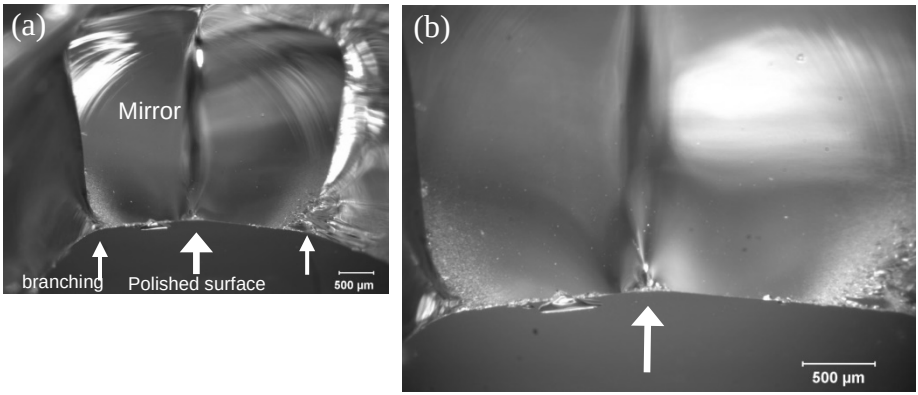

Figure 5.15 *Bent mirror in a BK-7 borosilicate crown glass ring-on-ring disk strength specimen. The origin was a Vickers indentation flaw (large white arrows) with multiple radial and median cracks. (a) and the close-up (b) show the fracture surface with the specimen tilted back to show the outer polished surface where the indentation (large white arrow) started fracture. Fracture started from Vickers indentation radial cracks oriented in different directions. A hackle line extends from the origin straight up through the mirror. Notice how main crack branching occurs (small white arrows) soon after the mirror boundaries formed in this equibiaxial-loaded specimen. Notice also that the branching angle initially is small then flares out to its final configuration.*

Non circular mirrors

Mirror shape distortions may reveal important information about flaws or the stress distributions in a part. Mirrors that are not circular or semicircular indicate stress gradients, residual stresses, or elongated flaws at the origin.

Parts with mirrors centered on an <u>interior</u> origin are usually circular. Oblong or elliptical mirrors in the interior are less common. Figure 5.12 shows three internal fracture origins and mirrors in ceramic test specimens. In one case (Figure 5.12c), the part was tested in flexure, but the mirror was relatively small and showed no obvious distortion or elongation.

On the other hand, parts with <u>surface</u> origins often have flared or elongated mirrors, especially if the part was stressed in flexure. The bending loading mode usually creates a stress gradient with a maximum tension at the surface, zero stress at the middle ("the neutral axis"), and compression on the opposite surface as shown in Figure 4.11 in the last chapter. As the crack accelerates from the surface origin, it traverses through a diminishing stress field towards the interior. This slows down the crack and elongates the mirror shape towards

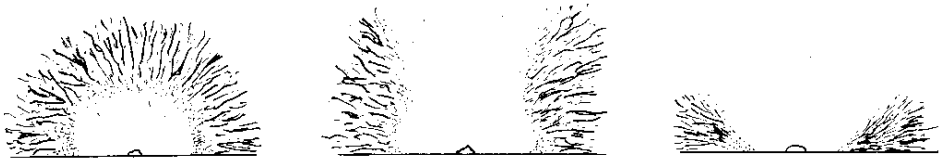

(a) (b) (c)

Figure 5.16 *Mirror shapes around surface origins. (a) is common for tension specimens, or flexure specimens or plates in bending if the mirror is small relative to the thickness. (b) and (c) show mirrors that are incomplete into the interior. This occurs when the mirror is large in a part loaded in bending.*

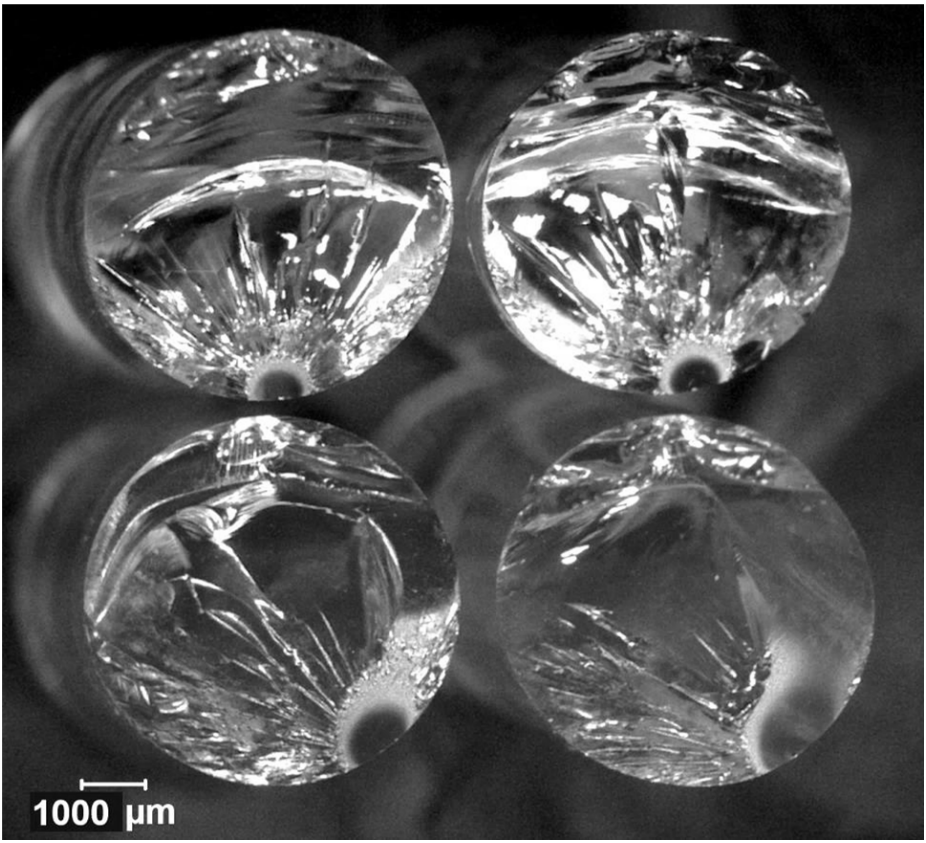

Figure 5.17 *Fracture mirrors in four glass rods broken in flexure. The maximum tensile stress was on the bottom in each case. Fracture mirrors on the rod sides had pronounced flair or were incomplete due to the stress gradient.*

the interior as shown in Figures 5.3, 5.13, 5.16, and 5.17. It can even eliminate the mirror boundary markings altogether if the mirror is large relative to the specimen cross-section size. The stress gradient does not affect the markings along the tensile surface. There often is a small cusp on either side of the mirror pointing back to the origin in glasses. The cusp is explained by fracture mechanics. (A crack that connects to a free surface experiences a slightly greater stress intensity factor K_I right at the surface.) The small cusp is inconsequential for most analysis, except when fracture mirror sizes are measured as discussed in chapter 7 and Appendix D. The elongations in Figures 5.16 and 5.17 are common. Flexural stress gradients always cause elongations towards the interior. On the other hand, there are several important cases whereby side-to-side elongations occur along the outer surface of the part as shown in Figure 5.18**.** Elongated flaws may generate elongated mirrors and sometimes even mirrors with side protuberances. Figure 5.19 shows two possible scenarios for the formation of such elongated mirrors. Grinding cracks and polishing scratches cause such markings.[43,45] Figures 5.20 and 5.21 show examples.

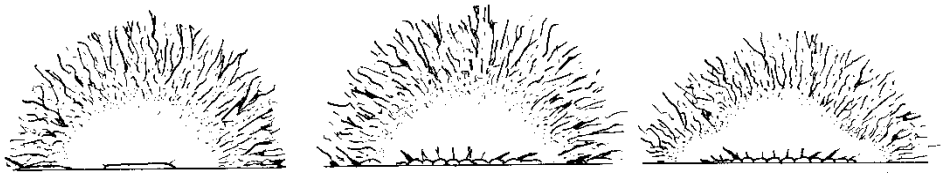

Figure 5.18 *Mirror elongations along the surface can occur if the origin is a scratch or a long parallel grinding crack. (a) shows a single elongated crack at the origin, (b) shows a grinding zipper crack (see section 6.7.6), and (c) shows a "zipper crack" that generated lobes on the sides of the mirror.*

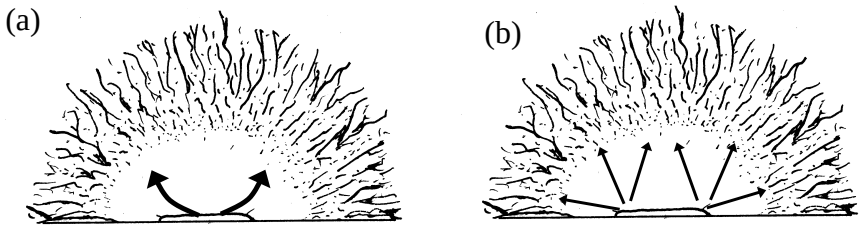

Figure 5.19 *Two scenarios that could account for mirror elongations along the surface from long flaws. (a) shows how a crack could unzip or propagate quickly along the surface. (b) shows that criticality could be reached at several points on the flaw periphery and fracture commences accordingly.*

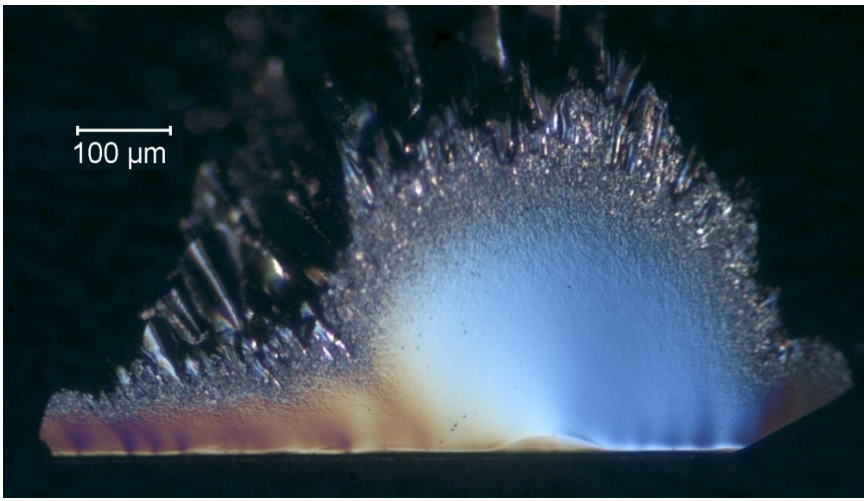

Figure 5.20 *Elongated mirror in a fully-annealed BK-7 borosilicate crown glass ring-on-ring disk strength specimen tested in dry nitrogen. (146 MPa, 21.2 ksi). The origin was a 7.3 µm deep long crack from a scratch in the polished surface. All surface traces of the scratch had been eliminated by the final polishing. A SEM image of the flaw is shown later in Figures 6.31 and 7.25. The crack appears as a thin white band on the bottom. The slightly deeper penetration of the flaw in the middle of the mirror suggests that it grew to criticality here first. The crack fanned out to form the non-circular mirror, but also unzipped along the surface to the left and right. Differential interference contrast image from a compound optical microscope.*

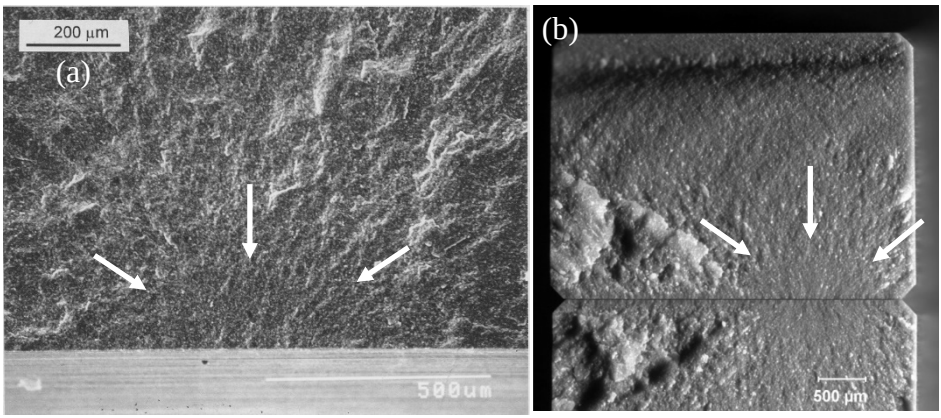

Figure 5.21 *Sideways-elongated mirrors from grinding flaws in ceramic bend bars. (a) SEM image of a "zipper machining crack" (see section 6.7.6) in sintered reaction bonded silicon nitride (542 MPa). (b) optical image of a zipper crack in sintered silicon nitride (432 MPa).*

Residual surface stresses may also alter mirror shapes. The shape distortion depends upon the magnitude, sign, and depth of the residual stresses. Figure 5.22 shows a typical parabolic residual stress distribution in glass from thermal tempering.[46] Stresses are strongly compressive at the surface, decrease to zero about 21% of the thickness in from each surface (assuming the two surfaces are cooled at the same rates), and change to tensile in the interior. The compressive stress at the surface is twice the magnitude of the interior tensile stress. Figure 5.23 shows mirrors in heat-strengthened glass consumer wares. For a surface origin, the compressive surface residual stresses suppress mirror boundary markings along the outer surface. Compensating residual internal tensile stresses shorten the mirror dimensions in the interior. A more detailed discussion of discussion of mirror shapes in tempered plates is in Appendix D and Figure D.8 in particular. Diced pieces from fully-tempered glass show mist and velocity hackle in the interior in Figure 5.24. Final crack breakthrough to the outer surface only occurs after the compressive stresses are released as a result of the local release of interior tensile stresses, and produces many fine parallel hackle lines that are perpendicular to the outer surface. Tempered and heat strengthened glass fractures are also discussed in section 4.11 in chapter 4.

Gardon[47] and Shinkai[48] have discussed the effect of non-uniform heat strengthening or tempering upon fracture patterns. Non-uniform air quenching may be intentional or unintentional. If interior and exterior quenching is not balanced, then the through thickness stress distribution may be altered considerably as compared to the ideal pattern shown in Figure 5.22.

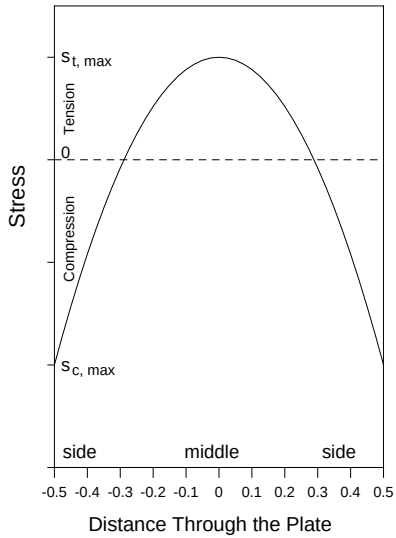

Figure 5.22 *Residual stresses in thermally-tempered glass pieces.*

(a)

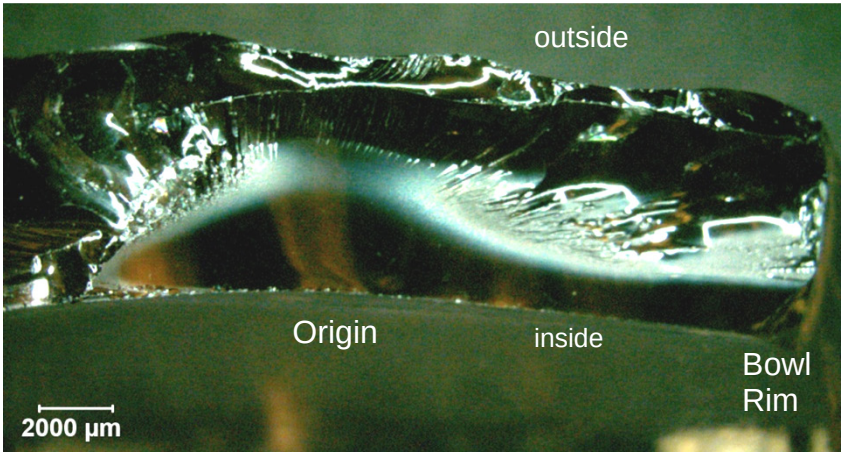

(b)

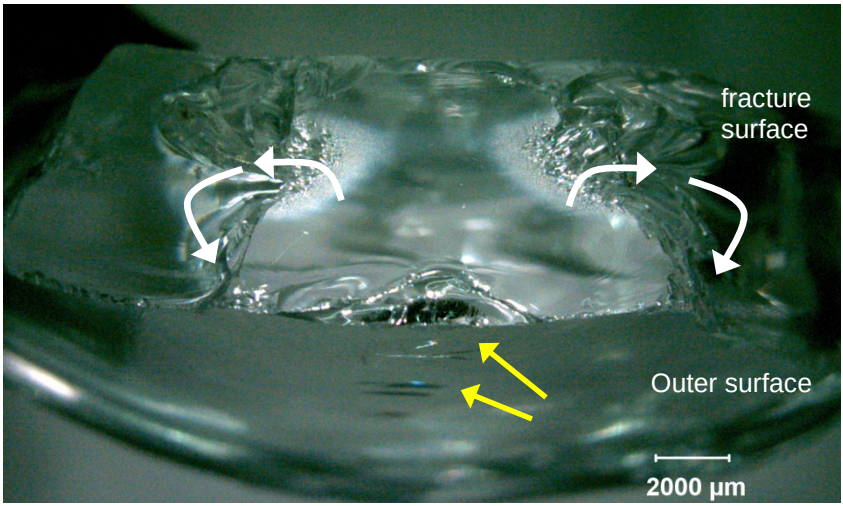

Figure 5.23 *Residual stresses alter the mirror shape. These images show thermally-strengthened glass consumer wares. The piece in (a) shows a complete suppression of mirror boundary markings along the lower right (interior) surface, but they are present to the left of the origin. This indicates the piece was thermally-strengthened with emphasis to protect the rim. In the middle, the mirror is well-developed into the depth since internal residual tensile stresses help form the mist and hackle. (b) shows a piece with mirror markings into the interior, but not along the bottom surface. The crack branched from the mirror sides in the interior of the piece then hooked back around to sever the fragment as shown by the white arrows. The origin is one or a series of "chatter cracks" (yellow arrows) from contact damage on the outer surface.*

(a)

(b)

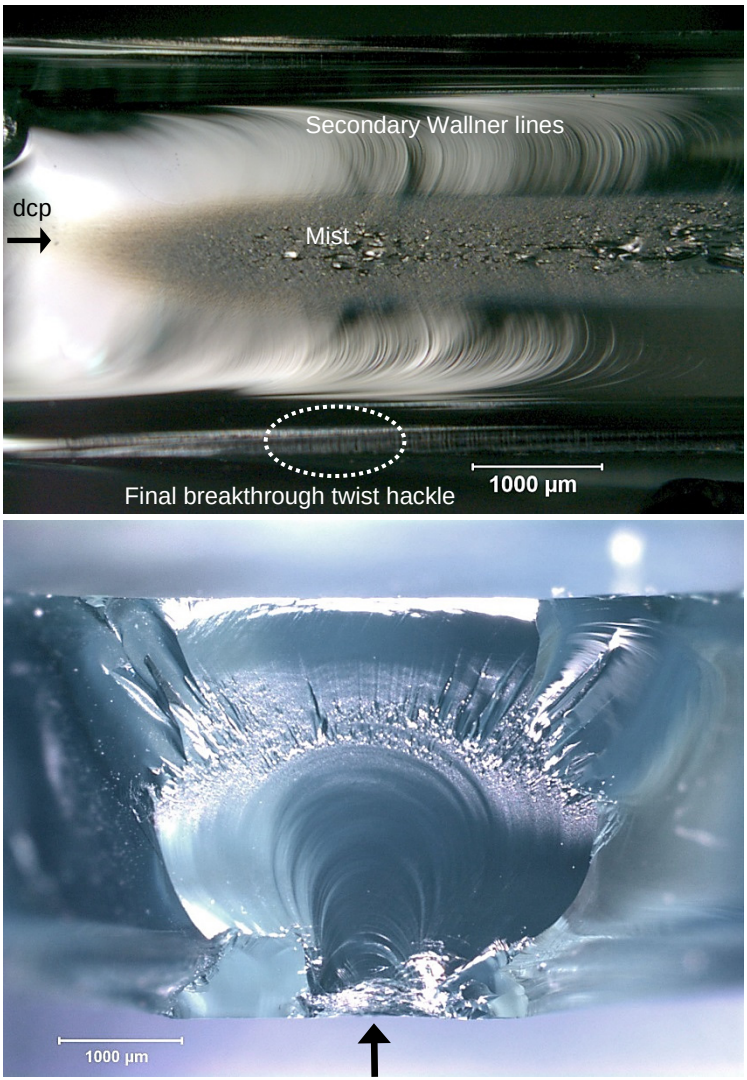

Figure 5.24 *Mist and velocity hackle in tempered glass. These photos are of the same diced-up auto window pieces in chapter 4 as Figures 4.24a,b,d. (a) shows the crack reached terminal velocity in the interior where the tensile stresses were greatest. The black arrow shows the direction of crack propagation and the onset of mist. Each diced piece usually has this pattern since cracks slow at a branch then accelerate to terminal velocity again. Crack propagation was retarded at the outer surfaces due to the compression. Final breakage through to the surface has vertical twist hackle (white dashed ring). The arc shaped lines are secondary Wallner lines described later. (b) shows the single impact origin (arrow) and mirror for the auto window.*

5.2.6 Fracture Mirrors in Other Materials

Relatively smooth regions surrounding a fracture origin can occur in other brittle materials. Figure 5.25 shows a fracture mirror in a human femur. The bone (from a cadaver) was from a forensic study whereby bones were broken in three-point bending in order to study fracture surface markings.[49] A new "Guide to Forensic Fractography of Bone" has been recently published by the U. S. Federal Bureau of Investigation Laboratory in Quantico, VA.[50] It includes many of the concepts and figures of this ceramic and glass Guide. The similarities and differences are fascinating.

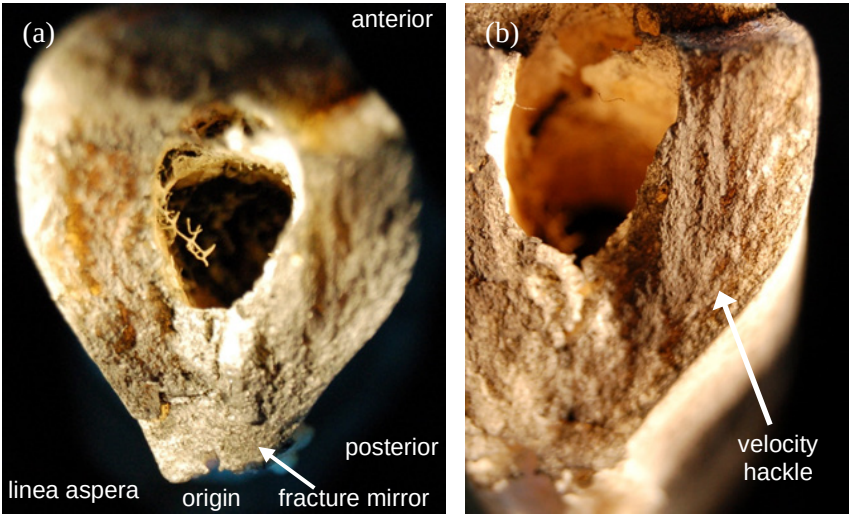

Figure 5.25 *Two views of a human femur fracture. The fracture mirror is centered on the tubular hole on the bottom in the linea aspea region of the femur. The tubular hole is a nutrient foramen, a passageway for a blood artery and nerves. (b) shows velocity hackle lines on the side of the bone. A light application of fingerprint powder to the fracture surfaces and oblique lighting enhances detail. (Courtesy, A. Christensen, FBI)*

Fracture mirrors are common in highly-filled dental resin composites such as the Paradigm MZ 100 bend bar shown in Figure 5.26. Such composites have a high-volume fraction of fine ceramic or glass filler particles. Fracture surfaces are similar to ceramic fracture surfaces. The fracture origin at the center of the fracture mirror was an internal calcium rich inclusion.[51] Fracture mirrors can exist in unfilled brittle polymers, but their interpretation is very different. They are a relatively smooth area surrounding a fracture origin, but the crack is moving slowly in this region as discussed in Roulin-Moloney's book.[52] This is

not the same as in glasses or ceramics, where the crack is running up to terminal velocity within the mirror.

Some in the rock fracture and geologic fields have deemed smooth circular geologic fractures as fracture mirrors. I am skeptical of such interpretations.

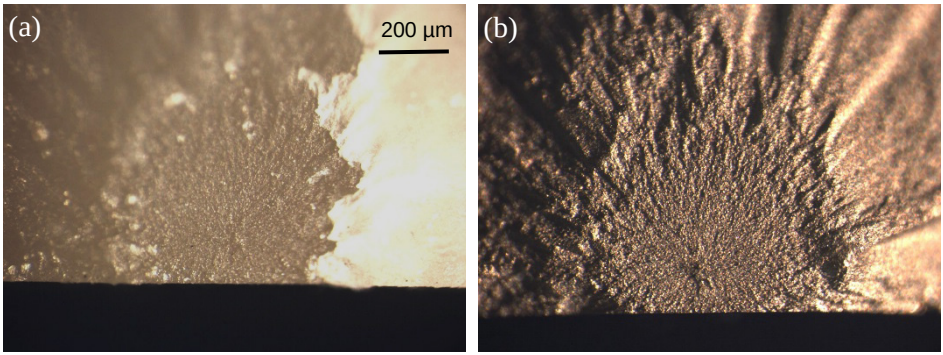

Figure 5.26 *Fracture mirror in a translucent, filled dental resin-composite bend bar. (a) is an uncoated optical image of the fracture surface. (b) is the same region but with a gold coating to enhance detail. Note the internal fracture origin flaws in this bend bar.*

5.3 Hackle

In addition to the mist hackle and velocity hackle (described above in the fracture mirror section) that are self-initiated by the crack near its terminal velocity, there are other types of hackle that are very useful for ascertaining the direction of crack propagation. These help the fractographer trace crack propagation back to an origin. Hackle lines are sometimes called "lances" and less commonly "striations," but this latter term is not recommended. Hackle can be generated from origin flaw irregularities. A good example is "*grinding crack hackle*" shown in section 6.7.6 in the origins chapter.

In this Guide and in most publications, the word "hackle" means both the singular and the plural. It "raises my hackles" when I see multiple hackle lines described as "hackles."

5.3.1 Coarse microstructural hackle

Coarse microstructural hackle: *Large broad hackle lines that form from non-specific sources, but most likely variations in the microstructure.*

Ceramics often develop coarse hackle even in the absence of mirrors or other well-defined fracture surface markings. They occur in low-strength or porous ceramics and often are the only marking on a fracture surface that indicate the direction of crack propagation. The microstructure or some geometric irregularity causes portions of the crack to advance on non-coplanar regions separated by rounded ridges as opposed to sharp steps. Figures 5.27 and 5.28 show examples. ("Fine microstructural hackle" is shown later on page 5-40.)

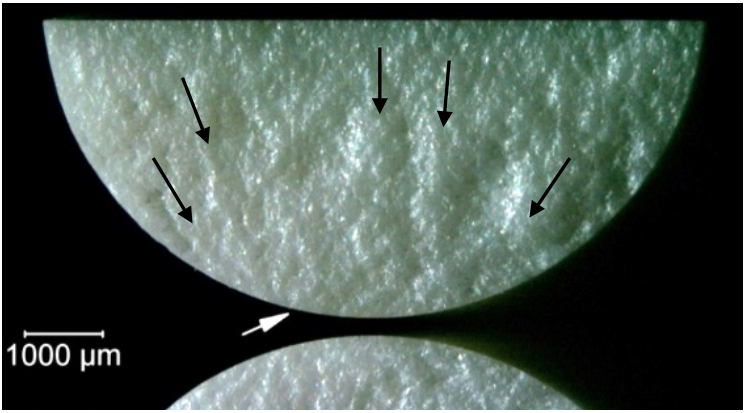

Figure 5.27 *Coarse microstructural hackle. Matching fracture surface halves of a split cylindrical rod flexural strength specimen of a coarse-grained (50 µm to 80 µm) Mg partially-stabilized zirconia. It has a very rough clumpy fracture surface. Low-angle grazing illumination shows the coarse hackle lines (black arrows) radiating from the origin region (white arrow).*

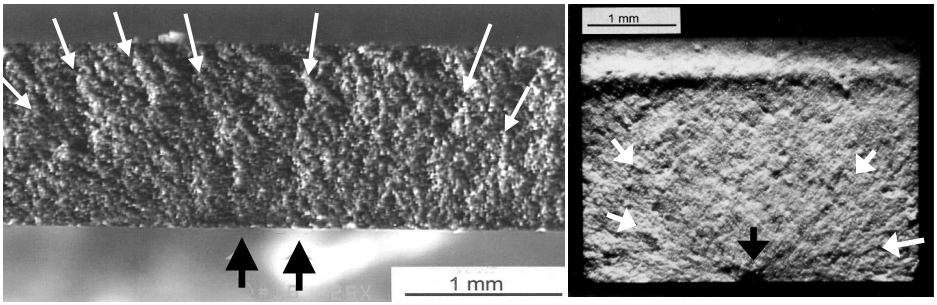

Figure 5.28 *Coarse microstructural hackle. (a) is a broken O-ring specimen of a ceramic membrane material. (b) is a silicon nitride bend bar with a Knoop indentation flaw on the bottom middle (black arrow). Coarse microstructural hackle lines (white arrows) guide the observer back to the origins. The only other fractographic feature observable is the compression curl in (b). Both specimens are so weak that fracture mirrors are larger than the cross sections.*

5.3.2 Wake hackle

Wake hackle: *A hackle mark extending from a singularity at the crack front in the direction of cracking.* (after Fréchette, ref. 1)

When an advancing crack encounters an elastic singularity such as an inclusion or a pore, the crack front may split at the object and sweep past it on both sides. The two fronts often pass the obstacle on slightly different planes and create a downstream step or "tail" between them. The tail may fade away quickly or persist for long distances. These markings are very recognizable and may be large or very small. They serve as miniature "weather vanes" which tell the direction of local crack propagation. Figures 5.29 – 5.31 show examples.

Wake hackle in glassy *glazes or veneers* often is the only recognizable fracture surface feature in kitchenware, electrical insulators, and some dental ceramics. The core ceramic materials in these instances are often coarse-grained, porous, or weak, and few fracture surface markings are evident. Sometimes in even the most difficult materials, tiny porosity will aid the fractographer by serving as a source of wake hackle. A superb example was shown by Ko[53] in his Figure 14 wherein many tiny hackle lines led back to an origin.

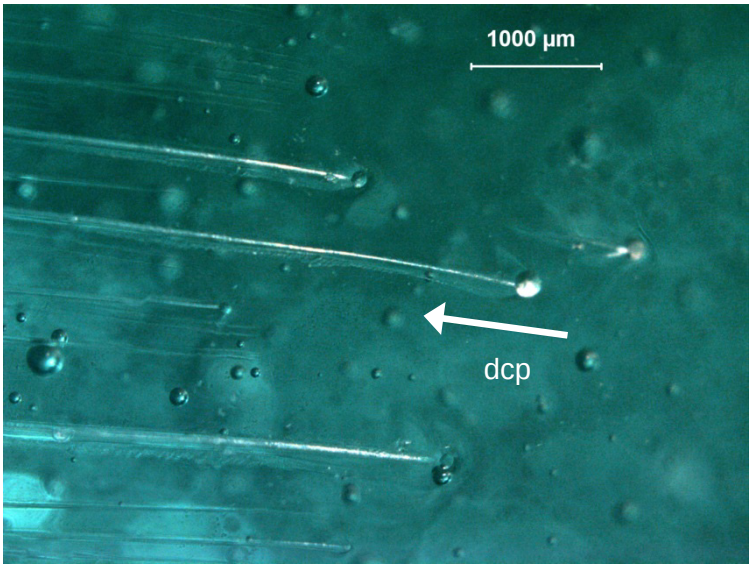

Figure 5.29 *Wake hackle is a "weathervane" for crack propagation. This optical image shows wake hackle from bubbles in glass. The direction of crack propagation (dcp) is shown by the arrow. Many bubbles are beneath the fracture surface in this view and as such do not create wake hackle.*

(a)

(b)

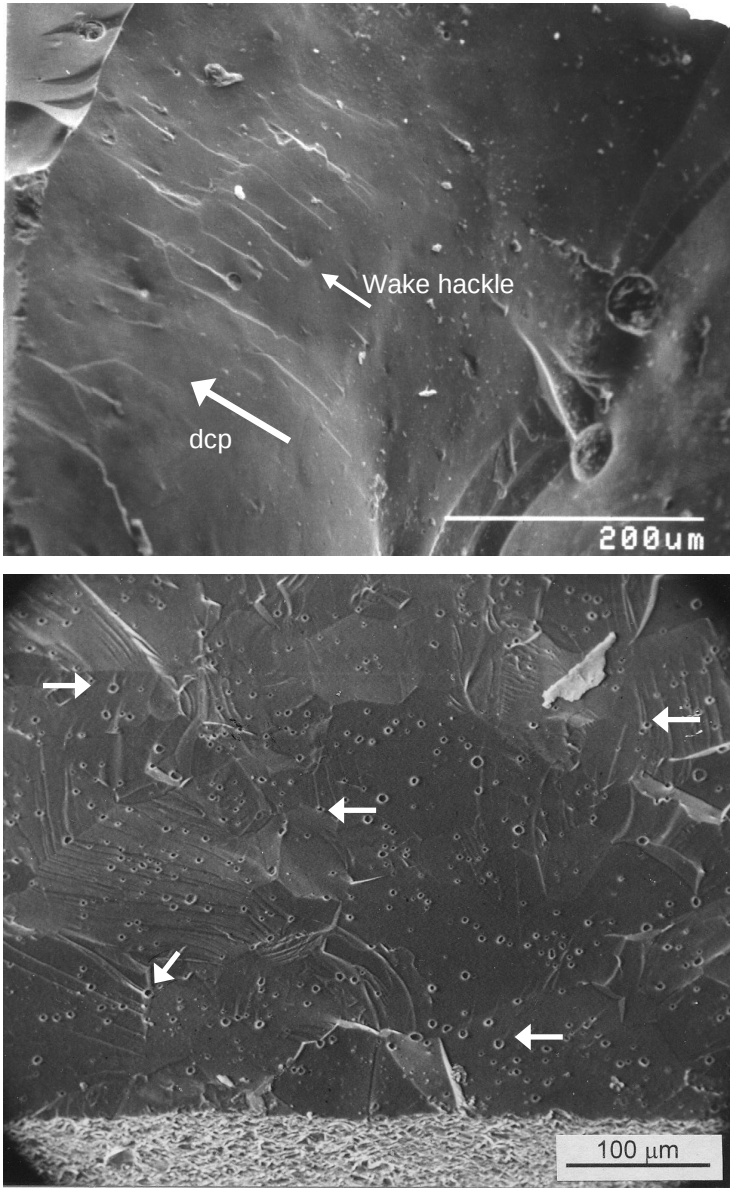

Figure 5.30 *SEM images of* ***w****ake hackle. (a) shows an array of wake hackle from pores in a glassy veneer on a Empress II dental crown. The direction of crack propagation (dcp) is marked by the big arrow in (a). (b) shows an example of transgranular fracture from a large grain origin in polycrystalline AlON. Wake hackle was triggered by grain boundaries and tiny pores within grains (small arrows). In (b) the arrows show the tiny wake hackle but* *<u>not</u>* *the dcp.)*

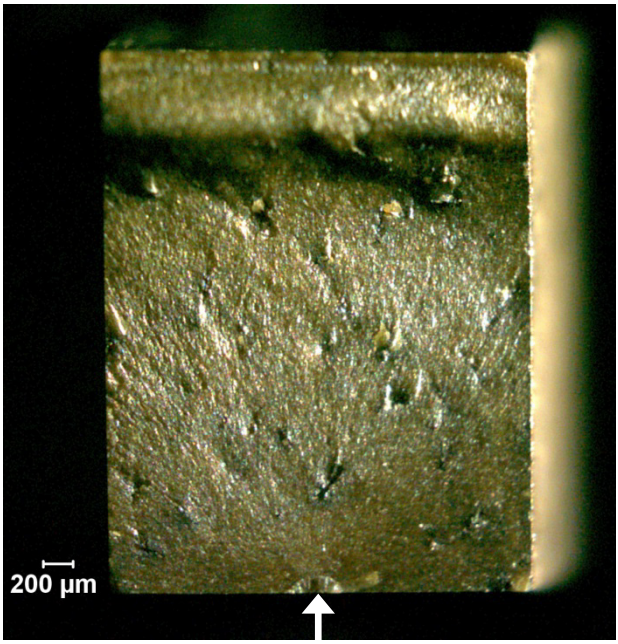

Figure 5.31 *Wake hackle from inclusions in a lead zirconium titanate (PZT) bend bar. The entire fracture surface is shown. The tensile surface is on the bottom and a compression curl is on the top. The wake hackle lines point back to the origin on the bottom marked by a white arrow. It is a semielliptical surface crack made by a Knoop indentation.*

Irregularities such as pores or inclusions are not the only sources of wake hackle in ceramics. Grain boundaries and local crack path redirection as a crack propagates from one grain to another with a different crystallographic orientation, or local-density or other microstructural variations all can trigger "fine microstructural hackle:"

Fine microstructural hackle: *Small hackle lines of the order of size of the microstructure that occur as a crack interacts with the local microstructure.*

Sometimes meticulous observations of within-grain cleavage, micro-wake hackle, and micro-twist hackle lines can allow one to backtrack to an origin.

Kerkhof and Sommer used ultrasonic fractography to show that a crack accelerates in the immediate vicinity of a hole in glass, but then is retarded as the crack runs past the hole.[54] Figure 5.51b later on page 5-62 in this chapter shows an example.

(a)

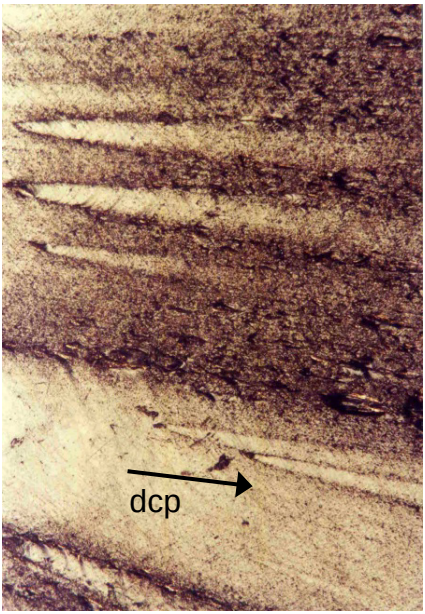

(b)

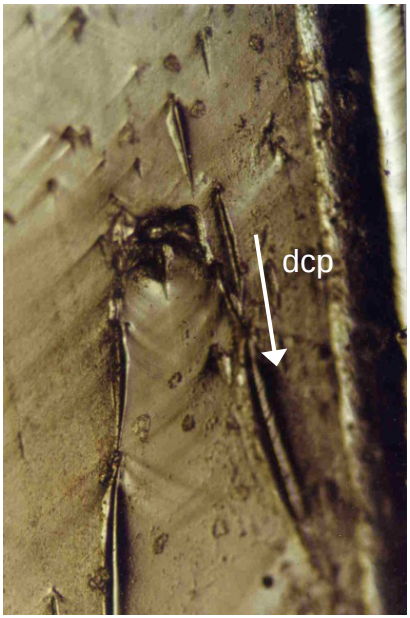

(c)

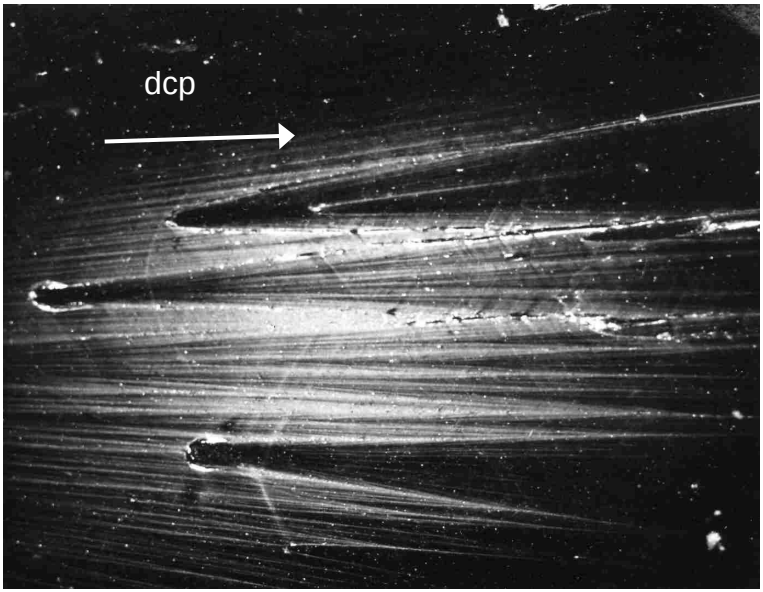

Figure 5.32 *Parabolic double wake hackle tails triggered by inclusions in obsidian glass. "dcp" denotes direction of crack propagation. These are rare in glasses and are associated with glasses that have many inclusions. They have not been observed in ceramics. They are very similar to, but not the same as Kies markings also known as parabolic or hyperbolic markings in polymers. (all courtesy A. Tsirk, see ref. 35)*

5.3.3 Twist hackle

Twist hackle: *Hackle that separates portions of the crack surface, each of which has rotated from the original crack plane in response to a lateral rotation or twist in the axis of principal tension. (Fréchette, Ref 1.)*

Twist hackle are very telltale markings as illustrated in Figures 5.33 and 5.34. They can form from fast or slowly moving cracks, or even from cracks that have arrested. They are also known as delta patterns, river deltas, river patterns, lances, and in the geological community as echelons or striations. Striations in this instance are not to be confused with fatigue striations, a well-known metallurgical fracture surface marking. The roughly parallel segments point in the direction of *local* crack propagation. Twist hackle can be generated by the primary crack as it travels directly through the body, especially as it goes around corners or geometric irregularities, or when stress conditions changed.

The crack is unable to rotate all at once in response to the new stress direction, so it breaks into small, unconnected segments. The steps are “hackle lines” or “lances.” Lateral breakthroughs occur between the micro segments as shown in 5.33(b) and (c). Note in 5.33(c) how the micro segments can link either by a top segment breaking though to a bottom segment or vice versa. On any given lance, the link up can alternate between either segment creating a barbed appearance. Sometimes an incomplete segment can breakthrough long after the main fracture has occurred, generating faint tinkling sounds and creating very sharp needle like fragments that fall free from the fracture surface. The small hackle lines gradually merge into coarser hackle lines, and so on, until the new crack plane is aligned perpendicular to the new tensile stress axis. Usually crack propagation is in the direction of fine to coarse hackle. The boundary between the initial flat crack, and the twist hackle zone is called a “fringe” in the rock fracture literature.

Twist hackle can also occur from final breakage between local crack segments, or through to the side of a specimen that had had strong thermal or stress gradients. Twist hackle shows the *local* direction of crack propagation. Plates in bending often have curved cracks that run quickly on the tension side, but do not quite break through to the opposite surface. The crack later snaps through to the opposite surface leaving twist hackle markings as shown in Figure 5.35a. Double torsion fracture mechanics specimens often have such markings. Figures 5.24a and 5.35b show a similar circumstance whereby final breakthrough of tempered glass has twist hackle near both outer surfaces.

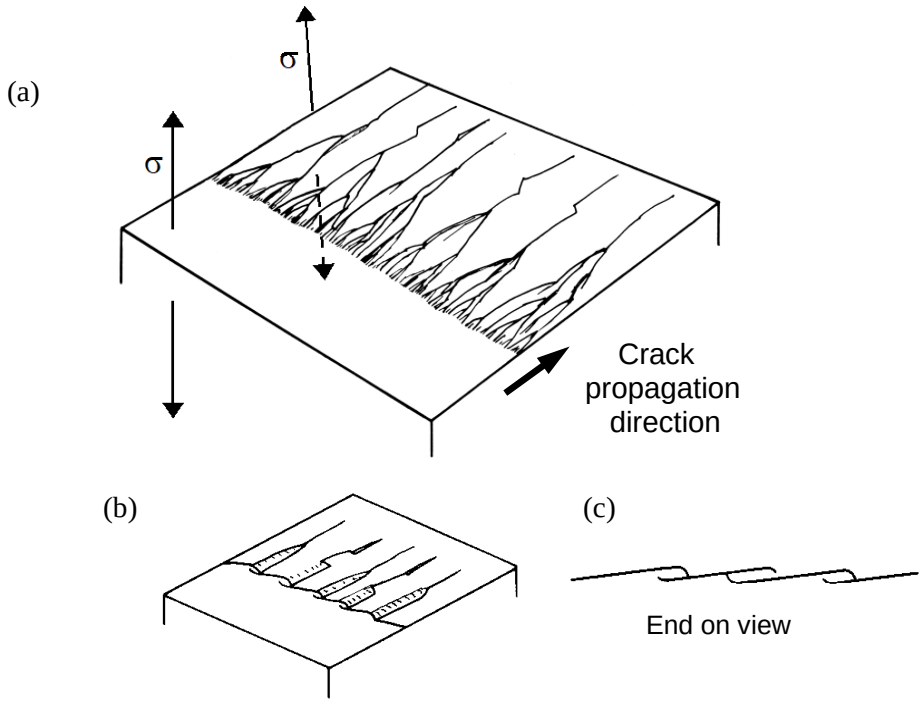

Figure 5.33 *Twist hackle. (a) shows how twist hackle is formed. It can form in either fast or slowly-moving cracks, or from arrested cracks. A crack propagating from left to right runs perpendicular to the initial stress field as shown on the left. The axis of principal stress then tilts as shown on the top middle. This creates a mixed mode I and Mode III loading (chapter 7) condition at the crack tip. (b) and (c) show how a top segment can break through to a bottom segment and vice versa.*

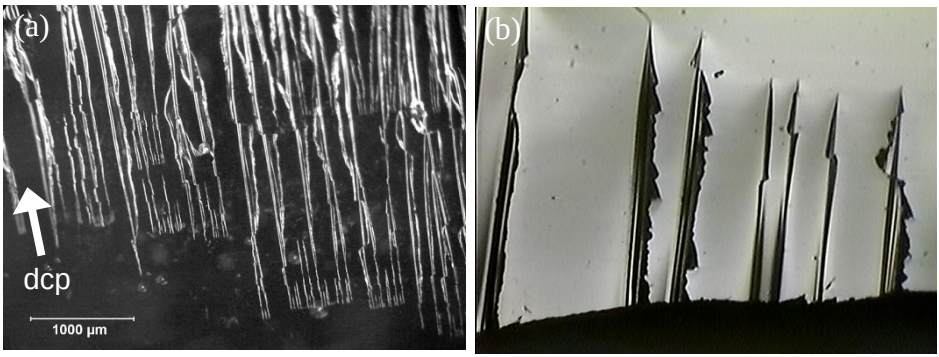

Figure 5.34 *Close-up views of twist hackle in glass. The crack was running in the direction of the arrow in (a). (b courtesy J. Varner, size scale unreported)*

(a)

(b)

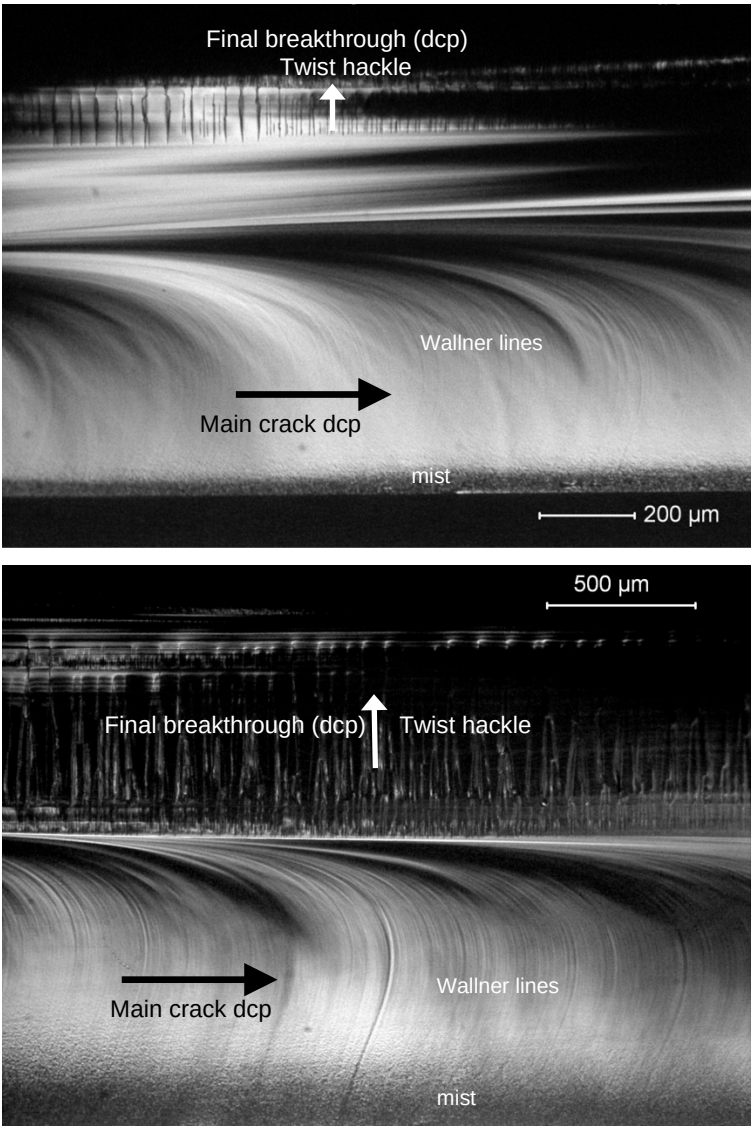

Figure 5.35 *Twist hackle. (a) shows a glass microscope slide that was broken in bending with a little superimposed torsion. The main crack fracture from left to right, leading on the bottom surface as attested to by the profusion of mist and secondary Wallner lines and an occasional primary Wallner line (described in the next section). Final breakthrough to the top surface created the twist hackle along the top and the local dcp is shown by the white arrow. (b) shows a similar pattern but in a tempered glass fragment.*

(a)

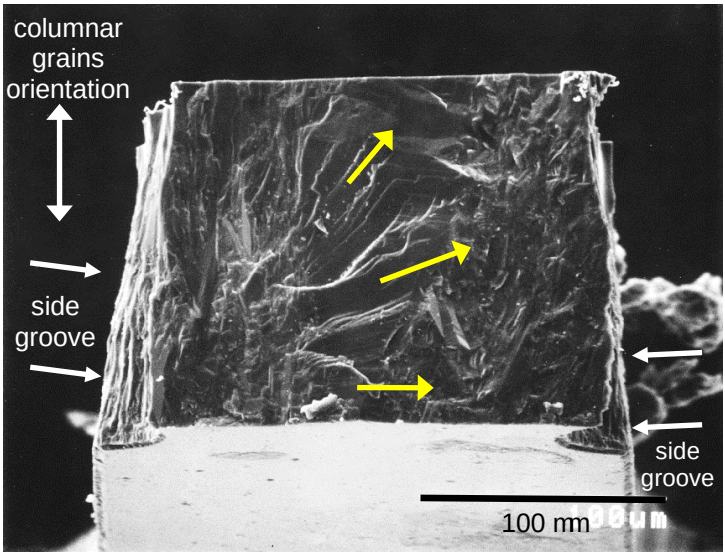

(b)

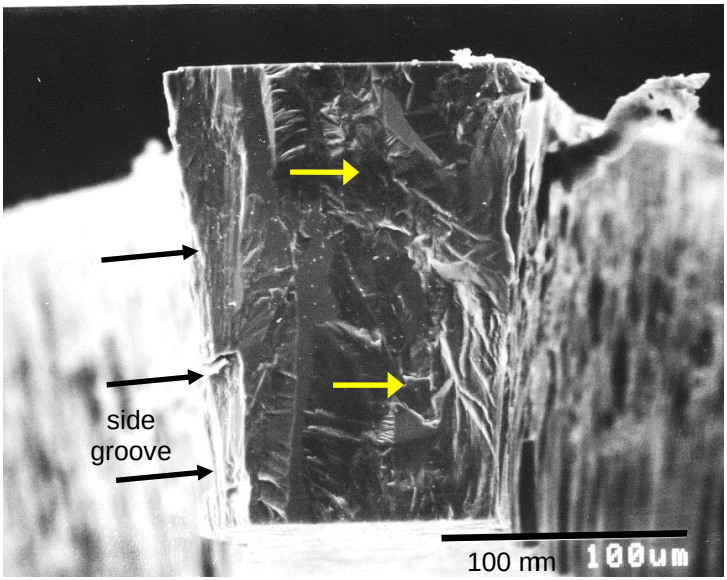

Figure 5.36 *Twist hackle in grains. (a) and (b) show fracture surfaces of chemical vapor deposition (CVD) silicon carbide micro-tensile specimens. CVD materials often have coarse columnar grains. Such grains run from top to bottom in this view. Figure 4-2c on page 4-4 showed a whole specimen where the grains were obvious. Twist hackle in the grains in both images show that fracture propagated from left to right as shown by the yellow arrows. Fracture occurred from cracks located at the bottom of the grooves on the left side in both cases.*

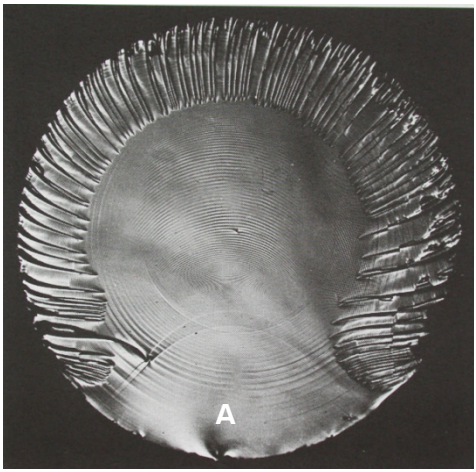

Figure 5.37 *Twist hackle around the circumference of a 15 mm diameter glass rod broken in tension. The tension was induced by lateral fluid pressure compression around the rod periphery while the rod ends were free. There also was some superimposed torsion. The wavy lines are tertiary Wallner lines (described in section 5.4.4) created by ultrasonic fractography. Fracture started at the bottom at point A and progressed into the rod interior. Final breakthrough to the outer surface generated the twist hackle. (Sommer,[39] Kerkhof and Sommer[54], and Richter and Kerkhof.[2])*

In polycrystalline ceramics, twist hackle markings within coarse grains can serve as very helpful markers. They are local indications of crack propagation and it is often possible to track a propagating crack back to an origin by reading the local "weather vanes." Figure 5.36 shows examples. The fractographer may be surprised to see that twist hackle line within separate grains may not all line up the same way. It is quite common for cracks to take detours through the microstructure in response to local conditions.

Sommer[39] analyzed the formation conditions of twist hackle and concluded that in glasses a stress redirection of 3.3° is needed to initiate the twist hackle or "lances". Beauchamp[36] observed hackle with only 1° of twist. Torsional stresses superimposed on tension stresses can create twist hackle markings as shown in Figure 5.37 which shows a rod loaded in mixed mode I, opening mode, and mode III, out-of-plane shear, as described in section 7.1. An interesting paper[55] reported on how a continuum phase-field approach could be used to model twist hackle formation and propagation. Very small initial perturbations along the initial crack front would form parallel "daughter crack segments" that gradually coalesce, as the main crack plane rotated.

5.3.4 Shear hackle

Shear hackle: *A particular form of twist hackle that occurs in the lazy loops generated in the latter stages of fracture of a hollow specimen. (after Fréchette, Ref 1.)*

This definition may seem peculiar, but once the fractographer has seen an example such as Figure 5.38, it becomes clear what Fréchette had in mind.[1] He said: "Far from the fracture origin, it is common to see the crack turn through 90° and develop a cupped surface, inclined at 45° to the free surface, from whose centerline a spray of twist hackle emerges. It has little significance in reconstructing a failure event in industry, but it is useful in problems of rock fractures."

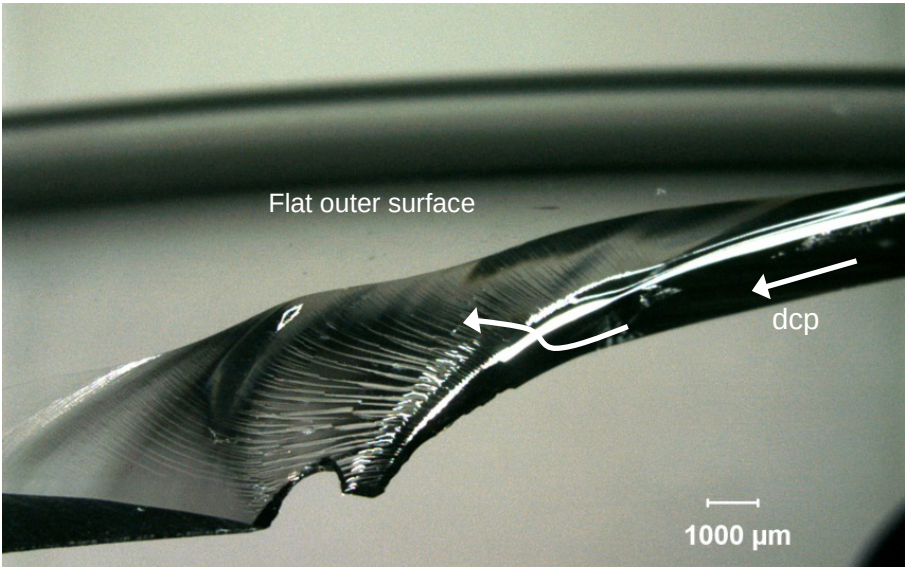

Figure 5.38 *Shear hackle in a glass plate. The crack was perpendicular to the glass surface and was slowing as it moved in the direction of the white arrow. It then turned 90° parallel to the surface and finally broke through to the surface at about 45°, producing the spectacular fan-shaped shear hackle. Shear hackle is a variant of twist hackle.*

5.3.5 Corner hackle

Corner hackle: *A fan like array of hackle lines created when a crack curves in a plate or goes around a corner of a component.*

Figure 5.39 shows examples. The fan like array spreads outwards in the direction of crack propagation. Figures 10.23b and 10.24c in Chapter 10 show an example in a broken dental crown.

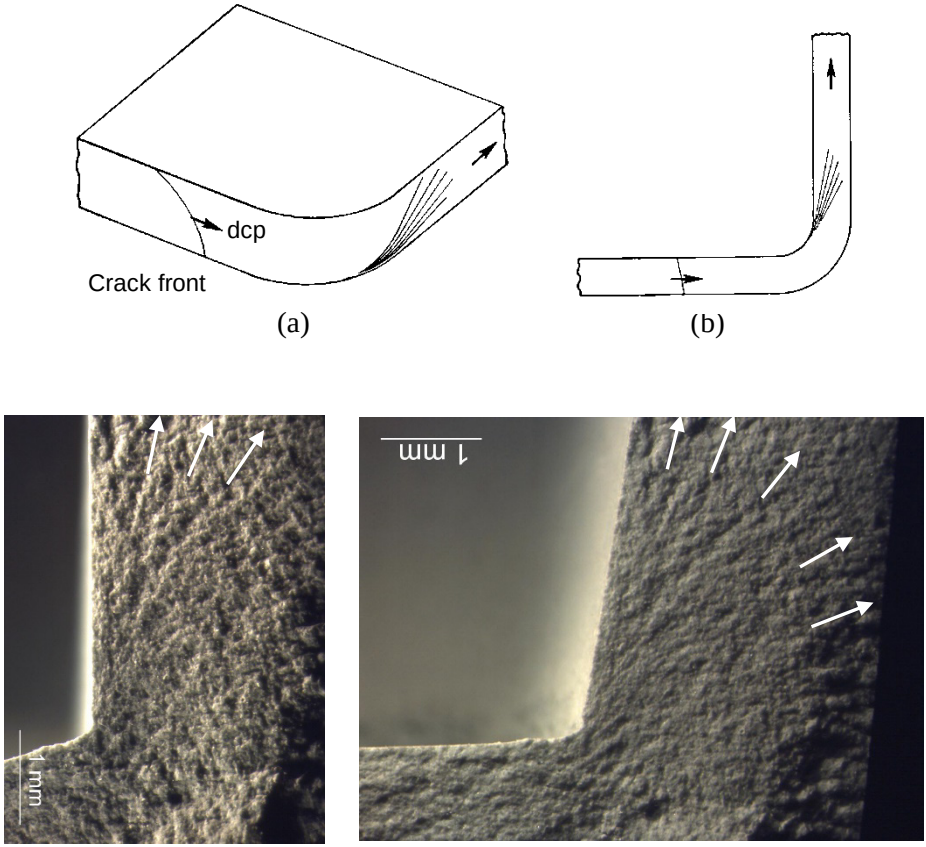

Figure 5.39 *Corner hackle. (a) shows a fan like pattern that occurs when a crack that is leading on the bottom surface turns to another direction. (b) shows a fan-like pattern that occurs when a crack goes around a corner of a container or vessel. (c) and (d) show examples in a dental hard-rock mold material. The microstructure makes a rough fracture surface, but with low angle grazing illumination from the left side, the corner hackle stands out.*

5.3.6 Step hackle

Step hackle: *A type of twist hackle in the form of a single line that is an arc shaped line on a fracture surface of a plate broken in bending and twisting.*

Step hackle is a line that is a step on the fracture surface such as shown in Figure 5.40. The line is parallel to the local direction of crack propagation. Unlike twist hackle, it is an isolated line. The arc curvature of a step hackle line is opposite to the curvature of arrest lines or Wallner lines that may exist on the same fracture surface. The fracture surface is usually tilted or curved and not perpendicular to the plate outer surfaces (end-on view Figure 5.40a.). The step can initiate by itself if the tilt is strong enough, or may be triggered by bubbles, inclusions or mist. Step hackle is shown here for glasses, but can occur in single crystals as "*cleavage step hackle*" as described in Chapter 8.

(a)

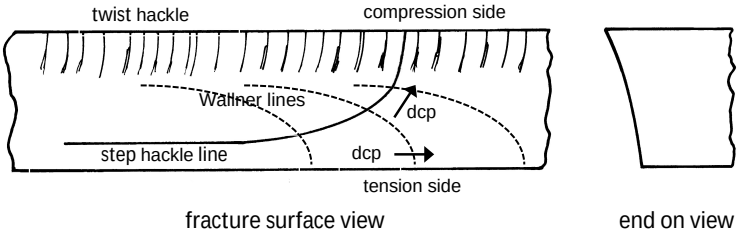

(b)

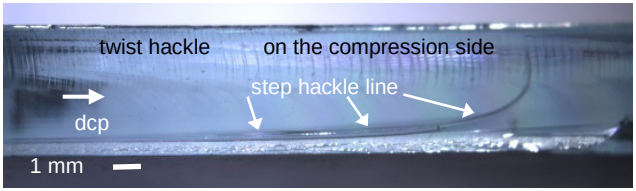

(c)

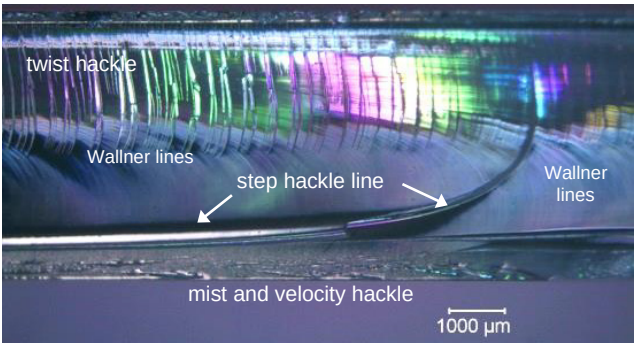

Figure 5.40 *Step hackle schematic (a). (b) and (c) show a piece of a large (1.5 m by 0.75 m) glass mirror that fell off a wall in the author's home. The mirror broke into over 100 pieces. Many fragments had evidence of bending and twisting. Notice the opposite arcs of the step hackle and the Wallner lines.*

5.4 Wallner Lines

5.4.1 Introduction

Wallner line: *A rib shaped mark with a wavelike contour caused by a temporary excursion of the crack front out of plane in response to a tilt in the axis of principal tension. It may also form from passage of the crack front through a region with a locally shifted stress field, as at an inclusion, pore, or surface discontinuity. (adapted from Fréchette, Ref. 1)*

Also known as "ripples" or "rib marks," Wallner lines were named for Helmut Wallner who first explained how they formed in 1939.[56] He showed beautiful images (similar to Figures 5.2 and 5.3 of this Guide) of fracture mirrors in flexurally-tested glass rods with the lines within the mirrors. He presented a splendid sketch showing how an expanding crack front was overtaken by an expanding elastic wave. The Wallner line is the locus of the intersection of the elastic wave and the crack front. The elastic wave momentarily causes the crack to ripple out of plane like a wave on a pond surface. The shape of the line depends upon the respective shapes and speeds of the elastic wave and the crack front, as well as the direction the wave approaches the crack front. Wallner lines are invaluable in determining the direction of crack propagation. As will be shown, they usually do not have the exact same shape as the crack front, but they are usually curved (bowed) in the direction of crack propagation.[e] They are best understood by the examples that follow.

Wallner lines are very shallow hillocks on a fracture surface. They look like a thin shadow band and they tend to shift slightly as illumination is adjusted. This is in marked contrast to crack arrest lines (shown later in section 5.5) that are sharp and do not appear to move as light is adjusted. Wallner lines are very easy to see on fracture surfaces once the lighting is adjusted, but they are almost impossible to see on the scanning electron microscope, since they produce almost no contrast and are very shallow.

There are several types of Wallner lines depending upon the source of the elastic wave. Fréchette[1] thoughtfully categorized these as primary, secondary, and tertiary. This Guide follows his scheme and adopts his definitions. His figures showing the evolution of the loci were instructive, but have been revised and expanded into separate illustrations in this Guide to make them easier for the beginner to understand.

---

[e] There can be exceptions to this curvature, however, that the fractographer must be on the lookout alert for. For example, Wallner and arrest lines in glue chips may be curved in the opposite sense to what is described in the text above and shown in the examples here.

Keep in mind that a crack front through a plate may be straight or have different shapes according to the stress state as shown in Figure 5.41.

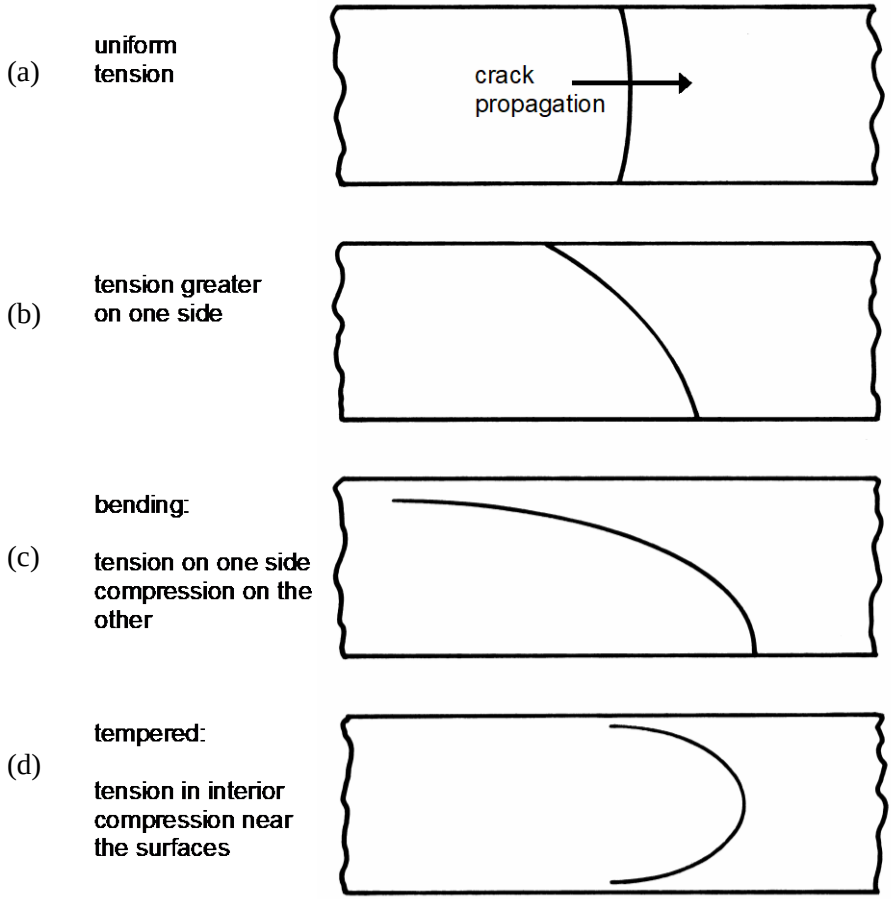

Figure 5.41 *Crack front variations due to stress distributions through the thickness. (a) shows a crack front in a uniform tensile loaded plate. (b) a plate with greater tensile stress on the bottom. (c) a plate in bending such that the bottom is in tension and the top in compression. (d) a tempered plate with tensile stresses in the interior and compressive stresses at the surface.*

5.4.2 Primary Wallner lines

Primary Wallner line: *A Wallner line formed by an elastic pulse generated by some portion of the crack front with a singularity in the specimen such as a discontinuity at the free surface or within the specimen, or with any localized stress field or elastic discontinuity. (adapted from Fréchette, ref. 1)*

Primary Wallner lines commonly are generated by surface blemishes and irregularities such as scratches, pits, or edge chips. Figure 5.42 shows an example and Figure 5.43 illustrates how they are formed. If a Wallner line is seen to emerge from such a surface blemish, it is evidence that the surface fault was present at the instant the crack ran by. Alternatively, if a large blemish or chip is on a glass fracture surface, but there is no Wallner line from it, the blemish occurred afterwards and was not initially on the piece.

Unless the crack is moving very slowly (and the elastic wave traverses the entire crack front very quickly), primary Wallner lines do not show the exact crack front profile. Nevertheless, they are curved in the same direction and can help the fractographer deduce which way a curved crack was running. It is fairly easy to show (by a vector analysis of the wave and crack velocities) that straight crack fronts generate straight but tilted Wallner lines.

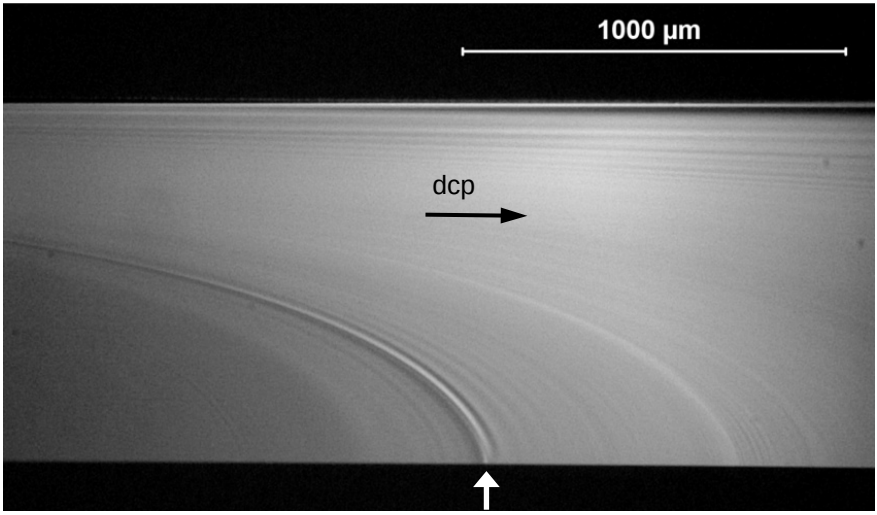

Figure 5.42 *Primary Wallner line in a glass slide broken in bending. A scratch on the surface (white arrow) triggered the strong Wallner line as the crack ran from left to right. Other tiny faults triggered fainter primary Wallner lines.*

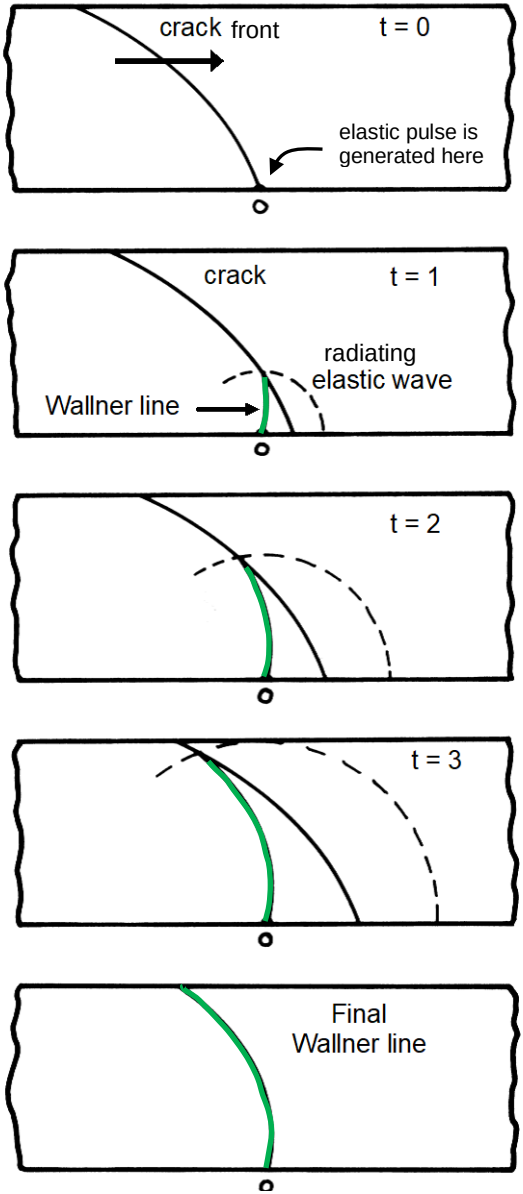

Figure 5.43 *Primary Wallner lines. This series shows the progressive advance of the crack at successive time intervals. The elastic wave that forms the Wallner line (shown in green) is generated when the crack hits a surface irregularity "O" at t = 0. The crack leads on the bottom surface and moves at constant velocity in this example. The elastic wave runs faster than the crack and thereby overtakes the entire crack front. Notice the Wallner line shape is not the same as the crack front shape.*

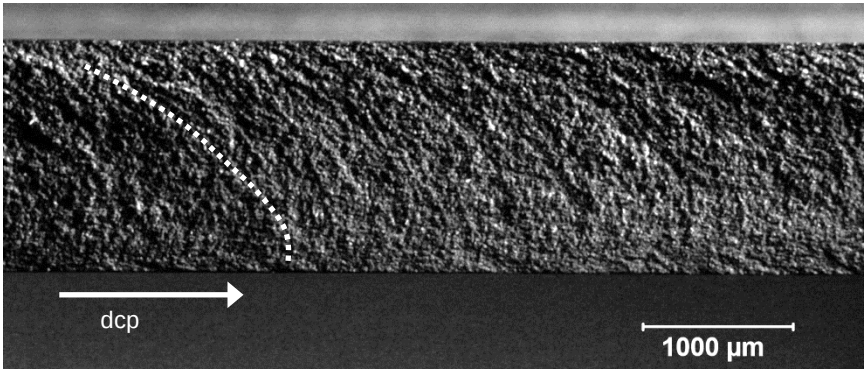

Figure 5.44 *Wallner lines are more difficult to see in polycrystalline ceramics. Low-angle grazing illumination is effective. This is an optical image of a silicon nitride double torsion fracture toughness specimen. The crack was running in the direction of the white arrow. The double torsion configuration bends a specimen so that the bottom is in tension and the top in compression. The cracks lead on the bottom surface. Primary Wallner lines formed with arcs shown by the white dashed curve.*

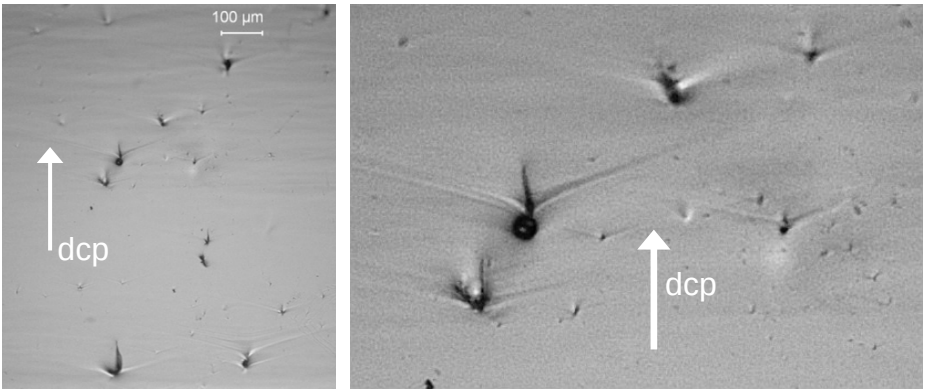

(a) (b)

Figure 5.45 *Gull wings are a variant of primary Wallner lines. (b) is a close-up of (a). These images are from obsidian with crack propagation from bottom to top as shown by the arrows. The wing angles can be used to measure crack velocity (section 7.9). Most of these pores or inclusions also have wake hackle. (specimen courtesy A. Tsirk)*

Wallner lines are less easy to see in ceramics. Figures 5.13b and 5.44 show examples. In porous, granular, or coarse-grained ceramics, large broad ridges that are Wallner lines may be the only recognizable marking on the fracture surface. If so, the ridge may have been caused by microstructural irregularities or surface flaws on one side of the origin or to a geometric irregularity (e.g., an inside corner in a formed ware, or a ridge on a plate).

Figure 5.45 shows "gull wings," a variant of primary Wallner lines. They are usually formed by a stress pulse created as the crack encounters pores, inclusions, or other irregularities. There even are instances where they may be triggered by secondary fracturing behind the primary crack front, and hence will be detached from obvious irregularities.[57]

5.4.3 Secondary Wallner lines

Secondary Wallner line: *A Wallner line generated by an elastic pulse released by a discontinuity in the progress of the crack front, typically one of the rough details which arise as the crack approaches its effective terminal velocity. (After Fréchette, Ref 1.)*

Unlike the primary Wallner lines that form as a result of a crack encountering an external feature, secondary Wallner lines occur from features the crack generates itself. Mist and hackle are disturbances created by crack running at or near terminal velocity. The mist and hackle generate copious secondary Wallner lines. Figure 5.46 shows their formation sequence and Figure 5.47 shows examples. It is very common for both primary and secondary Wallner lines to be present. They can be distinguished by their different curvatures. Secondary Wallner lines are more hooked (like a fish hook) than primary Wallner lines. As was the case with primary Wallner lines, secondary Wallner lines do not show the exact crack front profile. Even so, it is helpful to deduce from their curvature which way a crack was running.

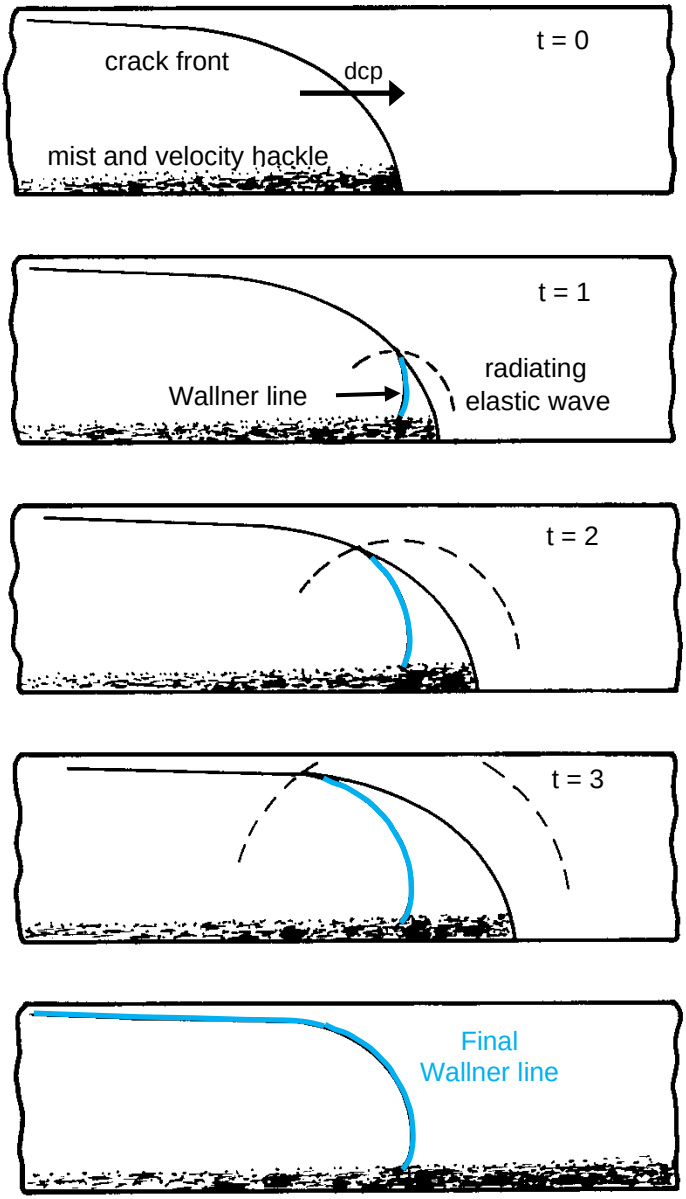

Figure 5.46 *Secondary Wallner lines are formed by the crack itself. This schematic series shows the progressive advance of the crack and the elastic pulse that forms the secondary Wallner line (in blue color) in a plate with a stress gradient. Notice the hook final shape, a consequence of the stress gradient caused by the variation in the crack velocity from a maximum on the bottom to close to zero at the top.*

(a)

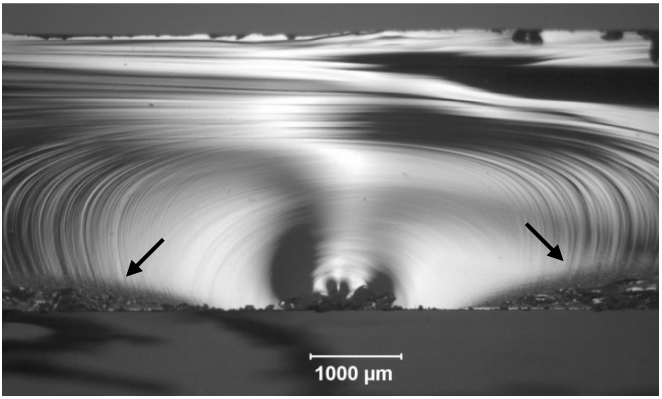

(b)

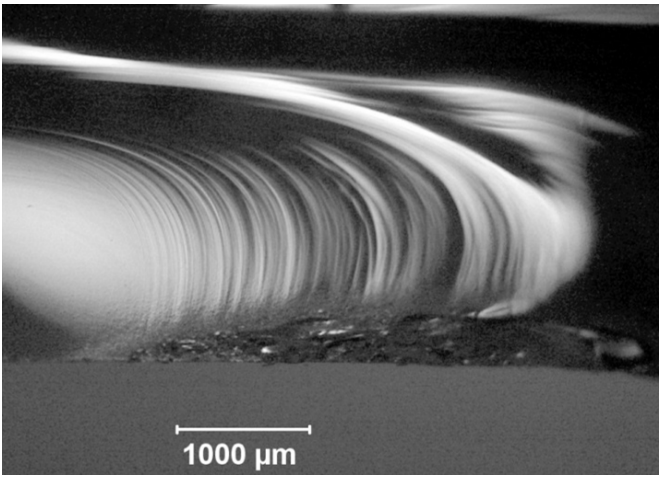

(c)

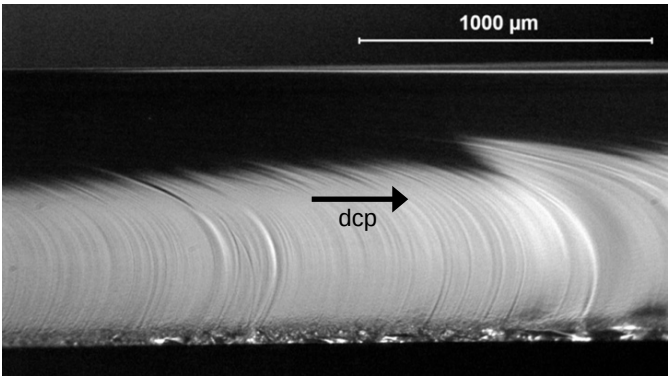

Figure 5.47 *Examples of secondary Wallner lines in glass microscope slides. (a) and (b) show Wallner lines from the sides of a fracture mirror. (b) is a close-up of the right side of (a). Mist and hackle triggered the secondary Wallner lines. There also are fainter primary Wallner lines inside the mirror as seen in (a). Notice their different arcs. (c) is a slide broken in bending.*

5.4.4 Tertiary Wallner lines

Tertiary Wallner lines: *Wallner lines caused by elastic pulses generated from outside the crack front. (Fréchette, Ref. 1)*

Vibration or shock from a source other than the crack itself can create waves that intersect with and cause momentary deviations in the crack front. Depending upon the source of the elastic pulse relative to the crack plane, the interaction may generate Wallner lines that may be very close to the shape of the crack front, or it may produce an arc formed by a progression of intersections of the crack front and the wave front as in the examples shown above. For example, if the crack is moving relatively slowly, the fast elastic wave will overtake all portions of the crack front nearly simultaneously, producing a Wallner line "snapshot" of the crack front.

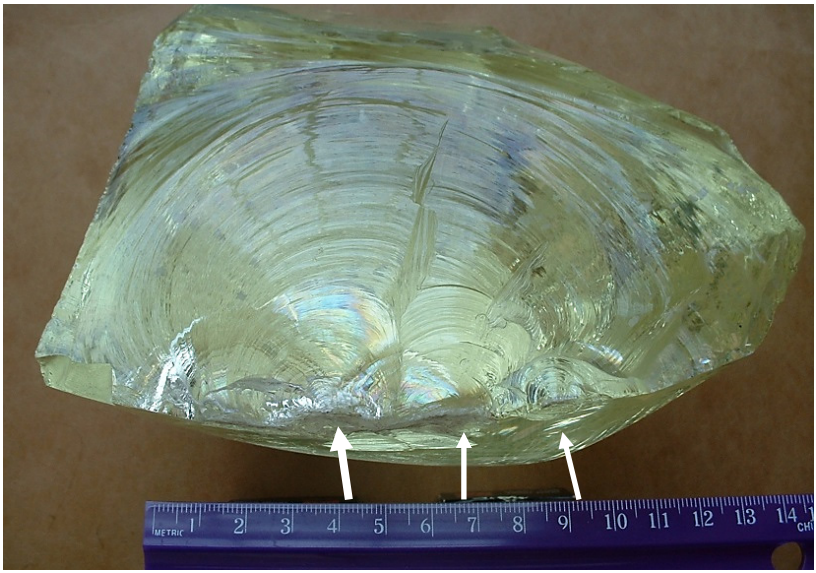

Figure 5.48 *Tertiary Wallner lines in a large chunk of glass that was hammered into pieces. There are multiple impact sites marked by arrows, the most prominent of which is marked by the larger white arrow. Notice how the tertiary Wallner lines are concentric about the impact sites. This was one of Professor Fréchette's classroom demonstration pieces.*

If the pulse source is located at a site normal to the fracture plane, the pulse may reach all portions of the crack front simultaneously also producing a "snapshot" of the crack front. The impacted glass shown in Figure 5.48 is a good example. Notice how the tertiary Wallner lines are *concentric* about the impact sites. The impact not only generated the cracks, but the elastic pulses as well. Figure 6.38 in the next chapter and the front cover of this book show an almost identical example from a fracture that occurred in antiquity. Impact typically results in a ringing within the specimen that may be short lived, but will be long enough to endure for the period a crack traverses through a body. Edgerton and Barstow showed superb examples of these propagating elastic waves in glass in 1941 with their novel ultra-high-speed photographic techniques.[58]

Sometimes chips are formed without impact, i.e., from a static force applied close to an edge. Knappers call this "pressure flaking." The sudden release of stored elastic energy as the chip pops off can cause elastic waves to propagate and these can create concentric tertiary Wallner lines on the edge chip fracture surface.

In contrast, note the primary and secondary Wallner lines in Figure 5.3a and 5.47a. Although at first glance the primary and secondary Wallner lines seem to be concentric, they are in fact not. They actually *cross over each other on top of the origin*. This means they are not tertiary Wallner lines.

A sudden stress relief may create a brief vibration when a crack pops in or propagates. This may be accompanied by an audible snap, but only generates faint elastic pulses so that only a few tertiary Wallner lines form near the origin. Fréchette[1] noted that window panes that are cracked by thermal stresses may have only a few tertiary Wallner lines near the origin and are featureless elsewhere.

A crack running in a plate with an overtaking elastic wave from the rear is shown in Figure 5.49. Although the crack front and the resulting Wallner line have a similar shape, they are not identical. The reader is reminded that Wallner lines do not always create a "snapshot" of the crack front shape. Tertiary Wallner lines are not always formed by pulses arriving from a source so conveniently located as in test pieces studied with ultrasonic fractography. They may come from any direction including from sources that are out of the crack plane.

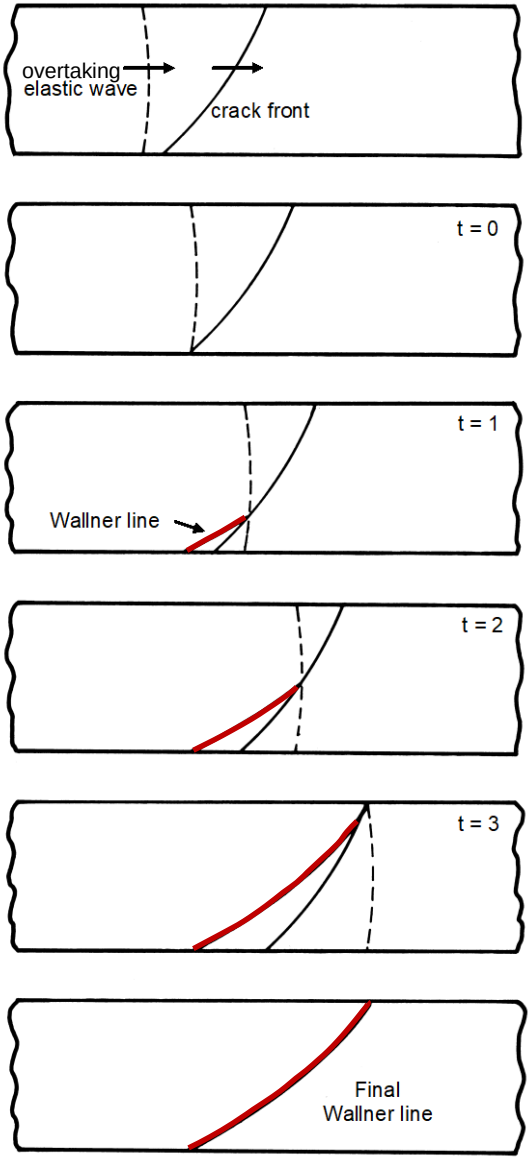

Figure 5.49 *Schematic showing the stages of formation of a tertiary Wallner line for a curved crack front overtaken by an elastic wave from behind the crack. The Wallner line (in red color) has a similar concavity as the crack front, but the lines are different.*

On the other hand, ultrasonic or stress wave fractography[2,6] (discussed in section 3.21) deliberately creates elastic waves to make tertiary Wallner lines on the running crack. The transducer making the elastic pulses is usually mounted on the specimen at right angles to the expected direction of crack propagation thereby taking "snapshots" of the moving crack front's position. Figures 5.50 and 5.51 show some examples from Richter and Kerkhof's work.[2] Local crack velocity can be simply calculated on the basis of the spacing between the lines and the frequency of the pulses. They were able to measure cracks running at terminal velocities in glass with 5 MHz lead zirconium titanate transducers. Their review article[2] has many fascinating examples of the application of this method to study crack front profiles and velocities.

(a)

(b)

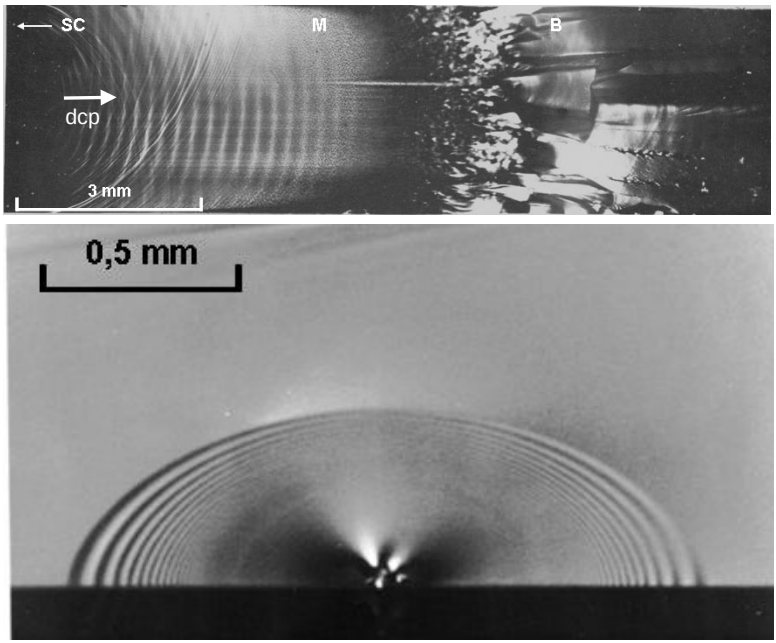

Figure 5.50 *Tertiary Wallner lines from ultrasonic fractography. A transducer created elastic pulses that made "snapshots" of the crack fronts as it propagated through a glass test specimen. (a) is a notched tension specimen loaded to fracture. The crack started at "SC" and ran to the right forming mist at M, and branching at B. The crack reached a terminal velocity of 1540 m/s, a little beyond the tip of the dcp arrow, well before the mist formed. (b) shows an accelerating crack that grew from an indentation flaw in a bend bar. The ellipse shapes are in perfect accordance with fracture mechanics predictions as discussed in section 7.5.3. These two images show how these Wallner lines are wave-like undulations (ripples) on the fracture surface, unlike the sharp arrest lines in Fig. 5.53c shown below. (both courtesy H. Richter)*

(a)

(b)

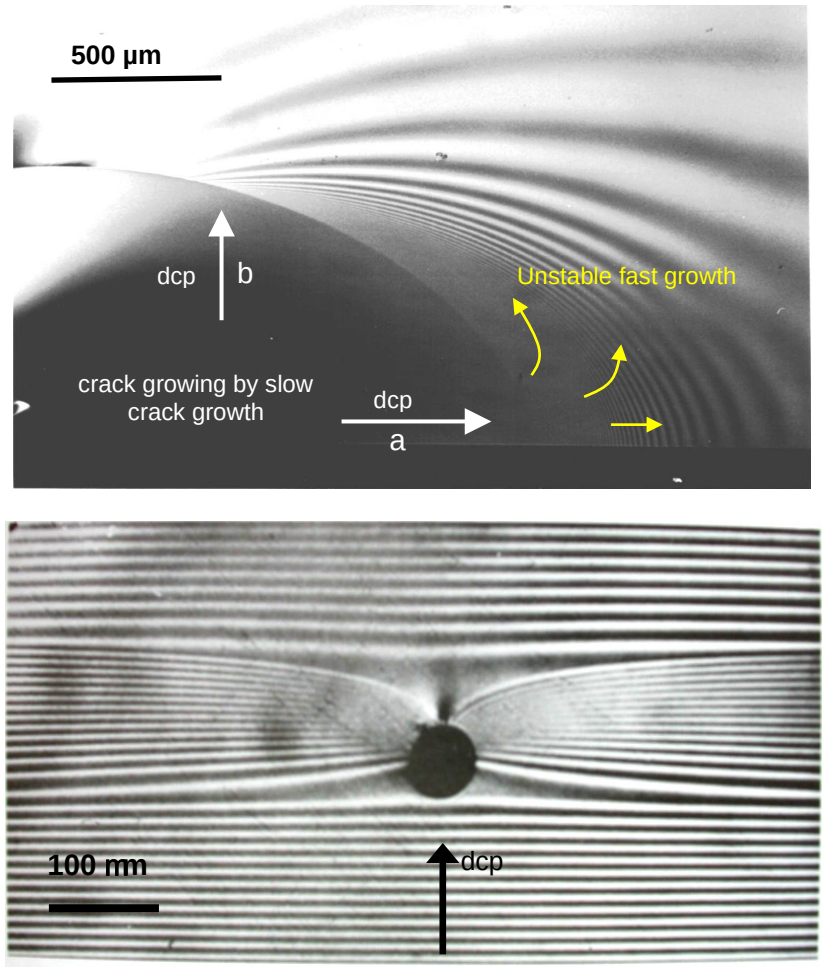

Figure 5.51 *Tertiary Wallner lines examples from ultrasonic fractography.* *(a) shows a surface crack in a bend bar that went unstable from one side when growing by slow crack growth in water. The bending stress field caused the crack to grow faster along the surface (arrow "a") than into the depth (arrow "b"). The crack went unstable on the right side (yellow arrows) and then rapidly fanned out and wrapped around the still slowly-advancing main crack. See also Figure 5.61 for a similar example. (b) shows a crack front approaching a capillary tube void at 60 m/s. The arrow shows the crack propagation direction. The crack locally accelerated to 60 m/s as it approached the hole, but then slowed down to 20 m/s as it passed around it, and then jumped at a faster velocity after passing around the void. (both are from Ref. 2, courtesy of H. Richter)*

5.4.5 Wallner lambda lines

Elastic waves can reflect off free surfaces creating a lambda-shaped line on the fracture surface as shown in Figure 5.52. These are typically formed by primary or secondary Wallner lines. Crack velocity can be calculated from the spacing of the Wallner lines as discussed in section 7.9 and Figure 7.32.

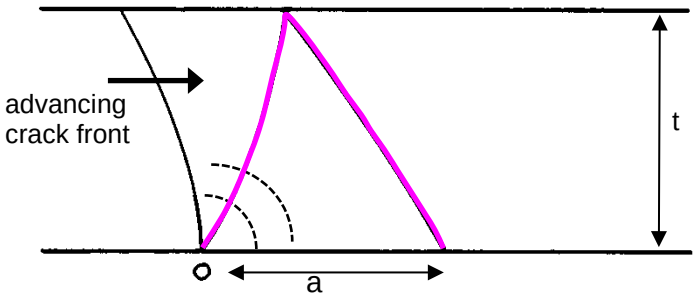

Figure 5.52 *Wallner lambda line mark (colored purple). The schematic shows the advancing crack (thinner black line) encountering a discontinuity at point O. An elastic pulse creates a radiating elastic wave (dashed concentric lines). The intersection of the wave and the advancing crack front creates a primary Wallner line that runs upward to the top surface. When the elastic wave reflects from the opposite surface, the Wallner line continues back downward.*

5.5 Arrest Lines (Interruption marks)

Figure 5.53 shows optical images of arrest lines.

Arrest Line (interruption mark): *A sharp line on the fracture surface defining the crack front shape of an arrested or interrupted crack. Resumed crack propagation occurs under a more or less altered stress configuration.*

This is an adaptation of Fréchette's original definition.[1] His definition included the words "rib mark" as in "rib shaped," but I have taken these latter descriptors out since I have often seen <u>straight</u> arrest lines in thermally-stressed plates. A more general definition seems in order.

(a)

(b)

(c)

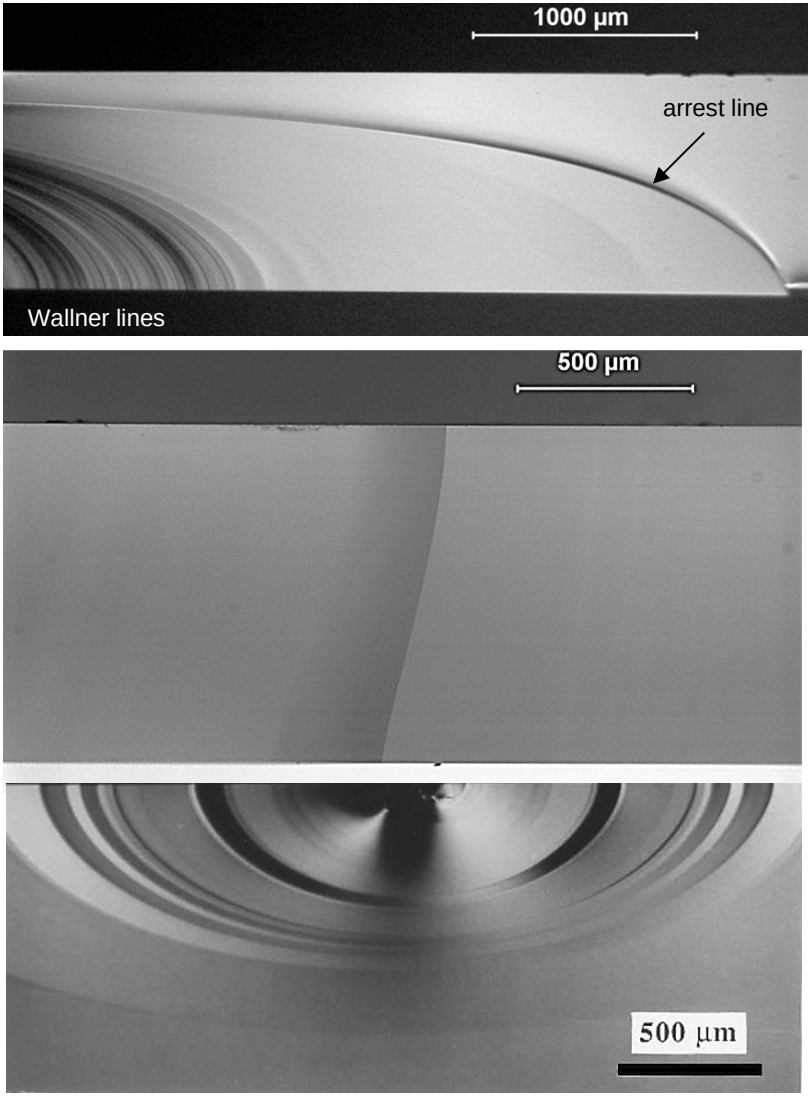

Figure 5.53 *Crack arrest line examples. (a) shows a glass microscope slide broken in bending and the arrest line is on the right (arrow). The lines to the left are primary Wallner lines. Wallner lines are not as sharp as arrest lines. (b) shows an arrest line in a glass slide that broke from thermal stresses. (c) shows concentric arrest lines from repeated cyclic loading of a glass plate in bending. Compare the sharp lines in this photo to the wavy tertiary Wallner lines in Figure 5.50b. (c is courtesy D. Green and is the same as Fig. 5.71).*

One issue that has long plagued the use of the arrest line term has been that it has been used to describe lines that formed even though the crack did not actually come to a full stop. To clarify this matter once and for all, in this 4th edition I have added the words “interruption mark" since it is not necessary for the crack to come to a complete halt. Fréchette also explained this notion in his book.[1] The word "interruption" is appropriate to describe how a propagating crack may be disturbed enough to form a discrete sharp line on a fracture surface. The disturbance to propagation may be the unloading of a crack so that it hesitates, or the direction of stress is suddenly altered. “Dwell mark” is a term sometimes used. In his book, Frechette[1] modified his definition to: “Arrest line (also called dwell mark).” Aldinger and de Haan mentioned a dwell line in passing in their book.[59] ASTM Standard C 1256 referred to “Dwell mark, also called arrest lines.”

Once the crack resumes motion it may be on a slightly different plane, usually in response to a slight change in the axis of principle tension. An abrupt change in the direction of principal tension while the crack is still moving can also create an interruption mark on the fracture surface. In these examples, the arrest lines are bowed in the direction of crack propagation, but there can be exceptions.

Arrest lines are different than Wallner lines in two key respects: arrest lines are sharp, and unlike most Wallner profiles, arrest lines show the crack front profile at an instant in time. Sometimes twist hackle lines will form that lead away from the arrest line if the crack repropagation occurs in a slightly different direction.

Michalske showed that cracks that arrested after slow crack growth sometimes require extra loading to repropagate after aging.[60] The crack tip blunts slightly during the aging, and the crack has to resharpen before repropagation. This process occurs with slight variations along the crack front so that when the crack repropagates there are slight humps and valleys along the crack front and tiny hackle lines leading away from the arrest line.

Concentric arrest lines in ceramics and glasses sometimes bear a resemblance to classical mechanical-fatigue markings in metals, but they are not the same. Classical mechanical fatigue in metals is iterative crack extension by cyclic loading. Repeated loading on a crack causes damage nucleation, accumulation, and stepwise growth in metals. This leaves periodic, spaced striation lines on the fracture surface. This mechanism is not operative in most fine-grained equiaxed-microstructure ceramics and glasses. Section 5.8.5 below has more on mechanical fatigue.

5.6 Scarps

Scarps shown in Figures 5.54 to 5.56 are subtle curved lines on a fracture surface. They can be very difficult to see and often require careful tilting, suitable lighting, patience, and sometimes even a bit of luck to detect. They are caused by interaction of a propagating crack and a liquid or a reactive environment. The liquid can act to retard a crack front or can cause it to accelerate, sometimes in a discontinuous fashion. The scarps mark sudden changes in crack velocities that can occur due to interactions of the crack with

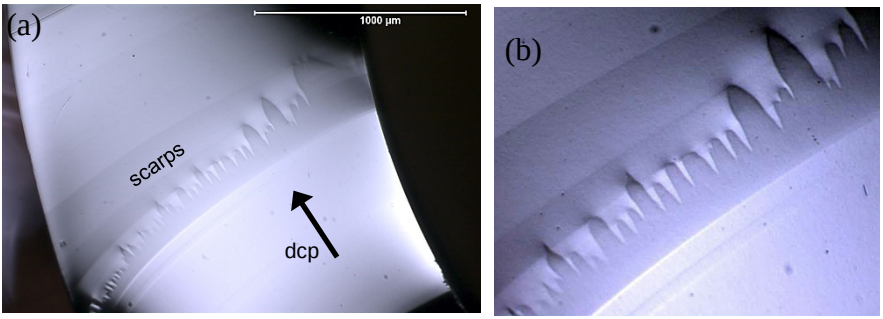

Figure 5.54 *Example of a scarp in a fractured glass medicinal vial. Liquid medicine within the vial was available to help form the scarps when fracture occurred. The arrow shows the direction of crack propagation. (b) is a closeup of (a) with contrast enhanced. Figure 10.10 also shows this vial.*

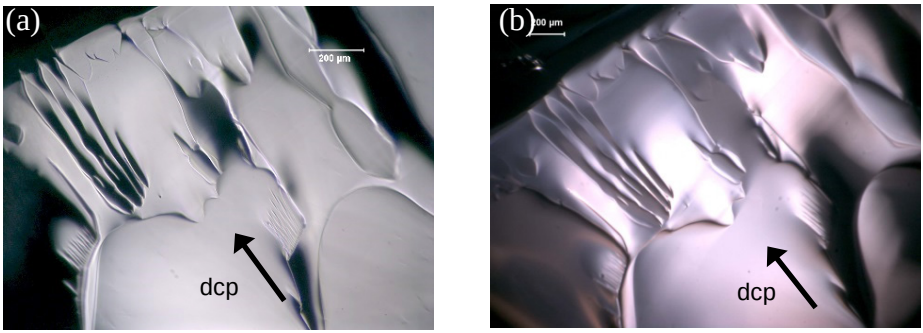

Figure 5.55 *Scarps in a single crystal sapphire hemispherical dome broken by water quench thermal shock. (#1037) The entire dome is shown in Figure 8.21 in the single crystal chapter. The arrows show the direction of crack propagation. (a) is a differential interference contrast optical photo from a compound optical microscope that shows the scarps have height variability. (b) is the same area photographed in a stereo optical microscope. See also Figures 6.32 and 8.21 for images of the scratch fracture origin for this dome.*

liquid. They usually correspond to transitions in the crack tip environment, including changing from wet to dry, dry to wet, humid air to dry air, etc. They even can occur in totally wet environments if the crack accelerates so fast that the viscous liquid cannot keep pace and instead cavitates behind the crack tip. Scarps are usually only detected in glasses and single crystals. Scarps could exist in polycrystalline ceramics, but the inherent roughness from the micro-structure masks their presence. To the best of my knowledge, the scarps that I photographed in Figure 5.55 in sapphire are the only documented cases of scarps in a single crystal or a ceramic. I detected them in two domes.

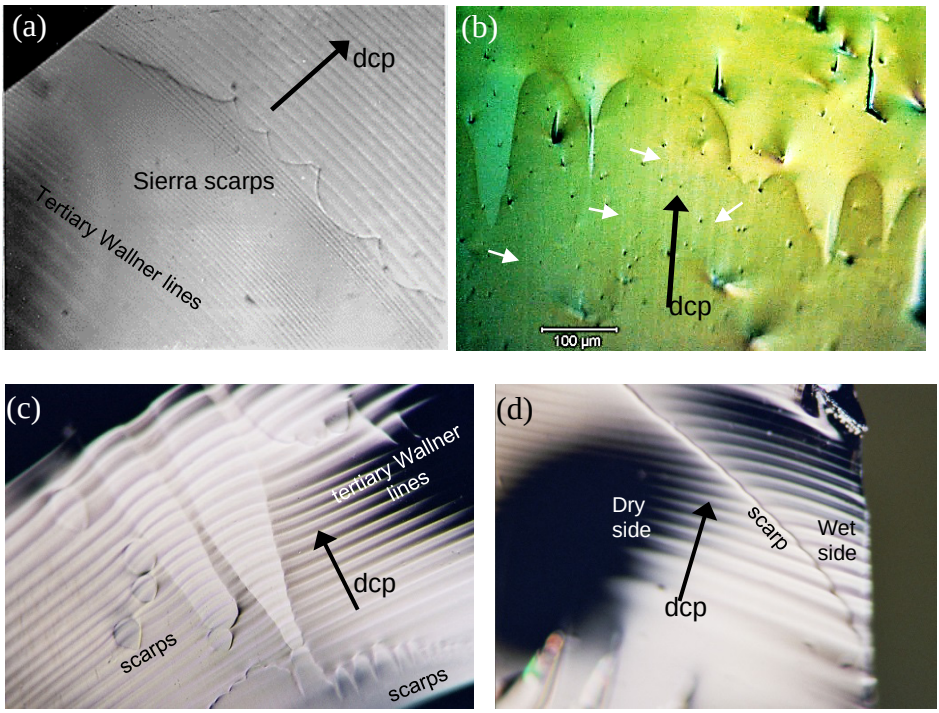

Figure 5.56 *Other **e**xamples of scarps. The large black arrows show the direction of crack propagation. (a) shows Sierra scarps in glass caused by water "fingerlets" overtaking the advancing crack (courtesy E. Beauchamp) (b-d) are obsidian flakes formed by knapping. (courtesy A. Tsirk) The very faint vertical lines within the scarps in (b) a few of which are marked by small white arrows, are either "streaks" or "subcavitation hackle," a precursor to complete cavitation. The parallel bands in (a), (c) and (d) are tertiary Wallner "timing" lines intentionally introduced by vibrations from an engraver (c), or a hand palm sander (c,d) to study the crack velocities. In (d) water that was available from the right side facilitated crack advance causing the scarp.*

The *practical significance* of scarps is that they are evidence that fracture occurred in the presence of a fluid, most commonly water. They also can help confirm the local direction of crack propagation.

Fréchette identified several types of scarps and accounted for their formation.[1] Scarps can vary from as simple as a single faint line across the fracture surface perpendicular to the direction of crack propagation (cavitation scarp), to a complex network of curves such as shown in Figures 5.54 and 5.55. Fréchette called some of these "Sierra scarps" if they are pointed in the direction of crack propagation as shown here and in Frechette's book, (his Figures 2.28 and 2.29) due to their similarity to his favorite mountain range. They form when water in the form of spaced fingerlets as in a Taylor instability overtakes a decelerating dry crack, causing local advances by the crack front.

"Cavitation scarps" occur when an accelerating crack causes void formation or cavitation in the water between the fracture surfaces that is trying to keep up with the crack tip. Once cavitation occurs the crack outruns the fluid water and a scarp line is left behind. The faint vertical lines within the scarps in Figure 5.56b have been described as "subcavitation hackle" by Michalske and Fréchette, who describe it as a microhackle precursor to complete cavitation.[1,61] The faint lines have alternatively been described as "streaks" by Beauchamp, since they may not in fact be steps, but slight perturbations in the crack plane.

Scarps are very subtle and can be very difficult to see. They are easily overlooked. They are best seen in an optical microscope with the specimen tilted to create a mirror-like reflection from the fracture surface. The specimen or the lighting must be tilted back and forth until one catches just the right reflection. They usually exist in only a portion of the specimen and usually where the crack is moving at a slow to moderate speed. Tsirk[35,57,62] studied a variety of scarps in knapped obsidian arrowheads and knives formed by pressure flaking as shown in Figures 5.56b-d. Some of the scarps were generated in antiquity when they chipped during usage. Tsirk has postulated that the shape of scarps may depend upon the nature of the fluid and possibly the viscosity. Scarps that have been observed associated with blood are different from those formed with water or saliva.[35,62] The reader is referred to Fréchette's book[1] and References 35, 57, 60, 62, 63, 64 for details on scarps.

Suratwala recently showed an example of Sierra scarps in a fractured laser phosphate glass (his Fig. 6.3).[65]

5.7 Transgranular and Intergranular Fracture

In addition to finding the fracture origin, in polycrystalline ceramics it is often important to observe whether crack propagation is transgranular and cleaves through grains or is intergranular whereby the crack runs around the grains along grain boundaries. It is usually necessary to have scanning electron micrographs of the fracture surface for this characterization. Figures 5.30b, 5.57, and 5.58 show examples. Sometimes the word *intra*granular is used interchangeably with transgranular, but the former word is not recommended, since it is so similar to *intergranular* that it often creates confusion.

(a)

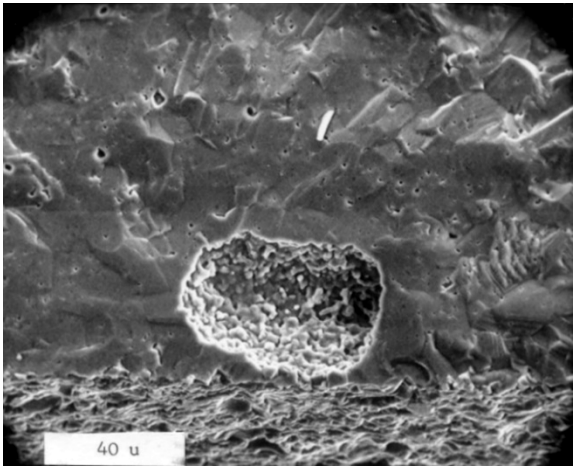

(b)

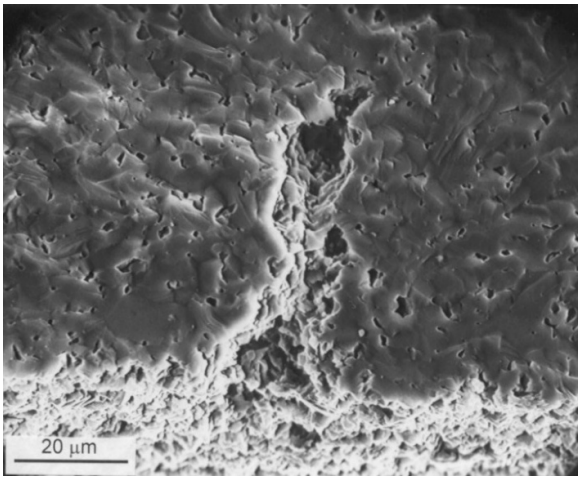

Figure 5.57 *Transgranular fracture examples around fracture origins. (a) is aluminum-oxynitride. Notice the wake hackle triggered by the grain boundaries and some small pores. (b) is a sintered alpha silicon carbide.*

(a)

(b)

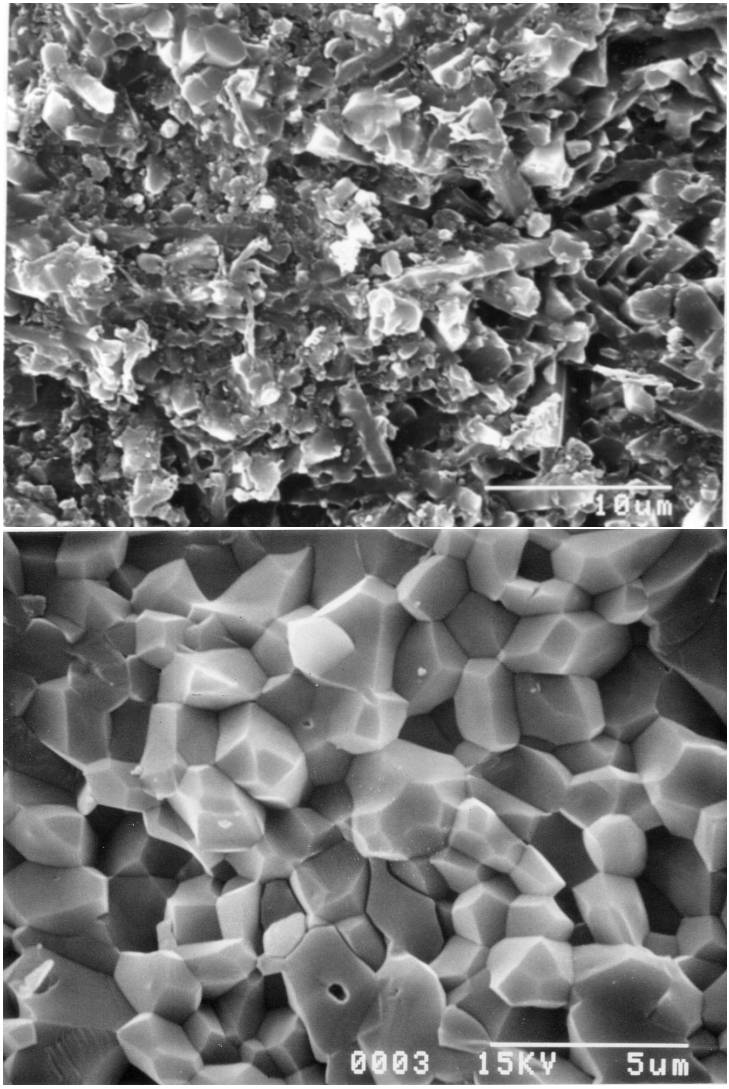

Figure 5.58 *Intergranular fracture surfaces. (a) is an elongated-grain silicon nitride. (b) is a 99.9 % sintered alumina.*

Material scientists are concerned with the mode of propagation since it provides information about how cracks interact with the microstructure. Intergranular fracture may indicate weak boundary strength. It may be a manifestation of between-grain stresses due to elastic or thermal anisotropies, especially in non-cubic ceramics. Mixed inter- and transgranular fracture modes are common. It is customary to make approximations or estimates of the fraction of inter- and transgranular fracture and to show an illustration.

There is clearly some interpretation involved and what may be a 50 % to 50 % mix for one observer might be reported as a 40 % to 60 % mix by another.

Fracture mirrors in polycrystalline ceramics may initially have transgranular fracture but change, to mixed trans- and intergranular fracture as the crack radiates outwards.[40]

Slow crack growth or environmentally-assisted crack growth usually occurs intergranularly. Grain boundaries are weaker than matrix grains and secondary phases or glasses often are distributed along the grain boundaries. There are exceptions, however.

Transgranular fracture though grains often generates twist hackle and/or cleavage steps within the grains as the crack twists and turns to follow preferred cleavage planes within the microcrystals. These markings can be interpreted to evaluate the local direction of crack propagation. Figure 5.36 earlier in this chapter is an example.

5.8 Stable Crack Growth

5.8.1 Slow crack growth (SCG) at ambient temperature

Many glasses, oxide ceramics, and nonoxide ceramics with an oxide sintering aid are susceptible to environmentally-assisted slow crack growth (SCG). The expression “slow crack growth” usually is used in the context of stable crack extension due to combined effects of stress and environment. (It is also commonly used to describe high temperature stable crack extension as described later in section 5.9.3.) Water, either in liquid or as a vapor, is the most common reactive species that causes slow crack growth, although other small polar molecules such as hydrazine (N_2H_4), ammonia (NH_3), and methanol (CH_3OH) can enhance crack growth in silicates.[66,67] Ceramics such as alumina and magnesium fluoride are also susceptible to environmentally-enhanced crack growth. Acetonitrile (CH_3CN) can attack magnesium fluoridate, but not alumina or silica.[66,67] Slow crack growth requires both a stress to open the crack faces and a reactive species to chemically react with the strained atomic bonds at the crack tip. Hence, it is sometime called “stress corrosion cracking.” Figure 5.59 illustrates the leading chemical reaction rate theory for how environmentally-assisted slow crack growth occurs in glasses. Strained atomic bonds at the tip of a crack are attacked by polar molecules such as water causing crack extension. Slow crack growth can lead to weakening and/or time dependent fracture. Slow crack growth is also sometimes called “static fatigue” if the loading is steady or constant. If the stable crack growth occurs while

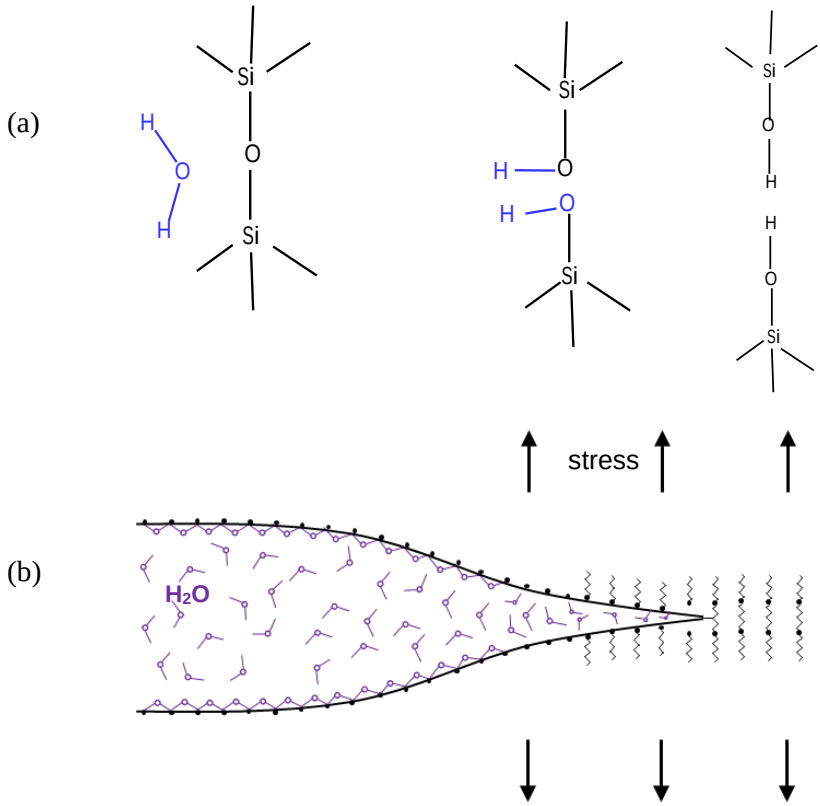

Figure 5.59 *Stress corrosion cracking can cause slow crack growth in glasses. The polar water molecule, either in liquid or gaseous form, attacks strained silicate bonds. (after Michalske, Bunker, and Freiman[66,67])*

loading increases at a constant rate, as in common strength tests, it is sometimes referred to as "dynamic fatigue." All silicate glasses and oxide ceramics are susceptible to slow crack growth. Many other ceramics are too, particularly if they are bonded by a glassy boundary phase, no matter how thin. Covalently-bonded ceramics are not susceptible to SCG at room temperature, unless there is an oxide boundary phase. Section 7.10 has more qualitative information about the mechanics of slow crack growth.

Reference 68 is a review of the chemical reaction rate theory described above for glasses as well as some alternative theories. These theories include plastic deformation at crack tips that can cause sharpening or blunting, diffusion of water along the crack faces, cavity creation ahead of the crack tip, or diffusion through the bulk near the crack tip. Tomozawa and colleagues[69,70] contend that structural relaxation of the glass near the crack tip occurs and this leads to slow

crack growth. The entire matter is complex and is the subject of ongoing studies. The nanostructure and the number of bridging and non-bridging oxygen bonds are important in glasses. A 2009 review paper by Ciccotti[71] summarized things: "The detailed nature of the stress-corrosion mechanisms that occur at the crack tip has been debated for decades. . . . Stress corrosion can involve a complex interplay between the diffusion or reactive molecules (mainly water) into the crack cavity and into the glass network, the corrosion (or dissolution) of the network itself and the migration of weakly bonded alkali ions under chemical or stress gradient. . . . The kernel of the difficulty turned out to be that there are many actors playing in the opera, most of them acting at the nanoscale in a deeply interrelated manner."

Slow crack growth is usually intergranular in polycrystalline ceramics. If the fast, unstable fracture mode is transgranular or mixed, then the difference in propagation morphology may be detectable as a SCG "halo" on a fracture surface as shown in Figure 5.60. SCG halos can often be detected with both optical and SEM microscopy as shown in that figure for the case of a high-purity alumina.[72] Usually the intergranular zone appears darker when viewed with an optical microscope since the rougher surface scatters light in different

Slow crack growth halo: *A region or band around a flaw in a ceramic caused by stable crack extension. The band is caused by changes in the mode of crack propagation.*

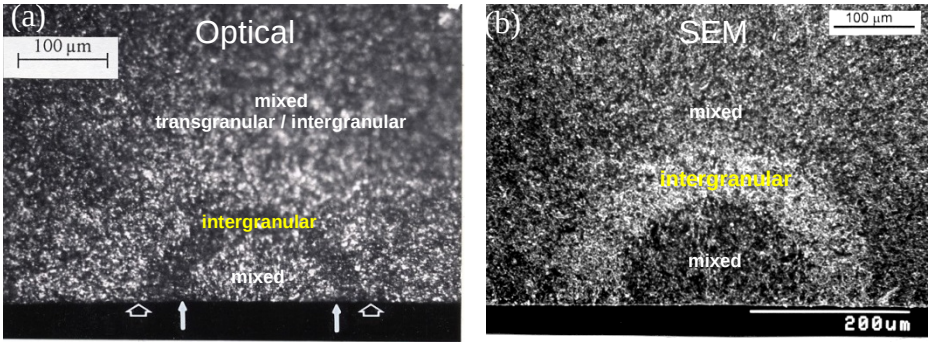

Figure 5.60 *Knoop semicircular flaws in two specimens with SCG "halos" in a sintered 99.9 % alumina. (a) is an optical image of a 29 N Knoop indentation flaw (courtesy J. Swab), and (b) is a SEM image of a 49 N flaw. The precracks are mixed transgranular-intergranular. The halo is mostly intergranular. The fast fracture is mixed transgranular-intergranular. The crack growth occurred in only a few seconds during an ordinary strength test conducted in a lab-air environment.*

directions. In contrast, the slow crack growth zone looks lighter in the electron microscope possibly due to slight charging effects on edges of the intergranularly-fractured grains. Mecholsky[73] showed superb pictures of intergranular slow crack growth (from constant stress-to-fracture tests, "static fatigue") versus transgranular fast fracture in magnesium fluoride. Morrell presented a case of a fractured alumina hip ball with an unusual circular intergranular zone of slow crack growth that appeared shiny in the optical microscope.[74]

(a)

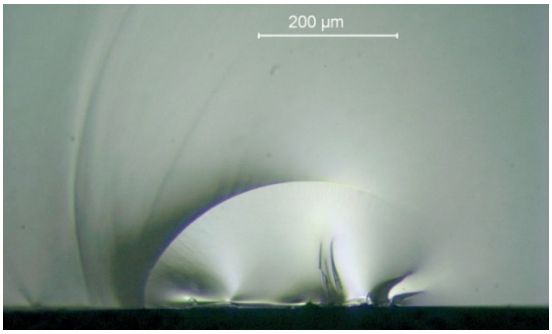

(b)

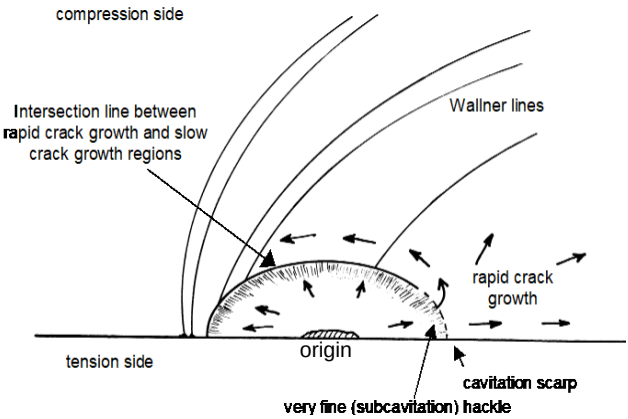

Figure 5.61 *Slow crack growth in glasses sometimes leaves a* <u>*partial*</u> *semielliptical line that approximates the critical crack size. (a) shows an example for a BK-7 glass disk tested in ring-on-ring biaxial flexure in water. It was a "dynamic fatigue" fast fracture strength test with steadily increasing loading until the disk broke at 224 seconds at 85.8 MPa. The original flaw was an 8 µm to 10 µm deep crack from a polishing scratch. It* <u>*grew twenty times*</u> *deeper in the bending stress field and then went unstable along the right side. Only a very faint cavitation scarp exists at that position, but a more distinct line forms around the crack front periphery as the unstable crack wraps around it. (b) shows a schematic of this sequence. See Fig. 5.51 for a similar example.*

The usual remedies to eliminate SCG in laboratory strength testing are to test either at a very fast loading rate or in an inert atmosphere. The SCG halos disappear when testing is done in inert atmosphere.[72]

In glasses a subtle partial elliptical line that sometimes appears on the fracture surface provides a strong clue that SCG has enlarged a flaw as shown in Figures 5.61 and 5.51a.[75,76] The line is a step that forms when the unstable crack wraps around the portion of the crack that has not yet gone unstable.

5.8.2 Stable extension from local residual stress or R-curve effects

Stable crack extension can occur, even in the absence of environmental effects, if a flaw has a strong local residual tensile stresses. Indentation crack flaws made by either Vickers or Knoop indentation are good examples. Damage zones underneath the indentation can provide the tensile stresses that are the driving force for crack extension. As the crack extends away from damage zone and the crack periphery gets larger, the effect of the tensile stresses diminishes, and the crack slows down and arrests in the absence of externally-applied stresses. Alternatively, in fast fracture tests where the specimen is loaded to fracture, there can be momentary stable crack extension of the flaw prior to rupture. Figure 5.62 shows an example of stable crack extension at room temperature due to local residual stresses in a hot-pressed silicon nitride.

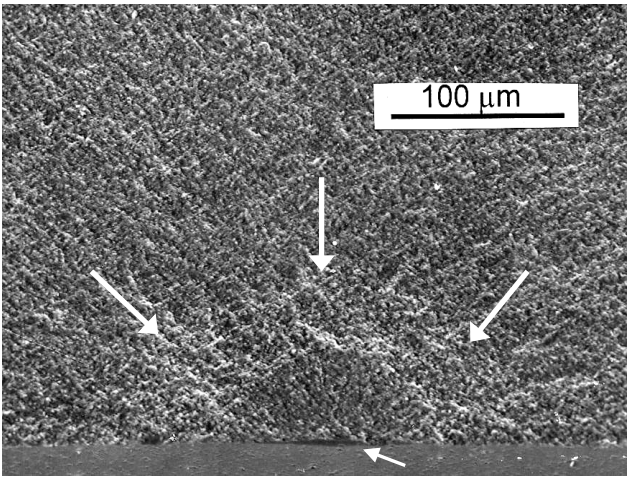

Figure 5.62 *Knoop flaw (dark semiellipse) in silicon nitride showing stable crack extension (large arrows). The local residual stresses underneath the indentation provided the impetus for the extension. Traces of the very shallow, indentation can be seen on the bottom outer surface (small white arrow).*

Rising R-curves, which will be discussed in more detail in chapter 7, can also lead to stable crack extension at room temperature. There is only a small fractographic literature on this effect, in part due to the fact that the amount of stable crack extension prior to a flaw going unstable is often very small.

Stable crack extension from local residual stresses or due to R-curve effects is usually not termed “slow crack growth” in the literature.

5.8.3 High-temperature slow crack growth in ceramics

At elevated temperatures, increased atom mobility and decreases in boundary phase viscosity can lead to intergranular crack growth. This also can cause weakening or time dependent fracture. The environment may or may not play a role in slow crack growth. Figures 5.63 and 5.64 show flaws that have been altered as a result of slow crack growth. The slow crack growth zones are usually rougher than the normal fast fracture surface and are usually easy to detect due to the topography difference in the SEM, or by a topography or reflectivity difference in an optical microscope. Sometimes oxidation of the material in a slow crack zone often causes a color or reflectivity difference that is also easy to detect in an optical microscope. The slow crack growth zones can be very small and may enlarge a flaw just enough to cause it to reach criticality.

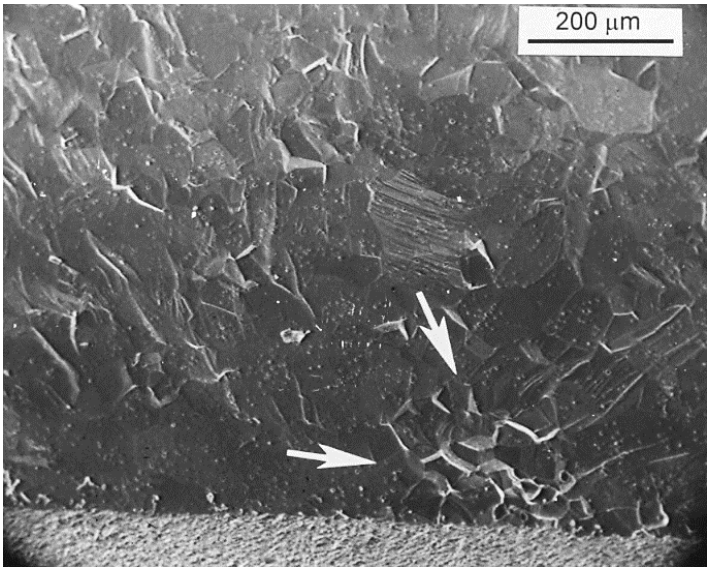

Figure 5.63 *Intergranular slow crack growth in a pure AlON at elevated temperature. The slow crack growth zone (arrows) formed in the short time that was needed to break the specimen in a strength test. (1200° C, 155 MPa)*

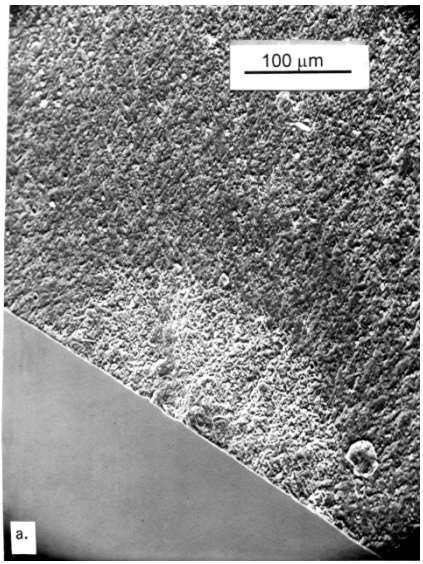

(a)

(b)

(c)

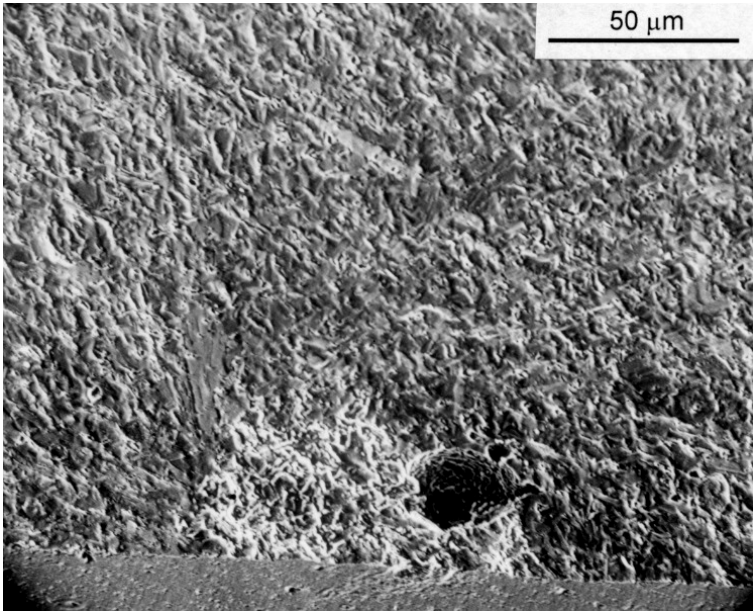

Figure 5.64 *Elevated-temperature slow crack growth in sintered alpha SiC tested in stress rupture at 1400 °C in air (a). The close-up (b) shows the boundary between the intergranular SCG and the transgranular fast fracture zones. (c) shows another alpha SiC specimen wherein the slow crack growth appears to have originated near a pore.*

Alternatively, at lower stresses slow crack growth zones may be very large that can cover as much as one half of a fracture surface as shown in Figure 5.65. In such cases, it often is impossible to locate the initial flaw from which the crack growth occurred.

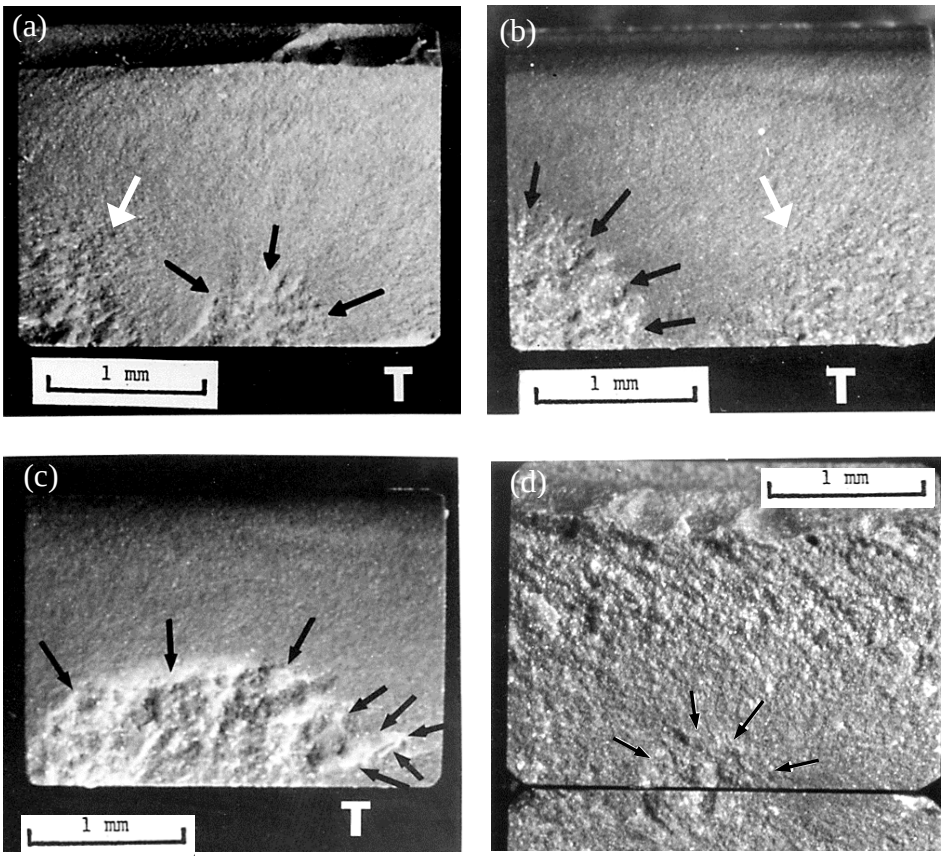

Figure 5.65 *Elevated-temperature slow crack growth zones in hot-pressed silicon nitride. These four bend specimens were tested at 1200 °C in air. The black arrows mark the intergranular crack growth zones, which appear lighter since they have oxidized somewhat, unlike the final fracture regions. Notice the roughness of mirror-like hackle on the left side of (a) and the right of (b) as marked by the white arrows. At low magnification, this roughness could be confused with a slow crack growth zone, but closer examination shows it has directional lines typical of hackle.*

5.8.4 High-temperature creep fracture

Creep can cause fracture at higher temperatures and lower stresses. There is so much boundary phase ductility that sharp flaws are blunted. Fracture is due to the nucleation and growth of cavities and microcracks and their coalescence. Creep fracture surfaces often look like the slow crack growth zones shown above, but with growth zones that extend across a major fraction of the fracture surface. Final rupture frequently occurs from creep crack zones connected to specimen corners. Tensile surfaces often reveal extensive tortuous microcrack patterns. A key difference between slow crack growth and creep fractures is that the former can occur with negligible bulk deformation, whereas the latter inevitably have significant permanent deformations with strains of 1% or more. Figure 5.66 shows several examples.

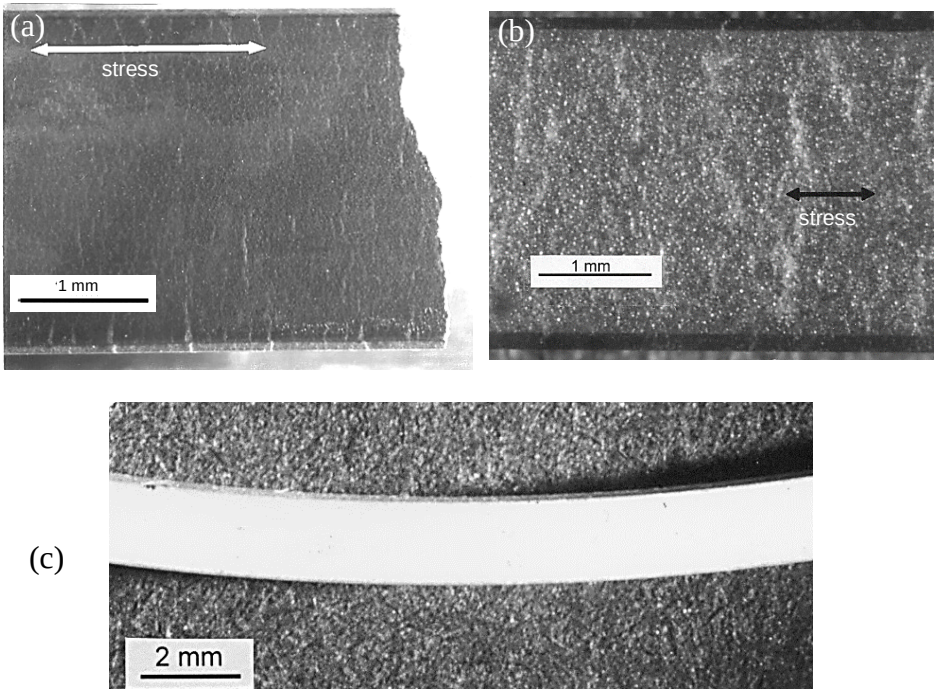

Figure 5.66 *Bend specimens tested under creep fracture conditions. (a) shows the tensile surface of a hot-pressed silicon nitride specimen. Notice the extraordinarily rough fracture surface on the right side of (a). (b) shows the tensile surface of a siliconized silicon carbide specimen. Note that the microcracking is perpendicular to the axis of tensile stresses (double arrow). (c) shows a side view of a silicon nitride bar tested in creep fracture conditions. The surface has oxidized to a white color and the bar has a lot of deformation!*

Figure 5.67 illustrates the differences between slow crack growth and creep fracture. Glassy boundary phases such as shown in Figure 5.68 on the next page usually account for both processes.

Slow crack growth occurs from preexistent flaws that grow until they reach a critical condition. Fracture toughness at elevated temperature is often greater than at room temperature due to the onset of some plasticity. Hence, critical flaw sizes can actually be much larger at elevated temperature than at room temperature. Specimens that fail from slow crack growth have negligible (< 0.2 %) permanent strain.

Creep fracture on the other hand usually does not involve the initial flaws. It blunts them. Voids and microcracks are nucleated, then coalesce, and then grow leading to rupture. Creep fracture specimens have considerable permanent strain at fracture. Failure is more a matter of accumulation of damage. The intergranular crack growth zone on creep fractured bend bars often extends over 33 % or more of the fracture surface.

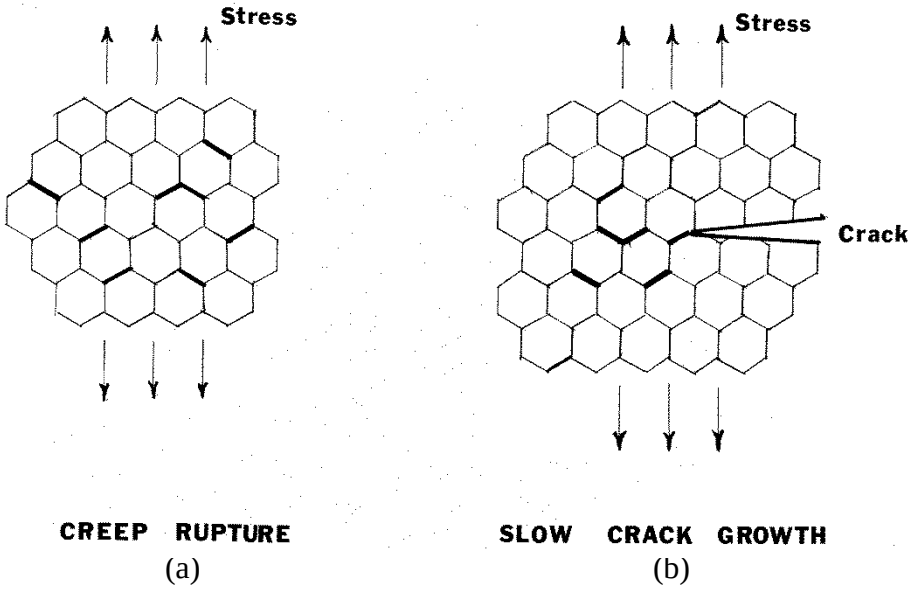

Figure 5.67 *Creep fracture and slow crack growth usually are intergranular at high temperature. In creep fracture (a), cavitation and microcrack nucleation occur throughout the body. In slow crack growth (b), the processes are confined to the immediate vicinity of the crack tip region.*

(a)

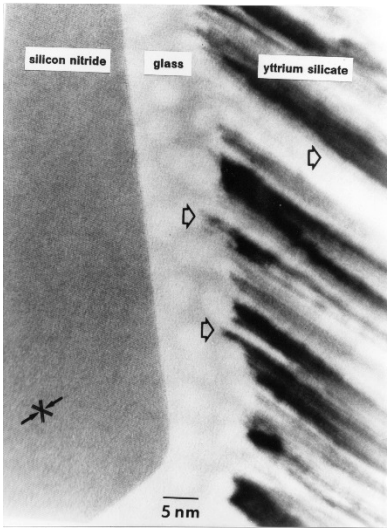

(b)

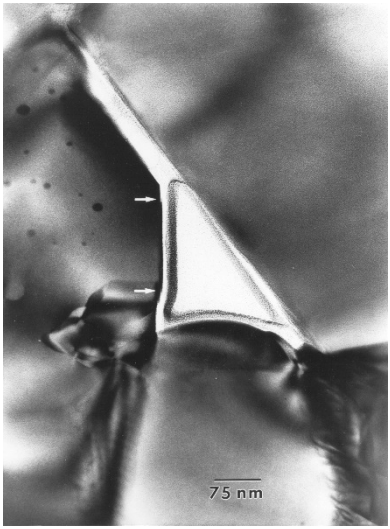

(c)

Figure 5.68 *Transmission electron microscopy images show the glassy boundary phase that often is the source of intergranular slow crack growth and creep crack growth. (a) shows the boundary phase which has partially devitrified in a silicon nitride with a yttrium aluminosilicate glass sintering aid. There still is a thin glassy layer that led to SCG and creep fracture. (b) shows a creep cavity opening up at a triple-grain junction. (c) shows strain sworls (black arrows) from grain boundary sliding. (Ref. 77, photos courtesy W. Braue).*

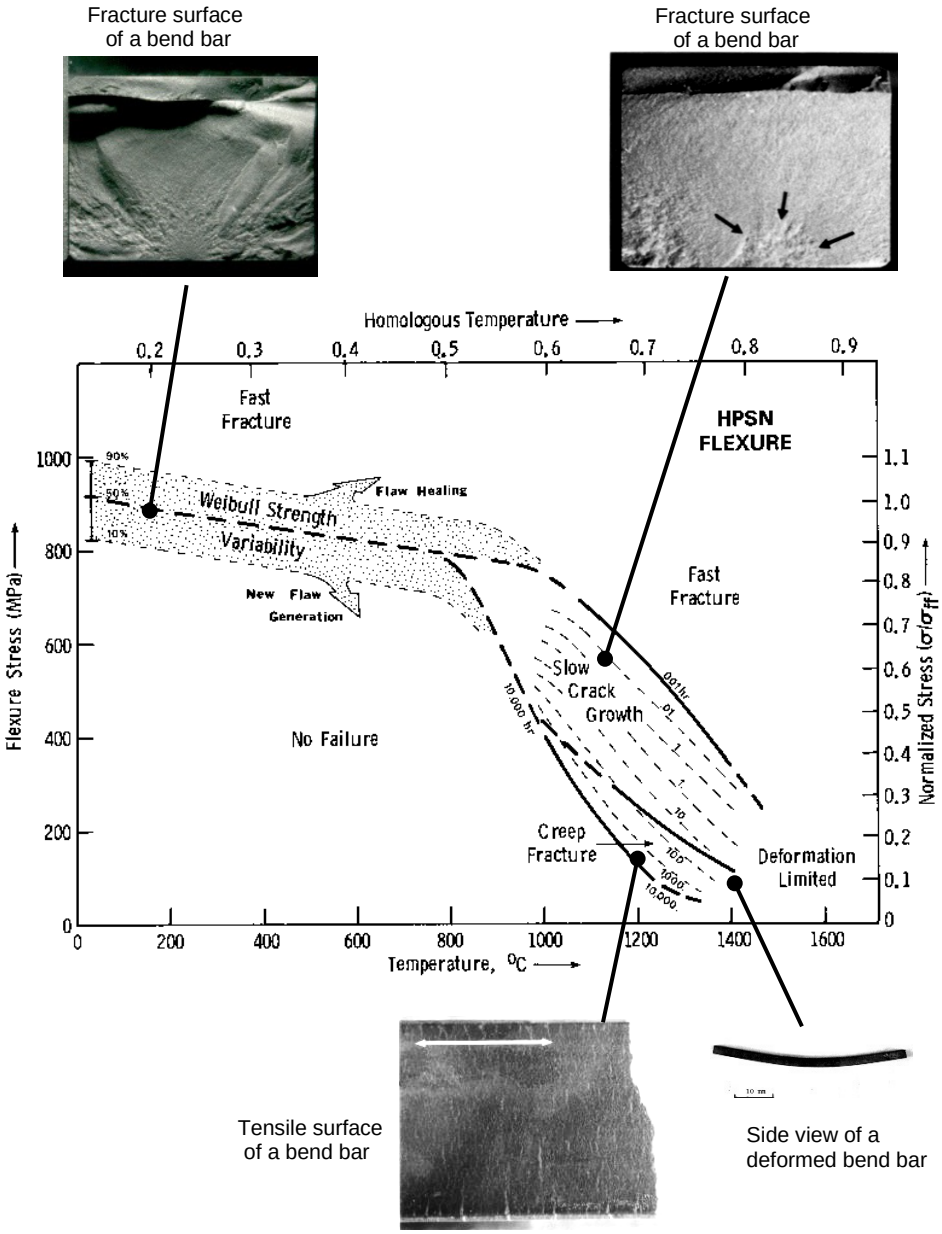

Figure 5.69 *Fracture mechanism map for hot-pressed silicon nitride from Reference 78. This map is for flexurally-loaded specimens. Five hundred and fifty tests were conducted to make this map. The thin dashed lines are times to failure in hours. Failures occurred at times as long as 15,000 hours.*

Figure 5.69 is a fracture mechanism map that puts these pheneomena into context.[78] It summarizes results from hundreds of tests with failure times from seconds to 15,000 hours. It is for a commercial silicon nitride hot-pressed with about 1 mass % magnesium oxide. The sintering aid reacted with silica on the surface of the starting powders and formed a very thin silicate boundary phase glass. Depending upon the stress and temperature, flexural specimens fractured from any one of several mechanisms. At low temperature, material and grinding flaws controlled strength. At moderate temperatures in an oxidizing environment, flaws either remained unchanged and controled strength, or they healed or blunted causing some strengthening. On the other hand, oxidation sometimes created pit flaws that weakened the body. At 1000ºC and greater, integranular slow crack growth caused flaw growth and eventual fracture in times shown in hours on the dashed lines. At low stresses and high temperature, creep fracture controlled lifetime.

5.8.5 Mechanical fatigue from cyclic loading

Fine-grained ceramics and glasses are usually not susceptible to classical mechanical fatigue, in the sense of stepwise stable crack growth from accumulated mechanical damage from repeated loading and unloading. Figure 5.70 shows classical metal fatigue markings that are called “fatigue crack striations.” (The whole fracture surface was shown in chapter 3 as Figure 3.21.) It is exceedingly rare to see genuine fatigue bands like this on ceramic fracture surfaces. In metals, each band-arc line may correspond to a number of loading cycles during which a damage process may occur, leading to one crack jump forward and then arrest. The process repeats with additional cycling until the part breaks.

With ceramics and glasses, if lines like these are observed, they are more likely to be simple arrest lines from iterative loading such as shown in Figure 5.71 which is from Reference 79. The lines are visible due to slight variations in the crack plane between loading cycles. Incremental crack growth during cyclic loadings might be simply due to the accumulated effect of the slow crack growth phenomena described in section 5.8.1. Evans showed another good example in glass.[80] Richter[81] showed a good example for alumina hip replacement balls that were tested to failure in the laboratory.

The fracture surfaces of laboratory test coupons (e.g., tension or bend bar specimens), even if they do fracture from fatigue cycling, will often not show such markings. The initial flaws grow a small amount before they go unstable because fatigue often occurs only for specimens that are loaded near the fast fracture strength.

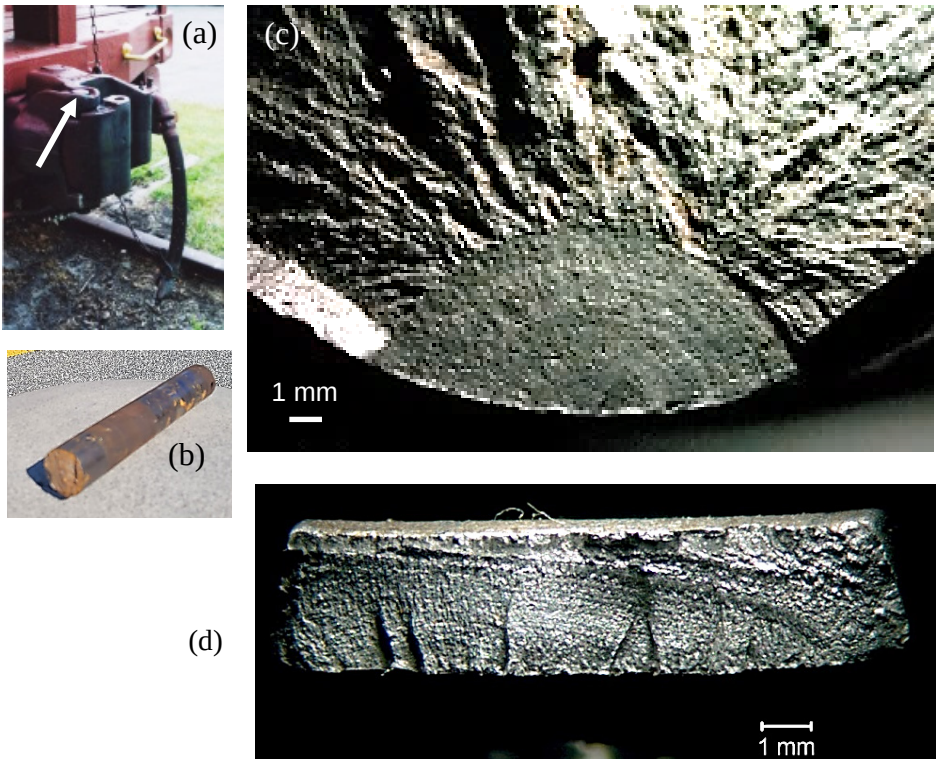

Figure 5.70 *Classic metal fatigue striations in (a-c,) a steel railroad coupler pin (see also Fig. 3.21). The broken 40 mm diameter piece was about 175 mm long. (d) is an aluminum bicycle bracket. A striation arc line does not necessarily correspond to one loading cycle.*

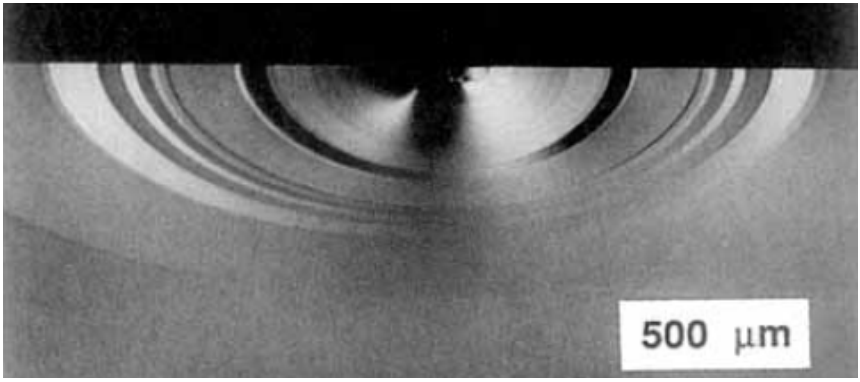

Figure 5.71 *Concentric* <u>*arrest lines*</u> *in a plate of soda lime silica that was cyclically loaded in flexure. The lines are due to slight variations in the crack growth planes on each loading cycle. (courtesy of D. Green)*

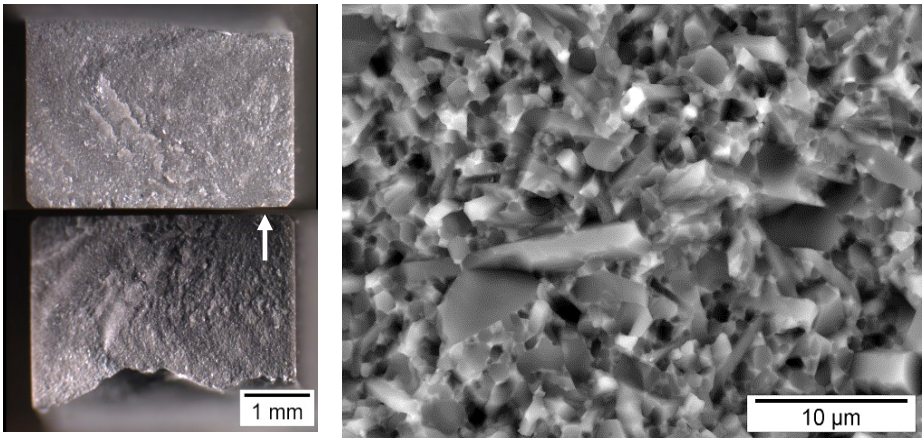

(a) (b)

(c)

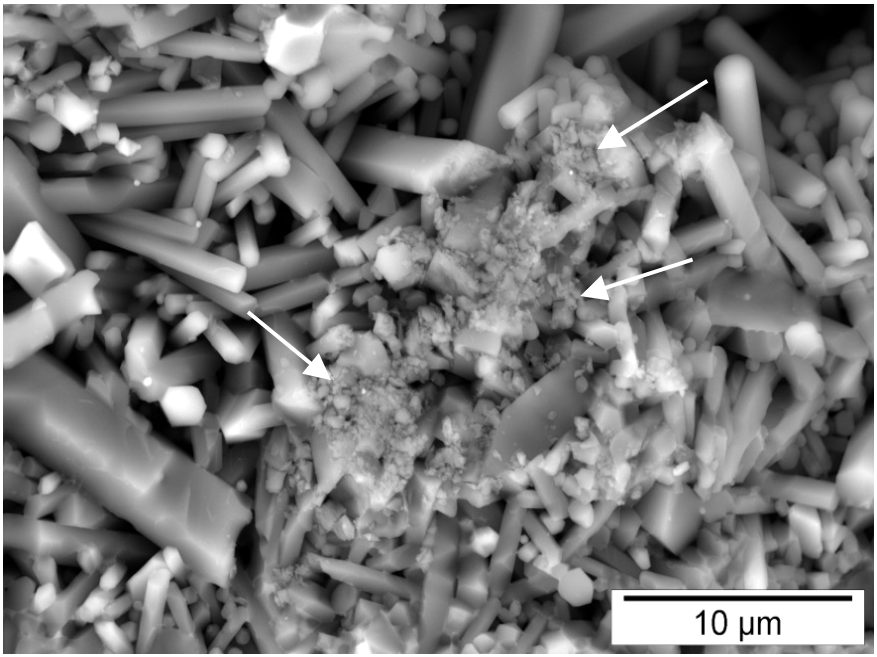

Figure 5.72 *Bend bar that was tested to fracture in cyclic fatigue loading. The material was a yttria and alumina additive sintered silicon nitride with an elongated grain structure for enhanced fracture toughness. (a) shows the bend bar fracture surfaces with the origin marked by the arrow. (b) shows a typical fast fracture portion of the fracture surface. There is no debris. (c) shows the origin region and fine debris (arrows) created by fatigue cycling. (ref. 82, images courtesy T. Lube and R. Danzer)*

On the other hand, polycrystalline ceramics having coarse-grained or elongated-grain microstructures and anisotropic properties may be susceptible to fatigue crack growth as shown in Figure 5.72. This is a curious tradeoff: the enhanced fracture toughness of an elongated-grain ceramic may be offset to some degree by increased vulnerability to mechanical fatigue. Unfortunately, the microstructure creates rough fracture surfaces such that it is difficult or impossible to discern evidence of progressive crack extension.

One subtle, but effective sign of genuine fatigue damage cyclic, is *small debris particles* on the fracture surfaces of polycrystalline ceramics such as shown in Figure 5.72, which are from Reference 82. The debris is small and detectable only in the SEM. The backscatter mode may help detect such debris. The fine debris can occur if the loading entails cyclic *tension and compression,* (e.g., the R factor, which is the ratio of the maximum stress to the minimum stress, is negative.) Dislodged or fractured grains near the crack tip may be crushed between the crack faces as the crack faces go into compression. The debris may or may not be present if the crack is loaded in cyclic tension-tension (e.g., the R factor is zero or positive). One suspects that too zealous a cleaning of a fracture surfaces beforehand might be harmful! On the other hand, it is possible that the crushing may help the debris adhere to the fracture surface and a light cleaning will not necessarily remove it.

5.9 Organizing all the Information – Fractographic Montages

Some component fracture analyses are complex, and an origin site may not be immediately obvious. In such cases, the entire fracture surface may be examined with the goal of observing the local directions of crack propagation. Wake hackle, gull wings, Wallner lines or arrest lines as described in this chapter provide such clues. A map of the overall fracture surface can be constructed in the form of a large montage, around which key local closeup photos of the crack propagation directions can be marked. Little arrows labeled “dcp” can then be put on the overall image. The localized direction of crack propagation can be “backtracked” to an origin site that might not have been immediately obvious. Ko showed marvelous montage examples for an alumina that broke from fatigue loading.[53] There were many tiny wake hackle lines from microporosity in an otherwise rough fracture surface. The tiny wake hackle lines were used to back track to the origin.

A good example is Figure 5.73 for an alumina dental crown which split into two pieces in a patient’s mouth. It was a relatively low energy fracture that created only two pieces. The core ceramic microstructure was not easy to interpret, but there were enough markings in it and the outer veneer porcelain

layer that it became obvious that fracture started at a margin. A fracture montage like this also has great value in communicating a failure analysis. It illustrates how much work has gone into an analysis, and it can also provide context. It can be much more effective in convincing a client or reader than merely showing a handful of closeup photos and relying on the client to trust the fractograpgher's judgement. Montages may also be used to integrate fractographic information with mechanical property test data such as a Weibull graph as shown in Section 6.19 and Figure 6.103 in the next chapter.

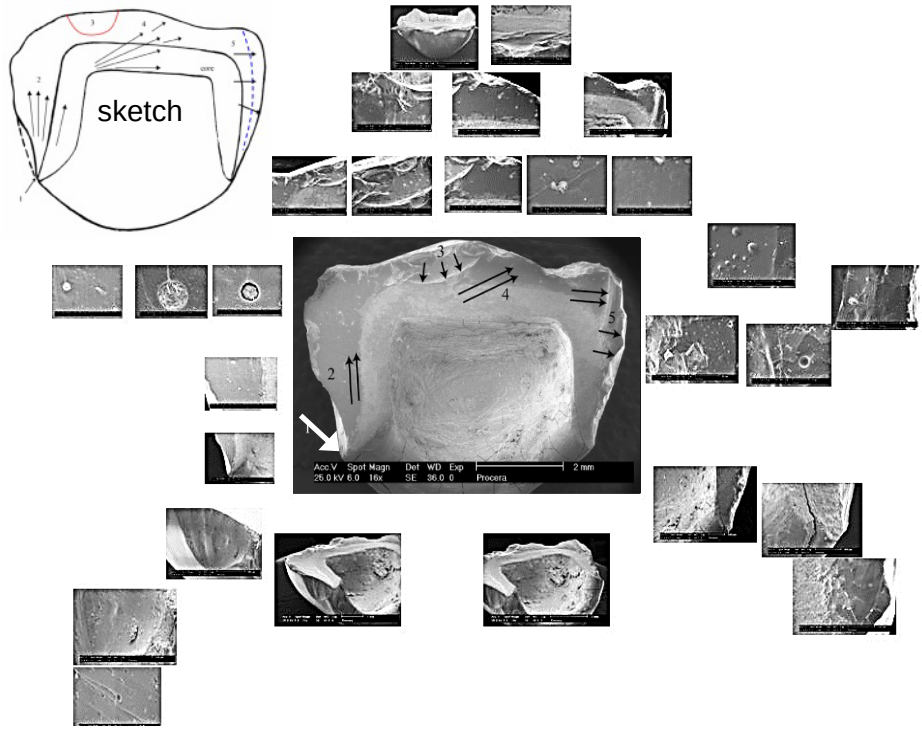

Figure 5.73 *A fractographic montage that integrates a lot of local information into a global interpretation. This was a broken Procera alumina dental crown. The photos are too small here to see the important details. The point here is to show how a montage can be created to organize the photos and information. The local photos are organized in a systematic manner around the overall image that provides context and location information. The white arrow is the fracture origin. Closeup photos and the actual fracture origin are presented as Figures 10.24 and 10.25 at the end of this book as the Procera alumina molar crown, Case 11 in Chapter 10. (courtesy of S. Scherrer)*

5.10 Specimen size effects on fractographic analysis

The specimen size can affect one's ability to interpret a fracture surface. This section is new to this 4th edition. The size effects are of several types. Sometimes it is due to looking at the specimen with too high a magnfication, and sometimes it is simply due to the fact that the specimen cross section is too small.

For example, surface roughness in coarse-microstructure or porous ceramics can mask or obscure the classic markings such as fracture mirrors, hackle lines, or Wallner lines. Figure 5.74 illustrates the problem. If one dives in and examines the fracture surface at "too close a distance" one may be "lost in the trees and not see the forest." Stepping back at lower magnifications can reduce the surface roughness appearance and make the fracture surface more interpretable. Good examples for coarse hackle lines were in section 5.3.1.

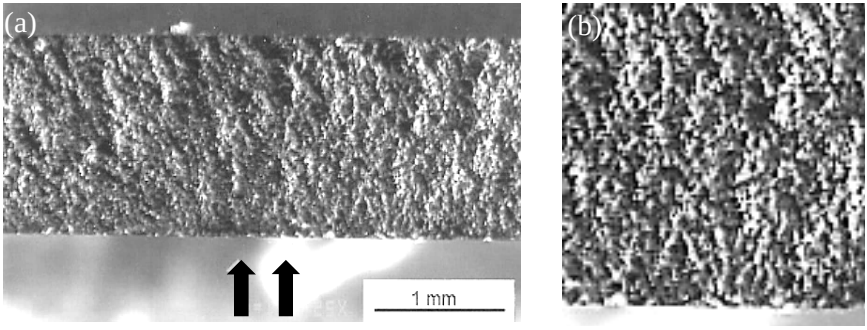

Figure 5.74 *Rough fracture surface of a ceramic membrane disk (same as Fig 5.28a). The coarse microstructural hackle leads one back to the origin area marked by arrows. (b) is a closeup from the right side of the same photo. It is difficult to see any pattern. One must have a large enougth cross section size as in (a) to be able to discern the coarse microstructural hackle.*

Other examples include broad Wallner lines as shown in Figure 5.44 that stand out more clearly at <u>low</u> magnifications. The wake hackle shown in Figure 5.31 also stand out at low magnifications. In these cases, the features may not be recognizable at all in small specimens. Markings may be difficult to detect in extremely thin pieces. This is a problem with modern thin glass cover sheets for cellphones or display panels.

Another situation arises for fracture mirrors. Their size is determined by the stress at fracture. Figure 5.75 shows fracture surfaces in tension specimens of the <u>same cross section</u> size. A high-strength material has a small fracture

mirror that is fully-contained on the fracture surface. A medium strength material has a larger mirror size with just a portion of boundary. Low-strength specimens may show no boundary features on the fracture surface. Although the illustration shows a tension specimen, the same issue pertains to flexural failures. Low-strength specimens will have no fracture mirror boundary.

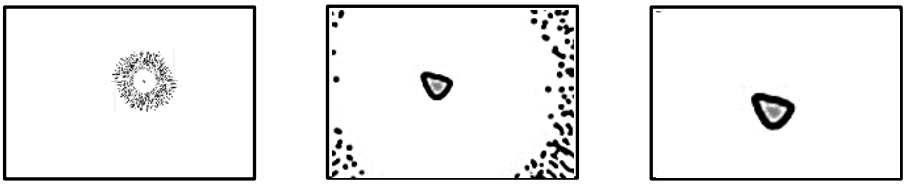

high strength (a) | medium strength (b) | low strength (c)

Figure 5.75 *Fracture mirror sizes vary with strength. The three specimens have the same overall cross section size but the origin flaw size varies from small on the left (a) to large on the right (c). The fracture mirror is easy to discern in the high-strength specimen. In the low strength specimen, the boundary lies beyond the physical confines of the piece.*

Alternatively, Figure 5.76 shows tension specimens with <u>identical strengths</u> but <u>different cross section sizes</u>. The fracture mirror size is constant. The fracture surface for the large specimen (a) reveals the entire fracture mirror and its boundaries. The smallest specimen (c) barely reveals the mirror boundary. Fractographic analysis is easier in (a) than in (c).

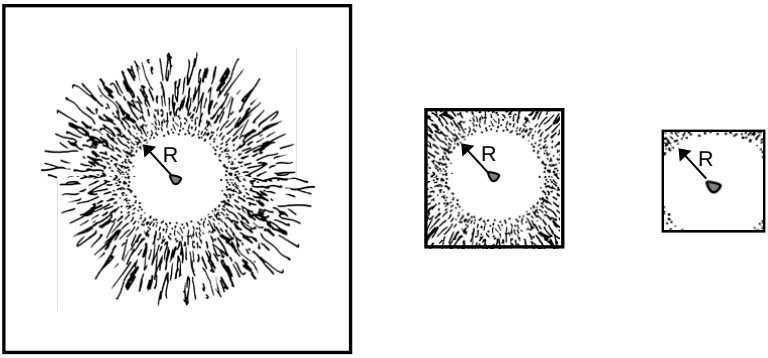

large sized specimen (a) | medium sized specimen (b) | small sized specimen (c)

Figure 5.76 *Fracture surfaces of three specimens with identical strengths and fracture mirror radii, R.*

Chapter 5 References

1. V. D. Fréchette, *Failure Analysis of Brittle Materials*, Advances in Ceramics, Vol. 28, American Ceramic Society, Westerville, OH, 1990.
2. H. G. Richter and F. Kerkhof, "Stress Wave Fractography," pp. 75 – 109 in *Fractography of Glass*, eds., R. C. Bradt and R. E. Tressler, Plenum, NY, 1994.
3. H. G. Richter, "Fractography of Bioceramics," pp. 157 – 180 in *Fractography of Advanced Ceramics*, ed. J. Dusza, *Key Engineering Materials*, **223** (2002) Trans Tech Publ. Switzer.
4. J. E. Field, "Brittle Fracture: Its Study and Application," *Contemporary Physics*, **12** [1] (1971) 1 - 31.
5. F. P. Bowden, J. H. Brunton, J. E. Field, and A. D. Hayes, "Controlled Fracture of Brittle Solids and Interruption of Electrical Current," *Nature*, **216** (1967) 38 - 42.
6. A. Smekal, "Procedures for the Measurement of Fracture Propagation Velocities on Fracture Surfaces," *Glastechn. Ber*., **23** [3] (1950) 57 – 67.
7. C. Brodmann, *Nachrichten von der Gessellschaft der Wissenschaften zu Göttingen, Mathematisch-Physikalische Klasse*, **1** (1894) 44 - 58.
8. G. D. Quinn, "On the Terminal Velocity of Cracks in Glasses," *Int. J. Applied Glass Technol.*, **10** [1] (2019) 7 - 16.
9. N. F. Mott, "Fracture of Metals: Theoretical Considerations," *Engineering*, **16** (1948)16–18.
10. D. K. Roberts and A. A. Wells, "The Velocity of Brittle Fracture," *ibid*, **178** (1954) 820-21.
11. J. J. Gilman, "Propagation of Cleavage Cracks in Crystals," *J. Appl. Phys.*, **27** [11] (1956) 1262 – 1269.
12. E. H. Yoffe, "The Moving Griffith Crack," *Phil. Mag*., **42** [330] (1951) 739 – 750.
13. J. W. Johnson and D. G. Holloway, "On the Shape and Size of the Fracture Zones on Glass Fracture Surfaces," *Phil Mag*., **14** (1966) 731 - 743.
14. A. B. J. Clark and G. R. Irwin, "Crack-Propagation Behaviors," *Exp. Mech*., **6** (1966) 321 – 330.
15. J. Congleton and N. J. Petch, "Crack-Branching," *Phil. Mag.*, **16** (1967) 749 – 760.
16. H. P. Kirchner and J. W. Kirchner, "Fracture Mechanics of Fracture Mirrors," *J. Am. Ceram. Soc.*, **62** [3-4] (1979) 198 – 202.
17. H. P. Kirchner and J. C. Conway, "Criteria for Crack Branching in Cylindrical Rods: I, Tension, and II, Flexure, " *J. Amer. Ceram. Soc.*, **70** [6] (1987) 413 – 425.
18. H. P. Kirchner, "Brittleness Dependence of Crack Branching in Ceramics," *J. Am. Ceram. Soc.*, **69** [4] (1986) 339 – 342.
19. W. Döll, "Investigations of the Crack Branching Energy," *Int. J. Fract.*, **11** (1975)184–186.
20. Y. L. Tsai and J. J. Mecholsky, Jr., "Fracture Mechanics Description of Fracture Mirrors Formation in Single Crystals," *Int. J. Fract.*, **57** (1992) 167 – 182.
21. E. K. Beauchamp, "Mechanisms of Hackle Formation and Crack Branching," pp. 409 – 446 in *Fractography of Glasses and Ceramics III*, eds., J. Varner V. D. Fréchette, and G. D. Quinn, Ceramic Transactions, Vol. 64, American Ceramic Society, Westerville, OH, 1996.
22. E. K. Beauchamp, "Fracture Branching and Dicing in Stressed Glass," Sandia Laboratories Research Report, SC-RR-70-766, Jan. 1971.
23. E. Gölz, "Übermikroskopische Feinstructuren an Glassbruchflächen," (Ultramicroscopic Fine Structures on Glass Fracture Surfaces), *Zeitschrift Physik*, **120** (1943) 773 – 777.
24. E. F. Poncelet, "The Markings on Fracture Surfaces," *J. Soc. Glass Technol*., **42** (1958) 279T – 288T.
25. Von Klaus Peter, "Mikro- und Makrostrukturen der Glasbruchfläche im Elektron-mikroskop." *Glastechn. Ber.*, **41** [11] (1968) 442 – 445.

26. J. W. Johnson and D. G. Holloway, “Microstructure of the Mist Zone on Glass Fracture Surfaces,” *Phil. Mag.*, **17** (1968) 899 – 910.
27. D. Hull, Chapter 5, in *Fractography, Observing, Measuring and Interpreting Fracture Surface Topography*, Cambridge Univ. Press., Cambridge, 1999.
28. L. B. Freund, *Dynamic Fracture Mechanics*, Cambridge Univ. Press, NY, 1990.
29. P. Gupta, D. Inniss, C. Kurkjian, and Q. Zhong, “Nanoscale Roughness of Oxide Glass Surfaces,” *J. Non. Cryst. Sol*., **262** (2000) 200 – 206.
30. J. F. Poggemann, A. Goss, G. Heide, E. Rädlein, and G. H. Frischat, “Direct View of the Structure of a Silica Glass Fracture Surface,” *J. Non. Cryst. Sol*., **281** (2001) 221- 226.
31. S. M. Wiederhorn, J. M. López-Cepero, J. Wallace, J-P. Guin, and T. Fett, “Roughness of Glass Surfaces Formed by Sub-critical Crack Growth,” *J. Non. Cryst. Sol*., **353** (2007) 1582 – 1591.
32. G. Pallares, F. Lechenault, M. George, E. Bouchaud, C. Ottina, C. Rountree, and M. Ciccotti, “Roughness of Oxide Glass Subcritical Fracture Surfaces,” *J. Amer. Ceram. Soc.*, **101** [6] (2018) 1279 – 1288.
33. J. A. Kies, A. M. Sullivan, and G. R. Irwin, “Interpretation of Fracture Markings,” *J. Appl. Phys*., **21** (1950) 716 – 720.
34. A. Smekal, “Zum Bruchvorgag bei Sprödem Stoffverhalten unter Ein- und Mehrachsigen Beanspruchungen,” *Osterr. Ing. Arch*., **7** (1953) 49 - 70.
35. A. Tsirk, *Fractures in Knapping*, Archeopress, Oxford, UK, 2014 (pages 70 - 73.)
36. E. K. Beauchamp, “Crack Front Stability and Hackle Formation in High Velocity Glass Fracture,” *J. Amer. Ceram. Soc*., **78** [3] (1995) 689 - 697.
37. K. Gopalakrishnan and J. J. Mecholsky, Jr., “Quantitative Fractography of Mixed-Mode Fracture in Soda Lime Silica Glass,” *J. Am. Ceram. Soc.*, **95** [11] (2012) 3622 - 3627.
38. K. Gopalakrishnan and J. J. Mecholsky, Jr., “Quantitative Fractography of Mixed-Mode Fracture in an R-curve Material,” *J. Mat. Sci.*, **48** (2013) 7081 – 7087.
39. E. Sommer, “Formation of Fracture ‘Lances’ in Glass,” *Eng. Fract. Mech.*, **1**(1969)539-546.
40. R. W. Rice, “Fracture Topography of Ceramics,” pp. 439 – 472 in *Surface Interfaces of Glasses and Ceramics*, eds., V. Fréchette, W. LaCourse, V. L. Burlick, Plenum, NY, 1973.
41. R. W. Rice, “The Difference in Mirror-to-Flaw Size Ratios Between Dense Glasses and Polycrystals,” *J. Am. Ceram. Soc*., **62** [9-10] (1979) 533 – 535.
42. D. Lewis, III and J. R. Spann, “Fracture Features at Internal Fracture Origins in a Commercial Glass Ceramic,” *Comm. Am. Ceram. Soc.*, Oct. 1982, C-173 – C-174.
43. G. D. Quinn, L. K, Ives, and S. Jahanmir, “On the Fractographic Analysis of Machining Cracks in Ground Ceramics: A Case Study on Silicon Nitride,” Special Publication 996, NIST, Gaithersburg, MD, May 2003.
44. M. Ramulu, R. C. Bradt, A. S. Kobayashi, and K. H. Yang, “A Dynamic Fracture Mechanics Interpretation of Multiple Mist Regions on Soda-Lime-Silicate Glass Fracture Features,” pp. 215 – 227 in *Fractography of Glasses and Ceramics, Advances in Ceramics*, Vol. 22, J. Varner, and V. Fréchette, eds., American Ceramic Society, 1988.
45. G. D. Quinn, L. K, Ives, and S. Jahanmir, “On the Nature of Machining Cracks in Ground Ceramics: Part I: SRBSN Strengths and Fractographic Analysis,” *Mach. Sci. Technol.*, **9** (2005) 169 - 210.
46. J. Barsom, “Fracture of Tempered Glass,” *J. Am. Ceram. Soc.* **51** [2] (1968) 75 – 78.
47. R. Gardon, “Thermal Tempering of Glass,” pp. 145 – 216 in *Glass: Science and Technology, Vol. 5, Elasticity and Strength in Glasses*, eds. D. R. Uhlmann and N. J. Kreidel, Academic Press, NY, 1980.
48. N. Shinkai, “The Fracture and Fractography of Flat Glass,” pp. 253 – 297 in *Fractography of Glass*, eds. R. C. Bradt and R. E. Tressler, Plenum, NY, 1994.

49. A. M. Christensen, M. A. Smith, J. T. Hefner, J. Blakely Webb, M. C. Bottrell, T. W. Fenton, "Forensic Fractography of Bone: A New Approach to Skeletal Trauma Analysis," *Forensic Anthropology*, **1** [1] (2018) 32 - 51.
50. A. Christensen, M. I. Isa, M. A. Smith, J. T. Hefner, H. Berryman, J. B. Webb, and I. S. Saginor, *A Guide to Forensic Fractography of Bone*, Federal Bureau of Investigation Laboratory, Quantico, VA, Feb. 2022.
51. J. B. Quinn and G. D. Quinn, "Material Properties and Fractography of an Indirect Dental Resin Composite," *Dental Materials*, **26** [6] (2010) 589 – 599.
52. *Fractography and Failure Mechanisms of Polymers and Composites*, ed. A. Roulin-Moloney, Elsevier, 1989.
53. H. Ko, "Fracture Behavior of Sintered Alumina Under Rotary Bending and Static Fatigue," pp. 15 – 29 in *Fracture Mechanics of Ceramics 12*, eds. R. C. Bradt, D. P. H. Hasselman, D. Munz, M. Sakai, V. Ya Shevchenko, Plenum, NY, 1996.
54. F. Kerkhof and E. Sommer, "Das Bild der Bruchfläche (von Gläsern)," in *Handbuch der Mikroscopie der Technik, Vol. IV, Mikroskopie der Silicate*, Umschau Verlag, Frankfurt am Main, Germany, 1964.
55. A. J. Pons and A. Karma, "Helical Crack-Front Instability in Mixed-mode Fracture," *Nature*, 464 (4 March 2010) 85 - 89
56. H. Wallner, "Line Structures on Fracture Surfaces," *Zeit. fur Physik*, **114** (1939) 368–378.
57. A. Tsirk, "Formation and Utility of a Class of Anomalous Wallner Lines on Obsidian," pp. 57 -69 in *Fractography of Glasses and Ceramics*, Advances in Ceramics, Vol. 22, eds., J. Varner, and V. Fréchette, American Ceramic Society, Westerville, OH, 1988.
58. H. E. Edgerton and F. E. Barstow, "Further Studies of Glass Fracture with High-Speed Photography," *J. Am. Ceram. Soc.*, **24** [4] (1941) 121 – 137.
59. B. S. Aldinger and P. de Haan, *Color Atlas of Glass Container Defects*, AGR, Butler, PA, 2019.
60. T. A. Michalske, "Fractography of Stress Corrosion Cracking in Glass," pp. 111 – 142 in *Fractography of Glass*, eds., R. C. Bradt and R. E. Tressler, Plenum, NY, 1994.
61. T. A. Michalske and V. D. Fréchette, "Dynamic Effects of Liquids on Crack Growth Leading to Catastrophic Failure in Glass," *J. Am. Ceram. Soc.*, **63** [11-12] (1980) 603 – 609.
62. A. Tsirk, "An Exploration of Liquid-Induced Fracture Markings," pp. 87 – 101 in *Fractography of Glasses and Ceramics, IV, Ceramic Transactions*, Vol. 122, eds., J. Varner, and G. D. Quinn, American Ceramic Society, Westerville, OH, 2001.
63. V. D. Fréchette, "Markings Associated with the Presence of H_2O During Cracking," pp. 71 – 76 in *Fractography of Glasses and Ceramics*, Advances in Ceramics, Vol. 22, eds., J. Varner, and V. Fréchette, American Ceramic Society, Westerville, OH, 1988.
64. T. A. Michalske, J. R. Varner, and V. D. Fréchette, "Growth of Cracks Partly Filled with Water," pp. 639 – 649 in *Fracture Mechanics of Ceramics, Vol. 4*, eds. R. C. Bradt, D. P. H. Hasselman, and F. F. Lange, Plenum, NY, 1978.
65. T. I. Suratwala, *Materials Science and Technology of Optical Fabrication*, Wiley, Hoboken, NJ, 2018.
66. T. A. Michalske and S. W. Freiman, "A Molecular Mechanism for Stress Corrosion in Vitreous Silica," *J. Amer. Ceram. Soc.*, **66** [4] (1983) 284 - 288.
67. T. A Michalske, B. C. Bunker, and S. W. Freiman, "Stress Corrosion of Ionic and Mixed Ionic/Covalent Solids," *J. Amer. Ceram. Soc.*, **69** [10] (1986) 721 – 724.
68. S. W. Freiman, S. M. Wiederhorn, and J. J. Mecholsky, Jr., "Environmentally Enhanced Fracture of Glass: A Historical Perspective," *J. Am. Ceram. Soc.*, **92** [7] (2009) 1371–1382.
69. M. Tomozawa, W-T. Han, and W. Lanford, "Water Entry into Silica Glass During Slow Crack Growth," *J. Am. Ceram. Soc.*, **74** [10] (1991) 2573 - 2576.

70. M. Tomozawa and R. Hepburn, "Surface Structural Relaxation of Silica Glass: A Possible Mechanism of Mechanical Fatigue," *J. Non-Cryst. Sol.*, **345-346** (2004) 444 - 460.
71. M. Ciccotti, "Stress-Corrosion Mechanisms in Silicate Glasses," *J. Phys D, Appl Phys*, **42** *(*2009) 1 – 18.
72. J. J. Swab and G. D. Quinn, "Effect of Precrack 'Halos' on K_{Ic} Determined by the Surface Crack in Flexure Method," *J. Am. Ceram. Soc*., **81** [9] (1998) 2261 - 2268.
73. J. J. Mecholsky, Jr., "Intergranular Slow Crack Growth in MgF_2," *J. Am. Ceram. Soc.*, **64** [9] (1981) 563 - 566.
74. R. Morrell, "Dealing with Component Failures," pp. 353 -368 in *Fractography of Glasses and Ceramics V*, eds., J. R. Varner, G.D. Quinn, M. Wightman, Ceramic Transactions, Vol. 199, American Ceramic Society, Westerville, OH, 2007.
75. T. A. Michalske, "Fractography of Slow Fracture in Glass," pp. 121 – 136 in *Fractography of Ceramic and Metal Failures*, ASTM Special Technical Publication 827, eds., J. J. Mecholsky, Jr. and S. R. Powell, Jr., ASTM, West Conshohocken, PA, 1984.
76. T. A. Michalske, V. D. Fréchette, and R. Hudson, "Dynamic Effects of Liquids on Surface Crack Extension in Glass," pp. 1091 – 1097 in *Advances in Fracture Research*, Vol. 2, ed., D. Francis, Pergamon, NY, 1981.
77. G. D. Quinn and W. R. Braue, "Fracture Mechanism Maps for Advanced Structural Ceramics, Part 2, Sintered Silicon Nitride," *J. Mat. Sci.*, **25** (1990) 4377 – 4392.
78. G. D. Quinn, "Fracture Mechanism Maps for Advanced Structural Ceramics, Part I, Methodology and Hot-Pressed Silicon Nitride," *J. Mat. Sci*, **25** (1990) 4361 - 4376.
79. P. J. Dwivedi and D. J. Green, "Determination of Subcritical Crack Growth Parameters by In Situ Observation of Indentation Cracks," *J. Amer. Ceram. Soc.*, **78** [8] (1995) 2122-2128.
80. A. G. Evans, "Engineering Property Requirements for High Performance Ceramics," *Mat. Sci. and Eng.*, **71** (1985) 3 – 21.
81. H. G. Richter, "Fractography of Bioceramics," pp. 157 -180 in *Fractography of Advanced Ceramics*, Key Engineering Materials Vol. **223**, Transtech Publ. Switzerland, 2004.
82. T. Lube, I. Khader, A. Kailer, U. Degenhardt, and K. Berroth, "Ermüdungsbruch in Siliziumnitrid," *Prakt. Met. Sonderband*, **46** (2014) 353 - 358.

6. Origins of Fracture

6.1 Origins, Flaws, and Defects

The origin is not only a location, but also an object. As noted at the beginning of Chapter 4, the majority of ceramic or glass fractures involve one origin, but there are exceptions. In the parlance of the engineer or scientist, the irregularities that initiate fracture are termed flaws or defects. The fractographer should use the terms "defect" and "flaw" with discretion. Scientists and engineers understand that virtually all brittle materials are imperfect and have irregularities that can behave as flaws, but nontechnical people may misunderstand the terms. That the material contains flaws or defects does not necessarily mean that the material has been prepared improperly or is somehow faulty. Conversely, there are instances where defects or flaws do indicate defective material. The author usually avoids using the word "defect" because of its similarity to the word "defective." "Flaw" seems a little less severe and sounds to many as a more technical term. If there is any doubt, then the fractographer may fall back upon the most innocuous term: "fracture origin." Ceramists, engineers, and researchers occasionally use the term "Griffith flaw:"

Griffith flaw: *A hypothetical sharp crack, usually envisioned as a tiny, slender, elliptically-shaped flaw, that intensifies stress at the sharp tip.*

Griffith flaws and fracture mechanics are discussed in chapter 7. There are hundreds if not thousands of papers on flaws in ceramics and glasses. Many are cited in this chapter, but other key papers and books are listed in Appendix A, in the sections: "Origins in Ceramics" and "Origins in Glass." The contributions of Mr. R. Rice, and Dr. F. Lange are particularly valuable in the 1970s to 1990s. (See Appendix A, Bibliography.) In the 1990s, Profs. K. Uematsu and S. Tanaka at Nagaoka University did fine work to characterize flaws in ceramics, starting from the earliest processing stages and monitoring flaw evolution during subsequent processing. They confirmed the link between the flaw size and the strength distributions. This topic is discussed further in Weibull Analysis section 7.15 of this Guide.

Some common flaws are pores, inclusions, large grains, agglomerates, contact cracks, etc. Basic types were emphasized in this Guide from the beginning in 2007 when the 1st edition was published. The flaws identified in this Guide has expanded and this chapter has doubled in size! An important refinement in this 4th edition is the recognition that there may be <u>different types of one flaw</u>. For example, there may be different types of pores in a material. It may be important to distinguish how these arise and how they are distributed. This Guide now recommends that multiple versions flaws should be named by their

primary identity (e.g., pore) and qualified with a suitable descriptor such as: "pore - spherical bubble."

This 4th edition includes new flaws from additively-manufactured (AM) alumina test pieces.[1] AM manufacturing entails building up a 3-D structure by a layer-by-layer approach. This Guide has examples of fracture origin flaws from one specific process called VAT polymerization. A 3-D structure is built stepwise by thin layer deposits of resin with ceramic filler. Each layer is partially polymerized by application of light. After this stereolithography process to create a "green body," the resin is burned off and the ceramic is sintered by conventional means to near full density. In a recent interlaboratory study of VAT polymerized alumina,[1,2] there were an astonishing five different types of pore fracture origins: pore - spherical bubble (from trapped gas); pore - disk bubble (from gas in a single build layer); pore - linear-elongated; pore - fibrous void; and pore - irregular. There undoubtedly will be many new and exotic flaws created by other AM processes in the future!

6.2 The Spatial Distribution of Flaws

Flaws are either *surface*- or *volume-distributed*. For example, inclusions are almost always volume-distributed, i.e., they are distributed throughout the bulk. Grinding cracks are inherently surface-distributed. Some flaws may even be edge-distributed. The distinction is important for understanding how flaws originated and whether they are from processing or from subsequent handling,

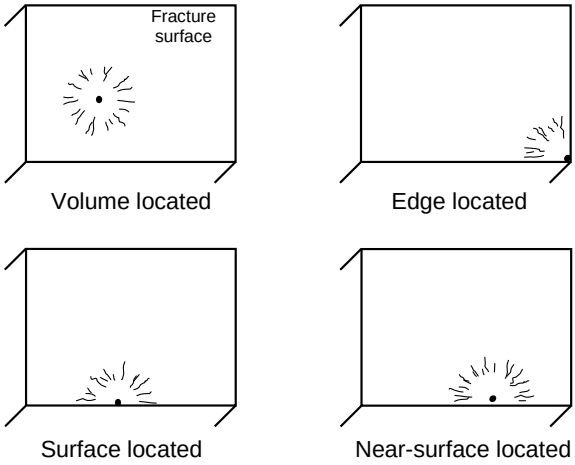

Figure 6.1 *Fracture surface schematics that show the four possible locations of a volume-distributed flaw type.*

finishing, or service damage. The distinction is also crucial for brittle material design engineers who often must scale the strengths of laboratory test data to predict component strengths via the Weibull theory.[3,4,5,6,7] Strength scaling and reliability predictions may be dramatically different for area and volume flaws. Glasses usually, but not always, break from surface-distributed flaws. Ceramics can fracture from surface or internal flaws.

One aspect about the spatial distribution of flaws needs clarification as shown in Figure 6.1. A single *volume-distributed* flaw may be *located* in the volume (in the bulk), at the surface, near the surface, or at an edge. For example, an inclusion originally may have been in the interior of a ceramic plate, but when a test bar was cut out, the inclusion ended up on the surface of the test bar. Surface-distributed flaws can only exist at the surface or at an edge. While the above statements may seem obvious, there are two reasons to keep the distinction clear. Firstly, if a flaw is found at a surface location, it does not necessarily mean it is a surface type flaw. It could be a volume-type flaw located at the surface. Some causal analysts simply look at the locations of the fracture origins. If they are located at the surface they simply interpret the origin as a surface type flaw. This is often wrong, particularly if the test data set is from bend bars or biaxially-loaded plates. It is a common misunderstanding that these two configurations always break from surface flaws. Origins are often located at the surface of these bending configurations, but if reasonable precautions are taken to control grinding damage, then they are quite likely to break from volume-distributed flaws. The following pages show many such examples. Secondly, a common mistake is to assume that all surface-located flaws are machining damage.

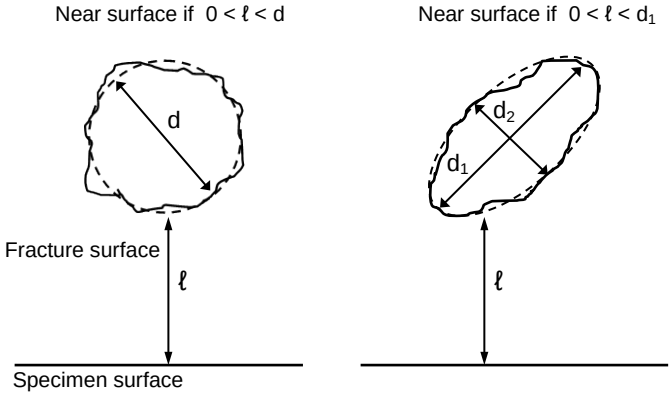

Figure 6.2 *Near surface (NS) origins are no deeper (ℓ) than the flaw diameter or major axis length.*

Thus, the fractographer should be careful when answering questions like: "What were the origins?" A cavalier answer such as "surface flaws" does not convey enough information. The answer should be more specific such as: "volume-distributed inclusions located at the surface," or "volume–type flaws located at or near the surface," or "surface-distributed grinding cracks."

One might ask at what point is a volume-type flaw "near surface." A review of the fracture mechanics stress intensity shape factors for flaws located at various distances in proximity to a surface suggests the criterion shown in Figure 6.2. At distances closer than one diameter, the stress intensity shape factors for such flaws increase by more than a few percent. Sometimes the characterization of location is important for service-performance issues or fracture mechanics analyses of the flaws. For example, some near-surface located origins may be more susceptible to time-dependent crack growth than equivalent volume-located origins. A classic example of this for time-dependent fractures in sintered silicon carbide is Case Study 3 in Chapter 10 of this Guide. Pores located at or near the surface behaved differently than identical pores located in the bulk. Near-surface-located origins may also be likely to link up with surface machining or impact damage, or to extend subcritically to the surface prior to catastrophic fracture.

6.3 Are Flaws Intrinsic or Extrinsic?

The irregularities that act as fracture origins in advanced ceramics and glasses can develop during or after fabrication of the material. Large irregularities (relative to the size of the base microstructure) such as pores, agglomerates, and

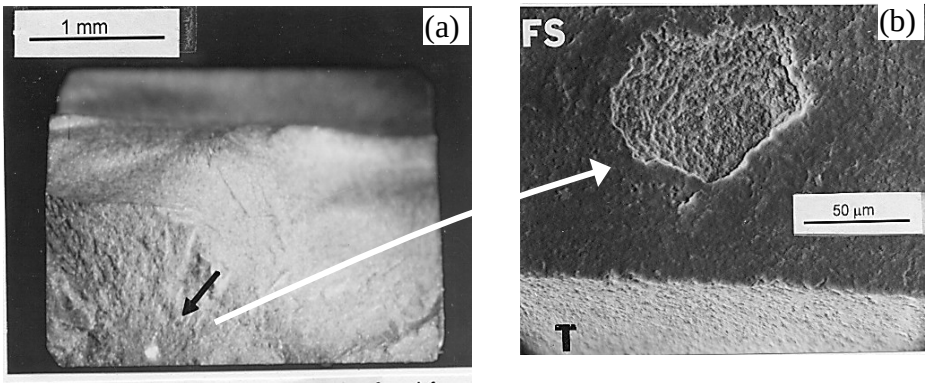

Figure 6.3 *Describe flaws by what they are, not how they appear. (a) shows a "white spot" at the origin in a reaction-bonded silicon nitride bend bar. The SEM image of the origin in (b) shows the origin actually is a volume-distributed pore. FS denotes fracture surface and T denotes tensile surface.*

inclusions may be introduced during processing. Some might deem inclusions and other irregularities as extrinsic flaws, but to the extent that they occur naturally during fabrication they are intrinsic. For example, if a ceramic customarily has a ball milling step in the process, and mill fragments flake off to become inclusions, then these may be considered intrinsic. Other origins can be introduced after processing as a result of handling, impact, wear, oxidation, and corrosion. These usually can be considered extrinsic origins. Machining damage may be considered either extrinsic or intrinsic. It is intrinsic to the manufacture if machining is a natural consequence of producing a final part. In any case, the differentiation between intrinsic and extrinsic is often of no practical concern.

The origin should be characterized by <u>what it is,</u> rather than a description of how it appears, since the latter may depend upon the mode of viewing. Descriptions such as the origin was a “white spot” should be avoided. It may

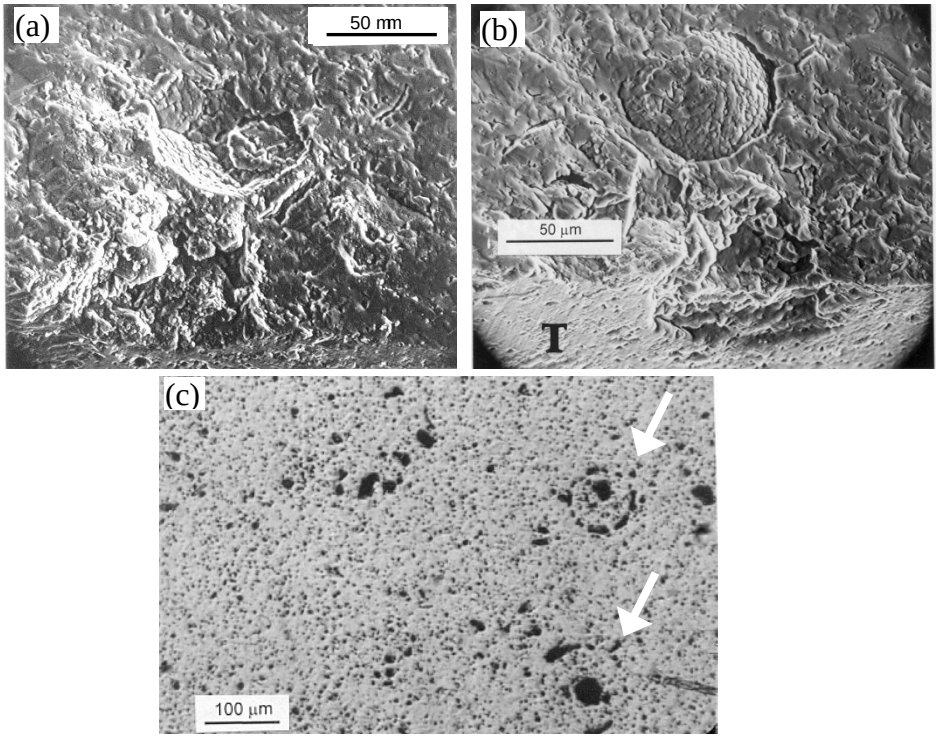

Figure 6.4 *Fracture origin in a sintered alpha silicon carbide flexure specimen. (a) suggests the origin is a pore, but (b), which shows the mating half, shows it is a spray-dry agglomerate. (c) shows a polished microstructural section for this material that reveals the agglomerates (arrows).*

be white in an optical microscope, but it most likely will not in a SEM (Figure 6.3). Sometimes descriptive terms may be used, but as qualifiers to the true flaw identity, e.g., "pores that appear white when viewed optically."

6.4 Matching Fracture Halves

Both halves of the fracture surface should be examined whenever possible, since each contains information about the fracture origin. For example, Figure 6.4 illustrates a case wherein an agglomerate was strength limiting. If only the (a) half was examined, the fractographer may have erroneously interpreted the flaw as a pore. A similar issue arises with nickel sulphide inclusions in glasses. The spherical black inclusion is usually found in one piece, but a perfectly matching socket hole is in the other.

6.5 External Surfaces

If an origin is located at the surface, it is wise to examine the exterior surface by tilting the specimen back or by directly looking at the exterior surfaces for clues as to the flaw type as shown in Figure 6.5. A common question is: "Was it a scratch or a grinding flaw?" If the surface-trace lines up with the striations that show the grinding direction as in Figure 6.5a, it is likely a grinding fault. If the fault has a different axis, as in Figure 6.5b, then it is a scratch. Section 6.7.3 later in this chapter has more on scratches.

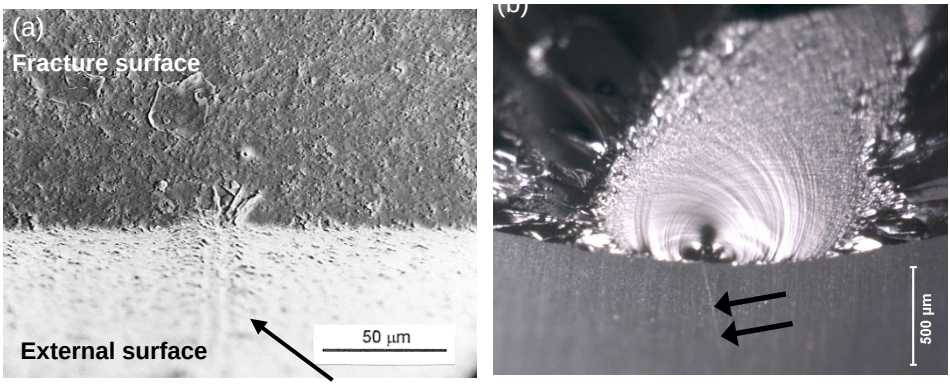

Figure 6.5 *The exterior surface should be checked if the flaw is located on the surface. (a) shows a deep grinding flaw with a distinctly different ground-surface trace at the origin in a reaction-bonded silicon nitride part. It is likely that a large "renegade" abrasive grit in the grinding wheel caused it. (b) shows the fracture origin of a fused silica rod broken in flexure. This tilted-back view shows a scratch on the surface (arrows) coincident with the origin.*

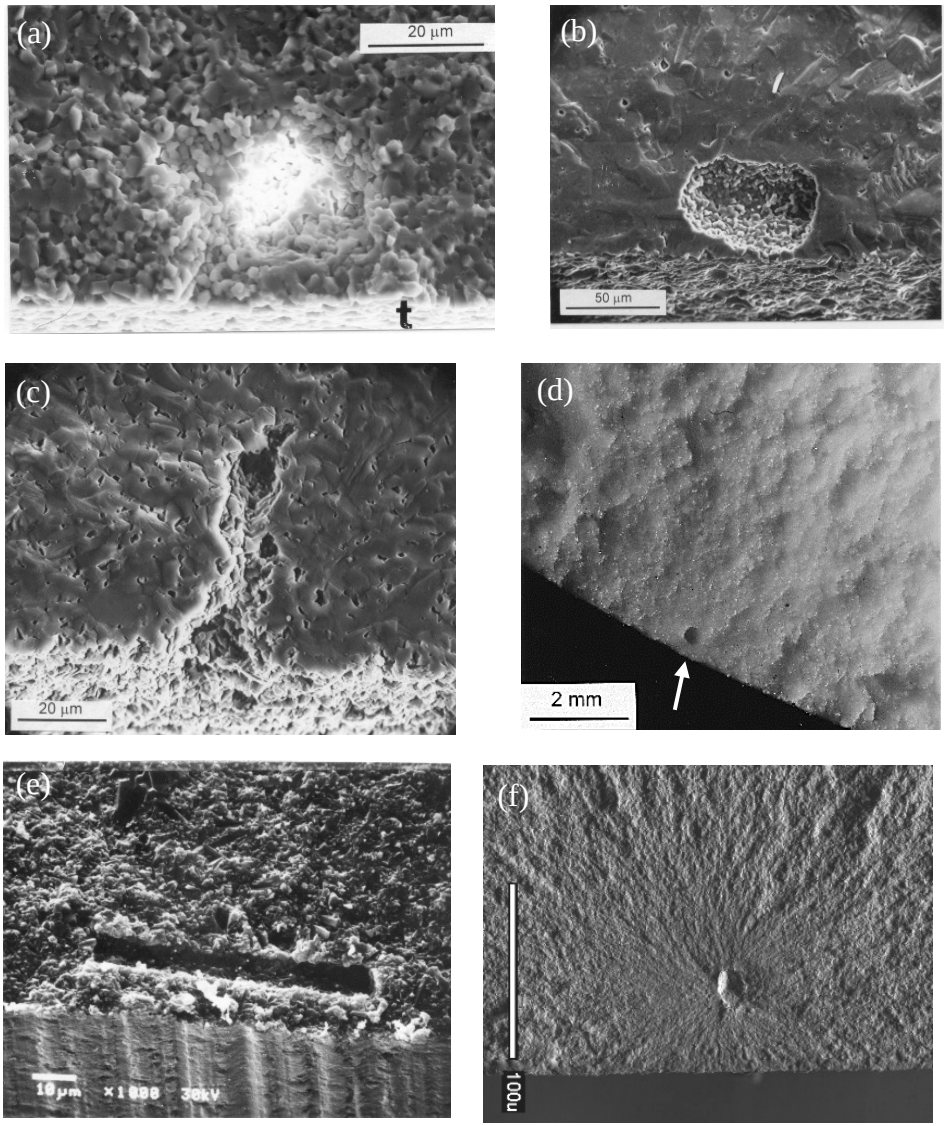

Figure 6.6 Examples of pore fracture origins in ceramics. (a) shows a SEM image of a pore in a 99.9% alumina bend bar. Electron charging created the bright spot. (b) is a pore in an AlON bend bar that is within 5 mm of the surface. This is a "near-surface" flaw. Transgranular fracture around it helps it stand out. (c) is an irregular pore in a sintered alpha SiC bend bar. (d) is a pore in a porcelain electrical insulator (courtesy J. Taylor and R. Rice). (e) is a cylindrical pore in a silicon nitride probably from a fiber or hair burn out. (f) is a pore in an dental yttria-stabilized tetragonal zirconia polycrystal (3Y-TZP). All of these are volume-distributed flaws in flexure specimens.

6.6 Volume-Distributed Flaws

6.6.1 Pores and bubbles

Pores are one of the easiest flaws to find and identify. They can have a variety of sizes and shapes. In ceramics they are often equiaxed, but can easily assume a myriad of odd shapes as shown in Figure 6.6. Pores are volume-distributed flaws that are discrete voids. Pores and bubbles in glasses are also known as “seeds” or “blisters” and commonly contain an internal gas. Small ones are termed “seeds” and large ones are termed “blisters.” This word is used somewhat differently for ceramics and glasses. Dictionaries say "blister" implies a raised feature or protrusion on a surface, e.g., in a ceramic from a localized resin binder burnout issue as discussed later in section 6.8.2.

Pores in glass or porcelain are often very smooth and round, and may contain trapped gas. They may be called “bubble-pores.” These are also found in slip cast advanced (technical) ceramics or additively-manufactured (3-D printed) ceramics using resin-based stereo-lithography. Their effect on strength can vary dramatically. Since they are very smooth, they usually act as simple stress concentrators and not as sharp flaws. This distinction is important as discussed in detail in Chapter 7. A material may have large *internal* pores that are relatively harmless. They may not necessarily act as fracture origins. On the other hand, they can be extremely deleterious *if they contact an exterior surface* or *each other,* as illustrated in Figure 6.7. Bubbles that are close to an outer surface are also prone to interact with grinding or machining damage that can link with the bubble, turning an otherwise harmless bubble into an extremely serious flaw. A good example of this was shown as Figure 5.8 in the previous chapter. Figures 6.8 and 6.9 show other examples of bubble origins. Reference 8 has more information about the feldspathic porcelain strengths and bubble/pore fracture origins. This dichotomy in behavior poses a dilemma to design engineers working with flaw sizes and Weibull statistics. A volume-distributed bubble can be either a harmless or a dominant flaw depending upon where it is located in a piece.

Pore-bubbles in ceramics or glass ceramics, can act as strength-limiting flaws even if they are located in the interior. For more information about pores as origins in ceramics, see Rice’s article, Reference 9. It is often suggested (but rarely shown) that rim cracks a few grain diameters long extend from the bubble surface into the ceramic. These are a “Rings of Saturn” type flaw (e.g., Figure 7.18) and fracture mechanics solutions for the stress intensity factors may be found in the literature. It is not likely that the actual flaws around the periphery of a real pore will be so idealized, however.

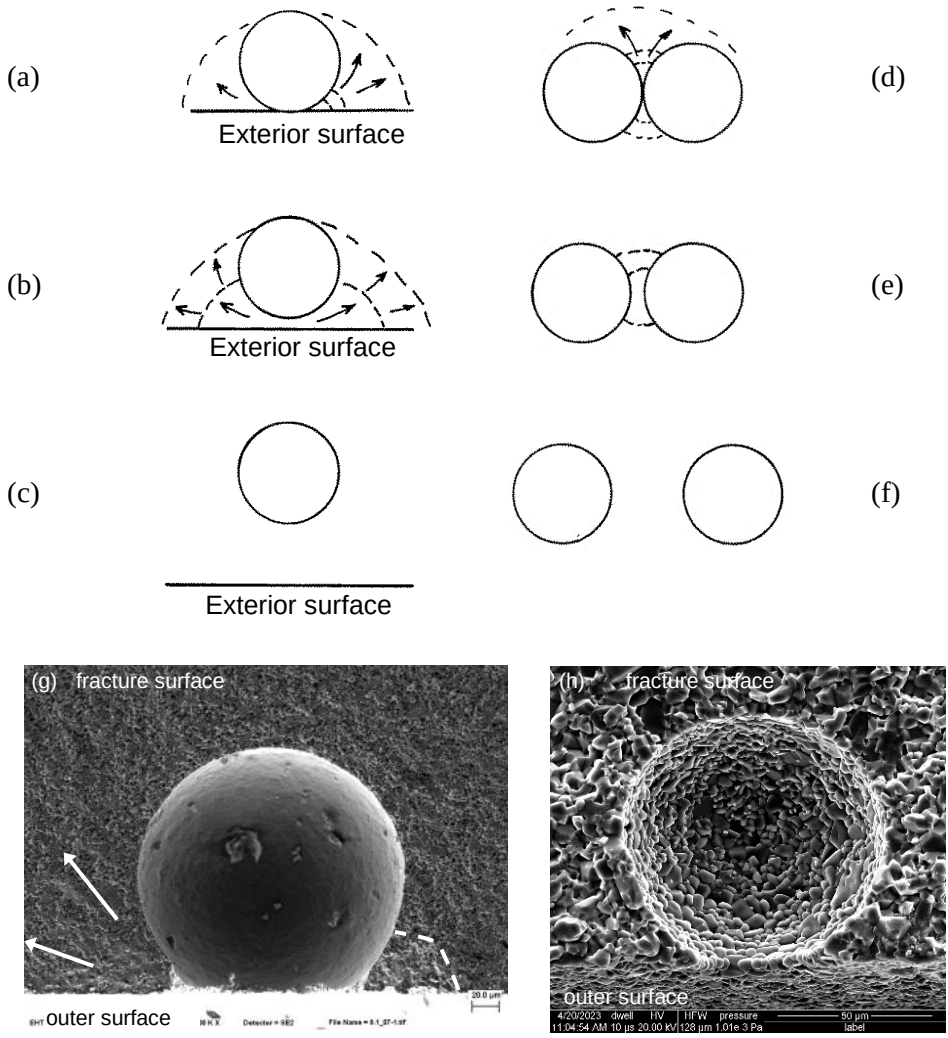

Figure 6.7 *Bubbles are smooth pores and may be relatively harmless or* <u>*extremely deleterious*</u> *depending upon location. (a, g, h) show bubbles just pierced by the exterior surface, creating very sharp cusps from which cracks will likely pop in and grow. (b) shows a near-surface bubble which can easily link up with grinding or other surface damage. (c) shows an interior bubble that is relatively harmless. Similar behavior can occur with two bubbles in proximity to each other. (d and e) are likely to form a strength-controlling flaw, whereas configuration (f) is relatively harmless. (g) is an example of a "pore - spherical bubble - pierced" in sintered alumina (courtesy of T. Bernthaler). (h) shows another example in a 3-D additively-manufactured sintered alumina from the author's study.*[1]

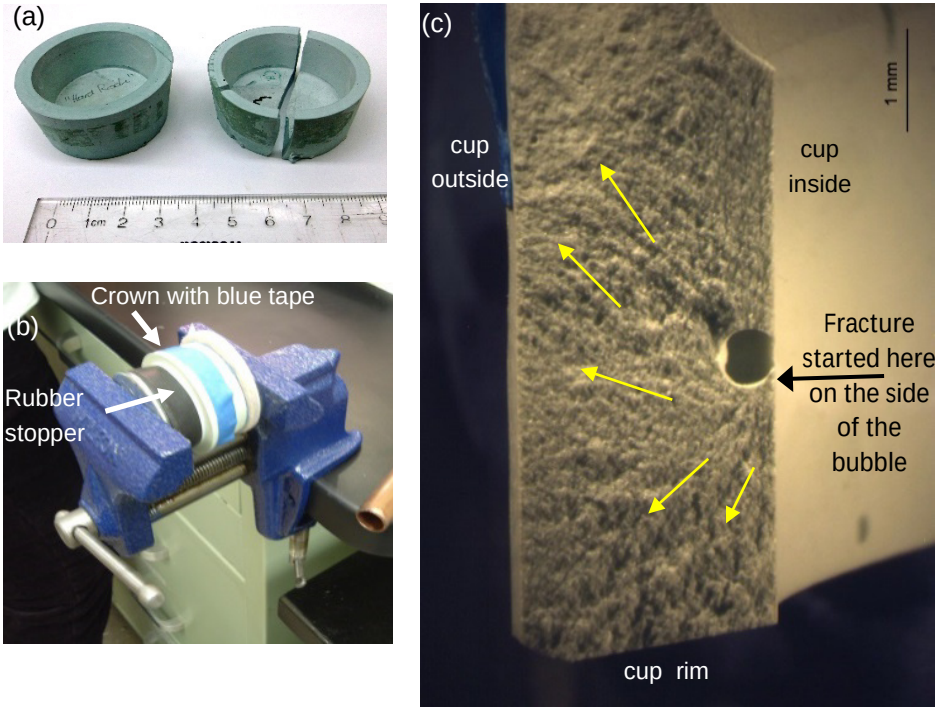

Figure 6.8 *Bubble origin in an oversized mock-up of a dental molar crown. Dental stone was slip cast into a hollow cup shape. The cup was loaded in a vise with an inner rubber stopper marked by the white arrow in (b). This simulated loading of an occlusal surface. When the vise was tightened, the rubber stopper expanded, and the "crown" split in half. Blue painter's tape held the fragments together. Hoop tensile stresses in the wall triggered fracture from a "pore, spherical bubble" that touches the inner surface as seen in the fracture surface view (c). Grazing illumination accentuates hackle lines that show the fracture started at a cusp marked by the black arrow in (c). This oversized mock-up crown simulates real crown fractures.*

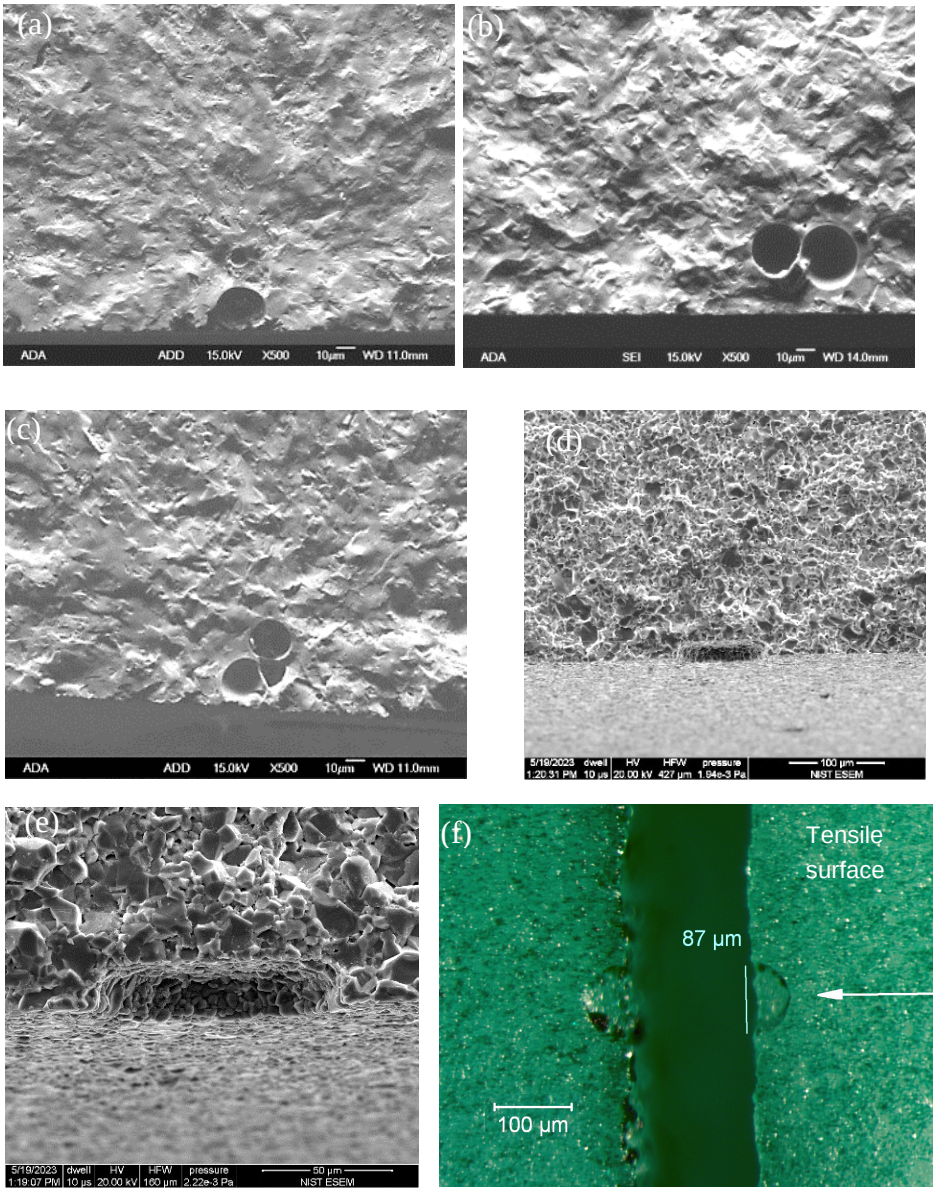

Figure 6.9 *Strength-limiting pore-bubble flaws. (a-c) are in Vita Mark II feldspathic dental porcelain bend bars.*[8] *The strengths were: (a)120 MPa, (b)119 MPa, (c) 115 MPa. (d) - (f) from reference 1 show a nonspherical bubble in a 3-D printed sintered alumina (420 MPa) bend bar. It is a pore-disk bubble ("hockey puck pore") that was one 25 μm build layer thick. (f) shows the same disk bubble on matching halves of the tension surface of the bend bar. They were green dye stained to make the disk easier to see.*

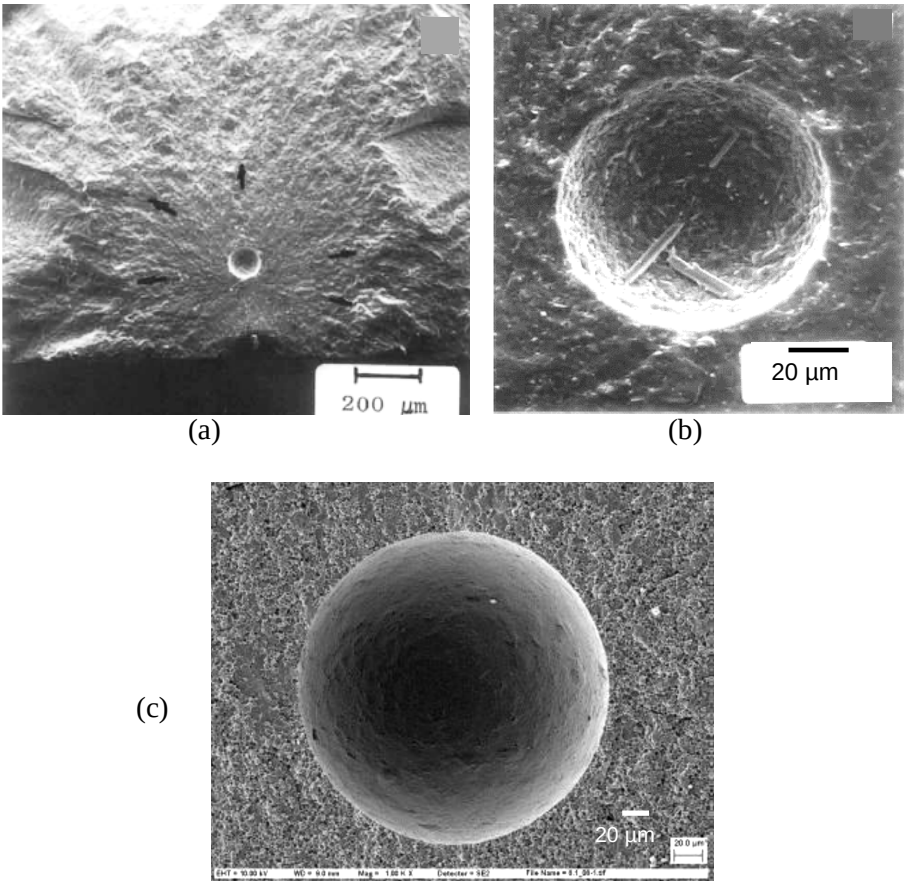

Figure 6.10 *Internal pore-bubbles in ceramics and glass ceramics. (a) and (b) show an internal spherical pore fracture origin in a cordierite glass ceramic bend bar (315 MPa). The pore was from a bubble in the original glass. The material crystalized around the bubble during the ceraming step. The arrows mark the hackle boundary of the fracture mirror. (a,b are courtesy D. Lewis, III) (c) shows a large internal seeded-pore origin in alumina. (courtesy T. Bernthaler)*

Figures 6.10a,b show a fascinating example by Lewis[10] of a large (100 µm diameter) internal bubble fracture origin in a cordierite glass ceramic bend bar. The spherical bubble was probably smooth in the parent glass, but roughened during crystallization. Bernthaler[11] used polymeric spheres in alumina that were burned out during sintering to create spherical fracture origin flaws such as shown in Figure 6.10c and previously in Figure 6.7g. Trapped gas bubbles in a polymer-ceramic starting material for a 3-D stereolithographic manufactured alumina created flaws as shown in Figure 6.7(h) from the author's

study.[1] It is tempting to call these "pore-blisters," but as noted above, the word "blister" usually denotes something that protrudes above the surface slightly. The flaws in Figures 6.7 (g,h) do not protrude above the surface, so a better description is "pore–bubble-pierced." Analogous flaws in glass have been termed an “open seed” or “open blister."

Even if they are not fracture origins, bubbles in glasses and porcelains can be very helpful to fractographers. They are a good source of wake hackle lines on fracture surfaces that show the direction of crack propagation.

Pores may often be very irregular and jagged. One way these may occur is by the formation of pressing defects when preparing the green body. Pores associated with spray-dry powder agglomerates may not be eliminated during final pressureless sintering. Figure 6.11 shows examples. Hot pressing or hot isopressing would likely eliminate such flaws. These flaws are sometimes called: “pressing flaws” or “blank pressing flaws.”

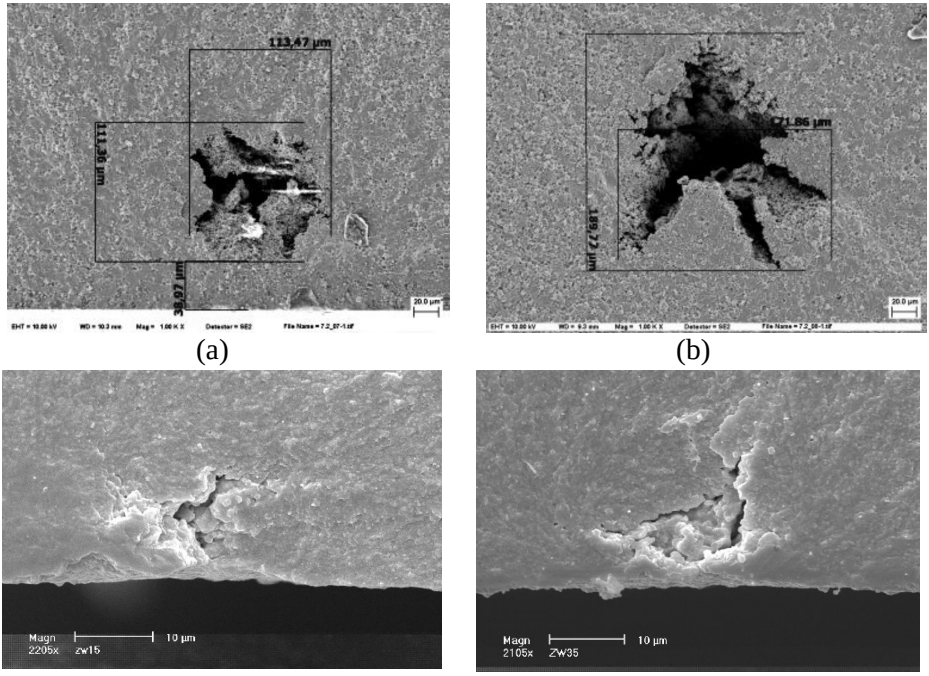

Figure 6.11 *Irregular pore origins. (a) and (b) were formed during cold pressing of alumina spray-dried powders. (courtesy T. Bernthaler).*
(c) and (d) are in a sintered 3Y TZP zirconia. (courtesy S. Scherrer)

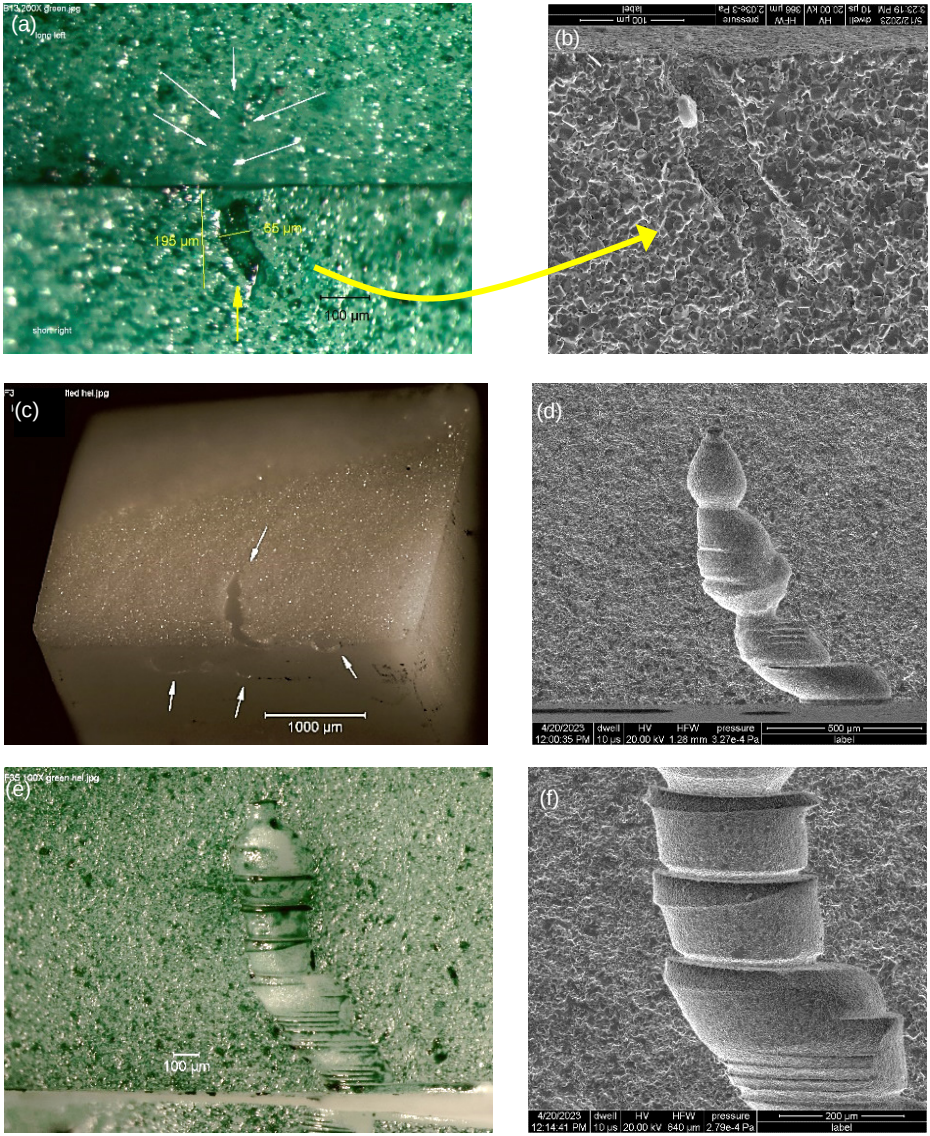

Figure 6.12 *Small and large linear pore fracture origins in 3-D additively-manufactured sintered alumina bend bars.*[1] *(a) and (b) were in a vertically-built up bar with a strength of 237 MPa. (a) is a green dye-stained view of the fracture surfaces of the mating halves at the origin site. (b) is an SEM closeup of the bottom half. The flaw is a "pore – small inclined linear hole." (c) and (d) show a "pore – very large linear hole", also known as a "wormhole," in a bar that was built up with horizontal layers. (162 MPa). (e) and (f) are another horizontally-built bar (156 MPa). Some very thin 5 µm to 20 µm thick build layers partially bridge the large open flaw.*

6.6.2 Porous regions

Porous regions are volume-distributed flaws that are three-dimensional zones of porosity or microporosity. Examples are shown in Figure 6.13. These can be obvious or very subtle. SEM microscopy is usually needed to identify these flaws. Optical microscopy may not be effective since light reflected from the interior will shine up through them "washing them out."

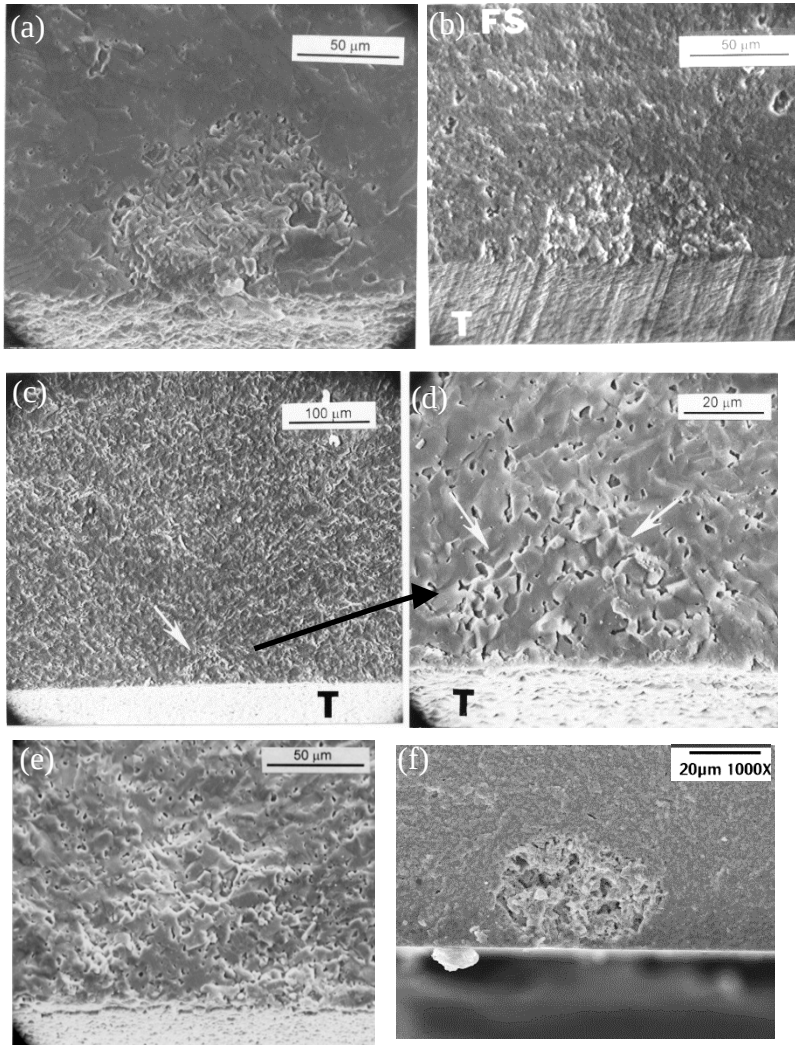

Figure 6.13 *Porous region origins in ceramics. (a) is in sintered aluminum oxynitride. (b) is in a reaction-bonded silicon nitride. (c) and (d) are one sintered alpha silicon carbide bend bar. (e) is also from a sintered silicon carbide. (f) is a common type in tetragonal zirconia polycrystals (3Y-TZP).*

6.6.3 Porous seams

Porous seams are similar to porous regions but are more planar or two-dimensional. They also may be very difficult to detect. They can meander through a body at odd angles for either short or long distances. Examples are shown in Figures 6.14 and 6.15. If the material separated completely between these seams, the flaw might be more aptly described as a processing (firing) crack, as described later in section 6.8.1. Differential shrinkage often causes these seams. The fracture surface may only expose a small portion of a large seam. It can be very helpful to examine the outer surface of the specimen as shown in Figure 6.15c-e.

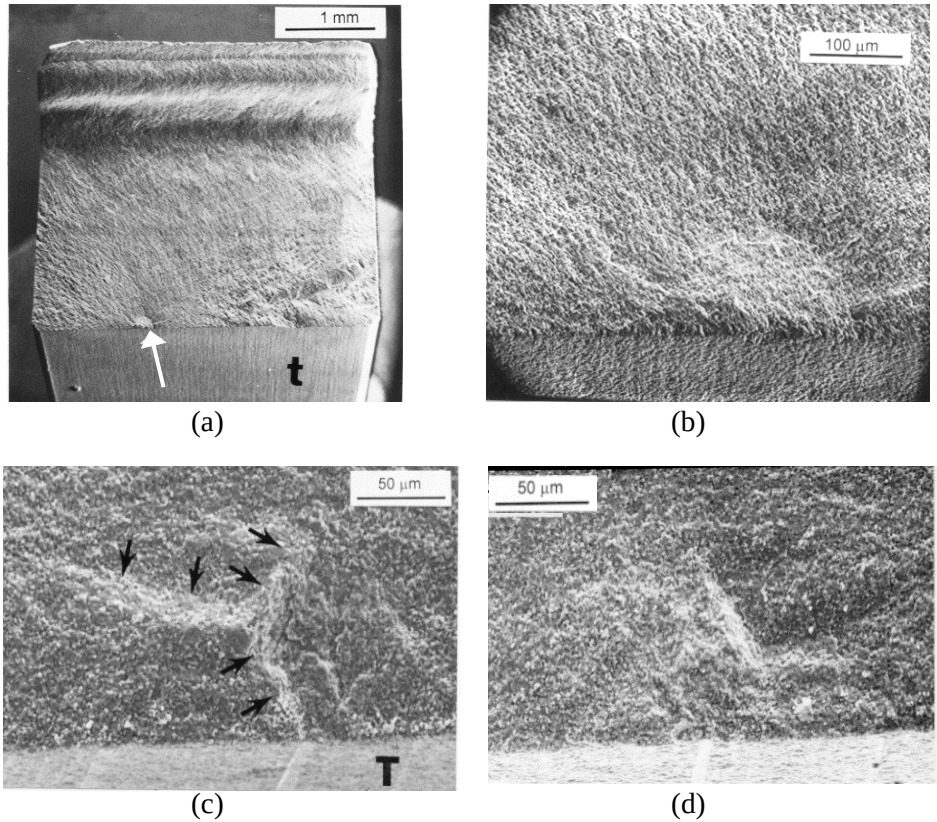

(a) (b)

(c) (d)

Figure 6.14 *Examples of porous seam fracture origins. (a) and (b) show a relatively easy-to-detect origin in a fine-grained sintered 99.9% alumina. (c) and (d) show the origin in matching halves of another fine-grained sintered 99.9 % alumina bend bar. Notice how different the flaw looks in the two halves.*

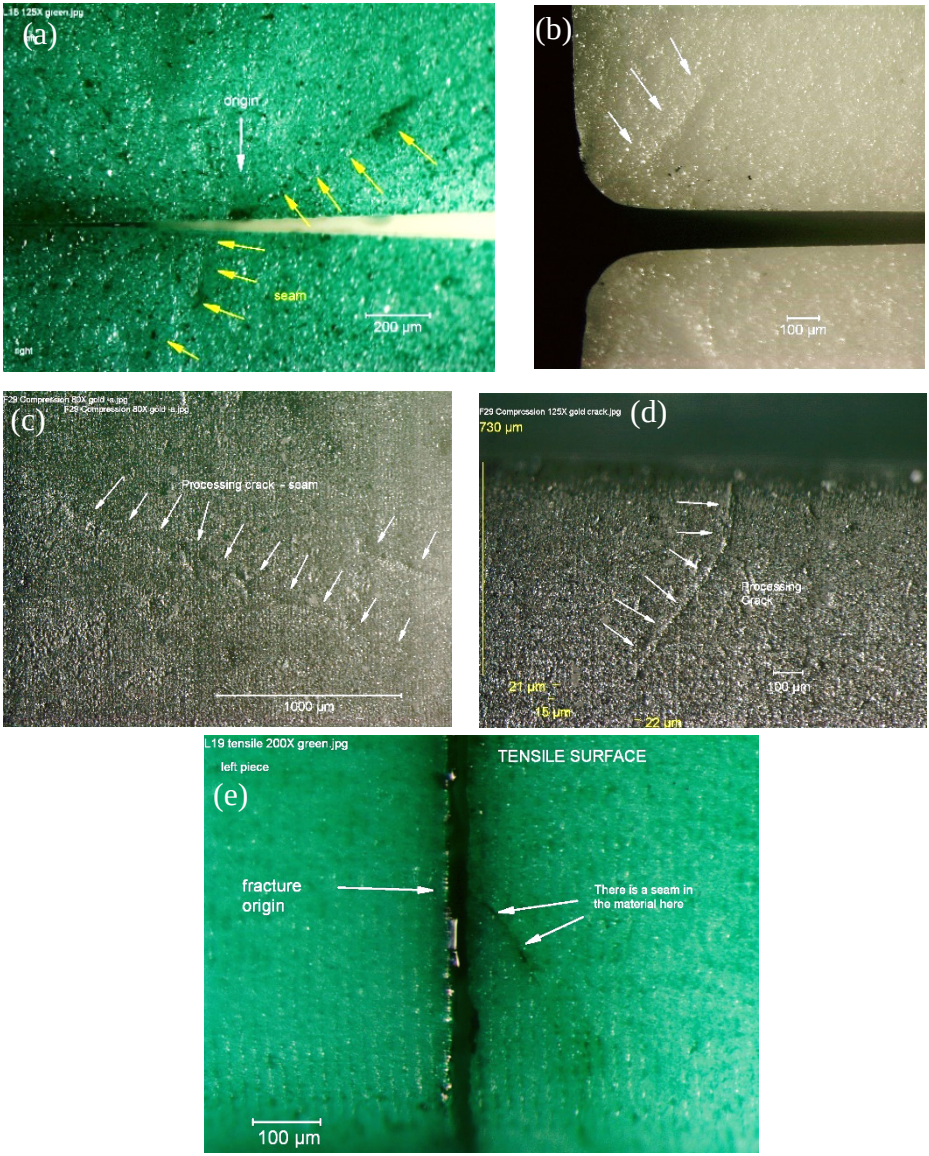

Figure 6.15 *Seams in additively-manufactured alumina specimens.*[1] *Seams can run at irregular angles through the body and only a portion of them may be seen on the fracture surface. (a) and (b) show seam origins as seen on the fracture surface. Seams are often easier to view on the specimen's outer surfaces as shown in (c) – (e). Matching bar halves are together in (e). Dye penetration or gold coating the surfaces can help reveal their existence especially in translucent ceramics. The 25 µm build layers are evident.*

6.6.4 Agglomerates

Agglomerates are volume-distributed flaws that are a cluster of grains, particles, platelets, or whiskers or a combination thereof. They are a common flaw in ceramics made with powders that are prepared by spray drying. Spray dry agglomerates are often hollow. Agglomerates often sinter away from the matrix, creating a shell-like void or seam around the agglomerate. Since the composition is identical to the matrix, the color and reflectivity of this flaw are identical to the matrix. If agglomerates are suspected, examine more of the fracture surface for similar spherical or ring like features, since if there is one, there usually are many. Examples are shown in Figures 6.4 on a previous page and 6.16 below. Lange *et al*.[12,13,14] wrote an excellent set of articles about agglomerates as fracture origins in alumina/zirconia composites.

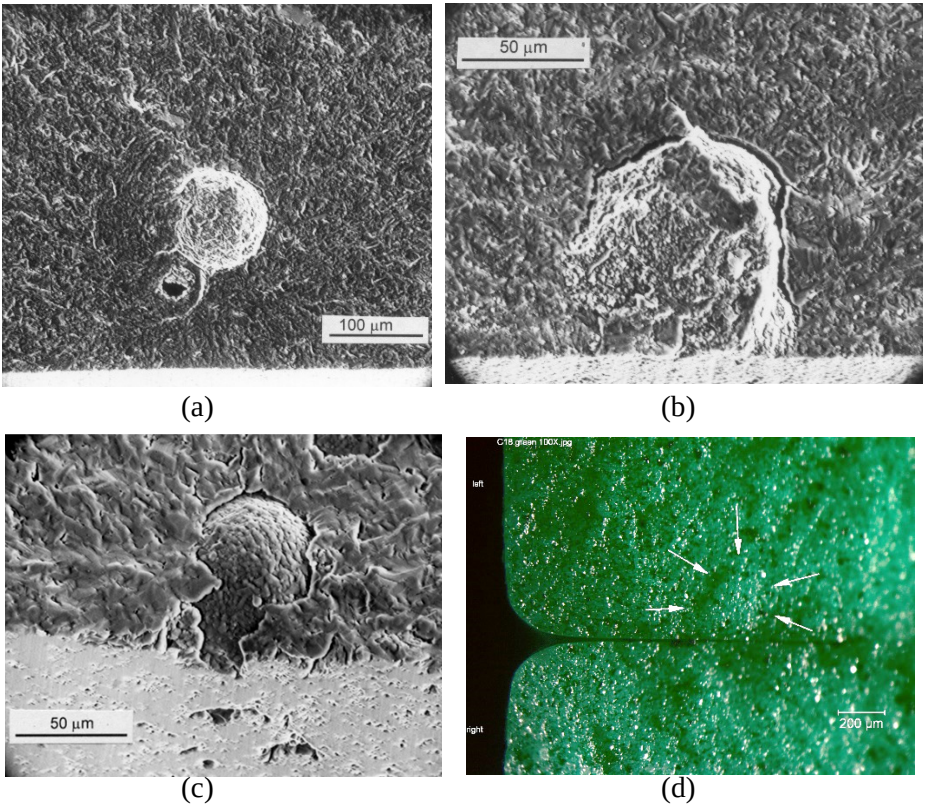

Figure 6.16 *Examples of agglomerate fracture origins. (a – c) show spray dry agglomerate fracture origins in sintered alpha silicon carbide. Agglomerates sometimes sinter away from the matrix leaving a void-like crack. (d) is in a 3-D additively-manufactured sintered alumina.*

Up to this point, agglomerates have been considered as discrete, isolated flaws. On the other hand, they may be pervasive and may make up the entire microstructure of a body that has not been fully-densified. If green bodies made up of dry-pressed, spray-dried particles are not sintered or hot-pressed to full density, then the microstructure may comprise particles with incomplete bonding and inter-particle porosity such as shown in Figure 6.17 below. Polished microstructural sections may reveal the incomplete bonding, which may be subtle. It may be very difficult to discern this on a fracture surface, but it may be seen with optical microscopy if the lighting is carefully adjusted as shown in Figure 6.17c. Gee and Morrell[15] showed similar features in dry-pressed, spray-dried b-alumina. Hangl[16] showed good images for an industrial grade zinc oxide for a varistor application.

(a)

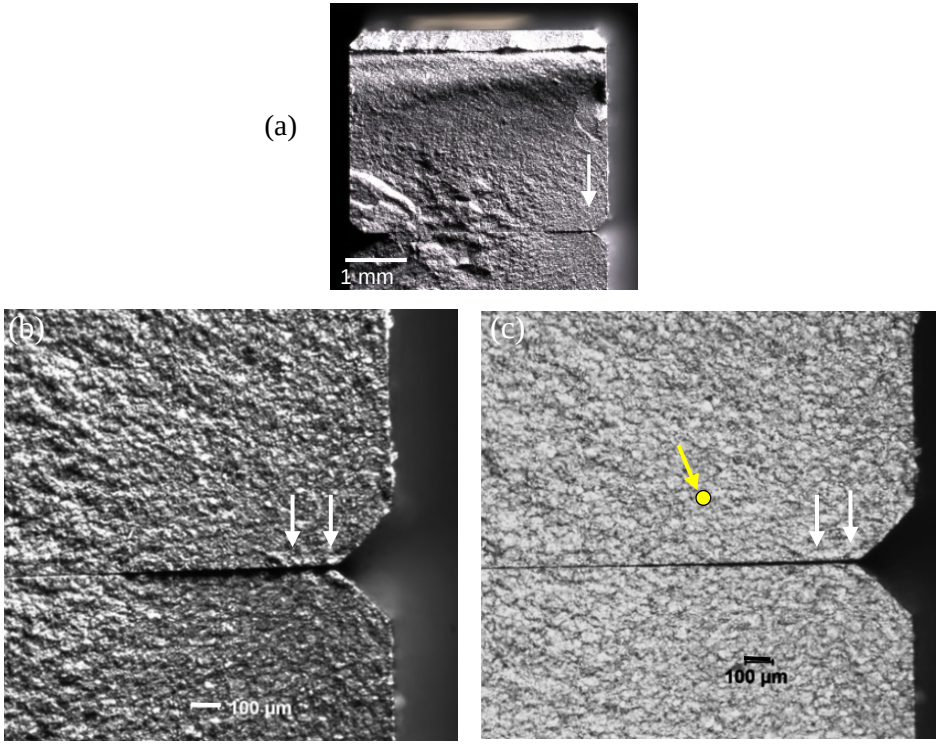

Figure 6.17 *Incomplete densification causes interparticle porosity throughout a body. (a) shows fracture surfaces of reaction-bonded silicon nitride bend bar. The fracture origin was grinding cracking marked by the white arrows. Although this material had low fracture toughness, the grinding cracks penetrated only one granule deep, since the intergranular porosity impeded further extension. The spherical granules are revealed by careful lighting in (c). The superimposed yellow circle shows their size.*

6.6.5 Inclusions

Inclusions are volume-distributed flaws that are a foreign body with a composition different than the glass or ceramic. They are termed “stones” in glasses. They can be present in the original ceramic starting powders or be picked up as contaminants during processing. They are often easy to detect due to color or reflectivity differences compared to the matrix as shown in Figures 6.18 to 6.20. They can be round and equiaxed, irregular, or fragmented.

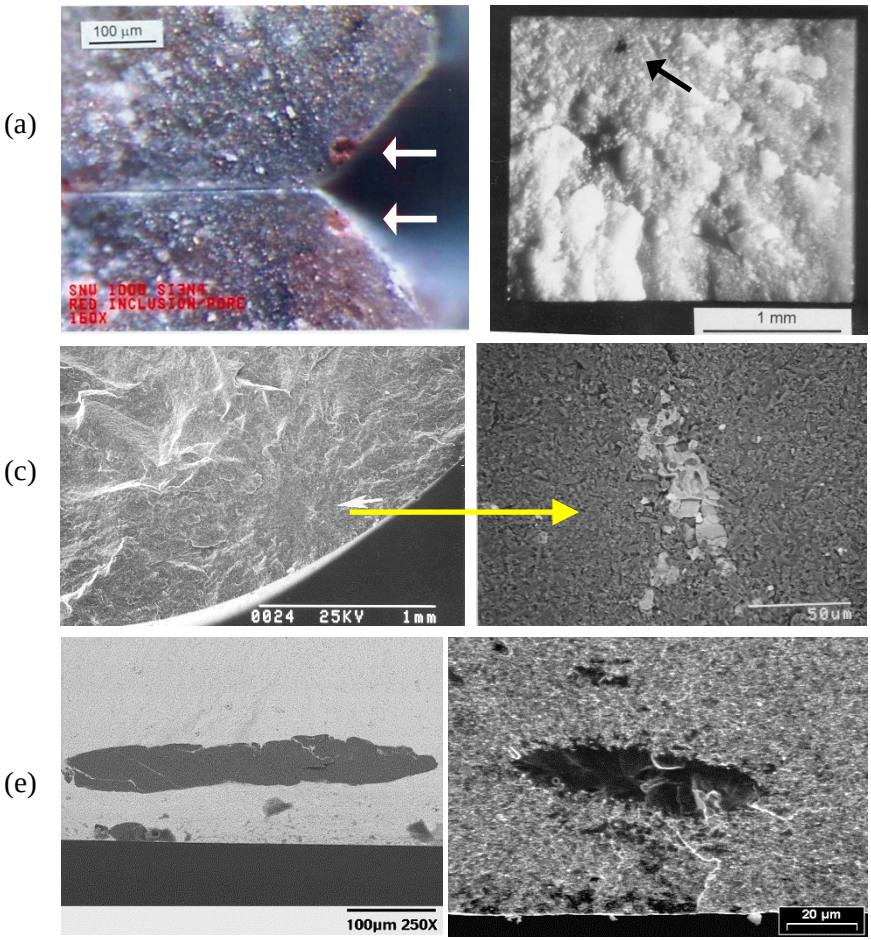

Figure 6.18 *Examples of inclusions in ceramics. (a) is a red iron inclusion in sintered silicon nitride bend bar at an edge chamfer. (b) is an inclusion in a silicon nitride tension specimen. (c) and (d) are an iron inclusion in a silicon nitride. (e) is an alumina inclusion in a 3Y-TZP zirconia biaxial disk specimen (courtesy J. Eichler), and (f) is a vanadium inclusion in a binderless tungsten carbide bend bar. (courtesy J. Swab)*

The tungsten inclusion shown in Figure 6.19b,c can be unusually deleterious in a silicon nitride ceramic. The tungsten impurity, from tungsten carbide ball milling media, can form very brittle tungsten silicides that lower the local fracture toughness around and in the flaw.[17] Figures 3.47 and 3.48 in chapter 3 show fragmented iron inclusions in silicon nitride.

(a)

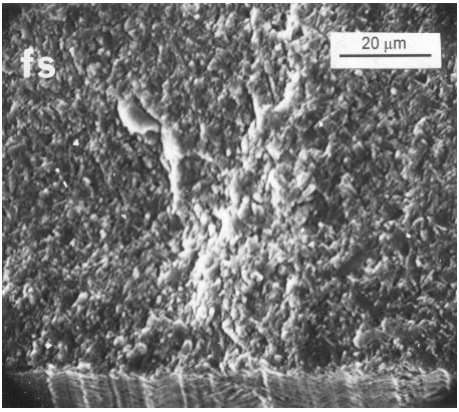

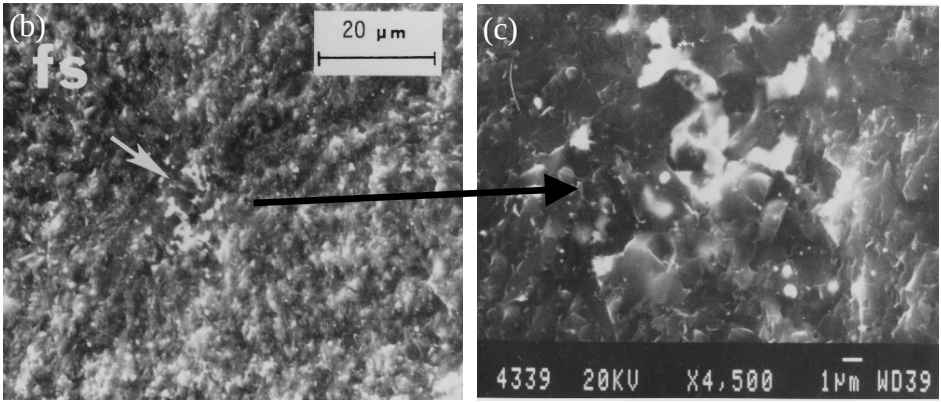

Figure 6.19 *Examples of inclusion origins in ceramics. (a) SEM image of an irregular iron and chrome inclusion in a sintered SiAlON bend bar. (b) and (c) show a fragmented tungsten inclusion in a hot-pressed silicon nitride bend bar.*

A variety of inclusions occur in glasses. Platinum inclusions can occur if glass is melted in platinum crucibles, but not from direct reaction with the melt. It occurs by atmospheric oxidation, vapor phase transport, then reduction of the oxide to produce a particle in the melt.[18] Many inclusions in glasses are called *Stones*. They can arise from a variety of causes including unreacted raw material, contamination of raw material or recycled material, glass devitrification, and contamination from grains refractory material broken off the tank or pot walls. Aldinger and Collins' book[19] is a colorful compilation

with thirty-eight types of stones in glass. Kaarlson[20] said that about fifty different inclusion types have been identified in glass, but most of them are harmless according to Johnson.[21]

The nickel sulfide inclusions shown in Figures 6.20 and 3.9 (in chapter 3) are particularly deleterious flaws in tempered or heat-strengthened glasses. They can undergo a spontaneous phase transformation at room temperature with an attendant volume expansion of 2.2 % to 4 %. If the inclusion is located in the

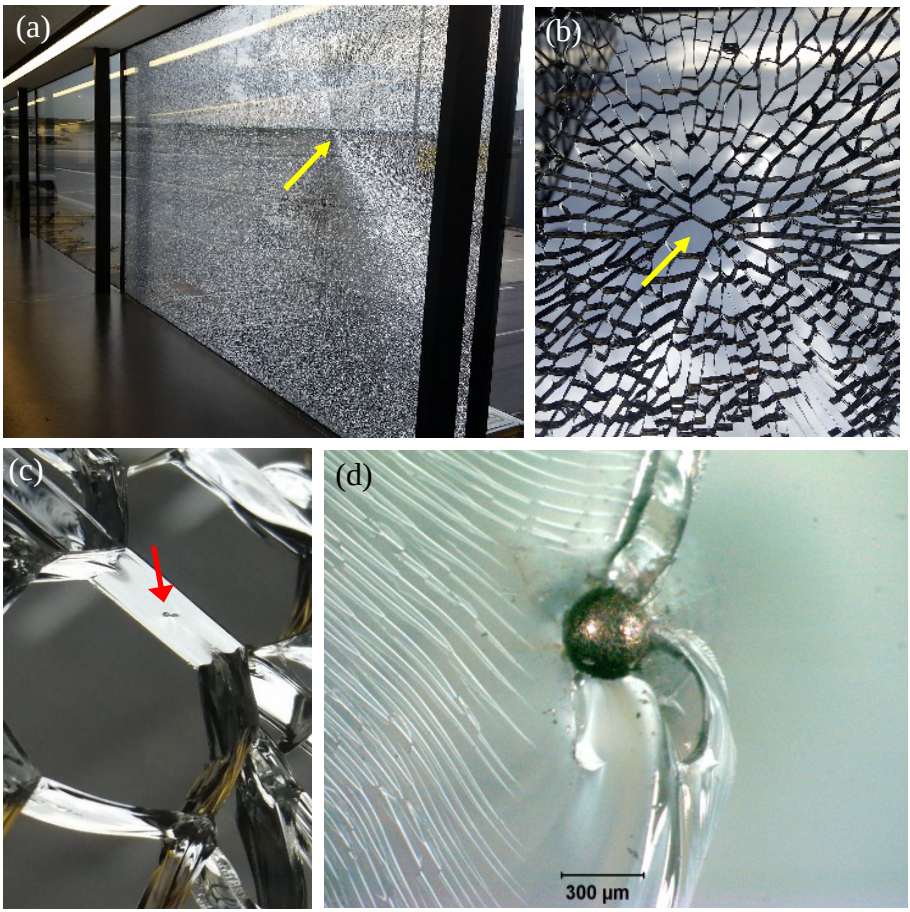

Figure 6.20 *Nickel sulfide inclusions. (a) – (c) show a 350 m NiS inclusion that I saw in a 3 m x 6 m window that spontaneously fractured in a gate ramp window at the Vienna airport in September 2019. (d) is a closeup of an NiS inclusion that caused spontaneous fracture in a different 12.5 mm tempered glass pedestrian walkway curtain. See Fig. 3.9 in chapter 3 for another NiS example.*

interior and is exposed to tensile residual stresses, it can cause spontaneous catastrophic breakage at any time (days, months, or years after fabrication) with no warning.[20,21,22,23,24,25,26,27,28] These inclusions are often so small (100 mm or less) that they cannot be detected easily in architectural glass. Karlsson's excellent review paper[20] has a wealth of information about how nickel sulfide inclusions arise, how many there may be, and ways to mitigate them or detect them before fracture. They often come from alloys (e.g., stainless steels) that react with Na_2SO_4 fining agents in the melt. The inclusions have a different thermal contraction than the glass, and they can pull away slightly from the glass on cooldown. Cooldown rates from the melt are fast enough that the nickel sulfide cannot transform to the stable beta phase at room-temperature. Nickel sulfide inclusions are usually easy to detect on fractured tempered windows. The telltale origin pieces (see patterns of breakage, chapter 4) have an internal fracture origin site and distorted fracture mirror markings will be centered on the round black metallic-looking inclusion. Sometimes their color is described as "yellow-gold."[20,25] Kasper[28] reported the size distributions of hundreds of nickel sulfide inclusions that caused breakages in building. They ranged from 70 mm to 450 mm in size. A second size distribution was shown for glass panels that broke during heat soak testing (a procedure used as a preventative screening method) and their size range was 40 mm to 450 mm.

Bao et al.[29] have reported a new class of metallic spherical inclusions that are not nickel sulfide, but are polycrystalline silicon. These can easily be confused with nickel sulfide, but chemical analysis in the scanning electron microscope convincingly showed they were not the latter. The silicon inclusions contract much less on cooldown than the surrounding glass, leading to very localized tangential tensile residual stresses in the glass. If the inclusion is in the inner tensile-stressed portion of the tempered plate, they can cause spontaneous fracture at any time, much like the nickel sulfide. It is not a silicon phase transformation that triggers this, however. Kasper[28] reported on silica stones, iron stones, and even a rare instance of a cobalt sulfide inclusion causing fractures in heat soak tests.

Not all inclusions behave the same. Their effect depends upon whether their elastic and thermal properties match or mismatch those of the matrix. Inclusions can cause cracking in the matrix, may crack themselves, or may detach and pull away from the matrix creating a void like flaw. Figure 6.21 on the next page from a paper by Evans[30] illustrates the possibilities. Fréchette's book has a brief chapter 6 on inclusions and discusses how inclusion sizes are important. If their dimensional changes relative to the matrix are small, the stresses in them are insufficient to generate microcracks. If they are in a low-stress region they may have little or no effect on service performance. His

Figure 6-1 showed a chromite inclusion that caused fracture in a glass bottle, Crossed-polar optical illumination highlighted the strains around the inclusion. Otherwise, inclusions can cause local deviations in trajectories of running cracks.

Inclusions can also control strength in highly-filled resin-matrix dental restorative materials such as shown in Figures 6.22 and 4.2d-f in chapter 4. Transillumination is effective in finding them in such translucent materials.

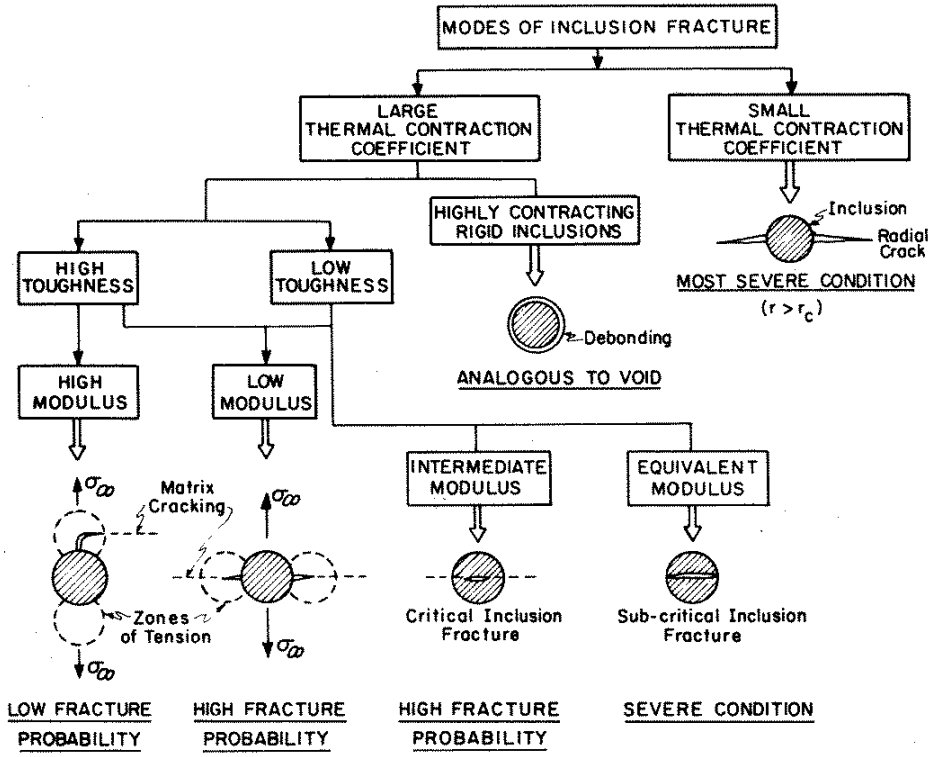

Figure 6.21 *The mismatch in properties between an inclusion and a matrix determine how severe an inclusion will be. From Evans, ref. 30.*

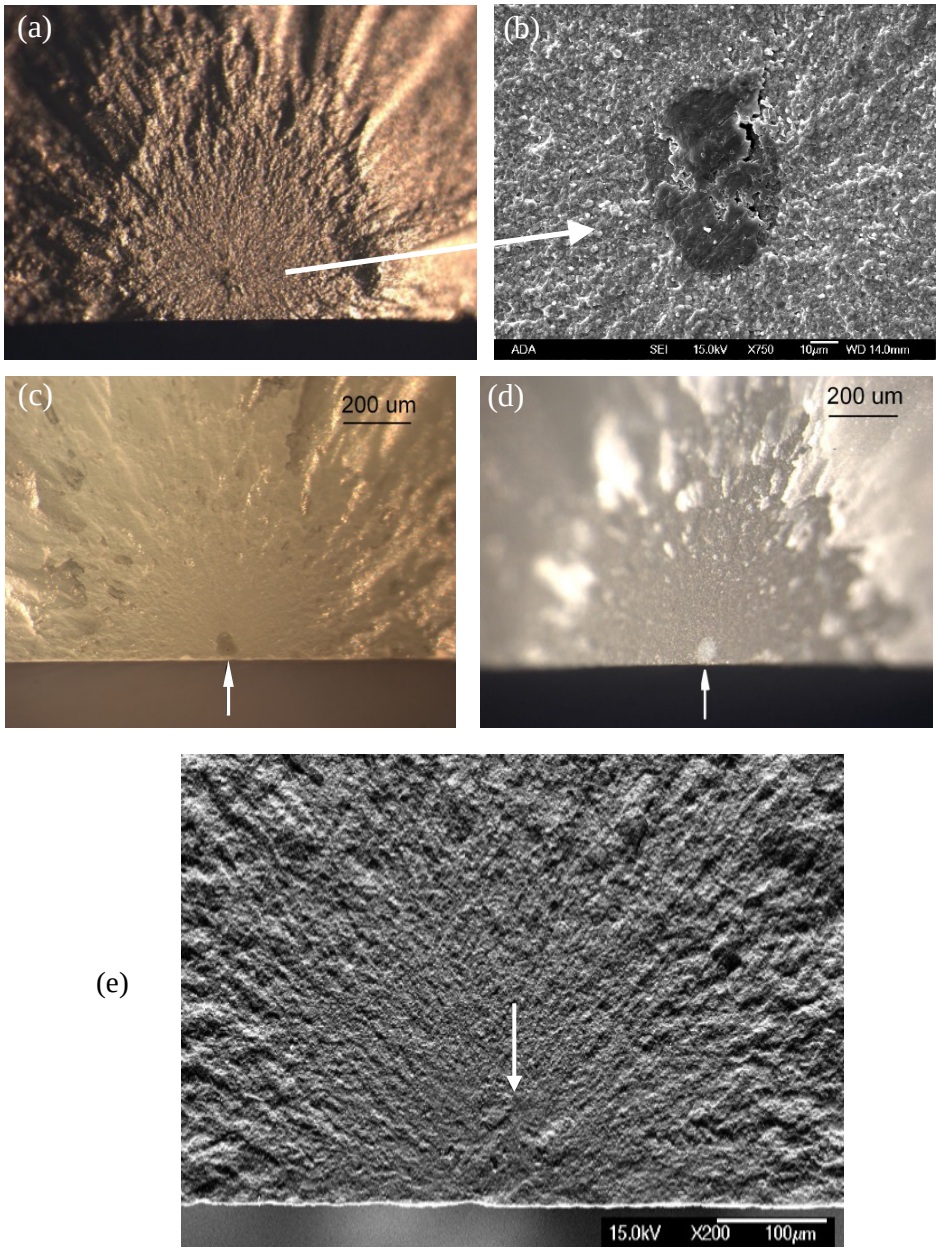

Figure 6.22 *Examples of inclusion origins in a highly-filled resin-matrix dental composite (Paradigm MZ 100) bend bars. (a) and (b) show a calcium rich inclusion on a gold-coated fracture surface. (a) is with reflected light and (b) is in the SEM. (c) – (e) show an aluminum inclusion in a different bend bar with: transillumination (c), conventional reflected light (d), and in the SEM (e).*

6.6.6 Compositional inhomogeneities

These are microstructural irregularities related to the nonuniform distribution of the primary constituents, an additive, or a second phase. They may have a color or reflectivity difference compared to the matrix. Sometimes they are pockets of glass in a ceramic. Examples are shown in Figures 6.23 and 6.24 here, and Figure 3.46 on page 3-51 in chapter 3.

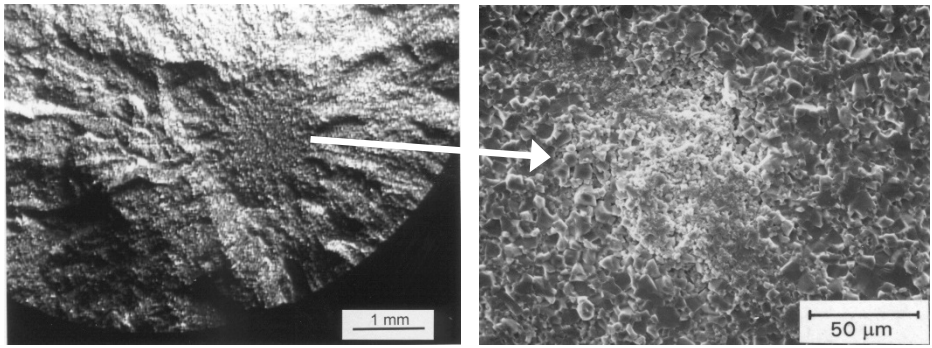

(a) (b)

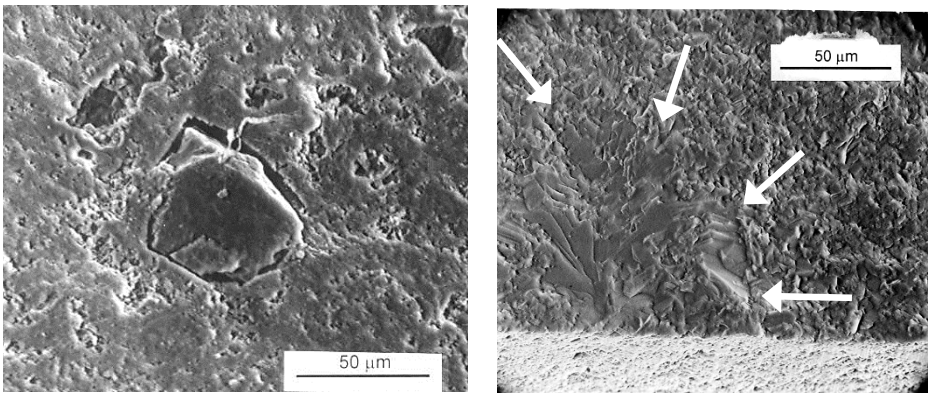

(c) (d)

Figure 6.23 *Examples of compositional inhomogeneity fracture origins. (a) and (b) show an example of an aluminum rich zone in a hot-pressed silicon carbide. Aluminum is an element in the sintering aid. (c) shows an unreacted silicon globule that pulled away from the matrix in a reaction-bonded silicon nitride. (d) shows a silicon lake in a siliconized silicon carbide.*

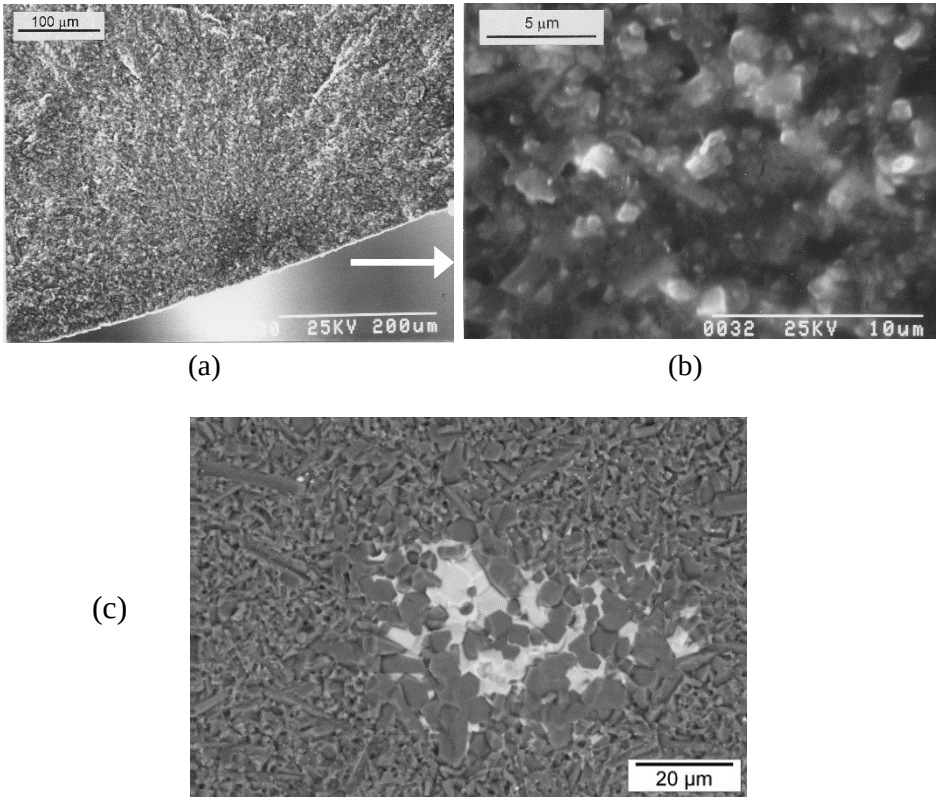

Figure 6.24 *Examples of compositional inhomogeneity fracture origins. (a) and (b) are an example of a local excess of sintering aid in a sintered reaction-bonded silicon nitride. Note the glassy appearance in (b). (c) is a yttria-alumina agglomerate in a silicon nitride bend bar where yttria and alumina were the sintering aids. (c is courtesy T. Lube and R. Danzer)*

6.6.7 Large grains

Large grains can occur due to local exaggerated grain growth. They may form due to a slight compositional or density variations during sintering. The compositional variability can be from a localized impurities or excesses of a sintering aid. Large grains can be a single grain or a cluster of grains having a size significantly greater than the range of the normal grain size distribution. They can often be seen with the optical microscope due to a difference in reflectivity compared to the matrix. Examples are in Figure 6.25. Rice's book[31] on grain size and mechanical properties of ceramics has a good discussion of large grains as fracture origins on his pages 13 – 16.

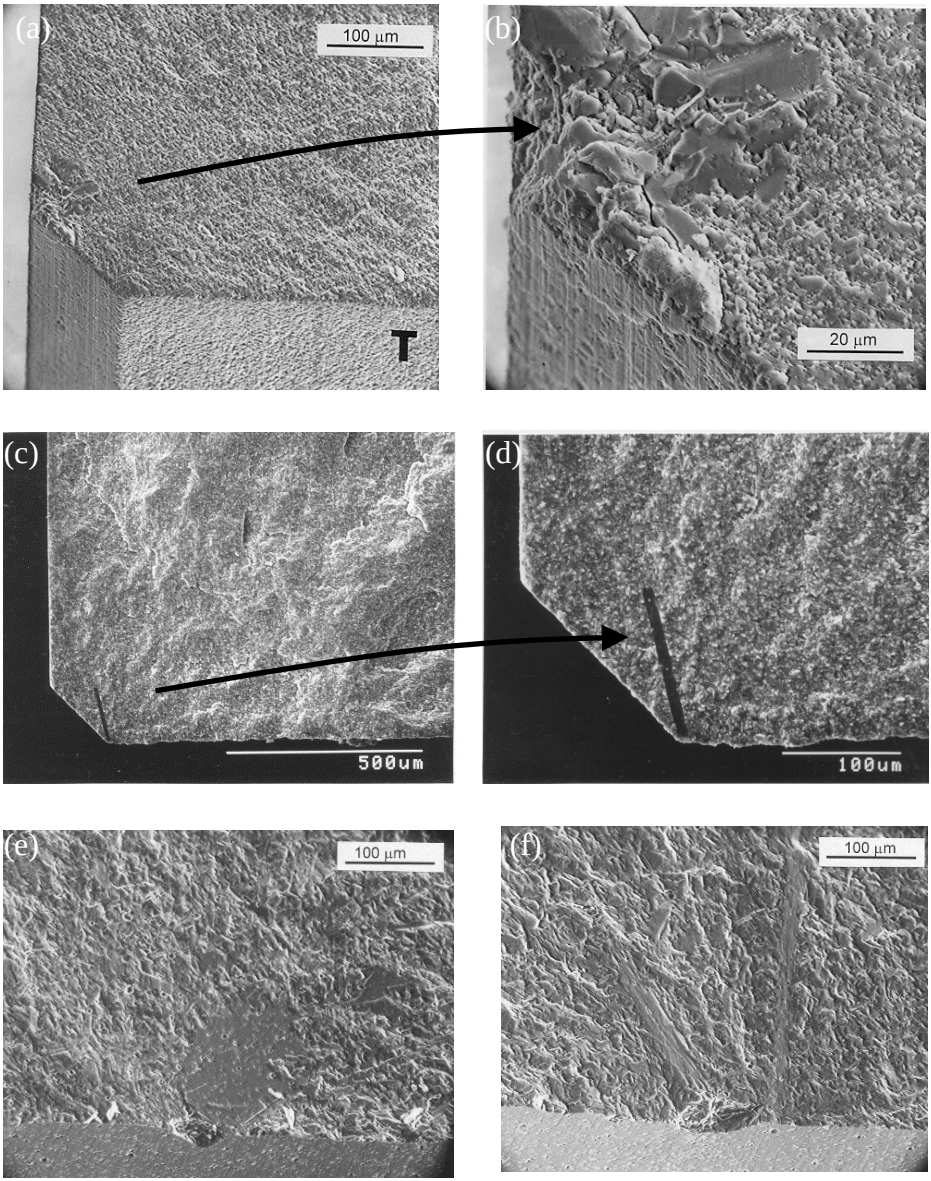

Figure 6.25 *Examples of large grain fracture origins. (a,b) show a cluster of large grains at a chamfer in a 99.9% alumina bend bar. (c,d) show an oversized grain in a silicon nitride. The material had small interlocking elongated grains intended to enhance fracture toughness. Notice how these are legitimate material flaws, and the chamfer preparation was completely satisfactory. (e, f) show examples of acicular large grains in sintered alpha silicon carbide.*

(a)

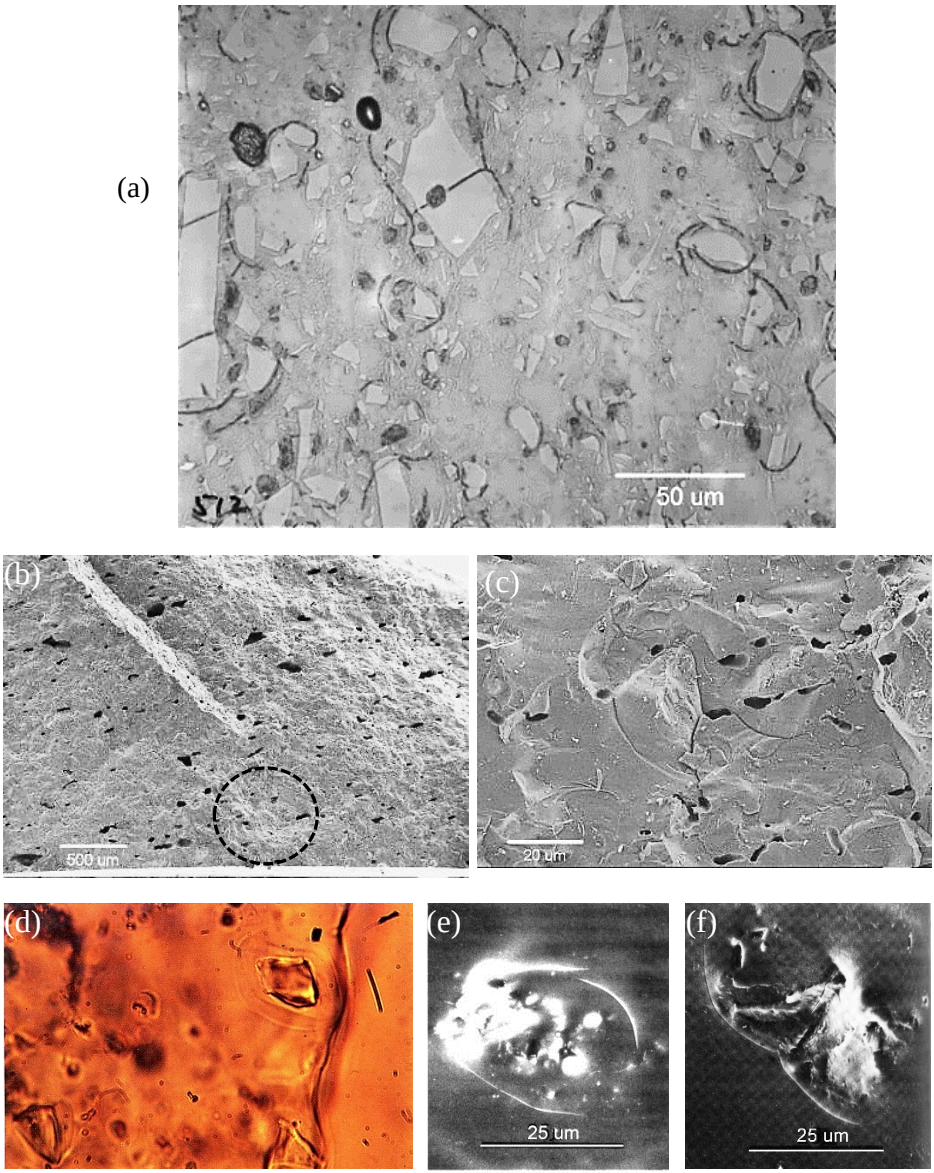

Figure 6.26 *Cracking around and through quartz grains. (a)-(c) are from a broken porcelain mortar (courtesy R. Morrell). (a) shows a polished and etched microstructural view. (b) shows an SEM image of one fracture origin (circled). (c) is a close-up SEM image showing microcracking around quartz particles. (d) – (f) are from porcelain dental crowns (courtesy D. Southan.*[33]*) The thin-section polarized-light color image (d) reveals a reaction zone and microcracking around the quartz grains.*

Large quartz grains can act as strength-limiting flaws in whitewares as discussed on page 6-75 (e.g., “dunts”). Porcelains may be comprised of many crystalline phases, but quartz can cause fractures. Quartz has several polymorphs and displacive transformations during cooldown from processing temperatures can cause cracking around large grains as shown in Figure 6.26. This is referred to as the b - a quartz inversion. If the quartz grains are much larger than the normal microstructure, they may stand out clearly on a fracture surface. If the quartz grains are similar in size to the normal microstructure, then the origin flaw may blend into the rough fracture surface and be difficult to discern. Good examples have been shown by Gee and Morrell,[15] Carlstrom and Carlsson,[32] Southan[33] (who had superb high-quality glossy color-prints), and Banda and Messer.[34]

6.6.8 Grain boundaries

Grain boundaries may be vulnerable areas and, if the grain size is large enough, the boundaries can act as strength limiting flaws. Figure 6.27 shows examples. Such flaws are very difficult to unequivocally identify as origins since the fracture path may be intergranular and follow other grain boundaries thereby creating a very rough fracture surface. There are many papers on the effect of grain boundary cracking upon strength, but few actually show a grain boundary origin. Davidge and Tappin[35] showed grain boundary origins in alumina.

Sometimes the grain boundary cracking occurs from internal strains set up from differential contractions in anisotropic, noncubic ceramic grains. In other cases, impurities or sintering aids can gravitate to grain boundaries and weaken them. For example, Salem[36] found tiny alumina particles at grain boundaries of coarse-grained $MgAl_2O_4$ cubic spinel transparent plates. These so weakened the material that jagged crack paths formed, and debris separated from the material upon fast fracture. Fracture origins were either large grains or the grain boundaries in disk strength specimens. Swab et al.[37] also studied a coarse-grained spinel which had irregular crack surfaces and even had granular debris generated during fracture. Lithium and fluoride from the sintering aid concentrated at the grain boundaries and dramatically weakened the material. I examined one large (40 cm square) plate made that had so much boundary cracking that green dye that I used to stain the fracture surface bled profusely into the bulk. Grains literately fell out of the fracture surface while I did this.

Coarse-grained (50 mm to 70 mm) magnesia partially-stabilized zirconia fails from grain boundary cracks as shown in Figure 6.27 Microstructural analysis of polished specimens is essential for the diagnosis in such cases. Gee and Morrell[15] showed a good example in a partially-stabilized zirconia.

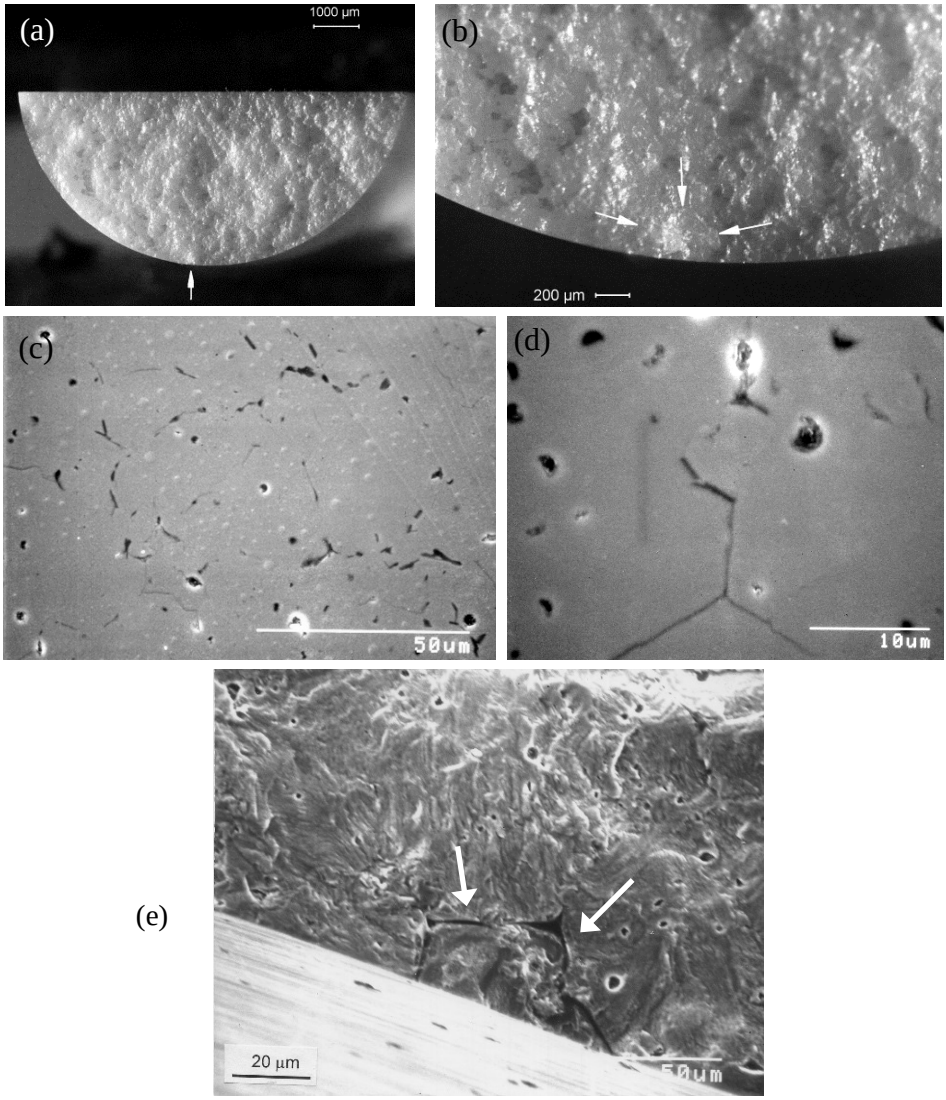

Figure 6.27 *Grain boundaries may be flaws in coarse-grained materials such as Mg partially-stabilized zirconia (50 m to 70 m grain size). (a) and (b) show optical images of the rough fracture surface of a split rod flexural strength specimen, a cylinder that has been sliced in half lengthwise. The origin is marked by the arrows. The rough surface is due in part to weak grain boundaries. (c) and (d) show SEM images of a polished surface revealing the gaps and cracks along the grain boundaries. (e) shows a grain boundary fracture origin. Tiny wake hackle lines from several small pores radiate away from the origin. Although this was a difficult analysis, the origin was identified by the coarse hackle lines in (a) and the tiny wake hackle lines in (e).*

6.7 Surface-Distributed Flaws

6.7.1 Surface voids or pits from processing

Surface voids are cavities on the surface of a component created by a reaction with the *processing* environment. They are similar to pores, except that they only arise on the surface. Surface voids can be in a reaction layer from hot-isostatic pressing with a glass encapsulation cladding or from trapped outgassing bubbles. Examples are shown in Figure 6.28.

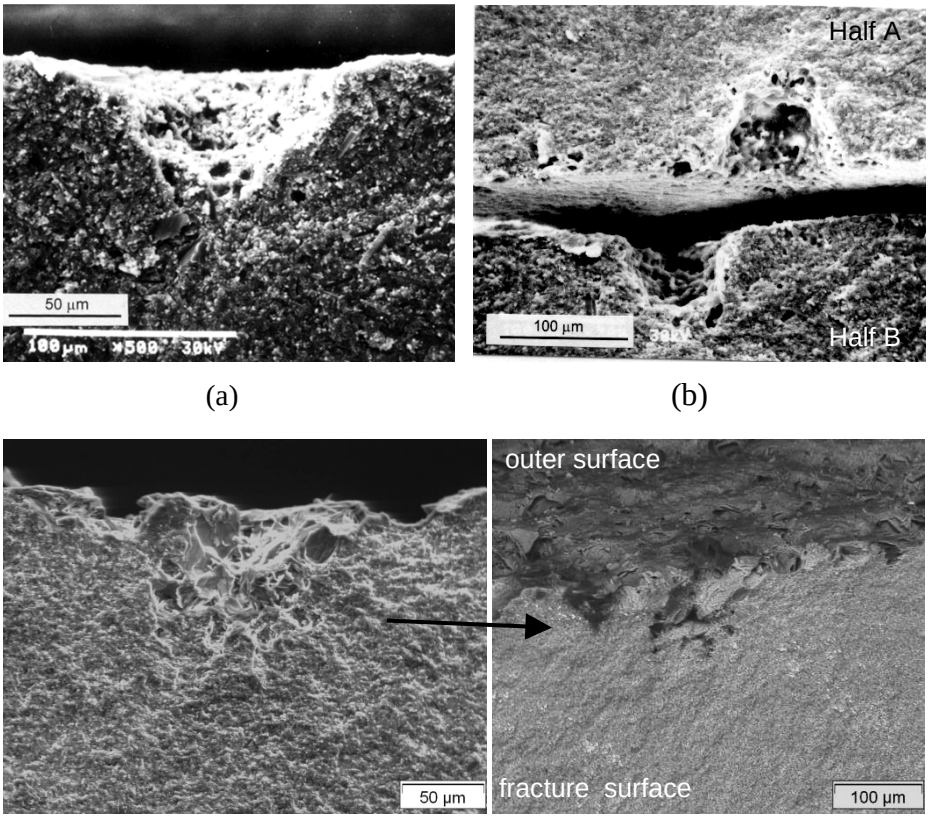

Figure 6.28 *Examples of surface void fracture origins. (a) and (b) are in as-fired bend bars of injection-molded sintered silicon nitride. (c) and (d) show a surface void in an as-fired silicon nitride component with yttria and alumina sintering aids. (d) is tilted so that the outer surface is visible. EDX analysis showed an excess concentration of aluminum at the site, so the flaw also has characteristics of a compositional inhomogeneity. (a,b are courtesy A. Pasto; c,d are courtesy T. Lube, W. Harrer, and R. Danzer).*

6.7.2 Pits from environmental exposure

Pits are surface cavities that may form as a result of a reaction between a ceramic or glass and the *usage* environment. Corrosion or oxidation can create pits. Examples are shown in Figure 6.29. Richerson[38] shows several good examples of oxidation and corrosion pits in silicon nitride. Pits have chemistry or structural differences that make them distinguishable from pores or surface voids. Sometimes the damage can be confined to grain boundaries and the flawed regions can be difficult to discern on a fracture surface.

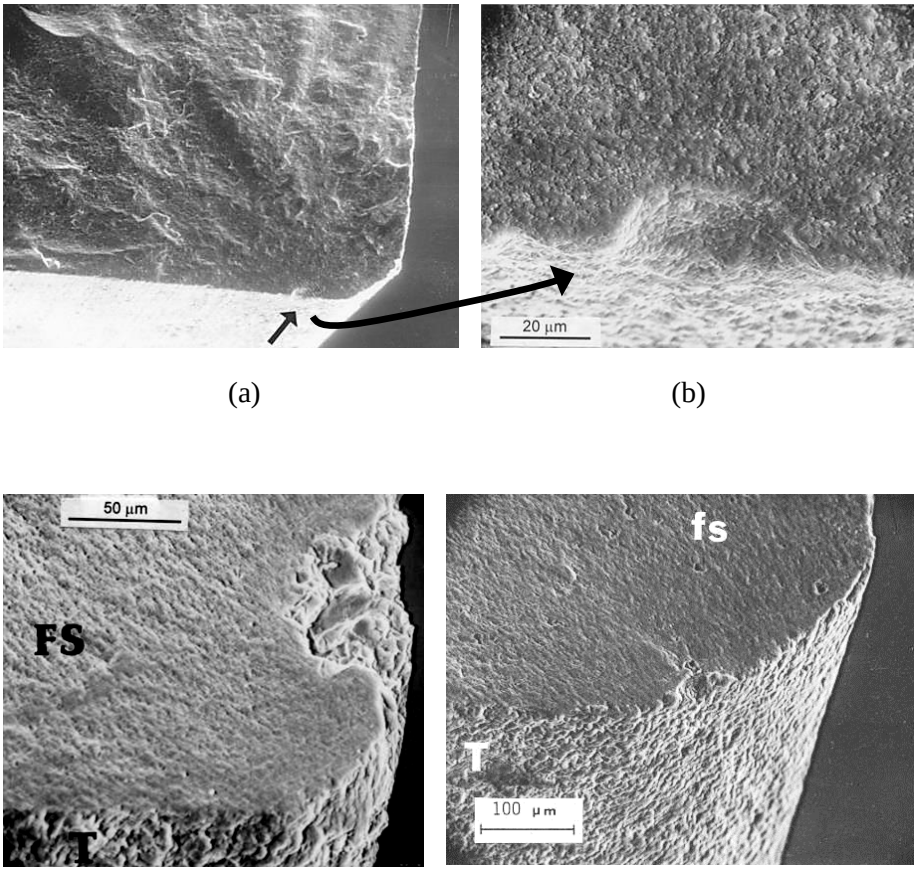

Figure 6.29 *Examples of pit fracture origins. (a) – (c) are in oxidized hot-pressed silicon nitride. (b) is a close-up of (a). (d) is a reaction-bonded silicon nitride.*

6.7.3 Handling scratches and polishing scratches

Handling damage may be scratches, chips, cracks, or other flaws due to handling or impact. Examples are shown in Figures 6.5b earlier in this chapter and 6.30, 6.31, 6.32 on the next pages. Scratch damage varies widely depending upon the material, the sharpness or bluntness, the speed, depth of cut, and force of the scratching object or abrasive. Schinker and Doll[39] showed superb illustrations of the variations of damage that occur in scratching of glass. Figure 3.11 in Suratwala's comprehensive book covers a range of scratch types in optical elements in glasses and laser materials.[40] At low force, a simple smooth groove may be created with mostly plastic deformation and minimal cracking. At higher forces and with more abusive tools and conditions, grooves with severe cracking may be generated. The cracking will be of several types: a crack that penetrates beneath the groove and follows the direction of the scratch, a series of shorter jagged cracks that jut out to either side of the scratch, and sometimes lateral cracks that are parallel to the surface and cause material to spall off. The cracking depth can be much greater (ten times or more) than the visible groove. Scratches that occur after fabrication and finishing are usually easy to identify. They are often isolated and stand out on a surface, provided that the fractographer is careful to illuminate the part from different directions. Figures 6.5b and 6.30 show examples. It is easy to overlook a scratch on a surface if the lighting is not right. It is wise to rotate the part under the illumination or move the illumination around while watching through a microscope. A quick momentary reflection may be the first sign a fractographer gets of a scratch. Scratches may be overlooked on the SEM since they have very low contrast.

If the tensile stresses are oriented at an angle to the axis of the scratch, then only be a small portion of the scratch may trigger a fracture as shown in Figure 6.30. The fractographer always should look at the object's outer surface when a fracture origin is near the surface. On the fracture surface the scratch origin will be seen as an irregular crack that may be so irregular as to confuse a fractographer who may mischaracterize the origin or guess it is machining damage. This is in fact exactly what happened in with the specimen shown in Figure 6.30c. This bend bar was one of eighteen prepared for a fractography round robin Dr. J. Swab and I organized in the mid-1990s as described in Chapter 10. Dr. Swab scratched the bars then broke them in bending. All eighteen bars broke from the scratch origin. Each round robin participant got one bar. Only five of eighteen round robin participants correctly identified the origin as a scratch. This was disappointing and we realized some participants only looked at fracture surfaces.

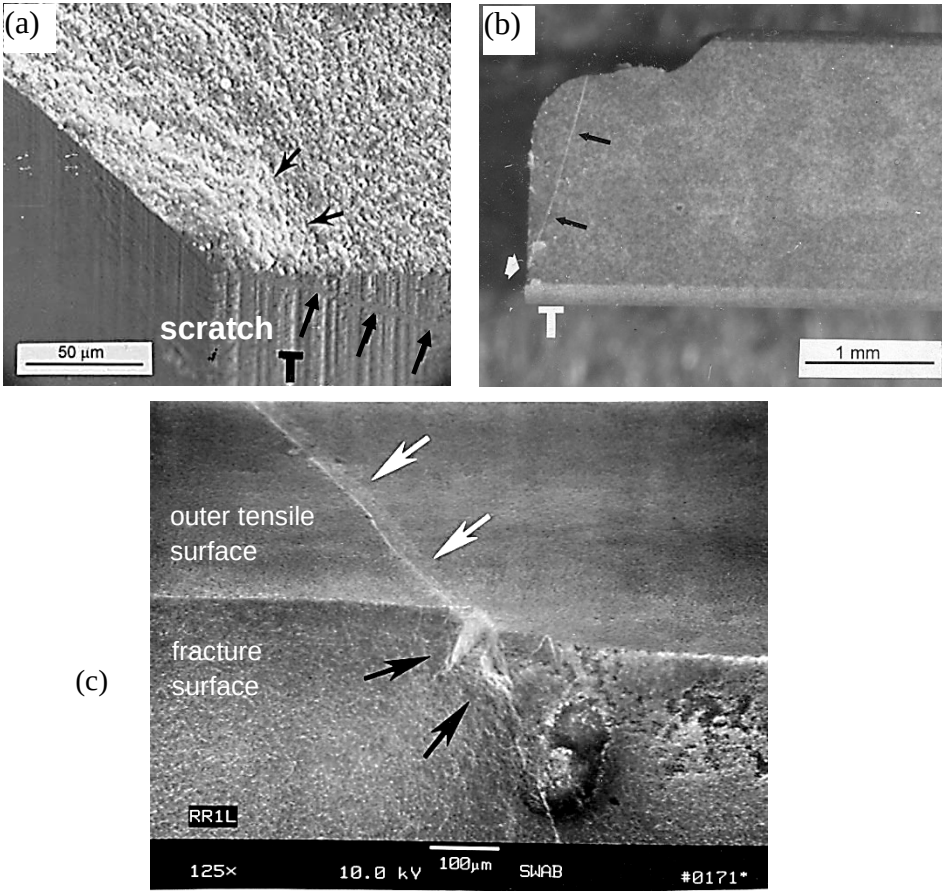

Figure 6.30 *Examples of scratch origins. The cracks penetrate much deeper than the scratch groove depth. Scratches can create damage that may be mistaken for grinding cracks, so it is wise to look at the orientation of the scratch relative to the grinding striations. Scratches will be at odd angles and are often isolated. (a) is in a SiAlON bend bar with a scratch near the chamfer. (b) is a side view of a reaction-bonded silicon nitride bend bar. Scratches often require illumination at just the right angle to be seen. (c) shows a scratch that was a fracture origin on an alumina bend bar surface. It is obvious on the outer surface (white arrows). The tilted bar shows the crack penetration into the interior (black arrows). (c is courtesy J. Swab).*

In other cases, with biaxially-loaded parts such as pressurized vessels or plates, or laboratory ring-on-ring strength tests, there will always be a tensile stress available that is perpendicular to the scratch axis. Figures 6.31 and 6.32 show two examples. In these cases, the fracture follows the scratch for a distance.

These can be tricky to diagnose if the fracture follows the entire length of the scratch, since the scratch trace on the outer surface may be overlooked or hard to see on the exact fracture edge, even if the pieces are put back together. On the other hand, fractures often veer off from the scratch axis, since irregular jagged cracks on the side of the scratch can redirect the main fracture.

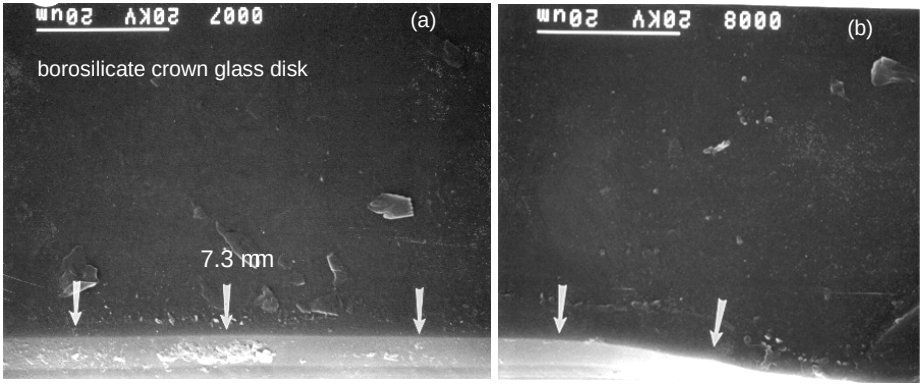

Figure 6.31 *Example of a scratch origin with the tensile stress normal to the scratch. The origin was in a polished BK-7 borosilicate crown glass disk broken in ring-on-ring flexure. The origin is a very long, but smooth 7.3 mm deep crack. Figure 5.20 in chapter 5 shows the fracture mirror. There were no traces of the scratch on the polished outer surface.*

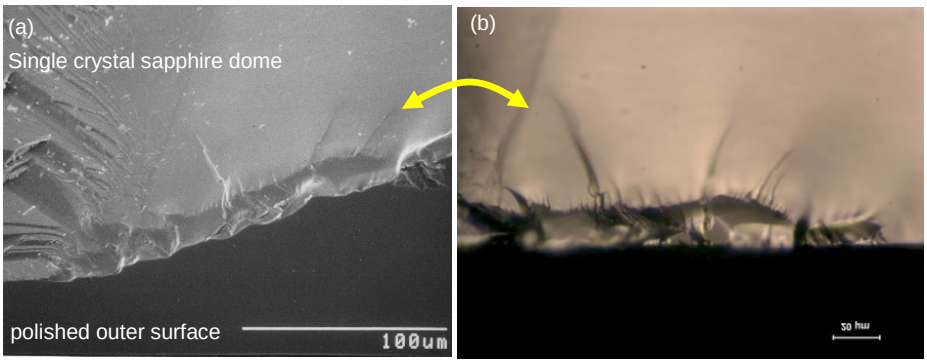

Figure 6.32 *Scratch origin in a single-crystal sapphire dome (#1037). (a) is an SEM image of the fracture surface and a portion of the outer surface on the bottom. (b) is an optical image at similar magnification. The dome broke in a high-temperature wind tunnel test rig. The dome is shown in its entirety in Figure 8.21 in chapter 8. There were no traces of the scratch on the polished outer surface.*

Polished surfaces often have no trace of the original scratch. Additional polishing after the scratch flaw was created removed all the surface traces. Figures 6.31 and 6.32 show two examples.

Scratch/dig specifications are used to describe the surface imperfections on the outer surfaces of glass or transparent ceramic materials. There is considerable confusion in the literature about scratch/dig specifications, and therefore this section is expanded significantly in this 4th edition. These specifications characterize appearances of irregularities on the outer surfaces. They do not necessarily characterize the depth of cracks that lie underneath the surface. The depth usually controls strength as discussed in chapter 7.

Scratch-dig specifications are commonly denoted by two numbers as in 60-40 (or 60/40) where the first number is the scratch specification and the second the dig specification. A 60-40 specification means a certain number of scratches of up to size #60 are permitted and digs of up to size #40 are permitted. The larger the number, the larger the feature on the surface. The scratch specification in MIL-PRF-13830B {1997}[41] is based on a visual comparison (under prescribed darkfield lighting and magnification conditions) to scratches on reference pieces maintained by the U. S Army. The inspection is subjective and can vary with the inspector.

Digs are damage sites that can be sharp or blunt contact damage as described in sections 6.7.4 and 6.7.5 below. They also may be bubbles or inclusions originally in the glass bulk that are partially exposed by the polishing. The dig number is straightforward. It is the approximate diameter of the observed feature on the surface in units of 0.01 mm or 10 μm. Thus, a #40 dig has an apparent diameter of 0.40 mm or 400 μm.

There is wild confusion about the scratch numbers in MIL-PRF-13830B.[41] Actual scratch width values are nowhere to be found in the latter. Although it was not intended to be a direct measure of a scratch length or width, the scratch number often has been associated to the nominal scratch width. It is most commonly converted to μm through a factor of 1/10. A #20 scratch thus has a width of 2 μm, a #60 has a width of 6 μm, and so on. In stunning contrast, the conversion factor to μm is 1 in many written references and sources on the internet. Beware! For example, a #60 scratch supposedly has a 60 μm width and so on. Reference 42 by Aikens explained the confusion, which is evidently traced to multiple revisions of U.S. Army drawing C7641866 that was a companion to the 1997 MIL-PRF-13830B. Aikens stated that: “The scratch-dig standard is, and has always been, a visibility standard, not a width standard. The scratch number is not the width in microns or tenths of microns.” He

added: “The misinterpretation of the scratch number as a width specification is a blight on our industry that costs millions of dollars a year and must be put to an end.” Aikens cited a newer ANSI approach that uses a lettering code as an alternative.

A different U.S. specification, MIL-C-48497A,[43] also has scratch and dig specifications for coatings. It is a little confusing since it specifies different procedures for transparent versus opaque coatings. For *transparent coated surfaces*, the scratch and dig specifications shall be specified by two numbers separated by a hyphen (i.e., 60-40) in accordance with MIL-O-13830 and MIL-PRF-13830B (as described above). Inspection is done with reflected light from specified cool white fluorescent light tubes with the inspected surface against a black background at a distance 18 inches (46 cm) or less. Alternatively, for *opaque coated surfaces*, scratch and dig requirements shall be specified by two letters separated by a hyphen (i.e., F-C) where the first letter is the maximum scratch size, and the second letter is the maximum dig size. Scratches A, B, C, D, E, F, G have widths of [5, 10, 20, 40, 60, 80 and 120 mm], respectively. Digs A, B, C, D, E, F, G, H have diameters of [50, 100, 200, 300, 400, 500, 700, and 1,000] mm, respectively. There also are limits on the accumulated length of the scratches and the permissible number of them.

Another alternative is ISO standard 10110-Part 7[44] which also characterizes surface imperfections. It is more quantitative and consistent than MIL-PRF-13830B, but requires a microscope with higher magnification and takes more time for inspection. Unfortunately, it defines scratches as features greater than 2 mm in length. In my experience, I have encountered scratch fracture origins that were less than 2 mm long. ISO 10110-7 uses a complex nomenclature specifying the size and number of scratches, digs, and sometimes edge chips. Fortunately, all the numbers simply correspond to the feature size in micrometers.[a] Whatever surface inspection specification is used, the outer surface features often have no correlation to the depth of cracks that lie underneath the surface. The depth usually controls strength as discussed in chapter 7.

When scratches are suspected, it is usually a good idea to look for other scratches elsewhere on the exterior surface of the part. Figure 6.33 shows an example where scratches controlled strength in an engine part.

[a] Suratwala’s book[40] covers surface preparation and characterization in great detail but curiously has little or no information about these standards.

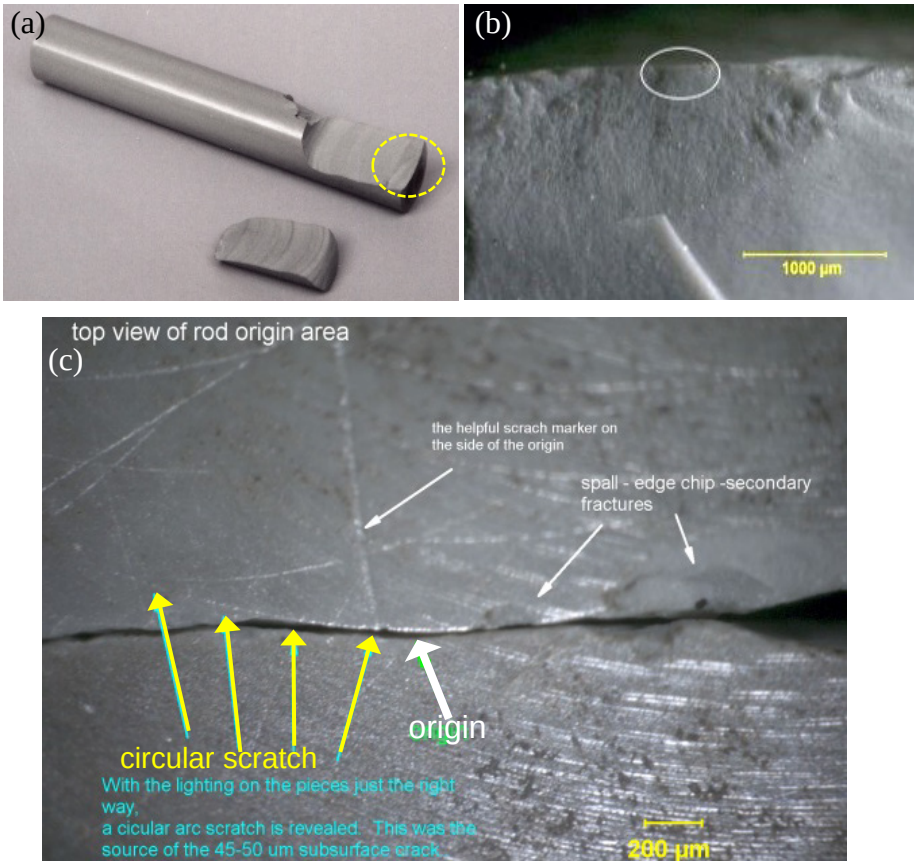

Figure 6.33 *A fractured 12 mm diameter silicon nitride pin. Examination of the fracture surface (b) might lead one to conclude that machining damage was the origin flaw. Examination of the outer surface (c) shows it actually was a scratch. Notice how the origin flaw has the same arc as the scratch.*

Suratwala's book[40] has a wealth of detail about how scratches arise in optical elements such as lenses, mirrors and prisms and active optics such as laser materials. Silicate and nonsilicate glasses (e.g., phosphate glasses) are covered as well as crystalline materials such as potassium dihydrogen phosphate. He introduced an interesting concept of **scratch forensics** (his section 6.2) to help ascertain the cause of scratches. *Rogue particles* in grinding and polishing media (section 3.1.2.7 in his book) can cause scratches. Scratches with large sharp changes in direction are typically *handling scratches*. (page 253 in his book). This know how is probably applicable to all ceramics and glasses rather than just optical materials.

The author became aware of an episode of rogue particles in a project on machining of ceramics that was coordinated by NIST in the 1990s. Some elements of that project are described later in this chapter in section 6.7.6. Ceramic flexural strength specimens were prepared by a variety of procedures by multiple institutions cooperating in a Consortium study. One institution had problems with random stray scratches that occurred in some of their bend bar specimens. The cause of the problem was elusive. Extensive efforts were made to track down the cause. Bars were carefully cleaned and handled with white gloves, packaged carefully, and inspected often. Eventually the cause of the scratches was tracked back to a conscientious machinist, who scrupulously cleaned the grinding machine table and specimen holder with a rag after every step. Unfortunately, he used the same rag for months on end, and it accumulated a host of dislodged diamond abrasive particles. The remedy was simple: change rags frequently.[b]

Occasionally a fractographer is called upon to examine an *intact* part and assess where a line on the surface is a crack or a scratch. The former may be very serious and may prompt a part to be replaced, whereas the later could be a simple cosmetic irregularity. How does one decide? In my experience, scratches usually have jagged edges when viewed with a 5 to 10 power hand loupe and strong lighting. They also will not allow water or alcohol to penetrate since they are superficial and shallow. Cracks, on the other hand, have very-sharp, narrow edges on the surface. If water or alcohol is applied,

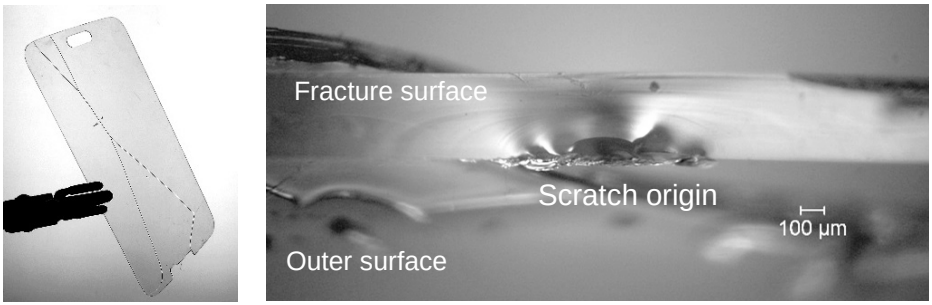

(a) (b)

Figure 6.34 *Cell phone supplemental glass cover plate that broke when the phone was dropped. The branching pattern is easy to interpret in this case as shown in (a). The curved Wallner lines on each side of the origin (b) confirm this was the origin site and that fracture occurred in bending.*

[b] This episode has not been documented in any previous publication.

the surface may dry quickly, but the crack will stay wet a while longer. If the material is transparent, one can shine a strong flashlight or laser pointer through the part side and look for reflections from the interior of the crack. Sometimes cracks may be invisible, however, as discussed in section 4.9 in chapter 4.

Figure 6.34 shows an example of a scratch in a tempered-glass cell phone supplemental cover plate. In this case, the scratch damage was very severe and deep so that not much energy was necessary to break the plate in bending. This was indicated by the minimal crack branching and large branch distance to either side of the origin site.

Single crystals are particularly susceptible to scratches. (An example is in Chapter 10 of the 3rd edition of this Guide, where Figure 10.38 showed a single scratch in an elaborate polished sapphire component caused fracture.)

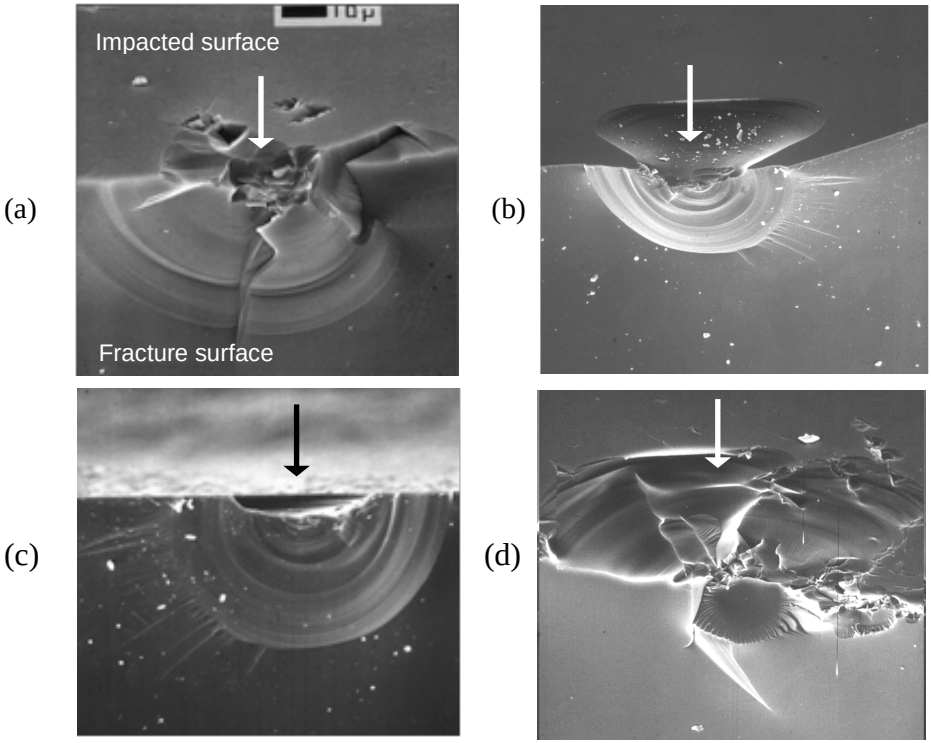

Figure 6.35 *Sharp particle imact origins in glass. The arrows show the impact direction. All have median – radial cracks and tertiary Wallner lines. (b) and (d) have surface lateral cracks as well. The picture height of (b) is 0.16 mm. The other sizes were not recorded. In each case the impact site has been pulverized or crushed, unlike blunt impact sites.(courtesy J. Varner)*

6.7.4 Sharp object impact or contact

Figures 6.35 and 6.36 shows examples of origins created by impact or contact of a sharp object. In glasses, such flaws are sometimes deemed "point contacts." Notice the beautiful concentric circular tertiary Wallner lines in Figure 6.35, a telltale characteristic of an impact as discussed in section 5.4.4. The cover of this book and Figure 6.38 below also show the concentric Wallner lines. Median and radial cracks may penetrate deep below the impact site, which is often heavily damaged with small fragments missing. Witness marks on the exterior surface may give clues as to the nature of the impactor. The exterior surface should be examined for other nearby impacts. Fréchette described sharp contact site damage as "pecks." "Digs" are visually-detected contact damage sites in glasses and optical ceramics (and were briefly described in the previous section on handling damage and scratches). Specifications for the allowable dig diameter may have some utility, but as the figures in this Guide show, and as discussed in the previous section, the surface damage size may or may not correlate with the size of the cracking beneath the surface.

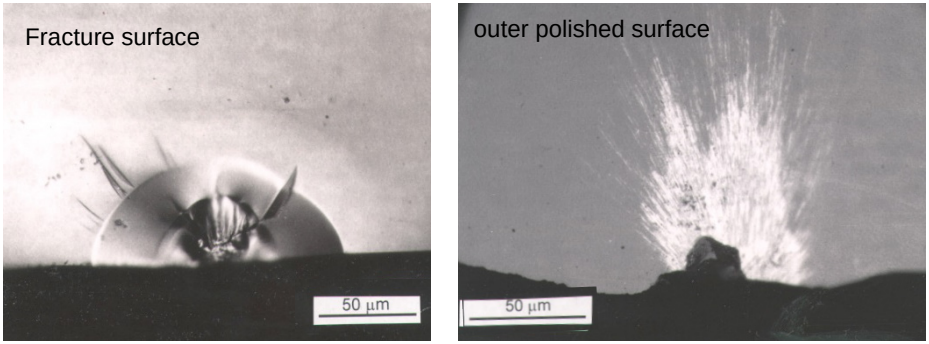

(a) (b)

Figure 6.36 *Particle impact origin in a single-crystal sapphire hemispherical dome. #29 (a) shows the subsurface cracking on the fracture surface. (b) shows the outer polished surface that was impacted. It has pronounced residual traces (witness marks) of the impactor.*

Sharp impact damage can cause fracture in tempered glass if the cracks penetrate the outer compression layers. Figure 6.37 shows an example. Figure 4.24 in chapter 4 and Figure 5.24 in chapter 5 show examples of a tempered auto side window.

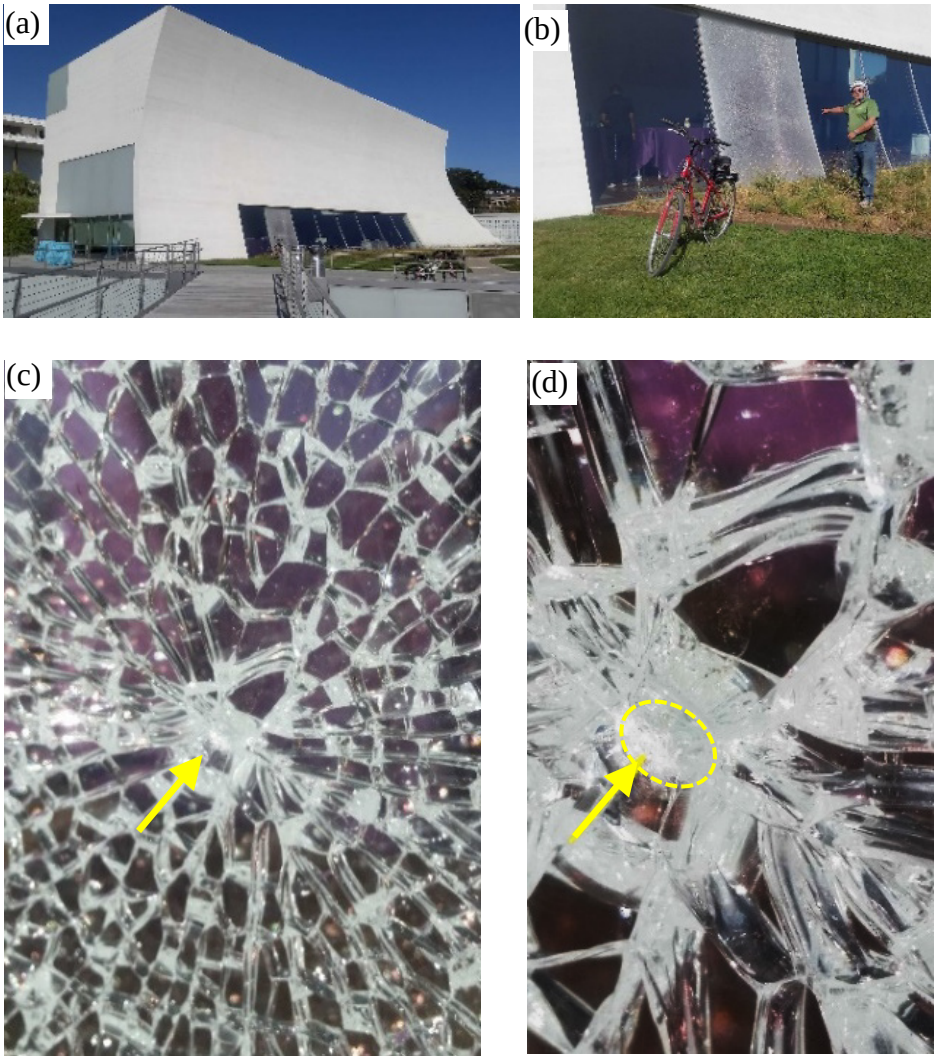

Figure 6.37 *The author poses with a broken tempered-glass window at the Kennedy Center for the Performing Arts in Washington, DC in October 2019. The window has "diced up" but is still in place. The sharp contact damage site on the outside surface is marked by the arrows. There is local pulverization at the impact point on the outer surface.*

Chips or flakes from contact loading or impact at the edge of a piece are described in section 4.15 and are shown in Figures 4.33 – 4.38. They usually are curved shell-shaped fragments since fracture runs out to the free surface. The initial contact damage or impact cracks in this section may either be straight into the bulk, or have some curvature.

Figure 6.38 shows a fractured piece of glass cullet from an archeological excavation of an ancient Roman glass factory at Jalame, Israel. The factory operated from 351 AD to 383 AD.[45] The irridescence on the surface is characteristic of heavily-weathered glass and is due to leaching of glass cations to the outer surface. The outer glass layers have varying compositions and different optical properties. Despite the severe weathering over 18 centuries, the magnificent circular tertiary Wallner lines are still evident. The corrosion over them indicates that fracture occurred in antiquity from impact. The plane of fracture is very flat, and not shell-shaped such as in an edge chip fracture.

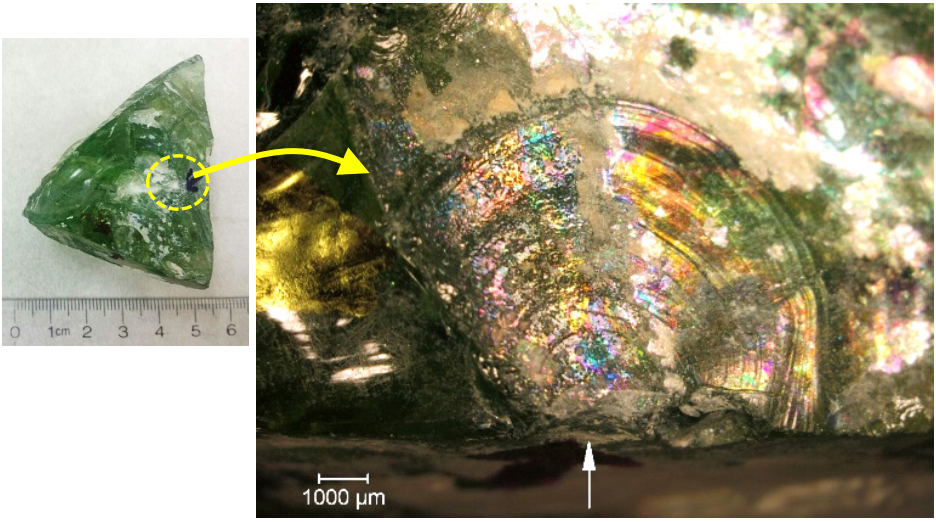

(a) (b)

Figure 6.38 *Impact origin in a glass fragment from an impact fracture that probably occurred in the 4th century. (a) shows the fragment, and (b) is a closeup of the impact origin site with concentric tertiary Wallner lines. (Fragment courtesy of R. Brill and S. Koob, Corning Museum of Glass.)*

6.7.5 Blunt object impact or contact

Blunt impacts or blunt contact loadings produce round Hertzian cone cracks as illustrated in Figures 6.39 and 6.40. In glasses, such flaws are sometimes called "percussion cones." These may be complete or partial rings as shown in Figures 3.61 (a C-crack in a ball bearing) and 6.42 – 6.44. The cone crack initiates as a ring just outside the footprint of the two contacting bodies as shown in Figure 6.41a. The size of the contact area depends upon the load, geometries, and elastic properties of the two materials. A simple rule of thumb is that the contacting object is almost always several times larger than the observed ring size on the contacting surface as shown in Figure 6.41. Of course, if the blunt object penetrates through the plate and makes a large hole, then the impactor may be comparable in size to the hole. When contact damage is detected, the exterior surface should be examined for witness marks at the contact site, as well as other nearby impacts.

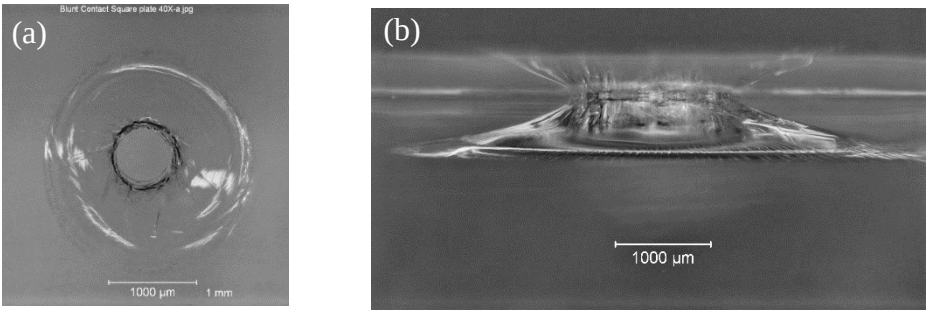

Figure 6.39 *Blunt contact or impact cone cracks in glass. (a) is a top view of the contacted surface. (b) is a side view looking through the glass.*

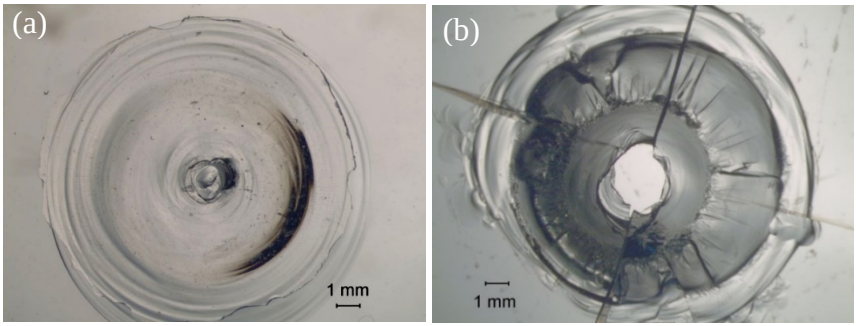

Figure 6.40 *Blunt impact origins in glass plates. These are also referred to as "percussion cones." (a) shows a mild – moderate impact with cone cracks. The plate did not break into pieces. (b) is a severe impact that was sufficient to create cone and radial cracks. The latter caused plate fracture. (Specimens courtesy of J. Varner and V. Fréchette)*

Blunt contact cracks often leave little trace on an outer surface. An inspection for "digs" may not find blunt contact damage cracks. The contact cracks might be revealed prior to fracture by very careful examination with adjustment of lighting angles. After fracture, they are easier to detect since they leave *a small telltale arc* on the fracture surface plane at the origin site.

Ring cracks initially pop in normal to the surface but then turn and propagate into the depth with an included angle of 125° to 135° for quasi static loading in glasses as shown in Figure 6.41a. The included cone angle decreases markedly with increasing impact velocity as shown in Figure 6.41d. It may be possible to estimate the projectile velocity from the included cone angle.[46,47,48]

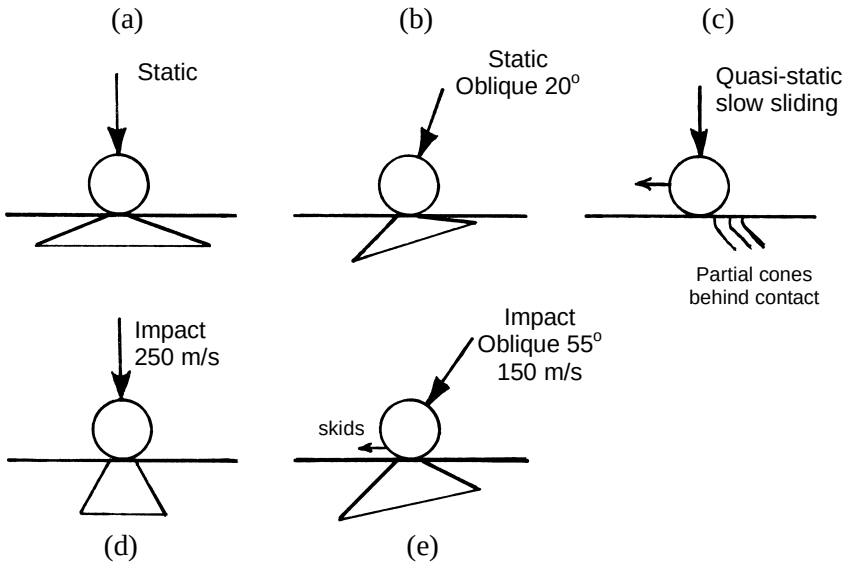

Figure 6.41 *Blunt contact or blunt impact cone crack profiles. These are side views. Notice the blunt impactor is larger than the size of the contact circle and first ring to form at the impact site.*

For example, at 250 m/s, 0.8 mm to 1 mm diameter steel balls created 60° to 80° cone cracks in glass[46] and 70° to 90° cracks in silicon carbide.[48] LaSalvia et al.[49] studied impact cone cracks from spherical ball impact on armor materials including boron carbide, silicon carbide and tungsten carbide. Aydelotte and Schuster[50] used 6.35 mm diameter tungsten carbide balls at 200 m/s to 500 m/s to impact boron carbide and obtained cone angles of 78° to 86°.

During quasi-static or impact loadings, as load increases the footprint area may expand and generate multiple concentric ring and cone cracks. Kirchner and Gruver[51] described interesting variations of cone cracks from impact, whereby cracks can nucleate on one side, then branch, and then even spiral around the contact site.

If a ball that is loaded perpendicular to the surface is slid over the surface at quasi static rates, the cone axis tilts such that the rear of the cone dips down deeper, and the front portion of the cone disappears (Figure 6.41c).[52] Partial cone cracks are the result. This is not surprising since the forward motion of the ball creates an additional tensile stress behind the ball but adds compressive stresses ahead of the ball.

Conditions are different if the contactor is loaded or impacts at nonperpendicular angles. Full cones form, but they tilt so that the backside approaches the surface while the front side penetrates deeper into the surface as shown in Figures 6.41b,e.[53] Aydelotte and Schuster[50] showed similar results for inclined spherical impacts in armor ceramics.

Most blunt contact loadings produce a cone crack that penetrates partially or completely through a plate or body as shown in Figure 4.23. These may not cause component breakage and may merely be a cosmetic fault. Subsequent loading in tension or flexure may cause new crack extension from the cone crack as shown in Figures 6.42d,e. Many structures such as dental crowns may have numerous harmless cone cracks in the veneers. They are only revealed when a fracture that commenced elsewhere passes through the cone (Figure 6.42f).

Impacts at moderate or high energy create radial cracks and bending stresses that can propagate cracks far beyond the impact site and any cone cracks, thereby causing component fracture. Figure 6.43b shows an example.

Partial cone cracks can be a problem as well. A common, serious flaw in ceramic balls and ball bearings is a so called “C-crack” also known as a “crescent crack” such as shown previously as Figure 3.61 in section 3.24 on fluorescent dye penetration. It was a partial cone crack. They are often formed by ceramic balls impacting each other! Manufacturers wisely started to package ceramic balls more carefully once the problem was recognized.

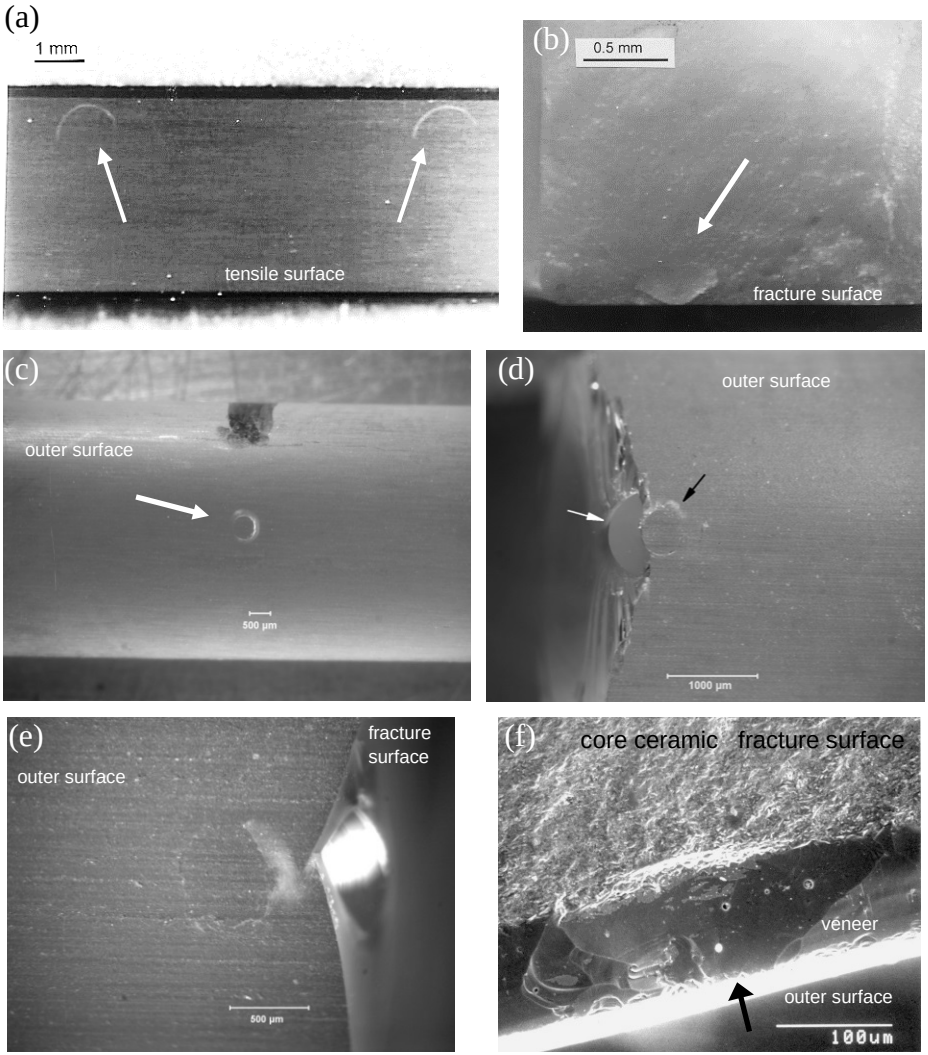

Figure 6.42 *Examples of blunt impact or contact crack damage. (a) shows the tensile surface of a silicon nitride bend bar with partial crack rings that were created by a ball-tipped micrometer. Such rings were fracture origins in some other bend bars. (b) is a cone crack fracture origin from a blunt contact or impact on a rectangular bend bar. (c) shows a blunt contact crack from a loading roller on a cylindrical rod glass flexure specimen. Notice that the ring is incomplete. The cone crack can act as a strength-controlling flaw if loaded in tension as shown in (d) and (e). (f) shows a cone crack in a dental bilayer crown. The cone crack, which initiated from contact on the porcelain veneer layer, was harmless. Fracture initiated elsewhere and a crack simply passed though the cone crack.*

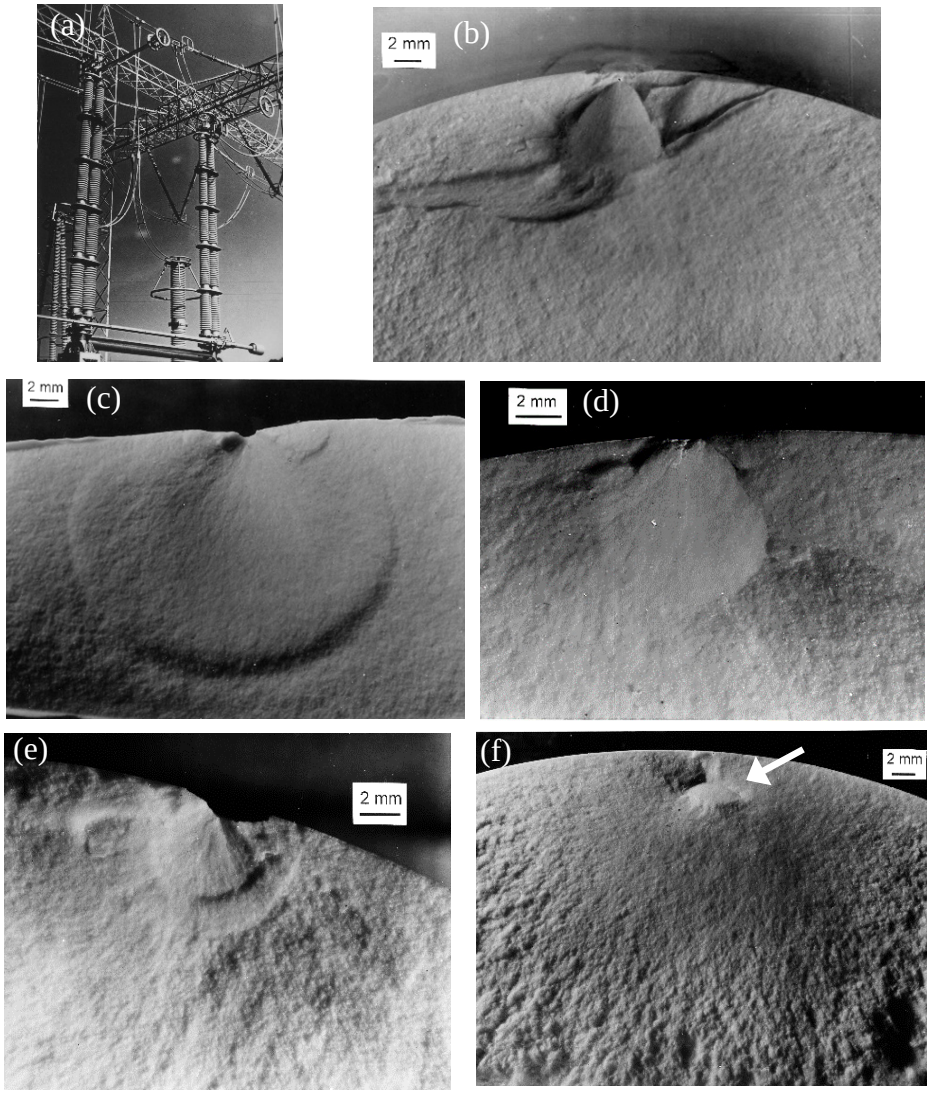

Figure 6.43 *Blunt impact origins in electrical insulator porcelains. (a) shows the installed insulators. (b) and (c) are blunt impact damage from "BB" gun projectiles. (d) is damage from a sling shot projectile. (e) and (f) are impact origins from contact with support structures. Note the partially exposed cone in (f) (arrow). (Photos courtesy of J. J. Taylor and R. W. Rice)*

Blunt-contact cracks can also be a problem in the glass container and pharmaceutical industries. Figure 6.44 on the next page shows examples. Sometimes such partial Hertzian contact cracks are called "bump checks" or "bruise checks." Case 4 in Chapter 10 has another example of contact damage

cracking in a medicinal vial. Figure 4.31 on page 4-45 shows another good example in a medicinal vial. Glass-to-glass contact between bottles or vials can cause severe contact damage as shown in references 54 and 55. Telltale surface abrasion marks accompanied the partial cone cracks. Case #13 in this Guide (Fig. 10.32) shows a partial cone crack that caused fracture in an elaborate single-crystal sapphire component.

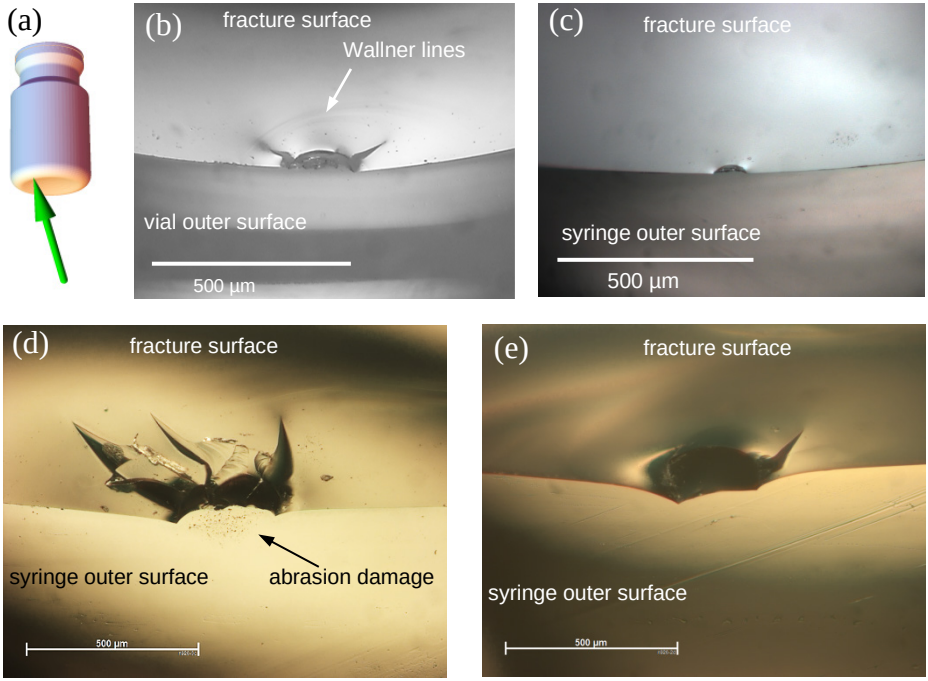

Figure 6.44 *Blunt contact damage in pharmaceutical glass. Contact damage like this is often called "bump checks" or "bruise checks." (a) and (b) are a vial. The pictorial (a) schematic shows a possible impact direction and is a useful aid for explaining a fracture event. (c) - (e) are three glass syringes. When arc-shaped contact cracks propagate to fracture, they often have hackle lines that emanate from the sides of the flaw. Notice how these tilt in opposite directions on the flaw sides indicating that fracture radiated outwards. Such hackle at an origin site suggests "eyelashes." Notice the witness mark of abrasion damage in (d). (Photos courtesy of F. Maurer)*

Water drops hitting a surface at high velocity can also cause impact damage that resembles solid object blunt contact crack damage. Many concentric ring cracks form with different penetration angles. Harris'[56] book illustrated water damage impact sites in missile dome materials including single crystals. Cross references to the water impact damage literature were provided.

6.7.6 Grinding and machining cracks

Grinding or cutting introduces damage to the surface. The damage can be controlled, usually by using progressively finer grinding and polishing steps to remove damage introduced by prior steps. Edges are particularly susceptible to damage and can easily be cracked or chipped. Bevels, chamfers, and rounding are effective treatments for the latter. They are commonly applied to biaxial disks and bend bars and are carefully aligned circumferentially or lengthwise lest the beveling introduce more cracks.

Surface grinding procedures use grinding wheels as shown in Figure 6.45. The grinding process entails material removal, often by means of microcrack and microchip formation. By its very nature, cracking is introduced into the surface. Initial grinding is done with coarse-grit wheels and modest depths of cut in order to facilitate material removal. Intermediate- and final-stage grinding is done with finer-grit wheels and smaller depths of cut to reach final part dimensions and surface finish requirements, but also to remove prior damage while introducing a minimum amount of new damage.

Fractographers realize that there often is no correlation between the strength of a part and the final surface finish. The reason is simple. Grinding induced cracks penetrate far deeper (10 to 20 times) below the surface than the surface undulations and striations. Sometimes the crack depths *are proportional* to the depth of the surface grooves, and the surface finish may correlate to strength. On the other hand, strength may be controlled by deep grinding cracks from earlier steps that are not removed in the final finishing phase which may produce a very fine outer surface finish. The author once ordered a batch of conventional alumina bend bars to be cut and ground out of a billet by a new machine shop. The shop was instructed to surface grind longitudinally and not use their preferred Blanchard grinding process that creates random swirl marks and attendant cracking. The shop ignored the instructions and Blanchard ground the bend bars and then lapped them to a beautiful finish. The strength of the bars was quite low, however. They fractured from severe, randomly-oriented grinding cracks introduced by the Blanchard process. The final lapping did not go deep enough to remove the prior damage. Suratwala's book[40] argues that crack depths are proportional in size to polished surface roughness, but admitted there is significant variability (from a factor of 1.4 to 49) in the reported trends even for a single material such as fused silica.

Figure 6.45, an adaptation of a figure by Rice and Mecholsky,[57] illustrates some key aspects of machining flaws. Parallel cracks oriented in the direction of grinding are longer and are the same depth or deeper than the orthogonal

cracks. Thus, the parallel cracks are more deleterious to strength. Not shown in the figure are shallow lateral cracks, which run parallel to the outer surface. These usually do not control strength. Nonetheless, their formation and interactions with each other across the surface are important mechanism of material removal in the grinding process.

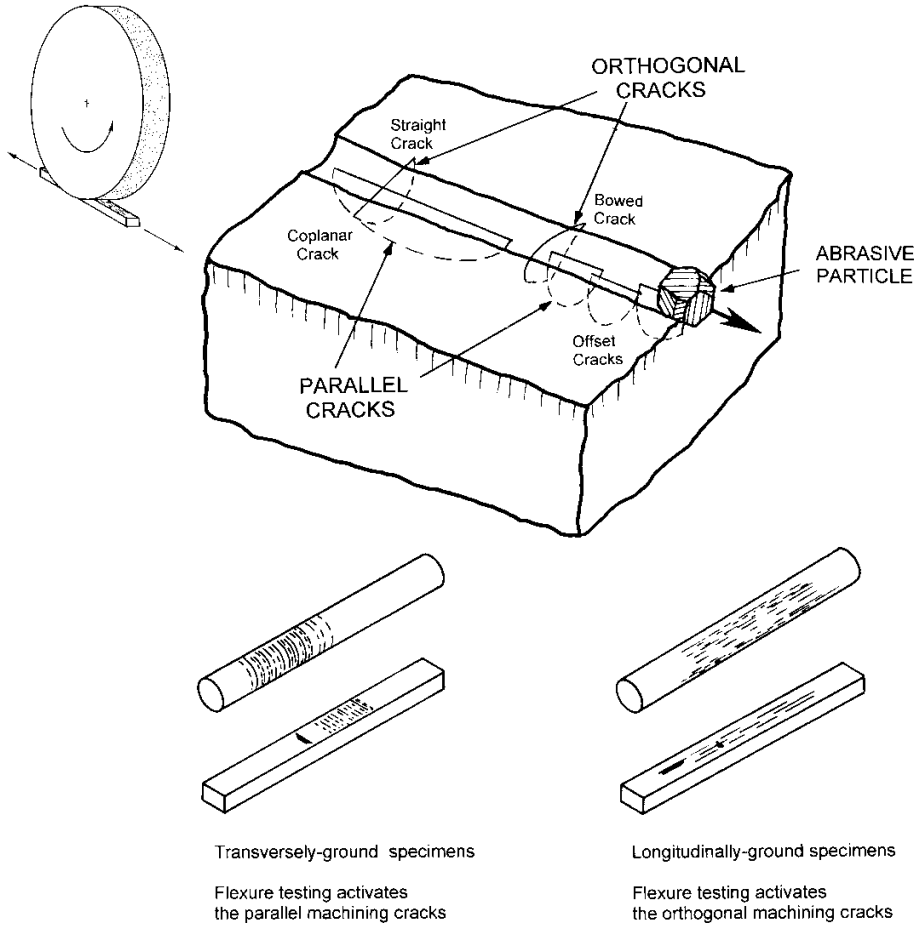

Figure 6.45 *Surface grinding (insert) creates grinding grooves (striations) and subsurface cracking. The cracking includes long deep "coplanar parallel cracks" or "offset parallel cracks" aligned with the striations in the direction of abrasive motion. Orthogonal cracks form at right angles to the striation and may be bowed in the direction of abrasive motion. Lateral cracks or spalls that are roughly parallel to the surface may also form (not shown). The axis of grinding is often chosen to align the worst cracking damage (parallel cracks) with a specimen axis as shown on the bottom right.*

The differences between the orthogonal and parallel cracks cause strength to vary with orientation if grinding cracks are the controlling flaws. Only one striation groove is shown in the schematic and the ground surface actually contains a network of cracks and grooves.

With some experience it is not too difficult to find parallel grinding crack flaws in dense materials, such as glass, single crystals, and either very coarse-grained or extremely fine-grained ceramics. Detection of grinding cracks in porous, heterogeneous, or mid grain-sized materials is very difficult, however, since the machining crack blends in to the background microstructure. This is especially true for the short orthogonal cracks. Orthogonal cracks are hard to find in nearly all materials. Figure 6.46 shows some examples of orthogonal cracks, which sometimes are described in the literature as "longitudinal-grinding flaws." (That expression means: "the flaws that are created by longitudinal grinding" with respect to the specimen's long axis.) Additional examples are shown in some of the papers by Rice and Mecholsky listed in Appendix A.

Parallel machining cracks are much easier to detect and often can be found with routine optical microscopy, but only with very low-angle grazing illumination. Indeed, they can be easier to detect with such optical microscopy than with an electron microscope! Figures 6.47, 6.48 and 5.21 in chapter 5 show examples. Figure 6.47a shows the grinding damage often is a series of small, slightly offset or staggered microcracks. When fracture starts from this group of microcracks, short hackle lines form between the nearby microcracks. They converge quickly and leave behind telltale "**grinding crack hackle**." This pattern is sometimes known as "**shark's teeth**" such as shown in Fig. 6.47a. One gets the sense that the main fracture crack runs quickly sideways along the microcracks and they "unzip" along the surface. Hence, the overall flaw may also be described as a **"zipper crack."**

Grinding crack hackle: *Hackle formed on the fracture surface originating from irregularities and steps in grinding cracks.*

The size of grinding cracks, and their effect on strength, depends upon material properties such as hardness, elastic modulus, and fracture toughness. It also depends on the grinding wheel and machine conditions such as abrasive type, grit size and concentration, depth of cut, wheel speed, grinding forces and machine horsepower. The crack size also depends upon the material's grain size. Deep grinding cracks can form in coarse-grained ceramics since the single-crystal fracture toughness is less than the polycrystalline fracture toughness. Figure 6.51 below has more information about crack sizes.

(a)

(b)

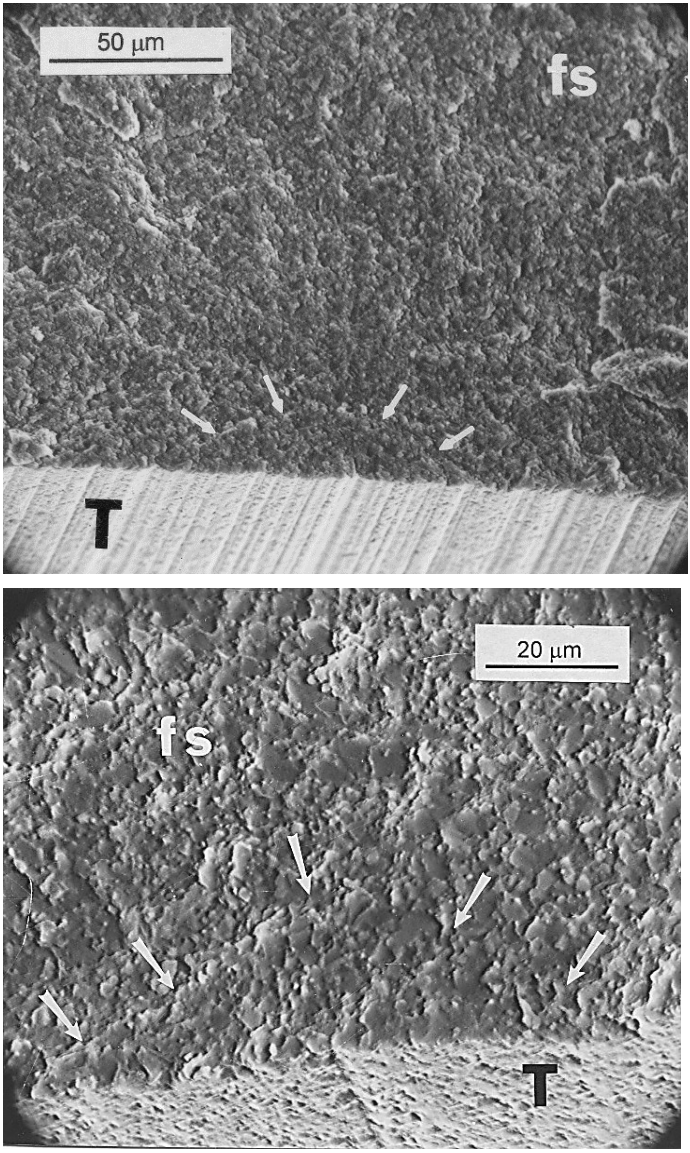

Figure 6.46 *Orthogonal grinding cracks from* <u>*longitudinal grinding*</u> *as seen in some fine-grained ceramics. (a) shows a crack in a hot-pressed silicon nitride bend bar. (b) shows a crack in a hot-pressed silicon carbide. The bars have been tilted back in the SEM to reveal parts of the ground surface "T" which was in tension. "fs" means fracture surface. Slightly larger than normal striations are evident on the ground surface in each case. The orthogonal cracks are hard to find even with the SEM, since they blend in with the microstructure. Notice the large striation on the bottom of (b).*

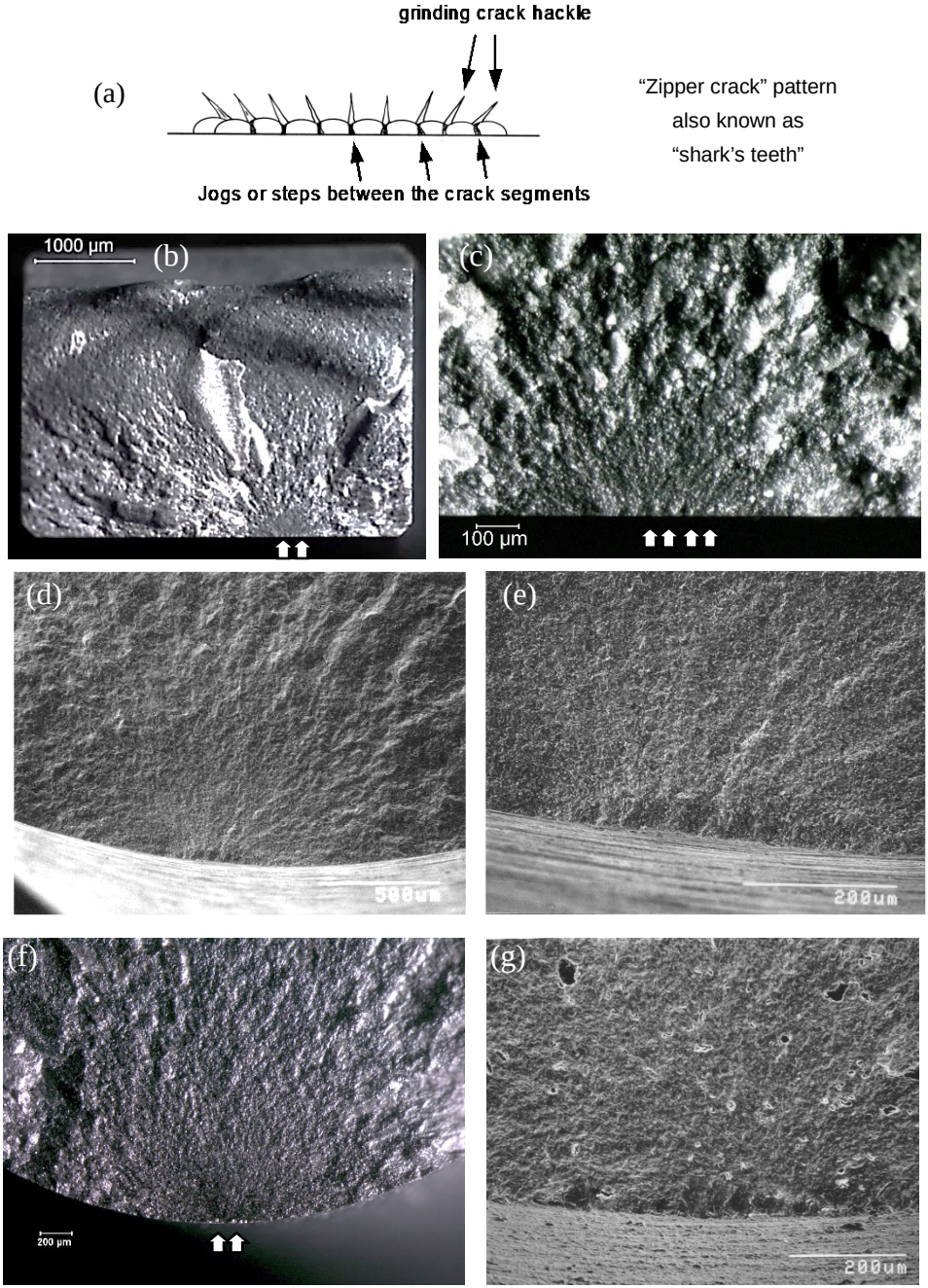

Figure 6.47 *A "**zipper grinding crack**" from transverse grinding is in the schematic (a). (b) and (c) show optical images in a sintered silicon nitride bend bar. (d) and (e) show SEM images of a crack in a silicon nitride rod. (f) is an optical and (g) a SEM image of a sintered alpha silicon carbide rod.*

Coarse grinding can create a "skin zone" of cracks along the outer bar surface. R. Rice also detected such skin zones. Figure 6.49 on the next page shows a schematic of the telltale signs of parallel flaws.

(a)

(b)

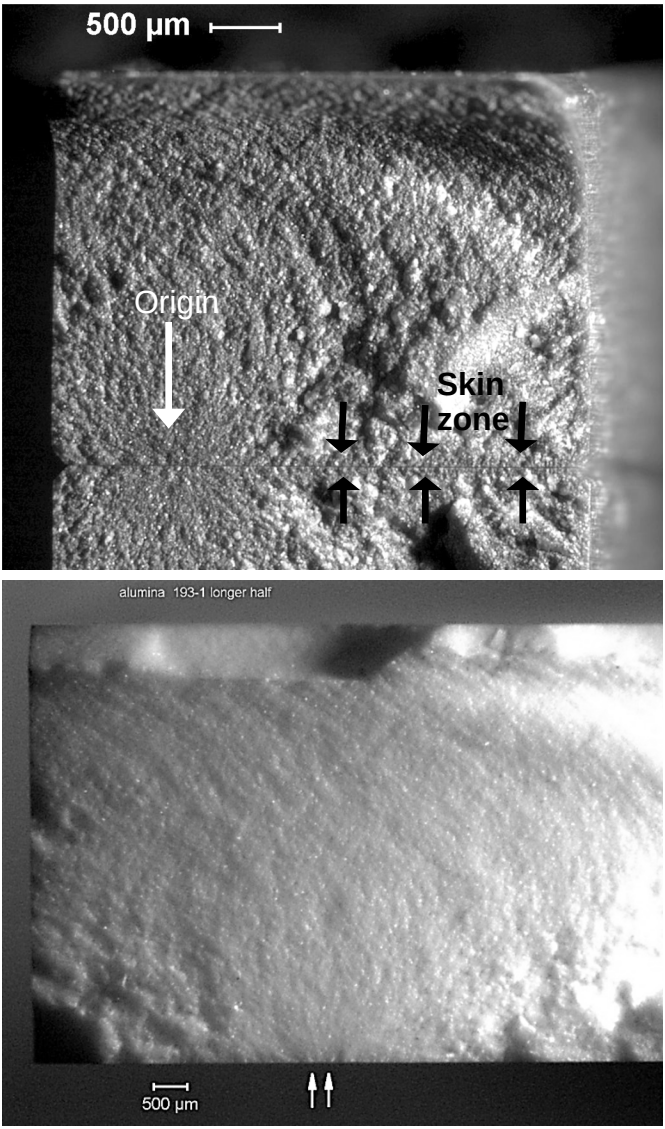

Figure 6.48 *Examples of parallel grinding cracks from* <u>*transverse grinding*</u>*. (a) shows back-to-back halves of a silicon nitride bend bar with coarse grinding (150 grit) cracks. A* ***zipper crack*** *is at the origin (large white arrow). The small black arrows show that there also is a machining crack "****skin zone****" along the entire surface. (b) is an alumina bend bar with low-angle grazing illumination from the side also revealing a zipper crack.*

(a) elongated “coplanar parallel crack”
(or coplanar linked semi-elliptical cracks).
A deep striation may or may not necessarily be present.
The fracture mirror may be elongated along the outer specimen surface.

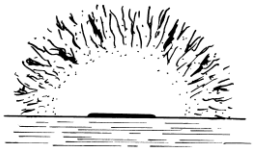

(b) elongated “coplanar parallel crack”
linked with a natural flaw.
A step in the fracture origin emanates from the material flaw.

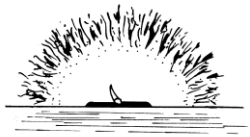

(c) “zipper crack”
This is a series of short semi elliptical cracks, which have linked.
A series of short tails, or “machining crack hackle,” emanate from the links or overlaps of the flaws and extend up into the fracture mirror. These tails may be tilted to the left or right and help confirm that fracture originated in the central region of the set. The short tails are telltale features of slightly misaligned or overlapping transverse machining cracks (or a scratch) and are often easier to see with an optical microscope with low angle lighting than with a scanning electron microscope. The fracture mirror may be elongated along the specimen outer surface or it may have one or two prominent side lobes.
This origin type is common in transversely-ground rectangular flexure specimens or scratched biaxial disk specimens.

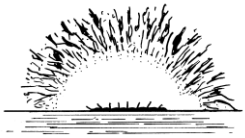

(d) coarse “zipper crack”
This is made up of a series of irregular, less coplanar semi- elliptical cracks. Larger tails than in (c) are created. In severe cases, the tail may extend all the way to the mirror boundary. The fracture mirror may be elongated. This origin is common in transversely ground or scratched specimens and the markings are sometimes termed “shark’s teeth.”

(e) “V machining crack”
The crack intersects the fracture surface at an angle. Only a portion of the machining crack or crack series is exposed. A pronounced step occurs in the fracture mirror. One or two (shown) tails extend well up into the fracture mirror. The machining direction is not quite perpendicular to the specimen length and uniaxial stress axis due to grinding wheel cross feed. This origin is common in cylindrical specimens prepared by centerless or cylindrical transverse grinding wherein the wheel and work piece displace axially relative to each other.

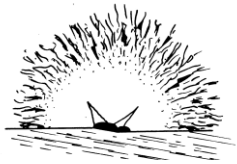

(f) “coarse grinding parallel crack”
The origin is a deep machining crack that extends along the entire surface. The origin is often bumpy since the origin is comprised of offset parallel cracks. Thin bands of uniform depth extend along the specimen surface on either side of the fracture mirror. The bands have the same depth as the grinding cracks. Short tails, or “machining crack hackle” which may be in the thin bands are tilted away from the origin. This origin type is common in coarse ground surfaces.

Figure 6.49 *Schematics of telltale features of parallel machining cracks. These origins are common in biaxial disks, pressure-loaded plates, and transversely-ground flexural or tension strength specimens. Low-angle grazing illumination facilitates their detection with optical microscopy. Some have elongated mirors along the surface, an important telltale sign.*

Figure 6.50 shows how "V" machining cracks form in ground round parts.

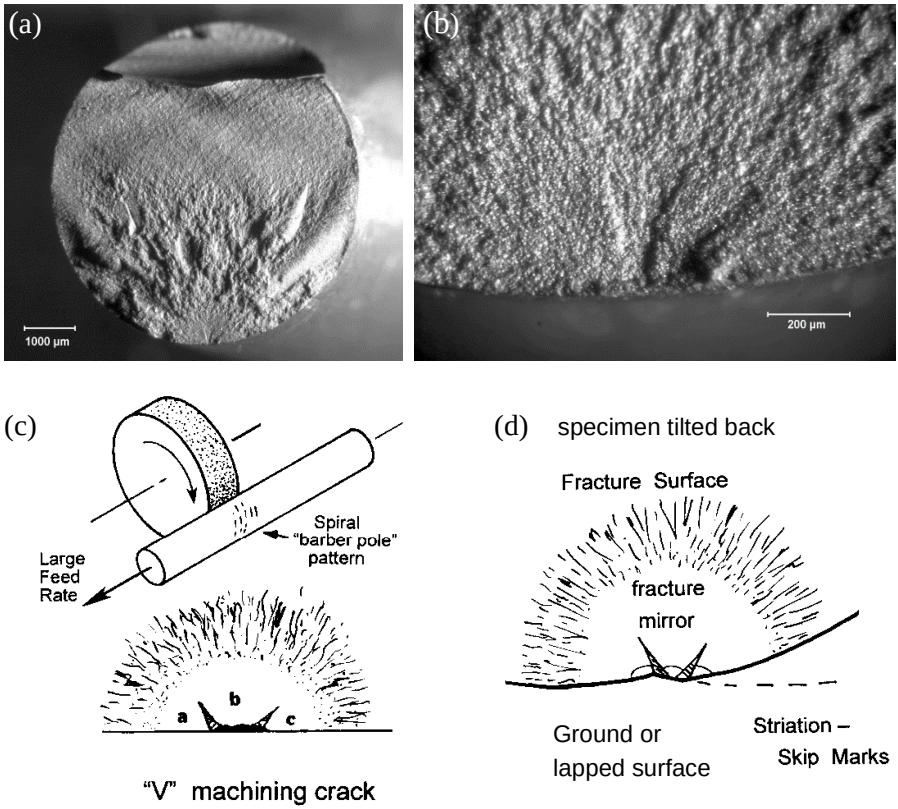

Figure 6.50 *Round parts may have "V" machining cracks. These are formed from small parallel crack segments a, b, c on different planes as shown in (a) and (b) for a silicon nitride rod. The steps between the individual crack segments form two or more telltale hackle lines, which extend up into a mirror. Examination of the ground surface shows striations (grinding grooves) that have a small angle relative to the rod axis. V crack flaws are easy to see even at very-low magnification with low-angle grazing illumination.*

Abrasive grit size usually is the dominant parameter that controls crack size. Figure 6.51 on the next page shows the effect of grit size upon parallel crack depth in a transversely-ground commercial silicon nitride.[58] Each data point in Figure 6.51a corresponds to a single flexural strength specimen that broke from a grinding crack. Crack sizes were comparable in rods and rectangular bars. The depths of transverse grinding cracks for a given procedure varied by up to a factor of 2. Their size ranged from 1/3rd to 3/4^{ths} of the nominal diameter of

the abrasive grit (the normal way of expressing abrasive grit size) or, in other words, the crack depths ranged from 2/3rds to 1.5 times the radii of the abrasive grits. It should be borne in mind that for a given nominal abrasive grit size, there actually is a range of particle sizes. Figure 6.51b summarizes the trend and also shows that material flaws became dominant for 600 grit or finer abrasive wheels. The smallest detected grinding crack depths were 12 mm. Sizes smaller than this do not appear in the graph since the specimens broke from material flaws instead. In the latter case, the material flaws had sizes from 10 mm to 45 mm (half minor axis length). Grinding crack depths in other silicon nitrides were discussed in a companion paper.[59] Other factors besides the abrasive particle size such as the depth of cut and grinding forces undoubtedly contribute to variations in the maximum crack depths. Nonetheless, the data shown in Figure 6.51 were collected from batches of ten to thirty specimens prepared by different machine shops and the data are remarkably consistent.

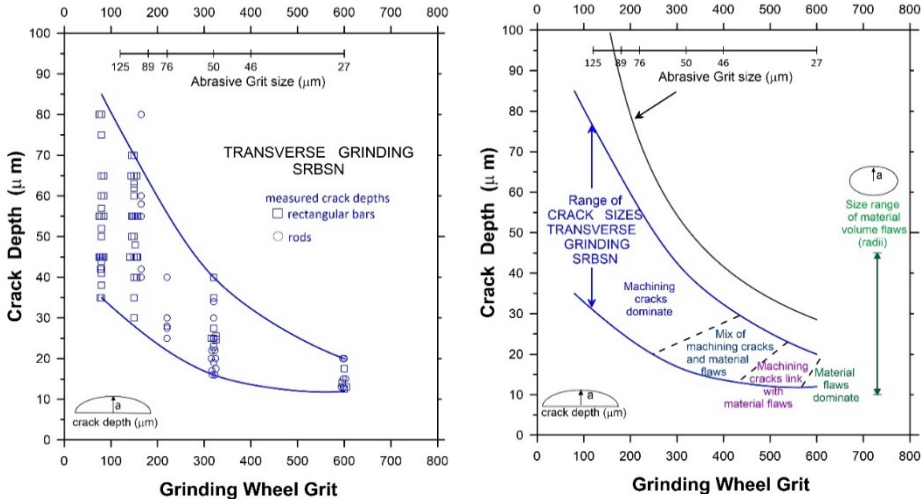

(a) (b)

Figure 6.51 *The depth (a) of parallel grinding cracks from transverse grinding as a function of grinding wheel grit size in a dense silicon nitride.*[58] *(a) shows the measured sizes from fracture surfaces. (b) shows how natural flaws controlled strength once the machining cracks were reduced in size. The depths of transverse grinding crack depths in a given procedure varied by up to a factor of 2 and ranged from 33% to 75% of the size of the nominal abrasive grit diameter. The abrasive grit sizes are from St. Gobain-Norton.*

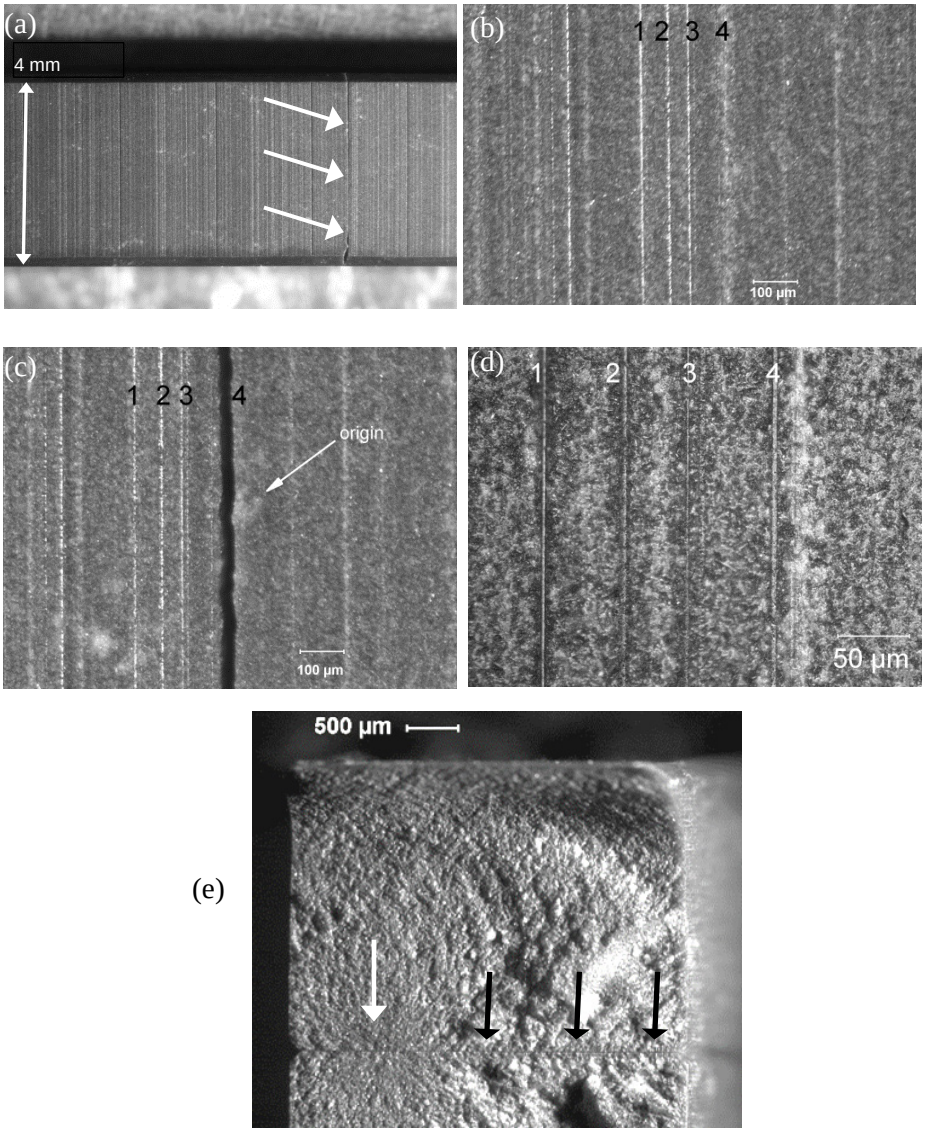

Figure 6.52 *Evidence of "renegade-grit" damage in a 150 grit transversely-ground 4 mm wide silicon nitride bend bar. (a) shows the tensile surface and the plane of fracture marked by the arrows. (b) shows a pattern of four repeating striations that periodically occurred (every 2 mm) along the bar length. Every bend bar in the set broke from one of the repeating #4 striations such as shown in (c). (d) is a close-up in this slightly-translucent material, illustrating that considerable subsurface grinding damage occurred beneath striation #4. (e) is the same as Fig. 6.48a and shows a typical fracture surface for this set and the "skin zone" damage associated with a striation #4.*

The *average* grit size may not necessarily be the controlling parameter. Instances of *renegade (or "rogue") abrasive grits* in a grinding wheel that caused atypical damage have been reported.[58] Renegade abrasive grits are much larger than normal particles that have been sorted by the normal classification procedures. They could be elongated particles that fell through the mesh gaps during sieving, or they could be particles that get through a hole or gap in the mesh, or they could be from cross contamination and handling. Rogue particles can also be a problem in polishing processes[40] and mentioned earlier in this chapter in section 6.7.3 on scratches. Figures 6.5a earlier in this chapter and Figure 6.52 on the previous page show an example of damage from a renegade grit in a silicon nitride. Calculations based on the wheel and table speeds and the specimen and wheel diameters confirm that a single grit can cause such long striations.

Machining cracks often link up with each other or with other materials flaws as shown in Figure 6.53. We tend to focus only on the ones that we see on a fracture surface, and it should be borne in mind that the surface actually contains a complex network of cracks as shown in Figure 6.54.

Although it is widely believed that materials with rising R-curves form smaller grinding cracks than materials with flat R-curves, there is evidence that just the

Figure 6.53 *Machining cracks can link with each other or with material flaws.*

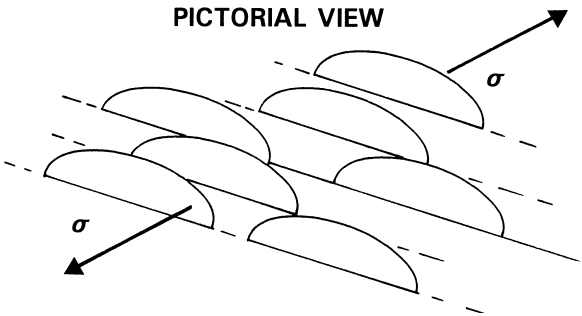

Figure 6.54 *Ground surfaces contain a dense network of machining cracks. This simplified schematic does not show cracks running parallel to the stress axis or lateral cracks parallel to the surface.*

opposite is true.[59] Materials with rising R-curves are more difficult to grind, so machinists often use larger grinding machines with higher horsepower motors. Greater grinding forces overcome the material's resistance for nominally the same grinding wheel conditions and depths of cut. These greater forces cause cracks to penetrate deeper than in materials with low fracture toughness or flat R-curves that cut or grind more freely.

Kanematsu[60] identified a "herringbone pattern" of grinding cracks in silicon nitride that has a completely different morphology those shown previously in this chapter. Figure 6.55 shows the cracking is made up of long, closely-spaced (but not touching) parallel cracks that curve off in the direction of abrasive motion. Indeed Figure 3.62 in chapter 3, which showed his innovative dye penetration technique applied to machining cracks illustrated, has several of these. These grinding cracks were in a fine-grained dense silicon nitride ground with 100 grit, 75 concentration resin bonded diamond wheels.

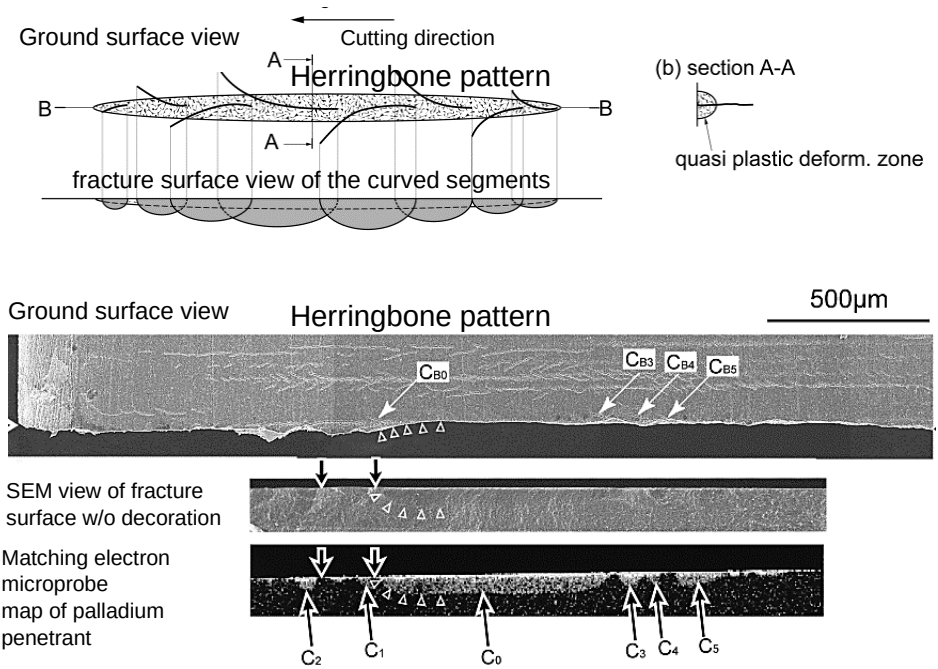

Figure 6.55 *"Herringbone crack pattern" discovered by Kanematsu, Ref. 60. See also Figure 3.62 in chapter 3. (images courtesy W. Kanematsu)*

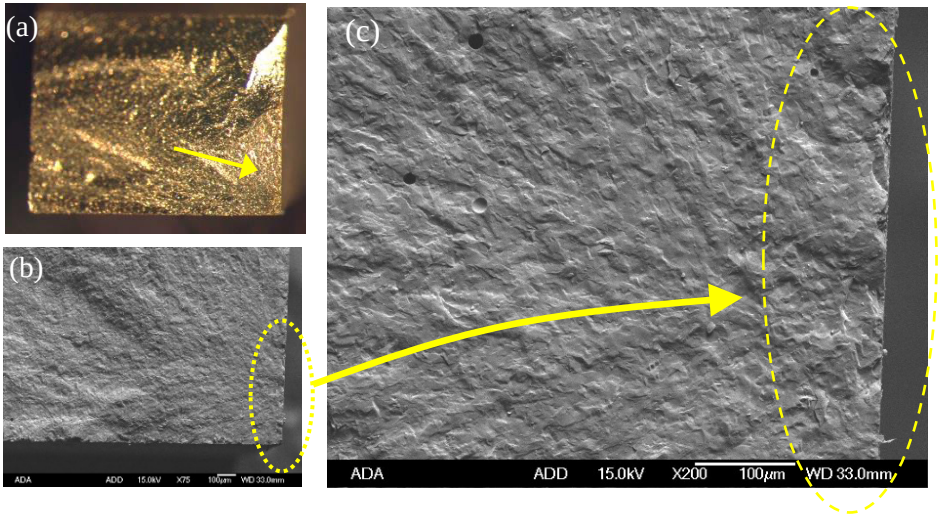

Figure 6.56 *Fracture surface of a dental feldspathic porcelain bend bar. (a) shows the entire surface of the 3 mm x 4 mm bar with a gold coating. The origin is on the right side wall (arrow). (b) and (c) show SEM images of the damage along the right side wall. Notice the slightly greater roughness of the fracture surface along the right side as compared to the fracture mirror centered on it*

Figure 6.56 shows an interesting example of parallel grinding damage on the *side wall* of a dental porcelain bend bar. Five of a group of twenty-six test bars broke from such side wall damage.[8] This is unusual since bend bars typically have the four main surfaces ground the same way. Careful examination of the exterior surfaces of the porcelain bars in this case revealed that the bottom tensile surface had been ground and polished adequately to minimize residual grinding damage. The side walls on the other hand had residual grinding damage from transverse grinding. Although the side walls were also polished, it was not done deep enough, and the damage was not completely removed. Many porcelains have a rough fracture surface due to the microstructure, and such distinct fracture mirrors and grinding damage may be difficult to interpret. This particular porcelain, Vita Mark II, was an exception and was easier to interpret due to its fine-grain size.

6.7.7 Chips

Blunt or sharp impacts or contact loadings near an edge can chip off a piece as shown in Chapter 4. The chip can in turn become a strength limiting flaw on subsequent loadings. Figures 6.57 and 6.58 show examples. See also section 4.15 for more on edge chipping."

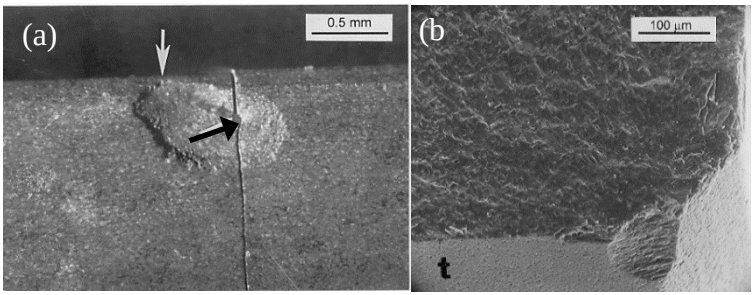

Figure 6.57 *Examples of chips that acted as fracture origins. (a) is an edge chip in a sintered reaction-bonded silicon nitride bend bar (195 MPa). This is a side view of the reassembled halves with the fracture plane running top to bottom in this view. The white arrow shows the impact point that first created the chip before the bar was broken in flexure. The fracture origin from the bend test was at the black arrow. Notice the continuity of the chip shape on each side of the final fracture. This confirms that the chip was in the bar to begin with and was not a secondary fracture. (b) shows the fracture surface of a sintered silicon carbide bend bar. The origin was a chip on the chamfer.*

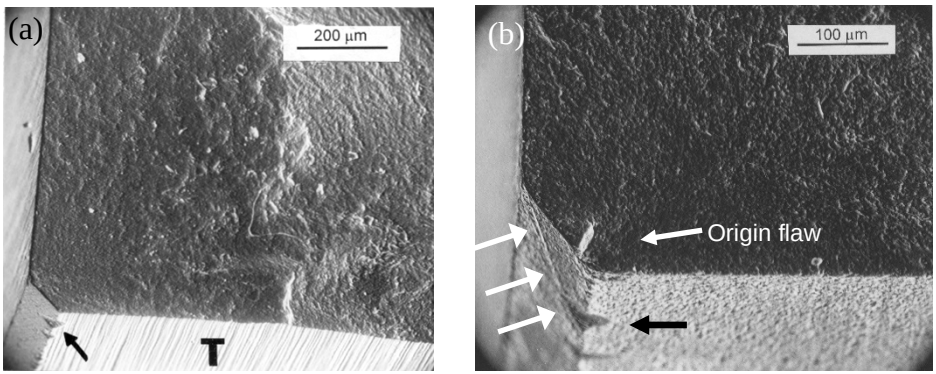

Figure 6.58 *Examples of chips that acted as origins. (a) and (b) show chips on bend bar chamfers in hot-pressed silicon nitride. Close examination of the chamfers revealed that the grinding was not done longitudinally, but at an angle causing the chips. Notice the striation marked by the white arrows on the chamfer in (b) and the chip-out marked by the black arrow.*

6.7.8 Glue Chips

Glue chips are shallow scallop-shaped surface flaws in glasses or ceramics that are bonded to other materials including metals. They are caused by either thermal expansion mismatches or shrinkage of a glue or epoxy.[61] Figure 6.59 illustrates the geometries. If the glue chips run back up to the surface, they may be relatively harmless. If they are incomplete and do not run back to the surface, they can be very serious flaws leading to later catastrophic fractures from mechanical or thermal loading. Glue chipping can be a serious problem for bonded engineering structures. Glue chipping is common in epoxy bonds with glass and can occur even at room temperature if the epoxy shrinks too much. Alternatively, failure can occur if the structure contracts on a cold day. Subfreezing temperatures are often a factor in glue chip fractures. As an epoxy or glue becomes rigid, its expansion coefficient markedly increases and stress relief through creep becomes ineffective.[62] Strong epoxy bonds in fact may be harmful. Compliant materials are better solutions for many sealing problems, such as architectural windows.

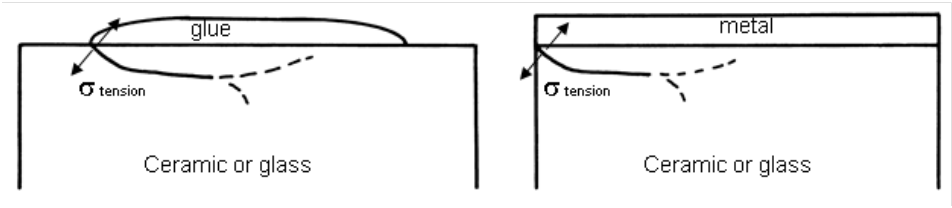

(a) (b)

Figure 6.59 *Side views of plates with glue chip cracks. (a) show a glue applied to the surface of the glass or ceramic. Contraction of the glue causes tensile stresses in the direction of the arrows causing a crack to enter the ceramic or glass surface. The entry angle may be perpendicular to the interface or at an angle as shown. (b) shows a metal bonded to a ceramic or glass. If the metal contracts more than the ceramic, glue chips at the edge may form. The entry angle is approximately 45° as shown. If cracks curve back up to the interface (dashed line), the chip may be harmless, but if it is incomplete or turns downward into the plate, it becomes a severe flaw.*

It is instructive first to consider how glue chipping is intentionally done by artists to make surface decorations on glass. Glue chipping on glass creates an effect such as shown in Figure 6.60a. The original glass surface is abraded lightly, or sprinkled with SiC grit, or sand blasted with alumina grit in order

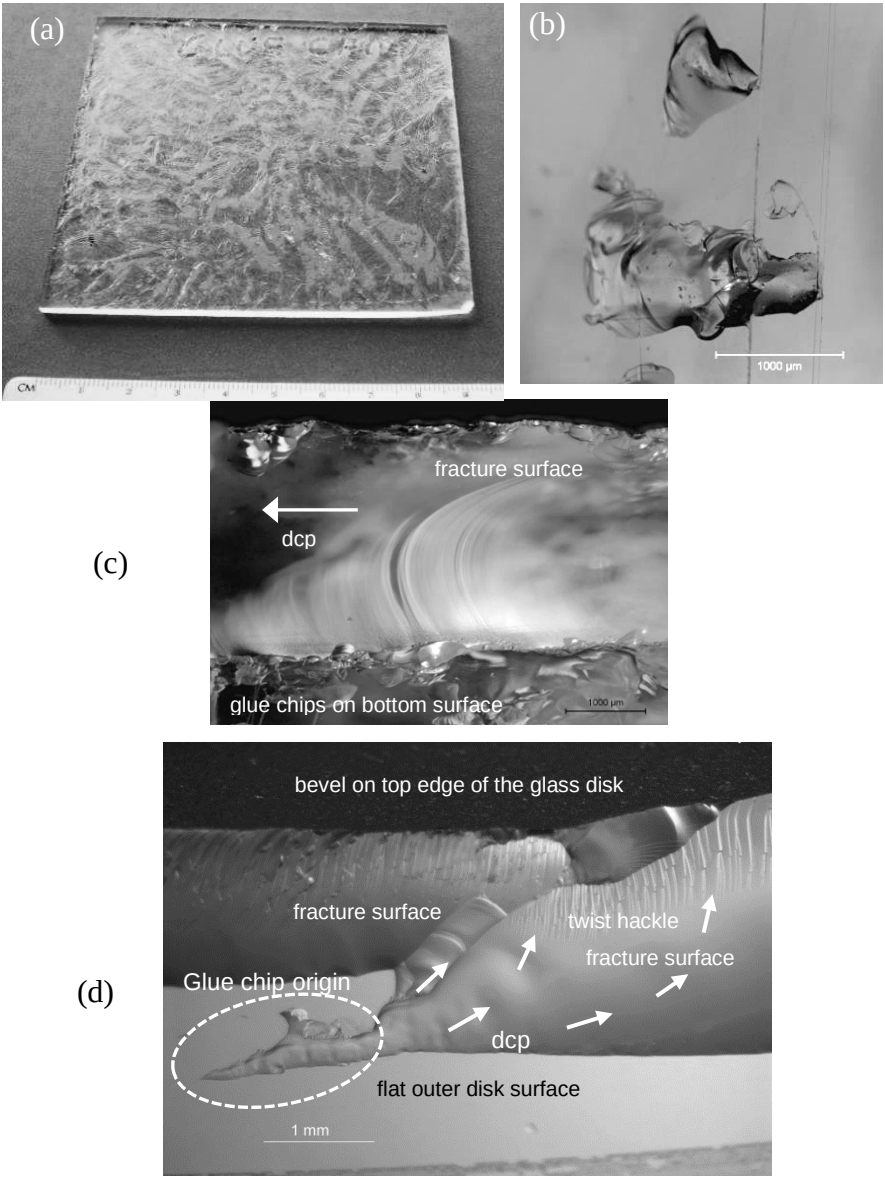

Figure 6.60 *Examples of glass glue chips. (a) shows an Alfred University demo plate covered with glue chips. (b) is a close-up of isolated glue chips on the surface. (c) shows a side view of a broken plate that shows glue chips on the bottom that affect crack propagation. (d) shows large glass disk that fractured from a glue chip caused by an epoxy bond to a metal part. The piece is tilted to show both the outer disk surface with the edge chip origin and the final fracture surface.*

to facilitate bonding and also to make small starter surface flaws. A glue, often an "animal hide glue", is heated and then applied to the prepared surface which is at ambient conditions. The glue temperature is carefully controlled and is usually cited as being within 60 ^{o}C to 66 ^{o}C (140 ^{o}F to 150 ^{o}F). Once the glue sets up, it is possible to trim some of it off, leaving a pattern on the surface where the subsequent chipping will occur. The epoxied glass is left to dry and chips form over a 24 hour or longer period as the glue shrinks. They penetrate a shallow distance into the glass and then run parallel to the interface and finally emerge at the interface. The glue layer is stripped away and many sharp glass chips adhere to the underside. The glass plate appears as in Figure 6.60a.

Tempered glass may explode days or months after being chipped for "no apparent reason." The actual reason is that deep segments of glue chip cracks may grow due to environmentally-assisted slow crack growth if there is localized tension at the glue chip. Eventually the crack reaches the inner tension zone of the tempered plate whereupon unstable fracture occurs.

Although glue chipping is done by artists with certain glues and over large areas, glue chipping can occur in isolated spots in epoxy-bonded glass or ceramics. It can also happen with glasses and ceramics that are bonded to metals. For example, Fréchette and Donovan[61] cemented brass bar strips to glass plates and then chilled them. They obtained surface chipping very similar to that made by glues, and they were even able to control the extent of the chipping in the glass by controlling the degree of chilling. They showed a side view of an example where the entry angle of the chip was about 90°, but they often came in at a shallow angle as shown above. Fréchette also told the author that "glue chips" could form at the interface of two glasses bonded together that had different thermal expansion coefficients. Sealing glasses for metal bonding (e.g., electrical leads) may be susceptible if the coefficient of thermal expansion does not match the metal. Glue chips often start at the edges of bonds as shown in Figure 6.59.

Glue chips are irregular in shape as shown in Figure 6.60 and their fracture surfaces have ample twist hackle, arrest lines, and tertiary Wallner lines. Their fracture surfaces can be tricky to interpret since Wallner lines and arrest lines may have curvatures that appeared with the "wrong sense:" i.e., the direction of crack propagation was toward the concave side of the lines. Frechette and Donovan[61] noted that, when <u>carried to completion</u> (meaning the chips came off), the glass plate may have an increased strength since the treatment effectively removes other surface flaws. The glue chips are shallow and run parallel to the surface. On the other hand, surfaces that had incomplete chips were dangerous, since they were vulnerable to subsequent mechanical loadings.

The conventional wisdom in many joining problems is to choose a metal or other material that contracts more than the ceramic or glass. During cool down from the elevated temperature joining process, the ceramic or glass is put into residual compression. This indeed is what happens, *except right at the edge of the joint* where a localized tensile stress can introduce cracks in the ceramic or glass as shown in Figure 6.59b. If the cracks remain shallow and come back to the surface joint, they are harmless. Alternatively, if they remain in the ceramic or glass interior, where subsequent tensile loadings activate them, or they tilt down away from the joint, they can cause severe strength degradation.

Gulati and Hagy wrote an excellent paper[62] about practical aspects of glue chipping. The paper has a mathematical analysis of the extent of the tensile stresses. They pointed out that even if the glue or epoxy is applied uniformly over a glass surface, it becomes brittle as the glue shrinks during curing. It experiences high biaxial tensile stresses, and "mud cracking" patterns form that breaks the glue into many small islands. As shrinkage continues, each island exerts a tensile stress in the glass at the island boundary which can propagate cracks in the glass. Their schematic side view of an interface shows the cracks initially penetrating into the glass a short distance at 90°, but then rapidly curving over to run parallel to the interface.

Professor Fréchette[61] and Mr. L. Orr observed that glue chips were the origins of fracture in spectacular failures of very large windows in the sixty-two story John Hancock skyscraper in Boston in the early to mid-1970s. The windows were 25 mm – 32 mm (1 inch to 1.25 inch) double-glazed glass panels with two 6.35 mm (0.25 inch) thick individual panels bonded with a lead spacer between them. A copper coating was flame sprayed to the inside rims of the glass panels. The glass panels were then soldered to the lead spacer around the rim. The high thermal contraction of the lead in cold weather created incomplete glue chips. (A silver reflective coating on the inside of the outer glass panel {or "light"} may also have been a factor.) Subsequent mechanical and thermal loadings caused the cracks to propagate, and the windows eventually fractured, with large portions of the outer panes sometimes falling many stories to the street. There were some injuries. My future spouse Janet Quinn and I were undergraduate students at Northeastern University at the time, and we often looked at the building as we came out of engineering classes. At any time, hundreds of glass panels were replaced temporarily by plywood sheets. All 10,334 of the windows in the skyscraper eventually were replaced. The above interpretation of the cause of the failures is based on my private oral communi-

cations with Prof. Fréchette[c], Mr. Leighton Orr, the information in Fréchette and Donovan's paper,[61] and the private papers of Mr. L. Orr.

Fréchette and Donovan[61] reported a second instance where glue chipping cracks caused tempered float glass spandrels to fracture in a high-rise building. The cause was spots of copper metal from weld spatter. The high shrinkage of the metal droplets on cooling caused glue chip type cracks.

Figure 6.61 shows a glue chip fracture in a complex multiplayer component. Suratwala[40] discussed several glue chip fractures in his book on optical materials and their fabrication.

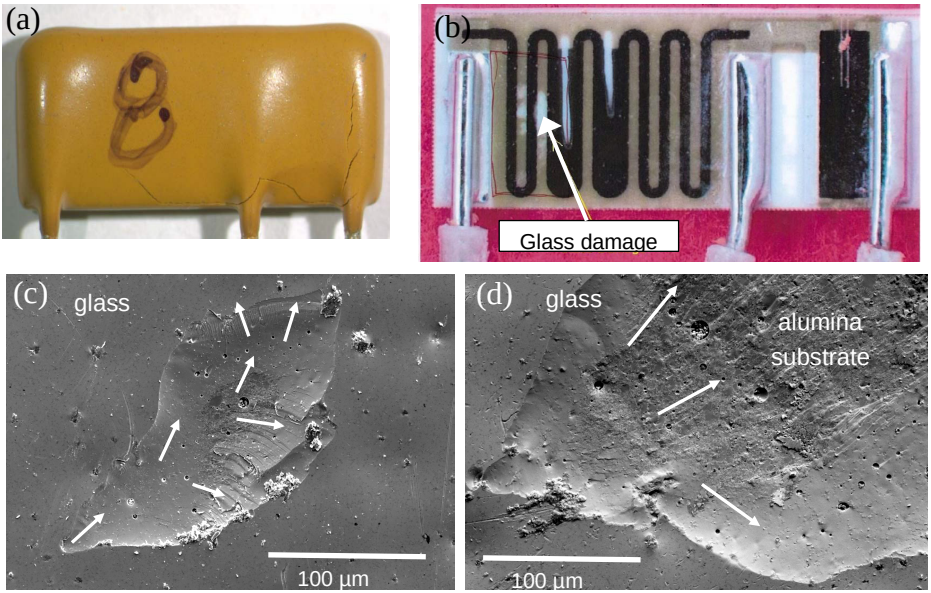

Figure 6.61 *Glue chipping damage in a thick-film resistor that cracked during thermal cycling. (a) shows the component in its epoxy encapsulant. (b) shows the exposed electrical circuitry. Scallop cracks (white-colored reflective patches) formed in an inner glass encapsulating layer. (c) and (d) show two glue chips in the glass. The arrows show the direction of crack propagation. (all photos and interpretation courtesy R. Tandon and S. Monroe)*

---

[c] Prof. Fréchette was bound to not directly disclose his findings due the litigation involved. He obtained a waiver such that he could discuss the case for teaching purposes without identifying the building. I heard him recount the case on at least five occasions in his Alfred University fractography classes. Although he did not specifically mention the Hancock building by name, in private he confided in me that it indeed was the Hancock building.

Glue chipping is a common cause of fracture in automotive windows, especially with epoxy adhesive bonds to metal pieces on tempered side windows. Sunroof windows fractures and metal antenna tab connections in laminated front windows with built-in antennas also have had glue chip-initiated fractures associated with epoxy bonds or fillers. More compliant silicone or urethane filers would have eliminated the problems.

6.8 Other Flaws

6.8.1 Processing and firing cracks in ceramics

Cracks that form in the green state or during firing are quite variable and troublesome. Firing stresses can be very irregular, may be transient, and may depend upon thermal gradients in the kiln or furnace. Firing or shrinkage crack

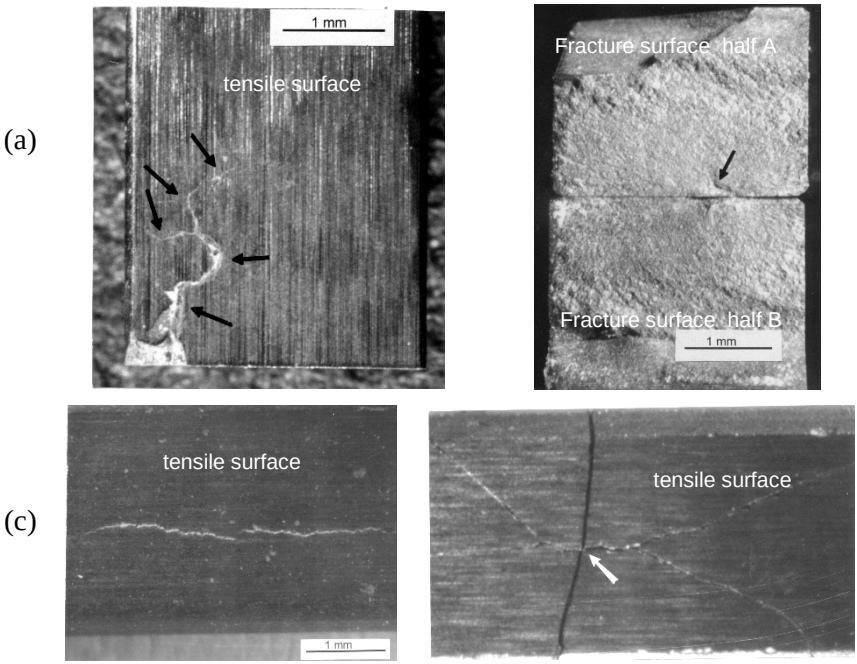

Figure 6.62 *Examples of processing cracks. (a) shows the tensile surface and (b) the fracture surface of two different silicon nitride bend bars which had an unstable boundary phase associated with the yttrium silicate sintering aids. The fracture origin is marked by the arrow. (c) shows a bend bar that had a moderate strength despite a huge processing crack running perpendicular to the tensile axis. (d) shows another example of a firing crack in a bend bar. The fracture origin is marked by the arrow.*

examples are shown in Figures 6.62 - 6.66. Cracks that *meander, are segmented, and/or are granular on the fracture surface* may have formed in the green state, or during firing, or during resin binder burnout of injection molded or additively manufactured parts. Since the body is not fully dense, the fracture surfaces are very granular and do not have the characteristic fracture surface markings. Close examination of interior crack surfaces may reveal thermal rounding of the particles and grains.

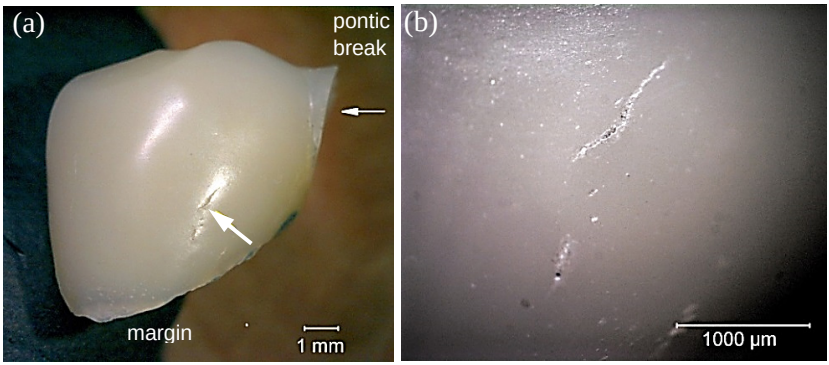

Figure 6.63 *Processing (firing) cracks in a three-unit Cercon zirconia dental bridge. (a) shows a frontal (buccal) view of the end unit which fractured at the narrow connection to the next unit (small white arrow). A sintering crack is evident on the face of the crown (large white arrow in a, and closeup in b). It did not cause fracture in this instance because it was in a low-stress area.*

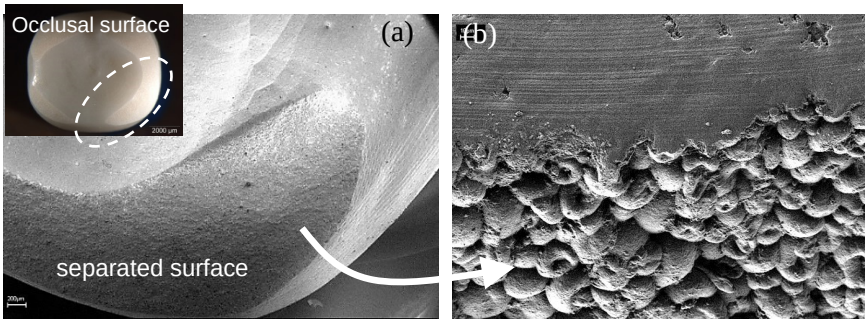

Figure 6.64 *Processing cracks in a single-unit zirconia crown. A large piece has separated off the top (occlusal) surface (a). This piece partially separated but did not fully detach until was in the patient's mouth. The apparent "fracture surface" is in fact a huge processing crack. One can see exposed spray-dry agglomerates from the starting powders. The material did not sinter correctly. The manufacturer claimed the fracture was due to patient overload or faulty installation by the dentist. This was wrong since the CAD/CAM blank had the processing crack in it. (courtesy Dr. S. Scherrer)*

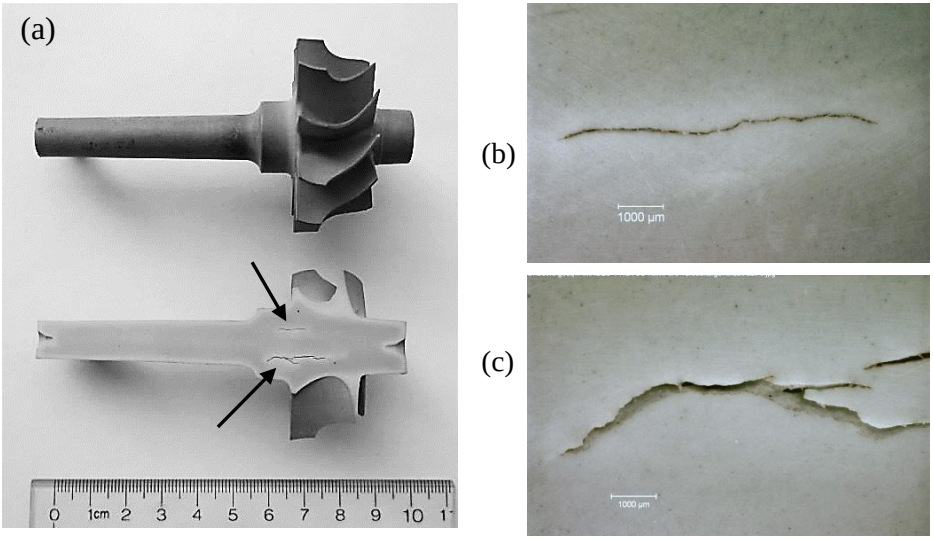

Figure 6.65 *A processing crack in a prototype Ford Motor Company silicon nitride automotive turbocharger rotor (a). The material is a reaction-bonded form of silicon nitride and was formed by injection molding. The lower view in (a) shows the interior after sectioning with a diamond cutoff wheel. The close-up views in (b) and (c) show how differential shrinkage during firing caused cracks to form in the thickest portion of the part. Notice the lighter-colored areas of low density that envelop the cracks.*

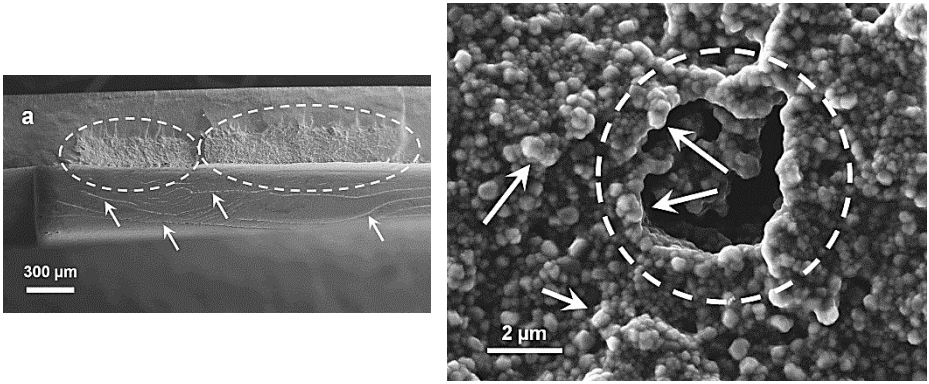

(a) (b)

Figure 6.66 *Processing crack in a zirconia watch bracelet. (b) is a close-up from inside the processing crack that shows rounded zirconia grains and porosity. (courtesy J. Kübler)*

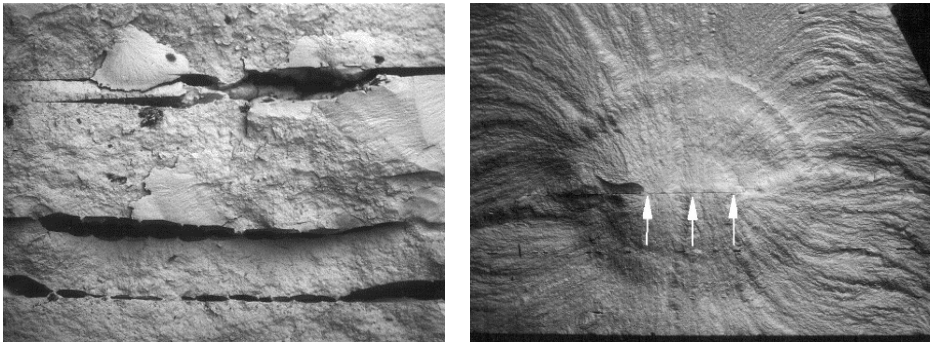

(a) (b)

Figure 6.67 *Delaminations revealed on the fracture surfaces of tape-cast PZT bend bars. (a) has severe open delaminations between tape cast layers. (b) was processed better but still had a very small horizontal delamination (arrows). The elliptical curved lines are arrest lines on the fracture surface. (courtesy C. Wu.)*

Delaminations are a particular type of processing crack. They generally are planar cracks within a material that arise from separation during green body forming, especially from mold or press release operations. They can also occur between bonded layers of dissimilar material or joints. Delaminations often occur in layered or tape cast structures such as the two lead zirconium titanate (PZT) examples shown in Figure 6.67 that are from reference 63. They also may occur in 3-D printed additively-manufactured bodies such as shown in Figure 6.68. The delaminations may occur along print build planes. Resin burnout delaminations also occur in traditionally-manufactured injection molded ceramics.

Diagnosis and remedial action for processing cracks usually requires close consultation with the processor to review the details of the fabrication and any steps that could lead to differential shrinkage, outgassing, or phase changes. Processing cracks and their effect on overall breakage and fragmentation are also covered briefly in section 4.5.

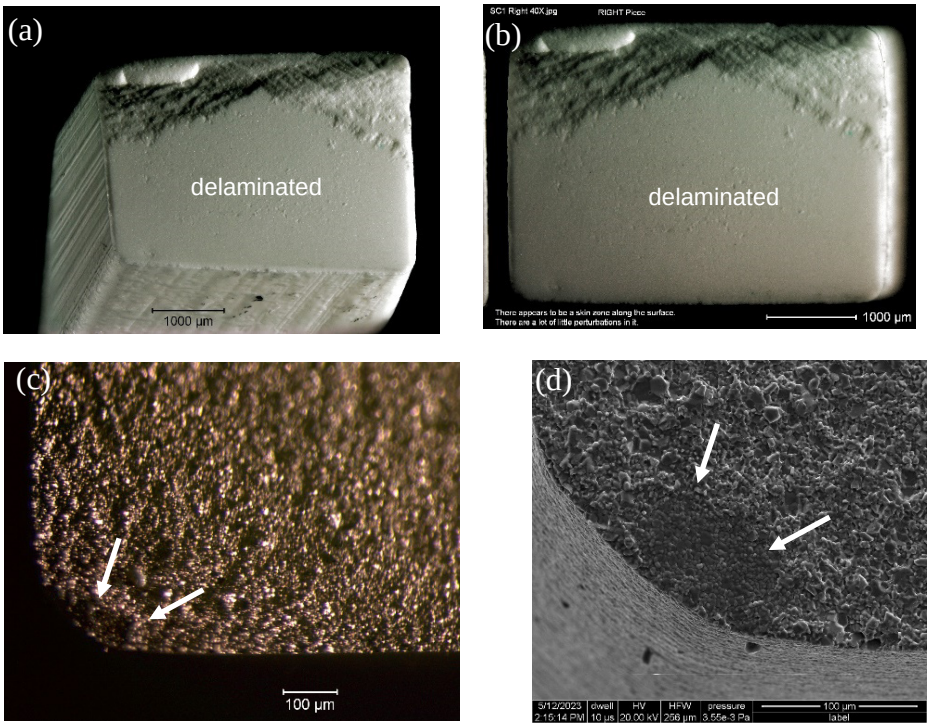

Figure 6.68 *Delaminations in additively-manufactured sintered alumina bend bars.*[1] *They can either be massive and extend over almost the entire bar cross section as shown in (a) and (b). This bar had a respectable nominal strength (236 MPa) suggesting that the flaw may be better termed a "weak build layer" than a complete delamination. The plane of separation is on one vertical build plane layer. In its final stages, the crack took a tortuous path, zig-zagging between build layers, as it progressed through the compression side of the bar. This pattern is similar to fractures in single- crystals (chapter 8) where a crack zig- zags on preferred cleavage planes. (c) and (d) are from a smaller delamination in another bar. (c) is an optical image of the gold-coated surface and (d) a SEM image. Both show a very localized delamination at a corner of a vertically-build bend bar (216 MPa).*

On the other hand, cracks that are <u>sharp and planar</u> (not rough and granular) may have *popped in during or after cooldown from the firing temperatures*. Such cracks may have fracture surface markings such as hackle or arrest lines. The microstructure will look fully dense with no roughness or rounding. Figure 6.69 shows such an example. Sometimes these are termed “thermal cracks.”

Varner and Fréchette[64] identified *dunt cracks* in whitewares. They are processing cracks that form during cool down when quartz particles undergo a sharp change in volume (due to the b - a phase change) when matrix glass is viscoelastic. The dunt crack appears as an atypical shiny transgranular fracture.

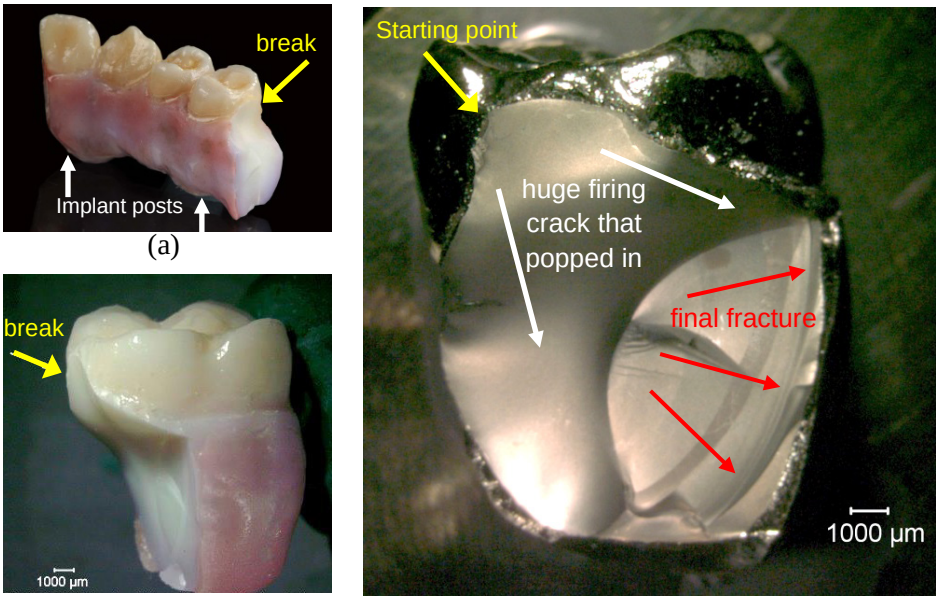

Figure 6.69 *A sharp firing crack in a complex zirconia dental five-unit "telescoping denture" that is a single-piece colored restoration for a patient with substantial tooth and jawbone loss. Two implant posts held it in place at the left end tooth and the fourth tooth in (a). The cantilevered fifth molar tooth broke off after only three months. (a) shows the four surviving units and (b) shows the cantilevered end molar tooth that broke off. (c) shows the fracture surface of it with a gold coating to make optical examination easier. The origin of the final fracture was the huge firing crack that popped in almost two-thirds of the way through the massive cross section. This sharp, smooth and probably very-tight crack was unnoticed during fabrication and installation in the patient's mouth. It started from irregularities in the porcelain veneer and core area marked by the yellow arrow in (c). Final fracture occurred on a different plane and in stages as attested to by multiple arrest lines. One normally does not expect fracture in such a massive zirconia piece, but the cantilever loading on the end piece with an enormous initial crack caused it to break. (courtesy M. Karl, U. Lohbauer, J. R. Kelly) Refs. 65 and 66.*

6.8.2 Blisters in Ceramics

Blisters are a type of flaw in ceramics made by injection molding or additive-manufacturing processes that use a resin binder with ceramic filler. The resin burnout step can cause gas formation that leads to surface blisters such as shown in Figure 6.70.

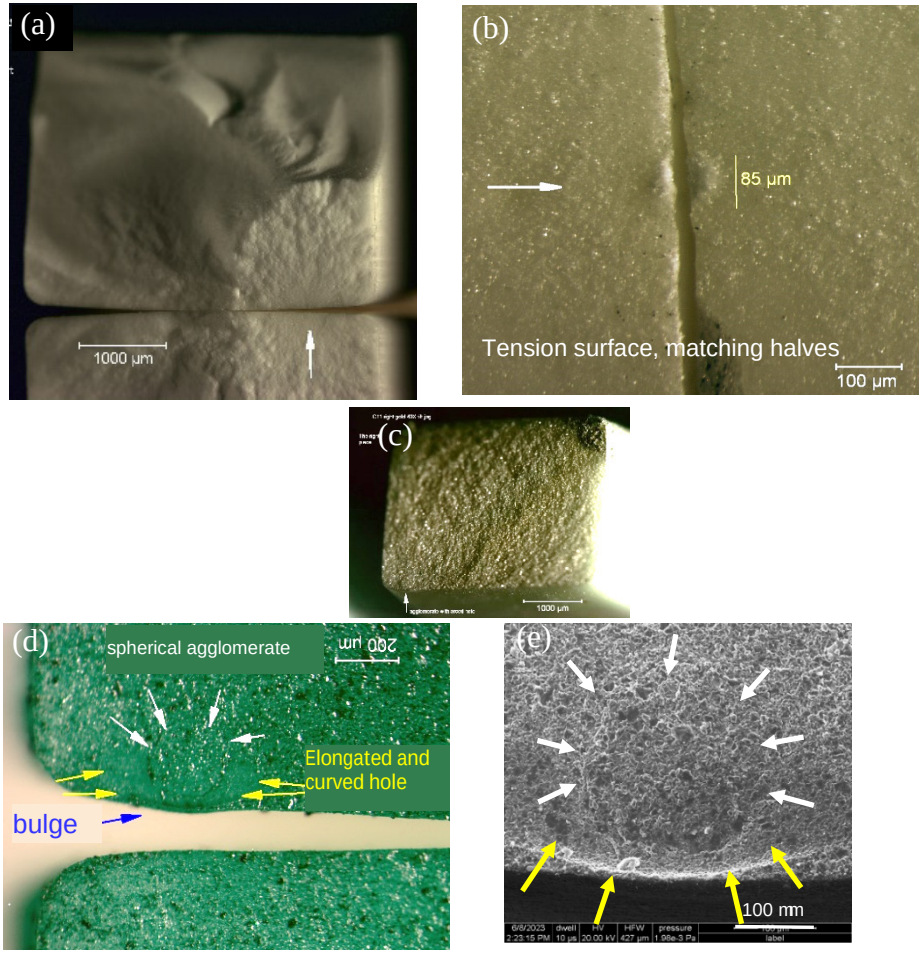

Figure 6.70 *Blister fracture origins in 3-D additively-manufactured sintered alumina.*[1] *(a-b) are for a 148 MPa bend bar. The middle of the blister has a central hole giving it the appearance of a "volcano." (c)-(e) are for a 313 MPa bar with a large spherical agglomerate marked by white arrows. It is surrounded by an elongated curved hole of some sort marked by yellow arrows that created a bulge in the surface. (c) is a gold coated optical photo, (d) is green dye-stained optical photo, and (e) is an SEM image.*

6.8.3 Knoop and Vickers controlled flaws, glasses and ceramics

Sometimes it is advantageous to make strength-controlling flaws. This is often done in fracture mechanics studies to create a controlled starting crack and then load it to fracture in order to evaluate the material's fracture resistance. Cracks made for fracture mechanics tests are typically called "precracks." Small flaws are sometimes made by fractographers to help get acquainted with fracture markings on a new or difficult material. Usually a microhardness testing machine with a Knoop or Vickers indenter is used to make the controlled flaw in a bend bar or disk specimen. The indentation not only makes a crack, but a significant damage zone with residual stresses. The residual stress zone extends three to five times the indentation depth beneath the surface. For fracture toughness tests, the best remedy to deal with the residual stresses is to polish or hand-grind the residual stress damage zone off, leaving behind a stress-free semielliptical surface crack.

The Knoop indenter produces a more-controlled "cleaner" crack than the Vickers indenter. The Knoop indentation procedure for creating controlled flaws is described in more detail in section 7.12. When used to measure fracture toughness with bars in bending, the method is known as the surface crack in flexure (SCF) method. Figures 6.71 and 6.72 here and Figures 3.27, 3.60, 5.28b, 5.31, 5.60, 5.62 elsewhere in this Guide show examples of Knoop surface flaws that were fracture origins in bend bars.

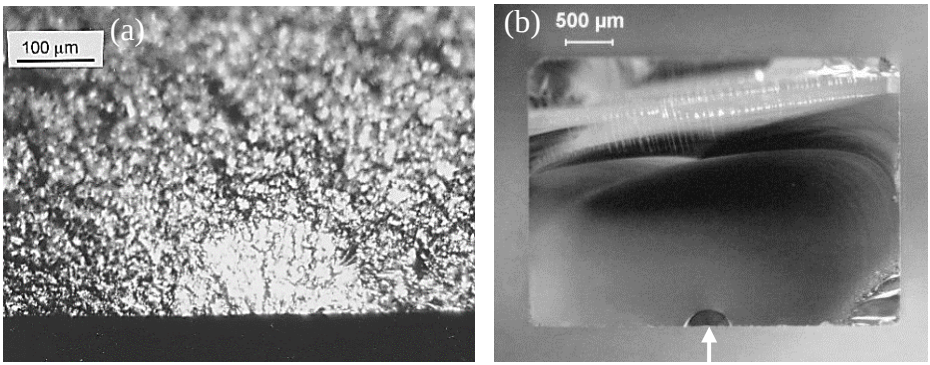

Figure 6.71 *Knoop indentation precrack flaws. (a) shows a precrack in a sintered alpha silicon carbide bend bar. (b) shows a BK-7 borosilicate crown glass bend bar.*

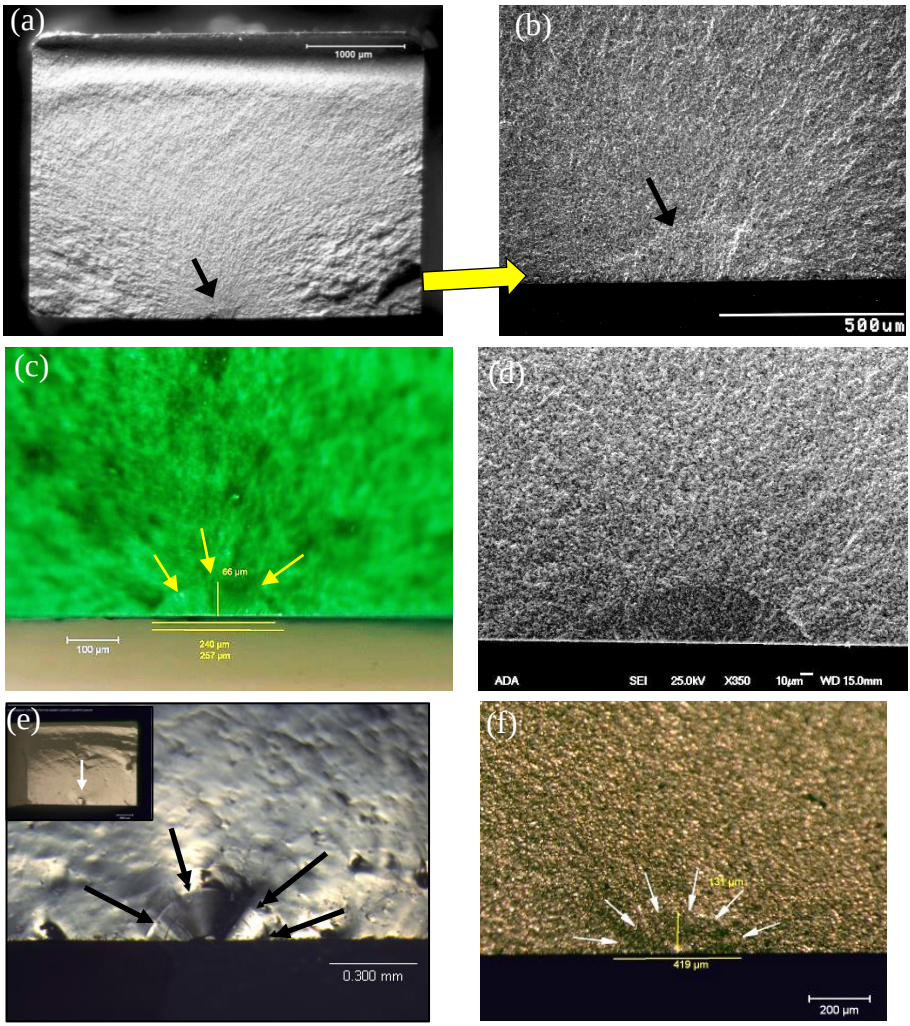

Figure 6.72 *Knoop indentation precrack flaws. (a) and (b) are optical and SEM images of cracks in a sintered reaction-bonded silicon nitride. (c) and (d) are matching optical and SEM images for an e.max CAD dental lithium disilicate glass ceramic. (e) is a dental porcelain designed to be fused to zirconia, and (f) is a Vita Enamic ceramic network, resin-infiltrated composite.*

The Vickers indenter creates a complex "messy" three-dimensional network of median, radial, and lateral cracks. There is much shear faulting and densification as well. Most fracture mechanics experts prefer simple, straight cracks such as made by the Knoop indenter for testing purposes.

6.8.4 Other Glass Origins

Examples of glass origins have been shown previously in this chapter including stones, inclusions, scratches, polishing-grinding cracks, impact and contact cracks, bump checks and bruise checks, Knoop precracks, and chips. Some key references are listed in the paragraphs below. Other flaw types that are common in glasses are shown below. This section in this 4th edition of this Guide has been expanded significantly compared to the earlier editions.

Varner,[67] Fréchette,[68] and Ernsberger[69] described the character of flaws in glass. Aldinger and de Haan recently published an Atlas of Glass Container Defects[70] that includes some glass flaw origin types that might cause fracture. Aldinger and Collins published an atlas of stones in glass.[19] ASTM C162, a terminology standard with over one hundred terms, describes fifteen flaws but does not provide illustrations.[71] These include: blisters, boils, bruises, bump checks, checks, chips, crescent cracks, fire checks, inclusions, open bubbles, percussion cones, pressure checks, seeds, scratches, sleeks, and stones. They also included examples of "lensing cracks" that run part way or all the way around the base. Company brochures and books often have tabulations of flaw types as part of their lists of glass irregularities, but they unfortunately do not show illustrations. (e.g., ref. 72). There is some overlap in these terms but often are differences and omissions. For example, ASTM C162 and the above compilations do not include "pecks," a term that Preston used, or "chill checks" a term Frechette used, do not appear in the above compilations. Schaut et al.,[55] illustrated "bump checks," "lensed cracks," and "neck cracking" in small pharmaceutical containers. Aldinger and de Haan described "cleavage" flaws, which most other users refer to as "scratches." Aldinger and de Haan summarized the state of affairs:[70]

> "Over the years, glass manufacturers and fillers have created a unique lexicon to describe the many kinds of defects found in glass containers. As in other industries, this organic language is a mixture of tradition, science, and jargon that can be completely incomprehensible to outsiders or newcomers to the business. Although some terms have gained widespread acceptance across the industry, others are more common in one sector than another. Even worse, the translated terms for glass defects used in non-English speaking countries are often completely different than their English equivalents, . ."

Flaws from the melt may come in several forms. These flaws are inclusions, pores, or compositional inhomogeneities, but have been given more specific names by the glass community.[68,69,73,74] *Devitrification inclusions* or *devitrification stones* (Figure 6.73) can form if the glass crystallizes. *Stones* (Figure 6.74 can arise from a variety of sources including grains of unreacted raw material, contamination of the raw stock or recycled material, or refractory

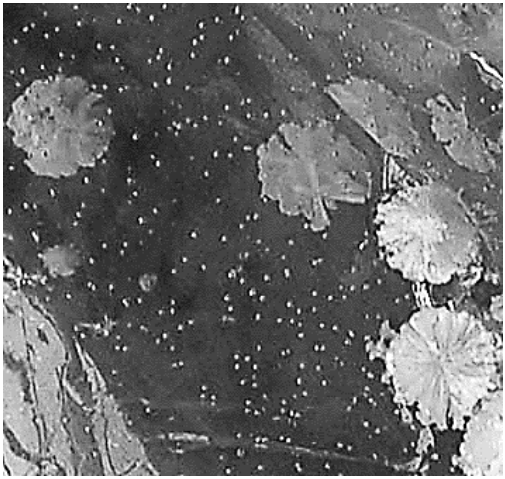

Figure 6.73 *Unusually large (» 1 cm) glass devitrification inclusions with a blossom-like structure as well as smaller seed bubbles. (Specimen courtesy of J. Varner and V. Fréchette*)

material broken off the tank or pot walls. *Devitrification stones* and *stones* have completely different chemistries and causes, so they should not be confused.

Gas bubble origins are termed *blisters* if large, and *seeds* if small. Bubble origins have already been discussed in section 6.6.1 of this chapter. Ernsberger[69] discussed tiny nanoscale bubbles and felt that they were unlikely candidates for fracture origins, but recent work suggests they may play a role in dynamic impact or compression tests. *Striae* are streaks of inhomogeneous, transparent glass. Their refractive index is different than the glass bulk. Very intense striae are termed *cords* and may appear as ropes or strands such as shown in Figure 6.75.

Vitreous enamels applied over glass bodies and then fired can also lead to localized cracking if the thermal expansions of the glass differ appreciably.

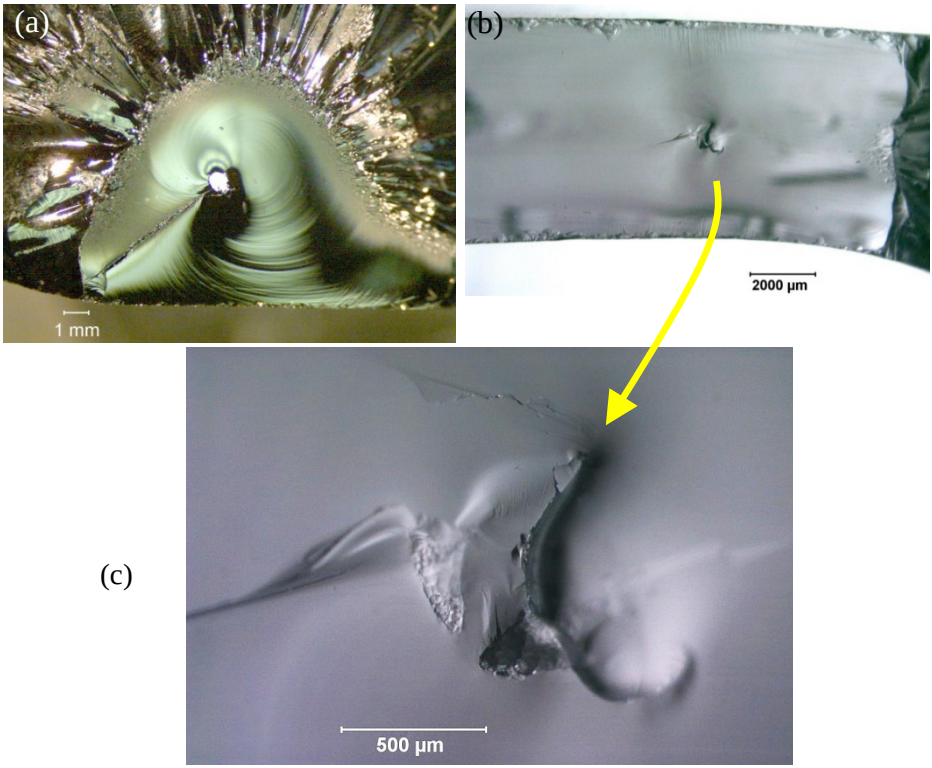

Figure 6.74 *Stone origins exposed on glass fracture surfaces. (a) is an example in an old cathode ray tube type television picture tube and broke from transient thermal stress during manufacture. (specimen courtesy of J. Varner and V. Fréchette). (b) and (c) show a stone in the middle of the wall of a heat-strengthened consumer glassware.*

Large glass origins are not too difficult to detect on glass fracture surfaces, but very small microflaws can pose difficulties as discussed by Ernsberger.[69] Ernsberger is often credited with being the first investigator to detect in 1960, by means of clever decoration techniques, the micro sized Griffith flaws that had been elusive up to that time due to limits of optical microscopy.[69,75] Ernsberger's 1974 paper[69] has some interesting illustrations of the differences between surface flaws and their concentrations in plate versus sheet glass. Plate glass had more flaws that were uniformly distributed since they were formed by the grinding process. Sheet glass, on the other hand, is drawn glass with a fire-finished surface. Some areas were entirely free of microcracks. Other areas had flaws from mechanical abrasion. The end of his article had some interesting observations about how dust settling on an exposed glass surface could chemically react with the surface causing a local

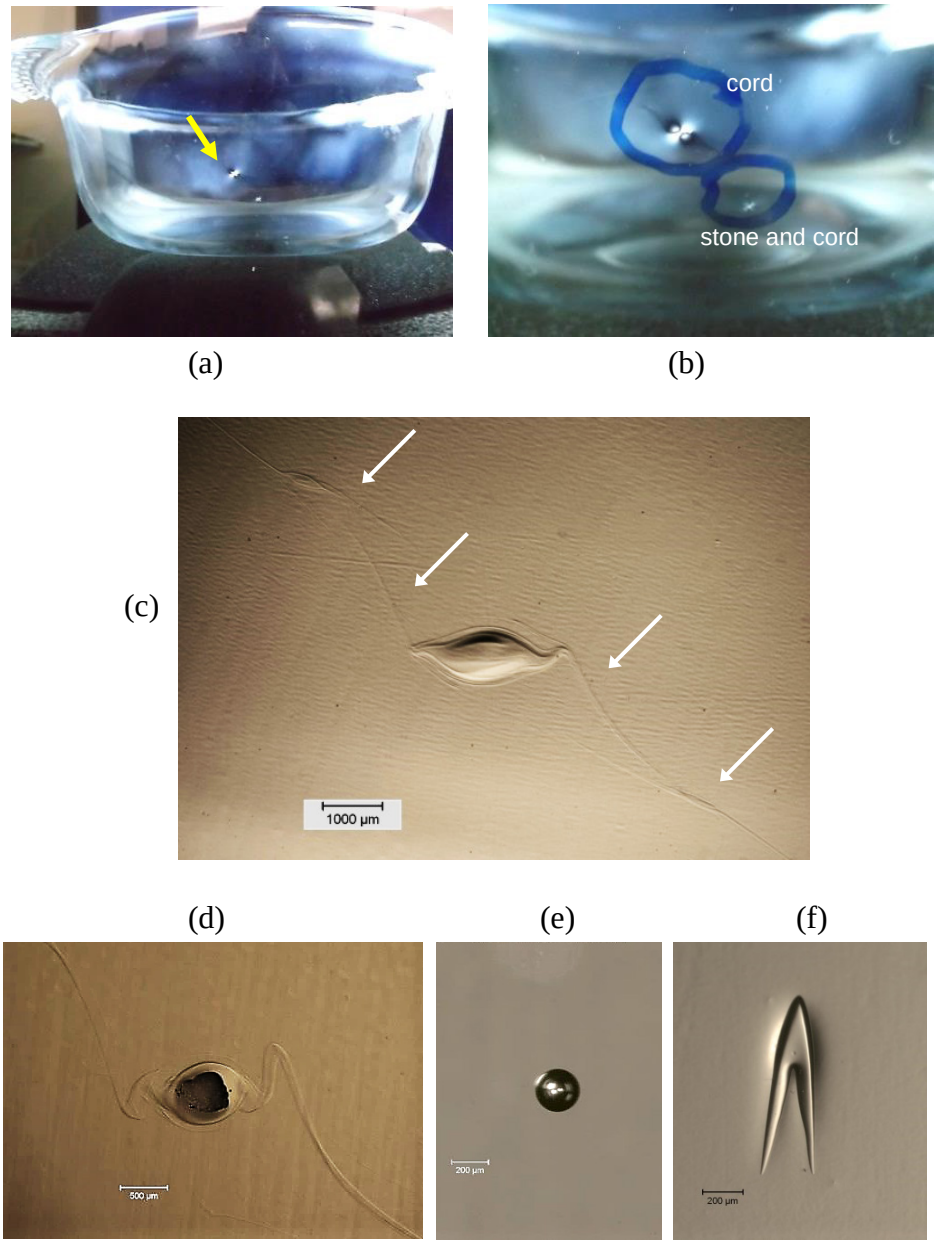

Figure 6.75 *Flaws in a borosilicate glass cookware. (a) – (c) show a* <u>*chord*</u>*. (crossed polarizers highlighted the internal strains in views (a) and (b). (c) is a close-up of the cord with a mix of transmitted and reflected illumination. The striae - stringers are marked by arrows. (d) shows a close-up of a* <u>*stone*</u> *with striae - stringers. (e) is a* <u>*seed*</u> *(a bubble). (f) is an odd internal hairpin flaw.*

reaction and even devitrification if the glass was exposed to elevated temperature. Other local chemical disturbances to glass surfaces can occur from environmental exposures and corrosive gasses or liquids.

Preston[74] in 1926 described *heat sleeks,* which are burnished streaks of glass where a metallic polishing or grinding wheel makes direct rubbing contact with a glass surface if the loose abrasive and water are inadvertently squeezed out. The glass locally reaches a high temperature and develops a number of hair-like fissures entering the glass normally to the surface and penetrating only a short distance. Surface contact damage flaws were previously presented in section 6.7.4. Sharp contact damage sites are *pecks.*

Small surface cracks called "checks" can form in glasses from a variety of causes. Sometimes there is a qualifying word, as in "chill checks," "bump checks," or "bruise checks." Checks can form as a result of mechanical or thermal contact, sometimes even from glass-on-glass contact, such as when bottles bump into each other, or medicinal vials are packaged without dividers. Rims or raised surface features on a glass outer surface are vulnerable spots for damage to occur. Sometimes they form on bottle bottoms or on embossed lettering or decorations. Localized thermal stresses during forming or after fabrication can also cause checks.

"Bump checks" and "bruise checks" are forms of blunt contact damage as described previously in this chapter in section 6.7.5. Aldinger and de Haan[70] list as many as ten different types of checks in glass containers depending upon the cause and location. Schaut et al.[55] conducted a survey that tabulated the occurrences of "bump checks" in 3 mL to 40 mL pharmaceutical containers and conducted laboratory tests that succeeded in mimicking them. Sometimes the contact site will have some abrasive damage or frictive materials transfer on the outer surface. Depending upon the angle of incidence of the offending contacting object, cracks may penetrate as classical Hertzian cone cracks or partial inclined cracks as shown in Figure 6.41. Subsequent loading may cause inclined cracks to spall off creating chips or flakes not unlike those shown in section 4.15 on edge chips in Chapter 4 and Figure 6.77 later in this chapter.

Figure 6.76 shows *chill checks,* a term used by Fréchette,[68] that are pernicious flaws that are often very difficult to detect. A chill check is a small wavy and tight crack that is introduced into a hot glass surface by <u>localized contact</u> with a cooler object. A metal tool or contact roller can create them. Thermal stresses create the crack, but since the contact and thermal stresses are localized, the cracks are small. Glasses with high thermal expansion coefficients are most susceptible. The cracks often are <u>difficult to detect</u> in an unbroken component

and require lighting at just at the right angle. Sometimes transmitted illumination is effective. If chill checks are suspected, then the piece or the illumination source should be rotated a variety of ways and angles so as to try to get a momentary reflection from the crack. Chill checks form quickly and close back up very quickly. They may close so tightly (less than the wavelength of light) that they are invisible. Nevertheless, some portions of the crack may have captured small amounts of gasses or water molecules that create slight opening pockets that are just barely detectable. These are often brightly colored, since they refract the light and may only be detectable from certain viewing angles. Once a momentary reflection is detected, the fractographer can zero in on the flaw site. Often the full extent of

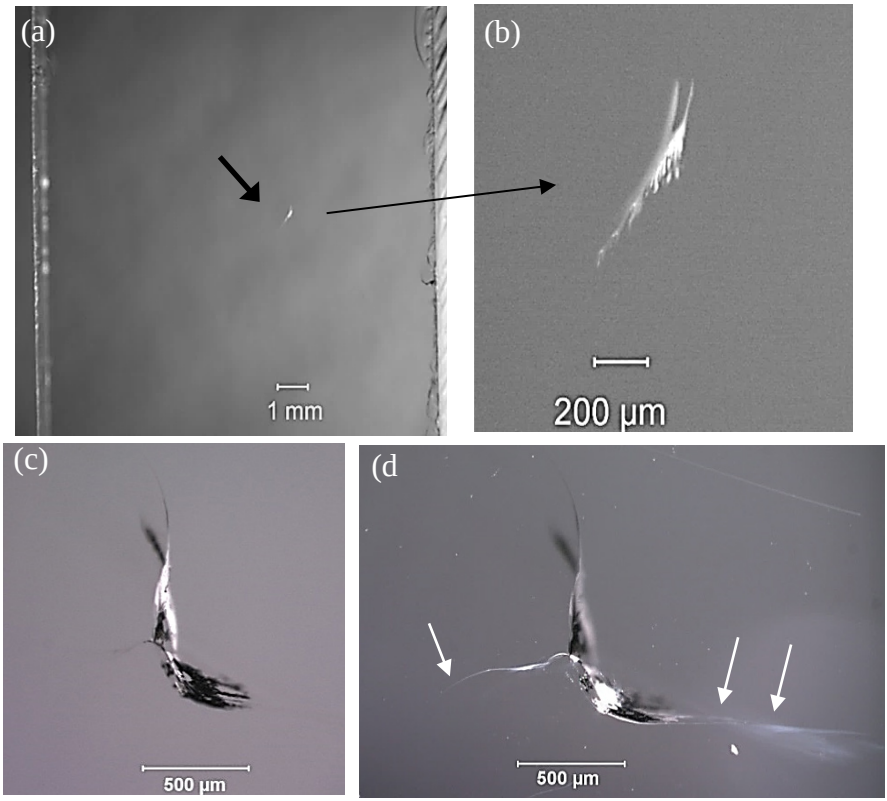

Figure 6.76 *Chill check cracks on the outer surface of unbroken glass plates. (a) and (b) show the same chill check. (c) and (d) show two close-up views of another chill check at the same magnification. Note how different illumination dramatically alters the apparent extent of the flaw. Much of the cracking is invisible in (c). Much more of the cracking is evident in (d). This one is very similar to a propeller-shaped example (Figure 4-7) in Fréchette's book.*[68] *Photos by the author. (Specimens courtesy V. Fréchette and J. Varner)*

the crack is not visible because the crack is so tight. Fréchette[68] observed that chill checks are hard to characterize since mechanical effects can also occur at the contact site. If a glass object breaks from a chill check during subsequent use and stressing, then it is likely the origin site will be irregular and may not be recognized as a chill check without examination of the outer surface. This underscores an earlier recommendation: if an origin on a fracture surface is located at the surface of the component, then it is prudent to examine the exterior surface of the part as well as the fracture surface. Varner[76] has compared features of chill checks and impact origins. Chill checks are curved and not flat, often have no visible outer surface damage, and, once the flaw is exposed on a fracture surface, have few markings on the flaw itself other than some twist hackle. Impact cracks are semicircular and are straighter, and the outer surface has chipping and lateral cracks. Once exposed on a fracture surface, the impact flaw exhibits tertiary Wallner lines.

Polishing flaws from a loose abrasive rolled across a surface while under load can leave a variety of damage including indentations, scratches, Hertzian full or partial ring cracks and gouges according to Fréchette.[68] The crack depths are typically four to five times larger than the particle diameter. They often are very elongated along the surface. Polishing, lapping or grinding glass can create are *sleeks* which are fine, scratch like, smooth-boundary imperfections usually caused by a foreign particle during polishing.[77]

Chatter marks such as shown in Figures 6.77 and 6.78 often are clues to contact cracks underneath. The periodicity is a manifestation of vibration or a stick-slip interaction when a contacting object slides over the surface. The parallel arc-shaped cracks are the telltale feature. Their shape, spacing, and possible existence of additional arc lines running across the top and bottom of the track vary with the circumstances. Preston[77] in 1922 called these "*chatter sleeks*." They are also known as: "frictive tracks: a series of crescent cracks lying along a common axis, paralleling the direction of frictive contact." Fracture often starts from the first or last chatter crack in a series. Abrasion tracks, which often occur around the bottom rim or sides of a glass vessel, are also vulnerable sites for localized contact damage as shown in Figure 6.77. Polishing, lapping or grinding glass can create miniature crack patterns of chatter cracks. Preston[77] and Ghering and Turnbull[78] showed numerous examples and correlated them with the forces, the surface lubrication conditions, and the abrasive or contactor types. Preston showed that a blunt contactor or ball dragged across a surface creates small partial cones cracks behind the contactor. The cracks are created by tensile stresses behind the ball or contactor as it moves, and the cracks are bowed in the direction of the contactor movement such as shown in Figure 6.45 earlier in this chapter for the case of

orthogonal cracks created by abrasive particle motion. In sharp contrast, a rolling ball creates arc cracks that bow in the opposite direction. They arch towards the direction from which the ball came.[77] Variations of chatter cracks with additional descriptions and more illustrations are shown by Preston.[77]

Aldinger and de Haan[70] have recently identified a new class of glass effects associated with applied ceramic labels (ACL) on glass surfaces. Thermal expansion mismatches between the glass and the ceramic label can cause tiny checks to form in the glass. The thermal stresses are very localized and can cause tiny cracks in either the ceramic coating, or in the body glass. Sometimes the cracks are best seen by looking through the glass at the back side of the label layer. The ceramic coating may have its own flaws (bubbles, inclusions, surface contact damage) and these flaws can propagate into the glass.

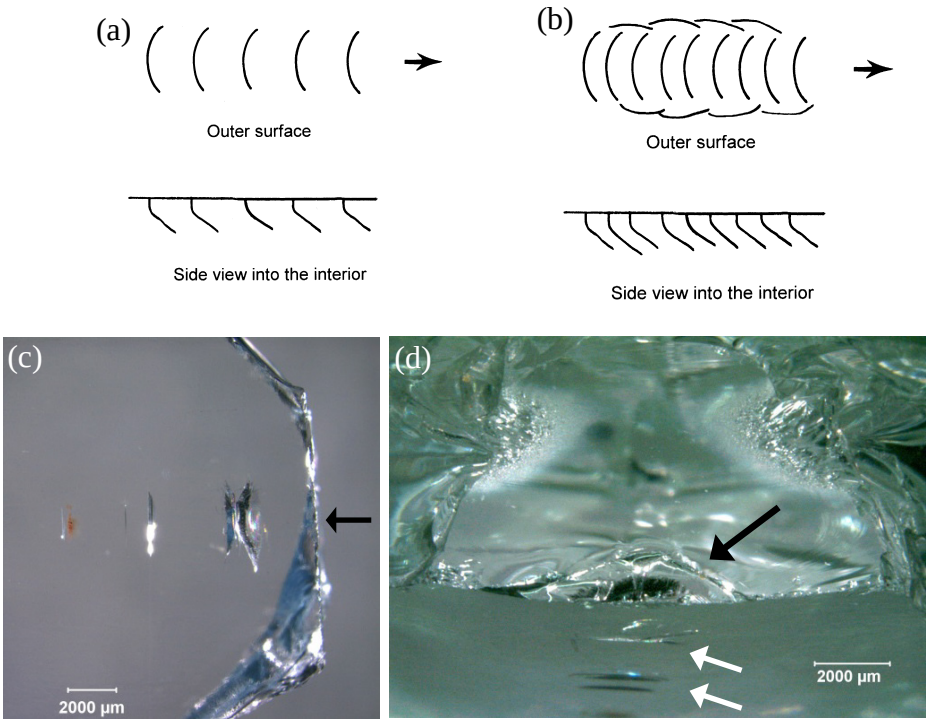

Figure 6.77 *Variants of "chatter cracks" are shown in (a) and (b). (c) and (d) show chatter cracks from an object that slid across the surface of a heat-strengthened soda lime glass kitchenware. (c) shows the outer surface. The black arrow points to the fracture surface and the origin site. (d) shows the specimen tilted to show the origin crack on the fracture surface (large black arrow) and the other chatter cracks on the outer surface (white arrows).*

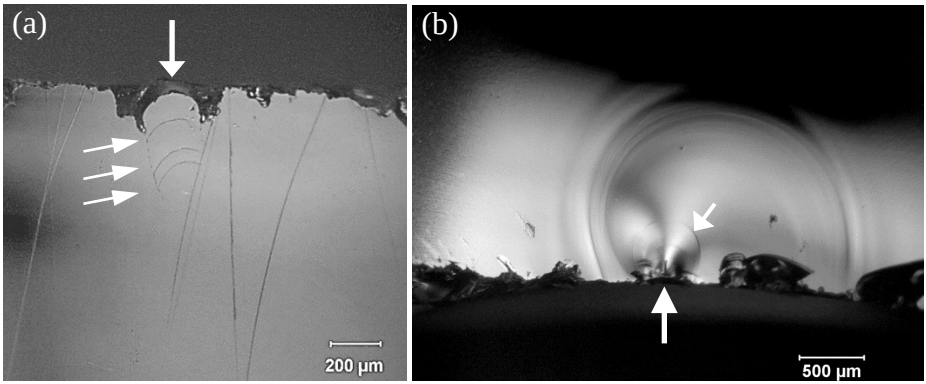

Figure 6.78 *Tiny chatter cracks from a small object that contacted and slid across the surface of a heat-strengthened soda lime glass kitchenware. (a) shows the outer surface with an assortment of common scratches and edge chips, some of which are secondary edge chips after the main fracture. The large arrow points to the exact origin site which is seen to be one of a series of curved chatter cracks (small arrows). (b) shows the fracture surface. The multiple secondary edge chips may confuse interpretation, but the Wallner lines and a faint pop in arrest line (small arrow) are centered on the chatter crack (large arrow).*

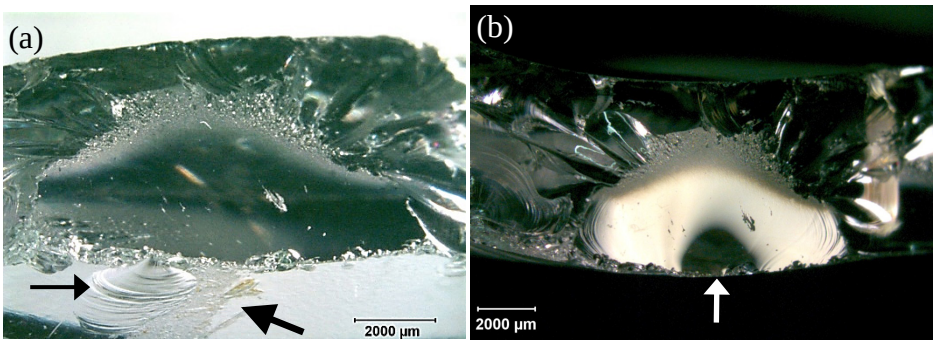

Figure 6.79 *Surface abrasion can create subsurface cracks. (a) shows a piece from a broken heat-strengthened glass kitchenware tilted back to show the fracture surface and the elongated mirror and the outer surface with the abrasion track (large black arrow). Incidental secondary handling edge chips on the left (smaller black arrow) came from handling after fracture. (b) is the fracture surface showing an elongated mirror and the origin (white arrow). The origin region is dark due to a slight curvature of the fracture mirror surface.*

It is worth mentioning tiny submicroscopic flaws may exist in pristine drawn, etched, or fire-polished glasses. In the first half of the 20th century there was much speculation and even doubt as to whether "Griffith flaws" were real or not. This was before high power optical and electron microscopes were readily available and fractographic examination techniques were not widely known or used. There was a lot of speculation about what these intrinsic flaws might have been in high-strength glasses. Eventually, in a seminal set of experiments, in 1960 Ernsberger used special flaw decoration techniques[79] to show that microscopic cracks did exist on the surfaces of glass, but there is another possibility. Could some of the intrinsic flaws be pockets of nonuniform material in glasses, of the order of 1 mm or smaller? Ernsberger wrote about these and contributions by contemporaries such as Levengood, Mould, Marsh, Holloway, Turner, Turnbull and others in his 1963 paper.[80] Some ideas for what these intrinsic flaws might be included: pockets of non-uniform or viscous glass, tiny sub-micrometer-sized invisible bubbles, very shallow cooldown surface cracks, tiny devitrification zones with crystals, or tiny phase separation zones. One type that has remained plausible to this day is so called "latent contact damage." Small localized contact on a pristine glass surface causes deformation damage sites without cracks, but from which cracks can initiate at a later time especially if the glass is exposed to external loading. One practical problem with the very high-strength glass fractures is that it is difficult to find a specific fracture origin site due to extreme fragmentation.

6.9 Fracture Oddities and other flaws

The fractographer should expect the unexpected. Rice[81] described cases of ball mills, thermocouple beads, insect carcasses and feces, dandruff, and hair as flaws. Alcock and Riley[82] analyzed dust particles that are found in ceramic processing environments. Figures 6.80 – 6.82 show other unusual examples. Figure 6.80 shows an example of how stray fibers occasionally land inside a ceramic during processing. These can be hair, clothes fibers, or paper filaments. They often, but not always, burn out during sintering of the ceramic leaving behind a fibrous pore. These stray flaws are usually rare. They often come as a surprise to the fractographer. Figure 3.19c showed a black hair or piece of lint that was intact and partially sticking out of a composite disk strength specimen. Such flaws can be surprisingly common in laboratory-prepared cast resin-composites. If the fiber is still in the ceramic, one might consider it a contaminant as described below in section 6.10, but if it has burned out, it no longer is a contaminant but a residual pore-hole. One might ask how does one distinguish a linear hole from a fiber burn out? The answer is that fiber burn outs usually have a long slender shape with a roughly constant diameter. They can be short straight cylinders such as Figure 6.6c earlier in

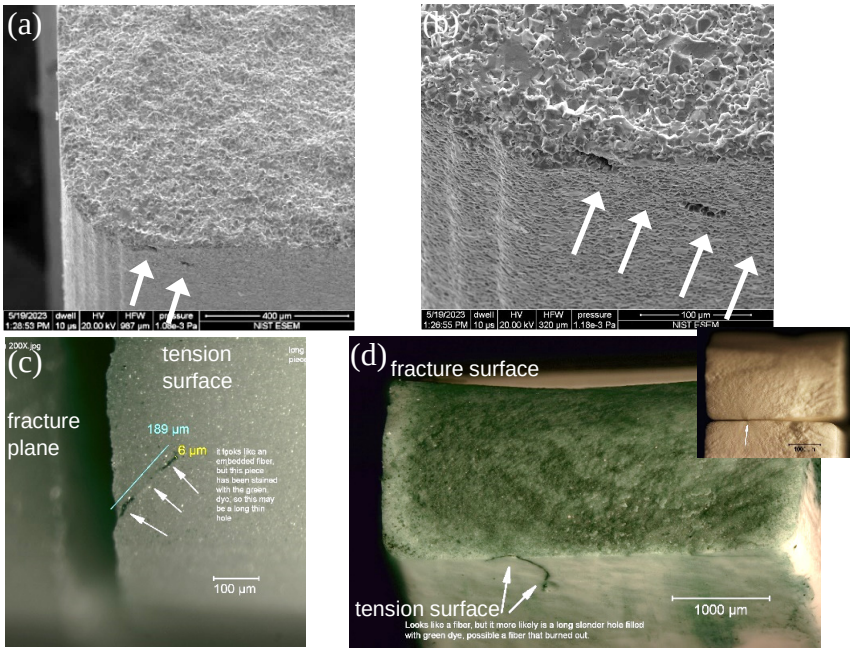

Figure 6.80 *Fibrous pores in an additively-manufactured sintered alumina bend bars.*[1] *(a)–(c) show a 366 MPa bend bar with a long fiber burnout hole that actually dived below the surface in some spots. (d) shows a different bar (292 MPa) tilted back to show a wandering fibrous-pore origin highlighted by green dye.*

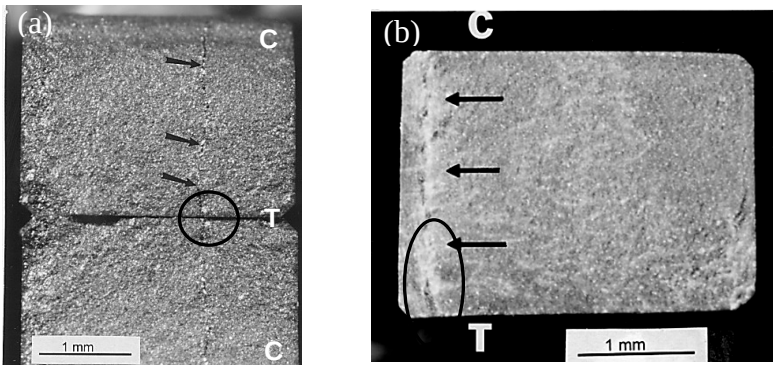

Figure 6.81 *Bend bars with unusual fracture origins. (a) has silicon vein in a siliconized SiC bend bar. The halves are mounted back-to-back. This probably was caused by silicon infiltration of a seam in the green body. (b) shows a silicon nitride bend bar with an unstable yttria-silicate boundary phase. Phase changes badly distorted the rectangular bar shape. Fracture occurred from the crack marked by arrows. T and C denote the tension and compression sides.*

this chapter or long and winding as in Figure 6.80d. The long fibrous hole origins flaws were difficult to detect until they were stained by green dye. The dye penetrated the length of the holes, and they became obvious on the tension surface of one fracture half in each case. These examples underscore what was written earlier in this Guide: the fractographer must be observant, try different techniques and lighting modes, examine both halves, and examine not only the fracture surfaces, but the outer surfaces as well. It also comes as a surprise when something stuck on an outer surface may be a strength-limiting flaw. Figure 6.82 shows two examples of stray shards. The shards were tiny particles (i.e., powders) of the same ceramic that were used to support the green body during sintering. The powder particles sintered to the ceramic. From a fracture mechanics perspective, it might be surprising that such a small discontinuity on an outer surface could act as a strength controlling flaw, but the shard probably had differential shrinkage relative to the main body that introduced local residual stresses at the contact site.

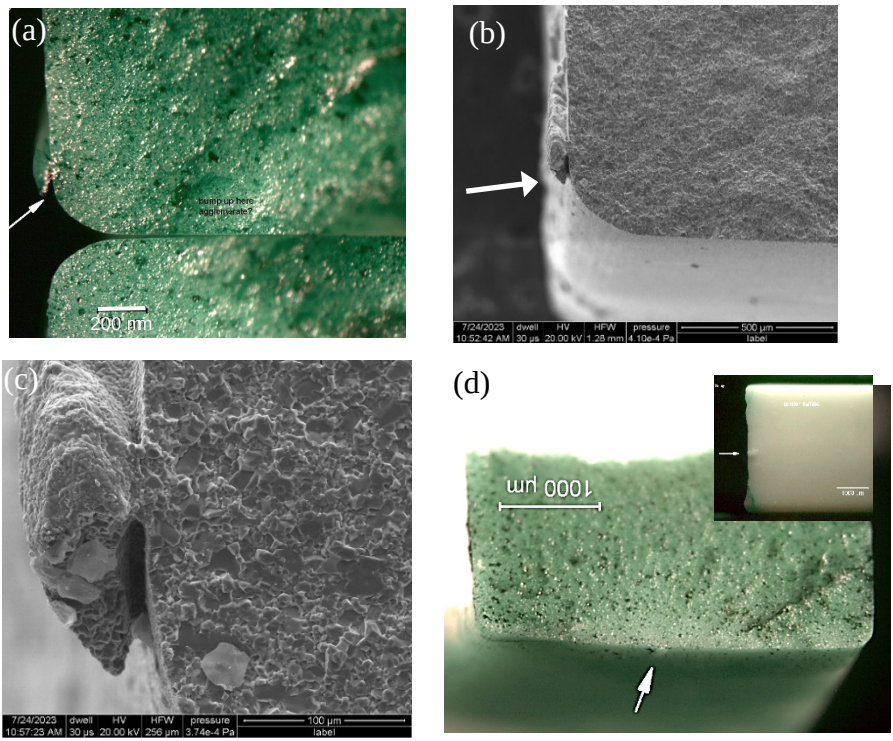

Figure 6.82 *Stray shards bonded to an outer surface acted as fracture origins in additively-manufactured sintered alumina bend bars.*[1] *The shards are sintered to the bars. (a-c) were for a bar at 330 MPa. (d) was for a bar at 331 MPa. The insert shows the shard on the outer tension surface.*

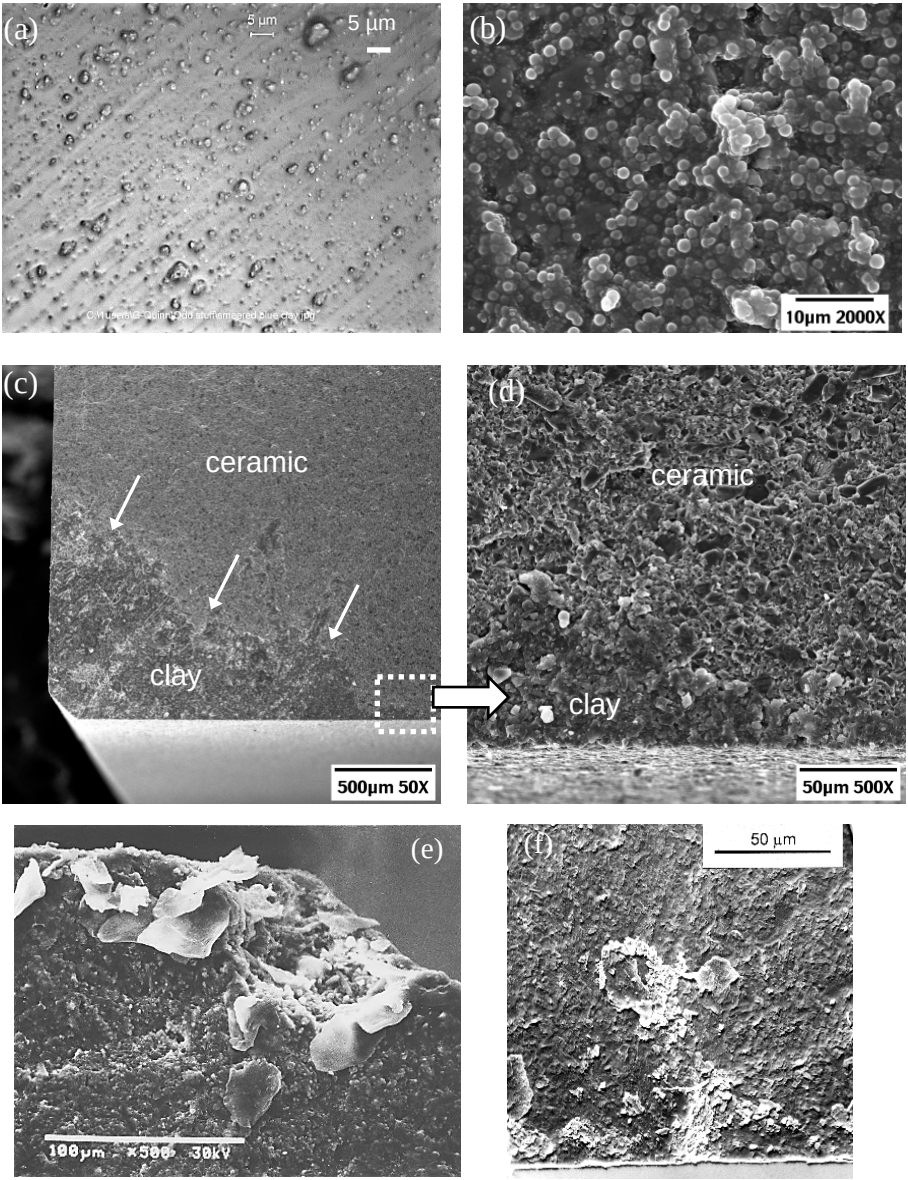

Figure 6.83 *Common contaminants. (a) shows a blue clay smeared on a glass microscope slide as photographed on an optical microscope. The tiny particles and grease smear are evident. (b) shows an SEM image of the clay. (c) shows a fracture surface of an fine-grained alumina bend bar with clay swiped across the lower left corner (arrows). The boxed area is shown enlarged in (d). (e) shows human skin (courtesy A. Pasto). (f) shows an indeterminate contamination on a sintered silicon carbide bend bar.*

6.10 Contaminants

Care should be taken to avoid contaminating the fracture surface, especially before preparation of the specimens for SEM examination. During an optical examination, cleaning is not too difficult. Once a specimen is gold coated and, in the SEM, it can be disappointing to realize the flaw is masked by contamination or that a photo of the origin has distracting debris in the vicinity. Extraction, recleaning, and preparation are time consuming and frustrating. Sometimes contaminants can be recognized if they appear to sit up on top of the fracture surface and are obviously not part of the material, but many contaminants get into the fracture surface crevices and blend in diabolically well. As noted in Chapter 3, modeling clays are especially pernicious since they are fine and blend in to the fracture surface, adhere extremely well, and are next to impossible to clean off. An EDX analysis of clay contamination on a fracture surface revealed aluminum, silicon, and titanium. Figures 6.83 – 6.85 illustrates some common contaminants and how they look in the SEM.

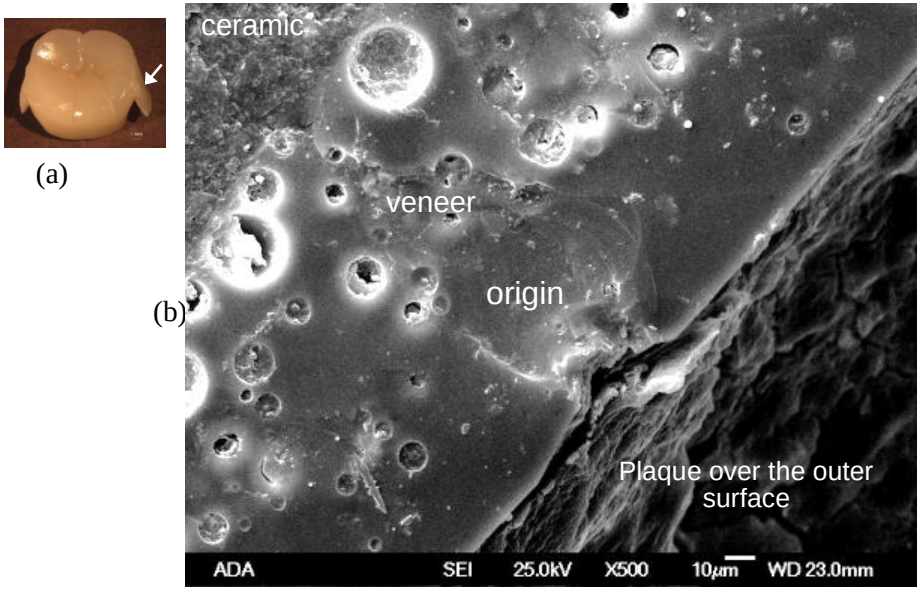

Figure 6.84 *Dental plaque is a common contaminant on ceramic restorations. (a) shows the broken middle ("pontic") piece of a lithium disilicate bridge that broke after 7 weeks in vivo. (b) shows the fracture surface at the contact damage origin site. Plaque can be removed by bleach as described on page 3.6. Figure 6.97 later in this chapter shows additional images of this bridge* <u>*after*</u> *cleaning.*

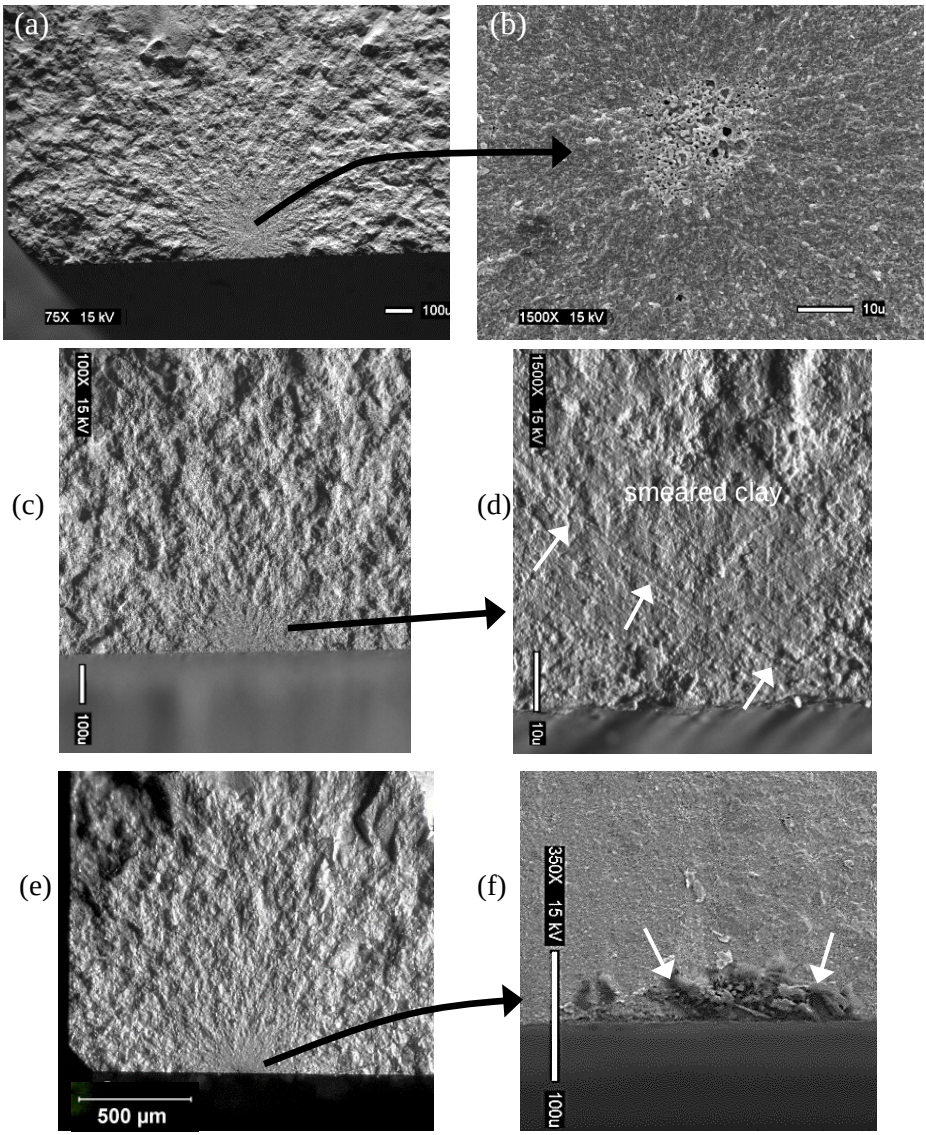

Figure 6.85 *Contaminants in 3Y-TZP bend bars. (a) and (b) show a clean fracture with a well-defined fracture mirror and the most common flaw in this material: a pore or porous region origin. (c) and (d) show clay smeared over the fracture surface and fracture mirror in another specimen. Notice the parallel smear tracks (arrows) from lower left to upper right in (d). The clay is not evident in the low-magnification image of the mirror (c), but it covers the origin in (d). It is possible the wrong end of the bend bar initially was put into mounting clay! (e) and (f) show a mirror with an unknown contaminant covering the origin (arrows). (all courtesy of J. Quinn)*

6.11 Combined or Hybrid Flaws

Sometimes flaws may link up or there simply may be side-by-side flaws at a fracture origin such as shown in Figures 6.86 - 6.87. Some judgment is required as to which origin is primary. ASTM C 1322[83] suggests several options for reporting such hybrid flaws. For example, if one origin type is primary, then a reporting code may list it first with the secondary flaw separated by a plus sign (+), slash mark (/), hypen (-), or ampersand (&). For example, Figures 6.87 and 6.88a show P+LG denoting the origin is primarily a pore, but with one or more associated large grains.[d] Origins can be difficult to characterize if they have mixed attributes. For example, porous *regions* often have large pores associated with them (Figure 6.88d). References 84, 85, and 86 also discuss flaw linking.

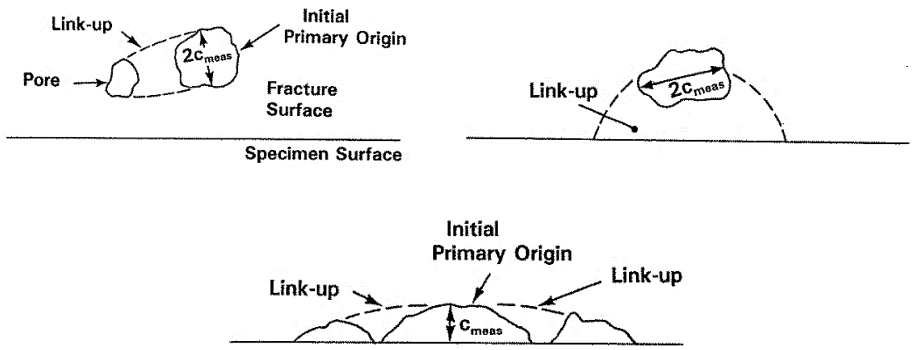

Figure 6.86 *Flaws may link up.*

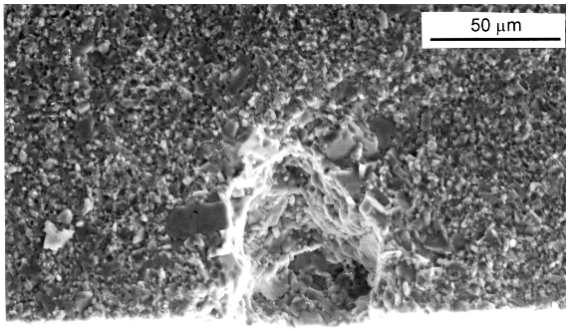

Figure 6.87 *Combined flaw fracture origin in a sintered 99.9 % alumina that can be described as primarily a pore, but with some large grains (P+LG).*

[d] This combined flaw coding scheme has been simplified in this 4th edition of the Guide.

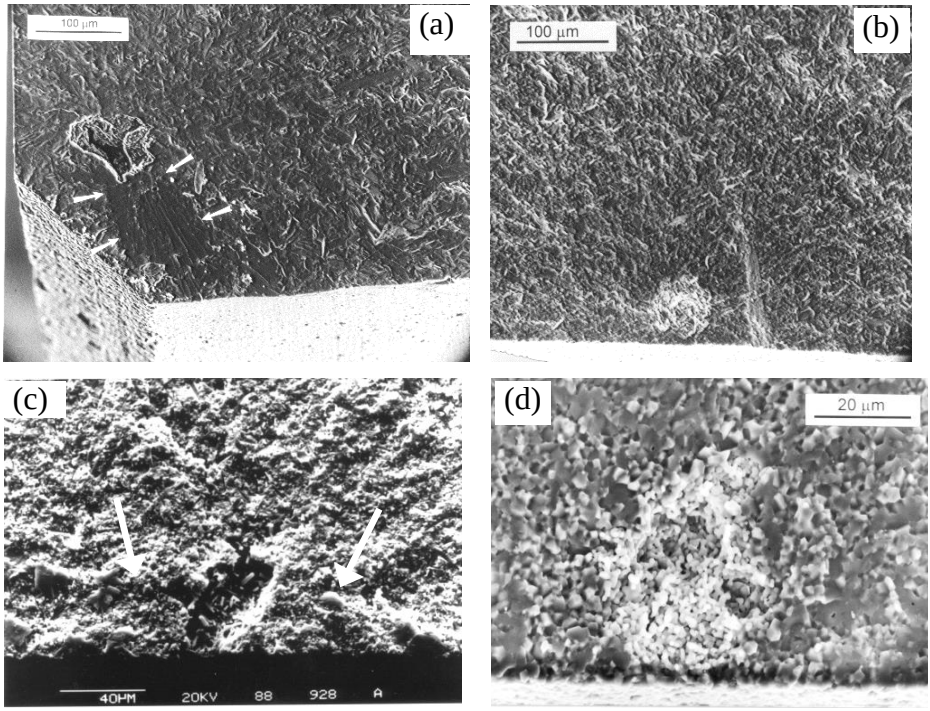

Figure 6.88 *Combined flaw fracture origins. (a) is a pore/large grain (P+LG) combination in a sintered alpha silicon carbide bend bar. Note the good quality of the chamfer. Edge damage was not a factor in this case. (b) is a combination of an agglomerate and a large grain (A+LG) in sintered silicon carbide. (c) is a surface grinding crack that linked with a pore in a sintered silicon nitride (P+MD). (d) shows a flaw in a sintered alumina could be described as either a porous region or a pore.*

6.12 Baseline Microstructure Origins

As fabricators improve materials by careful process control and eliminate large abnormal flaws, ceramics will break from origins that are part of the ordinary microstructure. These are "baseline microstructure" origins. Figure 6.89 illustrates the concept. Once the inclusions are eliminated, grains from the large end of the grain size distribution become the strength-limiting flaws. The materials processor does not believe these are flaws, but the fracture mechanics expert does. Rice[81] described such origins as "mainstream microstructural features." Figure 6.90 shows an example in an aluminum oxynitride.

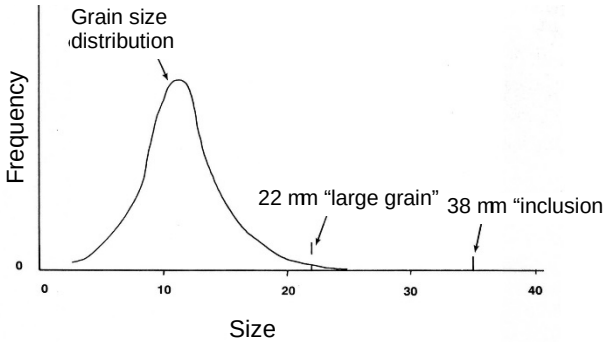

Figure 6.89 *Careful processing may eliminate severe flaws such as inclusions or gross pores. In the absence of such flaws, the material may fail from "baseline microstructure" origins.*

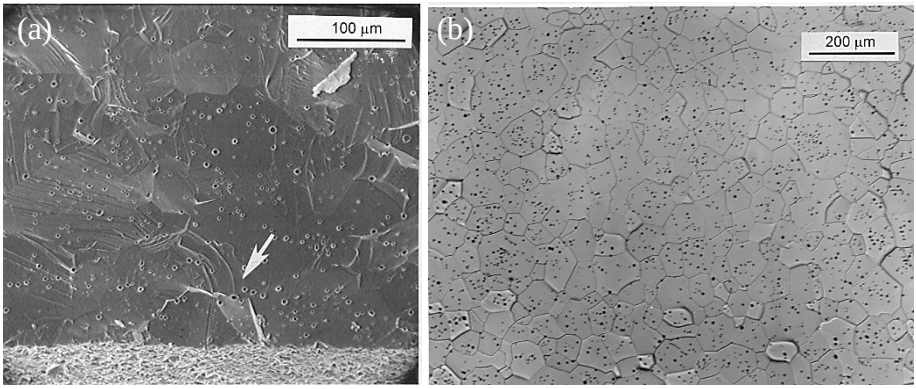

Figure 6.90 *Baseline microstructure flaw in a sintered aluminum oxynitride four-point flexure bar. (a) shows a single grain that was the fracture origin. The origin in this case may actually be the grain boundary around the grain. Notice the short wake hackle steps from the tiny pores that are tiny weathervanes that help confirm the origin. (b) shows a polished section view of the microstructure.*

Figure 6.91 shows two examples from a study on Vita Mark II feldspathic dental porcelain.[8] The fracture origins look exactly like the surrounding microstructure. The flaws evidently are clusters of one or two of the normal crystalline phases that are present in the material. This feldspathic porcelain has a mixture of five or more crystalline phases: potassium and sodium feldspars, a feldspathoid, trydimite and some residual glass.[8] The phases have similar compositions with silicon, aluminum, potassium, and sodium, and oxygen. Backscattered electron microscopy images revealed no apparent chemistry differences. Figures 6.91c,d are SEM images of the microstructure

and show substantial amounts of both matrix glass and crystalline phases. Some regions that were preferentially acid etched away with HF are seen in Fig. 6.91d, suggesting different phase assemblages were present. The feldspar and feldspathoid phases are very similar in chemistry so it is difficult to discriminate between them on the fracture surfaces in the SEM. Local variations in the phase assemblages are likely.

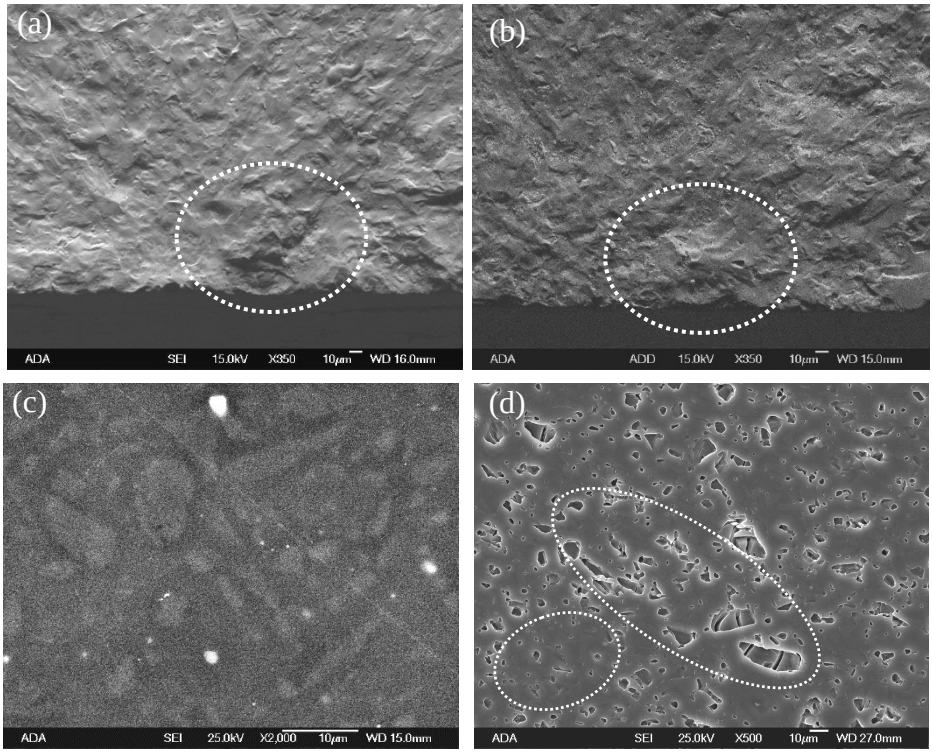

Figure 6.91 *SEM images of "baseline microstructure flaws" in a dental feldspathic porcelain are in (a) and (b). (c) is an unetched polished section as seen in the SEM. (d) shows an HF etched surface. The ellipses highlight microstructural regions of that etched very differently. Reference 8.*

Varner and Fréchette[64] wrote about another case where a clump of feldspar grains caused a large high-tension porcelain insulator to break in half. It fell twenty-six meters onto a man's head, killing him. During firing, the feldspar clump had transformed into mullite crystals around a void.

Another excellent example of baseline microstructure flaws origins but for a cordierite glass ceramic is from the work of Lewis and Spann.[87,88] Very distinct fracture mirrors were centered on flaw origins in high-strength

specimens. The origins contained no obvious flaws, defects, or chemical inhomogeneities. The origins looked exactly the same as the normal microstructure exposed on the fracture surfaces. They suspected that internal stresses resulting from thermal expansion anisotropy and or thermal expansion mismatches were a factor. Cordierite glass ceramics have anisotropic crystals such that the overall body has a low thermal expansion. The material is often used in applications where thermal shock or thermal stress resistance is important.

6.13 Geometric Sharp Points or Cusps

Sharp points are extremely vulnerable to crack pop-in at very low stresses during fabrication or subsequent handling. Once the part is put under stress, these pop-in cracks can propagate to fracture. There may not necessarily be a material flaw as a starter. Sometimes an arrest line will be detected at the end of the pop-in crack, but often the final plane of fracture is identical to the initial pop-in crack plane, and the latter will not stand out. Figure 6.92 shows a sharp "feather-tip margin" origin in a dental crown. The margin of this crown is much too thin. This type of margin is used by some dentists since less reduction of the tooth is needed and the crown blends into the gum line very well. Such practice is unwise for all-ceramic crowns. Cases 11 and 12 in Chapter 10 have more examples of crowns with margin cracks. Figure 6.93 shows exceptionally-thin cusps between etch pits in theta strength specimens.[89]

Not all sharp point/cusp origins are in small pieces. The author once found such an origin in a ~ 1 m large SiC honeycomb structure for a space mirror.

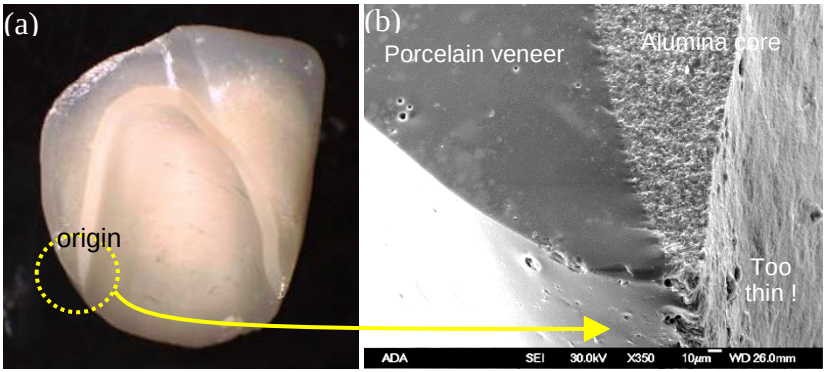

Figure 6.92 *A "feather tip" margin in an alumina dental crown that broke in a patient's mouth. The margin is only 30 µm wide and was extremely vulnerable! Hoop stresses caused fracture from some of the tiny flaws at the margin tip. See also Case 12 in Chapter 10. (crown #22, courtesy of M. Øilo)*

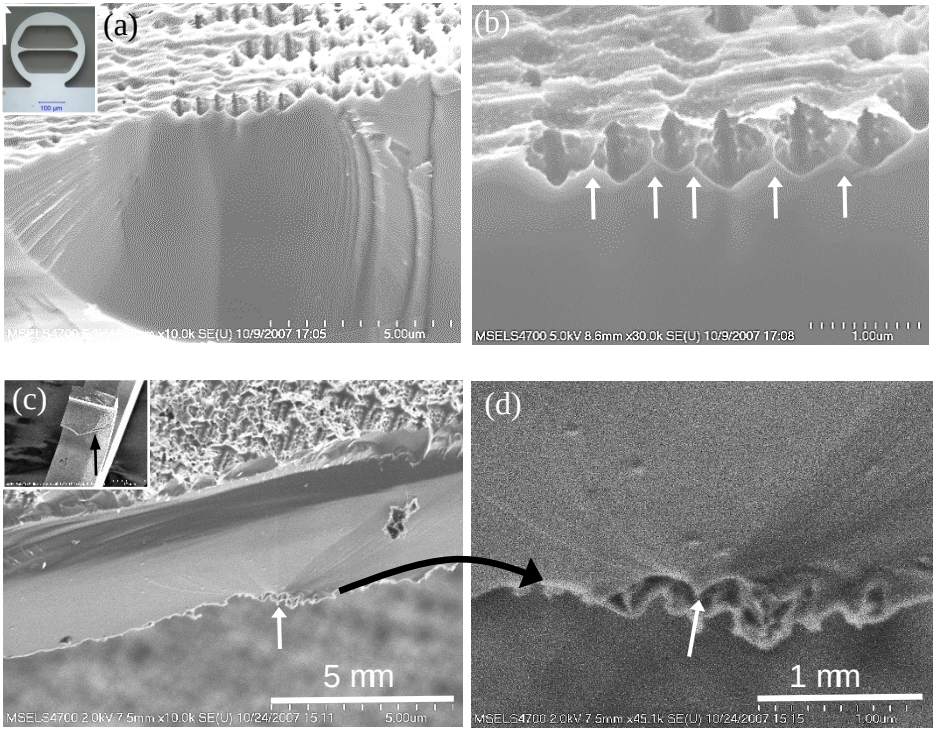

Figure 6.93 *Small cracks may pop-in from sharp points or cusps. The insert of (a) shows a miniature 300 µm diameter) silicon theta strength-test specimen. A force applied to the top of the ring causes the middle 10 µm thick web to stretch and break. (a) shows the fracture mirror around the surface pits fracture origin. The pits are caused by the deep reactive ion-etched (DRIE) processing. Sharp cusps between the pits are an easy path for tiny micro-cracks to pop-in and link. (c) and (d) show another theta specimen. The insert in (c) shows the fragment and the origin location. The hackle lines in (d) indicate fracture started at a single sharp cusp between two pits. (The image is a bit grainy at this high magnification.) The cusp is less than 50 nm in size and may be the smallest fracture origin ever recorded.*

6.14 Partially-Exposed Flaws

Flaws may not necessarily be oriented so that they are perpendicular to the principle tensile stress. The flaw may be truncated on a fracture surface as shown in Figure 6.94 on the next page. The cone cracks of Figure 6.42 and also the seam fracture origins in Section 6.6.3 shown earlier are examples.

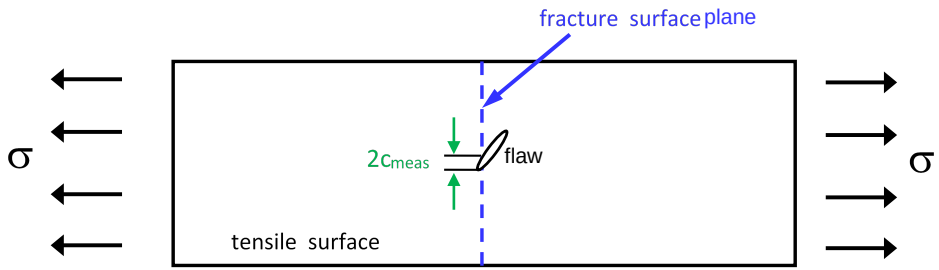

Figure 6.94 *The flaw may not be fully-exposed on the fracture surface.*

6.15 Glaze and Coating Flaws

Glazes and veneers are glassy and have low fracture toughness and resistance to fracture. A crack can form in the vulnerable glaze and then propagate into the remainder of the component. Figures 6.95 to 6.97 show some examples for three clinical dental fractures. Excessive mismatch in the thermal expansion coefficients of the glaze and the body can cause cracking, such as shown in Figure 6.95. Glaze or veneer cracking formed by tension is called "crazing." Some-times excessive porosity can occur at a boundary and can be the strength-limiting flaw as shown in Figure 6.96. Excessive compression in a glaze can cause cracking called "shivering." Buckling of the outer layer fragments, often at an edge or rim, can cause a piece to detach. Krohn *et al.*[90] showed pore and pigment aggregate fracture origins in enamel layers that were applied to float glass. Kobayahsi *et al.*[91] showed excellent images of fracture origins that were a series of bubbles at the boundaries between an alumina porcelain and a glaze.

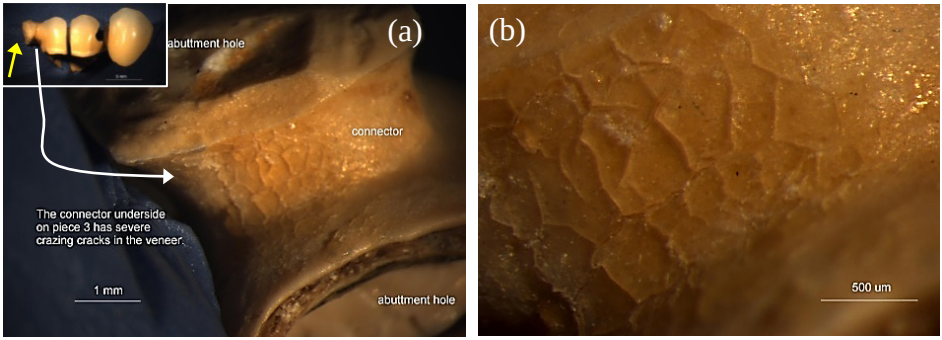

Figure 6.95 *Glazes can be preferred sites of fracture initiation. This was an in vivo broken three-unit zirconia bridge (courtesy T. Kosmac) with a crazed veneer probably from a mismatch of the veneer type to the ceramic. Fracture started on the plane on the left insert marked by the yellow arrow.*

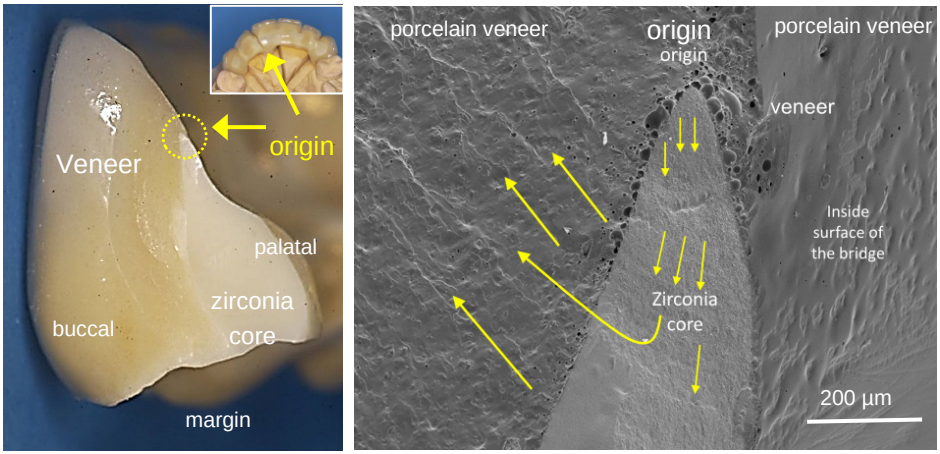

Figure 6.96 *Glaze interfaces can be preferred sites of fracture initiation. This is an in vivo broken six-unit zirconia dental bridge with a poor design. The origin is the pore cluster at the interface between the porcelain veneer and core apex. (images courtesy U. Lohbauer and S. Scherrer)*

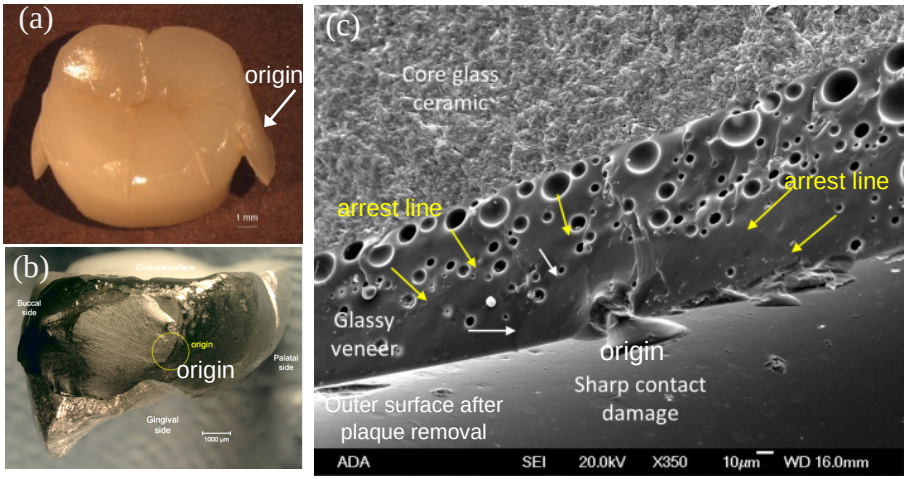

Figure 6.97 *An in vivo broken lithium disilicate glass ceramic bridge pontic unit (courtesy S. Scherrer). (a) is an occlusal surface view and shows it broke on the palatal side of a connector. (b) shows the connector fracture surface with gold coating. (c) the origin was a sharp contact damage crack in the vulnerable veneer. Arrest lines are marked by white and yellow arrows. Also notice the helpful tiny wake hackle lines from the bubbles in the glassy porcelain veneer. See earlier Figure 6.84 for images of this particular bridge fracture* <u>*before*</u> *the plaque was cleaned off.*

6.16 Microfault Pockets

Even if a fracture origin site can be found, there may not be an obvious flaw at the origin. Subtle porous regions or grinding damage crack flaws be hidden in the background microstructure of coarse-grained ceramics, porous ceramics, and heterogeneous ceramics.

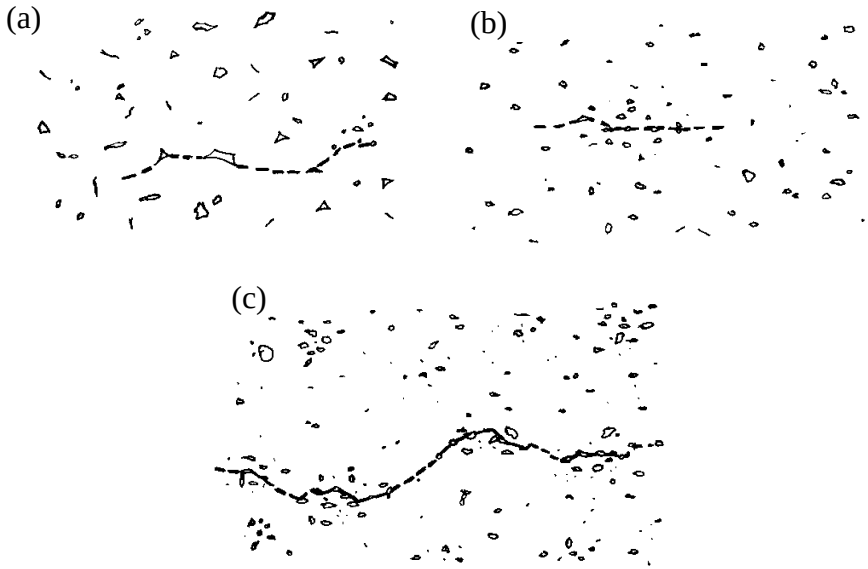

Figure 6.98 Schematics *of "microfault pockets." The fracture origin may be an array of tiny microstructural faults that are linked by microcracking. Tension stress is applied vertically. (a) is similar to a schematic by Sines and Okada*[92,93] *(b) shows an origin site that has a greater local concentration of the irregularities. (c) shows random pockets of greater-than-average concentration. Fracture may entail linkage of these pockets by microcracking.*

There is another possibility why a discrete flaw may not be detectable at an origin site: There may not be one. Emphasis in this chapter up to this point has been on flaws that are discrete irregularities larger than the baseline microstructure. Alternatives are illustrated in Figure 6.98. Fracture origins may be regions of slightly or moderately greater concentration of ordinary irregularities such as micropores, grain boundary cracks or other tiny faults. The regions may be termed "microfault pockets." By themselves, the tiny irregularities are insufficient to case fracture, but they can link by micro-cracking during loading. Sines and Okada[92,93] suggested that this could account for time-dependent fracture, but there is no

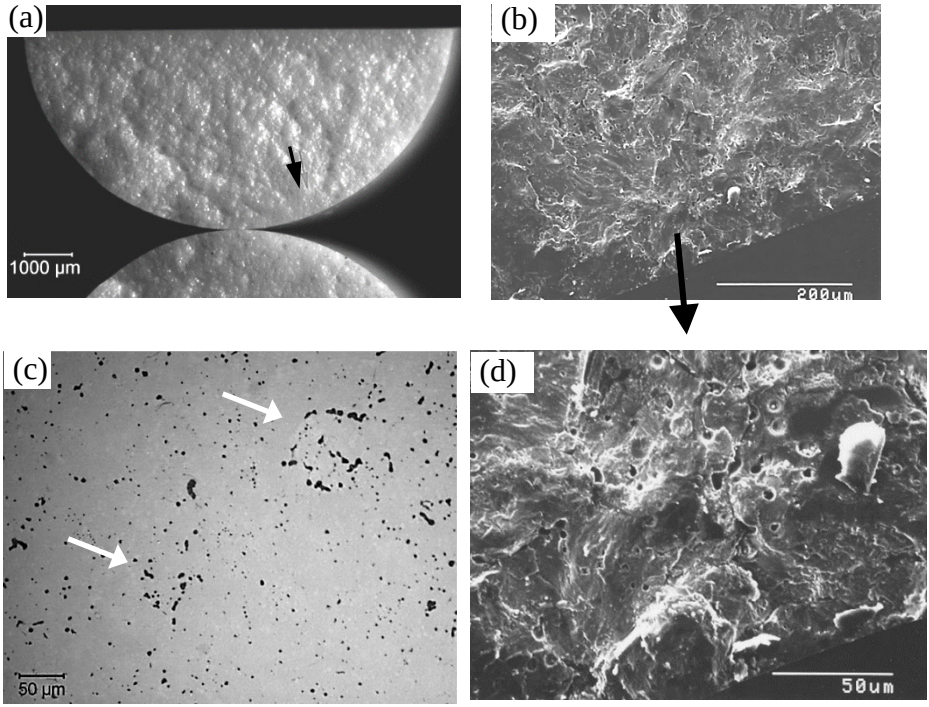

Figure 6.99 *Origin in a magnesia partially-stabilized zirconia split-rod bend specimen. Coarse hackle lines lead back to the origin. (a) shows the entire fracture surface which is very rough and undulating due to the coarse and irregular microstructure. (b,d) show close-ups of the origin which is a pocket of micropores and grain boundary faults. Close examination showed tiny wake and twist microhackle radiate away from the origin. (c) is a polished section with microflaw pockets marked by the arrows.*

reason it cannot apply to fast fracture strength as well. It should be borne in mind that a *random* distribution does not mean a *uniform* distribution. A random distribution of such tiny irregularities will have local regions of greater-than-average concentration.

Fracture origins of the types shown in Figure 6.98 are extremely difficult to diagnose on fracture surfaces, since the features at the origin look exactly like the normal microstructure. Figure 6.99 is an example. Polished specimen microstructural analysis helped with the interpretation as shown in Figure 6.99. The origin may take on the character of porous regions as shown in Figure 6.13. The literature is sparse on such flaws, no doubt because engineers and scientists are loath to show fractographs that fail to show a distinct flaw!

6.17 Polished Microstructural Sections

Many figures in this chapter and Figures 6.100 and 6.101 below show examples of how polished microstructural sections can provide complimentary information about flaw types and their distributions. Polished section preparation is a staple for metals failure analysis, usually to ensure that the microstructure is as expected, and the correct phases are present.

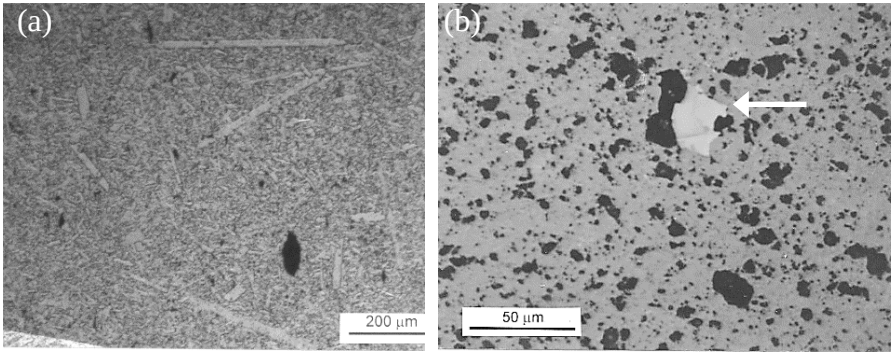

Figure 6.100 *Polished microstructural sections can aid origin interpretation. (a) Sintered alpha silicon carbide often has large grain fracture origins. The acicular or platelet shape of these and their concentration are revealed by the micrograph. (b) reaction-bonded silicon nitride sometimes fails from unreacted silicon (arrow).*

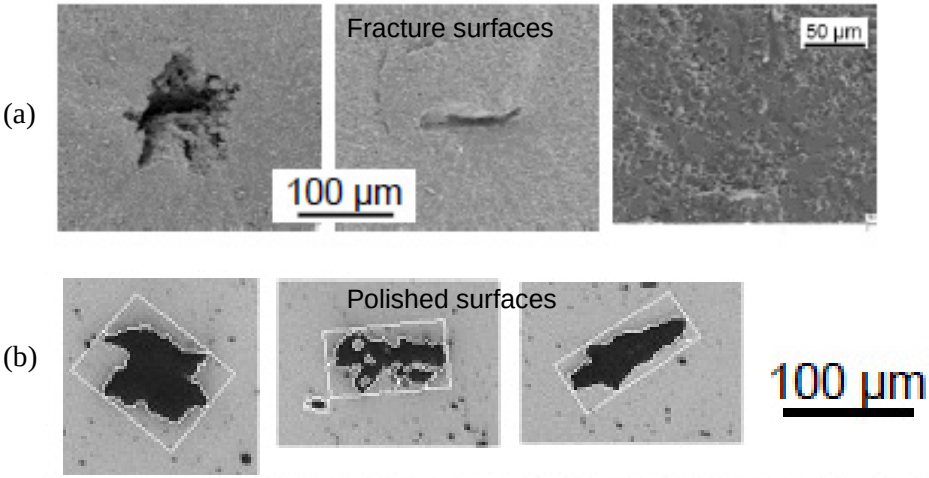

Figure 6.101 *Polished microstructural sections can aid origin interpretation. (a) and (b) show irregular pressing flaws on fracture surfaces and polished sections of a sintered alumina, respectively. (courtesy T. Bernthaler)*

6.18 Flaw Size

It may suffice to identify the nature of the flaw, but a better characterization includes at least a rough estimate of its size. A 100 mm inclusion may not have the same source or behavior as a 20 mm inclusion. The size need not be measured precisely if the characterization is intended to describe the general nature of the origin. On the other hand, there are some instances when a good estimate is needed, such as when it is intended to do a fracture mechanics analysis of the flaw as described in the next chapter. This may be to confirm that the fractographer has found the correct flaw. For example, if a fractographer has tentatively identified a 2 mm feature as an origin, but fracture mechanics suggests the flaw should be 50 mm in size, then the fractographer ought to reevaluate his assessment. Measure an approximate flaw diameter, or if the flaw is elongated, approximate it with a semi-elliptical shape and measure the minor and major axis lengths as shown in Figure 6.2. The origin's true size may not be revealed on the fracture surface. Exact fracture mechanics analyses of most origins are not possible due to their complex shape. An important exception to this is machining damage, wherein the origin size measurement may be very useful for the estimation of fracture toughness. When measuring the flaw size of surface-located flaws, measure and record the origin depth and the width. Chapter 7 and Figures 7.21 and 7.22 furnish guidance.

6.19 What to Report

For each component, or laboratory-tested specimen, record the origin type, the location in the particular specimen, and the flaw size. As discussed in section 6.1, if there are more than one type of a different flaw (e.g., various types of inclusions or pores), identify each by its primary type with a qualifier, e.g.: pore, long fibrous. If a fracture mirror is present, it may also be helpful to measure its size. Mirror size measurements in laboratory strength test specimens also may be done so that mirror constants can be estimated and published for new materials. Figure 6.102 shows images that follow the recommendations in ASTM C 1322.[83]

Organizing a wealth of fractographic images can at times be difficult. Ideally the images should be presented in a coherent fashion with some context. Section 5.9 and Figure 5.73 showed how montages can be useful in organizing a lot of local detail into a global map for a component failure analysis. Figure 6.103 shows how a montage can be constructed for laboratory strength test data. In this example for bend strength specimens, the fracture images are coupled to a Weibull strength distribution graph. The low power (25X) photos show the whole fracture surface of one or both halves of a bar. Higher

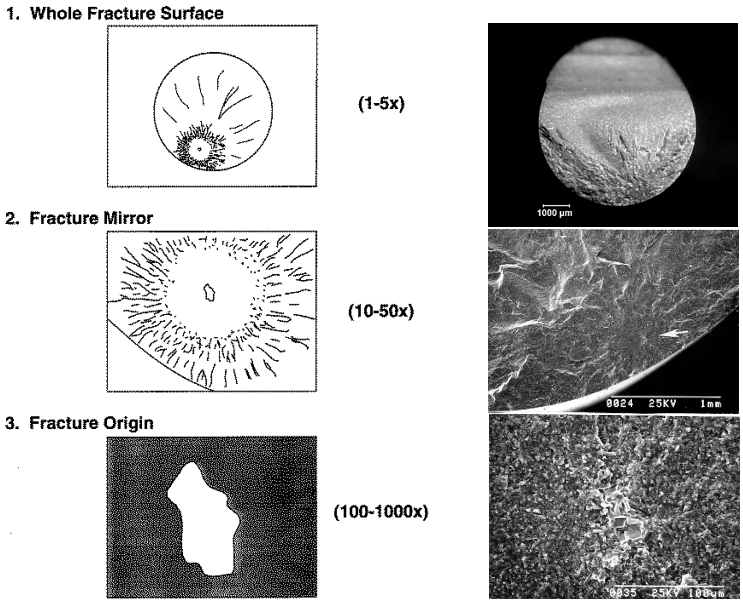

Figure 6.102 *Multiple photos should be taken showing whole fracture surface, the mirror region and the origin. The right side shows an example for an inclusion in a silicon nitride rod flexural strength specimen.*

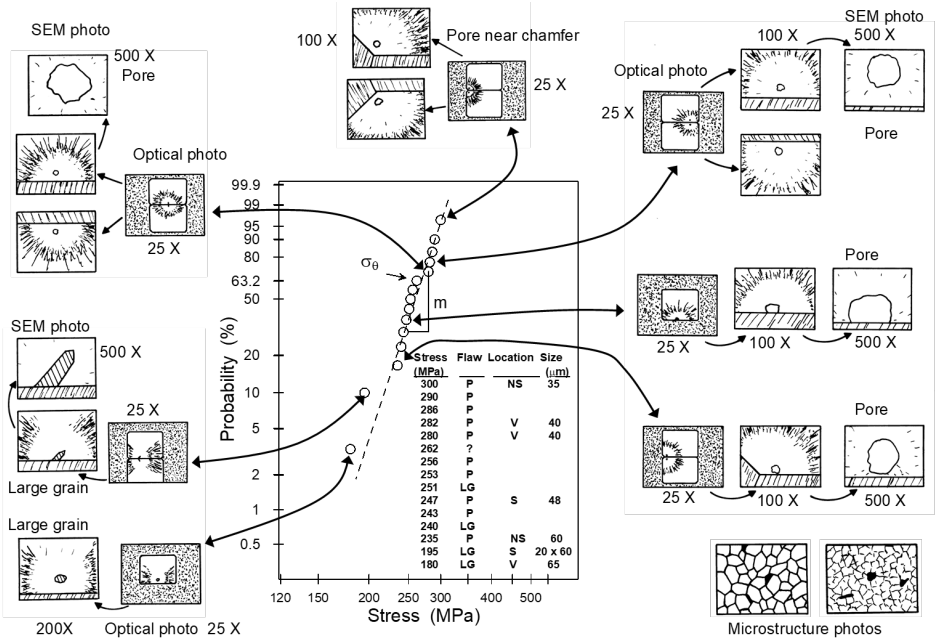

Figure 6.103 *Schematic of a fractographic montage.*

magnification photos show the fracture mirrors and the fracture origin flaws. This provides valuable information for interpreting the Weibull graph, and also organizes the photos in a logical manner.

Component failure analyses should have some overall photographs of the entire structure and close-ups of various critical features. Much time and confusion can be saved if the successive images are presented in an orderly, systematic way. It is always wise to start with an overall image of the structure and then add images at progressively higher magnification at key locations.

When one jumps from one magnification to a higher magnification, later it may be difficult to correlate the two images. In the author's experience, magnification jumps of about 5 are the most one should use. When a series of photos are taken, at each step the image relationships should be clear.

Chapter 6 References

1. G. D. Quinn and R. Maier, "Fractographic Observations from a Pilot Round Robin on Flexural Strength of a Photolithography Manufactured High-purity Alumina," presented at ICACC conference, American Ceramic Society, Daytona Beach, January 30, 2024.
2. R. A. Maier, A. J. Allen, B. Cox, and I. Levin, "Interlaboratory Study of Flexural Strength in Additively Manufactured Alumina," *J. Am. Ceram. Soc.*, **108** [2] e20133 doi.org/10.1111/jace.20133.
3. W. Weibull, "A Statistical Distribution Function of Wide Applicability," *J. Appl. Mech.*, **18** (1951) 293 - 297.
4. G. D. Quinn and R. Morrell, "Design Data for Engineering Ceramics: A Review of the Flexure Test," *J. Am. Ceram. Soc.*, **74** [9] (1991) 2037 - 2066.
5. R. W. Davidge, *Mechanical Behavior of Ceramics*, Cambridge Univ. Press, London, 1979.
6. D. Munz and T. Fett, *Ceramics, Mechanical Properties, Failure Behavior, Materials Selection*, Springer, Berlin, 1999.
7. W. E. C. Creyke, I. E. J. Sainsbury, and R. Morrell, *Design with Non-ductile Materials*, Applied Science Publ., London, 1982.
8. G. D. Quinn, K. Hoffman, and J. B. Quinn, "Strength and Fracture Origins of a Feldspathic Porcelain," *Dent. Mat.*, **28** [5] (2012) 502 – 511.
9. R. W. Rice, "Pores as Fracture Origins in Ceramics," *J. Mat. Sci.*, **19** (1984) 895 - 914.
10. D. Lewis, III, "Fracture Strength and Mirror Size in a Commercial Glass-Ceramic," *J. Am. Ceram. Soc.*, **64** [2] (1981) 82 - 86.
11. T. Bernthaler, "Defect Imaging and Analysis for Predicting the Reliability of Ceramics," PhD thesis, School of Materials Science and Engineering, University of New South Wales, Sydney, Australia and Aalen University, Aalen, Germany, April 2011.
12. F. F. Lange, "Processing-Related Fracture Origins: I, Observations in Sintered and Isostatically Hot-Pressed Al_2O_3/ZrO_2 Composites," *J. Am. Ceram. Soc.*,**66** [6](1983)396-8.
13. F. F. Lange and M. Metcalf, "Processing-Related Fracture Origins: II, Agglomerate Motion and Cracklike Internal Surfaces Caused by Differential Sintering," *ibid*, 398 - 406.
14. F. F. Lange, B. I. Davis, and I. A. Aksay, "Processing-Related Fracture Origins: III, Differential Sintering of ZrO_2 Agglomerates in Al_2O_3/ZrO_2 Composite," *ibid*, 407 - 408.

15. M. G. Gee, and R. Morrell, “Fracture Mechanics and Microstructures,” pp. 1 – 22 in *Fracture Mechanics of Ceramics*, Vol. 8, R. Bradt, A. Evans, D. Hasselman, and F. Lange, eds., Plenum Press, NY, 1986.
16. M. Hangl, “Processing Related Defects in Green and Sintered Ceramics,” pp. 133 – 143 in *Fractography of Ceramics and Glasses*, IV, eds. J. R. Varner and G. D. Quinn, Ceramic Transactions, Vol. 122, American Ceramic Society, Westerville, OH, 2001.
17. H. R. Baumgartner and D. W. Richerson, “Inclusion Effects on the Strength of Hot Pressed Si_3N_4,” pp. 367 – 386 in *Fracture Mechanics of Ceramics, Vol. 1,* eds., R.C. Bradt, D. P. H. Hasselman, and F. F. Lange, Plenum, NY, 1974.
18. R. J. Ginther, “The Contamination of Glass by Platinum,” *J.Noncryst.Sol*., **6**(1971)294–306.
19. B. S. Aldinger and B. K. Collins, *Color Atlas of Stones in Glass,* American Glass Research, Butler, PA, 2016.
20. S. Karlsson, “Spontaneous Fracture in Thermally Strengthened Glass – A Review and Outlook,” *Ceramics-Silikaty,* **61** [3] (2017) 188 – 201.
21. R. R. Johnson, “Managing the Problems Inherent in Tempered Glass,” US Glass Magazine, **43** [6] June 2008, on line at: industry.glass.com: https://industry.glass.com/USGlass/2008/June/onlyonlineTemper.htm
22. R. Huet, J. M. Wolf, P. D. Moncarz, “Delayed Fracture of Tempered Glass Panels Due to Nickel Sulfide Inclusions,” pp. 431-433 in *Handbook of Case Studies in Failure Analysis, Vol. 1*, ed. K. A. Esakul, ASM Int., Materials Park, OH, 1992.
23. R. C. Bradt, “Macro- and Microfracture Patterns of Thermally Tempered Plate Glass Falling from Nickel Sulfide Inclusions,” pp. 417 – 426 in *Fractography of Glasses and Ceramics,* eds. J. D. Varner and V. D. Fréchette, Advances in Ceramics, Vol. 22, American Ceramic Society, Westerville, OH, 1988.
24. C. C. Hsiao, “Spontaneous Fracture of Tempered Glass,” pp. 985 -992 in *Fracture 1977, Vol. 3*, ed. D. Taplin, Int. Congress on Fracture 4, Waterloo, Canada, 1977.
25. J. C. Barry and S. Ford, “An Electron Microscopic study of Nickel Sulfide Inclusions in Tempered Glass,” *J. Mat. Sci.,* **36** (2001) 3721 – 3730.
26. M. V. Swain, “Nickel Sulphide Inclusions in Glass; An Example of Microcracking Induced by a Volumetric Expanding Phase Change,” *J. Mat Sci.,* **16** (1981) 151 – 158.
27. A. Kasper, “Spontaneous Cracking of Thermally Toughened Safety Glass. Part One: Properties of Nickel Sulfide Inclusions,” *Glass Struct. Eng*., **4** (2019) 279 - 313.
28. A. Kasper, “Spontaneous Cracking of Thermally Toughened Safety Glass. Part Three: Statistic Evaluation of Field Breakage Records and Consequences for Residual Breakage Probability,” *Glass Struct. Eng*., *ibid,* 345- 376.
29. Y. Bao, L. Liu, S. Han, X. Shi, and J. Yang, “A New Mechanism of Spontaneous Breakage of Tempered Glass – Monolithic Silicon Particles,” *J. Chinese Ceram. Soc,* **35** [9] (2007) 1273 – 1276.
30. A. G. Evans, “Structural Reliability, A Processing Dependent Phenomenon,” *J. Am. Ceram. Soc*., **65** [3] (1982) 127 - 137.
31. R. W. Rice, *Mechanical Properties of Ceramics and Composites, Grain and Particle Effects,* Marcel Dekker, NY, 2000.
32. E. Carlstrom and R. Carlsson, “A Fractographic Study of Electrical Porcelains Containing Alumina,” *J De Physique,* **47** [C-1] (1986) 563 – 567.
33. D. Southan, “The Porcelain Jacket Crown,” pp. 207 -230 in *Dental Ceramics*, Proc. First International Symposium on Ceramics, ed. J. McLean, Quintessence Publ., London ,1983.
34. J. S. Banda and P. F. Messer, “Fracture-Initiating Flaws in Whitewares,” pp. 363 – 375 in *Fractography of Glasses and Ceramics,* Advances in Ceramics, Vol. 22. eds, J. R. Varner and V. D. Fréchette, 1988, American Ceramic Society, Westerville, OH, 1988.

35. R. W. Davidge and G. Tappin, "The Effects of Temperature and Environment on the Strength of Two Polycrystalline Aluminas," *Proc. Br. Ceram. Soc*., **15** (1970) 47 – 60.
36. J. A. Salem, "Transparent Armor Ceramics as Spacecraft Windows," *J. Am. Ceram. Soc.*, **96** [1] (2013) 281-289.
37. J. J. Swab, R. Pavlacka, G. Gilde, S. Kilczewski, J. Wright, and D. Harris, "Determining the Strength of Coarse-Grained AlON and Spinel," *J. Am. Ceram. Soc*., **97** [2] (2014) 592-600.
38. D. W. Richerson, *Modern Ceramic Engineering*, Marcel Dekker Inc., NY, 1982; and 3rd edition, CRC Press, Taylor and Francis, Boca Raton, FL, 2006.
39. M. G. Schinker and W. Döll, "Plasticity and Fracture Induced by Scratching Optical Glass at High Speeds," pp. 115 – 133 in *Strength of Inorganic Materials*, ed. C. R. Kurkjian, Plenum, NY, 1985.
40. T. I. Suratwala, *Materials Science and Technology of Optical Fabrication*, Wiley, Hoboken, NJ, 2018.
41. MIL-PRF-13830B, 9 January 1997, "Optical Components for Fire Control Instruments: General Specification Governing the Manufacture, Assembly, and Inspection of," U.S. Army ARDEC, Picatinny Arsenal, New Jersey. (Originally MIL-O-13830 of 7 December 1954; superseded by MIL -O-13830A of 11 Sept 1963)
42. D. M. Aikens, "The Truth About Scratch and Dig," *Optical Fabrication and Testing Technical Digest (2010*), Proc. of the Optical Fabrication and Testing conference, 13-17 June 2010, Jackson Hole, WY, Optical Society of America, Washington, DC.
43. MIL-C-48497A, 8 September 1980, "Military Specification, Coating, Single or Multiplayer, Interference: Durability Requirements for," U. S. Army ARDEC, Picatinny Arsenal, NJ.
44. ISO 10110:2017, Optics and Photonics – Preparation of Drawings for Optical Elements and Systems – Part 7: Surface Imperfections," ISO, Geneva, CH, 2017.
45. G. D. Quinn and J. J. Swab, "On the Fracture Resistance of Ancient Roman Glass from the Jalame Excavations," *Journal of Glass Studies*, **61** (2019) 254 - 259.
46. C. G. Knight, M. V. Swain, and M. M. Chaudhri, "Impact of Small Steel Spheres on Glass Surfaces," *J. Mat. Sci*., **12** (1977) 1573 – 1586.
47. M. M. Chaudhri, "High-Speed Photographic Investigations of the Dynamic Localized Loading of Some Oxide Glasses," pp. 87 – 113 in *Strength of Inorganic Glass*, ed. C. Kurkjian, Plenum, New York, 1985.
48. Y. Akimune, "Hertzian Cone Crack in SiC Caused by Spherical Particle Impact," *J. Mat. Sci. Lttrs.*, **9** (1990) 659 – 662.
49. J. C LaSalvia, M. J. Normandia, H. T. Miller, and D. Mackenzie, "Spherical Impact Induced Damage in Ceramics, Parts I to III, in *Advances in Ceramic Armor, Ceramic Engineering and Science Proceedings*, Wiley and Sons, 2008, pp. 170 – 202.
50. B. Aydelotte and B. Schuster, "Observation and Modeling of Cone Cracks in Ceramics," pp. 19 - 24 in *Dynamic Behavior of Materials*, Vol. 1, *Proc. 2015 Annual Conf. Exptl. and Appl. Mech*., eds. D. Casem, L. Lamberson, and J. Kimberley, Springer, 2016.
51. H. Kirchner and R. Gruver, "Branching of Hertz Cracks," pp. 959-964 in *Fracture 1977, Vol. 3*, Proceedings of the 4th Int. Conf. on Fracture, Waterloo, Canada, ed., D. Taplin, Univ. Waterloo Press (1977).
52 B. R. Lawn, S. M. Wiederhorn, and D. E. Roberts, "Effect of Sliding Friction Forces on the Strength of Brittle Materials," *J. Mat. Sci.*, **19** (1984) 2561 - 2569.
53. M. M. Chaudhri and C. Liangyi, "The Orientation of the Hertzian Cone Crack in Soda-Lime Glass Formed by Oblique Dynamic and Quasi-static Loading with a Hard Sphere," *J. Mat. Sci.*, **24** (1989) 3441 – 3448.
54. C. Colin and J. L. Heitz, "Failure Analysis: Glass Bottle Breakage," *Verre*,**16**[4](2010)33-6.

55. R. A. Schaut, K. C. Hoff, S. E. Demartino, W. K. Denson, and R. L. Verkleeren, "Enhancing Patient Safety Through the Use of a Pharmaceutical Glass Designed to Prevent Cracked Containers," *PDA J. Pharm. Sci. and Tech.*, **71** (2017) 511 - 528.
56. D. C. Harris, *Materials for Infrared Windows and Domes, Propertius and Performance*, SPIE, Bellingham, WA, 1999, Chapter 7.
57. R. W. Rice and J. J. Mecholsky, Jr., "The Nature of Strength Controlling Machining Flaws in Ceramics," pp. 351 – 378 in *The Science of Ceramic Machining and Surface Finishing II*, eds., B. J. Hockey and R. W. Rice, Special Publication 562, NBS, Gaithersburg, MD, 1979.
58. G. D. Quinn, L. K, Ives, and S. Jahanmir, "On the Nature of Machining Cracks in Ground Ceramics: Part I: SRBSN Strengths and Fractographic Analysis," *Mach. Sci. Technol.*, **9** (2005) 169 - 210.
59. G. D. Quinn, L. K, Ives, and S. Jahanmir, "On the Nature of Machining Cracks in Ground Ceramics: Part II: Comparison to Other Silicon Nitrides and Damage Maps," *Mach. Sci. Technol.*, **9** (2005) 211 - 237.
60. W. Kanematsu, "Visualization of Subsurface Damage in Silicon Nitride from Grinding by a Plasma Etching and Dye Penetration Method," *J. Amer. Ceram. Soc*., **89** [8] (2006) 2564-2570.
61. V. D. Fréchette and M. Donovan, "Some Effects of the "Glue-Chipping" Process on Strength," pp. 407 –411 in *Fractography of Glasses and Ceramics, II, Ceramic Transactions*, Vol. 17, eds., V. Fréchette, and J. Varner, American Ceramic Society, Westerville, OH, 1988.
62. S. T. Gulati and H. E. Hagy, "Analysis and Measurement of Glue-Spall Stresses in Glass-Epoxy Bonds," *J. Amer. Ceram. Soc*., **65** [1] (1982) 1 – 5.
63. B. A. Bender, C. Kim, and C. Cm Wu, "Solid Preform Fabrication of a Piezoelectric Ceramic Torsional Actuator Motor," *Ceram. Eng. Sic., Proc*., **25** [3] (2004) 89 – 94.
64. J. R. Varner and V. D. Fréchette, "Fractography of Whitewares," pp. 305 – 315 in *Science of Whitewares*, Eds. V. Henkes, G. Y. Onoda, and W. M. Carty, American Ceramic Society, Westerville, OH, 1996
65. G. D. Quinn, K. Hoffman, S. Scherrer, U. Lohbauer, G. Amberger, M. Karl, and J. R. Kelly, "Fractographic Analysis of Broken Ceramic Dental Restorations, pp. 161 - 174 in, *Fractography of Glasses and Ceramics*, VI, *Ceramic Transactions*, Volume 230, eds., J. R. Varner, M. Wightman, Wiley, New York, 2012.
66. G. D. Quinn, "Fractographic Analysis of Broken Ceramic Dental Restorations," *Ceram. Eng. Sci. Proc.*, **35** [1] (2015) 39 - 51.
67. J. R. Varner, "The Practical Strength of Glass," pp. 389 – 406 in *Strength of Inorganic Glass*, ed., C. Kurkjian, Plenum, NY, 1986.
68. V. D. Fréchette, *Failure Analysis of Brittle Materials*, Advances in Ceramics, Vol. 28, American Ceramic Society, Westerville, OH, 1990.
69. F. M. Ernsberger, "Origin and Detection of Microflaws in Glass," pp. 161 – 173 in *Fracture Mechanics of Ceramics*, Vol. 1, Eds., R.C. Bradt et al., Plenum, NY , 1974.
70. B. S. Aldinger and P. W. de Haan, "Color Atlas of Glass Container Defects," AGR, Butler, PA 2019.
71. ASTM C162-05, "Standard Terminology of Glass and Glass Products," Annual Book of Standards, Vol. 15.02, ASTM Int., West Conshohocken, PA, 2015, (originally 1941).
72. *Glass Container Defects, Causes and Remedies*, Bucher Emhart Glass Company, Steinhausen, Switzerland, 2017.
73. H. Pfaender, *Schott Guide to Glass*, Chapman and Hall, London, 1996.
74. F. Preston, "A Study of the Rupture of Glass," *J. Soc. Glass Techn.*, **10** (1926) 234- 269.
75. F. M. Ernsberger, "Detection of Strength-Impairing Surface Flaws in Glass," *Proc. Roy. Soc., London, A*, **257** (1960) 213 - 223.

76. J. Varner, private communication.
77. F. W. Preston, "The Structure of Abraded Glass Surfaces," *Trans. Opt. Soc.*, **23** [3] (1921-1922) 141 – 164.
78. L. G. Ghering and J. C. Turnbull, "Scratching of Glass by Metals," *Bull. Am. Ceram. Soc*., **19** (1940) 290 – 294.
79. F. M. Ernsberger, "Detection of Strength-Impairing Surface Flaws in Glass," *Proc. Roy. Soc. London A*, **257** (1960) 213 – 223.
80. F. M. Ernsberger, "Current Status of the Griffith Crack Theory of Glass Strength," pp. 58 – 76 in *Progress in Ceramic Science*, *Vol. 3*, Ed. J. E. Burke, Pergamon Press, NY, 1963.
81. R. W. Rice, "Failure Initiation in Ceramics: Challenges of NDE and Processing," pp. 1057 - 1064 in *Ceramic Developments*, eds., C. Sorrell, and B. Ben-Nissan, *Materials Science Forum*, Vol. **34–36**, Trans. Tech. Publ. Ltd., Switzerland, 1988.
Note this is only a short eight-page text-only article of a paper that was presented at a conference. The long preprint of this paper had a comprehensive, well-illustrated review of failure origins. Origins included: agglomerates, pores, large grains, inclusions, machining damage, handling damage, thermocouple beads, ball mills, dandruff, insects, feces, inadequate mixing of constituents, etc. Unfortunately, due to page limitations, none of the figures were published in the conference proceedings. Nonetheless, the printed text paper lists many of the above flaws and provides original references for further investigation.
82. J. R. Alcock and F.L. Riley, "A n Investigation of Dust Particles Found in a Ceramic Processing Environment," *J. Eur. Ceram. Soc*., **6** (1990) 339 - 350.
83. ASTM C 1322-96, "Standard Practice for Fractography and Characterization of Fracture Origins in Advanced Ceramics," *Annual Brook of Standards*, Vol. 15.01, ASTM Int., West Conshohocken, PA (1996).
84. A. G. Evans and G. Tappin, "Effects of Microstructure on the Stress to Propagate Inherent Flaws," *Proc. Brit. Cer. Soc*., **20** (1972) 275 - 297.
85. R. W. Davidge, *Mechanical Behavior of Ceramics*, Cambridge University Press, Cambridge, UK, 1974, pp. 98 - 100.
86. R. W. Rice, "Machining of Ceramics," pp. 287 - 343 in *Ceramics for High Performance Applications*, eds., J.J. Burke, A. E. Gorum, and R. N. Katz, Brook Hill Publ., Chestnut Hill, MA, 1974.
87. D. Lewis, "Fracture Strength and Mirror Size in a Commercial Glass-Ceramic," J. Am. Ceram. Soc., **64** [2] (1981) 82 – 86.
88. D. Lewis III and J. R. Spann, "Fracture Features at Internal Fracture Origins in a Commercial Crystallized Glass," *J. Am. Ceram. Soc*., **65** [10] (1982) C173 - C174.
89. G. D. Quinn, "Fractographic Analysis of Miniature Theta Specimens," *Ceram. Eng. Sci. Proc.*, **29** [3] (2008) 189 – 199.
90. M. H. Krohn, J. R. Hellmann, D. L. Shellemann, and C. Pantano, "Strength and Fatigue of Float Glass Before and After Enameling," *The Glass Researcher*, **11** [2] (2002) 24 – 27.
91. Y. Kobayashi, M. Mukai, T. Mizuno, O. Ohira, and H. Isoyama, "Effect of Cristobalite Formation and Glaze on Bending Strength of a-Alumina Reinforced Porcelain," *J. Ceram. Soc. Japan*, **113** [6] (2005) 413 – 418.
92. T. Okada, G. Sines, and D. Green, "Crack Origins and Microcracking in Delayed Fracture of Alumina," *Comm. Am. Ceram. Soc.*, May 1982, C64 - C65.
93. G. Sines and R. Okada, "Flaws Responsible for Slow Cracking in the Delayed Fracture of Alumina," *J. Am. Ceram. Soc.*, **66** [3] (1983) 228 - 232. {correction, ibid, **66** [7] (1983) 538.}

7. Quantitative Analysis

7.1 Introduction

Quantitative analysis can aid the fractographic analysis and extend its value. It may be used to confirm that the right flaw has been identified as a fracture origin. It can make good estimates of the stresses in the part at failure. Four methods to estimate stress are shown in this chapter: fragmentation analysis, branching distance analysis, fracture mirror size analysis, and origin size analysis. Some analyses are empirical. Others are based on the powerful tool of fracture mechanics. One goal of this chapter is to convey a working knowledge of fracture mechanics so that it can be used to solve practical problems. Table 7.1 includes some useful conversion factors.

length		
1 micrometer	=	1×10^{-6} m
1 inch *	=	25.4 mm
0.001 inch *	=	25.4 micrometers (mm)
force		
1 kgf (kilogram force)*	=	9.80 N (Newtons)
stress or pressure		
1 ksi (1,000 psi) *	=	6.895 MPa (Megapascal)
1 Pa	=	1 N/m^2
1 MPa	=	1 MN/m^2 = 1×10^6 Pa
1 MPa	=	145.04 psi = 0.14504 ksi *
1 GPa	=	1,000 MPa = 1×10^9 Pa
example: 100 ksi = 690 MPa		
stress intensity		
1 ksi Ö inch *	=	1.10 MPaÖm

example: $5\ MPa\sqrt{m} \quad x \quad \left(\frac{1\ ksi\sqrt{in}}{1.10\ MPa\sqrt{m}}\right) = 4.55\ ksi\sqrt{in}$

energy		
1 erg	=	0.0000001 (= 1×10^{-7}) J (Joule)
1 ft-lbf *(foot pound force)	=	1.355 J
energy/area		
erg/cm^2	=	.001 J/m^2
Length on Photos		
1 mm = 1 micrometer on a 1,000X photo		

* Not an official SI unit, but included here for completeness.

Table 7.1 Conversion Factors

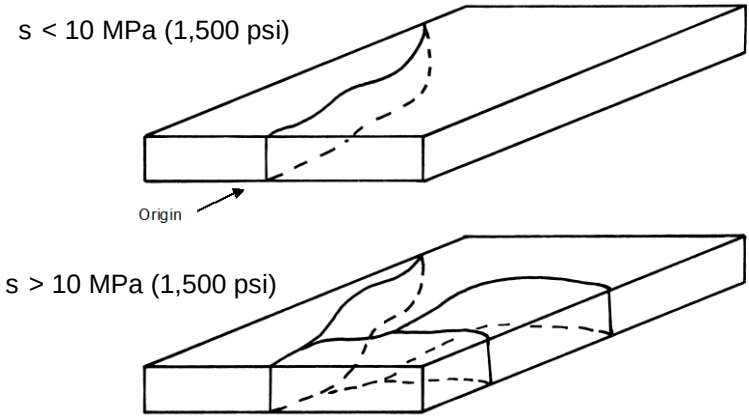

Figure 7.1 *Schematic of thermal fractures of windows. Low stress fractures (s < 10 MPa, 1,500 psi) do not cause branching. (After Orr[2] and Fréchette[1])*

7.2 Stresses from the Extent of Fragmentation

7.2.1 Annealed parts

A general assessment of stress levels can be made from the fracture pattern. Low stressed parts break into only two pieces. Fréchette[1] and Orr[2] and have suggested that 10 MPa (»1,500 psi) is a threshold stress level for branching and fragmentation in glass as illustrated in Figure 7.1. This is an interesting value which we will encounter again later in this chapter in the sections on fracture mirror sizes and crack branching distances. Additional fragmentation occurs with increasing stress in the part, or increasing stored elastic energy. Very highly-stressed parts fragment to such a degree that laypersons are apt to describe the fracture as an "explosion." Retrieval of the two fragments with the fracture origin may be problematic.

Fréchette and his students[3,4] have shown fragmentation correlations with internal pressure of bottles and as shown in Figure 7.2 and for impact velocity for impacted bottles. While their work may have been specific to certain bottle types and shapes, similar testing could be done with alternative shapes and sizes to aid in the failure analysis of new service failures.

Figure 7.3 shows how the fragmentation of ring-on-ring (32 mm and 64 mm diameters) tested borosilicate crown glass disks (76 mm diameter x 5.4 mm thick) can be correlated to fracture stress. This work was done as part of a reliability analysis for a pressurized aircraft window.[5] Figures 4.16 and 4.17

showed examples of such test specimens and their breakage patterns. Fragmentation in Figure 7.3 was quantified by the number of radial cracks that reached the outer rim. This was an arbitrary criterion. Morrell showed a very similar graph for the number of fragments as a function of stress in ring-on-ring tests of high purity alumina.[6] Shand made a similar graph counting radial cracks for 2.3 mm thick by 6 cm square window glass plates broken by impact in the middle.[7] He noted that by such counting, one could obtain a stress at failure estimate even if the impacted site was lost or destroyed. Kerkhof showed a graph of number of radial cracks versus center point deflection for 60 mm diameter glass disks supported on the rim and loaded by a central point.[8] Wang[9] did stress analyses and counts of the number of pieces in glass plate coupons of different sizes when pressure loaded to fracture. Graphs such as these are very specific to specimen or component size, shape, and material.

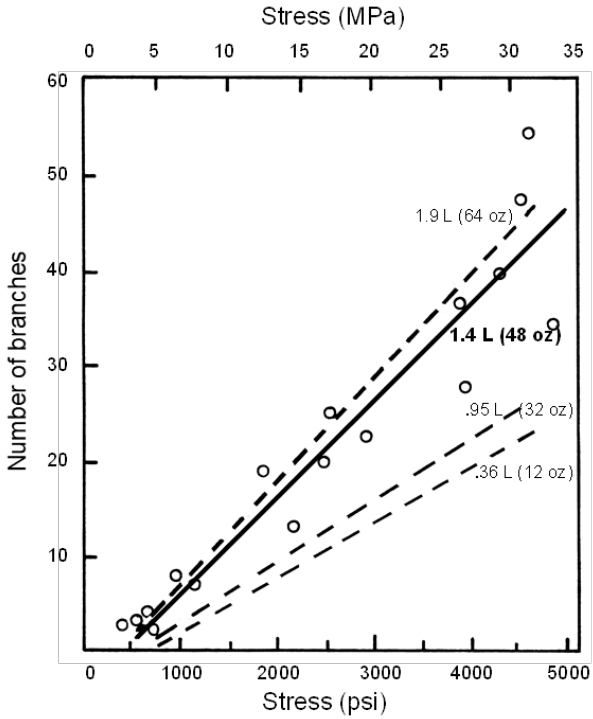

Figure 7.2 *Fragmentation of internally-pressurized bottles. The number of branches (fully developed that extend more than 13 mm beyond the first fork) are shown versus the hoop stress in the glass wall for four different glass containers. Data points and a solid line are shown only for the 1.4 L (48 oz) bottles. Dotted lines show the trends for the three other sizes. Some of the scatter is due to variations in the glass wall thickness. (After Fréchette and Michalske, Ref. 3)*

Figure 7.3 was actually used to analyze an unexpected fracture. A similar glass disk was impacted by a hailstone that was intended to weaken the disk by creating surface damage that could be assessed in a subsequent strength test. The hailstone unexpectedly fractured the disk. The fragments were recovered and reassembled and the origin determined to be an ordinary polishing scratch on the surface opposite the hail impacted side. The hailstone diameter (25 mm) was similar to the inner ring diameter in the strength test set. From the number of radial cracks, the stress at failure was estimated. The estimate matched the dynamic stress estimated from an impact stress analysis, thereby confirming that the impact indeed had imparted sufficient energy to flex the disk to fracture from the ordinary surface flaw on the opposite face.

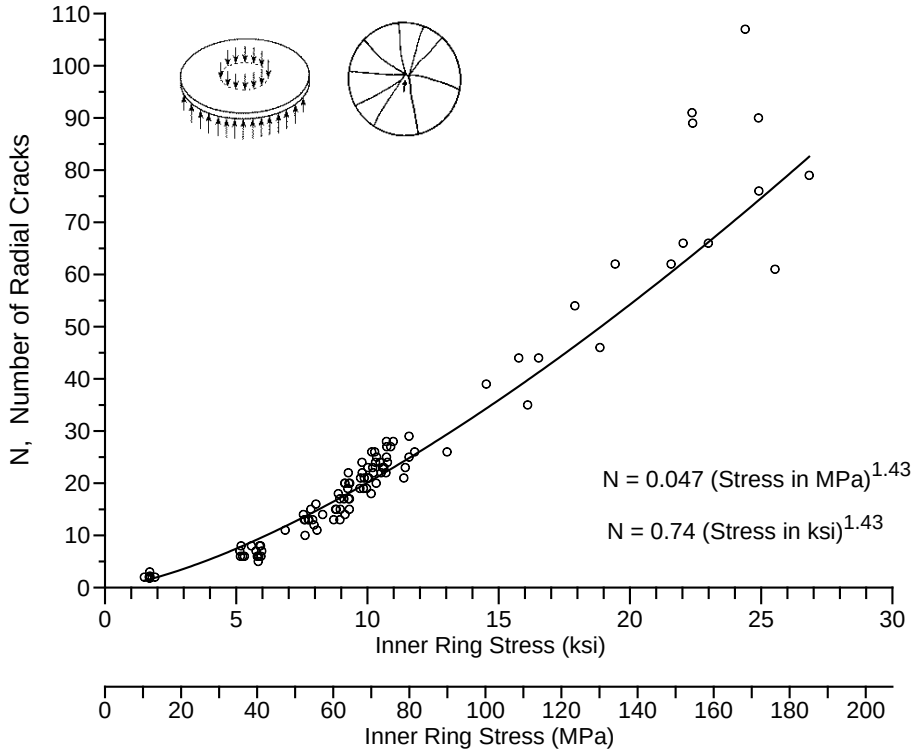

Figure 7.3 *The number of radial cracks that reach the outer rim as a function of fracture stress for 76 mm diameter by 5.4 mm thick BK-7 borosilicate crown glass disks broken in ring-on-ring flexure. Data for this graph included only fractures that initiated inside the inner loading ring.*

More often, one may make a qualitative stress assessment with a cursory examination. This is often sufficient for a diagnosis. For example, if a fracture occurs at an unexpectedly low stress and there are few or no branches, the fractographer might search for an unexpectedly large flaw in the component or specimen. A handling or preparation flaw may have weakened it.

7.2.2 Fragmentation of tempered parts

McMaster et al.[10] state that the most common method of inferring stress levels in tempered glass is by breaking it. The greater the internal midplane tensile stress, the greater the number of fragments. They and Shinkai[11] cited work by Akeyoshi et al.,[12,13] wherein 10 cm square tempered plates of various thickness were broken by sharp impact near to, but not at the corner. The number of fragments in 5 cm square regions correlated to the internal tension temper stress as shown in Figure 7.4. (Note that Shinkai's 1994 paper showed Akeyoshi's data, but with a mislabeled X axis that said Pa and not MPa. The 1st and 2nd

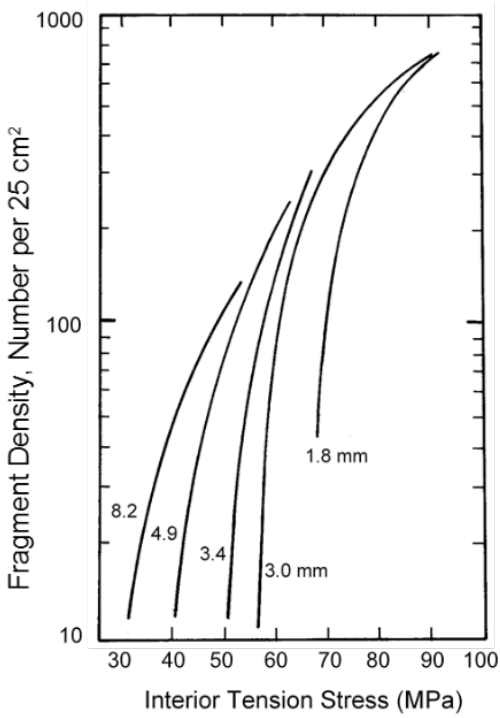

Figure 7.4 *The interior tension stress in tempered soda lime glass plates may be estimated from the fragment density when the plate is broken. Each line corresponds to the plate thickness shown. (References 11 and 12)*

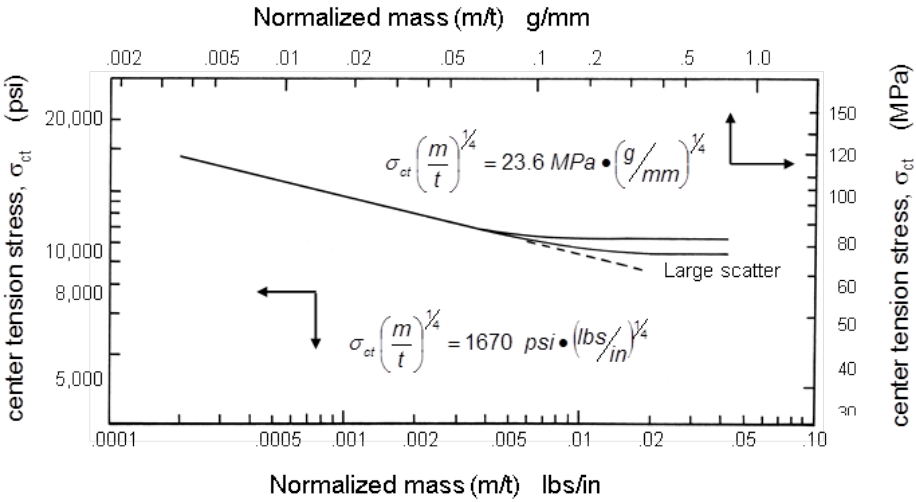

Figure 7.5 *The interior tension stress in tempered soda lime sheet and plate glass may be estimated from the average fragment mass. Center tension stress is plotted versus mass normalized by the plate thickness, t. Data for five different thickness plates and sheets from 3.2 mm to 9.5 mm (1/8 in to 3/8 in) fall on the same curve. (After Barsom[17])*

editions of this Guide copied the same mistake. Figure 7.4 now has the correct units.)

Akeyoshi's work was verified and extended with additional analysis and excellent illustrations by Pourmoghaddam and Schneider.[14] Plate thickness plays an important role: the thicker the plate, the more the stored elastic energy and the greater the number of fragments.[14,15] Breakage patterns and fragment densities change significantly with very thin glass pieces.[15]

For a particular thickness plate, the data suggests there is a minimum temper stress to cause dicing. Blank[16] presented some interesting fragmentation work on tempered soda lime silica plates, 300 mm by 300 mm in size and with thicknesses varying from 3.2 mm to 7.2 mm. The average fragment size (area) in mm^2 dramatically decreased with increasing surface compression strengthening.

Of course, other means of assessing temper stresses are available, including polariscope inspections and use of the stress optical coefficient, but in this Guide we are concerned with fractographic techniques.

Barsom[17] showed that interior tension stress s_{ct} was related to the fragment mass:

$$s_{ct}\left(\frac{m}{t}\right)^{1/4} = \text{constant} \tag{7.1}$$

where *m* is the fragment weight (mass), *t* is the plate thickness. The constant has units of stress × (mass/thickness)$^{1/4}$.

It should be borne in mind that these relationships and trends are altered if there are significant *externally* applied stresses superimposed on the temper stresses.

The fractographer also should be on the lookout for irregular breakage patterns and fragment sizes that are signs of nonuniform temper stresses. Fréchette[1] showed two examples. In one case a glass cylinder was not tempered uniformly during the fabrication process (his case 10.18). A second case (his 10.22) featured a high-powered lamp that cracked spontaneously as a result of heating in service. The fragments were atypically large in the fracture origin area, but elsewhere the normal dicing fragmentation pattern was observed. Fréchette concluded that the intense in-service heating caused the middle of the lamp to lose its temper. Blank[16] and Gardon[18] discussed the use of tempered glass in front automobile windshields in Europe and showed fascinating drawings of fractured windshields that have dramatically uneven fragment sizes and crack patterns due to nonuniform heat transfer during tempering.

It is commonly assumed that the residual stresses are symmetric *through the thickness* as shown in Figure 5.22, but Menčík[19] illustrated the effects of asymmetric tempering of plates on the final stress distributions. Gardon[18] also discussed non-uniform tempering and showed polariscope images of some stress field variations. Different residual compression stresses could exist on the two plate surfaces. There may even be a net <u>tensile</u> stress on one surface!

7.3 Stresses from the Branching Distances

7.3.1 Annealed plates and bars

The stress at fracture is related to the branching distance away from the origin:

$$s\sqrt{R_b} = A_b \tag{7.2}$$

where s is the stress, R_b is the branching radius, and A_b is a constant called the fracture branching constant. It has units of stress × length. These units are the

same as for stress intensity which is described in section 7.5. The relationship between A_b and fracture toughness is discussed in 7.6. A similar relationship applies to mirror sizes as will be discussed in section 7.4. Rearranging shows that the branching distance is inversely dependent upon the square of the stress:

$$R_b = \left(\frac{A_b}{s}\right)^2 \tag{7.3}$$

This <u>empirical</u> relationship has been found to apply to uniaxially-stressed parts such as a tensile strength specimen or a component with tensile stresses primarily in one direction. The relationship also can be applied to bend bars or components loaded in bending provided that the branching distance is measured along the surface where the tensile stresses are a maximum. A_b may not necessarily be a material constant. It certainly does depend upon the material properties such as elastic modulus or fracture toughness, but there is evidence that stress state and component geometry affect it too. A_b is always greater than the fracture mirror constant that is described later in this chapter.

Equation 7.3 also may apply to biaxially-stressed parts such as a ring-on-ring strength test disk or pressurized windows or bottles. Branching distances in biaxially-stressed parts may be less (and the corresponding constants A_b) than the branching distances in uniaxially-stressed parts. Shetty et al. [20] showed that branching can occur just beyond the mirror in highly stressed, biaxially loaded disks. Hull[21] suggested that the cross-section thickness of a component might influence when branching occurs. Reported A_b values are tabulated in Appendix C. Very few values are available since most investigators have focused on fracture mirror constants instead. Branch distances for tempered glasses may be different. Initial branches tend to trifurcate, and the middle branch has a shorter length than the two sideways branches.

The branching angle can at least be a qualitative indicator of the stress state as shown in Figure 4.8 in chapter 4.

7.3.2 Tempered Plates

Figure 7.6a is a photo the author took of a 3.3 mm tempered automobile side window glass. The initial run 2a to the left and right of the origin is 2.6 mm, or a = 1.3 mm. Branching starts in the plate interior, and the crack trifurcates. The next <u>sideways</u> branches are longer, with a_i between 3.3 mm and 4.2 mm. Figure 7.6b shows an interesting approach suggested by Soltesz et al.[22] to estimate temper stresses in tempered glass plates. The lengths of the first and second branches can be correlated to the internal midplane temper stresses.

(a)

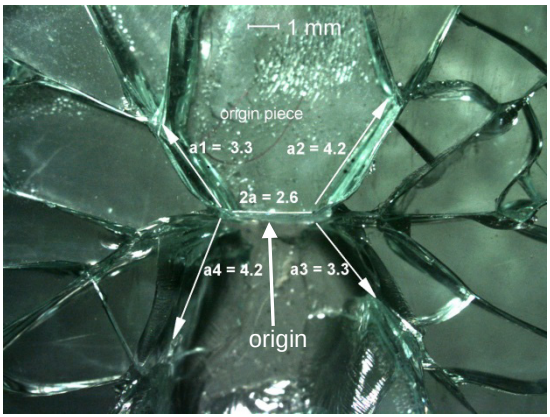

(b)

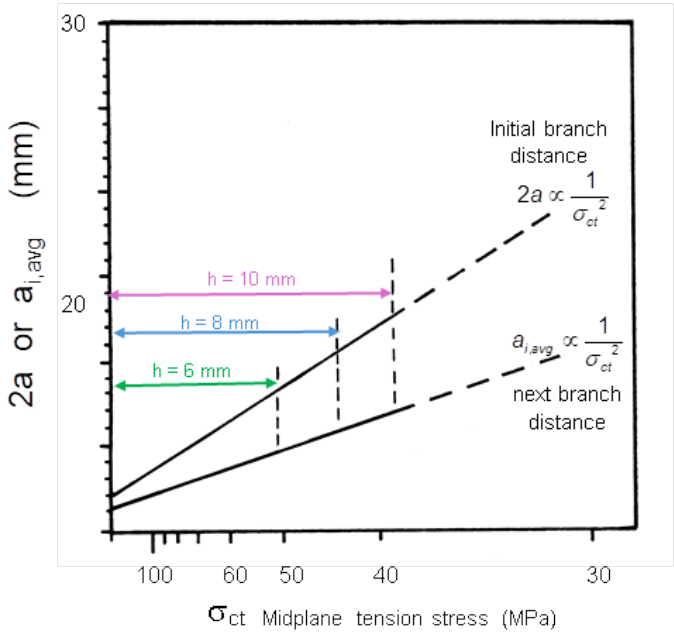

Figure 7.6 *Branch distances in tempered glass may be used to estimate internal tension stresses. (a) shows an example by the author from a 3.3 mm thick tempered automobile side window. The initial branch crack run is 2a = 2.6 mm, i.e., a = 1.3 mm. The crack then trifurcates. The lengths a_1 to a_4 of the next four sideways branches are marked. (b) is after Soltesz et al.,[22] for different thickness glass. It shows the initial branch distance 2a and the average first branch distance $a_{i,avg}$ for the next four sideways branches (a_1 to a_4) versus the center tension stress. The trends are the same irrespective of the glass thickness (h), but the limit of applicability for each thickness is shown by the colored lines. Data to the right of these limits (at low stresses) has excessive scatter.*

7.4 Stresses from the Fracture Mirror Size

7.4.1 Fracture mirror analysis and constants

The fracture mirror size is related to the stress at the origin. Orr's empirical mirror size relationship is:

$$s\sqrt{R} = A \tag{7.4}$$

where s is the tensile stress *at the fracture origin location* at the instant of fracture, R is the mirror radius, and A is the "mirror constant" with units of stress intensity (MPaÖm or ksiÖin) and is considered by most as a material property. (A version of this equation with a residual stress term is discussed later in this chapter.) This relationship is similar to, but not quite the same, as that for stress intensity or fracture toughness as will be discussed in section 7.6 below. Figure 7.7 shows more details of a mirror centered on a surface flaw. This rendition also depicts the prospect that the initial flaw might grow somewhat from a to a_c before going critical.

This author reviewed the evolution of fracture mirror size analysis in a 2006 paper.[23] Leighton Orr of the Pittsburg Plate Glass (PPG) Company was the first to systematically use equation 7.4 with the square root dependence of mirror size to solve glass fracture problems as far back as the 1940s.[2,24,25]

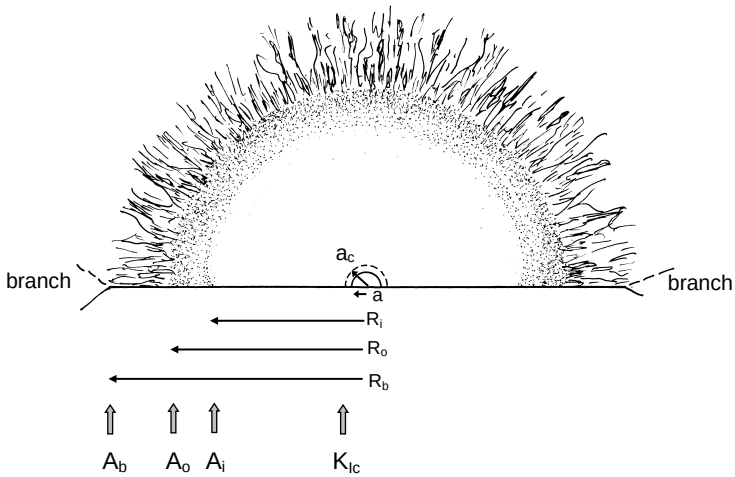

Figure 7.7 *Fracture mirror schematic. R_i is the inner or mirror-mist boundary, R_o is the mist-hackle boundary, and R_b is the branching distance. The fracture toughness K_{Ic} (discussed in section 7.5.1), the mirror constants A_i and A_o and the branching constant A_b correspond to each of these boundaries. All have units of stressÖlength.*

The physics of how fracture mirrors form was covered in section 5.2.1. In brief, once cracks propagate at speeds greater than 60% of the shear wave velocity, the maximum stress in front of the crack shifts to locations slightly above and below the plane of crack propagation. This causes local deviations in the crack front plane that form tiny perturbations and steps.

Figure 7.8 shows the two most common graph types that are used to show stress - mirror size data. The merits of each approach are discussed in Appendix D. This Guide recommends the use of stress versus 1/ÖR, Fig. 7.8a. The linear graph of stress versus 1/ÖR in Figure 7.8a has the advantage that the fracture mirror constant is the slope of the line, and residual stresses can be detected by non-zero intercepts as described later.

The log stress versus log R graph in Figure 7.8b facilitates plotting a broad range of stress and mirror sizes. The mirror constant corresponds to the stress necessary to create a mirror of unit size, since (from eq. 4):

$$\log s_a = \log A - \tfrac{1}{2}\log (R). \quad \text{If } R = 1, \text{ then } \log s_a = \log A, \text{ and } s_a = A$$

Examples of mirror data are shown in Figures 7.9 – 7.12. The glass data in Figure 7.9 is extraordinary since the mirror size range is almost a factor of 100. Two hundred and fifty-nine Pyrex borosilicate rods varying in size by almost a factor of ten (4.1 mm to 38.1 mm) were broken in three-point flexure by Kerper and Scuderi at the National Bureau of Standards in 1964.[26]

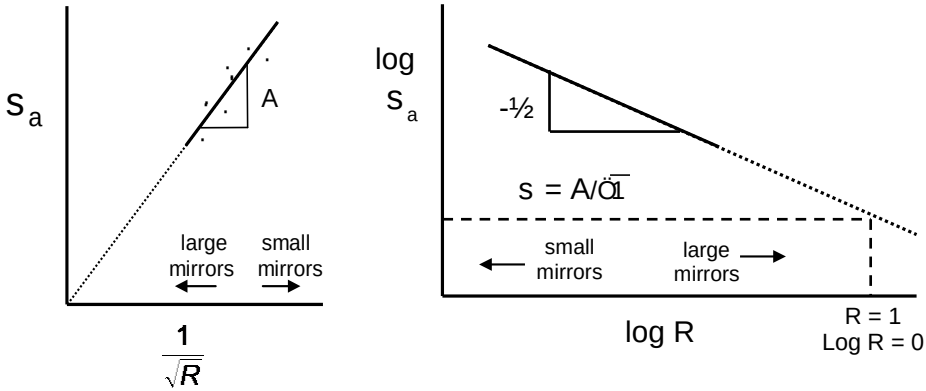

(a) (b)

Figure 7.8 *Stress and mirror size graphs. (a) shows the preferred graph of applied stress, s_a, versus inverse square root of mirror radius. The mirror constant is the slope of the line. (b) shows log s_a versus log radius as commonly used in the older literature.*

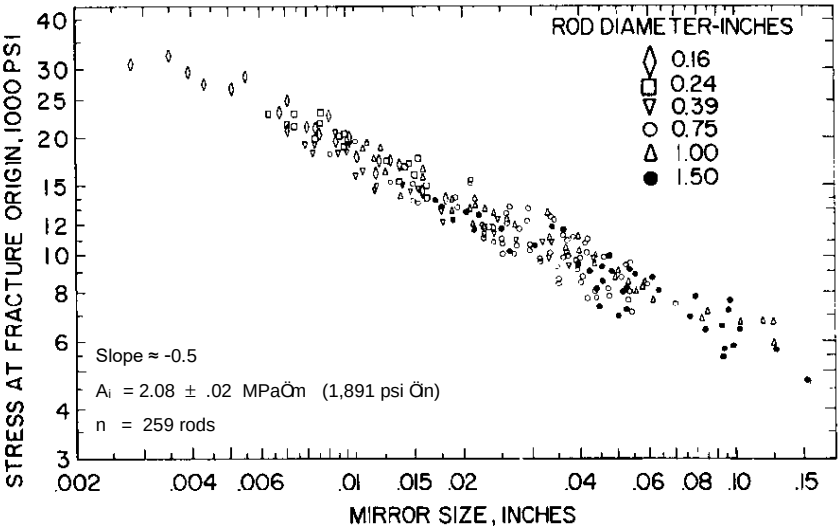

Figure 7.9 *A superb example of fracture mirror data for Pyrex 7740* borosilicate *glass rods of many sizes and strengths. From Kerper and Scuderi.*[26]

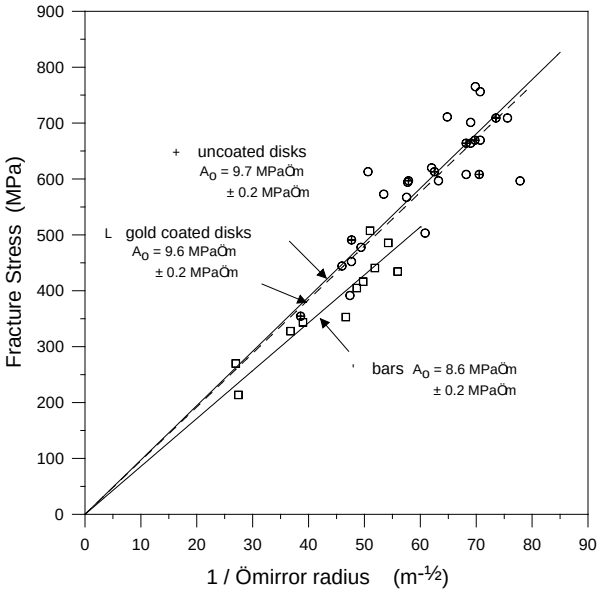

Figure 7.10 *Fracture mirror size data for a 3 mol % yttria-stabilized tetragonal zirconia (3Y-TZP) from Ref. 27. Figure 7.13 shows one of the mirrors. Figure 3.25 shows a mirror both coated and uncoated. Bend bars produced a smaller mirror constant, either due to a geometric effect or simply the scatter in the data.*

The 3Y-TZP zirconia data in Figure 7.10 shows that measurements on uncoated and gold coated specimens concurred. This was gratifying since the uncoated specimens were difficult to interpret due to material translucency and difficulty in judging a boundary. Not surprisingly, the data scatter was greater for the uncoated specimens. Photos and examples of marked fracture mirrors are shown in in the next section 7.4.2 and in Appendix D which also has detail on how residual stresses, stress gradients, the origin flaws, and microstructure can affect mirror sizes and shapes.

Figure 7.11 shows data by J. Quinn for borosilicate crown (BK-7) glass disks tested in a ring-on-ring configuration.[28] Mirror-mist, mist-hackle, and branching distances were all carefully measured and there was a systematic offset at the origin of about 10 MPa. This was despite the fact that the disks were all annealed. Oakley[29] observed the exact same offset in annealed soda lime silica float-glass plates that were loaded in pressure-on-ring conditions. Although offsets like this are commonly attributed to residual stresses (as discussed later in this chapter and in Appendix D), the evidence is growing that the 10 MPa represents a threshold stress for branching to occur at all, as noted previously in section 7.2.1.

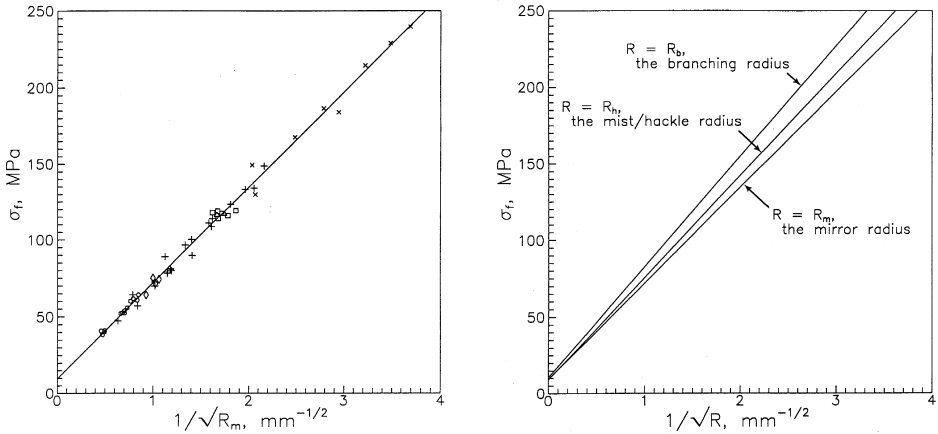

(a) (b)

Figure 7.11 *Fracture mirror (a) and branching plus mirror summary data (b) for annealed BK-7 borosilicate crown glass disks tested by ring-on-ring loading by J. Quinn.[28] The offset of 10 MPa occurred for all three data sets.*

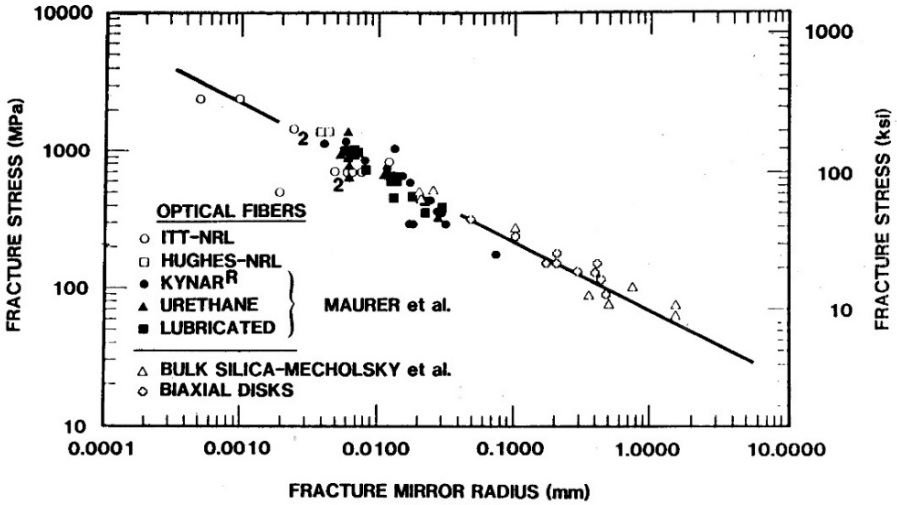

Figure 7.12 *Fracture mirror size data for fused silica from [30]. The graph includes data from fibers pulled in tension from Maurer et al,[31], three-point bend bars, and piston on three-ball biaxial disks from Mecholsky and Rice [30]. All data fall on the same trend line which means the mirror size relationship is independent of testing configuration and component size.*

Figure 7.12 shows data for fused silica from Mecholsky and Rice[30] and Mauerer et al.[31] that shows the mirror size relationship is independent of the mode of loading and size of the component. This is quite remarkable and reassuring. The Mecholsky and Rice paper showed additional examples for Pyrex 7740 borosilicate glass, a Pyroceram 9606 cordierite glass ceramic, and polycrystalline magnesium fluoride. Many other studies have shown that the mirror size relationship is independent of component size or testing mode. The reader is referred to the tabulations in Appendix C for examples.

Deviations in the trend occur when very thin plates, or rods, or disks are tested in bending and this should not be surprising due to the stress gradient through the thickness. The deviations start to occur when the mirror sizes approach the thickness of the part. For mirrors with radii larger than the plate thickness, data points fall above the trend on a log stress – log mirror size plot (Fig. 7.8b) which means that mirrors are larger than they would otherwise be if the part were loaded in uniform tension.

Johnson and Holloway in 1966[32] offered a physical interpretation of the relationship of equation 7.4 based on the energetics of crack propagation. Levengood,[25] Shand,[33] Kerper and Scuderi,[26,34,] and later Kirchner et al.[35] gave

credit to Orr for equation 7.4. Orr did not publish his findings until he retired in 1972,[2] but discussed his empirical equation at a Glass Division meeting of the American Ceramic Society in Bedford, PA in September 1955.[36] Orr told me in 2001[24] that equation 2 had been extensively used for glass fracture analysis at PPG in the 1940s. In the 1950s and 1960s, many people used a general form of equation 7.4 with the mirror size raised to an arbitrary power. Shand's 1954 and 1959 papers[33,37] presented an early argument for the 1/2 power based on stress concentrations at the tip of a sharp crack. These two papers incorporated elements of what become known later as fracture mechanics. Kerper and Scuderi[26,34] in the 1960s at the National Bureau of Standards in Washington performed meticulous experiments on hundreds of glass laths and rods and showed conclusive evidence that Orr's equation was applicable over a broad range of specimen and mirror sizes as shown in Fig. 7.9. Some have credited Terao[38] (1953) with equation 7.4, but a careful reading of his paper fails to back the claim since it shows an exponential form relating mirror size to stress instead. Although many associate equation 7.4 with Johnson and Holloway[32] in 1966, the relationship had already been in use by Orr for 20 years.

The practical significance of equation 7.4 is that one can calculate the origin stress if a fracture mirror size is measured and a fracture mirror constant is available. The calculated stress is the net tensile stress acting on the flaw and the region around the flaw. It may include several stress sources including mechanical, thermal, and residual stresses. It is possible to discern separate mirror-mist and mist-hackle boundaries in glasses and each has a corresponding mirror constant A. The most common notation is to refer to the mirror-mist boundary as the *inner* mirror boundary and the corresponding mirror constant is designated A_i. The mist-hackle boundary is referred to as the *outer* mirror and the corresponding mirror constant is designated A_o. The mirror-mist boundary is usually not perceivable in polycrystalline ceramics and only the mirror-hackle boundary is usually measured.

At this point it is appropriate to reiterate that equation 7.4 is empirical. In chapter 5, it was noted that there were competing models to account for the mirror formation. Kirchner and colleagues[39,40] presented compelling evidence that a fracture mechanics criterion based on a critical stress intensity, K_B, (stress intensity is described later in section 7.5) gives the best fit to data and the exact shape of mirrors in various stress fields. (Here it should be noted that they used "K_B" to refer to the *microscale* branching that causes the mirror-mist or mist-hackle to form, not the macroscale forking of a crack.) A crucial observation is that the stress intensity model fully accounts for the small inward facing cusp at specimen surfaces (Figures 5.2 and 7.7), whereas the other

models do not. Kirchner et al.[39,40] argued that a more fundamental material parameter might be K_B, the stress intensity factor at micro branching, rather than the A's in equation 7.4 since the latter do not take into account the free surface, geometry factors, and non-uniform stress gradients over the crack surface. There is validity to their argument, but in practice the ease of use of equation 7.4 has led to its widespread adoption. (The size and shape predictions based on A or K_B match very closely for the limiting cases of small mirrors in tension specimens. This is also true for most of the periphery of small semicircular mirrors centered on surface flaws in strong tension or flexure specimens.)

The accuracy of the stress estimate varies depending upon the material, the experience of the fractographer, the microscopy and illumination used, and component geometry and stress gradient effects. The mirror constants themselves have uncertainties. In principle, the mirror or branching constants should not vary with type of specimen or testing configuration, but there are some variations as listed in the entries in Appendix C. Many of the entries have no standard deviations listed for them. I believe that stress estimates may be accurate to within ≈ 10 % with glasses if they form ideal fracture mirrors.

Kirchner and Gruver[41] also showed that the relationship holds for elevated temperature fractures in ceramics. The mirror constant was invariant from room temperature to 1400 °C for a hot-pressed alumina with a 1 μm grain size. This is a remarkable finding since the alumina was fired at 1475 °C. Kerper and Scuderi[42] also showed that mirror constants were unaffected by elevated temperature for eight glasses. Shinkai[43] showed the mirror-mist constant, A_i, varied little with temperature for three glasses. A_i varied little with temperature for the Pyrex borosilicate glass, but for the soda lime silica float glass and the 96% silica (Vicor), the A_i values at -150 °C were greater (0.03 – 0.04) than at room temperature. The trends were comparable to similar increases of the fracture surface energy, γ_f, with decreasing temperature. Shinkai[43] also did experiments in various environments. There was negligible environmental effect. The A_i's measured at room temperate in air and dry N_2 gas were comparable. The lack of an environmental sensitivity is not surprising since mirror boundaries form when the crack is travelling at or near terminal velocity.

Crack branching constants A_b have sometimes been reported, but some caution is advised, however, as discussed in previous section 7.3. There is evidence to suggest that A_b depends upon the loading mode (uniaxial or biaxial) and the size of the mirror relative to a part thickness if the part breaks in bending.

The three boundaries correspond to an expanding crack front, and hence: $A_i < A_o < A_b$. Appendix C has a comprehensive compilation of fracture mirror and branching constants. The table shows there is some variability in the published mirror constants, even for model materials such as fused silica or soda lime silica. Some of this is due to the aforementioned metrology and judgment issues, but much of it is due to genuine material-to-material variability. Thus, one should not expect all silicon nitrides or aluminas to have the same mirror constants. Microstructural differences can change the mirror constants considerably.

The word "boundary" must be used with some caution. It is now clear from a number of studies that there probably is not a discrete or sudden transition point on the fracture surface corresponding to a mirror boundary. The mode of viewing and magnification affects the judgment of the boundary location. The higher the magnification the smaller the mirror seems to be, since fine detail that was washed out or not resolvable at lower power can be discerned at higher power. The mirror-mist boundary probably corresponds to surface roughness features that are of the order of 0.1 mm to 0.2 mm, which is a fraction of the wavelength of light and at the threshold of observable features with an optical microscope. Section D.3 in Appendix D has a discussion of several studies that have used various surface roughness measurement methods to measure mirrors, but these methods have yielded different results.

Although there is some variability in how different observers judge and measure fracture mirror sizes, most fractographers agree that there is a fracture mirror that can be measured. Size estimates can vary depending upon the type of microscope used, the mode of illumination, the objective power of the lens, and the judgment criteria of the fractographer.

7.4.2 How to measure fracture mirror sizes

This section gives guidance on how to measure fracture mirror sizes. Very detailed guidelines are presented in Appendix D. These procedures were adopted as an ASTM standard C 1678 in 2007.[44] In principle, a mirror size measurement is a straightforward exercise, but in practice it is not as easy as one would think, even with glasses. In addition to the boundary interpretation issue discussed above, component geometry effects, stress gradients, residual stresses, and origin flaw effects can all contribute to mirror distortions.

The mirror-mist boundary in *glasses* is the periphery where one can discern the onset of mist. This boundary corresponds to A_i, the inner mirror constant.

The mist-hackle boundary in *glasses* is the periphery where one can discern the onset of systematic hackle. This boundary corresponds to A_o, the outer mirror constant.

The mirror-hackle boundary in *polycrystalline ceramics* is the periphery where one can discern the onset of systematic new hackle, and there is an obvious roughness change relative to that inside the mirror region. This boundary corresponds to A_o, the outer mirror constant Ignore premature hackle and/or isolated steps from microstructural irregularities in the mirror or from irregularities at the origin.

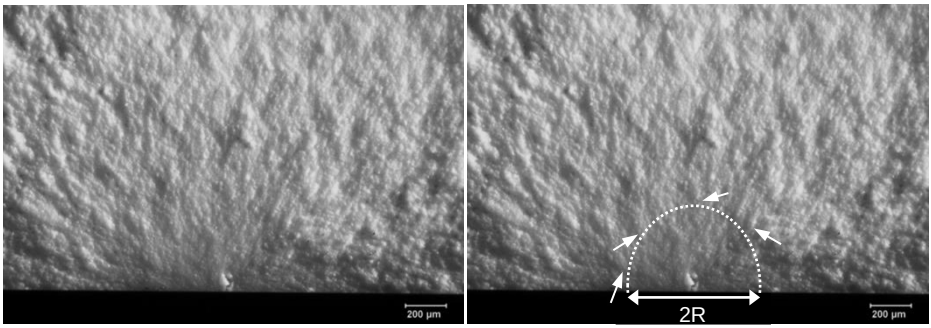

(a) ***(b)***

Figure 7.13 *Example of a mirror in a ceramic. This is one of the specimens of the 3Y-TZP for the data in Figure 7.10. (a) shows the uncoated fracture surface of a 2.8 mm thick bend bar with low angle, grazing illumination (486 MPa). (b) shows the same photo with a marked mirror-hackle boundary whereby new hackle is detected (small white arrows) as compared to the roughness inside the mirror. The mirror is slightly elongated into the interior due to the stress gradient. Judgments are best made while viewing the surface through a microscope.*

Figure 7.13 shows an example in a moderately difficult-to-judge ceramic. The yttria-stabilized zirconia is a difficult to interpret since, although it has a very fine grain size (< 0.5 mm), it has a gradual progression of roughness from well within the mirror to the obvious hackle region far from the origin. Keeping in mind the criteria for polycrystalline ceramics above, the first step is to look at a region well *within* the mirror and note the typical, *inherent* roughness due to the microstructure. The next step is to observe the obvious new hackle that is greater in magnitude than anything in the relatively smooth mirror region. Additional examples are in Appendix D.

7.5 Fracture Mechanics Analysis of the Flaw Size

7.5.1 Introduction to fracture mechanics

Fracture mechanics is a powerful analytical tool to aid the fractographer. It can be used to estimate critical flaw sizes and can help determine whether a flaw the fractographer has detected is of appropriate size to cause fracture. It can also be used to estimate the stress in a fractured part. Fracture mechanics fundamentals are presented below followed by some practical examples.

Figure 7.14 shows a hypothetical "brick" loaded in tension. A force P may or may not cause breakage depending upon the size and shape of the object and the material's strength. Load divided by the area carrying the load is known as stress. The stress is constant across the cross section and throughout the brick in this simple example. The opposing forces or stresses at either end are

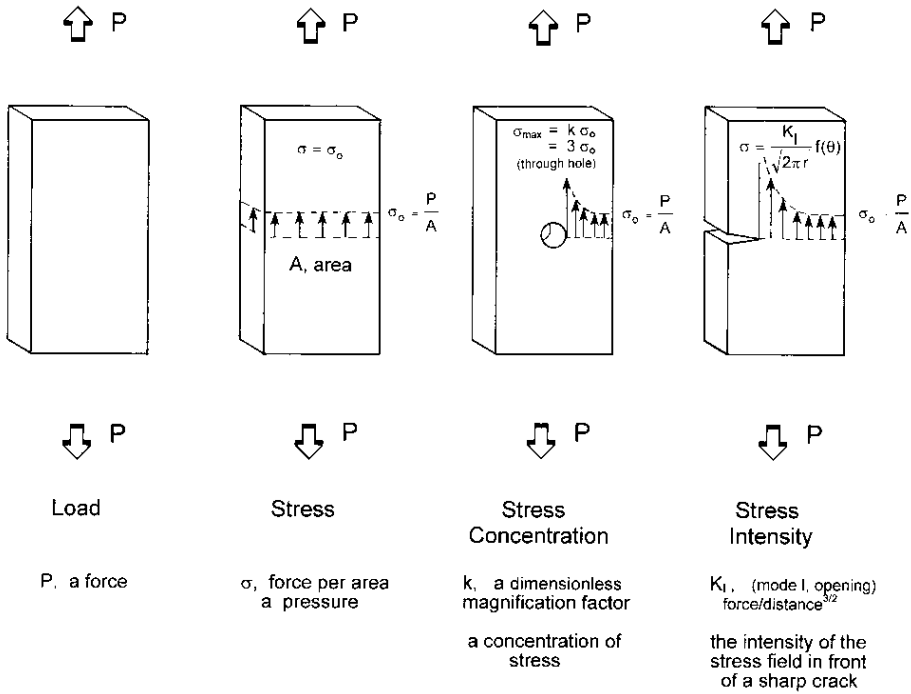

Figure 7.14 *A force P acts upon the object. Fracture occurs at a critical force that depends upon the material properties and the object's size. (b)shows stress is the force normalized by the cross sectional area. (c) shows a thorough-hole that* <u>*concentrates*</u> *stress in the vicinity of the discontinuity. (d) shows how sharp cracks* <u>*intensify*</u> *the stress field in front of the discontinuity.*

transmitted through the bulk by "*flow lines of stress*" such as shown in Figure 7.15. Real engineering structures usually have stress variations or gradients, and the stresses are magnified or concentrated in the vicinity of geometric discontinuities. For example, a hole *concentrates* stresses at the hole side since "flow lines of stress" are diverted around the hole. Stress concentrations are dimensionless magnification factors often designated by lower case letter k. For the case of a through hole in a plate, k = 3, meaning that in the immediate vicinity of the hole, the stress is three times the nominal stress. For an isolated spherical bubble in the interior, k = 2. Simple problems may be analyzed by the so-called "strength of materials" analysis, wherein assumptions about the structure (e.g., cross section plane sections remain plane, deflections are small, the structure remains elastic to fracture) lend themselves to simplified analysis. The maximum stress in three- or four-point beams in bending may be readily derived from "simple beam theory" a subset of the strength of materials analysis. More elaborate analyses may be solved by the "theory of elasticity" or by computer analysis using the "finite element analysis" (FEA).

Flow lines of stress is a useful concept that may aid those who are not familiar

(a)

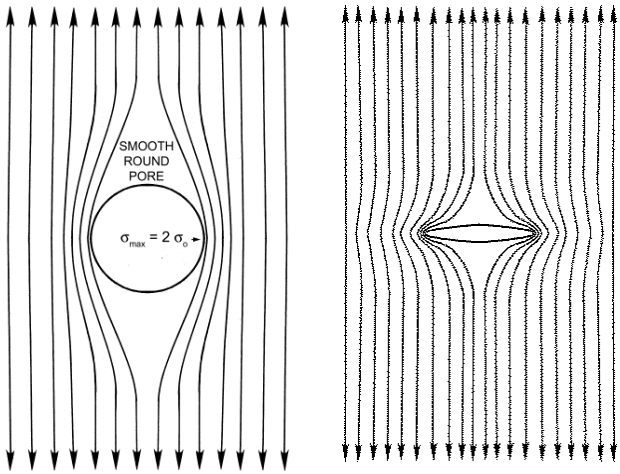

(b)

Figure 7.15 *Lines of stress or "flow lines of stress" in a body. They cannot be transmitted through an irregularity such as a bubble or a pore in (a). The flaws create a stress concentration on the sides where the flow lines converge. Sharper irregularities, such as the flattened wide flaw on in (b) create even greater stress concentrations. In the limit, for a flat, sharp crack, the flow lines kink severely, and fracture mechanics must be used as opposed to a simple stress concentration factor.*

with stress concentrations or fracture mechanics. Flow lines kink or bend around notches, grooves, or flaws. Engineers often use the flow lines of stress concept to qualitatively assess what would happen with notches or grooves in parts such as rotating shafts, or a step reduction in diameter in a shaft, or even the neck and gage section of a direct tension strength test specimen. The more severe the kinking, the greater the stress concentration.

The local stress conditions in the vicinity of *sharp* discontinuities such as cracks cannot be adequately modeled using stress concentration analysis. Stress concentration analyses lead to estimates of infinite stress at crack tips. Fracture mechanics is a discipline that deals with the stresses and strains around sharp flaws and has as its roots the 1920s work of Griffith.[45,46] He showed that the strength of a brittle material with a slender elliptical flaw through crack of size 2c in a uniformly stressed plate as shown in Figure 7.16a is:

$$s_f = \sqrt{\frac{2Eg_f}{pc}} \tag{7.5}$$

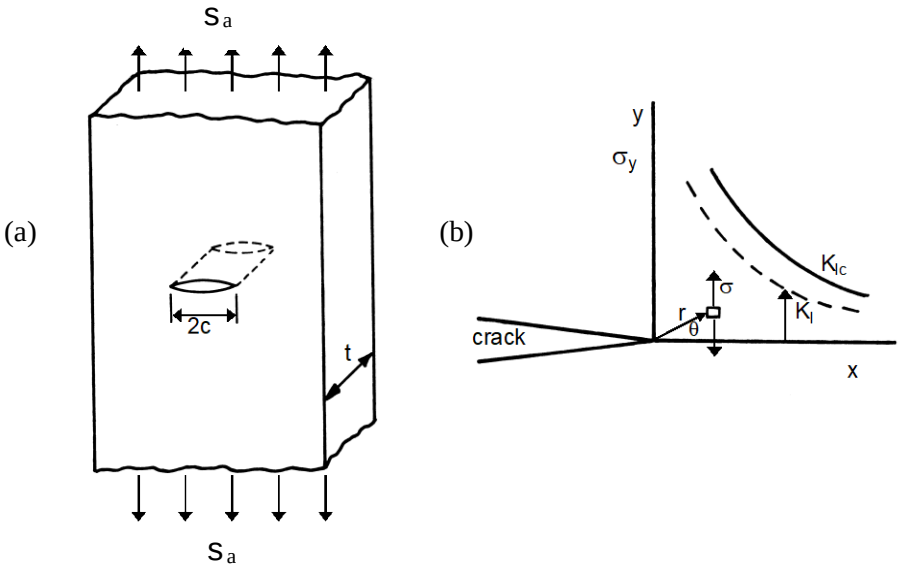

Figure 7.16 *Through crack in a plate loaded in tension in opening mode I. Long slender elliptical cracks of this type were envisioned by Griffith as flaws. (b) shows a closeup of the crack tip region. If the crack tips are atomically sharp, fracture mechanics developed by Irwin must be used to model the stress state in the immediate vicinity for the crack tip.*

where s_f is the fracture stress (the nominal stress in the plate), E is the elastic modulus, and g_f is the fracture surface energy that is the energy to create unit surface area. In this Guide, flaw size is denoted as either "a" or "c" following conventional practice in the fracture mechanics literature. Usually, the flaw dimension is the radius or half width if the flaw is in the middle of a plate as shown in Figure 7.16a. If the crack is on the edge of the plate as shown in the right side of Figure 7.14, then a or c are the full crack length. The critical feature of this relationship is that strength is inversely proportional to the square root of flaw size. The larger the flaw, the weaker the structure is. Griffith's formula was derived on the premise that crack propagation occurs if the rate of elastic strain energy release in a body (if a crack grows longer) is greater than the creation of surface energy due to the new surfaces. His formula sets a necessary condition for a decrease in overall energy of the system.

Many flaws are atomically sharp and fracture mechanics analyses developed by Irwin in the 1950s are applicable.[47,48] This approach analyses the actual stress field in front of a crack tip as shown in Figure 7.16b. The intensity of the field is quantified by the term K_I, which is called the "stress intensity factor, mode I." Mode I means the opening mode, that is of primary concern for most ceramic and glass failures. The dashed line in Figure 7.16b shows that the stress field in the plane ahead of the crack has the form $s_y = K_I / \sqrt{(2px)}$, where x is the distance in front of the crack tip. This has a singularity at the crack tip, but what is important is the magnitude of the field in general. The flaw will propagate when the stress intensity reaches a critical condition, K_{Ic}. For many loading configurations, once the crack begins to propagate, it will run unstably and cause fracture. K_{Ic} is called the "critical stress intensity factor, Mode I," or simply "*fracture toughness*."

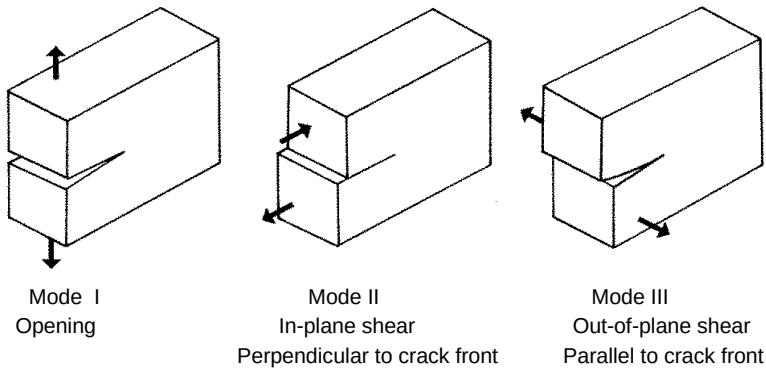

Figure 7.17 *Loading modes on a crack*

Figure 7.17 shows that in addition to the opening Mode I, a crack can be subjected to two other modes involving shear. Ceramics and glasses usually break due to the opening Mode I.

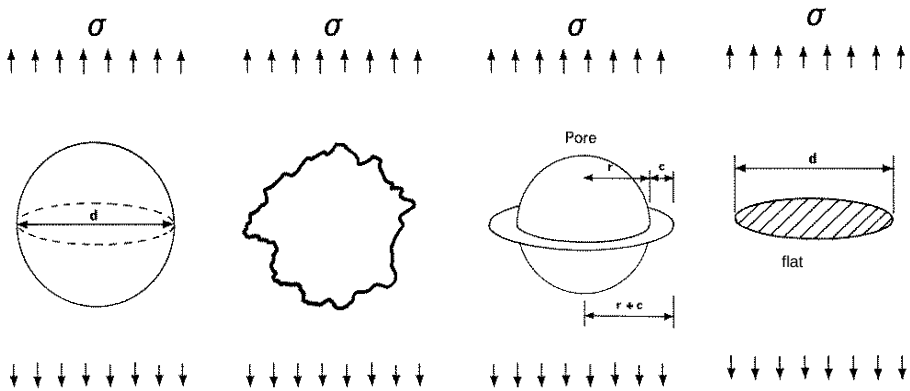

Figure 7.18 *Four flaws that have similar size. The left two are not particularly severe flaws despite their size, but the right two are more deleterious, especially if the rim-cracked pore ("Rings of Saturn") flaw has a large rim crack, c. The flat penny-shaped flaw (shown schematically) on the right is the severest.*

Figure 7.18 shows flaws of similar size, but they have dramatically different stress concentrations (the first pair) or stress intensities (the second pair).

There is surprising variability in the literature about just what constitutes "K_{Ic}, fracture toughness." Many formal test method standards define it in operational terms; i.e., the result obtained if one does a specific fracture test in accordance with the procedures in the standard. ASTM standard E 399 for metals is a good example and it has verbiage about "plane strain" conditions.[49] Some books say K_{Ic} is a condition for crack extension or the <u>start</u> of crack propagation. Others say it is a critical condition for <u>rapid</u> or <u>unstable extension</u>. Further confusion has ensued since some have argued that cracks emanating from Vickers indentations can be used to measure fracture toughness, but these are cracks that are <u>arresting</u>, not propagating. Further complications arise since ceramics and glasses may exhibit slow crack growth or stable crack extension behavior as described below. After careful review of dozens of books, standards, and key references, in 2018 this author decided to craft a simple, new universal definition for glasses, glass-ceramics, and ceramics:[50]

> *Fracture toughness*, K_{Ic}, the critical condition for the onset of rapid crack extension in an inert environment.

The first ten words were written by George Irwin in the 1950s.[47,48] I added the four key qualifier words: "in an inert environment." These were written by Wiederhorn et al. in 1974[51] when he described fracture toughness of glasses. Irwin's words including "critical condition" and "onset of rapid crack extension" are at the core of what he felt was fracture toughness, whether he was speaking about K_{Ic} or G_{Ic} (his critical strain energy release rate) and appeared in many of his publications over the years. He often used the word "unstable" in place of the word "rapid." He mostly dealt with brittle metals and environmentally-assisted slow crack growth (SCG) at room temperature was not an issue. Wiederhorn, a pioneer investigator of SCG in glasses, recognized that measurements of fracture toughness must take SCG into account and influences of the environment must be eliminated.[51]

For a small flaw in a body loaded in tension, s_a, the stress intensity, K_I, acting on the flaw is:

$$K_I = Y s \sqrt{c} \tag{7.6}$$

and fracture occurs when:

$$K_{Ic} = Y s_f \sqrt{c} \tag{7.7}$$

Y is the stress intensity shape factor, a dimensionless parameter that takes into account the shape of the crack and the loading conditions, c is the crack size, and s_f is the stress at fracture. If the specimen has a stress gradient, then the stress at the fracture origin location should be used. In this Guide, Y combines all geometric terms and p or Öp terms. Examples of Y are shown below. Fracture occurs when any combination of Y, s, or c leads to the critical condition. It is emphasized that equations 7.6 and 7.7 only apply to small flaws loaded by remote tensile (or bending) stresses, also known as "far-field stresses."

> ***Far field stress:*** *the stress that is remotely applied (not near the crack) and is the nominal stress if no crack were present.*

Equation 7.7 has four variables: the far-field tensile stress at fracture, s_f; the flaw size, *a* or *c*; the shape factor, Y; and the fracture toughness, K_{Ic}. This simple equation may be used in three different ways:

(1) Flaw size may be estimated if Y, s_f, and K_{Ic} are known. This approach is very useful in laboratory testing, whereby specimens are broken under controlled conditions, and break loads and specimen and fixture geometries are used to compute failure stresses.
(2) The failure stress, s_f, can be estimated if the flaw size and shape can be measured fractographically, and K_{Ic} is known. This approach is useful in estimating stress in fractured components.
(3) Fracture toughness, K_{Ic}, may be computed if the flaw size and shape, and the failure stress are known.

Examples of the application of equation 7.7 are shown later in this chapter. The reader should be forewarned that there is no consistency in the fracture mechanics and materials science literatures. Crack sizes are described by *a*, *b*, *c*, *2c*, or other symbols, but sometimes these same symbols are used differently and sometimes they are even used for the component dimensions. The flaw size dimension is usually the radius in the equations for K_{Ic}. Sometimes the Y factor includes the p or a Öp term, but often it does not. In this Guide and in ASTM standards C 1322[52] for fractography and C 1421[53] for K_{Ic}, all geometric terms for the stress intensity shape factor including p or Öp are <u>combined into</u> Y.

Equation 7.7 should not be applied if the stresses are localized, or if the part dimensions are so small that the flow lines of stress around the flaw are not well established as shown in Figure 7.15.

Most textbooks on fracture mechanics show illustrations such as Figures 7.14 and 7.15, whereby the stress field is <u>remotely</u> applied (not near the crack) and s_a is the <u>nominal stress if no crack were present</u>. The flaws may be embedded in the bulk or may be on the specimen surface. Cracks may be loaded in other component shapes or loading configurations that do not create far-field stresses. For example, the local stresses from the plastic deformation zone underneath a Vickers indentation (that act on a median crack) are not far-field stresses, nor are the localized contact stresses where a sphere presses on a ceramic or glass surface. Furthermore, equations 7.6 and 7.7 may be inapplicable once cracks become very large relative to a component size. For example, a bend bar with a crack that reaches half way through the bar thickness has a much more complicated equation relating force, crack size, and beam dimensions to K_I. The point here is that if one finds a fracture origin crack in a broken ceramic or glass object, and is tempted to apply equation 7.7, decide first whether the stresses really are remotely applied and are genuinely far field.

Note that the stress and flaw size dependencies are the same as the Griffith equation. Indeed, the energy and stress intensity approaches are consistent, and for plane strain (page 1.5) loading conditions:

$$K_{Ic} = \sqrt{\frac{2E\gamma_f}{(1-n^2)}} \tag{7.8}$$

where E is the elastic modulus, γ_f is the fracture surface energy, and n is Poisson's ratio. Sometimes the reader may find this equation without the $1-n^2$ term. The equation without the $1-n^2$ term is appropriate for plane stress conditions, but nearly all practical problems for ceramics and glasses are plane stress conditions. In any case, since n is typically between 0.15 and 0.25 for ceramics and glasses, n^2 is small, and the denominator is close to 1.

Sometimes the fracture mechanics literature uses a related term, G_{Ic}, *the critical strain energy release rate.* For plane strain conditions, it is related to K_{Ic} by:

$$K_{Ic} = \sqrt{\frac{EG_{Ic}}{(1-n^2)}} \tag{7.9}$$

and $G_{Ic} = 2\gamma_f$. The ceramics and glass technical literature of the 1960s and early 1970s used analyses based on γ_f and the Griffith equation 7.5, but few flaws have a simple through-plate elliptical shape. Fracture mechanics analysis based upon stress intensity K_I is more versatile and can model more complex-shaped cracks. It became more common in the 1970s and is dominant today.

Fracture toughness, K_{Ic}, is an important material property that characterizes a material's intrinsic resistance to fracture. It has units of stress Ölength and in SI units is expressed either as MPaÖm or $MN/m^{1.5}$. The English system of units has ksiÖin and the conversion factor to the SI units is only 1.1 (Table 7.1). Fracture energies are usually expressed as erg/cm^2 or as J/m^2. Table 7.2 shows some approximate K_{Ic} values. It is much better, however, to use a value for a specific material, since fracture toughness depends strongly upon composition and microstructure.

Table 7.2 includes columns three through five that require explanation. The third column is for R-curve behavior whereby fracture resistance increases as a crack extends. This behavior is caused by several of the crack microstructure interactions shown in Figure 7.19 such as transformation toughening around a crack tip or bridging behind the crack tip. The fourth column in Table 7.2 is for environmentally-assisted "slow crack growth" which is a phenomenon whereby cracks grow stably at stress intensities less than K_{Ic}. The fifth column

Material	K_{Ic} MPaÖm	Rising R-curve?	Slow crack growth (SCG) at room temperature?	Mechanical cyclic fatigue?
Glasses	0.75 – 0.90	No, flat	Yes	No *
Sintered fused silica	0.92	No	Yes	?
Glass ceramics	2.0 – 2.5	No	Yes	Possibly *
Mullite	2.2	?	?	?
Alumina, sapphire single crystal	2.4 to 4.5 different planes	No	Yes	No
Alumina (hot pressed or sintered, 99.9% pure, fine grained)	3.0 – 4.0	No	Yes	No
Alumina (sintered, glass bonded)	2.5 – 5.	No	Yes	Maybe
Alumina (coarse grained)	3.0 – 5.0	Yes	Yes, especially if there is a glassy boundary phase	Yes
Boron carbide (hot pressed)	2.5	No, flat	No	No
Silicon carbide (solid state sintered)	2.5 – 3.0	No, flat	No	No
Silicon carbide (liquid phase sintered, elongated grains	3. – 5.	Yes	Yes	?
Silicon nitride (equiaxed fine-grained)	4.5	No	No	No
Silicon nitride (elongated grains, glassy boundary phase)	5. – 8.0	Yes	Yes	Yes
Zirconia, cubic stabilized	3.	No, flat	?	No
Zirconia, Mg partially stabilized	3. – 18	Yes	Yes	Yes
Zirconia, Y tetragonal zirconia polycrystal	4.5. – 5.0	No	Yes	No, ?
Cast iron	37. – 45.	No	No	Yes?

* Accumulated environmentally-assisted slow crack growth can lead to apparent mechanical fatigue.

Table 7.2 *Approximate fracture toughness, K_{Ic}, values. Fractographers should obtain a more specific value for the material being examined whenever possible. SCG, rising R-curves, environmentally-assisted slow crack growth, and mechanical fatigue are covered later in this chapter. If rising R-curve behavior is suspected for a material, it is best to use a small-crack fracture toughness in a flaw size calculation rather than a plateau value.*

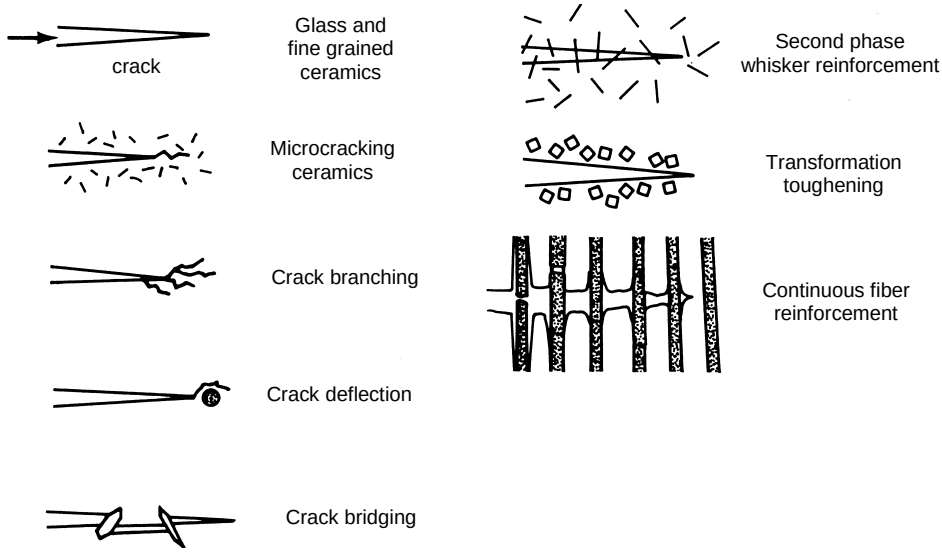

Figure 7.19 *Crack interactions with microstructure.*

is for mechanical-cyclic fatigue, whereby cracks extend in response to repeated cyclic loading. These phenomena are dependent upon the chemistry and microstructure. Slow crack growth, R-curves, and cyclic fatigue are discussed later in this chapter.

For now, the discussion will focus on the simplest situation: a material that does not have slow crack growth, that has a flat R-curve, and that has no mechanical (cyclic) fatigue. Such a material has a single value for fracture resistance, i.e., fracture toughness: K_{Ic}. Many ceramics (e.g., solid-state sintered silicon carbide and many fine-grained materials) and all glasses if tested under inert atmosphere conditions fit this category.

Users should be cautioned that much fracture toughness data is unreliable, especially the data obtained from simple saw cut notched bend bars or Vickers indentation crack length methods. The former method almost always overestimates fracture toughness. Vickers indentation fracture toughness data are notoriously faulty. Reliable methods such as single-edged precracked beam, chevron-notched beam, or surface crack in flexure, have been refined and standardized. International round robins and reference materials such as NIST SRM's 2100, 2100A, and 2100B, have confirmed their reliability. [a,54]

[a] The three SRMs were prepared the same way, but were from different plates. They had different certified fracture toughness values. The original SRM 2100 has sold out.

Slow crack growth and R-curve behavior are important phenomena that add complications to fracture analysis, but for now we focus on a straightforward, simple application of equation 7.7 to aid fractographic analysis.

7.5.2 Fracture mechanics solutions for internal penny-shaped cracks

The stress intensity K_I on a flaw depends upon the flaw size and shape, the stress magnitude and distribution, and on the component size and shape. A remarkable variety of fracture crack shapes and loading configurations have been analyzed and the reference handbooks listed in Appendix A may be consulted for a specific problem. Figure 7.20 illustrates two examples for internal flaws. Figure 7.20a shows *a flat penny-shaped circular flaw* in uniform tension, which is a case that is commonly used to simulate internal flaws in ceramics. Equation 7.7 is applicable and the stress intensity shape factor Y for this configuration is 1.128.

Figure 7.20b shows the same flaw but with a different loading configuration. At first glance it looks similar, but it is not. Opposing <u>forces</u> P pull on the center of the crack faces. This is not a far-field stress and equation 7.7 is inapplicable. K_I has a completely different form as shown in the figure.

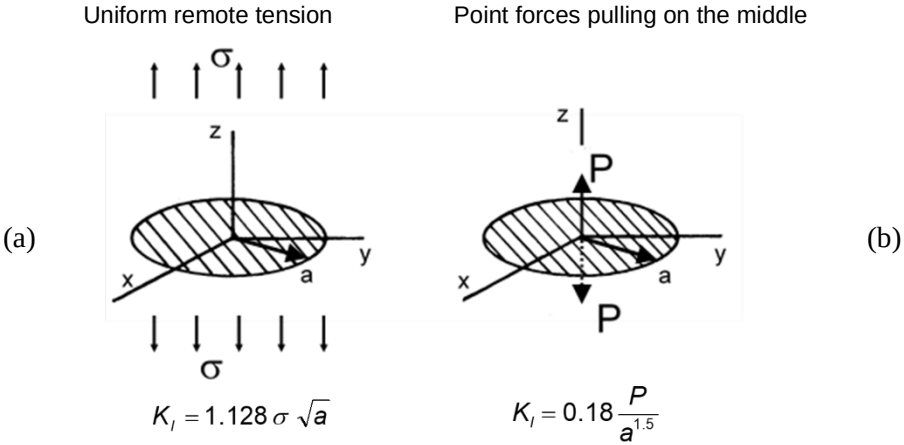

Figure 7.20 *The stress intensity K_I for penny-shaped circular cracks for two different loading configurations. (The three-dimensional axes make the flaws appear elliptical in this view.) (a) shows a far-field tensile stress s, and (b) shows opposed forces P pulling directly on the middle of the crack. K_I increases with crack size in (a), but decreases with crack size in case (b).*

Indeed, the larger the crack size, a, the less the stress intensity! This can easily be understood by considering that the effect of the force P is distributed along the flaw's perimeter. The larger the crack radius, a, the greater the perimeter and the less the force per unit length of crack perimeter. (This K_I solution with force divided by the cracks size raised to the 3/2 power is commonly used to approximate the effect of concentrated residual indentation stresses from a Vickers indentation on a semicircular median crack flaw. Therefore, most equations for "indention fracture toughness" have a $P/a^{1.5}$ term.)

The left hand column of illustrations in Figure 7.21 shows a variety of <u>internal</u> flat elliptical flaws loaded in far-field uniform tension. The shape of the flaw affects the Y factor. It varies around the flaw periphery if it is not a circle. The figure shows the location and value of the maximum Y. A flaw goes critical when one portion of the flaw reaches K_{Ic}, so the maximum Y is of primary concern. The author has seen a number of instances where localized fractographic markings confirmed that fracture indeed had started at the portion of the flaw periphery that had the maximum Y. The reader again is reminded that the flaw size for equation 7.7 ($K_{Ic} = Y s_f \sqrt{a}$) is the radius or *half minor axis length* (a) for the internal cracks.

The right column of Figure 7.21 shows analogous <u>surface</u> flaws and their Y values. The flaw size in these cases is usually the flaw depth. Surface flaws are covered in the next section 7.5.3 of this Guide. It is worth noting that the right column in Figure 7.19 shows that surface flaws have greater Y factors than for analogous internal flaws. This is because the surface cracks have less supporting material in the vicinity to share the forces. The crack opening displacements on a surface-connected flaw are also greater.

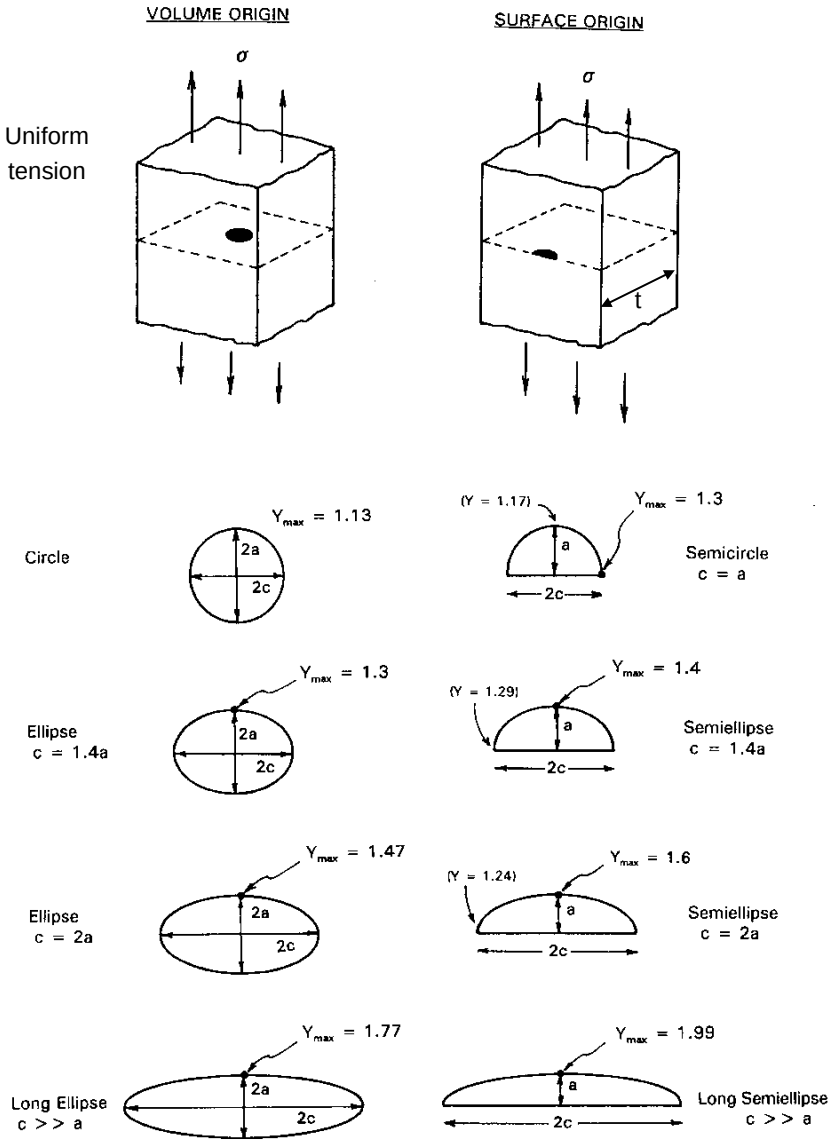

Figure 7.21 *The stress intensity shape factors Y for surface and internal circular and elliptical internal (volume) cracks and surface cracks for* *far-field tension stresses*. *Minimum Y factors for the surface cracks are shown in parenthesis. The Y factors for the surface flaws may also be used for parts loaded in* *bending* *if the flaw depth a is small relative to the specimen thickness, t (i. e., a/t is small).* *Caution*! *the convention is that the flaw size dimensions a and c are the minor and major axis radii, respectively.*

7.5.3 Fracture Mechanics solutions for surface cracks

The surface crack problem is of great importance and therefore is covered in detail below. Surface cracks can often be modeled by semielliptical flaws as shown in Figures 7.21 and 7.22. It is very important to distinguish between surface flaws that are loaded in uniform tension as shown in the left column in Figure 7.22 and flaws loaded in bending on the right. For the latter, the relative depth of the flaw compared to the part thickness (i.e., the a/t ratio) is very important, since the flaw tip extends into a decreasing stress field. The convention used for bending problems is that the far field stress is the maximum outer fiber stress.[54,55,56]

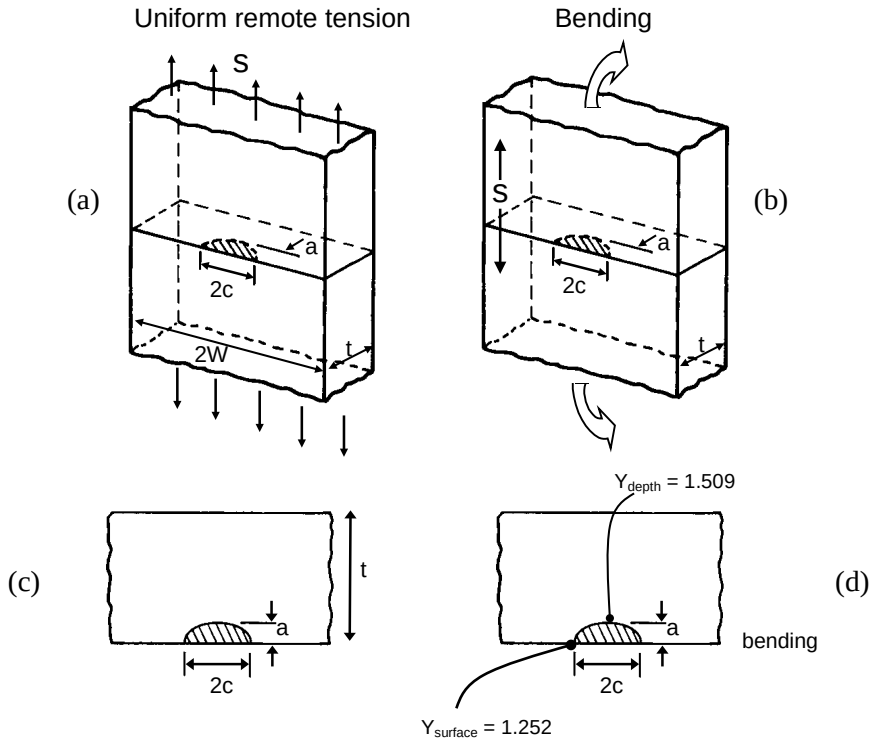

Figure 7.22 *Surface cracks in plates or bars in far-field tension (a) or bending (b). The stress intensity factor equations by Newman and Raju[56] are applicable to these configurations. The Y factors for case (a) in tension and (b) in bending are the same for very shallow cracks, a/t ® 0. (c) is a view of the cross section. (d) shows the same but labeled with the Y factors at two locations for the flaw dimensions given in the example on page 7.34 in Section 7.5.3.1. The flaw size in most calculations is the depth, a.*

Several solutions of varying sophistication are presented below, and the reader may choose which is most appropriate for his or her surface crack problem. The simplest approach is to consult Figure 7.21 and pick the best flaw match bearing in mind that the Y values shown are for uniform tension. The values may be overestimates if the surface crack is large and is in bending.

7.5.3.1 The Newman-Raju Y factors for semielliptical surface flaws in bending

Ceramics and glasses often have surface origins and the stress intensity factor solutions of Newman and Raju[56] for both tension and bending stress fields are very helpful. Their versatile solutions may be applied to tension, bend bar, and biaxial disk specimens, and indeed any component shape wherein a remote stress field causes fracture. With reference to Figure 7.22 for dimensions for surface flaws in a plate or beam in bending, the Y_{depth} and $Y_{surface}$ for locations at deepest part of the crack and at the surface are:

$$Y_{depth} = \frac{M}{\sqrt{Q}} H_2 \sqrt{p} \tag{7.10}$$

$$Y_{surface} = S \frac{M}{\sqrt{Q}} H_1 \sqrt{p} \tag{7.11}$$

where M, Q, H_2, H_1, and S are geometric terms:

$$M = \left[1.13 - 0.09\left(\frac{a}{c}\right) + \left[0.54 + \frac{0.89}{0.2 + \left(\frac{a}{c}\right)}\left(\frac{a}{t}\right)^2\right] + \left[0.5 - \frac{1.}{0.65 + \left(\frac{a}{c}\right)} + 14.\left(1. - \left(\frac{a}{c}\right)\right)^{24}\right]\left(\frac{a}{t}\right)^4\right] \tag{7.12}$$

$$H_1 = 1. - \left(0.34 + 0.11\left(\frac{a}{c}\right)\left(\frac{a}{t}\right)\right) \tag{7.13}$$

$$H_2 = 1. - \left(1.22 + 0.12\left(\frac{a}{c}\right)\left(\frac{a}{t}\right) + \left[0.55 - 1.05\left(\frac{a}{c}\right)^{0.75} + 0.47\left(\frac{a}{c}\right)^{1.5}\right]\left(\frac{a}{t}\right)^2\right) \tag{7.14}$$

$$F = \sqrt{Q} = \sqrt{1. + 1.464\left(\frac{a}{c}\right)^{1.65}} \qquad \text{for } a/c \le 1 \tag{7.15}$$

$$S = \left(1.1 + 0.35\left(\frac{a}{t}\right)^2\right)\sqrt{\frac{a}{c}} \qquad (7.16)$$

(Equations 7.10 and 7.11 do not include an additional term f_w in the original Newman-Raju analysis, since for nearly all cases for ceramics and glasses, the flaw width 2c is small relative to the component width, and f_w is 1.0.) These polynomials appear intimidating at first glance, but are easily programmed (with care!) into hand calculators or spreadsheets. Notice how many of the dimensions appear as ratios, e.g., a/c, the flaw ellipticity ratio; or a/t, the ratio of the flaw depth to the plate thickness). The $(1-(a/c))^{24}$ term for M in eq. 7.12 is genuine and not a typographical mistake. The Newman–Raju Y factors have been widely used in many textbooks and are included in several ASTM standards including C 1421 for fracture toughness of ceramics,[53] E740[57] and E2899[55] for metals, as well as ISO standard 18756.[58] The reader is again cautioned that the flaw dimensions a and c are the flaw radii, or minor and major axis dimensions.

The above equations are for surface cracks in <u>bending</u> stress fields. Newman and Raju listed alternative formulas for direct uniform tension loadings.[56] It is not necessary to list them here. Equations 7.10 – 7.16 may be easily used for cracks in uniform tension loaded parts by the simple expedient of inputting an arbitrary large value (e.g., 1000) for the part thickness, t. The a/t ratio ® 0 and the Y factors in equations 7.10 and 7.11 converge to the tension solutions.

As an example, if a bend bar is broken and it has a surface crack with a depth (a) of 40. x 10^{-6} m; width (2c) of 144. x 10^{-6} m; and specimen thickness (t) of 2.998 x 10^{-3} m; then M = 1.080, H_1 = 0.995, H_2 = 0.983, ÖQ = 1.247, and S = 0.820. Then, Y_{depth} = 1.509, $Y_{surface}$ = 1.252 as shown in Figure 7.22d.

In practice, the more elliptical the flaw, the more likely the maximum Y is at the flaw depth (unless the crack penetrates deeply into the specimen interior and into the stress gradient.)

Using the larger value for Y and the flexural strength which was 453 MPa, equation 7.7 gives K_{Ic} = 1.509 x 453 MPa Ö40 x 10^{-6}m = 4.32 MPaÖm. In this case, the parameters are used to estimate the material's fracture toughness.

As noted on page 7.25, equation 7.7 for K_{Ic} can be used two other ways. If the fracture toughness and flexural strength were known, the flaw size could have been estimated. Similarly, if the crack size had been measured and the fracture toughness was known, then the stress of 453 MPa could have been estimated.

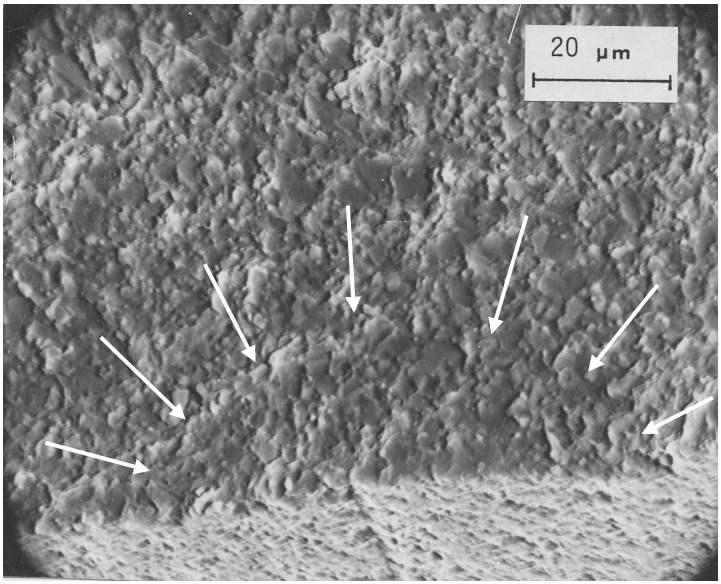

Figure 7.23 *Grinding crack in a longitudinally-ground hot-pressed silicon carbide bend bar at 649 MPa. This flaw was located directly in the center of a well-defined fracture mirror. The depth a is 23 µm, the width 2c is 95 µm, and the bar thickness, t, was 2.2 mm.* Y_{max} *was at the deepest point and was 1.58. The computed fracture toughness is: 1.58 * 649 MPa * Ö23 x* 10^{-6}*m = 4.9 MPaÖm, which is reasonably consistent with published average values of 4.0 to 4.5 MPaÖm for the material. This orthogonal grinding crack is subtle and does not stand out clearly against the background microstructure. There may have been some doubt about its identification, but the fracture mechanics calculation shows it is about the right size.*

Figures 7.23, 7.24, and 7.25 show three examples of how the calculation can be used to confirm that the right flaw has been identified. Sometimes the calculated and measured flaw sizes agree very closely, but there are a number of reasons why they may differ as discussed below in section 7.8. ASTM standard C 1322[52] states that if the calculated and measured flaw sizes do not agree within a factor of two or three, then the origin should be reexamined to verify that the correct feature has been identified.

The surface crack in the BK-7 borosilicate crown glass disk shown in Figures 5.20, 6.31, and 7.25 was 7.3 µm deep and the stress at fracture was 146 MPa. For a long surface crack, Y is 1.99. The calculated fracture toughness from these values is 0.78 MPaÖm, which is very close to published values for this particular glass.

(a)

(b)

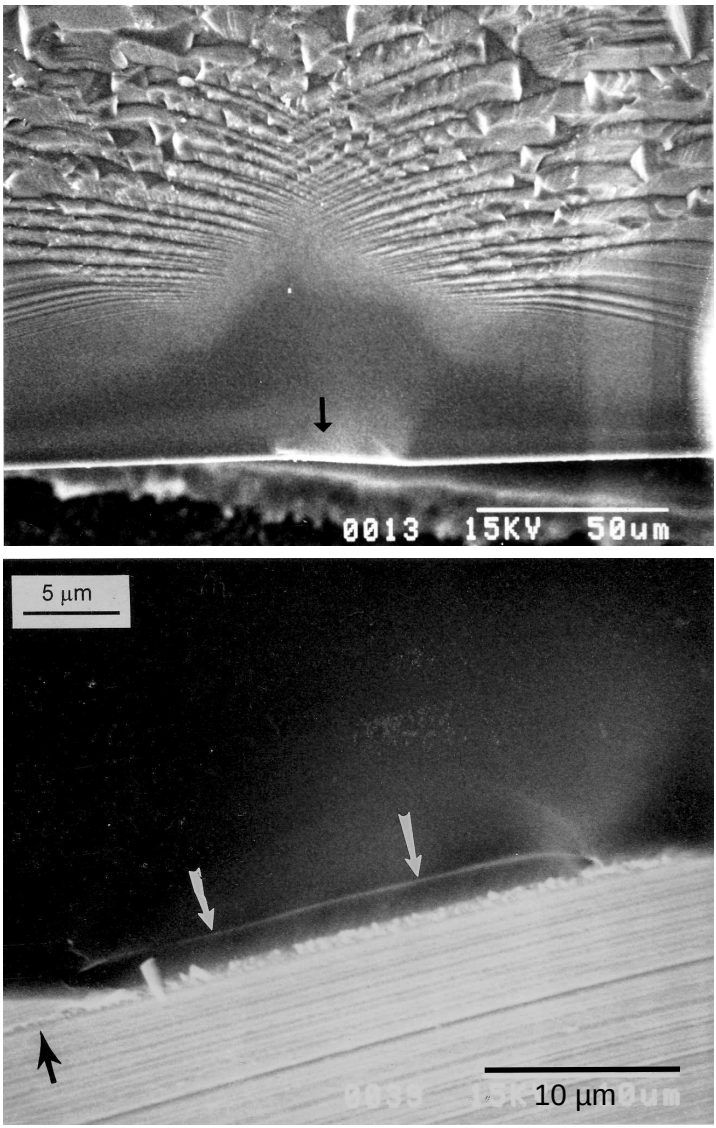

Figure 7.24 *Fracture origin in a single crystal silicon wafer. (a) shows the fracture mirror which has a very faceted shape typical of some single crystals. The origin is a grinding crack shown by the white arrows in (b). The specimen was tilted back to show both the fracture and outer ground surfaces. A 3,000 X scanning electron microscope photo showed that the crack was 2 micrometers deep, and when combined with a 282 MPa fracture stress, and a Y factor of 1.99, gives* K_{Ic} *= 0.79 MPa√m, in reasonably good agreement with published values for fracture on the {110} plane. See also Figure 8.6.*

(a)

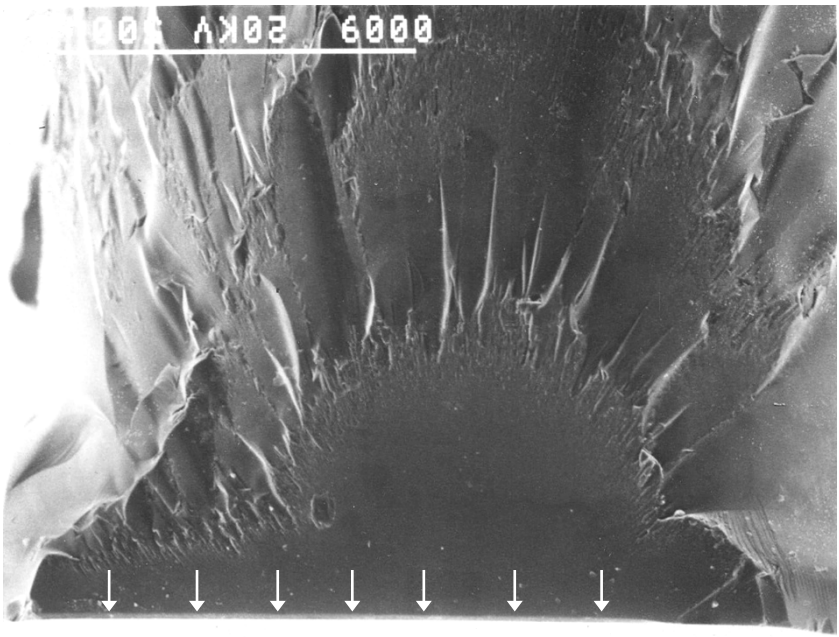

(b) (c)

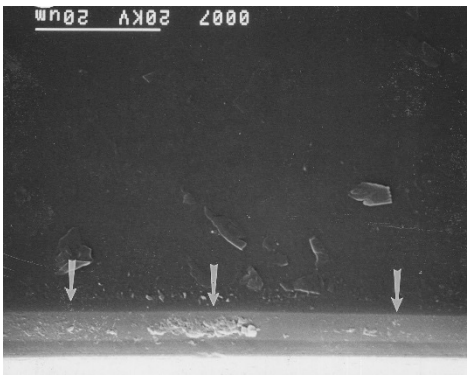

Figure 7.25 *Fracture origin crack for the BK-7 borosilicate crown glass biaxial disk specimen that was broken in inert conditions as shown in Figure 5.20. (a) is an SEM photo of the distorted mirror. The arrows show the long polishing scratch. (b) and (c) show two portions of the polishing scratch which was 7.3 mm deep (arrows). Using Y = 1.99 and the breaking stress of 146 MPa, gives* K_{Ic} *= 0.78 MPa*Ö*m. The optical image (see Figure 5.20) showed a slight bulge in the flaw at the center of the mirror suggesting the flaw may have grown slightly before going critical. This growth is not evident in the SEM images.*

7.5.3.2 Newman-Raju formulas deep (a/c > 1) for semielliptical surface cracks

Occasionally the fractographer may find a flaw that is deeper than a semicircle, i.e., a/c > 1. Fett[59] devised modified Newman-Raju formulas that permits one to compute the Y_d and Y_s factors in such cases for either tension or flexural loadings. A conscientious reader may consult his paper for the modified formulas. Rather than listing all the revised formulas or showing charts or tables, some approximations are provided here. In the cases with semi-ellipses that are deeper than a semicircle, the maximum Y is at the surface, Y_s. For cracks that are shallow relative to the plate thickness ($a/t \leq 0.2$) in tension or bending, the *surface* Y_s factor decreases linearly from that for a semicircle by only 10% as a/c goes from 1 (the semicircle) to 2 (a very elongated crack into the thickness). The stress intensity shape factor Y_d for the *deepest* part of the flaw also decreases approximately linearly, but by greater amounts. Y_d decreases by 33 % in both tension and bending as a/c goes from 1 to 2. If the flaw is larger relative to the plate thickness (e.g., a/t = 0.2), Y_d decreases by 33 % and 45 % in tension and bending, respectively, as the a/c ratio goes from 1 to 2. In other words, as a very deep semi-ellipse penetrates into the stress gradient in <u>bending</u> (a/t = 0.2, or 40 % of the way to the neutral axis), Y_d diminishes rapidly.

7.5.3.3 Accuracy of the Newman-Raju Y formulas

The Newman-Raju stress intensity factors Y for semielliptical surface flaws are considered to be accurate to within a few percent and this suffices for most fractographic analysis. Developed by finite element analysis over forty years ago, the Newman-Raju factors are widely used in textbooks, fracture mechanics and fractography standards around the world. Fett has reviewed[60,61] them carefully and concluded that for most common configurations, they are accurate to within 3%. Fett noted that a solution of Isida et al.,[62] obtained by means of a modified body-force method exhibits superior accuracy with a maximum deviation of less than 1% for Y_d.

Alternative solutions have been developed by Stobl et al.[63]. They modeled surface cracks as truncated semiellipses and allowed different Poisson's ratios other than 0.3. For most common semi-elliptical cracks and $n = 0.3$, their Y_d solutions concur with Newman and Raju's within a few percent.

7.5.3.4 Bansal's approximation for semielliptical surface flaws

Bansal reviewed the Newman-Raju stress intensity shape factors for semi-elliptical surface flaws in uniform tension[64] and arrived at a simple approximation:

$$K_I = \frac{2.0}{1.68}\sigma\sqrt[4]{A} \qquad 7.17$$

where A is the area of the flaw. Since the area of a semi-ellipse is pac/2:

$$K_I = 1.33\,\sigma\sqrt[4]{ac} \qquad 7.18$$

Sometimes the expression is written as:

$$K_I = 1.33\,\sigma\sqrt{b} \qquad 7.19$$

where the effective flaw size b = Öac. This equation should only be used if the a/c ratio is: 0.2 < a/c < 1.0. It should only be used for a/t < 0.05 for bending. (See the 1st-3rd editions of this Guide for further explanation.) This approach, with the fourth root of the flaw's area, is very similar to Murakami's model as discussed in the next section.

7.5.3.5 Murakami's equation for irregular surface cracks

Fracture mechanics reference books have tabulations of stress intensity formulas and shape factors for a myriad of crack shapes and loading configure-ations. There are even listings for multiple cracks in proximity to each other

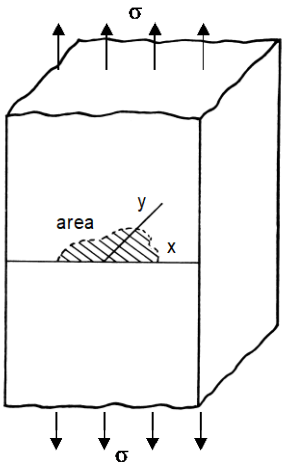

Figure 7.26 *An irregular planar shaped surface crack in a tension stress field. (After Murakami, ref. 65.)*

that show how the stress intensity fields interact. Real flaws in real materials often do not have convenient shapes, however. Several approximations are very helpful. Figure 7.26 shows a case of an irregular planar surface crack loaded by far-field tension. The stress intensity may be approximated, with a maximum of a 10% error (Poisson's ratio of 0.3), by a solution in Murakami's 1986 book that also uses the fourth root of flaw area, A:[65]

$$K_i = 1.15\, s \sqrt[4]{A} \tag{7.20}$$

Murakami's numerical analysis showed that equation 7.20 is an adequate approximation for stress intensity factor solution for such diverse shapes as partial circles, triangles, rectangles and semi ellipses. His equation is very similar to Bansal's and equation 7.17 shown above. If the flaw is semicircular with radius *a*, equation 7.20 simplifies to

$$K_I = 1.29\, s \sqrt{a} \tag{7.21}$$

This is nearly the same as Bansal's equation 7.19. This equation should <u>only be used</u> if the area is not very elongated. It should only be used for shallow cracks in bending.

7.5.4 Three-dimensional, blunt, and inclined flaws

Real flaws are not always flat and planar. Figure 7.27a shows a sphere that is not unlike many pores in ceramics and glasses. Sometimes round pores are

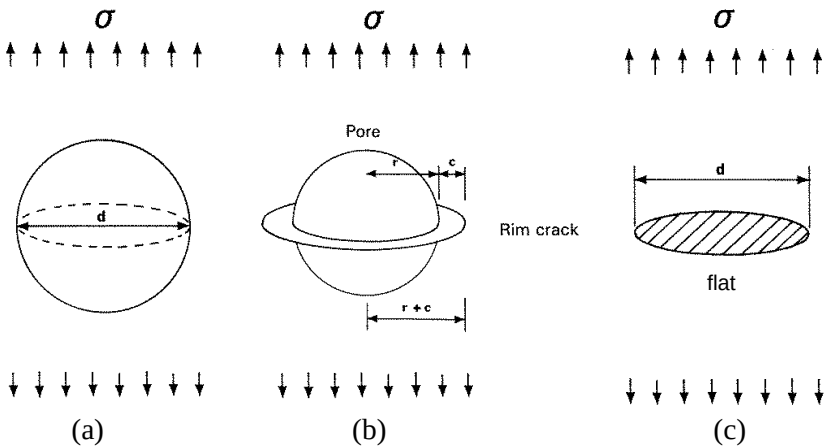

Figure 7.27 *Flaws may be three-dimensional. A flat penny-shaped crack (c) is a two-dimensional approximation.*

modeled by a penny-shaped crack, Figure 7.27c. This is a gross over-simplification. Indeed, if the pore is round and crack free, it does not act to *intensify* the stress, but simply *concentrates* stress around the flaw sides. The stress concentration factor for an interior sphere in a part in uniform tension is only k = 2. Smooth round pores require much greater force to cause fracture than the penny-shaped flaw of the same diameter. Smooth round pores may be quite docile and not act as strength-limiting flaws. Figure 7.27b shows another variation. This rim-cracked pore ("Rings of Saturn") flaw is a combined stress concentration and fracture mechanics problem. For small rim cracks, the pore acts as a stress concentrator, and the rim crack size, c, may be regarded as the crack size in a fracture mechanics calculation. For a very large rim crack (c/r > 1), the pore's effect is diminished, and the penny-shaped crack is a very good approximation. In practice, it is very difficult to detect a rim crack around a pore, much less measure it. It is not unreasonable to expect that rim cracks of one or two grain diameters extend from the pore and in fact many pores in ceramics do have local microstructural irregularities or microporosity in the vicinity. Only very rarely have fractographers attempted to precisely model such flaws and it is customary to use the penny-shaped cracks as an approx.-imation, but with full cognizance that the actual flaw is much blunter.

The reader may consult fracture mechanics handbooks (e.g., Bibliography Appendix A) for more information about rim-cracked pores (also called "annular cracks around a spherical void").

Appendix A also has references that cover flaws that are *inclined* to the stress direction. A slight inclination of 5 degrees does not affect the mode I loading very much, but beyond 10 degrees flaws experience not only mode I loading but varying degrees of modes II and III depending upon the flaw shape and inclination angle. Modes II and III have shearing actions on a crack as shown in Figure 7.17.

7.6 Relationship of K_{Ic} and A

K_{Ic} and the fracture mirror and branching constants are related to sÖa or sÖR and hence have the same set of units: MPaÖm (or ksiÖin). As Figure 7.7 at the beginning of this chapter illustrates, K_{Ic} pertains to conditions at the flaw whereas the A values correspond to events away from the origin as the crack propagates and reaches terminal velocity. Kirchner and Conway[40] showed that mirror shapes can be predicted on the basis of stress intensity at the crack front as it expands outwards from the origin, so it is not unreasonable to expect that K_{Ic} and the A's are related. If they are related, then in principle one can estimate K_{Ic} from A or vice versa. Mecholsky et al. [66] tabulated A's and K_{Ic}'s

for over two dozen ceramics and glasses and showed there was an approximate correlation. On average the ratio of A_o to K_{Ic} was 20/7 = 2.86, although there was considerable scatter. Bansal and Duckworth[67,68] carefully measured A_o to K_{Ic} ratios of 2.2 to 2.4 for a glass ceramic and a sintered alumina, and 2.3 for float glass and a hot-pressed alumina. Subsequent tabulations[69] on more contemporary materials, many of which have R-curve behavior, have given ratios as low as 1.5 to 2.0.

In a dissenting view, Bradt and colleagues[70,71] have suggested that A is not really a material constant and noted the discrepancies in A/K_{Ic} ratios. In summary, variability in the quality and accuracy of the K_{Ic} and A data, plus genuine microstructural effects, probably mean there is no unique A/K_{Ic} ratio.

Kirchner et al.[72] showed that the branching constant A_b varied by over a factor of 2 with the degree of transformation toughening in a calcia partially-stabilized zirconia. The greater the toughening, the greater the suppression of branching to greater distances, i.e., the A_b/K_{Ic} ratio increased with increased toughness. As discussed above, branching distances may depend on geometry.

7.7 Fracture Mirror to Flaw Size Ratios

A simple but very useful observation is that mirror and flaw sizes are related. Krohn and Hasselman[73] showed that the mirror size to flaw size ratio (R/c) is about 10 for glasses. Mecholsky et al.[66,74] obtained ratios of 10 to 11.6 using the mirror-mist (inner mirror) boundary in glasses. They estimated the ratio to be about 13 for the mist-hackle (outer) boundary to flaw size ratio for glasses. There are many exceptions to these ratios, however, as discussed below. Ratios for ceramics are more problematic and depend upon the microstructure and the ability to judge a specific boundary. Mecholsky et al.[66] estimated the ratio of the hackle boundary (outer mirror) to flaw size was 13 for polycrystalline ceramics and single crystals but varied from 8 to 40! Rice[75] pointed out that blunt flaws cause smaller mirror to flaw size ratios. For example, smooth pores (e.g., bubbles) often act as blunt flaws and it requires extra energy or stress to overcome the bluntness. The excess energy causes a mirror to form at shorter distances from the origin than if the flaw were sharp. Slow crack growth can also alter the apparent ratios.[74] If the mirror to flaw size ratio (R/c) is much greater than the values listed above, then the flaw should be checked for evidence that it grew stably prior to fracture. Residual stresses in the vicinity of the flaw or the mirror also can change the ratios. One example is the case of Vickers indentation starting flaws.[76] Unexpected mirror to flaw size ratios may be evidence of residual stresses acting on the flaw or the whole mirror. The mirror to flaw size ratio (R/c) may also be affected by the presence of mixed

Mode I/II loading. Gopalakrishnan and Mecholsky,[77] and Rice[78] have shown that increasing Mode II loading on a crack decreases R/c.

The R/c ratio is also affected if a material has a rising R curve. The larger the fracture toughness, the lower the R/c ratio.[77,79] In rising R-curve materials, the ratio may even depend upon how large the initial crack was and how far it might have stably grown before it went unstable. (Stable crack growth and crack instability is discussed more in sections 7.10 and 7.11 later in this chapter.) In rising R-curve materials, the larger the initial crack, the smaller the R/c ratio. Gopalakrishnan and Mecholsky's 2013 paper[77] even goes so far as to analyze the combined effects of R-curve and mixed Mode I/II behavior on R/c ratios.

In summary, the mirror size to flaw size ratio can vary considerably, but for starters, the fractographer should look for a flaw that is 10% to 20% of the size of a fracture mirror.

$C_{calc} < C_{meas}$	$C_{calc} > C_{meas}$	$C_{calc} > C_{meas}$ or $C_{calc} < C_{meas}$
· Crack blunting · Use of 2-D model · Stress gradients · Crack healing	· Stable crack extension – SCG · Stable crack extension – R curve · Flaw causes a local fracture toughness degradation · Flaw is within a single grain · Flaw links with other flaws	· High temperature SCG · Multiple flaws nest or interact · Residual stresses · Flaw is truncated on the fracture surface · Flaw shape irregularity · Flaw elastic properties are different than the matrix · Faulty fracture toughness data

Table 7.3 *Factors that can cause a measured flaw size c_{meas} to differ from the calculated c_{calc} size. (Quinn and Swab, Refs. 80,81)*

7.8 Comparing Measured to Calculated Flaw Sizes

Differences in calculated and measured flaw sizes of 20 % to 50 % should not be considered too serious, but variations greater than a factor of 2 or 3 should prompt the fractographer to study the origin more carefully. Either the wrong feature has been identified as an origin or the origin may be more complicated than expected. Either something about the calculation is wrong or the fractographically measured size is wrong. Table 7.34 and Figure 7.28 show some of the factors than can cause the discrepancy.[80,81] These can be appreciated if Equation 7.7 is rewritten:

$$c_{calc} = \left(\frac{K_{Ic}}{Y s_f}\right)^2 \tag{7.22}$$

(a) Flaw bluntness or 2-D approximations

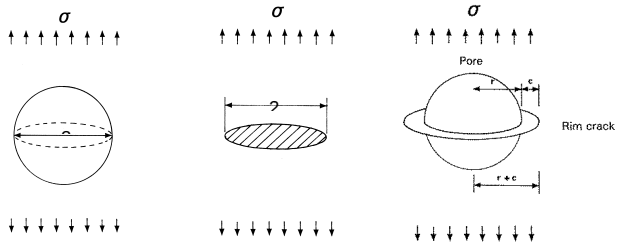

(b) Flaw interactions

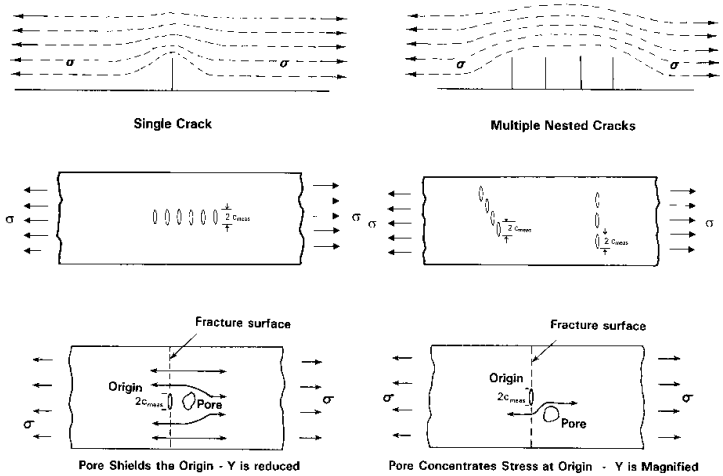

(c) Flaw linkage

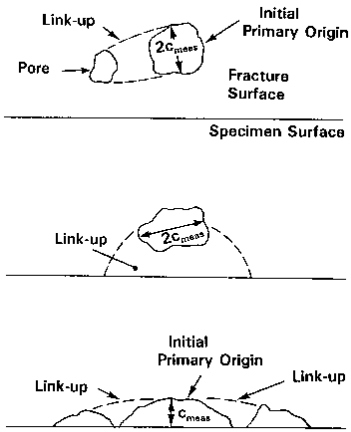

(d) Flaw slow crack growth

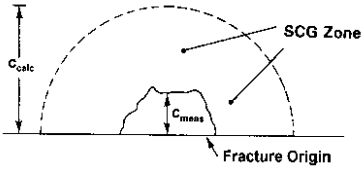

(e) Flaw truncation on the fracture surface

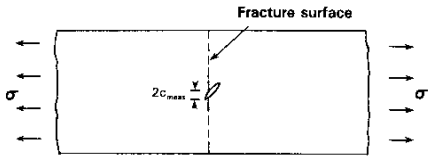

Figure 7.28 *Factors that cause calculated and measured crack sizes to differ.*

where c_{calc} is the calculated critical crack size at fracture, s_f is the fracture stress at the origin site, and K_{Ic} is fracture toughness. The reader again is cautioned that the convention is to use a flaw radius, or half minor or half major axis dimension as the flaw size in the calculation.

The cases where $c_{calc} < c_{meas}$ are considered first. A blunt flaw of actual size 2c requires a greater stress to cause fracture than a comparably-sized sharp flaw. Some flaws are blunt to begin with. Other initially-sharp flaws may have been blunted or even partially healed by oxidation or other environmental effects. Glass cracks can partially heal in vacuum or inert atmospheres, especially if they form during dynamic events and are unloaded quickly. Inserting the greater stress to break healed or blunted cracks into equation 7.22 leads to a smaller c_{calc} than the actual flaw size c. Assuming that flaws are 2-D penny shaped or are flat ellipses of radius c, when they really are 3-D flaws such as shown in Figure 7.28a usually leads to Y estimates that are too large, and this also leads to c_{calc} that is less than the actual flaw radius c. Unexpected stress gradients can cause s_f to be overestimated. That in turn will again cause c_{calc} to be too small. The stress at the origin site should be used in equation 7.22.

Next are the cases where $c_{calc} > c_{meas}$. Slow crack growth and rising R-curve behavior can cause stable crack extension as shown in Figure 7.28d. Using the actual breaking stress in equations 7.7 or 7.22 gives a correct flaw size calculation, but if the fractographer detects and measures only the initial flaw size, then $c_{calc} > c_{meas}$. In this case it is the fractographic size measurement that is off. Alternatively, if stable crack extension due to R-curve behavior does occur, but the fractographer uses a long crack (plateau) value of fracture toughness, then the fracture toughness is overestimated and again $c_{calc} > c_{meas}$. R-curve behavior is discussed later in more detail in section 7.11. Inclusions or chemical inhomogeneities can be particularly deleterious if they degrade the fracture toughness of the surrounding matrix. If the fractographer uses the baseline K_{Ic} value in equation 7.22, this also leads to $c_{calc} > c_{meas.}$ In this case, the calculated size is wrong and the observed crack size is correct. The fracture toughness of a single crystal, or a single grain, is almost always less than that of a polycrystal. If a flaw resides within a single grain, but a polycrystalline K_{Ic} value is used in equation 7.22, then c_{calc} will be too large. Flaws may link up with other flaws or a surface weakening the specimen as shown in Figure 7.28c. If the linkage is undetected by the fractographer, then his c_{meas} will be too small compared to the calculated and actual critical flaw size.

Some factors can cause the measured size versus calculated size discrepancy to go either way. Flaws are often assumed to exist in isolation, but as Figure 7.28b shows they can interact causing either an increase or a decrease in the Y

factors that act on them. It all depends upon the geometries and arrangements. This is an instance where the "flow lines of stress" concept can aid interpretation. If flaws are lined up in a row parallel to the stress, the flaws will shield each other. If they are staggered or lined up sideways, they can intensify the K_I fields and the Y factors. Flaws may be truncated such as shown in Figure 7.28e and only a portion detected on the fracture surface. Undetected residual stresses can throw off the calculated flaw size as well. Faulty fracture toughness data can also throw off the correlations.

The point here is that fracture mechanics is a valuable tool to aid fractographic analysis. It can help confirm that the fractographer has found the correct origin flaw. A finding that the calculated and measured sizes are appreciably different should prompt further consideration and analysis. What factors caused the discrepancy? Is the discrepancy an isolated outcome or part of a pattern?

7.9 Crack Velocities from Wallner Line Analysis

Wallner lines can be used to estimate crack velocities, whether they are created incidentally during the fracture event or deliberately by ultrasonic fractography. Wallner lines may not be evident in very slow fractures in glass or in ceramics due to the latter's rough fracture surfaces.

Ultrasonic fractography uses a transducer to generate sonic waves that interact with the propagating crack as discussed later in sections 5.4.4 (on tertiary Wallner lines) and 3.21 (on examination techniques). Usually, the transducer is placed onto the specimen perpendicular to the crack propagation plane. The sonic waves create tertiary Wallner lines and show the crack front shape on the fracture surface. Velocities are easily estimated from the pulse frequency and the spacing between the Wallner lines. Richter and Kerkhof[82,83] and Michalske et al.[84,85] used this technique over a broad range of crack velocities from terminal velocity down to 10^{-7} m/sec. Indeed, Richter and Kerkhof[82] used this technique to show that surface cracks that grow by slow crack growth evolve in shape in accordance with the Newman-Raju stress intensity shape factors as shown in Figure 5.50. They also showed Figure 5.51a which proved a semielliptical crack could go unstable from one side. This is explained with an example of my own as shown in Figure 5.61.

Wallner lines are formed by transverse elastic waves interacting with the moving crack front. The transverse (shear) wave velocity from section 5.1 of this book is:

$$v_t = \sqrt{\frac{E}{2r(1+n)}} \tag{7.23}$$

where E is the elastic modulus, r is the density, and n is Poisson's ratio. Experimental values for transverse wave velocities for glasses may be found in the book and papers by Kerkhof that are cited in Chapter 5 and Appendix E.

Even in the absence of externally-applied sonic pulses, it is possible to interpret *naturally* created Wallner lines to estimate crack velocities as shown in Figures 7.29 – 7.31. The simplest case is for a straight crack front that intersects a discontinuity such as a bubble or inclusion that creates an elastic pulse. This makes a fracture surface feature called a "gull wing." The radiating transverse elastic wave always travels faster than the crack front. Figure 7.29 shows how the radiating circular wave front (the concentric dashed lines) catches up and intersects with other portions of the advancing crack front. The locus of intersections generates Wallner lines that have a telltale "V" pattern centered on the elastic discontinuity. There often is a slight curl at the pulse origin. The included angle (2b) between the wing segments may be used to calculate crack velocities.

$$v_c = v_t \cos b \tag{7.24}$$

where v_c and v_t are the velocities of the crack front and the transverse wave.

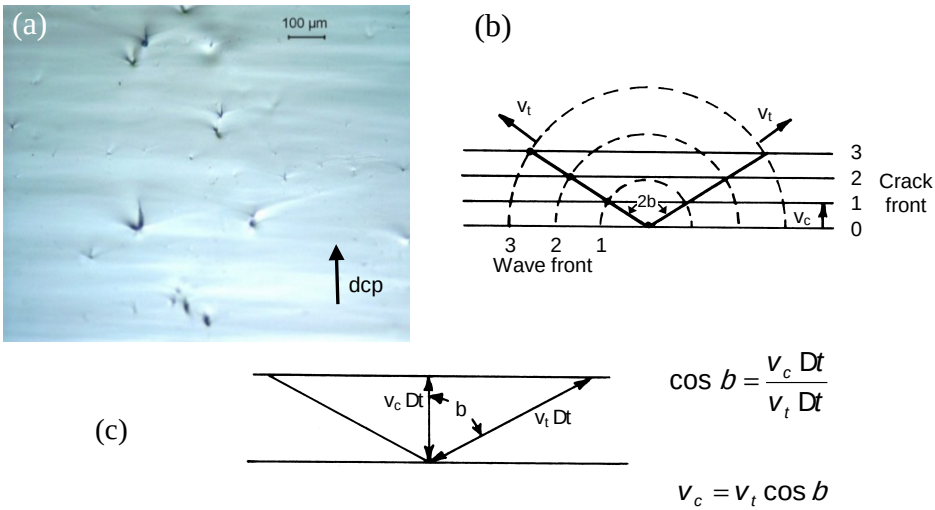

Figure 7.29 *Crack velocity may be estimated from Wallner line analysis. Gull wing lines occur when a straight crack front passes a point discontinuity such as a bubble or inclusion. (a) shows gull wings in knapped obsidian (specimen courtesy A. Tsirk). The direction of crack propagation is from bottom to top. The included angle (2b) is used to estimate crack velocity. Slow cracks have flat (horizontal) wings. Fast cracks create wings with a "V" shape. (b) and (c) show the geometries and simple trigonometry used to estimate crack velocity.*

Slowly-moving cracks do not advance very far in a time interval Dt, and the elastic pulse quickly overtakes the entire front. Thus, the "V" shape is very flat and, if it assumed that the included angle 2b is 180° – 2° = 178°, then the slowest velocity that can be measured in a glass with v_t = 3460 m/s is $v_{c,min}$ = 60 m/s. Conversely, if the crack is advancing at the terminal velocity of 60 % of the transverse wave velocity, then the minimum included angle 2b is 106°. Tsirk[86] showed such "V" shaped Wallner lines in obsidians.

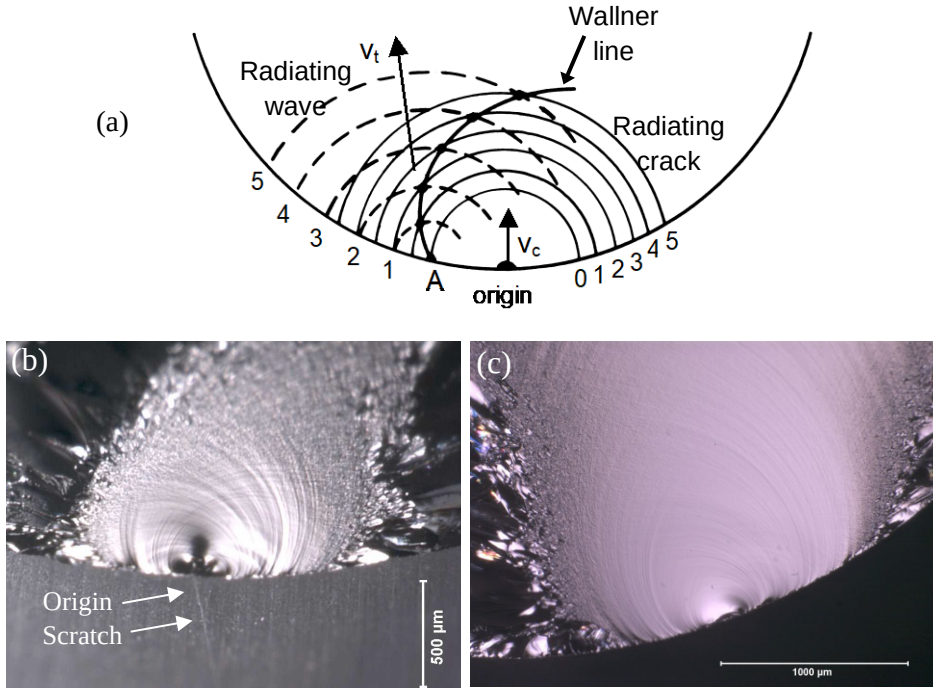

Figure 7.30 *Crack velocities can be estimated from Wallner line analysis. (a) shows a crack front that radiates outward from the origin at velocity v_c (thin circular lines) and reaches irregularity A on the left. An elastic pulse is generated at A and it radiates a transverse (shear) wave outward from A (dashed lines) with a faster speed v_t than the crack front. The numbers label the crack and elastic pulse fronts at the successive times starting at 0, the instant the crack reaches A. The intersections for the specific times are marked by dots, but of course this is a continuous process and the solid line shows the ensuing Wallner line. The crack front is assumed to be moving at constant velocity $v_c = 0.5\ v_t$ in this case. If the crack were accelerating, the Wallner line would be less hooked in the beginning and would extend more towards the upper right. (b) and (c) show Wallner lines inside mirrors in silica glass rods.*

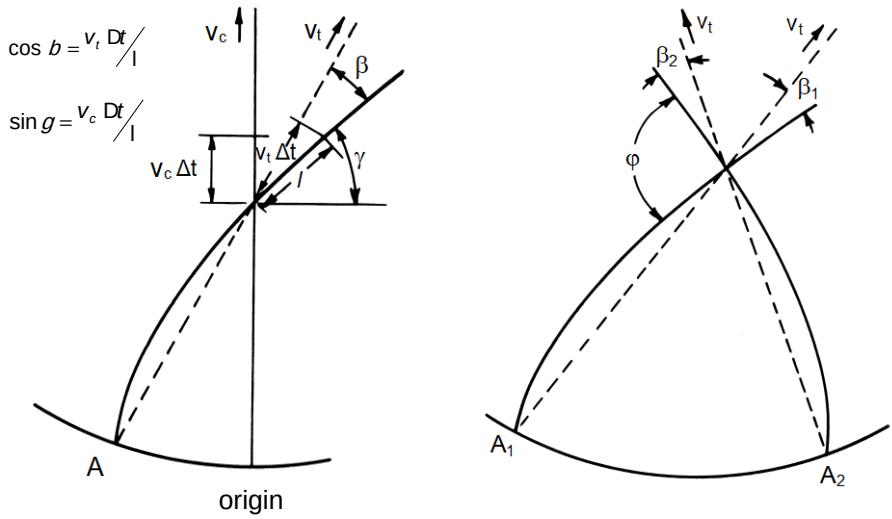

Figure 7.31 *Analysis of Wallner lines to determine the crack velocity if a crack radiates outwards from an origin. (a) shows a case where the location of the Wallner line elastic wave pulse (site A) and the direction of the crack extension are known. (b) shows the case where the precise crack growth direction is not known, but the origins (A_1 and A_2) of the Wallner lines are known.*

Wallner lines such as those inside a mirror shown in Figure 7.30 may be analyzed as shown in Figure 7.31.[8,19,37,87,88] In the case where the exact direction of crack propagation (radiating at speed v_c from the origin) and the initiation site of the Wallner line (A) are known as in Figure 7.31a:

$$\frac{v_c}{v_t} = \frac{\sin g}{\cos b} \tag{7.25}$$

Crack velocity can be determined even if the crack propagation direction is not known as in Figure 7.31b, Two intersecting Wallner lines were analyzed by Kerkhof in his 1975 paper[8] (and repeated by Mencik[19]):

$$\frac{v_c}{v_t} = \frac{\sin j}{\sqrt{\cos^2 b_1 + \cos^2 b_2 + 2\cos b_1 \cos b_2 \cos j}} \tag{7.26}$$

and if the Wallner line intersection is symmetric ($b_1 = b_2 = b$), then:

$$\frac{v_c}{v_t} = \frac{\sin\left(\frac{j}{2}\right)}{\cos(b)} \tag{7.27}$$

(Kerkhof showed a different version of this as equation 7.2 in his 1970 book.[89] Poncelet had yet another variant in his 1958 paper[87] which Michalske copied in his 1990 article.[90]) Elastic waves may overtake and pass over slowly-moving cracks may run across the crack front fairly quickly and thus the Wallner line corresponds closely with the crack front shape. The *minimum* velocity that can be estimated by Wallner line analysis was estimated by Mencík as $v_c/v_t = 0.175$, using equation 7.27 with j =2°, corresponding to nearly flat crossing Wallner lines. For glass with $v_t = 3460$ m/s, then $v_{c,min} = 60$ m/s. In general, quantitative Wallner line analysis for crack velocities is most suitable for fast moving cracks.

The spacing between the legs of Wallner lambda lines, discussed in section 5.4.5 and shown in Figure 7.32, can easily be used to estimate a crack velocity. In the time that the crack advances approximately a distance a/2, the elastic wave has traveled across the thickness once. For a straight crack front:[b]

$$V_c = V_s \frac{a}{2\sqrt{\left(a/2\right)^2 + t^2}} \tag{7.28}$$

The formula can also be used to approximate crack velocities for slightly curved crack fronts as well.

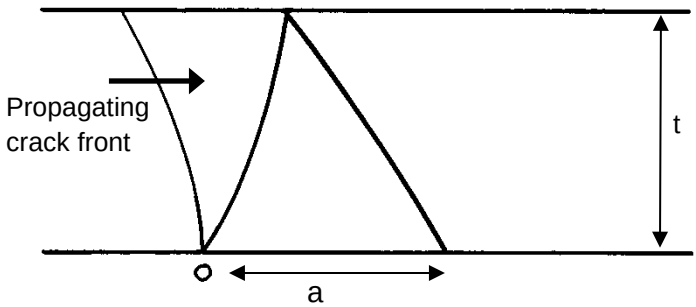

Figure 7.32 *The spacing between the lambda line legs can be used to estimate crack velocity.*

[b] Frechette's book (Ref. 1) has a faulty version of this equation. It is missing the factor of 2 in the denominator.

7.10 Slow Crack Growth

Cracks may grow stably when loaded at stresses and stress intensities less than that necessary for the flaw to become unstable. As discussed in sections 5.8.1 and 5.8.3, glasses, oxide ceramics, and ceramics with glassy boundary phase are susceptible. The mechanism of slow crack growth at ambient temperature is a stress corrosion phenomenon whereby stressed cracks that are open to the environment are attacked by water (or another polar molecule.) The water may be in the form of liquid or gaseous molecules. The water molecules attack the strained silicate or oxide bonds at the crack tip causing them to rupture which in turn leads to stable crack extension. Other fluids that promote slow crack growth are listed in section 5.8.1. At elevated temperature, oxidation attack, grain boundary softening, or other mechanisms can lead to slow crack growth (section 5.8.3).

Crack velocity depends strongly upon the stress intensity, K_I. The larger K_I, the faster the crack grows. Slight changes in it have dramatic effects upon crack velocity. As a crack size increases, it increases K_I in accordance with equation 7.6. If stress and the crack shape are invariant, the crack will gradually accelerate. Data are often graphed on log - log axes as shown in Figure 7.33a. Straight lines in Region I imply a power law dependence of velocity upon stress intensity:

$$V = A\,K_I^{\,N} \tag{7.29}$$

Region I crack velocity behavior often controls lifetime or rate effects on strength. Region II occurs when insufficient amounts of the reactive element are available. Region III occurs close to K_{Ic} and does not require a reactive species. With a few exceptions, during most of the time a crack is growing it will be in Region I. The slope of the line, N, is known as the slow crack growth exponent and is a critical parameter for reliability and rate effect analyses. Very high values of N (e.g., > 100) indicate considerable resistance to slow crack growth and hence, little rate sensitivity. Low values (e.g., 5 to 30) indicate high susceptibility. Velocity data as shown in Figure 7.33a are usually collected with laboratory specimens under controlled testing conditions.

Figure 7.33b shows how slow crack growth affects the <u>lifetime</u> of specimens loaded at <u>constant</u> stress levels below the fast fracture strength. This is referred to as “static fatigue” or “stress rupture” testing. The decrease in log strength varies with log time to the –1/N power.

Slow crack growth can even affect outcomes in <u>ordinary strength tests</u> as shown in Figure 7.33c. The slower the test is run, the weaker are the specimens since the crack can grow a surprising amount during the time of loading.

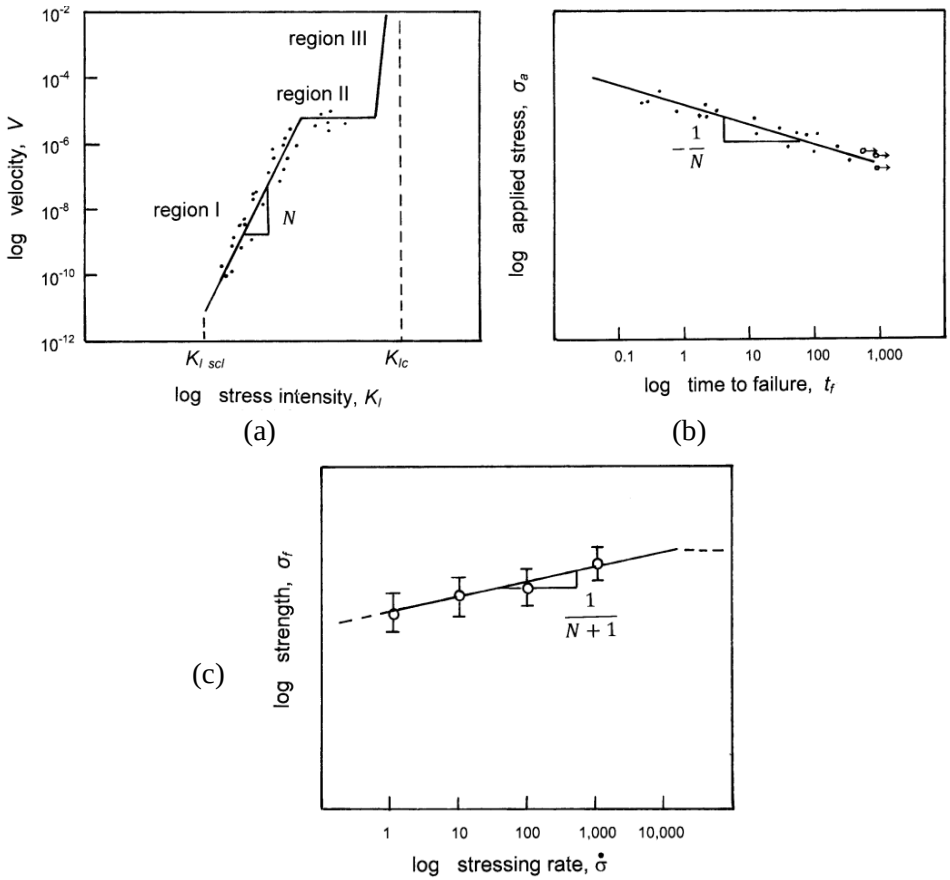

Figure 7.33 *Slow crack growth manifests itself in different ways. (a) shows a crack velocity versus stress intensity (K-V) graph showing three regions. Usually such data is plotted on log-log axes. Fracture mechanics type tests are used to collect such data. (b) shows a graph of log stress – log time to failure, also known as a "static fatigue" or "stress rupture" plot wherein a constant stress is applied until a piece breaks. (c) shows a graph of strength as a function of stressing rate also with log - log axes, also known as a "dynamic fatigue" plot. The exponent N plays a prominent role in each instance.*

Figure 5.61 showed an example of a flaw in glass that grew as much as 20 times its original size due to slow crack growth in water. Figure 5.60 showed a flaw in alumina that grew about twice its original size in a simple 30 second strength test conducted in lab-ambient air.

A comprehensive theoretical justification for the power law relationship between K_I and V is lacking at the present time. There are alternatives, but the

power law relationship lends itself to simple integrations and transformations and is usually adequate. It should be used with caution for any extrapolations beyond the times and velocities for which the data was collected, however.

Crack-fluid interactions can cause abrupt changes in crack growth that can create markings such as scarps on fracture surfaces as shown in section 5.6. For example, an accelerating crack may outrun the ability of a fluid to keep up with the crack tip and this may cause cavitation and a scarp. Conversely, a decelerating crack may slow down enough that water can catch up to the crack causing a scarp. Sometimes a jump in the crack from region I behavior to region II behavior creates a scarp.

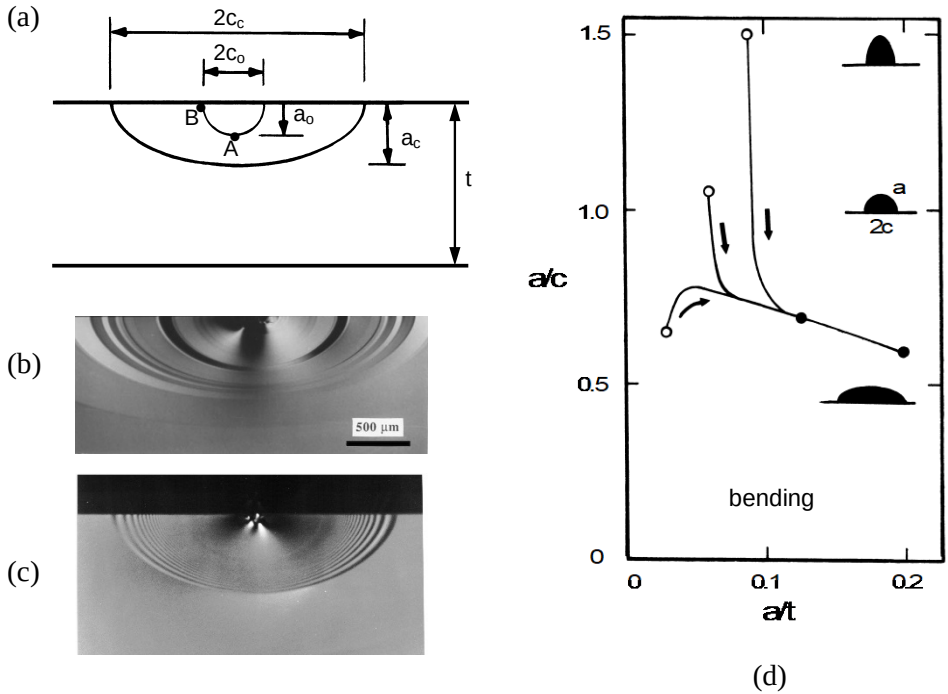

Figure 7.34 *Crack shape often changes as it grows either by monotonic or cyclic loading. (a) shows an initially semicircular crack of size a_o that changes to a semi elliptical shape as it grows in a* <u>*bending*</u> *stress field in a plate of thickness t. (b) shows concentric arrest lines from cyclic loading (same as Figure 5.53c) (c) shows tertiary Wallner lines from a rapidly moving crack (same as Figure 5.50b) (d) shows the evolution of crack shapes in glass bend specimens converges to a shallow semiellipse, irrespective of the starting shape (hollow circles). (b) courtesy D. Green. (c) is courtesy H. Richter. (d) is after Fett et al., Ref. 91.*

The Newman-Raju stress intensity shape factors also explain one commonly observed trend: surface cracks that grow stably *evolve shape and become semielliptical*. Figure 7.34 illustrates the trend for a beam or plate in bending. The stress intensity shape factor Y varies around the crack front. For a semicircular flaw, Y is greatest at the point where the crack intersects the outer surface, point B. At the internal point A, there is more material on either side of the crack front that can share the load, and hence the stress intensity shape factor is about 13 % less. Thus, the crack initially grows faster along the outer surface, but then, as the crack shape evolves into a semiellipse, the stress intensity evens itself out around the periphery. Newman and Raju[56] showed examples of this for fatigue crack growth in metals, both for bending and direct tension stress fields. The semielliptical shapes differ in the two cases, depending upon the size of the crack relative to the specimen thickness. The identical trends have also been observed in ceramics and glasses.[84,91,92,93,94,95] Small surface cracks in large, uniform, direct-tension loaded specimens or plates will assume a constant semi elliptical shape with an aspect ratio a/c of about 0.83. Cracks in bending stress fields will also gravitate to this shape if they are small relative to the thickness, but if they penetrate into the stress gradient (a/t > 0) they will become more elongated sideways as they grow and the semiellipse ratio a/c will decrease as shown in Figure 7.36d.

7.11 R-Curve Behavior

R-curve behavior, which arises from crack-microstructure interactions, is a phenomenon that may improve fracture resistance in ceramics. It can give rise to stable crack extension prior to fracture. It is not operative in glasses. Unfortunately, R-curve behavior does not leave any intrinsic telltale markings on the fracture that the fractographer can interpret.

Figure 7.35 illustrates the general concepts. Flat R-curve materials such as glasses and many fine-grained ceramics behave as shown in Figure 7.35a. Fracture toughness is independent of the crack size and has a specific value: K_{Ic}. When the combination of stress, flaw shape, and size reach the critical condition, unstable crack extension can occur. If there are substantial tensile stresses throughout the body, it will break. If, on the other hand, the stresses decrease either temporally as in thermal shock cases or spatially as in localized contact loading cases, the crack initially may be unstable, but then slows down and may even stop.

Rising R-curve behavior occurs when the microstructure impedes crack extension. Several crack-microstructure interactions shown earlier in Figure 7.19 can cause this. For example, yttria-stabilized tetragonal zirconia

polycrystal (Y-TZP) is carefully processed so that after firing, the microstructure is composed of metastable tetragonal grains. These can transform to the monoclinic phase when a crack tip and its stress field approaches. This martensitic phase transformation consumes some energy that might otherwise drive the crack forward. In addition, the transformed grains expand by » 4% thereby putting a compressive constraint on the crack tip. The process zone may only be a few grains wide in Y-TZP. R-curves can arise from other crack-microstructure interactions. For example, with coarse-grained ceramics, large grains behind the crack tip may not necessarily be immediately cleaved. They may act as bridges across the crack faces that reduce the stress intensity field on the crack tip. They can persist for long crack propagation distances.

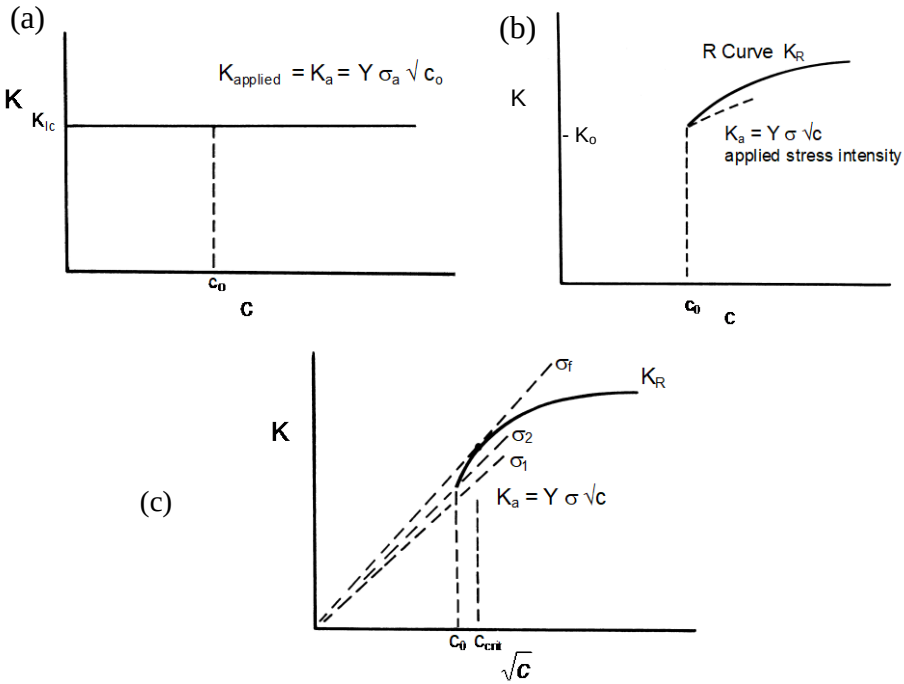

Figure 7.35 *R-curves in ceramics. (a) shows the case of a material with a constant, or flat R-curve. (b) shows a general schematic of a rising R-curve. Crack extension leads to a greater applied stress intensity K_a, but the material's fracture resistance curve K_R may also increase. (c) shows K_a versus $\sqrt{c}$, in which case the applied K_a plots as a straight line with slope proportional to applied stress. Fracture occurs at c_{crit} where the rate of increase of applied K_a is greater than the slope of the K_R curve. Initial flaws larger than c_{crit} may not exhibit any stable crack extension and may immediately go critical.*

Phenomena such as these can lead to behavior shown in Figure 7.35b. Starting with an initial crack size, c_o, if the stress intensity K_a from an applied stress reaches the level of K_o, the crack begins to propagate. As it grows, K_a increases in proportion to Öc if the stress is held constant as per eq. 7.6. The material's fracture resistance K_R may increase at a greater rate thereby retarding or arresting further crack propagation. Further propagation requires additional applied stress to increase K_a. The R-curve typically reaches a plateau such that further toughening is not possible. Fracture may occur *before* the plateau is reached if:

$$K_a = K_R \tag{7.30}$$

and

$$\frac{dK_a}{dc} > \frac{dK_R}{dc} \tag{7.31}$$

In other words, fracture occurs when the applied K_a reaches the level of the R-curve *and* the rate of increase in K_a with further extension is greater than the rate of toughening. To better show the relative increases, it is common to plot fracture resistance with K^2 versus c, or K versus Öc as shown in Figure 7.35c. In this fashion, the increase in K_a with crack size appears as a straight line with slopes that increase with s. This K_a line can be more easily compared to the K_R trend. Instability occurs at $c = c_{crit}$, a value well before the plateau is reached, after only a small amount of crack growth has occurred.

There is no universal R-curve for a material.[96] The R-curve depends upon the starting size of the crack relative to the microstructure and its prior propagation history. It also depends upon the size, shape, and mode of loading of the specimen. R-curves for large cracks are not the same as those for small cracks. In other words, data from large crack fracture mechanics specimens are usually not applicable to natural small flaws. Large fracture mechanics specimens usually are effective in measuring plateau toughness values. A double-cantilever beam specimen has a dramatically different crack opening displacement than a notched beam or a surface flaw in a bend bar. The number of bridges behind the crack tip bridges depends upon the crack opening displacement and the greater the opening, the fewer the intact bridges. For example, a 20 mm grinding-induced crack may have already interacted with the microstructure and formed bridges or transformed some material during the crack formation. Figure 7.36 shows two possible examples. In contrast, a 20 mm round pore may not have activated any prior toughening.

It is extremely difficult to measure R-curves for small natural-sized flaws, and especially the initial K_o fracture resistance. The limited data that has been collected suggests the initial K_o may be very small, approaching single crystal

or even grain boundary fracture toughness values. Some materials may have such small toughening zones that, for all practical purposes, they can be treated as having a set fracture toughness value. Many yttria-stabilized tetragonal zirconias (Y-TZPs) may be like this since the transformation zone is only a few grains large. On the other hand, magnesia partially-stabilized zirconia (Mg-PSZ) may experience considerable crack extension prior to fracture.[97]

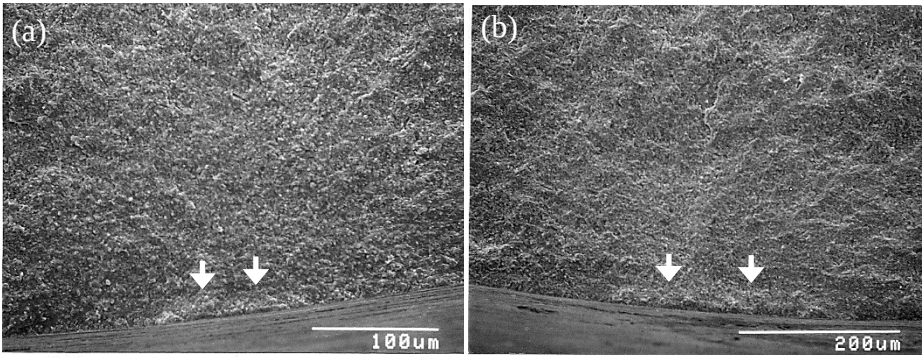

Figure 7.36 *Grinding cracks in transversely-ground rods that show evidence of stable crack extension (arrows) in a silicon nitride with rising R-curve behavior. (a) 657 MPa and (b) 641 MPa. (Ref. 98)*

Many studies have used Vickers indentation artificial flaws, but they often do not behave like genuine flaws as discussed in the next section. The R-curves that are generated are not relevant to natural flaws or are simply wrong. For example, one study showed that without proper care, the usual analysis with Vickers indentation flaws produced the implausible result that a soda lime silica glass has a rising R curve.[99] (The problem was that the standard indentation strength model fails to account for changes in crack shape, especially as cracks penetrate into strong flexural stress gradients.) The most credible R-curve data to date (that is applicable to strength limiting flaws) has been that collected by careful microscopic examination of crack growth from natural flaws in controlled loading experiments.[96,97,100,101]

The instability point depends upon the starting crack size and the slope of the R-curve at small crack sizes as shown in Figure 7.35c. Indeed, the overall plateau value may be inconsequential in many cases. A particular crack may grow only a small amount before going unstable [98,100,102] or it may immediately be unstable. Fett and Munz's mathematical analysis is quite revealing.[102] They showed that R-curve behavior led to negligible strength enhancements in an alumina that had bridging grains, quite simply because the natural flaws did

not have a chance to grow very far before going unstable. Their analytical and experimental results may easily be understood by the simple realization that in strong aluminas the flaws are only 5 to 20 times larger than the average grain size. The stable crack extension may involve only a few grains before the flaw goes critical and it is impossible to generate many behind-the-crack tip bridges. Perceptible strengthening would only occur in very weak specimens ($s < 100$ MPa) with large initial flaws. Fett and Munz also showed that the R-curve behavior in their aluminas had negligible effect on the Weibull distribution[102] contradicting predictions of dramatic improvements in Weibull modulus based on indentation mechanics analysis.[103]

Mecholsky et al.[104] and Marshall[97] suggest that a simple way to measure an effective R-curve is to measure strength and critical flaw size in strength test specimens and compute apparent K_c at fracture. Rising R-curves will be evident on a plot of K_c versus crack size. They showed evidence that the mirror to flaw size ratio changed significantly as a function of crack size.

The fractographer should keep the above factors in mind. As noted above, R-curve behavior does not leave any intrinsic telltale markings on the fracture surface. R curve behavior can throw off flaw size calculations if they are based on a single point value for fracture toughness in equations 7.7 or 7.22. In principle, the fractographer may be able to find a region of stable extension around a flaw, but in practice this may be difficult especially if the toughening phenomena and the microstructure produce a rough fracture surface. One indication of potential R-curve behavior may be a systematic $c_{calc} \neq c_{meas}$ trend. As noted previously, if the fractographer detects and measures only the initial flaw size, then $c_{calc} > c_{meas}$. In this case it is the fractographic size measurement that is off. Alternatively, if stable crack extension due to R-curve behavior does occur, but the fractographer uses a long crack (plateau) value of fracture toughness, then the fracture toughness is overestimated and the calculated crack size is wrong, and again $c_{calc} > c_{meas}$.

A rising R-curve does not necessarily translate to superior mechanical properties. Careful microstructural control is usually required. If reinforcing agents are not well dispersed and are clumped together, they can act as strength-limiting flaws. Alternatively, local regions depleted of the reinforcing elements may also have ordinary flaws. Many toughened ceramics have not shown commensurate increases in strength or Weibull moduli (which is a measure on consistency of strengths as discussed in section 7.15), contrary to expectations. The reason is simple. The very microstructural changes that enhance crack-microstructure interactions also create non-uniform microstructural regions, flaws, and microflaw concentration regions. That is

why Y-TZP with a modest fracture toughness of 5 MPaÖm to 6 MPaÖm is stronger than Mg-PSZ. The Y-TZP has a very uniform sub-micron grain size and small » 20 mm diameter pore flaws (Figure 6.6f). The Mg-PSZ has a fracture toughness of up to 10 to 20 MPaÖm, but a coarse-grain microstructure loaded with grain boundary faults and concentrations of micropores (Figures 6.98 and 6.99). The flaw size may be hundreds of mm in size.

7.12 Indentation Mechanics

A substantial literature exists on the mechanics of flaws made with Vickers or Knoop indentations. The author strongly prefers the Knoop indenter for reasons explained below, but, in brief, the Vickers crack is far from a controlled flaw. There is a complex damage zone underneath the Vickers indenter and the myriad of cracks around it that vary dramatically between different ceramics (covalent or ionic bonded), glasses and single crystals.

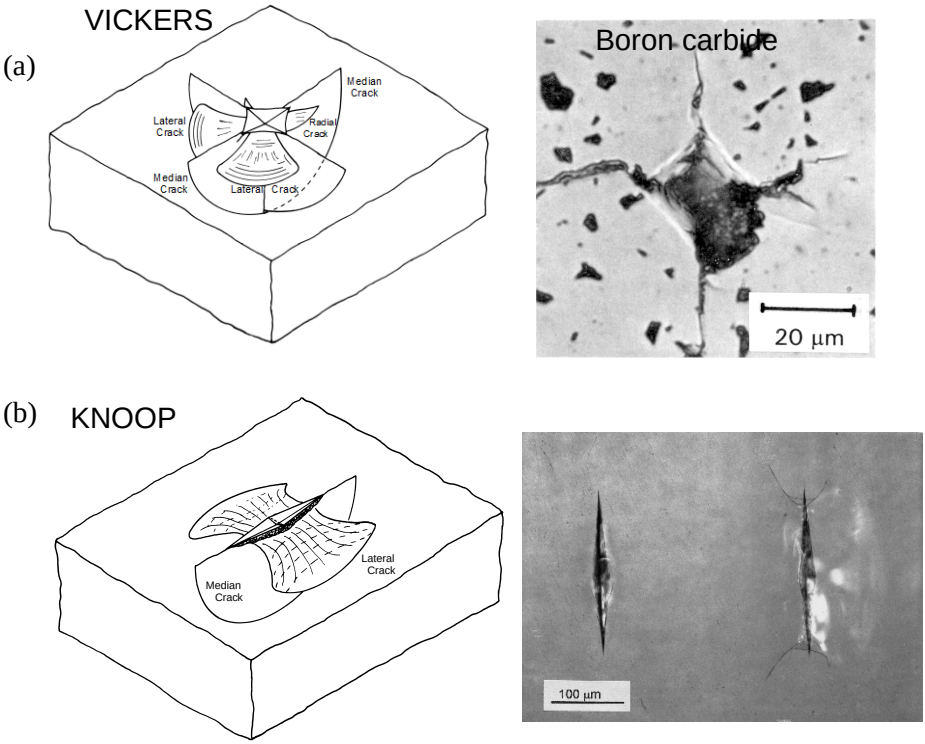

Figure 7.37 *Indentation generated damage sites. (a) shows a Vickers indentation in a ceramic. (b) shows a Knoop indentation in BK-7 borosilicate glass. The author prefers the Knoop since it makes a simpler crack system.*

Figures 7.37 illustrate some of these "controlled flaws." The indentations create not only a residual impression that is measured in a hardness test, but cracks and a concentrated damage zone directly underneath the indentation.

Controlled flaws for fracture mechanics experiments should be made with the Knoop indenter.[105,106] The flaw geometry is simpler and more easily controlled. Loads of 19.6 N to 294 N are used to create a semi-elliptical surface cracks in ceramic bend bars (Figure 7.38). Loads of 19.6 N to 29.4 N are used for glasses. The indentation residual stress damage zone and any lateral cracks are removed by polishing and then the test piece broken in flexure. The removal of the damage zone and the residual stresses is critical and a major reason why this Knoop method gives superior results compared to the Vickers system. Fractographic techniques are used to find and measure the flaw size. Other Knoop precrack examples are shown throughout this Guide including Figures 3.27, 5.60, 6.71 and 6.72. Calculations are simple. The Newman-Raju stress intensity shape factors described in section 7.5.3.1 are used with equation 7.6 to compute stress intensities. The name of the method was changed from "controlled surface flaw" to the "surface crack in flexure (SCF)" method by the author in 1994 in order to avoid confusion with some Vickers indentation methods and to also use nomenclature then in use in the fracture mechanics community.[107] The SCF procedure was the primary method used to prepare the world's first standard reference material (SRM 2100) for the property fracture toughness, K_{Ic}.[54,108] It was formally standardized by the American Society for Testing and Materials as C 1421,[53,109] the European Committee for Standards as CEN 14425,[110] and the International Organization for Standards as ISO 18756.[58] The method does not work on soft, porous, or very tough materials, since median cracks will not form. Details on the SCF method are in these standards and in References 106 and 107.

Vickers indentation procedures are widely used since they usually do not require fractographic examination. This supposed advantage leads to severe drawbacks with the method, however. The method produces inaccurate results (compared to standardized, valid fracture toughness tests) and although it has been claimed that it can be used at least for comparative purposes, many studies have shown that even this is not true. In 2006[111] and 2007[112] the author and Prof. R. Bradt wrote about the limitations of Vickers indentations for fracture mechanics studies. Vickers generated flaws are much more complex than Knoop median cracks and, since the Vickers flaws are tested without removal of the residual stresses and damage zones, all sorts of complications arise. Rather than a single median crack, Vickers indentations have multiple median, radial, and lateral cracks. The cracks also have a complex stress residual stress

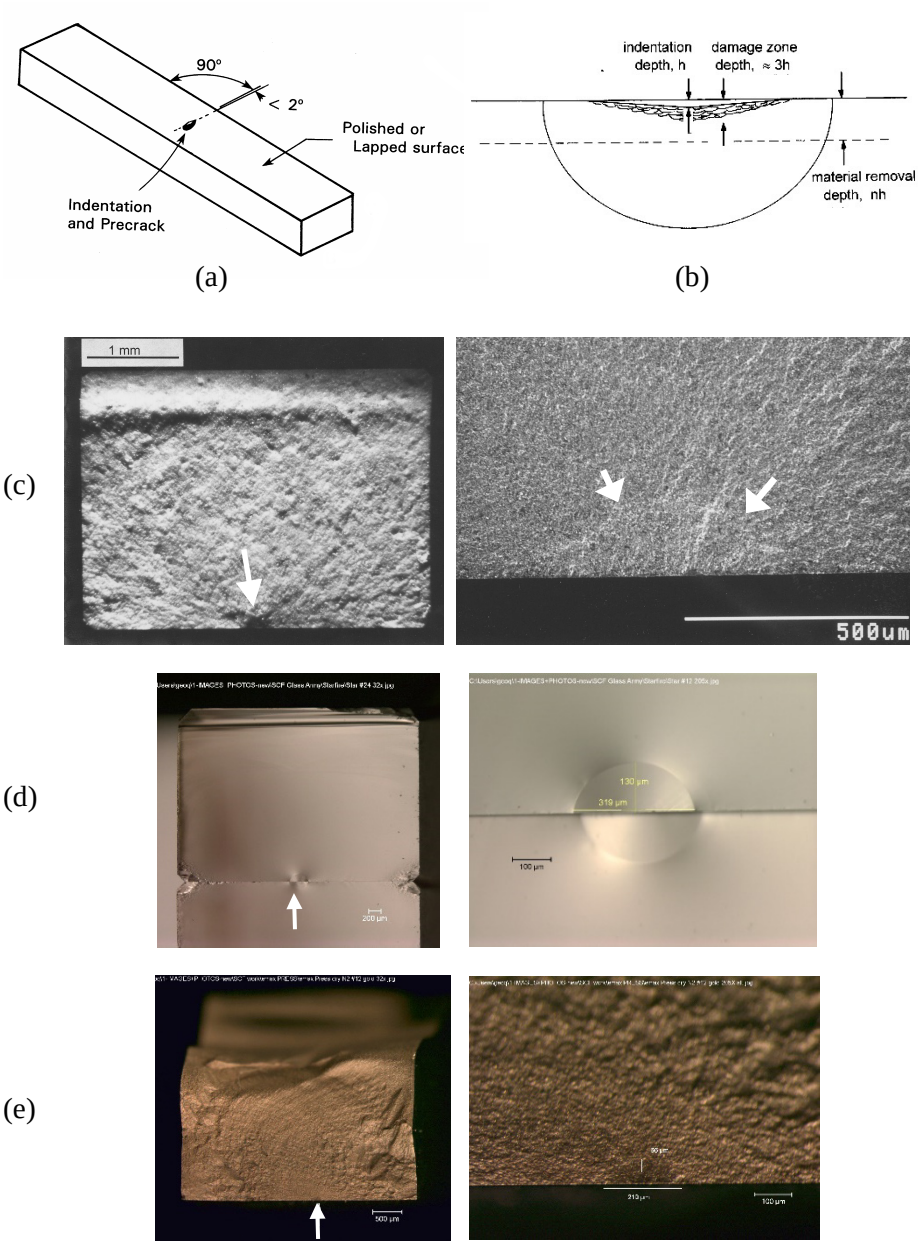

Figure 7.38 *The surface crack in flexure (SCF) method uses a Knoop indenter to create surface cracks in bend bars (a). (b) shows a section view of the indentation and the median crack below it. The damage zone is removed by polishing or hand grinding. (c) low and high magnification images of precracks in two different silicon nitrides. (d) precracks in soda lime silica glass. (e) precrack in a gold-coated IPS e.max Press lithium disilicate bar.*

damage associated with them.[113,114] Rather than envision these Vickers indentation sites as model flaws with discrete median cracks with a modest residual stress pulling on the faces, it is actually more appropriate to regard them as Vickers *damage zones*. A semicircular median crack is typically assumed to pop in underneath the indentation, although the crack type and formation sequence is quite complicated and varies dramatically with material.[115,116,117] The residual stress damage zone is approximated by a point force acting to open the crack. The stress intensity factor K_{Ir} acting on the flaw in this case has the same form of relationship shown in Figure 7.20b at the beginning of this chapter, namely:

$$K_{Ir} = c\frac{P}{c^{1.5}} \tag{7.32}$$

where c is the crack size, P is the indentation load, and c is a constant that incorporates geometry and residual stress field factors. If a test piece with a Vickers flaw is broken, K_{Ir} combines with the stress intensity created by a far field tensile stress to produce a total K_I:

$$K_I = Y\sigma_a\sqrt{c} + c\frac{P}{c^{1.5}} \tag{7.33}$$

The first term on the right dominates for large cracks. The second term is significant for small crack sizes, but rapidly diminishes as the crack extends away from the residual stress damage zone. The net effect of the two terms is to cause a crack to extend stably somewhat prior to catastrophic propagation. The extent of stable propagation has been estimated to be 2.5 times the original flaw size when the testing is done in inert environment and all the assumptions in the analysis are upheld.[114]

It is clear from above that the local residual stresses dramatically alter the local stress intensity field, and that a simple application of equations 7.6 (eq. 7.33 without the second term on the right) based on only the far-field tensile stresses, will be faulty. Typically c_{calc} will be larger than c_{meas}, if the latter is the original flaw size and stable crack extension is not detected.

By the time the crack propagates to the extent that it is forming the mirror boundary markings, the effect of the localized residual stress at the origin site is insignificant.[118] Hence, the mirror size is unaffected by the indentation residual stresses and the stress-mirror size relationship equation 7.4 is unaffected. The mirror to *initial* flaw size ratio (see Section 7.7 earlier in this chapter) is affected, however, and can be larger than values for annealed flaws.[118] That study produced some very unusual low R/c ratio that fall well below the usual ratios of 10 to 13 in glasses, even for plates annealed after indentation. It is

suggested that this is yet again a manifestation of the disorder of the Vickers indentation damage zone. Very localized indentation residual stresses do not affect branching distances or the fragmentation patterns. Evidence of stable crack extension from indentation localized residual stresses may be difficult to detect on fracture surfaces. Figure 5.62 in chapter 5 shows a rare example in a fine-grained silicon nitride. Stable extension is most often detected in laboratory conditions with careful microscopy on a polished outer surface, or through the material if the material is transparent.

The observant reader will note that Vickers indentation flaws do not resemble the majority of origins shown in Chapter 6. Notwithstanding claims to the contrary, it is not at all clear whether indentation damage sites simulate genuine flaws in ceramics and glasses. They may model contact damage sites and/or machining cracks, but Figure 6.35 in the previous chapter shows that actual contact damage sites are often more irregular, with significant amounts of material removed by lateral cracks and spalls. The contact-generated residual stresses are often partially or completely relieved. Service impact conditions are rarely as controlled as those in an indentation process, where an ideal diamond slowly applies load perpendicular to the surface.

The localized indentation residual stress field of a laboratory indentation has a very stabilizing influence on a flaw, allowing it to have extensive stable extension that may not be experienced by genuine flaws. The previous section on R-curve effects mentioned some examples where predictions of enhanced Weibull modulus based on indentation flaw analysis were misleading or wrong.

In summary, there has been an over reliance on Vickers indentation flaws. From some of the literature one might think that are they are more important than genuine flaws. Fractographers know otherwise.

7.13 Fractal Analysis

7.13.1 General

Fractal analysis has been applied to fracture problems in two ways: to the analysis of breakage patterns as a crack branches and divides a part into pieces (fragmentation), and to analysis of the tortuosity or roughness of fracture surfaces. These are covered separately in the next two sections, but first some general principles of fractal analysis are presented. Advocates of fractal analysis contend that it can assist in interpretation of fragmentation patterns, or can link fracture behavior at a fundamental level to material properties. There are many skeptics.

Fractal geometry is a non-Euclidean geometry that exhibits self-similarity and scale invariance. Self-similarity means that a geometric shape in one location is similar to a geometric shape elsewhere. Scale invariance means that the geometric shape is similar irrespective of its size.

Classical Euclidean geometry has a simple relationship between area and length. For example, a circle of diameter D has the well-known relationships in accordance with Euclidean geometry:

$$Area = \rho D^2 / 4 \tag{7.34}$$

and

$$Perimeter = \rho D \tag{7.35}$$

so that:

$$Perimeter \ \mu \ \sqrt{Area} \tag{7.36}$$

This is the case for a perimeter line that is unwavering and follows the circle rim exactly. If on the other hand, the perimeter line has perturbations and wiggles, the perimeter length is greater. If the perimeter line is magnified and studied in greater detail, it is possible that each wiggle or perturbation itself may be seen to have yet smaller wiggles creating additional length and so on. That is the nature of fractal dimensions. The greater the magnification used, and the finer the measuring stick used to measure the lengths, the longer is the overall perimeter length. This leads to the somewhat paradoxical outcome that the perimeter length varies with magnification and the size of the measuring scale. The perimeter of a fractal shape around an area can be characterized by the following relationship:

$$L = L_0 s^{1-D} \tag{7.37}$$

where L is the length of the line, L_o is a constant, s is the measuring scale or ruler size, and D is the *fractal dimension* which in this instance is between 1 and 2. If the line has no wiggles (and is a Euclidean line) then D = 1, and $L = L_o$ irrespective of the size of ruler used to measure it. On the other hand, if the line is fractal and D is between 1 and 2, then L varies with the size of the ruler. The exponent of s in equation 7.37 is negative and the smaller it is, the larger is L. The value of D-1 is often written as D^*, the fractional part of the fractal dimension. For example, a fractal dimension D might be 1.1 in which case D* = 0.1. Fractal analysis usually involves measuring L by using rulers of different sizes, s, and plotting the log of L versus the log of s.

A similar relationship as 7.37 may be written if areas are used in which case D would have a value between 2 and 3.

7.13.2 Fractal analysis of fragmentation

Patterns of fragmentation were discussed in chapter 4 and in section 7.2 on quantitative aspects of fragmentation. At first glance, fractal analysis seems to be a potentially useful approach to analyzing component fragmentation, but there are many complications. Fragmentation starts with crack branching from the fracture origin. These rebranch to make a treelike pattern, a process that might be analyzed by fractal analysis. Secondary breakages of fragments may be less amenable to fractal analysis. Obviously, the greater the stress and energy in the part when it fractures, the greater the degree of fragmentation. Examples of the initial fracture patterns are by Sakai *et al*. for fractures of laminated safety glass panels, [119,120] and G. W. Quinn *et al*. for ring-on-ring tested glass disks.[121] Figure 7.39 is an example from the latter work showing an actual glass disk fracture and a computer- generated pattern using fractal

(a)

(b)

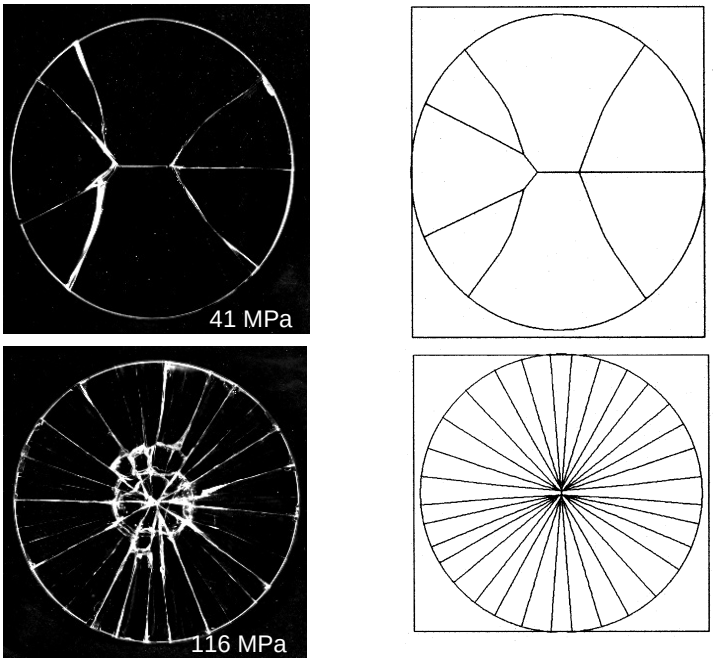

Figure 7.39 *Glass disks (76 mm diameter by 5.3 mm thick Schott BK-7) fractured in ring-on ring strength tests (31.8 mm x 63.5 mm diameters). Some of the radial cracks in (b) are faint but do reach the outer rim. The right side shows comparable computer-generated model fractures. The part-circumferential cracks in the disk in (b) are secondary bending fractures of the initial wedge-shaped fragments. This is a different fracture process and loading mode and is not reflected in the model pattern. (Ref. 121)*

analysis with some simple assumptions about the nature of propagating cracks. It is necessary to make some key assumptions about how cracks propagate and branch such as: how the cracks curve, how they interact with each other, how they partition the specimen, how the initial stresses (and the biaxiality) vary with location within the specimen, how the cracks themselves alter the stress distributions as they propagate, and how reverberations of elastic waves from specimen edges affect the cracks. Primary radiating cracks seem to repel each other (as discussed in section 4.3 on crack branching angles). Sometimes they tend to partition the specimen into fragments of approximately equal area, probably to evenly distribute the strain energies. In fact, with reference to Figure 7.39b, it can be argued that the fast, nearly parallel radial cracks unload each other. Furthermore, secondary cracking that occurs in the fragments created by the initial fracture pattern can be a serious complication to fractal analysis. Figure 7.39b shows an example where circumferential secondary breaks were completely missed in the fractal model. The formation of these secondary "cross cracks," that are a form of circumferential cracking, was discussed in section 4.6.3 in Chapter 4. Sometimes the fast-running radial cracks branch sideways, and the branches can run over and stop at a nearby radial crack, or they may jump over a few radial cracks before they are arrested. In other cases, once the primary radial cracks run out to the rim, the pie-wedge shaped pieces are subjected to bending stresses in the ring-on-ring test fixture causing them to break off in bending. In other words, this shift in the loading conditions caused a whole new family of secondary cracks. Similar events can occur in windows.

As a consequence of these additional factors, the realistic modelling of crack and fragmentation patterns is very complex. Rudimentary fractal models that simply partition a component into interesting geometric shapes overlook these complications and should be viewed with skepticism.

7.13.3 Fractal analysis of the fracture surface

Fractal analysis may be used as a tool to characterize the area of a surface and its roughness or unevenness. D will be between 2 and 3. Fractal analysis is unlike classical surface roughness measurements that characterize the heights between peaks and valleys. Fractal analysis measures the extent of the "wiggliness," "tortuosity," or irregularity of the surface.[122,123] Fractal analysis may be used to analyze a parameter, R_s, the ratio of the actual fracture surface area to the projected surface area.[124]

Two ways to measure the fractal dimension of a fracture surface are the fracture profile technique and the slit island analysis.[123] The fracture profile

technique simply makes a vertical cross section through a fracture surface. The cross section is a jagged line whose profile with all its ups and downs is analyzed. The length of the line is measured using rulers of different sizes. In the slit island technique, a horizontal cross section is made through a fracture surface to reveal islands corresponding to the peaks of hills and ridges and their wiggly outlines. The length of the island perimeters is measured with different ruler sizes. Alternatively, the area of the exposed islands can be measured using many miniature box squares of size s^2. This process is repeated with different box sizes. Repeat measurements are made much like in a classical metallographic serial section analysis. Both procedures can be tedious, but computer analysis and image analysis software can simplify this task. Confocal optical microscopy would seem to be an ideal tool, since it may be able to examine the fracture surface directly and section it automatically without the need for repetitive polishing.[125,126] A typical fractal analysis measures a perimeter length or roughness number with finer and finer measuring intervals. A graph of log L versus log s is constructed and the slope is used to estimate the fractal dimension.

There are limits to these fracture surface analyses, however, and deviations from the linear trends (on log-log plots) have been noted at both large and small ruler sizes.[126] Limitations of atomic size, or coarse pixel sizes in automatic image analyses, can cause asymptotic deviations from the expected trend. Obviously, there are practical limits on how broad a size range one may apply fractal analysis. Experience also has shown there can be variations in the reported fractal dimensions due to subjective interpretation.

Fractal analysis has usually been used to correlate fracture toughness with the fractal dimension of the fracture surface. The processes that enhance fracture toughness often increase the roughness of a fracture surface. Passoja, Mecholsky and colleagues have pioneered correlations of this type for ceramics.[122,123,127,128] For example, they have shown that:

$$K_{Ic} = K_o + A\left(D^*\right)^{1/2} \tag{7.38}$$

where K_o is a baseline toughness of the material for a smooth (Euclidean) fracture surface, D^* is the fractional part of the fractal dimension and A is a constant that can be related to the elastic modulus and the atomic dimensions of the structure of the material. The implication of this relationship is that only a small portion of a fracture surface is needed to determine the fracture toughness. In principle, this could be used in forensic analyses to determine if the material was poorly processed and had a lower-than-expected fracture

toughness. The fractal analysis gives no information about the fracture origin, however.

Mecholsky and Freiman[128] showed that variations in the mirror to flaw size ratio correlated with the fractal dimension of the fracture surface well outside the mirror:

$$\frac{R}{c} \mu \frac{1}{D^*} \tag{7.39}$$

where R is either the mirror-mist, mist-hackle, or branching distance, and c is the flaw size. They used a slit island method but with replicas of the fracture surfaces and only a narrow range of ruler sizes which raises some concerns.

Sometimes there may be a correlation of fractal dimension to the fracture toughness or fracture surface energy, but often there is not. Morrell's Guide to fractography[129] cited several studies where fracture toughness did not correlate to the fractal dimension. One puzzling aspect of fractal analysis is that it ignores the directionality of fracture surface markings. Features like hackle lines run in the direction of crack propagation creating ridges and valleys. It is very questionable whether surface scans parallel and perpendicular to the direction of these features would have the same fractal character. The author is not aware of any instances where fractal analysis has helped solve a practical fracture problem.

7.14 Estimation of Residual Stresses

7.14.1 Introduction

Residual stresses may exist on many levels as discussed in section 4.19.6. They may be local to a flaw, as in a Vickers indentation or an inclusion with a mismatch in properties with the matrix. They may be distributed through the thickness, as in surface compression and internal tension in chemically- or thermally-tempered glasses. They may be global from differential shrinkage during firing. Their effects on flaws may be very difficult to analyze unless some assumptions are made about their character and distribution.

For example, residual stresses from grinding vary with direction, whether parallel to or perpendicular to the grinding direction. They are strongly compressive right at the surface, but rapidly decrease and become tensile a short distance (5 mm to 20 mm) below the surface. The tip of a grinding crack may be in tension or in compression depending upon how deep it is. The net effect of the stress gradient on the flaw as a whole is a complex fracture

mechanics problem, but analytical attempts have been made to determine the effect on flaws with mixed success. The reader is referred to the work of Hollstein et al.[130] for a good example. It is often difficult to determine whether the net effect is tensile or compressive. The weak point in these analyses is the lack of adequate quantitative information about the residual stress spatial profile.

7.14.2 Estimates of residual stresses from fragmentation

Empirical estimation of residual stresses in tempered glass plates by fragmentation patterns has been covered in sections 7.2.2 and 7.3.2.

7.14.3 Estimates of residual stresses from fracture mechanics analysis of flaws

The usual approach in dealing with residual stress problems is to rely on the principle of superposition. That is, the effect of stresses on a location or flaw in a body is additive, whether the stresses are mechanical, transient thermal, or residual. To a first approximation, residual stresses, s_r, simply add to or subtract from the applied stresses acting on the flaw from known external sources, s_a, so that the net stress acting on a site or a flaw is:

$$s_{net} = s_a + s_r \tag{7.40}$$

Tensile residual stresses add to externally-applied tensile stresses and reduce the external stresses or forces necessary to cause fracture from a particular flaw. Compressive residual stresses acting on a flaw must be overcome and require greater applied stresses. (The usual convention is that compressive stresses are negative.) For the case of a flaw loaded with a far-field stress s_a with a residual stress s_r that is constant in the vicinity of the flaw:

$$K_{Ic} = Y s_{net} \sqrt{a} \tag{7.41}$$

Rearranging:

$$s_r = \frac{K_{Ic}}{Y\sqrt{a}} - s_a \tag{7.42}$$

If a convenient flaw is found that has a shape that is conducive to a fracture mechanics analyses and K_{Ic}, s_a, and the flaw size, a, are known, then equation 7.42 can be used to estimate s_r. This is the residual stress present at the flaw site. There may be a residual stress gradient with location. Similarly, if the applied stresses have a gradient, then s_a must be adjusted for flaw location.

7.14.4 Estimates of residual stresses from fracture mirror size analysis

Residual stresses can cause systematic deviations in the stress - mirror size trends presented previously. Trend deviations are shown in Figure 7.40. The easiest interpretation is in Figure 7.40a, whereby a nonzero intercept indicates the magnitude and sign of the residual stress. A compressive residual stress shifts the line upward since a greater applied stress, s_a, is necessary to cause fracture.

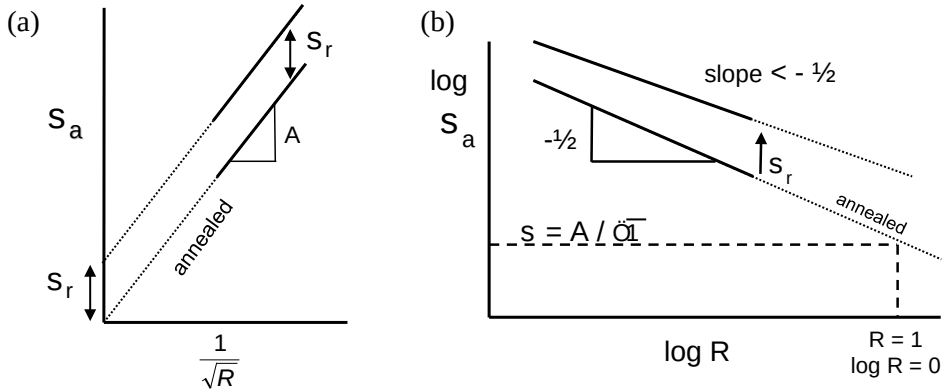

Figure 7.40 *Systematic deviations in the fracture mirror size trends for applied stress, s_a, as a function of mirror radius are indicative of residual stresses. (a) shows that residual stresses create nonzero intercepts. (b) shows that residual stresses alter the slope.*

If a single mirror is measured and the externally applied stress, s_a, is known, then:

$$(s_a + s_r)\sqrt{R} = A \tag{7.43}$$

and

$$s_r = \frac{A}{\sqrt{R}} - s_a \tag{7.44}$$

A good example of the application of this approach of measuring mirror-mist and mist—hackle boundaries on glass rods with cladding is in a paper by Mecholsky and Drexhage.[131] Similarly, the branching distances were used by Conway and Mecholsky [132] to estimate residual stresses in tempered glass plates. Additional details by this method are in Appendix D. The reader is reminded that an offset <u>does not necessarily mean</u> there is a residual stress. As noted earlier in this chapter in section 7.4.1 above, small offsets of the order of

10 MPa have been observed in annealed glass plates and disks where presumably there are no residual stresses.[28,29] The 10 MPa may be an intrinsic threshold stress necessary for forking to occur.

7.14.5 Estimates of residual stresses from indentation crack sizes

Surface residual stresses may be estimated by measuring the crack lengths emanating from the corners of Vickers indentations in a variation of the procedure described in section 7.12. If there are surface compression stresses, then the indentation crack lengths (c) at a particular indentation load (P) will be shorter than those in for an annealed piece of material.[133,134] Assuming that the indentation crack slows down and stops at $K_I = K_{Ic}$, and that environmentally-assisted slow crack growth doesn't affect its length, then:

$$K_{Ic} = \chi \frac{P}{c^{1.5}} + Y\sigma_r\sqrt{c} \qquad (7.45)$$

where c is the dimensionless contact constant which incorporates details of the indenter specimen contact conditions. Testing is usually done over a range of loads and crack lengths. This methodology is susceptible to all of the shortcomings addressed in section 7.12. If a test piece with residual stresses is indented and then broken, say in a plate or bend bar form, then the stress intensities acting on the crack sum:

$$K_{Ic} = Y\left(s_a + s_r\right)\sqrt{c} + c\frac{P}{c^{1.5}} \qquad (7.46)$$

where s_a is the applied stress from external loading, s_r is the surface residual stresses at the location of the flaw, and the last term on the right is the stress intensity from localized indentation residual stresses. In practice, considering all the assumptions in indentation analysis, and the probable stress gradients, it may be difficult to reliably solve this equation to obtain s_r.

7.14.6 Estimates of residual stresses by other means

Qualitative assessments can be made from mirror shapes as discussed in section 5.2.5 and also by changes in the mirror to flaw size ratio in section 7.7.

7.15 Weibull Analysis

Ceramic and glass strengths depend upon the size and shape of the specimens and the mode of loading. Specimen strengths vary due to variations in the size, severity, location, and density of flaws. Strength variability is usually analyzed in accordance with the Weibull distribution,[135,136,137] that is based on

the premise that the weakest link in a body controls strength. A strength test produces two key bits of information: a strength datum and a fracture origin flaw. The flaws are just as important as the strength. "Flaw management" is an important strategy for process control and reliability improvements. The Weibull two-parameter distribution is:

$$P_f = 1. - \exp^{-\left(\frac{s_a}{s_q}\right)^m} \tag{7.47}$$

where P_f is the probability of fracture, s_a is the applied stress, and m and s_q are constants called the Weibull modulus and the characteristic strength of the specimen, respectively. Strength data is typically ranked from weakest to strongest and then plotted on a special set of axes intended to linearize the data as shown in Figure 7.41.

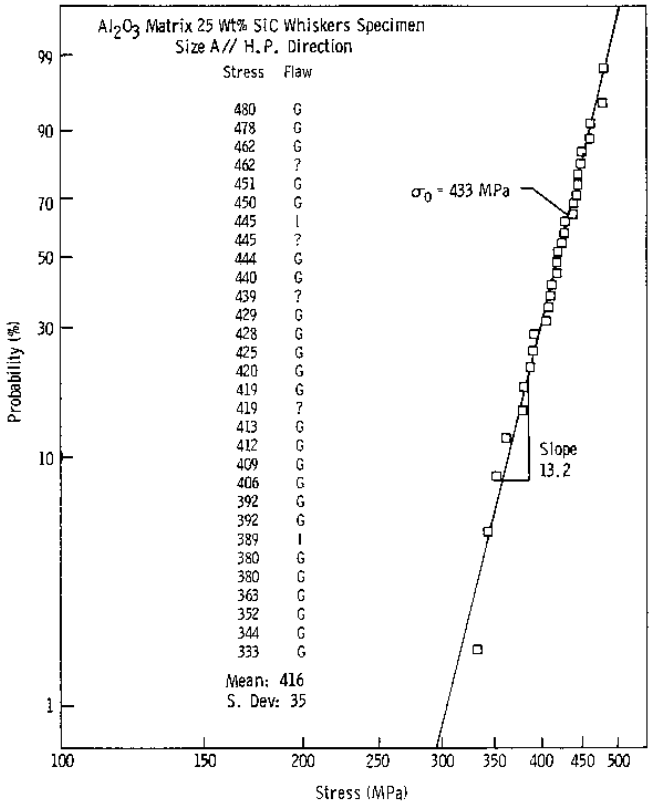

Figure 7.41 *Fractographically-labeled Weibull graph. Four-point flexural strength data for a SiC whisker-reinforced alumina. "G' is an abbreviation for a large grain origin type, "I" is for inclusion, and "?" is unknown. The slope of the fitted line is Weibull modulus (m), a measure of strength variability.*

With Weibull analyses, the maximum nominal stress in the body is used. Stress is not adjusted for location. For example, it is correct to use the maximum outer fiber stress for bend bar or biaxial disk strengths. If the data fits the Weibull distribution, then it should fit on a line with the slope equal to the Weibull modulus, m, and the characteristic strength s_q corresponding to the strength of the specific test specimen configuration at the 63.2 % level. Figure 7.41 shows a data set with 100 % fractographic analysis: every specimen was examined. The goodness of fit to the Weibull function can be assessed by eyeball by comparing the fitted line to the data. The graph is fractographically-labeled and has not only the individual strength values, but also the flaw identities. The strength-controlling flaws were almost always large alumina grains designated "G." Figure 7.42 shows one example. The whiskers that were added to enhance K_{Ic} had chemistries or impurities that caused grain growth in the alumina matrix. The good news was that one flaw type primarily controlled strength and the Weibull distribution fit quite well.

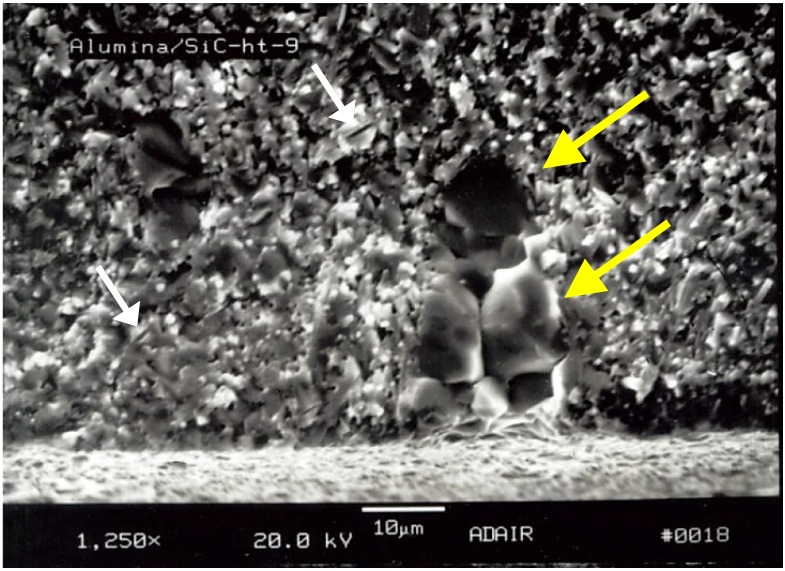

Figure 7.42 Fracture origin in one of the alumina/SiC whisker bend bars. The origin is a cluster of large grains marked by the large yellow arrow. The SiC whiskers are quite small. Two are marked by the small white arrows. (Courtesy J. Swab)

In contrast, Figure 7.43 shows a SiAlON material that had many different concurrent flaw types and a very low Weibull modulus.[138] Brittle materials design with such a material would be problematic, since each flaw type has its

own distribution. In principle, "censored statistics" could deal with each flaw type, but in this instance, there are so many flaw types active that it would be a desperate exercise. This is particularly true since each flaw type only manifests itself in a few test pieces. Strength scaling with size would be complicated. The tester might have wondered why the curve had so many wiggles. The fractographic analysis makes it clear why the single Weibull line does not fit very well. Weibull originally derived his distribution on semi-empirical grounds. He recognized that flaws could control strength in brittle materials,[136,137] but did not consider their size or distribution. His 1951 paper said nothing about flaws.[135] He simply assumed that small elements in a body had a local strength. He chose a plausible distribution for the local variations in strength. He then integrated the risk of rupture for all elements to compute the failure probability for the whole specimen assuming that fracture would occur at the weakest link or element. His perceptive analysis has been theoretically verified by subsequent analyses by a number of authors, but most especially by Jayatilaka and Trustrum.[139,140] They showed that flaw size distributions could

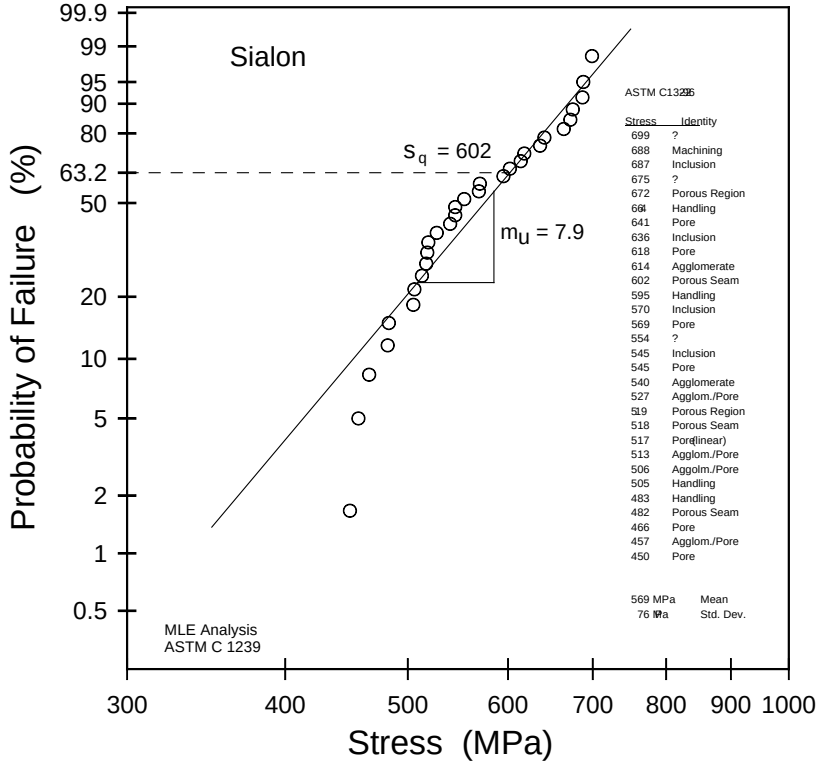

Figure 7.43 *Fractographically-labeled Weibull graph. Four-point flexural strength data for a SiAlON ceramic (Reference 138).*

have the large flaw size tails matched by an inverse power law distribution as shown in Figure 7.44. Using this inverse power law distribution and applying classical fracture mechanics (equation 7.7), and weakest-link theory, they were able to mathematically derive the Weibull distribution. The Weibull modulus (m) is directly related the flaw size distribution exponent (n'). The Weibull distribution is now based on a solid theoretical footing. Danzer has considered more general distributions, but concluded that if the frequency of flaws follows the inverse power law, then the material may be deemed a "Weibull material.[141] In the 1990s and 2000s, a number of studies confirmed the large flaw size distribution tails can indeed be matched by the inverse power law. The reader is referred to papers by Prof. Uematsu in the Origins in Ceramics section of Appendix A for many examples. The Quinn and Morrell paper [142] has a useful

$$H'(c) = \text{constant} * \exp^{-\left(\frac{a}{c}\right)} c^{-n'}$$

(a)

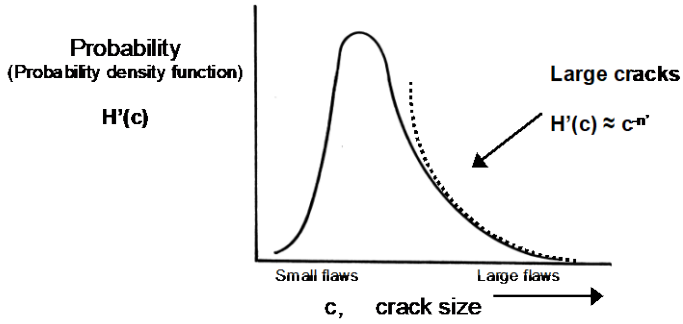

(b)

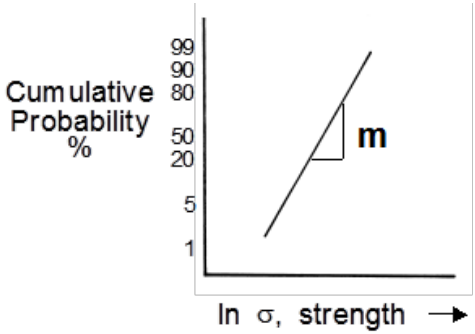

m = 2n' -2

Figure 7.44 *The Weibull distribution can be derived from the flaw size distribution shown in (a). H'(c) is the probability for occurrence of a flaw of size c. n' and a are constants. The largest flaws control strength and that portion of the distribution can be modeled by an inverse power law with exponent n'. (b) shows the Weibull distribution for strength. The Weibull modulus m is equal to 2n' – 2.*

review of a number of successful applications using Weibull analysis and it lists all of the assumptions necessary for Weibull strength scaling with size.

Average bulk properties such as density, surface finish, or grain size often do not correlate with strength. Strength often depends upon infrequent or aberrant microstructural features, namely flaws, and not on the average microstructure. In some cases, the aberrant features do scale with the average microstructure, so there may be a correlation between strength and average grain size or surface finish.

One important aspect of the Weibull model is that the larger the structure or test piece is, the more likely it is to contain a severe flaw. Hence, strength usually varies inversely with component size: the larger the component, the weaker it is likely to be. Strengths can be correlated or scaled by comparing effective volumes or effective surfaces. It is beyond the scope of this Guide to delve into this topic, but suffice to say that such strength scaling analyses depend upon crucial assumptions. For example, a Weibull effective volume scaling approach is justified if fractography confirms that strength limiting flaws are volume-distributed. One often overlooked assumption in the Weibull analysis is that specimens must contain a minimum number of flaws. There must be a number of "chain links" present in the specimen for it to have strength controlled by a "weakest link." A specimen with a single flaw has only one strength controlling link. Therefore, it is inappropriate to apply Weibull statistics to specimens with a single indentation flaw. It is also dangerous for engineers to ignore or discard a few specimens from the low strength tail of a Weibull distribution. These "atypical" or "non representative outcomes" may reflect a genuine flaw type that will cause trouble if the product is scaled up for mass production or if the components are designed to have very low probabilities of fracture (e.g., $P_f << 1\%$).

Strength scaling analyses become very complex if more than one flaw type (e.g., pores and inclusions; or pores, inclusions, and machining damage) controls strength such as the SiAlON case shown in Figure 7.43. Various flaw types may suddenly appear or disappear as strength controlling flaws as component sizes are scaled up or down. See the Quinn and Morrell review[142] for more information on these fascinating topics. Sung and Nicholson published results on a good study[143] where fractography was effectively used to identify five different flaw types in a 4 mass % yttria-stabilized, tetragonal polycrystal material: fiber burn-out pores, agglomerates, iron inclusions, alumina inclusions, and pores. By careful process control and flaw management, they were able to eliminate two flaw types, and control the remaining three. Small pores, alumina inclusions, and agglomerates became

the primary strength-controlling flaws. That was an outstanding materials science study.

The author is often asked whether the Weibull distribution is the best for modeling strength variations, and my answer is always yes, but with some caveats. The Weibull distribution is the only one that the author knows of that permits size scaling of strength. Indeed, the ultimate proof that the Weibull distribution is valid is not whether one set of data can be plotted linearly on a Weibull graph, but whether size scaling is successful. In the dental materials community, confusion about the validity of the Weibull model prompted Dr. J. Quinn and the author to write a review article[144] on this topic. Everything in the review is applicable to other ceramics and glasses as well.

An amazing study on *5,100* alumina flexural strength specimens by Gorjan and Ambrožič [145] that confirmed the Weibull two-parameter distribution was perfectly suitable. It was better than the log normal, the normal, or the gamma distributions. The author congratulated them on their study and offered to do some fractography. Imagine the challenge! It was learned that they broke even more and had reached *11,700* tests. The Weibull distribution two parameter still held true. Regrettably, they did not save any specimens for the author to look at. What a pity!

Chapter 7 References

1. V. D. Fréchette, *Failure Analysis of Brittle Materials*, Advances in Ceramics, Vol. 28, American Ceramic Society, Westerville, OH, 1990.
2. L. Orr, "Practical Analysis of Fractures in Glass Windows," *Materials Research and Standards*, **12** [1] (1972) 21 - 23.
3. V. D. Fréchette and T. A. Michalske, "Fragmentation in Bursting Glass Containers," *Bull. Am. Ceram. Soc.*, **57** [4] (1978) 427 – 429.
4. V. D. Fréchette and S. L. Yates, "Fragmentation of Glass Bottles by Impact," *J. Am. Ceram. Soc*., **72** [6] (1989) 1060.
5. E. R. Fuller, Jr., S. W. Freiman, G. D. Quinn, J. B. Quinn, and W. C. Carter, "Fracture Mechanics Approach to the Design of Glass Aircraft Windows: A Case Study," pp. 419 – 430 in *Proc. SPIE Symp. on Windows and Dome Technologies and Materials, IV,* 24-29 July 1994, San Diego, CA, SPIE Volume 2286.
6. R. Morrell, "Fractography of Brittle Materials," Measurement Good Practice Guide, #15, National Physical Laboratory, Teddington, Middlesex, UK, 1999.
7. E. B. Shand, "New Information on Glass Fracture," pp. 117 – 128 in *Proc. Amer. Scientific Glass Blowers Soc. Symp*., June, 1969.
8. F. Kerkhof, "Bruchmechanische Analyse von Schadensfällen an Gläsern, *Glastechnische Ber.* **48** (1975) 112 - 124.
9. J. Wang, "Fracture and Stress Pattern Correlations in Glass Plates," Masters Thesis, Texas Tech Univ., August, 1986.

10. R. A. McMaster, D. M. Shetterly, and A. G. Bueno, "Annealed and Tempered Glass," pp. 453 - 459 in *Engineered Materials Handbook*, Vol. 4, *Ceramics and Glasses*, S. Schneider, ed., ASM, Metals Park, OH, 1991.
11. N. Shinkai, "The Fracture and Fractography of Flat Glass," pp. 253 - 297 in *Fractography of Glass*, eds. R. C. Bradt and R. E. Tressler, Plenum, NY, 1994.
12. K. Akeyoshi, E. Kanai, K. Yamamoto, and S. Shima, Asahi Garasu Kenkyu Hokoku, Report of the Research Lab, Asahi Glass Co., **17** [1] (1967) 23 - 26.
13. K. Akeyoshi and E. Kanai, "Mechanical Properties of Tempered Glass," pp. 80.0 to 80.8 in Proceedings of the 7th Int. Glass Congress (Brussels), Vol. 14 (1965).
14. N. Pourmoghaddam and J. Schneider, "Experimental Investigation into the Fragment Size of Tempered Glass, *Glass Struct. Eng*., **3** (2018) 167 - 181.
15. H. Lee, S. Cho, K. Yoon, and J. Lee, "Glass Thickness and Fragmentation Behavior in Stressed Glasses," *New Jour. Glass and Ceram.*, **2** (2012) 138 – 143.
16. K. Blank, "Some Practical Aspects of Thermally Strengthened Glass," pp. 485 – 499 in *Strength of Inorganic Glass*, ed. C. Kurkjian, Plenum, NY, 1985.
17. J. M. Barsom, "Fracture of Tempered Glass," *J. Am. Ceram. Soc.*, **51** [2] (1968) 75 - 78.
18. R. Gardon, "Thermal Tempering of Glass," pp. 145 – 216 in *Glass: Science and Technology, Vol. 5, Elasticity and Strength in Glasses*, eds. D. R. Uhlmann and N. J. Kreidel, Academic Press, NY, 1980.
19. J. Menčík, "*Strength and Fracture of Glass and Ceramics*," Glass Science and Technology 12, Elsevier, NY, 1992.
20. D. Shetty, A. Rosenfield, and W. Duckworth, "Crack Branching in Ceramic Disks Subjected to Biaxial Flexure," *Comm. Am. Ceram. Soc.*, Jan. 1983, C10 - C12.
21. D. Hull, "Influence of Stress Intensity and Crack Speed on the Fracture Surface Topography: Mirror to Mist to Macroscopic Bifurcation," *J. Mat. Sci.*, **31** (1996) 4483 – 4492.
22. U. Soltesz, H. Richter, and E. Sommer, "Influence of Internal Stresses on the Development of Cracks in Glasses," pp. 2303 – 2310 in *Advances in Fracture Research*, eds. D. Francois et al., Pergamon Press, NY, 1980.
23. G. D. Quinn, "Guidelines for Measuring Fracture Mirrors," pp. 163 – 190 in: *Fractography of Glasses and Ceramics*, Vol. 5, eds. J. R. Varner, G. Quinn, M. Wightman, American Ceramic Society, Westerville, OH, 2007.
24. Private Communication, Letter from L. Orr to G. Quinn on December 15, 2001.
25. W. C. Levengood, "Effect of Origin Flaw Characterization on Glass Strength," *J. Appl. Phys.*, **29** [5] (1958) 820 – 826. See footnote on page 821.
26. M. J. Kerper and T. G. Scuderi, "Relation of Fracture Stress to the Fracture Pattern for Glass Rods of Various Diameters," *Cer. Bull.*, **45** [12] (1966) 1065 - 1066.
27. G. D. Quinn, J. Eichler, U. Eisele, and J. Rödel, "Fracture Mirrors in a Nanoscale 3Y-TZP," *J. Am. Ceram. Soc*., **87** [3] (2004) 513 - 516.
28. J. B. Quinn, "Extrapolation of Fracture Mirror and Crack-Branch Sizes to Large Dimensions in Biaxial Strength Tests of Glass," *J. Am. Ceram. Soc.*, **82** [8] (1999) 2126 - 2132.
29. D. R. Oakley, "Crack Branching in Float Glass Subjected to Biaxial Loading," *J. Non-Cryst. Sol.*, **196** (1996) 139 – 143.
30. J. J. Mecholsky, Jr. and R. W. Rice, "Fractographic Analysis of Biaxial Failure in Ceramics," pp. 185 – 193 in *Fractography of Ceramic and Metal Failures*, ASTM STP 827, eds., J. J. Mecholsky, Jr. and S. R. Powell, Jr., ASTM Int., 1984.
31 R. D. Maurer, R. A. Miller, D.D. Smith and J.C. Trondsen "Optimization of Optical Waveguides-Strength Studies," ONR Contract N00014-73C-0293, Corning Glass Works Technical Report, March 1974.

32. J. W. Johnson and D. G. Holloway, “On the Shape and Size of the Fracture Zones on Glass Fracture Surfaces,” *Phil. Mag.*, **14** (1966) 731 - 743.
33. E. B. Shand, “Breaking Stress of Glass Determined from Dimensions of Fracture Mirrors,” *J. Am. Ceram. Soc*., **42** [10] (1959) 474 – 477.
34. M. J. Kerper and T. G. Scuderi, “Relation of Strength of Thermally Tempered Glass to Fracture Mirror Size,” *Bull. Am. Ceram. Soc*., **44** [12] (1965) 953 – 955.
35. H. P. Kirchner, R. M. Gruver, and W. A. Sotter, “Fracture Stress-Mirror Size Relations for Polycrystalline Ceramics, *Phil. Mag*., **33** [5] 775 – 780 (1976).
36. *Glass Industry*, **36** [10] (1955) 523.
37. E. B. Shand, “Experimental Study of Fracture of Glass: II, Experimental Data,” *J. Am. Ceram. Soc*., **37** [12] (1954) 559 – 572.
38. N. Terao, “Sur une Relation entre la Resistance a la Rupture et le Foyer d’Eclatement du Verre,” *J. Phys. Soc. Japan*., **8** [4] (1953) 545 – 549.
39. H. P. Kirchner and J. W. Kirchner, “Fracture Mechanics of Fracture Mirrors,” *J. Am. Ceram. Soc*., **62** [3-4] (1979) 198 – 202.
40. H. P. Kirchner and J. C. Conway, Jr., “Criteria for Crack Branching in Cylindrical Rods: I, Tension; and II, Flexure,” *ibid*, **70** [6] (1987) 413 – 418 and 419 - 425.
41. H. P. Kirchner and R. M. Gruver, “Fracture Mirrors in Alumina Ceramics,” *Phil Mag*., **27** (1973) 1433 – 1446.
42. M. J. Kerper and T. G. Scuderi, “Modulus of Rupture of Glass in Relation to Fracture Pattern,” *Bull. Am. Ceram. Soc.*, **43** [9] (1964) 622 – 625.
43. N. Shinkai, “Fracture Mirror Constants of Silicate Glasses,” *Japan J. Appl. Phys.*, **14** [1] (1975) 147 - 148.
44. ASTM C 1678-07, Standard Practice for Fractographic Analysis of Fracture Mirror Sizes in Ceramics and Glasses, *Annual Book of Standards*, Vol. 15.01, ASTM, West Conshohocken, PA, 2007.
45. A. A. Griffith, “The Phenomena of Rupture and Flow in Solids,” *Philos. Trans. R. Soc. Lond*., **A221** (1920) 163 – 198.
46. A. A. Griffith, “The Theory of Rupture,” in *Proc. 1st Int. Congress on Applied Mechanics*, eds. C. B. Biezeno and J. M. Burgers, (1924) 55 - 63.
47. G. R. Irwin, “Analysis of Stresses and Strains Near the End of a Crack Traversing a Plate,” *J. Appl. Phys.*, **24** (1957) 361 – 364.
48. G. R. Irwin, “Fracture” pp. 551 – 590 in *Encyclopedia of Physics, Vol. VI, Elasticity and Plasticity*, Springer-Verlag, 1958.
49. ASTM E 399- 17, “Standard Test Method for Linear-Elastic Plane-Strain Fracture Toughness K_{Ic} of Metallic Materials,” *Annual Book of Standards*, Vol. 3.01, ASTM, West Conshohocken, PA, 2017.
50. G. D. Quinn, J. J. Swab, and P. Patel, “Fracture Toughness of Modern and Ancient Glasses and Glass Ceramics as Measured by the SEPB Method,” Proc. Int. Conf. Advanced Ceramics and Composites, Daytona, FL, Jan. 2018, *Ceram. Eng. and Sci. Proc.*, **39** [2] (2019) 1 – 13.
51. S. M. Wiederhorn, H. Johnson, A. M. Diness, and A. H. Heuer, “Fracture of Glass in Vacuum,” *J. Am. Ceram. Soc.*, **57** [8] (1974) 336 - 341.
52. ASTM C 1322-96, “Standard Practice for Fractography and Characterization of Fracture Origins in Advanced Ceramics,” *Annual Book of Standards*, Vol. 15.01, ASTM Int.,1996.
53. ASTM C1421-99, “Standard Test Method for the Determination of Fracture Toughness of Advanced Ceramics,” *ibid*, 2000.
54. SRM’s 2100, 2100A, and 2100B, “Fracture Toughness of Ceramics,” National Institute for Standards and Technology, Gaithersburg, MD, 1999.

55. ASTM E2899-19, "Standard Test Measurement for Measurement of Initiation Toughness in Surface Cracks Under Tension and Bending," *Annual Book of Standards*, Vol. 3.01, ASTM Int., 2019.
56. J. C. Newman and I. S. Raju, "An Empirical Stress Intensity Factor Equation for the Surface Crack," *Eng. Fract. Mech.*, **15** [1-2] (1981) 185 - 192.
57. ASTM E740-88, "Standard Practice for Fracture Testing with Surface-Crack Tension Specimens," Annual Book of Standards, Vol. 3.01, ASTM Int., 1988.
58. ISO 18756, Fine Ceramics (Advanced Ceramics, Advanced Technical Ceramics) – Determination of Fracture Toughness of Monolithic Ceramics at Room Temperature by the Surface Crack in Flexure (SCF) Method, Inter. Organ. for Standards, Geneva, SW, 2003.
59. T. Fett, "An Extension of the Newman-Raju Formula," *Int. J. Fract*., **33** (1987) R47-R50.
60. T. Fett, "Stress Intensity Factors for Semi-elliptical Surface Cracks in a Plate Under Tension Based on the Isida's solution," *ibid*, **48** (1991) 139 – 151.
61. T. Fett and D. Munz, *Stress Intensity Factors and Weight Functions*, Computational Mechanics Publ., Southampton, UK and Boston, MA, USA, 1997.
62. M. Isida, H. Noguchi, and T. Yoshida, "Tension and Bending of Finite Thickness Plates with a Semi-elliptical Surface Crack," *Int. J. Fract*., **26** (1984) 157 - 188.
63. S. Strobl, P. Supancic, T. Lube, and R. Danzer, "Surface Crack in Tension or Bending – A Reassessment of the Newman and Raju Formula in Respect to Fracture Toughness Measurements in Brittle Materials," *J. Eur. Cer. Soc.*, **32** (2012) 1491–1501. See also "Corrigendum to Surface Crack in Tension or in Bending," *J. Eur. Cer. Soc*, **32** [8] (2018) 355 – 358.
64. G. K. Bansal, "Effect of Flaw Shape on Strength of Ceramics," *J. Am. Ceram. Soc*., **59** [1-2] (1976) 87 - 88.
65. Y. Murakami, *Stress Intensity Factors Handbook*, Vols. 1 and 2, ed., Pergamon Press, NY, 1986. (Case 9.49)
66. J. J. Mecholsky, Jr., S. W. Freiman, and R. W. Rice, "Fracture Surface Analysis of Ceramics," *J. Mat. Sci*., **11** (1976) 1310 – 1319.
67. G. K. Bansal and W. H. Duckworth, "Fracture Stress as Related to Origin and Fracture Mirror Sizes," *J. Am. Ceram. Soc.*, **60** [7–8] (1977) 304 – 310.
68. G. K. Bansal, "On Fracture Mirror Formation in Glass and Polycrystalline Ceramics," *Phil Mag*., **35** [4] (1977) 935 - 944.
69. S. R. Choi and J. P. Gyekenyesi, "Crack Branching and Fracture Mirror Data of Glasses and Advanced Ceramics," NASA Technical Report TM 1998-206536, NASA Glenn Research Center, Cleveland, OH, 1998.
70. A. I. A. Abdel-Latif, R. C. Bradt, and R. E. Tressler, "Dynamics of Fracture Mirror Boundary Formation in Glass," *Int. J. Fract.*, **13** [3] (1977) 349 - 359.
71. M. Ramulu, R. C. Bradt, A. S. Kobayashi, and K. H. Yang, "A Dynamic Fracture Mechanics Interpretation of Multiple Mist Regions on Soda-Lime-Silicate Glass Fracture Features," pp. 215 – 227 in *Fractography of Glasses and Ceramics, Advances in Ceramics*, Vol. 22, J. Varner, and V. Fréchette, eds., Am. Ceram. Soc., Westerville, OH, 1988.
72. H. P. Kirchner, R. M. Gruver, M. V. Swain, and R. C. Garvie, "Crack Branching in Transformation-Toughened Zirconia," *J. Am. Ceram. Soc.*, **64** [9] (1981) 529 - 533.
73. D. A. Krohn and D. P. H. Hasselman, "Relation of Flaw Size to Mirror in the Fracture of Glass," *J. Am. Ceram. Soc.*, **54** [8] (1971) 411.
74. J. J. Mecholsky, Jr., A. Gonzalez, and S. W. Freiman, "Fractographic Analysis of Delayed Failure in Soda-Lime Glass," *ibid*, **62** [11-12] (1979) 577 – 580.
75. R. W. Rice, "Ceramic Fracture Features, Observations, Mechanism and Uses," pp. 5 – 103 in *Fractography of Ceramic and Metal Failures*, ASTM STP 827, ASTM, 1984.

76. D. B. Marshall, B. R. Lawn, and J. J. Mecholsky, “Effect of Residual Stresses on Mirror/Flaw Size Relations,” *J. Am. Ceram. Soc*, **63** [5-6] (1980) 358 – 360.
77. K. Gopalakrishnan and J. J. Mecholsky, Jr., “Quantitative Fractography of Mixed-Mode Fracture in an R-curve Material,” *J. Mat. Sci.*, **48** (2013) 7081 – 7087.
78. R. W. Rice, “Ceramic Fracture Features, Observations, Mechanism and Uses,” pp. 5-103 in *Fractography of Ceramic and Metal Failures*, eds., J.J. Mecholsky, Jr, S. W. Freiman, and S. R. Powell, ASTM STP 827 ASTM, Int., West Conshohocken, PA, 1984.
79. J. J. Mecholsky, Jr., T. J. Hill, and Z. Chen, “Application of Quantitative Fractography to the Characterization of R-Curve Behavior,” pp.152 - 168 in *Fracture Resistance Testing of Monolithic and Composite Brittle Materials*, eds., J. A. Salem, G. D. Quinn, M. G. Jenkins, ASTM STP 1409, ASTM, Int., West Conshohocken, PA (2002).
80. G. D. Quinn and J. J. Swab, “Fractography and Estimates of Fracture Origin Size from Fracture Mechanics,” *Cer. Eng. Sci. Proc.*, **17** [3] (1996) 51 - 58.
81. G. D. Quinn and J. J. Swab, “Comparisons of Calculated and Measured Flaw Sizes,” pp. 175 – 192 in *Fractography of Glasses and Ceramics IV*, Ceramic Transactions, Vol. 122, eds. J. Varner and G. Quinn, American Ceramic Society, Westerville, OH, 2001.
82. H. G. Richter and F. Kerkhof, “Stress Wave Fractography,” pp. 75 – 109 in *Fractography of Glass*, eds. R. C. Bradt and R. E. Tressler, Plenum, NY, 1994.
83. H. Richter, “Crack Propagation in Glass Under Liquids in an Intermediate Range of Crack Velocities,” pp. 219 – 229 in *Strength of Inorganic Glass*, ed. C. R. Kurkjian, Plenum Press, NY, 1985.
84. T. A. Michalske, M. Singh, and V. D. Fréchette, “Experimental Observation of Crack Velocity and Crack Front Shape Effects in Double-Torsion Fracture Mechanics Tests,” pp. 3 - 12 in *Fracture Mechanics for Ceramics, Rocks, and Concrete*, STP 745, ASTM Int., West Conshohocken, PA, 1982.
85. T. A. Michalske and J. M. Collins, “Fractographic Determination of Crack-Tip Stress Intensity,” pp. 229 – 239 in *Fractography of Glasses and Ceramics*, Advances in Ceramics, Vol. 22, eds. J. R. Varner and V. D. Fréchette, American Ceramic Society, Westerville, OH 1988.
86. A. Tsirk, “Formation and Utility of a Class of Anomalous Wallner Lines on Obsidian,” *ibid*, pp. 57 – 69.
87. E. F. Poncelet, “The Markings on Fracture Surfaces,” *J. Soc. Glass Technol.*, **42** (1958) 279T – 288T.
88. A. Smekal, “Procedure for Measurement of Fracture Surface Propagation Velocities on Fracture Surfaces,” *Glastech. Ber.*, **23** [3] (1950) 57 – 67.
89. F. Kerkhof, *Bruchvorgänge in Gläsern*, (Crack Propagation in Glasses), DKG, Frankfurt am Main, 1970.
90. T. A. Michalske, “Quantitative Fracture Surface Analysis,” pp. 652 – 662 in *Engineered Materials Handbook, Vol 4, Ceramics and Glasses*, ASM Int., 1991.
91. T. Fett, D. Munz, and K. Keller, “Determination of Subcritical Crack Growth on Glass in Water from Lifetime Measurements on Knoop-Cracked Specimens,” *J. Mat. Sci.*, **23** (1988) 798 - 803.
92. P. J. Dwivedi and D. J. Green, “Determination of Subcritical Crack Growth Parameters from In situ Observation of Indentation Cracks,” *J. Am. Ceram. Soc*., **78** [8] (1995) 2122 - 2128.
93. V. M. Sglavo and R. Dal Maschio, “Controlled Indentation-Induced Cracks for the Determination of Fracture Toughness in Alumina,” pp. 233 – 244, in *Fracture Mechanics of Ceramics, Vol. 11*, eds. R. C. Bradt et al., Plenum, NY, 1996.

94. M. Stech and J. Rödel, "Method for Measuring Short -Crack R-Curves Without Calibration Parameters: Case Studies on Alumina and Alumina-/Aluminum Composites," *J. Am. Ceram. Soc*., **79** [2] (1996) 291 - 297.
95. W. Chen, D. Lupascu, J. Rödel, and C. S. Lynch, "Short Crack R-Curves in Ferroelectric and Electrorestrictive PLZT," *ibid*, **84** [3] (2001) 393 – 397.
96. A. H. Heuer, "Transformation Toughening in ZrO_2-Containing Ceramics," *ibid*, **70** [10] (1987) 689 – 698.
97. D. B. Marshall, "Strength Characteristics of Transformation-Toughened Zirconia," *J. Am. Ceram. Soc.*, **69** [3] (1986) 173 – 180.
98. G. D. Quinn, L. K, Ives, and S. Jahanmir, "On the Fractographic Analysis of Machining Cracks in Ground Ceramics: A Case Study on Silicon Nitride," Special Publication SP 996, NIST, Gaithersburg, MD, May, 2003.
99. S. M. Smith and R. O. Scattergood, "Controlled Crack Shapes for Indentation Fracture of Soda Lime Glass," *J. Am. Ceram. Soc.*, **75** [9] (1992) 2593 – 2596.
100. R. W. Steinbrech and O. Schmenkel, "Crack-Resistance Curves of Surface Cracks in Alumina," *ibid*, **71** [5] (1988) C271 - C273.
101. T. Fett, D. Munz, J. Siedel, M. Stech, and J. Rödel, "Correlation Between Long and Short Crack R-Curves in Alumina Using the Crack Opening Displacement and Fracture Mechanical Weight Function Approach," *ibid*, **79** [5] (1996) 1189 -1196.
102. T. Fett and D. Munz, "Evaluation of R-curve Effects in Ceramics," *J. Mat. Sci*., **28** (1993) 742 – 752.
103. R. F. Cook and D. R. Clarke, "Fracture Stability, R-Curves and Strength Variability," *Acta Metall.*, **36** [3] (1988) 555 – 562.
104. J. J. Mecholsky, Jr., T. J. Hill and Z. Chen, "Application of Quantitative Fractography to the Characterization of R-Curve Behavior," pp. 152 – 167 in *Fracture Resistance Testing of Monolithic and Composite Brittle Materials*, ASTM STP 1409, eds., J. Salem et al., ASTM, West Conshohocken, PA, 2002.
105. J. J. Petrovic, L. A. Jacobson, P. K. Talty, and A. Vasudevan, "Controlled Surface Flaws in Hot-Pressed Si_3N_4," *J. Am. Ceram. Soc*., **58** [3-4] (1975) 113 - 116.
106. G. D. Quinn, R. J. Gettings, and J. J. Kübler, "Fractography and the Surface Crack in Flexure (SCF) Method for Evaluating Fracture Toughness of Ceramics," pp. 107 - 144 in *Fractography of Glasses and Ceramics III*, Ceramic Transactions, Vol. 64, eds., J. R. Varner, V. D. Fréchette, and G. D. Quinn, ACS, Westerville, OH, 1996.
107. G. Quinn, R. Gettings, and J. Kübler, "Fracture Toughness by the Surface Crack in Flexure (SCF) Method: Results of the VAMAS Round Robin," *Cer. Eng. Sci. Proc.*, **15** [5] (1994) 846 - 855.
108. G. D. Quinn, K. Xu, J. A, Salem, and J. J. Swab, "SRM 2100: the World's First Fracture Toughness Reference Material," pp. 499 – 530 in *Fracture Mechanics of Glasses and Ceramics, Vol. 14*, eds., R. C. Bradt, D. Munz, M. Sakai, and K. W. White, Klewer/Plenum, NY, 2005.
109. I. Bar-On, G. D. Quinn, J. Salem, and M. J. Jenkins, "Fracture Toughness Standard Test Method C 1421-99 for Advanced Ceramics," pp. 315 - 335 in *Fatigue and Fracture Mechanics, Vol. 32*, ASTM STP 1406, ed. R. Chona, ASTM Int., 2001.
110. CEN 14425 "Advanced Technical Ceramics – Test Methods for the Determination of Fracture Toughness of Monolithic Ceramics – Part 4: Surface Crack in Flexure (SCF) Method," European Committee for Standards, Brussels, 2003.
111. G. D. Quinn, "Fracture Toughness of Ceramics by the Vickers Indentation Crack Length Method: A Critical Review," *Cer. Eng. Sci. Proc.*, **27** [3] (2006) 45 – 62.
112. G. D. Quinn and R. C. Bradt, "On the Vickers Indentation Fracture Toughness Test," *J. Am. Ceram. Soc*., **90** [3] (2007) 673 – 680.

113. B. R. Lawn and D. B. Marshall, “Indentation Fractography,” pp. 1 –36 in *Fractography of Glass*, eds., R. Bradt and R. Tressler, Plenum, NY, 1994.
114. P. Chantikul, G. R. Anstis, B. R. Lawn and D. B. Marshall, “A Critical Evaluation of Indentation Techniques for Measuring Fracture Toughness: II Strength Method,” *J. Am. Ceram. Soc.*, **64** [9] (1981) 539 – 543.
115. R. F. Cook and G. M. Pharr, “Direct Observation and Analysis of Indentation Cracking in Glasses and Ceramics,” *ibid*, **73** [4] (1990) 787 – 817.
116. T. Wilantewicz, “Crack Initiation Behavior of Optical Glasses from Vickers Indentations,” Ph. D. Thesis, Alfred University, November, 2005.
117. T. Wilantewicz and J. R. Varner, “Vickers Indentation Fracture in Optical Glass Compositions,” pp. 131 -151 in *Fractography of Glasses and Ceramics*, Vol. 5, eds. J. R. Varner, G. D. Quinn, M. Wightman, American Ceramic Society, Westerville, OH, 2007.
118. D. B. Marshall, B. R. Lawn, and J. J. Mecholsky, “Effect of Residual Stresses on Mirror/Flaw Size Relations,” *J. Am. Ceram. Soc*, **63** [5-6] (1980) 358 – 360.
119. T. Sakai, M. Ramulu, A. Ghosh, and R. C. Bradt, “A Fractal Approach to Crack Branching (Bifurcation) in Glass,” pp. 131 – 146 in *Fractography of Glasses and Ceramics II*, eds, V. D. Frechette and J. R. Varner, Ceramic Transactions Vol. 17, American Ceramic Society, Westerville, OH, 1991.
120. T. Sakai, M. Ramulu, A. Ghosh, and R. C. Bradt, “Cascading Fracture in a Laminated Tempered Safety Glass Panel,” *Int. J. Fract.*, **48** (1991) 46 – 69.
121. G. W. Quinn, J. B. Quinn, J. J. Mecholsky, Jr. and G. D. Quinn, “Computer Modeling of Crack Propagation Using Fractal Geometry,” *Ceram. Eng. and Sci. Proc.*, **26** [2] (2005) 77 - 84.
122. D. E. Passoja, “Fundamental Relationships Between Energy and Geometry in Fracture,” pp. 101 – 126 in *Fractography of Glasses and Ceramics*, eds., J. R. Varner and V. D. Fréchette, Advances in Ceramics, Vol. 22, American Ceramic Society, 1988.
123. J. J. Mecholsky, T. J. Mackin, and D. E. Passoja, “Self-Similar Crack Propagation in Brittle Materials,” *ibid*, pp. 127 – 134.
124. E. E. Underwood and K. Banerji, “Fractal Analysis of Fracture Surfaces,” pp. 211 – 215 in *ASM Metals Handbook, Volume 12, Fractography*, ASM Int., Materials Park, OH, 1992.
125. D. A. Lange, H. M. Jennings, and S. P. Shah, “Relationship Between Fracture Surface Roughness and Fracture Behavior of Cement Paste and Mortar,” *J. Am. Ceram. Soc.*, **76** [3] (1993) 589 – 597.
126. Y. Xin, K. J. Hsia, and D. A. Lange, “Quantitative Characterization of the Fracture Surface of Si Single Crystals by Confocal Microscopy,” *ibid*, **78** [12] (1995) 3201 – 3208.
127. J. J. Mecholsky, D. E. Passoja, and K. S. Feinberg-Ringel, “Quantitative Analysis of Brittle Fracture Surfaces Using Fractal Geometry,” *ibid*, **72** [1] (1989) 60 – 65.
128. J. J. Mecholsky, Jr. and S. W. Freiman, “Relationship Between Fractal Geometry and Fractography,” *ibid*, **74** [12] (1991) 3136 – 3138.
129. R. Morrell, *Fractography of Brittle Materials*, Measurement Good Practice Guide #15, National Physical Laboratory, Teddington, UK, 1999.
130. T. Hollstein, W. Pfeiffer, M. Rombach, and B. Thielicke, “Analysis of Machining Damage in Engineering Ceramics by Fracture Mechanics, Fractography, and X-ray Diffraction,” pp. 145-169 in *Fractography of Glasses and Ceramics, III*, Cer. Trans, Vol. 64, eds., J. Varner et al., ACS, Westerville, OH, 1996).
131. J. J. Mecholsky and M. G. Drexhage, “Comparison of Optical and Fractographic Measurements of Residual Stress in Compressively Clad Glass Rods,” *J. Am. Ceram. Soc.*, **63** [5-6] (1980) 347 - 349.
132. J. C. Conway, Jr. and J. J. Mecholsky, Jr., “Use of Crack Branching Data for Measuring Near-Surface Residual Stress in Tempered Glass,” *ibid*, **72** [9] (1989) 1584 - 1587.

133. D. B. Marshall and B. R. Lawn, “An Indentation Technique for Measuring Stresses in Tempered Glass Surfaces,” *J. Am. Ceram. Soc*., **60** [1-2] (1977) 86 - 87.
134. M. V. Swain, J. T. Hagan, and J. E. Field, “Determination of the Surface Residual Stresses in Tempered Glasses by Indentation Fracture Mechanics,” *J. Mat Sci. Lttrs.*, **12** (1977) 1914 - 1917.
135. W. Weibull, “A Statistical Distribution Function of Wide Applicability,” *J. Appl. Mech.*, September, (1951) 293 – 297.
136. W. Weibull, “A Statistical Theory of the Strength of Materials,” *Proc. Royal Swedish Inst. Eng. Res*, No. 151, 1939.
137. W. Weibull, “The Phenomenon of Rupture in Solids,” *ibid*., No. 153, 1939.
138. G. D. Quinn, “Static Fatigue and Creep Resistance of a Commercial Sialon,” *J. Mat. Sci*., **22** (1987) 374 - 380.
139. K. Trustrum and A. De S. Jayatilaka, “Application of Weibull Analysis for Brittle Materials,” *J. Mat. Sci*., **18** (1983) 2765 - 70.
140. A. De S. Jayatilaka and K. Trustrum, “Statistical Approach to Brittle Fracture,” *ibid*, **12** (1977) 1426 - 1430.
141. R. Danzer, “A General Strength Distribution Function for Brittle Materials,” *J. Eur. Ceram. Soc*., **10** (1992) 461 – 472.
142. G. D. Quinn and R. Morrell, “Design Data for Engineering Ceramics: A Review of the Flexure Test,” *J. Am. Ceram. Soc*., **74** [9] (1991) 2037 - 2066.
143. J. Sung and P. S. Nicholson, “Strength Improvement of Yttria-Partially-Stabilized Zirconia by Flaw Elimination,” *J. Am. Ceram. Soc*., **71** [9] (1988) 788 - 795.
144. J. B. Quinn and G. D. Quinn, “A Practical and Systematic Review of Weibull Statistics for Reporting Strengths of Dental Materials,” *Dent. Mat.*, **26** [2] (2010) 135 - 147.
145. L. Gorjan and M. Ambrožič, “Bend Strength of Alumina Ceramics: A Comparison of Weibull Statistics with Other Statistics Based on a Very Large Experimental Data Set,” *J. Eur. Ceram., Soc*., **32** (2012) 1221 - 1227.

8. Single Crystals

8.1 General

Fractographic procedures are similar to those for glasses and polycrystalline ceramics, but there are some nuances and differences. At first exposure to single crystal fractography, the fractographer is startled by the complexity, symmetry, and sometimes the beauty of the fracture surfaces. Surfaces may have glass-like regions with conchoidal fracture, Wallner lines, and twist hackle. Other regions may be extremely flat or have dramatic faceting. Fracture resistance often varies significantly between the different crystallographic planes, causing jagged fracture patterns as cracks change directions onto preferred cleavage planes. Fracture surfaces may be very difficult to interpret. Figure 8.1 shows examples.

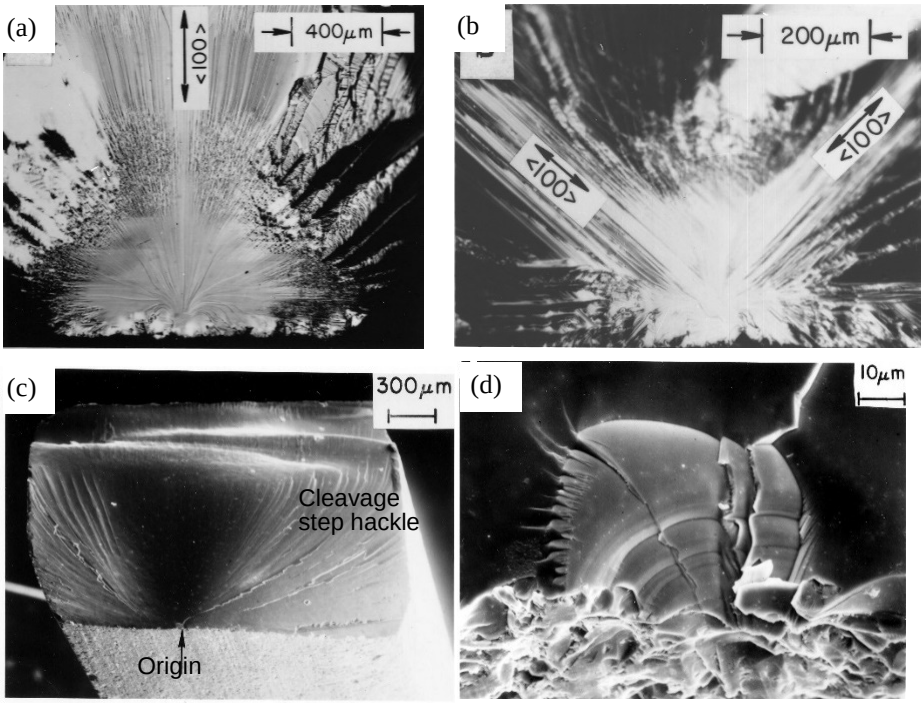

Figure 8.1 *Examples of single crystal fractures in bend bars. (a) and (b) show fracture mirrors on the {100} type planes in MgO, but with two different tensile surface orientations. (c) and (d) show a cubic zirconia with curved lance markings that are "cleavage step hackle" emanating from the origin area and the grinding crack origin. (courtesy R. Rice)*

Ionic-bonded cubic alkali halides like NaCl, KCl, or KB and oxide ceramics such as MgO may even have plastic flow prior to fracture even at room temperature. The extent of plasticity is strongly dependent on surface damage, environment, rate of loading, and even time after a piece is cleaved from the bulk.

The overall fracture plane may not necessarily be perpendicular to the direction of principal normal stress, since a preferred cleavage plane may be at an irregular angle to that stress. Sometimes the overall fracture extension may be approximately perpendicular to the maximum principal stresses, but local fracture proceeds in a zigzag fashion on other planes. This crack redirection is different than conventional crack branching in glasses or polycrystalline ceramics. Branching is much less common in single crystals. If the maximum principal stress is perpendicular to a preferred cleavage plane, the fracture surface may be very flat and featureless with little or no hackle, and no branching at all.

Fracture mirrors may be present but may have odd shapes and markings. There may be no mist or hackle on preferred cleavage planes. Mirror sizes may be extremely difficult or impractical to measure. Cleavage hackle steps (described below) may be confused with Wallner lines. Twinning may cause fracture.

Since fractures often proceed along preferred cleavage planes, it is very helpful to have a 3-D crystallographic model of the structure handy as shown in Figure 8.2. Under ideal conditions, the initial orientation of the component is known, but if it is not, manipulation of the model to align known preferred fracture planes can help deduce the component orientation and the cleavage planes.

There is some interesting nomenclature carryover from mineralogy. *Cleavage* and *conchoidal* fractures were previously discussed in section 5.1 of this Guide. In the mineralogical field, *cleavage* has been described as a “smooth break producing what appears to be a flat crystal face.” There may be many possible cleavage planes in a mineral. The easiest cleavage plane is the “preferred cleavage plane." In minerology, the cleavage may even be described as perfect, imperfect, good, distinct, indistinct, or poor depending on the plane. Mineral identification is often aided by observations of how the mineral cleaves. Cubic crystals exhibit cubic or octahedral cleavage, whereas hexagonal crystals may have basal fractures perpendicular to a major crystal axis, whereas prismatic cleavages may be parallel to the major axis. In contrast, *conchoidal* fracture is commonly defined in mineralogy as “ not cleavage,” but curved such as in seashells and many glass fractures.

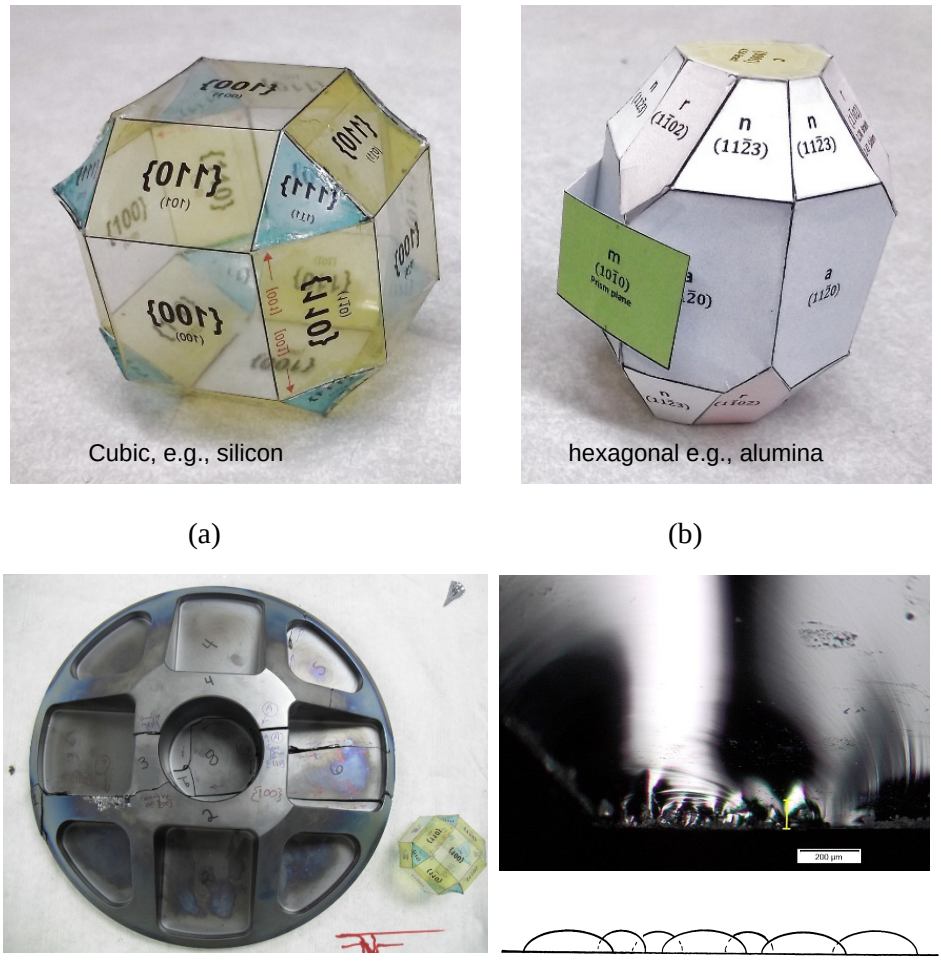

Figure 8.2 *Three-dimensional crystallographic models shown in (a) and (b) are extremely valuable in interpreting fractures. They can be aligned and rotated to interpret fracture planes in a broken component. (a) shows a transparent plastic model for a cubic single crystal. (b) shows a stiff paper model for single crystal sapphire. The m and* ***a*** *planes for sapphire are sometimes confused in depictions on the internet and even in the scientific literature, so this model shows them both. The* ***a*** *planes are pale blue on the sides and the* ***m*** *planes (only two are shown) are green. (c) shows a large (30 cm diameter) broken single crystal silicon mirror. The cubic model is next to it and helped interpret the breakage planes relative to the preferred cleavage planes in this complex machined component. (d) shows a photograph of the fracture origin that was 95 μm to 104 μm deep grinding cracks.*

8.2 Preferred Cleavage Planes

Bradt et al.[1,2] reviewed the various criteria for cleavage and concluded that fracture toughness is the best indicator of the preferred cleavage plane. Fracture toughness can vary dramatically on different planes. The energy to propagate cracks along preferred cleavage planes is less than that for other planes. Nevertheless, there is contradictory information in the literature on preferred cleavage planes in some crystals, even for such well-studied materials as silicon, alumina (sapphire), and magnesium aluminate spinel. Some of the contradictory information is due to experimental error or specific aspects of the test method. It is disappointing that some studies do not even identify the direction of crack propagation or even the plane. The direction of crack advance on a plane is as important as the plane itself. The speed of crack advance can even determine which fracture plane is preferred.[3] Although the DCB method and AMDCB methods shown in Figure 8.3 are often used, results are not strictly valid if the crack zigzags down the guiding groove or is tilted to the intended fracture plane.

Knoop indentations in bend bars may be used to make small semielliptical surface flaws in bend bars for the surface crack in flexure (SCF) method as shown in Figures 8.3 and 8.4. The specimen axis and cross section and the indentation and precrack plane may be aligned with a particular cleavage plane. The local direction of crack extension may vary along the semielliptical flaw periphery, however. Such micro flaws, which mimic naturally occurring flaws,

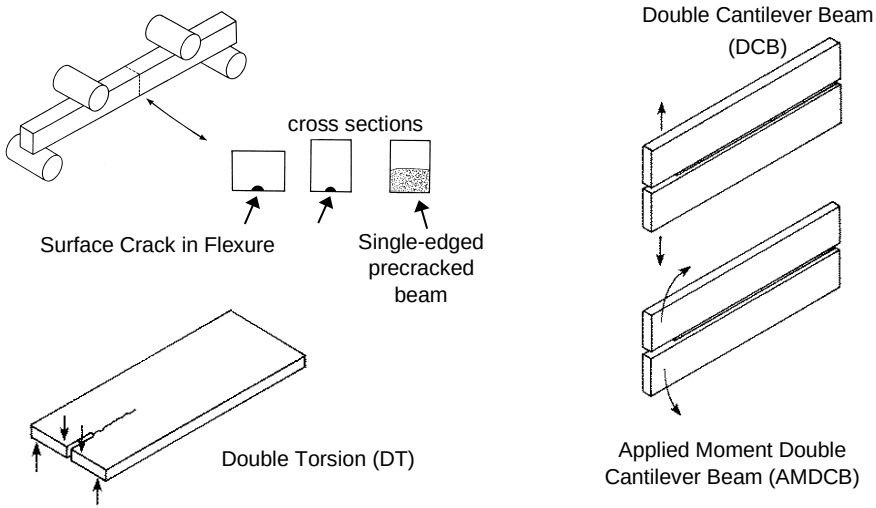

Figure 8.3 *Test methods for single crystal fracture toughness determination.*

are valuable in demonstrating just how complex fracture resistance can be in single crystals. A good example is from the work of Chen and Leopold[4] and Xin et al.[5] on silicon as summarized in Table 8.1. Xin et al. [5] showed that indentation residual stresses could change the propagation plane. It is recommended that residual stresses associated with the Knoop indentation be removed by polishing or hand-grinding, a step normally required for this method. Annealing is not advised due to the risk of crack tip blunting or crack healing. Readers interested in single crystal silicon are referred to the 2013 review paper by Masolin et al.[6] who noted the considerable variability in the published values of K_{Ic} depending upon the method. A 2015 paper by Jaya et al.[7] included consistent results for (100) plane fractures with four different test methods using tiny micrometer-sized specimens. Bradt et al.[8,9,10,11] used the SCF method on alumina and spinel. Akimune and Bradt[11] showed that there is considerable Knoop *hardness* anisotropy even on one plane (100) in spinel, but negligible variability on the (111). Iwasa and Bradt[12] used the SCF method on five planes in quartz single crystals, including both natural and synthetic materials. Conchoidal fracture can occur in quartz since K_{Ic} varied only a small amount between the planes.

Table 8.2 and Figure 8.5 show K_{Ic} data for key planes in sapphire from Iwasa and Bradt,[10] Wiederhorn,[13] and Salem.[14] The r plane is considered by some to be the preferred cleavage plane, but the a and m planes have comparable fracture resistances. Fracture toughness, K_{Ic}, critical strain energy release rate, G_{Ic}, and fracture surface energy data for other crystals is scattered in the literature. Atkinson and Meredith[15] have an excellent Table11.1 for calcite, diamond, feldspar, fluorite, galena, halite, muscovite, olivine, periclase, pyrite, quartz, and spinel.

Reference	Plane Type	K_{Ic} (MPaÖm)	Fracture characteristics
Chen and Leipold (4)	{111}	0.82	Flat and smooth fractures. This is the preferred cleavage plane.
Chen and Leipold (4)	{110}	0.90	Large but asymmetric cathedral mirrors centered on the flaws. Propagation switched to {111} planes and zigzagged at the mirror boundaries.
Chen and Leipold (4)	{100}	0.95	A very rough fracture surface. Cracks switched to {111} very quickly.
Xin, Hsia, and Lange (5)	{110}	0.95	Residual indentation stresses intact. Cracks propagated on {110}.
Xin, Hsia, and Lange (5)	{110}	-	Residual indentation stresses removed by annealing. Crack switched to {111}.

Table 8.1 *Fracture toughness of single crystal silicon from Knoop SCF tests.*

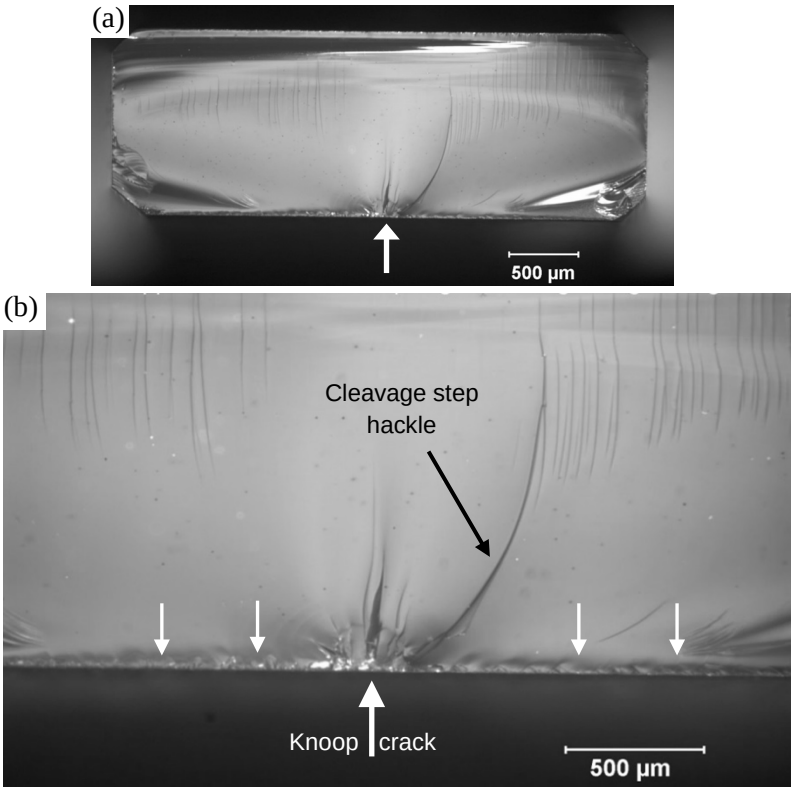

Figure 8.4 *Relatively smooth fracture surface (a) of a surface crack in flexure (SCF) sapphire bend bar with a 49 N Knoop indentation as a starter flaw (large arrow). The tensile surface of the bar was the a-plane. Fracture occurred on the m-plane. (b) is a close-up which shows grinding cracks along the surface (small white arrows). The larger indentation crack (large white arrow) was dominant. The long curved line leading from the origin is a "**cleavage step hackle**" line as discussed in section 8.4 later in this chapter.*

8.3 Fractographic Techniques

Reflections or translucency sometimes make photographing single crystals difficult. Different lighting and specimen tilting are needed to bring out various details. Low-angle grazing illumination on cleaved surfaces may be more problematic since fracture surfaces are mirror like and reflect light away from the microscope objective lens. Silicon is a good example of this and the fractographer is confronted with either getting too little or too much light reflected into the eyepieces. When using a stereo microscope with directional

Reference	Plane	K_{Ic} (MPaÖm)*	Method (Figure 8.3)
Iwasa and Bradt (10) air	c basal (0001)	4.54 ± 0.32	SCF - Knoop
Iwasa and Bradt (10) air	r $(1\bar{1}02)$	2.38 ± 0.14	SCF - Knoop
Salem (14) dry N_2	r $(1\bar{1}02)$	2.47 ± 0.02	SEPB
Wiederhorn et al. (13) vacuum	r $(1\bar{1}02)$	2.10 ± 0.17	DCB
Iwasa and Bradt (10) air	a $(11\bar{2}0)$	2.43 ± 0.26	SCF - Knoop
Salem (14) dry N_2	a $(11\bar{2}0)$	2.31 ± 0.12	SEPB
Iwasa and Bradt (10) air	m $(10\bar{1}0)$	3.14 ± 0.30	SCF - Knoop
Wiederhorn et al. (13) vacuum	m $(10\bar{1}0)$	2.59 ± 0.29	DCB

* Uncertainties are one standard deviation

Table 8.2 *Fracture toughness of single crystal sapphire.*

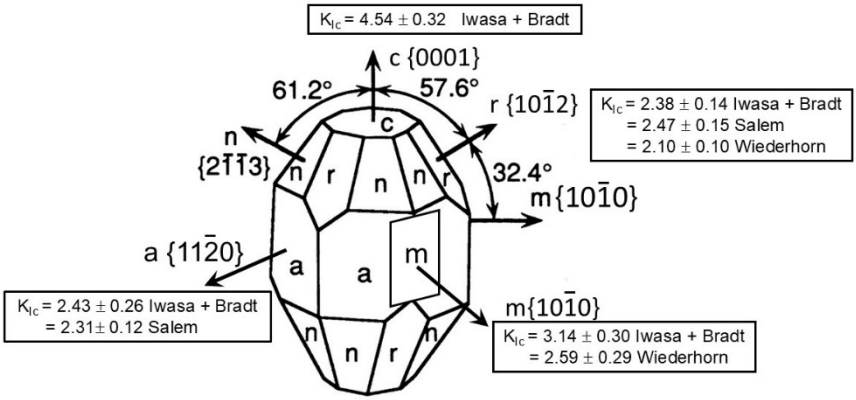

Figure 8.5 *A model of single-crystal sapphire with K_{Ic} on key planes.*

illumination, it is often effective to tilt the specimen at an angle to reflect more light up into the eyepieces.

A reflected-light compound microscope may be very effective with single crystals if the fracture surface is not too rough. Dark-field illumination may aid finding fracture mirrors, since the symmetry of cleavage steps may be accentuated as shown in Figure 8.6. In my experience, the shape symmetry of

a fracture mirror is more easily detectable with dark-field illumination. What the fractographer may first notice is a strange, swirling and blurry region that has symmetry as seen in Figure 8.6a. The crystallographic facets become sharper and clearer with lighting adjustments or in the SEM.

Confocal microscopes may not be very effective due to the specular reflections. Transmitted illumination is often useful for transparent single crystals. Polarizers are essential aids to help discern twinning that may cause fracture.

Gold coating of a transparent crystal may make the fracture surface easier to view, but if the surface is very flat, the gold coating may make it behave like a mirror, which will pose problems for inspection and photography.

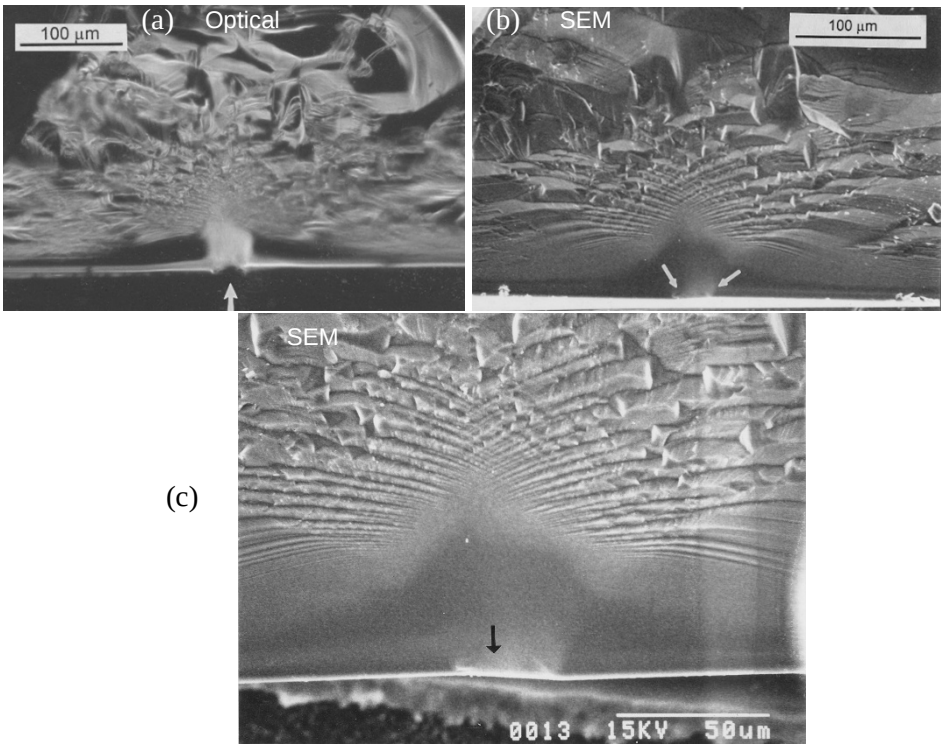

Figure 8.6 *Different views of the fracture origin in a silicon wafer tested in a biaxial ring-on-ring mode (282 MPa). Fracture initiated from the surface grinding crack (also shown later in Figure 8.20), propagated on a {110} type plane, but started to zigzag. (a) is a dark field optical image with a strange swirling appearance. It nonetheless has a symmetry that is a tip off to the existence of an origin and fracture mirror. (b) and (c) are SEM images of the fracture mirror and origin with arrows calling attention to the origin flaw.*

X-ray topography is a unique tool for single crystals. Imperfections in the crystal and its surface produce image contrast. Figure 8.7 shows an example that reveals handling damage (HD, scratch) on the polished surface of a sapphire hemi-spherical dome.[16] The full extent of the handling damage was not visible with optical or scanning electron microscopy

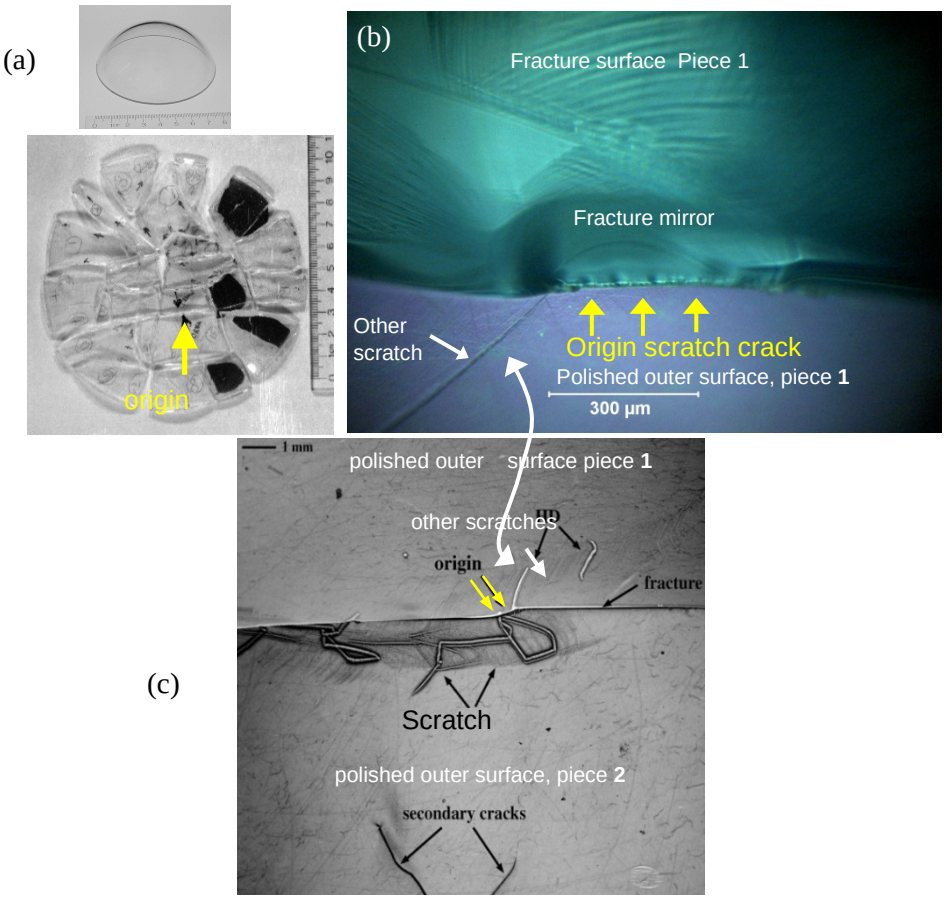

Figure 8.7 *Thermal shock fractured* ***s****apphire dome (#1087). Yellow arrows mark the fracture origin. The black patches in (A) are tape pieces. (b) is a stereo optical photo with the origin piece #1 tilted back to show the fracture surface and the polished outer surface. The origin scratch (HD) is marked by yellow arrows. Another intersecting scratch is marked with the white arrow. (c) is a composite of two x-ray topographs showing the polished* <u>*outer*</u> *surfaces of matching fracture pieces #1 and #2 butted up against each other where they meet at the origin. Surface and subsurface damage are exposed. The scratch in (b) is part of a complex handling damage network. The jagged nature of the scratches is typical of handling damage. (c courtesy of D. Black*)

8.4 Fracture Surface Markings

Cleavage step hackle: *A form of hackle in single crystals caused by the crack running on two very close parallel planes. It is in the form of one or more single lines, parallel to the local direction of crack propagation.*

Single crystal fracture planes often have "***cleavage step hackle***" as shown in Figure 8.8. Its curved shape resembles and may be confused with Wallner lines in plates in bending, but cleavage step hackle is different. Cleavage step hackle is often generated by the origin or other surface irregularities and runs parallel to the direction of crack propagation. The hackle may suddenly change from curved lines to parallel vertical segments on the compression side of a specimen. The step may be very persistent and extend over great distances without merging, unlike twist hackle lines. Cleavage step hackle is not unlike "step hackle" in glasses as described in section 5.3.6, but here with single crystals, the step is caused by the preference of a crack to stay on two nearby parallel planes without merging. Figures 8.9 on the next page and 8.1c and 8.4 earlier in this chapter show good examples in sapphire.

As early as 1962, Orowan[17] studied the propagation of cleavage step hackle and some twist hackle on alkali halide single crystals such as KCl. Sometimes the hackle lines diverged with crack propagation, but there were instances of convergence. If the local crystal planes separated by the hackle lines were offset with the "same sign" they might join to form a larger single step. Offset planes of "opposite sign" could annihilate each other. Some-times the hackle lines had dislocation etch pits for fractures at elevated temperatures.

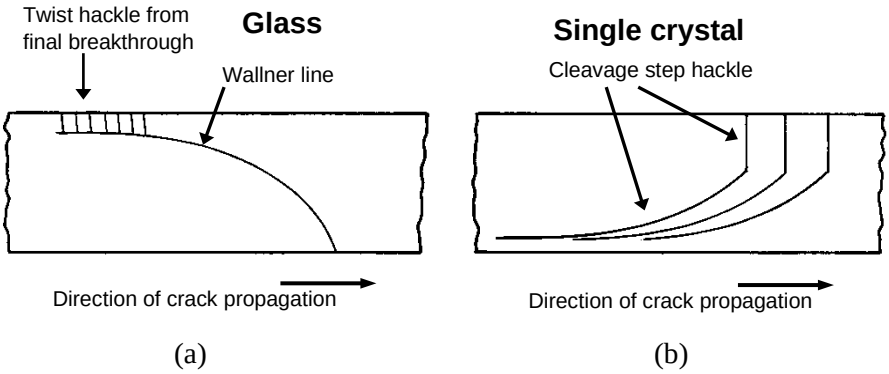

Figure 8.8 *Schematics showing (a) a Wallner line and twist hackle in a glass plate loaded in bending and (b) "**cleavage step hackle**" in a single crystal plate loaded in bending. The crack was leading on the bottom for both cases.*

Fracture surfaces and fracture mirrors may have extraordinary shapes and facets, but usually have some degree of recognizable symmetry that will help the fractographer identify an origin site. Mirror shapes may vary dramatically within a crystal depending upon the fracture plane. Figure 8.9 shows an example of a "**Batman mirror"** in sapphire as well as cleavage step hackle.

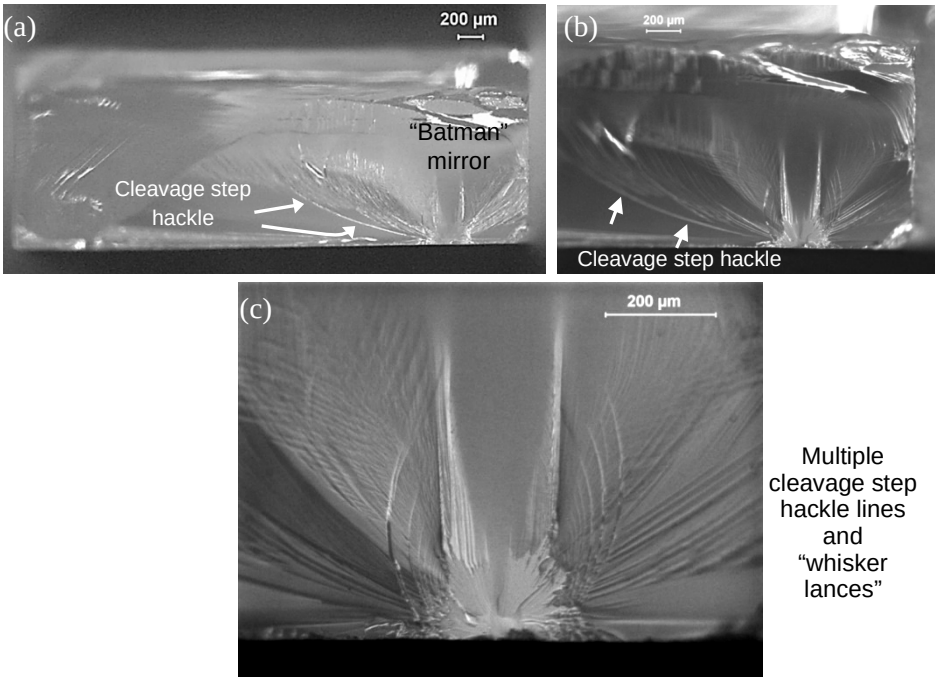

Figure 8.9 *Examples of cleavage step hackle and a "Batman mirror" in a sapphire bar. (a) shows an optical image of the bend bar with a tensile surface parallel to the a-plane and bend bar cut so that fracture should be on the r-plane. The tensile direction was the r axis. The origin was grinding damage. (specimen courtesy R. Krause).*

To illustrate these fascinating variations, fracture markings for cubic spinel are shown as a series in the systematic series of Figures 8.10 through 8.17 on the following pages. They show a picture of the whole fracture surface, the fracture mirror, and a close up of the origin. The fractographic findings are summarized in Table 8.3. These images are from Rice *et al*.[3,18,19,20] who studied fracture in this material using double cantilever beam and flexural strength specimens. They found a remarkable variety of fracture surfaces with features that they described as "**cathedral mirrors**," "**gull wing mirrors**," "**skewed cathedral mirrors**," and "**whisker lances**." (Here, for the sake of

consistency with Rice *et al*.'s work, the author has departed from the philosophy expressed in section 6.2 that fractographic features should be described by what they are rather than how they appear.) Cathedral and gull wing mirrors have also been observed in other cubic crystals such as silicon and fully-stabilized zirconia. Gull wing mirrors look like cathedral mirrors that are tilted 90° on the fracture surface. Bear in mind that there may be threshold stresses or stress intensities for the formation of markings on certain planes. Thus, the flat fractures shown in Figures 8.10 and 8.11 may indicate fracture on a preferred cleavage plane, or that the stresses were too low to generate mirror markings. The preferred cleavage plane in spinel is the {100} which has a fracture toughness of 0.9 to 1.2 MPaÖm depending upon the method of measurement.[3,8,9,18,19,20] The fracture toughness of the {110} is not much greater: 1.0 to 1.5 MPaÖm. Consequently, fracture usually runs on {100} or {110} type planes. Fracture is not preferred on the {111} since the fracture toughness is much greater (1.9 MPaÖm or more).

Intended fracture plane type	Bend bar tensile surface	Bend bar tensile axis	Fracture type	Figure
{100} (Case **A**)	{100}	<100>	**Cathedral mirror** Major crack redirection beyond the mirror sides	8.10
{100} (Case **D**)	{110}	<100>	**Cleavage, no mirror** Flat and featureless fracture surface	8.11
{110} (Case **B**)	{100}	<110>	**Cleavage, no mirror** Flat and featureless fracture surface	8.12
{110} (Cases **F1 + F2**) (Case **C**)	{110}	<110>	**Skewed fracture mirror** and Major crack redirection beyond the mirror sides, or **Gull wing mirror** and jagged fracture surface beyond top of mirror	8.13 8.14 8.15
{110} (Cases **G1 + G2**)	{111}	<110>	**Skewed cathedral mirror** Major crack redirection beyond the mirror sides, or flat	8.16 8.17
{111} (Case **E**)	{110}	<111>	**Gull wing mirror** Jagged propagation beyond mirror top	8.18

Table 8.3 *Fracture markings in $MgAl_2O_4$ spinel bend bars. The brackets {100} denote the family of (100) planes and the angles <100> denote the family of [100] directions. (After Wu, McKinney, and Rice, Ref. 3)*

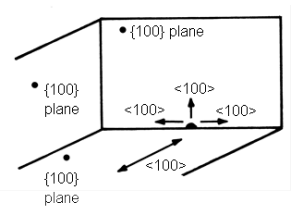

Bend bar orientation

Case A

(a)

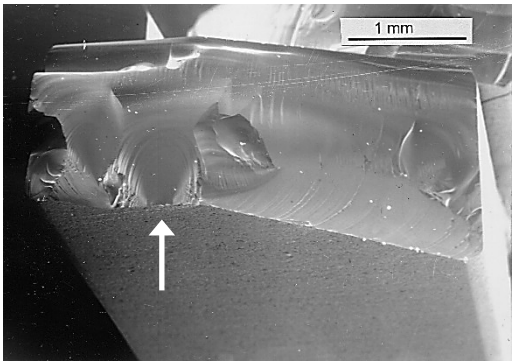

(b)

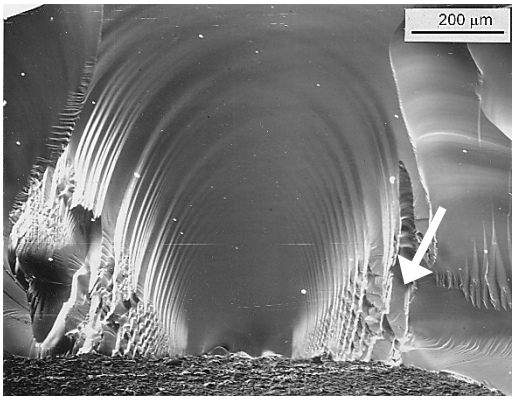

(c)

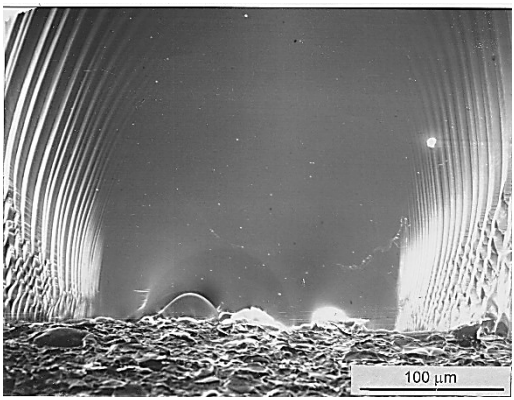

Figure 8.10 *Spinel bend bar with a {100} tensile surface and <100> tensile axis designed to cause fracture on a {100} plane. (185 MPa) (a) shows the whole fracture surface and origin (arrow). (b) shows the "**cathedral mirror**" and the arc-ribs that gradually get progressively larger until a branch or major crack redirection occurs (white arrow). (c) shows the grinding crack fracture origin. Fracture starts on the {100} but shifts or branches to the {110} just beyond the sides of the mirror. (Case **A**, Table 8.3) (Courtesy R. Rice)*

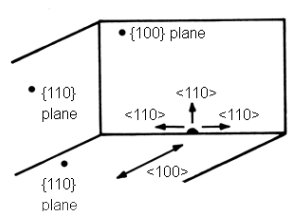

Bend bar orientation

Case D

(a)

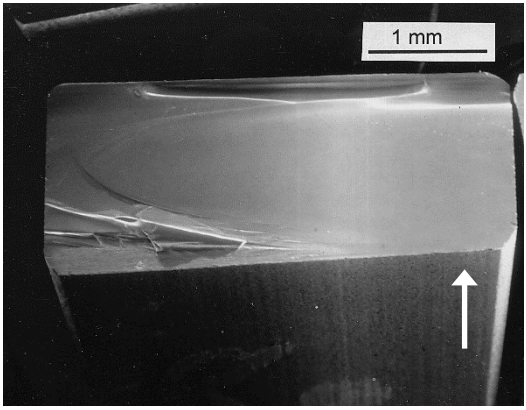

(b)

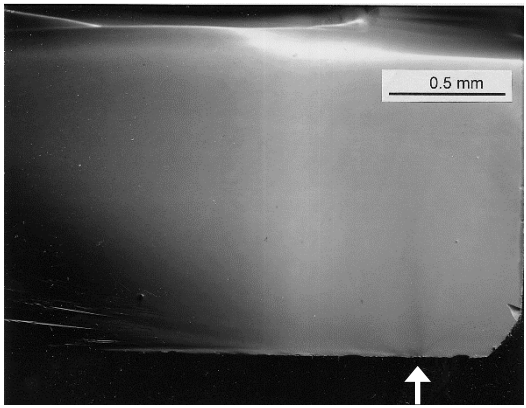

(c)

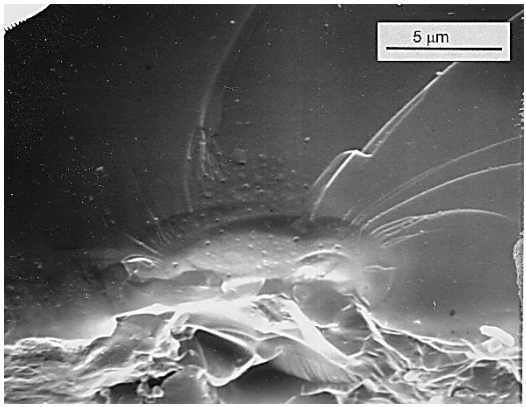

Figure 8.11 *Spinel bend bar with a {110} tensile surface and <100> tensile axis designed to cause fracture on the {100} cleavage plane. (170 MPa) (a) shows the whole fracture surface which is flat except for the cleavage steps on the side and the cantilever curl. Other similar specimens had no cleavage steps. (b) shows the origin site and (c) shows the grinding crack fracture origin. (Case* ***D****, Table 8.3) (Courtesy R. Rice*)

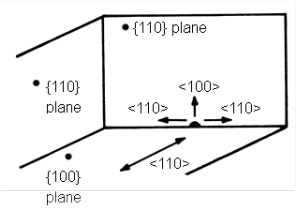

(a)

Bend bar orientation

Case B

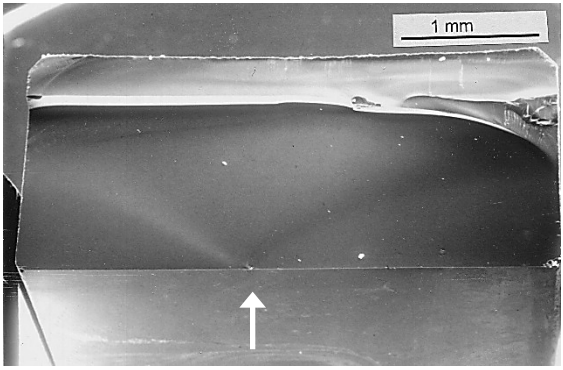

(b)

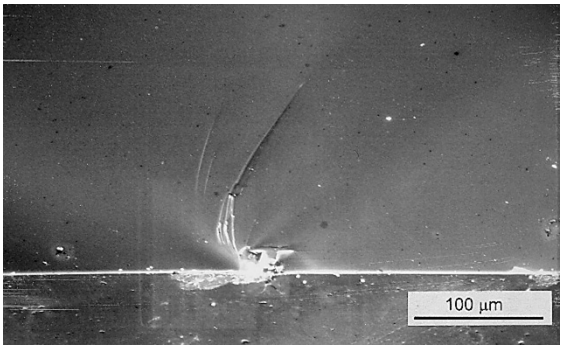

Figure 8.12 *Spinel bend bar with a {100} tensile surface and <110> tensile axis designed to cause fracture on a {110} type plane. (169 MPa) (a) shows the whole fracture surface which is flat and featureless except for the cantilever curl. The arrow shows the origin. (b) shows the grinding crack fracture origin. Fracture stays on a {110} type plane. (Case* ***B****, table 8.3) (Courtesy R. Rice)*

Fracture mirror shapes seem to correlate with elastic moduli[21] or fracture surface energy[22] variations in different directions in a fracture plane. The very limited data on fracture mirror constants that have been published are listed in Appendix C. The asymmetry and diversity of fracture mirror shapes and difficulties in judging mirror sizes hamper any attempts to accurately correlate fracture stresses to mirror sizes by the methods described in chapters 7 and appendix D. Recent work by Gopalakrishnan and Mecholsky [23] provides an explanation why mist does not appear around fracture mirrors in single crystals. The existence of any mode II loading on a crack tends to suppress mist in general and accentuates twist hackle lance lines at a mirror boundary. They argue that mixed mode I and II loading is naturally introduced in single crystals due to crystal anisotropy.

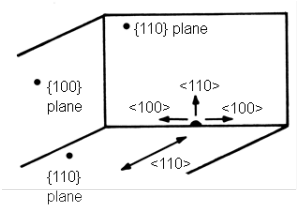

Bend bar orientation

Case F1

(a)

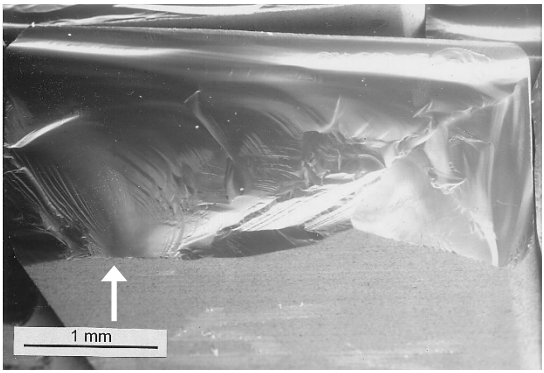

(b)

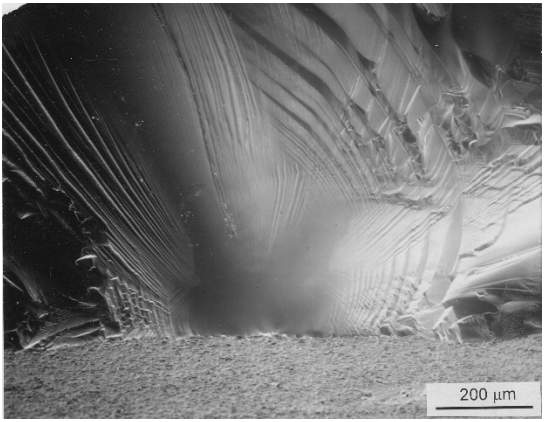

(c)

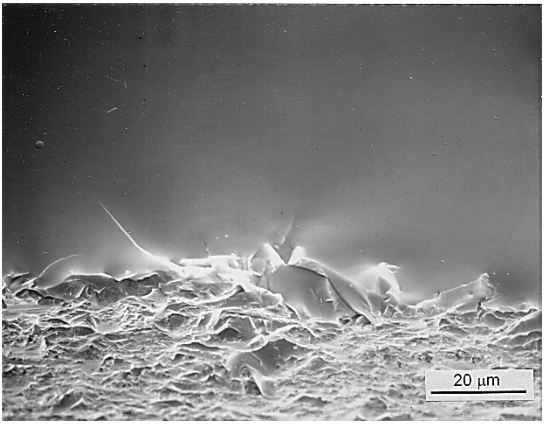

Figure 8.13 *Spinel bend bar with a {110} tensile surface and <110> tensile axis designed to cause fracture on a {110} plane. (283 MPa) (a) shows the whole fracture surface, (b) shows the mirror with "**whisker lances**" radiating outward, and (c) shows the grinding crack fracture origin.*
*(Case **F1**, table 8.3) (Courtesy R. Rice)*

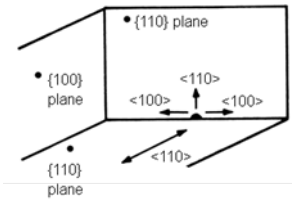

Bend bar orientation

Case F2

(a)

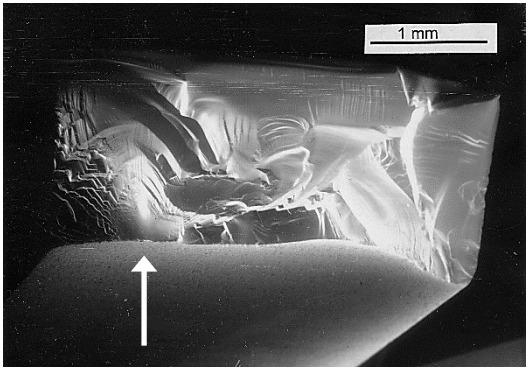

(b)

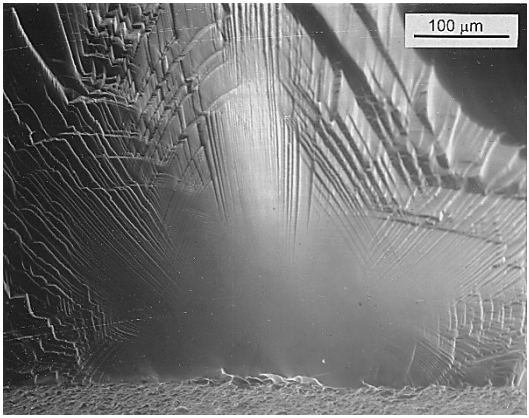

(c)

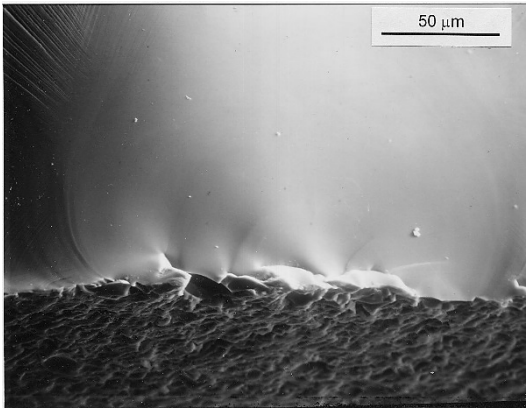

Figure 8.14 *A second example of a spinel bend bar with a {110} tensile surface and <110> tensile axis designed to cause fracture on a {110} plane (172 MPa). The fracture surface (a) is very rough as in the previous figure. The mirror (b) is more symmetric than in the previous figure. This mirror was shown in an earlier publication (Figure 29 of Ref. 19), but with a typographical mistake identifying it as {110}<100>. (Case F2, table 8.3). (Courtesy R. Rice)*

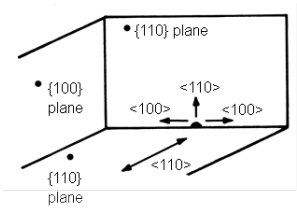

Bend bar orientation

Case C

(a)

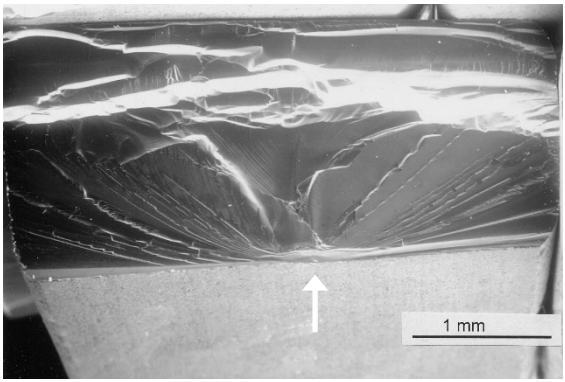

(b)

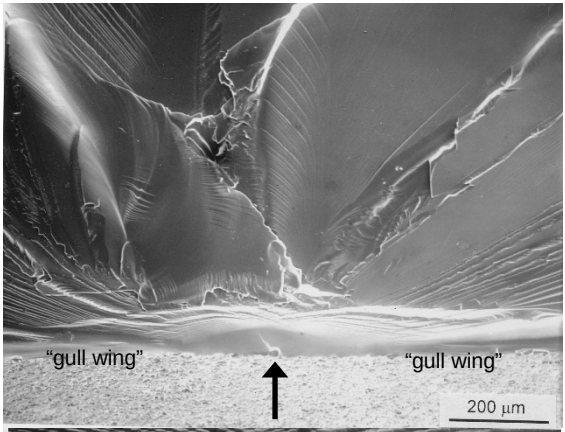

(c)

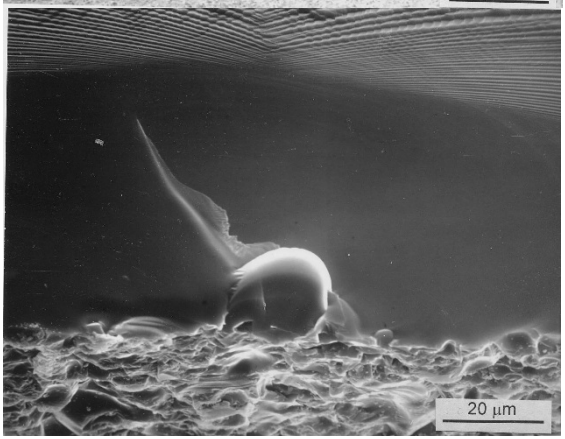

Figure 8.15 *Spinel bend bar with a {110} tensile surface and <110> tensile axis designed to cause fracture on a {110} plane. (361 MPa) (a) shows the whole fracture surface, (b) shows the "**gull wing mirror**," and (c) shows the grinding crack fracture origin. (Case **C**, table 8.3) (Courtesy R. Rice)*

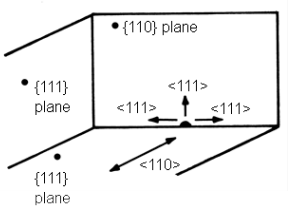

Bend bar orientation

Case G1

(a)

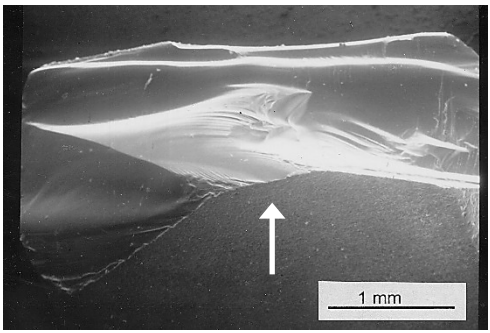

(b)

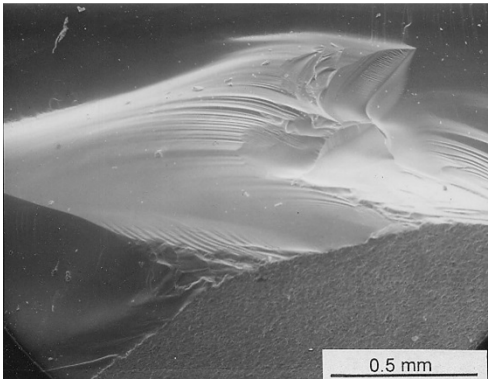

(c)

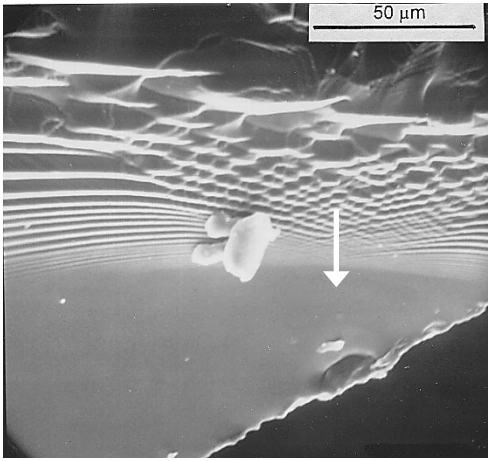

Figure 8.16 *Spinel bend bar with a {111} tensile surface and <110> tensile axis designed to cause fracture on a {110} plane. (unknown stress) (a) shows the whole fracture surface and the major crack redirection on the mirror sides. (b) shows the "**skewed cathedral mirror**," and (c) shows the grinding crack fracture origin from the matching fracture piece. (Case **G1**, table 8.3) (Courtesy R. Rice*)

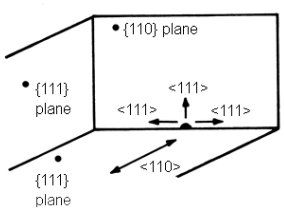

Bend bar orientation

Case G2

(a)

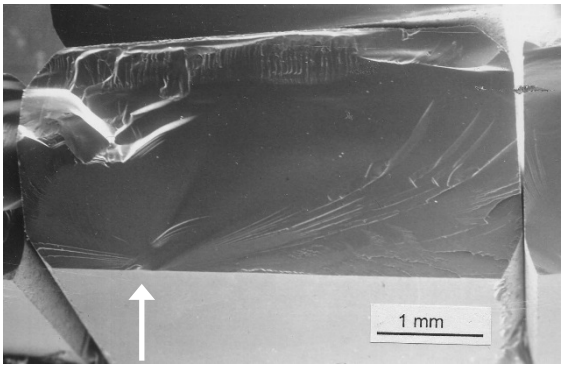

(b)

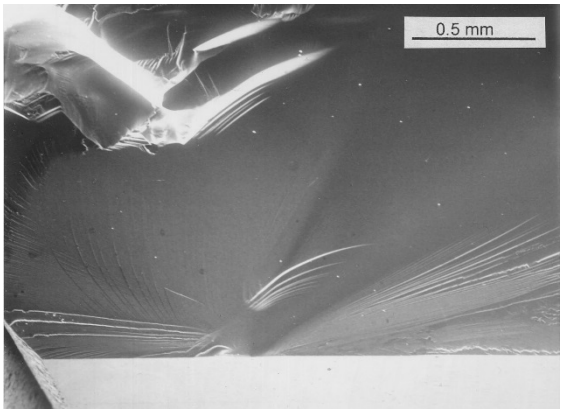

(c)

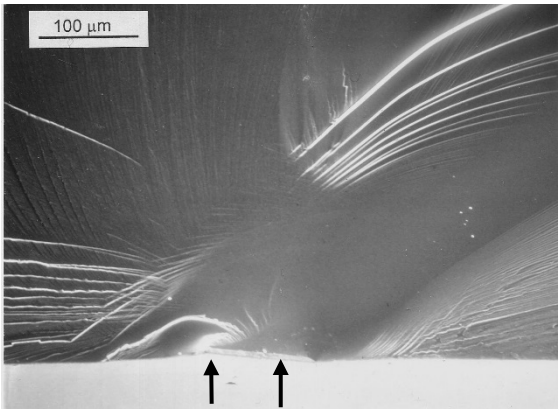

Figure 8.17 *Another example of a spinel bend bar with a {111} tensile surface and <110> tensile axis designed to cause fracture on a {110} plane. (261 MPa) (a) shows the whole fracture surface, (b) shows a "**skewed mirror**" with "**whisker lances**" and (c) shows the grinding crack fracture origin (black arrows) which is at a slight angle to the tensile stress axis and the fracture surface). (Case **G2**, Table 8.3) (Courtesy R. Rice*)

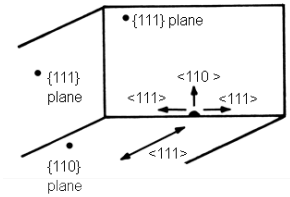

Bend bar orientation

Case E

(a)

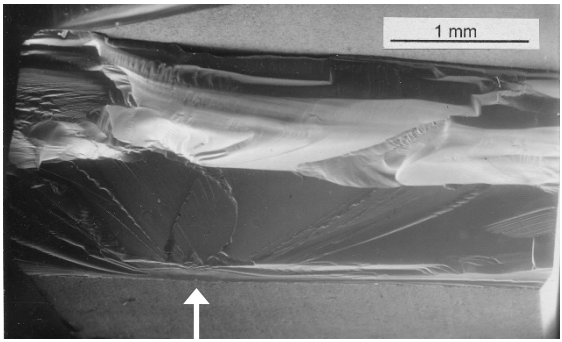

(b)

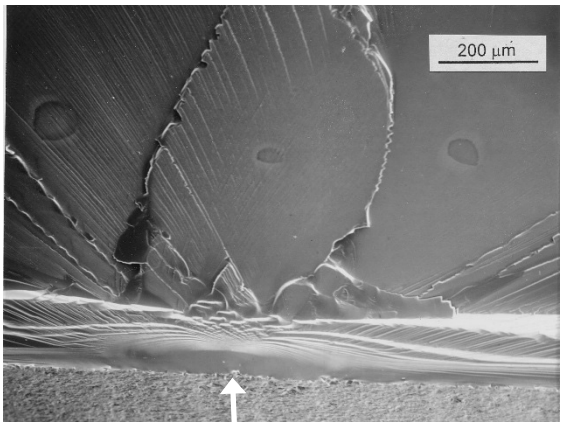

(c)

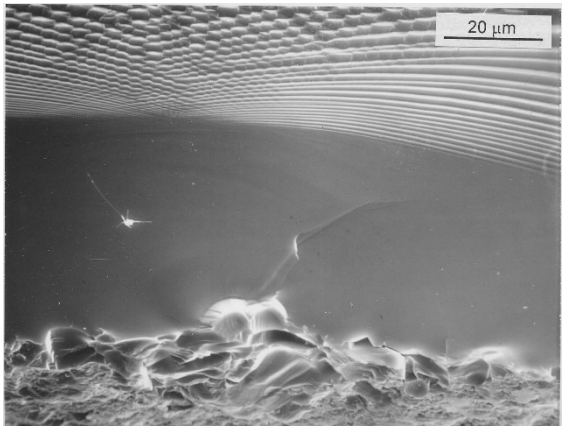

Figure 8.18 *Spinel bend bar with a {110} tensile surface and <111> tensile axis designed to cause fracture on a {111} plane. (325 MPa) (a) shows the whole fracture surface and the major crack redirection on the top half, (b) shows the "**gull wing mirror**," and (c) shows the grinding crack fracture origin. (Case **E**, Table 8.3) (Courtesy R. Rice)*

Scarps can occur in single crystals and are indicative of the presence of liquid during fracture. Figure 5.55 in chapter 5 showed scarps in sapphire. Figure 8.21d below shows another example.

Arrest lines are not common, but multiple distinct examples were shown on a KCl crystal cleaved with a hammer and chisel by Orowan at 400 ^{o}C.[17] He also noted that extensive plastic deformation involving dislocations could occur at arrest lines, which made the arrest lines very pronounced on a fracture surface. His 1962 study focused a great deal on dislocation activity in high temperature fractures and was typical for that era. There was surprisingly little about preexisting flaws or fracture origins!

One should not be surprised if fracture surface *oddities* crop up occasionally. A recent example is "hackle nodes" that Salem et al. detected in slabs of an exotic Nd:YVO_4 single crystals that broke from thermal stresses.[24] These are sites where hackle lines converge or diverge. Figure 8.19 shows an example for a prototype amplifier slab. Cleavage step hackle lines emanated from a surface crack fracture origin site, then curved around and converged from different directions to a final stopping point termed a "hackle terminus node." All the converging hackle lines made it seem like an origin, *i.e*, an initiation point, but careful examination showed it was in fact a terminus!

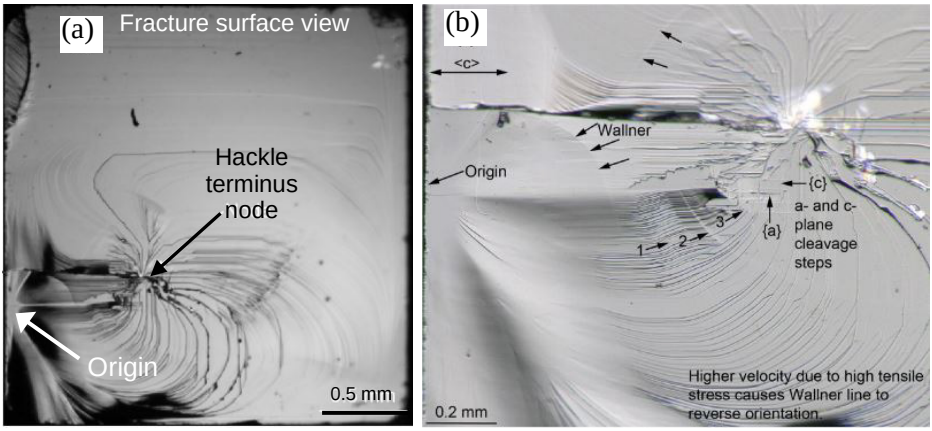

Figure 8.19 An unusual fracture surface of a beam-shaped "slab" of a Nd:YVO_4 single crystal. The surface crack fracture origin is marked on the left. Hackle lines emerge from it, curve around, and then converge at a "hackle terminus." (b) is a closeup of (a). (both images are courtesy of J. Salem)

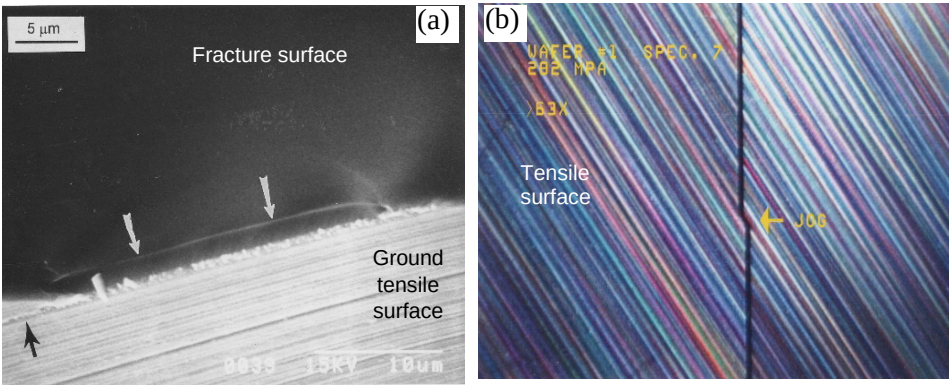

Figure 8.20 *Fracture origin of the silicon wafer shown previously in Figure 8.6. (282 MPa) (a) shows the origin is a grinding crack that extends only 2 mm below the tensile surface and is associated with a grinding striation (groove) that seems to be deeper and has caused greater cracking than other nearby striations. (b) is an optical microscope photo of the outer tensile surface and shows the grinding direction is slightly different than the final plane of fracture. The jog in the crack plane is in fact the origin seen in (a). The fractographer should be alert to subtle features like the jog. They are important clues.*

8.5 Origins

Single crystals are very sensitive to surface contact damage of any type. The low fracture toughness and high stiffness means that tiny strength-limiting cracks can easily pop into the crystal. There are no grain boundaries or other microstructural features to impede or redirect surface-initiated cracks. Grinding or polishing flaws are common fracture origins. Flexure and tensile specimens are very sensitive to edge flaws and special care must be taken with the edge beveling or rounding procedures. Figure 8.20 shows the grinding crack origin of the silicon wafer shown earlier in Figure 8.6. Single crystals are very susceptible to polishing flaws. Subsequent polishing or finishing may eliminate any surface trace or scratch associated with the flaw, rendering final optical inspections ineffective. Figure 8.21 shows an example in a sapphire dome. Figure 8.7 earlier in this chapter is another example of a sapphire dome with subtle scratch surface damage. Surface impact or contact loading may create cracks that may be extended by subsequent loading. Alternately, there may be stresses already present in the part that can propagate the crack when it is created by the impact event. Figure 8.22 shows an example where a small high velocity particle “dinged” the surface of a sapphire missile dome. Thermal stresses further propagated the small crack causing the dome to break.

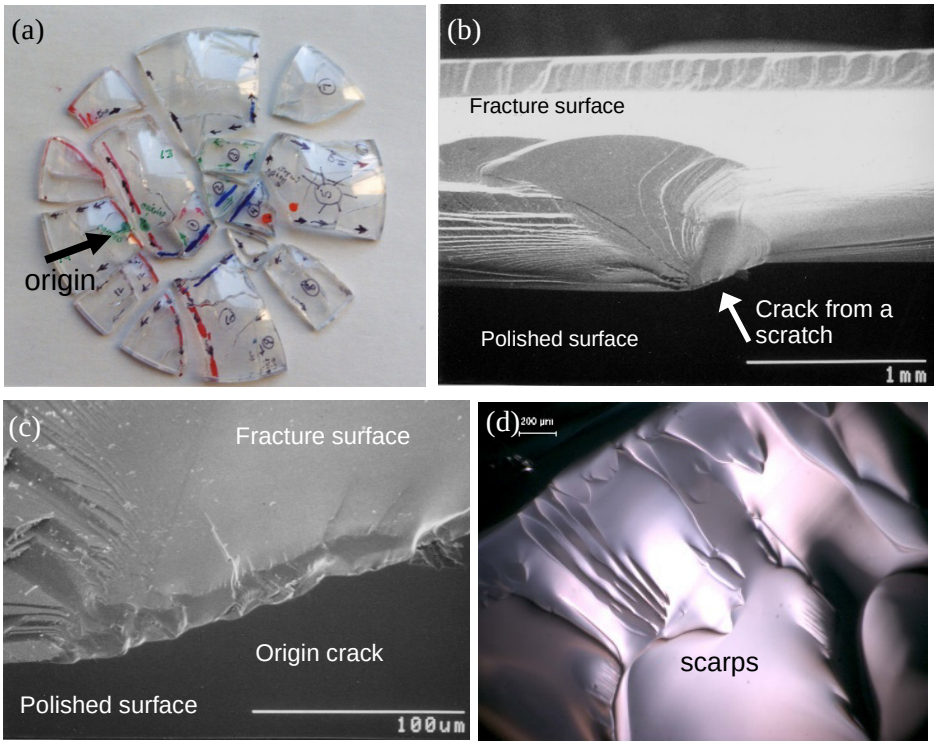

Figure 8.21 *Polishing (or grinding) crack origin in a sapphire dome (#1037) that broke during a thermal shock proof test. (a) shows the entire fractured structure. (b) shows an SEM photo of the origin piece tilted back. Fracture followed the axis of a polishing scratch for a short distance, but then quickly shifted to a different plane. (c) is a SEM close-up of the origin. The piece is tilted back to show both the fracture and outer polished surfaces. There is* <u>*no trace*</u> *of damage on the polished surface. Figure 6.32 in chapter 6 shows this scratch origin. (d) shows scarps on another piece. Scarps are discussed in section 5.6 in chapter 5 and Figure 5.55. They are indicative of the presence of water when fracture occurred.*

Other surface flaws may originate as a result of processing conditions. Figures 8.23 and 8.24 show fractures in microelectromechanical (MEMS) sized single crystal silicon theta specimens.[25,26] Deep reactive ion etching (DRIE), a lithographic process used to prepare integrated circuits and small structures, was used to fabricate the specimens from a standard {100} type silicon wafer. This process created the surface damage that was strength limiting in this case. Figure 6.93 in chapter 6 shows other theta specimen origins.

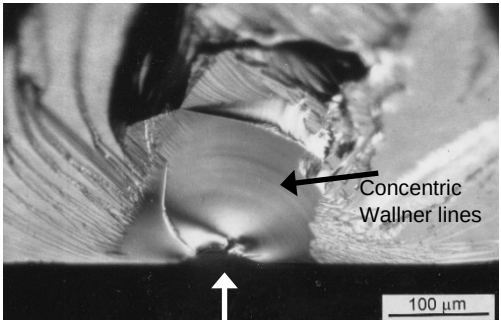

Figure 8.22 *Impact crack fracture origin in a hemispherical sapphire missile dome (#SN37) while the dome was under thermal stress in a high Mach wind tunnel. A debris particle flying down the wind tunnel created the impact crack. Note that this is a starter crack and not a fracture mirror. The 150 µm deep crack has concentric tertiary Wallner lines that are telltale signs of impact. Thermal stresses propagated the crack causing dome breakage. See Figure 3.10 in chapter 3 and Figure 4.21 in chapter 4 for views of the entire dome and the sketch of the fracture sequence.*

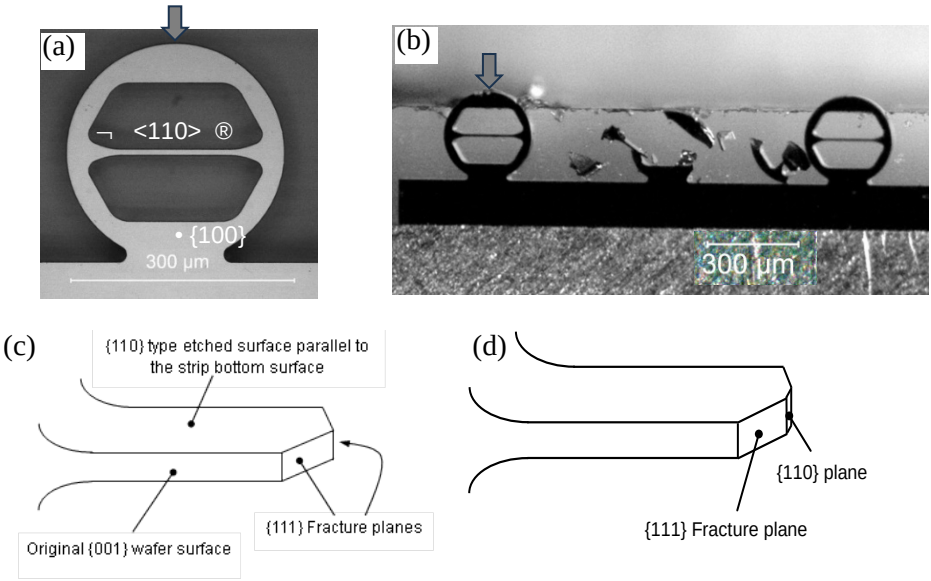

Figure 8.23 *Tiny silicon theta test specimens. The ring shown in (a) is compressed on its rim on the top and bottom (large arrow) in a nanoindenter causing the 7.5 µm tall by 100 µm thick web section in the middle to stretch sideways in uniaxial tension. (b) shows a fractured specimen on a strip. (c) shows that the web fractures usually occurred on {111} cleavage planes. (d) A few initiated on {110} planes but then changed to {111} planes. Origin flaws are shown in the next figure.*

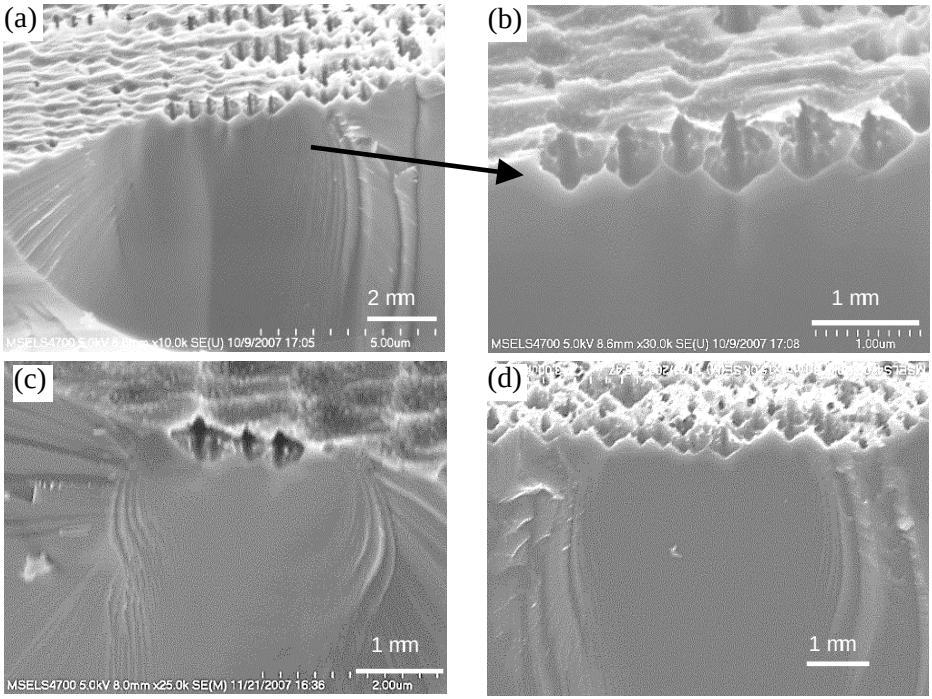

Figure 8.24 *Fracture origins in single crystal silicon theta specimens. (b) is a close-up of (a). The "cathedral mirrors" are very clear. The origins are etch pits from the DRIE processing. The cusps between them are sharp and probably initiated cracks. Figure 6.93 shows other sharp cusp origins.*

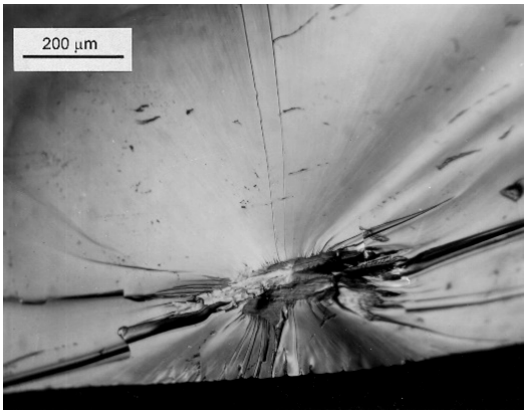

Figure 8.25 *Internal origin in a flame-polished non-stoichiometric spinel single crystal. The bend bar strength was 238 MPa. (courtesy R. Rice)*

Volume-distributed flaws such as pores, inclusions, or compositional inhomogeneities can also cause fracture. They usually will stand out quite clearly on the fracture surface. Newcomb and Tressler[27] and Rice[28] showed pore examples in sapphire fibers. An example of an internal origin in a nonstoichiometric spinel (alumina rich) is shown in Figure 8.25.

Twinning can initiate fractures, especially if twins from different planes intersect and nucleate cracks. Figure 8.26 shows twins that controlled the strength in a sapphire bend bar tested at high temperature. This failure mechanism is especially a problem in sapphire since twins are easily nucleated by even small compression stresses at fairly low temperatures (300 ºC to 500 ºC). They cause drastic reductions of compression and flexure strengths in some orientations.[29,30,31] They sometimes form with an audible pop.[24] It has even been reported that twins can form in sapphire from sudden temperature

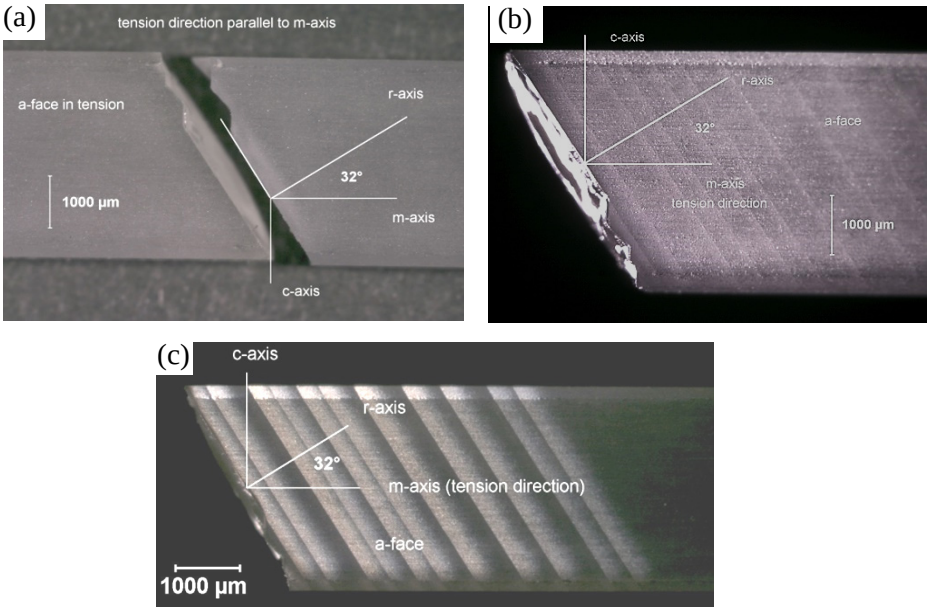

Figure 8.26 *Twinning in a sapphire bend bar in an elevated temperature bend bar specimen. The bar was cut with an a-plane tensile surface and an intended m-plane fracture surface. It instead broke on the r-plane. Cracks were created by twins that probably initiated from the* <u>*compression*</u> *side of the bend bar specimen. (a) shows the tensile face under ordinary lighting and the twins are indiscernible. (b) shows the same specimen, but with common reflected lighting adjusted to reflect off the twins. (c) shows the bar between crossed polarizers that make the twins much easier to detect.*

changes and hydrostatic compression.[32] Some twins may simply be growth twins that formed during fabrication and not during usage or mechanical loading. Possible examples in sapphire are shown in Case 15 in Chapter 10, "The Case of the Ruined Refractors."

Figures 8.27 and 8.28 show two fractured c-axis sapphire tubes with intersecting twins that created fracture origin cracks. The tubes were 38 mm in diameter and 400 mm long and fractured during two runs of a prototype plasma asher. This is a device used to dry-remove photoresist from large 300 mm diameter silicon wafers during manufacture of integrated circuits. The tubes contained oxygen and nitrogen gasses which were energized into a plasma state by a 2.5 kW microwave chamber which was cycled on and off in 60 s intervals. The sapphire tubes reached temperatures of 600 ºC to 700 ºC. One tube broke during a gas purge step three seconds after the shutdown of the microwave energy. The second tube broke two minutes after a shutdown. The tubes should have had lifetimes in excess of 400,000 cycles. Breakage during cool down suggested thermal stresses had contributed to fracture, but this was not the full story. The cracks curved and wiggled at the tube ends, indicating the cracks slowed down and arrested. Some of the cracks crossed over each other, indicating that primary cracks did not run all the way through the wall thickness. During optical microscopic examination of one of the fracture surfaces, using common reflected light, a *momentary chance reflection off one surface* revealed thin parallel reflective lines that ran counter to the fracture surface faceting as shown in Figure 8.27b. This was a sign of twinning. The next step was to view the tubes between crossed polarizers (with the results shown in Figure 8.28. Multiple twins in the hot region triggered crack formation at twin intersections. The twins were oriented at 32º to the sapphire tube axis corresponding to classic r-plane twinning in sapphire, which can be caused by rather low compression stresses at temperatures as low as 300 º to 500 ºC.[29]

Fracture of these tubes occurred in two stages. First, axial constraint from a new type of seal at the tube ends prevented their free expansion during the heating portion of the operating cycle. The earlier model tubes that did not have breakages used a different seal design that allowed expansion. The constraint in the new design created axial compression stresses that created intersecting twins that in turn generated cracks. The cracks grew in stages and propagated by cool down thermal stresses until the tube ruptured. The problem was solved when the seal design was changed to allow for tube expansion.

(a)

(b)

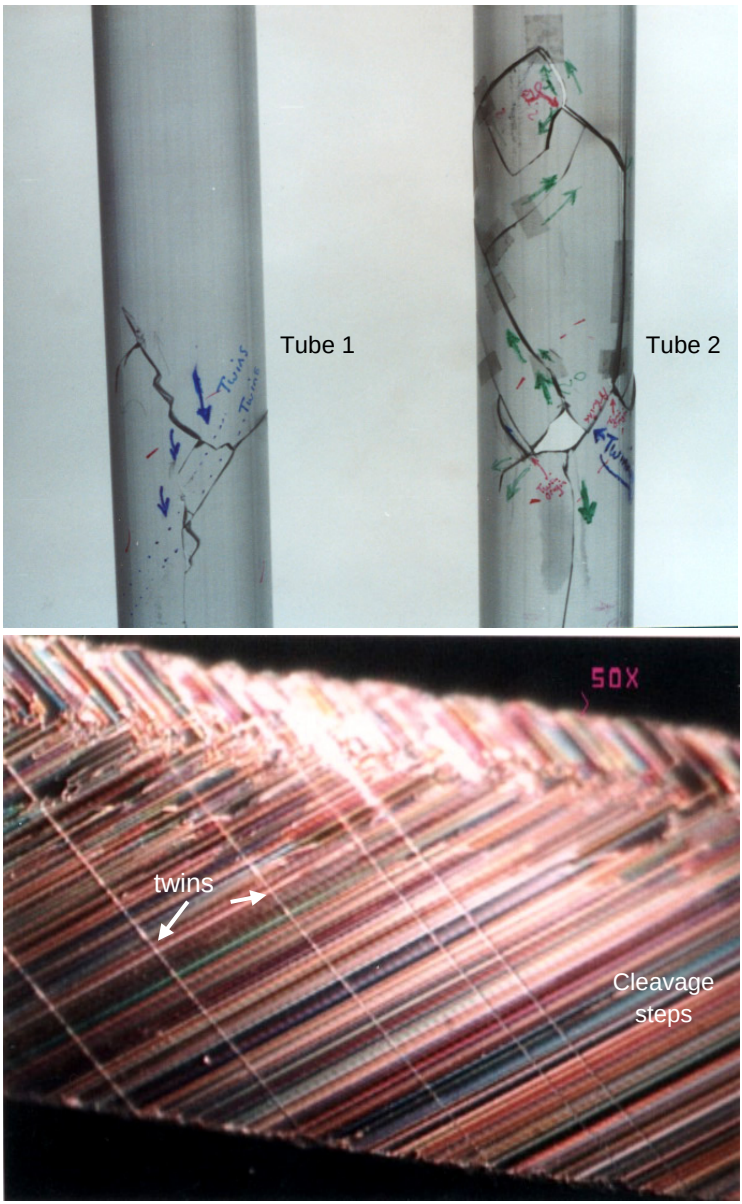

Figure 8.27 *Two broken 38 mm diameter sapphire tubes from an integrated circuit plasma asher. Although the locations of twins are marked with felt tip pens, the twins are* <u>*not visible*</u> *in this lighting. (b) shows a stereo optical microscope photo close-up of the very faceted fracture surface of a fragment from the middle of one tube in normal white light illumination at just the right angle. Five thin twin bands are visible against the facetted surface. The next figure reveals the twins much better.*

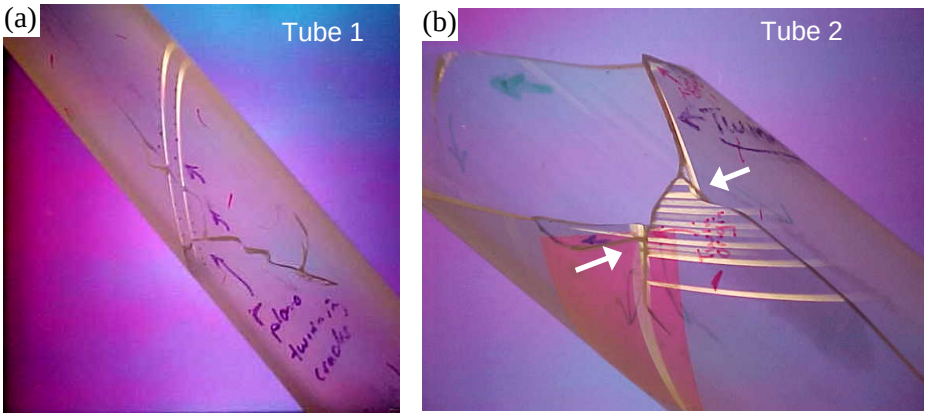

Figure 8.28 *Twin bands became very apparent when the sapphire tubes were illuminated by light from crossed polarizers. Cracks initiated at twin band intersections (white arrows) and then were propagated by cooldown thermal stresses. (Photos courtesy R. Pingree)*

Case study 13 in Chapter 10 is a complex sapphire solar refractor part. It also shows twins, but they were incidental and not the cause of fracture. Very tiny "micro twins" were also detected in that part. These presumably were the nuclei of twin bands that would have grown much larger with time or they may have been growth twins. The fractographer should be on the lookout for twins in materials such as sapphire. They may be present, but not necessarily the cause of fracture.

Earlier in this chapter that if a preferred cleavage pane is perpendicular to the maximum principal tensile stress, the fracture surface will be flat and smooth and at right angles to the tensile stress. If the preferred cleavage plane is not perpendicular to the maximum principal tensile stress, then the fracture plane may be at an *inclined angle to the tensile stress.* This is an exception to the law of normal crack propagation discussed in section 4.3. In some extreme cases, the loading geometries and stresses may be such that fracture is forced to occur on an unfavorable plane, such as the basal plane in a sapphire tube shown in Figure 8.29. The fracture surface is extremely jagged with many zig-zags. Other examples of basal plane fracture in sapphire are shown in references 10, 27, and 33.

Good estimates of the fracture toughness K_{Ic} may be obtained from fracture mechanics analyses of flaws. For example, the long uniform 2 mm deep surface crack in the silicon wafer shown in Figure 8.20a combined with a break stress of 282 MPa and a shape factor Y = 1.99 produced an estimate of K_{Ic} = 1.99

(282) Ö2 x 10^{-6} = 0.79 MPaÖm in good agreement with values in table 8.1. Rice showed good examples.[19,28] Newcomb and Tressler[27] measured fracture toughness on the basal plane of sapphire by this approach. Other methods usually fail to get values for the basal plane due to the difficulty of controlling fracture on this plane. The Knoop surface crack in flexure method has been effective in studying fracture behavior of single crystals.

(a)

(b)

(c)

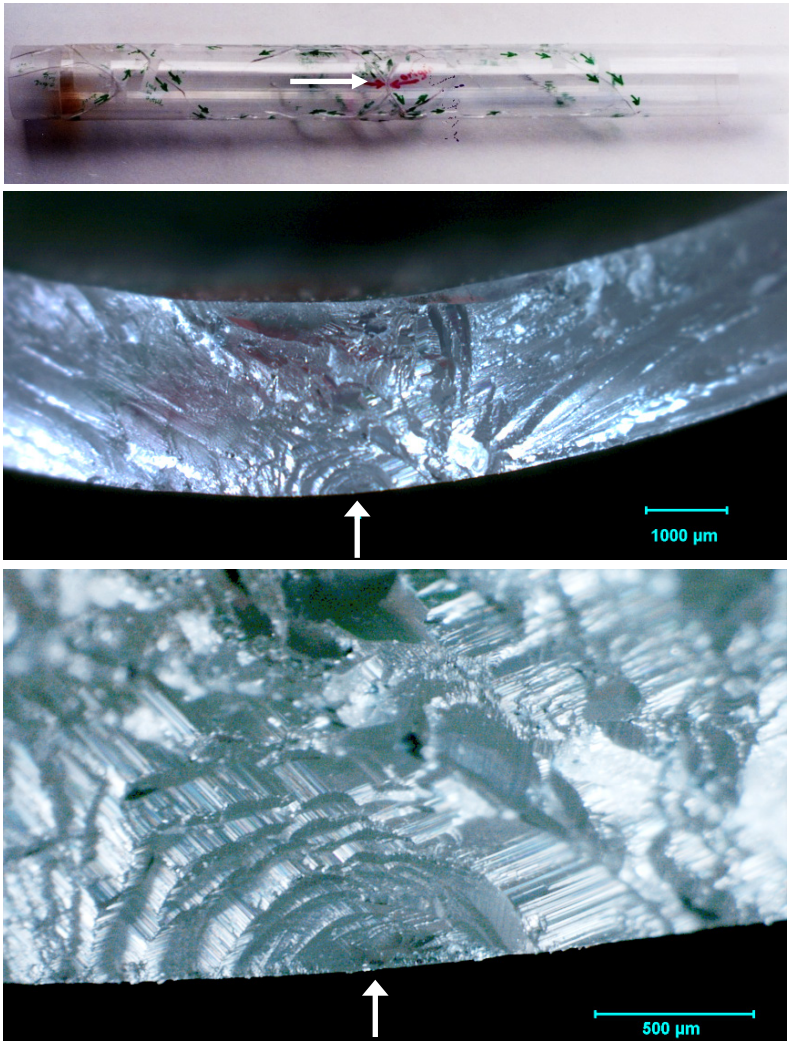

Figure 8.29 *Example of basal plane fracture in a c-axis sapphire tube that fractured from severe thermal shock (a). The origin in the middle (large arrow) and is perpendicular to the tube axis. Thermal stresses acted in the axial direction. (b) and (c) show the mirror and origin.*

8.6 Other Sources

Rice has written several outstanding, richly-illustrated papers on fractography of single crystals. His 1984 book-length article[19] has over thirty figures showing fracture surfaces in MgO, $MgAl_2O_4$, Si, SiC, Al_2O_3, ZrO_2, CaF_2, and W. His 1998 54-page paper[20] has six pages of illustrations and a discussion of fracture markings in various single crystal ceramics.

Chapter 8 References

1. R. A. Schultz, M. C. Jensen, and R. C. Bradt, "Single Crystal Cleavage of Brittle Materials," *Int. J. Fract.*, **65** [4] (1994) 291 - 312.
2. R. C. Bradt, "Cleavage of Ceramic and Mineral Single Crystals," pp. 355 – 365 in *Cleavage Fracture*, Proceedings of a Symposium at the 1997 TMS Fall meeting, Indianapolis, IN, Sept. 15- 17, 1997, ed. K. S. Chan, The Minerals, Metals, and Materials Society, Warrendale, PA, 1997.
3. C. C. M. Wu, K. R. McKinney, and R. W. Rice, "Zig-zag Crack Propagation in $MgAl_2O_4$ Crystals," *J. Mat. Sci. Lttrs.*, **14** (1995) 474 – 477.
4. C. P. Chen and M. H. Leipold**,** "Fracture Toughness of Silicon," *Bull. Am. Cer. Soc.*, **59** [4] (1980) 469 - 472.
5. Y-B. Xin, K. J. Hsia, and D. A. Lange, "Quantitative Characterization of the Fracture Surfaces of Silicon Single Crystals by Confocal Microscopy," *J. Am. Cer. Soc.*, **78** [12] (1995) 3210 – 3208.
6. A. Masolin, P.O. Bouchard, R. Martini, M. Bernacki, "Thermo-mechanical and Fracture Properties in Single-Crystal Silicon," *J. Mater Sci.*, **48** (2013) 979 - 988.
7. B. N. Jaya, C. Kirchlechner, and G. Dehm, "Can Microscale Fracture Tests Provide Reliable Fracture Toughness Values? A Case Study in Silicon," *J. Mater. Res*, **30** [5](2015)686–698.
8. R. L. Stewart, M. Iwasa, and R. C. Bradt, "Room Temperature K_{Ic} Values for Single-Crystal and Polycrystalline $MgAl_2O_4$," *Comm. Am. Cer. Soc.*, Feb. 1981, C22 - C23.
9. R. L. Stewart and R. C. Bradt, "Fracture of Single Crystal $MgAl_2O_4$," *J. Mat. Sci.*, **15** (1980) 67 - 72.
10. M. Iwasa and R. C. Bradt, "Fracture Toughness of Single-Crystal Alumina," pp. 767 – 779 in *Advances in Ceramics*, Vol. 10, ed. W. Kingery, American Ceramic Society, Westerville, OH, 1984.
11. Y. Akimune and R. C. Bradt, "Knoop Microhardness Anisotropy of Single-Crystal Stoichiometric $MgAl_2O_4$ Spinel," *J. Amer. Cer. Soc*., **70** [4] (1987) C84 – C86.
12. M. Iwasa and R. C. Bradt, "Cleavage of Natural and Synthetic Single Crystal Quartz," *Mat. Res. Bull.*, **22** (1987) 1241 - 1248.
13. S. W. Wiederhorn, B. J. Hockey, and D. E. Roberts, "Effect of Temperature on the Fracture of Sapphire," *Phil. Mag.* **28** (1973) 783 - 796.
14. J. A. Salem, "Slow Crack Growth and Fracture Toughness of Sapphire for the International Space Station Fluids and Combustion Facility," NASA TM 214023, NASA Glenn Center, Cleveland, OH, 2006.
15. B. K. Atkinson and P. G. Meredith, "Experimental Fracture Mechanics Data for Rocks and Minerals," pp. 477 – 525 in *Fracture Mechanics of Rock*, ed. B. K. Atkinson, Academic Press, London, 1987.
16. D. Black and G. D. Quinn, "X-ray Topography for Fractography of Single-Crystal Components," *J. Fail. Anal. Prev.*, **6** [3] (2006) 79 - 86.

17. E. Orowan, “Task 7, Fracture Mechanisms,” pp. 296 – 325 in “Studies of the Brittle Behavior of Ceramic Materials,” final report of Armour Research Institute of Illinois Institute of Technology, editor. N. A. Weil, to Aeronautical Systems Division of Air Force Systems Command, Wright-Patterson Air Force Base, Ohio, ASD TR-61-628, April 1962.
18. R. W. Rice, “Fractographic Determination of K_{Ic} and Effects of Microstructural Stresses in Ceramics,” pp. 509 – 545 in *Fractography of Glasses and Ceramics II,* eds. V. Fréchette and J. Varner, 1991.
19. R. W. Rice, “Ceramic Fracture Features, Observations, Mechanisms and Uses,” pp. 5 –102 in *Fractography of Ceramic and Metal Failures,* ASTM STP 827, eds. J. Mecholsky and Powell, 1984, American Society for Testing and Materials, West Conshohocken, PA, 1984.
20. R. W. Rice, “Perspectives in Fractography,” pp. 3-56 in *Fractography of Glasses and Ceramics,* Advances in Ceramics, Vol. 22, eds. J. Varner and V. Fréchette, American Ceramic Society, Westerville, OH, (1988).
21. S. W. Freiman, J. J. Mecholsky, and P. Becher, “Fractography: A Quantitative Measure of the Fracture Process,” pp. 55 - 78 in *Fractography of Glasses and Ceramics, II* , eds. V. Fréchette and J. Varner, American Ceramic Society, Westerville, OH, 1991.
22. Y. L. Tsai and J. J. Mecholsky, Jr., “Fracture Mechanics Description of Fracture Mirror Formation in Single Crystals,” *Int. J. Fract*., **57** (1992) 167 - 182.
23. K. Gopalakrishnan and J. J. Mecholsky, Jr., “Quantitative Fractography of Mixed-Mode Fracture in Soda Lime Silica Glass,” *J. Am. Cer. Soc*., **95** [11] (2012) 3622 - 3627.
24. J. Salem, C. He, N. Sawruk, S. Litovich, and M. Jenkins, “Thermally Driven Failure of Nd:YVO4 Amplifier Crystals,” *J. Eur Ceram. Soc.,* **40** [14] (2020) 4939 – 4948.
25. G. D. Quinn, E. Fuller, D. Xiang, A. Jillavenkatessa, L. Ma, D. Smith, and J. Beall, “A Novel Test Method for Measuring Mechanical Properties at the Small -Scale: The Theta Specimen,” *Cer. Eng. Sci. Proc*., **26** [2] (2005) 117 – 126.
26. G. D. Quinn, “Fractographic Analysis of Miniature Theta Specimens,” *Cer. Eng. Sci. Proc.,* **29** [3] (2008) 189 – 199.
27. S. A. Newcomb and R. E. Tressler, “High-Temperature Fracture Toughness of Sapphire,” *J. Am. Cer. Soc*., **77** [11] (1994) 3030 – 3032.
28. R. W. Rice, “Corroboration and Extension of Analysis of c-Axis Sapphire Filament Fractures from Pores,” *J. Mat. Sci. Lttrs*., **16** (1997) 202 – 205.
29. F. Schmid and D. C. Harris, “Effects of Crystal Orientation and Temperature on the Strength of Sapphire,” *J. Am. Cer. Soc*., **81** [4] (1998) 885 – 93.
30. P. F. Becher, “Fracture Strength Anisotropy of Sapphire,” *J. Am. Ceram. Soc*., **59** [1-2] (1976) 59 –61.
31. W. D. Scott and K. K. Orr, “Rhombohedral Twinning in Alumina,” *J. Am. Ceram. Soc.*, **66** [1] (1983) 27 – 32.
32. L. M. Belyaev, *Ruby and Sapphire*, Translated from Russian, Amerind Publ. Co., New Delhi, 1980, pp. 286.
33. R. W. Rice and P. F. Becher, “Comment on Creep Deformation of 0° Sapphire,” *J. Am. Cer. Soc.,* **60** [3-4] (1977) 186 – 188.

9 Ceramic and Glass Composites

9.1 Particulate, Whisker, or Self-Reinforced Ceramic Composites

Ceramics or glasses that are reinforced by second phases, whiskers, or particulates may be examined using the same equipment and techniques as used for monolithic materials. The reinforcing agents act to deflect or bridge cracks and create very rough fractures surfaces that may mask classical fracture surface features such as Wallner or hackle lines.

The composite ideally should have a controlled microstructure such that the reinforcing phase is uniformly distributed. This is routinely achieved with glass ceramics, but is more problematic with fiber or particulate-reinforced ceramics. Sometimes the reinforcing agent forms clumps or aggregates that can act as strength-limiting flaws as shown in Figure 9.1. Flaws of this type may be broadly described as compositional inhomogeneities using the logic in chapter 6, but more specific descriptors are probably better (fiber clump, fiber tangle, platelet cluster, etc.).

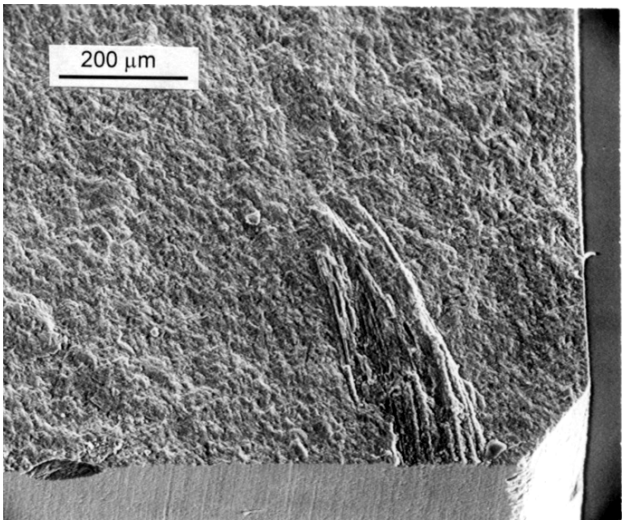

Figure 9.1 *Nonuniform dispersal of toughening agents often causes strength-limiting flaws in ceramic composites. This figure shows a whisker clump that was the strength-limiting flaw in a siliconized SiC bend bar. The material was made by mixing chopped carbon fibers with SiC starting powders and then infiltrating with silicon. The carbon fibers were intended to react with the silicon to form dispersed silicon carbide fibers that would toughen the matrix.*

Second phase aggregates can also inhibit local sintering causing pockets of porosity that also act as strength limiting flaws. Self-reinforced materials that rely on interconnected elongated-grain microstructures may develop excessively large grains that control strength as shown in Figures 6.25c and d. Very often reinforcing agents such as SiC whiskers can create local chemistry imbalances in the matrix leading to exaggerated grain growth. SiC whisker-reinforced alumina for cutting tools is an example. These large grains then can act as flaws. In the examples above, the very agents used to reinforce the material caused flaws that limited the material's strength.

9.2 Fiber-Reinforced Composites

Long, one-dimensional fiber-reinforced ceramics and glasses may have much greater resistance to fracture if stressed in the same direction as the fiber reinforcements. Usually the fibers have greater strength and elastic modulus than the matrix. Optimum bonding does not necessarily mean perfect bonding, however, since the latter would lead to cleavage through the reinforcing fibers. Optimum bonding is such that the fiber-matrix interface is able to transmit some load, but then fractures or debonds along the interface. The fibers pull out of the matrix with additional loading. While pulling out they exert frictional or mechanical interlocking resistance so that more energy is consumed. The microstructure is designed to shed load from the matrix to the strong fibers and to divert cracks in the matrix to run along the matrix fiber interface. The processing must be done carefully so that the interface strength is controlled, and that the fiber does not deteriorate too much from micro-structural changes, surface pitting, or interactions with the matrix.

Fractography of continuous fiber-reinforced ceramics and glasses is different than that for monolithic materials. Fracture surfaces are often very rough and there often is no point looking for a specific fracture origin. There are exceptions. Figures 9.2 and 9.3 shows a silicon carbide filament-reinforced silicon nitride that did have discrete fracture origins.

Fracture typically entails damage accumulation and coalescence leading to rupture. Often the objective is to observe the general fracture mode and to ascertain whether it was due to tensile fiber pull out and fiber rupture, shear delamination in the matrix parallel to the fibers, compression buckling of fibers, or buckling of a protective coating in compression. The failure mode depends upon whether the structure is one-, two-, or three-dimensionally

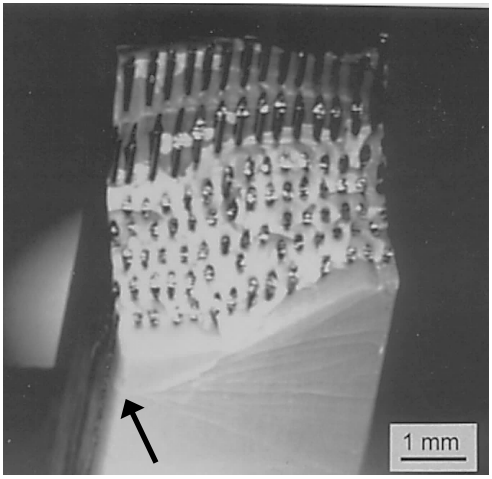

Figure 9.2 *A CVD SiC (SCS-6) filament-reinforced Si_3N_4 bend bar tilted back at an angle so as to view the fracture and tensile surfaces. A series of branching cracks radiate outwards from one origin site (arrow).*

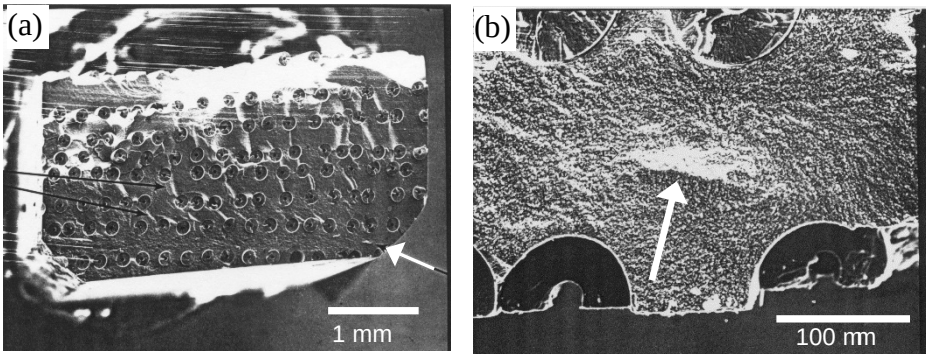

Figure 9.3 *Fracture surface of CVD SiC filament reinforced Si_3N_4 bend bar. (Ref. 1) (a) shows that there was not very much fiber pullout in this case. Wake hackle in the matrix behind the filaments are telltale indicators of the local direction of crack propagation through the matrix and lead back to the origin, which is a porous seam in the matrix shown by the white arrows in (a) and (b).*

reinforced and the size and shape of the component and the loading conditions. Although bend testing is reliable for creating tensile fractures in monolithic ceramics and glasses, composites are more susceptible to alternative failure modes when loaded in bending. Figures 9.4 and 9.5 shows tensile stress fractures with good pull-out in a fiber-reinforced epoxy and a ceramic, respectively.

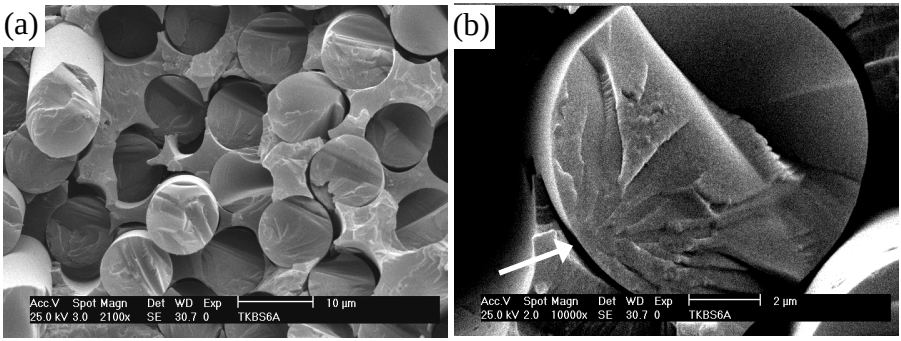

Figure 9.4 *Fracture surface of an E-glass fiber reinforced epoxy matrix one-dimensional composite. (b) shows the origin in one fiber. (courtesy S. Scherrer)*

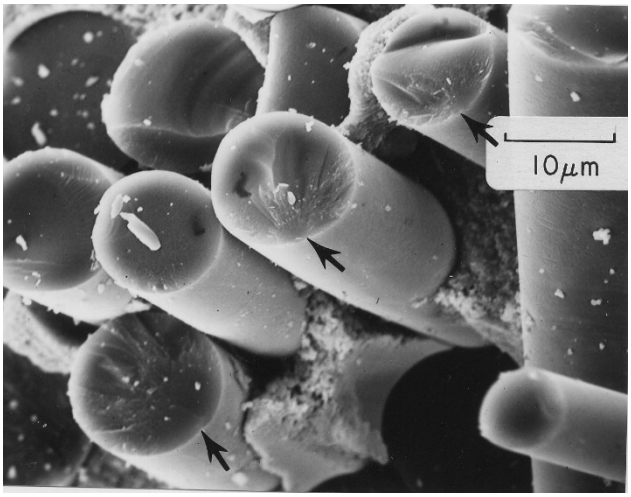

Figure 9.5 *SEM image of the fracture surface of a SiC (Nicalon) ceramic fiber – zirconia matrix composite. The arrows mark fracture origins and mirrors in several fibers. (Ref. 2, courtesy of R. Rice)*

Images such as these can be used to qualitatively assess the fiber-matrix interface bonding and also if any damage has been done to the fibers during processing. Very often the fibers have fracture mirrors, and it is instructive to ascertain whether the fibers have fractured from surface or internal flaws. Furthermore, the fracture mirror sizes in the fibers may be analyzed and used to obtain good estimates of the stress at fracture in the fibers. This strength can be compared to analytical predictions for the composite behavior to determine whether the load redistribution to the fibers was as expected. The strength of the fibers in the matrix may be compared to the strength of virgin fibers tested alone. Processing interactions with the matrix or with a fiber coating often weakens the fibers.[3,4,5,6,7,8]

Some material science or material development investigations focus on crack interactions with the structure. The scanning electron microscope is the preferred tool. Emphasis is placed on cracking in the fibers, the fiber pullout lengths, cracking in and around the fiber-matrix interface, or the microcrack density in the matrix. Micro-analytical chemical analyses are often used to study the chemistry of the fibers and the interfaces.

The usual desired mode of fracture is one with a very rough fracture surface with ample fiber pullout. Observation that portions of a composite structure have fractured in a planar fashion with minimal pull out is often a sign that some deterioration in the composite has occurred or that the fiber-matrix bond is too strong. For example, Glass et al.[9] analyzed a spectacular rupture of a large fiberglass–epoxy tank that stored pressurized sulphuric acid. Large portions of the tank had the classic rough fracture fractures with extensive fiber pullout, but the origin region had flat planar fracture zones. The cause was traced to spilled acid on the exterior surface that penetrated matrix microcracks and reached and degraded the reinforcing E-glass fibers. Fracture mirror analysis showed the fibers broke at only 20 % to 40 % of the baseline fiber strengths. Progressive fracture from the exterior occurred over a period of time as outer fibers broke, matrix microcracks opened up, and more acid penetrated and damaged more fibers until the vessel ruptured.

Composites that are exposed to elevated temperature sometimes fracture with planar fracture regions near the surface surrounding a core of rough fibrous fracture in the core.[10,11,12] Oxidation, corrosion, or surface reactions can alter the fiber–matrix bonding or fiber strength causing composite degradation.

Composites that are tested transversely, that is with tensile stresses perpendicular to the fiber directions, are usually very weak. Fractography in such cases often is focused on the crack propagation paths around or through the fiber and the fiber-matrix interface. Hull shows several examples in section 7.2 in his book on fractography.[13]

9.3 Dental composites

Although resin-matrix composite materials might seem to be outside the scope of this Guide, they are in fact brittle. Many dentists use dental composites as an alternative to ceramics, glass ceramics, or conventional porcelain fused to metal crowns. Crowns fractures are a serious problem. Fractographic analysis is underutilized by the dental materials community, but that is now changing in large part due to the leadership of Drs. S. Scherrer, J. Quinn, K. Anusavice, J. Mecholsky, M. Øilo, and J. R. Kelly as well as the widespread distribution of

the first edition of this Guide in 2007. Dental composites in the form of *"direct"* restoration monomers with ceramic or glass fillers can be applied to cavities in a patient's tooth in a dentist's office. They are cured in situ with a "blue" ultraviolet light to polymerize the material. Alternatively, larger *"indirect"* restorations such as crowns (for more damaged teeth) can be made by first making an impression. An outside laboratory then fabricates a custom shaped tooth restoration that is cemented onto the reduced and prepared tooth. These indirect restoration materials are typically prepared as blanks by a manufacturer and then are custom ground to shape. In some instances, an alternative procedure is taken whereby the dentist digitally scans a tooth and uses a CAD/CAM machine to mill crowns in the office. The blanks have a resin matrix with a very high glass or ceramic filler content, and are designed to have good strength, wear and fracture resistance, and good aesthetics. They behave as brittle materials and are usually linear to fracture when strength tested in a laboratory. A simple rule of thumb is that the more the filler, the more the material will fractographically resemble glasses and ceramics. Filler contents of as much as 70% by volume are not uncommon.[a]

There are some similarities, but many important differences in the fractography of dental composites versus dental glass ceramics and ceramics. The lower elastic modulus of resin composites and often lower strengths mean they have much less stored elastic energy when fracture occurs. Thus, there will be less fragmentation and branching. Fracture surfaces will have some of the same markings described in this book, but sometimes are described in the polymer literature with different nomenclature. The reader is referred to Roulin-Moloney's excellent book[14] on the fractography of polymers and composites for more information about resin-matrix composites in general. Much of the fractography is aimed at observing filler-matrix interfaces and what cracks do at the interfaces as opposed to finding origin flaws. Fracture mirrors may exist, and are described as smooth areas on the fracture surface at the origin. With highly-filled composites, the interpretation is the same as described in this book: the mirror is a smooth zone surrounding the fracture origin flaw. By the time the rough hackle lines form, the crack has reached terminal velocities (e.g., 800 m/sec) that are much slower than in glasses and ceramics. Figure 9.6 shows fracture surfaces of one such highly-filled resin matrix composite from Reference 15. It had a mean strength of 145 MPa, a Weibull modulus of about 10, and a fracture toughness of 0.9 MPaÖm to 1.3 MPaÖm indicative of a

[a] The distinctions between resin composite and ceramic have been blurred in the dental community. One company makes a very highly-filled, resin-matrix composite and terms it a ceramic, but most practitioners still regard it to be a resin-matrix composite. Another company makes a porous skeletal ceramic network then infiltrates it with a resin. Both phases are interconnected.

material with a slight R-curve. These materials have very small glass filler particles and are translucent. Inclusions and agglomerates are easy to detect in uncoated bend bars, either with reflected illumination or sometimes more effectively with transmitted illumination. Once the specimens have been examined in the natural state, they can be gold coated. The fracture surfaces will be much easier to interpret. On the other hand, mirrors in *unfilled* resins[14,16] might look similar, but they are not fracture mirrors. They are a

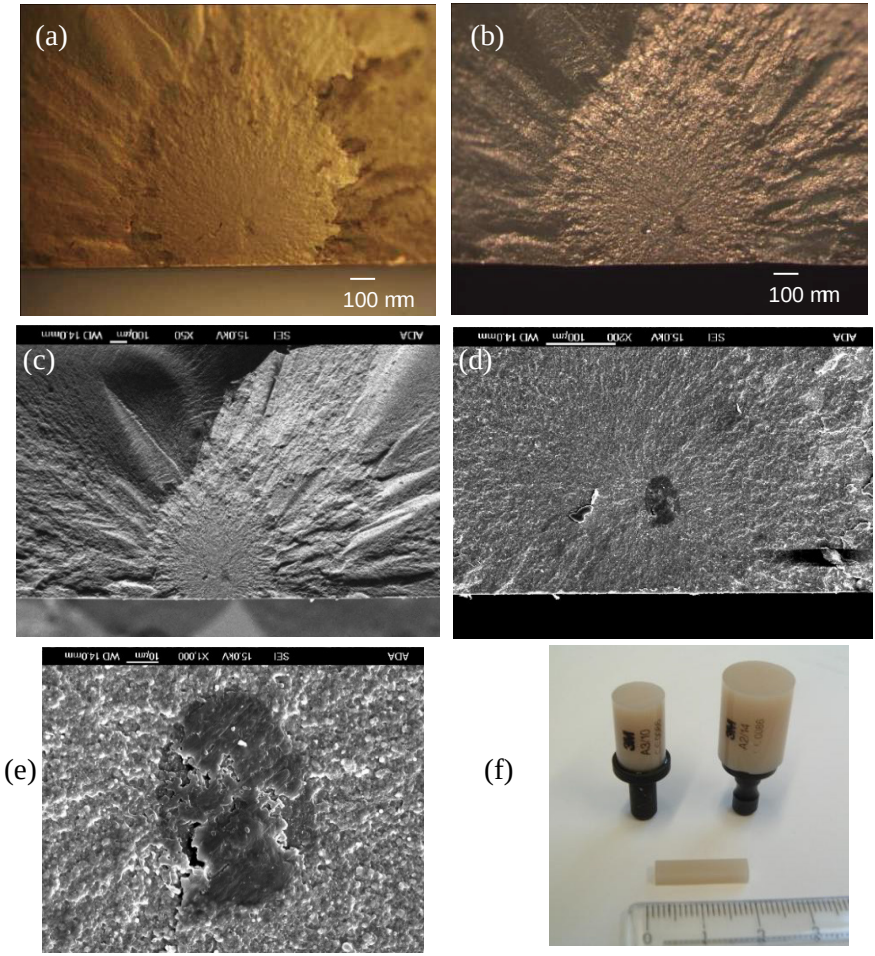

Figure 9.6 *Filled resin-matrix composite fractography. (a) shows the fracture mirror in an uncoated 3M Paradigm MZ 100 bend bar, with transmitted light through the bar, (b) shows the same view, but with reflected light after gold coating. (c) - (e) show SEM images of the mirror and the origin, a calcium-rich inclusion that is a volume-distributed flaw. (f) shows the original blanks and a machined bend bar with a mm scale. (a-e courtesy J. Quinn)*

region of slow crack extension that occurs prior to the crack going critical. The apparent "mirror" is the critical crack. So, one must be careful in interpreting fracture mirror constants in the polymers field. They may not be the same as those in the ceramic and glass field.

Chapter 9 References

1. J. J. Swab, G. D. Quinn, and D. J. Snoha, "Mechanical Behavior of a SiC-Fiber/Si_3N_4 Composite," U. S. Army MTL Technical Note TN 90-2, Watertown, MA, Sept. 1990.
2. R. W. Rice and D. Lewis, III, "Ceramic Fiber Composite Based Upon Refractory Polycrystalline Ceramic Matrices," pp. 117 – 142 in *Reference Book for Composite Technologies, Vol. 1*, ed S. N. Lee, Technomic Publ. Co., Lancaster, PA, 1989.
3. M. D. Thouless, O. Sbaizero, L. S. Sigl, and A. G. Evans, "Effect of Interface Mechanical Properties on Pullout in a SiC-Fiber-Reinforced Lithium Alumino Silicate Glass-Ceramic," *J. Am. Ceram. Soc.*, **72** [4] (1989) 525 - 532.
4. W. A. Curtin, "*In situ* Fiber Strengths in Ceramic-Matrix Composites from Fracture Mirrors," *J. Am. Ceram. Soc.*, **77** [1] (1994) 1075 –1078.
5. I. J. Davies and T. Ishikawa, "Mirror Constant for Tyranno Silicon-Titanium-Carbon-Oxygen Fibers Measured *In Situ* in a Three Dimensional Woven Silicon Carbide/Silicon Carbide Composite," *J. Am. Ceram. Soc.*, **85** [3] (2002) 691 - 693.
6. A. J. Eckel and R. C. Bradt, "Strength Distribution of Reinforcing Fibers in a Nicalon Fiber/Chemically Vapor Infiltrated Silicon Carbide Matrix Composite," *J. Am. Ceram. Soc.*, **72** [3] (1989) 455 - 458.
7. J. F. Jamet, D. Lewis, and E. Y. Luh, "Characterization of Mechanical Behavior and Fractographic Observations on Compglas SiC/LAS Composites," *Cer. Eng. Sci. Proc.*, **5** [7] (1984) 625 – 642.
8. A. C. Jaras, B. J. Norman, and S. C. Simmens, "The Measurement of Glass Fibre Strength in Composites from Studies of their Fracture Surfaces," *J. Mat. Sci.*, **18** (1983) 2459 – 2465.
9. S. J. Glass, E. K. Beauchamp, M. J. Carr, T. R. Guess, S. L. Munroe, R. J. Moore, A. Slavin, and N. R. Sorenson, "Failure Analysis of A Fiberglass-Reinforced Plastic Pressure Vessel," pp. 527 – 541 in *Fractography of Glasses and Ceramics, III, Ceramic Transactions*, Vol. 64, J. Varner, Fréchette, V., and G. Quinn, eds., American Ceramic Society, Westerville, OH, 1996.
10. K. M. Prewo, "Tension and Flexural Strength of Silicon Carbide Fibre-Reinforced Glass Ceramics," *J. Mat. Sci.*, **21** (1986) 3590 – 3600.
11. T. Mah, M. G. Mendiratta, A. P. Katz, R. Ruh, and K. S. Mazdiyasni, "High-Temperature Mechanical Behavior of Fiber-reinforced Glass-Ceramic Matrix Composites," *Comm. Am. Ceram. Soc.*, **68** [9] (1985) C 248 - C251.
12. T. Mah, M. Mendiratta, A. Katz, and K. Mazdiyasni, "Recent Developments in Fiber-Reinforced High Temperature Ceramic Composites," *Bull Am. Ceram. Soc.*, **66** [2] (1987) 304 – 308, 317.
13. D. Hull, Fractography, Observing, Measuring and Interpreting Fracture Surface Topography, Cambridge University Press, Cambridge, 1999.
14. A. C. Roulin-Moloney, *Fractography and Failure Mechanisms of Polymers and Composites*, Elsevier, London and New York, 1989.
15. J. B. Quinn and G. D. Quinn, "Material Properties and Fractography of an Indirect Dental Resin Composite," *Dent. Mat.*, **26** [6] (2010) 589 – 599.
16. E. H. Andrews, *Fracture in Polymers*, Elsevier, NY, 1968.

10. Case Studies

The following case studies illustrate the application of fractographic techniques for failure analysis.

Case 1: Ruptured Rotor (Ceramic Gas Turbine Rotor)

This is a case of a dynamic fracture of a part that broke under exotic laboratory testing conditions. The fractographic analysis involved a complex reassembly and a painstaking hunt for the fracture origin. The cause of fracture was unexpected and posed problems for the life-prediction analysts.

Figure 10.1 shows a model axial gas turbine rotor made of silicon nitride that was designed to fail. It was one of twelve such model structures made by the Ford Motor Company's scientific research laboratory in the mid-1980s.[1,2] It was part of an ambitious endeavor to use advanced ceramics in automotive gas turbine engines. A small project was set up to verify the ceramic design and reliability codes by using a simulated model rotor that was mounted in a hot-spin rig shown in Figure 10.1.

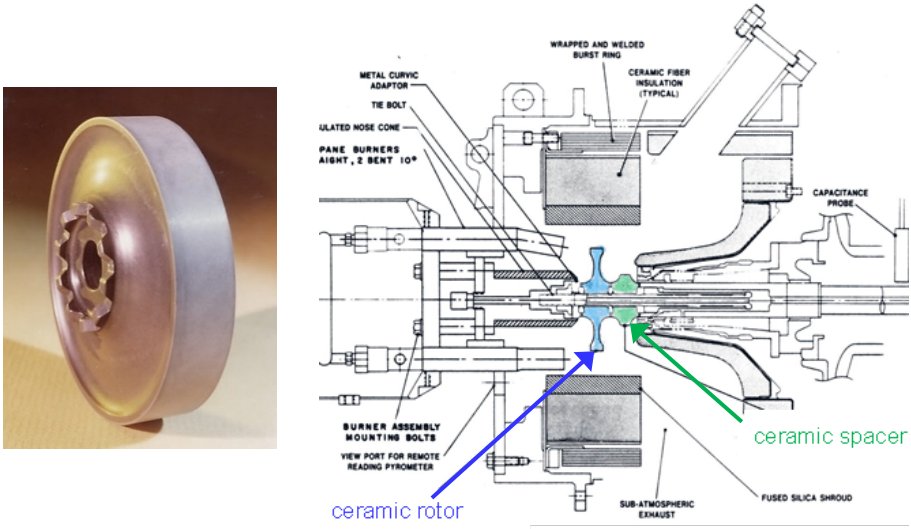

Figure 10.1. *A Ford silicon nitride 95 mm diameter model gas turbine rotor that survived 25 h intact in the gas turbine test rig shown on the right. The outer rim is thicker than a real rotor in order to simulate the vane masses that would be attached in a real rotor. Notice the ceramic coupling teeth that enabled the rotor to be connected to a metallic shaft. A thin platinum foil separated the ceramic rotor from a mating ceramic spacer part and its teeth.*

The rotors were made of a 1980s hot-pressed, fully-dense, and fine-grained silicon nitride[a] that was carefully machined to final dimensions. The particular grade was one of the most thoroughly-analyzed structural ceramics of all time. A fracture mechanism map for it was created.[3] It also was used as the world's first reference material for fracture toughness, K_{Ic}[4]. The model rotors were spun at 50,000 rpm while heated by hot gasses to a peak rim temperature of 1260 °C (2300 °F). The speed, mass, and shape of the rotors were designed so that some of them would fracture in a time-dependent manner due to slow crack growth of volume-distributed material flaws. The goal was to validate the life prediction computer models. The rotors were expected to break in the thin web where the maximum principal steady state stress was 131 MPa (19 ksi) and the temperature was 1240 °C (2260 °F). Twelve rotors were tested and six broke in a time-dependent manner. The hot spin times to failure these were in excellent agreement with predictions made using laboratory stress rupture

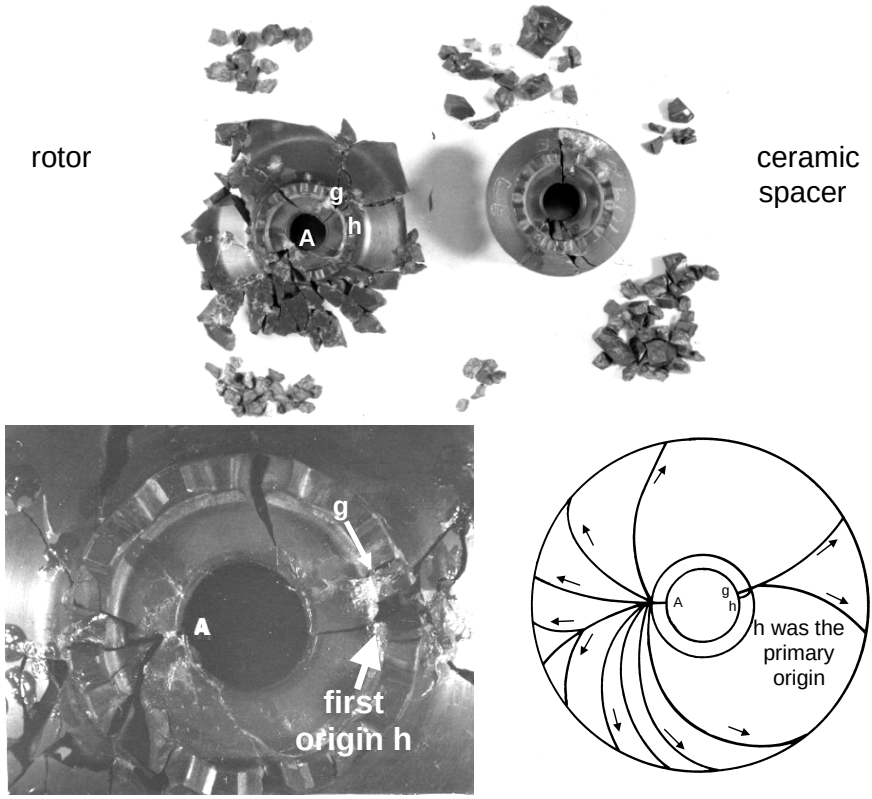

Figure 10.2 *Reconstructed model rotor and spacer (18.6 h). First fracture was at "h." Fractures "g" and "A" occurred later.*

[a] Grade NC 132, Norton Co., now St. Gobain Advanced Ceramics, Worcester, Ma.

test data on bend bars and tension specimens.[1,2] The test rig was constructed in such a manner that most of the fragments were retrievable. The longest (18.6 h) and third longest (13.8 h) rotors were fractographically analyzed. It was felt that these would have large slow crack growth zones that would be easy to find. Analysis revealed that fracture did not occur quite as anticipated. Fractures initiated in the bore or at the curvic coupling teeth and not in the web as had been intended and predicted. Why not?

Fracture markings were quite clear, and the local direction of crack propagation could be assessed in every single piece. The 18.6 h rotor was reconstructed piece-by-piece over the course of *one week* culminating in the assembly shown in Figure 10.2. It was a classic puzzle-solving exercise. Many outer rim fragments were missing, but they did not matter. The ceramic spacer part had also fractured, and its pieces were commingled with the rotor, thereby complicating the matter. Nevertheless, the central and web portions of the primary rotor were almost completely reassembled. After completion, the rotor was disassembled, the fracture surfaces examined, and a map of crack propagation directions was made.

Fracture started on one side of the rotor in the bore area at site "h" then branched into two main radial cracks that ran out to the rim. This opened up the disk on that side. The unbalanced rotor then fractured violently on the opposite side at site "A" from machining cracks. Origin "h" was determined to be the first break based on crack intersection patterns. The flaw shown in Figure 10.3 was a large <u>contact damage crack</u> with a large fracture mirror at the root of a tooth of the curvic coupling. The local stress was estimated to be

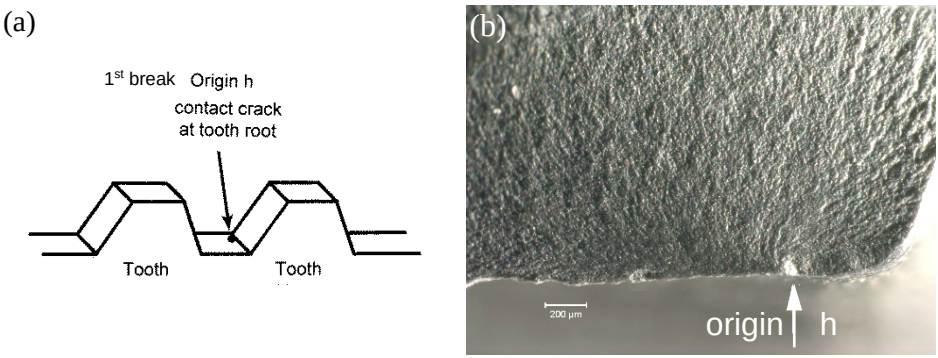

Figure 10.3 *The primary fracture origin was a contact crack at site "h" on the curvic coupling teeth. Low-angle grazing illumination from the right highlights the radiating hackle lines that converge on it.*

500 MPa (72 ksi) from the flaw size and 580 MPa (84 ksi) from the fracture mirror. These are fairly consistent estimates. The computer model indicated there were only modest bore stresses (138 MPa, 20 ksi) and temperatures (1150 ^{o}C, 2200 ^{o}F) at the first origin site "h". These did not match the fractographic stress estimates.

An important observation on the coupling teeth helps explain the fracture. When the rotor and the mating ceramic spacer were assembled in the hot test rig, they were separated with a thin platinum foil to prevent direct ceramic-to-ceramic contact. The fractographic examination showed uneven platinum wear traces and some bare spots on the curvic coupling teeth. The foil probably deformed or crept with time during the test and eventually ceramic-to-ceramic contact occurred. This caused the initial contact crack to form. Unbalanced stresses in the rotor and spacer (due to the platinum foil creep and displacement) then caused breakage.

This exercise was a good example of one of the author's laws of fractography: "The first one is the hardest." While at first glance, reassembly of a burst rotor appeared to be a formidable task, but it was simply time consuming. The second rotor (13.8 h) took less time to do. It also had fracture initiation sites at the bore or at the teeth. Years later, the author learned of comparable work done on model silicon nitride rotors at Daimler-Benz's research center in Stuttgart.[5] They also reconstructed burst silicon nitride rotors and used fractography to find that grinding cracks in the bores were the fracture origins.

Some lessons learned from this case study were:

a. Fracture occurred from a different cause than expected.
b. Stress rupture data may have been the best for reliability estimates, but the correlation of failure times was fortuitous.
c. Volume flaws were not found in the two fractured rotors. Surface machining cracks and contact cracks were found and Weibull area scaling should also have been included in the reliability model.

Case 2: Busted Barrel (Silicon Carbide Machine Gun Liner)

This also was a dynamic fracture case where fracture was from an unexpected cause. The fractographic analysis sent the designers back to the drawing board for additional analysis.

The U. S. Army has occasionally investigated the possibility of using ceramic liners to improve gun barrel life and reduce mass. The low density, high compression strength, refractoriness, and erosion and wear resistances of

ceramics could be advantageous. Figure 10.4 shows a drawing for a 50-caliber (12.7 mm) machine gun breech with a ceramic liner from a 1980s project conducted for the U. S. Army.[6] The ceramic was put into compression by shrink fitting a steel sleeve around the ceramic. The steel sleeve was heated and placed over the cool ceramic tube. As the steel cooled, it contracted and put the ceramic liner into axial, radial, and hoop compression.

The dimensions and temperature differentials were chosen so that the ceramic liner was always in compression, even when firing a projectile. Several ceramics were tried, but most testing was on a sintered a-SiC.

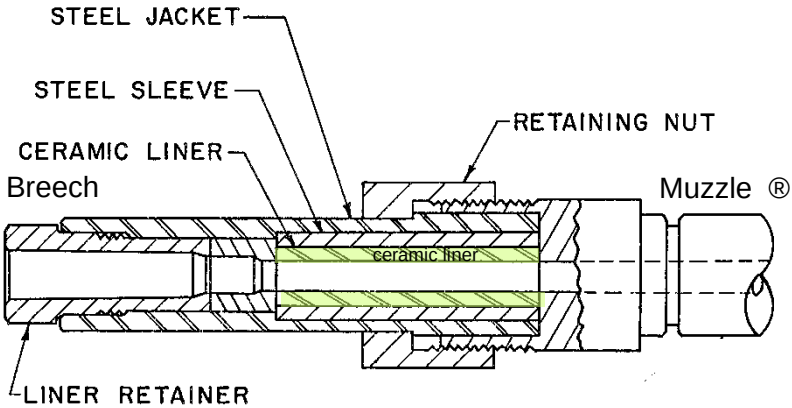

Figure 10.4 *Schematic of the breech end of the 50 caliber (12.7 mm) gun barrel (Ref. 6). The ceramic tubular liner is shown in green.*

An analysis combining the residual shrink fit and projectile firing stresses indicated the maximum *axial* stress s_x was 670 MPa in compression in the ceramic liner mid-portion. This stress tapered to zero at each end. The axial stress maximums were only 112 MPa tensile in the steel sleeve and 154 MPa tensile in the steel jacket. The maximum *radial* stress in the ceramic liner was 345 MPa compression. The maximum *hoop* stress, s_q, was 590 MPa compression during projectile firing. The environment is severe, but if the ceramic was always under compression, perhaps it would not fracture.

Some liners survived as many as a thousand single-shot firings, confounding skeptics who felt that the assembly would not survive one shot. Figure 10.5 shows one assembly that cracked after a few hundred shots. It had circumferential fractures as shown in Figure 10.5a. The steel sleeve and jacket

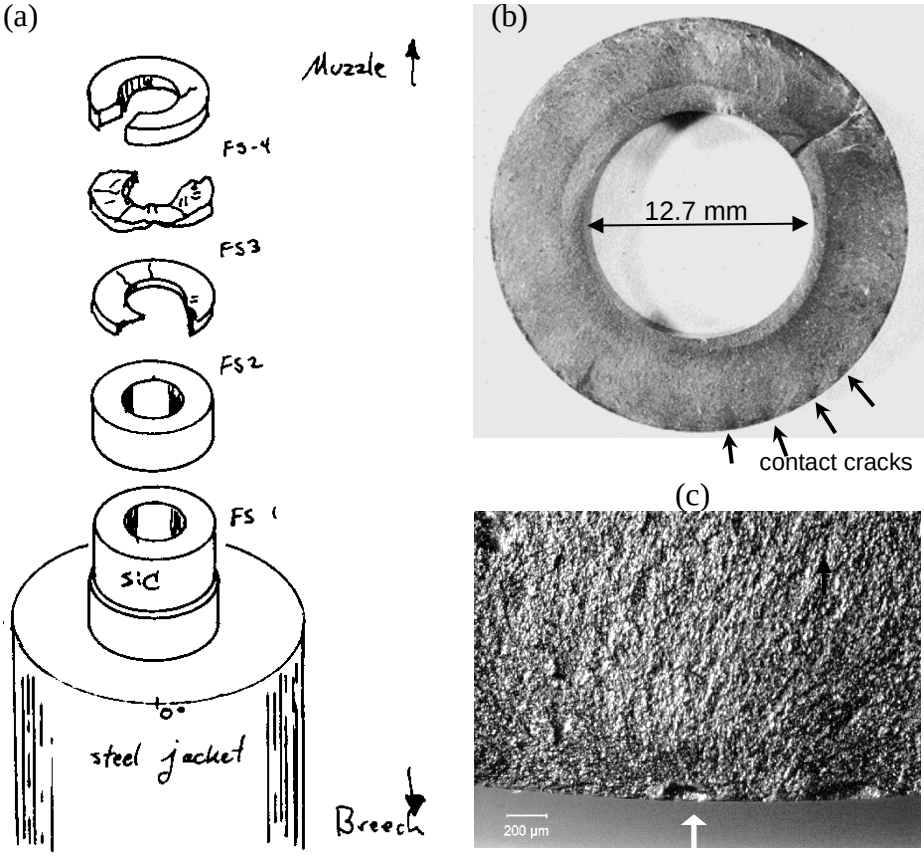

Figure 10.5 *Fractured a-SiC gun barrel. (a) is a sketch to show context. (b) shows the fracture surface of one of the ring-shaped fragments. Contact cracks are spaced periodically around the outer rim and appear as shadows in this view (arrows). (c) shows a close-up of one of the contact cracks.*

were machined away to allow extraction of the ceramic as shown in Figure 10.5b. The fractures were perpendicular to the axial direction, suggesting that hoop stresses from internal pressure during projectile firing were not the cause of failure since hoop stresses would have created radial cracking. Analyses showed that every fragment fractured from one or more contact cracks that were periodically spaced on the *outer rim* of the ceramic where it contacted the steel sleeve.

Where did the tensile stresses come from? The plane of the fractured surfaces and also of the initial semi-elliptical contact cracks indicated that the tensile stresses were *axial:* s_x. The axial residual compressive stresses did taper off at

the tube ends. The most likely sources of tensile stresses are dynamic stress waves generated during the firing. Even if these are initially compressive, they can become tensile when the stress waves reflect off the end faces. Furthermore, the elastic wave velocity and impedance of the silicon carbide and the steel sleeve are not matched, and stress waves propagated axially at different speeds. Hence, a dynamic tensile stress could develop at the steel-ceramic interface due to mismatch of the transient elastic strains.

The contact stress cracks often were periodic around the rim. The parts were machined to tight tolerances, but it is likely that slight variations in the mating surfaces led to an uneven fit and stress concentration sites that triggered the contact cracks.

In this case, the ceramic was designed to always be in compression, but fractography showed otherwise. Some design and modeling improvements were suggested. The tolerances and surface specifications for the mating parts could be changed. The elastic properties of the ceramic and the confining sleeve could be matched better. More sophisticated stress analysis models could examine the transient stress states in the assembly.

Case 3: Conflicting Carbide Data (Silicon carbide flaws and slow crack growth)

This case is not about a specific component, but about the risk of treating all flaws as if they behave the same. Different flaws can behave differently. As part of a program on characterization of structural ceramics for heat engine ceramics in the 1980s, the author conducted extensive stress rupture testing of pressureless-sintered a-SiC.[b] [7,8,9] (Incidentally, this is the same material as used in the gun barrel liner case 2.) Stress rupture testing entails applying a constant stress to a specimen, at a level below that needed to cause fast fracture, and measuring the time to failure. Slow crack growth can cause flaw enlargement and time-dependent fracture. Sometimes such tests are termed creep rupture if the loading conditions are such that bulk creep deformation leads to accumulated damage and fracture. The author's data at 1300 °C in air was consistent with data published by another team.[10] Both teams detected time-dependent fractures due to easily detected intergranular slow crack growth of volume-distributed material flaws such as large grains, pores, or agglomerates. Figure 10.6 shows an example.

[b] Hexoloy SA, Carborundum, Co., Niagara Falls, NY. Now St. Gobain Advanced Ceramics.

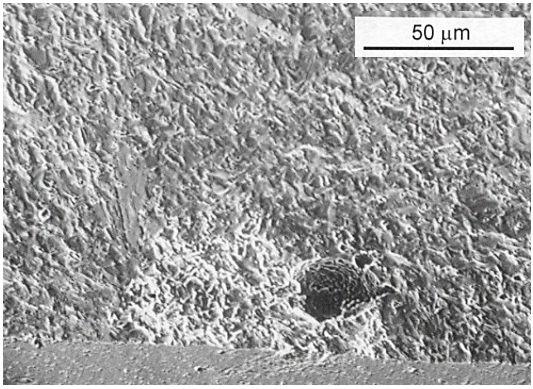

Figure 10.6 *Fracture origin in a 1300 °C stress rupture SiC specimen. The origin is a light-colored large intergranular slow crack growth region that may have started from the side of or beneath the large discrete pore.*

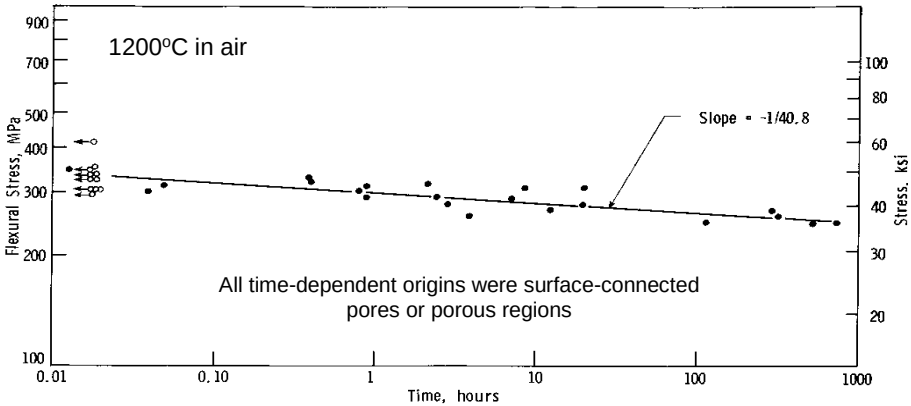

Figure 10.7 *Stress rupture curve at 1200 °C in air for sintered a-SiC.*[7-9] *Every time-dependent fracture was from a pore or porous zone and only if it was surface connected. The hollow points with arrows to the left are breaks on loading and are consistent with the fast fracture strength which was about 350 MPa. The slow crack growth exponent N was 40.8.*

A much different story emerged at 1200 °C. The author recorded time-dependent fractures such as shown in Figure 10.7 with origin flaws as shown in Figure 10.8. The other team did not observe a single time-dependent fracture at all in their experiments. Why did the two groups have such contrasting outcomes at 1200 °C? The answer was that they used Knoop indented, artificially-flawed specimens, whereas the author used specimens that fractured from naturally-occurring flaws. They behaved differently. Every one of the 1200 °C time-dependent fracture origins was a pore or porous region

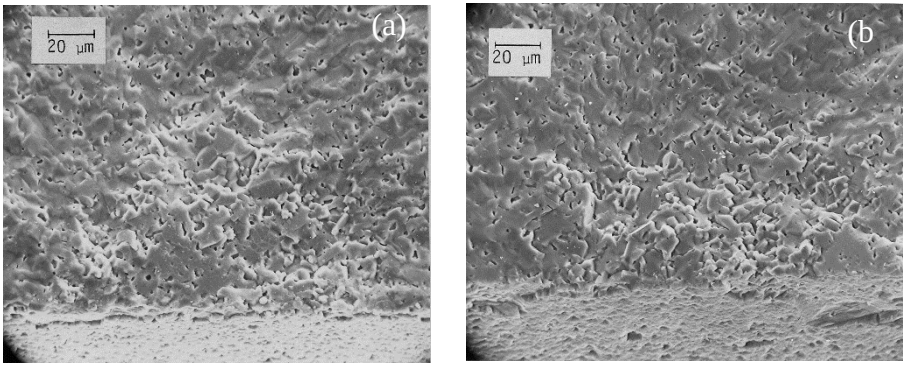

Figure 10.8 *Fracture origins in 1200 °C a-SiC specimens that fractured at 863 h (a) and 1460 h (b) from surface-connected porous regions. These are different than the pore with a large SCG zone in Figure 10.6.*

region *connected to the outer surface* as shown in Figure 10.8. These flaws did not have large slow crack growth zones like those seen at 1300 °C. Evidently the porosity flaws were susceptible to very localized stress-corrosion crack extension (from oxidation) that sharpened or locally extended tiny micro-cracks on the pore periphery. These flaws did not need much change in size or severity for them to go critical, since the failures occurred at stresses

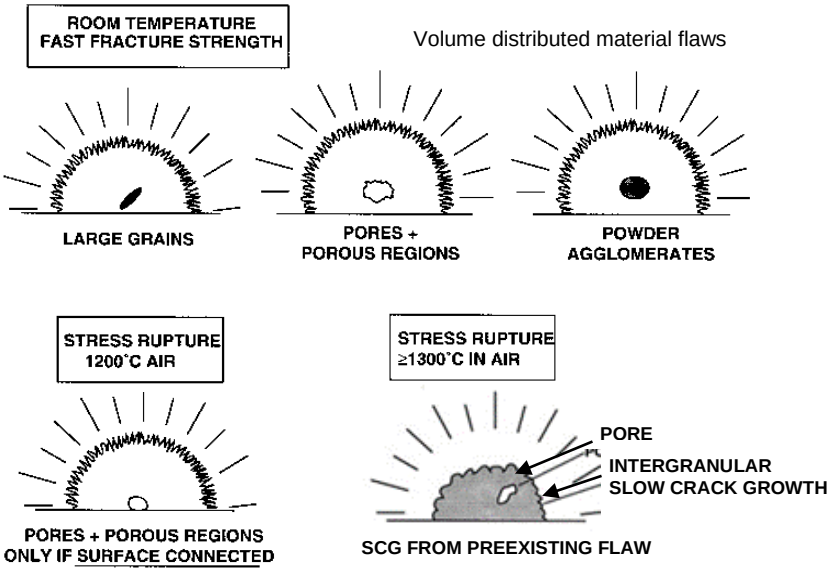

Figure 10.9 *Fracture origins in a-SiC.*

(250 to 350 MPa) very close to the fast fracture strength (350 MPa). Figure 10.9 summarizes the fractographic findings.

The other testing team did not observe the 1200 °C stress corrosion mechanism since they used Knoop artificial flaws in all of their bend specimens.[10] Such flaws often are effective tools for studying fracture, but in this instance, they produced misleading results. The Knoop flaws did not grow by slow crack growth at 1200 °C. Why? The answer was that they were loaded to a very low stress level, insufficient to activate the pore stress corrosion mechanism that was active from 250 to 350 MPa (Figure 10.7). Since the large Knoop flaws reduced the fast fracture strength of the specimens to less than 200 MPa, the other group's stress rupture specimens were loaded to only 100 to 200 MPa. This case demonstrates that it is often best to let a material reveal the type of flaws it is apt to fail from, rather than rely on artificial indentation flaws.

Case 4: Vulnerable Vials (Broken Medicinal Bottles)

This was a very practical problem involving commercial glass medicinal vials in an ongoing pharmaceutical clinical trial with an expensive new medicine. The vials developed cracks. Would the cracking require a recall and termination of the clinical trial?

Rim cracks developed in the 17 mm diameter medicinal vials. The cracking rarely caused the vials to break, but trace leakage and loss of the airtight seal due to through-cracks in the rim caused great concern. Loss of seal carries a risk of contamination with potentially fatal consequences (e.g., see case 10.8 in Fréchette's book, Ref. 11). Optical stereomicroscope examination of vials with intact caps revealed a circumferential damage zone in the glass just under the aluminum cap seal (Figure 10.10 a,b). Focusing through the glass revealed that some cracks had penetrated deep beneath the surface although the full extent of the penetration was difficult to assess. Examination of a different vial with a severed cap (Fig 10.10c) confirmed the cracks could reach all the way to the interior. No glass defects were detected. The concentricity of the neck with the vial body was within specifications. The problem was traced to a misalignment of the cap crimping machine star-wheel assembly.

An incidental finding was the beautiful example of scarps; Fig 10.10d (shown previously as Figure 5.54), on one of the fracture surfaces of another severed vial at the cap. The scarps were consistent with the outer surface cracks having reached the vial interior and the interior medicinal fluid, therein aiding the final fracture of the glass neck.

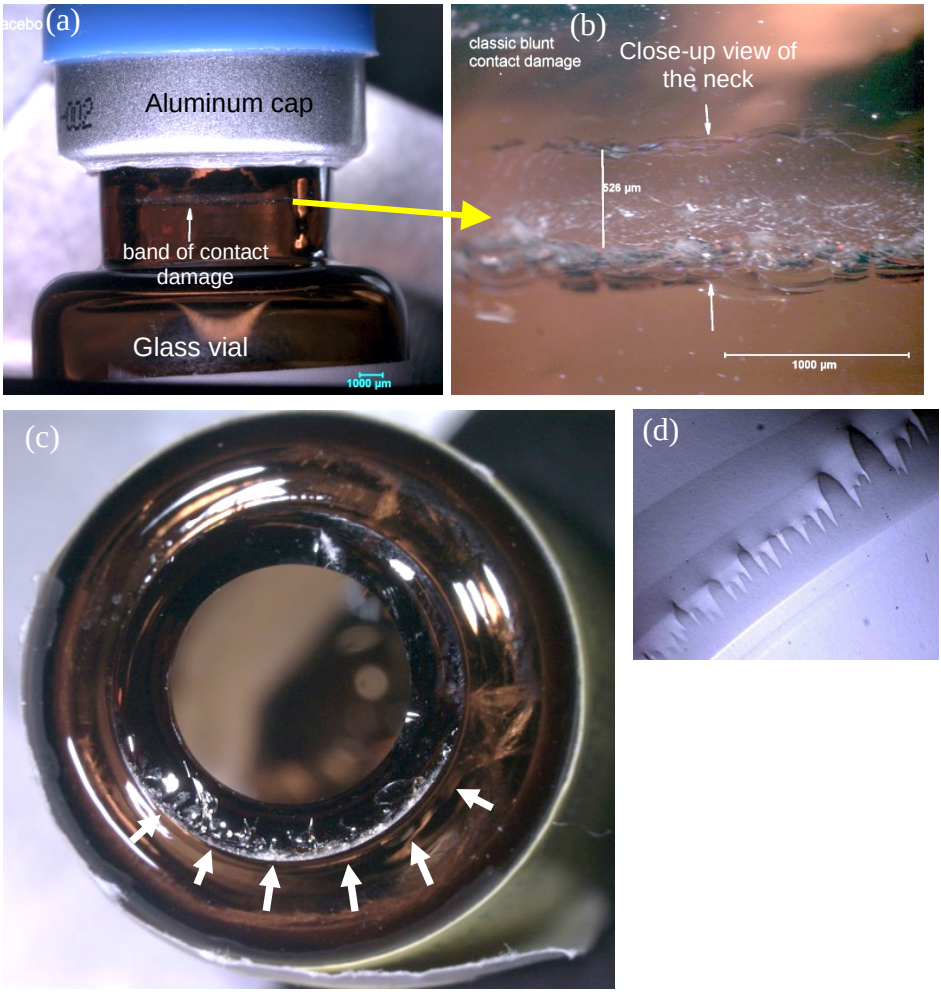

Figure 10.10 *Rim cracking in glass medicinal vials. (a) and (b) show blunt contact cracking damage (arrows). (c) shows a top view of the fracture surface of a vial with a severed cap. (d) shows scarps in another severed vial.*

Case 5: Damaged Dome (Coarse-Grain AlON IR dome)

This case illustrates what can be accomplished with optical microscopy alone, even on very difficult ceramics. A coarse-grained aluminum oxynitride missile infrared (IR) sensor dome broke during a thermal stress proof test. It broke into several pieces, and the branching patterns directed attention to an area near the base as shown in Figure 10.11a. One might expect the origin to be at the dome rim, possibly at a bevel, but that was not the case. The roughness of the coarse

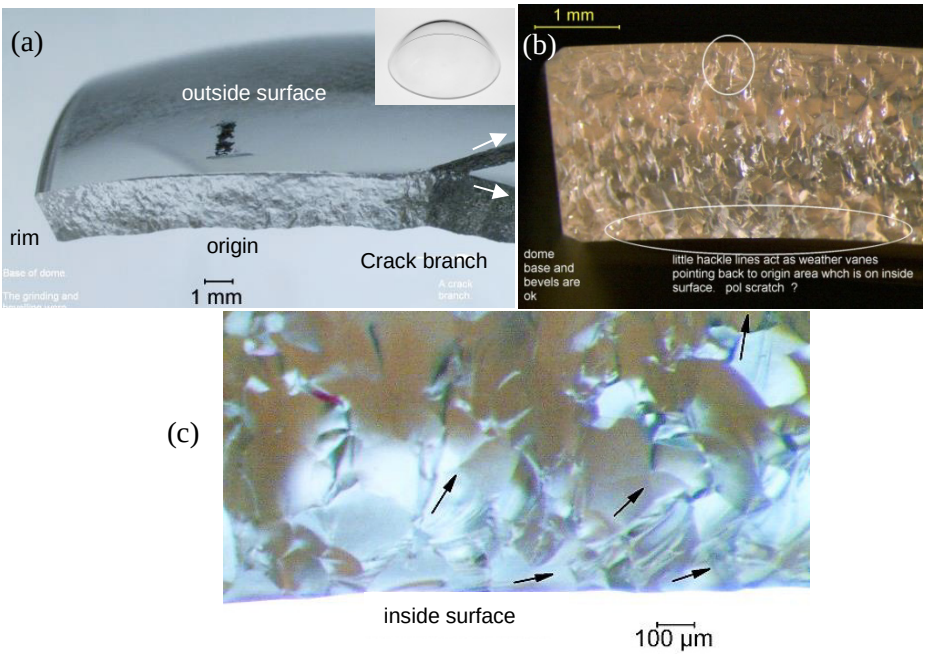

Figure 10.11. *AlON infrared missile dome. (a) shows how the branch on the right leads away from the origin area. The black mark on the outside surface is a pencil mark opposite the fracture origin. (b,c) show the fracture surface with the coarse microstructure. Various types of hackle lines radiate outward from the origin site. The black arrows are directions of crack propagation.*

grain microstructure hid nearly all fracture markings. Careful adjustment of low-angle grazing lighting at higher magnifications revealed coarse micro-structural hackle lines. There also was twist hackle within the transgranularly-fractured grains as shown in Figure 10.11b and c. It was possible to read these lines back to the inside surface of the dome to a location well away from the rim. Close-up examination in Figure 10.12 (on the next page) revealed the origin site had zipper machining crack hackle lines within one or two grains, indicating the origin was grinding or scratch damage that was not completely removed by polishing. Similar grinding/polishing flaws inside single grains of aluminum oxynitride have been reported by Swab et al. [12]

Unfortunately, the dome was not available for SEM confirmation or further examination of the inside surface for traces of a scratch at the origin site. The polished surfaces in general did have an assortment of polishing flaws.

The author once used a similar approach to find origins in coarse-grained polycrystalline alumina (PCA) vapor arc lamp tubes.

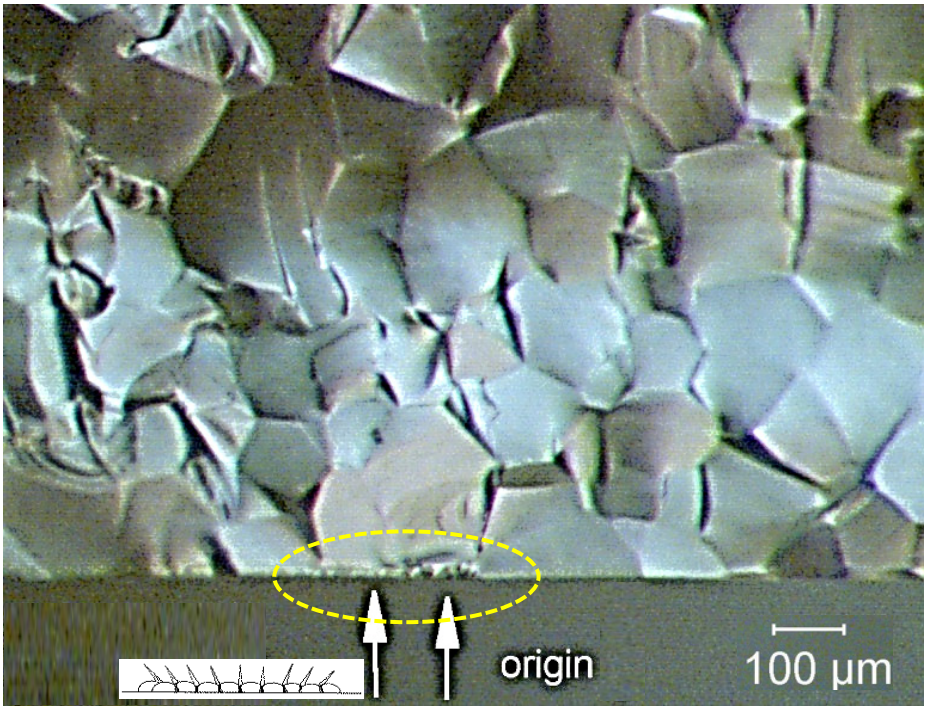

Figure 10.12 *Wake and twist hackle within cleaved AlON grains lead back to the inside surface of the missile dome. The origin was tiny zipper machining crack hackle lines (circled) within one or two large grains. This image was taken at the maximum magnification (125X) of the available stereo optical microscope.*

Case 6: Suffering Setter Plate (Silicon Carbide Furnace Plate)

A large silicon carbide furnace setter plate fractured during a furnace run. Was the material faulty or was there some other cause? Figure 10.13 shows one half of the broken plate. It has the wavy fracture that is a telltale sign of a center-heated plate fracture as described in Chapter 4 in section 4.12.

Figure 10.14 shows the fracture surface revealing that fracture initiated from grinding damage at a hole near the rim. No material flaws of consequence were detected. The mirror size was about 9.3 mm. Using an A_o value of 11 MPaÖm for a dense hot-pressed SiC (from Appendix C), the stress at fracture was estimated to be only 115 MPa. The material was completely satisfactory, but the machining, grinding, and attachments were not. This failure analysis required only a one-minute visual inspection.

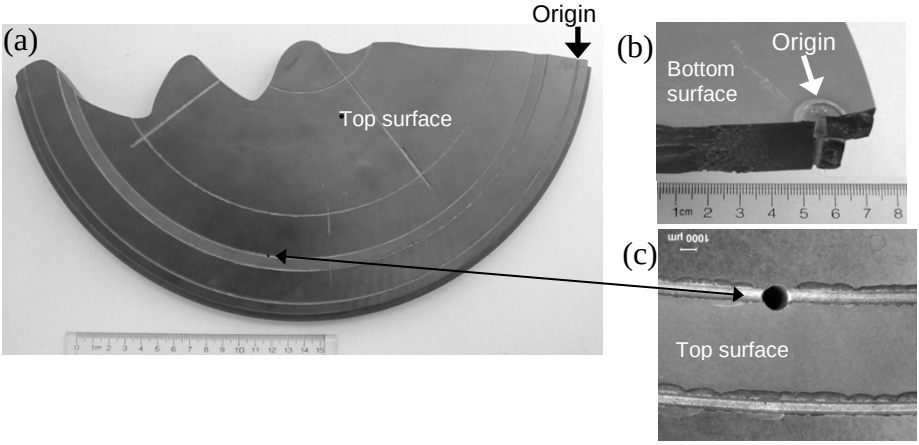

Figure 10.13 *SiC furnace setter plate. The plate was 36 cm round and 1.9 cm thick. The curvy pattern is typical of a center-heated plate fracture (Chapter 4). The origin is a chipped hole through the plate. (b) shows the origin hole from the bottom surface. There is spall and evidence of a chemical reaction with a mounting bolt or washer. The machined grooves also were chipped and had ragged edges as shown in (c). (plate courtesy of B. Mikijelj)*

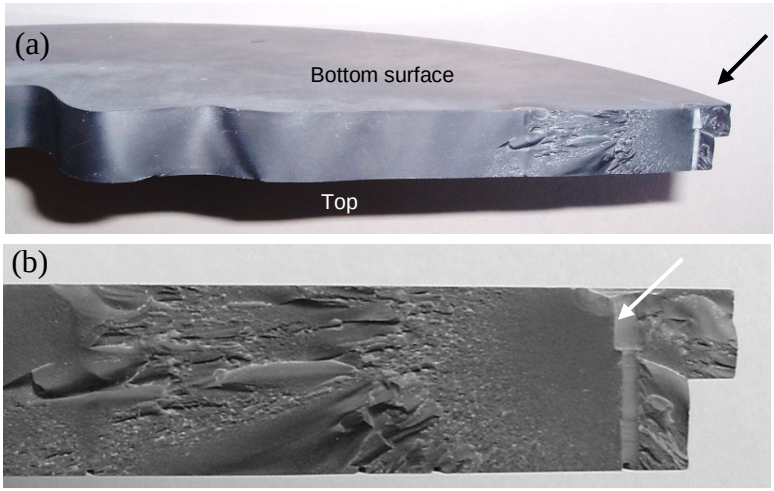

Figure 10.14 *Fracture surface of the SiC setter plate. A fracture mirror at the origin (arrows) attests to a moderate stress level. Hoop tensile stresses on the rim were generated by thermal strains. Thermal expansion of the hot plate center was resisted by the cooler rim. As the crack propagated towards the plate middle it slowed since it reached hot regions that were originally in compression. The fracture surface became relatively featureless and the crack meandered. The hole through the plate at the origin (b) had chipping and grinding damage that weakened the plate.*

Case 7: Ruptured Radomes (Fused Silica Missile Nosecones)

This was initially a very difficult case since the flaws at the fracture origin were hard to detect since they blended into the normal microstructure. It was necessary to "learn how to look" at this material.

First generation U. S. Army Patriot air defense missiles in the early 1980's utilized fused-silica radomes (Figure 10.15). Radomes are nosecones that are radar transmissive. The radome was prepared by slip casting and then sintering silica particles to greater than 85% density. This porous structure had a low but acceptable strength and, like an insulating firebrick, was more effective in arresting cracks than if the radome were a fully-dense glassy body. Although sintered fused silica is weak, it was selected since it had a low coefficient of thermal expansion and thus would be less susceptible to thermal stresses from aerodynamic heating. Some radomes were deliberately loaded to fracture or proof tested as part of the engineering development program. This was done by attaching a sling to the side of the radome and pulling it laterally several times in different directions. Unexpected fractures occasionally occurred. Most fractures occurred in the ceramic where it was joined to a threaded fiber-epoxy thread ring attachment part (Figure 10.16a,b). Fractography was difficult in the porous weak ceramic since it had a rough fracture surface, but a number of fractures were successfully diagnosed. Figure 10.17 shows an instance where

(a) 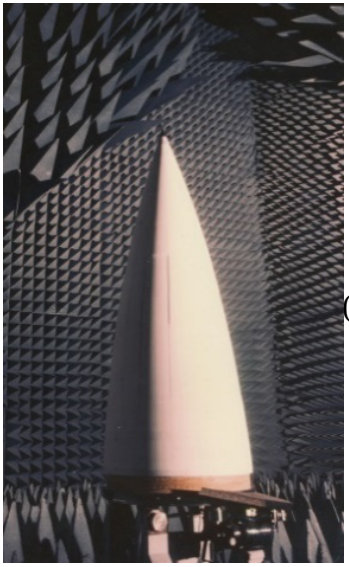 (b)

Figure 10.15 *U. S. Army first generation Patriot air defense missile. The radome was 1.1 m tall with a 40 cm diameter. (b is courtesy Raytheon)*

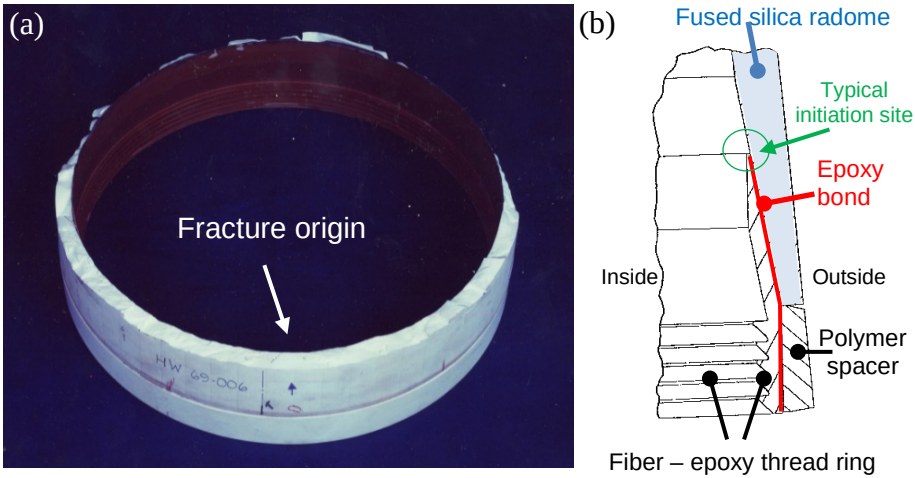

Figure 10.16 *Sintered fused silica radome that fractured during a proof test. (a) is a top view with the origin region marked by the arrow. The ceramic is bonded on the inside to a fiber epoxy attachment ring that attached the ceramic radome to the missile body. (b) is a schematic showing the bottom of the radome where it was attached to the fiber epoxy thread ring. Fractures in the ceramic typically occurred near the top of the fiber epoxy thread ring.*

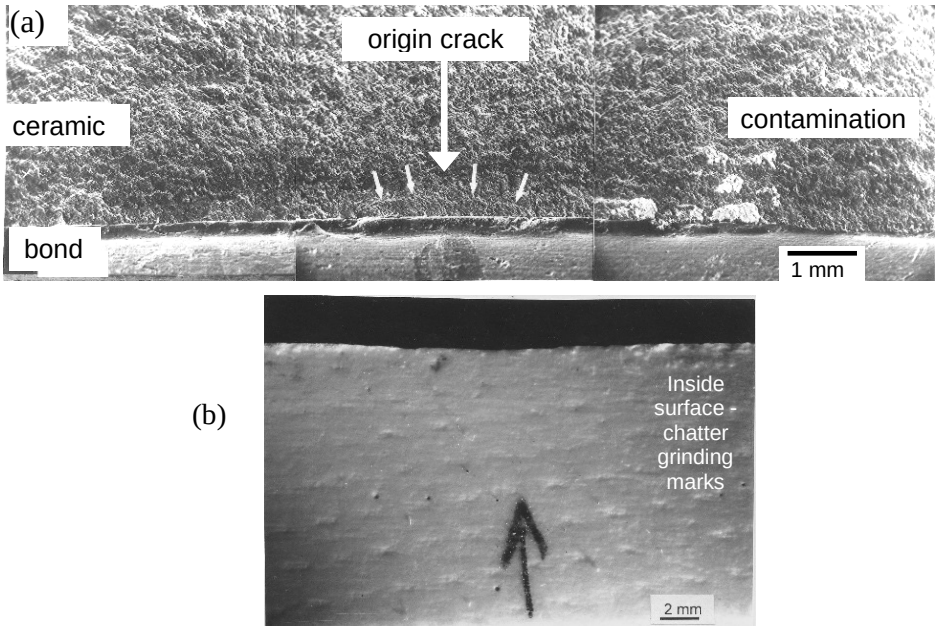

Figure 10.17 *(a) shows a grinding crack at the origin area (arrows). (b) shows a grinding pattern on the inside ground ceramic surface.*

atypical grinding damage created strength limiting cracks. Better control of the surface grinding eliminated the problem.

Figure 10.18 shows a different example wherein excessive shrinkage of the epoxy bond caused debonding. This created a stress concentration site in the ceramic that initiated fracture. The strength was greater for this example since there was a distinct fracture mirror. The remedy in this case was to adjust the bond-cure thermal cycle to eliminate the debonding.

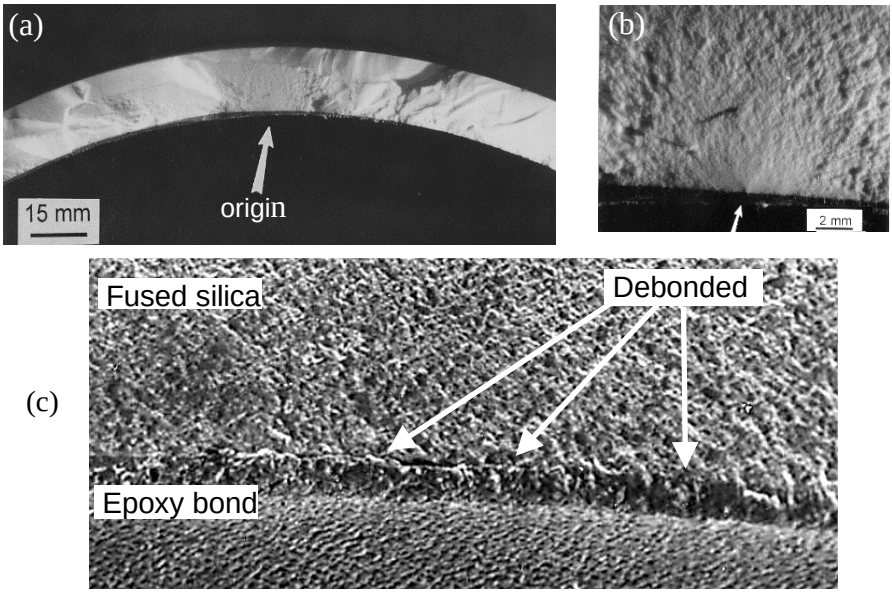

Figure 10.18 *Sintered fused silica radome fracture. (a) shows the origin site on the inside wall. (b) is a close-up showing a fracture mirror centered on a feature on the inside wall of the ceramic at the top of the bond line (c) shows there is no significant material flaw at the origin, but the ceramic and the epoxy are debonded at the origin.*

Case 8: Maligned Machinists (Bend Bars from Machine Shops)

This case was part of an investigation whether different machine shops could prepare bend bars to a set of specifications with minimal damage and at a reasonable cost. This work was done in the mid-1980s in support of the first standard test method for flexural strength of high performance ceramics in the United States, MIL STD 1942(MR).[13] This 1983 standard served as a basis for ASTM Intl. standard C 1161 in 1990[14] and (along with elements from European and Japanese standards) was used as the basis for ISO 14704 in

2000.[15] Standardization led to dramatic improvements in the quality of data and significant cost savings. Bend bar costs decreased dramatically as machine shops prepared specimens to a common, reliable procedure. As part of the MIL STD standardization work, a major international round robin on flexural strength with 11 laboratories around the world was conducted in 1984 and 1985.[16,17] Two ceramics were used, and several thousand specimens tested. One was a 99.9 % pressureless-sintered alumina[c] and the other was reaction bonded silicon nitride made at the Admiralty Research Laboratory, UK.[d] Consistent flexural strength results were obtained with the standard procedure with defined test fixtures and alignments.

A side topic in the round robin was whether different machine shops could meet the grinding specifications and prepare damage-free B-type bend bars (3 mm x 4 mm x 50 mm). Requests for price quotations were sent to eight machine shops to prepare 20 specimens from the sintered alumina according to the MIL STD 1942. The specifications called for a multi-step grinding process

Shop	Bar Price $	Were the specifications met?	alumina plate	Avg. MPa	Std. Dev. MPa	Char. Str. MPa	Weibull Modulus	Fracture Origins
A	15	Yes	P	372	42	391	10.3	Round pores Porous zones Porous seams 2 machining
B	19	Yes, a, b	2	315	22	325	17.1	Porous zones Porous seams Agglomerates 4 machining
C	20	Yes, c	1	301	30	314	11.5	Porous seams Pores Agglomerates
D	41	Yes, b	3	335	32	350	12.0	Porous seams Porous zones Agglomerates
E	50	Yes, b	4	373	36	389	11.9	Pores Agglomerates 2 machining

a Minor edge chips on some b Some skip marks or deep striations
c Chamfers a bit uneven

Table 10.1 *Flexural strengths of sintered 99.9% alumina from test sets prepared by different machine shops. The strength-limiting flaws are listed in their order of frequency in each set.*

---

c Grade AD 999, Coors Technical Ceramics, Golden, Co., 1984.
d Courtesy Dr. David Godfrey.

ranging from coarse initial grinding to final finishing. Finer grinding wheels with reduced depths of cut were used at each step with the objective of removing prior damage and minimizing final residual damage.

Five separate alumina plates of size 100 mm x 100 mm x 25 mm from a common batch were sent to the five shops which bid from $15 to $50 per bar. The machined bars were broken in four-point flexure on 20 mm x 40 mm spans. The surfaces and edges of all bars were inspected beforehand to ascertain whether the bars met specifications or if there were any signs of machining damage. The results are shown in Table 10.1. For the most part, the five venders met all of the specifications. Deviations were usually on isolated specimens. Machining damage can be hidden, however, and the strength testing was intended to reveal such damage if present.

Shops A and E had the highest strengths. The much lower strengths of the bars from venders B, C, and D suggested that they had damaged their specimens. It would have been tempting to reject venders B, C, and D for further jobs on the basis of the strength outcomes, but the fractographic analysis revealed a surprising explanation for the outcomes. Optical examination of the fracture surfaces revealed that machining damage was <u>not</u> the prime factor in any of the five sample sets. Machining cracks did cause fracture in a few isolated specimens, but the primary strength-limiting flaws were volume-distributed sintering flaws such as pores, porous zones, porous seams, agglomerates, and occasional inclusions. Several figures in Chapter 6 Origins of Fracture showed these flaws. The crucial difference was that <u>the flaws were different in the five plates.</u>

Porosity was the most common flaw type, but it manifested itself differently in the plates. In some plates the flaws were primarily round discrete pores. In other plates, the flaws were equiaxed regions of microporosity, porous seams, or porosity associated with inclusions. The plates were prepared from the same powder lot by the identical procedure by a well-established ceramic company. To all external appearances the plates were identical. Only when the specimens were fractured were the plate-to-plate flaw variations revealed.

This case illustrates the hazards of interpreting strength results without supportive fractographic analysis. The variability in flaw character between plates and its effect on strength also underscores a serious problem for structural ceramic designers. If the flaws in a material vary between nominally identical ceramics pieces, reliability analyses are in jeopardy.

Case 9: Modeler's Match
(Fracture Origins in MEMS Scale SiC Micro Tension Specimens)

This was a case by Sharpe et al.[18] where tension test specimens with different gage section sizes were prepared and tested to check the Weibull size scaling theory for very small pieces. The initial analysis showed that strengths could be scaled for two of three configurations, but Weibull scaling failed for the third configuration. Why?

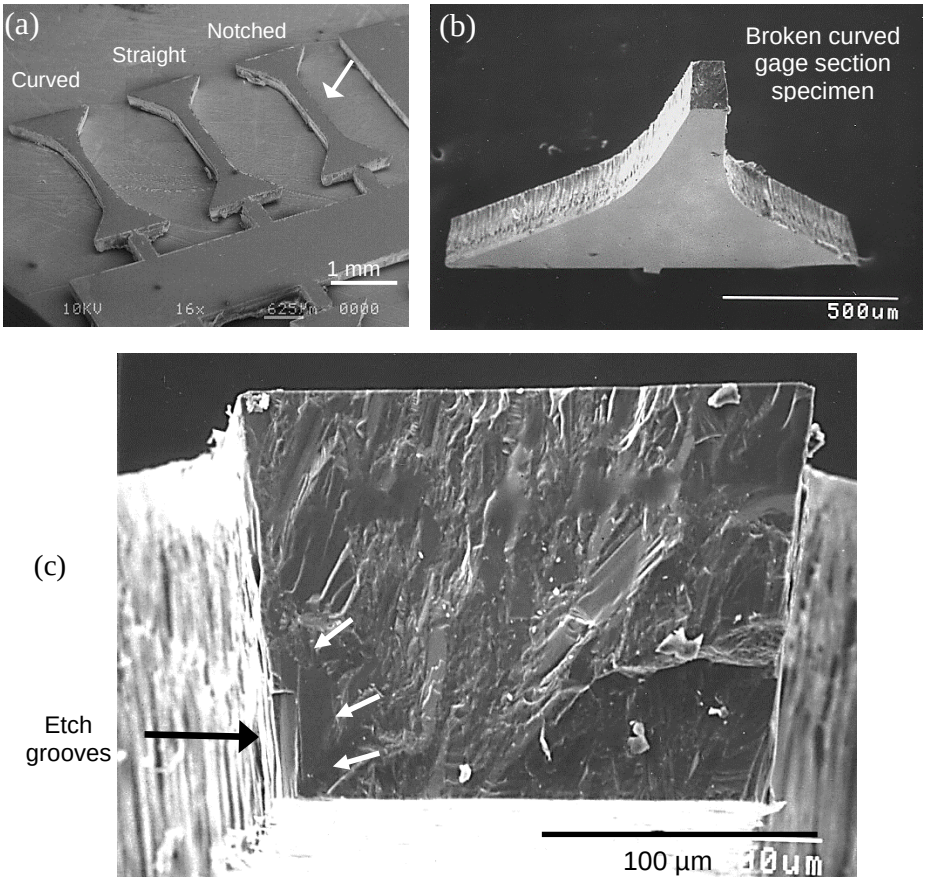

Figure 10.19 *Miniature 3.1 mm long SiC tensile test specimens. (a) shows curved, straight and notched gage sections. The notch (small white arrow) is too small to see in (a), but is clearer in Figure 10.20. (b) shows a fractured curved gage length specimen (c) shows the fracture surface of a straight section specimen. The small white arrows show the origin is a 25 µm x 50 µm large grain at the root of an etch groove. (a,b are courtesy W. Sharpe)*

The strengths of miniature microelectromechanical systems (MEMS)-scale silicon carbide specimens as shown in Figure 10.19 were measured. These had cross section dimensions of » 200 mm or less and were prepared at NASA-Glenn Center by chemical vapor deposition (CVD) followed by deep reactive ion etching (DRIE) to final shape.[19] Specimens with straight, curved, and double notched gage sections were tested in direct tension and fractured in a special miniature tensile tester. Weibull statistics were applied to scale the strengths and to determine whether surface or volume flaw scaling gave better correlation. The notches were intended to force fractures to occur in a tiny volume. The Weibull analysis using area scaling worked reasonably well for the curved and straight specimens, but gave a poor correlation for the notched specimens. They were much weaker than expected.

Fractographic analysis was difficult, but productive.[19,20] The CVD SiC had a coarse microstructure that created a very rough fracture surface that masked common fracture markings. Large hexagonal SiC grains affected the crack propagation across the fracture surface, causing significant crack redirection and severe roughness as the propagating crack sought out preferred cleavage planes. The most helpful features for pinpointing the origin were twist hackle

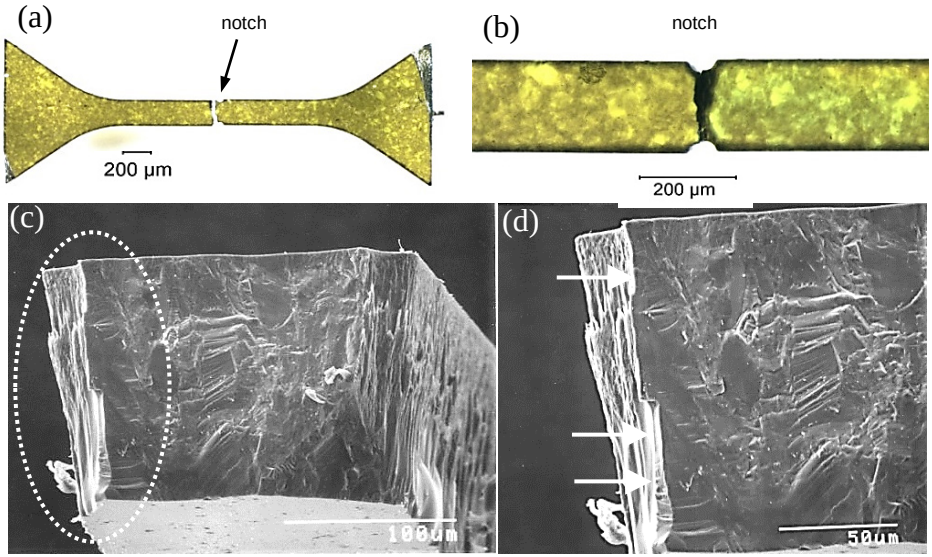

Figure 10.20 *A notched SiC tensile specimen. (a) shows the whole specimen. (b) shows a close-up of the gage section notches. Transillumination through the individual green single-crystal SiC grains created the light patches. (c) and (d) show the fracture surface. Fracture started at the bottom of the round notch (arrows), from a etch groove linked with a single long and large columnar SiC grain that ran from the top to the bottom.*

lines on cleaved grains and occasional large hackle lines that showed the local direction of crack propagation. These markings led back to the origins.

The fracture origins in all three specimen types usually were a combination of a deep etch groove with a large, favorably-oriented columnar grain. Cracks popped-in on a preferred cleavage plane in such grains. Thus, most critical flaws were a hybrid surface-volume type flaw: a sidewall groove and a large grain as shown in Figure 10.20c,d. The fractographic results supported the Weibull area scaling for comparing the straight and curved specimens if only the etched *sidewall areas* were used in the calculation.

The reason the Weibull strength scaling did not work for the notched specimens became obvious as shown in Figure 10.20. The notches were quite small (15 mm to 25 mm radius). They concentrated stress to a very small region around the notches. Hence, the Weibull effective volumes or areas were tiny and comparable to the size of some of the single grains. Hence, there is not a well-distributed set of flaws scattered throughout the volume, as is assumed in conventional Weibull analysis. Furthermore, an analysis based on continuum mechanics assuming the material was isotropic and homogeneous is wrong.

Case 10: Fractious Fractographers (A Fractography Round Robin)

Can different fractographers agree on fracture origin analysis? Can they reach similar conclusions? How do they exercise their craft? These were questions addressed in an international round robin conducted in the mid-1990s.[21] Round robins are interlaboratory exercises using a common procedure. There are many reasons for conducting a round robin, but usually the goals are to evaluate whether different laboratories can apply a prescribed procedure and obtain consistent results, or to generate repeatability or reproducibility precision estimates.

This author and Dr. J. Swab of the U.S. Army Materials Technology Laboratory (now with U. S. Army Research Lab, Aberdeen, MD) conducted a major international round robin on characterization of fracture origins of advanced ceramics in 1994 - 1995. Seventeen laboratories participated. The participants had experience that ranged from zero to thirty-five years. The project was coordinated under the auspices of the Versailles Advanced Materials and Standards (VAMAS) program. This work evaluated a new (1992) set of guidelines for finding and characterizing fracture origins in ceramics: “Fractography and Characterization of Fracture Origins in Advanced Structural Ceramics,” Military Handbook MIL HDBK 790[22] which was a

predecessor to ASTM Standard Practice C 1322,[23] the world's first fractography standard for characterizing ceramic fracture origins.

Topic 1 of the round robin was a photo interpretation exercise with focus on detection and characterization of grinding damage in bend bars. Photos of one specimen each of silicon nitride, a zirconia-alumina composite, and an alumina were furnished. Six photos for each specimen were provided showing for each half: a low magnification overall shot, a picture of the fracture mirror area, and a close-up of the origin area. Results were mixed. There was consensus that the origins were machining cracks, but there was considerable variability in how they were marked and measured. Some participants disagreed and felt the origins were not grinding damage. Although a short paragraph on each specimen with strength and fracture toughness information was furnished along with the photos, very few of the participants used this information to estimate a critical crack size. Participants were also asked to mark and measure the fracture mirror sizes on the photos. The organizers were surprised at the scatter in mirror size estimates. Evidently many participants were not familiar with measuring fracture mirrors.

Specimen	Material	Origin Flaw
1	Hot-pressed alumina + SiC whiskers	Large grain
2	Sintered 99.9% alumina	Handling damage (scratch) See Fig. 6.30c for an example
3	Sintered 3 mol% yttria stabilized zirconia (Y-TZP)	Pore
4	Reaction bonded silicon carbide	Surface Pit
5	Hot isopressed (HIP) silicon nitride	Machining damage
6	Sintered titanium diboride	Porous seam, porous region

Table 10.2 *Bend bar specimen types distributed in Topic 2 of the VAMAS round robin. Each participant received a set of six specimens: 1 to 6.*

Topic 2 was an actual examination of bend bar strength specimens. Each participant received both halves of a single bend bar of the six specimen types listed in Table 10.2. Again, results varied. Most participants had no trouble identifying the pore as the fracture origin in specimen #3. Many had difficulty with the others. For example, the scratch that caused cracking damage in their specimen #2 was sometimes identified as machining damage or even a pore or large grain. Figure 6.30c shows one of these scratched specimens. The scratch should have been obvious. Dr. Swab had made it with a diamond indenter, and it stood out very clearly on the tension surface of the bend bar. Evidently some participants *did not bother looking at the external surface* and only

looked at the fracture surfaces. Sometimes participants looked at only one half which might have been the less clear piece.

Many participants evidently did not read the brief four to six sentences of information furnished with each specimen, including treatments if any and the breaking stress and fracture toughness. For example, the surface pit origin specimens #4 had been exposed to an oxidizing environment at high temperatures. Some labeled the origin a pore and ignored the surface condition and severe reaction zones around the pits. Only a few participants estimated flaw sizes from fracture mechanics and compared them to their fractographically-measured sizes for verification.

The entire exercise was a learning experience for Dr. Swab and me. Some participants did very well, but many had difficulty. Much was learned by studying the causes of the misinterpretations. Even for such simple objects as bend bars, there was considerable variability in how the participants analyzed the photos, the specimens, and the ancillary information provided. Some just looked at the fracture surfaces and ignored everything else. We came to realize that fractographic analysis (and failure analysis in general) is a process whereby an expert integrates all information including, but not limited to, fracture surface examination. This realization led us to prepare Figures 1.3 and 1.4 of this Guide also shown here as Figure 10.21. We also came to the realization that we had a huge advantage compared to the participants. We could look at many specimens of a type, and were not limited to a solitary example. The participants only had one. Furthermore, there is no substitute for actually looking at the actual specimen under a microscope, as opposed to looking at 2-D photographs as in Topic 1. Several of the author's fractographic Rules of Thumb listed in the final chapter of this Guide stem from this exercise.

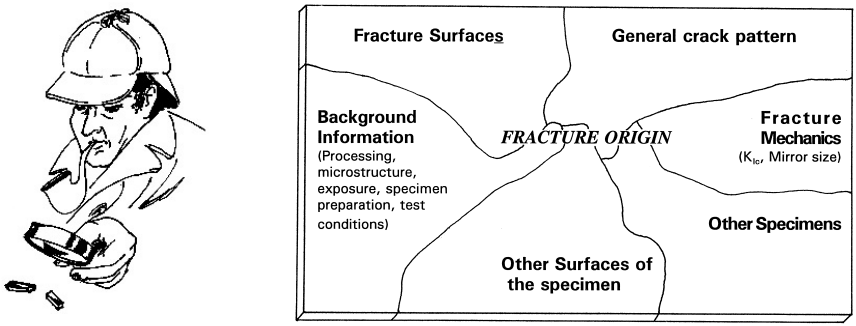

Figure 10.21 *Fractographers are detectives who must integrate all available information to "solve a case."*

Case 11: Perilous Prostheses (Three Ceramic Dental Crowns)

All-ceramic dental crowns are increasingly being used as alternatives to gold or porcelain fused-to-metal restorations (Figure 10.22). They can break. A variety of ceramic materials have been used including feldspathic or leucite porcelains, glass ceramics, alumina, and zirconia. These ceramics function as the main load bearing portion of a crown and are called the "core" or the

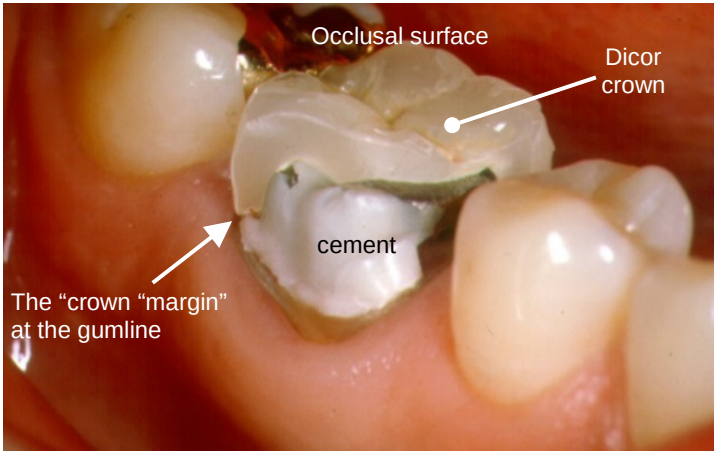

Figure 10.22 *A fractured Dicor[e] glass-ceramic molar crown. Note the good color match of the crown to the other teeth. (courtesy S. Scherrer)*

"foundation." A glassy exterior veneer layer is added for cosmetic purposes. Brittle, highly-filled resin-matrix composites with ceramic or glass fillers are common crown materials as well, but do not need a veneer layer. The fracture resistance and durability of the new ceramic and composite crowns are a primary concern. Despite the sanguine claims of the manufacturers, premature fractures do occur, much to the consternation of the patient and the dentist.

Until the early 2000s, progress in the field was typified by a trial-and-error approach. The usual approach was to statistically analyze the rates of failures and infer or guess causes of breakage. There were conflicting explanations as to why the crowns failed. It was not even clear what properties were desired and what were the best laboratory-scale tests to evaluate these properties. Dental ceramic crown fractures are in fact among the most challenging problems to solve. The early generation ceramics had coarse-grained and/or

[e] Dentsply Int., York, PA.

porous microstructures. They often fractured at low stress and classic fractographic markings were often masked by the roughness of the fracture surface. High-density aluminas and 3Y-TZP zirconias are exceptions and are easier to interpret. Another complication is that stress states in the crowns are transient and uneven. Fracture mirrors are almost never observed in a clinical fracture since fracture stresses are low, or the mirrors are larger than the crown wall sizes. Another difficulty is that key fragments are often missing, either due to loss in the mouth or damage during crown extraction. Furthermore, crowns usually accumulate damage from multiple events at multiple sites, creating complex, conflicting fracture networks. For example, the author has often detected Hertzian cone crack damage sites on crown occlusal and facial surfaces, but has only seen a few instances where the cone acted was an actual crown fracture origin. The Hertzian cones crack damage sites usually are dormant. Contact damage does occur and cause clinical failures, but it almost always is due to *edge chipping*. Starting in the late 1990s and early 2000s, substantial progress was made in fractographic analyses.[24,25,26,27,28] Fracture origins and fracture mechanisms were identified. (See also references listed in the Appendix B.)

Example 1 in Figure 10.23 on the next page is from Ref. 24 and is a Procera 99.9% purity alumina.[f] It split vertically, evidently in response to a hoop stress. The fractographic markings lead to a margin origin site but a specific single flaw is not obvious. We had to examine the pieces many times and gradually constructed a map. The origin is a barely-discernable semicircular crack (best seen in the "b" half of the crown) in the core material at the end of the margin as shown in Figure 10.23e,f. The origin crack was on almost exactly the same plane as the final fracture and it was not discernable in SEM photos. It was only detected with optical microscopy. From its size (179 µm radius) and using K_{Ic} of 4.0 MPaÖm for dense fine-grained alumina, and a Y of 1.4 for a corner crack, the hoop stress at fracture was estimated to be 213 MPa, a plausible value. The margin in this example was well-prepared and over 1 mm thick.

This case was a good example of how optical and electron microscopy can be used in conjunction with each other. It also showed how the origin crack was more easily detectable with optical microscopy.

This case was a good example of how one should not be afraid to go back and reexamine specimens. As one gains experience, things which at first seemed mysterious or unclear can sometimes become easier to interpret.

---

[f] Nobel Biocare, Stockholm, Sweden.

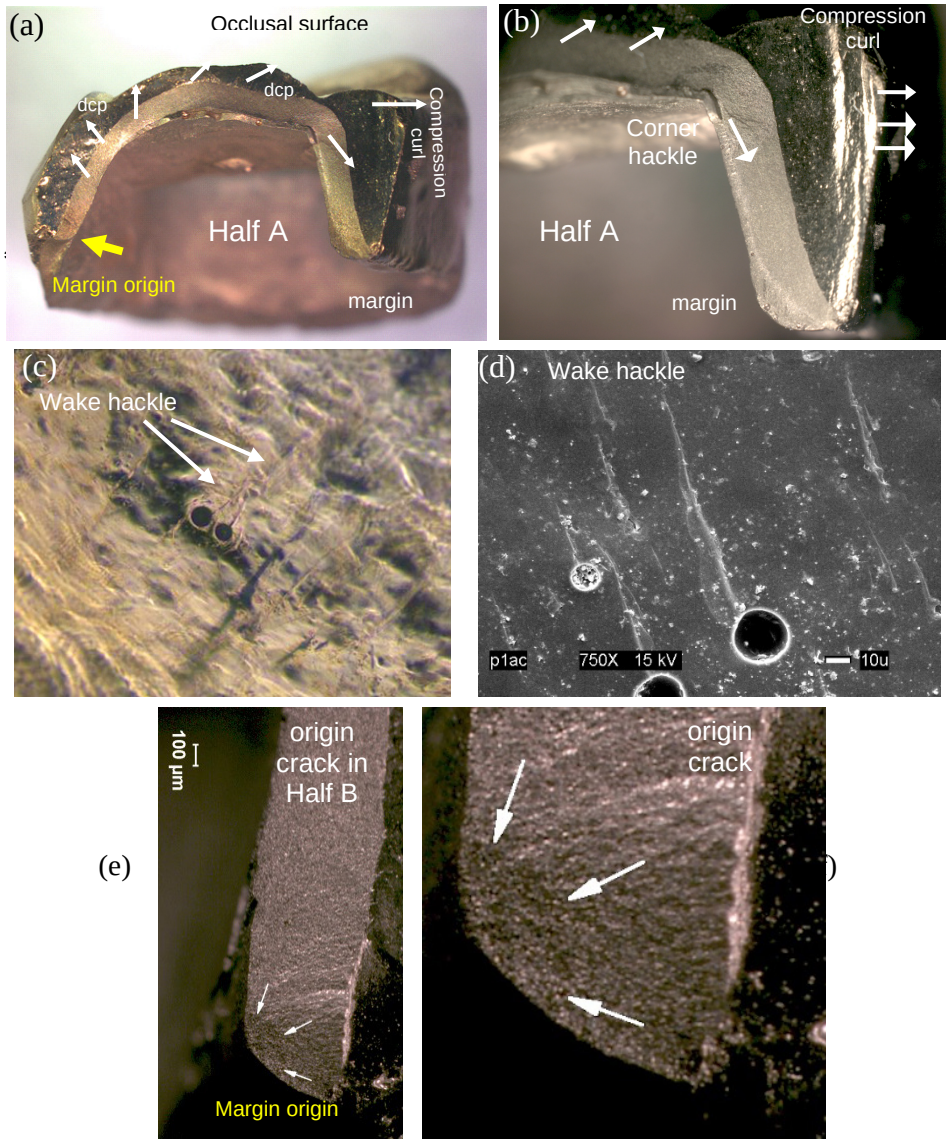

Figure 10.23 *Example 1 is a Procera alumina molar crown. The crown split vertically into two halves. The fracture surfaces have been gold coated for the optical images (all except d). (b) is a close-up of the compression curl on the side away from the origin site. The veneer porcelain is dark. The core ceramic is light grey. The arrows in (a,b) show the dcp based on the fractographic markings such as shown in (c) and (d). (e, f) show optical images of the origin which is a subtle margin crack as marked with white arrows. This origin crack was so flat and coplanar with the final fracture surface it did not stand out well in SEM images. (all courtesy of J. Quinn and S. Scherrer)*

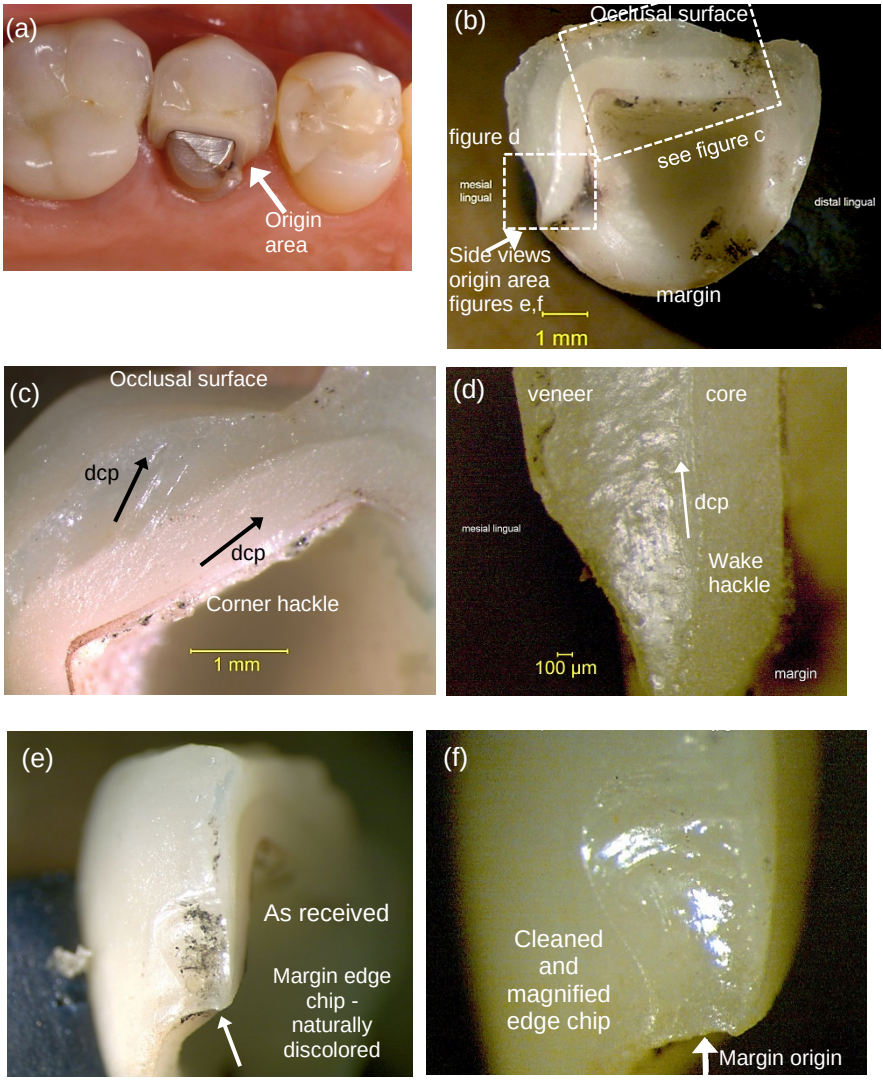

Figure 10.24 *<u>Example 2</u> is another Procera alumina molar crown. This one broke from an* ***edge chip on the margin****. All are optical images without any coating. (a) is a clinical view with the origin marked. (b) is the other half of the fractured crown. A closeup of the top inner corner is shown in (c) which shows a fanlike array of* ***corner hackle****. The hackle is between the two arrows which show the propagation direction (dcp) in both the veneer and core. (d) is from near the margin on the left side and shows tiny wake hackle from veneer pores. (e) and (f) show the origin was an edge chip from a force applied on the bottom of the margin aimed upwards. <u>Notice the discoloration stain in (e).</u> See the next figure for SEM images of the origin. (a is courtesy of S. Scherrer).*

Example 2, another Procera alumina crown is shown in Figures 10.24 on the previous page and 10.25 below. It has a margin edge chip fracture origin. A crack formed on the side of the chip and hoop stresses caused it to split the crown in half. Images 10.24 a-f are all optical images of the crown without coatings. This crown failure was diagnosed solely on the basis of an optical examination with a stereomicroscope. The black discoloration on the edge chip visible in Figure 10.24e was important. It meant the chip formed *in vivo* (in the patient's mouth) from the oral environment. Subsequent SEM examination (once the crown was cleaned) produced the sharper images shown in Figures 10.25.

Step by step a full fractographic montage - map for this crown was constructed as shown as Figure 5.73 at the end of chapter 5. Corner hackle (section 5.3.5) around the inside corners of the core, a compression curl, and wake hackle again led us back to the origin. The direction of the edge chip was puzzling. It appeared to have been from a force directed upwards on the crown. Such a loading is not likely in the mouth since the margin is protected by the gum line and jaw. The chip was probably created during fabrication or installation and was discolored in vivo.

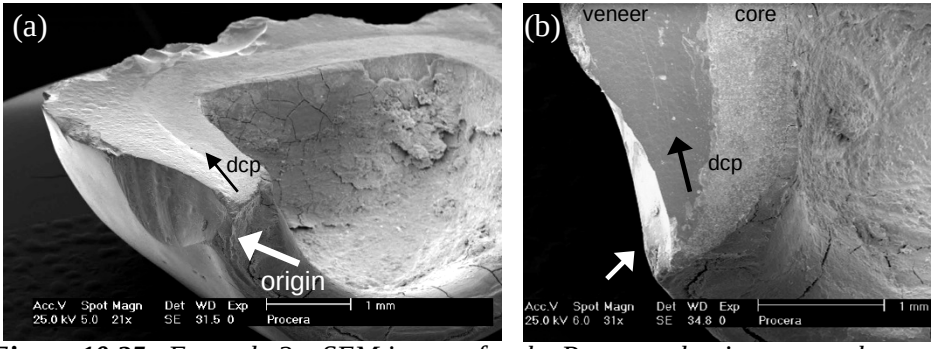

Figure 10.25 *Example 2. SEM images for the Procera alumina crown that broke from a margin chip (white arrows). The final fracture that split the crown started at the bottom at the margin, from part of the margin chip, and ran as shown by the black arrows. (images courtesy of S. Scherrer)*

Example 3 is shown in Figures 10.26 -10.28 on the next pages. It is an Empress II lithium disilicate glass ceramic incisor[g] that was obtained from the author's dentist. It had been in service only 4 months when it split into two pieces. This was a difficult analysis and was the first crown that J. Quinn and the author did together in the late 1990s. Our initial examinations had only

[g] Ivoclar, Schaan, Liechtenstein.

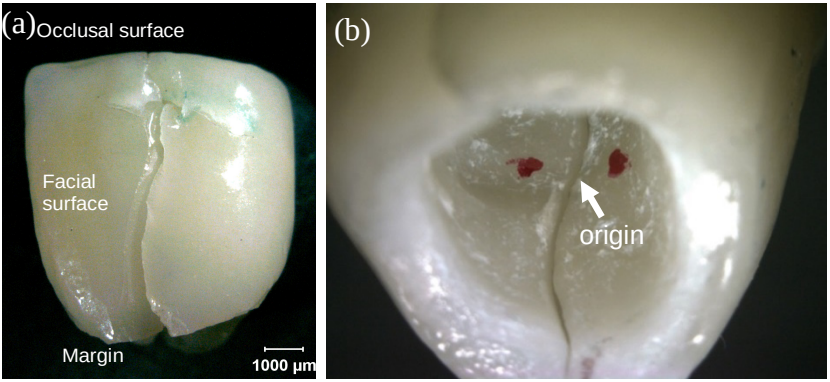

Figure 10.26 *Example 3 is a fractured Empress II glass ceramic anterior (#7) incisor crown. The insert (a) shows a facial view of the cleaved crown. (b) is a view looking up into the interior with the two halves together. The origin is located between the two red dots on the inside surface.*

limited success. The puzzle was solved after one year of examinations and reexaminations! Patience and persistence led us to solve the puzzle. We were unlucky that it was an extremely-unusual example with confusing and contradictory markings. We thought that it would be easy since the crown broke into only two pieces, and we had both. First, we had to get acquainted with crown fractures in general, and then we had to learn how to look at the material. We used different examination techniques (optical, optical green dye coated, optical gold coated, and SEM) and eventually we found the surprising origin. It was a contact crack on the inside of the crown!

The fracture plane was vertical and perpendicular to the dental arch. The two halves fitted closely together. A few small chips were missing, probably from secondary fracture, and were inconsequential to the analysis. The lingual surface (the side toward the tongue) had some surface damage and an unusually thick veneer. There were numerous conchoidal chip fractures, small pits and gouges at mid crown height. There also were several shallow depressions with tool marks indicating they were from grinding adjustments to the lingual surface by the dentist once the crown had been cemented in place and opposing tooth contact checked. This adjustment was only partially successful in relieving contact from the opposing tooth as evidenced by the numerous pits, chips, and gouges. This location was near the fracture origin region. On the other side of the crown, the facial surface was in good condition and had little damage or evidence of abuse. It had an unusually thin veneer with a few secondary spall chips and one harmless Hertzian cone crack that did not penetrate into the core material.

Some of the chips that initially confused us were on one fragment but not on the other, indicating that they were secondary fractures that occurred after the crown had broken. There was negligible damage on the occlusal (top) surface. Remnants of the cement were on the crown interior. Tool grinding marks and/or casting impression marks also were detected on the inside of the crown.

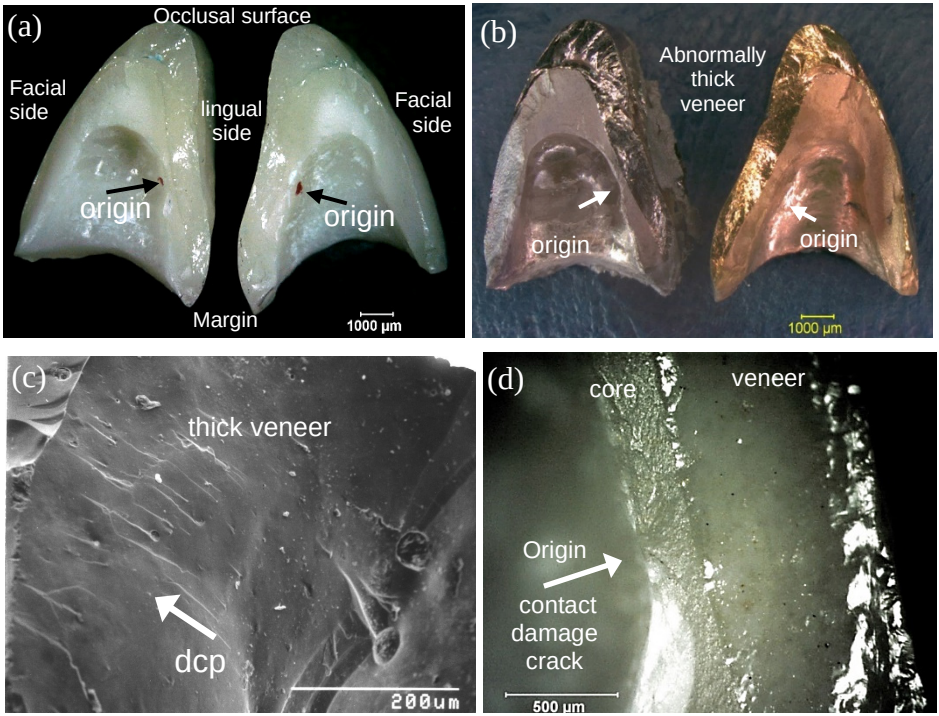

Figure 10.27 *Example 3. The fracture surfaces of the two halves. (a) is an optical photo. (b) is an optical photo after gold coating. Two different coaters caused the different coloration. The gold coating of the glassy veneer reflects more light in both pieces. The veneer thickness is very uneven and out of normal guidelines. It is very thick on the lingual side and very thin on the facial side. The arrows mark the origin site which was located at the thinnest part of the core material. (c) is an SEM image of wake hackle in the glassy veneer near the top (occlusal) surface. It shows the local direction of crack propagation (dcp). All the wake hackle in the crown showed that fracture ran from the inside to the outside. (d) is an optical image of the origin which originated from a contact crack on the inside of the crown at the thinnest point of the core. This is very unusual.*

Green dye staining for an optical examination and subsequent SEM examination brought out a number of telltale brittle material fracture features. Fractographic markings in the glass ceramic core material were difficult to detect, but there were some subtle hackle markings. Extensive wake hackle from bubbles in portions of the glassy veneer was very helpful as shown in Figure 10.27c and 10.28a,b. Seven or eight crack arrest lines were also detected.

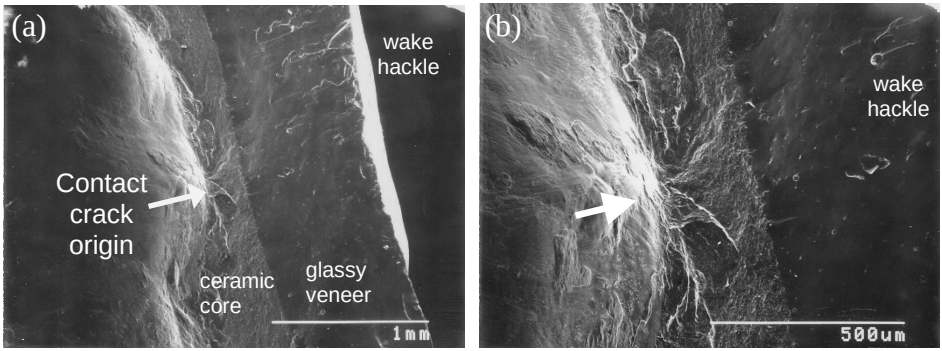

Figure 10.28 *SEM images of the Example 3 origin. Notice all the wake hackle in the veneer showing that the crack ran from the inside to the outside. The inside surface is uneven and there are mold or tool marks in the vicinity.*

Maps of local crack propagation direction were constructed, primarily through observations of the wake hackle markings in the veneer. Fracture initiated in the core material (very thin) from an *internal* surface Hertzian cone crack. Both fracture halves showed this blunt contact damage at the exact same location on the inside (cementitious) surface of the crown. This was unexpected and very unusual. The critical observation occurred when stereo SEM paired images were viewed of this area, and the arc-shaped crack that is typical of blunt contact damage was revealed. It was also noted that the inside crown surface was uneven. This location was in the same vicinity where *external* lingual surface damage has also been detected. Fracture then radiated upwards and downwards in response to hoop stresses causing the crown to split into two halves.

In summary, this Empress II incisor crown had uneven veneer and core wall thicknesses. Fracture initiated from contact damage on the *inside* of the crown, a rare event probably due to an uneven fit or improper placement. Opposing tooth contact in the same vicinity on the crown exterior surface (as evidenced by shallow pit and chip damage) created the stresses in the origin area. Surface grinding adjustments made to the same area suggested a fitting problem.

All three crowns in this Case series broke from hoop stresses and split vertically, perpendicular to the dental arch. The origin flaws were cracks introduced into the crowns at some point such as chips, contact damage, or margin cracks. The origins were not material flaws such as pores, inclusions, or sintering flaws.

Case 12: Mangled Margins (Twenty alumina dental crowns)

Dental fractographic analysis improved in the 2000s. The failures shown in Case 11 were *isolated* examples. This short case study is of many *in vivo* failures in one particular crown system. There was one dominant failure mode.

Prof. M. Øilo at the University of Bergen, Norway collected dozens of clinical fractures of one material system, CAD/CAM machined Procera 99.9% high purity alumina[h] [29] and organized them by type. As discussed in Chapter 4, she also devised a laboratory set-up that causes crowns to break into the same patterns as clinical fractures.[30,31] She and I worked together to identify the fracture origins in twenty-two crowns out of a set of twenty-seven retrieved crowns. These fractured *in vivo* from times as short as days to years. Twenty-one crowns broke from a common cause: hoop stresses on the margins that split the crowns, usually at the area of shortest wall length in the approximal area, from an irregularity in the margin. The flaws were chips, grinding cracks, and veneer irregularities. Figures 10.29 and 10.30 on the next page show two examples. A common element in all twenty-seven crowns was irregular grinding damage on feather margins that were as thin as 100 µm (0.1 mm). Feather margins are bad in ceramics. (Compare these margins to the thick ones in Figures 10.23 or 10.25.) Although such margins may be satisfactory for gold or porcelain fused-to-metal crowns, they are disastrous for ceramics since they are vulnerable to all sorts of damage and chipping.

Overall, dental material fractography is making progress. It is now possible to analyze clinical fractures by the dozens. Patterns are emerging. Analysis in this alumina crown project was still time consuming, but it went quicker the more that we did. Of note was that the origin area was identified in all crowns by light microscopy. We learned that gold coating the specimens dramatically speeded up the process. Green dye staining worked, but gold coating prior to an optical examination was better. It was then not too difficult to get the appropriate piece into the SEM and focus on the origin itself. (The 2020 third edition of this Guide showed several more examples for this case study.)

---

[h] Nobel Biocare, Stockholm, Sweden.

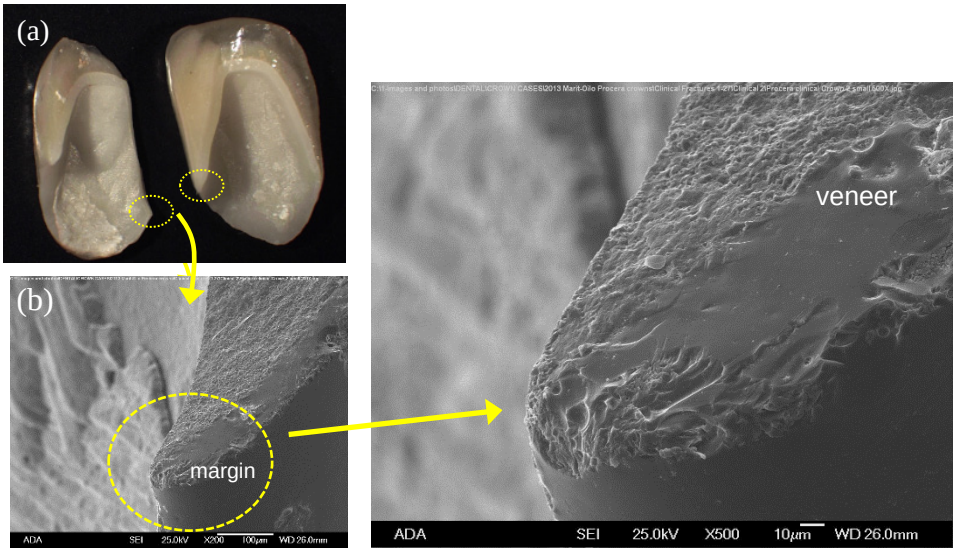

Figure 10.29 *Alumina central incisor that broke in vivo after 1 year. Fracture started at the margin from cracking in both the veneer and core. The margin is too thin, and even worse, the core portion is exceptionally thin. The origin is chipping damage at the margin. (clinical case 2)*

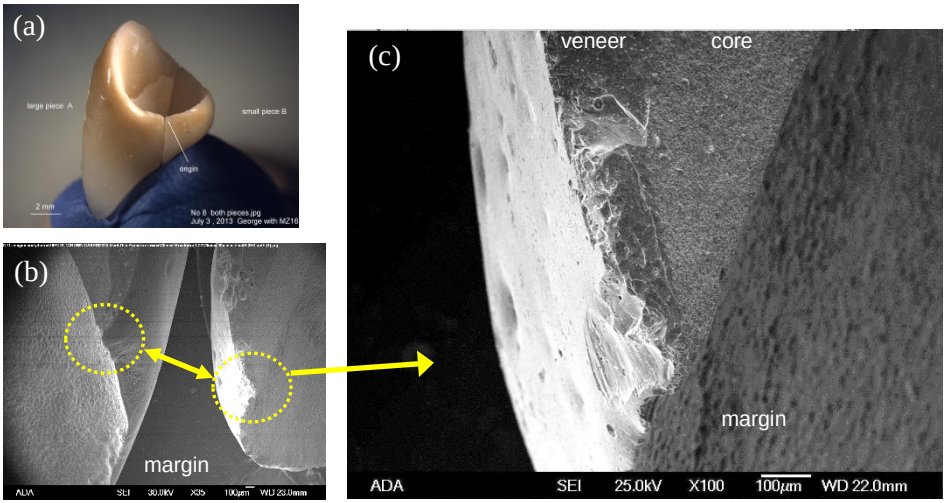

Figure 10.30 *Alumina incisor that broke in vivo at an unreported time. Fracture started at the margin from cracks and chipping in both the veneer and core. The crown split in half from the mesial to distal side. The margin is too thin and the core portion of it is exceptionally thin. (clinical case 8).*

Case 13 Ruined Refractors (Sapphire Lenses)

This case is of a large elaborate single crystal sapphire component. Sapphire is a "harsh mistress." She has alluring physical and mechanical properties such as good transmission of optical and infrared light, strengths of 1000 MPa or more, and good high-temperature properties. She also has vulnerabilities, such as large strength variability, sensitivity to contact and machining damage, and a shocking weakness at 300 ºC - 500 º C due to compression-induced twinning.

(a)

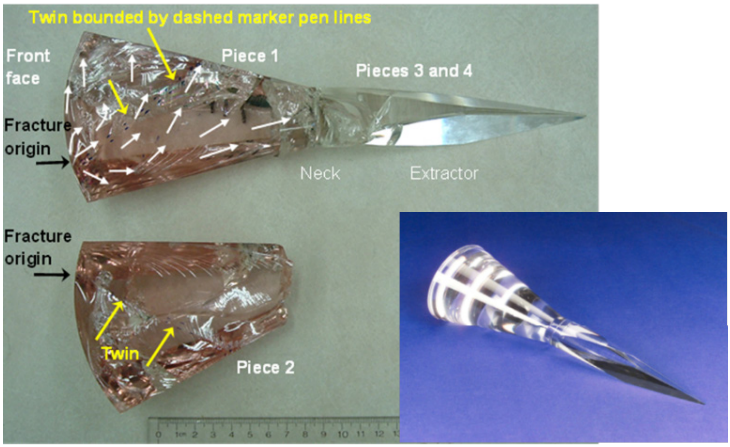

(b)

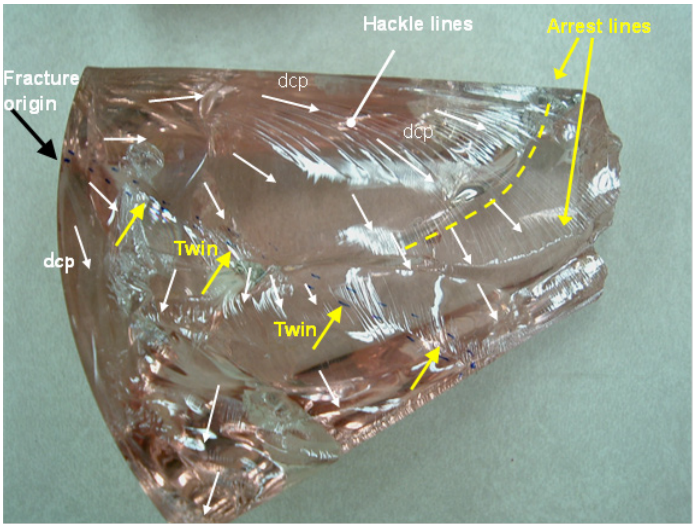

Figure 10.31 *Fractured sapphire solar light secondary concentrator which broke into four pieces. The origin was on the rounded front surface where incoming light is focused into the body. The blue insert in (a) shows an intact lens prior to testing. It is a complex but beautiful piece.*

NASA is laying the groundwork for spacecraft of the future that could harness solar energy. One concept is to use a large primary mirror solar collector that focuses light to a secondary lens collector. The collector focuses and concentrates energy by total internal reflection into a heat exchanger.[32] Two of these full-scale (30 cm long by 9.5 mm diameter) c-axis sapphire lenses were tested in the giant solar thermal vacuum facility that simulates outer space at the Glenn Research Center. They fractured during high-temperature trials. This analysis was done by Dr. J. Salem of NASA-Glenn and me.[32]

Figure 10.31 shows one of the fractured lenses. It changed to a rose-brown color from solarization at the 1300° C peak temperature of the test. The fracture surface had a mix of cleavage and conchoidal fracture and some crack bifurcations. The fracture origin was on the front lens face. It is shown in Figure 10.32 and was a large, partial Hertzian cone crack that extended from one of two partially polished impact divots or "bruises" on the polished surface. Thermal stresses subsequently caused the lens to fracture. This structure also had twins, but they were incidental and not a cause of fracture. They probably were growth twins, not twins induced by the stresses. Figure 3.63 in the equipment chapter showed one big twin in a polariscope.

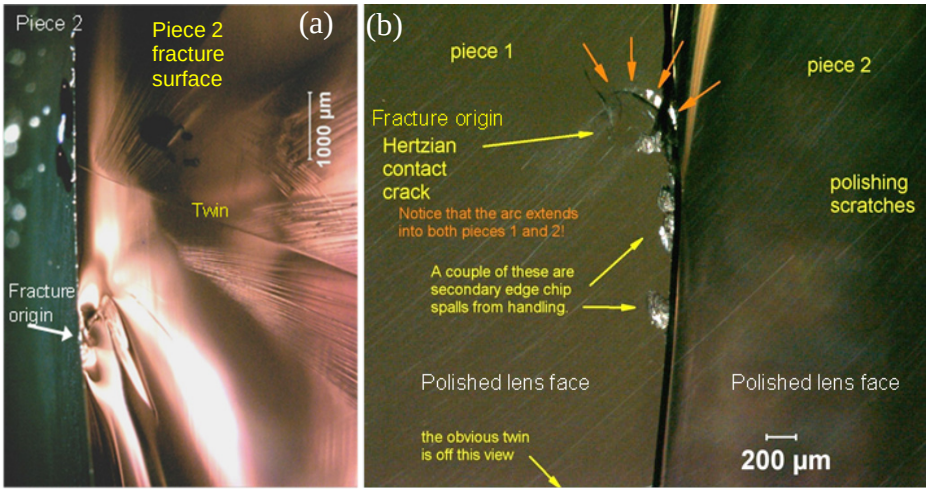

Figure 10.32 *The origin of the first refractor was a blunt contact damage crack shown on the fracture surface (a) and on the lens front face in (b).*

The second broken refractor also broke from an origin on the curved front surface, again from thermal stresses, but the origin was a scratch. The full analysis was shown in Chapter 10 of the 3rd edition of this Guide and in reference 32.

Both refractors and some of the earlier IR domes shown in this Guide typify the vulnerability of sapphire to residual grinding cracks, polishing and handling damage. The thermal gradients created both tensile and compression stresses, and it is very likely that with additional high-temperature exposure and cycling, more twins would have formed with the possibility they would have intersected at some point leading to crack formation and eventually fracture.

Chapter 10 References

1. R. R. Baker, L. R. Swank, and J. C. Caverly, "Ceramic Life Prediction Methodology - Hot Spin Disk Life Program," AMMRC TR 83-44, Army Materials and Mechanics Research Center, Watertown, MA, August, 1983.
2. L. R. Swank, R. R. Baker, and E. M. Lenoe, "Ceramic Life Prediction Methodology," pp. 323 - 330 in *Proc. of the 21st Automotive Technology Development Contractors Coordination Meeting*, SAE, Warrendale, PA, 1984.
3. G. D. Quinn, "Fracture Mechanism Maps for Advanced Structural Ceramics, Part I, Methodology and Hot-Pressed Silicon Nitride," *J. Mat. Sci*, **25** (1990) 4361 - 4376.
4. G. D. Quinn, K. Xu, R. J. Gettings, J. A. Salem, and J. J. Swab, "Does Anyone Know the Real Fracture Toughness? SRM 2100: The World's First Ceramic Fracture Toughness Reference Material," pp. 76 - 93 in *Fracture Resistance Testing of Monolithic and Composite Brittle Materials, ASTM STP 1409,* eds., J. Salem, G. Quinn, and M. Jenkins, ASTM Int., West Conshohocken, PA, 2002.
5. K. D. Mörgenthaler and E. Tiefenbacker, "Bauteile Aus Keramik Für Gasturbinen," Daimler-Benz AG, Technical Report, Stuttgart, 1983.
6. E. J. Bunning, D. R. Claxton, and R. A. Giles, "Liners for Gun Tubes – A Feasibility Study," *Ceram. Eng. and Sci. Proc*., **2** [7-8] (1981) 509 - 519.
7. G. D. Quinn, "Characterization of Turbine Ceramics After Long Term Environmental Exposure," AMMRC TR 80-15, Army Materials and Mechanics Research Center, Watertown, MA, May, l980.
8. G. D. Quinn, "Review of Static Fatigue in Silicon Nitride and Silicon Carbide," *Ceram. Eng. and Sci. Proc*., **3** [1-2] (1982) 77 - 98.
9. G. D. Quinn and R. N. Katz, "Time Dependent High Temperature Strength of Sintered Alpha SiC," *J. Amer. Ceram. Soc*., **63** [1-2] (1980) 117 - 119.
10. J. Coppola, M. Srinivasan, K, Faber, and R. Smoak, "High Temperature Properties of Sintered Alpha Silicon Carbide," pres. at the Int. Symp. *Factors in Densification and Sintering of Oxide and Non-Oxide Ceramics*, Hakone, Japan, October, 1978.
11. V. D. Fréchette, *Failure Analysis of Brittle Materials*, Advances in Ceramics, Vol. 28, American Ceramic Society, Westerville, OH, 1990.
12. J. J. Swab, R. Pavlacka, G. Gilde, S. Kilczewski, J. Wright, and D. Harris, "Determining the Strength of Coarse-Grained ALON and Spinel," *J. Am. Ceram. Soc*., **97** [2] (2014) 592-600.
13. MIL STD 1942 (MR), "Flexural Strength of High Performance Ceramics at Ambient Temperature," U. S. Army Materials Technology Laboratory, Watertown, MA, 1983.
14. ASTM C 1161-90, "Standard Test Method for Flexural Strength of Advanced Ceramics at Ambient Temperature," ASTM Int., West Conshohocken, PA, 1990.
15. ISO 14704, "Fine Ceramics (Advanced Ceramics, Advanced Technical Ceramics) – Test Method for Flexural Strength of Monolithic Ceramics at Room Temperature," Int. Org. for Standards, Geneva, SW, 2000.

16. G. D. Quinn, “Fractography and the Army Flexure Standard,” pp. 319 - 334 in *Fractography of Glasses and Ceramics*, eds., J. Varner and V. Fréchette, American Ceramic Society, Westerville Ohio, (1988).
17. G. D. Quinn, “Flexure Strength of Advanced Structural Ceramics: A Round Robin,” *J. Am. Ceram. Soc.*, **73** [8] (1990) 2374 - 2384.
18. W. N. Sharpe, Jr., O. Jadaan, N. N. Nemeth, G. M. Beheim, and G. D. Quinn, “Fracture Strength of Silicon Carbide Microspecimens,” *J. Microelectromechanical Systems*, **14** [5] (2005) 903 - 913.
19. G. D. Quinn, W. Sharpe, Jr., G. Beheim, N. Nemeth, and O. Jadaan, “Fracture Origins in Miniature Silicon Carbide Structures,” pp. 62 - 69 in *Fractography of Advanced Ceramics, II*, eds., J. Dusza, et al., TransTech Publ., Zurich, 2005.
20. G. D. Quinn, “Design and Reliability of Ceramics, Do Modelers, Designers and Fractographers See the Same World?” *Ceram. Eng. and Sci. Proc*., **26** [2] (2005) 239 - 252.
21. J. J. Swab and G. D. Quinn, “The VAMAS Fractography Round Robin: A Piece of the Fractography Puzzle,” pp. 55 -70 in *Fractography of Glasses and Ceramics III*, Ceramic Transactions, Vol. 64, eds., J. R. Varner et al., ACS, Westerville, OH, 1996.
22. MIL HBK 790, “Fractography and Characterization of Fracture Origins in Advanced Structural Ceramics,” U. S. Army Materials Technology Laboratory, Watertown, MA, June, 1992.
23. ASTM C 1322-96, “Standard Practice for Fractography and Characterization of Fracture Origins in Advanced Ceramics,” *Annual Book of Standards*, Vol. 15.01, ASTM Int., West Conshohocken, PA.
24. J. B. Quinn, G. D. Quinn, J. R. Kelly, and S. S. Scherrer, “Fractographic Analyses of Three Ceramic Whole Crown Restoration Failures,” *Dent. Mater.*, **21** (2005) 920 - 929.
25. S. S. Scherrer, J. B. Quinn, G. D. Quinn, and J. R. Kelly, “Failure Analysis of Ceramic Clinical Cases Using Qualitative Fractography,” *Int. J. Prosth.*, **19** [2] (2006) 151 - 158.
26. J. B. Quinn, G. D. Quinn, J. R. Kelly, and S. S. Scherrer, “Useful Tools for Dental Failure Investigation,” pp. 36 - 53 in *Proc. Conf. on Scientific Insights and Dental Ceramics and Photopolymer Networks*, ed. D. C. Starrett, Trans. Acad. Dental Materials, Vol. 16, 2004.
27. J. R. Kelly, “Fractography of Dental Ceramics,” pp. 241 – 251 in *Fractography of Glasses and Ceramics*, IV, eds., J. R. Varner and G. D. Quinn, American Ceramic Society, 2001.
28. J. Y. Thompson, K. J. Anusavice, A. Naman, and H. F. Morris, “Fracture Surface Characterization of Clinically Failed All-Ceramic Crowns,” *J. Dent. Res*., **73** [12] (1994) 1824 – 1832.
29. M. Øilo and G. D. Quinn, “Fracture Origins in Twenty-two Dental Alumina Crowns,” *J. Mech. Beh. Biomed. Mater.*, **53** (2016) 93 – 103.
30. M. Øilo, A. K. Kvam, J. E. Tibballs, and N. Gjerdet, “Clinically Relevant Fracture Testing of All-Ceramic Crowns,” *Dent. Mater.*, **29** (2013) 815 - 823.
31. M. Øilo, N. R. Gjerdet, “Fractographic Analysis of All-Ceramic Crowns: A Study of 27 Clinically-Fractured Crowns,” *Dent. Mater*., **29** (2013) e78 - e84
32. J. A. Salem and G. D. Quinn, “Fractographic Analysis of Large Single Crystal Sapphire Refractive Secondary Concentrators,” *J. Eur. Cer. Soc.*, **34** (2014) 3271 - 3281.

11. Conclusions

Figure 11.1
The fractographer as a detective.

This Guide is intended to introduce engineers and scientists to the science of fractographic analysis of brittle materials as a tool to solve fracture problems. This tool may be applied to a broad range of practical problems including component failure analyses, materials processing refinements, routine materials characterization, laboratory scale mechanical testing, and reliability and design. Fractography is the examination of fracture surfaces, the examination of the general crack patterns, other part surfaces, other specimens, and a review of processing, exposure, and testing conditions. Much like the master detective, the fractographer starts with an open mind, integrates and analyzes the available information and relates it to similar episodes from his own experience and to what is published in the literature. The fractographer applies deductive logic to arrive at a conclusion.

We are in the midst of microscopy revolution, as the marriage of computers with digital cameras and glass lenses expands the fractographer's tool box dramatically. Quantitative, virtual, three-dimensional imaging is increasingly available. Nonetheless, no matter how powerful these tools become, in the author's opinion they will never supplant the fractographer as an expert system.

The question has been raised as to whether machine or artificial intelligence systems could do fractographic analysis. What if all the contents, including all the text and images of this Guide and all of the literature cited herein, were uploaded to an AI system? Could it do a competent fractographic analysis? My answer is yes but only in some very limited, repetitive circumstances. It is unlikely it will be able to solve general problems. An expert fractographer knows how to tilt a specimen or light source under a stereooptical microscope and recognize a fleeting reflection that unlocks a fractographic puzzle. The fractographer knows when and how to look at something differently, how to stain a specimen on a hunch, how to diagnose which of several fractures is the first if there are multiple origins, how to recognize exceptions, how to recognize something unusual or new (e.g., new additive-manufactured ceramic flaws), or when to do controlled-laboratory fractures tests to duplicate mysterious in-service failures. The fractographer knows how to manage the sometimes confusing and contradictory nomenclature that we have inherited, e.g., the word "striation." Its meaning is very different for a metallurgist and a ceramist. Nomenclature variations, exceptions, and new flaws or markings may confuse or even fool an AI system. It will take some time before cameras

and AI systems will be able to routinely view broken pieces in three dimensions, a simple skill that every fractographer does without thinking! The fractographer knows how to integrate all of the available information as illustrated in the puzzle Figure 1.4 in the Introduction. The fractographer makes sensible interpretations consistent with all the facts and clues and is not likely to imagine things and have hallucinations as some AI systems now in use are apt to do as this 4th edition went to press in late 2025.

My experiences over fifty-six years have been distilled into the following fractography rules of thumb:

1. **The first one is the hardest.** The more examples of a particular fracture problem that are examined the better. This is true for both experienced and novice fractographers. Patterns may be recognized that are not apparent in a single example. An unfamiliar or subtle feature may be overlooked in one example. When the fractographer sees a curious or unfamiliar marking in multiple examples, he is less likely to dismiss it as a random artifact. One of the most gratifying experiences a fractographer has is when he or she first recognizes and understands a new marking or flaw and adds it to his or her experience base.

2. **The more experience the fractographer has the better.** Fractography is a cumulative learning experience. The more one learns, the easier and faster fractography becomes. The fractographer should look at as many different test specimens, components, and materials as possible.

3. **Photos almost never show all there is to see.** Photos are two-dimensional representations of a three-dimensional world and perspective is inevitably lost.

4. **Good equipment makes the job easier or even possible, but is no substitute for skill and experience.** One must know where to look and great pictures of the wrong things are worthless. Many published close-up SEM images fit this category.

5. **Good fractography under laboratory testing situations begins even before the specimen is broken.** The specimen should be tested in clean conditions to minimize contamination and secondary fractures.

6. **Fractography is more than looking at fracture surfaces.**

7. **A good fractographer is patient.** Don’t be afraid to reexamine the pieces. Look at all the pieces, even the ones that may not seem to be relevant. Sometimes, in a group of laboratory-tested specimens, a key feature is discerned or recognized on the very last specimen. Fractographers in a rush often overlook important details.

8. It's better to let the material tell you why it failed than the other way around. Theoretical modelers cause the most trouble. They already know why something should fail since it is in their computer model. Indentation mechanics people come next. They have more interest in indentations than in the real flaws in a material.

9. A good fractographer does not overreach, guess, or force an interpretation. Don't let other people put words in your month. The good fractographer is not afraid to say: "I don't know," or to say up front: "I'll take a look, but I make no promises." The credibility of the fractographer is a precious commodity.

10. Fractography may seem subjective to the uninformed, but it is very objective. One last metaphor to summarize the fractographic craft is offered. When a fractographer first sees broken fragments, he or she sees pieces that are trying to tell a tale. With the tools of the trade and with the fractographic skills summarized in this Guide, a fractographer can listen to the pieces, interpret their story, and unlock the secrets of the fracture.

Fracture surfaces can be beautiful such as Figure 11.2 from an unpublished study by Janet Quinn of dental porcelains with varying amounts of crystallization and leucite content. It shows many markings shown in this Guide.

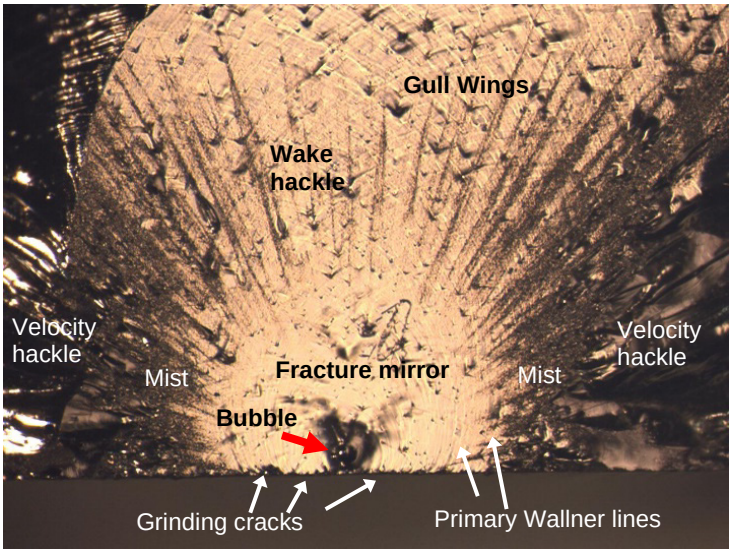

Figure 11.2 *Fracture surface of a dental glass-porcelain flexural strength bar. The fracture origin is a row of grinding cracks that interacted with a near-surface bubble. (unpublished, found in Dr. J. Quinn's computer after her death.)*

APPENDIX A BIBLIOGRAPHY

Books on Glass and Ceramic Fractography

Good books on fractography in general are now listed in Chapter 2.

Conference Series Books on Fractography of Glasses and Ceramics

Fractography of Glasses and Ceramics, Advances in Ceramics, Vol. 22, J. Varner and V. Fréchette, eds., American Ceramic Society, Westerville, OH, 1988.

The first of a quadrennial-quinquennial conference series by the same name held at Alfred University in the summer of 1986. Sections on: fundamental phenomena, high-temperature fracture, fractography and fracture mechanics, fractography in materials development and testing, and component failures. Twenty-eight papers including Rice, Fréchette, Mecholsky, Kirchner, Bradt, Michalske, Beauchamp. Notable papers on whitewares by Banda and Messer; ceramic armor by Tracy, Slavin, Viechnicki; NiS tempered glass by Bradt; fractals by Mecholsky and Passoja; flexure testing by Quinn.

Fractography of Glasses and Ceramics, II, Ceramic Transactions, Vol. 17, V. Fréchette and J. Varner, eds., American Ceramic Society, Westerville, OH, 1991.

Twenty-six papers from the second 1990 Alfred University conference held on campus in the summer of 1990.

Fractography of Glasses and Ceramics, III, Ceramic Transactions, Vol. 64, J. Varner, V. Fréchette, and G. D. Quinn, eds., American Ceramic Society, Westerville, OH, 1996.

Twenty-five papers from the 3rd Alfred University conference in 1995.

Fractography of Glasses and Ceramics, IV, Ceramic Transactions, Vol. 122, J. Varner and G. D. Quinn, eds., American Ceramic Society, Westerville, OH, 2001.

Thirty-two papers from the fourth Alfred University conference, held on campus in 2000. Special session on edge chipping.

Fractography of Glasses and Ceramics, V, Ceramic Transactions, Vol. 199, J. Varner G. D. Quinn, and M. Wightman, eds., American Ceramic Society, Westerville, OH, 2007.

Thirty-six papers from the fifth Alfred University conference, held in 2006 but this time in Rochester, NY. Papers by Quinn on fracture mirror size measurements; Wilantewicz and Varner on indentation damage evolution under Vickers indentations in glass and the importance of the ratio of G/K; by Hecht-Mijic and Richter on fractography of hip joint balls; Morrell on component fractures including SiC seal rings, CaF_2 windows, and alumina hip balls; Cleary and Nichols on automotive windows; and Engelder about controversies in interpreting mesoscopic cracks in rock fractures in the earth.

Fractography of Glasses and Ceramics, VI, Ceramic Transactions, Vol. 230, J. Varner and M. Wightman, eds., American Ceramic Society and Wiley, Westerville, OH, 2012.
Twenty-five papers from the 2011 sixth Alfred university conference, held in Jacksonville, FL. Papers by Quinn on the history of fractography; Glaesemann et al., on fractography in the development of ion-exchanged cover glasses (e.g., Gorilla glass); Gross on crack evolution in alkali aluminosilicate glasses for cover glass; Bradt on an energy criterion for mirror formation; Hecht-Mijic on dental implants; Maurer on a glass pharmaceutical syringe fracture.

Fractography of Advanced Ceramics, ed., J. Dusza, Trans Tech Publ., Zurich, 2002.
First (2001) of a conference series in Stará Lesná, Slovakia. Organized by the Slovakian Academy of Sciences -Institute of Materials Research in Košice, Slovakia. Thirty-six papers, many of which are on mechanical testing and have no fractography. Excellent fractography papers including a bioceramics fracture paper by H. Richter and a paper by R. Morrell and J. Kübler on the background of the then new CEN EN 843-6 fractography standard: "Advanced Technical Ceramics, Monolithic Ceramics, Part 6: Guidelines for Fractographic Examination,".

Fractography of Advanced Ceramics II, eds. J. Dusza, R. Danzer, and R. Morrell, Trans Tech Publ. Zurich, 2005.
Second (2004) of the Stará Lesná, Slovakia conference series. Sixty-one short papers. Papers by Quinn et al. on machining damage detection and characterization, Wang et al. on ZnO varistor failures, Supanic et al., on fractures in stacked PZT piezoceramic actuators, and Tatami et al. on nanofractography of alumina by scanning probe microscopy. Many of the papers have negligible fractography, however, and deal more with mechanical properties, processing, and indentation.

Fractography of Advanced Ceramics III, eds. J. Dusza, R. Danzer, R. Morrell, and G. D. Quinn, Trans Tech Publ. Zurich, 2009.
Third (2008) of the Stará Lesná, Slovakia conference series. Sixty-three short papers. Papers by Quinn on the history of fractography of brittle materials; Bradt on some legal aspects and challenges; Varner on use of replicas.

The fourth through sixth and eighth conferences in this series were held in 2013, 2016, 2019, and 2025 in Smolenice castle outside Bratislava in Slovakia. The seventh was held in 2023 in Leoben, Austria. The eighth conference is now called: Fracture Mechanics and Fractography of Advanced Ceramics 2025. Selected papers from these were published in topical issues of the Journal of the European Ceramic Society.

Fractography of Ceramic and Metal Failures, J. Mecholsky, Jr., and S. Powell, Jr., eds., *ASTM STP 827*, ASTM, Philadelphia, PA, 1984.
An excellent book with eight papers on ceramics from a 1982 symposium at ASTM headquarters in Philadelphia. Includes an outstanding, comprehensive, and well-illustrated, 99-page review paper by Rice, and papers by Pantano and Kelso, and Healy and Mecholsky (cited below).

Fracture Mechanics of Ceramics, Vol. 1, R. C. Bradt, D. P. H. Hasselman, and F. Lange, eds., Plenum Press, NY, 1974.

Proceedings of a conference at Pennsylvania State University in 1973 with twenty-three papers on fracture mechanics applied to origin detection and fractography. Later volumes of this quadrennial series also had some fractography papers. Bradt was a famous fractographer who had many publications. He passed away in 2019.

Microscopy Techniques

C. G. Pantano and J. F. Kelso, "Chemical Analysis of Fracture Surfaces," *Fractography of Ceramic and Metal Failures, ASTM STP 827*, ASTM, 1984, pp. 139–156.

The applicability of various instrumental techniques for chemical analysis of fracture surfaces is reviewed. The relative merits and spatial and depth resolutions of Auger microscopy and energy or wavelength dispersive electron microscopy are given.

J. T. Healy and J. J. Mecholsky, Jr., "Scanning Electron Microscopy Techniques and Their Application to Failure Analysis of Brittle Materials," *Fractography of Ceramic and Metal Failures, ASTM STP 827*, ASTM, 1984, pp. 157 – 181.

Discusses cleaning, coating, and other procedures for SEM specimens. The merits of secondary and backscattered electron imaging are presented.

C. R. Brooks and B. L. McGill, "The Application of Scanning Electron Microscopy to Fractography," *Mater. Char.*, **33** (1994) 195 - 243.

An excellent, well-illustrated review of the application of scanning electron microscopy for topographical and chemical analysis of fracture surfaces of ceramics, metals, and polymers. Includes a good discussion of stereo SEM fractography.

Fractography of Ceramics and Glasses - Overview Papers

J. J. Mecholsky, Jr., and S. W. Freiman, "Determination of Fracture Mechanics Parameters Through Fractographic Analysis of Ceramics," pp. 136 – 150 in *Fracture Mechanics of Ceramics Applied to Brittle Materials*, S. Freiman, ed., *ASTM STP 678*, ASTM, 1979.

A short overview of the utility of fractography as a quantitative tool to determine strength-limiting origins, the stress at failure, and critical fracture toughness.

R. W. Rice, "Fractographic Identification of Strength Controlling Flaws and Microstructure," pp. 323 – 345 in *Fracture Mechanics of Ceramics*, Vol. 1, R. Bradt, D. Hasselman, and F. Lange, eds., Plenum Press, NY, 1974.

A short but valuable discussion of key origins (pores, pore groups, large grains). and their relationship to fracture energy. The fracture energy can either be a single-crystal or polycrystalline value depending upon the relative sizes of origin and microstructure.

G. D. Quinn, J. J. Swab, and M. J. Slavin, "A Proposed Standard Practice for Fractographic Analysis of Monolithic Advanced Ceramics," MTL TR 90-57, November 1990, NTIS Access No. ADA-231989.

Discusses MIL HDBK 790, "Fractography and Characterization of Fracture Origins in Advanced Structural Ceramics," a 1992 Military Standard handbook that was the predecessor of the 1996 ASTM C 1322 "Practice for Fractography and Characterization of Fracture Origins in Advanced Ceramics." Discusses essential background information and the rationale for consistency in characterization. A standard nomenclature and origin characterization scheme were proposed.

R. W. Rice, "Topography of Ceramics," pp. 439 – 472 in *Surfaces and Interfaces of Glass and Ceramics*, V. Fréchette et. al., eds., Plenum Press, NY, 1974.

A very helpful introduction describes the role of unaided eye, hand lens, optical, scanning, and transmission electron microscopy. Fracture surface features such as transgranular and intergranular fracture, crack microstructure interactions, crack branching, mirrors, and single crystal fractography are discussed.

R. W. Rice, "Ceramic Fracture Features, Observations, Mechanism and Uses," *Fractography of Ceramic and Metal Failures, STP 827*, ASTM, 1984, pp. 5 – 103.

An extraordinary book-length (99 pages) article with many useful tips and analyses. Many single crystal examples.

T. A. Michalske, "Quantitative Fracture Surface Analysis," pp. 653 – 662 in *Ceramics and Glasses, Engineered Materials Handbook*, Vol. 4, ed. S. Schneider, ASM, Metals Park, OH, 1991.

J. R. Varner, "Descriptive Fractography," pp. 635 - 644 in *Ceramics and Glasses, Engineered Materials Handbook*, Vol. 4, ed. S. Schneider, ASM, Metals Park, OH, 1991.

J. S. Wasylyk, "Special Terminology Used in Fractography," pp. 632 – 634 in *Ceramics and Glasses, Engineered Materials Handbook*, Vol. 4, ed. S. Schneider, ASM, Metals Park, OH, 1991.

R. C. Bradt, "The Fractography and Crack Patterns of Broken Glass," *J. Fail. Anal. Prev.*, **11** (2011) 79-96.

R. J. Parrington, "Fractography of Metals and Plastics," *J. Fail. Anal. Prev.*, **2** [5] (2002) 16 - 19, 44 - 46.

A short article with some interesting history of fractography. Metals and plastic fracture modes and patterns are compared.

W. Harrer, R. Morrell and R. Danzer, "A Brief Guide to Conducting Failure Analysis on Ceramic Components," *Pract. Metallogr.*, **60** [9] (2023) 580 - 593.

Fractography Round Robins

J. J. Swab and G. D. Quinn, "Fractography of Advanced Structural Ceramics, Results from the VAMAS Round Robin Exercise," U.S. Army Technical Report, ARL-TR-656, U.S. Army Research Laboratory, Aberdeen, MD, Dec. 1994.

An international Versailles Advanced Materials and Standards (VAMAS) Round Robin for identification of fracture origins in test coupons and photographs. Lessons learned.

J. J. Swab and G. D. Quinn, "Fractography of Advanced Structural Ceramics: Results from Topic #2 of the VAMAS Round Robin Exercise"' *Ceram. Eng. Sci. Proc.*, **16** [5] (1995) 929 - 938.

A short summary of part of the 1994 VAMAS round robin on ceramic fractography.

J. J. Swab and G. D. Quinn, "Results of a Round Robin Exercise on the Fractography of Advanced Structural Ceramics," *Cer. Eng. Sci. Proc.*, **15** [5] (1994) 867 - 876.

A short summary of findings from the 1994 VAMAS fractography round robin.

J. J. Swab and G. D. Quinn, "The VAMAS Fractography Round Robin: A Piece of the Fractography Puzzle," pp. 55 - 70 in *Fractography of Glasses and Ceramics III*, eds. J. Varner and G. D. Quinn, American Ceramic Society, Westerville, OH, Ceramic Transactions, Vol. 64, (1996).

Seventeen laboratories analyzed photos of grinding cracks. They also analyzed actual specimens with other types of flaws. Results varied. Much was learned by the organizers from this exercise. How do fractographers sift through and use the clues?

Origins in Ceramics

H. Kirchner, R. Gruver, and W. Sotter, "Characteristics of Flaws at Fracture Origins and Fracture Stress—Flaw Size Relations in Various Ceramics," *Mater. Sci. Eng.*, **22** (1976) 147 – 156.

A concise but useful report on strength-limiting origins in alumina, silicon nitride, and silicon carbide with a detailed tabulation of different types of origins. Emphasis is on porosity, large grains, and machining origins. An important observation (Fig. 1b) is that origins in the center of fracture mirrors may be intersected-at an angle and a true view of the origin may not be seen.

H. Baumgartner and D. Richerson, "Inclusion Effects on the Strength of Hot Pressed Si_3N_4," *Fracture Mechanics of Ceramics*, Vol. 1, 1974, pp. 367–386.

Good characterization of machining damage and inclusions in silicon nitride. The inclusions are much smaller than expected due to local-degradation of the matrix K_{Ic}.

M. G. Gee and R. Morrell, "Fracture Mechanics and Microstructures," pp. 1 – 22 in *Fracture Mechanics of Ceramics*, Vol. 8, R. Bradt, A. Evans, D. Hasselman, and F. Lange, eds., Plenum Press, NY, 1986.

Principally a discussion of the application of fracture mechanics theories to strength. Microstructural influences significantly complicate matters and may limit utility to

qualitative issues. The nature of strength-limiting origins and their severity is discussed. In some instances, sharp cracks will not form until the stress is applied.

A. G. Evans, "Structural Reliability, A Processing Dependent Phenomenon," *J. Amer. Ceram. Soc*, **65** [3] (1982) 127–139.

Evans didn't spend much time looking through microscopes, but he was the preeminent modeler of mechanical behavior in ceramics and glasses in the 1970s - 2000s. He passed away in 2009. This paper and the two below were important contributions pertaining to flaws and their effect upon strength and reliability. This paper has an emphasis on the micromechanics of fracture with a good discussion of the effect of thermal and mechanical property mismatches between an origin and the matrix. Graph of stress versus origin size for silicon nitride showing the relative severity of different origins (WC, Fe, Si, C inclusions, porosity, and machining damage).

A. G. Evans, "Non-Destructive Failure Prediction in Ceramics," pp. 595 - 626 in *Progress in Nitrogen Ceramics*, ed. F. L. Riley, Matirnus Nijhoff Publ., The Hague, 1983.

Includes the graph of stress versus origin size for silicon nitride showing the relative severity of WC, Fe, Si, and C inclusions, porosity, and machining damage origins.

A. G. Evans, M. E. Meyer, K. W. Fertig, B. I. Davis, and H. R. Baumgartner, "Probabilistic Models for Defect Initiated Fracture in Ceramics," *J. Nondest. Eval.*, **1** [2] (1980) 111 – 122.

Includes some of the actual data used to construct the strength versus flaw size graph for different flaws. Many of the flaws were intentionally seeded into hot-pressed silicon nitride. Additional data were obtained from work done at the U.S. Army Materials and Mechanics Research Center at Watertown, MA and documented in U.S. Army Technical Report TR78-11 by Brockelman and Hansen in 1978.

G. D. Quinn, L. K. Ives, and S. Jahanmir, "On the Fractographic Analysis of Machining Cracks in Ground Ceramics: A Case Study on Silicon Nitride," Special Publication SP 996, NIST, Gaithersburg, MD, May, 2003.

An exhaustive, well-illustrated treatment of the nature of machining flaws in ground ceramics and how to find them. Photos and many schematics.

G. D. Quinn, L. K. Ives, and. S. Jahanmir, "On the Nature of Machining Cracks in Ground Ceramics: Part I: SRBSN Strengths and Fractographic Analysis," *Mach. Sci. Technol.*, **9** (2005) 169 - 210.

G. D. Quinn, L. K. Ives, and S. Jahanmir, "On the Nature of Machining Cracks in Ground Ceramics: Part II: Comparison to Other Silicon Nitrides and Damage Maps," *Mach. Sci. Technol.*, **9** (2005) 211 - 237.

G. D. Quinn, L. K. Ives, and S. Jahanmir, "Machining Damage Cracks: How to Find and Characterize Them by Fractography," *Ceram. Eng. Sci. Proc*., **24** [4] (2003) 383-394.

G. D. Quinn, L. K. Ives, and S. Jahanmir, "Machining Cracks in Finished Ceramics," pp. 1 - 14 in *Fractography of Advanced Ceramics, II*, eds. J. Dusza, R. Danzer, and R. Morrell, TransTech Publ., Zurich, 2005.

A short summary of the work in the above three references.

R. W. Rice and J. J. Mecholsky, "The Nature of Strength Controlling Machining Flaws in Ceramics," pp. 351 - 378 in *The Science of Ceramic Machining and Surface Finishing II*, eds. B. Hockey and R. Rice, National Bureau of Standards, Gaithersburg, MD, Special Publication SP562. 1979.

Rice and Mecholsky were two of the foremost fractographers of the late twentieth and early twenty-first centuries. Rice passed away in 2011. Mecholsky was still active in 2025. This and the next papers are some of their best.

R. W. Rice, "Machining of Ceramics," pp. 287 - 343 in *Ceramics for High Performance Applications*, eds., J.J. Burke, A. E. Gorum, and R. N. Katz, Brook Hill Publ., Chestnut Hill, MA, 1974.

An excellent fifty-six page long review of machining effects and damage beneath the surface. Grain size effects can be important. Dislocations and twins and cracking. Several pages on edges and bevels and their damage.

R. W. Rice, "Failure Initiation in Ceramics: Challenges of NDE and Processing," and "Ceramic Developments," C. Sorrell, and B. Ben-Nissan, eds., *Materials Science Forum*, Vol. 34–36, Trans. Tech. Publ. Ltd. Switzerland, 1988, pp. 1057 – 1064.

This entry is revised for the 4th edition. This is a short eight-page text-only article that was presented at a conference. The preprint of this paper had a comprehensive, well-illustrated review of failure-initiating origins. It was nearly an encyclopedia of flaws. Origins included: agglomerates, pores, large grains, inclusions, machining damage, handling damage, thermocouple beads, ball mills, dandruff, insects, feces, inadequate mixing of constituents, etc. Due to page limitations, none of the figures were published in the conference proceedings. Nonetheless, the printed text-only paper lists many of the flaws cited above and <u>provides very useful original references</u> for further investigation.

R. W. Rice, "Processing Induced Sources of Mechanical Failure in Ceramics," pp. 303–319 in *Processing of Crystalline Ceramics*, eds., H. Palmour, R. Davis, and T. Hare, Plenum Press, NY, 1978.

A short, seventeen-page, well-illustrated review of origins. A good starting point.

R. W. Rice, J. J. Mecholsky, Jr., and P. F. Becher, "The Effect of Grinding Direction on Flaw Character and Strength of Single Crystal and Polycrystalline Ceramics," *J. Mat. Sci.*, **16** (1981) 853 – 862.

Machining damage in a variety of ceramics is well illustrated by nine figures.

J. J. Mecholsky, Jr., S. W. Freiman, and R. W. Rice, "Effects of Grinding on Flaw Geometry and Fracture of Glass," *J. Amer. Ceram. Soc.*, **60** [3–4] (1977) 114 – 117.
Two primary sets of cracks from surface grinding are schematically shown and complemented by SEM photos and related to fracture mechanics parameters.

R. W. Rice, "Pores as Fracture Origins in Ceramics," *J. Mat. Sci.*, **19** (1984) 895 – 914.
A well-illustrated examination of pores in glassy and polycrystalline materials. Pores tend to be "sharper" in the latter than in the former.

R. W. Rice, S. W. Freiman, and J. J. Mecholsky, Jr., "The Dependence of Strength-Controlling Fracture Energy on the Flaw Size to Grain Size Ratio," *J. Am. Ceram. Soc*., **63** [3-4] (1980) 129 - 136.
The flaw-size to grain-size ratio determined whether the relevant fracture toughness a polycrystalline value or a single crystal value. Small flaws within very large grains are ruled by single crystal fracture toughness that is much less than for polycrystals. Large grains are susceptible to machining cracks.

D. Munz, O. Rosenfelder, K. Goebells, and H. Reiter, "Assessment of Flaws in Ceramic Materials on the Basis of Non-Destructive Evaluation," pp. 265–283 in *Fracture Mechanics of Ceramics*, Vol. 1, eds. R. Bradt, D. Hasselman, and F. Lange, F., Plenum Press, NY, 1986 .
Six different flaw types were characterized in reaction bonded and sintered silicon nitrides. Some flaws were artificially created to support a fracture mechanics analysis. Pores have a different effect upon strength than inclusions.

J. E. Ritter, Jr., and R. W. Davidge, "Strength and Its Variability in Ceramics with Particular Reference to Alumina," *J. Am. Ceram. Soc*., **67** [6] (1984) 432 - 437.
A good study of strength variability in alumina with flaws deliberately introduced by adding glucose or corn starch to starting powders, or by grit blasting surfaces. Flaw linking was observed.

F. F. Lange, "Processing-Related Fracture Origins: I, Observations in Sintered and Isostatically Hot-Pressed Al_2O_3/ZrO_2 Composites," *J. Am. Ceram. Soc.*, **66** [6] (1983) 396 - 398.
Lange was a famous processing scientist who passed away in 2010. This and the next three are companion articles about flaws generated during processing in the alumina-zirconia system. They are a classic study. Differential shrinkage of agglomerates created cracking.

F. F. Lange and M. Metcalf, "Processing-Related Fracture Origins: II, Agglomerate Motion and Cracklike Internal Surfaces Caused by Differential Sintering," *ibid*, 398-406.

F. F. Lange, B. I. Davis, and I. A. Aksay, "Processing-Related Fracture Origins: III, Differential Sintering of ZrO_2 Agglomerates in Al_2O_3/ZrO_2 Composite," *ibid*, 407-408.

F. F. Lange, B. I. Davis, and E. Wright, “Processing-Related Fracture Origins: IV, Elimination of Voids Produced by Organic Inclusions,” *J. Am. Ceram. Soc.*, **69** [1] (1986) 66 - 69.

M. Hangl, “Processing Related Defects in Green and Sintered Ceramics,” pp. 133-156 in *Fractography of Glasses and Ceramics, IV, Ceramic Transactions*, Vol. 122, J. Varner, and G. D. Quinn, eds., American Ceramic Society, Westerville, OH, 2001.

An excellent article about spray-dried agglomerates in varistor grade sintered zinc oxide. Many photographs show the agglomerates from their initial state through green body and final sintered stages. Agglomerates can be hollow or donut shaped. The final fracture surface will reveal the spray-dried pattern if one looks carefully.

S. Nakamura, S. Tanaka, R. Furushima, K. Sato, and K. Uematsu, “Estimation of Weibull Modulus from Coarser Defect Distribution in Dry-pressed Alumina Ceramics,” *J. Ceram. Soc. Japan*, **117** [6] (2009) 742 - 747.

Starting in the 1990s, Profs. K. Uematsu and S. Tanaka at Nagaoka University did exceptional work characterizing flaws in ceramics, starting from the earliest processing stages and monitoring their evolution during processing. Prof. Uematsu passed away in 2020. Innovative microscopy techniques were devised to see the flaw population in ceramic bodies, as well as the flaws exposed by conventional polished section work and fractographic analysis of test specimens. The flaws were closely coupled to the final strength distribution. Their work confirmed analytical predictions by Jayatilaka and Trustrum in 1977 and 1983. The latter work plus the Nagaoka University work established beyond any doubt that the Weibull distribution is appropriate for brittle materials. Some of the dozens of Nagaoka Univ. papers are listed below.

H. Abe, M. Naito, T. Hotta, N. Shinohara, and K. Uematsu, “Flaw Size Distribution in High-Quality Alumina,” *J. Am. Ceram. Soc*., **86** [6] (2003) 1019 - 1021.

Y. Saito, S. Tanaka, N. Uchida, and K. Uematsu, “Direct Observation of Three-Dimensional Structure in Powder Compact,” pp. 657 - 660 in *Key Engineering Materials*, Vols. 206-213, Proc. of the 7th European Ceramic Society, Brugge, Belgium, 2001, Transtech Publ., Zurich, Switzerland, 2002.

Confocal laser scanning fluorescence microscopy with a special immersion fluid was used to see the three-dimensional flaw distribution in alumina.

Y. Saito, S. Tanaka, N. Uchida, and K. Uematsu, “Direct Evidence for Low-Density Regions in Compacted Spray-Dried Powders,” *J. Am. Ceram. Soc*., **84** [10] (2001) 2454 - 2456.

K. Sato, S. Tanaka, N. Uchida, and K. Uematsu, “Characterization of Large Defects in Alumina,” *Bull. Am. Ceram. Soc.*, **82** [4] (2003) 39 – 42.

K. Sato, S. Tanaka, N. Uchida, and K. Uematsu, "Morphological Change of Large Pores in Alumina Ceramics in the Final Stage of Densification," *J. Ceram. Soc. Japan*, **111** [7] (2003) 525 - 527.

Transmission optical microscopy was used to study the flaw population through a thin 200 µm piece of alumina.

K. Sato, S. Tanaka, N. Uchida, and K. Uematsu, "Direct Study on the Formation of Large Defects in Final Stages of Sintering in Alumina Ceramics," pp. 225 – 228 in Key Engineering Materials, Vols. 264 - 268, Proceedings of the 8th European Ceramic Society conference, Trans Tech Publ., Zurich, 2004.

The formation and development of defects in sintered alumina was studied with transmission optical microscopy and the SEM.

N. Shinohara, M. Okumiya, T. Hotta, K. Nakahira, M. Naito, and K. Uematsu, "Morphological Changes in Process-Related large Pores of Granular Comp-acted and Sintered Alumina," *J. Am. Ceram. Soc*., **83** [7] (2000) 1633 - 1640.

Exceptional pictures and characterization of pores of different shapes formed as a result of power agglomerate collapse during processing. Compacts sintered at different temperatures had different flaws.

H. Takahasi, N. Shinohara, K. Uematsu, and T. Junichiro, "Influence of Granule Character and Compaction on the Mechanical Properties of Sintered Silicon Nitride," *J. Am. Ceram. Soc*., **79** [4] (1996) 843 - 858.

N. Shinohara, M. Okumiya, T. Hotta, K. Nakahira, M. Naito, and K. Uematsu, "Seasonal Variation of Microstructure and Sintered Strength of Dry-Pressed Alumina," *J. Am. Ceram. Soc*., **82** [12] (1999) 3441 – 3446.

An exceptional study that showed strength <u>varied with the season of the year</u>. The variation was traced to subtle flaw variations in the powder compacts. These were caused by differences in the flowability of the spray-dried powders and their deformability <u>in winter and summer</u> due to temperature and humidity differences in the processing environment!

H. Abe, M. Naito, T. Hotta, N. Shinohara, and K. Uematsu, "Flaw Size Distribution in High-Quality Alumina," *J. Am. Ceram. Soc*., **86** [6] (2003) 1019 - 1021.

Transmission optical microscopy characterized the flaws in three-dimensional pieces of three aluminas. The exponents of the flaw size distributions did not correlate well to the actual four–point strength distributions in this case, probably since only flaws in a small 0.5 mm^3 slice were measured by transmission optical examination. In contrast, the bend bars had Weibull effective volumes of 1.9 – 2.5 mm^3. The flaws were also round pores and not penny-shaped cracks.

Y. Zhang, M. Inoue, N. Uchida, and K. Uematsu, "Characterization of Processing Pores and Their Relevance to the Strength in Alumina Ceramics," *J. Mater. Res.*, **14** [8] (1999) 3370 - 3374.

T. Bernthaler, "Defect Imaging and Analysis for Predicting the Reliability of Ceramics," PhD Thesis, School of Materials Science and Engineering, Univ. of New South Wales, Sydney, Australia, and the University of Aalen, Germany, April 2011

A remarkable study under the guidance of Profs. M. Hoffman and G. Schneider, comparing flaw size distributions measured with automated image analysis on polished sections and strength distributions and fractographic analysis in alumina, alumina with seeded defects, dense and porous silicon carbide, and an alumina-zirconia composite. A variety of flaw types were identified and characterized. The size distributions matched an inverse power law function. Unfortunately, this work was never published in a technical journal, but the thesis is available

J. R. Varner and V. D. Fréchette, "Fractography of Whitewares," pp. 305 – 315 in *Science of Whitewares, eds. V. Henkes, G. Y. Onoda, and W. M. Carty,* American Ceramic Society, Westerville, OH, 1996.

An interesting article with multiple case studies involving processing cracks and mechanical failures in whitewares and porcelains. Toilet bowls, electrical insulators, storage jars, other.

Origins in Additively-Manufactured Ceramics

S. Boardman and C. Packard, "Linking Flexural Strength and Strength-Limiting Flaws in Additively Manufactured Alumina with Print Parameter Variations," *J. Amer. Ceram. Soc.*, **107** [2] (2023) 1185 - 1200.

J. Schlacher, T. Lube, W. Harrer, G. Mitteramskoglerb, M. Schwentenweinb, R. Danzer, and R. Bermejo, "Strength of Additive Manufactured Alumina." *J. Eur. Ceram. Soc*. **40** (2020) 4737 - 4745.

W. Harrer, M. Schwentenwein, T. Lube, and R. Danzer, Fractography of Zirconia - Specimens Made Using Additive Manufacturing (LCM) Technology," *J. Eur. Ceram. Soc.*, **37** (2017) 4331 - 4338.

Origins in Glass

J. R. Varner, "The Practical Strength of Glass," pp. 389 – 406 in *Strength of Inorganic Glass*, ed. C. Kurkjian, Plenum, NY, 1986.

V. D. Fréchette, *Failure Analysis of Brittle Materials, Advances in Ceramics*, Vol.28, American Ceramic Society, Westerville, OH, 1990.

R. J. Ginther, "The Contamination of Glass by Platinum," *J. Noncryst. Sol*., **6** (1971) 294 – 306.

Platinum inclusions can occur in glasses meted in platinum crucibles, by atmospheric oxidation, then vapor phase transport, followed by reduction and particle entrapment in the melt. Such inclusions can cause fractures in lasers.

S. Karlsson, “Spontaneous Fracture in Thermally Strengthened Glass – A Review and Outlook,” *Ceramics-Silikaty*, **61** [3] (2017) 188 – 201.
An excellent review of nickel sulfide inclusions in glass.

M. V. Swain, “Nickel Sulphide Inclusions in Glass: An Example of Microcracking Induced by a Volumetric Expanding Phase Change,” *J. Mat Sci.,* **16** (1981) 151 – 158.

J. C. Barry and S. Ford, “An Electron Microscopic study of Nickel Sulfide Inclusions in Tempered Glass,” *J. Mat. Sci.,* **36** (2001) 3721 – 3730.

R. C. Bradt, “Macro- and Microfracture Patterns of Thermally Tempered Plate Glass Falling from Nickel Sulfide Inclusions,” pp. 417 – 426 in *Fractography of Glasses and Ceramics*, eds. J. D. Varner and V. D. Fréchette, Advances in Ceramics, Vol. 22, American Ceramic Society, Westerville, OH, 1988.

Y. Bao, L. Liu, S. Han, X. Shi, and J. Yang, “A New Mechanism of Spontaneous Breakage of Tempered Glass – Monolithic Silicon Particles,” *J. Chinese Ceram. Soc*, **35** [9] (2007) 1273 – 1276.
Silicon inclusions, not nickel sulphide, sometimes cause fracture in tempered glass.

B. S. Aldinger and B. K. Collins, *Color Atlas of Stones in Glass*, American Glass Research, Butler, PA, 2016.
A beautiful 126-page book that is a compilation and characterization of 38 types of inclusions in glass.

B. S. Aldinger and P. de Haan, *Color Atlas of Glass Container Defects*, AGR, Butler, PA, 2019.
A 154-page book that is a beautifully-illustrated compilation of dozens of glass defects in commercial glass containers and pharmaceutical containers. Some occur in manufacture and forming and some in handling. An interesting discussion about nomenclature is in the Introduction. Some of the defects are cracks or flaws that can act as fracture origins. Some defects are merely cosmetic faults.

Glass Container Defects, Causes and Remedies, Bucher Emhart Glass Company, Steinhausen, Switzerland, 2017.
A 197-page atlas of dozens of glass container defects that are schematically illustrated with causes and remedies. This book has terms that sometimes are the same and sometimes different than those in the AGR book listed above. This is not unusual in the glass container industry where a variety of terms have come into use.

R. A. Schaut, K. C. Hoff, S. E. Demartino, W. K. Denson and R. L. Verkleeren, “Enhancing Patient Safety Through the Use of a Pharmaceutical Glass Designed to Prevent Cracked Containers,” *PDA J. Pharm. Sci. and Tech*., **17** (2017) 511 - 518.
Mostly about a new Corning glass for pharmaceutical containers, it nonetheless has good illustrations of bump checks, bottom lens cracks, and neck cracks in borosilicate and aluminosilicate glasses. Includes a tabulation of eleven recalls.

Fracture Mirrors

J. J. Mecholsky, Jr., S. W. Freiman, and R. W. Rice, "Fracture Surface Analysis of Ceramics," *J. Mat. Sci.*, **11** (1976) 1310 – 1319.

A detailed correlation of origin size, fracture mirror sizes and characterization, and fracture mechanics parameters for single and polycrystalline ceramics. A table of mirror constants is given for a range of ceramics, and it is demonstrated that the outer mirror (hackle) to origin size ratio is about 13 to 1. The inner mirror (mist) ratio is between 6 to 1 and 10 to 1.

J. J. Mecholsky, Jr., R. W. Rice, and S. W. Freiman, "Prediction of Fracture Energy and Flaw Sizes in Glasses from Measurements of Mirror Size," *J. Amer. Ceram. Soc.*, **57** [10] (1974) 440 – 443.

Details of fracture mirror features are discussed and related to fracture mechanics parameters for glasses. A table of mirror constants for glasses.

H. P. Kirchner, R. M. Gruver, and W. A. Sotter, "Fracture Stress—Mirror Size Relations for Polycrystalline Ceramics," *Phil. Mag.*, **33 [5]** (1976) 775 – 780.

Many mirror constants for a range of ceramics.

H. P. Kirchner, and J. C. Conway, Jr., "Fracture Mechanics of Crack Branching in Ceramics," pp. 187 – 213 in *Fractography of Glass and Ceramics, Advances in Ceramics*, Vol. 22, American Ceramic Society, Westerville, OH, 1988.

Analysis that fracture mirror features are controlled by stress intensity.

J. J. Mecholsky, Jr., and S. W. Freiman, "Determination of Fracture Mechanics Parameters Through Fractographic Analysis of Ceramics," pp. 136 – 150 in *Fracture Mechanics Applied to Brittle Materials, ASTM STP 678*, S. Freiman, ed., ASTM, 1979.

A short discussion of fracture mirrors and mirror constants with a comparative table of mirror constants. Comments on useful techniques to measure mirror parameters.

Fracture Mechanics—Estimates of Flaw Size

D. W. Richerson, *Modern Ceramic Engineering*, Marcel Dekker Inc., NY, 1982 and later editions (2nd in 1992, 3rd in 2006, 4th in 2018).

Chapter 3 in the 1st edition, (chapter 8 in the 3rd + 4th ed.) is a good primer on strength and fracture toughness measurements and their applicability to fractographic analysis. Several numerical examples are given for estimating strength of a specimen on the basis of a fracture mechanics calculations using the measured flaw size.

H. K. Baumgartner and D. W. Richerson, "Inclusion Effects on the Strength of Hot Pressed Si_3N_4," *Fracture Mechanics of Ceramics*, Vol. 1, eds. R. Bradt, D. Hasselman, and F. Lange, Plenum Press, NY, 1974, pp. 367 – 386.

Applies fracture mechanics to one class of flaws with several numerical examples. The strength-limiting inclusions are smaller than expected from fracture mechanics, suggesting that the fracture toughness is altered in the vicinity of the inclusions.

J. J. Mecholsky, Jr., S. W. Freiman, and R. W. Rice, "Fracture Surface Analysis of Ceramics," *J. Mat. Sci.*, **11** (1976) 1310 – 1319.
Compares measured flaw sizes to fracture mechanics estimates for a range of ceramics and glasses.

H. P. Kirchner, R. M. Gruver, and W. A. Sotter, "Characteristics of Flaws at Fracture Origins and Fracture Stress-Flaw Size Relations in Various Ceramics," *Mater. Sci. Eng.*, **22** (1976) 147 – 156.
Measured flaw sizes were compared to fracture mechanics estimates for several different types of flaws in alumina, silicon nitride, and silicon carbide.

A. G. Evans and G. Tappin, "Effects of Microstructure on the Stress to Propagate Inherent Flaws," *Proc. Brit. Ceram. Soc.*, **20** (1972) 275 – 297.
Discusses flaws in alumina ceramics and compares the stress actually needed to cause fracture to estimates based on fracture mechanics. Microstructural factors such as flaw linking prior to catastrophic fracture are discussed.

D. Munz, O. Rosenfelder, K. Goebells, and H. Reiter, "Assessment of Flaws in Ceramic Materials on the Basis of Non-Destructive Evaluation," pp. 265 – 283 in *Fracture Mechanics of Ceramics*, Vol. 1, eds. R. Bradt, D. Hasselman, and F. Lange, Plenum Press, NY, 1986.
A superb, comprehensive fracture mechanics analysis of six different flaw types in two silicon nitrides. Fractographic size measurements agreed with fracture mechanics estimates for some flaw types, but not others. Over 100 specimens. Discusses the different crack models that can be used to simulate real flaws as well as the shortcomings of such models. Includes Raju-Newman and elliptical integral flaw stress intensity factor solutions.

G. D. Quinn and J. J. Swab, "Fractography and Estimates of Fracture Origin Size from Fracture Mechanics," *Ceram. Eng. Sci. Proc.*, **17** [3] (1996) 51 – 58.
Fracture mechanics should be used routinely in fractographic analyses to verify that the correct feature has been identified as the fracture origin. This paper reviews the factors that may cause calculated and measured flaw sizes to differ.

Fracture Mechanics—Stress Intensity Factors

The following are compilations of stress intensity factors for various cracks under different loading conditions. Important single papers are also included.

Y. Murakami, *Stress Intensity Factors Handbook*, Vols. 1 and 2, Pergamon Press, NY, 1986. Vol. 3 in 1992 by Pergamon Press, and Vols 4 and 5 in 2001 by Elsevier.
A master collection of stress intensity factors for various cracks under different loading conditions. Organized by the Society of Materials Science in Japan.

H. Tada, P. C. Paris, and G. R. Irwin, *The Stress Analysis of Cracks Handbook*, 3rd edition, ASM International, Metals Park, OH, 2000.

An update of their famous 1973 collection of stress intensity factors for various cracks under different loading conditions.

T. Fett, and D. Munz, *Stress Intensity Factors and Weight Functions*, Wessex Institute of Technology, Southhampton, UK, 1997.

A collection of stress intensity factors for various cracks under different loading conditions.

D. P. Rooke, and D. J. Cartwright, *Compendium of Stress Intensity Factors*, Her Majesty's Stationary Office, London, 1976.

A collection of stress intensity factors for various cracks under different loading conditions.

G. C. Sih, *Handbook of Stress Intensity Factors*, Lehigh University, Bethlehem, PA, 1973.

An older but still useful collection of stress intensity factors for various cracks under different loading conditions.

I. Bar-on, "Applied Fracture Mechanics," *Engineered Materials Handbook*, Vol. 4, *Ceramics and Glasses*, S. Schneider, ed., ASM, Metals Park, OH, 1991, pp. 645–651.

A good, short introduction to the application of fracture mechanics analysis to idealized crack configurations. Stress intensity shape factors are given for through slits, surface cracks, and pores with rim cracks.

J. C. Newman, Jr., and I. S. Raju, "An Experimental Stress-Intensity Factor Equation for the Surface Crack," *Eng. Fract. Mech.*, **15** [1–2] (1981) 185 – 192.

A famous paper that presents a widely-used equation for the calculation of the stress intensity shape factors (Y) for surface semicircular or semielliptical cracks. Y is given for the location where the origin meets the surface and at the deepest point of the origin. Both direct tension and flexural solutions are presented.

S. Strobl, P. Supancic, T. Lube, and R. Danzer, "Surface Crack in Tension or Bending – A Reassessment of the Newman and Raju Formula in Respect to Fracture Toughness Measurements in Brittle Materials," *J. Eur. Cer. Soc*., **32** (2012) 1491 – 1501.

Also presents shape factor (Y) for surface semicircular or semielliptical cracks, but for more general cases than the Newman-Raju solutions. The Strobl et al. solutions can be considered refined solutions in some important cases. They allow different values of Poisson's ratio and truncated semielliptical surface crack shapes. For many surface cracks the new solutions are only a few percent different than Newman and Raju's. An important correction to this paper was published 6 years later:

S. Strobl, P. Supancic, T. Lube and R. Danzer, "Corrigendum to Surface Crack in Tension or in Bending," *J. Eur. Cer. Soc*, **32** [8] (2018) 355 – 358.

The six papers below are for the case of a pore with a circumferential rim crack ("Rings of Saturn")

F. Baratta, "Stress Intensity Factor Estimates for a Peripherally Cracked Spherical Void and a Hemispherical Surface Pit," *J. Am. Ceram. Soc*., **61** [11-12] (1978) 490 - 492.

F. Baratta." Refinement of Stress Intensity Factor Estimates for a Peripherally Cracked Spherical Void and a Hemispherical Surface Pit," *J. Am. Ceram. Soc*., **64** [1] (1981) C3-C4.

D. J. Green, "Stress Intensity Factor Estimates for Annular Cracks at Spherical Voids," *J. Am. Ceram. Soc.*, **63** [5-6] (1980) 342 - 344.

T. Fett, "Stress Intensity Factors and Weight Functions for a Void with an Annular Crack," *Int. J. Fract.*, **67** (1994) R41 - R47.

L Y. Chao and D. K. Shetty, "Extreme-Value Statistics Analysis of Frcature Strengths of a Sintered Silicon Nitride Failing from Pores," *J. Amer. Ceram. Soc.*, **75** [8] (1992) 2116-2124.

D. K. Shetty, A. R. Rosenfeld, and W. H. Duckworth, "Biaxial Stress State Effects on Strengths of Ceramics Failing from Pores," pp. 531 - 542 in *Fracture Mechanics of Ceramics*, Vol. 5, Eds., R. C. Bradt, A.G. Evans, D.P.H. Hasselman, and F. F. Lange, Plenum Press, NY, 1983.

APPENDIX B FRACTOGRAPHIC CASE STUDIES

The case studies for components and structures are organized by topic. Glass cases come first, followed by ceramics and glass ceramics, fibers, single crystals, gemstones, and rocks and lithics. This tabulation is available only in the on-line version of the 3rd edition of this Guide. This list is current as of early 2025.

Glass Windows and Plates of All Sizes

Automotive and building windows

N. Shinkai, "The Fracture and Fractography of Flat Glass," pp. 253 – 297 in *Fractography of Glass*, eds. R. C. Bradt and R. E. Tressler, Plenum Press, NY, 1994.
A superb practical article on annealed, tempered, and laminated glass for automobiles or building windows.

V. D. Fréchette and M. Donovan, "Some Effects of the Glue Chipping Process on Strength," pp. 407 – 411 in *Fractography of Glasses and Ceramics II, Ceramic Transactions Vol. 17*, eds. V. D. Fréchette and J. R. Varner, American Ceramic Society, Westerville, OH, 1991.
Fractures of hundreds of very large float glass windows in a Boston skyscraper.

V. D. Fréchette, *Failure Analysis of Brittle Materials,* Advances in Ceramics, Vol. 28, American Ceramic Society, Westerville, OH, 1990, pp. 119 - 120.
Fractures in large float glass windows in a skyscraper. Glue chips.

T. Sakai, M. Ramulu, A. Ghosh, and R. C. Bradt, "A Fractal Approach to Crack Branching (bifurcation) in Glass," pp. 131 – 146 in *Fractography of Glasses and Ceramics II*, eds., V. D. Fréchette and J. R. Varner, *Ceramic Transactions,* Vol. 17, American Ceramic Society, Westerville, OH, 1991.
Fracture patterns in laminated safety glass for bus passenger shelters.

S. T. Gulati, R. Akcakaya, and J. Varner, "Fracture Behavior of Tin vs. Air Side of Glass," pp. 317 – 325 in *Fractography of Glasses and Ceramics,* IV, eds., J. R. Varner and G. D. Quinn, American Ceramic Society, Westerville, OH, 2001.

S. T. Gulati, J. D. Helfinstine, T. A. Roe, "Strength Degradation of Automotive Wind-shield from Manufacturing to On-Road Service," *Glass Tech.,* **43C** (2002) 303 – 308.
Testing of singlets and windshield coupons. Edging, scoring, solder tabs.

T. Cleary and S. Gulati, "Influence of Glass Score and Seam Orientation on Edge Strength of Multi-Layered Glass Articles," pp. 327 – 341 in *Fractography of Glasses and Ceramics,* IV, eds. J. R. Varner and G. D. Quinn, American Ceramic Society, Westerville, OH, 2001.
Fracture patterns in laminated safety glass (sandwich of two glass plates and a central plastic sheet).

T. M. Cleary and R. T. Nichols, “Adhesive Induced Fracture of Automotive Glass,” pp. 369 - 380 in *Fractography of Glasses and Ceramics, V*, eds. J. R. Varner, G.D. Quinn, M. Wightman, *Ceramic Transactions*, Vol. 199, American Ceramic Society, Westerville, OH, 2007.

Glue chips and adhesive and thermally-induced fractures in both front laminated and tempered rear windows.

R. A. Allaire and T. Ono, “Fracture Analysis of the Glass Scoring Process,” pp. 467 – 471 in *Fractography of Glasses and Ceramics*, IV, eds. J. R. Varner and G. D. Quinn, American Ceramic Society, Westerville, OH, 2001.

Fracture patterns on scored glass plates.

J. Suzuki and H. Shirahashi, “Studies on Windshield Glass Fracture Caused by Flying Objects,” pp. 495 - 503 in *Mechanical Behavior of Materials*, Vol. IV, Proc. Int. Conference, Kyoto, Japan, 1971, The Society of Materials Science, Japan, 1972.

Thirty-two broken tempered front windshields were collected over a 214 day interval on an expressway. Dicing patterns and impact origin sites were studied. Origin sites were either sharp impact or blunt impact, cone crack damage. Some delayed fractures were observed, whereby the windows shattered long after they had been impacted.

S. A. Batzer, “Failure Mechanisms of Automotive Side Glazing in Rollover Collisions,” *J. Fail. Anal. Prev.*, **6** [3] (2006) 6 - 11, 33, 34.

R. C. Bradt, M. E. Barkey, S. E. Jones, M. E. Stevenson, “Projectile Impact – A Major Cause for Fracture of Flat Glass,” *J. Fail. Anal. Prev.*, **3** [1] (2003) 5 - 11.

R. Huet, J. M. Wolf, P. D. Moncarz, “Delayed Fracture of Tempered Glass Panels Due to Nickel Sulfide Inclusions,” pp. 431 - 433 in *Handbook of Case Studies in Failure Analysis, Vol. 1*, ed. K. A. Esakul, ASM Int., Materials Park, OH, 1992.

C. C. Hsiao, “Spontaneous Fracture of Tempered Glass,” pp. 985 - 992 in *Fracture 1977, Vol. 3*, ed. D. Taplin, Int. Congress on Fracture 4, Waterloo, Canada, 1977.

R. C. Bradt, “Macro- and Microfracture Patterns of Thermally Tempered Plate Glass Falling from Nickel Sulfide Inclusions,” pp. 417 – 426 in *Fractography of Glasses and Ceramics*, eds. J. D. Varner and V. D. Fréchette, Advances in Ceramics, Vol. 22, American Ceramic Society, Westerville, OH, 1988.

R. Gardon, “Thermal Tempering of Glass,” pp. 145 – 216 in *Glass: Science and Technology, Vol. 5, Elasticity and Strength in Glasses*, eds. D. R. Uhlmann and N. J. Kreidel, Academic Press, NY, 1980.

T. I. Suratwala, *Materials Science and Technology of Optical Fabrication*, Wiley, Hoboken, NJ, 2018.

Technical optical elements for passive optics (lenses, transmission flats, mirrors, prisms) and active optics, (lasers, frequency converters, polarizers, adaptive optics).

Handbook of Glass Fractography, R.C. Ropp, AuthorHouse, Bloomington, Indiana, USA, 2008.

This book must be used with caution since there are many mistakes in it. Many of the figures are poor. Nevertheless, there are some interesting case studies in it.

A swinging glass door on a cruise ship broke injuring a child. The tempered glass door had no rim protection for the edges and was supported by only two hinges.

A glass wall panel in a Jamaican resort hallway broke when a 9-year old girl backed into it. The glass was an ordinary annealed glass. Only some fragments were retrieved for examination, so a specific origin could not be found.

A windstorm caused two large supermarket windows to break injuring several people. Although the fracture origins were not found, it was determined that one window was heat strengthened and the other was not. The windows were also too large in area for their given thickness, and the wind loadings caused them to be overloaded, even if they had not been impacted by flying debris in the storm.

M. Meshulam, web site www.chicagowindowexpert.com

An amazing collection of glass fracture cases are documented on this web site. Over 50 cases range from building facades to interior doors and shower doors. Some cases involved fatalities.

See also the section on **tempered glass windows** below.

International Space Station and Mir and Space Shuttle Windows

J. A. Salem, "Residual Strength of Hypervelocity Impacted Silica," NASA Tech. Report TM-2-230017129, April 2024.

Cracking patterns and damage in American and Russian grades of fused-silica are shown and analyzed. These include windows from the ISS and Mir space stations and the USA space shuttle. Also includes man-made impacts created at a NASA test facility. Also references 3 technical reports by J. Lankford at SwRI on shuttle orbiter windows.

Cell phone cover glass

G. S. Glaesemann, T. M. Gross, J. F. Bayne, and J. J. Price, "Fractography on Ion-Exchanged Cover Glass," pp. 85 – 93 in *Fractography of Glasses and Ceramics VI,*

eds. J. Varner and M. Wightman, *Ceramic Transactions*, Vol. 230, American Ceramic Society, Wiley, Westerville, OH, 2012.

T. M. Gross, "Scratch Damage in Ion-Exchanged Alkali Aluminosilicate Glass: Crack Evolution and the Dependence of Lateral Cracking Threshold on Contact Geometry," pp. 113-122 in *Fractography of Glasses and Ceramics VI*, eds. J. Varner and M. Wightman, *Ceramic Transactions*, Vol. 230, American Ceramic Society, Wiley, Westerville, OH, 2012.

S. Kim, W. J. Chung, S. Jung, G. Shim, H. Shon, S. Kim, and K. D. Park, "Analysis of Fracture Mechanisms of Ultrathin Glass for Flexible Cover Window Under Pen Drop Conditions, " *J. Am. Ceram. Soc.*, **106** [1] (2023) 569 - 581.

Sight glass windows, water hammer

V. D. Fréchette, *Failure Analysis of Brittle Materials*, Advances in Ceramics, Vol. 28, American Ceramic Society, Westerville, OH, 1990, p. 112.

Tempered glass

R. C. Bradt, "Macro- and Microfracture Patterns of Thermally Tempered Plate Glass Falling from Nickel Sulfide Inclusions," pp. 417 – 426 in *Fractography of Glasses and Ceramics*, Advances in Ceramics, Vol. 22, ed. J. D. Varner and V. D. Fréchette, American Ceramic Society, Westerville, OH, 1988.

C. C. Hsiao, "Spontaneous Fracture of Tempered Glass," pp. 985 – 992 in *Fracture 1977*, Vol. 3, International Congress on Fracture 4, Waterloo, Canada, 1977.

R. Huet, J. M. Wolf, P. D. Moncarz, "Delayed Fracture of Tempered Glass Panels Due to Nickel Sulfide Inclusions," pp. 431 - 433 in *Handbook of Case Studies in Failure Analysis, Vol. 1*, ed. K. A. Esakul, ASM Int., Materials ark, OH, 1992.

R. Tandon and S. J. Glass, "Frcature Initiation and Fragmentation in Chemically Tempered Glass," *J. Eur. Cer. Soc.*, **35** (2015) 285 – 295.

Disks of an alumino-silicate glass that were chemically strengthened were broken by Vickers indentation to the disk center, or by conventional ring-on-ring biaxial strength tests. Fracture patterns varied with the extent of chemical tempering.

A. L. Zulstra and A. J. Burggraaf, "Fracture Phenomena and Strength Behavior of Chemically Strenthened Glass in Connection with the Stress Profile, Part II," *J. Noncryst.. Sol.*, **1 (**1969) 163 – 185.

Disks of a lithium alumina silicate glass were given various thermal and thermal plus chemical strengthening treatments. The differing stress profiles through the thickness created different fracture and branching patterns when the supported disks were impacted by dropped balls or darts with rounded tip.

S. A. Batzer, "Failure Mechanisms of Automotive Side Glazing in Rollover Collisions," *J. Fail. Anal. Prev.*, **6 [**3] (2006) 6 - 11, 33,34.

R. Gardon, “Thermal Tempering of Glass,” pp. 145 – 216 in *Glass: Science and Technology, Vol. 5, Elasticity and Strength in Glasses,* eds. D. R. Uhlmann and N. J. Kreidel, Academic Press, NY, 1980.

Plate glass mirrors for solar cells

V. D. Fréchette, *Failure Analysis of Brittle Materials,* Advances in Ceramics, Vol. 28, American Ceramic Society, Westerville, OH, 1990, p. 117.

Hail stones, thermal stresses, and edge cracks.

Laser glass slabs

J. E. Marion, “Fracture Mechanisms of Solid Sate Slab Lasers,” pp. 307 – 318 in *Fractography of Glasses and Ceramics,* eds. J. D. Varner and V. D. Fréchette, Advances in Ceramics, Vol. 22, American Ceramic Society, Westerville, OH, 1988.

J. E. Marion, “Fracture of Solid State Laser Slabs,” *J. Appl. Phys.*, **60** [1] (1986) 69–77.

T. I. Suratwala, *Materials Science and Technology of Optical Fabrication,* Wiley, Hoboken, NJ, 2018.

Several laser or optical glass window cases are presented in section 6.4 Case Studies in Chapter 6, Scratch Forensics and Fractography.

Borosilicate Glass Flowmeter

J. Kübler, “Failure Analysis on a Flowmeter,” pp. 65 - 71 in *Fractography of Advanced Ceramics III*, eds. J. Dusza, R. Danzer, R. Morrell, and G. D. Quinn, Trans Tech Publ. Zurich, 2009.

Home cocktail table

A. A. Johnson and R. J. Storey, “A Fatal Accident Involving a Glass-Topped Cocktail Table,” *J. Fail. Anal. Prev.*, **14** (2014) 267 - 271.

A college-graduating student fell over a glass-topped cocktail table which shattered. A long sharp shard pierced his heart and killed him. The untempered glass was supported by eight tabs, only four of which had plastic inserts.

Eyeglass lens

Handbook of Glass Fractography, R.C. Ropp, AuthorHouse, Bloomington, Indiana, USA, 2008.

A photochromatic glass lens in set of spectacles broke and injured a victim’s eye in 1986. The fracture was in the form of a large edge chip with some smaller fragments, and was caused by improper tightening of a set screw in the frame.

Glass Containers, Lamps, and Pressure Vessels

Pharmaceutical Glass Vials and Syringes

F. Maurer, "Application of Fractography in Pharmaceutical Industry," pp. 289 – 298 in *Fractography of Glasses and Ceramics,* VI, eds. J. R. Varner, M. Wightman, *Ceramic Transactions,* Vol. 230, Wiley, New York, 2012.

Glass syringe compliant specimen.

G. D. Quinn, This Guide, Chapter 10. Medicinal Glass Vials

Neck cracking from the cap sealing operation.

R. A. Schaut, K. C. Hoff, S. E. Demartino, W. K. Denson and R. L. Verkleeren, "Enhancing Patient Safety Through the Use of a Pharmaceutical Glass Designed to Prevent Cracked Containers," *PDA J. Pharm. Sci. and Tech*., **17** (2017) 511 - 518.

A comprehensive study of fracture-failure modes in borosilicate pharmaceutical bottles. Has a nice review of failure modes reported in the literature (including some with fatalities from contamination) and a table of eleven recalls due to cracking for injectable pharmaceuticals. Three primary failures modes were studied (bump checks, lensing, and neck cracking) and replicated in the laboratory for both a borosilicate and a new chemically-strengthened aluminosilicate glass.

Bottles and flasks

V. D. Fréchette, *Failure Analysis of Brittle Materials,* Advances in Ceramics, Vol. 28, American Ceramic Society, Westerville, OH, 1990, pp. 94 – 101, 112, 118, 123.

Internal pressure, water hammer, thermal shock, and impact fractures. Various bottles including intravenous medical bottles, wine bottles, frozen citrus fruit concentrate bottles, malformed bottles.

F. W. Preston, "Bottle Breakage – Causes and Types of Fractures," *Am. Ceram. Soc. Bull.,* **18** [2] (1939) 35 – 60.

An early paper, but with an exceptional treatment of a variety of failure causes.

V. D. Fréchette and T. A. Michalske, "Fragmentation in Bursting Glass Containers," *Bull. Amer. Ceram. Soc.*, **57** [4] (1978) 427 – 429.

Four different sizes of internally-pressurized, water-filled bottles.

V. D. Fréchette and S. L. Yates, "Fragmentation of Glass Bottles by Impact," *J. Am. Ceram. Soc*., **72** [6] (1989) 1060.

Three different sizes of water-filled bottles were swung at different velocities against a stationary steel rod.

J. B. Kepple, and J. S. Wasylyk, "Fracture of Glass Containers," pp. 207 –252 in *Fractography of Glass*, eds. R. C. Bradt and R. E. Tressler, Plenum Press, NY, 1994.

An excellent, multifaceted treatment. Shows fracture causes and patterns.

C. Spangenberg, "Exploding Bottles," *Ohio State Law Journal*, **24** [3] (1963) 516 – 533.

An interesting treatise by an attorney who was familiar with manufacture, legal issues, and fractography. Pressurized bottles are potential bombs. A variety of causes of fracture of beer bottles and carbonated beverage bottles are discussed. Manufacturing flaws, mishandling, thermal shock, impact failures, invisible cracks, and damaged recycled bottles are covered. Continued fermentation in beer bottles or even decaying mouse carcasses can cause internal pressure to develop.

R. E. Mould, "The Behavior of Glass Bottles Under Impact," *J. Amer. Ceram. Soc.*, **35** [9] (1952) 230 – 235.

A well-illustrated paper on controlled breakages of bottles. This article (and Dimmick's that followed it) proved that hinge origins away from the impact site were sources of breakage in some cases.

C. Colin and J. L. Heitz, "Failure Analysis: Glass Bottle Breakage," *Verre*, **16** [4] (2010) 33 - 36.

Sparkling wine bottle broke spontaneously in boxes in a warehouse. Glass-to-glass contact damage from improper packing caused cracks that grew to failure.

D. D. Cannon, C. S. Musso, J. C. Williams, and T. W. Eagar, "Analysis of Brittle Fracture of Soda Glass Bottles Under Hydrostatic Pressure," *J. Fail. Anal. Prev.*, **45** [5] (2004) 72 - 77.

Soda glass bottles were fractured in the lab by increasing pressure after a scratch had been made. Other bottles were impacted in various manners.

Handbook of Glass Fractography, R.C. Ropp, AuthorHouse, Bloomington, Indiana, USA, 2008.

This book must be used with caution since there are many mistakes in it. Many of the figures are poor. Nevertheless, there are some interesting case studies in it.

Soda lime silica beer bottle thrown into a bonfire exploded, causing a shard to hit a by-stander in the eye leading to loss of sight.

A consumer glass jar broke in a victim's hand causing tendon damage. The glass canister was faulty with extremely thin wall thickness on one side caused by lack of glass in the "gob" that was molded by the canister making machine.

A glass mug broke after boiling water was added to it. The glass had many manufacturing defects. The mug had significant variability in wall thicknesses and internal residual stresses that were not annealed out.

A glass soda bottle fractured ("exploded") when hit by a snowball causing eye damage to a victim. The bottle was poorly manufactured, had significantly variable wall thickness, and was recycled many times with accumulated abrasion and contact damage. It broke from thermal or mechanical stresses.

A large 2.5-liter bottle with concentrated nitric acid broke as it was being removed from a shipping case causing severe injury to the victim. The victim lifted the bottle via a glass eyelet on the bottle side. Fracture apparently started at the eyelet and ran around the neck. The bottle fell to the floor and broke further. The glass fragments were swept up and discarded. Two exemplars were examined. One had uneven wall thicknesses. Both had significant residual stresses around the eyelet handles. It was inferred that the fractured flask may have been faulty since it broke at low load.

A glass coffee carafe "exploded" causing coffee to spill onto and burn the victim. The carafe had impact or contact damage on the side wall either from the time of the incident, or from prior handling. Twenty-one glass bottles containing carbonated mineral water from Turkey exploded while being unloaded in one case from a truck, in a cascading fracture sequence. None of the broken bottles were retrieved. Two exemplars had many large bubbles and differed significantly in mass. Although the fractographer interpreted the failures as due to faulty bottle manufacturer, there was insufficient fractographic information to justify this conclusion, since none of the fractured bottles were examined.

Fluorescent lamps

D. Johnson, "Arc Induced Fractures from Lampmaking Test Equipment," pp. 517 – 525 in *Fractography of Glasses and Ceramics, III, Ceramic Transactions,* Vol. 64, J. R. Varner, V. D., Fréchette, and G. D. Quinn, eds., American Ceramic Society, Westerville, OH, 1996.

Cathode Ray Tube

A. Ghosh, C. Y. Cha, Vaidyanathan, and R. C. Bradt, "Finite Element Stress Analysis and Crack Path Prediction of Imploding CRT," pp. 1 - 24 in *Fractography of Glasses and Ceramics II,* eds. V. D. Fréchette and J. R. Varner, *Ceramic Transactions,* Vol. 17, American Ceramic Society, Westerville, OH, 1991.

Glass cooking thermometer

V. D. Fréchette, *Failure Analysis of Brittle Materials,* Advances in Ceramics, Vol. 28, American Ceramic Society, Westerville, OH, 1990, p. 120.

Tempered glass cylinders

V. D. Fréchette, *Failure Analysis of Brittle Materials,* Advances in Ceramics, Vol. 28, American Ceramic Society, Westerville, OH, 1990, pp. 120 –121, 123 –124.

Uneven thermal temper in a structural cylinder and also a high-power gymnasium lamp that lost its temper due to heating.

Glass neutron beam guideline

G. D. Quinn, O. Zilcha, J. M. Rowe, and D. J. Pierce, "Failure Analysis of a 41 Meter Long Neutron Beam Line Guide," 4th Int. Conf. on Fractography of Advanced Ceramics," Smolenice Castle, Oct. 2013, *J. Eur. Cer. Soc.,* **34** (2014) 3263 - 3270.

Glass optical elements

T. I. Suratwala, *Materials Science and Technology of Optical Fabrication*, Wiley, Hoboken, NJ, 2018.

Technical optical elements for passive optics (lenses, transmission flats, mirrors, prisms) and active optics, (lasers, frequency converters, polarizers, adaptive optics).

Glass Bulletproof or Impact Resistant Windows

M. E. Stevenson, S. E. Jones, and R. C. Bradt, "Fracture Patterns of a Composite Safety Glass Panel During High Velocity Projectile Impacts," pp. 473 – 488 in Fractography *of Glasses and Ceramics*, IV, eds. J. R. Varner and G. D. Quinn, American Ceramic Society, Westerville, OH, 2001.

D. L. Ahearn, J. L. Ladner, S. E. Jones, R. E. Wright and R. C. Bradt, "Fracture Patterns of Impact Resistant Glass Panel Laminates with Annealed and Heat Strengthened Glass Plates," pp. 383 – 395 in *Fractography of Glasses and Ceramics V*, eds. J. R. Varner, G.D. Quinn, M. Wightman, Ceramic Transactions, Vol. 199, American Ceramic Society, Westerville, OH, 2007.

H. Yoshimura and R. G. Morrone, "Analysis of Projectile Impact Damage in Bulletproof Glasses," pp. 397 – 406 in *Fractography of Glasses and Ceramics V*, eds. J. R. Varner, G.D. Quinn, M. Wightman, *Ceramic Transactions* ,Vol. 199, American Ceramic Society, Westerville, OH, 2007.

J. LK. Ladner, D. L. Ahearn, and R. C. Bradt, "Laminate Design Effects on the Fracture Patterns of Impact Resistance Glass Panels," pp. 281 - 287 in in *Fractography of Glasses and Ceramics*, VI, eds. J. R. Varner, M. Wightman, *Ceramic Transactions*, Vol. 230, Wiley, New York, 2012.

D. G. Christie and H. Kolsky, "The Fractures Produced in Glass and Plastics by the Passage of Stress Waves," *J. Soc. Glass Technol.*, **36** (1952) 65 - 73.

D. A. Shockey, D. Bergmannshoff, D. R. Curran, and J. W. Simons, "Physics of Glass Failure During Rod Penetration," in *Advances in Ceramic Armor IV, Ceram. Eng. Sci. Proc.*, **29** [6] (2008) 23 – 32.

A fascinating study. Thick soda lime and borosilicate blocks of glass were partially penetrated by hemispherical nose 6.35 mm diameter maraging steel rods fired at 300 m/s to 600 m/s. After impact, encased targets were infiltrated with epoxy to hold the fragments in place. Cone and lateral impact cracks were observed. The targets were sectioned and revealed several zones including a tunnel region with in-situ fragments in a matrix of more randomly-oriented fragments. A particle size analysis revealed micrometer and larger sizes. Fine fragments in the tunnel were firmly compacted and agglomerated. They showed evidence of melting and bonding to the steel projectile remnants. Some of the fragments on the sides of the tunnel may be Mescall zone fragments.

D. T. Berry and S. J. Bless, "Effects of Impact Damage on Glass Laminate Armor," Amer. Inst. of Aeronautics and Astronautics 5th Biennial Nat. Forum on Weapon System Effectiveness, Oct. 16-18, 2007, Huntsville, AL

and:

S. Bless and T. Chen, "Impact Damage in Layered Glass," *Int. J. Fract.*, **162** (2010) 151 - 158.

A very interesting and informative study. Seven layers of polyurethane-bonded soda lime glass for a total of 76 mm were impacted by a 12.7 mm steel fragment simulating projectile at 1,110 m/s to 1118 m/s in depth of penetration tests. Two layers were penetrated. Damage patterns and crack types in each layer were evaluated. Radial and transverse cracking occurred around the penetration cavity. These papers introduced some interesting crack nomenclature. Maps of crack types were shown including "bundled radial cracks," "fan cracks," "coarse radial cracks," "bow tie cracks," and "dicing cracks." Material in and around the penetration cavity was examined with optical and scanning electron microscopy. Around the penetration cavity the material was finely comminuted with classic fracture surface markings on a very fine scale. A surprise was the existence of large numbers of submicron fragments including elongated glass whiskers with submicron diameter but tens of microns in length.

Ceramic Windows, IR Domes, Radomes

Magnesium Fluoride (MgF_2) IR window test coupons

R. W. Rice, "Failure Analysis of Ceramics," pp. 369 – 388 in *Fractography of Glasses and Ceramics,* IV, eds. J. R. Varner and G. D. Quinn, American Ceramic Society, Westerville, OH, 2001.

Calcium Fluoride (CaF_2) windows in a laser flash diffusivity apparatus

R. Morrell, "Dealing with Component Failures," pp. 353 - 368 in Fractography of Glasses and Ceramics V, eds. J. R. Varner, G.D. Quinn, M. Wightman, *Ceramic Transactions,* Vol. 199, American Ceramic Society, Westerville, OH, 2007.

48 mm diameter single crystal disks that broke from thermal stresses activating edge damage or impact damage.

Glass ceramic missile radome, thermal shock

R. W. Rice, "Failure Analysis of Ceramics," pp. 369 – 388 in *Fractography of Glasses and Ceramics,* IV, eds. J. R. Varner and G. D. Quinn, American Ceramic Society, Westerville, OH, 2001.

Fused silica missile radome

This Guide. Chapter 10, case 7.

Grinding flaws and joint debonding.

Spinel and Yttria missile domes

J. S. Lin and L. B. Weckesser, "Thermal Shock Capabilities of Infrared Dome Materials," *Johns Hopkins APL Technical Digest,* **13** [3] (1992) 379 - 385.

IR domes fractured in thermal shock at up to Mach 4.6 in a hot wind tunnel up to 1120°C. Good photos of the breakage patterns in hot-pressed spinel and yttria.

Infrared window and dome materials

D. C. Harris, *Materials for Infrared Windows and Domes, Properties and Performance*, SPIE Press, Bellingham, WA, 1999.

Rain, sand, and bug impact damage on windows and domes are shown. CVD diamond, silicon cladding damage. Zinc selenides, zinc sulfides, gallium arsenide spinel, and silicon.

Polycrystalline Alumina (PCA) Lamp Tubes

F. Lofaj, V. Ivančo, and P.P Varga, "Fracture of Thin Walled Translucent Polycrystalline (PCA) Tubes," pp. 223 – 230 in *Fractography of Advanced Ceramics III*, eds. J. Dusza, R. Danzer, R. Morrell, and G. D. Quinn, Trans Tech. Zurich, 2009.

Microwave tube (alumina)

R. W. Rice, "Failure Analysis of Ceramics," pp. 369 – 388 in *Fractography of Glasses and Ceramics*, IV, eds. J. R. Varner and G. D. Quinn, American Ceramic Society, Westerville, OH, 2001.

Ceramic Crystal Optical Elements

T. I. Suratwala, *Materials Science and Technology of Optical Fabrication*, Wiley, Hoboken, NJ, 2018.

Technical optical elements for passive optics (lenses, transmission flats, mirrors, prisms) and active optics, (lasers, frequency converters, polarizers, adaptive optics).

Ceramic Seals

Tetragonal zirconia polycrystalline (TZP) hydraulic seal disks

R. W. Rice, "Failure Analysis of Ceramics," pp. 369 – 388 in *Fractography of Glasses and Ceramics*, IV, eds. J. R. Varner and G. D. Quinn, American Ceramic Society, Westerville, OH, 2001.

Mechanical seal rings – silicon carbide

R. Morrell, "Fractography of Brittle Materials," R. Morrell, Measurement Good Practice Guide 15, National Physical Laboratory, Teddington, Middlesex, United Kingdom, 1999, pp. 76 – 85.

Large open rotating rings with shoulders and notches. Impact damage - chipping, preexisting cracks, grinding cracks, handling damage.

Large (300 mm) silicon carbide seal rings

R. Morrell, "Dealing with Component Failures," pp. 353 - 368 in *Fractography of Glasses and Ceramics V*, eds. J. R. Varner, G.D. Quinn, M. Wightman, *Ceramic Transactions*, Vol. 199, American Ceramic Society, Westerville, OH, 2007.

Fractures during over-speed poof testing by spinning the disks. Good sketches of 5 disk fractures, illustrating how multiple crack patterns can be deciphered to find

the primary fracture. Origins were edge chamfer damage, contact damage cracks, and machining cracks.

Ceramic Containers and Pressure Vessels

Large porcelain tubes

V. D. Fréchette, *Failure Analysis of Brittle Materials,* Advances in Ceramics, Vol. 28, American Ceramic Society, Westerville, OH, 1990, pp. 125 – 126.

"Spontaneous" fracture during end-face machining. Internal residual stresses.

Beta alumina hollow cylinders, burst pressure loading

B. J. McEntire, R. H. Snow, J. L. Huang, L. Viswanathan, and A. V. Virkar, "Characterization of Processing Flaws in Beta Alumina," pp. 335 – 349 in *Fractography of Glasses and Ceramics,* eds. J. D. Varner and V. D. Fréchette, Advances in Ceramics, Vol. 22, American Ceramic Society, Westerville, OH, 1988.

Beta alumina electrolyte tubes, service failures

E. K. Beauchamp, "Beta Alumina failures in Sodium/Sulfur Batteries," pp. 377 – 387 in *Fractography of Glasses and Ceramics,* eds. J. D. Varner and V. D. Fréchette, Advances in Ceramics, Vol. 22, American Ceramic Society, Westerville, OH, 1988.

Ceramic Armor Plates

S. Winkler, H. Senf, and H. Rothenhäusler, "High Velocity Fracture Investigation in Alumina," pp. 165 – 183 in *Fractography of Glasses and Ceramics II,* eds. V. D. Fréchette and J. R. Varner, *Ceramic Transactions,* Vol. 17, American Ceramic Society, Westerville, OH, 1991.

High-speed photography of alumina and glass plates hit on end.

J. J. Swab, G. A., Glide, P. J. Patel, A. A Wereszczak, J. W. McCauley, and J. D. Risner, "Fracture Analysis of Transparent Armor Ceramics," pp. 489 – 508 in *Fractography of Glasses and Ceramics, IV,* eds. J. R. Varner and G. D. Quinn, American Ceramic Society, Westerville, OH, 2001.

Biaxial strength tests on sapphire, aluminum oxynitride, and magnesium alumina spinel.

R. L. Woodward, R. G. O'Donnell, B. J. Baxter, B. Nicol, and S. D. Pattie, "Energy Absorption in the Failure of Ceramic Composite Armors," *Mater. Forum,* **13** (1989) 174 – 181.

C. Tracy, M. Slavin, and D. Viechnicki, "Ceramic Fracture During Ballistic Impact," pp. 295 – 306 in *Fractography of Glasses and Ceramics,* eds. J. D. Varner and V. D. Fréchette, Advances in Ceramics, Vol. 22, American Ceramic Society, Westerville, OH, 1988.

and:

D. Viechnicki, W. Blumenthal, M. Slavin, C. Tracy, and H. Skeele, "Armor Ceramics - 1987," pp. 27 – 54 in Vol. 2 of the *Proceedings of the Third TACOM Armor Coordinating Conference for Light Combat Vehicles*, Feb. 1987, Monterey, CA, Battelle Columbus Labs, Columbus, OH (1987).

This was an early attempt to connect ballistic impact resistance to various microstructural and mechanical properties of materials such as Al_2O_3, TiB_2, SiC, and B_4C. There are some fascinating and important observations about fragment sizes and fragment fracture morphologies (transgranular, intergranular) that are directly related to the processing and microstructures. E.g., not all SiC's are the same. They can behave very differently in ballistic impacts. There are some fascinating similarities and contrasts between ballistic impact fractures and static uniaxial compression test fractures.

M. J. Slavin, "Fractographic Analysis of Long Rod Penetrator-Armor Ceramics Interactions," U. S. Army Technical Report, TR 89-93, U.S. Army Materials Technology Laboratory, Watertown, MA, Oct. 1989.

S. Rodriguez, V. B. Munoz, E. V. Esquivel, L. E. Muir, and N. L. Rupert, "Microstructural Characterization of TiB_2 Armor Targets," *J. Mat. Sci. Lttrs*., **21** (2002) 1161 – 1666.

V. D. Fréchette and C. F. Cline, "Fractography of Ballistically Tested Ceramics," *J. Am. Ceram. Soc.*, **49** [11] (1970) 994 – 997.

V. D. Fréchette, "Fractography and Quality Assurance of Glass and Ceramics," pp. 227 236 in *Quality Assurance in Ceramic Industries*, eds. V. D. Fréchette, L. D. Pye, and D. E. Rase, Plenum, NY, 1978.

Hot-pressed boron carbide blanks fractured during machining. Internal residual stresses were created by too rapid a cool down from the firing temperature.

R. N. Katz and W. A. Brantley, "Fractography of High Boron Ceramics Subjected to Ballistic Loading," pp. 271 – 282 in *Materials Science Research*, Vol. 5, ed. W. W. Kriegel, Plenum, NY, 1971.

D. G. Christie and H. Kolsky, "The Fractures Produced in Glass and Plastics by the Passage of Stress Waves," *J. Soc. Glass Technol.*, **36** (1952) 65 - 73.

H. Wu, S. Ghosh, C. Dancer, and R. Todd, "Ballistic Damage of Alumina Ceramics – Learning from Fragments," pp. 49 – 61 in *Advances in Ceramic Armor X*, ed. J. LaSalvia, American Ceramic Society, 2015.

An excellent study. High alumina plates 100 mm square were impacted by a mild steel 7 mm bullet at 820 m/s at DSTL, United Kingdom. Fragments were examined with transmission electron, focused ion-beam, scanning electron, and optical luminescent microscopes. The identified characteristics of transgranular and intergranular frcature, plastic deformation and microcracking had a strong correlation to fragment size. The fragment size was correlated to Grady's energy

balance model. Dislocation, subgrain boundaries, and twins were detected. Smeared surfaces on fragments and lots of very fine debris were indicative of plasticity effects.

Ceramic Ball Bearings

J. J. Swab and M. P. Sweeney, "Fracture Analysis of An All-Ceramic Bearing System," U. S. Army Research Laboratory Technical Report, ARL TR 512, September 1994.

Y. Wang and M. Hadfield, "Rolling Contact Fatigue Failure Modes of Lubricated Silicon Nitride in Relation to Ring Crack Defects," *Wear*, **225-229** (1999) 1284 – 1292.

Y. Wang and M. Hadfield, "The Influence of Ring Crack Location on the Rolling Contact Fatigue Failure of Lubricated Silicon Nitride: Experimental Studies," *Wear*, **243** (2000) 157 – 166.

T. Lube, S. Witsching, P. Supancic, R. Danzer, O. Schöppl, "The Notched Ball Test – Characterization of Surface Defects and Their Influence on Strength," pp. 225 – 234 in *Fractography of Glasses and Ceramics, VI*, eds. J. R. Varner, M. Wightman, *Ceramic Transactions*, Vol. 230, Wiley, New York, 2012.

P. Supancic, R. Danzer, W. Harrer, Z. Wang, S. Witschnig, and O. Schöppl, "Strength Tests on Silicon Nitride Balls," pp. 193 – 200 in *Fractography of Advanced Ceramics III*, eds. J. Dusza, R. Danzer, R. Morrell, and G. D. Quinn, Trans Tech Publ. Zurich, 2009.

Cellular Ceramics, Catalytic Converters, Filters

D. J. Green and R. Brezny, "Fractographic Determination of Strut Strength in Cellular Ceramics," pp. 199 – 129 in *Fractography of Glasses and Ceramics II*, eds. V. D. Fréchette and J. R. Varner, *Ceramic Transactions*, Vol. 17, American Ceramic Society, Westerville, OH, 1991.

J. Kübler, R. Baechtold, G. Blugan, L. Lemster, and S. Fuso, "Failure Analysis on a De-No_x Catalyst of a Large Waste Burner," pp. 78 - 85 in *Fractography of Advanced Ceramics II*, eds. J. Dusza, R. Danzer and R. Morrell, Transtech, Zurich, 2005.

Special Ceramic Components

MEMS structures

S. J. Glass, D. A. LaVan, T. E. Buchheit, and K. Jackson, "Strength Testing and Fractography of MEMS Materials," pp. 227 –240 in *Fractography of Glasses and Ceramics*, IV, eds. J. R. Varner and G. D. Quinn, American Ceramic Society, Westerville, OH, 2001.

G. Quinn, W. Sharpe, G. M Beheim, N. Nemeth and O. Jadaan, "Fracture Origins in Miniature Silicon Carbide Structures," pp. 62 –69 in *Fractography of Advanced Ceramics II,* eds. J. Dusza, R. Danzer and R. Morrell, Transtech, Zurich, 2005.

Theta specimens

G. D. Quinn, "Fractographic Analysis of Very Small Theta Specimens," pp. 201-208 in *Fractography of Advanced Ceramics III*, eds. J. Dusza, R. Danzer, R. Morrell, and G. D. Quinn, Trans Tech Publ., Zurich, 2009.

Ceramic automotive valves

R. Danzer, M. Hangl, and R. Paar, "Edge Chipping of Brittle Materials," pp. 43 – 55 in *Fractography of Glasses and Ceramics,* IV, eds. J. R. Varner and G. D. Quinn, American Ceramic Society, Westerville, OH, 2001.

M. J. Andrews, A. A. Wereszczak, K. Breder, and T. P. Kirkland, "Fractographic Analysis Applied to Ceramic Component Life Prediction," pp. 301 – 315 in *Fractography of Glasses and Ceramics,* IV, eds. J. R. Varner and G. D. Quinn, American Ceramic Society, Westerville, OH, 2001.

Ceramic gas turbine model rotor

G. D. Quinn, This Guide, Chapter 10, and
G. D. Quinn, "Design and Reliability of Ceramics, Do Modelers, Designers and Fractographers See the Same World?" *Ceram. Eng. Sci. Proc.,* **26** [8] (2005) 239 - 252.

a - Silicon carbide heat exchanger tube

K. Breder and J. R. Kaiser, "Failure Analysis of an a-SiC Tube Subjected to Thermal Cycling in and Oxygen-Steam Atmosphere," pp. 301 – 315 in *Fractography of Glasses and Ceramics, III,* eds. J. R. Varner, V. D. Fréchette, and G. D. Quinn, *Ceramic Transactions,* Vol. 64, American Ceramic Society, Westerville, OH, 1996.

Silicon carbide machine gun barrel

G. D. Quinn, This Guide, Chapter 10, and
G. D. Quinn, "Design and Reliability of Ceramics, Do Modelers, Designers and Fractographers See the Same World?" *Ceram. Eng. and Sci. Proc.,* **26** [8] (2005) 239 - 252.

Contact cracks from shrink fitting and stress reverberations

Silicon nitride rolling mill rollers

M. Lengauer, R. Danzer, D. Rubesa, W. Harrer, and W. Zleppnig, "Failure Analysis of Si_3N_4 Rolls for Wire Hot Rolling by Numerical Simulation of Thermal and Mechanical Stresses," pp. 94 -101 in *Fractography of Advanced Ceramics II,* eds. J. Dusza, R. Danzer and R. Morrell, Transtech, Zurich, 2005.

R. Danzer, M. Lengauer, D. Rubesa, and W. Harrer, "Silicon Nitride Tools for Hot Rolling of High-alloyed Steel and Superalloy Wires," pp. 43 – 54 in *Fractography of*

Advanced Ceramics III, eds. J. Dusza, R. Danzer, R. Morrell, and G. D. Quinn, Trans Tech Publ. Zurich, 2009.

W. Harrer, R. Morrell, and R. Danzer, "Failure Analysis on a Compaction Roll made of Silicon Nitride," *Pract. Metallogr*., **56** [4] (2019) 262 -275.

Compaction rollers for tool forming with submicron abrasive powers broke from thermal stresses associated with a joint between ceramic rollers and steel clamping rings.

Lead zirconate titanate (PZT) sonar rings

R. W. Rice, "Failure Analysis of Ceramics," pp. 369 – 388 in *Fractography of Glasses and Ceramics*, IV, eds. J. R. Varner and G. D. Quinn, American Ceramic Society, Westerville, OH, 2001.

Epoxy bonding stresses

Silicon Nitride foundry tubes and rolls

W. Harrer, R. Danzer, K. Berroth, "Thermal Shock Behavior of Si_3N_4 Specimens – Influence of Annealing and Edges," pp. 245 – 254 in *Fractography of Glasses and Ceramics*, VI, eds. J. R. Varner, M. Wightman, *Ceramic Transactions*, Vol. 230, Wiley, New York, 2012.

Beryllium oxide hollow cylinder

J. R. Varner and V. D. Frechette, "Fractography of Whitewares," pp. 305 – 315 in *Science of Whitewares*, eds. V. Henkes, G. Onoda, and W. Carty, American Ceramic Society, Westerville, OH, 1996.

Hollow cylinder loaded at high temperature under laboratory conditions.

Electronic Ceramics

Porcelain railroad electrical insulator

J. Woodtli, K. Berroth, and T. Luthi, "Combination of Fractography and Computed Tomography for the Determination of the Cause of Fracture," pp. 257 – 271 in *Fractography of Glasses and Ceramics, III*, eds. J. R. Varner, V. D. Fréchette, and G. D. Quinn, *Ceramic Transactions*, Vol. 64, American Ceramic Society, Westerville, OH, 1996.

Porcelain insulator, high tension power line

J. R. Varner and V. D. Frechette, "Fractography of Whitewares," pp. 305 – 315 in *Science of Whitewares*, eds. V. Henkes, G. Onoda, and W. Carty, American Ceramic Society, Westerville, OH, 1996.

A large high-tension insulator broke and fell 26 m onto a man's head, killing him. Material fault, a clump of feldspar grains that reacted during firing to form a void with a rim of mullite grains.

Silicon wafers

R. E. Moore, P. G. Hansen, W. Carty, and J. W. Ha, "Fracture of Thermally Shocked Silicon Disks," pp. 351 – 361 in *Fractography of Glasses and Ceramics*, eds. J. D.

Varner and V. D. Fréchette, Advances in Ceramics, Vol. 22, American Ceramic Society, Westerville, OH, 1988.

Stacked PZT piezoelectric actuator material

P. Supancic, Z. Wang, W. Harrer, K. Reichmann, and R. Danzer, "Strength and Fractography of Piezoceramic Multilayer Stacks," pp. 46 –53 in *Fractography of Advanced Ceramics II*, eds. J. Dusza, R. Danzer and R. Morrell, Transtech, Zurich, 2005.

PTC (Positive Temperature Coefficient) thermistors – barium titanate

A. Platzer, P. Supancic, C. Lembacher, U. Theiszi, and R. Danzer, " Thermography and Simulation as a Combined Method for Failure Analysis of PTCs," pp. 54 - 61 in *Fractography of Advanced Ceramics II*, eds. J. Dusza, R. Danzer and R. Morrell, Transtech, Zurich, 2005.

R. Danzer, A. Platzer, P. Supancic, Z. Wang, "Fractography of Thermistors," pp. 231 – 241 in *Fractography of Glasses and Ceramics V*, ,eds. J. R. Varner, G.D. Quinn, M. Wightman, *Ceramic Transactions*, Vol. 199, American Ceramic Society, Westerville, OH, 2007.

ZnO varistors

Z. Wang, P. Supancic, F. Aldrian, A. Schriener and R Danzer, "Strength and Fractography of High Power Varistors," pp. 358 - 365 in *Fractography of Advanced Ceramics II*, eds. J. Dusza, R. Danzer and R. Morrell, Transtech, Zurich, 2005.

R. W. Rice, "Failure Analyses of Ceramics," pp. 369 - 388 in *Fractography of Glasses and Ceramics*, IV, eds. J. R. Varner and G. D. Quinn, American Ceramic Society, Westerville, OH, 2001.

Components suffer dielectric breakdown.

Sold Oxide Fuel Cells

J. Malzbender, R. W. Steinbrech, E. Wessel, "Brittle Fracture Studies of Solid Oxide Fuel Cells," pp. 81-93 in *Fractography of Advanced Ceramics III*, eds. J. Dusza, R. Danzer, R. Morrell, and G. D. Quinn, Trans Tech Publ. Zurich, 2009.

L. Blanco, S. Taylor, and K. Wiggins, "Unexpected Thermal Fracture of a Ceramic Sensor," *J. Fail. Anal. Prev*., **11** (2011) 478 - 480.

A ceramic substrate, to which an electronic infrared sensor was bonded, fractured when thermally cycled due to excessive force from a polymer pad used to clamp the assembly together.

F. Fleischhauer, A. Tiefenauer, T. Graule, R. Danzer, A. Mai, J. Kubler, "Failure Analysis of Electrolyte-Supported Solid Oxide Fuel Cells," *J. Power Sources*, **258** (2014) 382 – 390.

Thin circular zirconia electrolyte disks develop radial cracks during long term operations up to 40,000 hours. Fracture started where small bumps on a metallic

interconnector created little cracks that propagated into the electrolyte due to residual stresses from thermal expansion mismatches of the parts. Thermal stresses then caused these to propagate in the zirconia electrolyte.

Bioceramics

Ceramic hip joint ball heads or liners

H. G. Richter, "Fractography of Bioceramics," pp. 157 - 180 in *Fractography of Advanced Ceramics,* ed. J. Dusza, Trans Tech Publ., Zurich, 2002.

S. Hecht-Mijic and H. G. Richter, "Fractography of Bioceramic Components for Hip Joint Replacement," pp 313 – 328 in *Fractography of Glasses and Ceramics V,* ,eds. J. R. Varner, G.D. Quinn, M. Wightman, *Ceramic Transactions,* Vol. 199, American Ceramic Society, Westerville, OH, 2007.

R. Morrell, L. Byrne, and M. Murray, "Fractography of Ceramic Femoral Heads," pp. 253 – 266 in *Fractography of Glasses and Ceramics,* IV, eds. J. R. Varner and G. D. Quinn, American Ceramic Society, Westerville, OH, 2001.

A. Walter, "Fracture Phenomena in Orthopedic Alumina," pp. 403 – 414 in *Fractography of Glasses and Ceramics,* eds. J. R. Varner and V. D. Fréchette, Advances in Ceramics, Vol. 22, American Ceramic Society, Westerville, OH, 1988.

R. Morrell, "Dealing with Component Failures," pp. 353 -368 in *Fractography of Glasses and Ceramics V*, eds. J. R. Varner, G.D. Quinn, M. Wightman, *Ceramic Transactions,* Vol. 199, American Ceramic Society, Westerville, OH, 2007.

Includes general observations of femoral head fractures, plus two specific alumina cases. One *in-vivo* ball fracture had an unusual, circular, shiny region of slow crack growth. The second case was an *in vitro* fracture that broke from cracks in the bore created by contact with a Co-Cr stem.

R. Morrell, R. Danzer, I. Milošev, R. Trebše, "An Assessment of in vivo Failures of Alumina Ceramic Total Hip Joint Replacements," *J. Eur. Cer. Soc.,* **32** (2012) 3073 - 3084.

Four *in vivo* cases. Femoral heads may be damaged by the surgeon, or contaminated during or prior to installation.

A. Bistolfi, R. Ferracini, G. Lee, D. Mellano, C. Guidotti, F. Baino, and E. Verne," Ceramic-on-Ceramic Catastrophic Liner Failure in Toral Hip Arthroplasty: Morphological and Compositional Analysis of Fractured Ceramic Components," *Ceramics Int.,* **47** (2021) 11029 – 11036.

Two *in-vivo* cases both of which were with a ceramic ball and ceramic cup liner. with no polyethylene. Case 1 was a misaligned ceramic (ZTA, zirconia toughened alumina) liner inside a metal cup that fractured into two main pieces and debris. Case 2 was also a ceramic liner in a metal cup, but the liner and the ball were different ceramics; an alumina for the former and a ZTA for the latter.

F. Traina, M. DE Fine, A. Martino, and C. Faldini, "Fracture of Ceramic Bearing Surfaces Following Total Hip Replacement: A Systematic Review," *Biomed Rs. Intl.*, 2013, 8 pages, Article ID 157247; //dx.doi.org/10.1155/2013/157247.

This is a useful review article that identified several dozen other papers that report ceramic head or liner fractures up to 2012. There are 75 references that cover 30 ceramic head ball fractures and 34 liner fractures.

Dental Ceramics and Glass Ceramics

J. R. Kelly, "Fractography of Dental Ceramics," pp. 241 – 251 in *Fractography of Glasses and Ceramics, IV*, eds. J. R. Varner and G. D. Quinn, American Ceramic Society, Westerville, OH, 2001.

J. B. Quinn, "Failure Analysis of a Broken Tooth," *J. Fail. Anal. Prev.*, **4** [1] (2004) 41 – 46.

A patient's natural tooth fractured days after open-heart surgery. Was the laryngoscopy by the anesthesiologist done correctly?

S. S. Scherrer, J. B. Quinn, G. D. Quinn, and J. R. Kelly, "Failure Analysis of Ceramic Clinical Cases Using Qualitative Fractography," *Int. J. Prosthodont.*, **19** [2] (2006) 151 – 158.

Five dental crown restorations that failed in service were analyzed. The materials were: Procera alumina, Cerestore alumina-spinel, In-ceram glass in-fused alumina, and porcelain fused to metal. Fractography identified the failure causes. These were correlated to clinical observations and crown design.

J. B. Quinn, G. D. Quinn, J. R. Kelly, and S. S. Scherrer, "Fractographic Analyses of Three Ceramic Whole Crown Restorations," *Dent. Mat.*, **21** (2005) 920 – 929.

Three dental crown restorations that failed in service were analyzed. The materials were Procera alumina, Cerestore alumina-spinel, and Empress II lithium disilicate. Origin sites were found in each case.

S. S. Scherrer, J. B. Quinn, G. D. Quinn, and H. W. A. Wiskott, "Fractographic Ceramic Failure Analysis Using the Replica Technique: Two Case Studies," *Dental Materials*, **23** [11] (2007) 1397 - 1404.

S. S. Scherrer, J. B. Quinn, G. D. Quinn, and H. W. A. Wiskott, "Descriptive Fractography on All Ceramic Dental Crown Failures," pp. 339 – 352 in *Fractography of Glasses and Ceramics, V*, eds., J. R. Varner, G. D. Quinn, M. Wightman, *Ceramic Transactions*, Vol. 199, American Ceramic Society, Westerville, OH, 2007.

S. S. Scherrer, G. D. Quinn, and J. B. Quinn, "Fractographic Failure Analysis of a Procera AllCeram Crown Using Stereo and Scanning Electron Microscopy," *Dent. Mater.*, **24** (2008) 1107 – 1113.

J. B. Quinn, S. S. Scherrer, and G. D. Quinn, “The Increasing Role of Fractography in the Dental Community,” pp. 253 - 270, *Fractography of Glasses and Ceramics, V*, eds, J. R. Varner, G. D. Quinn, M. Wightman, *Ceramic Transactions*, Vol. 199, American Ceramic Society, Westerville, OH, 2007.

J. B. Quinn, G. D. Quinn, J. R. Kelly, and S. S. Scherrer, “Useful Tools for Dental Failure Investigation,” pp. 36 - 53 in *Proc. Conference on Scientific Insights and Dental Ceramics and Photopolymer Networks*, ed. D. C. Starrett, Trans. Academy of Dental Materials, Vol. 16, 2004.

S. S. Scherrer, J. B. Quinn, and G. D. Quinn, “Fractography of Dental Restorations,” in *Fractography of Advanced Ceramics, III*, ed. J. Dusza, R. Danzer, R. Morrell and G. Quinn, TransTech Publ., Zurich, 2009. *Key Engineering Materials*, **413** (2009) 72 - 80.

B. Taskonak, J. J. Mecholsky, Jr., and K. J. Anusavice, “Fracture Surface Analysis of Clinically Failed Fixed Partial Dentures,” *J. Dent. Res.*, **3** (2006) 277 – 281.

J. Y. Thompson, K. J. Anusavice, A. Naman, and. H. F. Morris, “Fracture Surface Characterization of Clinically Failed All-Ceramics Crowns, *J. Dent. Res.*, **73** [12] (1994) 1824 - 1832.

Ten Dicor crown were fractographically analyzed in accordance with MIL HDBK 790 and the principles outline by Fréchette. Fracture initiated on the inside surfaces from abrasive damage or failure of the cement at the restoration/cement interface. Twelve Cerestore crowns were more difficult and appeared to break from the porcelain/core interface or inside the core material. Biaxial disk specimens furnished valuable property and fractographic information.

G. D. Quinn, K. Hoffman, S. Scherrer, U. Lohbauer, G. Amberger, M. Karl, J. R. Kelly, “Fractographic Analysis of Broken Ceramic Dental Restorations, pp. 161 - 174 in *Fractography of Glasses and Ceramics, VI*, eds. J. R. Varner, M. Wightman, *Ceramic Transactions*, Vol. 230, Wiley, New York, 2012.

Three case studies: an alumina 3-unit bridge; a 6-unit zirconia bridge; a 5-unit zirconia telescoping-denture.

G. D. Quinn, “Fractographic Analysis of Broken Ceramic Dental Restorations,” *Ceramic Engineering and Science Proceedings*, **35** [1] (2015) 39 - 51.

S. Hecht-Mijic, “Fractography of Ceramic Dental Implants,” pp 175 – 191 in *Fractography of Glasses and Ceramics, VI*, eds. J. R. Varner, M. Wightman, *Ceramic Transactions*, Vol. 230, Wiley, New York, 2012.

Fractures in ceramic dental implants.

M. Borba, H. N. Yoshimura, J. A. Griggs, P. F. Cesar, and A. Della Bona, “Qualitative and Quantitative Fractographic Analysis of All-Ceramic Fixed Partial Dentures,” pp. 205 – 212 in in *Fractography of Glasses and Ceramics, VI*, eds. J. R. Varner, M. Wightman, *Ceramic Transactions*, Vol. 230, Wiley, New York, 2012.

U. Lohbauer, R. Belli, G. Arnetzl, S. Scherrer, and G. D. Quinn, "Fracture of a Veneered-ZrO2 Dental Prosthesis from an Inner Thermal Crack," *Case Studies in Engineering Fracture Analysis*, **2** (2014) 100 - 106.

U. Lohbauer, G. Amberger, G. D. Quinn, S. S. Scherrer, "Fractographic Analysis of a Dental Zirconia Framework: A Case Study on Design Issues, *J. Mech. Behav. Biom. Mat.*, **3** (2010) 623 - 629.

M. Øilo, A. K. Kvam, J. E. Tibballs, and N. Gjerdet, "Clinically Relevant Fracture Testing of All-Ceramic Crowns," *Dent. Mater.*, **29** (2013) 815 - 823.

M. Øilo, N. R. Gjerdet, "Fractographic Analysis of All-Ceramic Crowns: A Study of 27 Clinically-fractured Crowns," *Dent. Mater.*, **29** (2013) e78 - e84.

M. Øilo, G. D. Quinn, "Fracture Origins in Twenty-Two Dental Alumina Crowns," *J. Mech. Beh. Biomed. Mater.*, **53** (2016) 93 – 103.

Whitewares and Kitchenware

J. S. Banda and P. F. Messer, "Fracture-Initiating Flaws in Whitewares," pp. 363 - 375 in *Fractography of Glasses and Ceramics*, eds. J. D. Varner and V. D. Fréchette, Advances in Ceramics, Vol. 22, American Ceramic Society, Westerville, OH, 1988.

P. B. Adams and S. E. DeMartino, "Glass-Ceramic Cookware Failure Analysis," pp. 669 – 673 in *Ceramics and Glasses, Engineered Materials Handbook*, Vol. 4, ed. S. Schneider, ASM, Metals Park, OH, 1991.

An interesting case involving impact fracture of a Corningware glass ceramic cooking bowl (Corning glass ceramic 9608) in which the food caught fire while being heated on an electric stove. There were two major crack systems initiated at two locations, causing crossing of some cracks. There is a superb illustration of the reassembled vessel with arrows showing the directions of crack propagation and the two origin sites. Two fractographers interpreted the failure differently. The preponderance of information, especially the ancillary information at the accident scene and a quantitative analysis of the fracture mirror sizes, provided the solution. The cook evidently threw the burning bowl out a back door of the residence. This was a superb case study illustrating the importance of integrating all the "pieces of the puzzle," as shown in Figure 1.4 of this Guide.

V. D. Fréchette, *Failure Analysis of Brittle Materials*, Advances in Ceramics, Vol. 28, American Ceramic Society, Westerville, OH, 1990, pp. 113 - 114.

Teapots on stoves – thermal stresses.

V. D. Fréchette, *Failure Analysis of Brittle Materials*, Advances in Ceramics, Vol. 28, American Ceramic Society, Westerville, OH, 1990, pp. 114 - 115.

Lasagna dish, cone crack – impact origin crack, propagated by thermal stresses.

J. R. Varner and V. D. Frechette, "Fractography of Whitewares," pp. 305 – 315 in *Science of Whitewares*, eds. V. Henkes, G. Onoda, and W. Carty, American Ceramic Society, Westerville, OH, 1996.

Porcelain Coffee Storage Jars – contact damage from a metal band cover seal
Porcelain Bushing, 2.7 m long by 0.9 m diameter – residual stresses from firing
Porcelain Bushing, small - screw holes acted as origins

V. D. Fréchette, *Failure Analysis of Brittle Materials*, Advances in Ceramics, Vol. 28, American Ceramic Society, Westerville, OH, 1990, p. 113.

Porcelain faucet handles

M. D. Hayes and D. L. Ahearn, "Thermomechanical Analysis of a Ceramic Cooker," *J. Fail. Anal. Prev*., **13** (2013) 383 - 388.

Escape of hot gasses through a crack in a ceramic cooker/grill caused a house fire. The cause of the crack was not determined.

R.C. Bradt and R. L. Martens, "Shattering Glassware," *Bull. Amer. Ceram. Soc*., **91** [7] (2012) 33-38.

Consumerwares. Thermal shock fractures of heat-strengthened soda lime silica versus borosilicate glass. Pyrex glass fractures are covered.

Porcelain Toilet Bowls

D. L. Ahearn, "Residual Failure Due to Incomplete Sintering of Vitreous China Plumbing Fixtures, pp. 273 – 279 in *Fractography of Glasses and Ceramics, VI*, eds. J. R. Varner, M. Wightman, *Ceramic Transactions*, Vol. 230, Wiley, New York, 2012.

J. R. Varner and V. D. Frechette, "Fractography of Whitewares," pp. 305 – 315 in *Science of Whitewares*, eds. V. Henkes, G. Onoda, and W. Carty, American Ceramic Society, Westerville, OH, 1996.

Toilet Bowl – water hammer. The bowl fractured while a woman was seated on it and caused serious injury.
Toilet Tank – mounting-bolt hole failure from mechanical overload

Other Ceramic Components

Porcelain faucet handles

V. D. Fréchette, *Failure Analysis of Brittle Materials*, Advances in Ceramics, Vol. 28, American Ceramic Society, Westerville, OH, 1990, p. 113.

Earthenware sewer pipe

V. D. Fréchette, *Failure Analysis of Brittle Materials*, Advances in Ceramics, Vol. 28, American Ceramic Society, Westerville, OH, 1990, p. 116.

Uranium dioxide fuel element – bushing

V. D. Fréchette, *Failure Analysis of Brittle Materials*, Advances in Ceramics, Vol. 28, American Ceramic Society, Westerville, OH, 1990, pp. 120 - 121.

Thermal fracture.

Beryllium oxide hollow cylinder

J. R. Varner and V. D. Frechette, "Fractography of Whitewares," pp. 305 – 315 in *Science of Whitewares*, eds. V. Henkes, G. Onoda, and W. Carty, American Ceramic Society, Westerville, OH, 1996.

Hollow cylinder loaded at high temperature under laboratory conditions.

Ceramic machine base (Electrically insulating base)

R. Morrell, "Fractography of Brittle Materials," R. Morrell, *Measurement Good Practice Guide 15*, National Physical Laboratory, Teddington, Middlesex, United Kingdom, 1999, pp. 67 – 69.

Bending failure from bolt holes.

Ceramic ball valve – alumina

R. Morrell, "Fractography of Brittle Materials," R. Morrell, *Measurement Good Practice Guide 15*, National Physical Laboratory, Teddington, Middlesex, United Kingdom, 1999, pp. 70- 71.

150 mm alumina ball with slots and large hole, internal pressure. Gas valve

Gas valve plate - alumina

R. Morrell, "Fractography of Brittle Materials," R. Morrell, *Measurement Good Practice Guide 15*, National Physical Laboratory, Teddington, Middlesex, United Kingdom, 1999, pp. 72 - 74.

Possible grinding or lapping damage near a complex hole.

Steel continuous casting nozzles – Carbon-bonded alumina, zirconia, magnesia, graphite

Mašelejová and A. Leško, "Fracture Characteristics of Isostatic Pressed Submerged Entry Nozzle," pp. 370 – 373 in *Fractography of Advanced Ceramics II*, eds. J. Dusza, R. Danzer and R. Morrell, Transtech, Zurich, 2005.

Tungsten carbide – cobalt dies used for manufacture of polycrystalline diamond

R. Morrell, K. Mingard, and J. Zunega, "Fractography of Hardmetal Dies Used for the manufacture of Polycrystalline Diamond," *J. Eur. Ceram. Soc*., **37** [14] (2017) 4259 – 4264.

Very large tungsten carbide dies operating at very high pressures and temperatures developed stable cracks that grew outwards from the inside bore and changed orientation. Unusual "fountain like cracks."

Fibers - Glass - Optical

H. C. Chandan, R. D. Parker, and D. Kalish, "Fractography of Optical Fibers," pp. 143 – 184 in *Fractography of Glass*, Ed. R. C. Bradt and R. E. Tressler, Plenum, NY, 1994.

W. R. Wagner, "Failure Analysis of Fiber Optic Connectors," pp. 389 – 402 in *Fractography of Glasses and Ceramics*, Advances in Ceramics, Vol. 22, ed. J. D. Varner and V. D. Fréchette, American Ceramic Society, Westerville, OH, 1988.

J. J. Mecholsky, "Fracture Surface Analysis of Optical Fibers," pp. 663 – 668 in *Ceramics and Glasses, Engineered Materials Handbook*, Vol. 4, ed. S. Schneider, ASM, Metals Park, OH, 1991.

P. G. Simpkins and J. T. Krause, "Dynamic Response of Glass Fibers During Tensile Fracture," *Proc. R. Soc. London A*, **350** (1976) 253 - 265.

High-speed photos of strong (> 2.8 GPa) glass fibers tested in tension reveal that secondary fractures occur as the result of fiber whipping and flexural and longitudinal wave interactions. Fibers disintegrate into a particulate cloud.

Fibers – Nonoptical

P. K. Gupta, "Fractography of Fiberglass," pp. 185 – 206 in *Fractography of Glass*, Ed. R. C. Bradt and R. E. Tressler, Plenum Press, NY, 1994.

G. V. Srinivasan and V. Venkateswaren, "Fractographic Investigation of Flaws in Sintered SiC Fiber," pp. 317 –337 in *Fractography of Glasses and Ceramics, III*, eds. J. R. Varner, V. D. Fréchette, and G. D. Quinn, *Ceramic Transactions*, Vol. 64, American Ceramic Society, Westerville, OH, 1996.

C-T. Li and N. R. Langley, "Development of a Fractographic Method for the Study of High-Temperature Failure of Ceramic Fibers," pp. 177 – 184 in *Fractography of Glasses and Ceramics*, eds. J. D. Varner and V. D. Fréchette, Advances in Ceramics, Vol. 22, American Ceramic Society, Westerville, OH, 1988.

T. Clark, "Fracture Properties of Thermally Aged Ceramic Fiber Produced by Polymer Pyrolysis," pp. 279 – 305 in *Fractography of Glasses and Ceramics*, eds. J. D. Varner and V. D. Fréchette, Advances in Ceramics, Vol. 22, American Ceramic Society, Westerville, OH, 1988.

Fiber Composites

Silicon carbide fibers in a glass matrix

A. S. Fareed, M. J. Koczak, F. Ko, and G. Layden, "Fracture of SiC/LAS Ceramic Composites," pp. 261 – 293 in *Fractography of Glasses and Ceramics*, eds. J. D. Varner and V. D. Fréchette, Advances in Ceramics, Vol. 22, American Ceramic Society, Westerville, OH, 1988.

Glass fibers in a fiberglass-reinforced plastic pressure vessel

S. J. Glass, E. K. Beauchamp, M. J. Carr, T. R. Guess, S. L. Munroe, R. J. Moore, A. Slavin, and N. R. Sorenson, "Failure Analysis of A Fiberglass-Reinforced Plastic Pressure Vessel," pp. 527 – 541 in *Fractography of Glasses and Ceramics, III*, eds. J. R. Varner, V. D. Fréchette, and G. D. Quinn, *Ceramic Transactions*, Vol. 64, American Ceramic Society, Westerville, OH, 1996.

Violent rupture of a pressurized tank holding sulphuric acid. Occasional and incidental spillage penetrated microcracks in the matrix and caused progressive degradation in glass fibers.

Single Crystal Ceramic Components

Sapphire secondary refractor lens for spacecraft

J. A. Salem and G. D. Quinn, "Failure Analysis of Sapphire Refractive Secondary Concentrators," NASA Technical Report: TM-2009-215802, NASA Glenn Research Center, Cleveland, OH, Dec. 2009. Also in this Guide, chapter 10.

and:

J. A. Salem, G. D. Quinn, "Fractographic Analysis of Large Single Crystal Sapphire Refractive Secondary Concentrators," second keynote presentation and paper, 4th International Conference on Fractography of Advanced Ceramics," Smolenice Castle, Oct. 2013, *J. Eur. Cer. Soc.*, **34** (2014) 3271 - 3281.

Large single crystal lens designed to concentrate sunlight in space. Fracture occurred from thermal stresses that propagated cracks from polishing and impact flaws from handling. Although strong and hard, sapphire is vulnerable to surface damage. Also this Guide, chapter 10.

Sapphire Tubes, Plasma Asher

This Guide, chapter 8.

Calcium Fluoride (CaF_2) windows in a laser flash diffusivity apparatus

R. Morrell, "Dealing with Component Failures," pp. 353 -368 in *Fractography of Glasses and Ceramics V*, eds. J. R. Varner, G.D. Quinn, M. Wightman, *Ceramic Transactions*, Vol. 199, American Ceramic Society, Westerville, OH, 2007.

48 mm diameter single crystal disks that broke from thermal stresses activating edge damage or impact damage.

Neodymium doped Yttrium Ortho-vanadate (Nd:YVO4) laser crystal

J. Salem, C. He, N. Sawruk, S. Litovich, and M. Jenkins, "Thermally Driven Failure of Nd:YVO4 Amplifier Crystals," *J. Eur. Ceram. Soc.*, **40** [14] (2020) 4939 – 4948.

Unusual fracture surface patterns in a very brittle single crystals tested under laser pumping conditions. Thermal stresses caused a low energy single fracture that curved around a cleavage plane with cleavage step hackle that converged to a point called a "hackle node."

Coatings and Glazes

Diamond coatings

H. A. Hoff, K. A. Snail, A. A. Morrish, and J. E. Butler, "Fractography and Fracture Mechanics of Combustion Grown Diamond Thin Films," pp. 25 – 54 *in Fractography of Glasses and Ceramics II*, eds. V. D. Fréchette and J. R. Varner, *Ceramic Transactions*, Vol. 17, American Ceramic Society, Westerville, OH, 1991.

Whiteware glazes

V. D. Fréchette, *Failure Analysis of Brittle Materials*, Advances in Ceramics, Vol. 28, American Ceramic Society, Westerville, OH, 1990, pp. 94 – 101.

Internal pressure, water hammer, thermal shock, and impact fractures.

Stoneware reactor catalyst media balls

R. W. Rice, "Failure Analysis of Ceramics," pp. 369 – 388 in *Fractography of Glasses and Ceramics, IV*, eds. J. R. Varner and G. D. Quinn, American Ceramic Society, Westerville, OH, 2001.

Coatings on Infrared Windows and Domes

D. C. Harris, *Materials for Infrared Windows and Domes, Properties and Performance*, SPIE Press, Bellingham, WA, 1999.

Rain, sand, and bug impact damage on windows and domes are shown. CVD diamond, silicon cladding damage. Zinc selenides and zinc sulfides.

Gemstones and Jade

Emerald gemstone (3.66 carat)

R. W. Rice, "Failure Analysis of Ceramics," pp. 369 – 388 in *Fractography of Glasses and Ceramics*, IV, eds. J. R. Varner and G. D. Quinn, American Ceramic Society, Westerville, OH, 2001.

Impact on ceramic kitchen tile countertop caused cracking.

Jade

D. J. Rowcliffe and V. Frühauf, "The Fracture of Jade," *J. Mat. Sci.*, **12** (1977) 35 – 42.

Gemstones

J. E. Field, "Brittle Fracture: Its Study and Application," *Contemp. Phys.*, **12** [1] (1971) 1 - 31.

Rocks, Lithic Materials, Geological

B. R. Kulander and S. L. Dean, "Hackle Plume Geometry and Joint Propagation Dynamics," pp. 85 – 94 in *Proc. Int. Symp. on Fundamentals of Rock Joints*, Björkilden, 15-20 September 1985.

An excellent review of fracture surface (joint) markings in rocks. A sensible discussion and interpretation of how the markings form, and how they can be interpreted. Has a superb explanation of the nomenclature and how it relates to that

in glasses and ceramics. Hackle, twist hackle, inclusion (wake) hackle, arrest lines can equally be applied to rocks and to glasses and ceramics. These marking can form with incremental, relatively slow crack propagation.

T. Engelder, "Propagation Velocity of Joints: A Debate Over Stable vs. Unstable Growth of Cracks in the Earth," pp. 457 - 482 in *Fractography of Glasses and Ceramics V*, eds. G. D. Quinn, M. Wightman, and J. R. Varner, *Ceram. Trans*., Vol. 199, American Ceramic Society, Westerville, OH, 2007.

A strong case is made that stable crack propagation accounts for most rock joints observed in nature. Presented at a conference on fractography of glasses and ceramics, Engelder takes pains to correlate nomenclature in the rock fracture filed (e.g., plumose, en echelon, fringe cracks) to nomenclature in the engineering materials literature. Includes excellent schematics showing progressive, self-correcting fracture where crack growth changes in response to changes in loading conditions. Interesting origins such as a "wormhole burrow" and a "flute cast" in siltstone beds are shown.

D. D. Pollard and A. Aydin, "Progress in Understanding Jointing Over the Past Century," *Geological Society of America Bulletin*, **100** (1988) 1181 – 1204.

An excellent review article about "joints" in the earth's crust and historical developments in their analysis. Many good illustrations showing "joints, echelon joint segments, plumose patterns, and conchoidal rib marks." These are terms in the geological community comparable to the terms "cracks, twist hackle, and shear hackle, arrest lines" in this book. A variety of flaws can act as fracture origins including: cavities, fossils, grains, clasts, and inclusions.

D. Bahat, *Tectonofractography*, Springer-Verlag, Berlin, 1991.

A controversial book. It begins with an excellent review of fractography of glass and ceramics, including key principals of fracture mechanics. Well-illustrated, with many famous figures from the glass and ceramic literature. Rock fractures from around the world are well-illustrated with matching schematics. There is an excessive differentiation of terminology, however, which can be confusing. Furthermore, the "fracture mirrors" are probably misinterpretations. Despite the extensive discussions of quantitative fracture mechanics, it is very rarely applied. What are terminal crack velocities in rocks, and do cracks really run that fast in the joints shown? Fracture mirror boundaries in glasses and ceramics form when the crack is running at or near terminal crack velocities. Are the "mirror boundaries" in the rocks shown in this book comparable, or are the boundaries something else, like simple arrest lines?

O. H. Muller, "Fractography Applied to Large Scale (m to km) Cracks in the Earth," pp. 427 – 438 in *Fractography of Glasses and Ceramics*, eds. J. D. Varner and V. D. Fréchette, Advances in Ceramics, Vol. 22, American Ceramic Society, Westerville, OH, 1988.

Similar features observed over nine orders of magnitude of size.

A. I. Younes and T. Engelder, “Fringe Cracks: Key Structures for the Interpretation of the Progressive Alleghanian Deformation of the Appalachian Plateau,” *Geolog. Soc. of Amer. Bull.,* **111** [2] (1999) 219 – 239.

D. T. McConaughy and T. Engelder, “Joint Initiation in Bedded Clastic Rocks,” *J. Struct. Geol.,* **23** (2001) 203 – 221.

T. Engelder, “Tectonic Implication Drawn from Differences in the Surface Morphology on Two Joint Sets in the Appalachian Valley and Ridge, Virginia,” *Geology,* **32** (2004) 413 - 416.

D. Bahat, T. Bankwitz, and E. Bankwitz, “Preuplift Joints in Granites: Evidence for Subcritical and Postcritical Fracture Growth,” *Geolog. Soc. of Amer. Bull.,* **115** [2] (2003) 148 – 165.

J. B. Quinn, J. W. Hatch, and R. C. Bradt, “The Edge Flaking Test as an Assessment of the Thermal Alteration of Lithic Materials, Bald Eagle Jasper,” pp. 73 – 85 in *Fractography of Glasses and Ceramics, IV,* eds. J. R. Varner and G. D. Quinn, American Ceramic Society, Westerville, OH, 2001.

A. Tsirk, “An Exploration of Liquid-Induced Fracture Markings,” pp. 87 – 101 in *Fractography of Glasses and Ceramics, IV,* eds. J. R. Varner and G. D. Quinn, American Ceramic Society, Westerville, OH, 2001.

Obsidian tools.

A. Tsirk, “Fractographic Evidence for Liquid on Obsidian Tools,” *J. Archeol. Sci.,* **27** (2000) 987 – 991.

A. Tsirk, “Formation and Utility of a Class of Anomalous Wallner Lines on Obsidian,” pp. 57 - 69 in *Fractography of Glasses and Ceramics,* eds., J. D. Varner and V. D. Fréchette, Adv. in Ceramics, Vol. 22, Amer. Ceram. Society, Westerville, OH, 1988.

A. Tsirk, “*Fractures in Knapping*,” Archaeopress, Oxford, UK, 2014.

A comprehensive compilation of the author’s lifelong work in fractures of rocks and glasses. This book was published very shortly before the author’s death. Well-illustrated and with links to modern fracture mechanics. The extensive terminology seems excessive, however.

APPENDIX C FRACTURE MIRROR AND BRANCHING CONSTANTS

The following table includes all published values of mirror and branching constants that the author could find up to mid-2025 for this 4th edition. Values are all in units of MPaÖm. The table has only a few new entries compared to the 2nd and 3rd editions. Many of the values are for obsolete materials. The original references are listed for each entry. In the 3rd and 4th editions of this Guide, some values that the author feels are suspect are listed in dark grey. There are many variations in the published mirror constants. Hopefully the recommendations in this Guide (Appendix D) and the usage of ASTM standard C 1678 will improve consistency in the future. Mirror and branching constants were analyzed using Orr's equation:

$$s\sqrt{R} = A \qquad \text{(C.1)}$$

Exceptions for non-zero intercepts are noted by the footnote NZ and the intercepts listed in parenthesis if available. These usually were estimated from analysis of stress and mirror size data with a non-zero intercepts for s versus 1/ÖR graphs as described in Appendix D.

Glasses and glass ceramics have mirror-mist (inner mirror) A_i and mist-hackle (outer mirror) A_o constants. Ceramics have only A_o values corresponding to the mirror-hackle boundary since mist is difficult or impossible to discern in most ceramics. Multiple entries in a cell denote estimates by different test methods, microscopy techniques, or analysis. Readers should check the references for more details. It has been suggested to the author this table be condensed and only list single entries or ranges for some of the materials where there are many entries. The author has chosen to continue to list separate entries so that users can appreciate the reported variabilities and also consult original references as needed.

For proper mirror size analyses, the stress, s, should be the value <u>at the fracture origin site</u>. The mirror size measurement should extend over a region of approximately constant stress as discussed and illustrated in Appendix D. It is not clear if researchers in the past have considered this when they did their analyses. So, for example, if they used 3-point flexure specimens and used the maximum beam stress, the results would be in error if the plane of fracture was off to either side of the middle loading point. The local stress at the plane of fracture should have been used.

One is tempted to conclude that most of the discrepancies are due to viewer judgment, but this cannot account for all of the variability. The mirror

constant is only sensitive to the square root of the measured radii. A 10% systematic error in radii measurements causes only a 5% error in an A value. The variations probably are caused by differences in: viewer judgement, the type of microscope and lighting used, directions the radii were measured, test method (flexure, tension, disk), stress gradients, possible residual stresses, how the data was plotted and analyzed, the number of specimens used, and of course, the materials themselves (microstructure, density, etc.).

All values in the table are listed with the same number of significant figures as in the original reference, up to a limit of three significant figures. Uncertainties (± std. dev.) are listed when available from the original reference. Authors almost never reported how these uncertainties were estimated.

If the user cannot find the mirror constant for a particular material, he or she may consider values for comparable materials within the same class.

As discussed in chapter 7, the fracture mirror constants do not vary significantly with temperature or environment. Variabilities with temperature usually follow trends in fracture surface energy or fracture toughness.

Footnotes are listed here for convenience.

NR	Not reported
NZ	A non-zero intercept was detected on the graph of s versus 1/ÖR. The intercept value in MPa is listed in parenthesis. Mirror or branching constants calculated with non-zero intercepts are usually different than those calculated with intercepts through the ordinate. Consult the original reference for more information.
*	It is not clear whether Ball and Payne, ref. 78 listed this as A_o for PMMA or actually A_b. Their other listed values for glass and polycrystalline ceramic A_b are <u>actually A_o</u> values from Kirchner, or Johnson and Holloway.
**	Additional mirror constants for the lead borate glasses are available at liquid nitrogen temperature (-196 ºC) in the original reference 60 by Shinkai and Ishikawa.
***	Likely an overestimate since stresses were probably not adjusted for failure location in the 3-point rod specimens.
#	Alternative analyses (besides a graph of s versus 1/ÖR) are in the original Shinkai reference 60.
?	These values (from the original references) for A_b cannot be correct since they are less than or equal to A_o.
Ä	Large internal residual stresses have been reported in WC-Co materials, often lead to large non-zero intercepts. Consult the original reference for guidance.
Å	Tempered soda lime silica rods

Material	Technique	*Mirror-Mist* A_i	*Mist-Hackle or Mirror-Hackle* A_o	Branching A_b	Reference
		GLASSES *(see also listings for "fibers" at the end of this table)*			
Soda-Lime Silicate	All methods, typical ranges	**1.8 to 2.1**	**2.0 to 2.3**	Depends on method and shape	**This Guide**
Soda-Lime Silicate – window glass	Flexure (biaxial ring-on ring, large)	2.09			Orr, 5
Soda-Lime Silica (window, plate)	Flexure (Bars or laths)	2.05			Shand, 4
Soda-Lime Silicate – float, plate, sheet	Flexure (Disks, biaxial ring-on-ring + bend bars)		2.09		Barsom, 62
Soda-Lime Silicate – window glass	Pressurized windows, large	1.96 ± 0.09			Reed + Bradt, 39
Soda-Lime Silicate	Flexure (Bars, 3-point)	1.74			Bansal, 14
Soda-Lime Silicate A – plate glass Soda-Lime Silicate B – plate glass	Flexure (Bars – large) (Room Temperature to the Strain Point)	1.86 ± 0.66 1.82 ± 0.91			Kerper + Scuderi, 6
Soda-Lime Silica Float	Flexure (Bars)	1.80 ± 0.15[NZ] 1.81 ± 0.25	2.42 ± 0.16[NZ] 2.29 ± 0.24		Ball, Landini, Bradt 40
Soda-Lime Silica Float (G.E.C. – X8)	Tension (Rods) Flexure (Bars)	1.89 ± 0.06	2.04 ± 0.06 2.09		Johnson + Holloway, 1
Soda-Lime Silica Float	Flexure (Bars) Flexure–Delayed failure (Bars)	1.92 2.0 ± 0.1	2.21 2.2 ± 0.1		Mecholsky et al., 18, 21 Mecholsky et al.,21
Soda-Lime Silica	Flexure	1.8	2.0	2.3	Mecholsky, 22
Soda Lime Silica Float	Flexure (Bars, large and small, 3- and 4-point)	2.06 ± 0.07	2.29 ± 0.19		Duckworth et al.,16
Soda-Lime Silica	Tension (Plates)			1.2 – 1.6	Congleton+Petch,2
Soda-Lime Silica	Flexure (Bars) Flexure (Biaxial ring-on-ring plates)	1.81 ± 0.28		3.54 ±0.64	Choi + Gyekenyesi, 33
Soda-Lime Silica	Tension			1.9	Clark + Irwin, 34
Soda-Lime Silica	Pressurized Tube			2.0	Aoki + Sakata, 35
Soda-Lime Silica	Flexure (Biaxial ring-on-ring disks) 3 environments. Vickers indented	1.82 - 1.94	2.03 – 2.13	2.28 – 2.42	Marshall et al., 19
Soda-Lime Silica	Flexure (Biaxial, pressure on ring disks)			2.1±0.1[NZ] (10 ± 4) [NZ]	Shetty et al., 15
Soda-Lime Silica	Flexure (rods)	1.8			Terao, 63
Soda-Lime Silica	Flexure (rods, 4-point)	1.85 ± 0.21 3.20 Å 2.82 Å			Varner +Oel, 68, 71
Soda-Lime Silica	Flexure (3-point rods) Flexure (4-point rods) Tension (Fibers)	3.15 ± 0.11 2.74 ± 0.15 1.72 ± 0.28			Abdel-Latif, Bradt, Tressler, 49
Soda-Lime Silica	Flexure (3-point, laths)	(2.9 ***)			Levengood 64
Soda-Lime Silica	Flexure (plates, 2 sizes)	1.47 [NZ (19.5)] 1.92 [NZ (7.0)]		2.88 [NZ (18.)] 3.1 [NZ (5.7)]	Gaume + Pelletier,73
Soda-Lime Silica	Flexure (4-point, laths) (air 20° C) (air -150° C) (water 17° C) (dry N_2 24° C)	 1.80 ± 0.07 2.08 ± 0.04 1.89 ± 0.05 1.92 ± 0.04			Shinkai, 69
Soda-Lime Silica	Flexure (4-point, laths)			2.29 ± .03	Shinkai + Hara, 86
Soda-Lime Silica annealed	Flexure (disks, pressure on ring)			2.14±.11[NZ] (10.9±0.6)	Oakley, 82
Borosilicate (C 7740)	Flexure (Rods)	2.2, 2.35			Shand, 3
Borosilicate A (P 3235) Borosilicate B (C 7740)	Flexure (Bars – large) (Room Temperature to Strain Point)	1.98 ± 0.46 2.04 ± 0.75			Kerper + Scuderi, 6

Material	Technique	*Mirror-Mist* A_i	*Mist-Hackle or Mirror-Hackle* A_o	Branching A_b	Reference
GLASSES - continued					
Borosilicate (C 7740)	Flexure (Rods, many diameters)	2.08 ± 0.02			Kerper + Scuderi, 7
Borosilicate (C 7740)	Flexure (Bars)	1.87 ± 0.3	2.10		Mecholsky et al., 17,18
Borosilicate (C 7740)	Flexure (Bars) and Biaxial disks	1.9 ± 0.3			Mecholsky + Rice, 20
Borosilicate (Pyrex)	Flexure (4-point, laths) (air 20° C) (air -150° C) (water 17° C) (dry N_2 24° C)	 1.98 ± 0.09 2.08 ± 0.11 2.02 ± 0.08 1.98 ± 0.12			Shinkai, 69
Borosilicate	Flexure +Tension (Rods)	1.9*			Alarcón et al., 56
Borosilicate crown (Schott BK-7)	Flexure (Biaxial, ring on ring disks)*	1.98±0.02 NZ (9.6±1.2)	2.11±0.03 NZ (9.1±1.7) 2.3 for a zero intercept	2.28±0.03 NZ (10.7±1.2)	Quinn, 25
Aluminosilicate (C 1723)	Flexure (Bars)	2.14	2.40		Mecholsky et al., 18
Aluminosilicate A (P 6695) Aluminosilicate B (C 1723)	Flexure (Bars –large) (Room Temperature to Strain Point)	2.31 ± 0.76 2.34 ± 0.97			Kerper + Scuderi, 6
Alkali-borosilicate	Tension (Fibers)	1.33 NZ			Jaras et al., 12
Alkaline-earth boro aluminosilicate (C1737)	Flexure (Biaxial ring-on-ring)	2.07 ± 0.01			Gulati et al., 57
Barium silicate $3BaO\text{-}5SiO_2$	NR (Flexure Bars?)	1.3	1.5		Mecholsky, 22
E glass $CaO\text{-}Al_2O_3\text{-}B_2O_3$ alumino borosilicate	Tension (Fibers)	1.47 NZ			Jaras et al., 12
Flint glass (Kimble R-6)	Flexure (Rods)		2.0 1.9 2.3		Kirchner et al., 8 Kirchner et al., 9 Kirchner + Gruver,10
Lead silicate (G.E.C. L1)	Tension (Rods)	1.71 ± 0.06			Johnson + Holloway, 1
Lead silicate	Flexure (Bars)	1.61	1.78		Mecholsky et al., 18
Leaded silicate 6.7 g/cm³	Flexure (Rods)	1.4 ± 0.1	1.6 ± (0,1)		Salem et al., 77
Lithium silicate $Li_2O\text{-}2SiO_2$	Flexure (Bars, 3-point)	2.2	2.6		Mecholsky, 22
Zinc silicate	Flexure (Bars)	2.1	2.6	3.2	Mecholsky, 22
Zirconia silicate (Cem-FIL AR)	Tension (Fibers)	2.37 *			Jaras et al., 12
Yttrium-Alumino-Silicon Oxynitride (2Y-Al-Si-O-N)	Flexure (Bars)	1.5 ± 0.2			Coon, 48
Fused silica	All methods, typical ranges	**1.9 to 2.3**	**2.4**	Depends on method and shape	**This Guide**
Fused Silica (C 7940)	Flexure (Bars)	2.23	2.42	2.7	Mecholsky et al., 18, 22
Fused Silica (C 7940)	Flexure (Bars – large) (Room Temperature to Strain Point)	1.89 ± 0.51			Kerper + Scuderi, 6
Fused silica (Vitreosil)	Tension (Rods)	2.33 ± 0.06			Johnson + Holloway, 1
Fused silica	Flexure (Rods)	2.20 ± 0.33			Choi + Gyekenyesi, 33

Material	Technique	*Mirror-Mist* A_i	*Mist-Hackle or Mirror-Hackle* A_o	Branching A_b	Reference
GLASSES - continued					
Fused silica	Flexure +Tension (Rods)	1.2 NZ			Alarcón et al., 56
Fused silica fibers	Tension	2.10			Choi + Gyekenyesi, 33
Fused silica fibers	Tension	1.83			Castilone et al., 30
Fused silica	Tension (Fibers) Flexure (Bars) Flexure (Biaxial, piston on 3 balls)	2.2 ± 0.5 2.3 ± 0.5 2.4 ± 0.3			Mecholsky + Rice, 20
Fused silica fibers	Tension	2.224			Chandan + Parker, 37
Leached High Silica (C 7930)	Flexure (Bars)	0.91	1.19		Mecholsky et al., 18
96% Silica (C 7900)	Flexure (Bars – large) (Room Temperature to Strain Point)	1.84 ± 0.65			Kerper + Scuderi, 6
96% Silica (Vycor)	Flexure (4-point, laths) (air 20° C) (air -150° C) (water 17° C) (dry N_2 24° C)	 1.77 ± 0.06 2.14 ± 0.06 1.80 ± 0.05 1.83 ± 0.07			Shinkai, 69
Glassy Carbon	Flexure (Bars)	1.17	1.67		Mecholsky et al., 17,18
Glassy Carbon	Flexure (Bars)			2.1	Bullock + Kaae, 61
Chalcogenides As-S-Se Ge-AS-Se-Te	Flexure (Fibers, 2-point bending)	1.58 1.77 ± 0.14 (NZ -66.4 ± 45.5)			Quinn et al., 75
Chalcogenide glass, As_2Se_3 untreated UV irradiated	Tension (Fibers)	 0.69 0.35	 0.77 0.38		Hulderman et al., 45
As_2S_3	Flexure (Bars)	0.56	0.65		Mecholsky et al.,18
$Ge_{33}As_{12}Se_{55}$	Flexure (Bars)	0.55	0.65		Mecholsky et al.,18
0.3PbSe - $0.7Ge_{1.5}As_{0.5}Se_3$	Flexure (Bars)	0.48	0.55		Mecholsky et al.,18
ZBLA (halide glass)	Flexure (Bars)	0.8			Mecholsky, 22
Lead Borate glass $30PbO-70B_2O_3$ (mol) $40PbO-60B_2O_3$ $50PbO-50B_2O_3$ $60PbO-40B_2O_3$ $70PbO-30B_2O_3$	Flexure (Bars)	 1.7 ± .05 1.45 ± .05 1.15 ± .05 0.85 ± .01 0.65 ± .01			Shinkai + Ishikawa, 60 **
LCD (AMLCD) glass	Flexure (very thin slabs)	1.90 NZ (21.2)			Kim + Choi, 90
GLASS CERAMICS					
Pyroceram 9608 (Li, Mg, Al silicate)	NR		2.8		Adams + DeMartino, 27
Pyroceram 9607 (Li, Mg, Zn, Al silicate)	NR		2.1 NZ		Adams + DeMartino, 27
Pyroceram 9606 (Cordierite, Mg, Al silicate)	Flexure (Bars)	3.6	6.5		Mecholsky et al.,17
Pyroceram 9606 (Cordierite, Mg, Al silicate)	Flexure (Bars)		6.5		Lewis, 44
Pyroceram 9606 (Cordierite, Mg, Al silicate)	Flexure (Bars, (3-point and 4-point, 2 sizes)		5.7		Bansal, 13,14

Material	Technique	*Mirror-Mist* A_i	*Mist-Hackle or Mirror-Hackle* A_o	Branching A_b	Reference
Pyroceram 9606 (Cordierite, Mg, Al silicate)	Flexure (Bars and Biaxial, piston on 3 balls)		6.3		Mecholsky + Rice, 20
Pyroceram 9606 (Cordierite, Mg, Al silicate)	Flexure (Biaxial, pressure on ring, and ball on ring)			3.1 ± 0.2 NZ (84 ± 6)	Shetty et al., 15
Pyroceram 9606 (Cordierite, Mg, Al silicate)	Flexure (Rods)		4.8		Shand, 3
Li_2O-SiO_2 (NRL, 2 grades)	Flexure (Bars)	3.3, 3.8	4.5, 5.4		Mecholsky et al.,17
DENTAL CERAMICS and FILLED COMPOSITES					
Dicor (dental, tetra silica fluoromica) glass ceramic	Flexure (Bars)		0.97		Kelly, 47
Feldspathic Porcelain (alumina filled, Vitadur N 338)	Flexure (Bars)		2.82		Kelly, 47
Feldspathic Leucite Porcelain (Optec OPC)	Flexure (Bars)		2.1		Fischer et al., 52
Leucite glass ceramic (Empress I)	Flexure (Bars)		1.7		Fischer et al, 52
Lithium disilicate glass ceramic (Empress II)	Flexure (Bars)		3.9		Fischer et al, 52
Omega - Opaker	Flexure (Bars)		1.3		Fischer et al., 52
Porcelain (Cerec Mark II)	Flexure (Bars)		1.6		Fischer et al., 52
Glass infused Alumina, (In-Ceram)	Flexure (Bars)		6.6		Fischer et al., 52
Dental resin, 85 wt% zirconia-silica filler in bisGMA-TEGDMA (Paradigm MZ100)	Flexure (Bars, 4-point)		2.6		Quinn+Quinn, 59
3Y-ZTP (Lava)	Flexure (Bars, 4-point)		10.7		Quinn et al., 58
ALUMINA					
b-Al_2O_3	Flexure		~ 6.5		Mecholsky et al.,17
Hot-pressed (1 mm, Cer. Fin.))	Flexure (Rods, 4-point) 25°C to 1400°C		10.4		Kirchner + Gruver, 11
Hot-pressed (99+% pure, Cer. Fin.)	Flexure (Rods, 4-point) Flexure-Delayed Fracture (Rods)		10.3 9.9		Kirchner et al., 8,9
Hot-pressed (99+% (Cer. Fin.)	Flexure (Rods-3-point)		9.1		Kirchner + Gruver, 10
Hot-pressed (99+%)	Flexure	5.2	12		Mecholsky et al., 17
Hot pressed	Flexure (Rods)		10.4		Kirchner + Gruver, 11
Hot-pressed (Avco, 1-2 mm)	Flexure (4-point, 2 sizes)		9.8		Bansal, 14
Sintered (Lucalox)	Tension (Plates)			7.3	Congleton+Petch,2
Sintered (96%) (Alsimag 614)	Flexure (Rods)		8.5		Kirchner et al., 9
Sintered (96%) (Alsimag 614)	Flexure (Rods) Flexure-Delayed Fracture (Rods)		8.3 8.9		Kirchner et al., 8
Sintered (96%) (Alsimag 614)	Flexure (Bars, 3-point and 4-point, 2 sizes)		9.0		Bansal, 13,14
Sintered (96%) (Alsimag 614)	Flexure (Rods)		9.1		Kirchner + Gruver, 10

Material	Technique	*Mirror-Mist* A_i	*Mist-Hackle or Mirror-Hackle* A_o	Branching A_b	Reference
Sintered (96%) (Alsimag 614)	Flexure (Bars)		13.1		Mecholsky et al.,17
Sintered (96%) (Alsimag 614)	Flexure (Bars) Flexure (Biax. ball on ring) Flexure (Biax. ring on ring)		7.6 ± 0.5	7.4 ± 0.6? 7.2 ± 0.7?	Choi + Gyekenyesi, 33
Sintered 96% (Alsimag 614)	Flexure (Biaxial, pressure on ring disks)			4.0 ± 0.3[NZ] (164 ± 11)	Shetty et al., 15
Hot isopressed (Biolox forte)	Flexure (Bars, 4-point)		7.7		Hecht-Mijic, 76
Hot isopressed, ZTA (Biolox delta)	Flexure (Bars, 4-point)		9.5		Hecht-Mijic, 76
SILICON CARBIDE					
Sintered SiC (Hexoloy SA)	Flexure (Bars)		5.39		Quinn et al., 23
Sintered SiC (Hexoloy SA)	Flexure (Biaxial, ring on ring plates)			6.3 ± 0.5	Salem et al., 31
Sintered SiC (Hexoloy SA)	Flexure (Biaxial, ring-on-ring plates)			5.5 ± 0.3	Choi+ Gyekenyesi, 33
Sintered SiC (Hexoloy SA)	C-ring	5.50 ± 0.94	8.20 ± 0.54	10.5 ± 1.0	Conway et al., 67
Sintered SiC toughened (Hexoloy SX)	Tension (Rods) and Flexure (Bars)		7.0	7.0?	Srinivasan et al., 42
Sintered with Al (Rioceram SiC)	C-ring	5.67 ± 0.60	8.16 ± 0.54	11.6 ± 0.8	Conway et al., 67
Sintered (Carolt S)	Flexure (Bars) (optical +SEM)		6.1, 6.8		Woodtli, 36
Hot-pressed SiC (NC-203)	Flexure (Rods) Flexure (Rods) Delayed Fracture		11.4 11.9		Kirchner et al., 8
Hot-pressed SiC (NC-203)	Flexure (Rods)		11.5		Kirchner et al., 9
Hot-pressed SiC (ACE)	Flexure (Rods)		10.8		Kirchner + Gruver, 10
Siliconized SiC (KT)	Flexure		10.7		Mecholsky et al.,17
Reaction bonded SiC (Coors SCRB205)	C-ring	4.11 ± 0.31	5.22 ± 0.23	6.4 ± 0.4	Conway et al., 67
SILICON NITRIDE					
Sintered Reaction Bonded (Ceralloy 147-31N)	Flexure (Rods) Flexure (Bars)		8.47 ± 0.07 7.79 ± 0.02		Quinn et al., 26
Sintered (SSN-500 yttria/alumina)	Flexure (Bars)		5.8		Quinn et al., 23
Sintered (SN 220)	Flexure (Biaxial, ring on ring disks)			8.1 ± 2.4	Choi + Gyekenyesi 33
Sintered (AS 44)	Flexure (Biaxial, ring on ring disks)			10.9 ± 2.7	Choi + Gyekenyesi, 33
Hot-pressed (Ceralloy 147A)	Flexure (Bars)		7.83		Quinn et al., 23
Hot-pressed (NC-132)	Flexure (Rods)		9.2		Kirchner et al., 9
Hot pressed (NC-132)	Flexure (Rods) Flexure-(Rods) Delayed Fracture		8.9 9.2		Kirchner et al., 8
Hot-pressed (NC-132)	Flexure (Rods)		14.3		Kirchner + Gruver, 10
Hot-pressed (NC-132)	Flexure (Bars, 1100°C) Flexure (Biaxial ring on ring, 1100°C)		9.4 ± 1.2	7.9 ± 2.1?	Choi + Gyekenyesi, 33

Material	Technique	*Mirror-Mist* A_i	*Mist-Hackle or Mirror-Hackle* A_o	Branching A_b	Reference
Hot-pressed (HS-130)	Flexure		18.1		Mecholsky et al.,17
Hot-pressed (HS-130)	Flexure (Rods)		9.1		Kirchner et al., 8
Hot-isopressed (NT 154)	Flexure (Bars)		5.9 ± 0.14		Choi et al., 32, 33
Hot-isopressed 30 vol% SiC whiskers	Flexure (Bars)		6.6 ± 0.11		Choi et al., 32, 33
Hot-isopressed (GN-10)	Flexure (Biaxial ring-on-ring) Tension (Rods)		11.8 ± 1.4	10.3?	Choi + Gyekenyesi, 33
b' Sialon $Si_{6-z}Al_zO_zN_{8-z}$ (z=0.5) 4 wt% Y_2O_3 and Boron	Flexure (Bars)		5.8 to 9.8 various grades		McGarrity et al., 84
Reaction Bonded (NC 350)	Flexure (Bars)		3.89		Messier et al., 24
Reaction Bonded (NC 350)	Flexure (Bars)		3.19		Larsen + Walther, 28
Reaction Bonded (AME A25B)	Flexure (Rods)		4.2		Kirchner et al., 8
ZIRCONIA					
Ytttria stabilized (3Y-TZP)	Flexure (Bars)		9.95		Morrell et al., 43
Ytttria stabilized (3Y-TZP)	Flexure (Bars) Flexure (Biaxial Disk, piston on 3 ball)		8.6 ± 0.23 9.6 ± 0.23		Quinn et al, 50
Yttria stabilized (3Y-TZP, Lava)	Flexure (Bars)		10.7		Quinn et al., 58
Yttria stabilized (3.5Y-TZP)	Flexure (Biaxial, ring on ring disks)			11.5 ± 1.5	Choi + Gyekenyesi, 33
Calcia - partially stabilized PSZ As fired-quenched As fired, under-aged 1300°C Peak aged Peak aged Over aged	Flexure (Bars, 3-point)			9.9 15.5 19.2 22.1 25.3-	Kirchner et al., 80
Zircar (Alfred-Union Carbide, 0.4 mm, 5-6 mol% Y TZP)	Flexure (Bars)		15.2		Mecholsky et al.,17
Zyttrite (AFML, 10 mm, cubic)	Flexure (Bars)		7.4		Mecholsky et al.,17
SINGLE CRYSTALS					
Ammonium diphosphate	Flexure (Bars)		0.5		Mecholsky et al.,17
MgO, single crystal	Flexure (Bars)		5		Mecholsky et al.,17
$MgAl_2AlO_4$ Spinel	Flexure (Bars)		2.6		Mecholsky et al.,17
Quartz, $(11\bar{2}0)$ plane with tension in [0001] direction	Tension (Plates)			1.64	Ball + Payne, 78
MgO	?			4.3	Ball + Payne, 78
Sapphire (average of several planes)	Flexure		6.1		Mecholsky et al.,17
Sapphire (Tyco filaments c-axis parallel to fiber axis)	Tension Flexure		5.5 10.0		Abdel-Latif et al.,38
Sapphire	Flexure (Rods)		3.3		Abdel-Latif et al.,38

Material	Technique	*Mirror-Mist* A_i	*Mist-Hackle or Mirror-Hackle* A_o	Branching A_b	Reference
(Ruby rods, c axis ~60º off rod axis)					
SINGLE CRYSTALS - continued					
Sapphire Filament, c-axis parallel to fiber axis	Tension, 800 to 1000ºC	2.4	3.2		Rice, 51
Sapphire, a plane	Flexure (Bars, 4-point)			7.3 ± 0.6 7.1 ± 0.3 NZ (11)	Salem, 70
Sapphire	?			7.3	Ball + Payne, 78
Sapphire filament, c-axis parallel to fiber axis	Tension, 800 to 1000ºC	2.4	3.2		Rice, 51
Silicon {110} plane <110> dir {110} plane <100> dir	Flexure (Bars)		2.01 ± .14 1.61 ± .14		Tsai + Mecholsky, 72
Silicon	?			5.8	Ball + Payne, 78
YAG yttrium aluminum garnet (111)	Flexure (Bars)		2.20 ± 0.06		Mezeix + Green, 66
OTHER					
AlON (Surimet, 150-250 mm)	Flexure (Disks)	-	-	8.1± 0.1	Salem, 88
$3BaO\text{-}SiO_2$	Flexure (Bars)	3.9	6.0		Mecholsky et al.,17
B_4C hot-pressed	Flexure (Bars)	4.8	9.27		Mecholsky et al.,17
B_4C hot-pressed (CoorsTek PAD)	Flexure (Bars) Tension (Buttonhead rods)		8.8 7.0		Swab et al., 83
$BaTiO_2$ (2 grades)	Flexure (Bars)		5.0, 5.4		Mecholsky et al.,17
$CaLa_2S_4$, Hot press + HIP	Flexure (Biaxial, ring-on-ring)			2.4	Swab + Shoulders,89
Chromium	?			4.5	Ball + Payne, 78
Mullite	Flexure		6.1		Mecholsky et al.,17
MgO	Flexure		9.6		Mecholsky et al.,17
MgO	Tension (Plates)			4.3	Congleton+Petch,2
MgO, single crystal	Flexure (Bars)		5		Mecholsky et al.,17
MgF_2 (Kodak)	Flexure (Bars)	1.8	3.1		Mecholsky et al.,17
MgF_2 (Kodak, IRTRAN 1)	Flexure (Bars and Biaxial Disks)			4.4	Mecholsky + Rice, 20
$MgAl_2AlO_4$ Spinel	Flexure (Bars)	4.0	7.8		Mecholsky et al.,17
$MgAl_2AlO_4$ Spinel, single crystal	Flexure (Bars)		2.6		Mecholsky et al.,17
PMMA	?		8.5 *	8.5 *	Ball + Payne, 78
PMMA	Tension plate			8.7	Congleton, 81
Porcelain aluminous electrical insulator	Flexure (Rods, 3-point)		~ 3.5		Carlström + Carlsson, 74
PZT	Flexure	1.7	3.7		Mecholsky et al.,17
Graphite (POCO)	Flexure		3.32		Mecholsky et al.,17
$SrZrO_3$	Flexure (Bars)	4.4	6.0		Mecholsky et al.,17
Steatite (Mg silicate insulator, DC -144)	Flexure (Rods)		4.8 4.5		Kirchner et al., 8,9 Kirchner, 10
WC-Co 6% Ni (Kennametal)	Flexure (Disks, biaxial, pressure-on-ring (POR) POR + ring-on-ring			8.2 NZ Ã (1154) 14.NZ Ã (329)	Salem et al., 79
WC-Co 10% Co (Kennametal KFS64/ S105) (0.5 mm –0.8 mm)	Flexure (Rods) Tension (Rods)		17 ± 2.0 16 ± 2.7		Pittari, Swab et al., 87
WC-Co 11.5 – 12.0 % Co (Ceratizit 3 grades) WC-Co	Flexure (Rods) 1.9 mm 0.8 mm 0.4 mm Tension (Dumbbell) 1.9 mm		26 ± 4.6 22 ± 2.3 21 ± 2.6 26 ± 3.2		Pittari, Swab et al., 87

Material	Technique	*Mirror-Mist* A_i	*Mist-Hackle or Mirror-Hackle* A_o	Branching A_b	Reference
11.5 – 12.0 % Co (Ceratizit 3 grades)	0.8 mm 0.4 mm		20 ± 3.6 21 ± 2.9		Pittari, Swab et al., 87
WC-Co 1% Co 2% Ni (Cercom)	Flexure (Bars?- 4-point)		3.6 NZ Ä (493)		Salem, et al., 79
WC (no Co)	Flexure		10 Ä		Swab et al., 46
Yttrium Aluminum Garnet, 0.2 mm poly.	Flexure (Bars)		2.15 ± 0.08		Mezeix + Green, 66
Yttrium Aluminum Garnet, single crystal (111)	Flexure (Bars)		2.20 ± 0.06		Mezeix + Green, 66
Zircon Porcelain (Alsimag 475)	Flexure (Rods)		4.0		Kirchner et al., 8,9
ZnS, CVD	Flexure (Disk, biaxial, ring-on-ring)			2.3	Swab + Shoulders, 89
ZnS, CVD + HIP	Flexure (Disk, biaxial, ring-on-ring)			1.1	Swab + Shoulders, 89
ZnSe	Flexure (Bars)			1.7	Mecholsky et al.,17
ZnSe (44 mm)	Flexure (Biaxial, ring-on-ring disks)			0.8, 1.0 #	Salem, 65
FIBERS					
Alkali-borosilicate	Tension	1.33 NZ			Jaras et al.,12
Chalcogenide As-S-Se and Ge-AS-Se-Te	Flexure, 2-point bending	1.58 1.77±0.14NZ (-66.4 ± 45.5)			Quinn et al., 75
Chalcogenide As_2Se_3	Tension	0.69 (0.35 if UV irradiated)	0.77 (0.38 if UV irradiated)		Hulderman et al., 45
E-glass $CaO-Al_2O_3-B_2O_3$ alumina borosilicate	Tension	1.47 NZ			Jaras et al., 12
E-glass glass wool fibers	Tension	2.1			Lund + Yue, 85
Basaltic glass wool fibers	Tension	2.3 to 2.4			Lund + Yue, 85
Fused silica fibers	Tension	2.10			Choi+ Gyekenyesi, 33
Fused silica clad fibers	Tension	1.96 ± 0.13			Baker + Glaesemann, 29
Fused silica fibers	Tension	1.83			Castilone et al., 30
Fused silica fibers	Tension	2.2 ± 0.5			Mecholsky + Rice, 20
Fused silica fibers	Tension	2.224			Chandan + Parker, 37
Si-Ti-C-O (Tyranno LoxM)	Fibers in a 3-D SiC matrix composite		2.50 ± 0.09		Davies +Ishikawa, 53
Si-C-O (Nicalon) Si-C-N-O fibers Si-N-C-O fibers	Tension		~2		Sawyer et al., 54
Si-C-O (Nicalon)	Fibers in a 2-D CVI SiC matrix composite		2.51		Eckel + Bradt, 55
Sapphire filament, c-axis parallel to fiber axis	Tension, 800 to 1000°C	2.4	3.2		Rice, 51
Zirconia silicate (Cem-FIL AR)	Tension (Fibers)	2.37 NZ			Jaras et al., 12

REFERENCES

1. J. W. Johnson and D. G. Holloway, “On the Shape and Size of the Fracture Zones on Glass Fracture Surfaces,” *Phil. Mag.*, **14** [130] (1966) 731 - 743.
2. J. Congleton and N. J. Petch, “Crack Branching,” *Phil. Mag.*, **16** [142] (1967) 749 - 760.
3. E. B. Shand, “Breaking Stress of Glass Determined from Dimensions of Fracture Mirrors,” *J. Amer. Ceram. Soc*., **42** [10] (1959) 474 - 477.
4. E. B. Shand, “Breaking Stresses of Glass Determined from Fracture Surfaces,” *The Glass Industry*, April 1967, 90 - 94.
5. L. Orr, “Practical Analysis of Fractures in Glass Windows,” *Materials Research and Standards*, **12** [1] (1972) 21 - 23.
6. M. J. Kerper and T. G. Scuderi, “Modulus of Rupture of Glass in Relation to Fracture Pattern,” *Bull. Amer. Ceram. Soc.*, **43** [9] (1964) 622 - 625.
7. M. J. Kerper and T. G. Scuderi, “Relation of Fracture Stress to the Fracture Pattern for Glass Rods of Various Diameters,” *Bull. Am. Ceram. Soc*., **45** [12] (1966) 1065 - 1066.
8. H. P. Kirchner, R. M. Gruver, and W. A. Sotter, “Fracture Stress-Mirror Size Relations for Polycrystalline Ceramics,” *Phil. Mag.*, **33** [5] (1976) 775 - 780.
9. H. P. Kirchner, R. M. Gruver, and W. A. Sotter, “Use of Fracture Mirrors to Interpret Impact Fracture in Brittle Materials,” *J. Am. Ceram. Soc.*, **58** [5–6] (1975) 188 - 191.
10. H. P. Kirchner, and R. M. Gruver, “Fracture Mirrors in Polycrystalline Ceramics and Glass,” pp. 309 – 321 in *Fracture Mechanics of Ceramics 1*, eds., R. C. Bradt, D. P. H. Hasselman, and F. F. Lange, Plenum, NY, 1973.
11. H. P. Kirchner and R. M. Gruver, “Fracture Mirrors in Alumina Ceramics,” *Phil. Mag.*, **27** [6] (1973) 1433 - 1446.
12. A. C. Jaras, B. J. Norman, and S. C. Simmons, “The Measurement of Glass Fibre Strength in Composites from Studies of Their Fracture Surfaces,” *J. Mat. Sci*., **18** (1983) 2459-2465.
13. G. K. Bansal and W. H. Duckworth, “Fracture Stress as Related to Origin and Fracture Mirror Sizes,” *J. Am. Ceram. Soc.*, **60** [7–8] (1977) 304 - 310.
14. G. K. Bansal, “On Fracture Mirror Formation in Glass and Polycrystalline Ceramics,” *Phil. Mag.*, **35** [4] (1977) 935 - 944.
15. D. K. Shetty, A. R. Rosenfeld, and W. H. Duckworth, “Crack Branching in Ceramic Disks Subjected to Biaxial Flexure,” *Comm. of the Amer. Ceram. Soc.*, Jan. 1983, C10 - C13.
16. W. H. Duckworth, D. K. Shetty, and A. R. Rosenfeld, “Influence of Stress Gradients on the Relationship Between Fracture Stress and Mirror Size for Float Glass,” *Glass Technology*, **24** [5] (1983) 263 - 273.
17. J. J. Mecholsky, Jr., S. W. Freiman, and R. W. Rice, “Fracture Surface Analysis of Ceramics,” *J. Mat. Sci.*, **11** (1976) 1310 - 1319.
18. J. J. Mecholsky, Jr., R. W. Rice, and S. W. Freiman, “Prediction of Fracture Energy and Flaw Size in Glasses from Measurements of Mirror Size,” *J. Amer. Ceram. Soc*., **57** [10] (1974) 440 - 443.
19. D. B. Marshall, B. R. Lawn, and J. J. Mecholsky, “Effect of Residual Contact Stresses on Mirror/Flaw Size Relations,” *J. Amer. Ceram. Soc.*, **63** [5-6] (1980) 358 - 360.
20. J. J. Mecholsky, Jr., and R. W. Rice, “Fractographic Analysis of Biaxial Failure in Ceramics,” pp. 175 – 193 in *Fractography of Ceramics and Glass Failures*, ASTM STP 827, eds., J. Mecholsky and S. Powell, ASTM, Westerville, OH, 1984.
21. J. J. Mecholsky, A. C. Gonzalez, and S. W. Freiman, “Fractographic Analysis of Delayed Failure in Soda Lime Glass,” *J. Am. Ceram. Soc.*, **62** [11-12] (1979) 577 - 580.
22. J. J. Mecholsky, “Quantitative Fractographic Analysis of Fracture Origins in Glass,” pp. 37 – 173 *in Fractography of Glass*, eds., R. C. Bradt and R. E. Tressler, Plenum, NY, 1994.

23. G. D. Quinn, D. R. Messier, and L. J. Schioler, "Characterization of Ceramic Vane Materials for 10 kW Turboalternator," U.S. Army Materials and Mechanics Research Center Technical Report TR 83-18, April 1983.
24. D. R. Messier, L. J. Schioler, and G. D. Quinn, "Fracture Behavior and Strength of Reaction-Bonded Si_3N_4 Turbine Shrouds," *Bull. Am. Ceram. Soc.*, **60** [8] (1981) 812 - 817.
25. J. B. Quinn, "Extrapolation of Fracture Mirror and Crack-Branch Sizes to Large Dimensions in Biaxial Strength Tests of Glass," *J. Am. Ceram. Soc.*, **82** [8] (1999) 2126 - 2132.
26. G. D. Quinn, L. K. Ives, S. Jahanmir, and P. Koshy, "Fractographic Analysis of Machining Cracks in Silicon Nitride Rods and Bars," pp. 343 – 365 in *Fractography of Glasses and Ceramics, IV, Ceramic Transactions,* Vol. 122, eds., J. R. Varner and G. D. Quinn, American Ceramic Society, Westerville, OH, 2001.
27. P. B. Adams and S. E. DeMartino, "Glass-Ceramic Cookware Failure Analysis," pp. 669 – 673 in *Engineered Materials Handbook, Vol. 4, Ceramics and Glasses*, ASM, Metals Park, OH, 1991.
28. D. C. Larsen and G. C. Walther, "Property Screening and Evaluation of Ceramic Turbine Engine Materials," IIT Research Institute, Chicago, IL, Interim Technical Report No. 5, IITRI D 6114-ITR-30, 1978.
29. L. K. Baker and G. S. Glaesemann, "Break Source Analysis, Alternate Mirror Measurement Method," *Proc. Inter. Wire and Cable Sympos.*, Philadelphia, PA, 1998, 933 - 937.
30. R. J. Castilone, G. S. Glaesemann, and T. A. Hanson, "Relationship Between Mirror Dimensions and Failure Stress for Optical Fibers," pp. 11 – 20 in *Optical Fiber and Fiber Component Mechanical Reliability and Testing II,* eds., J. Matthewson and C. R. Kurkjian, Proc. of SPIE, Vol. 4639, 2002.
31. J. A. Salem, S. R. Choi, and L. M. Powers, "Toughened Ceramics Life Prediction," in Ceramic Technology Project Semiannual Progress Report for October 1992 Through March 1993, Oak Ridge National Laboratory Technical Report TM 12428, Sept. 1993, 307 - 316.
32. S. R. Choi and J. A. Salem, "Indentation Flaw Formation and Strength Response of Silicon Nitride Ceramics at Low Indentation Loads," *J. Mat. Sci. Lettrs*, **11** (1992) 1398–1400.
33. S. R. Choi and J. P. Gyekenyesi, "Crack Branching and Fracture Mirror Data of Glasses and Advanced Ceramics," NASA Technical Report TM 1998-206536, 1998.
34. A. B. J. Clark and G. R. Irwin, "Crack Propagation Behaviors," *Experimental Mechanics*, **6** [6] (1966) 321 - 330.
35. S. Aoki and M. Sakata, "Crack Bifurcation Under Hydrostatic Pressure," *Engineering Fracture Mechanics*, **13** [3] (1980) 491 – 499.
36. J. Woodtli, "Quantitative Fractographie in Keramik: Auswertung von Spiegelzonen in SiC," Swiss Federal Laboratories for Materials Testing and Research, Report 157361, Dec. 1997.
37. H. C. Chandan and R. D. Parker, "Fractography of Optical Fibers," pp. 143 - 184 in *Fractography of Glass*, eds., R. C. Bradt and R. E. Tressler, Plenum Press, NY, 1994.
38. A. Abdel-Latif, R. Tressler, and R. C. Bradt, "Fracture Mirror Formation in Single Crystal Alumina," *Fracture 1977*, Vol. 3, ed. D. Taplin, Univ. Waterloo Press, 1977, 933 - 939.
39. D. A. Reed and R. C. Bradt, "Fracture Mirror-Failure Stress Relations in Weathered and Unweathered Window Glass Panels," *Comm. Am. Ceram. Soc.*, Nov. 1984, C 227 – C 229.
40. M. J. Ball, D. J. Landini, and R. C. Bradt, "Fracture Mist Region in a Soda-Lime Silica Float Glass," pp. 110-120 in *Fractography of Ceramic and Metal Failures, ASTM STP 827,* J. Mecholsky, Jr., and S. Powell, eds., ASTM, 1984.
41. S. Bartolucci Luyckx, and A. Sannino, "Crack Branching and Fracture Mirrors in Cemented Tungsten Carbide," *J. Mat. Sci.*, **23** (1988) 1243 - 1247.
42. G. V. Srinivasan, J. Gibson, and S. K. Lau, "The Origin of Strength Limiting Defects in a Toughened SiC (Hexoloy SX-SiC), pp. 181 – 192 in *Fractography of Glasses and Ceramics*

III, *Ceramic Transactions* Vol. 64, eds., J. R. Varner, V. D. Fréchette, and G. D. Quinn, American Ceramic Society, Westerville, OH, 1996.

43. R. Morrell, L. Byrne, and M. Murray, "Fractography of Ceramic Femoral Heads," pp. 253 – 266 in *Fractography of Glasses and Ceramics, IV,* Ceramic Transactions, Vol. 122, eds., J. R. Varner and G. D. Quinn, American Ceramic Society, Westerville, OH, 2001.
44. D. Lewis, III, "Fracture Strength and Mirror Size in a Commercial Glass-Ceramic," *J. Am. Ceram. Soc.*, **64** [2] (1961) 82 - 86.
45. F. Hulderman, J. S. Sanghera, and J. D. Mackenzie, "The Effect of UV Radiation on the Mechanical Strength of As_2Se_3 Glass Fibers," *J. Non-Cryst. Sol.*, **127** (1991) 312 - 322.
46. J. J. Swab, J. C. LaSalvia, and W. A. Gooch, "Characterization of WC-Based Armor Ceramics," unpubl. priv. com., U.S. Army ARL, Aberdeen Proving Ground, MD, 21005.
47. J. R. Kelly, "Fractography of Dental Ceramics," pp. 241-251 in *Fractography of Glasses and Ceramics, IV*, eds., J. R. Varner and G. D. Quinn, Ceramic Transactions Vol. 122, American Ceramic Society, Westerville, OH 43081, 2001.
48. D. N. Coon, "Mirror/Mist Radius Constant for Y-Al-Si-O-N Glass," *J. Mat. Sci. Lettrs*., **21** (2002) 1121 - 1122.
49. A. Abdel-Latif, R. C. Bradt, and R. E. Tressler, "Dynamics of Fracture Mirror Boundary Formation in Glass," *Int. J. Fract.*, **13** [3] (1977) 349 - 359.
50. G. D. Quinn, J. Eichler, U. Eisele, and J. Rödel, "Fracture Mirrors in a Nanoscale 3Y-TZP," *J. Am. Ceram. Soc.*, **87** [3] (2004) 513 - 516.
51. R. W. Rice, "Corroboration and Extension of Analysis of c-Axis Sapphire Filament Fractures from Pores," *J. Mat. Sci. Lttrs*., **16** (1997) 202 - 205.
52. H. Fischer, J. Gröbel, and R. Marx, "Fraktograpische Schadensanalyse an Dentalkeramik," *Deutsche Zahnarztl. Zeitschrifft*, **55** [10] (2000) 667 - 670.
53. I. J. Davies and T. Ishikawa, "Mirror Constant for Tyranno Silicon-Titanium-Carbon-Oxygen Fibers Measured in Situ in a Three-Dimensional Woven Silicon Carbide/Silicon Carbide Composite," *J. Am. Ceram. Soc.*, **85** [3] (2002) 691 - 693.
54. L. C. Sawyer, M. Jamieson, D. Brikowski, M. I. Haider, and R. T. Chen, "Strength, Structure, and Fracture Properties of Ceramic Fibers Produced from Polymeric Precursors: I: Base-Line Studies," *J. Amer. Ceram. Soc.*, **70** [11] (1987) 798 - 810.
55. A. J. Eckel and R. C. Bradt, "Strength Distribution of Reinforcing Fibers in a Nicalon Fiber/Chemically Vapor Infiltrated Silicon Carbide Matrix Composite," *J. Am. Ceram. Soc.*, **72** [3] (1989) 455 - 458.
56. O. E. Alarcón, R. E. Medrano, and P. P. Gillis, "Fracture of Glass in Tensile and Bending Tests," *Metall. Mat. Trans A*, **25A**, May (1994) 961 - 967.
57. S. T. Gulati, J. F. Bayne, W. R. Powell, and J. D. Helfinstine, "Mirror Constant for AMLCD Glass," *Bull. Am. Ceram. Soc.*, **83** [5] (2004) 14 - 15.
58. J. B. Quinn, D. Cheng, R. Rusin, and D. Suttor, "Fractographic Analysis and Material Properties of a Dental Zirconia," International Association for Dental Research (IADR) paper, 0560, Baltimore, MD, March 2005.
59. J. B. Quinn and G. D. Quinn, "Materials Properties and Fractography of an Indirect Dental Resin Composite," *Dent. Mater*., **26** (2010) 589 - 599.
60. N. Shinkai and H. Ishikawa, "Crack Branching of Binary $PbO-B_2O_3$ Glasses," *J. Noncryst. Solids*., **52** [1-3] (1982) 385 - 394.
61. R. E. Bullock and J. L. Kaae, "Size Effect on the Strength of Glassy Carbon," *J. Mat. Sci.*, **14** (1979) 920 - 930.
62. J. M. Barsom, "Fracture of Tempered Glass," *J. Am. Ceram. Soc*., **51** [2] (1968) 75 - 78.
63. N. Terao, "Sur ene Relation entre la Résistance à la Rupture et le Foyer d'Eclatement du Verre," *J. Phys. Soc. Jap.*, **8** [4] (1953) 545 - 549.

64. W. C. Levengood, "Effect of Origin Flaw Characteristics on Glass Strength," *J. Appl. Phys.*, **29** [1] (1958) 820 - 826.
65. J. A. Salem, "Mechanical Characterization of ZnSe Windows for Use with the Flow Enclosure Accommodating Novel Investigations in Combustion of Solids (FEANICS) Module," NASA Tech. Rep. TM-2006-214100, NASA-Glenn Center, Cleveland, OH, 2006.
66. L. Mezeix and D. J. Green, "Comparison of the Mechanical Properties of Single Crystal and Polycrystalline Yttrium Aluminum Garnet," *Int. J. Appl. Cer. Technol*, **3** [2] (2006)166-176.
67. J. C. Conway, Jr., J. J. Mecholsky, O. M. Jadaan, and D. L. Shelleman, "Test Methodology for Ceramic Tubular Components," CAM Res. Report, Pennsylvania State University, 1989.
68. J. R. Varner and H. J. Oel, "Einfluss von Oberflächenbeschädigungen auf die Festigkeit von Glasstäben, " *Grastechn. Ber*., **48** [5] (1975) 73 – 78.
69. N. Shinkai, "Fracture Mirror Constants of Silicate Glasses," *Japan J. Appl. Phys.*, **14** [1] (1975) 147 - 148.
70. J. A. Salem, Private communication, March, 2008.
71. J. R. Varner and H. J. Oel, "Surface Defects: Their Origin, Charcaterization and effects on Strength," *J. Non-Cryst. Sol*., **19** (1975) 321 - 333.
72. Y. L. Tsai and J. J. Mecholsky, Jr, "Fractal Fracture of Single Crystal Silicon," *J. Mater. Res.*, **6** [6] (1991) 1248 - 1263.
73. O. Gaume and S. Pelletier, "Analysis of Fracture Featrures for Uniaxial Bent Glass Plates," in *2002 Glass Odyssey*, proc. 6th ESG conf., June 26, 2002, Montpellier, France.
74. E. Carlström and R. Carlsson, "A Fractographic Study of Electrical Porcelains Containing Alumina," *J. De Physique*, **47** (C-1) (1986) 563 - 567.
75. J. B. Quinn, V. Q. Nguyen, J. S. Sanghera, I. K. Lloyd, P. C. Puzera, R. E. Miklos, and I. D. Aggarwal, "Strength and Fractographic Analysis of Chalcogenide AS-S-Se and Ge-As-Se-Te Glass Fibers," *J. Non-Cryst. Sol*., **325** (2003) 150 - 157.
76, S. Hecht-Mijic, "Fracture Mirror Constants of Bioceramics for Hip Joint Replacement: Determination and Application, " pp. 303 -312 in *Fractography of Glasses and Ceramics V*, eds., J. R. Varner, G.D. Quinn, M. Wightman, Ceramic Transactions Vol. **199**, American Ceramic Society, Westerville, OH, 2007.
77. J. A. Salem, N. Smith, and A. Ersahin, "Mechanical Properties of a High Lead Glass Used in the Mars Organic Molecule Analyzer," NASA Glenn Research Center, Cleveland, OH, Technical Report, TM 2015-218847, August 2015.
78. A. Ball and B. W. Payne, "The Propagation and Bifurcation of Cracks in Quartz," pp. 971 – 978 in *Fracture 1977, Vol. 3*, Waterloo, Canada, 1977.
79. J. A. Salem, S. Slingluff, R. Rogers, and J. J. Swab, "Stress Gradients and Crack Branching in Tungsten Carbide," unpublished research, 2015.
80. H. P. Kirchner, R. M. Gruver, M. V. Swain, and R. C. Garvie, "Crack Branching in Transformation-Toughened Zirconia," *J. Am. Ceram. Soc.*, **64** [9] (1981) 529 - 533.
81. J. Congleton, "Practical Applications of Crack-Branching Measurements," pp. 427 – 438 in *Dynamic Crack Propagation*, ed. G. C. Sih, Noordhoff, Leyden, NL, 1973.
82. D. R. Oakley, "Crack Branching in Float Glass Subjected to Biaxial Loading," *J. Non-Cryst. Sol.*, **196** (1996) 139 – 143.
83. J. J. Swab, J. J. Pittari, and W. R. Gamble, "Uniaxial Tensile Strength and Fracture Analysis of a Hot-Pressed Boron Carbide," *J. Eur Cer. Soc.*, **39** [6] (2019) 1965 – 1973.
84. K. McGarrity, P. Tumurugoti, K. Ning, and H. Shulman, "Fractography of Silicon Nitride Based Ceramics to Guide Process Improvements," *J. Eur Cer. Soc.*, **40** (14) (2020) 4746 - 4752.
85. M. D. Lund and Y. Yue, "Fractography and Tensile Strength of Glass Wool Fibres," *J. Cer. Soc. Japan*, **116** [8] (2008) 841 – 845.

86. N. Shinkai and M. Hara, “Determination of the Breaking Strength of Glass from the Fracture Pattern,” *Reports of the Res. Laboratory, Asahi Glass Co.*, **19** [2] (1969) 73 - 84.
87. J. J. Pittari III, J. J. Swab, J. Wright, and K. Atwater, “Mechanical Evaluation of WC-Co Materials with Varying Microstructure,” *Int. J. Refr. Metals Hard. Mat.* **104** (2022) 105809.
88. J. A. Salem, “Crack Growth Testing of an Aluminum Oxynitride (AlON) for International Space Station Kick Plates,” NASA TM-2017-219165, NASA Glenn Research Center, Cleveland, OH, 2017.
89. J. J. Swab and W. T. Shoulders, “Equibiaxial Flexure Strength and Fractography of Long-Wave Infrared Materials,” *J. Eur Cer Soc.*, **43** (2023) 7059 - 7067.
90. S. Kim and S. Choi, “AMLCD Glass Mirror Constant and Crack Flaw Size in Non-Crack LCD Panels,” *J. Info. Display*, **18** [1] (2017) 19 - 24.

APPENDIX D GUIDELINES FOR MEASURING FRACTURE MIRRORS

D.1 Introduction

This appendix presents a set of guidelines for measurement of fracture mirrors in glasses and ceramics. (The appendix has a few minor editorial revisions compared to the 3rd edition.) The guidelines were originally presented by the author at the Fifth Conference on the Fractography of Glasses and Ceramics in Rochester New York in 2006.[1] That paper extensively reviewed the historical development (going back as far as 1894) of fracture mirror analysis as a quantitative tool for glasses and ceramics. These guidelines were adopted in an ASTM standard C 1678 [2] in 2007.

Fracture mirror measurements are a powerful diagnostic tool for quantitative analysis. Mirrors are circular in ideal loading conditions such as uniform tension specimens. Otherwise, they can be elongated or distorted due to stress gradients or geometrical effects. There is a strong subjective element to estimating the location of the mirror boundary.[3]

Since many of the early mirror measurements were made while viewing through the optical microscope, it is safe to say that the first perception of a mirror boundary was where the surface roughness was a fraction of the wavelength of light (0.39 mm - 0.80 mm). Threshold levels of detectability have been estimated to be as small as a few tens of nanometers to as much as 0.25 mm. Attempts to make objective determinations of the mirror boundary by quantitative surface roughness characterization are discussed in section D.3 below, but a single threshold roughness value cannot be specified.

Some of the following recommendations are based on common sense. Others are based upon the experiences of the author and other experts. The empirical mirror relationship for a residual stress-free part is:

$$s\sqrt{R} = A \qquad \text{(D.1)}$$

where s is the stress <u>at the origin site,</u> R is the mirror radius, and A is the appropriate mirror constant as described below. As discussed in detail in Reference 1, Leighton Orr recognized as early as 1945 that stress varied inversely with the square-root dependence of the mirror radius, so the author now refers to equation D.1 as “Orr’s equation.”

The boundary criteria are:

The mirror-mist boundary in *glasses* is the periphery where one can discern the onset of mist. This boundary corresponds to A_i, the inner mirror constant.

The mist-hackle boundary in *glasses* is the periphery where one can discern the onset of systematic hackle. This boundary corresponds to A_o, the outer mirror constant.

The mirror-hackle boundary in *polycrystalline ceramics* is the periphery where one can discern the onset of systematic new hackle and there is an obvious roughness change relative to that inside the mirror region. This boundary corresponds to A_o, the outer mirror constant. Ignore premature hackle and/or isolated steps from microstructural irregularities in the mirror or irregularities at the origin.

In coarse-grained or porous materials, it may be impossible to identify a mirror boundary. In polycrystalline ceramics, it is highly unlikely that a mirror-mist boundary can be detected due to the inherent roughness created by the crack-microstructure interactions even within the mirror. Another reason a boundary may not be evident is that in very weak materials, the mirror may be larger than the specimen or component.

If the mirror is being measured for a component failure analysis, and if the mirror constant A is known, follow steps 1 through 9 in the next section and compute the stress *at the origin* in accordance with equation D.1. Note that this origin stress may or may not necessarily be the *maximum* stress in the part.

On the other hand, if the fracture mirror constant A is being evaluated by means of testing laboratory specimens and the origin stresses are known, follow steps 1 through 12.

Examples of how to judge the boundaries are shown in Figures D.1 through D.6. Low power images provide an overview. Matching unmarked and marked images are shown so that the reader can make a judgment for comparison. The boundaries were assessed while looking through a microscope and the digital images in Figures D.1 to D.6 were marked. Mirrors should be evaluated while looking in a microscope and not solely on photos. Although some of the mirrors are approximately circular or semicircular, examples of common alternative shapes are presented. As discussed in detail in my 2006 review paper,[1] Kirchner et al.[4,5] presented compelling evidence that fracture mechanics analyses account for stress gradient and geometric effects upon mirror shapes.

(a)

(b)

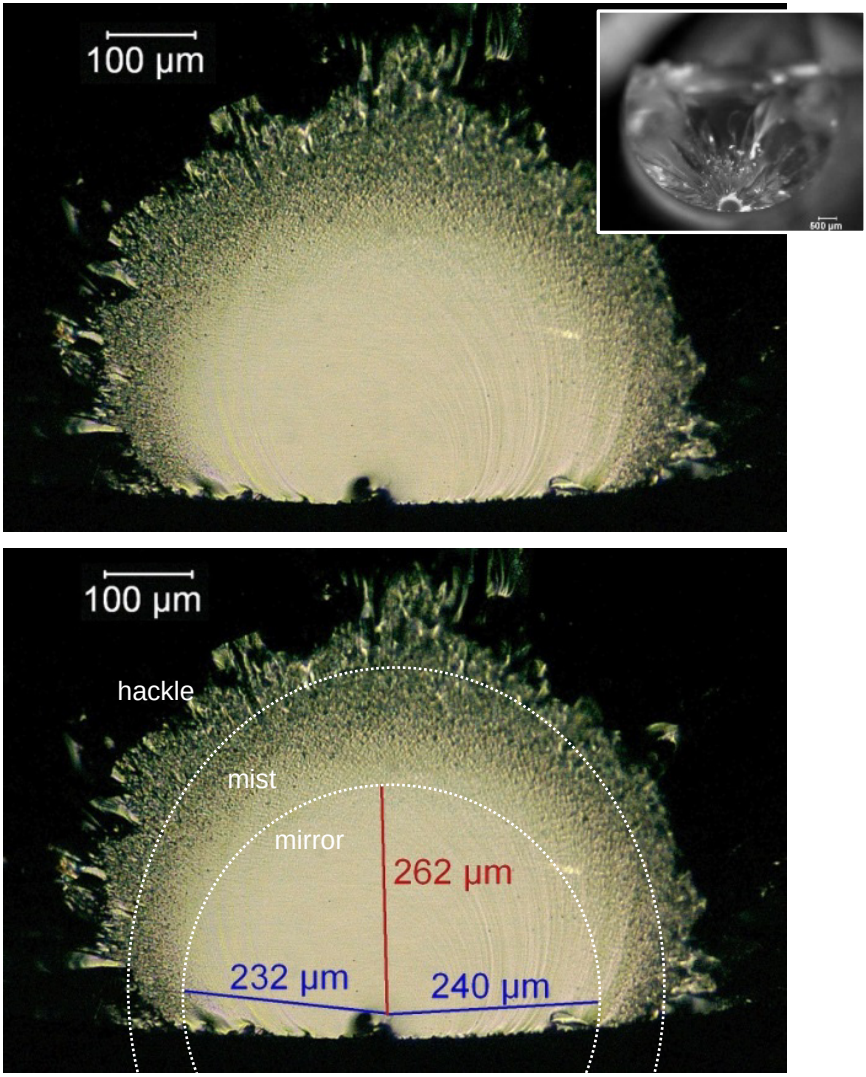

Figure D.1 *Optical images of a fused silica glass rod broken in flexure (122 MPa). The origin is a surface flaw located at the bottom of the specimen (the insert in a) where the stress was a maximum. A stress correction is unnecessary. The mirror-mist boundary is small relative to the cross-section size and is approximated by a circle in (b). The inward cusps at the surface on the left and right are ignored as discussed in section D.3. The mist – hackle boundary is slightly elongated towards the top. Close examination of the fracture surface in the vicinity of the flaw (not shown) showed that fracture started from the deepest part of the flaw. (c) and (d) on the next page show SEM images of the same mirror.*

(c)

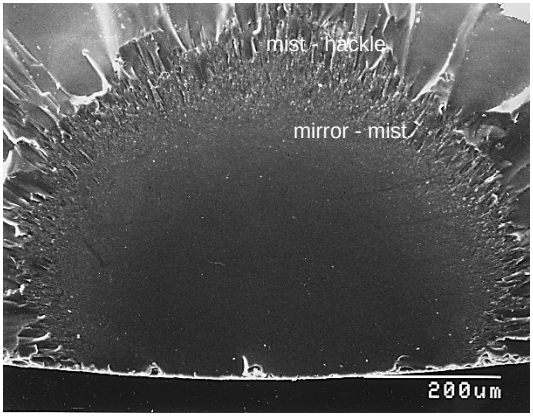

(d)

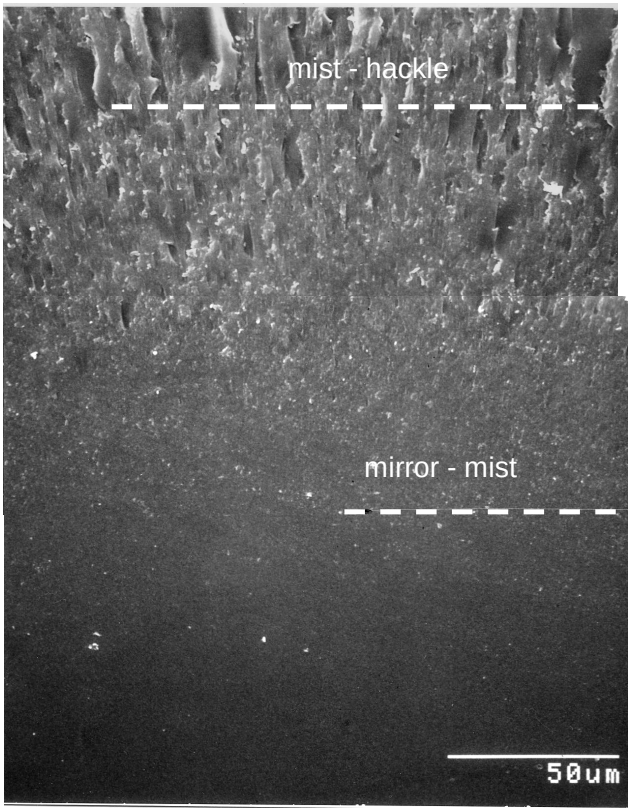

Figure D.1 continued *(c) is an SEM image of the same mirror and at the same magnification as (a) and (b). The mist is indistinct in the SEM image. (d) is a composite of two SEM images at a higher magnification showing the transition from mirror to mist to hackle. The locations of the boundaries as assessed by* <u>*optical*</u> *microscopy (as shown in b) are marked by two dashed lines on the SEM images.*

(a)

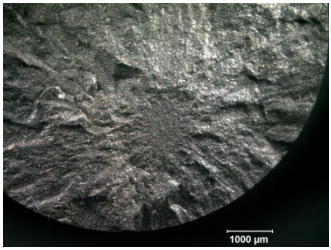

(b)

(c)

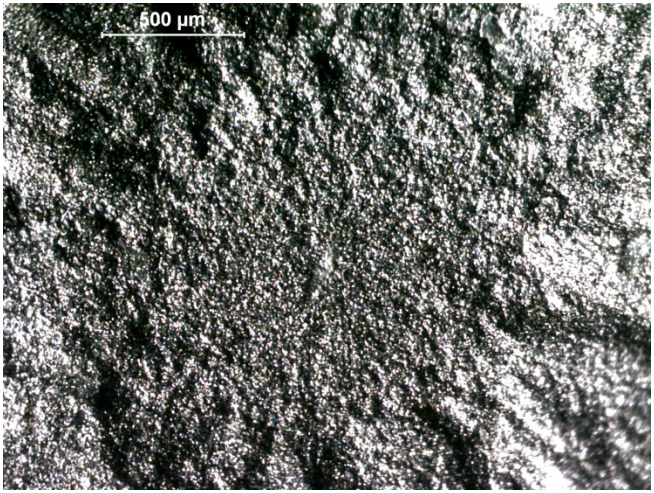

(d)

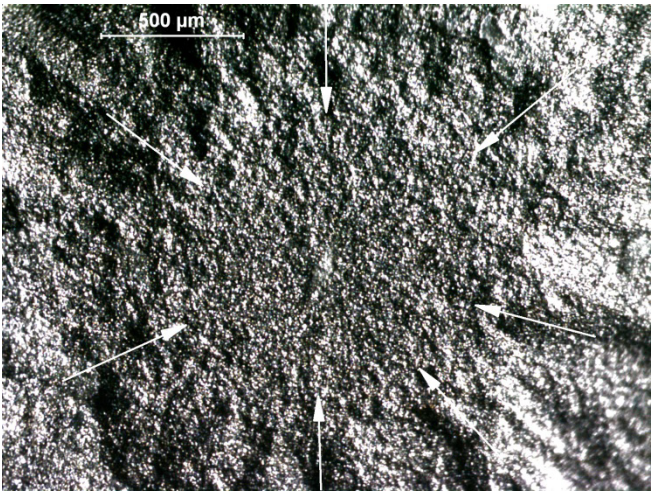

Figure D.2 *Optical images of a dense silicon carbide tension strength specimen (371 MPa) with a mirror centered on a compositional inhomogeneity flaw shown in Figures 6.23a,b. Note how clear the mirror is in the low power images. The mirror boundary (arrows in d) is where systematic new hackle forms and there is an obvious difference compared to the roughness inside the mirror region.*

(a)

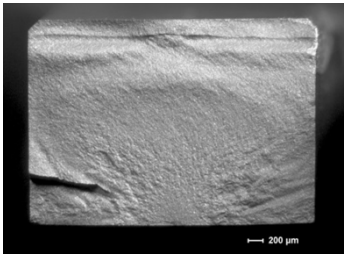

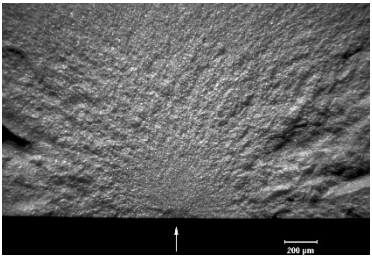

(b)

(c)

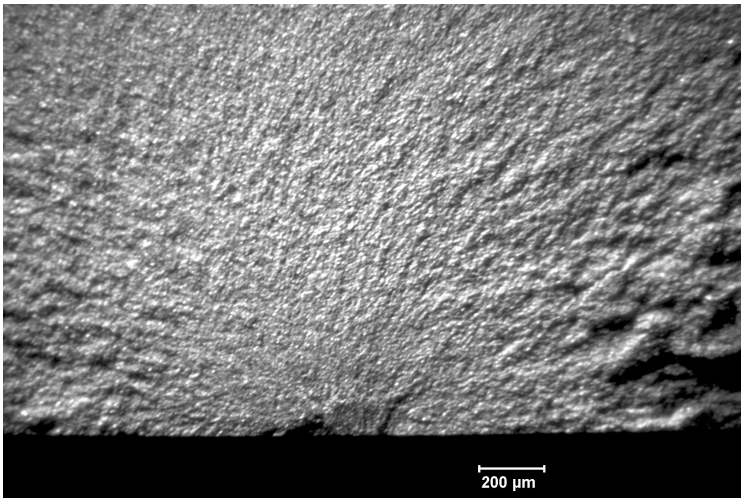

(d)

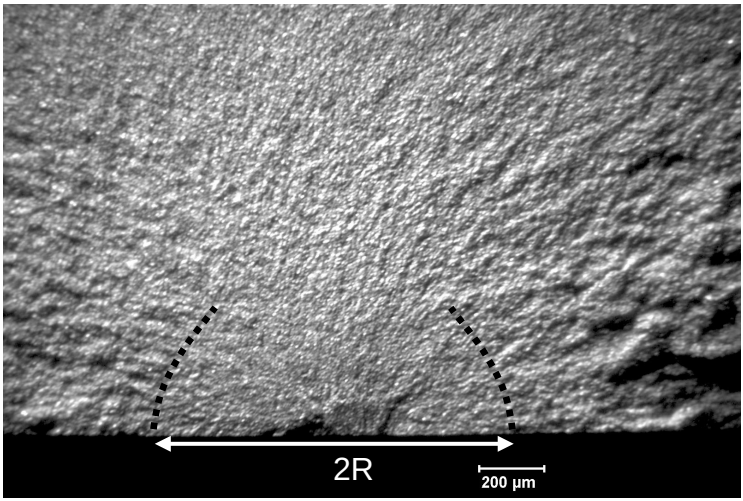

Figure D.3 *Optical images of a dense, fine-grained, silicon nitride bend bar with a Knoop surface crack origin flaw (449 MPa, Ceralloy 147-31N, Refs. 6,7). The mirror is incomplete into the stress gradient, but the mirror sides can be used to construct boundary arcs in (d). Radii are measured in the direction of constant stress along the bottom.*

(a)

(b)

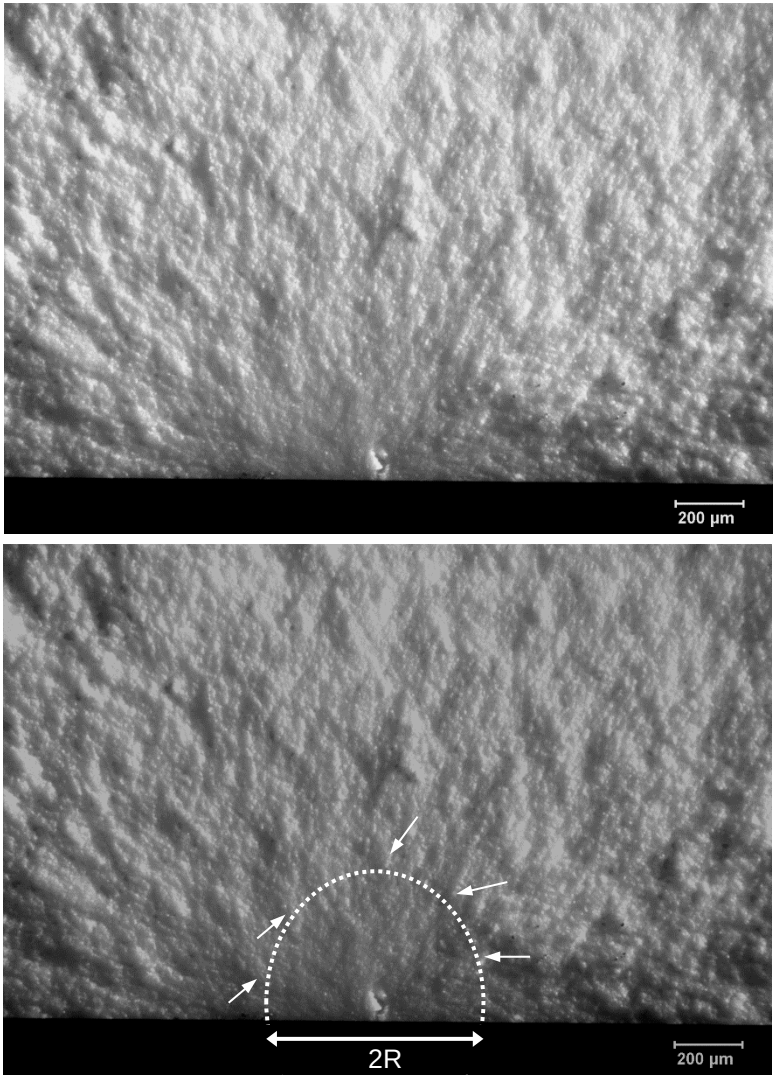

Figure D.4 *Optical images of a mirror in a fine-grained 3 mol % yttria-stabilized tetragonal zirconia (3Y-TZP) polycrystal (Bosch, Ref. 8). The mirror is difficult to mark in this material. (a) shows the uncoated fracture surface of a 2.8 mm thick flexural strength specimen (486 MPa) with low-angle grazing illumination. (b) shows an interpretation for a mirror-hackle boundary where systematic new hackle is detected (small white arrows) as compared to the roughness inside the mirror. The marked circle is elongated somewhat into the depth due to the stress gradient. The radius was 345 m.*

(a) (b)

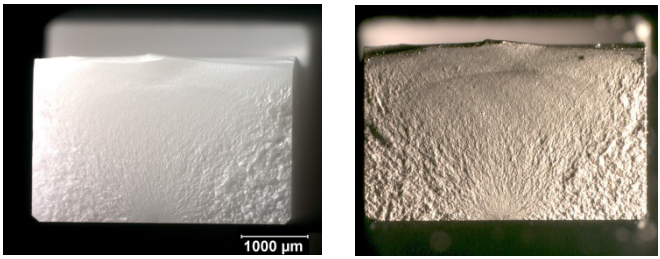

(c)

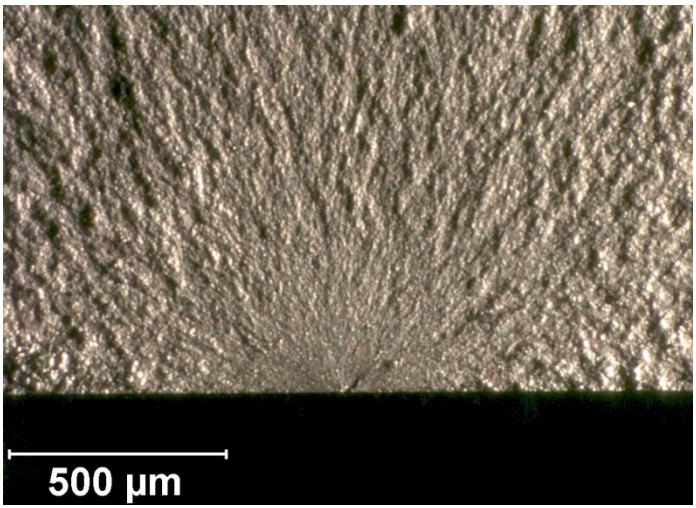

(d)

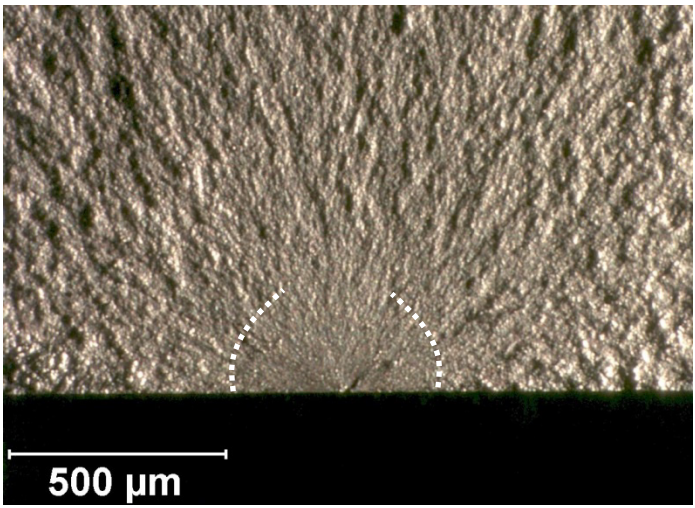

Figure D.5 *Optical images of a fracture mirror in a 3Y-TZP zirconia flexural strength specimen (3M-ESPE Lava, 798 MPa). (a) and (b) are uncoated and gold-coated images of the whole fracture surface, respectively. (c,d) are gold coated. Notice how much easier it is to distinguish the mirror boundaries in (d) since the gold coating curtails internal light scattering. (courtesy J. Quinn)*

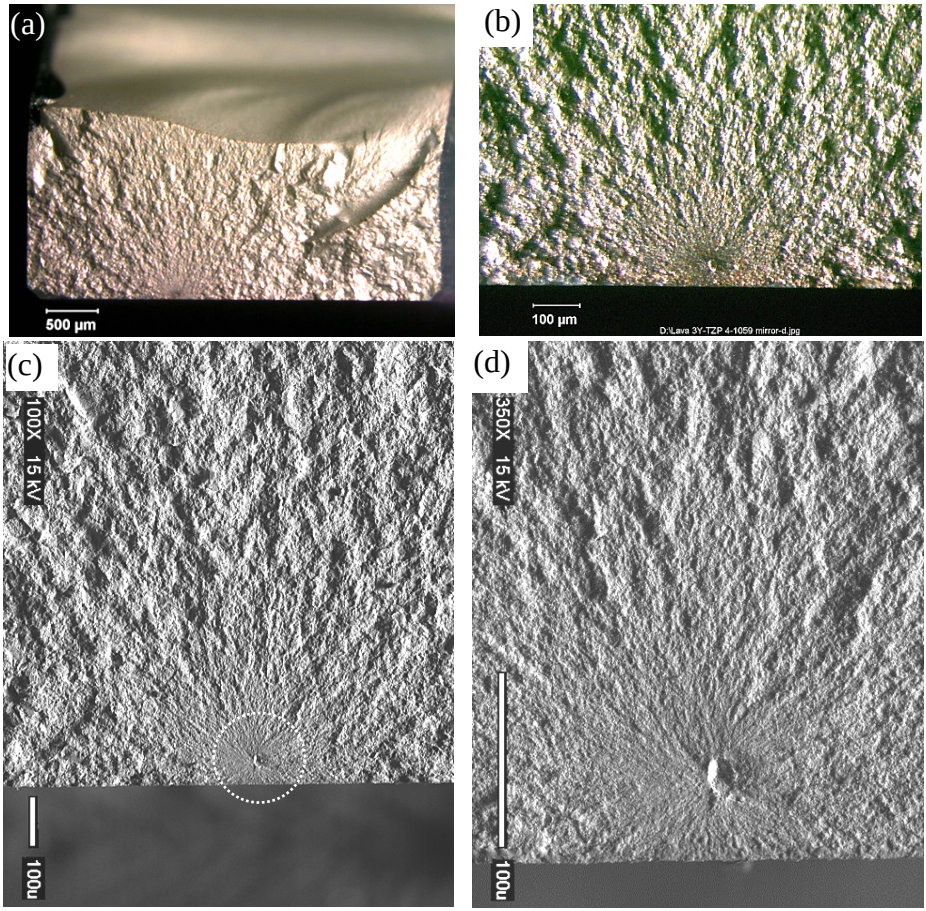

Figure D.6 *Fracture mirror in another 3Y-TZP bend bar. (3M-ESPE Lava, 1059 MPa maximum stress, 1024 MPa at the origin). (a) and (b) are stereo optical microscope images. (c) and (d) are SEM images. Images (b) and (c) are at the same magnifications. The flaw is a pore. Fine hackle lines in the mirror run right to the origin. They are created by the flaw itself and the microstructure. The mirror boundary is where systematic new hackle forms and there is an obvious difference compared to the roughness inside the mirror region. This is a very difficult example. My interpretation is shown in the lower magnification SEM image (c). (SEM images (c,d courtesy J. Quinn)*

D.2 Measure the Mirror Size

Use the following steps to measure mirror sizes. These steps are repeated, but with detailed notes, clarifications, and illustrations in section D.3.

1. **Use an optical microscope whenever possible.** A compound optical microscope is best for glasses. A stereooptical microscope is best for ceramics. A thin coating may be applied to translucent or transparent ceramics. A scanning electron microscope may be used if optical microscopy is not feasible.

2. **The fracture surface should be approximately perpendicular to the microscope optical path or camera.**

3. **Optimize the illumination to accentuate topographical detail.** Ceramics may be coated with gold or carbon.

4. **Use a magnification such that the fracture mirror area occupies about 75 % to 90 % of the width of the field of view for glasses, and approximately 33 % to 67 % of the width of the field of view for ceramics.** An additional, lower-power image may be helpful for ceramics.

5. **Measure the mirror size while viewing the fracture surface with an optical microscope whenever possible.**
   Measurements from photos may be used as a last resort if the steps above cannot be followed.

6. **Measure radii in directions of approximately constant stress whenever possible.** Units should be meters (or inch).

7. **Exercise caution when mirrors are large relative to the specimen cross-section size.**
8. **Show at least one photo with arrows or lines marking the mirror size.**
9. **Report how the mirrors were measured.**

Additional steps for the determination of fracture mirror constants with multiple test specimen examples:

10. **Use the stress *at the origin site*.**
11. **Evaluate the fracture mirror constants by regressing stress on inverse square root of mirror radius. (Preferred method)**
    Use linear regression methods to obtain A in accordance with equation D.2 with a forced zero intercept as shown in Figure D.7a. Use units of MPa for stress and 1/Öm for the graph axes. The mirror constant A is the slope of the regression line.

$$s_a = \frac{A}{\sqrt{R}} \qquad \text{(D.2)}$$

where s_a is the stress at the origin site, computed from the known applied stresses. R is the mirror radius in the direction of constant stress.

Use some judgment in the regression analysis since fracture mirror data frequently has moderate scatter. If the data does not appear to fit a trend that has a zero intercept, regress the data with a non-zero intercept and equation D.3.

$$s_a = \frac{A}{\sqrt{R}} - s_r \qquad \text{(D.3)}$$

where s_a is the stress at the origin from known applied stresses, s_r is the residual stress at the origin location. Report the intercept if it deviates significantly (> 10 MPa) from zero. Investigate possible residual stresses or specimen size or shape issues if the intercept deviates significantly from zero. A positive intercept on the graph often (but not necessarily) corresponds to a residual compression stress acting on the mirror. It means that a greater applied stress s_a must be applied in order to overcome the residual stress and to form a mirror of the same size as for an annealed part. A negative intercept corresponds to a residual tensile stress.

12. Mirrors sizes should be collected over a broad range of sizes and fracture stresses if possible. Data from different specimen types and sizes may be combined.

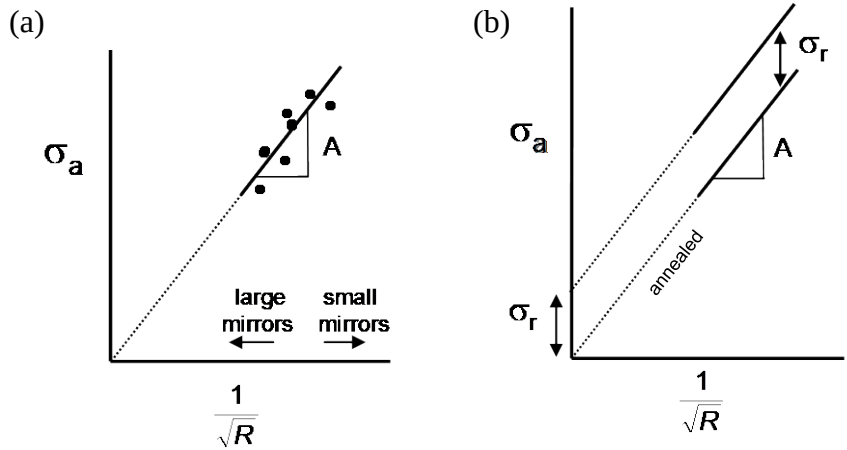

Figure D.7 *Plot of applied stress s_a (at the origin) versus 1/ÖR. (a) shows the trend for residual stress-free parts. (b) shows it for parts with residual stresses. Compressive residual stresses move the locus up with a positive intercept s_r, but with the same slope. Tensile residual stresses shift the data downwards with a negative intercept (not shown).*

D.3 Clarifications, Additional Notes, and Illustrations

1. Use an optical microscope whenever possible. A compound optical microscope with bright field illumination is best for glasses. A stereo optical microscope is best for ceramics. A thin coating may be applied to translucent or transparent ceramics. A scanning electron microscope may be used if optical microscopy is not feasible.

Differential interference contrast (DIC, also known as Nomarski) mode viewing with a research compound microscope *originally was not recommended* by this Guide. It is only suitable for glasses. It is not suitable for rough ceramic fracture surfaces. There are complications with glass fracture surfaces. There is no question that DIC mode viewing can discern very subtle mist features in glasses, but the threshold of mist detectability is highly dependent upon how the polarizing sliders are positioned. Hence, DIC measured radii are quite variable.[1] DIC measured radii can be substantially smaller than those obtained with conventional viewing modes. During a review process in 2010, paragraph 6.1.3 of standard ASTM C 1678[2] was revised to allow DIC mode for glasses, provided that the polarizing elements are used in a consistent manner in the grey mode (with a l plate for color control removed).

Dark-field illumination may be used with glasses, but dark-field images may lose a little resolution with glasses and radii may be slightly larger as a result. It is very effective with highly-reflective mirror surfaces in single crystals.

Confocal optical microscopes and optical interferometers have been occasionally used to examine fracture mirrors, but the author is unaware of any published systematic study to correlate apparent mirror sizes from these tools to those measured with conventional optical microscopes. The quantitative surface roughness capabilities of these instruments in principle could be used to correlate an average or root mean square roughness to the mist or hackle boundaries.

Scanning electron microscope images of mirrors are not recommended for measuring the mirror-mist boundary in glasses since the boundary is usually indiscernible at the magnifications needed to see the overall mirror. SEM images often appear flat and do not have adequate contrast to see the fine mist detail. SEM images may be used to measure mirror-hackle boundaries with very small mirrors that would be difficult to see with optical microscopy, e.g., as in high strength optical fibers. Scanning electron microscope images may be used for ceramics if necessary, but steps should be taken to enhance contrast and shadowing to produce images such as shown in Figures D-6c and d.

Attempts to correlate the mirror boundaries with a simple surface roughness parameter have produced mixed results. The author reviewed this matter in Reference 1 and in Appendix D in the 1st and 2nd editions of this Guide. The work has been limited to glasses. There appears to be no simple correlation of surface roughness and a judgment of mirror size using optical microscopy.

Other than my own study as reported in Reference 1, the author is not aware of any systematic study comparing fracture mirror sizes as a function of the viewing mode or microscope type.

2. The fracture surface should be approximately perpendicular to the microscope optical path or camera.

This simple and fairly obvious requirement is intended to avoid the foreshortening that can occur if the specimen is tilted. A small amount of tilting is acceptable in order to get a favorable reflection off a glass piece.

The requirement poses a small problem if the mirrors are examined with stereo binocular microscopes. These have two different tilted optical paths. If viewing with *both* eyes in a stereomicroscope, the specimen should be flat and facing directly upwards. The observer's brain will interpret the image as though he or she is facing it directly.

Alternatively, if a camera is mounted on one light path of the stereomicroscope and it is used to capture or display the mirror, then the specimen should be tilted so that the camera axis is normal to the fracture surface. For example, tilt the specimen to the right if the camera is attached to the right optical path.

3. Optimize the illumination to accentuate topographical detail.

The mist and hackle features should be accentuated. Glasses may either be illuminated from directly down onto a fracture surface or by low-angle grazing illumination. Ceramics should not be directly illuminated since the light will reduce contrast, especially in translucent or transparent materials. Ceramics should be illuminated with low-angle grazing illumination. Stereo optical microscopes are strongly preferred for ceramics. Low-angle illumination is less convenient with compound light microscopes. The observer should experiment with whatever illumination options are available to accentuate subtle surface roughness and topography features. If it is necessary to use a SEM because the mirror is too small to be measured optically, then make careful adjustment to the contrast to emphasize topographic detail.

4. Use a magnification such that the fracture mirror area occupies about 75 % to 90 % of the width of the field of view for glasses, and approximately 33 % to 67 % of the width of the field of view for ceramics. An additional, lower-power image may be helpful for ceramics.

Observers usually mark the mirror boundaries closer to the origin at greater magnifications than they would at lower magnifications. This is because mist or micro hackle markings are easier to see at distances closer to the origin at high magnification. This is particularly the case with glasses. Conversely, at very low magnifications, much detail is lost and observers typically overestimate the mirror size.

Fracture mirrors are reasonably easy to see in glasses and magnifications should be used such that they nearly fill the field of view.

Mirror interpretation is more problematic with polycrystalline ceramics. Excessive magnification often leads to confusion as to where the boundary is located. Even though a mirror may be obvious at low or moderate magnifications, at higher magnifications it may be impossible to judge a boundary. It is more practical to view the mirror region (and the natural microstructural roughness therein) relative to the hackle roughness in the regions outside the mirror. "Stepping back" and using the 33 % to 67 % rule should help an observer better detect the topography differences. Images recorded at these magnifications are also more convincing when shown to other fractographers or engineers. Even lower magnification images may also be made to aid interpretation such as shown in Figures D-2b, D-3b, and D-6b. The images should not be more than 5 times different in magnification; otherwise it is difficult to correlate features in one image to another.

Sometimes the microstructure of polycrystalline ceramics creates even worse judgment problems in ceramic matrix composites (particulate, whisker or platelet) or self-reinforced ceramics whereby elongated and interlocking grains impart greater fracture resistance. These difficulties were experienced in studies of the fracture surfaces of a self-reinforced silicon nitride[6,7] and also a yttria-stabilized tetragonal zirconia polycrystal.[8] Mirrors were plainly evident at low magnifications, but accurate assessment of their size was difficult. The mirror region itself was somewhat bumpy in the self-reinforced silicon nitride, so some judgment as to what was the mirror boundary was necessary. The zirconia had intrinsic micro-hackle lines well within the mirror. The criterion for the zirconia mirror boundaries was as follows: *The mirror boundary was judged to be the point where systematic new radiating hackle commenced and there was an obvious roughness change relative to the inside-mirror region.*

The word systematic requires elaboration. Mirror boundary hackle lines are velocity hackle lines created after the radiating crack reaches terminal velocity. Premature, isolated hackle can in some instances be generated well within a mirror, however. It should be disregarded when judging the mirror boundary. Wake hackle from an isolated obstacle inside the mirror (such as a large grain or agglomerate) can trigger early "premature" hackle lines such as shown in Figure 5.8 in the main text. Steps in scratches or grinding flaws can trigger hackle lines that emanate from the origin itself.

5. Measure the mirror size while viewing the fracture surface with an optical microscope whenever possible.

As noted above, a compound optical microscope is best for glasses. A stereo optical microscope is best for ceramics. Use either calibrated reticules in the eyepieces or traversing stages with micrometer-positioning heads. For routine measurements for ceramics, the author uses a stereo optical microscope with a traversing X-Y stage with digital micrometer heads that read out to 0.001 mm (1 m). Alternatively, measurements may be made on digital images projected onto a high-resolution computer monitor preferably while the fracture surface can be simultaneously viewed through the microscope eyepieces in order to aid judgment.

Measurements from photos may be necessary for very small specimens or very strong specimens with tiny mirrors, such as in fibers or microelectro-mechanical system (MEMS) devices. Scanning electron microscope images may be used. Again, the fractographer should take an overall framing photograph or image shot in accordance with the 75 % to 90 % rule for glasses and 33 % to 67 % rule for ceramics. Higher and lower magnification images may be used to help aid in interpretation.

Mirror size measurements from <u>photographs</u> are usually less accurate. They frequently overestimate mirror sizes unless conditions are carefully optimized to accentuate contrast and topographic detail. Two-dimensional photographic renditions of a three-dimensional fracture surface usually lose much of the topographic detail discernable by the eye with a compound optical or stereomicroscope.

Mirror size measurements made on <u>computer monitor</u> screens are also subject to inaccuracies, also because they are two-dimensional renditions of a three-dimensional fracture surface.

6. Measure radii in directions of approximately constant stress whenever possible. A mirror diameter may be measured and halved to estimate the radius if the origin site is indistinct or complex.

There is no consensus on how many mirror radii measurements should be taken and in how many directions. Ideally, measurements should be taken from the center of the mirror region, but some judgment may be necessary. A common practice is to make a judgment whether a mirror is indeed approximately semicircular or circular. If it is, then multiple radii measurements may be made in different directions and averaged to obtain the mirror size estimate. The center of the mirror may not necessarily be the center of the origin flaw. Careful inspection of tiny localized fracture surface markings (Wallner lines and micro hackle lines) right around the origin may reveal that fracture started at one spot on a flaw periphery. For example, fracture from grinding or impact surface cracks in glass often starts from the deepest point of the flaw and not at the specimen outer surface. Figure D.1 shows an example. Large pores often trigger unstable fracture from one side. An example is the pore in Figure D.6d, where fracture seems to have started on the left side of this internal flaw. If an exact mirror center cannot be determined, it is adequate to measure a mirror diameter and halve the measurement. This is commonly done for semicircular mirrors centered on irregular surface-located flaws whereby the mirror center may be difficult to judge.

Circular embedded mirrors are easiest to interpret (such as in D-2 and Figure 5.12). Small semicircular mirrors on the surface of a part, such as in a bend bar or a flexurally loaded plate, are also not too difficult to interpret. The mirror relationship holds up remarkably well in glass optical fibers tested in tension for mirror radii almost as large as the fiber diameter.[9] The mirror radius should simply be measured from the origin to the mirror-mist or mist-hackle boundary on the opposite side of the fiber, R_d (where the subscript denotes "depth") as shown in Figure D.8.

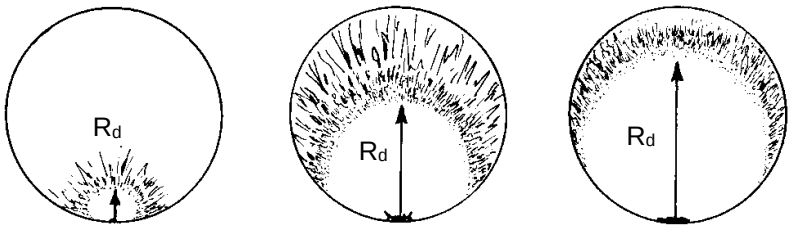

Figure D.8 *Mirrors surrounding surface origins in rods or fibers loaded in direct tension. (after Ref. 9) Measure both the mirror-mist radius (shown) and mist hackle radii into the depth as shown.*

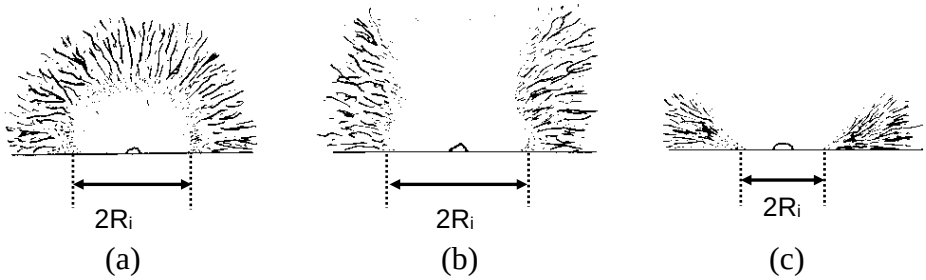

Figure D.9 *Elongated mirrors in bending stress fields. If the mirror is small relative to the part size (i.e., a strong part), then the mirror may be semi-circular as shown in (a). Weaker parts have larger mirrors that flare into the interior and are incomplete as shown in (b) and (c). Measure the mirror size (R_i or $2R_i$ for the mirror-mist in the illustrations here) in the direction of constant stress. (Note: special guidance on how to deal with small inward bending cusps at the surface is shown in Figure D.12 below.)*

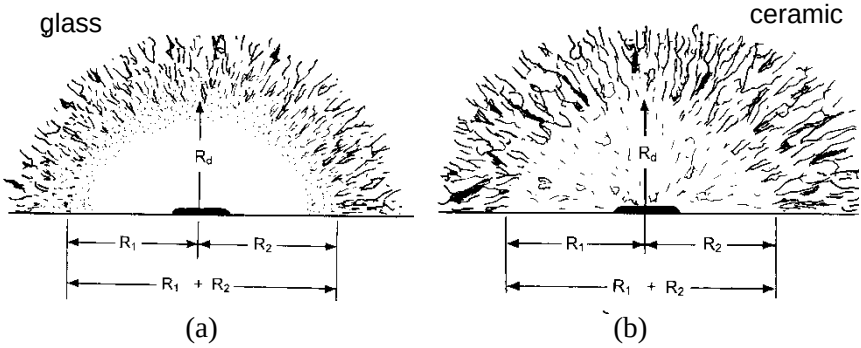

Figure D.10 *Grinding cracks and scratches can cause sideways mirror elongations along the surface, even in bend bars with stress gradients. (a) shows a schematic of such a mirror with the mist-hackle boundary marked in glass, and (b) shows a comparable image in a polycrystalline ceramic. (b) has some intrinsic microstructural roughness inside the mirror and the mirror-hackle boundary is marked. Use an average radius: $R_{avg} = (R_1 + R_2 + R_d)/3$.*

Quarter circular mirrors centered on an edge or chamfer should be measured from the origin.

On the other hand, mirror shapes are commonly affected by stress gradients in a plate or a beam. Mirror radii are elongated in the direction of <u>decreasing</u> stress.

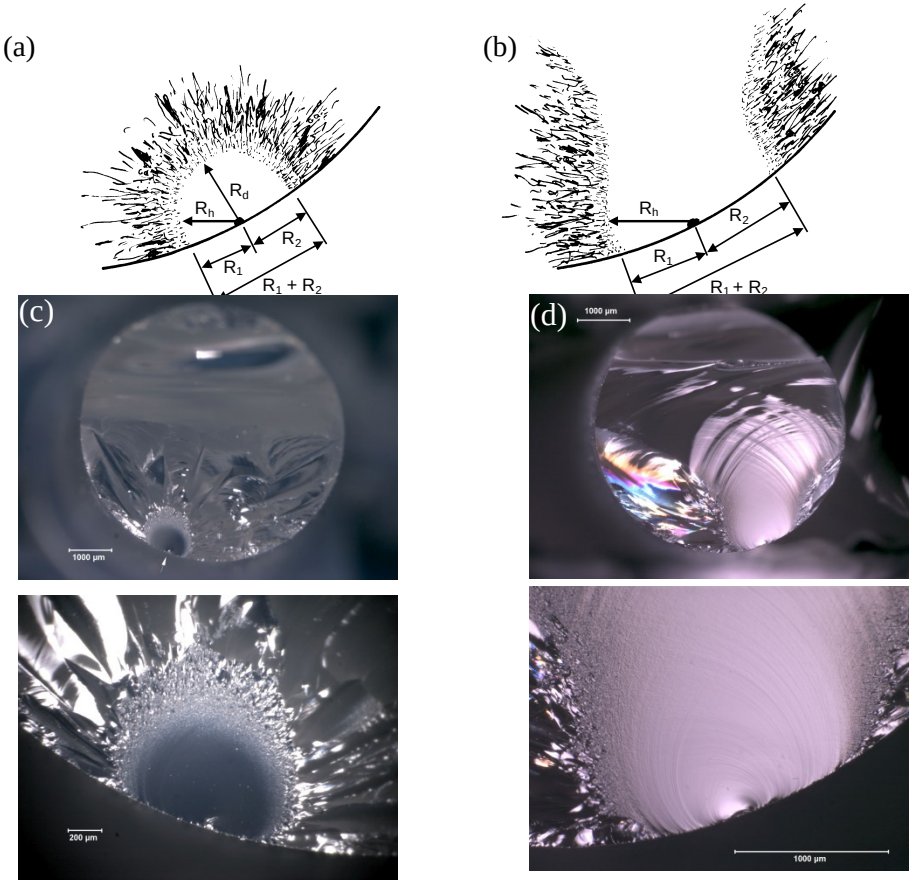

Figure D.11 *Optical images of fused silica glass rods tested in flexure. The load was applied vertically, and the maximum tensile stresses are at the bottom center. Fractures started at flaws part way up the sides of the rods causing the mirrors to have unequal radii. Schematics (a and b) are similar to two glass rods (c and d). The rod shown in (c) was sufficiently strong that a nearly semicircular mirror formed, but with unequal radii due to the stress gradient. Use $R = R_h$ (where the subscript h denotes horizontal) if the origin and mirror center is distinct. Otherwise use $R_{avg} = (R_1 + R_2 + R_d) / 3$ if the mirror is nearly semicircular. Use $R_{avg} = (R_1 + R_2) / 2$ if the mirror is elongated into the interior and R_d is large. (d) shows a weaker glass rod. Use $R = R_h$ if the origin and mirror center are distinct, otherwise use $R_{avg} = (R_1 + R_2) / 2$.*

Examples are shown in Figure D.9b and c. In such cases, measure the mirror radius along the tensile surface where the stress is constant. Do not measure the mirror radii into the gradient. Even with this precaution, there is considerable evidence that the data begins to depart from the stress-mirror size

curves and the relationship in equation D.1 when the sizes approach the plate, beam, or rod thickness. For mirrors radii larger than the plate thickness, data points fall above the trend on a log stress – log mirror size plot which means that mirrors are larger than they would otherwise be if the part were loaded in uniform tension.

A trend for mirrors to elongate the opposite way, along the external surface of a specimen, was detected by the author in recent work on the fractographic analysis of grinding flaws in structural ceramics.[6,7] Long surface cracks often caused mirrors to have perceptible deviations from a semicircular shape as shown in Figure D.10. In such cases, measure an average radius:

$$R_{avg} = (R_1 + R_2 + R_d) / 3. \qquad \text{(D-4)}$$

In some cases, it may be difficult to measure mirrors in directions of constant stress. The two sides of a mirror may have unequal lengths since the stresses are different on either side of the mirror. Figure D.11 shows examples from the author's research of round rods broken in flexure. Many origins were not at the rod bottom where the stresses were a maximum, but part way up the side of the specimen. The specimen orientation was easily determined from observation of the compression curl. The maximum tensile stress on the bottom of the specimen was on the rod directly opposite the cantilever curl. It was a simple task (see section 10 below) to compute the actual stress at the origin location. The mirror radii had obviously different lengths due to the stress gradient. *Use a radius in the direction of constant stress, R_h, as shown in Figure D.11, if the mirror is centered on a well-defined origin site.* If there is any doubt, then an average radius may be computed. Use $R_{avg} = (R_1 + R_2 + R_d) / 3$ if the mirror is nearly semicircular. Use $R_{avg} = (R_1 + R_2) / 2$ if the mirror is elongated into the interior and R_d is large or is incomplete.

For origins located in the interior of a rod broken in flexure, *only use the radii in the direction of constant stress.* As a check, and only if the mirror is a complete ellipse, one may measure two orthogonal mirror diameters and compute an average diameter and halve this to obtain an average radius.

There is one important detail about mirror sizes that warrants discussion. Mirrors located on a specimen external surface have *small cusps* at the intersection with the outer surface as shown in Figure D.12a. Cusps are often detected in glass mirrors, but they are rarely if ever discerned in polycrystalline ceramic mirrors. The small cusp is a consequence of fracture mechanics. A small element of material near the tip of a crack at the specimen exterior surface experiences greater stress intensity K_I than a similar element buried in

the interior whereby neighboring elements can "share the load." Kirchner et al.[4,5] discussed the shapes of fracture mirrors that intersect outer surfaces and they showed that the local enhancement of the stress intensity K_I accounts for the cusps. The slightly-greater stress intensity at the surface triggers the mirror markings a bit sooner than for interior elements. *The usual convention, and the one adopted in this Guide and in ASTM C 1678, is to truncate the cusp. Extend the semicircular (or other mirror shape) arcs as shown in Figure D.12c.* Another reason to be wary of measurements right along the surface is that surface roughness, machining damage, or other surface irregularities may trigger mist or hackle formation a bit earlier than in the interior. Others have noted that measurements taken right on an exterior surface are slightly different

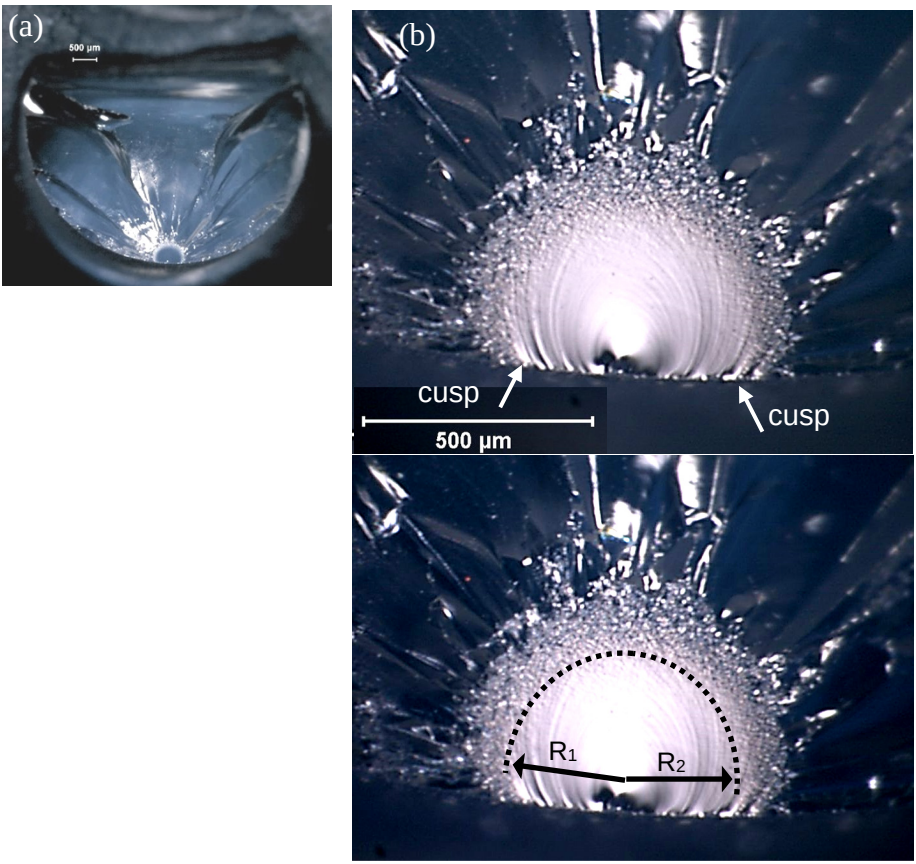

Figure D.12 *Optical images of a fused silica rod (a), illustrating the cusps in the mirror near the outer surface (b). Mirror measurements should not include the inward bend of the mirror and may be made as shown in (c).*

than those taken into the interior. Even Shand[10] recommended in 1959 that size measurements be taken 0.1 mm (.004 in) beneath the exterior surface. Mecholsky and Freiman[11] in 1979 recommended ignoring the cusp at the surface on the basis of fracture mechanics considerations: "In measuring the mirror-mist and mist-hackle boundaries, these should be projected to the tensile surface to compete a circular arc, since there is curvature at the surface due to free surface effects."

A dilemma occurs when mirrors are large in plates or beams broken in flexure as shown in Figure D.9c. Cusps cannot be detected. In this case the only plausible way to measure a mirror radius is directly along the surface. In such cases, the general warning of step 7 (on page D-10 and the next page) applies.

It is worth reiterating that equations D.1 and D.2 are empirical. Kirchner and colleagues[4,5] showed a more rigorous fracture mechanics analysis (based on a critical stress intensity for branching) completely explained the mirror shapes and distortions including the cusp mirrors in various stress fields. Despite the merits of their rigorous fracture mechanics analysis, there is significant practical advantage to using the simpler mirror size - stress relationships D.1 and D.2 even if some rigorousness is sacrificed. In addition, for small mirror sizes relative to the specimen dimensions, the simpler approach is almost as rigorous.

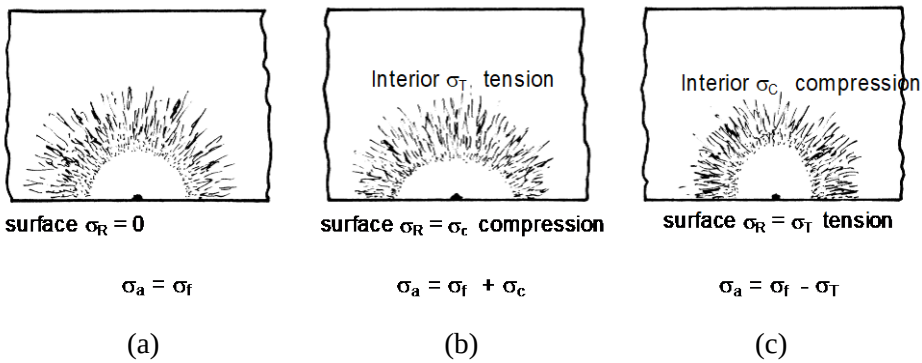

Figure D.13 *Surface residual stresses also may alter a mirror shape.* s_a *is the applied stress to cause fracture and* s_f *is the fracture stress in an annealed plate. (a) shows a surface mirror in an annealed plate. (b) shows the mirror shape in a plate with surface compression stresses that decrease into the interior and become tensile. (c) shows a mirror in a plate with surface tensile stresses that diminish into the interior and become compressive.*

Residual stresses alter mirror shapes. If the mirror is very small relative to the stress gradient, the mirror shape may remain circular or semicircular if along the surface. On the other hand, if the mirror is larger or the stress gradient is steep, then the gradient alters the mirror shape as shown in Figure D.13. Figure D.13a shows an annealed plate that requires an applied stress of $s_a = s_f$ to cause fracture. Figure D.13b shows the case where the same plate has residual surface compression stress $s_r = s_c$ from ion exchange or thermal tempering, so that an applied stress to cause fracture is $s_a = s_f + s_c$. In other words, the applied stress must be increased to overcome the residual surface stress. Nevertheless, the net stress at the surface at the moment of fracture is $s = s_a - s_c = (s_f + s_c) - s_c = s_f$, the same stress as in the annealed plate. Hence the mirror radii along the surface are *unchanged* compared to the annealed plate. In contrast, in the direction into the interior, tensile stresses combine with the applied tensile stress to cause the mirror markings to form sooner, at a shorter radius into the interior than in the annealed plate. In this example, the mirror shape is flattened to a semiellipse. Mirror radii should be measured *only along the surface* (or just beneath the surface if there is a cusp) in these cases.

Figure D.13c shows that surface residual tensile stresses have the opposite effect: mirror radii are elongated into the interior. Mirror radii again should only be measured along the surface, since again the net stress to cause fracture is $s = s_f$.

There are two possible paths for data analysis if there are residual stresses:

(a) The mirror is measured on a component. The applied stress and the residual stresses are unknown. In this instance the net stress s at the origin can be evaluated from R_{avg} and equation D.1.

(b) The mirrors are collected in laboratory conditions with multiple specimens such that the apparent origin stresses s_a, from applied external stresses are known. In this instance, one or more matched pairs of s_a and R are obtained. Graphical analysis as shown in Figures D.1 or D.2 reveals the existence and magnitude of the residual stresses.

7. Exercise caution when mirrors are large relative to the specimen cross-section size.

At some point, one can expect departures from of the stress - mirror size relationship. The point where the departure occurs depends upon the loading geometry and the stress state.

Pronounced deviations occur once the mirror size approaches or is greater than the component thickness in plate or beam *bending* fractures. Experimentally-measured radii are much greater than predicted by equation D.1. Shand recommended that the maximum mirror size should be no more than 15% of the rod diameter (or 30% of the distance to the centroid) for *flexure* tests.[10,12] Kirchner and Conway[5] warned about limitations in the fracture mechanics models for mirror radii exceeding 20 % of a rod diameter tested in flexure. On the other hand, Castilone et al.[9] had success with mirrors that were almost as large as the fiber diameters for fibers tested in *tension*.

There still is merit to measuring and recording mirrors even if they are large relative to a cross-section size. The data may have value for use with analyzing genuine component fractures.

Mecholsky and Freiman[11] warned that systematic deviations from the mirror size relationship occur at large mirror sizes and also at very small sizes, the latter due to internal stress effects, e.g., from thermal expansion anisotropy of grains in ceramics.

8 Show at least one photo with arrows or lines marking the mirror size.
This simple step will help clear up a lot of the doubt and confusion about what an investigator has actually measured.

9. Report how the mirrors were measured.
This simple step is often overlooked or ignored, and the reader is left wondering exactly what had been done. The fractographer should report the type of microscope used, whether interpretation was made while looking through the microscope or from photos, and approximately what magnifications were used. The direction the mirror radii were measured should be documented. The approximate shape of the mirrors (semicircular, circular, or elliptical) should be noted. It should also be noted whether the mirrors were an appreciable fraction of the size of the cross section or not. Lastly, and most importantly, the judgment criterion used should be reported.

10. Use the stress at the origin site (additional steps to determine A).
If the specimen was broken in controlled conditions where the stress distribution was known (e.g., beams, rods, or plates in flexural loadings) one must *correct the stress for location in specimens with stress gradients.*

No correction is needed if a part was stressed in uniform tension. On the other hand, many parts or laboratory specimens do have stress gradients. The general principal that should be followed is that the mirror formation is guided by the

stresses that acted on and in the immediate vicinity of the flaw origin. While this may seem obvious, it is probable that some analysts in the past have erroneously used *nominal stresses* in a specimen (e.g., 3-point flexure) or component rather than the *actual stress* that was acting upon the mirror region in a body. In contrast, some researchers have correlated the stress at every site along the mirror periphery with the mirror radius at that periphery site, but this complex process is not practical on a routine basis.

Example 1: Flexural strength test specimens

The nominal flexural strength is the maximum stress at the outer fiber or tensile surface of the bar. The stress correction for locations beneath the surface is simple if the material is linearly elastic. The stress decreases from a maximum at the outer tensile surface to zero at the middle "neutral axis" which

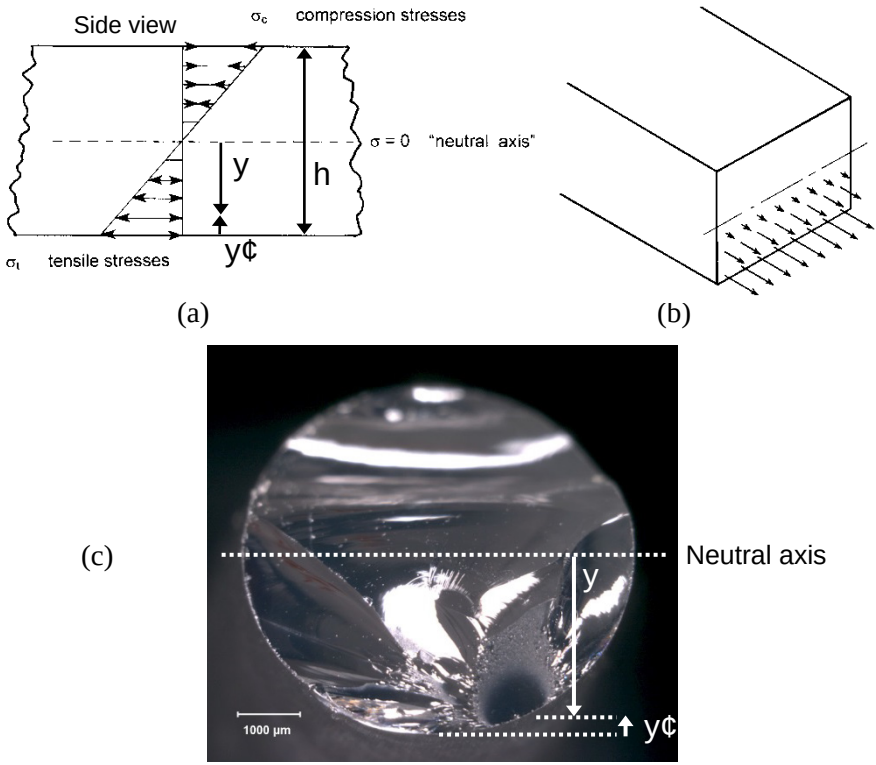

Figure D.14 *The flexural stress gradient is shown in (a) and (b) for a rectangular beam. (c) shows how the origin location may be measured from a rod neutral axis in a fused silica rod.*

corresponds to the centroid in a square, rectangular, or circular cross-section beam specimen as shown in Figure D.14. At the origin,

$$s = (2y/h)\, s_{max} \qquad (D.5)$$

where y is the distance from the neutral axis (centroid) and h is the beam thickness or rod diameter. Alternatively, in terms of the distance from the tensile surface, y':

$$s = (1 - 2y'/h)\, s_{max}. \qquad (D.6)$$

In similar fashion, if a fracture origin is not directly under the middle loading point in three-point bending, or if the origin is outside the inner gage length in four-point bending, then the stress should be correspondingly adjusted to the stress that actually acted on the origin site. Corrections for breaks outside the gage section or away from the middle loading point are also linear. The stress is reduced in proportion to the distance from the fracture plane to the outer loading points. This correction requires knowledge of the loading point locations. This is an important reason why loading points should be marked on any test piece prior to its fracture. For three-point loading:

$$s = (2x/L)\, s_{max} \qquad (D.7)$$

where x is the distance from the outer loading point to the fracture plane and L is the total three-point span. For four-point flexure,

$$s = (x/a)\, s_{max} \qquad (D\text{-}8)$$

where x is the distance from an outer loading point to the fracture plane, and a is the distance from the outer loading point to an inner loading point. If an origin in a flexural beam is subsurface and outside the inner span, then both corrections should be applied. If the origin is on the tensile surface, within the inner span length, and the mirror size is small and semicircular, then no stress correction is needed.

Example 2: Ring-on-ring biaxial strength test specimens.

If the origin is on the tensile surface in the inner loading circle, and the mirror size is small and semicircular, then no stress correction is needed. Fracture mirrors from volume flaws located beneath the tensile surface should be corrected in the same manner as above for the uniaxial bend test methods. Corrections for mirrors located outside the inner loading ring also should be

corrected for location. The corrections are not as simple in this case, however. In the annulus outside the inner loading ring, the radial and circumferential (hoop) stresses decrease out to the specimen rim at different rates.[13,14] Radial stresses decrease faster, and are zero at the outer rim, and are therefore less likely to induce fracture. Fracture planes and mirrors are usually perpendicular to the hoop stresses outside the inner ring, so use the hoop stress.

On the other hand, hoop stresses decrease more slowly and *are non-zero at the outer circumference* of the specimen. So although the outer hoop stresses are only 10 % to 50 % of the maximum stress in the inner circle (depending upon the disk and fixture geometries, and especially the disk thickness), large grinding or handling flaws on the specimen rim can cause fracture.

The same comments apply to piston on three-balls, ball on three balls, or even pressure loaded plates in bending. Consult appropriate references as needed for the stress distributions in these configurations.

Example 3: Component failure analyses

If the mirror constant for the material is known and a mirror size is measured, the stress at the origin site can be calculated. The peak stress or the nominal stress in the part may be different, however. So as a rudimentary example, imagine a bend bar that broke from an internal origin site, but at an unknown stress. The fractographer uses the mirror size and the mirror constant to estimate the stress at the origin site. The nominal strength of the beam (the maximum outer fiber stress) or the "flexural strength" is greater, however. In this case, the stress adjustment should use s, A, h, x, y or y' to compute the greater nominal stress, s_{max}.

11. Evaluate the Fracture Mirror Constants

If only a few data points are available, it may suffice to compute individual estimates of A for each specimen (using equation D-1: A = sÖR), then compute an average and standard deviation.

If more data with matching mirror radii and fracture stresses are available, it is customary to plot the data on either: (a) a graph of log stress versus log mirror size (Figure D-7a) or (b), linear stress versus inverse square root of mirror size (Figure D.7b). A linear regression analysis is then performed and a mirror constant calculated from the regressed line. Both procedures are widely found in the literature. Each is discussed below, and the author concludes that option (b) is *better*. The mirror constants should be reported as either MPaÖm (or ksiÖin if the older units are in use).

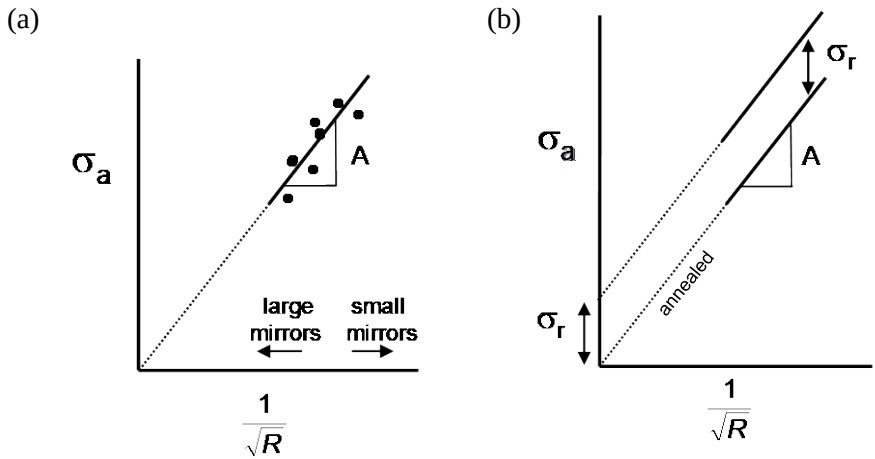

Figure D.7 *(duplicate) Plot of applied stress, s_a, versus 1/ÖR, the preferred regression method. (a) shows the trend for parts with no residual stress. (b) shows the effects of residual stresses. Compressive residual stresses move the line up with a positive intercept s_r, but with the same slope. Tensile residual stresses shift the data downwards (not shown).*

11a. Plot s versus 1/ÖR. (Preferred)

Use linear regression methods to obtain A in accordance with equation D.9 (same as D.2) with a zero intercept. Use units of MPa for stress and 1/Ömm for the graph axes. In a typical strength test experiment in a laboratory, applied stress, s_a, and mirror radius, R, are independently measured. The reader is reminded that the stress should be corrected for the origin/mirror location if there are stress gradients. It is customary to regress s_a on R and this procedure shall be followed in this Guide. A is the slope of the regression line:

$$s_a = \frac{A}{\sqrt{R}} \qquad \text{(D-9)}$$

Use some judgment in the regression analysis since fracture mirror data usually has moderate scatter. If the data does not appear to fit a trend that has a zero intercept, regress the data with a non-zero intercept as shown in Figure D.7b. Again, use some judgment in the interpretation, since a strict linear regression fit may produce implausible outcomes, particularly if the data is collected over a limited range of mirror sizes and stresses. Report the intercept if it deviates significantly (> 10 MPa) from zero. Investigate possible residual stresses or specimen size or shape issues in such cases.

Consistent units should be used. That is to say, if the stress axis is MN/m^2 or MPa, then the abscissa (horizontal axis) should be $1/\sqrt{R}$ where radius is in units of *meters*. (If the mirror is measured in mm or mm, then appropriate conversion factors should be added, but this is not trivial and can cause confusion, since the square root of a conversion factor of 1000 {e.g., meters to mm} is an odd value.) If the stress units are psi or ksi, the mirror radii should be measured in inches.

The mirror constant as a slope is easily visualized. Statistical analysis may be used to estimate the uncertainties (e.g., standard deviation) of the line slope.[a]

Deviations from the trend usually cause a nonzero intercept, which may be conveniently interpreted as an effective residual stress. If residual stresses σ_r are present in addition to the externally applied stress, σ_a, then the net stress acting on the origin site is: $\sigma_a + \sigma_r$. The fracture and the mirror markings respond to the actual net stress, σ_{net}:

$$\sigma_{net} = (\sigma_a + \sigma_r) = \frac{A}{\sqrt{R}} \tag{D.10}$$

$$\sigma_a = \frac{A}{\sqrt{R}} - \sigma_r \tag{D.11}$$

An intercept below the origin corresponds to a net tensile residual stress. A positive intercept corresponds to residual compressive stress since the usual sign convention is for compressive stresses to have a negative sign.

Some caution is advised since residual stresses are often nonuniform. The residual stress estimated from the intercept is an effective residual stress, which in reality may vary in magnitude through the mirror region. If the mirror is in a heat-strengthened or tempered piece (where stress may be constant along the surface, but change dramatically through the thickness) the mirrors should only <u>be measured along the surface or just underneath to avoid the cusp</u>. Residual stresses from an indentation or impact site are very local to the origin and may have very little effect on a mirror size.

Although most researchers have felt that the regressed lines should go through the origin in *annealed* test pieces, there is evidence by J. Quinn[15] and Oakley[16] that a small but measurable intercept may exist in even annealed materials. The intrinsic intercept was evaluated[15] as 10 MPa (1,500 psi) for BK-7 borosilicate

[a] This may not be a trivial exercise. Many software packages (e.g., Excel) can readily compute the standard deviation of a line if the function is Y = mX + b where there is a distinct intercept, b, but there is some controversy in how to do this if one uses Y = mX with a zero intercept.

crown glass, a value that interestingly concurs with Orr's[17] estimate of the minimum stress necessary for branching in glass.

b. Plot log s versus log R. (Alternative method)

Use linear regression methods to fit the data in accordance with equation D.12 (slope set at – ½) as shown in Figure D.15a. Use units of MPa for stress and meters for the graph axes. This will simplify the computation of the mirror

(a)

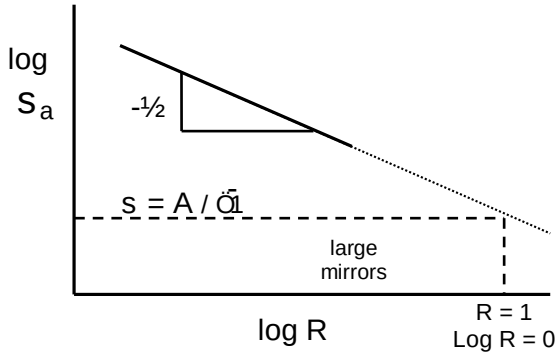

(b)

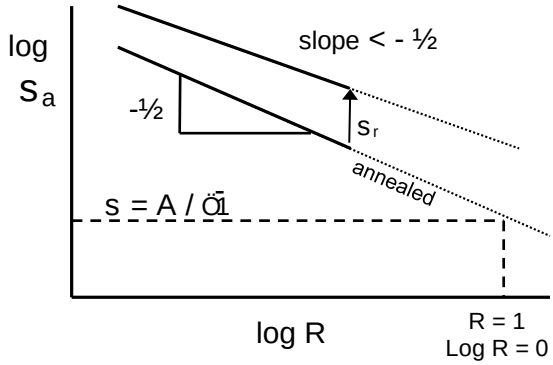

Figure D.15 *Plot of log s_a versus log R for residual stress-free parts (a) and parts with residual stress (b). Compressive residual stresses move the locus upwards, but with a different slope and intercept. Tensile residual stresses move the loci below the baseline curve (not shown).*

constants in units of MPaÖm. The mirror constant A corresponds to the stress that would create a mirror of size = 1 meter.

$$\log s_a = -\frac{1}{2}\log R + \log A \qquad \text{(D.12)}$$

where s_a is the stress at the origin site, A is the mirror constant and R is the mirror radius in the direction of constant stress. Use some judgment in the regression analysis since fracture mirror data frequently has moderate scatter. If the data does not appear to fit a trend with slope -½, then regress the data with equation D.13:

$$\log s_a = m \log R + \log A' \qquad \text{(D.13)}$$

where s_a is the stress at the origin estimated from known applied stresses. R is the mirror radius in the direction of constant stress. A¢is a modified mirror constant. Report the slope m and the alternative constant A¢ Again, use some judgment in the interpretation, since a strict linear-regression fit may produce implausible outcomes, particularly if the data is collected over a limited range of mirror sizes and stresses. Investigate possible residual stresses or specimen size or shape issues if m deviates significantly from the value –½.

If stresses are in units of MN/m^2 (MPa) and the mirror size is measured in meters, then the mirror constant A has units of $MN/m^{1.5}$ or MPaÖm. If the mirror size is 1 m, then log R = 0. Then log σ = log A and hence, σ = A. Thus, the mirror constant A corresponds to the value of stress that would create a mirror of size 1 m. Use an appropriate statistical analysis to compute an uncertainty (e.g., standard deviation) in the intercept, A.

Use consistent units with this approach for the same reasons mentioned in section 11a. If the stresses are in MPa, then the abscissa (horizontal axis) should be with radii in units of *meters or micrometers.* (If the stress units are psi or ksi, the mirror radii should be in inches.)

Since most actual mirrors that are measured are usually much smaller than unit size (e.g., 1 meter), it is apparent from Figure D.15 that the mirror constant (or the stress at R = 1) lies somewhat beyond the range of data usually collected. This method of showing the results and calculating a mirror constant was common in the older technical literature and is occasionally still found today. Deviations from the linear relationship on a log - log plot occur when residual stresses are present but unaccounted for (since the plotted stress may not be the true stress at the origin), or when the mirror size becomes large relative to the component size, or when there are stress gradients. The residual stress deviations cause the line to have a slope other than -½ as shown in Figure D.15b. Attempts to compute the residual stresses may then be made by iteratively guessing values of the residual stresses s_r, replotting the data with a vertical axis of $(s_a - s_r)$, and checking the goodness of fit of a line of slope -½. This is a fairly cumbersome process and the alternative procedure in section 11a and Figure D.7b may be simpler and more effective.

If a single mirror is measured, and the externally applied stress, s_a, and the mirror constant A are both known, then:

$$(s_a + s_r)\sqrt{R} = A \tag{D.14}$$

$$s_r = \frac{A}{\sqrt{R}} - s_a \tag{D.15}$$

Mecholsky and colleagues[18,19] have shown excellent examples of how residual surface stresses in tempered or clad glasses may be estimated from equation D.15 and fracture mechanics analysis.

11c. Comparison of the two curve fitting and regression approaches

The merits of the two plotting - regression schemes vary. They put different weights on large and small mirror measurements. In one case, the mirror constant is a slope of a line, in the other it is an intercept at R = 1, a rather large mirror size not likely to be realized in practice. Some researchers may have evaluated test pieces with residual stresses, and then force-fitted regression lines through the data with zero intercepts in the former scheme, or lines of slope -½ through the data in the latter scheme. This probably contributed to variability in published mirror constants.

Figure D.16 shows both graph types for a common set of data from the author's work on the effects of machining on the strength of silicon nitride.[6,7] A large number (N = 140) of rod- or bar-shaped specimens were tested. The author

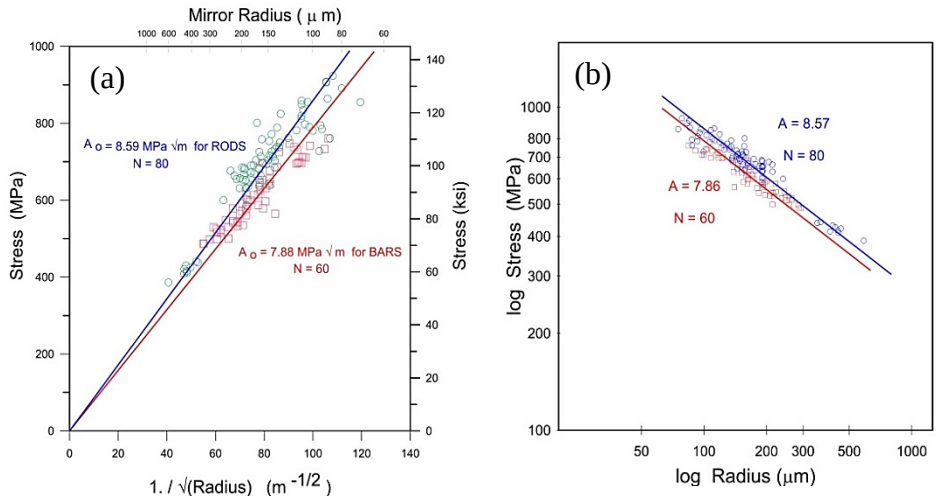

Figure D.16 *Fracture minor data for silicon nitride.[6,7] The round blue symbols are for 80 rods and the square red symbols are for 60 bars.*

measured every mirror. They had various grinding treatments. The mirror constants from the two analyses are almost identical. It is not known why there is a small difference (9%) between the constants for the rods and bars.

Data from flexurally-loaded specimens frequently deviate from the trends when mirror sizes are large and are a significant fraction (50 % or greater) of the cross-section size. Upward deviations from the log stress - log radius graphs have been noted in a number of studies (e.g., Shand,[12,20] Orr[16]). The experimentally-measured mirrors are larger than they otherwise would be in a uniform tension stress field. Regression lines chase the upward deviations from the trend and dramatically alter the estimate of the mirror constant. On the other hand, with the s versus 1/ÖR graph, large or oversized mirror data points are closer to the origin and have less influence on the regression line, and hence have less effect upon the slope which is the mirror constant A.

Regression analysis with the s versus 1/ÖR approach minimizes the deviations of s from the fitted line. Regression analysis for the log s versus log R approach minimizes deviations of log s from the fitted line.

In the 1950s and 1960s many researchers plotted log stress versus log radius probably because they were not confident of the theoretical justification for the -½ slope. They let the exponent vary on the log-log plots and discussed the differences, if any, relative to the -½ power. Differences were usually due to residual stresses or overly-large mirrors relative to the specimen size. Gradually the case for the sÖR relationship solidified, and more researchers began to plot stress versus 1/ÖR.

In summary, *the linear stress versus inverse square root radius approach is superior and is recommended by this Guide.* Analyses are simple and intuitive. The mirror constant is the slope of the regressed line. Residual stresses may be interpreted from non-zero intercepts. The uncertainty of the slope can be estimated from routine analyses available in many statistical software packages. Data deviations due to large mirrors in flexure specimens have less effect upon the regression process and the mirror constant estimates. The alternative method (log stress – log radius) may be useful in some cases for displaying data with an unusually large range of mirror sizes and stresses.[21]

12. Mirrors sizes should be collected over a broad range of sizes and fracture stresses if possible. Data from different specimen types and sizes may be combined.

This is a fairly obvious conclusion in light of the discussion in the previous paragraph. Superb examples are shown by Kerper and Scuderi[21,] for

borosilicate glass rods with diameters that varied by a factor of ten, and by Mecholsky and Rice[22] for various sized fused silica rods, disks, and fibers.

Ideally, data from many small specimens could be complemented by testing of a few large specimens. Another common procedure is to anneal or fine grind/polish some specimens to obtain high strengths, but abrade or damage others to obtain low strengths. Sometimes the mode of loading can be changed to alter the fracture stress. For example, some studies have used mirrors with large four-point and small three-point flexure specimens. Some specimens may be tested in inert conditions and others tested in conditions conducive to slow crack growth.

D.4 Some Final thoughts

The goal of these guidelines is to bring some consistency to procedures used to measure fracture mirrors. They were adopted as ASTM Standard C1678 in 2007. This should facilitate improved data bases and better estimates of failure stresses. These Guidelines were prepared on the basis of the author's own experiences as well as a careful review of sixty years of literature as summarized in reference 1. One is struck by the conclusion, which nearly all writers have reached, that measurement of the mirror sizes requires subjective interpretation. The perception of the observer and the type of equipment are important factors. Although advanced microscopy and software tools hold considerable promise in the future, it is unlikely that a simple definitive criterion (such as a set level of surface roughness) will emerge. Despite this, most students of the technique have concluded that consistent readings are possible between observers. Johnson and Holloway said:[3]

> "The position assigned to the boundary between mirror and mist zones depends upon the illumination and the magnification at which the fracture is examined, even within the range of the optical microscope. …. However, under given conditions a reproducible position for the boundary can be assigned."

Mecholsky and Freiman[11] said:

> "While one might think initially that the measurements of a mirror boundary using a microscope is quite a qualitative operation and would vary from observer to observer; in fact, experiments performed over a number of years by a large number of investigators have shown that the values of mirror constants obtained in different laboratories are quite nearly the same."

They then listed values for a few glasses and ceramics that unfortunately varied as much as 20 % to 30 %. Hopefully, adoption of the guidelines in this Guide and ASTM C 1678 will improve the consistency of future data to within 10%.

One positive conclusion is that fracture mechanics principles do seem to account for the observed shape variations in mirrors.[4,5] Orr's equation seems over simplistic, since it does not account for stress gradients or geometric effects. Nevertheless, it *does have the proper functional form* for the stress intensity of a crack in a far-field tension stress. For a small mirror in a uniform tensile stress field, equation 1 is completely justifiable.

Another interesting finding from the literature review is how few authors have shown good fracture mirror photos. Furthermore, nearly all the mirrors shown in the literature, even in the classical papers, are not exactly semicircular or circular, despite all the schematics that imply that they are. Fractographers should not be too alarmed if their mirrors are not perfect.

Many of the steps in this Guide have already been proposed. Shand recommended that stresses be corrected for the origin location,[12] that radii be measured beneath the surface to avoid surface effects,[10] that low-angle grazing illumination be used.[12] He also warned about deviations from the trends if the mirror sizes were too large relative to the component thickness.[12] Shand also said that mist could not be discerned in glass ceramics.[12] Morrell et al. [23] agonized over the interpretation of mirrors in Y-TZP zirconia (such as shown in Figures D.4 – D.6), but settled on a set of specific criteria. Optical microscopy with a stereo optical microscope at a fixed magnification was used, with grazing incidence illumination. No reflective coating was applied to the surface. The specimen sides were masked to block transmitted-light scatter. Matching fracture halves were mounted together to aid the interpretation. Six of Mecholsky and Freiman[11] recommendations match the steps in this Guide.

Appendix D References

1. G. D. Quinn, "Guidelines for Measuring Fracture Mirrors," pp. 163 – 190 in *Fractography of Glasses and Ceramics, V*, eds., J. R. Varner, G. D. Quinn, M. Wightman, American Ceramic Society, Westerville, OH, 2007.
2. ASTM C 1678, "Standard Practice for Fractographic Analysis of Fracture Mirror Sizes in Ceramics and Glasses," Annual Book of Standards, Vol. 15.01 ASTM Int., West Conshohocken, PA, originally 2007.
3. J. W. Johnson and D. G. Holloway, "On the Shape and Size of the Fracture Zones on Glass Fracture Surfaces," *Phil. Mag.*, **14** (1966) 731 - 743.
4. H. P. Kirchner and J. W. Kirchner, "Fracture Mechanics of Fracture Mirrors," *J. Am. Ceram. Soc.*, **62** [3-4] (1979) 198 - 202.

5. H. P. Kirchner and J. C. Conway, Jr., "Criteria for Crack Branching in Cylindrical Rods: I, Tension and II, Flexure," *J. Am. Ceram. Soc.*, **70** [6] (1987) 413 - 425.
6. G. D. Quinn, L. K, Ives, and S. Jahanmir, "On the Fractographic Analysis of Machining Cracks in Ground Ceramics: A Case Study on Silicon Nitride," SP 996, NIST, Gaithersburg, MD, May 2003.
7. G. D. Quinn, L. K. Ives, S. Jahanmir, and P. Koshy, "Fractographic Analysis of Machining Cracks in Silicon Nitride Rods and Bars," pp. 343 - 365 in *Fractography of Glasses and Ceramics IV*, Ceramic Transactions, Vol. 122, eds., J. R. Varner and G. D. Quinn, American Ceramic Society, Westerville, OH, 2001.
8. G. D. Quinn, J. Eichler, U. Eisele, and J. Rödel, "Fracture Mirrors in a Nanoscale 3Y-TZP," *J. Am. Ceram. Soc*., **87** [3] (2004) 513 - 516.
9. R. J. Castilone, G. S. Glaesemann, and T. A. Hanson, "Relationship Between Mirror Dimensions and Failure Stress for Optical Fibers," pp. 11 - 20 in *Optical Fiber and Fiber Component Mechanical Reliability and Testing II*, eds., M. J. Matthewson and C. R. Kurkjian, Proc. SPIE, 4639 (2002).
10. E. B. Shand, "Strength of Glass – The Griffith Method Revised," *J. Amer. Ceram. Soc.*, **48** [1] (1965) 43 - 48.
11. J. J. Mecholsky, Jr. and S. W. Freiman, "Determination of Fracture Mechanics Parameters Through Fractographic Analysis of Ceramics," pp. 136 -150 in *Fracture Mechanics Applied to Brittle Materials*, ASTM STP 678, ed., S. W. Freiman, ASTM Int., 1979.
12. E. B. Shand, "Breaking Stress of Glass Determined from Dimensions of Fracture Mirrors," *J. Am. Ceram. Soc.*, **42** [10] (1959) 474 - 477.
13. H. Fessler and D. C. Fricker, "A Theoretical Analysis of the Ring-On-Ring Loading Disk Test," *J. Am. Ceram. Soc*., **67** [9] (1984) 582 - 588.
14. J. A. Salem and L. Powers, "Guidelines for the Testing of Plates," *Cer. Eng. Sci. Proc.*, 24 [4] (2003) 357 - 364.
15. J. B. Quinn, "Extrapolation of Fracture Mirror and Crack-Branch Sizes to Large Dimensions in Biaxial Strength Tests of Glass," *J. Am. Ceram. Soc.*, **82** [8] (1999) 2126 - 2132.
16. D. R. Oakley, "Crack Branching in Float Glass Subjected to Biaxial Loading," *J. Non-Cryst. Sol.*, **196** (1996) 139 – 143.
17. L. Orr, "Practical Analysis of Fractures in Glass Windows," *Materials Research and Standards*, **12** [1] (1972) 21 - 23, 47.
18. J. C. Conway, Jr. and J. J. Mecholsky, Jr., "Use of Crack Branching Data for Measuring Near-Surface Residual Stresses in Tempered Glass," *J. Am.Ceram. Soc.*,**72**[9](1989)1584-7.
19. J. J. Mecholsky, Jr. and M. G. Drexhage, "Comparisons of Optical and Fractographic Measurements of Residual Stress in Compressively Clad Glass Rods," *J. Am. Ceram. Soc.*, **63** [5-6] (1980) 347 - 349.
20. E. B. Shand, "Breaking Stresses of Glass Determined from Fracture Surfaces," *The Glass Industry*, April (1967) 190 - 194.
21. M. J. Kerper and T. G. Scuderi, "Relation of Fracture Stress to the Fracture Pattern for Glass Rods of Various Diameters," *Bull. Am. Ceram. Soc.*, **45** [12] (1966) 1065 - 1066.
22. J. J. Mecholsky, Jr. and R. W. Rice, "Fractographic Analysis of Biaxial Failure in Ceramics," pp. 185 - 193 in *Fractography of Ceramic and Metal Failures*, eds., J. J. Mecholsky, Jr. and S. R. Powell, ASTM STP 827 American Society for Testing and Materials, West Conshohocken, PA, 1984.
23. R. Morrell, L. Byrne, and M. Murray, "Fractography of Ceramic Femoral Heads," pp. 253 - 266 in *Fractography of Glasses and Ceramics, IV, Ceramic Transactions*, Vol. 122, eds., J. R. Varner and G. D. Quinn, American Ceramic Society, Westerville, OH, 2001.

APPENDIX E TERMINAL CRACK VELOCITIES

E.1 Published values

Table E.1 on the next pages lists terminal velocities obtained by a variety of methods including direct observation with high-speed cameras, ultrasonic fractography, Wallner line analysis, and electrical resistance grid recordings. Clarifying footnotes are at the end of the table. Some of the variability in outcomes for the same material may be due to experimental errors, but much is due to variability in the materials themselves.

The most comprehensive testing of glasses was done at the Fraunhofer Institute in Germany by Schardin and Kerkhof and their colleagues in the 1950s and 1960s. Their work was discussed in detail in my 2018 review of terminal crack velocities in glasses.[1] Schardin et al.[2,3] measured v_{ct} in twenty-nine different Schott glasses, and Kerkhof [10,11] added fourteen more glasses. Only the most important glasses are listed in Table E.1. They showed that terminal crack velocities increased with decreasing density and molecular weight, and longitudinal wave velocity. In other words, materials with strong elastic bonding (high E) and low density transmit elastic waves faster and thus, cracks can run faster. On the other hand, glasses with high density and heavy molecular weights have slower maximum crack speeds. It should be noted that the two borosilicate glasses that Schardin evaluated had significantly greater network modifier atom content, higher densities, and lower terminal crack velocities than Corning Pyrex 7740 or Schott Borofloat 33 borosilicate glasses that were evaluated in later years by Kerkhof and others. Not all borosilicate glasses are the same! Kerkhof [10] in 1962 continued Schardin's work on glasses and added Corning Pyrex 7740 glass. He reported the longitudinal, shear, and Rayleigh wave velocities of these and showed interesting correlations of the maximum crack velocities with the wave velocities, densities, elastic moduli, and Poisson's ratios. Kerkhof showed the terminal crack velocities for 42 glasses with velocities ranging from 700 m/s to 2155 m/s in the appendix of his 1970 book[11] and in his Figure 6.11. The fastest glass velocities are in fused silicas (or fused quartz). A value of » 2200 m/s is often shown in textbooks or reviews. Values of 2100 m/s, 2135 m/s, and 2155 m/s, as reported by Smekal,[24] Schardin et al.,[2] and Kerkhof,[10,11] respectively, are commonly cited. Other investigators,[14,21] have reported even higher velocities: up to 2500 m/s. Ceramics and glasses have much greater terminal velocities than brittle polymers.

In this 4th edition, the discussion of the Mott-Robert-Wells model is refined, expanded, and validated by a new correlation with fracture mirror constants.

Table E.1 *Terminal Crack Velocities in Ceramics and Glasses*

Material	Terminal Crack Velocity v_{ct} (m/s)	Reference
Glasses		
Soda lime glass	1510	Schardin et al., 2,3
Soda lime glass	1580	Field, 4 and Bowden et al.,5
Soda lime glass	1536	Barstow and Edgarton, 6
Soda lime silica	1600	Congleton and Denton, 7
Soda lime silica	1550	Anthony, Chubb, Congleton, 8
Soda lime silica	1540	Richter and Kerkhof, 9
Window and Mirror soda lime glass	1500, 1520	Kerkhof (1962), 10
Plate glass – soda lime silica	1542, 1510, 1520 Ä	Kerkhof (1970), 11
Soda lime glass	1550	Döll et al. (1977), 12
Soda lime glass	1512	Döll, (1975) 13
Soda lime glass	1500	Chaudhri, 14
Soda lime silica	1550	Chaudhri and Kurkjian, 15
Soda lime glass	1485 Ä	Dimmick and McCormick, 16
Soda lime glass	1460	Winkler et al., 17
Soda lime silica	1498, 1628, 1664	Strassburger, 18
Soda lime glass	1550	Küppers, 19
Soda lime silica (Pilkington float)	1550	Dobbs, 20
Soda lime silica (Starphire)	1580	Strassburger et al., 21 McCauley et al., 29
Soda lime silica	1450 – 1500	Mohanty, 22
Soda lime silica	1500 – 1550 t	Hyodo and Nakatsuka, 23
Various flint glasses	750 - 1400	Schardin et al., 2,3
Various flint glasses	1164 - 1627	Kerkhof, (1962) 10
Heavy flint glasses	700 - 1095	Kerkhof, (1962) 10
Borosilicate crown glass (Schott BK-7)	1677	Kerkhof, (1962) 10
Borosilicate crown glass (Schott BK-7)	1800	Smekal, 24
Borosilicate crown glass (Schott NBK-7)	1729, 1801	Strassburger, 18
Zinc Borosilicate crown glass (Schott ZK-7)	1760	Kerkhof., (1962) 10
Borosilicate (Schott Borofloat 33)	1920 ± 30	Anderson et al., 25
Borosilicate (Schott Borofloat 33)	2034	Strassburger et al., 21 McCauley et al., 29
Borosilicate (Schott Supremax)	2114, 1962	Strassburger, 18
Borosilicate (Corning Pyrex)	2065, 1966	Strassburger, 18
Borosilicate (Corning Pyrex 7740)	1935, 1950	Kerkhof (1970), 11
Borosilicate (Schott Duran 50)	1958	Döll, 13
Phosphate Crown (Schott FK-52)	1163	Döll, 13
Aluminosilicate glass (Corning 1723)	1742, 1743	Strassburger, 18
Fused silica (quartz glass)	2100	Smekal, 24
Fused silica	2135, 2155	Kerkhof (1970), 11
Fused silica (quartz glass)	2155	Schardin et al., 2,3
Fused silica	2400	Strassburger et al., 23 McCauley et al., 29
Fused silica	2500	Chaudhri, 14
Fused silica	2350	Chaudhri and Kurkjian, 15
Borate glass B_2O_3	1000	Chaudhri and Kurkjian, 15
32.5% Na_2O + 67.5% B_2O_3 glass	900	Chaudhri and Kurkjian, 15
GeO_2 glass	1800	Chaudhri and Kurkjian, 15
10% Na_2O + 90% GeO_2 glass	850	Chaudhri and Kurkjian, 15
30% Na_2O + 70% GeO_2 glass	1400	Chaudhri and Kurkjian, 15
Vitreous carbon	1400	Dobbs, 20

Glass ceramics		
Glass ceramic (unidentified grade)	2157, 2083	Strassburger, 18
Glass ceramic (Transarm)	2151	McCauley et al., 29
Ceramics		
Reaction bonded Si_3N_4 (74% dense, r = 2.35 g/cm^3 AME)	2950	Congleton and Denton, 7
Hot-pressed Si_3N_4 (HS 130)	3500	Congleton and Denton, 7
KCl, single crystal cleavage {100}	700	Field, 4
KCl, single crystal cleavage {100}	1039	Winkler et al., 26
LiF, single crystal cleavage {100}	1700	Field, 4
LiF, single crystal cleavage {100}	» 2000	Gilman et al., 27
MgO, polycryst. (15 mm G.S., 85% dense)	1800	Congleton and Denton, 7
MgO, single crystal, cleavage {100}	5100	Field, 4 and Bowden et al., 5
$MgAl_2O_4$ spinel Polycrystalline (20346+20347)	2816	Strassburger and Bauer, 28
Diamond, cleavage {111}	7200	Field, 4 and Bowden et al., 5
Al_2O_3, sapphire, cleavage on m plane {10$\bar{1}$0}	4500	Field, 4 and Bowden et al., 5
Al_2O_3, sapphire, cleavage on m plane {10$\bar{1}$0}, test 17074 configuration 1, cracks A - E	4590 - 4934	McCauley et al., 29 Strassburger et al., 30
Al_2O_3, sapphire, cleavage on r plane {10$\bar{1}$2} test 17075 configuration 2, cracks A+B	4837 - 4949	Strassburger et al., 30
Al_2O_3, sapphire, cleavage on r plane (10$\bar{1}$2}, test 17076 configuration 3, crack A	5438	Strassburger et al., 30
Al_2O_3, polycrystalline (See note*) (15 mm G.S., E = 385 GPa, r = 3.67 g/cm^3)	2000 *	Congleton and Denton, 7
Al_2O_3, polycrystalline , Hoechst 98% (8.3 x 3.6 mm GS, E = 360 GPa, r = 3.79g/cm^3)	3400 – 4600 3100 – 5300	Winkler et al., 26, 31
AlON, polycrystalline	4377	McCauley et al., 29
Metals		
Tungsten, polycrystalline, rolled	2200	Field, 4 and Bowden et al., 5
Steels	1037 - 2012	Roberts and Wells, 35
Tool Steel (Pitho)	1700	Congleton and Denton, 7
Rocks		
Vermont marble	965 **	Daniel and Rowlands, 32, 33
Minnesota granite	915 **	Daniel and Rowlands, 32, 33
Norite rock	1875	Bieniawski, 34
Polymers, Plastics, Rubber		
Cellulose acetate	305 - 419	Roberts and Wells, 35
Resin Plastic	420	Kerkhof (1962), 10
Homalite 100 (thermosetting polyester)	487	Ravi-Chandar and Knauss, 36
Homalite 100 (thermosetting polyester)	338	Daniel and Rowlands, 32
Columbia Resin 39 (allyl diglycol carbonate, ADC)	350 - 513	Daniel and Rowlands, 32
Columbia Resin 39	581	Wells and Post, 47
Perspex (PMMA, acrylic)	710	Anthony et al., 8
PMMA acrylic	770	Congleton and Denton, 7
Plexiglass II, acrylic	100	Bueche and White, 37
Silicone rubbers	3 - 16	Bueche and White, 37

* This entry should be considered a value for an alumina that is not fully-dense. The material was labelled "Lucalox" in the original Congleton and Denton paper, but this is incorrect. Lucalox was a fully-dense, coarse grain, transparent aluminum oxide. The reported density of 3.67 g/cm^3 indicates the material was not fully dense, and the 15 mm grain size was too small for a typical Lucalox.

** This may be a damage wave velocity.

Ä Velocities at temperatures other than room temperature also are included but not listed here.

t Virtually identical v_{ct} results were obtained in air, vacuum, carbon dioxide, hydrogen and water.

Terminal crack velocities, v_{ct}, are limited by three factors:

a. elastic wave propagation speeds in the material
b. localized deviations of the crack from the main plane of fracture
c. evolution of the crack shape from a 2-D planar surface to a complex 3-D structure

E.2 Elastic wave velocities

The elastic wave propagation speeds ("the speed of sound") determine the speed that elastic energy is transferred to the advancing crack tip. They limit how fast the crack runs. There are three elastic waves: longitudinal (dilational), shear (transverse), and Rayleigh surface waves.[38] The longitudinal wave is the fastest, followed by the shear wave, and then the slower Rayleigh wave. These wave velocities are illustrated in Figure E.1. For a uniaxial stress situation, as

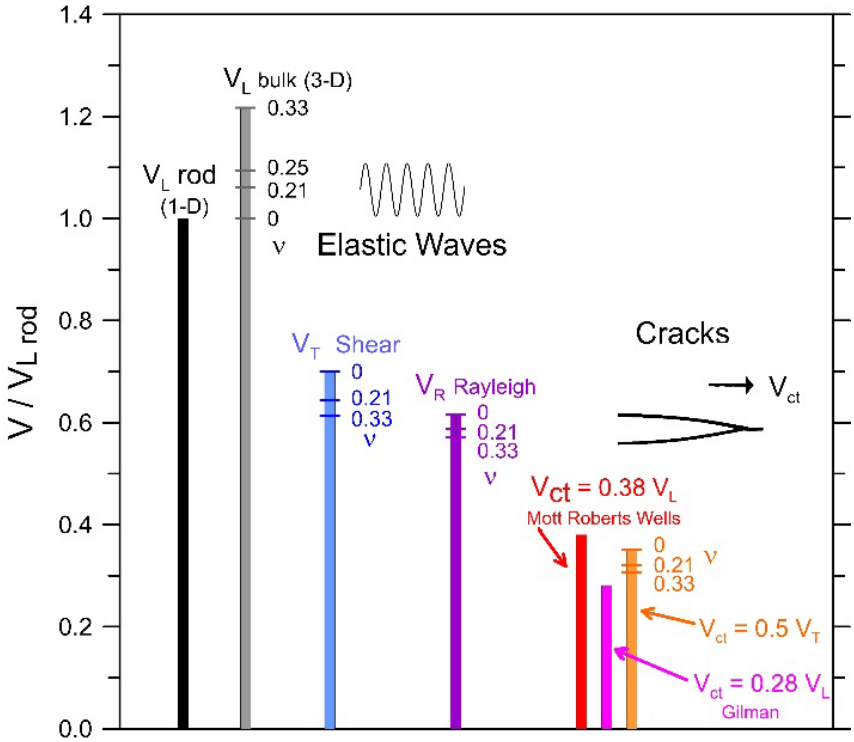

Figure E.1 *Wave and theoretical terminal crack velocities. All velocities are normalized by the one-dimensional longitudinal wave velocity, "V_L rod," in a slender rod or bar. Many of the velocities depend on Poisson's ratio, n.*

in a wave propagating in a slender rod or bar, the longitudinal wave velocity, v_L is:

$$v_L = \left(\frac{E}{\rho}\right)^{1/2} \tag{E.1}$$

where E is the elastic modulus and r is the density. For a wave propagating in a thick plate, or a three-dimensional infinite medium, the relationship has an additional term:

$$v_L = \left(\frac{E}{\rho}\right)^{1/2} \left[\frac{(1-\nu)}{(1+\nu)(1-2\nu)}\right]^{1/2} \tag{E.2}$$

where n is Poisson's ratio. The Poisson's ratio term on the right varies from 1.00 to 1.22 as n ranges from 0.00 to 0.33. In other words, for materials with positive Poisson's ratios, cracks run faster in the bulk in thick parts than in slender rods or bars. For a material with n = 0.2, the increase is 5%. If n = 0.25, the increase is 10%. These are marked by tic marks on the vertical bars in Figure E1.

The shear (transverse) wave velocity, v_t, is:

$$v_t = \left(\frac{E}{\rho}\right)^{1/2} \left[\frac{1}{2(1+\nu)}\right]^{1/2} = \left[\frac{E}{2(1+\nu)\rho}\right]^{1/2} \tag{E.3}$$

which is 30% to 50% slower than v_L in a slender rod or beam. The commonly-stated 50% reduction, i.e., $v_t/v_L = 0.5$, is for materials with n of 0.33 that is typical of metals. The 30% reduction is for a limiting case for n = 0. If n = 0.21, as for some glasses, then v_t is 40% less than v_L. These also are marked by tic marks on the vertical bars in Figure E1.

The slowest wave is the Rayleigh wave, which runs on the free surface of a material. It travels at:

$$v_R = \frac{0.87+1.12\nu}{(1+\nu)} \; v_t \tag{E.4}$$

It is 13% to 7% slower than v_t as Poisson's ratio varies from 0.00 to 0.33.

The terminal crack velocity, v_{ct}, is often expressed as a fraction of these elastic wave velocities. A crack is usually not able to outrun the speed at which elastic energy moves in a material. The specific relationships are derived from models that are based on continuum mechanics. In some cases, actual data matches the predictions, but in many instances, the cracks run much slower than predicted.

E.3 Deviations from the main crack plane

The terminal crack speed is also limited by local deviations of the crack front up and down out of the main propagation plane. These deviations create the mist and hackle in glasses and ceramics. The fast crack evolves from a flat continuous 2-D surface to a complex 3-D structure of separated micro segments. This process consumes energy and limits the maximum crack velocity. There are two sources of local crack front deviations in fast cracks in glasses and ceramics:

(a) changes in the direction of maximum principal tensile stress at the crack tip
(b) irregularities in the material's microstructure, or the microstructure itself

The first is a matter of 2-dimensional continuum mechanics, and the second is a matter of material structure. Yoffe's theoretical work[39] on the state of stress ahead of the moving crack in a continuous medium showed that the maximum principal stress moved out of plane for cracks moving at v_c ³ 0.5 v_t. This is conceptually illustrated in Figure E.2. In practice, this means that very localized segments of the advancing crack front can tilt up or down out of plane.[a] Rawson noted:[40]

"The fracture is at a loss in which way to go."

The crack front fluctuates and eventually breaks up into microsegments with steps between the microsegments. In addition. microstructural irregularities in

Figure E.2 *The maximum s_Y at the crack tip is above or below the crack plane for fast cracks, $v_c > 0.6\ v_t$. Local portions of the crack front start to wobble up or down out of plane. These deviations consume energy and occur even in a perfect continuum material. They retard crack velocity. The deviations evolve into mist and hackle that are easily discernable on glass and ceramic fracture surfaces as discussed in section 5.2.3 in Chapter 5.*

[a] Subsequent analyses (e.g., Ravi-Chandar and Knauss[36]) have suggested some specific shortcomings in Yoffe's analysis, but the key observation that the maximum stress moves out of plane is still sound.

ceramics and glasses, and even nano flaws (e.g., nano bubbles), as well as compositional or structural variations in the glass at the nanoscale may also cause local crack deviations that limit v_{ct}. These factors are not considered in the 2-D continuum mechanics models.

Cracks can run fast and match theoretical continuum mechanics predictions in dense polycrystalline ceramics with simple microstructures and in glasses with low density, open structures, minimal network modifier additives, and minimal nanostructural variations. Fused silica and some borosilicates are examples.

The mist and hackle lines associated with the formation of fracture mirror markings retard crack velocities. Chapter 5 showed that the mist and microhackle are caused by local deviations of the crack front out of plane. With ceramics, local crack front deviations are caused not only by the mist and hackle formation, but also by interactions with the microstructure or flaws. So, for example, several silicon carbides may have very different v_{ct} even if they have similar elastic moduli and densities, since they have different microstructures. Microstructural irregularities in ceramics, porosity in particular, affect terminal velocities by not only triggering crack front perturbations, but also by altering density and elastic modulus and hence the wave velocities.

E.4 Mott-Robert-Wells model

There are competing models and controversy as to which of the three types of elastic waves controls v_{ct}. These are discussed in detail in my 2018 review[1] and only a few summary remarks are shown below. The elastic energy model by Mott[41] in 1948 and expanded by Roberts and Wells[42] in 1954 is simple continuum mechanics model that is fundamentally sound. The model correlates terminal crack velocity to the longitudinal elastic wave velocity. When a crack propagates rapidly, the strain energy release is balanced by the energy to create the fractured surfaces plus the kinetic energy of the moving crack. This is conceptually illustrated in Figure E.3. Atoms on either side of the crack surface and in the surrounding strain energy field move as the crack grows. These atoms have mass and inertia and the longitudinal wave speed controls the speed of their movement. Mott simply analyzed the vertical displacements of material around a crack moving at a constant velocity and added a kinetic energy term to the classic Griffith equation. The term is often described as the “kinetic energy of a crack,” but it more specifically is the kinetic energy of the material being displaced around a crack. Mott concluded that crack velocity was linearly-proportional to the longitudinal wave

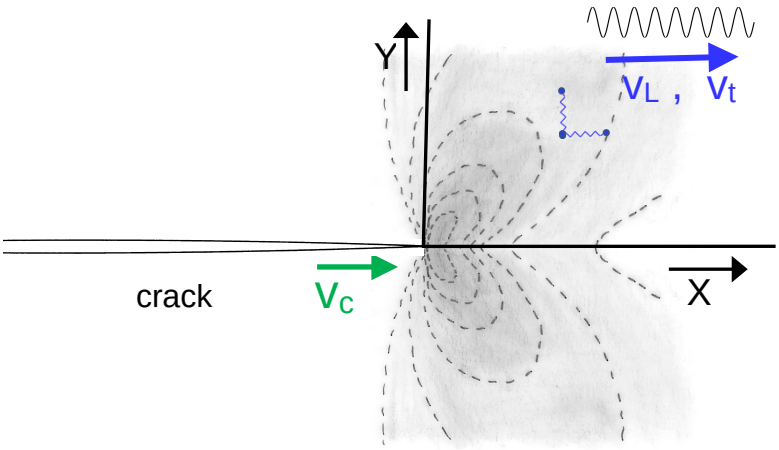

Figure E.3 *Strain map showing how strain energy moves as the crack advances. The elastically-strained atoms (suggested by the blue balls and springs) transfer energy by longitudinal and shear wave propagation. (The oscillating wave form is conceptual and not to scale.) Atoms in the strain field around the crack move vertically (and to a lesser extent horizontally) as the crack advances.*

velocity, $v_{ct} = k\ v_L$. Roberts and Wells[42] extended Mott's analysis by using Westergard's solutions for the X-Y displacements and motion of the material around a crack. (They noted in their Appendix I the assistance of George Irwin in this analysis.) They determined the constant, k, in the Mott formulation was 0.38, so that:

$$v_{ct} = 0.38\ v_L \qquad \text{(E.5)}$$

Gilman concurred with this approach in 1956,[43] and later in 1998 developed a similar relationship relating the terminal crack velocity to the longitudinal wave velocity, but with a proportionality constant of 0.28.[44] The author of this Guide believes that both shear and longitudinal waves are involved with the transmission of elastic energy in the material around and ahead of an advancing crack, but equations E.1 to E.3 show the velocities of these two wave types are related. Schardin[2,3] and Kerkhof [10,11] measured many terminal crack velocities and their data shows that some glasses have terminal crack velocities that closely match equation E.5. These are glasses that have simple open structures such that the crack can run straight and fast. Schardin et al.'s and Kerkhof's measurements showed that the actual range of crack velocities for all their glasses was v_{ct}/v_L = 0.19 to 0.39 as shown in Figure E.4. The more <u>complex the composition, and the denser the glass, the slower the velocity</u>. Again, as noted above, local deviations of the crack front or interactions with microstructure or

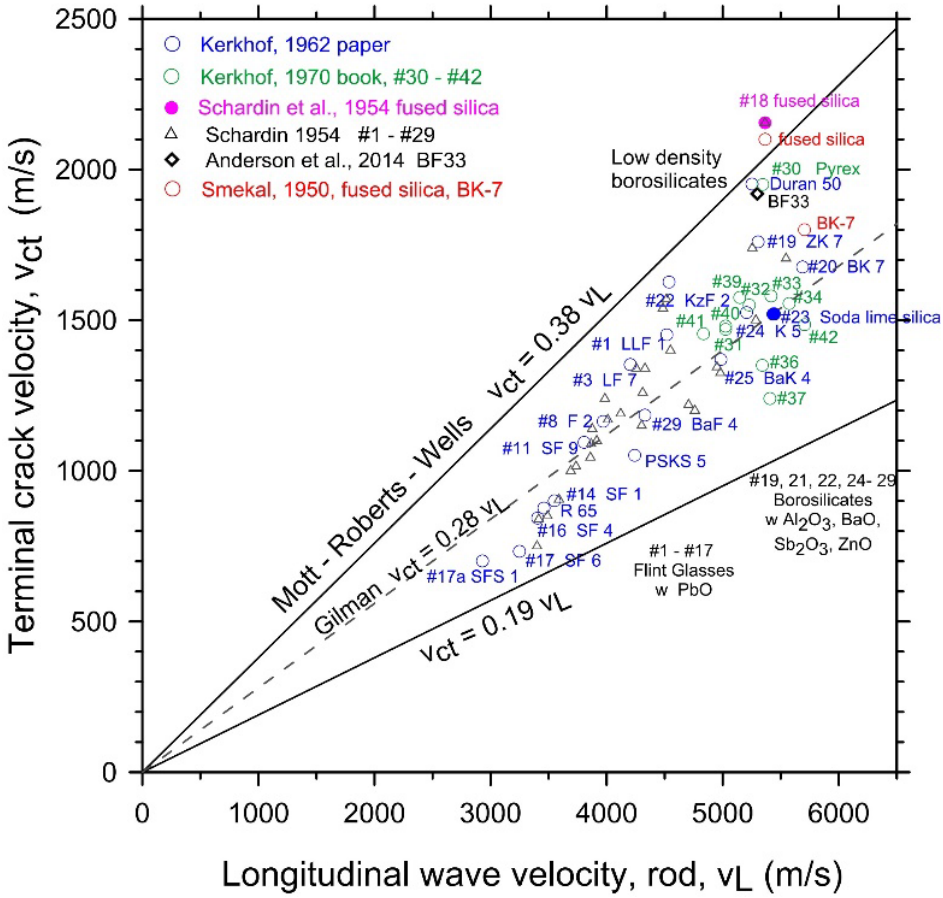

Figure E.4 *Terminal crack velocities in glasses. Each symbol corresponds to a particular glass. Most data are from Schardin[2,3] and Kerkhof.[10,11] Their data points are labelled with Schardin's glass code number as well as the Schott glass code if it was a Schott glass. Table E.1 lists the other data.*

nano flaws account for the lower observed velocities. The glasses with open structures, namely fused silica and low-density borosilicate glasses (Corning Pyrex, Schott Duran and Borofloat 33) on the upper right of Figure E.4, have high v_{ct} and fit the Mott-Robert-Wells model quite well.

Figure E.5 shows the available data for ceramics. Some cracks actually run faster than the model predicts, but much of such data is for cracks running on cleavage planes in single crystals.

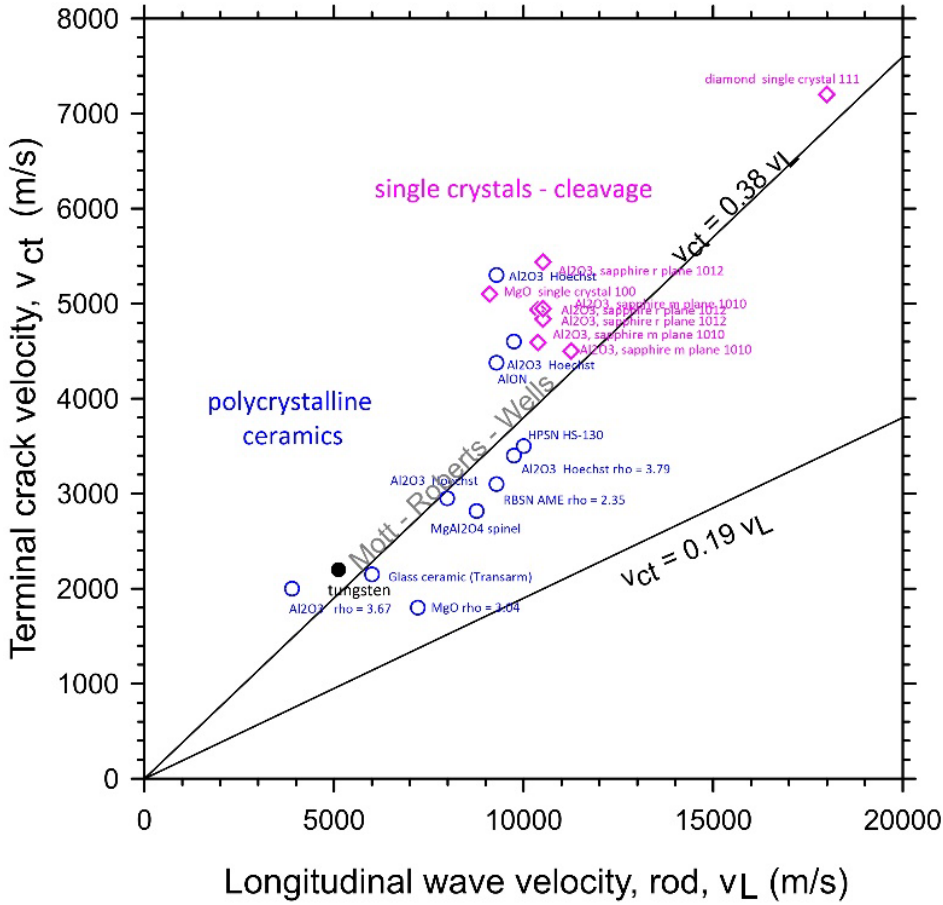

Figure E.5 *Terminal crack velocities in ceramics. The materials and original references are identified in Table E.1.*

Some have criticized the Mott-Roberts-Wells model as too simplistic. Snowden[45] and Erdogan[46] pointed out that the model used quasi-static stress and displacement fields for what actually is a dynamic problem. It is suggested that the actual stresses and strains very close to the crack tip are different in the dynamic problem. In contrast, work by Wells and Post[47] (that was directly supported by G. Irwin[48]) showed dynamic stress distributions are not appreciably different from static ones for specimens subjected to fixed displacements at the ends. That study featured spark camera and photo-elasticity methodologies on Columbia Resin 39 and confirmed that $v_{ct} = 0.38\ v_L$ for that material.

The fact remains, however, that the longitudinal and transverse elastic wave velocities are much faster than the moving crack as shown in Figure E-1, so the quasistatic stress distribution assumption in the Mott-Robert-Wells model is reasonable. Anderson[49] also concluded that kinetic energy is the major reason why crack velocity is a specific fraction of the sound wave velocity.

The beauty of global energy approaches (e.g., the Griffith model and the Mott-Robert-Wells adaptation) is that they do not get bogged down by precise stress and strain details at the crack tip. The critics also argue that the dynamic fracture toughness may be different from the quasi-static fracture toughness (and while this may be true for metals,) it is far from clear that is true for glasses and ceramics. Steverding and Lehnigk[50] derived equations of motion for cracks subjected to stress pulses and concluded that stress waves can accelerate cracks to terminal velocity in extremely short times, as short as microseconds. They further concluded that "the critical threshold stress for a given crack length is the same for dynamic and static conditions."

The author of this Guide therefore concludes that the Mott-Robert-Wells model has considerable merit and the predicted crack velocities match measured velocities in some important glasses and most ceramics.

Several studies showed that the terminal velocity is independent of environment. For example, Hyodo and Nakatsuka[23] obtained virtually identical results for soda lime silica in air, vacuum, carbon dioxide, hydrogen and water. This should come as no surprise since there is insufficient time for a fast-moving crack to interact with a potentially reactive species. Dimmick and McCormick[16] showed that the terminal velocity of soda lime silica had only a slight temperature dependence from liquid nitrogen temperatures up to 200 ^{o}C.

Since glasses and ceramics are not homogeneous and isotropic at nano or microstructural size regions, a simple modification to equation E.5 is proposed:

$$V_{ct} = 0.38\, q\, V_L \qquad \text{(E.6)}$$

where q is a structure factor that considers the nano or microstructure that can cause local 3-dimensional perturbations of the crack tip out of the main plane of crack propagation. For an ideal homogenous and isotropic medium, $q = 1$ but it can be < 1 for a real material with structural variations. An interesting topic for future research would be to quantify the parameter q, which may be some function of the variability of a material's structure and atomic bonding. Simple open-structure glasses like fused silica have fewer nano and microscale features that lead to crack front deviations.

A new insight into q factors is from studying the fracture mirror constants. Fracture mirror boundaries are formed by cracks running at or near the terminal velocity. Cracks running in simple open-structure glasses like fused silica may take longer for the 3-D perturbations to develop and form the mist and hackle as compared to higher-density glasses with substantial network modifiers such as soda lime silica. In other words, the mirror-mist and mist-hackle boundaries occur at larger distances R away from an origin for open-structure low-density materials, leading to higher mirror constant values in accordance with Ohr's equation (Chapter 5 and Appendix C) that is repeated here:

$$s\sqrt{R} = A \qquad \text{(E.1)}$$

where A is the mirror constant (either A_i or A_o with units of MPAÖm), s is the stress (MPa), and R is distance (m). A review of the fracture mirror constants in Appendix C shows that the mirror constants for fused silica (and the lower-density borosilicates) are indeed larger than those for other higher density and more complex glasses. The mirror-mist constants for the latter are 1.8 MPaÖm to 2.1 MPaÖm and are 1.9 MPaÖm to 2.3 MPaÖm for the former. The mirror constants are thus 5% to 10% greater and the terminal velocities about 500 m/s faster for the open-structure, low-density glasses (2,000 m/s) than for soda lime silica (1,500 m/s). In accordance with Ohr's equation, a 5% to 10% difference in the mirror radius R leads to 10% to 20% change in A. The differences in v_{ct} are even greater for the higher-density more complex glasses. Thus, q is 1.0 for the low-density, open-structure glasses, and 1,500/2,000 = 0.75 for the more complex, higher-density glasses like soda-lime-silica.

In contrast, to the above Mott-Robert-Wells model, it is commonly said in the dynamic fracture mechanics literature that the crack can travel as fast as, or is "limited by," the Raleigh wave velocity, a wave that travels on surfaces and is much slower than the longitudinal waves. Figure E.6 illustrates the concept which dates back to Stroh in 1957.[51] Many advocates of this concept refer to

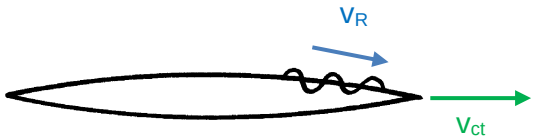

Figure E.6 *Stroh[51] and others in the dynamic fracture community contend that Rayleigh surface waves on the opened-up crack faces limit the terminal crack velocity. The present author finds this explanation to be implausible.*

Erdogan's comprehensive 1968 paper[46] that suggested that Mott's crack was analogous to an internal crack with pressure acting on its faces. It was argued that "motion of surface disturbances in a nondissipative medium" on the crack faces put limits on the terminal crack velocity. Hence, Rayleigh waves were controlling. The author does not believe this. The kinetic energy term of a fast-moving crack in the Mott-Robert-Wells model involves a lot of material in the bulk around a crack (see Figure E.3 above) and not merely that at the crack faces. The usual exposition of the Rayleigh wave theory elsewhere is based on continuum mechanics models that lead to $v_c \gg v_R$, but then it is acknowledged that virtually no material conforms to this relationship. Evidence has shown that the terminal crack velocity varies with material, and it is much slower: v_{ct} is only 0.3 to 0.6 times v_R. As discussed in my review paper,[1] there is no data that supports the model of $v_c \gg v_R$ for glasses or ceramics.

Figure E.7 *It is often claimed that plastic damage zone microcracks open up ahead of the rapidly-advancing crack and cause the local deviations that limit the crack's speed. This is implausible and does not occur in brittle glasses or ceramics.*

The dynamic mechanics community (e.g., Ref. 36) rationalize the discrepancy between predicted and observed terminal velocities by arguing that plastic damage zone microcracks open up ahead of the crack and these cause the local deviations that limit crack speed. This is illustrated in Figure E.7. This does occur for polymeric materials. The evidence on the fracture surfaces is called: Kies markings,[52] also called hyperbolic and parabolic markings. It has been reported that they sometimes occur in metals.[b,53]

I conclude that there is no evidence of fast cracks creating plasticity-generated flaws or microcracks ahead of the crack in glasses or dense ceramics.

---

[b] There are only two suggested examples in the literature, and they were for unusual glasses that were loaded with large internal inclusions, such as in the volcanic glass obsidian. See Smekal (Ref. 24, 1950, Fig. 10) and Kerkhof (Ref. 11, 1970, Fig. 7.10). Tsirk[53] stated that the markings were not caused by microcracking ahead of the crack tip, but instead were double wake hackle lines from the inclusions as shown in his book on pages 70-73. This author concurs with Tsirk.

Other prominent experts have reached the same conclusion. In his 1990 book, Fréchette wrote[54] that Kies markings were associated with obsidians with numerous internal inclusions, but Tsirk disagreed (see footnote b on previous page). Regarding ceramics, Fréchette wrote:

> ”They might be expected in ceramics which have potential origins scattered throughout their bulk, but it has not been reported.”

The respected metallurgist and fractographer Derek Hull wrote in his 1999 book:[55]

> “For brittle materials, . . . there is no convincing experimental evidence for the initiation of cracks ahead of the growing crack in these materials. . . It is difficult to envision why a growing crack should expand by micro-crack initiation rather than by bond breakage at the tip.”

In a discussion of the Wells and Post paper, published in the same journal, no less an authority than G. Irwin stated:[48]

> “It would appear that for a crack extending under the action of a steadily increasing crack extension force, it is the roughening and branching of the crack which places a limit on the velocity of crack extension.”

Much of the thinking in the dynamic fracture mechanics community has been based on experiences with convenient “brittle” materials which are polymers like Homalite 100a polyester, Columbia Resin CR 39 polycarbonate, polymethyl-methacrylate (PMMA), Araldite, or Perspex. They are not as brittle as glasses and ceramics whose terminal crack velocities are many times faster than those in polymers.

E.5 Exceptions

Sometimes cracks can run faster than the expected terminal velocity. Cracks can run very fast on cleavage planes in single crystals since-there is little tendency for them to deviate out of plane. As noted above, with glasses and polycrystalline ceramics, under normal loading conditions the crack velocity is restricted by the speed of elastic energy transfer to the advancing crack tip. Alternatively, if energy can be applied directly to the crack itself, as in shock loading or laser pulse loading, the crack can run faster and even super-sonically.[56] Some shock loading cases can create stress waves that drive a crack faster than the normal terminal velocity provided that the crack does not develop mist, hackle, or branching. Snowden[45] observed terminal crack

velocities in Pyrex borosilicate glass as high as 3,050 m/s in shock loading via flyer plate impact experiments. This unusual crack velocity was attributed to the rapid load transfer provided by stress waves. He made the very interesting observation that the fracture surfaces for this very high velocity example were mirror smooth and free of hackle. Evidently the extreme loading conditions did not "give enough time" for a crack to start deviating out of plane even on a local level. In his book, Fréchette wrote that: "There was neither time nor space to develop instabilities at the crack front." Snowden's results are consistent with section E.3 above, where it was explained how 3-dimensional crack plane deviations put limits on crack velocity. Rader[57] estimated that some of his cracks in soda lime silica traveled as fast as 1,800 m/s due to stress waves in his explosively-loaded plates.

In some ballistic impact conditions, a *damage wave* of cracking in glass can proceed at velocities 80 % to 90 % of the *longitudinal* wave speed.[58,59] High speed photography revealed that individual cracks in ballistically-impacted soda lime glass traveled no more than the conventional terminal velocity of 1,480 m/s, but that damage wave cracks nucleated right behind the shock wave. Schardin in 1969[3] also showed some interesting examples where "supervelocity cracks" *appeared* to run faster than the expected terminal velocity, but these were shown to be secondary fractures occurring along scratches or tension band streaks ahead of the main crack.

E.6 Crack arrest

At the other end of the spectrum, cracks can decelerate and even stop. It is usually due to decreases in the stresses acting on the advancing crack. This is common in thermal shock cases where there are large stress gradients in a component. Schardin in 1969[2] noted that decelerating cracks often have discontinuous velocity changes and can even stop abruptly. Snowden also observed discontinuous velocity changes in his stress wave loaded glass plates.[45] Continuum mechanics cannot account for this, but it is perfectly plausible if the crack front is three-dimensional (see Chapter 5) and if there are structural variations in the glass or ceramic.

E.7 Conclusions

The Mott-Robert-Wells model accounts for the terminal crack velocity in brittle materials. It is a modification of the Griffth equation that includes a term for the kinetic energy of a crack. The terminal velocity of a crack in a glass or ceramic is controlled by:

a. The longitudinal wave velocity in the material.

b. Localized deviations of the crack plane (even in a continuum) due to shifts in the direction of the maximum principal stress.
c. Evolution of the fast crack from a smooth 2-D planar surface to a complex 3-D segmented structure. Localized segments of the advancing crack front can tilt up or down out of plane even in a continuum, thereby breaking up the continuous crack front. This process is enhanced by the material's nano- and microstructure.

Appendix E References

1. G. D. Quinn, "On Terminal Crack Velocities in Glasses," *Int. J. Appl. Glass Science*, **10** [1] (2019) 7 - 16.
2. H. Schardin, L. Mücke, and W. Struth, "Bruchgeschwindigkeit von Gläsern," *Glastechn. Ber*., **141** [5] 1954, 19 -147. Also available translated into English as: "Fracture Velocities in Glasses," *Glass Industry*, **36** [3] (1955) 133 – 168.
3. H. Schardin, "Velocity Effects in Fracture," Chapter 16 in *Fracture*, Proc. Int. Conf. on Atomistic Mechanism of Fracture, Swampscott, MA, (1969) 297 – 330.
4. J. E. Field, "Brittle Fracture: Its Study and Application," *Cont. Phys*, **12** [1] (1971) 1 –31.
5. F. P. Bowden, J. H. Brunton, J. E. Field, and A. D. Hayes, "Controlled Fracture of Brittle Solids and Interpretation of Electrical Current," *Nature*, **216** (1967) 38 – 42.
6. F. E. Barstow and H. E. Edgarton, "Glass Fracture Velocity," *J. Am. Ceram. Soc.*, **22** [9] (1939) 302 – 307.
7. J. Congleton and B. K. Denton, "Dynamic Fracture Toughness Experiment," Final Technical Report, University of Newcastle on Tyne to U. S. Army European Research Office, July 1975.
8. S. R. Anthony, J. P. Chubb, and J. Congleton, "The Crack-Branching Velocity," *Phil. Mag*., **22** [180] (1970) 1201 – 1216.
9. H. G. Richter and F. Kerkhof, "Stress Wave Fractography," pp. 75 – 109 in *Fractography of Glass*, eds., R. C. Bradt and R. E. Tressler, Plenum, NY, 1994.
10. F. Kerkhof, "Bestimmung der Maximalen Bruchgeschwindigkeit Verschiedener Gläser nach der Ultraschall-Methode," *Glastechn. Ber.*, **35** [6] (1962) 267 – 272.
11. F. Kerkhof, *"Bruchvorgänge in Gläsern,"* DGG, Frankfurt, 1970.
12. W. Döll, M. Schinkler, and G. W. Weidmann, "Measurement of Fast Crack Propagation in Glass Under Dynamic Loading," pp. 965 – 969 in *Fracture 1977*, ed. D. Taplin, Univ. Waterloo Press, Canada, 1977.
13. W. Döll, "Investigations of the Crack Branching Energy, *Int. J. Fract*., **11** (1975)184-186.
14. M. M. Chaudhri, "High-Speed Photographic Investigations of the Dynamic Localized Loading of Some Oxide Glasses," pp. 87 – 113 in *Strength of Inorganic Glass*, ed., C. Kurkjian, Plenum, NY, 1985.
15. M. M. Chaudhri and C. K. Kurkjian, "Impact of Small Steel Spheres on the Surfaces of "Normal" and "Anomalous" Glasses," *J. Am. Ceram. Soc*., **69** [5] (1986) 404 - 410.
16. H. M. Dimmick and J. M. McCormick, "Variation, with Temperature, of the Cracking Velocity of Glass," *J. Am. Ceram. Soc*., **34** [8] (1951) 240 – 241.
17. S. Winkler, H. Senf, and H. Rothenhäusler, "High Velocity Fracture Investigation in Alumina," pp. 165 – 183 in *Fractography of Glasses and Ceramics, Advances in Ceramics*, Vol. 22, eds., J. Varner, and V. Fréchette, American Ceramic Society, Westerville, OH, 1988.

18. E. Strassburger, "Ballistic Impact Damage in Different Types of Glass and Glass Ceramic," Fraunhofer, Ernst Mach Institute Tech. Report E21/16, August 2016.
19. H. Küppers, "The Initial Course of Crack Velocity in Glass Plates," *Int. J. Fract.* **3** (1967) 13 - 17.
20. H. S. Dobbs, "Vitreous Carbon and the Brittle Fracture of Amorphous Solids," *J. Phys. D.: Apply. Phys.*, **7** (1974) 24 – 31.
21. E. Strassburger, J. W. McCauley, and P. Patel, "Preliminary Results of Ballistic Impact Damage and Fragmentation in Fused Silica, Borofloat, and Starphire Glass Plates," presented at the April 2015 MACH Conference, Annapolis, MD.
22. B. Mohanty, "Some Characteristics of Thermal Fracture in Glass," *Exp. Mech*., **12** (1972) 471 – 474.
23. S. Hyodo and H. Nakatsuka, "Photographic Study of Crack Propagation in Glass Plates in Controlled Environments," pp. 1865 – 1870 in Proc. 1st Intl. Conf. on Fracture," eds., T. Yokobori, T. Kawasaki, and J. L. Swedlow, Sendai, Japan, Vol. 3 (1966).
24. A. Smekal, "Verfahren zur Messung von Bruchfortpflanzungs-Geschwindigkeiten an Bruchflächen," *Glastechn. Ber*., **23** [3] (1950) 57 – 67.
25. C. E. Anderson, Jr., R. P. Bigger, and C. E. Weiss, "Crack and Damage Velocities in Ballistic Experiments," *Int. J. Appl. Glass Sci.*, **5** [4] (2014) 374- 383.
26. S. Winkler, D. A. Shockey, and D. R. Curran, "Crack Propagation at Supersonic Velocities, I," *Int. J. Fract. Mech*., **6** [2] (1970) 151 - 158. (The v_{ct} of 1037 m/s for LiF is attributed to M. Schinker, unpubl.)
27. J. J. Gilman, C. Knudsen, and W. P. Walsh, "Cleavage Cracks and Dislocations in LiF Crystals," *J. Appl. Phys*., **29** (1958) 601 – 607.
28. E. Strassburger and S. Bauer, "Analysis of the Interaction of Projectiles with Ceramic Targets by Means of Flash X-ray Cinematography and Optical Methods," *Advances in Ceramic Armor, Cer. Eng. and Sci. Proc*., **38** [2] (2017) 205 - 219.
29. J. W. McCauley, E. Strassburger, P. Patel, B. Paliwal, and K. T. Ramesh, "Experimental Observations on Dynamic Response of Selected Transparent Armor Materials," *Exptl. Mech*., **53** (2013) 3 - 29. (Terminal velocities of radiating cracks created by impact of a sphere on the specific planes. Velocities were calculated by G. Quinn from the photos. Blunt cylinder tests caused damage fronts which travelled much faster.)
30. E. Strassburger, P. Patel, and J. W. McCauley, "Visualization and Analysis of Impact Damage in Sapphire," U.S. Army ARL Tech. Report, ARL-RP-345, Nov. 2011.
31. S. Winkler, H. Senf, and H. Rothenhäusler, "Wave and Fracture Phenomena in Impacted Ceramics," Institut für Werkstoffmechanik report V23/89, Freiburg, Germany, for European Research Office, U.S. Army, London, August 10, 1989.
32. I. M. Daniel and R. E. Rowlands, "Studies of Wave and Fracture Propagation in Rock Media," Project Final Report D6069, IITRI, Chicago, ILL, June 1973.
33. I. M. Daniel and R. E. Rowlands, "On Wave and Fracture Propagation in Rock Media," *Exptl. Mech.*, **15** [12] (1975) 449 – 457.
34. Z. T. Bieniawski, "Fracture Dynamics of Rock," *Int. J. Fract*., **4** [4] (1968) 415 - 430.
35. D. K. Roberts and A. A. Wells, "The Velocity of Brittle Fracture," *Engineering*, **178** (1954) 820 - 821.
36. K. Ravi-Chandar and W. G. Knauss, "An Experimental Investigation into Dynamic Fracture: III. On Steady-State Crack Propagation and Crack Branching," *Int. J. Fract.*, **26** (1984) 141 – 154.
37. A. M. Bueche and A. V. White, "Kinematographic Study of Tensile Fracture in Polymers," *J. Appl. Phys.*, **27** [9] (1956) 980 – 983.
38. M. A. Meyers, "Dynamic Behavior of Materials," Wiley, NY, 1994.
39. E. H. Yoffe, "The Moving Griffith Crack," *Phil. Mag*., **42** [330] (1951) 739–750.

40. H. Rawson, "A Note on the Velocity of Crack Propagation in Glass," *J. Soc. Glass Tech.*, **36** (1952) 297 – 299.
41. N. F. Mott, "Fracture of Metals: Theoretical Considerations," *Engineering.*, **16** (1948) 16 – 18.
42. D. K. Roberts and A. A. Wells, "The Velocity of Brittle Fracture," *Engineering*, **178** (1954) 820 - 821.
43. J. J. Gilman, "Propagation of Cleavage Cracks in Crystals," *J. Appl. Phys.*, **27** [11] (1956) 1262 – 1269.
44. J. J. Gilman, "Fast, Faster, and Fastest Cracks," *Phil. Mag. Lttrs.*, **77** [2] (1998)79–82.
45. W. E. Snowden, "Crack Growth in Glass Subjected to Controlled Impacts," Ph.D. Thesis, Univ. California, Lawrence Livermore Berkeley Laboratory, Livermore, CA, Report for U.S. Energy Research and Development Administration, Nov. 1976.
46. F. Erdogan, "Crack-Propagation Theories," in *Fracture*, Vol. II, ed. H. Liebowitz, Academic Press, New York, 1968, p. 497 - 590.
47. A. A. Wells and D. Post, "The Dynamic Stress Distribution Surrounding a Running Crack - A Photoelastic Analysis," Proceedings of the SESA, **16** [1] (1958) 69 - 92.
48. G. R. Irwin, "Discussion of 'The Dynamic Stress Distribution Surrounding a Running Crack - A Photoelastic Analysis,'" *idem*, pp. 93 - 96.
49. O. L. Anderson, "The Griffith Criterion for Glass Fracture," in *Fracture*, Averbach, Feldbeck, Hahn, Thomas, eds., Wiley, New York, 1959, pp. 331 - 353.
50. B. Steverding and S. H. Lehnigk, "Response of Cracks to Impact," *J. Appl. Phys*, **41** [5] (1976) 2096 – 2099.
51. A. N. Stroh, "A Theory of the Fracture of Metals," *Adv. in Physics*, **6** (1957) 418 – 465.
52. J. A. Kies, A. M. Sullivan, and G. R. Irwin, "Interpretation of Fracture Markings," *J. Appl. Phys.*, **21** [7] (1950) 716 - 720.
53. A. Tsirk, *Fractures in Knapping*, Archeopress, Oxford, UK, 2014.
54. V. D. Fréchette, *Failure Analysis of Brittle Materials, Advances in Ceramics*, Vol.28, American Ceramic Society, Westerville, OH, 1990.
55. D. Hull, *Fractography*, Cambridge University Press, Cambridge, UK, 1999.
56. S. Winkler, D. A. Shockey, and D. R. Curran, "Crack Propagation at Supersonic Velocities, I," *Int. J. Fract. Mech.*, **6** [2] (1970) 151-158.
57. D. Rader, "On the Dynamics of Crack Growth in Glass," *Proc. Soc Exptl. Stress Anal.*, **24** [1] (1967) 160 – 167.
58. U. Hornemann, H. Rothenhäuser, H. Senf, J. F. Kalthoff, and S. Winkler, "Experimental Investigation of Wave and Fracture Propagation in Glass Slabs Loaded by Steel Cylinders at High Impact Velocities, pp. 291 – 298, in Int. Phys. Conf. Series No. 70, *3rd Conference on Mechanical Properties at High Rates of Strain*, Oxford, The Institute of Physics, London, 1984.
59. S. Winkler, H. Senf, and H. Rothenhäusler, "High Velocity Fracture Investigation in Alumina," pp. 165 – 183 in *Fractography of Glasses and Ceramics, Advances in Ceramics*, Vol. 22, eds., J. Varner, and V. Fréchette, American Ceramic Society, Westerville, OH, 1988.

INDEX

Abrasion	6-50, 6-81, 6-85, 6-87
Acid, aqua regia	3-28, 3-29
Acid etch	4-25, 6-97
Additively-manufactured ceramic	iii, 6-2, 6-8, 6-9, 6-11, 6-12, 6-14, 6-17, 6-73, 6-76
Alumina	(many examples throughout this Guide)
Alumina furnace plate	4-37
Alumina polycrystalline lamp (PCA)	10-12, B-11
Alumina single crystal	see Sapphire
Alumina, whisker-reinforced	7-72, 7-73
Aluminum oxynitride (AlON)	5-39, 5-76, 6-7, 6-21, 6-95, 6-96, Chapter 10 Case 5
Anesthesiologist	4-57
Anticracks	4-79, 4-80
Armor plates, Armor windows	Appendix B-9, B-10, B-12, B-13
Arrest lines (interruption marks)	5-3, 5-49, 5-50, 5-60, Section 5.5, 5-83, 5-84
Arrowhead, obsidian	3-9
Artificial intelligence	11-1
Automotive parts, ceramics	6-72, Appendix B-1, B-2
Automobile window	4-1, 4-36, 6-70, 7-9, Appendix B
Ball bearings	3-65, 6-45, 6-47, B-14
Ball mill	6-5, 6-21, 6-88
Baseline microstructural flaws	Section 6.12
Bend bar	4-16 - 4-22, 4-61, 4-62, Chapter 10 Case 8
Biaxial disk	3-24, 3-28, 4-5– 4-12, Section 4.6.3, 4-55, 5-74, 6-36, 6-51, 6-57, 6-66, 7-4
Biaxial stress, see also biaxial disk	1-3, 1-4, 4-9, 4-11, 4-25, 4-31, 4-38, 4-39, 4-45, 4-59, 4-60, 4-61, 4-79
Bioceramics	see Dental ceramics, B-18, B-19
Black Fingerprint Powder	3-30
Black light	3-64, 3-65
Bleach	3-6
Blood	5-35, 5-68
Bone	2-2, 3-30, 3-70, 3-71, 4-22, 4-71, 5-35
Boron carbide, B_4C	4-72, 4-74, 6-46, 7-27, 7-59
Bottles	4-5, 4-9, 4-11, 4-33, Section 4.13, 7-3, Chapter 10 Case 4, Appendix B-6 – B-8
Boundary phases, ceramics	5-72, 5-76, 5-79 – 5-81
Bovine dentin	4-18
Branching	Sections 4.2 - 4.5, pages 4-31, 4-32, 7-7 - 7-9
Branching angles	Section 4.3
Branching constant	4-13, 7-7, Appendix C
Branching distance	4-13, 7-7 – 7-9
Brittle fracture	1-1
Brittleness	4-81
Bruxism	4-57
Bump checks, Bruise checks	4-45, 4-57, 6-49, 6-50, 6-79
Bubbles	5-38, 5-49, Section 6.6.1, 6-32, 6-37, 6-79, 6-80, 6-88, 6-100, 6-101

Butterfly pattern	4-36, 6-22
C-crack, crescent crack	3-65, 6-45, 6-48, 6-85
Cellulose acetate	3-37 - 3-39, 3-42
Cell Phone	3-9, 3,10, B-3, B-4
Center heated plate	Section 4.12, 4-60, Chapter 10: Case 6
Ceramic Tube	Chapter 10 Case 2, Appendix B
Chain of events	1-9, 1-10
Chalk	3-31
Chamfers, bevels	6-20, 6-28, 6-51, 6-64, 6-95, 10-18
Channel crack	4-67, 4-68
Checks	4-33, 4-45, 4-57, 4-62, 6-49, 6-79
Chill checks	see Origins
Chips, chipping	see Edge chips, Glue chips
Clay	3-5, 3-35, 6-91 - 6-93
Cleaning coatings off	3-28 – 3-30
Cleaning specimens	2-1, 3-6 – 3-8, 3-68, 5-1, 5-86
Cleaning, green dye	3-29, 3-30
Cleavage	5-3, Chapter 8
Cleavage step hackle	8-1, 8-6, 8-7, 8-10, 8-11, 8-22
Coatings, on fracture surfaces	Section 3.9
Coatings	Section 4.19.3, Appendix B-26
Coating flaws	Section 6-15, 6.86
Combination flaw	Section 6.11
Component fracture patterns	4-14, Section 4.7, Section 4.16, 4-72, 6-107
Composites	6-18, 6-25, 6-78, 6-88, 7-28, 7-58, 7-72, 7-73, Chapter 9
Compression curl	3-17, 4-18 – 4-20, 5-1, 10-27
Compression fracture	Section 4.19.8
Conchoidal fracture	5-3, 8-1, 8-2, 8-5
Cone cracks	see Hertzian cone crack
Contact cracks	3-42, 3-65, 4-34, 4-45, Section 4.19.5, 6-37, Sections 6.7.4, 6.7.5, pages 6-64, 6-79, 6-83, 6-85 - 6-88, 6-92, 6-101, Chapter 10 Cases 1, 2, 4, 11, 13
Contaminants, see also clay	6-20, Section 6.10
Cordierite Glass Ceramic	6-12, 6-97, 6-98
Cords	see Origins, chord
Corrosion flaws	Section 4.19.4, 6-33
Crack arrest	see Arrest lines, Section E.6
Crack blunting	7-43
Crack branching	see Banching
Crack bridging	7-55, 7-56
Crack healing	4-33, 7-43
Crack, processing	4-13, 6-5, 6-16, Section 6.7.1, Section 6.8.1
Crack, intersecting	Section 4.8
Crack, spiral	4-25 - 4-27, 4-39, 4-40
Crack velocity	5-4 – 5-5, 7-46 – 7-50, Appendix E
Crack velocity, terminal	5-4 – 5-5, 5-7, Section 5.2.2, 5-11, 5-19, 5-26, 5-27, 5-34, 5-55, 5-61, 7-46, 7-48, Appendix E

Crackle glass, Craquelle, Craquelé	Section 4.19.2, 4-63
Crazing	Section 4.19.3, 6-100
Credibility, fractographer' s	11-3
Crizzling	4-57, 4-66, Section 4.19.4
Creep fracture	Section 5.8.4
Crescent crack	See C-crack
Critical strain energy release rate, G_{Ic}	7-24, 7-26
Crossing cracks	Section 4.8, 4-47, 4-48,
Cusps	6-9, 6-10, Section 6.13
Dark-field illumination	3-25, 3-33, 3-34, 8-7, 8-8
Debonding	Chapter 10, Case 7
Debris on fracture surface, fatigue	5-85, 5-86
Deep Reactive Ion Etching (DRIE)	6-99, 8-24, 8-26, Chapter 10 Case 9
Deer	4-28
Defect, see also flaws and origins	6-1
Delaminations	6-73, 6-74
Delta markings	5-3, 5-42
Dental ceramics, crowns, bridges	3-40, 3-41, 4-52, 4-53, 4-56, 4-66, 5-39. 5-86, 5-87, 6-7, 6-10 - 6-13, 6-24, 6-25, 6-29, 6-47, 6-48, 6-63 6-71, 6-75, 6-78, 6-92, 6-93, 6-96 - 6-98, 6-100 Chapter 10 Cases 11 and 12, 11-3, B-19 - 21
Dental composites, filled and unfilled	3-24, 3-29, 5-35, 5-36, 6-25, 6-78, 9-5 – 9-7
Dental plaque	3-6, 6-92, 6-101
Dental replicas	3-39 – 3-42
Denture material	4-51
Detective	1-7, 10-24, 11-1
Dicing, tempered glass	4-14, 4-35
Differential Interference Contrast (Nomarski)	D-12
Digs	6-37, 6-38, 6-42, 6-46
Disk specimen	see Biaxial disk
Dislocations	3-62, 3-63
Dome, IR	see Sapphire dome, AlON dome, Appendix B-10
Dome, submersible glass	4-7
Double cantilever beam (DCB) specimen	8-4
Double torsion (DT) specimen	5-42, 5-54, 8-4
Drawings	see Sketches
Dunt crack	6-75
Dwell mark	see Arrest line
Dye staining	3-29, 3-30, Section 3.24, 3-63 - 3-67, 4-62, 6-11, 6-14, 6-17, 6-76, 6-78
Dye penetration	3-63 – 3-67, 4-62, 6-17, 6-30, 6-47, 6-62, 6-89, 6-90
Dynamic fatigue (variable rate strength)	5-72, 5-74, 7-52
E-glass composite	9-4, 9-5
Edges, bevels, chamfers	6-2, 6-3, 6-20, 6-28, 6-35, 6-44, 6-51, 6-64 , 6-95
Edge chips	Section 4.15, Section 6.7.7, 6-37, 6-87, Chapter 10 case 11
Electrical insulators	3-38, 6-7, 6-49, 6-97, B-16
Electronic part, multilayer capacitor	3-24

Electronic part, thick film resistor	6-69
Electronic part, varistor	6-19, Appendix B
Ellipses, partial from SCG	5-62, 5-74, 5-75
Environmental barrier coating (EBC)	4-67
Exceptions	1-11, 4-1, 4-5, 4-17, 4-61
Exemplars	Section 4.17
Expert System	11-1
Extrinsic flaws	6-4
Failure analysis	1-2, 1-6 - 1-9, 2-1, 10-24
Fan cracks	4-12, 4-23
Far field stress	7-24, 7-32
Fatality	6-97
Fatigue crack, cyclic loading	3-25, Section 5.8.5
Fiber composite	Chapter 9 , Appendix B-24, B-25
Fiber, nonoptical	Chapter 8, B-24
Fiber, optical	B-24
Fiber reinforcement	7-19, chapter 9
Fiber testing	4-15, 4-16
Fingerprint powder	3-30
Fingerprints	1-9, 3-39, 3-68
Finite element analysis	1-4, 1-5, Section 4.18, 7-20
Firing (sintering) cracks	See cracks, processing
Flaw bluntness	7-23, 7-40 - 7-45
Flaw linkage	6-8, 6-9, 6-61, Section 6.11, 6-94, 6-102, 7-44, 7-45
Flaw management	7-72, 7-76
Flaw shielding	7-44, 7-46
Flaw size	6-3, 6-23, 6-37, 6-38, 6-53 – 6-59, 6-81, Sections 6.12 and 6.18, Chapter 7
Flaw size distribution	Section 6.18, 7-74, 7-75
Flaw truncation (partial exposure)	6-100, 7-43, 7-44
Flexural strength	Section 4.6.2
Flexural stress gradient	D-24, D-25
Flow lines of stress	7-20 – 7-21, 7-25, 7-46
Focus stacking	3-1, Section 3.5, 3-21
Ford Rotor	Chapter 10 Case 1
Ford Turbocharger	6-72
Fractal analysis	7-63 – 7-68
Fractography, definition	1-1, 1-2
Fractography, Rules of Thumb	11-2 – 11-3
Fractology	1-2
Fracture surface energy	7-22, 7-16, 7-26
Fracture map	5-82, 5-83
Fracture mirror	Chapter 5, definition on page 5-19, 1-1, 3-20, 3-34, 3-35, 3-38, 3-59, 3-60, 7-1, 7-8, Sections 7.4, 7.6, 7.7, 7.10, 7.14.4, page 7-48, Appendices C and D
Fracture mirrors, multiple	5-2, 5-26
Fracture mirror, single crystals	Chapter 8
Fracture toughness, definition	7-24
Fracture toughness test, double torsion	5-42, 5-54

Fracture toughness test, SEPB	3-26
Fracture toughness test, Vickers indentation	Section 6.8.3, 7-23, 7-25, 7-28, 7-30, 7-42, 7-57, 7-59, 7-60, 7-62, 7-63, 7-68, 7-71
Fracture toughness test, Knoop SCF	Section 6.7.3, 7-59 -7-61
Fractographic montages	5-86, 5-87, 6-105, 6-106
Fracture toughness	Chapter 7
Fracture toughness, single crystal	8-3, 8-4, 8-6
Fragmentation	4-12, Section 4.5, 4-16, 4-23, 4-27, 4-36, 4-72 - 4-44, 7-1 – 7-7, 7-63 – 7-65, 7-69
Fringe	5-42
Fuel cells, solid oxide	B-17
Furnace plate	4-37, 4-38, 4-60, 4-62, Chapter 10 Case 6
Gas turbine rotor	Chapter 10, Case 1
Gemstones	B-26
Glass	
Borosilicate, Pyrex	4-2, 7-11, 7-12, 7-14, 7-16
Borosilicate crown (BK-7)	4-6, 4-24, 4-25, 6-36, 6-77, 7-2, 7-4, 7-13, 7-35, 7-37, 7-59
Chalcogenide	5-1
Fused silica	5-1, 5-5 – 5-7, 5-17, 6-6, D-3
Fused silica, sintered	Chapter 10 Case 7
Phosphate	5-68
Soda lime	(many examples throughout this Guide)
Glass ceramic	6-8, 6-12, 6-78, 6-92, 6-97, 6-98
Glass ceramic, dental	3-30, 6-78, 6-92, 6-101, 10-25, 10-29 – 10.33
Glass disease	4-57, 4.69
Glass horn, “post horn”	4-57, 4-58
Glaze, veneers	3-38, 3-42, 5-38, 5-39, 5-86, 6-47, 6-48, 6-75, Section 6-15, 6-92, Section 6.15, Chapter 10 cases 10, 11, Appendix B-26
Gloves, cotton	3-2, 3-47
Glue, specimen reconstruction	4-2, 4-3
Glue chips	Section 6.7.8
Granite	E-3
Grazing illumination	3-11, 3-22, 3-23, 3-25, 3-33
Green pen, dyes	see dye staining
Griffith flaw	definition: 6-1, 6-81, 6-88, 7-21
Griffith equation	7-21
Grinding	Section 6.7.6
Gull wings	5-21, 5-54, 5-55, 7-47
Gull wing mirrors	8-12, 8-12, 8-18, 8-21
Gun barrel, ceramic	Chapter 10 Case 2
Hackle	Chapter 5, definition on page 5-19
Hackle, cleavage step	8-1, 8-6, 8-7, 8-10, 8-11, 8-22
Hackle, grinding crack	6-53, 6-55, 6-57, 6-58
Hailstone	7-4
Hair	see Origins, hair
Halo, slow crack growth	5-73, 5-75

Handling damage (see also contact damage)	Section 6.7.3, 8-9
Heat-strengthened glass	4-34, 4-61, 6-87
Hertzian cone cracks	4-24, 4-35, Section 6.7.5, 6-83, 6-85, 10-26, 10-30, 10-32, 10-36
Hinge fracture	4-41, 4-43, 4-44
Hip balls, ceramic	4-55, 4-58, 5-74, Appendix B
History of brittle materials fractography	1-9, 1-10
Hopf bifurcation, thermal cracks	4-38
Human bones	see bone
Human enamel	4-4, 4-60
Hybrid flaws	Section 6.11
Hyperbolic markings	5-12, 5-18, 5-41
Ice glass	4-63
Illumination	Chapter 3
Impact	4-1, 4-2, 4-26, 4-28, 4-34 - 4-38, 4-41 - 4-44, 4-52, 4-54, 4-59, Section 4.19.5, 4-71, 4-73, 4-76, 5-58
Impact, hailstone	7-4
Indentation fracture mechanics	7-23, 7-25, 7-28, 7-57, Section 7.12
Insulator, electric	3-28, 6-7, 6-49, 6-97, Appendix B
Intergranular fracture	5-3, 5-23, 5-24, 5-69 – 5-71, 5-73, 5-74
Intersecting cracks	Section 4.8, 4-64
Intrinsic flaws	6-4
Intubation (surgery)	4-57
Invisible cracks	Section 4.9, 6-41, 6-84
Joint	5-3
Kennedy Center tempered glass	6-43
Kies markings (polymers)	5-18, 5-41
Kitchenware	1-10, 6-81, 6-86, 6.87, B-21, B-22
Knoop indentation crack	see Origins, Knoop indentation
K-V diagram (slow crack growth)	Section 7.10
Laboratory fractures	4-1, Section 4.6, Section 4.16
Lambda lines	5-63
Lamp fracture	4-14, 7-7, Appendix B
Lances, see also hackle	5-22, 5-23, 5-36, 5-42, 5-46, 8-11, 8-16, 8-20
Laser pointer	3-25
Lateral cracks	6-34, 6-41, 6-52, 6-78, 6-85, 7-59, 7-60, 7-63
Law of normal crack propagation	1-11, 4-5
Lead zirconium titanate (PZT)	3-61, 5-40, 5-61, 6-73, B-16, B-17
Leader crack	4-41, 4-43, 4-44
Lithic fractures, rocks	3-6, 3-31, 4-72, 4-79 – 4.81, 5-3, 5-36, 5-42, 5-47, B-26 – B-28, E-3
Lithic fractures, obsidian	see Obsidian
Litigation	1-8, see also the Spangenberg 1963 article page B-7
Machine shops	Chapter 10 Case 8
Machining, grinding	Section 6.7.6

Magnesium fluoride 5-71, 5-74, Appendix B
Magnesium oxide 8-1
Magnesium aluminate spinel, see spinel
Marble E-3
Mars, the planet 4-67
Maximum distortion energy criterion 1-5
Mechanical engineers 1-3 – 1-5
Mechanical overload 4-2, Section 4.19.2
Medicinal vial 4-33, 4-42, 4-45, 4-57, 5-66, 6-50, 6-79, 6-83, Chapter 10 Case 4, Appendix B
Microcracking 7-28
Microelectromechanical structures (MEMS) 8-24, Chapter 10 Case 9, B-14, B-15
Microflaw pocket Section 6.16
Micrometer, contact damage from 6-48
Microscope Chapter 3
Mirror, space SiC honeycomb 6-98
Missile IR domes see Sapphire domes, see AlON
Missile radomes Chapter 10 Case 7
Mist Section 5.2.2, definition on page 5-19
Mohr's circle 1-4
Mohr-Coulomb failure criterion 4-78, 4-79
Montages 5-86, 5-87, 6-105, 6-106
Mudcrack 4-67, 4-68, 6-68

Near surface 6-2 – 6-4, 6-9
Neutral axis, bending 4-17, D-24
Nickel sulfide see Origins, nickel sulfide
Nomarski illumination, (see also DIC) D-12
Nomenclature 1-8, 1-9, 5-3, 6-1, 6-79

Obsidian 3-9, 5-18, 5-21, 5-41, 5-54, 5-67, 5-68, B-28
Optical comparator 3-3
Optical profilometer see Section 3.19
Origin Chapter 6
- Abrasion, abrasion tracks 6-83, 6-50, 6-81, 6-85, 6-87, 6-87
- Agglomerate 3-50, 6-4 - 6-6, 6-13, Section 6.6.4, 6-71, 6-76, 6-95 9-1
- Ball mill pieces 6-5, 6-21, 6-88
- Baseline microstructure Section 6.12
- Blank pressing flaws 6-13
- Blisters 6-8, 6-76
- Bruise checks See Origins, bump checks
- Bubbles 5-38, 5-49, Section 6.6.1, 6-32, 6-37, 6-79, 6-80, 6-88, 6-100, 6-101, 11-3
- Bump checks 4-45, 6-49, 6-50, 6-79, 6-83
- Chatter marks, cracks, chatter sleek 5-33, 6-85 - 6-87
- Chill checks 4-33, 4-62, 6-83 – 6-85
- Chips See edge chips, glue chips
- Contact cracks See Contact cracks
- Cords, glass 6-80, 6-82

Compositional inhomogeneity	3-50, 3-51, Section 6.6.6, 6-32
Cusp	see Origins, geometric sharp points, cusps
Dandruff	6-88
Debonded area	10-17
Delaminations	6-73, 6-74
Devitrification stones, inclusions	6-80
Disk pore	6-11
Dunt cracks	6-30, 6-75
Dust	6-81, 6-88
Etch groove	Chapter 10 Case 9
Fatigue crack	3-25, Section 5.8.5
Feces	6-88
Fiber, lint	see Origins, hair
Fiber clump	9-1
Firing cracks	see Cracks, processing
Frictive crack, materials transfer	6-83, 6-85
Geometric sharp points, cusps	6-9, 6-10, Section 6.13
Glue chips	Section 6.7.8
Grain boundary	Section 6.6.8, 6-96, 6-102, 6-103
Hair (and lint)	3-24, 6-7, 6-88, 6-89
Handling damage (see also contact)	Section 6.7.3, 6.42, 8-9, 10-23
Heat sleeks	6-83
Hybrid	Section 6.11
Impact	4-13, 4-14, 4-30, 4-34 – 4-36, 4-42 - 4-45, 4-59, 4-70, 4-71, 5-58, Section 6.7.4, 8-23, 8-25
Inclusion	3-6, 3-29, 3-35, 3-50 – 3-53, 3-63, 4-4, 4-35, 4-59, 4-72, 4-76, Section 6.6.5,
Inclusion, Nickel sulfide	see Origin, Nickel sulfide below
Inclusion, tungsten silicide	6-21
Insect	6-88
Knoop indentation cracks	3-30, 3-50, 3-64, 5-37, 5-40, 5-73, 5-75, Section 6.8.3, Section 7.12, 8-4 - 8-7, 8-31, 10-8 – 10-10, D-6
Labels, applied ceramic (ACL)	6-86
Large grain	Section 6.6.7, 6-104, 10-23
Lint (hair)	see Origins, hair
Machining (grinding) cracks	3-66, 5-25, 5-25, 5-30, 5-31, 6-6, Section 6.7.6, 10-3, 10-4, Chapter 10 Case 6, 10-16, 10-23, 11-3
Machining crack skin zone	6-56, 6-60
Microflaw pockets	Section 6.16
Nickel sulfide, NiS glass	3-9, 4-35, 6-22, 6-23, B-2
Pecks	Section 6.7.2, 6-42, 6-83
Pits	Section 6.7.2, 6-99, 10-24
Polishing surface flaws	3-62, 5-30, 5-34, 5-74, 6-85, Section 6.7.3, 6-83, 6-85, 8-23, 8-24, 10-12, 10-37
Pore	6-4, Section 6.6.1, 6-94, 10-18, 10-19, 10-23
Porous region	Section 6.6.2, 6-94, 6-95, 6-103, 10-18, 10-19, 10-23
Porous seam	Section 6.6.3, 9-3, 10-18, 10-19, 10-23
Pressing flaws	6-13, 6-104

Processing cracks	see Cracks, processing
Quartz grains, Quartz inversion	6-29, 6-30, 6-75
Scratch	5-30, 5-31, 5-52, 5-66, 5-74, 6-6, Section 6.7.3, 8-9, 8-23, 8-24, 10-23
Seeds, glass	6-8, 6-79, 6-80, 6-82
Shards, stray	6-90
Silicon vein	6-89
Sleeks	6-79, 6-83, 6-85
Stones, glass	Sections 6.6.5 and 6.8.5
Striae, glass	6-80, 6-82
Surface void	Section 6.7.1
Thermocouple bead	6-88
Vickers indentation cracks	5-28, 5-75, Section 6.8.3, 7-23, 7-25, 7-28, 7-30 7-42, 7-57, Sections 7.12 and 7.14.5
Volcano	6-79
Whisker clump	9-1
Wormhole	6-14
Origins, multiple	5-2, 5-26, 5-58
Oxidation	Section 4.19.4, 5-79, 6-33, 10-24
Parabolic markings	5-12, 5-18, 5-41
Parabolic double wake hackle	5-41
Parfocal	3-12, 3-19
Parting, rocks, minerals	5-3
Patriot missile	Chapter 10 Case 7
Pattern recognition	1-2, 1-3
Pharmaceutical vials and syringes	4-33, 4-42, 4-45, 4-57, 5-66, 6-50, 6-79, 6-83, Chapter 10 Case 4, Appendix B
Phase instability	6-89
Photogrammetry	3-56, 3-70, 3-71
Plane strain and plane stress	1-5
Plaque, dental	3-6, 6-92, 6-101
Plasma asher	8-28, 8-29
Plastic yield zone	1-5
Plasticity	5-72, 5-80
Plastics	5-7, 5-12, see also polymers, E-3, E-13
Plate, whiteware	3-42
Plexiglass, Perspex	5-18, E-3, E-13
Poisson’s ratio	7-26, 7-38, 7-40, 7-47, E-4, E-5
Polariscope	Section 3.25, 3-67
Polarizer	Section 3.25, 3-27, 6-82, 8-8, 8-27, 8-28, 8-30
Polished microstructural section	6-5, Section 6.17
Polymers	2-1, 2-2, 5-7, 5-18, E-1, E-3, E13
Polyvinylchloride (PVC) replicas	3-39
Polyvinylsiloxane (PVS) replicas	3-39 – 3-42
Porcelain	3-37, 3-38, 3-42, 3-63, 6-7, 6-8, 6-11, 6-13, 6-29, 6-30, 6-49, 6-63, 6-97, 6-100, Appendix B
Porcelains, dental	4-49, 4-56, 4-66, 6-8, 6-11, 6-13, 6-48, 6-63, 6-75, 6-78, 6-96, 6-97, 6-101, 11-3
Porcelain electrical insulator	3-38, 6-7, 6-49, 6-97

Porcelain toilet	3-63, 4-71, B-22
Potassium dihydrogen phosphate (KDP)	4-61, 6-39
Pressure flaking	5-59
Pressure vessel	Section 4.13
Puzzle	1-3, 1-7, 10-24, 11-2
Pyrex bowl, thermal shock	4-2, 4-3
R-curve	5-75, 5-76, 6-61, 6-62, 7-26, 7-27 - 7-29, 7-42, 7-43, 7-45, Section 7.11, 7-63
R factors, thermal shock	4-60
Radome, fused silica	Chapter 10 Case 7
Reliability	10-1, 10-19
Renegade abrasive grit (Rogue particles)	6-6, 6-39, 6-40, 6-60, 6-61
Replicas	Chapter 3
Replicates, exemplars, testing of	Section 4.17
Residual stress	1-5, 4-2, 4-34, 4-66 – 4-68, Section 4.19.6, 4-76, 4-77, 5-31, 7-7, 7-13, 7-42, 7-46
Estimates of magnitude	Section 7.14, D-27 – D-31
Grinding	7-68
Heat strengthened glass	5-32
Indentation	5-75, 6-77, 7-60, 7-62, 7-63, Section 7.14.5
Mirror shapes, effect on	5-28, 5-32 - 5.33, D-22, D-23
Tempered glass	4-2, 4-3, 4-11, 4-14, 4-34, Section 4.11, 5-32, 5-34
Resins	5-7, 5-26, 5-35, 5-36, E-1, E-3, E-13
Resin-matrix composite, dental	6-25, 6-78, 9-6 – 9-8
Rib marks	5-3, 5-50, 5-63
Rings of Saturn	6-8, 7-23, 7-41
River deltas	5-3, 5-42
Rock fracture	see Lithics, B-26 – B-28
Rogue particles	(see Renegade abrasive grit)
Roman bottle	4-65
Roman brick	4-49
Roman glass	4-65, 4-70, 6-44
Rotor, gas turbine	Chapter 10 Case 1
Round robin, flexural strength	Chapter 10 Case 8
Round robin, fractography	Chapter 10 Case 10
Round robin, machining	Chapter 10 Case 8
Saliva	5-68
Sapphire, single crystal alumina	3-10, 3-62, 3-63, 3-67, 4-30, 5-66, 6-36, 6-42 Chapter 8, Chapter 10 Case 13
Sapphire dome	3-10, 3-62, 4-30, 5-66, 6-36, 8-9, 8-23 – 8-25
Sapphire tubes	8-28 – 8-31
Scarps	Section 5.6, 7-53, 8-22, 8-24, 10-10, 10-11
Scratch, see also origin	5-30, 5-31, 5-52, 5-66, 5-74, 6-6, Section 6.7.3, 10-23
Scratch/Dig specifications	6-37, 6-38
Scratch forensics	6-39
Seals, ceramic	B-11
Shark’s teeth	6-53, 6-55, 6-57, 6-58

Shear bands, compression	4-75 - 4-79
Shear stress	4-17
Shivering	4-66, 6-100
Shock loading	5-7
Sialon	6-21, 6-35, 7-73, 7-74, 7-76
Side-wall damage	6-63
Silica, fused	see glass, fused silica; Chapter 10 Case 7
Silicon	3-3, 6-23, 6-26, 6-89, 6-99, 6-104, 7-36, Chapter 8, Appendix B-16
Silicon carbide, CVD	5-45, 9-3, Chapter 10 Case 9
Silicon carbide, fibers	9-1 – 9-3, 9-5
Silicon carbide, machine gun barrel	Chapter 10 Case 2
Silicon carbide, furnace plate	Chapter 10 Case 6
Silicon nitride	(many examples throughout this Guide)
Single crystals	Chapter 8, 6-41
Alumina	see Sapphire
Spinel	8-4, 8-5, 8-12 8-21, 8-27
Silicon	3-3, 6-99, 7-36, Chapter 8
Zirconia, cubic	7-27, 8-1
Size effect, fractography	iv, Section 5.10
Sketches	4-29 – 4.31, 5-87
Skin, Human - contamination	6-91
Sleeks	6-79, 6-83, 6-85
Sling shot projectile	6-49
Slow crack growth	4-36, Section 4.19.8, Section 5.8, 6-67, 7-23, 7-24, 7-26 – 7-29, 7-42, 7-45, 7-46, Section 7.10, Chapter 10 Cases 1, 3
Solar cells	Appendix B-5
Specular illumination	3-26, 3-27
Spinel, magnesium aluminum oxide	6-30, 8-4, 8-5, 8-12 8-21, 8-27
Spiral crack	4-25 - 4-27, 4-39, 4-40
Spontaneous fracture	4-72, see also Origins, nickel sulfide
Spray-dried particles	6-5, 6-13, 6-18, 6-19, 6-71
Stable crack growth	Section 5.8, 7-23, 7-43, 7-46, Section 7.10, Section 7.11, 7-62, 7-63
Standards	
ASTM C 162, glass terminology	6-79
ASTM C 1161, flexural strength	10-17
ASTM C 1322, fractography	6-94, 6-105, 7-25, 7-35, 10-23
ASTM C 1421, fracture toughness	7-25, 7-34, 7-60,
ASTM C 1678, fracture mirrors	7-17, C-1, D-1, D-34
ASTM E 399, fracture toughness	7-23
ISO 10110-7, Surface imperfections	6-36
ISO 14704, flexure	10-17
ISO 18756, fracture toughness	7-34, 7-60
MIL STD 1942 (MR), flexure	10-17
MIL HDBK 790, fractography	10-22
MIL-O-1380A, optical, scratch/dig	6-37
MIL-PRF -13830B, optical, scratch/dig	6-37, 6-38
MIL-C-48497A, coatings, scratch-dig	6-38

Standard Reference Material 2100, K_{Ic}	7-28, 7-60
Stage micrometer	3-31, 3-32
Static fatigue	5-71, 7-51, 7-52, Chapter 10 Case 3
Steel, fatigue crack	3-25, 5-84
Step hackle	5-3, section 5.3.6
Stereolithography	6-2, 6-8, 6-9, 6-11, 6-12, 6-14, 6-17, 6-73, 6-76
Stereophotogrammetry	3-56
Stereoscope	3-55 – 3-56
Streaks	5-21, 5-67, 5-68
Stress corrosion	5-71, 5-72, Chapter 10 Case 3
Stress far field	definition 7-24, 7-25, 7-32, 7-62
Stress flexural	4-16 – 4-22
Stress gradients	1-5, D-24, D-25
Stress hoop	4-10, 4-11, 4-24, 4-25, 4-38, 4-39, 4-42, 4-45, 4-46, 4-56, 4-60, 4-65, 6-98, Chapter 10 Cases 11,12, D-26
Stress intensity	Chapter 7
Stress rupture	7-51, 7-52, 10-3, Chapter 10 Case 3
Stress state, uniaxial, biaxial, triaxial	1-4 – 1-5, 4-73 - 4-79, Chapter 7
Stress state, plane stress, plane strain	1-5
Stress wave fractography	Section 3.21
Stresses, Maximum Principal	1-4, 1-5
Striae, see also origins	1-8, 6-80, 6-82
Striations, fatigue cracks	1-8, 5-42, 5-83, 5-84, 11-1
Striations, grinding	6-6, 6-35, Section 6.7.6, 6-64, 0-18
Subcavitation hackle	5-69, 5-68
Superglue	4-3
Surface crack – fracture mechanics	7-31, Sections 7.5.3, 7-46, 7-54, Section 7-12
Surface crack in flexure	see Origins, Knoop
Surface finish	6-51
Surface grinding	Section 6.7.6
Syringes	6-50
Tape	4-3, 4-14, 4-15, 4-47, 4-48, 4-54
Tempered glass, heat-strengthened glass	3-9, 4-2, 4-3, 4-11, 4-14, 4-34, Section 4.11, 4-71, 4-72, 5-32 - 5-34, 6-22, 6-23, 6-41, 6-43, 6-67 6-69, 6-70, 6-81, 6-86, 6-87, Section 7.2.2, 7-8, 7-9, Section 7.3.2, 7-70, Appendix B
Tension strength	4-11, 4-15, Section 4.6.1, Chapter 10 Case 9, D-5
Terminal velocity	Section 5.2.2, Appendix E
Thermal crack	6-74
Thermal rounding	4-13
Thermal shock	4-2 – 4-3, 4-5, 4-33, 4-40, 4-42, 4-57, 4-58, Section 4.19.2, 8-30
Thermal stresses, thermal fracture	4-1, 4-14, 4-30, 4-38 – 4.40, 4-42, Section 4.19.2, 6-74, 6-75, 6-80, 6-81, 6-83, 6-86, 6-98, 6-100, 8-9, 8-22 – 8-25, 8-28 -31, Chapter 10 Cases 6 and 13
Theta strength specimen	6-98, 6-99, 8-24, 8-25
Time dependent fracture	4-59, Section 4.19.7, Section 5.8
Toilet	4-71, Appendix B-22

Tooth	4-4, 4-51, 4-55 - 4-57, 4-60
Torsion	4-9, 4-11, Section 4.14, 5-23, 5-44, 5-46
Transformation toughening	7-26, 7-28, 7-42, 7-55, 7-57
Transgranular fracture	5-3, 5-23, 5-24, 5-39, Section 5.7, 5-73, 5-74, 5-77, 10-12
Transillumination	3-26, 3-27, 4-4, 4-5, 8-8, 9-7, 10-21
Tube fracture	4-43, 4-44, 4-62, 4-72, 8-28 – 8-31, 10-4– 10-7, Appendix B
Tungsten carbide, WC	6-20, 6-21, 6-46, Appendix B-23
Turbocharger, silicon nitride	6-72
Twins, Twinning	3-27, 3-58, 3-67, 3-68, 4-75 - 4-77, 4-79, 8-2, 8-8, 8-27 - 8-30, Chapter 10 Case 13
Ultrasonic fractography	Section 3.21, 5-4, 5-11, 5-40, 5-46, 5-59 -5-62, 5-67
Varistor, ZnO	6-19
Velocity hackle	Chapter 5, definition on page 5-19
Veneer, dental	5-39, 5-86, 6-47, 6-48, 6-75, 6-100, 6-101 Chapter 10 cases 10 and 11
Vials, medicinal	see Medicinal vials and Appendix B
Vicinal illumination	3-24
Vickers indentation flaws	see Origins, Vickers indentation
Vienna airport gateway, tempered glass	6-22
Von Mises failure criterion	1-5, 4-79
Wallner lines	3-59 – 3-61, Chapter 5 and section 5.4, pages 6-41, 6-44, 6-67, 6-87, Section 7.9. 8-1, 8-2, 8-10, 8-25
Watch bracelet, ceramic	6-72
Water drops, impact	6-50
Water hammer	4-27, 4-41, 4-43, B-4
Wavy fracture	4-38 – 4-40, Chapter 10 Case 6
Weibull, distribution, strength scaling	6-1, 6-3, 6-8, 6-105, 7-58, 7-63, Section 7.15, Chapter 10 Case 9
Whisker lances, single crystal	8-11, 8-16, 8-20
Whisker reinforcement	7-28, 7-72, 7-73, 9-1, 9-2
Whiteware	3-10, 3-42, B-21, B-22
Wing cracks	4-74, 4-75, 4-78, 4-81
Window failure	4-7, 4-13, 4-26 – 4-29, 4-32 – 4-37, 4-60, 4-62, 6-69, 7-2, Appendix B
Window failure, Notre Dame	4-62
Witness marks	4-27, 4-29, 4-71, 6-42, 6-45, 6-50
X-ray topography	Section 3.23, 8-9
Zinc oxide, varistor	6-19, B-17
Zipper crack	6-53, 6-55 – 6-57
Zirconia	(many examples throughout this Guide)